BOREHOLE GEOPHYSICS FOR MINING AND GEOTECHNICAL APPLICATIONS

Canada

Geological Survey of Canada
Paper 85-27

BOREHOLE GEOPHYSICS FOR MINING AND GEOTECHNICAL APPLICATIONS

edited by
P.G. Killeen

Proceedings of a symposium held in
Toronto, Canada, August 1983

1986

Available in Canada through

authorized bookstore agents and other bookstores

or by mail from

Canadian Government Publishing Centre
Supply and Services Canada
Ottawa, Ontario, Canada K1A 0S9

and from

Geological Survey of Canada offices:

601 Booth Street
Ottawa, Canada K1A 0E8

3303-33rd Street N.W.,
Calgary, Alberta T2L 2A7

100 West Pender Street
Vancouver, British Columbia V6B 1R8
(mainly B.C. and Yukon)

A deposit copy of this publication is also available
for reference in public libraries across Canada

Cat. No. M44-85/27E Canada: $20.00
ISBN 0-660-12200-6 Other countries: $24.00

Price subject to change without notice

Cover

The Geological Survey of Canada's borehole logging truck on site. (GSC 204323)

Original manuscript received: 1985-08
Final version approved for publication: 1985-09

CONTENTS

INTRODUCTION

This volume contains the proceedings of an International Symposium and Workshop on Borehole Geophysics for Mining and Geotechnical Applications, held in Toronto in August 1983. It also contains five of the papers originally presented at an informal workshop on Mineral Logging, held at the Geological Survey of Canada in 1981, and for which the information is still timely and valuable. It was the enthusiasm of the participants at that workshop that led to the organization of the Toronto Symposium which was jointly sponsored by the Canadian Exploration Geophysical Society (KEGS) and the Geological Survey of Canada (GSC). The symposium was attended by over 200 people from around the world, including delegates from Australia, Austria, Finland, France, Holland, Ivory Coast, Norway, Saudi Arabia, Sweden, Switzerland, South Africa, the U.K., U.S.A., West Germany and Canada.

The contents of this volume, which includes 41 papers and summaries of two afternoon-workshops on Instrumentation and on Interpretation are printed in the order of presentation, in groups of papers on logging applications, calibration aspects, EM methods, applied potential methods, acoustic methods, magnetic methods, and 'new' methods. The last category includes borehole radar, magnetometric resistivity, gravity, x-ray and other nuclear methods. The five papers from the earlier Mineral Logging Workshop concern inverse filtering of gamma ray logs, borehole IP, EM, resistivity and seismic measurements, and log calibration and quality control.

It is hoped that this publication will be a valuable reference for some years to come, with its unique blend of case histories as well as theoretical and applied papers on perhaps the broadest range of borehole geophysical techniques for mining and geotechnical applications ever assembled.

Two committees were involved in preparing the Symposium.

Organizing Committee

Chairman: Roger Caven (Geophysical Consultant)
Frank Bottos (Urtec Ltd.)
Nigel Edwards (University of Toronto)
Chris Madsen (Spectronics)

Technical Program Committee

Chairman: Patrick G. Killeen (GSC)
Quentin Bristow (GSC)
Alfred V. Dyck (GSC)
C. Jonathan Mwenifumbo (GSC)

The Organizing Committee was greatly aided by the experience and efforts of Kathy Jones (on loan from CANMET) who found solutions to last minute panics and smoothly oversaw arrangements especially through the critical period of the weeks preceeding and during the Symposium. Special thanks are also due to Kathryn Mooney (GSC) who looked after many of the details of the symposium in its earlier stages, up to and including production of the Program with Abstracts.

INTRODUCTION

Le présent ouvrage est un compte rendu d'un symposium international et d'un atelier sur la géophysique des sondages appliquée à l'exploitation minière et à la géotechnique, tenus à Toronto en août 1983. On y trouve aussi cinq des études présentées au cours d'un atelier sans caractère officiel sur la diagraphie des minéraux, tenu à la Commission géologique du Canada en 1981; l'information recueillie à ce moment-là est encore valable et utile. L'enthousiasme des participants à l'atelier a été tel que le symposium de Toronto a été organisé, parrainé conjointement par la Canadian Exploration Geophysical Society (KEGS) et la Commission géologique du Canada (CGC). Plus de 200 délégués venus de l'Australie, de l'Autriche, de la Finlande, de la France, de la Hollande, de la Côte d' voire, de la Norvège, de l'Arabie Saoudite, de la Suède, de la Suisse, de l'Afrique du Sud, de la Grande-Bretagne, des États-Unis d'Amérique, de l'Allemagne de l'Ouest et du Canada, y ont participé.

Les 41 études présentées à l'occasion du symposium ainsi que les résumés des deux ateliers d'une demi-journée sur l'appareillage et l'interprétation sont donnés par ordre de présentation, par sujet: application des diagraphies, étalonnage, méthodes électromagnétiques, méthodes de la mise à la masse, méthodes acoustiques, méthodes magnétiques et "nouvelles" méthodes. Cette dernière catégorie comprend les méthodes suivantes: radar, résistivité magnétométrique, pesanteur, rayons-X et autres méthodes nucléaires. Vous trouverez ci-après les cinq études présentées au cours de l'atelier sur la diagraphie des minéraux et qui traitent du filtrage inverse des diagraphies gamma, des mesures par polarisation induite, des mesures électromagnétiques, des mesures de résistivité et des mesures sismiques, de l'étalonnage des diagrammes et du contrôle de la qualité.

Nous espérons que cette publication sera une référence précieuse pour bon nombre d'années à venir car elle présente des cas concrets aussi bien que des documents de recherches théorique et pratique portant sur ce qui pourrait être le plus vaste choix de méthodes d'exploration géophysique des sondages jamais compilés sur les applications minières et géotechniques.

Le Comité d'organisation et le Comité du programme technique ont participé à la préparation du symposium.

Comité d'organisation

Président: Roger Caven (conseiller en géophysique)
Frank Bottos (Urtec Ltd.)
Nigel Edwards (Université de Toronto)
Chris Madsen (Spectronics)

Comité du programme technique

Président: Patrick G. Killeen (CGC)
Quentin Bristow (CGC)
Alfred V. Dyck (CGC)
C. Jonathan Mwenifumbo (CGC)

Le Comité d'organisation apprécie l'aide considérable que lui a apportée Kathy Jones (détachée de CANMET); en effet, elle a résolu tous les problèmes de dernière minute et surveillé tous les arrangements, notamment pendant les semaines critiques avant et pendant le symposium. Le Comité aussi tient à remercier spécialement Kathryn Mooney de la CGC qui a apporté une attention serieuse et pertinente des premières aux derières étapes d'organisation du symposium, y compris, sa participation à la mise au point de la publication du Programme accompagné des résumés.

In addition, many individuals in the Borehole Geophysics Section of the Resource Geophysics and Geochemistry Division of the GSC took part in the responsibilities of organizing the technical program including G.R. Bernius, W.G. Hyatt, S. Birk and L. Schock whose assistance is greatly appreciated.

Each paper was critically read by at least two reviewers thereby greatly improving the quality of this publication. In alphabetical order the critical readers are: A.P. Annan, Q. Bristow, L.S. Collett, J.G. Conaway, J.D. Crone, J.L. Davis, A.V. Dyck, R.L. Grasty, P. Gudjurgis, J.K. Hallenburg, J.R. Hearst, C. Huang, P.A. Hurley, O.G. Jensen, P.W. Kasameyer, R. Keith, P.G. Killeen, P.H. McGrath, J.D. McNeill, W.A. Morris, C.J. Mwenifumbo, S. Nargolwolla, E.R. Niblett, A. Overton, T.E. Owen, K.A. Richardson, J. Roth, J.H. Scott, A.K. Sinha, J.A. Slankis, E.J. Schwarz, T.I. Urbancic, R.D. Watts, R.D. Wilson, K.E. Witherly, J. Wong, D.V. Woods, and D.L. Wright. Their time spent on these manuscripts is greatly appreciated.

En outre, de nombreux employés de la Section de la géophysique des sondages, Division de la géophysique et de la géochimie des ressources, CGC, ont participé à l'organisation du programme technique, notamment G.R. Bernius, W.G. Hyatt, S. Birk et L. Schock dont l'aide a été très précieuse.

Chaque étude a été lue par au moins deux réviseurs, ce qui a beaucoup amélioré la qualité de cette publication. Ces lecteurs exigeants sont, par ordre alphabétique: A.P. Annan, Q. Bristow, L.S. Collett, J.G. Conaway, J.D. Crone, J.L. Davis, A.V. Dyck, R.L. Grasty, P. Gudjurgis, J.K. Hallenburg, J.R. Hearst, C. Huang, P.A. Hurley, O.G. Jensen, P.W. Kasameyer, R. Keith, P.G. Killeen, P.H. McGrath, J.D. McNeill, W.A. Morris, C.J. Mwenifumbo, S. Nargolwolla, E.R. Niblett, A. Overton, T.E. Owen, K.A. Richardson, J. Roth, J.H. Scott, A.K. Sinha, J.A. Slankis, E.J. Schwarz, T.I. Urbancic, R.D. Watts, R.D. Wilson, K.E. Witherly, J. Wong, D.V. Woods et D.L. Wright. Nous leurs remercions pour tout le temps et l'effort qu'ils ont consacrés à ces manuscrits.

Président, Comité du programme technique

P.G. Killeen

Chairman, Technical Program Committee

SUBSURFACE EXPLORATION THROUGH PENETRATION – OPENING REMARKS

A.G. Darnley

On behalf of the sponsors I would like to begin by welcoming you to this International Symposium. Toronto is the centre of gravity for mining geophysics in Canada; the University of Toronto is well known for its school of mining geophysics, and so it is appropriate that this meeting should be held here. The Canadian Exploration Geophysical Society is composed of people very much aware of the realities of exploration and the Geological Survey of Canada is pleased to be associated with the Chairman and members of KEGS in making the arrangements for what is intended to be a very down-to-earth occasion.

This meeting is a sequel to a highly successful informal workshop on Mineral Logging held at the Geological Survey of Canada in Ottawa in 1981. It in turn was an outgrowth of earlier workshops on borehole geophysics applied to uranium exploration organized under the umbrella of the International Atomic Energy Agency and the Nuclear Energy Agency. I am glad to welcome a number of participants from these past workshops to this broader field of interest. The majority of people engaged in mineral exploration, or research relating to it, are not long confined to any single commodity, and are required to change their priorities in response to economic circumstances. Fortunately, geophysical techniques are relevant to finding the whole range of economic minerals as well as investigating many engineering problems which involve the earth. It can be very productive to bring together different specialists at a meeting like this, and we hope some cross-fertilization of ideas will be achieved in the workshops which follow.

I entitled my opening remarks "subsurface exploration through penetration" because I want to emphasize the fact that this is what borehole geophysics enables us to do. As far as one can foresee there will always be a need to recover solid rock samples from as great a depth as can be penetrated. Coring will always be required for a proportion of the holes drilled in any exploration program but the requirement will undoubtedly grow for geophysical techniques to supplement what can be deduced from core examination, substitute for loss of core, and extend beyond the thin column of rock directly sampled. I believe the greatest use of subsurface exploration geophysics in the future will lie with uncored holes, made at minimum cost, where data are gathered with a wide variety of passive and active probes, not forgetting television and acoustic viewers. At the same time, the greatest opportunity for new developments probably lies with subsurface reconnaissance methods, using hole-to-hole techniques, requiring a broadly spaced network of holes.

EXPLORATION PAR PÉNÉTRATION DE LA SUBSURFACE – PRÉAMBULE

A.G. Darnley

Au nom des organisateurs, j'aimerais vous souhaiter la bienvenue à ce symposium international. La ville de Toronto est le point de mire de la géophysique minière au Canada; l'école de géophysique minière de l'Université de Toronto est très bien connue et il est donc juste que cette réunion soit tenue ici. Les membres de la Canadian Exploration Geophysical Society (KEGS) sont très conscients des réalités de l'exploration et la Commission géologique du Canada (CGC) se fait un plaisir de prendre avec le président et les membres de la KEGS les arrangements nécessaires pour que nous traitions, tel qu'entendu, de questions pratiques, dans une ambiance cordiale.

Cette réunion fait suite à un atelier sans caractère officiel, mais très réussi, sur la diagraphie des minéraux qui a eu lieu à la Commission géologique du Canada, à Ottawa, en 1981. Cet atelier a été tenu pour faire suite aux ateliers antérieurs sur la géophysique des sondages appliquée à l'exploration de l'uranium, lesquels avaient été organisés sous l'égide de l'Agence internationale de l'énergie atomique et de l'Agence de l'énergie nucléaire. J'ai grand plaisir à accueillir à cet événement de plus grande portée un certain nombre des personnes qui ont participé aux ateliers antérieurs. La plupart de ceux qui travaillent dans le domaine de l'exploration minière ou des recherches connexes ne s'attardent pas longtemps à un seul produit et doivent changer leurs priorités en fonction des circonstances économiques. Heureusement, les méthodes géophysiques peuvent servir à la prospection de toute la catégorie des minéraux économiques ainsi qu'à l'étude d'un grand nombre de problèmes techniques se rapportant à la Terre. Il peut être très utile de rassembler divers spécialistes à l'occasion d'une réunion comme celle-ci et nous espérons que les ateliers donneront lieu à un certain échange d'idées constructives.

J'ai intitulé mon préambule "Exploration par pénétration de la subsurface" car je désire souligner que c'est bien ce que l'étude géophysique des sondages nous permet d'accomplir. Il sera sans doute toujours nécessaire d'extraire des échantillons de roche solide des plus grandes profondeurs possibles. En outre, il faudra toujours extraire des carottes d'une certaine proportion des trous forés dans le cadre de tout programme d'exploration, mais il faudra utiliser de plus en plus des méthodes géophysiques pour compléter les renseignements venant de l'examen des carottes, pour remplacer les carottes perdues et pour fournir des données sur une plus grande étendue. Je crois qu'à l'avenir, les méthodes d'exploration géophysique de la subsurface seront utilisées le plus souvent dans le cas de trous non carottés, forés à un coût minimal, où les données sont recueillies à l'aide d'un bon nombre de sondes passives et actives diverses sans oublier les écrans de télévision et d'appareils acoustiques. En même temps, l'exploration de la subsurface au moyen de techniques recoupant plus d'un puits, qui exige un réseau très espacé de trous, offre les meilleures possibilités en ce qui a trait aux nouvelles découvertes.

It is worth bearing in mind that in petroleum exploration the Schlumberger Corporation, which has 90% of the international well-logging market, had net earnings in 1982 of over $1 billion from this activity. The cost of logging a single petroleum well may be as high as $100K. The application of borehole geophysics to mining exploration clearly has a long way to go and grow!

I am not going to say anything about specific geophysical techniques but merely to ask you to bear in mind some related matters which seem important to me as far as the future of subsurface exploration is concerned.

The first is a problem about which I think something could be done relatively quickly. It is the reliability of down-hole equipment. It is always frustrating and annoying to go to the field, start work, and then have an equipment failure. Delays are often incurred in locating the exact problem; this is particularly true if it is intermittent in nature; there can be lengthy delays in obtaining replacements; the worst situation is when a unit has to be returned to the manufacturer. This is disruptive and costly in the case of normal surface field work. In borehole geophysics, equipment failure is a much more serious matter because often a hole is only accessible for a few hours, and measurements must either be made within this period or not at all. If equipment failures are a relatively common occurrence, potential users of, and customers for, borehole geophysical services are rapidly discouraged. It is clear that to increase the utilization of borehole geophysical methods, reliability of equipment is important, and designers, manufacturers and users need to be particularly alert to this. Until such time as hardware failures become rare events, on-the-spot availability of duplicate equipment is a prudent precaution. I am sure manufacturers will be delighted to be asked to sell all equipment in sets of two!

The second concern I have will be a familiar one to many of you. It concerns the need for calibration and standardization of all geophysical measurements used in exploration. The American Petroleum Institute has established some standards for petroleum borehole work, but these are not suitable for hard-rock situations. There are many reasons why standardization and calibration of different types of measurement are not merely desirable, but positively advantageous. It is not an effective use of the available methods to limit them to the discovery of "anomalies". Whatever parameter is being measured, the "background" or "geological noise" level could be as significant as an "anomaly". How do we recognize very small anomalies? We need to know what the geological noise level is in different geological environments. Geophysical instrumentation generally gives results in numerical form. Greater efforts are required to ensure that wherever possible we acquire numbers relatable to some definable property, or combination of properties, real or nominal, that can be independently verified on sample material of appropriate dimensions. In order to advance the state of the art, and to provide geologically meaningful interpretations we need to

Il est bon de se rappeler que dans le domaine de l'exploration pétrolière, les recettes de la Schlumberger Corporation, qui détient plus de 90 pour cent du marché international des diagraphies, se sont chiffrées à plus d'un milliard de dollars en 1982. Le coût demandé pour diagraphier un seul puits de pétrole peut atteindre 100 000$. L'application de la géophysique des sondages à l'exploration minière a manifestement un long chemin à faire!

Je n'ai pas l'intention de vous parler de méthodes géophysiques particulières mais uniquement de vous demander de bien vouloir tenir compte de certaines questions connexes qui, à mon avis sont importantes pour l'avenir de l'exploration de la subsurface.

La première de ces questions est un problème qui pourrait être résolu sous peu. Il s'agit de la fiabilité des appareils de fond. C'est toujours décevant et fâcheux de se rendre sur le terrain, de commencer le travail puis de subir une panne d'équipement. Il faut parfois beaucoup de temps pour en détecter la cause, notamment lorsqu'il s'agit d'un problème intermittent. Les pièces de rechange peuvent n'être livrées qu'après de long délais; le pire qu'il puisse arriver c'est qu'on doive retourner l'appareil au fabricant. Il y a interruption des activités et les coûts augmentent dans le cas des travaux normaux en surface. En géophysique des sondages, les pannes d'équipement sont plus sérieuses d'autant que le puits n'est souvent accessible que pendant quelques heures et que les mesures ne peuvent se prendre qu'à ce moment précis. Lorsque les pannes sont relativement nombreuses, les utilisateurs et clients éventuels des services de géophysique des sondages se découragent vite. Si l'on veut accroître l'utilisation des méthodes géophysiques, il faudra donc améliorer la fiabilité de l'équipement, il importe que les concepteurs et les fabricants en soient conscients et que les utilisateurs soient au courant. En attendant que les pannes d'équipement se fassent rares, il serait prudent d'avoir accès sur place à des appareils de rechange. Je suis certain que les fabricants seront ravis de vendre deux exemplaires de chaque appareil!

La deuxième de ces questions est connue d'un bon nombre d'entre vous. Il s'agit de l'étalonnage et de la normalisation de toutes les mesures géophysiques utilisées en exploration. L'American Petroleum Institute a établi quelques normes pour le forage des puits de pétrole, mais celles-ci ne conviennent pas à l'étude des roches dures. La normalisation et l'étalonnage des divers types de mesure seraient non seulement utiles mais aussi très avantageuses et pour plusieurs raisons. On n'utilise pas les méthodes disponibles si on les réserve uniquement à la découverte des "anomalies". Peu importe le paramètre mesuré, le niveau de "bruit de fond" peut être aussi élevé qu'une "anomalie". Comment reconnaître les anomalies très faibles? Il faut connaître le niveau de bruit de fond dans les divers milieux géologiques. En général, les appareils géophysiques fournissent les résultats sous forme numérique. Dans la mesure du possible, il faudra tenter d'obtenir des chiffres qui sont rattachable à une propriété ou combinaison de propriétés réelles ou nominales susceptibles d'être définies et vérifiées indépendamment sur des échantillons de dimensions suffisantes. Afin de pouvoir progresser et de fournir des interprétations géologiquement utiles, il faut savoir à quoi rattacher les mesures; pour vérifier le fonctionnement régulier des appareils et compiler les données recueillies par divers appareils, il faudra établir des normes et des

know what our measurements actually relate to; to ensure that instrumentation is performing consistently, and for the purpose of compiling data acquired by different instruments, we need agreed standards and calibration facilities that are convenient and easy to use. Systematic compilation, for the purpose of three dimensional subsurface mapping is going to become an accepted requirement in the future. Although there has been increasing agreement in recent years that standardization of reporting methods and calibration are desirable objectives, unfortunately there has been no rush of eager participants to do anything about it! Similarly the systematic measurement of rock properties from all types of rocks is not regarded by most geophysicists as a very exciting assignment, but it seems to me this is an essential preliminary in the development of comprehensive standards, and ultimately it affects our ability to have effective subsurface exploration. Possibly one way of overcoming this deficiency in systematic basic data is to encourage university geophysics departments to make certain types of rock property measurement their speciality and make a quota of measurements an advanced-course requirement for their students. A lot of progress could be made in a decade.

The third concern I have is a more general one. Hole-making. At first sight this may not seem to be of concern to an audience of geophysicists; it is not something about which geophysicists are expected to be knowledgeable, or to have any responsibility. However the extent and manner in which borehole geophysics will be utilized in the future depends, ultimately upon the ease, and therefore the cost of making holes. The readiness of exploration and mining companies to locate patterns of holes optimized for particular geophysical techniques hinges upon the costs involved. Of course the same could be said of cored boreholes which the geologists will always require. Earth scientists interested in obtaining subsurface data may not realize it, but they have a vested interest in encouraging and promoting cheaper hole-making, because if costs can be substantially reduced, this will permit more use of geophysics and geophysical interpretations will become more reliable.

You may be wondering why I am using the term "hole-making" rather than drilling or boring. This is quite deliberate in order to suggest that the methods by which holes are now made may not be the best or the only way to do it in the future. Rotating an abrasive substance on the end of a long rod or pipe is hardly high-technology!

Compared with mineral exploration geophysics, hole-making is big business. In Canada in 1980 $100M was expended on exploration drilling (about one quarter of which was spent on uranium exploration). The expenditure on R&D for hole-making technology is much less than R&D into exploration geophysics. This generalization appears to be true in every western country, and I find this rather surprising. One explanation may be that whilst there are academic institutions that specialize in applied geophysics there are to my knowledge none that specialize in applied hole-making, certainly not holes of the diameter or

installations d'étallonnage commodes et faciles à utiliser. À l'avenir, la compilation systématique à des fins de cartographie tridimensionnelle de la subsurface sera exigée comme procédure normale. Bien que l'on reconnaisse depuis quelques années qu'il serait souhaitable de normaliser des méthodes de présentation des données et d'étallonnage, les chercheurs ne se sont malheureusement pas précipités pour le faire. De même, la plupart des géophysiciens ne considèrent pas que la mesure systématique des propriétés de tous les types de roches soit une tâche passionnante; toutefois, il me semble qu'il s'agit là d'un travail préliminaire essentiel à l'établissement de normes complètes, qui influera sur notre capacité d'effectuer l'exploration efficace de la subsurface. Il serait peut-être possible d'augmenter le nombre de données fondamentales systématiques en encourageant les départements de géophysique des universités à se spécialiser dans certains types de mesure des propriétés de roche et de faire en sorte que les étudiants avancés soient obligés d'effectuer un certain nombre de mesures. En dix ans, beaucoup de progrès serait accompli.

La dernière question est de nature plus générale. Il s'agit du creusement de trous. À première vue, cette question ne semble pas d'un grand intérêt pour des géophysiciens; on ne s'attend pas à ce que les géophysiciens soient bien informés dans ce domaine ou qu'ils en aient la responsabilité. Toutefois, le degré d'utilisation future de la géophysique des sondages dépendra en définitive de la facilité du creusement des trous et donc du coût. L'empressement des sociétés d'exploration et des sociétés minières à placer les trous de façon à tirer le plus grand avantage de méthodes géophysiques particulières dépend des coûts qu'elles auront à supporter. Manifestement, on peut dire la même chose des sondages carottés qui seront toujours utilisés par les géologues. Bien qu'ils ne s'en rendent peut-être pas compte, les spécialistes des sciences de la Terre qui désirent obtenir des données sur la subsurface ont intérêt à encourager et à promouvoir le creusement de trous à moindre coût, car s'il devenait possible de réduire les coûts, les méthodes géophysiques seraient utilisés davantage et les interprétations géophysiques deviendraient plus fiables.

Vous vous demandez peut-être pourquoi j'utilise l'expression "creusement de trous" plutôt que forage ou percement. Cette utilisation est intentionnelle car je crois que les méthodes utilisées présentement pour creuser les trous ne sont pas les meilleures et qu'elles ne seront pas les seules à être employées à l'avenir. Peut-on parler de techniques de pointe lorsqu'il s'agit simplement de faire tourner un abrasif à l'extrémité d'une longue tige ou d'un long tuyau?

Si l'on compare la géophysique à la prospection des minéraux, le creusement de trous représente de grosses affaires. Au Canada, en 1980, on a dépensé 100 millions de dollars pour le forage d'exploration (dont environ le quart pour l'exploration de l'uranium). La somme consacrée à la recherche et au développement de la technologie du creusement des trous est bien inférieure à celle qui est consacrée aux travaux de R et D en prospection géophysique. Ceci semble vrai dans tous les pays de l'Ouest et c'est ce qui m'étonne. La raison en est peut-être que, bien qu'il y ait des institutions qui se spécialisent en géophysique appliquée, à ma connaissance, aucune ne se spécialise en creusement de trous et certainement pas de trous de diamètre ou de profondeur nécessaires à l'exploration minérale. Le nombre

length required for mineral exploration! So in the absence of dedicated teaching or research institutions there have been very few researchers. The best overall review on hole-making possibilities that I am aware of is one written by William Maurer of Esso Research about 15 years ago. His review covers every method that I have seen mentioned in more recent years. Unfortunately none of the possibilities seems to have progressed very far, as much as anything because no organization has taken, or been given this task as a prime responsibility. Yet when one considers how much has been achieved in the last 25 years in the penetration of outer space by vehicles launched from the surface of the earth one cannot help wondering whether comparable progress could not be made in the penetration of inner space if a small percentage of the R&D invested into space vehicles were to be directed downwards rather than upwards.

By way of conclusion I would like to remind you that in order to make progress in any direction we need to have vision, to go one step beyond current reality. Effective subsurface exploration demands, in the final analysis, much easier physical penetration of the crust. The people who conquered the air and the people who conquered space had vision. Almost all of their contemporaries were skeptics. Those of us interested in subsurface exploration should be willing to spare a little of our own energy to encourage the idea that, given the determination to do so there is no reason why, by the end of the century, deep penetration of the earth's crust should not be as commonplace as flying in space. Think what scope it would give to geophysics and earth science as a whole!

de chercheurs est donc très restreint vu l'absence d'institutions d'enseignement ou de recherche. A ma connaissance, le meilleur compte rendu global des possibilités en matière de creusement a été rédigé par William Maurer d'Esso Recherches, il y a environ 15 ans. Son ouvrage couvre toutes les méthodes que j'ai vu mentionner depuis quelques années. Malheureusement, aucune de ces méthodes ne semble avoir beaucoup progressé, étant donné surtout qu'aucun organisme n'a entrepris ou ne s'est vu confier cette tâche à titre d'objectif principal. Toutefois, si l'on constate les progrès réalisés depuis 25 ans en ce qui a trait à la pénétration de l'espace par des véhicules lancés à partir de la surface de la Terre, on ne peut que se demander si de pareils progrès ne pourraient être réalisés en ce qui concerne la pénétration de la croûte terrestre si seulement un petit pourcentage des travaux de recherche et de développement portant sur les véhicules spatiaux étaient orientés vers le bas plutôt que vers le haut.

En conclusion, j'aimerais vous rappeler que pour progresser, dans quelque direction que ce soit, il faut avoir une claire perception du but à atteindre et aller au-delà de la réalité actuelle. En définitive, si l'on veut explorer efficacement la subsurface, il faut pouvoir pénétrer plus facilememt la croûte. Les conquérants de l'air et de l'espace étaient clairvoyants. Presque tous leurs contemporains étaient sceptiques. Ceux d'entre nous qui sont intéressées à l'exploration de la subsurface doivent être prêts à encourager quelque peu la notion que, si nous sommes déterminés à le faire, rien ne pourra empêcher, d'ici à la fin du siècle, que la pénétration en profondeur de la croûte terrestre devienne un exploit aussi courant que la navigation dans l'espace. Imaginez quel champ d'action s'offrira aux géolphysiciens et aux géoscientifiques en général.

1. AN APPROACH TO DETERMINING STRATIGRAPHIC AND PHYSICAL PROPERTIES OF OVERBURDEN USING BOREHOLE GEOPHYSICS

John P. Greenhouse[1] and Peeter E. Pehme[1]

Greenhouse, J.P. and Pehme, P., An approach to determining stratigraphic and physical properties of overburden using borehole geophysics; in Borehole Geophysics for Mining and Geotechnical Applications, ed. P.G. Killeen, Geological Survey of Canada, Paper 85-27, p. 7-11, 1986.

Abstract

We present our approach in the early stages of a project to establish the subsurface Quaternary stratigraphy and hydrogeological potential of the east flank of the Waterloo Moraine near the cities of Kitchener and Waterloo, Ontario. The complexity of the stratigraphy and the high cost of continuously cored holes to bedrock make it important to gather as much quantitative information from logged rotary-drilled holes as possible. The geophysical component of this project is therefore concerned with identifying certain widely distributed till sequences that can serve as stratigraphic markers, and with estimating the physical properties of all formations traversed by the borehole.

Certain tills, such as the very competent Catfish Creek, can be recognized readily on a variety of geophysical logs. Most are not so easy to identify, however, and their geophysical characteristics may vary widely throughout the region. By logging adjacent to continuously cored holes, and by using calibration pits, we are attempting to bracket the range of responses these units can display on electric, neutron, gamma and gamma-gamma density tools. From this calibration, and with a suite of geophysical logs, we hope to be able to estimate in a statistical sense the porosity, clay content, density and stratigraphy of the formations encountered.

The logger, an ancient but fairly reliable Gearhart Owen unit, feeds its data directly to a CBM 8032 microcomputer with double disk drives. The micro serves as a very low cost digitizer, data logger and data processor, and greatly enhances the capabilities of the system.

Résumé

Nous présentons la méthode suivie au cours des premières étapes d'un projet visant à établir la stratigraphie quaternaire de la subsurface et les possibilités hydrogéologiques du versant est de la moraine de Waterloo près des villes de Kitchener et de Waterloo. La complexité de la stratigraphie et le coût élevé du carottage en continu de la croûte font qu'il est important de recueillir le plus de renseignements quantitatifs possible à partir de trous diagraphiés, creusés par forage rotatif. L'élément géophysique de ce projet vise donc à identifier certaines séquences de till à grande étendue qui pourraient servir de repères stratigraphiques, et à estimer les propriétés physiques de toutes les formations traversées par le sondage.

Certains tills, tel le till très compétent de Catfish Creek, sont facilement identifiés sur une gamme de diagraphies géophysiques. Cependant, la plupart des tills ne sont pas faciles à identifier et leurs caractéristiques qéophysiques peuvent varier considérablement d'un bout à l'autre de la région. En effectuant des diagraphies à côté des trous carottés en continu et en utilisant des fosses d'étalonnage, nous tentons d'établir la gamme des réponses que peuvent présenter ces unités sur les appareils électriques, les sondes neutrons, les sondes gamma et les sondes gamma-gamma. À partir de cet étalonnage et d'une série de diagraphies géophysiques, il serait possible d'estimer, d'un point de vue statistique, la porosité, la teneur en argile, la densité et la stratigraphie des formations traversées.

La sonde, une unité Gearhart Owen ancienne mais plus ou moins fiable, fournit les données directement à un micro-ordinateur CBM 8032 à entraînement à disque double. Le micro-ordinateur sert de convertisseur analogique-numérique, d'enregistreur de données et de machine de traitement des données peu dispendieux et accroît énormément les capacités du système.

[1] Department of Earth Sciences, University of Waterloo, Waterloo, Ontario N2L 3G1

Introduction

We report here on the first year of a three year program to improve understanding of the Quaternary stratigraphy of the Kitchener-Waterloo region of Ontario, a community of about 200 000 people located 130 km southwest of Toronto.

An improved knowledge of the geology of the overburden is important both economically (water supply, gravel) and academically (Quaternary history). One major goal of the program is to improve the usefulness of geophysical logging for the task at hand. The Earth Sciences Department (University of Waterloo) has operated a Gearhart Owen/Widco logging unit for 12 years, mainly as a service to hydrogeology and Quaternary projects. The logging unit includes E-log, neutron, gamma, gamma-gamma and caliper tools. Data were routinely recorded in digital form on cassette tape and transferred to 9-track tape for storage, but little effort was made in the past to develop analysis of these logs beyond a preliminary interpretation (sand/clay) interfaces, well-screen location, etc.). The rotary-drilled boreholes for logging had to be taken when and where they

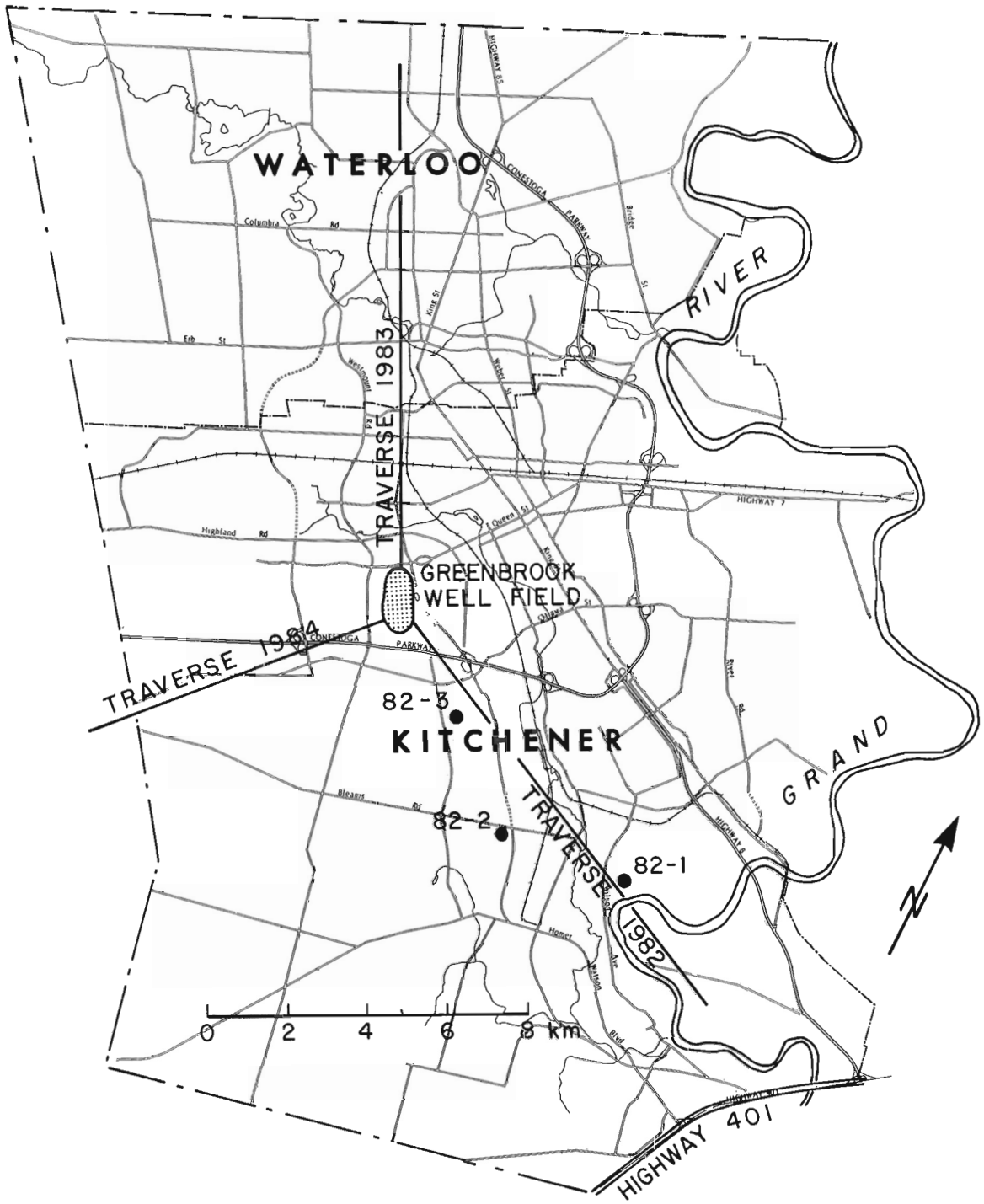

Figure 1.1. Map of the Kitchener-Waterloo region, located 130 km southwest of Toronto. The traverses planned for the three year project are shown. Boreholes completed in 1982 are indicated as 82-1, 82-2, and 82-3.

became available. They were usually uncased, variable in diameter, and liable to collapse within a few hours after drilling or mud circulation ceased. A systematic standardization, calibration and correlation of the log data across the region under these circumstances did not seem practical.

The detailed information required for the Kitchener-Waterloo study is to based on continous coring, which is time consuming and very expensive. As a result, there is ample incentive to improve the yield of geophysical logs. It became apparent in reviewing the published record of geophysical logging in the glaciated areas of central Canada and the United States that the sophistications of hardware and software that are now routinely applied in downhole coal, tar-sands, and mineral exploration have seen little use in geotechnical studies of the overburden. While there have been a number of elegant studies of overburden logging – the papers by Dyck et al. (1972) and Locat (1975) being notable

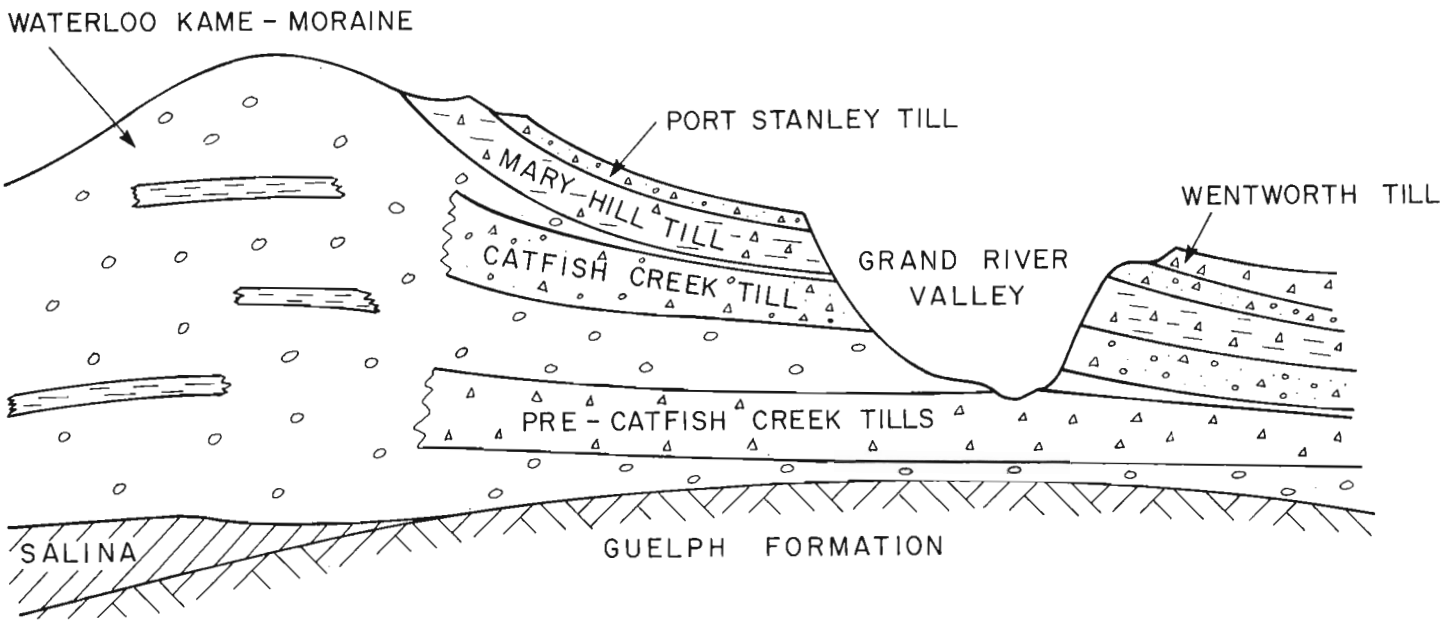

Figure 1.2. *Schematic cross-section showing overburden stratigraphy from West (left) to East (right) on a line passing through the Greenbrook well field in Figure 1.1.*

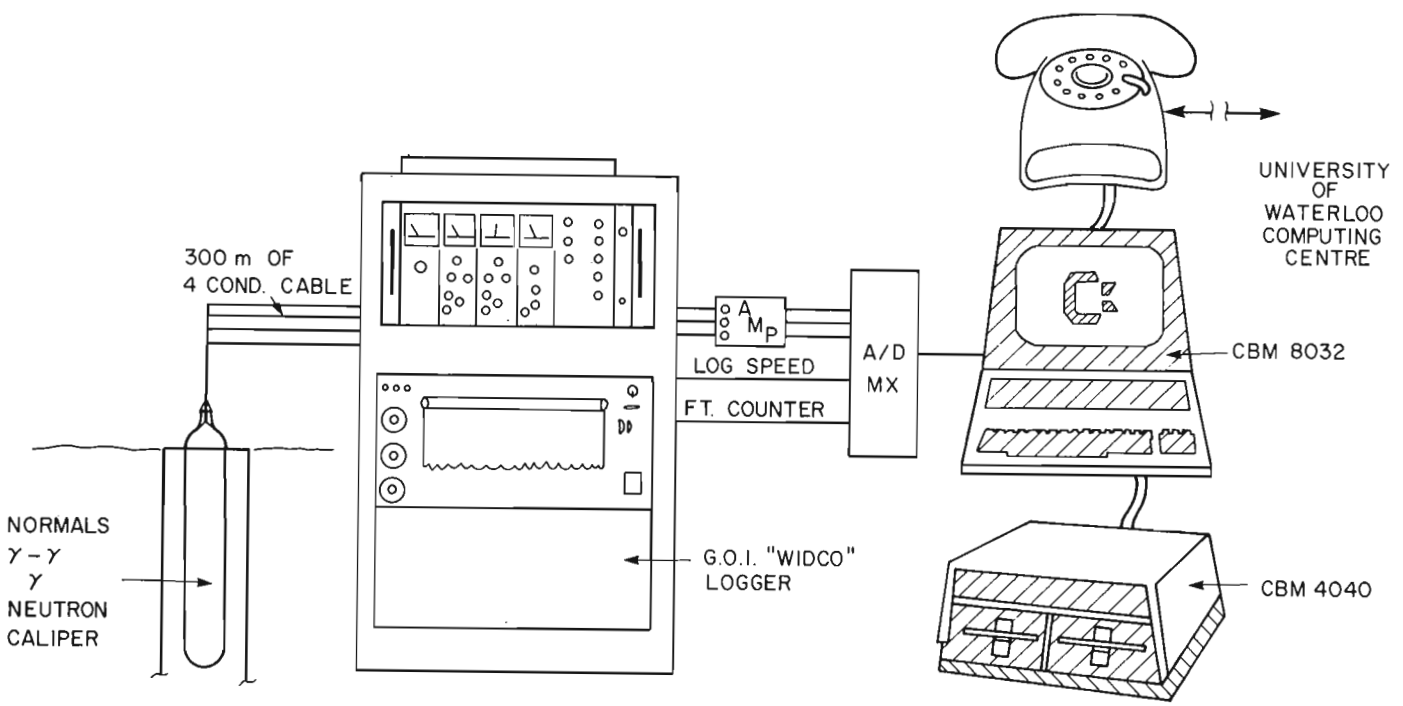

Figure 1.3. *Schematic of the data recording scheme. "A/D" is an analog to digital converter, "MX" a multiplexing unit to feed the 5 digitized records serially to the CBM 8032.*

examples – the "fall-out" from these studies to the day-to-day business of exploring the regolith is limited. Hence the present effort to explore the full potential of geophysical logging in this particular environment appears to be timely.

We describe only our approach to the problem here. The results will be reported later. This project was funded by the Ontario Geological Survey.

Approach

The region of interest is shown in Figure 1.1. Water supply is from sands and gravels within the 50 to 70 m thick overburden, and mainly from the Greenbrook well field near the centre of the diagram. The current project concentrates on three traverses radiating outward from this field. Plans call for 3 logged holes to bedrock, and at least one continuously cored hole, to be completed on one traverse each year. The three boreholes for 1982 are shown on the southwest traverse; a continuously cored hole to 52 m has been completed beside hole 82-3.

While Quaternary deposits are notoriously variable in their lateral distribution, the till units can often serve as stratigraphic markers. A schematic cross-section from west to east through the Greenbrook field is shown in Figure 1.2.

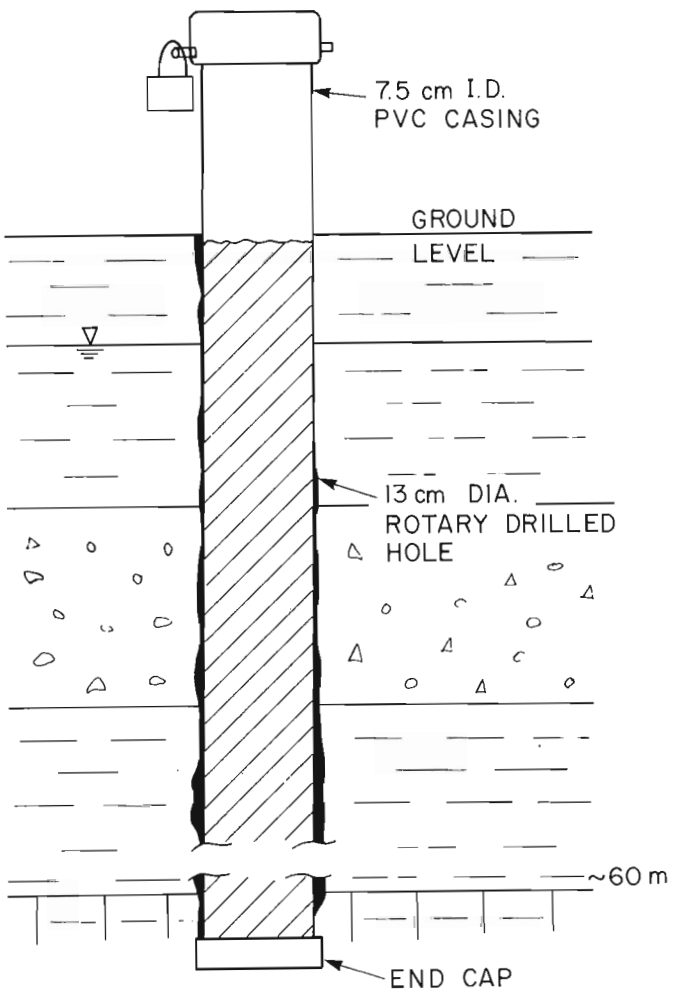

Figure 1.4. *Diagram of the casing installed in the boreholes for this project following E-logging and caliper logging and prior to nuclear logging. The casing is filled with fresh water.*

The Maryhill (clay) and Catfish Creek (sand, boulder) tills in particular are almost always encountered on boreholes throughout the area, they are not usually recognizable on the basis of the drillers logs alone. Pre-Catfish Creek tills are occasionally encountered, but their lateral continuity is not established.

Our objectives for the logging are:

i) To improve data collection and processing with the existing equipment.

ii) To establish and consistently use a standard logging environment.

iii) To calibrate the logging tools against physical properties (formation resistivity, porosity, density, clay content).

iv) To calibrate the logging tools responses for the main stratigraphic units; that is, to establish the mean and variance of the log responses to the existing marker horizons (Catfish and Maryhill tills) and to identify these – and eventually other – units on the basis of those log responses.

v) To correlate the marker horizons and intervening aquifers along the traverses.

The approach to each of these objectives is described briefly below.

Data collection

To improve the versatility and turn-around time of the recording, the system shown schematically in Figure 1.3 has been implemented. Signals from the tools are processed by the GOI electronics and then fed to a CBM 8032 micro-computer for storage on floppy disk and eventual transmittal to the University computer centre.

Standard logging environment

While the E-log and caliper log must be run in the uncased hole, it was important to create a stable, standard environment for the nuclear logs. We now install an inexpensive, 7.5 cm ID PVC drainage pipe as casing (Fig. 1.4), with lower end cap. The entire casing is filled with fresh-water immediately before logging. The casing allows radio-active sources to be safely deployed in the regional aquifers, and the boreholes are available for re-logging at later times.

Calibration for physical properties

We have installed four 1.5 m lengths of 92 cm diameter steel culvert side by side at a site on the north campus of the university. The culvert "bins" have plywood bases, and are set into a stiff clay thought to be Wentworth till. As shown in Figure 1.5 the standard 7.5 cm casing runs down the centre of the bin and 2.75 m into the till, providing two calibrating materials and a calibrating boundary.

Three bins have been filled to date, with sand, concrete and vermiculite concrete. The densities for the sand, concrete, vermiculite concrete and clay are 2.02, 2.38, 1.69 and 2.05 g/cm^3 respectively. The volumetric moisture contents are 38, 33, 42 and 51 per cent respectively. The sand bin can be drained to allow the sand to be logged dry. The fourth bin will be used to fill gaps in the above ranges.

Some care must be taken in calibrating the calibrators. Density and porosity can be quite variable in both time and space within concrete or sand in the bins, and bulk estimates (total weight divided by volume) may mislead. To monitor

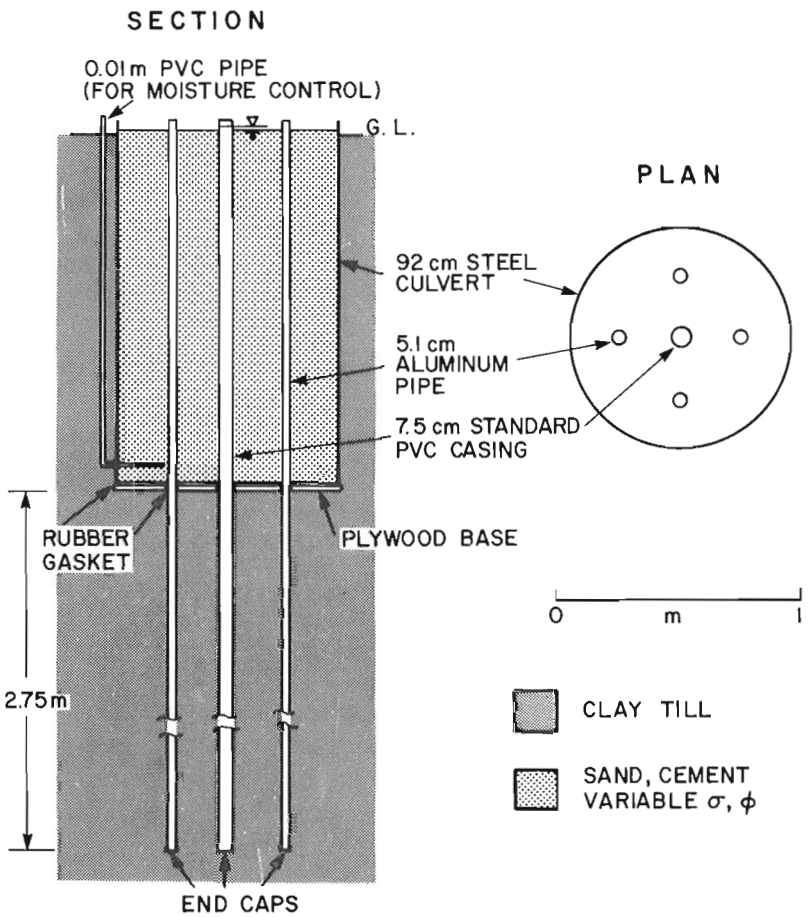

Figure 1.5

Calibration pits for this project consist of a 1.5 m length of 92 cm diameter steel culvert standing upright on a watertight plywood base. The central logging borehole is surrounded by four smaller diameter aluminum tubes which are used to measure moisture content and density with calibrated soil-moisture probes. All the casings extend 2.75 m into an underlying clay till, providing a second calibrating medium with a sharp upper boundary.

changes in space and time within the sands and curing cements, we have installed 5.1 cm aluminum tubes parallel to the borehole at four places in the bin. A calibrated soil moisture probe is passed down these tubes to record the distribution and changes in properties. Filled with water during logging, these tubes do not affect the tool response. The clay contents of the tills, sands and cements have also been determined to calibrate the natural gamma tool response.

The continuous core obtained adjacent to the logged holes on the traverses will in some cases also be suitable for physical property calibration.

Stratigraphic calibration

We plan to drill a series of shallow holes into the Catfish Creek and Maryhill tills at widely separated sites where these two prominent markers are near the surface. Together with the continuously cored holes, these calibration holes will provide a measure of the variability of the till responses to the electric and nuclear logs.

From these measurements we will also determine whether these stratigraphic units can be reliably "fingerprinted" by one or more log responses. This stratigraphic calibration will also be extended to the deeper, pre-Catfish tills if these preliminary attempts appear promising.

We intend to run additional logs in all these boreholes, specifically magnetic susceptibility, gamma ray spectrography, and induction tools as they become available.

Summary

Geophysical logging of water supply and geotechnical boreholes in Ontario with anything other than simple electric and/or natural gamma logs is unusual. Indeed we know of only one drilling or logging contractor between Calgary and Montreal who is prepared to supply its clients with more than point-sampled E-logs in shallow boreholes. The present project, as planned, does not break new ground in logging technology but when measured against the current level of activity in geotechnical logging in our area it becomes significant. We have not attempted to present the initial results in this brief paper, but they encourage us that the goals described above can be achieved.

The success or failure of the project ultimately depends, however, on the cost effectiveness of geophysical logging. A geophysically logged, rotary drilled hole in this area typically costs one third that of a continuously cored hole. It remains to be seen if the quality of geological information obtained from the geophysical data can make this trade off worth while.

References

Dyck, J.H., Keys, W.S., and Meneley, W.A.
1972: Application of geophysical logging to groundwater studies in southern Saskatchewan; Canadian Journal of Earth Sciences, v. 9, p. 78-94.

Locat, J.
1975: Une methode d'utilisation quantitative de la sonde neutron-neutron (porosite) pour l'etude des depts meubles; Commission géologique du Canada, étude 74-42.

2. MULTIPARAMETER LOGGING TECHNIQUES APPLIED TO GOLD EXPLORATION

T.I. Urbancic[1] and C.J. Mwenifumbo[2]

Urbancic, T.I. and Mwenifumbo, C.J., Multiparameter logging techniques applied to gold exploration; in Borehole Geophysics for Mining and Geotechnical Applications, ed. P.G. Killeen, Geological Survey of Canada, Paper 85-27, p. 13-28, 1986.

Abstract

Several boreholes intersecting gold mineralization at the Barber Larder gold prospect, Larder lake, Ontario were logged with gamma ray spectral, induced polarization (IP), resistivity, self potential (SP), and temperature methods in an attempt to delineate favourable lithologic units. The gold mineralization at this prospect occurs within highly altered, pyritized, brecciated and carbonatized volcanic rocks of Archean age. The gold is associated with pyrite mineralization.

A qualitative interpretation of the borehole logging data indicated that SP and gradient SP logs were useful in outlining the known favourable sections of volcanics. Further detailed investigations were carried out in these sections. Zones of gold mineralization within the volcanics were found to correlate with increased apparent conductivity values and in some cases, decreased potassium values. High apparent conductivities are due to increased pyrite content. Abnormally low potassium content is generally associated with high potassium enveloping halos, that are due to an increase in sericite. In general these zones also exhibit low or near zero temperature gradients. Temperature anomalies encountered in these zones are probably due to fracture zones and water movement along the borehole.

Résumé

Plusieurs trous de forage intersectant une minéralisation aurifère dans la zone aurifère prometteuse de Barber Larder, au lac Larder, en Ontario, ont fait l'objet d'enregistrements au moyen de la méthode du spectre du rayon gamma, de la méthode de polarisation induite (PI), de la méthode de résistivité, de la méthode électrique de polarisation spontanée (PS) et de la méthode des températures, en vue de délimiter des unités lithologiques favorables à une découverte. La minéralisation aurifère située dans cette zone prometteuse s'étend dans une formation rocheuse volcanique très altérée, pyritisée, bréchique et carbonatée de l'Archéen. L'or est associé à la minéralisation de pyrite.

Une interprétation qualitative des données de diagraphie indique que les méthodes PS et PS à gradient ont aidé à délimiter les sections prometteuses connues de la roche volcanique. D'autres analyses plus détaillées ont porté sur ces sections. Selon les résultats, la présence de zones de minéralisation aurifère dans la roche volcanique est liée à une plus forte conductivité apparente et, dans certains cas, à une teneur plus faible en potassium. La conductivité apparente élevée découle d'une plus forte teneur en pyrite. Les teneurs anormalement faibles en potassium sont généralement associées à des auréoles encaissantes à forte teneur en potassium qui sont dues à une teneur plus élevée en séricite. En général, ces zones affichent des gradients faibles ou presque nuls de température. Les anomalies de température enregistrées dans ces zones sont probablement attribuables à la présence de zones de fracture et à un écoulement d'eau le long du trou de sondage.

[1] University of Toronto, Toronto, Ontario
[2] Geological Survey of Canada, 601 Booth St., Ottawa, Ontario K1A 0E8

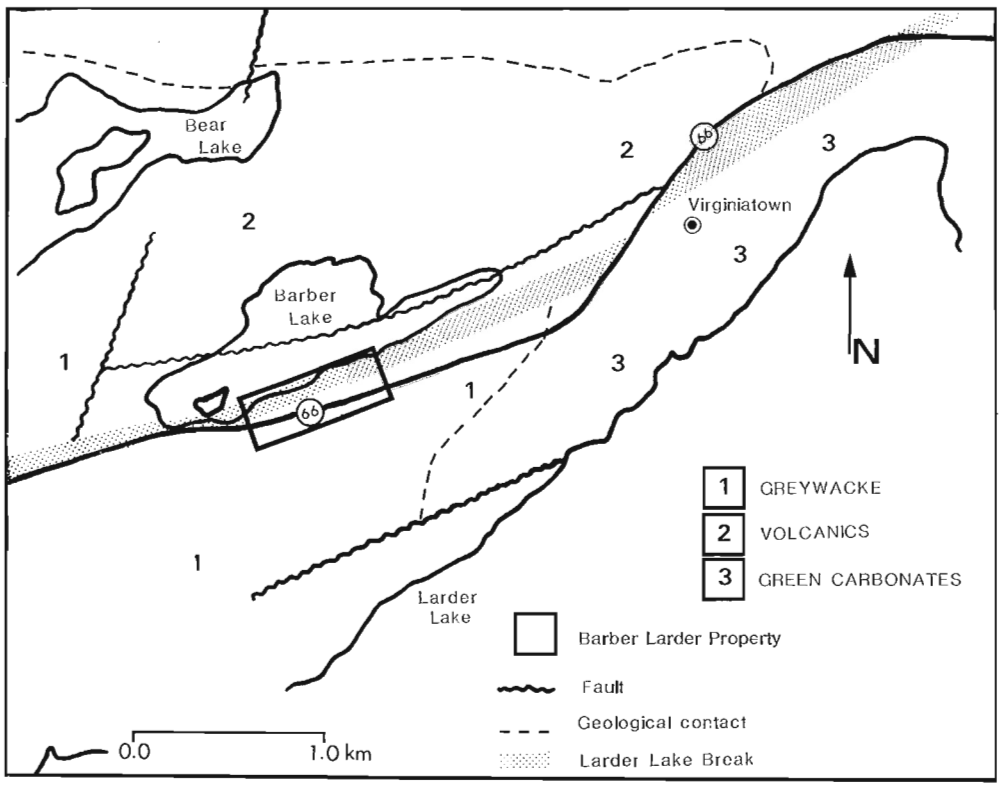

Figure 2.1

General geology of the Barber Larder Lake area. (modified from Hamilton, 1983). The rectangle straddling Highway 66 near Barber Lake outlines the Barber Larder property.

Introduction

Recent increases in gold prices have sparked interest in the metal, resulting in a significant increase in money spent for gold exploration. Despite this increased expenditure, there is still a lack of methodology in gold exploration. In fact, the old axiom 'gold is where you find it' is still applied to exploration in Archean volcanic terranes (Jensen, 1981).

Conventional geophysical methods rely on detecting significant changes in the physical properties of host rocks due to the presence of ore. Since the presence of gold usually does not influence the physical properties of the host rocks to any great extent, geophysical methods have not been utilized extensively in the direct detection of the metal (Boyle and Hood, 1980). However, geophysical techniques have been used to delineate lithologic units favourable for gold mineralization. In principle, the use of geophysical multiparameter logging methods should allow for rapid characterization of rock types by their logging signatures and the delineation of these units into zones with the maximum likelihood for gold occurrence. This approach provides an exploration methodology for gold mineralization.

Most gold deposits are characterized by hydrothermal alteration processes such as sericitization, carbonatization, silicification and pyritization. Sericitization consists of the development of sericite or hydromuscovite within the host rock, resulting in an enrichment in the element potassium (K), including its radioactive isotope ^{40}K. Carbonatization consists of the development of secondary carbonate: dolomite, ankerite and calcite. Silicification is often characterized by an increase in secondary silica (quartz) and depletions in the concentration of potassium. Pyritization consists of the development of disseminated pyrite (Boyle, 1979).

It should be possible to use gamma ray spectrometry to outline alteration zones enriched or depleted in potassium and Induced Polarization (IP) and resistivity techniques to

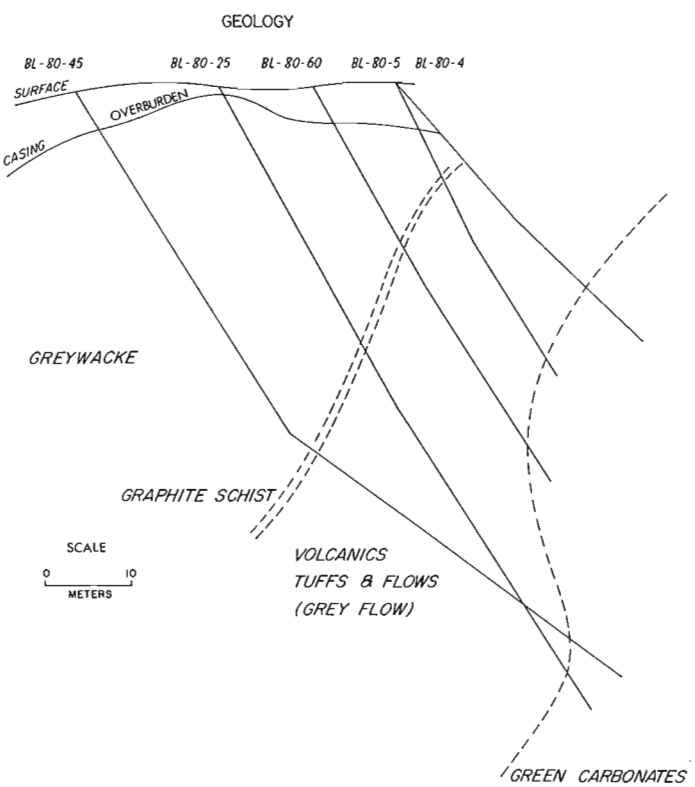

Figure 2.2. *Geological section through the major lithologic units underlying the Barber Larder property. Boreholes intersecting the section are indicated by lines running approximately perpendicular to the lithologic units and are labeled with the prefix 'BL' (notation for Barber Larder). No vertical exageration.*

locate zones of disseminated sulphides (Boyle and Hood, 1980). Structurally, alteration zones lie within wall rock units that are highly fractured and faulted. Temperature logging methods can be used to locate these types of structures, ground water movement (Drury, 1982), and lithologic boundaries.

A number of studies has been conducted on the use of aerial and surface gamma ray spectral methods in prospecting for gold mineralization (Thomson, 1980; Balykin et al., 1973; Tihor and Crocket, 1975; Gross, 1952). Many of the studies have indicated a strong spatial association between gold and potassic alteration zones (Balykin et al., 1973; Krendelav et al., 1976; Fel'dman et al., 1975; Blyumenstev et al., 1974). Although the application of electrical prospecting to gold exploration dates back to 1934 (Kihlstedt, 1934), such studies are scarce in the literature. Most of the work has been proprietary and hence has not been published. To date, the application of temperature methods to gold exploration has not been studied.

Preliminary investigations with downhole gamma ray spectral equipment by Mwenifumbo et al. (1983) provided the following tentative conclusions: zones of higher potassium concentration may be associated with gold, and an inverse correlation exists between gold and potassium in quartz – carbonate stockworks located within volcanic flows and tuffs.

The present study discusses a qualitative correlation of gamma ray spectral, electrical and temperature borehole logs with gold mineralization. Measurements were carried out in several boreholes intersecting gold mineralization on the Barber Larder property. The property is located in the Larder Lake region of northeast Ontario.

Local geology and type of mineralization

The Barber Larder property is situated approximately 2 km west to southwest of the Kerr Addison mine in Virginiatown, immediately south of Barber Lake in the southwest portion of McGarry township, Ontario (Fig. 2.1). The property is underlain by three major lithologic units (Fig. 2.2):

1) An upper unit, Larder Lake group, of fine grained, thinly bedded greywackes.
2) A middle unit of Timiskaming volcanic flows, breccias and tuffs.
3) A lower unit of fuchsite-bearing ultramafic volcanic agglomerates (green carbonate unit).

A relatively thin zone of brecciated graphitic schist occurs at the contact between the greywacke and volcanic unit. The graphitic schist corresponds to the Kerr break, an offshoot of the regional Larder Lake break and is an extension of the larger Cadillac-Malartic break (Campbell, 1957). The gold mineralization is confined to the volcanic unit of the sequence. This favourable unit is part of the Kirkland-Malartic gold belt. At Barber Lake, the volcanic unit is approximately 60 m in width at its maximum. The gold occurs largely within finely disseminated pyrite grains. This mineralized zone most closely resembles the 'flow' type ore found at the Kerr Addison mine, consisting of

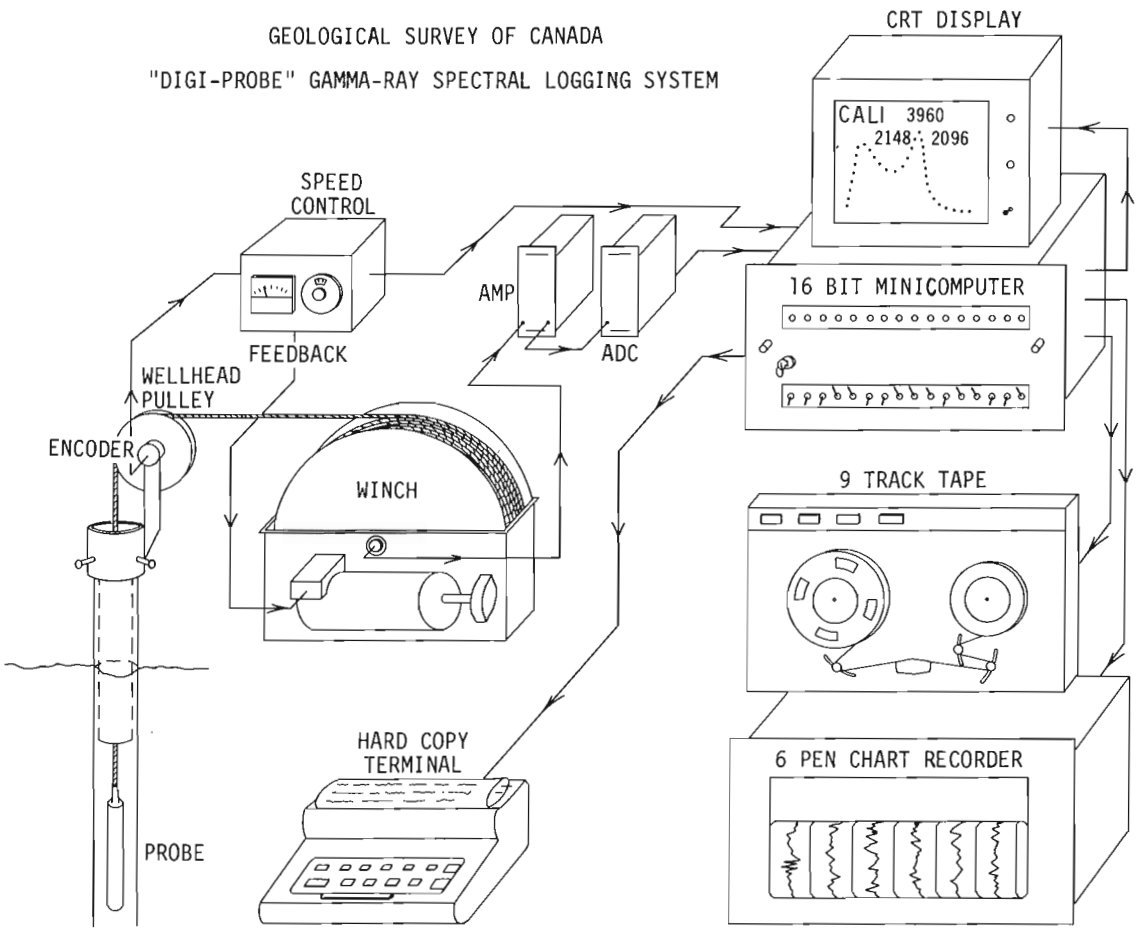

Figure 2.3. *Schematic block diagram of the GSC research and development logging system (after Bristow, 1979).*

lenses of mineralized and carbonatized rock lying within less altered bands of tuffs and flows. Along with pyrite, the ore bodies also contain traces of chalcopyrite, galena, sphalerite, scheelite and arsenopyrite (Baker, 1957).

In general, the entire sequence at the Barber Larder property has been subjected to intense alteration in the form of carbonatization. The lithologic units consist of approximately 60% to 80% carbonate by weight. These units have also been extensively folded and faulted, producing a sequence of steeply dipping beds, trending east to northeast. Total reserves are estimated to be approximately 75 000 tons with an average grade of 0.20 oz/ton (Campbell, 1957; Hogg, 1975).

Table 2.1: Standard gamma ray spectral windows

Decay Radioelement	Series	Window (MeV)	Energy Peak (MeV)
Total Count		0.4-3.0	
Potassium-40		1.36-1.56	1.46
Bismuth-214	Uranium	1.61-2.3	1.76
Thallium-208	Thorium	2.4-3.0	2.62

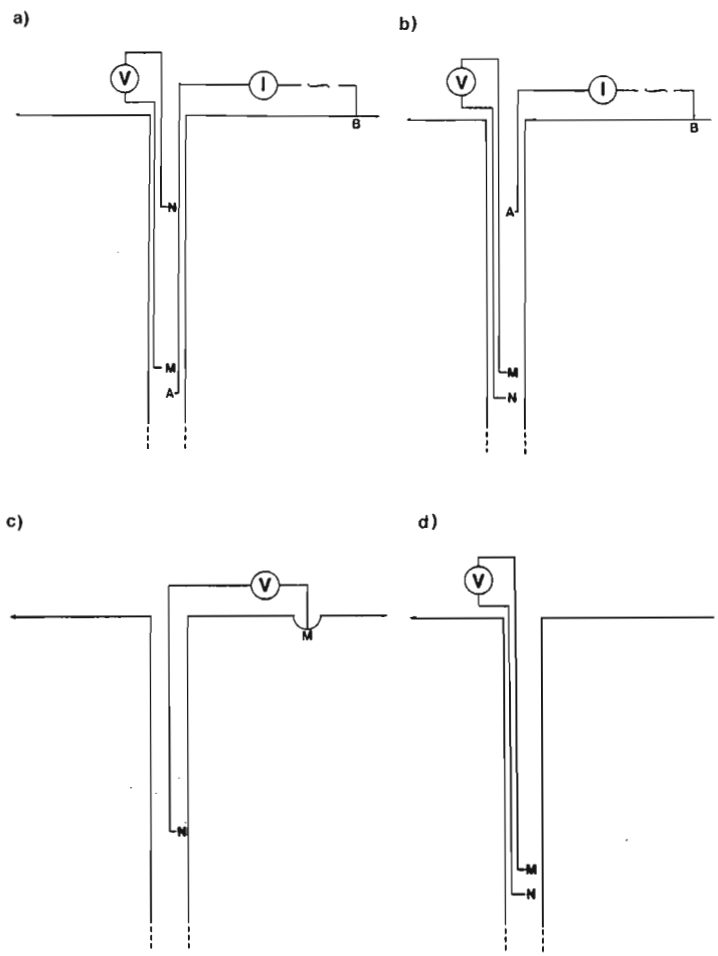

Figure 2.4. The electrode arrays used in the borehole electrical logging:

a) Short Normal array - AM = 0.4 m, MN = 2.6 m
b) Lateral array - AM = 2.6 m, MN = 0.4 m
c) SP array
d) Gradient SP array - MN = 0.4 m.

A and B are current electrodes; M and N are potential electrodes.

Field equipment

The boreholes were logged with the Geological Survey of Canada (GSC) Research and Development borehole logging system (Bristow, 1979). The data acquisition in this system is based on a 16 bit Nova minicomputer. Full gamma ray spectra, IP waveforms and temperature were digitally recorded on 9 track magnetic tapes (Fig. 2.3).

In addition to recording full gamma ray spectra (0 MeV to 3.0 MeV in 256 channels), accumulated counts in ten pre-selected energy windows are also recorded on tape. Logs of the selected windows and combinations of them, can be displayed on a multipen chart recorder during the data acquisition. The recording of the complete spectrum makes it possible to examine energy ranges other than the standard windows used in gamma ray data analysis (Table 2.1). The scintillation detector used in the present study was a 32 mm x 127 mm sodium iodide (thallium activated) crystal.

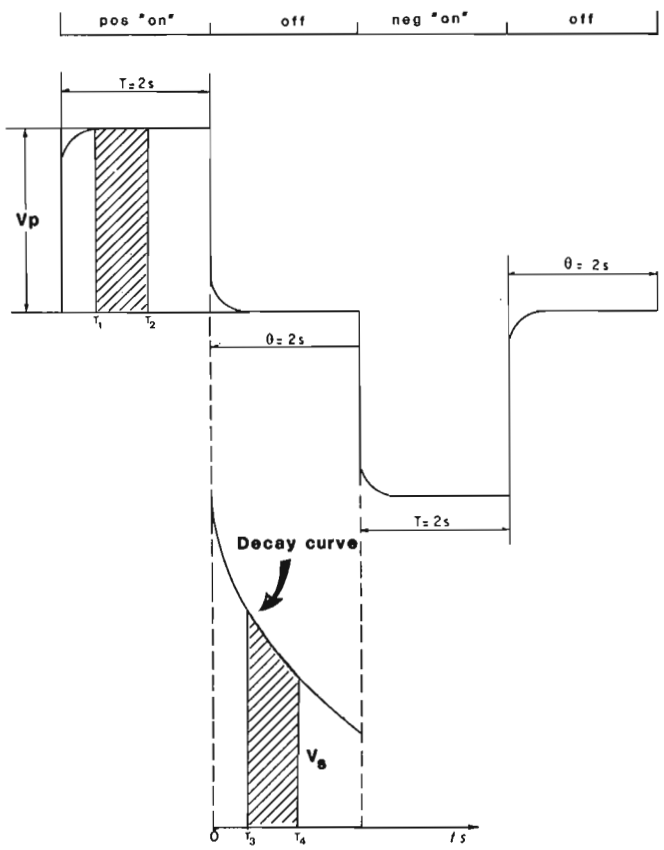

Figure 2.5. Typical Newmont type IP and resistivity waveform consisting of a T second positive polarity current pulse 'on' time, a second ø current 'off' time, a T second negative polarity 'on' time and a second ø 'off' time where T øand are set to 2 s. The primary voltage is obtained from the area between T_1 (0.45T) and T_2 (0.85T). The secondary voltage is obtained from the area between T_3 (0.28ø) and T_4 (0.5ø). V_p is used in the calculation of resistivity and V_s is used in the calculation of IP (after Bertin and Loeb, 1976).

Temperature logging was carried out with an active probe containing a voltage to frequency convertor and a sensor in the form of a 15 cm long tip of bead thermistors. The system has a noise equivalent of less than 0.0001°C (Bristow and Conaway, 1984).

A 4-electrode system consisting of 2 downhole potential electrodes and 2 current electrodes was used for resistivity and IP measurements (Figure 2.4). One of the current electrodes was placed on the surface at a considerable distance (approximately 0.5 km) from the borehole in order to minimize its influence on the measurements in the borehole. Measurements were taken with the time domain IP system developed at the GSC (Bristow, 1986). The current waveform is transmitted as a symmetrical sequence of Positive, Off, Negative, Off pulses. The time for such a sequence can be set at 1, 2, 4 or 8 seconds. The corresponding voltage waveforms detected at the potential electrodes are digitized at 4 ms intervals. The number of samples recorded per complete waveform were 256, 512, 1024 and 2048 corresponding to 1, 2, 4 or 8 second periods, respectively. The transmitter is a constant current source. The current can be varied in steps of 1 mA from 1 to 128 mA and in steps of 2 mA from 128 to 256 mA. The value is set automatically by the system based on received signal strength.

Computed primary voltage (V_p), IP and SP were also recorded and displayed on the multipen chart recorder during the data acquisition. Gradient SP measurements were also recorded with the current switched off.

In addition to the above, a separate portable system was used to obtain conventional SP and gradient SP measurements. For conventional SP measurements the system employed a surface potential electrode and a downhole potential electrode (Fig. 2.4c). The surface electrode consisted of a non-polarizable copper-copper sulphate electrode (porous pot). The downhole electrode was a 0.02 m long cylindrical platinum mesh. Measurements were recorded manually every 0.2 m from a digital multimeter. Gradient SP measurements were taken with a probe consisting of two platinum electrodes with a separation of 0.4 m.

Calibration of the logging equipment

To determine actual values for the measurements observed, proper calibration of the logging equipment is essential. For gamma ray spectral data, a correction is required for interferences due to Compton scattering from radioelement energy peaks adjacent to each of the standard energy windows used. For example, high concentrations of thorium produces anomalously high count rates in the uranium and potassium windows. To correct for this, stripping ratios are determined (Killeen, 1979) from measurements made in model boreholes with known concentrations of potassium, uranium and thorium (Killeen and Conaway, 1978). From these model boreholes, deconvolution parameters are also determined (Conaway, 1980). The calibration of the gamma ray spectral system also requires the determination of the sensitivities that are used to derive concentrations of each particular radioelement. The gamma ray spectral equipment was calibrated using the Geological Survey of Canada Calibration Facilities in Ottawa, Ontario. Calibrations were done before and after the field survey.

The electrical equipment was tested at the GSC Borehole Geophysics Test Site in Ottawa. The logs obtained were compared to test results the GSC has obtained through their own testing as well as results obtained from the test holes by geophysical logging companies. The temperature equipment, like the electrical equipment was tested at the GSC Borehole Geophysics Test Site. The repeatability of the measurements was verified by comparing the results with existing logs recorded by the GSC. The accuracy of the temperature data was determined in the laboratory with the use of water baths at known temperatures (Keys and MacCary, 1976).

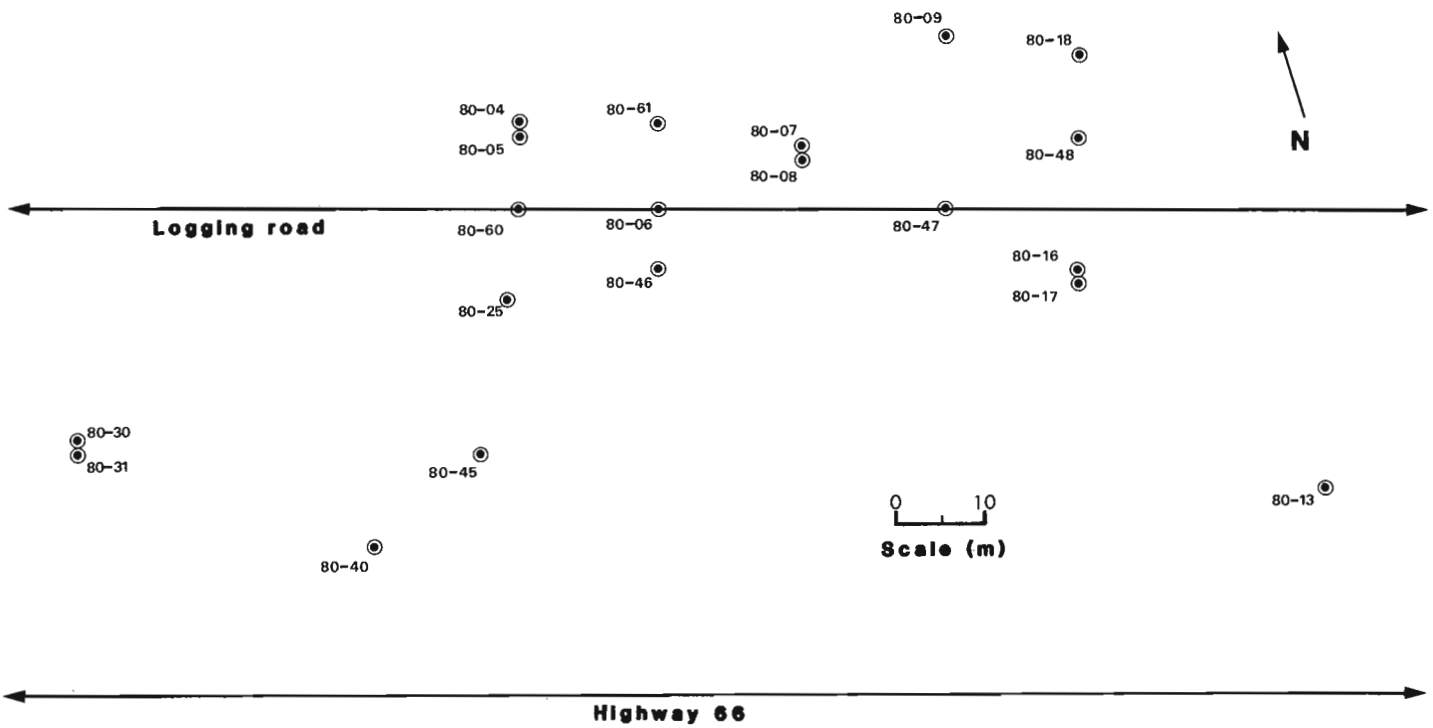

Figure 2.6. The surface location of the boreholes investigated on the Barber Larder property. Strike of the ore body is along the logging road. Results are presented from: a) boreholes 80-04, 80-05, 80-25, 80-45, 80-17 and 80-47 intersecting gold mineralization; b) barren borehole, 80-13.

Data processing

Gamma ray spectral data:

Gamma rays are random in nature and are governed by a Poisson statistical distribution. The amount of noise is inversely proportional to the square root of the level of radioactivity for a given counting time and inversely proportional to the square root of the counting time for a given level of radioactivity. As a result, low countrate environments produce logs that exhibit a high amount of statistical noise. This noise is accentuated when the stripping factors are applied to the data. Normally, the deconvolution operator is combined with a low pass filter and applied to the data to reduce the high frequency noise. Use of the deconvolution operator assumes that the set of borehole and formation field conditions are similar to those encountered in the model boreholes and that the source of radioactivity is within a zone perpendicular to the borehole. No corrections were applied to the data obtained in boreholes that intersected the lithologic layers at oblique angles.

Resistivity and IP data:

A 0.4 m normal array was used in the resistivity and IP measurements. For an ideal normal array, the reference potential electrode, N, is placed on the surface (effectively at infinity). In practice, however, the N electrode is placed downhole at a distance from the current electrode, A, considerably greater than the measuring potential electrode, M.

The apparent resistivity, ρ_a, is a function of the primary voltage, V_p:

$$\rho_a = KV_p/I \qquad (1)$$

where: I is the input current.

K is the geometric factor for the normal array, with the

N electrode down the borehole:

$$K = 4\pi R_1 R_2/(R_2 - R_1) \qquad (2)$$

where: R_1 = AM spacing
R_2 = AN spacing

V_p is the average of the positive and negative "on" cycle voltages, integrated from 0.45T to 0.85T (T_1 to T_2 in Fig. 2.5):

$$V_p = \left[1/(0.4T)\right] \int_{0.45T}^{0.85T} V(t)dt \qquad (3)$$

where T is the 'on' cycle period

The apparent resistivities are expressed in ohm-m.

The induced polarization (or chargeability) values are calculated from the secondary voltage, V_s, during the decay cycle:

$$M_a = \left[1/V_p\right] \int_{0.285\theta}^{0.55\theta} V_s(t)dt \qquad (4)$$

For a 2 second decay cycle (θ = 2 s.), M is the standard Newmont Chargeability parameter (Bertin and Loeb, 1976; Fig. 2.5). The apparent chargeability, M_a, can be expressed in milliseconds (ms) or mV/V. The present IP data are expressed in mV/V.

Temperature data:

The temperature probe sensor has an inherent response lag or time constant. A step change in temperature would be recorded as an exponential change with time in the

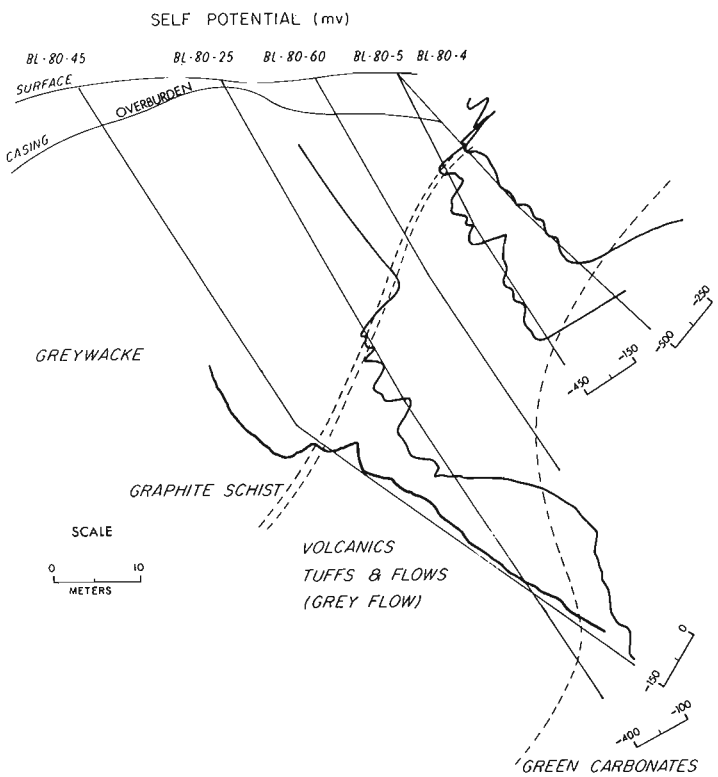

Figure 2.7. *Portable SP results plotted along the boreholes (dark lines) for a fence of boreholes across the main ore zone. Measurements were taken every 0.2 m.*

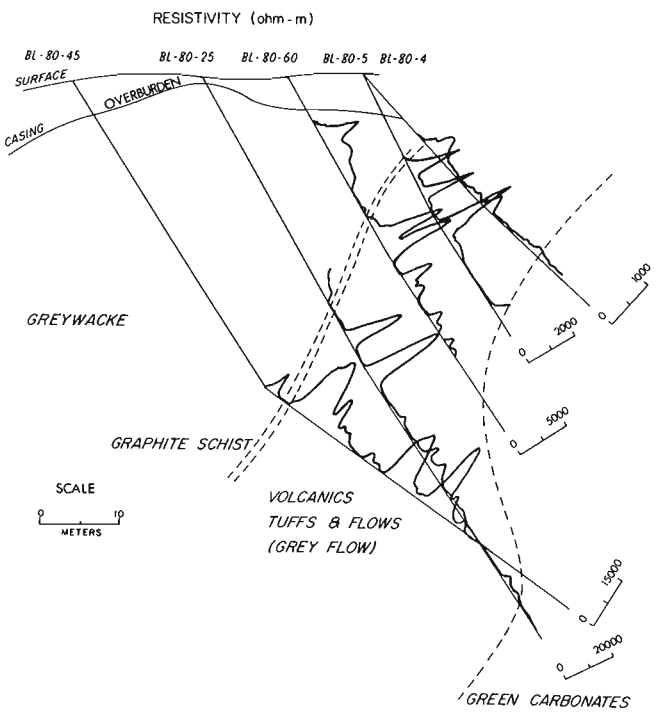

Figure 2.8. *Resistivity results plotted along the boreholes (dark lines) for a fence of boreholes across the main ore zone. The boreholes were logged at 3.0 m/min with a sample time of 1 s. A 0.4 m short normal array was used for the measurements.*

electrical resistance. The true temperatures were obtained by deconvolving the data with an inverse operator (Conaway, 1977, 1980; Bristow and Conaway, 1984). Temperature gradient data were obtained by applying a combined gradient, deconvolution and smoothing operator (low pass Blackman filter) to the recorded data (Conaway, 1977). The effective smoothing length of 0.5 m produced logs with acceptable signal to noise ratios.

Field results and discussions

Of the 12 boreholes logged (Fig. 2.6), results are presented from boreholes intersecting gold mineralization and from a barren borehole outside of the ore body (ie. core assay results indicated no gold). The boreholes were logged initially with the temperature probe at a logging speed of 3.0 m/min with a sample interval of 0.375 s. The gamma ray logging was conducted at 0.3 m/min with a sampling interval of 12 s (approximately one half of the detector length). This appeared to be adequate for the low radioelement concentrations encountered in this environment (i.e. the count rates observed in the K, U and Th windows after stripping provided enough information to delineate changes in the radioelement concentrations). The electrical logging was carried out with a 0.4 m normal array with a logging speed of 3.0 m/min and a period of 1 s. All the boreholes were logged twice to check for repeatability. A borehole fluid stabilization period of 24 hours preceeded each temperature log, during which the borehole was left undisturbed.

The gamma window data were stripped and converted to concentrations. The resistivity (rho), IP and gradient SP (SP Grad) logs were computed from the complete voltage waveforms recorded on the field tapes. The resistivity log was used in the calculation of log rho and 1/rho (apparent conductivity). Rho, 1/rho and log rho all show the same information, but the last two parameters are an enhanced form of the data which makes interpretation easier. The gradient SP log was integrated to produce the SP log. The temperature (Temp) data were obtained directly from the field tapes. The gradient temperature log was derived from the temperature logs.

One of the major problems encountered in attempting to make comparisons between geophysical log data and core was in relating the depths accurately. Due to the nature of drilling and core recovery (possible missing or lost core), errors exist in determining exact core depths. Cable stretching and slippage may also introduce errors in the depth measurements of the geophysical logs. Marker horizons such as the greywacke-graphite schist boundary (clearly recognizable in most of the logs) were used to correct for any depth offsets between the logs and the core assays.

Crosshole comparisons of electrical data

An initial investigation was conducted to determine if favourable units for gold mineralization could be outlined with the use of multiparameter logs. Figure 2.7 shows a fence of boreholes across the ore body that were logged with the portable SP system. Major changes in SP occur at the boundary between the volcanic unit and the overlying greywackes. The volcanic and the underlying green carbonate contact is also well defined in the upper section (boreholes 80-4, 80-5) from the SP data. The volcanics unit

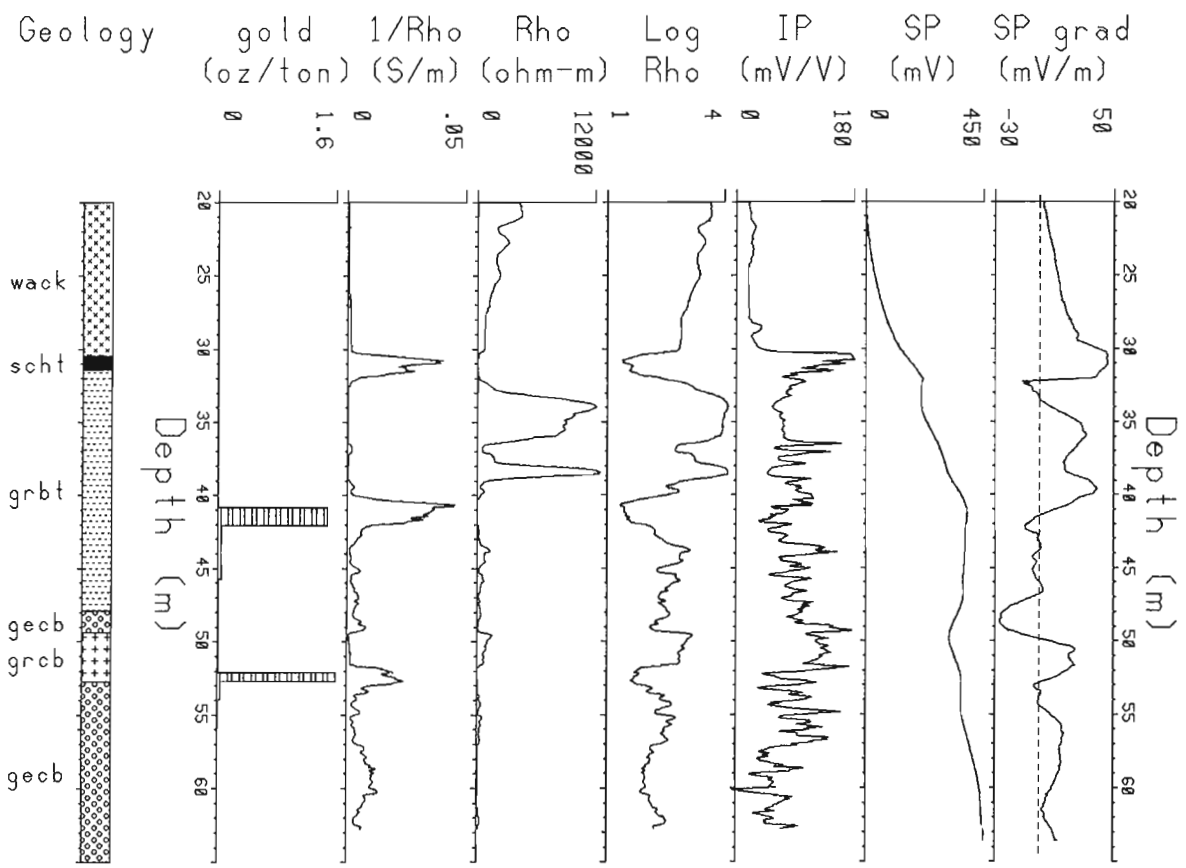

Figure 2.9. Correlations between the electrical logs, gold assays and geologic log for borehole 80-17. The geology abbreviations are: wack – greywacke; scht – graphitic schist; grbt – grey flow breccia and tuff; gecb – green carbonate; grcb – grey flow breccia.

is outlined by SP values that are less than the surrounding greywacke and green carbonate units (Fig. 2.7; boreholes 80-04, 80-05 and 80-25).

Figure 2.8 shows the resistivity logs for the fence of boreholes across the ore body. Within the unit of volcanic tuffs and flows, the resistivity logs are more variable than the SP logs. The volcanics can be subdivided into zones of high resistivity, associated with increased quartz-carbonate content and into zones of low resistivity, predominantly associated with increased pyrite content. Since the gold mineralization is predominantly associated with pyrite, it is within the low resistivity zones that there is an increased likelihood of gold occurrence. Unfortunately, the low resistivity zones are not uniquely associated with pyrite locations because low responses are also observed in the regions of increased graphite content (Fig. 2.9, graphite schist layer). This implies that a combination of geophysical parameters, other than the just the electrical parameters, is required in order to define the regions for the maximum likelihood of gold occurrence.

The next step therefore involved determining if a combination of geophysical parameters could be used to locate the sections of gold mineralization without ambiguity within the volcanics. Comparisons were made between the drill core geological log, gold assays and the geophysical parameters for boreholes 80-17, 80-47, 80-25, 80-05 and 80-13.

Borehole 80-17

Figure 2.9 shows a comparison between the geology, gold assays and the electrical logs for borehole 80-17. Gold assays are presented in a histogram format. Two zones of high gold assays are observed from 40.8 m to 42.2 m within the grey flow breccia tuff unit and from 52.1 m to 52.8 m within a section of quartz-carbonate stockwork. A detailed comparison of the gold assays and the drill core geological log indicates that the zones of gold mineralization correspond to zones of increased pyrite content.

Examination of the electrical logs allowed for the determination of the pyritic and graphitic rich and poor zones (Fig. 2.9). The graphitic schist is characterized by an

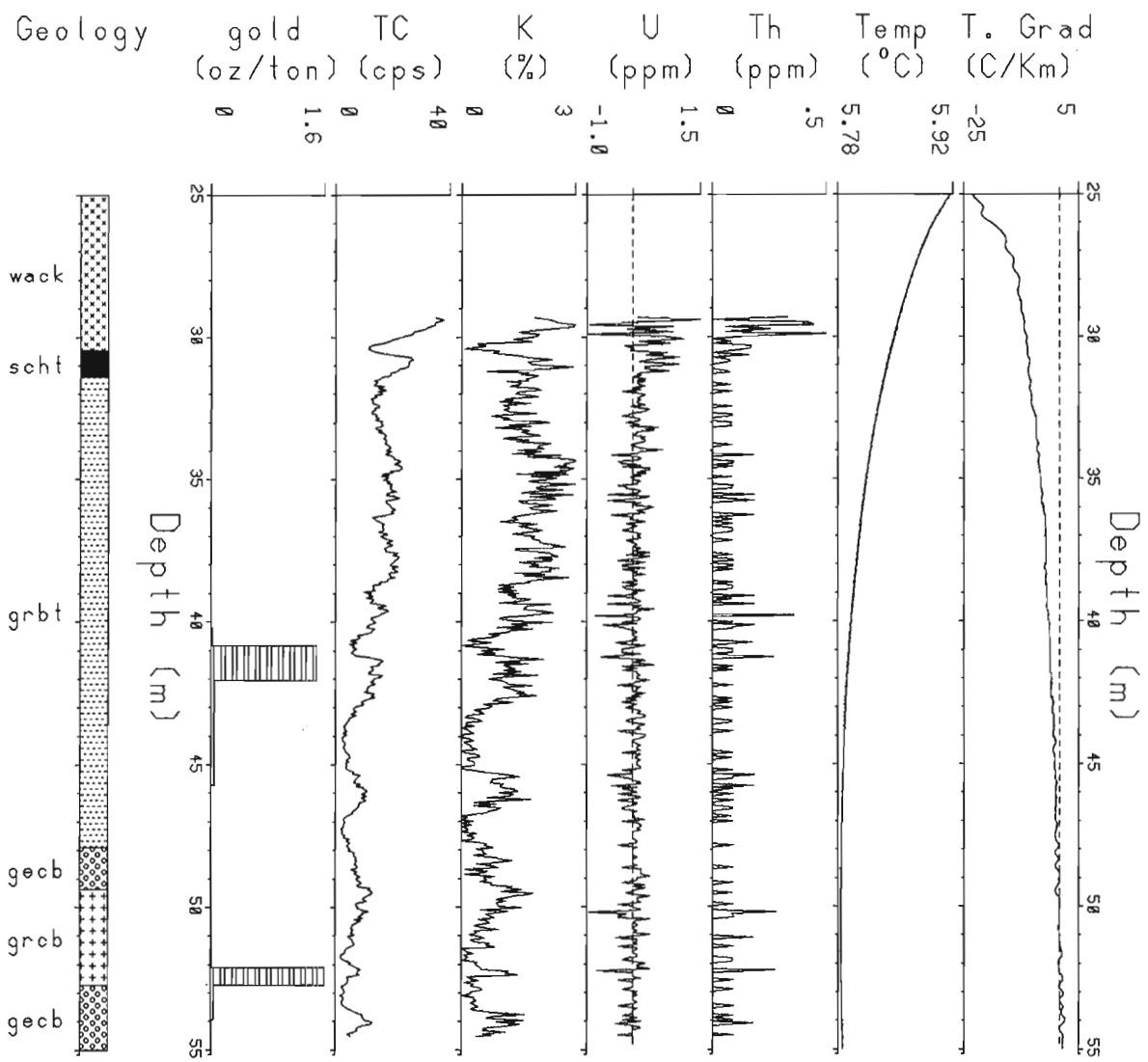

Figure 2.10. *Correlations between the gamma ray spectral logs, temperature logs, gold assays and geological log for borehole 80-17. The geology abbreviations are: wack – greywacke; scht – graphitic schist; grbt – grey flow breccia and tuff; gecb – green carbonate; grcb – grey flow breccia.*

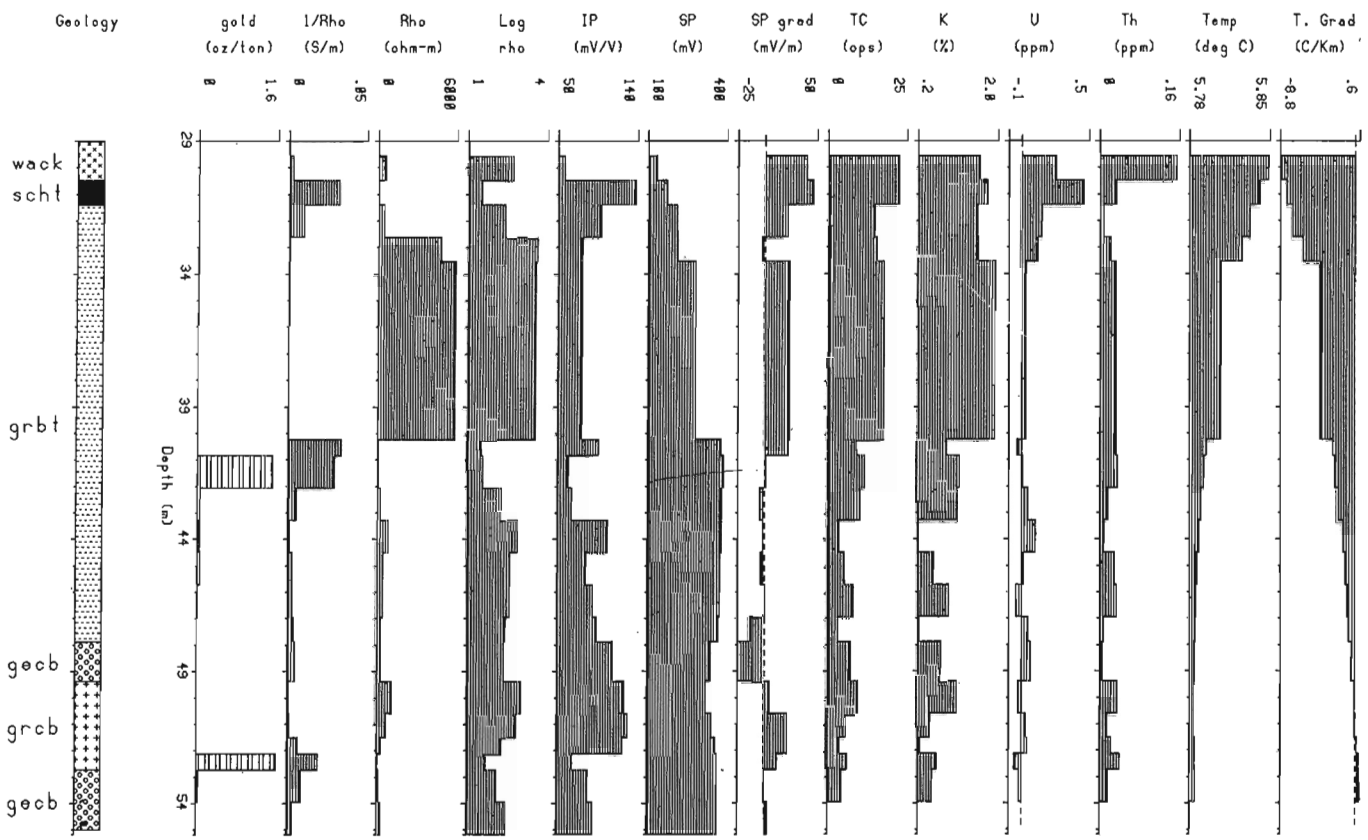

Figure 2.11. Correlations between the geophysical logs, gold assays and geological log for borehole 80-17. The geophysical logs are averaged over the gold assay sample intervals. The geology abbreviations are: wack – greywacke; scht – graphitic schist; grbt – grey flow breccia and tuff; gecb – green carbonate; grcb – grey flow breccia.

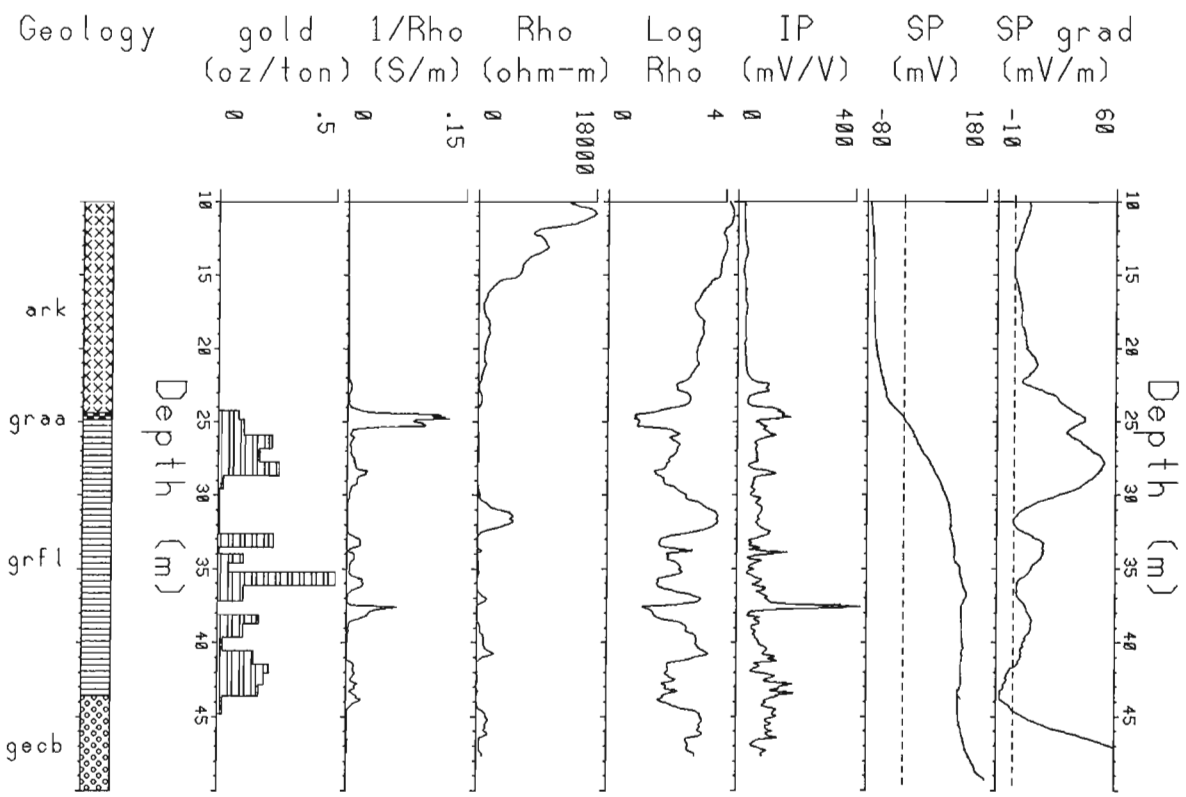

Figure 2.12. Correlations between the electrical logs, gold assays and geological log for borehole 80-47. The geology abbreviations are: ark – arkose; graa – graphitic argillite; grfl – grey flow; gecb – green carbonate.

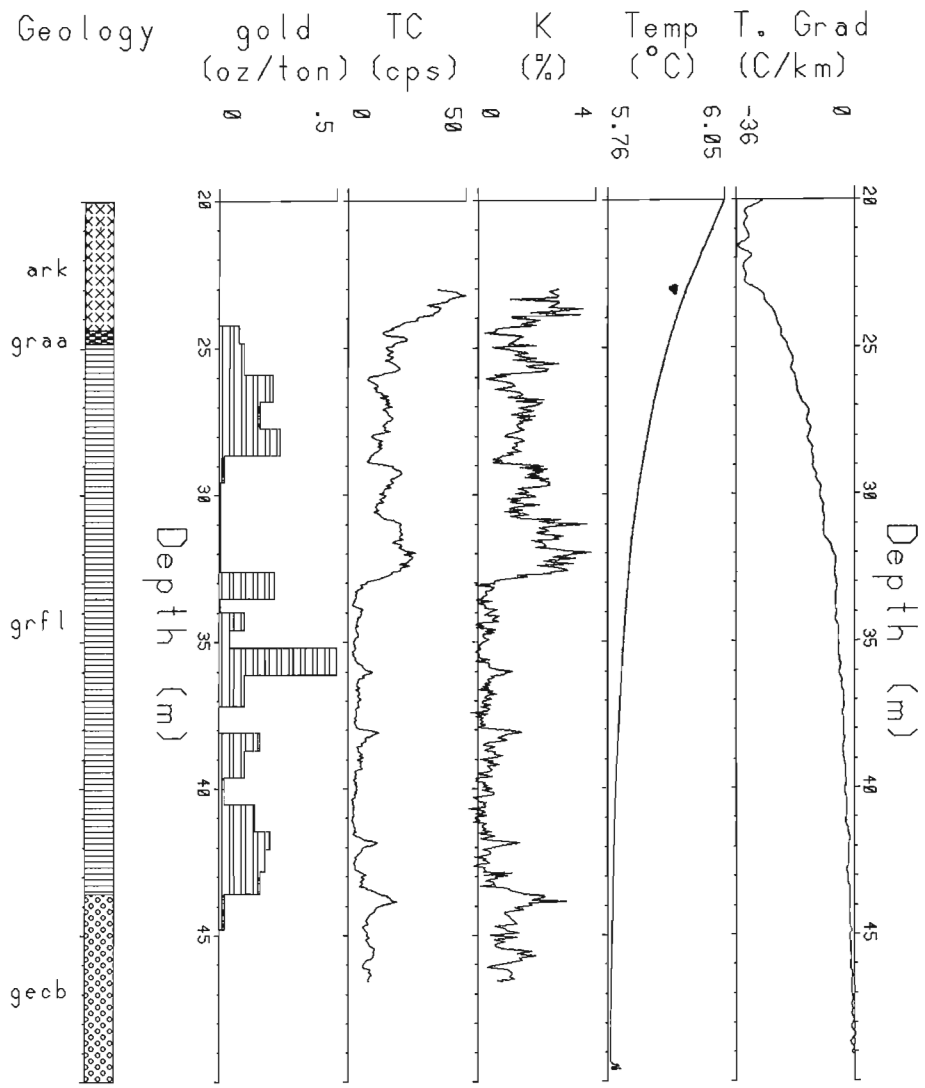

Figure 2.13

Correlations between the total count, potassium, temperature and temperature gradient logs with the gold assays and geological log for borehole 80-47. The geology abbreviations are: ark – arkose; graa – graphitic argillite; grfl – grey flow; gecb – green carbonate.

increase in apparent conductivity, IP effect and a decrease in log resistivity values. Both zones of gold mineralization are outlined by increases in apparent conductivity. The apparent conductivity, in general, also outlines sections of increased pyrite content. The IP log generally shows high chargeabilities within the volcanic unit, because there is disseminated pyrite throughout the unit.

The gamma ray spectral logs for borehole 80-17, shown in Figure 2.10, indicate that the uranium and thorium values appear to be scattered about zero, (ie. virtually no uranium or thorium is present). Increases in the potassium content on the log may correspond to the location of sericitized zones. The potassium log also indicates a general decrease in potassium with depth. This divides the volcanics into an upper portion of higher potassium concentrations and a lower portion with smaller potassium concentration levels. This change in potassium might possibly be that sericitization is more prevalent closer to the graphite schist. There is no clearly defined relationship between potassium and the location of gold mineralization for borehole 80-17.

The temperature and temperature gradient logs (Fig. 2.10), do not appear to be very informative, although the temperature gradient appears to approach zero along the lower section of the volcanics. The absence of anomalies atleast indicates that the conductivity anomalies are not due to major fractures with moving fluids.

Figure 2.11 is a plot of the geophysical parameters with the values averaged over the intervals used in the gold assays of the core. These plots were used to increase the statistical accuracy of the logs and to allow for direct comparison of the log parameter data with the gold assays. The averaged logs generally confirm the results of the unaveraged logs. The graphite schist is defined by an increase in apparent conductivity, IP effect, slight potassium and uranium. A change in potassium content is observed in the grey flow unit at 40.2 m (a corresponding change is observed in the potassium and resistivity logs). The gold mineralization at 40.8 m correlates with increases in apparent conductivity and decreases in IP. The potassium, uranium and thorium logs do not correlate with the location of mineralization.

In summary, for borehole 80-17, a number of qualitative correlations exists between the different lithologic units, alteration zones, gold assays and the geophysical logs. The strongest correlation with gold mineralization is seen in the apparent conductivity log.

Borehole 80-47

Figure 2.12 is a plot of both the electrical logs and drill core geological log for borehole 80-47. Increases in the apparent conductivity log correspond to sections of pyrite (>10 % pyrite) observed in the core. The gold mineralized sections also correspond with increases in the

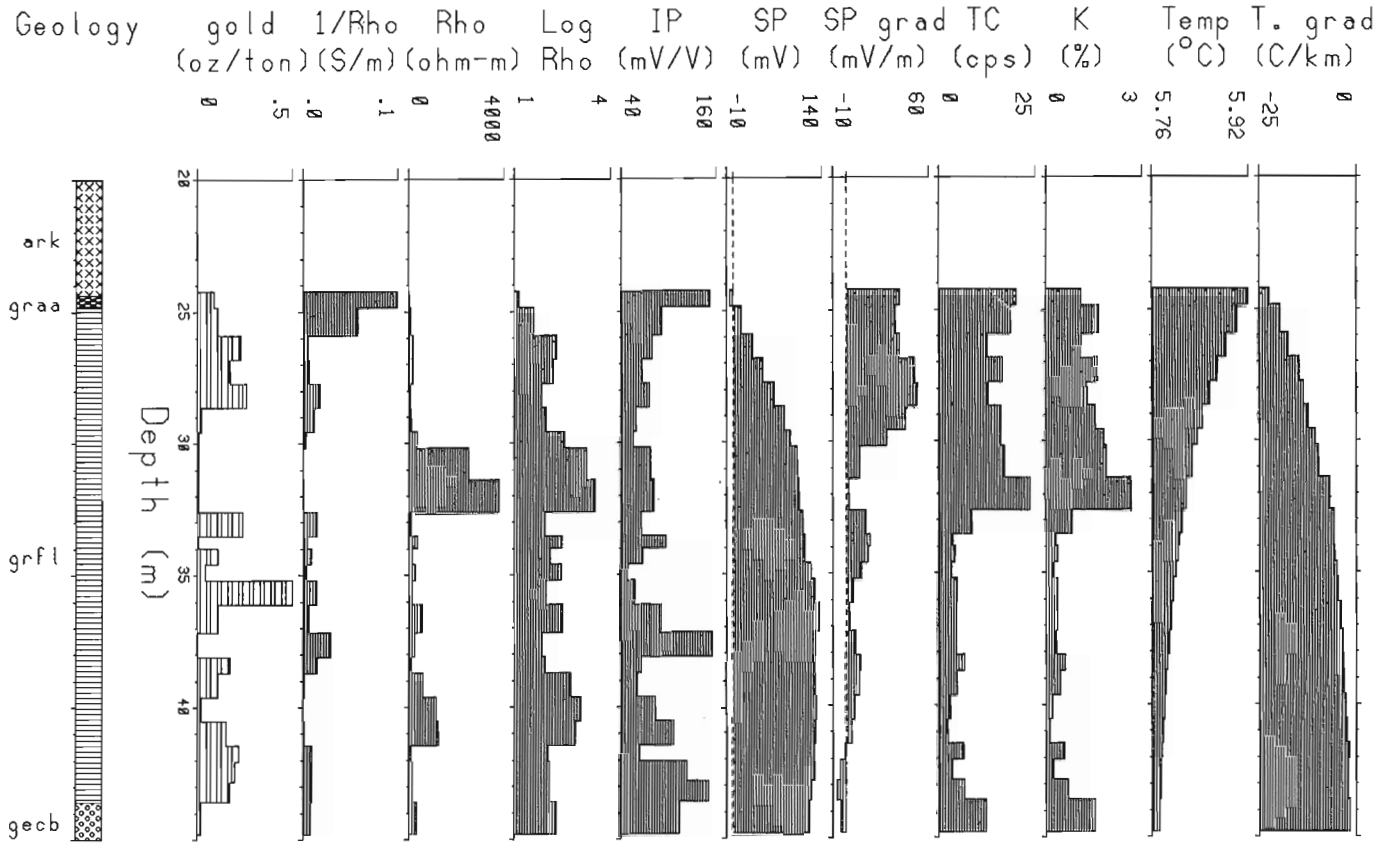

Figure 2.14. *Correlations between the geophysical logs, gold assays and geological log for borehole 80-47. The geophysical logs are averaged over the gold assay sample intervals. The geology abbreviations are: ark – arkose; graa – graphitic argillite; grfl – grey flow; gecb – green carbonate.*

apparent conductivity. The total count and potassium logs for borehole 80-47 (Fig. 2.13) indicate two distinct sections within the grey flow. The upper section from 25 m to 32.5 m has a higher potassium content than the lower section (32.5 m to 43.5 m). The lower section correlates with increases in quartz-carbonate content. Within the quartz-carbonate section there are three thin sericitic sections at 36 m, 38.2 m and 41.8 m, corresponding to slight increases in potassium. The gold mineralization occurs within sections of decreased potassium content (26 m to 29 m, 32.6 m to 43.5 m). The temperature and temperature gradient logs (Fig. 2.13), as was the case for borehole 80-17, do not appear to add any information, except to indicate the absence of groundwater flow associated with fracture zones.

Figure 2.14 is a plot of the multiparameter values averaged over the intervals used for the gold assays for the same borehole as in Figures 2.12 and 2.13. The graphitic schist is clearly outlined by the apparent conductivity and IP logs. The two mineralized sections appear to be generally associated with various degrees of increases in apparent conductivity and also slight local decreases in potassium. The other logs appear to have no observable correlations with the gold assays. To summarize, for borehole 80-47, the potassium and apparent conductivity logs can best be used as an aid in locating the gold mineralization.

Borehole 80-05

Figure 2.15 shows the comparisons between the resistivity, temperature, temperature gradient logs and the geological log for borehole 80-05. A negative correlation is observed between the temperature gradient and the resistivity profiles between 10 and 15 m in the logs, ie. low temperature gradient values almost correspond to resistivity highs. A similar relationship has been observed in a coal mining environment by Beck (1976). Of interest is the discrepancy that exists in this pattern from 22 m to 29 m, where the resistivity and temperature gradient are positively correlated. Low temperature gradients (approximately zero) in the region below 20 m are similar to the results from boreholes 80-17 and 80-47. This may be caused by an increase in carbonate content observed in the core. This section also corresponds with an increase in gold assays. The low resistivity values are associated with an increase in pyrite content.

It is interesting to note the changes in temperature that occur between 11 m and 20 m. Drury (1982) and Drury and Lewis (1981) have suggested that temperature variations are the result of water flow along the borehole and along fractures that intersect the boreholes. Using their models as a basis for explaining the temperature logs, the changes from Z_1 to Z_2 are perhaps due to cooler water entering the borehole at Z_1, flowing downwards and leaving the borehole at Z_2. Therefore, it is likely that depths Z_1 and Z_2 correspond to fracture zones. According to the core geology, Z_1 corresponds to the unit of graphitic schist, which is the Kerr break. Also, warmer water appears to enter at Z_4 and flow upwards leaving at Z_3 and Z_2. Thus, depths Z_3 and Z_4 likely correspond to fracture zones. The value of the temperature gradient logs in this case implies that the resistivity anomalies between 10 and 15 m are almost certainly due more to major fractures with moving fluids, than they are to changes in the host rock properties.

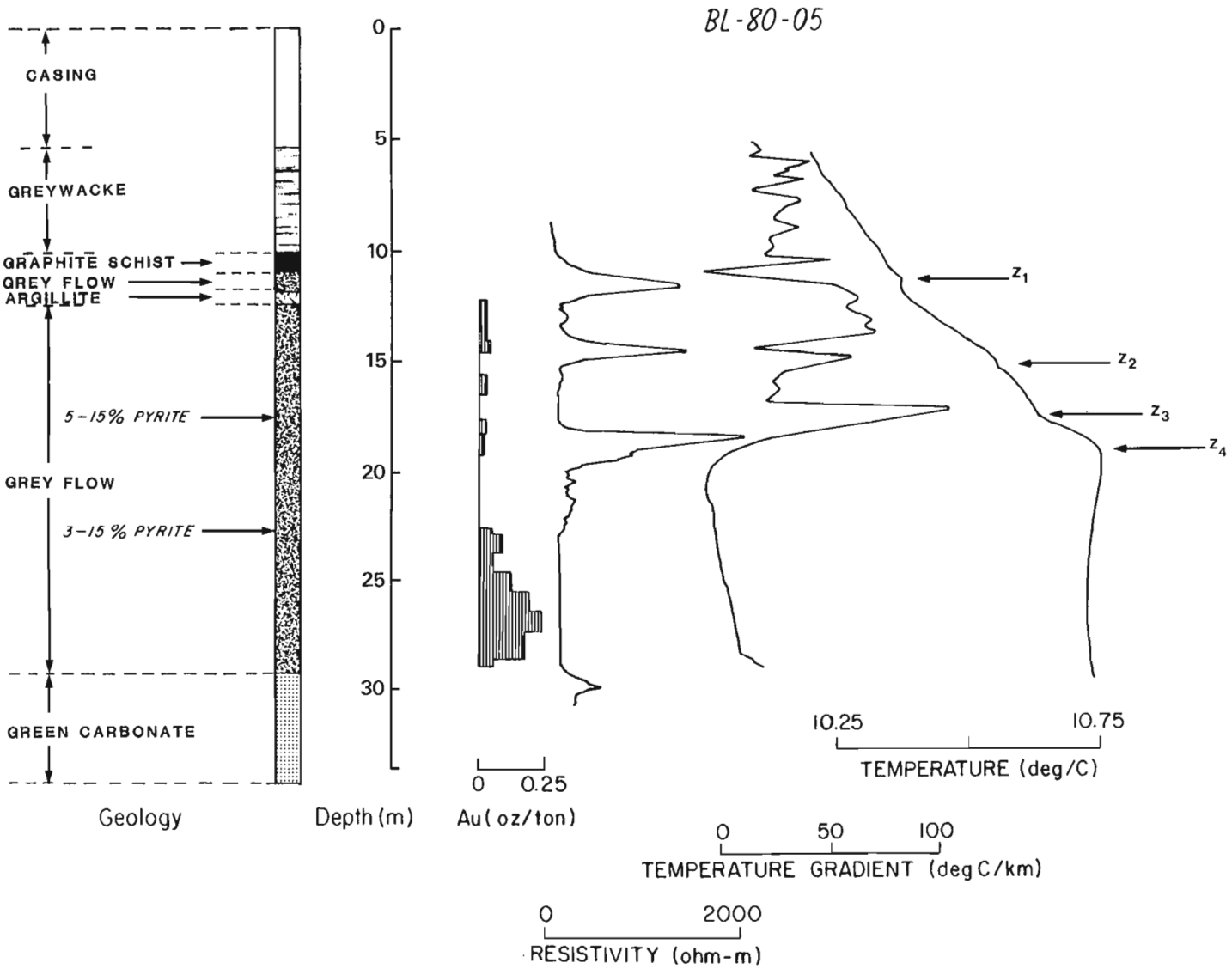

Figure 2.15. *Correlations between the resistivity, temperature and temperature gradient logs with the gold assays and geological log for borehole 80-05. Z_1 corresponds to the Kerr break, Z_2 to Z_4 correspond to possible fractures.*

Borehole 80-25

Comparisons between the gold assays, total count log and potassium log for borehole 80-25 are shown in figures 2.16 and 2.17. The sections of gold mineralization fall within regions of decreased potassium content. At the upper and lower ends of the mineralized zones the potassium level increased. The relationship between the potassium log and the gold mineralization corresponds to a negative type enveloping halo as described by Boyle (1982). According to Boyle, these enveloping halos mark zones where there is a dispersion of major, minor or trace amounts and indicator elements adjacent to the mineralization, typically symmetrical about the mineralization. For example, at approximately 46.5 m and 48.5 m, the decrease in potassium values corresponds to the increase in gold, while increases occur at the upper and lower edges of the ore zone. The lower ore zone from 59.8 m to 63.3 m falls within a section of increased quartz-carbonate content. This section corresponds to a lower potassium content.

Borehole 80-13

Besides logging boreholes that intersected mineralization, borehole 80-13, which intersected a similar geologic sequence which did not interest any mineralization, was logged. Analysis of the electrical logs indicates the following relationships (Fig. 2.18): The graphitic schist is clearly defined by a high apparent conductivity and high IP; the grey flow breccia and tuff has high apparent resistivity values, except for the three decreases in resistivity at 67.5 m, 68.7 m and 79 m (no increases in pyrite or graphite were observed in the core corresponding to these low resistivity zones) and the low resistivity zones are higher than (approximately 1000 ohm-m) in the boreholes which intersected mineralization. Since the electrical measurements generally have a larger sample volume than the core, the logs may indicate offhole mineralization. The following qualitative observations can be made on the gamma ray spectral logs (Fig. 2.19): In general, the radioactivity observed in the total count log is due to potassium and a slight increase in potassium values due to the presence of sericite is associated with the graphitic schist.

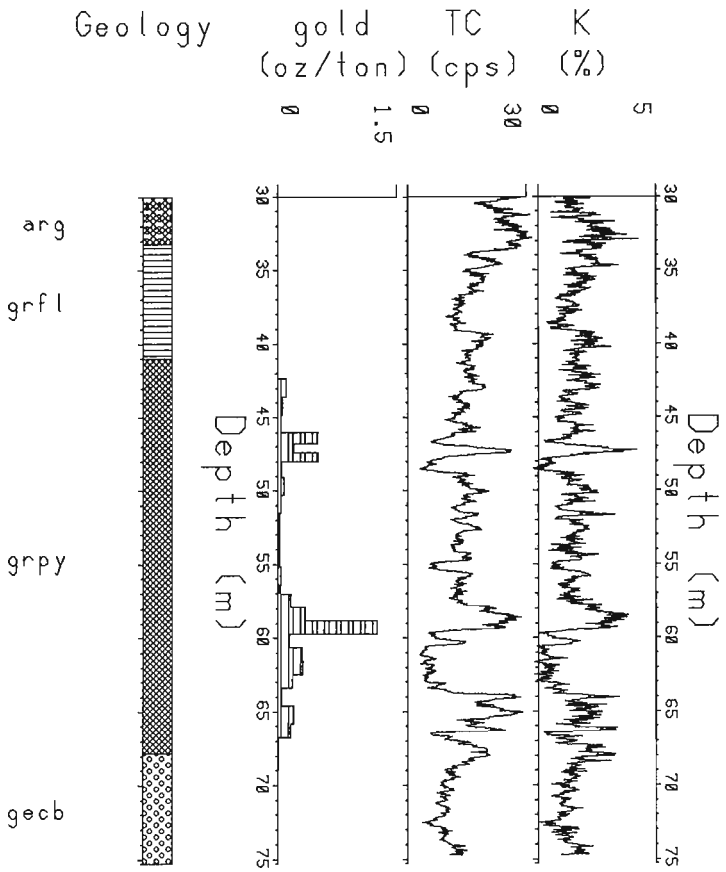

Figure 2.16. *Correlations between the total count and potassium logs with the gold assays and geologic log for borehole 80-25. The geology abbreviations are: arg – argillite; grfl – grey flow; grpy – pyritic grey tuff and flow; gecb – green carbonate.*

The temperature gradient log obtained for 80-13 (Fig. 2.19) does not contain any information that could be related to mineralized and non-mineralized boreholes.

Summary of results

The results obtained may be summarized as follows:

1) SP logs were used to determine changes in lithology ie. from the greywacke to volcanic unit and from the volcanic unit to the green carbonate unit.

2) Electrical logs outlined quartz - carbonate rich zones (incresed resistivity values) and pyrite, or graphite rich zones (decreased resistivity values). In non-mineralized sections the resistivity level was higher.

3) Potassium logs were used to outline increases in sericite content. Within the gold mineralized zones, a lower potassium content was observed, although lower potassium contents were also observed in non-mineralized zones.

4) Temperature logs in one example outlined fracture zones associated with water flow along the borehole. This was valuable additional information in that the obvious correlation of these zones with resistivity anomalies made it almost certain that these resistivity anomalies were not associated with pyrite and other conductive mineralization, a conclusion which might otherwise have been made.

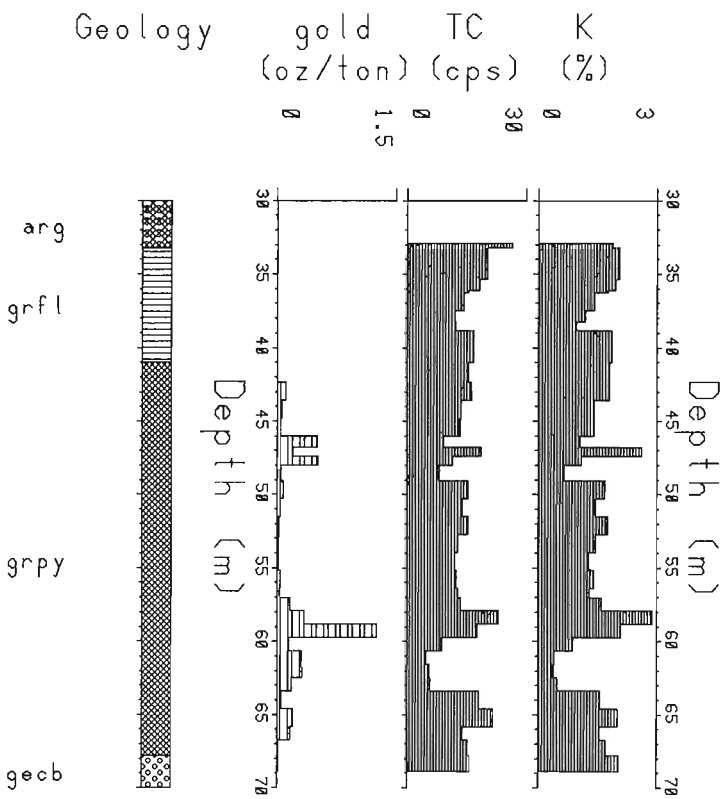

Figure 2.17. *Correlations between the total count and potassium logs with the gold assays and geologic log for borehole 80-25. The total count and potassium logs are averaged over the gold assay sample intervals. The geology abbreviations are: arg – argillite; grfl – grey flow; grpy pyritic grey tuff and flow; gecb – green carbonate.*

Conclusions

It may be concluded that the application of multiparameter logging techniques provides a method for outlining highly altered rocks and may prove useful in locating alteration zones associated with gold mineralization. If so, then it may provide a means of optimizing the core sampling process. In the Larder Lake region, the ore deposit investigated was related to pyrite, sericite and carbonate content. The unique balance of these types of alteration processes required for mineralization was observed by visually comparing electrical, temperature and radioelement measurements. Although these observations were made, effective and consistent analysis of the data was not easy due to the large number of variables examined. Thus, the study can be considered as preliminary, as statistical analysis of the data has to be carried out in order to clarify and substantiate the qualitative correlations, and to determine the degree of significance geophysical logging techniques can play as an exploration technique for gold. Statistical analysis of the data is now in progress. Further investigations are also being carried out with additional parameters eg. magnetic susceptibility and density, at the Barber Larder property as well as other gold mining areas.

Acknowledgments

We would like to thank Kerr Addison Mines, and in particular D.M. Hendrick, chief exploration geologist, for allowing us to perform experiments on their property,

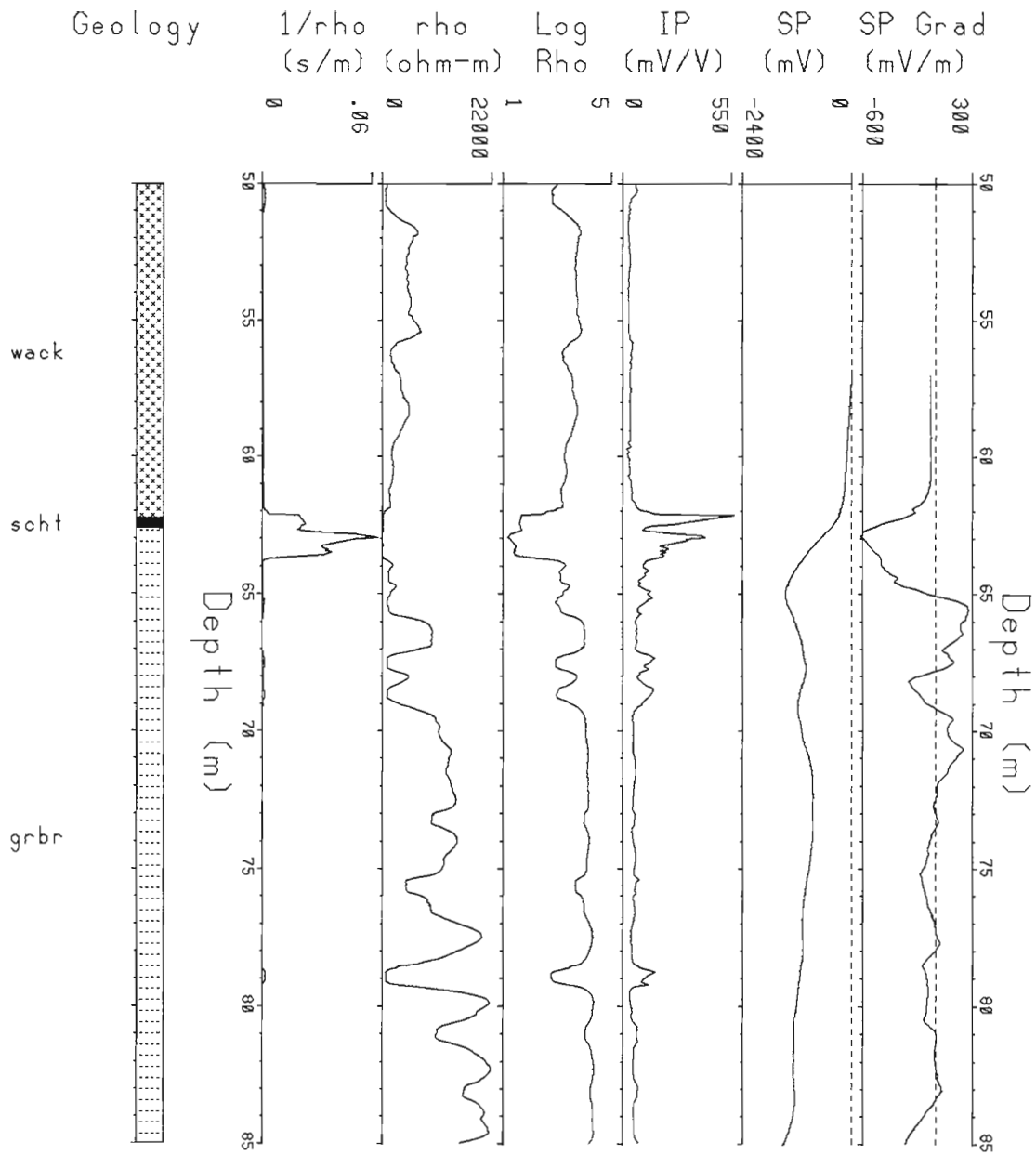

Figure 2.18. *Correlations between the electrical logs with the geologic log for borehole 80-13. The geology abbreviations are: wack – greywacke; scht – graphitic schist; grbr – grey flow breccia and tuff.*

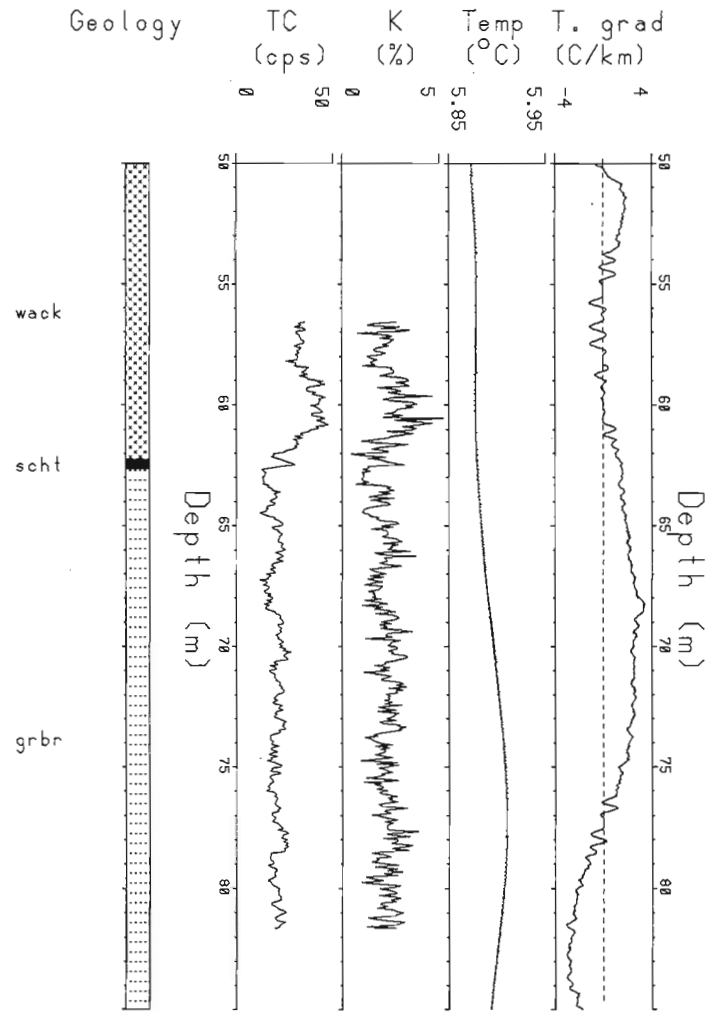

Figure 2.19. *Correlations between the total count, potassium, temperature and temperature gradient logs with the geologic log for borehole 80-13. The geology abbreviations are: wack – greywacke; scht – graphitic schist; grbr – grey flow breccia and tuff.*

examine the geological logs and gold assay data, and permitting us to publish these data. We would also like to thank R.C. Bailey of the University of Toronto, P.G Killeen and Q. Bristow of the Geological Survey of Canada for their constructive criticism and advice, and Bill Hyatt and Yves Blanchard (GSC) for assisting in the data acquisition process.

References

Baker, J.W.
1957: Kerr Addison mine; in Structural Geology of Canadian Ore Deposits, v. 2, 6th Commonwealth Mining and Mettallurgical Congress, Canada, p. 392-402.

Balykin, P.A., Borob'yev, V.I. and Krendelev, F.P.
1973: Gamma-spectrometric measurements of Clarkes of radioactive elements in gold deposits of the schist zone; Doklady Akademii Nauk SSSR, v. 209, no. 1, p. 190-192.

Beck, A.E.
1976: The use of thermal resistivity logs in stratigraphic correlation; Geophysics, v. 41, no. 2, p. 300-309.

Becker, A. and Telford, W.M.
1965: Spontaneous polarization studies; Geophysical Prospecting, v. 13, p. 173-188.

Bernius, G.R.
1981: Boreholes near Ottawa for the development and testing of borehole logging equipment – a preliminary report; in Current Research, Part C, Geological Survey of Canada, Paper 81-1C, p. 51-53.

Bertin, J. and Loeb, J.
1976: Experimental and theoretical aspects of induced polarization – Volume 1; Presentation and application of the IP method, case studies; in Geoexploration Monographs, Series 1, no. 7, Pub. by Gebruder Borntraeger, 250 p.

Blyumentsev, A.M., Khrust, A.R. and Chepizhnaya, E.A.
1974: Radioactive elements as indicators of gold in effusives; Yad. Geol, p. 187-197; Chemical Abstracts, v. 83, 100886a.

Boyle, R.W.
1979: The Geochemistry of Gold and its Deposits; Geological Survey of Canada, Bulletin 280.

1982: Geochemical methods for the discovery of blind mineral deposits; Canadian of Mining and Metallurgical Bulletin, v. 75, no. 844 and 845.

Boyle, R.W. and Hood, P.J.
1980: Geochemical and geophysical techniques for gold exploration; in Northern Miner Press, October issue.

Bristow, Q.
1979: Airborne and vehicle mounted geophysical data acquisition system controlled by NOVA minicomputers; in Proceedings of the 6th Annual Data Generals User's Group Meeting, Dec. 4-7, New Orleans, p. 615-634.

1986: A system for the digital transmission and recording of induced polarization measurements in boreholes; in Borehole Geophysics for Mining and Geotechnical Applications; P.G. Killeen, ed.; Geological Survey of Canada, Paper 85-27, report 14.

Bristow, Q. and Conaway, J.G.
1984: Temperature gradient measurements in boreholes using low noise high resolution digital techniques; in Current Research, Part B, Geological Survey of Canada, Paper 84-1B, p. 101-108.

Campbell, N.
1957: Preliminary report on reappraisal of Amalgamated Larder Mines Limited; The Consolidated Mining and Smelting Company of Canada Limited, March 21, 1957.

Conaway, J.G.
1977: Deconvolution of temperature gradient logs; Geophysics, v. 42, no. 4, p. 823-837.

1980: Exact inverse filters for the deconvolution of gamma-ray logs; Geoexploration, v. 18, p. 1-14.

Conaway, J.G. and Beck, A.E.
1977: Fine scale correlation between temperature gradient logs and lithology; Geophysics, v. 42, no. 7, p. 1401-1410.

Conaway, J.G. and Killeen, P.G.
1978: Quantitative uranium determinations from gamma-ray logs by application of digital time series analysis; Geophysics, v. 43, p. 1204-1221.

Drury, M.J.
1982: Borehole temperature logging for the detection of water flow; Proceedings of Workshop on Geophysical Investigations in Connection with Geological Disposal of Radioactive Waste, Ottawa, Canada, OECD/NEA, Manitoba.

Drury, M.J. and Lewis, T.J.
1981: Thermal studies in the Lac du Bonnet batholith at Pinawa, Manitoba; Atomic Energy of Canada Limited Technical Record, TR-163.

Fel'dman, A.A., Slepnev, P.V., and Kul'kov, B.N.
1975: Use of gamma spectrometry in prospecting for gold ore deposits near the surface; Razved. Okhr. Nedr., no. 10, p. 59-60; Chemical Abstracts, v. 84, 138431g.

Gross, W.H.
1952: Radioactivity as a guide to ore; Economic Geology, v. 47, p. 722-742.

Hamilton, J.V.
1983: Geological Study of the area of the Kirkland Lake - Larder Lake in central McGarry Township; Ontario Geological Survey, Miscellaneous Paper 116, p. 179-184.

Hogg, N.
1975: Hanna Mining Company, Report on a program of diamond drilling by the Hanna Mining Company of Larder Lake gold property of Amalgamated Larder Mines Ltd; Ontario Geological Survey, Report 63-3347.

Jensen, L.S.
1981: Gold mineralization in the Kirkland Lake-Larder Lake areas; Ontario Geological Survey, Miscellaneous Paper 97, p. 59-64.

Keys, S.W. and MacCary, L.M.
1976: Application of borehole geophysics to water resources investigation; United States department of the Interior, Book 2, chapter E1.

Kihlstedt, F.H.
1934: Electrical methods in prospecting for gold; Geophysical Prospecting, February issue, p. 62-74.

Killeen, P.G.
1979: Gamma-ray spectrometric methods in uranium exploration – application and interpretation; in Geophysics and Geochemistry in the Search for Metallic Ores; Peter J. Hood, ed; Geological Survey of Canada, Economic Geology Report 31, p. 163-229.

Killeen, P.G. and Conaway, J.G.
1978: New facilities for calibrating gamma-ray spectrometric logging and surface exploration equipment; Canadian Mining and Metallurgical Bulletin, v. 71, no. 793, p. 84-87.

Krendelev, F.P., Mironov, A.G., and Gofman, A.M.
1976: Gamma spectrometry applied to contouring ore zones in the Trans Baikal Region; Geologiya Geofizika, v. 17, no. 8, p. 67-75.

Mwenifumbo, C.J., Urbancic, T.I. and Killeen, P.G.
1983: Preliminary studies on gamma-ray spectral logging in exploration for gold; in Current Research, Part A, Geological Survey of Canada, Paper 83-1A, p. 391-397.

Thomson, I.
1980: Gamma ray mapping of alteration zones associated with gold-bearing horizons: orientation studies at the Kerr Addison Mine, Virginiatown, District of Timiskaming; Ontario Geological Survey, Miscellaneous Paper 96, p. 145-149.

Tihor, L.A. and Crocket, J.H.
1975: Gold distribution and gamma-ray spectrometry in the Kirkland Lake-Larder Lake gold camp; Report of Activities, Part A, Geological Survey of Canada, Paper 75-1A, p. 355-357.

3. A SYSTEM OF DEEP TEST HOLES AND CALIBRATION FACILITIES FOR DEVELOPING AND TESTING NEW BOREHOLE GEOPHYSICAL TECHNIQUES

P.G. Killeen[1]

Killeen, P.G., A system of deep test holes and calibration facilities for developing and testing new borehole geophysical techniques; in Borehole Geophysics for Mining and Geotechnical Applications, ed. P.G. Killeen, Geological Survey of Canada, Paper 85-27, p. 29-46, 1986.

Abstract

The Geological Survey of Canada has established a system of model boreholes and drilled test holes for calibrating and testing borehole geophysical equipment. These include: nine models at Bells Corners, Ontario, near Ottawa, for calibration of gamma ray spectral logging probes; two models in Fredericton, New Brunswick, for calibration of total count gamma ray logging probes; four models in Saskatoon, Saskatchewan for calibration of total count gamma ray logging probes; the Lebreton NQ test hole near the GSC building in Ottawa, drilled to a depth of 442 m; the Bells Corners geophysical test area: four NQ holes of approximately 300 m depth and two of 120 m depth separated by distances of 10, 20, 30, 70, and 100 m; the Bancroft, Ontario, test holes; two BQ and two HQ, drilled to depths of up to 100 m; the recently completed Aberdeen Street calibration facility in Ottawa, which will eventually contain multiple interchangeable zones with different physical properties; two partially completed model holes in Dartmouth, Nova Scotia, for calibration of coal logging tools in Eastern Canada; and two planned model holes in Calgary, Alberta, for calibration of coal logging tools in Western Canada.

Information available on the various test holes include gamma ray count rates, thorium, uranium and potassium distributions, temperature, temperature gradient, XRF measurements, IP, resistivity, SP, seismic measurements, VLF and time domain EM measurements, density, porosity, caliper and magnetic susceptibility logs. Not all measurements have been made in all holes.

The model holes are described and examples of the different types of borehole geophysical measurements which have been made in some of the test holes are presented. The test holes and models are available for use by mining industry, university and government groups involved in developing, calibrating, or improving the quality of borehole geophysical instrumentation and measurements.

Résumé

La Commission géologique du Canada a mis en place un système de modèles de trou de sondage et foré des trous d'essais, afin de procéder à l'étalonnage et à l'essai de matériel de sondage géophysique de fond. En voici l'éventail: neuf modèles à Bells Corners, à Ottawa (Ontario), pour l'étalonnage de sondes de diagraphie spectrale par rayons gamma; deux modèles à Fredericton (Nouveau-Brunswick), pour l'étalonnage de sondes de diagraphie par rayons gamma à comptage total; quatre modèles à Saskatoon (Saskatchewan), pour l'étalonnage de sondes de diagraphie par rayons gamma à comptage total; un trou d'essai de diamètre NQ Lebreton à Ottawa, à proximité d'un bâtiment de la Commission géologique du Canada, à une profondeur de 442 m; quatre trous de diamètre NQ d'environ 300 m et deux autres de 120 m, dans la zone d'essais géophysiques de Bells Corners, à Ottawa; les trous sont séparés de 10, 20, 30, 70 et 100 m; les trous d'essais forés à Bancroft (Ontario): deux trous de diamètre BQ et deux trous de diamètre HQ, forés à des profondeurs allant jusqu'à 100 m; l'aménagement récent d'une installation d'étalonnage à Ottawa, rue Aberdeen; ces installations comporteront éventuellement des modèle de trou à zones artificielles multiples et interchangeables affichant des propriétés physiques variées; deux modèles de trou en cours de forage à Dartmouth (Nouvelle-Écosse), pour l'étalonnage d'instruments servant à la diagraphie du charbon, dans l'Est du Canada; et deux modèles de trou que l'on projette de construire à Calgary (Alberta), pour l'étalonnage d'instruments servant à la diagraphie du charbon dans l'Ouest du Canada.

Les renseignements disponibles sur les divers trous d'essai portent sur les taux de comptage de rayons gamma; la répartition du thorium, de l'uranium et du potassium; la température; le gradient thermique; les mesures XRF; la polarisation induite; la résistivité; la polarisation spontanée; les résultats des mesures sismiques, des mesures électromagnétiques à très basses fréquences (VLF) et du domaine temporel (EM); la densité; la porosité; le diamétrage et la susceptibilité magnétique. Certaines des mesures n'ont pas été effectuées à tous les trous.

La présente étude décrit les modèles de trou de sonde et présente des exemples des divers types de mesures géophysiques de fond qui ont été prises à certains des trous d'essai. Les trous d'essai et les modèles sont mis à la disposition de groupes qui, dans l'industrie minière, dans le milieu universitaire et au gouvernement, sont engagés dans la mise au point, l'étalonnage et l'amélioration des instruments et des mesures de sondage géophysique de fond.

[1] Geological Survey of Canada, Ottawa, Ontario K1A 0E8

Introduction

A number of projects at the Geological Survey of Canada (GSC) have been concerned with various aspects of borehole geophysics, ranging from the development of new interpretation techniques to the design and construction of innovative logging tools. These projects ultimately depend on measurements in boreholes to evaluate the interpretation techniques and to test the downhole equipment. In support of these activities several test holes have been drilled in the Ottawa area as well as in the Precambrian pegmatitic rocks in the Bancroft area, about 125 km west of Ottawa. Over a period of years, in addition to the borehole geophysical measurements conducted by the GSC, several groups from universities, institutes and private industry have utilized these boreholes in their research and development work. Each type of measurement has provided additional information on the physical properties of the rocks in the vicinity of the boreholes, making the test holes more valuable. Detailed geological logs of the diamond drill core, combined with geophysical measurements on selected sections of core have been a fundamental part of this work.

Examples illustrating some results of the broad range of geophysical measurements which have been made are presented for several of the test holes. These demonstrate the potential for their future use by other interested parties.

In addition to the drilled test holes, several model boreholes have been constructed of concrete mixtures to provide controlled homogeneous zones with documented

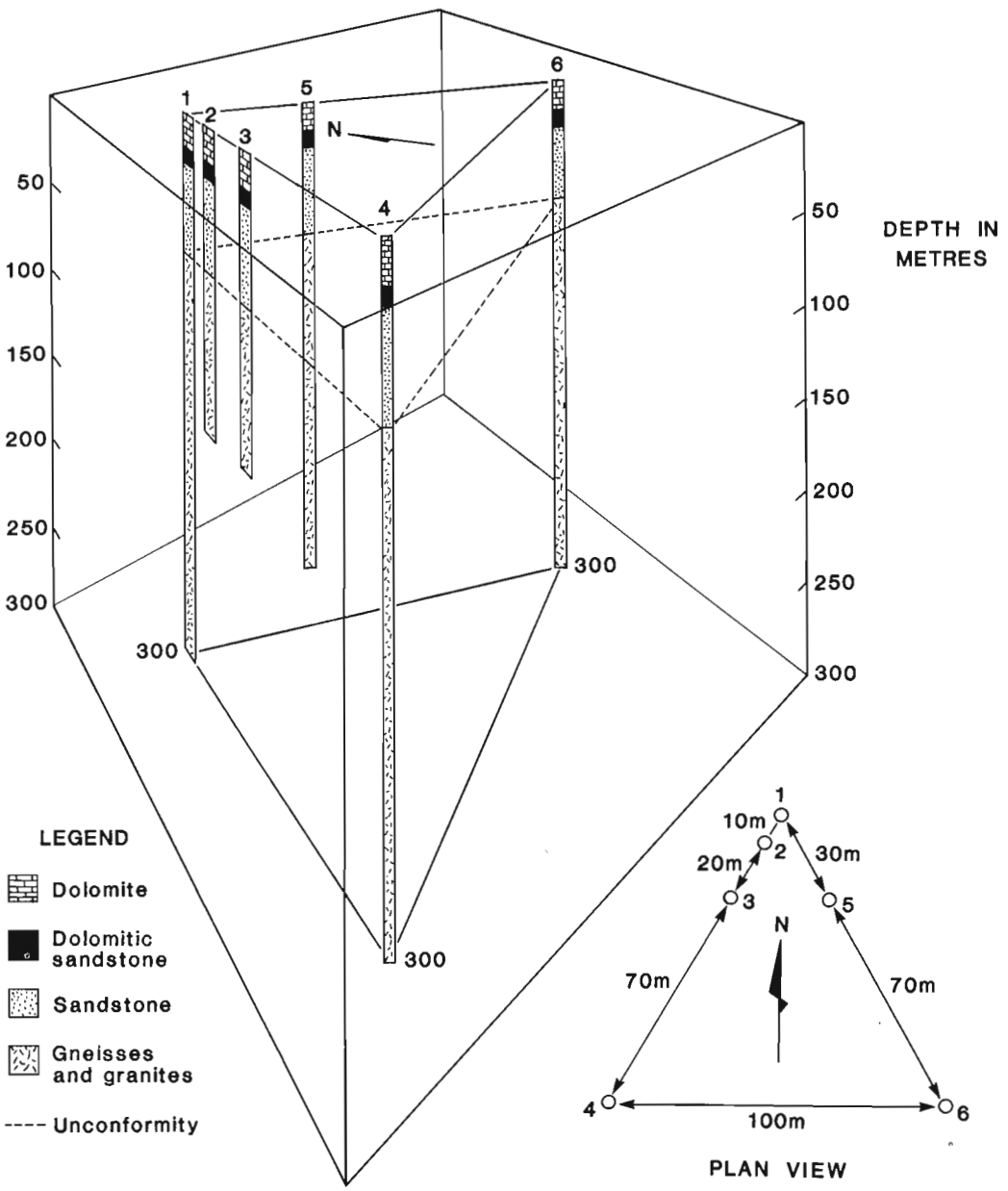

Figure 3.1. The geology and geometry of the Borehole Geophysics Test Area at Bells Corners near Ottawa. The depths of the six vertical NQ boreholes are as follows: BC-81-1, BC-81-4, and BC-84-6 are 300 m; BC-81-2 and BC-81-3 are 120 m; and BC-84-5 is 250 m. Boreholes BC-81-1, 81-4, and 84-6 form a triangle with 100 m sides, and BC-81-1, 81-3, and 84-5 form a 30 m triangle for 3 dimensional hole-to-hole experiments. The inset plan view shows the relative locations of the test holes. The unconformity at 65 m depth is also indicated in the diagram by a dashed line.

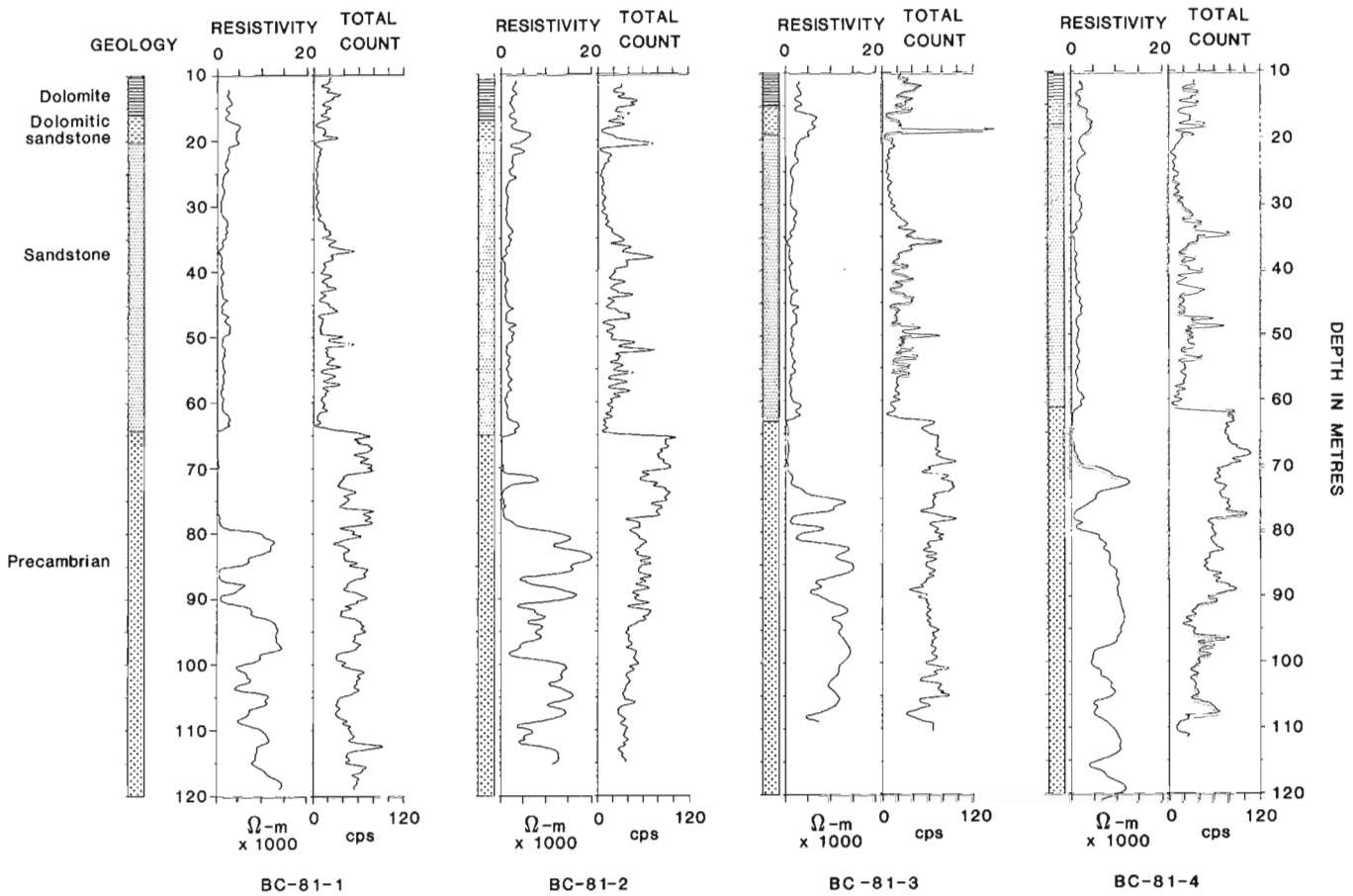

Figure 3.2. Geological logs, resistivity logs (derived from IP logs) and total count logs (derived from gamma ray spectral logs) for the fence of four holes at Bells Corners. Resistivity logs were recorded with a normal 40 cm array, a logging speed of 6 m/min, and a digital sample time of 1 second. The total count log was obtained with a 32 mm x 125 mm CsI (Na) detector at 1 m/min and a sample time of 3 s. All logs were obtained with the GSC research logging system.

physical properties. These make it possible to calibrate logging tools to produce quantitative logging measurements of the physical properties of rocks. The first model boreholes were designed for the calibration of gamma ray logging tools, including spectral gamma ray probes which distinguish between the radioelements potassium, uranium and thorium. These model boreholes were constructed in three localities (Ottawa, Ontario; Fredericton, New Brunswick; and Saskatoon, Saskatchewan) partially in support of uranium exploration activities by the mining industry. More recently, model boreholes for calibration of logging tools used in the coal mining industry have been designed. These are being constructed near the coal mining areas of eastern and western Canada.

The model borehole calibration facilities and some examples of their use in calibration of logging tools are described later.

Borehole geophysics test area at Bells Corners

Six holes have been drilled to depths up to 300 m to form a borehole geophysics test area at Bells Corners approximately 10 km west of Ottawa. They were drilled in 1981 and 1984 as part of an ongoing program by the Resource Geophysics and Geochemistry Division of the Geological Survey of Canada to construct calibration and test facilities for the development of borehole geophysical instruments and techniques (Killeen, 1978; Killeen and Conaway, 1978).

The test area is located near the entrance to the Canada Centre for Mineral and Energy Technology (CANMET) Research Laboratory. All of the holes are drilled vertically and are NQ size (76 mm diameter). The first four (described by Bernius, 1981) were spaced horizontally along a line at intervals of 10, 20 and 70 m to conduct experiments in the use of hole-to-hole electromagnetic and seismic equipment. In 1984, two new holes were drilled, offset from the previously drilled line of holes to allow an expanded range of hole-to-hole measurements to be used and thereby develop methods to produce a three dimensional picture of the geology and structure.

Figure 3.1 shows the relative positions of the boreholes which in plan view are drilled at the corners of equilateral triangles. The depths of the holes are also indicated in the figure as well as their generalized geological logs. Core (47.6 mm diameter) recovery was very high — 99 per cent in most cases — which will allow detailed petrological and geophysical studies to be made.

In this test area the top 65 m of Upper Cambrian and Ordovician sandstone and dolomite are separated from the underlying Precambrian mixed granite and gneiss by an unconformity marked by a thick weathered alteration zone. Numerous fractures were recognized in the core. The geology has been described in more detail by Bernius (1981).

Figures 3.2 to 3.7 illustrate the broad range of borehole geophysical measurements which have been made in the test area. Figure 3.2 shows the electrical resistivity log, the natural gamma ray log and the geological log for the upper 120 m of the four boreholes which form the fence (BC-81-1, 2, 3, and 4) shown in Figure 3.1. The logs in Figure 3.2 were recorded with the GSC research logging system. The resistivity logs were derived from results of an Induced Polarization log (IP) (Bristow, 1986) and the radioactivity log is a total count log obtained from the 0.4 MeV to 3.0 MeV window of a gamma ray spectral log (Killeen, 1979). The logs show an increase in radioactivity and decrease in resistivity at the unconformity at about 65 m. The thick weathered or altered zone below the unconformity is characterized by relatively high radioactivity and extremely low resistivity. In BC-81-2 a less altered section in the middle of the weathered zone shows up as a rise in resistivity accompanied by a decrease in radioactivity. The very narrow uraniferous zone at the base of the March Formation can be seen as a narrow gamma ray high at a depth of about 20 m. The general character of both types of logs is considerably different in Precambrian rocks compared to the overlying Paleozoic sedimentary rocks.

Figure 3.3 shows a suite of logs recorded in borehole BC-81-2 with the GSC research logging system. These include magnetic susceptibility log (Bristow and Bernius, 1984; Bristow, 1985), the resistivity, and induced polarization log from an IP logging tool, the total count, potassium, uranium and thorium logs from a gamma ray spectral logging tool, temperature and temperature gradient log (Bristow and Conaway, 1984).

Some of the more interesting features that can be seen in the suite of logs, relates to the measurements in the vicinity of the weathered zone at about 65 m to 80 m. The magnetic susceptibility values are low in the sedimentary column and in the weathered zone, except for the section from 72 to 74 m which is relatively unaltered. This section is also indicated by the resistivity high and a decrease in the radioactivity in the otherwise potassic altered zone.

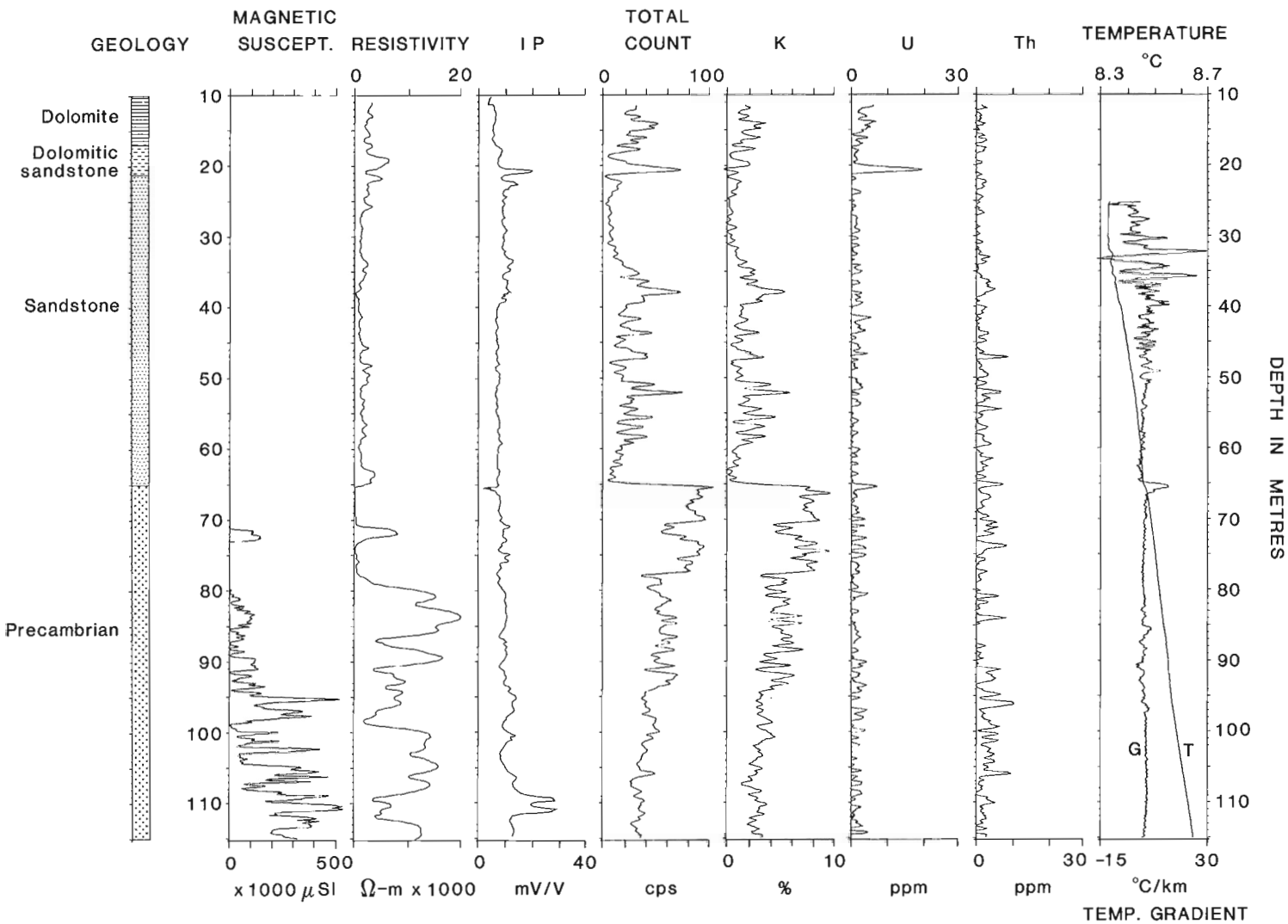

Figure 3.3. *The geological log and nine geophysical logs in Bells Corners borehole BC-81-2, obtained with the GSC research logging system. The magnetic susceptibility log was run at 6 m/min with a sample time of 0.2 s. The resistivity and IP logs were recorded with a 40 cm normal electrode array, at 6 m/min and a sample time of 1 second. The total count (0.4 to 3.0 MeV), K, U and Th logs were recorded at 1 m/min and a sample time of 3 s, using a 32 mm x 125 mm CsI (Na) detector. The temperature and temperature gradient logs were recorded at 6 m/min and a sample time of 0.375 s. A 15 point smoothing filter has been applied to the temperature log.*

The temperature and temperature gradient logs show that water is flowing at the unconformity due to increased porosity and fracturing associated with it.

Additional logs recorded in BC-81-2 by Century Geophysics Limited of Calgary are shown in Figure 3.4. They include the electrical resistivity log, natural gamma, gamma-gamma density, and caliper logs. Comparing the first two logs with those shown in Figure 3.2 recorded by the GSC, very good agreement is apparent, except for the degree of smoothing used for the presentation of the logs. It is also interesting to note that the caliper log indicates that the borehole does not have any cave-ins, and is essentially smooth-walled from top to bottom.

Figure 3.5 shows the results of a borehole VLF survey of hole BC-81-1. Two logs are shown; the inphase and quadrature E field data from two different VLF transmitters (NAA Cutler Maine, 25 kHz and NSS Anapolis Maryland, 21.4 kHz). NAA is located east, and NSS is south of the area. The E field is measured by Pb electrodes buffered by high impedance circuitry. The electrical structure and hence geological structure is obviously affecting the signal. The H-field received by antennae (ferrite core coils) was essentially zero response and is not shown. The logging system is a prototype developed by the Mineral Exploration Research Institute (MERI) in Montreal and modified and upgraded by the GSC. Some of the features which correlate with zeros or crossovers in the logs are indicated.

Also available, but not shown here, are the results of a transient EM survey of borehole BC-81-1 using the GSC's prototype of the Crone Pulse EM System. Data were obtained using a transmitter loop 300 m square, placed about 50 m to the side of the hole. Results indicate there are no detectable conductors present in the vicinity of the borehole.

Figure 3.6 illustrates the results of an interesting temperature logging experiment in borehole BC-84-6. Utilizing the GSC high sensitivity logging system, and logging at 6 m/min, a set of eight temperature and temperature gradient logs were recorded after drilling the hole. These logs were recorded at approximately the following times after the drilling had stopped: 4 hours, 28 hours, 52 hours,

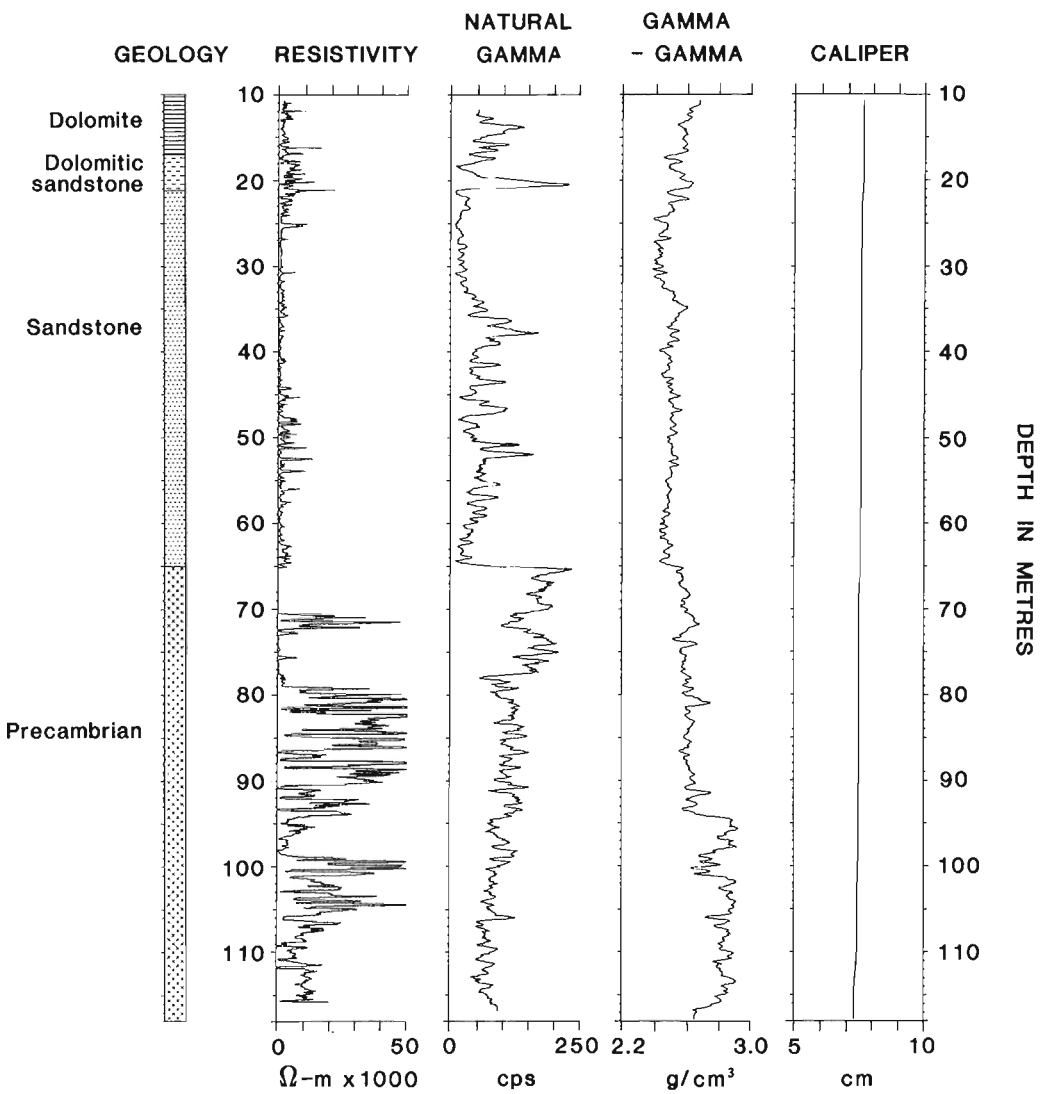

Figure 3.4. Geological and geophysical logs obtained at 6 m/min with a 0.5 s sample time in borehole BC-81-2 by Century Geophysics of Calgary. The resistivity log was a focused resistivity 3-electrode guard-type. The natural gamma log used a 13 mm x 75 mm NaI (Tl) detector in a 'gross count' mode (low level energy threshold set very low) to increase count rates. The gamma-gamma density log used a collimated Cs-137 source and detector. All raw data have been smoothed with a 15 point filter.

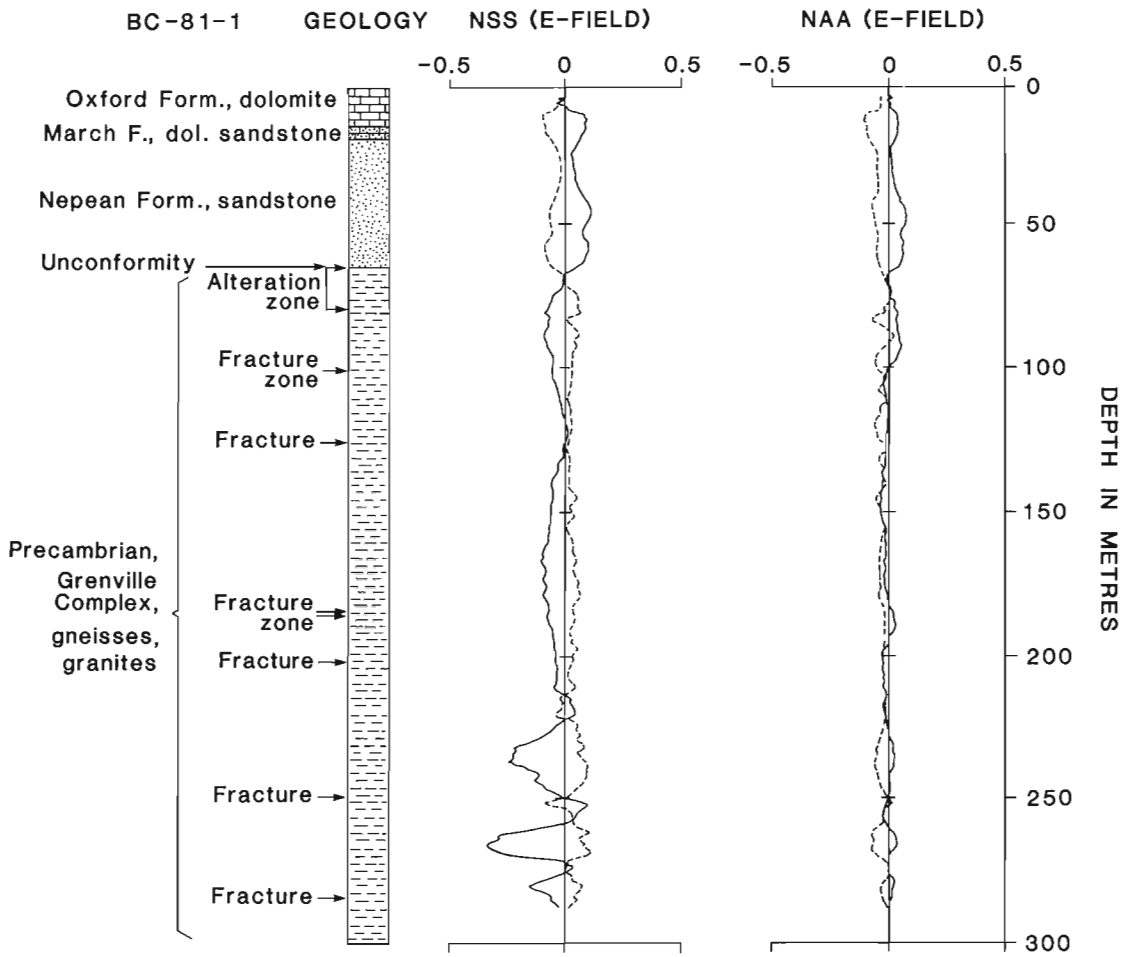

Figure 3.5. *The geological log and borehole VLF measurements in Bells Corners hole BC-81-1. Shown are the inphase (solid line) and quadrature (dashed line) E-field logs for two different VLF transmitting stations, NSS and NAA. Logs were obtained at about 3 m/min using Pb electrodes. Some of the zeroes or crossovers in the logs may relate to the conductivity of fracture zones indicated on the geological log.*

100 hours, 6 days, 8 days, 12 days and 16 days. The return to thermal equilibria can be seen and it is interesting to note the relatively rapid change that takes place in the first five logs. It is believed that two events occurred during drilling which are both seeking re-adjustment to equilbrium. First, zones that are more porous than average (fractured?) are disturbed to a greater degree than average by the heating effect of the drilling fluid (water), since the fluid enters the porous zones. Second, zones with higher thermal conductivity than average will transport heat away from the holes quickly, and after drilling will also return to equilibrium (cool down) relatively quickly. These effects can be seen in a qualitative sense in the logs where fractured zones are indicated. It is possible that high sensitivity temperature logs recorded immediately and shortly after drilling can provide useful information which was previously disregarded. At present it is generally considered that the only useful temperature data can be obtained after the hole has returned to thermal equilibrium which may take months or even years.

Figure 3.7 illustrates some of the results of an interesting borehole seismic tomography experiment conducted by a research group from the University of Toronto. (Wong et al., 1982). The experiment was conducted between boreholes BC-81-1 and BC-81-4 which are separated by a distance of 100 m. Using multiple receiver positions in one hole and multiple transmitter positions for each receiving position in the other hole, the tomographic technique produces a two-dimensional image of the seismic properties of the rock between the two boreholes. In this way an image of any anomalous feature (ore body? fracture zone?) located between the two boreholes would appear in the resulting reconstructed image.

With the addition of the boreholes BC-84-5 and BC-84-6 in 1984, it is now possible to conduct 3-dimensional tomographic measurements of the volume of rock contained inside the triangular arrangement of boreholes.

Lebreton test hole LB-1

This NQ size test borehole is located at the edge of a parking lot near the GSC building in Ottawa. Only the bottom approximately 75 m of this 442 m deep test hole penetrates Precambrian basement rocks. The upper part of the hole intersects a thick section of limestone and shale before it reaches the formation in which the Bells Corners test holes are collared.

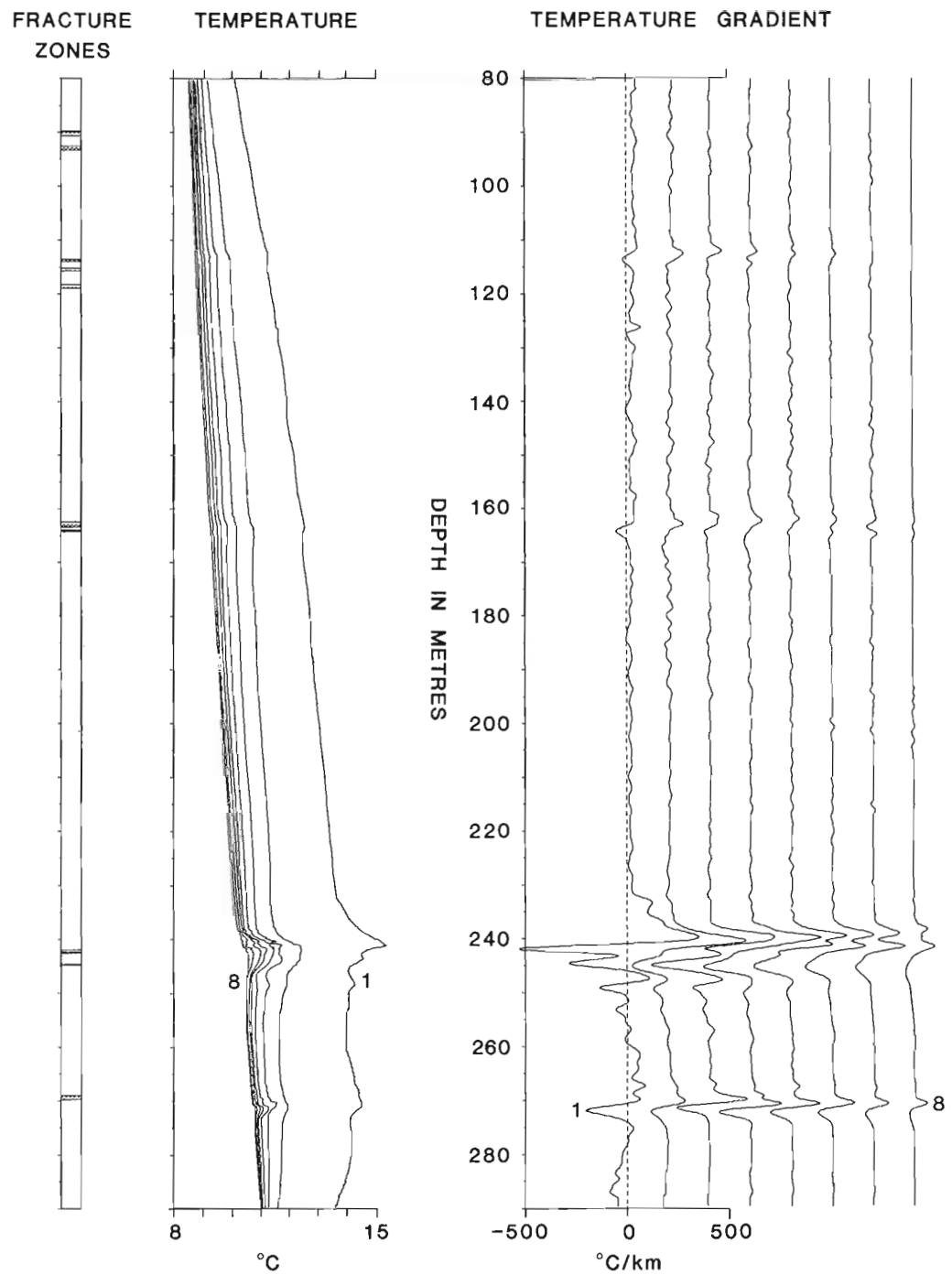

Figure 3.6. *Fracture log and time dependent temperature and temperature gradient logs of BC-84-6. These logs were recorded with the GSC high sensitivity temperature probe at 6 m/min and a sample time of 0.375 s. The data were deconvolved and smoothed as described by Bristow and Conaway (1984). The eight logs are numbered relative to the time elapsed since the drilling of the hole was completed. The time-after-drilling for logs numbers 1 to 8 are from 4 hours to 16 days as given in the text.*

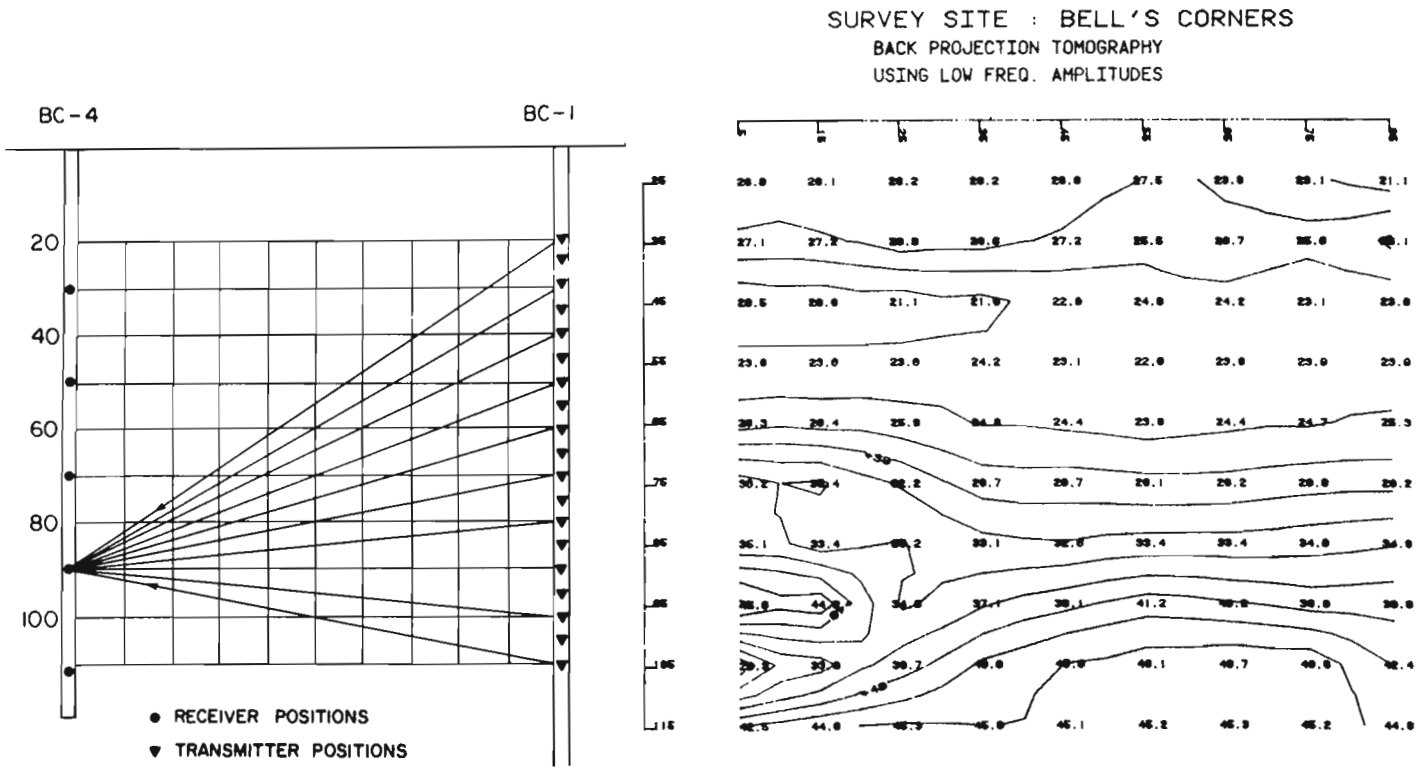

Figure 3.7. *Receiver and transmitter positions (left) for a seismic tomography experiment conducted between borehole BC-81-1 and BC-81-4 at Bells Corners. On the right is shown a reconstructed image of seismic properties of the rock, contoured to represent the generalized geology between the holes. The layering of the geology is generally replicated. Further details on this experiment are given by Wong et al. (1982).*

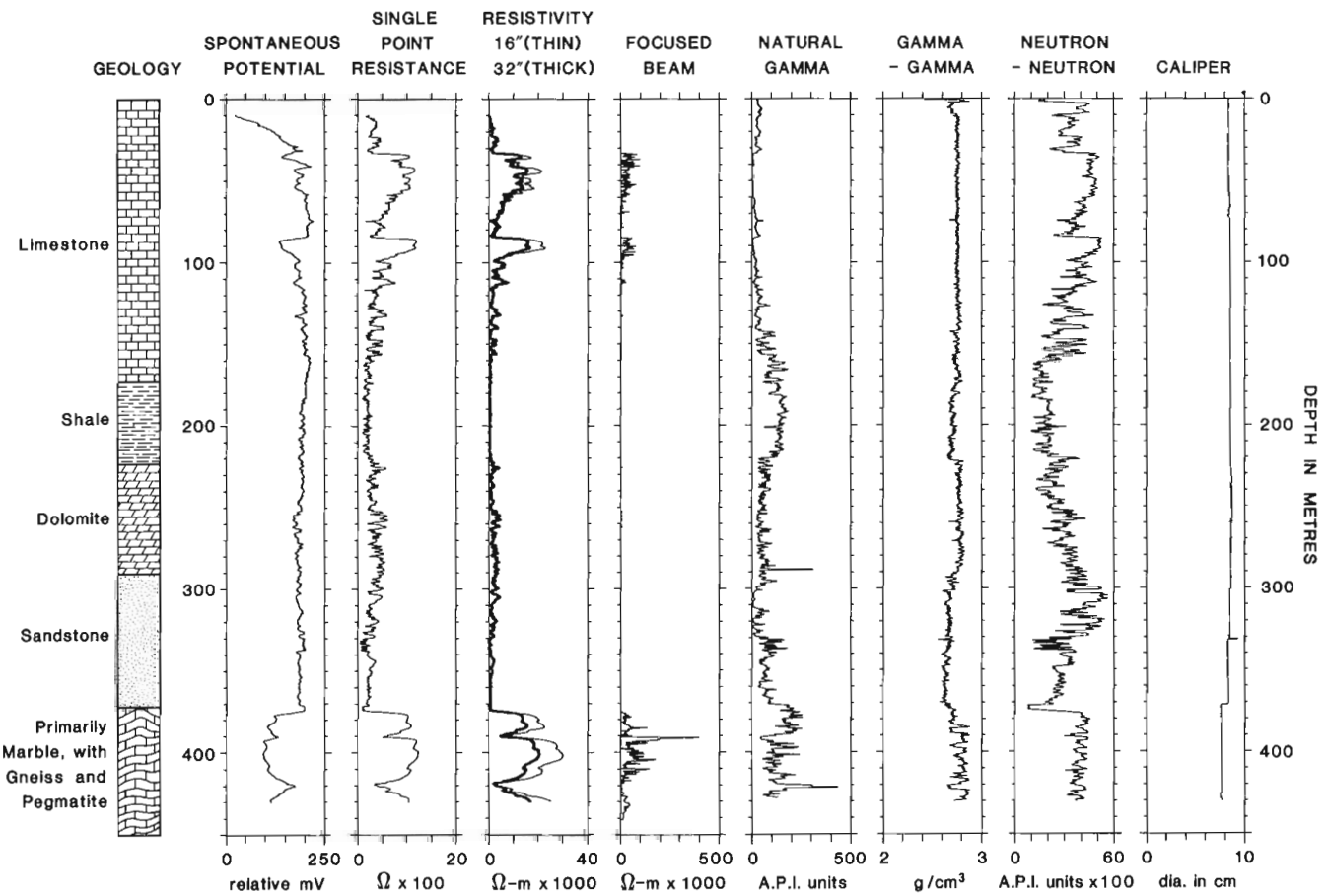

Figure 3.8. *Geological log and geophysical logs recorded in borehole LB-1 near the GSC building in Ottawa. They were recorded in 1979 by Roke Oil Enterprises of Calgary at 4 m/min with an analog system. The density tool was a side-walled type with a Cs-137 source. The neutron tool used a Am/Be source and was calibrated in API units as was the natural gamma tool. The upper 375 m of this 442 m borehole is in sedimentary rock.*

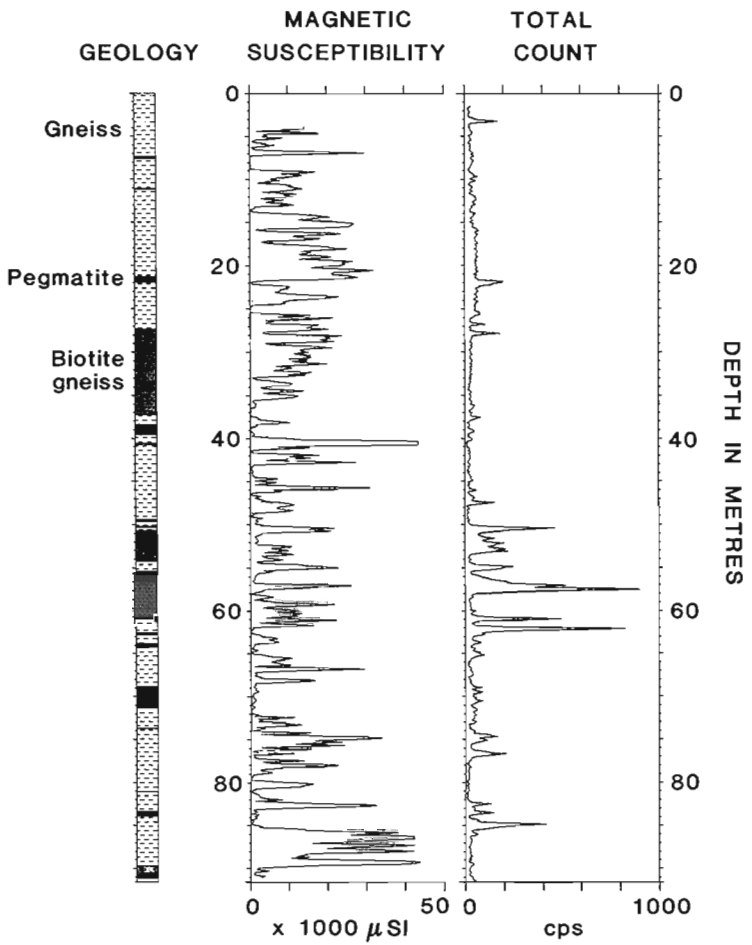

Figure 3.9. Geological log, magnetic susceptibility (MS) log and total count (TC) log recorded in Bancroft test hole BN-81-1 with the GSC research logging system. The MS log was recorded at 6 m/min and a sample time of 0.2 s. The TC log was run at 3 m/min and a sample time of 1 s using a 19 x 76 mm NaI (Tl) detector.

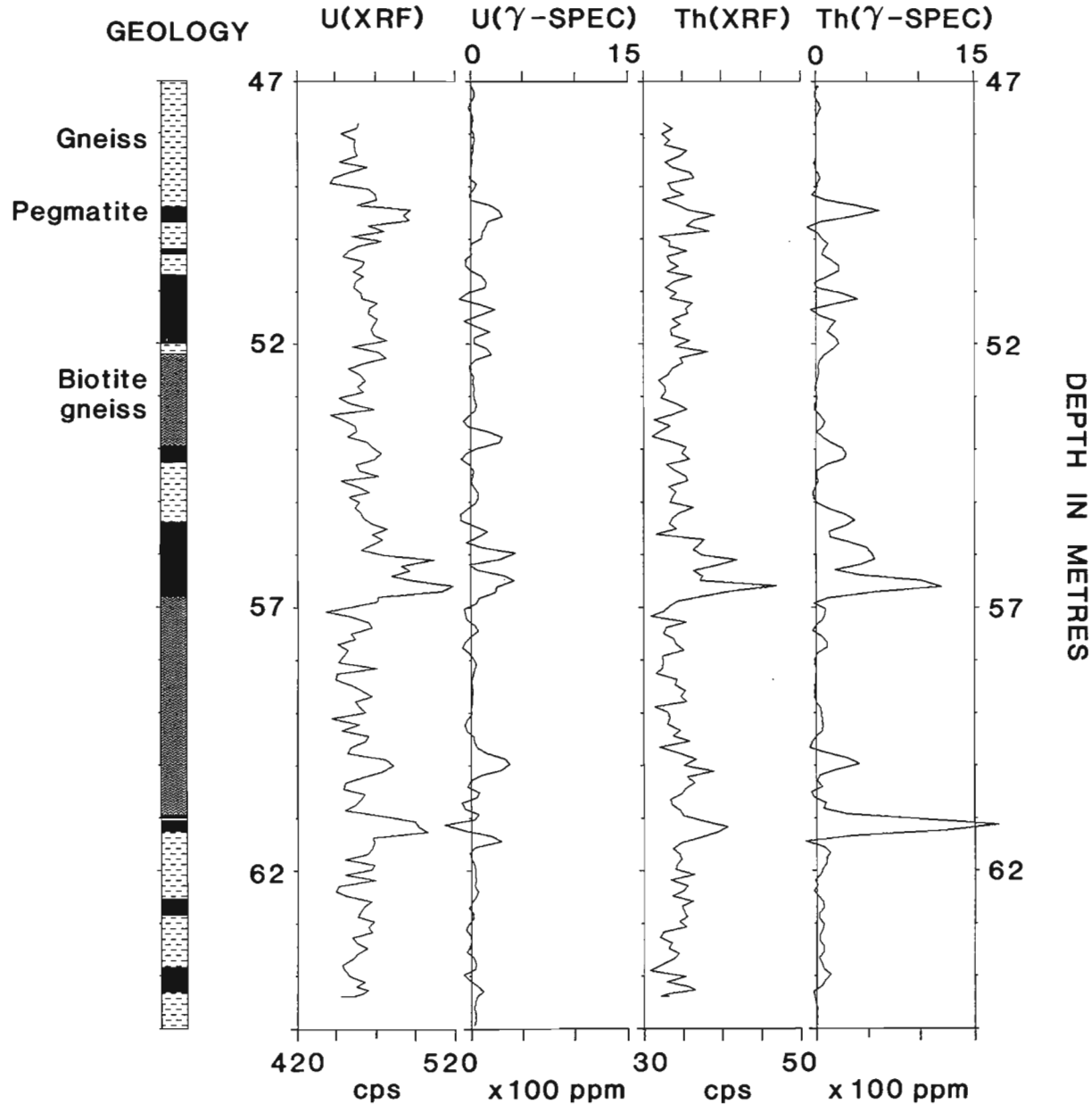

Figure 3.10. Geological log, experimental XRF logs, and gamma ray spectral logs of a portion of Bancroft borehole BN-81-1. The XRF logs are presented in counts per second (cps) proportional to uranium and thorium content, and the gamma spectral logs are reduced to ppm uranium and ppm thorium. The XRF logs were run at 0.3 m/min with a sample time of 20 s (equivalent to a 10 cm depth sample). The spectral logs were smoothed to produce the same 10 cm depth sample. The agreement between the logs indicates the uranium and thorium decay series are in radioactive equilibrium.

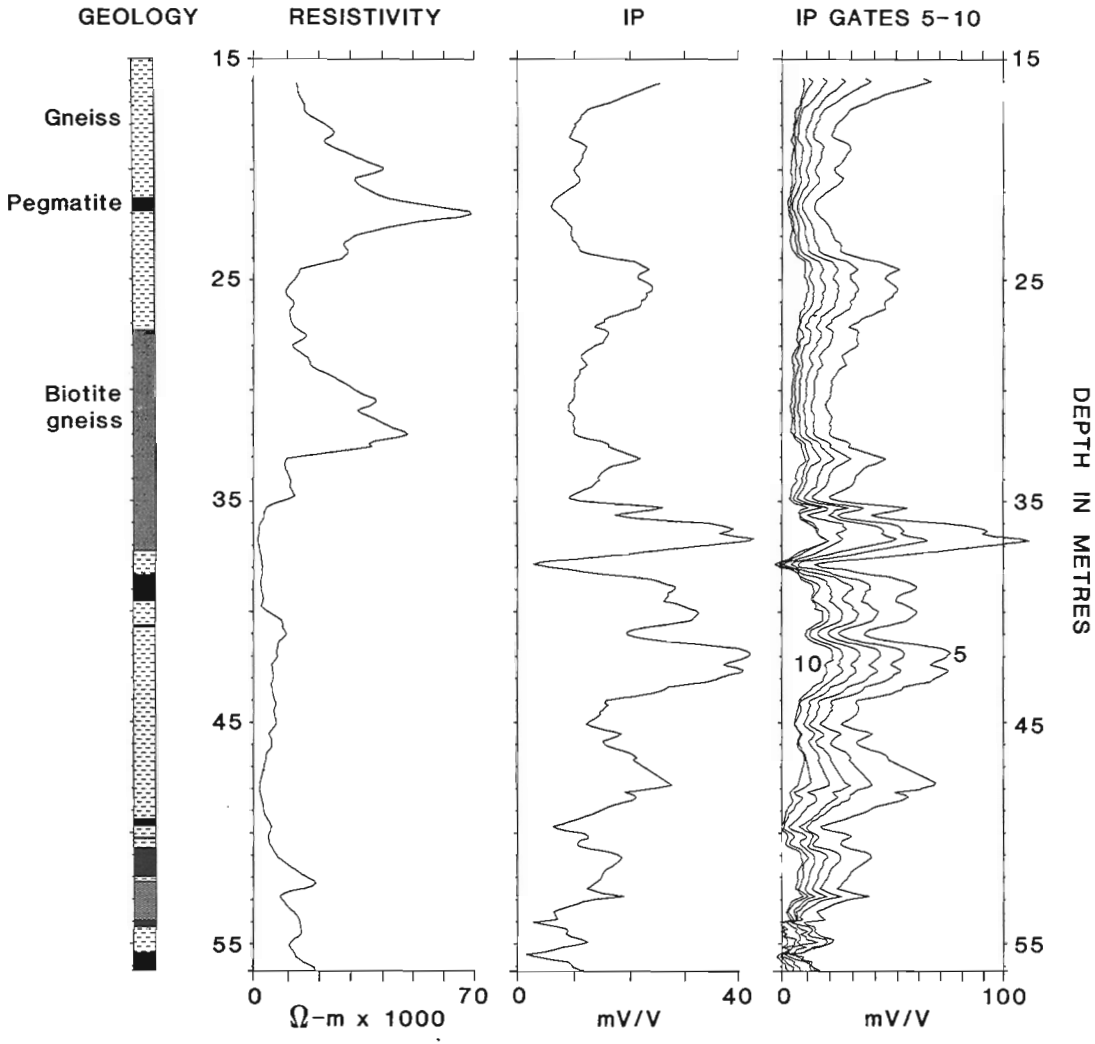

Figure 3.11. The geological log and some experimental induced polarization (IP) logs of the upper part of Bancroft borehole BN-81-1. They include the resistivity log (derived from the IP log), the standard IP log (using the Newmont window of 0.45s to 1.1s), and six experimental time gates for sampling the decaying pulse during the 'off time'. The electrode array is the lateral array with current electrode 2.6 m above the upper potential electrode, and 3.0 m above the lower potential electrode. Logging speed was 0.75 m/min and the period for the IP pulse was 8 s. Post processing of the logs is made possible by the unique full wave recording features of the GSC research logging system.

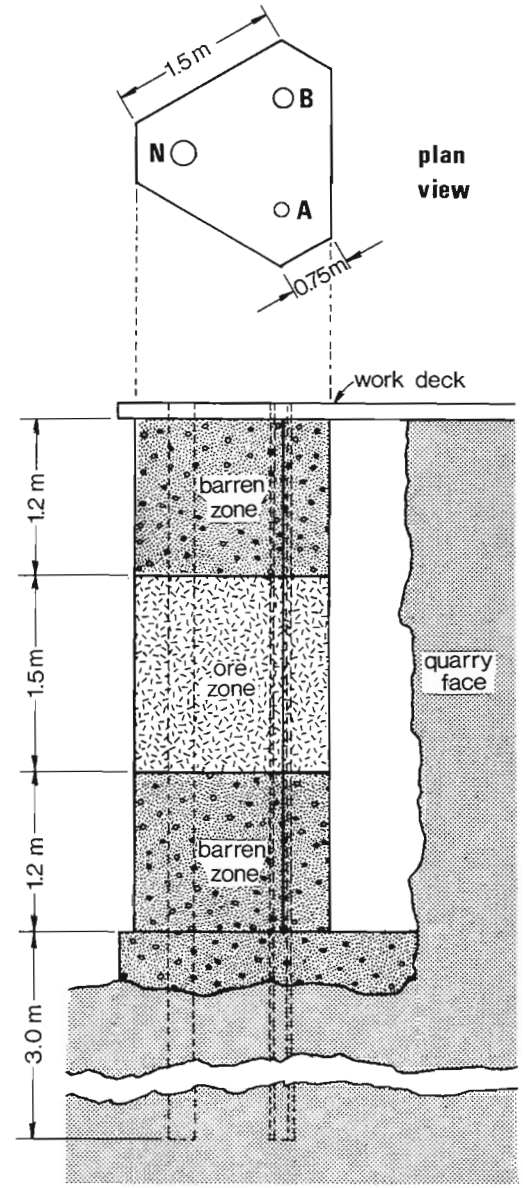

Figure 3.12. Details of one of the nine test columns at Bells Corners containing three model boreholes for calibrating gamma ray spectrometric logging equipment.

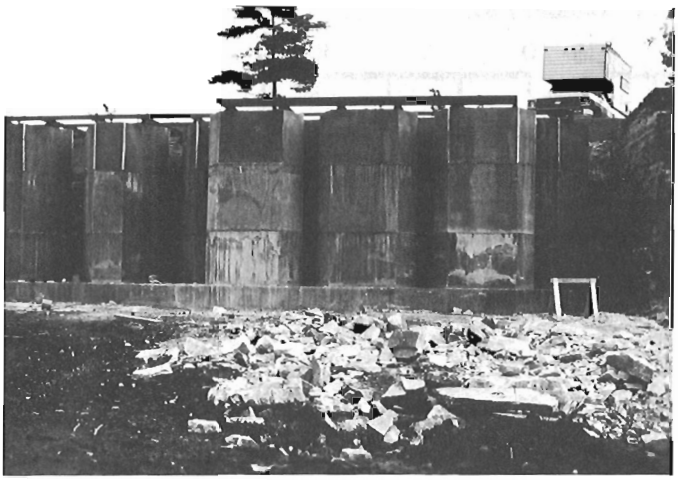

Figure 3.13. *The nine concrete test columns at Bells Corners viewed from inside the quarry showing the "ore zones" and a logging truck parked above in the working area for calibrating logging systems. (GSC 203254-0).*

Figure 3.8 shows the general geological column and eight borehole logs recorded by Roke Oil Enterprises of Calgary, a logging service company. These logs include the spontaneous potential (SP), single point resistance, 16 inch and 32 inch normal resistivity logs, focused beam electric log, natural gamma, gamma-gamma density, neutron-neutron porosity, and a caliper log. Additional statistics are given in the figure caption.

This suite of logs presents a good overview of a representative number of physical properties of the rocks intersected by this test hole. For researchers interested in a thicker sedimentary section (about 370 m) than the boreholes at Bells Corners (about 65 m), test hole LB-1 should be used. An interesting feature on these logs is the presence of the uraniferous marker zone at about 290 m which coincides with the basal March Formation gamma ray peaks at a depth of about 20 m, seen in the logs of Figures 3.2 to 3.4 at Bells Corners 15 km to the west.

The unconformity is also easily seen at about 375 m in both the electrical and radiometric logs. The caliper log shows that borehole LB-1 does not deviate by much more than 1 cm from its nominal NQ diameter of 76 mm. It should be noted that due to its location, surrounded by buildings and city traffic, for some experimental high sensitivity seismic or electrical measurements this test hole would be considered too noisy.

Bancroft area test holes

Bancroft, Ontario is a world famous mineral collecting location, from which many museum quality samples of minerals originate. Most of these come from the numerous pegmatites which cut the Precambrian gneisses and granitic rocks in the area. In 1979 two test boreholes (BN-79-4, BN-79-5) of BQ diameter (60 mm) were drilled to intersect uranium- and thorium-bearing mineralized zones, primarily for testing a gamma ray spectral logging system. In 1981 two additional large diameter (HQ;100 mm) boreholes (BN-81-1, BN-81-2) were drilled 60 m apart at the same location, primarily to test and evaluate a new borehole XRF (X-ray fluorescence) probe. These test boreholes have also proven to be extremely useful for other purposes because of the variations in the physical properties of the rocks intersected by the holes. Figure 3.9 shows a magnetic susceptibility log and a total count log for the 92 m deep borehole BN-81-1.

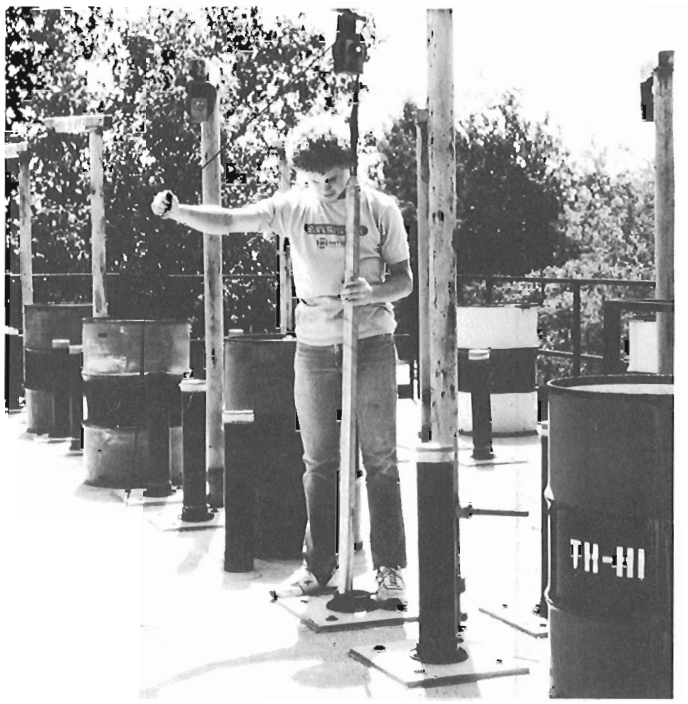

Figure 3.14. *Lowering a gamma ray spectral logging probe into one of the model boreholes at Bells Corners. This view of the working area shows the overhead pulley assemblies, the black plastic extension pipes for aligning the probes with the holes in the model below (as well as permitting calibration when snow covers the work area), and the storage drums for antifreeze used in the boreholes. (GSC 202942-R.)*

The magnetic susceptibility logs are discussed in greater detail and compared to measurements made on drill core by Bristow and Bernius (1984). Examples from these Bancroft test holes have also been used to illustrate papers on gamma ray and gamma ray spectral logging (Killeen, 1982, 1983; Conaway and Killeen, 1978; Conaway et al., 1980; Conaway, 1980).

Figure 3.10 shows uranium and thorium logs from a section (47 m to 65 m) of borehole BN-81-1, obtained by both the XRF and gamma ray spectrometric methods. The XRF probe was developed at the Karlsruhe Nuclear Research Institute, West Germany, and was brought to Canada for testing and evaluation as a joint project with the GSC. The probe, which has a 70 mm diameter, utilized a low energy Cobalt 57 gamma ray source (122 KeV) to excite X-ray fluorescence in the wall rocks of the borehole. The detector was a solid state hyperpure germanium crystal cooled to liquid nitrogen temperature and housed in an appropriate cryostat container in the probe. The energy spectrum of these X-rays was recorded using the GSC research logging system. The X-ray peaks were analyzed and converted into a count rate which is directly proportional to the uranium and the thorium content of the rocks as shown in the logs of Figure 3.10. This is a direct technique which is sensitive to the uranium metal and thorium metal irrespective of the fact that they are radioactive elements.

The GSC gamma ray spectral logging system, calibrated in the model boreholes at Bells Corners (Killeen, 1978, 1979; Killeen and Conaway, 1978), was used to produce an indirect measurement of the uranium and thorium content. It is indirect because the technique actually counts the gamma radiation of radioactive daughter products of uranium and thorium, rather than these two elements themselves. Results of these tests were reported by Lubecki et al. (1982).

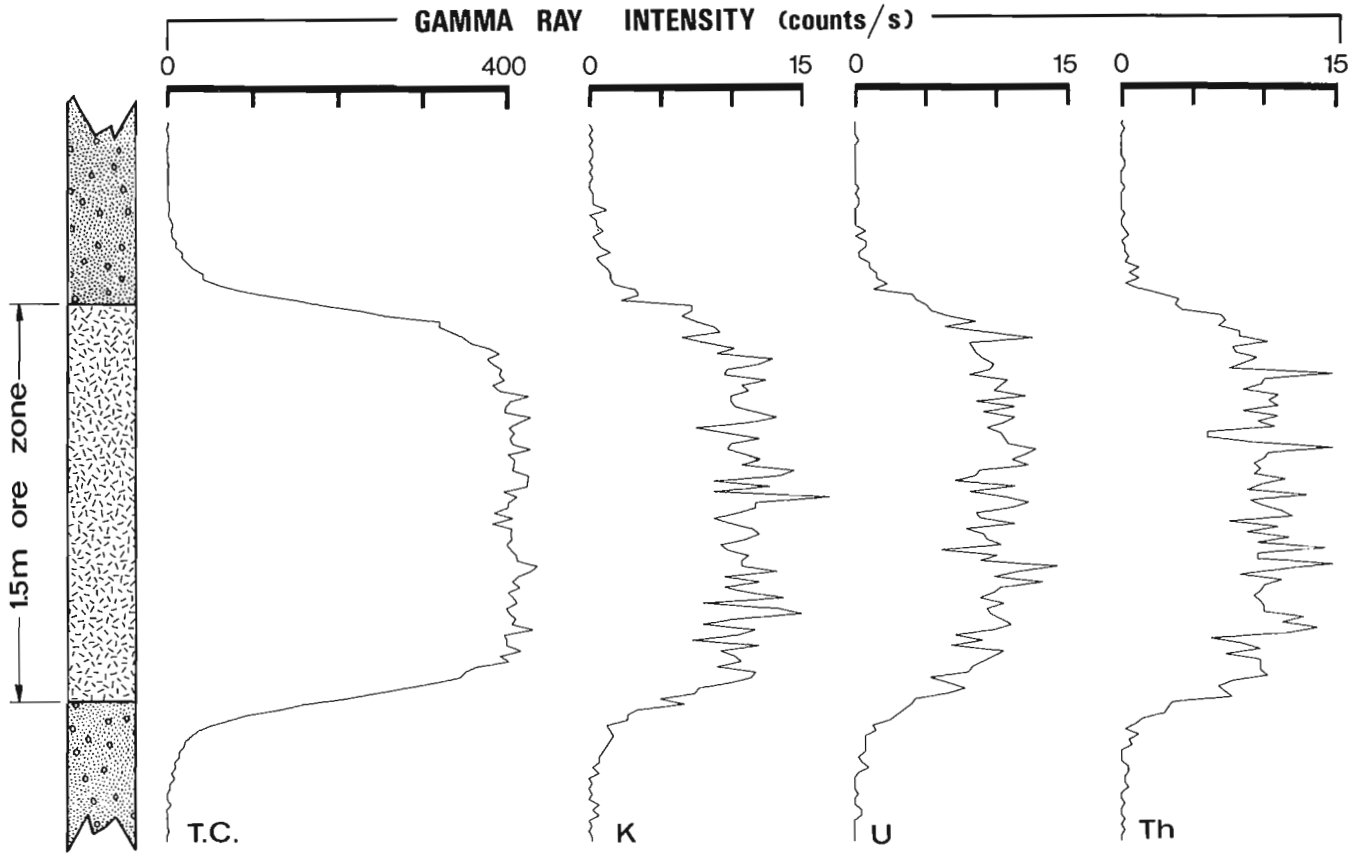

Figure 3.15. Gamma ray spectral log recorded digitally in the highest-grade thorium test column at Bells Corners (BT-9-0T). The four channels recorded are total count, potassium, uranium and thorium.

Another interesting series of experiments conducted in borehole BN-81-1 relates to the GSC developments in IP logging (Bristow, 1986; Mwenifumbo, 1986). The logs shown in Figure 3.11 demonstrate the variability in both the resistivity and polarizability of the rocks intersected by the borehole. The figure shows the generalized geological log, the resistivity log, the standard IP log (chargeability), and a set of six IP logs representing results from six different time gates or windows in the decaying IP transient pulse. The GSC research logging system records the entire IP wave form so that different (nonstandard) IP gates may be selected as desired during post processing of the recorded data. This makes it possible to optimize the time gates for the particular environment being measured.

Additional information is available on the Bancroft test holes although not as much as for the Bells Corners test area. The holes are also suitable for hole-to-hole experiments, since their greatest separation is about 60 m. It should be noted that these test holes are drilled approximately perpendicular to the dip of the rocks and are therefore inclined at an angle of about 60° from the horizontal. The two large diameter boreholes BN-81-1 and BN-81-2 present a unique opportunity to test prototype probes which are often of larger diameter than their final version.

Model boreholes for calibration purposes

In October 1977, construction was completed near Ottawa of extensive calibration facilities for borehole gamma-ray spectrometry equipment. These facilities were

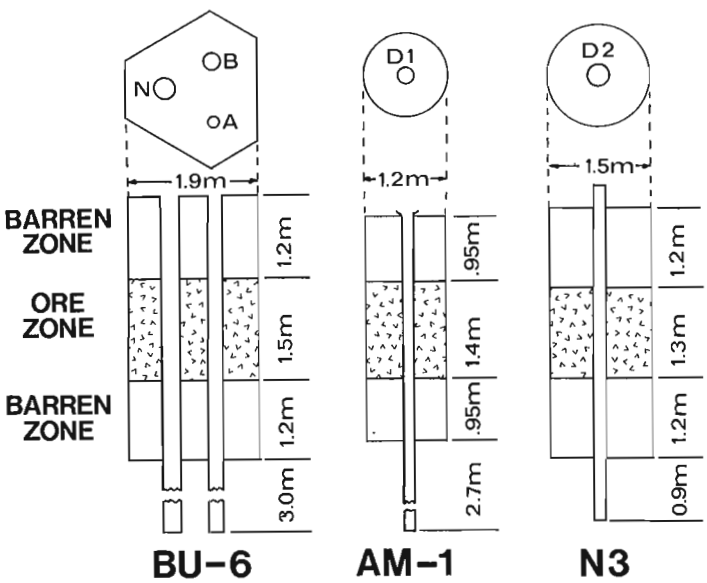

Figure 3.16. Schematic diagram of the model boreholes for calibration of gamma ray logging probes in Ottawa, Canada (BU-6); Adelaide, Australia (AM-1) and Grand Junction, United States (N3). The dimensions of the ore zones and barren zones are shown, as well as a cross-section of each model.

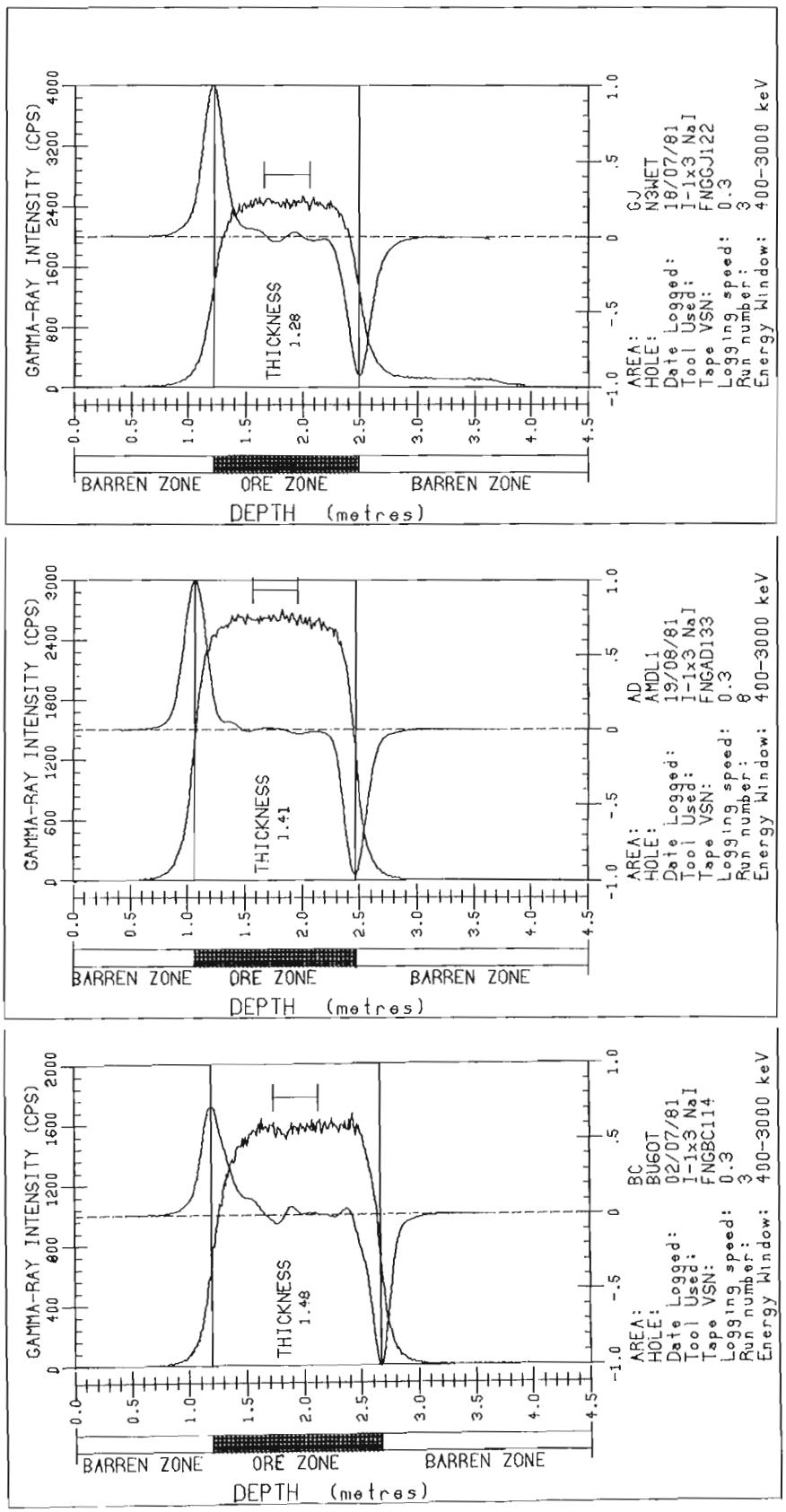

Figure 3.17. *Example gamma ray logs in the three model boreholes BU-6, AM-1 and N3 shown in Figure 3.3.16. The logs shown were recorded with the GSC research logging system with a 25 x 75 mm NaI (Tl) detector, a logging speed of 0.3 m/min, an energy window of 0.4 to 3.0 MeV. The plateau region where average intensities were calculated is indicated, as well as the derivative of the log used to compute the thickness of the ore zones.*

constructed as part of the Geological Survey of Canada program to implement the recommendations of the International Atomic Energy Agency (IAEA, 1976, 1982) regarding calibration of radiometric exploration equipment. The calibration facilities are located on the property of the CANMET laboratory complex near Bells Corners, Ontario. Their location and description are given in detail by Killeen (1978) and Killeen and Conaway (1978).

For calibration of borehole gamma ray spectrometers under controlled conditions, nine concrete test columns were constructed along the wall of an abandoned rock quarry. Each of these columns is 3.9 m in height, with a simulated 1.5 m thick ore zone sandwiched between upper and lower barren zones (Fig. 3.12). Each test column contains 3 boreholes, with nominal diameters of 46 mm (size A), 60 mm (size B) and 75 mm (size N), intersecting the ore zones. Three of the test columns contain ore zones of different concentrations for potassium, three for uranium and three for thorium. Nominal radioelement concentrations in the ore zones are: for models BK-1, BK-2, and BK-3-OT: 0.7%, 1.1% and 3% potassium; for models BU-4, BU-5 and BU-6-OT: 15 ppm, 100 ppm and 950 ppm uranium; and for models BT-7, BT-8 and BT-9-OT: 8 ppm, 35 ppm and 350 ppm thorium.

Figure 3.13 is a view of the nine concrete test columns as seen from inside the quarry, showing the 'ore zones' and a logging truck parked above in the working area for calibrating logging systems. Figure 3.14 illustrates the procedure for lowering a gamma ray probe through the holes in the deck covering the models. Each test column is supplied with a 'well head' pulley assembly which can be positioned over any one of three holes in each test column. The metal drums shown in the photograph are used to store the antifreeze which is used in the water-filled boreholes to prevent freezing in winter. The holes may be logged wet or dry by pumping the fluid out of the holes and into the storage drums.

Figure 3.18. *The two model boreholes located in Fredericton, New Brunswick at the Department of Mineral Resources. The 1.5 m thick 'ore zones' nominally contain 100 ppm U (BU-1-F) and 1000 ppm U (BU-2-F) for calibration of natural gamma ray logging tools. (GSC 203255-U.)*

A typical raw gamma ray spectral log recorded in borehole BT-9-OT (the 350 ppm thorium model) is shown in Figure 3.15. The contribution of the thorium decay series gamma rays to the uranium and potassium channels of the spectral logging system can be easily seen in the figure. This type of calibration data can be used to derive stripping factors as well as sensitivities as described by Killeen (1979).

The sensitivities (often called k-factors) for gamma ray logging systems are derived from logging measurements made in model boreholes with known radioelement concentrations. The determination of the known radioelement concentrations is found by laboratory analysis of samples taken from the 'ore zones' during their construction.

The equipment manufactured for gamma ray logging is distributed internationally and it is reasonable to assume the calibration measurements in standard model holes in any country should give the same answer. At the recommendation of the NEA/IAEA Working Group on R&D in Borehole Logging for Uranium Exploration, the Canadian model boreholes established in Ottawa in 1977 were to be intercalibrated with the United States Department of Energy (USDOE) models in Grand Junction, Colorado. Intercalibration measurements between the models in Grand Junction and the models in Ottawa were conducted by the GSC and by the USDOE. An inconsistency in results was found, and further intercalibration measurements in 1981 were conducted using the GSC research logging system. At the same time, mining companies in Australia, using the calibration facilities established in Adelaide found discrepancies for equipment previously calibrated in Grand Junction. The Geological Survey of South Australia, arranged through the NEA/IAEA, to have the GSC research logging system taken to Australia to help resolve these differences.

The schematic diagram of Figure 3.16 shows the major features of the model boreholes for calibration of gamma ray logging probes in Ottawa, Canada (BU-6); Adelaide, Australia (AM-1), and Grand Junction, United States (N3). The dimensions of the ore zones and barren zones are shown, as well as a cross section of each model. Model BU-6 contains three boreholes of different diameters 46 mm, 60 mm, and 75 mm. The hole diameters of AM-1 and N3 are 108 mm and 114 mm respectively. Further details on the models are given in Killeen (1978), Killeen and Conaway (1978), Mathews et al. (1978), Wenk (1980), Milton (1982) and Wenk and Dickson (1981).

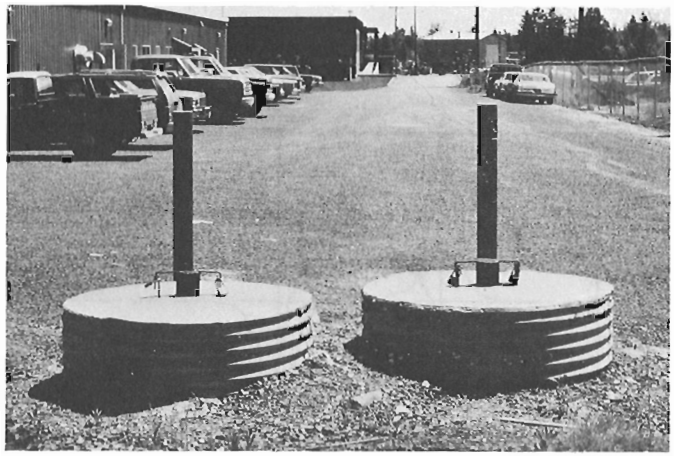

Figure 3.19. *The four model boreholes located in Saskatoon, Saskatchewan, designed for calibration of gamma ray logging tools. They nominally contain: BU-1-S, 0.01% U; BU-2-S, 0.1% U; BU-3-S, 1.0% U; and BU-4-S, 4.0% U. (GSC 202942-Q.)*

The results of the international intercalibration measurements have been described by Bristow et al. (1982), George (1982), and Killeen et al. (1983). An example of a gamma ray log recorded in model BU-6-OT at Bells Corners (Ottawa) compared to logs obtained with the same system in model N3 (Grand Junction) and AM-1 (Adelaide) is shown in Figure 3.17. It is this type of data which was analyzed to intercalibrate the model boreholes.

Model boreholes at Fredericton, New Brunswick

Two model boreholes were constructed in Fredericton for the calibration of gamma ray logging equipment, on the property of the Department of Mineral Resources of the province of New Brunswick. The models are housed below ground in corrugated steel tanks with approximately the upper 50 cm exposed above ground level (Fig. 3.18). Each model contains a single, H size (100 mm diameter) borehole which penetrates an 'ore zone' sandwiched between upper and lower barren zones. The 1.5 m thick ore zones have nominal uranium concentrations of 100 ppm (model borehole BU-1-F) and 1000 ppm (model borehole BU-2-F).

These model boreholes are designed primarily for calibration of 'gross-count' natural gamma ray logging tools, for which it is assumed that the radiation from potassium and thorium is negligible.

Model boreholes at Saskatoon, Saskatchewan

In collaboration with the Saskatchewan Geological Survey and the Saskatchewan Research Council, a set of four model boreholes was constructed in Saskatoon. These are designed primarily for calibration of gross-count natural gamma ray logging tools, and in particular were meant to support the uranium exploration activities being carried out in the area of the Athabasca sandstone to the north. The four model boreholes shown in Figure 3.19 are constructed in a configuration similar to the Fredericton boreholes, being single hole models in below-ground tanks. The ore zones have nominal uranium concentrations and thickness for the four models as follows: model BU-1-S, 0.01%U, 1.4 m thick;

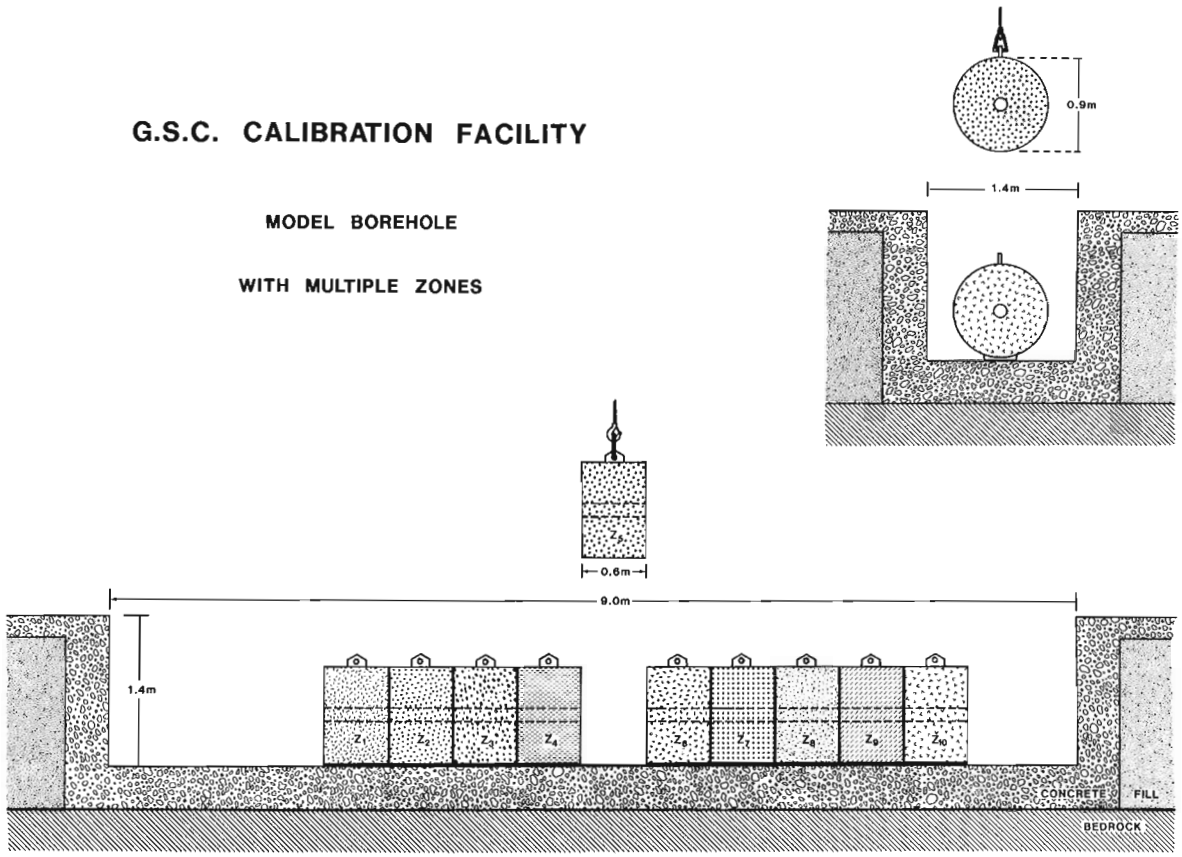

Figure 3.20. *Configuration of cylindrical concrete zones at Aberdeen Street, Ottawa used for calibration of borehole logging probes. Each zone will have specific known physical properties. The horizontal configuration makes it easy to interchange zones using an overhead crane assembly. Some calibration zones will be shipped to other areas in Canada to establish field calibration model boreholes.*

model BU-2-S, 0.1%U, 1.6 m thick; model BU-3-S, 1.0%U, 1.6 m thick; and model BU-4-S, 4.0%U. The last zone is meant to be a high grade zone, and is only 21 cm thick. The borehole is 76 mm in diameter.

Aberdeen Street calibration facility in Ottawa

A multiple-zone model borehole has been constructed for calibration of logging probes, and for testing and evaluation of the calibration zones to be used in future field calibration models. The new calibration facility, located in Ottawa, consists of a series of zones in the form of concrete cylinders placed in contact with each other in a horizontal configuration as shown in Figure 3.20. Each cylinder represents a 'zone' with specific known physical properties for which the logging tool response can be evaluated. The horizontal model borehole is produced by the alignment of the axial holes in the individual zones. Logging tools will be calibrated by pulling them through the successive zones.

The Ottawa primary facility has provision for saturating the model borehole with water to simulate most field conditions. The horizontal configuration of the model borehole makes it a versatile facility allowing removal and placement of different calibration zones during testing and evaluation.

Initial construction of the calibration facility includes a series of calibration zones made of concrete (Fig. 3.21) with different densities covering the range of interest for coal logging. These zones, when tested for homogeneity and accurately measured for density, will be shipped to field calibration facilities which are being established in western and eastern Canada for coal logging.

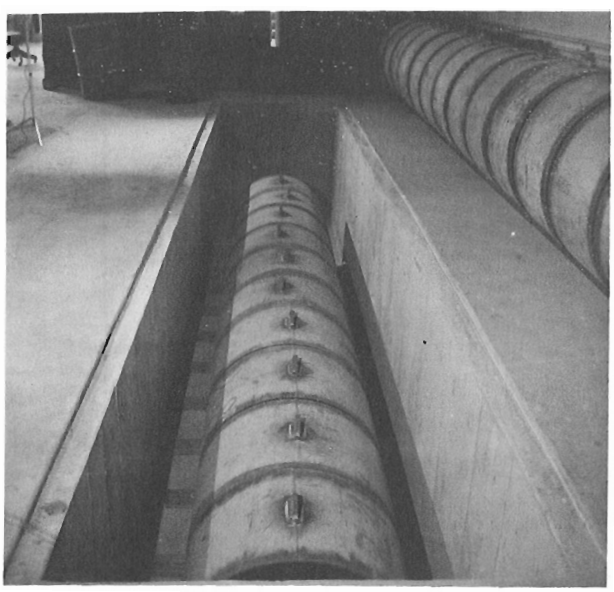

Figure 3.21. *The multiple-zone horizontal model borehole in its below-ground tank, located in the Borehole Geophysics Laboratory at Aberdeen Street, Ottawa (GSC 204145-B).*

The Ottawa facility will also be used to develop standardized calibration zones for other physical properties such as porosity or magnetic susceptibility. These will be added to the field calibration facilities as they become available.

Coal logging calibration facilities

Field logging calibration facilities are being developed in Dartmouth, Nova Scotia, for the coal mining areas of eastern Canada and in Calgary, Alberta for the western Canadian coal mining activities. Figure 3.22 illustrates the design of the inground fiberglass tank assembly and the vertical stack of calibration zones which form each model borehole. The central hole in each cylindrical zone is aligned such that the stack provides a continuous hole through all the

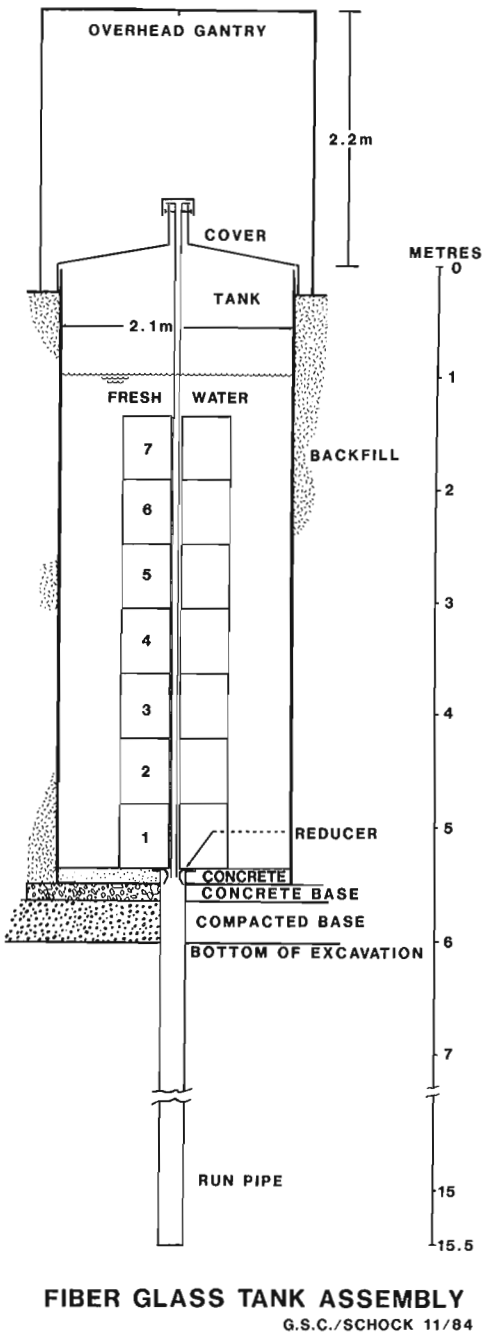

Figure 3.22. *Schematic diagram of the tank assembly used in the field calibration facilities showing a vertical stack of calibration zones aligned with the run pipe in the below-ground tank. The optional drill rod is shown suspended from the cover inside the model borehole formed by the zones. The reducer at the bottom allows smooth transition from the below-tank run pipe to the zone borehole.*

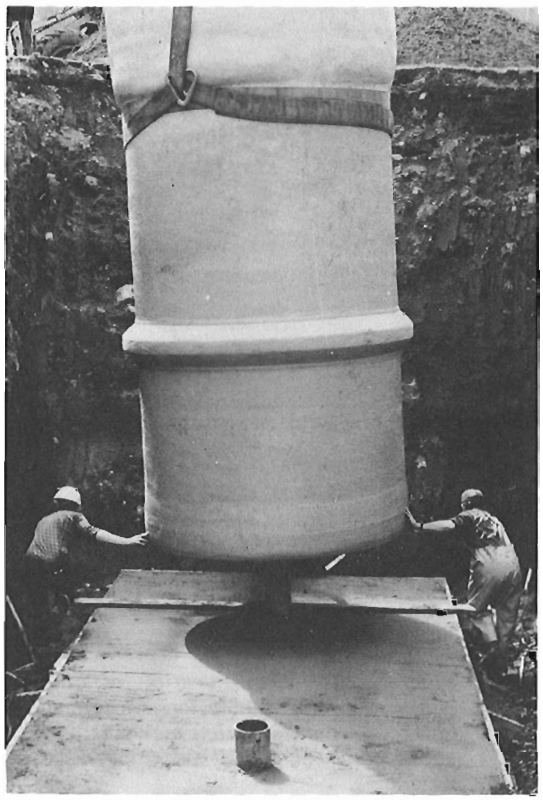

Figure 3.23. *Positioning the fiberglass tank in the excavation at the Nova Scotia Research Foundation Corporation. The run pipe for the second tank can be seen in the foreground protruding through the concrete base. The hole in the bottom of the tank is positioned over the run pipe. After installation it is attached to the tank with a watertight fiberglass bond. (GSC 203256-W.)*

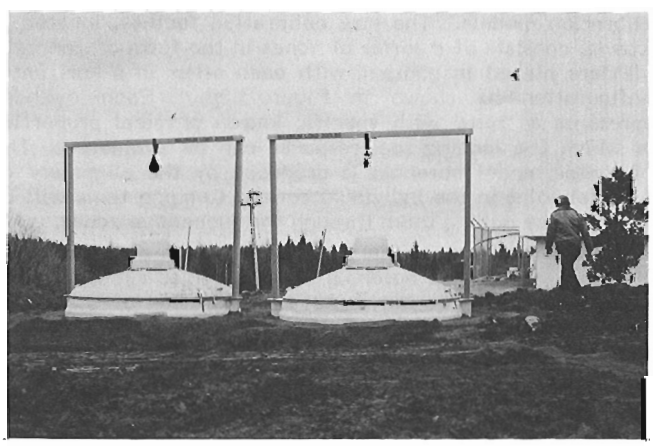

Figure 3.24. *The completed coal logging field calibration facility at the Nova Scotia Research Foundation Corporation showing insulated tank and cover, and overhead gantry. (GSC 204145-Z.)*

zones, which is further aligned with a run pipe protruding below the tank. Some calibration measurements require that a steel drill rod (or pipe) be temporarily suspended in the model borehole to simulate logging inside the drill rod. For this reason the insulated fiberglass cover for the tank was designed to support the weight of two drill rod sections as well as a maximum of four workers. During the calibration procedure, logging tools will normally be lowered into the model borehole on a cable which runs over a pulley suspended on an overhead gantry assembly. Continuous logging at a uniform speed through the entire simulated borehole during the calibration procedure is ensured by the 'run pipe' beneath the tank.

The optimum borehole diameter was determined based on common regional coal drilling practice, to be 100 mm in Western Canada and 75 mm in Eastern Canada requiring an appropriate reducer allowing smooth transition from below-tank run pipe (200 mm diameter) to the borehole.

Field logging calibration facilities at Dartmouth, Nova Scotia

Two fiberglass tank assemblies have been installed at the site of the Nova Scotia Research Foundation Corporation in Dartmouth, Nova Scotia. Figure 3.23 shows one of the tank assemblies being lowered into place on a concrete supporting base, and centralized over the run pipe which extends beneath the model as shown in Figure 3.22. The completed installation of two tanks is shown in Figure 3.24. Additional details and the descriptions of the installation procedure are given by Killeen et al. (1984) and Schock and Killeen (1985).

Calibration zones are being constructed and tested at the Ottawa primary calibration facility before being shipped to Nova Scotia for installation inside the tanks.

Field logging calibration facilities at Calgary, Alberta

The Western site is to be located in Calgary, at the Institute of Sedimentary and Petroleum Geology (a division of the GSC), adjacent to calibration pads for portable gamma-ray spectrometers which were constructed in 1977 (Killeen, 1979). At this location, the water table is variable and the ground is unstable, which required an engineering site evaluation with appropriate recommendations prior to installation of the new fiberglass tanks. Details of the procedure for installation have been determined and the Western tanks have already been designed and constructed to withstand the condition of saturated soil surrounding them to the top. These tanks are 60 cm longer than the Eastern tanks to allow a greater amount of concrete inside for additional load against uplift. It is expected that the Calgary set of inground tanks will be installed in the summer of 1985.

Acknowledgments

I would like to thank all those who have helped with various aspects of the project as it evolved over the past eight years. I am especially grateful to the following individuals for their part in constructing models and logging the test holes: Ralph Arnold, Saskatchewan Research Council; Dwight Ball, New Brunswick Department of Mineral Resources; Andy Cicoria of Century Geophysics for the gratis logging at Bells Corners; Gordon Bernius, George Cameron, Bill Hyatt, and Laurel Schock of the GSC. I thank Kerr Addison Mines Limited and in particular D.M. Hendrick, Chief Geologist-Exploration, for permission to establish test holes on their property in the Bancroft area. Thanks are also due to contributors of material and example logs of the test holes including Quentin Bristow, John G. Conaway, John Hayles, C. Jonathan Mwenifumbo, Ted I. Urbancic and Joe Wong.

References

Bernius, G.R.
1981: Boreholes near Ottawa for the development and testing of borehole logging equipment - a preliminary report; in Current Research, Part C, Geological Survey of Canada, Paper 81-1C, p. 51-53.

Bristow, Q.
1985: A digital signal processing unit for the Geo Instruments magnetic susceptibility sensors, with analogue and RS-232C outputs; in Current Research, Part B, Geological Survey of Canada, Paper 85-1B, p. 463-466.

1986: A system for the digital transmission and recording of induced polarization measurements in boreholes; in Borehole Geophysics for Mining and Geotechnical Applications, P.G. Killeen, ed.; Geological Survey of Canada, Paper 85-27, report 14.

Bristow, Q. and Bernius, G.R.
1984: Field evaluation of a magnetic susceptibility logging tool; in Current Research, Part A, Geological Survey of Canada, Paper 84-1A, p. 453-462.

Bristow, Q. and Conaway, J.G.
1984: Temperature gradient measurements in boreholes using low noise high resolution digital techniques; in Current Research, Part B, Geological Survey of Canada, Paper 84-1B, p. 101-108.

Bristow, Q., Killeen, P.G. and Mwenifumbo, C.J.
1982: Comparison of standardized gamma-ray log calibration measurements: Ottawa, Adelaide and Grand Junction; in Symposium on Uranium Exploration Methods, Review of the NEA/IAEA R&D Programme, Paris, June 1-4.

Conaway, J.G.
1980: Direct determination of the gamma ray logging system response function in field boreholes; Geoexploration, v. 18, p. 187-199.

Conaway, J.G., Bristow, Q. and Killeen, P.G.
1980: Optimization of gamma-ray logging techniques for uranium; Geophysics, v. 45, p. 292-311.

Conaway, J.G. and Killeen, P.G.
1978: Quantitative uranium determinations from gamma-ray logs by application of digital time series analysis; Geophysics, v. 43, p. 1204-1221.

George, D.C.
1982: Total count gamma-ray logging: correction factors and logging model grade assignments; Symposium on Uranium Exploration Methods, Review of the NEA/IAEA R&D Programme, Paris, June 1-4.

IAEA
1976: Radiometric reporting methods and calibration in uranium exploration; International Atomic Energy Agency, Technical Report Series no. 174, 57 p.

1982: Borehole logging for uranium exploration - a manual; International Atomic Energy Agency, Technical Report Series no. 212, Vienna, 279 p.

Killeen, P.G.
1978: Gamma-ray spectrometric calibration facilities -a preliminary report; in Current Research, Part A, Geological Survey of Canada, Paper 78-1A, p. 243-247.

Killeen, P.G. (cont.)
1979: Gamma-ray spectrometric methods in uranium exploration - application and interpretation; in Geophysics and Geochemistry in the Search for Metallic Ores; Peter J. Hood, ed.; Geological Survey of Canada, Economic Geology Report 31, p. 163-229.

1982: Gamma-ray logging and interpretation; Chapter 4 in "Developments in Geophysical Exploration Methods", Vol. 3, Applied Science Publishers Ltd. (Elsevier), p. 95-150.

1983: Borehole logging for uranium by measurement of natural gamma radiation; in Nuclear Geophysics, C.G. Clayton, ed., Pergamon Press, p. 231-260.

Killeen, P.G. and Conaway, J.G.
1978: New facilities for calibrating gamma-ray spectrometric logging and surface exploration equipment; Canadian Mining and Metallurgical Bulletin, 793, p. 84-87.

Killeen, P.G., Bernius, G.R., Schock, L.D. and Mwenifumbo, C.J.
1984: New developments in the GSC borehole geophysics test area and calibration facilities; in Current Research, Part B, Geological Survey of Canada, Paper 84-1B, p. 373-374.

Killeen, P.G., Bristow, Q. and Mwenifumbo, C.J.
1983: Gamma-ray logging for uranium: status of international efforts to resolve discrepancies in calibration models; in SPWLA Twenty-fourth Annual Logging Symposium, June 27-30, Paper AA, 15 pp.

Lubecki, A., Doebele, R. and Herrmann, W.
1982: Direct uranium logging using X-ray fluorescence technique; Symposium on Uranium Exploration Methods, Review of the NEA/IAEA R&D Programme, Paris, 1st-4th June 1982, p. 699-713.

Mathews, M.A., Koizumi, C.J. and Evans, H.B.
1978: D.O.E. - Grand Junction logging model data synopsis; Bendix Field Corporation Report GJBX-76(78).

Milton, B.E.
1982: The Adelaide pit system for radiometric logging calibration; Bulletin of Australian Society of Exploration Geophysicists, v. 13, no. 1, March.

Mwenifumbo, C.J.
1986: Drill hole mise-a-la-masse induced polarization and potential measurements in a Zn-Pb-Cu sulphide Deposit; in Borehole Geophysics for Mining and Geotechnical Applications, P.G. Killeen, ed.; Geological Survey of Canada, Paper 85-27, report 15.

Schock, L.D. and Killeen, P.G.
1985: Establishment of coal logging field calibration facilities: a progress report; in Current Research, Part B, Geological Survey of Canada, Paper 85-1B, p. 459-462.

Wenk, G.J.
1980: Calibration test pits for gamma logging; Information for Usage, 2nd Edition, Australia Mineral Development Laboratories (AMDEL), Frewville, South Australia.

Wenk, G.J. and Dickson, B.L.
1981: The gamma logging calibration facility at the Australian Mineral Development Laboratories; Bulletin of Australian Society of Exploration Geophysicists, v. 12, no. 3, Sept.

Wong, J., Hurley, P. and West, G.F.
1982: Crosshole audiofrequency seismology in granitic rocks using piezoelectric transducers as sources and detectors; Proceedings of Workshop on Geophysical Investigations in Connection with Geological Disposal of Radioactive Waste, Ottawa, Canada, OECD/NEA, Manitoba, p. 93-112.

4. PRACTICAL ASPECTS AND EXPERIENCE RESULTING FROM BOREHOLE MODELS FOR GAMMA RAY LOGGING IN URANIUM EXPLORATION

K. Schmid[1] and K. Olschewski[1]

Schmid, K. and Olschewski, K., Practical aspects and experience resulting from borehole models for gamma ray logging in uranium exploration; in Borehole Geophysics for Mining and Geotechnical Applications, ed. P.G. Killeen, Geological Survey of Canada, Paper 85-27, p. 47-52, 1986.

Abstract

Gamma ray logging as an indirect measurement technique does not produce absolute results in terms of uranium concentrations. Although this fact is widely recognized, it is of some concern to people having to evaluate logging data in an advanced stage of exploration. Most of the gamma-log results being radiometrically determined are expressed in eU concentration. However, discrepancies in results from calibrated probes are unacceptable to the user, and the question of how to report "true" uranium values arise.

This paper illustrates an attempt to meet the problems mentioned and how a set of model boreholes was constructed, i.e. simulating within certain limits the natural conditions of a crystalline environment. A least squares fit for chemically determined U-content and measured activity rates in the model boreholes was made. Linearity covers a range of 0.02 to 0.7% U and permits direct conversion of total counts to concentrations.

Such borehole models, primarily built for field calibration of logging equipment, offer additional advantages often overlooked by theorists. By means of regular maintenance checks, erratic measurements due to malfunction of the logging system or decreased sensitivity of the crystal can be detected early and before field operations start. Finally, for monitoring the long term behaviour of the ore-enriched models, all the measurements taken are referred to a calibrated cesium source giving absolute activity values.

Résumé

À titre de technique de mesure indirecte, la diagraphie par rayon gamma ne donne pas de résultats absolus pour ce qui est des concentrations d'uranium. Bien que généralement reconnu, ce fait n'en préoccupe pas moins certaines personnes chargées d'évaluer les données de diagraphie au cours d'une étape avancée des travaux d'exploration. La plupart des résultats tirés des diagraphies gamma et déterminés de façon radiométrique sont exprimés en équivalents d'uranium (eU). Toutefois, l'utilisateur ne peut se contenter de résultats divergents provenant de sondes étalonnées et il faut savoir comment présenter les teneurs "réelles" en uranium.

Cette étude explique comment on a tenté de résoudre ces problèmes et comment on a construit des maquettes de sondages qui simulent, à l'intérieur de certaines limites, les conditions naturelles d'un milieu cristallin. On a effectué l'ajustement par la méthode des moindres carrés des concentrations en uranium chimiquement et des taux d'activité mesurés dans les maquettes. La linéarité couvre la gamme de 0,02 à 0,7% d'U et permet la conversion directe des quantités totales en concentrations.

Ces maquettes, construites principalement à des fins d'étalonnage sur le terrain des appareils de diagraphie, présentent d'autres avantages que les théoriciens oublient souvent. La vérification régulière des appareils permet de déceler, avant la mise en oeuvre des travaux, le mauvais fonctionnement qui donne lieu à des mesures erratiques ou provoque la décroissance de la sensibilité du cristal. Enfin, pour permettre la surveillance du comportement à long terme des maquettes minéralisées, toutes les mesures sont comparées à une source de césium étalonnée qui donne des chiffres de l'activité absolue.

[1] Saarberg-Interplan Uran GmbH, Saarbrucken, F.R.G.

Introduction

Calibration facilities for gamma ray detection instruments have existed since the 1960s. Logging equipment is checked by the manufacturer in model boreholes before distribution around the world. Logging probes are normally accompanied by calibration certificates containing factors for conversion of gamma-activities into eU content.

However, intercalibration tests between facility owners in the United States, Canada and Australia revealed discrepancies between the various stations and models in the order of 7 to 18 per cent (Bristow et al., 1982). Because of these facts, the conversion problem is of serious concern to the exploration team that is in charge of gamma log interpretation. In advanced stages of exploration, reporting in terms of uranium concentration, which is usually demanded for decision making, can be a nightmare.

In summary this means that calibration of gamma ray detection equipment, in particular logging equipment, is subject to numerous imponderabilities which affect the final result.

What can be done for the logging geologist who presumes correct calibration and operation of the equipment and wants "true" uranium concentration?

This paper, mainly resulting from field experience, demonstrates that construction of borehole models for a particular geological environment can definitely contribute to the production of reliable data to form a basis for resource evaluation.

History

The reasons for such an attempt can be reported as follows: several years of exploration in a strongly tectonized area with vein-type deposits resulted in a number of promising targets. The program for detailed subsurface investigation of each target consisted of percussion drilling and a number of diamond core drillings. Some of the latter resulted in poor core recovery and consequently only a limited number of samples were available for analysis. In the face of the conflicting requirements of the problem, keeping drilling costs at a predetermined level, and getting reliable information on the zones intersected, a method for making grade estimations had to be found. Therefore, concentration calibration of gamma-probes based on chemically assayed U-content seemed to be a reasonable approach to minimize the risks.

Requirements

A number of requirements must be considered for the construction of model boreholes:

- simulation of rock matrix which should correspond in chemical and physical properties to the country rocks being drilled;
- simulation of borehole conditions such as: air/water filled, casing, etc.;
- simulation of an infinite medium normal to the hole;
- homogeneity of the ore zone;
- equilibrium of the ore;
- concentration range of ore zones should cover the maximum/minimum detection range of the probe; and
- mobility of the models.

Eight pallet-mounted concrete models were built in a sandwich-layer construction, covering a concentration range from 200 ppm U to 2.4% U. A schematic diagram is given in Figure 4.1.

Material and procedure

One important factor for simulating natural or standard conditions is the selection of material compounds, in particular the matrix of the model.

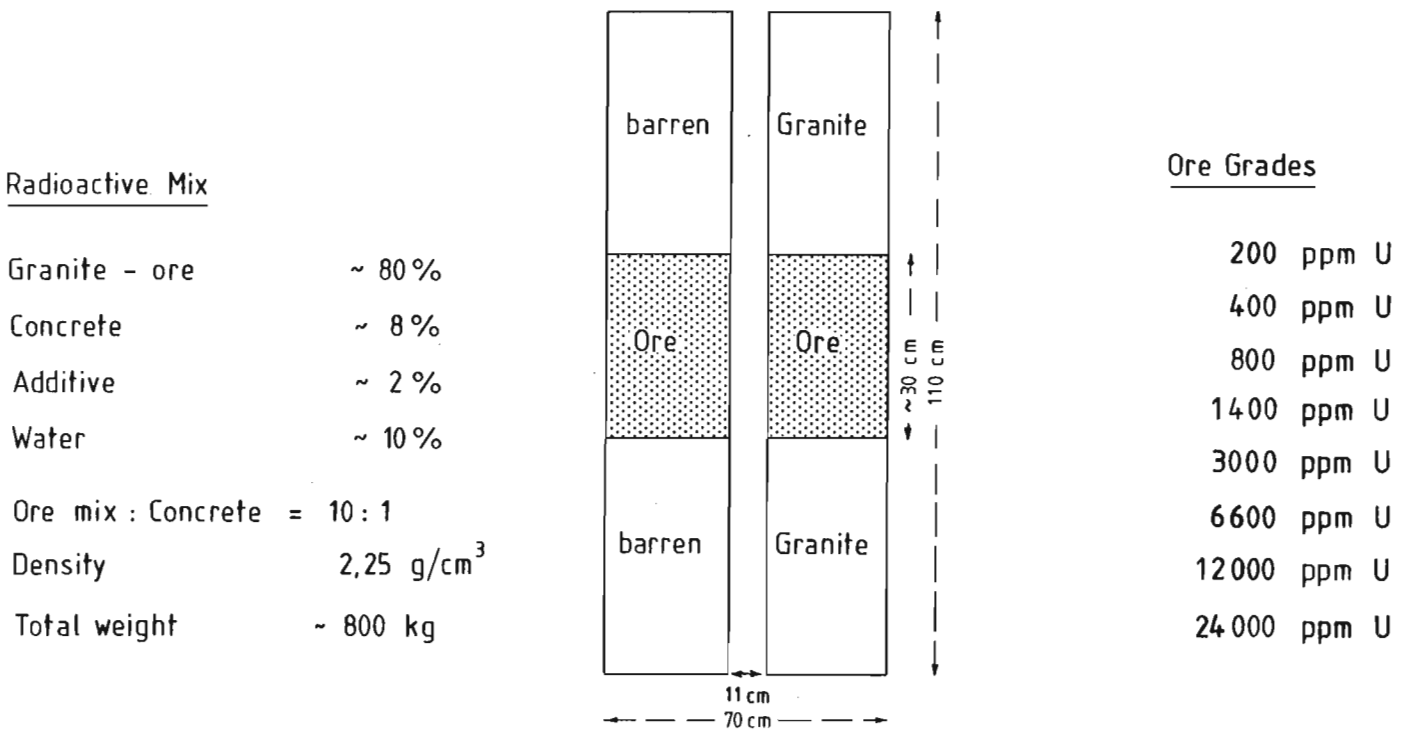

Figure 4.1. *Model borehole with ore-mix between two barren zones. Material compounds and mixing ratios are indicated.*

From geological knowledge of the area being explored, the main rocks drilled are granites and granitoids originating from metasediments. Therefore, a granite of the composition listed in Table 4.1 was selected for the matrix thus representing the average country rock. The 55 ppm Th concentration of the granite matrix was not considered to be a significant contribution to the count rate because thorium yields only about half the activity of uranium. Even in the worst case (the 200 ppm U model) it would contribute the equivalent of about 25 ppm U or about 10% of the activity.

A high grade ore containing 10% U, consisting of pitchblende and secondaries, was blended with granite. This initial mix with a concentration of approximately 2.7% U was used for further splitting and blending. After crushing to 5 mm grain size, the material was blended to the concentrations listed in Figure 4.1.

The uranium grade was determined chemically by collection 10 random samples before pouring. The samples were dried, crushed and ground before packing about 300 g of the powder into containers for analysis. Uranium determinations were performed by XRF and fluorometry. The averaged results were taken for assigning ore grade to the models. Homogeneity was tested by placing α-particle films on the surface of cylindrical disks made from the active mix. The results from the track patterns showed that the uranium minerals were regularly distributed.

Analysis of secular equilibrium of the ore resulted in a ^{238}U: ^{226}Ra ratio of 1.2 ± 0.1. The individual ratios (Table 4.2) reflect the varying proportions of secondary uranium minerals present in the samples.

Closely linked with equilibrium is radon with its tendency to emanate from crushed and porous samples. The following precautions were taken to prevent or minimize radon release from the ore zone:

1. Increase of the pore volume of the ore mix by adding synthetic Na-zeolite, a hydrated alumino-silicate with a frame-work structure as shown in Figure 4.2.

A characteristic feature of zeolites is the channel system, formed by different combinations of linked tetrahedra-rings. In the case of zeolite-A, the tetrahedra are linked to form cubooctahedral cages. Cavities and channels act as sieves for atoms and molecules of similar dimensions. The addition of zeolite produces an increase of pore volume of approximately 1%.

2. Sealing of the ore zones with meta-silic acid after drying and reconstitution of equilibrium.

The efficiency of sealing was tested by measuring α-activity of the free active surface before covering with barren material. Results showed that radon emanation was negligible.

Physical properties of the models

For 0.6 MeV (^{214}Bi) gamma-energy the model simulates 98.6% of an infinitely thick source.

Assuming that the International Atomic Energy Agency rule of thumb (IAEA, 1976) is correct, then the effective sample volume for gamma-probes is the product of the radial distance from the borehole to the model exterior and the density of the medium. Comparison of our model parameters (density, radius) with the recommended ones, (see Table 4.3) shows that the physical properties and dimensions of the models built, fit well within the recommended ranges.

Table 4.1. Average composition of the granite used for matrix in weight - %

SiO_2	66.50
TiO_2	0.60
Al_2O_3	15.85
Fe_2O_3	0.61
FeO	2.69
CaO	1.38
MgO	1.17
MnO	0.06
Na_2O	2.93
K_2O	5.56
LOI	2.21
P_2O_5	0.25
U ppm	5
Th ppm	55

Table 4.2. Equilibrium of uranium ore

Sample nr.	Uranium-238 µg/g	Uranium-238 pCi/g	Ra-226 pCi/g	Equilibrium U-238/Ra-226
2	285.59	95.96	67.64	1.42
3	477.65	160.49	127.31	1.26
4	854.11	286.98	238.29	1.20
5	1 655.45	556.26	433.78	1.28
6	3 416.70	1 148.01	960.29	1.20
7	8 169.26	2 744.87	2 233.39	1.23
8	13 074.28	4 392.96	4 131.79	1.06
9	24 803.57	8 334.00	7 944.05	1.05

Table 4.3. Physical properties and dimensions of the models

Model density	(d) 2.3 g/cm^3
Model radius	(r) 35 cm
Product	(d x r) = 35 x 2.3 = 78.75 g/cm^2
IAEA product recommended	(d x r) 75 - 120 g/cm^2
IAEA radius recommended	30 - 48 cm

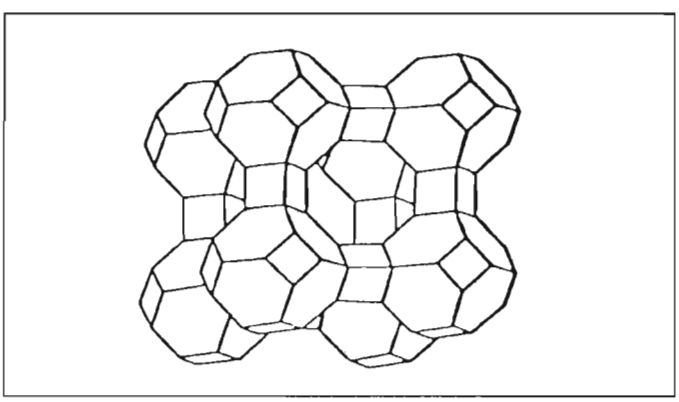

Figure 4.2. *Structure model of Zeolite – A, described in the text.*

Table 4.4. Test runs in model boreholes 1982 and 1983

Model nr.	U conc. ppm	Probe nr.	cps 1982	cps 1983
barren	background	1011	180	180
		1010	178	178
		1009	184	180
		118	174	172
III	800	1011	1650	1650
		1010	1650	1600
		1009	1680	1640
		118	1640	1630
		Ø	1655	1630
IV	1400	1011	3320	3370
		1010	3220	3245
		1009	3300	3375
		118	3250	3370
		Ø	3273	3340
V	3000	1011	6100	6200
		1010	6000	6200
		1009	6100	6250
		118	6000	6250
		Ø	6050	6238
VI	6600	1011	13600	13850
		1010	13200	13200
		1009	13600	13850
		118	13400	13800
		Ø	13450	13675
VII	12000	1011	20600	22080
		1010	20500	21250
		1009	20500	22080
		118	20500	21870
		Ø	20525	21820
VIII	24000	1011	37500	39160
		1010	37250	37900
		1009	37750	39160
		118	37000	38740
		Ø	37375	38740
Cs-137-source 1 µ Ci		1011		1040
		1010		1000
		1009		1140
		118		1040
				Ø 1054

The measurement

Static and dynamic gamma ray measurements were taken in air-filled model holes. For each probe a separate work sheet was made. Ten test runs were carried out in 1982 and 5 runs in 1983. The average count rates are listed in Table 4.4.

A slight increase of gamma-activity in 1983 in the highly enriched zone was detected. This could be due to equilibrium in the models not being fully reconstituted in 1982. Secondly, the varying moisture content of the medium (9-11%) likely decreased the first readings when moisture was higher than 1983.

In the future, special attention will be paid to these apparent growing count rates and their possible origin.

Figure 4.3 shows that total count rates plotted versus true (chemically determined) uranium concentration are in good agreement with the regression line. Linearity covers a range up to 0.66% U or about 14 000 cps respectively.

To exclude uncertainties in factors influencing correct measurement such as probe function, aging of the crystal and apparent growing gamma-rates, a defined standard has been introduced into the test package as a basis for futher control. A calibrated gamma-reference source with an energy of 0.66 MeV, similar to ^{214}Bi, should enable us to correct measured gamma values, if necessary. For that purpose a ^{137}Cs source seemed to be the most appropriate with a nominal activity of 1 µCi, and half life of 30.17 years.

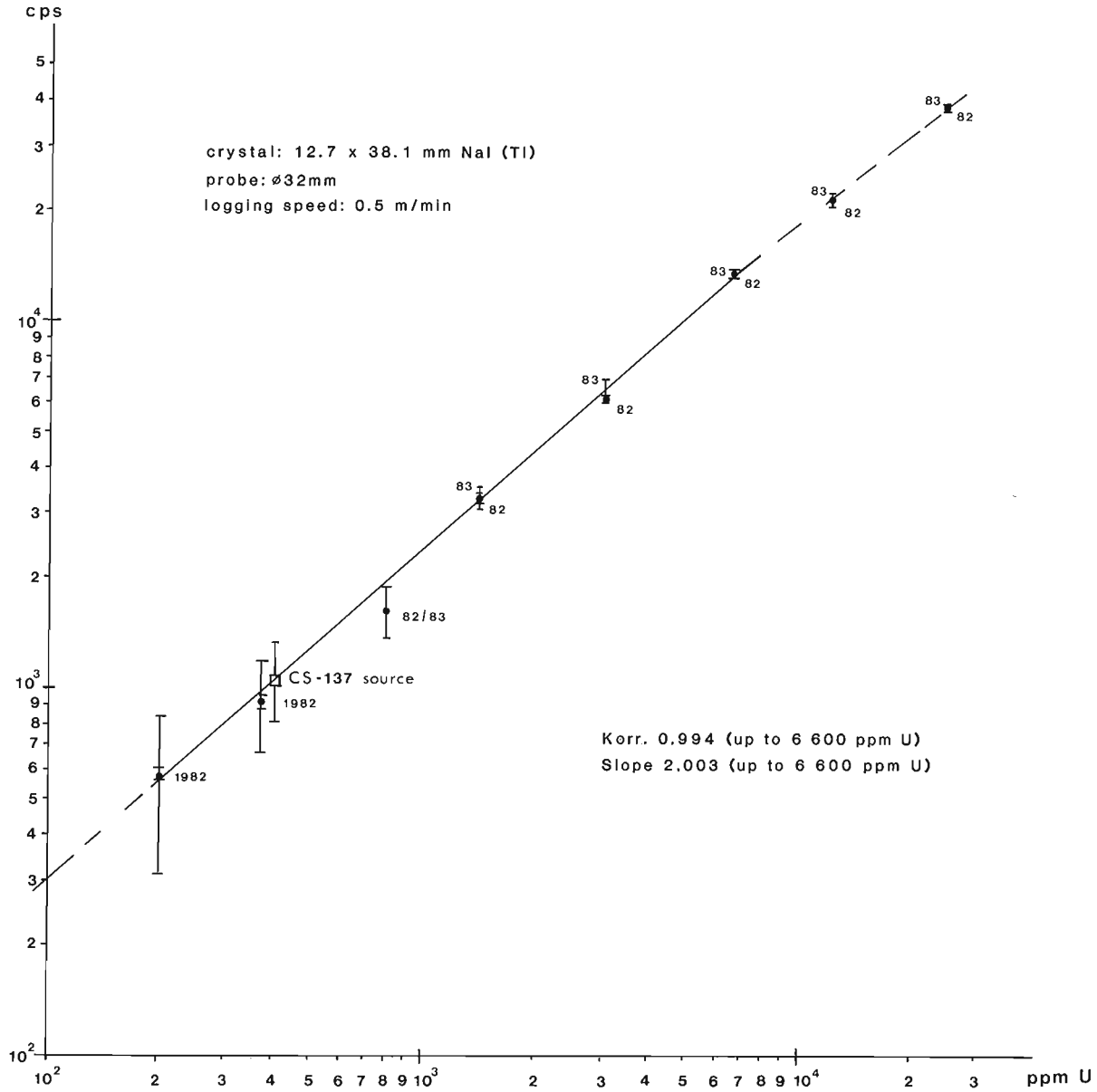

Figure 4.3. *Regression line obtained from 8 model holes. Uranium concentration based on chemical assay.*

Conclusions

From the results presented the following conclusions can be drawn:

1. Simulation of natural conditions in model boreholes for a specific geological setting has been accomplished successfully.

The reproducible conditions of the model boreholes permit direct conversion of the gamma-readings into U-concentration without correction within the range of 0.02-0.7% U. This result is in fairly good agreement with Grand Junction calibrated gamma probes. According to these probe specifications, 20 000 cps correspond with 1% eU.

However, radiation readings above 14 000 cps have to be considered with caution, for the discrepancy between true and equivalent uranium will increase significantly above that level.

For making absolute comparison and eventual corrections possible, control checks of the future will be related to a calibrated cesium-gamma-reference source.

2. Borehole models as described are considered to be a useful compromise between in situ borehole analysis, too costly for European users – and gamma ray logging based on relative, (indirect, i.e. radiometrically determined), U-concentration.
3. The design of the models (dimensions and weight) was made with respect to transportability. This is a definite advantage, because individual models, even though they weigh about 800 kg, can be transported to wherever they are needed.

Acknowledgments

The authors are indebted to the President of Saarberg-Interplan for the permission to publish this paper.

We further wish to thank the exploration and laboratory staff for their assistance and helpful discussions. This work was part of an exploration program supported by the European Commission.

References

Bristow, Q., Killeen, P.G., and Mwenifumbo, C.J.
1982: Comparison of standard gamma-ray log calibration measurements: Ottawa, Adelaide and Grand Junction; Proceedings of Symposium on Uranium Exploration Methods – Review of the NEA/IAEA R & D Programme, Paris, France, p. 715-726.

George, D.C.
1982: Total count gamma-ray logging: correction factors and model grade assignments; in Uranium Exploration Methods, OECD/NEA/IAEA, p. 729-751.

International Atomic Energy Agency (IAEA)
1976: Radiometric reporting methods and calibration in uranium exploration; IAEA, Vienna, Technical Series No. 174, p. 57.

5. A NEW TEST SITE FOR THE CALIBRATION OF GEOPHYSICAL EQUIPMENT

S.E. Osterlund[1]

Osterlund, S.E., A new test site for the calibration of geophysical equipment; in Borehole Geophysics for Mining and Geotechnical Applications, ed. P.G. Killeen, Geological Survey of Canada, Paper 85-27, p. 53-55, 1986.

Abstract

A new facility located at Mala, Sweden for calibrating borehole logging equipment is described. The borehole models include provision for calibration of gross count gamma ray and spectral gamma ray (K, U, Th) logging equipment and provision for future addition of density, porosity and magnetic susceptibility models. The site also includes seven concrete calibration pads for portable gamma ray spectrometers.

Résumé

Ce rapport décrit une nouvelle installation d'étalonnage des appareils de diagraphie des sondages à Mala, en Suède. Les maquettes de sondages peuvent aussi accomoder un dispositif d'étalonnage des appareils de diagraphie gamma-gamma à comptage brut et des appareils de diagraphie spectrale par rayons gamma (K, U, Th); on pourra aussi y ajouter des modèles de densité, de porosité et de susceptibilité magnétique. L'emplacement comporte également sept patins d'étalonnage en béton pour les spectromètres portatifs à rayons gamma.

[1] Swedish Geological Company, Luleå, Sweden

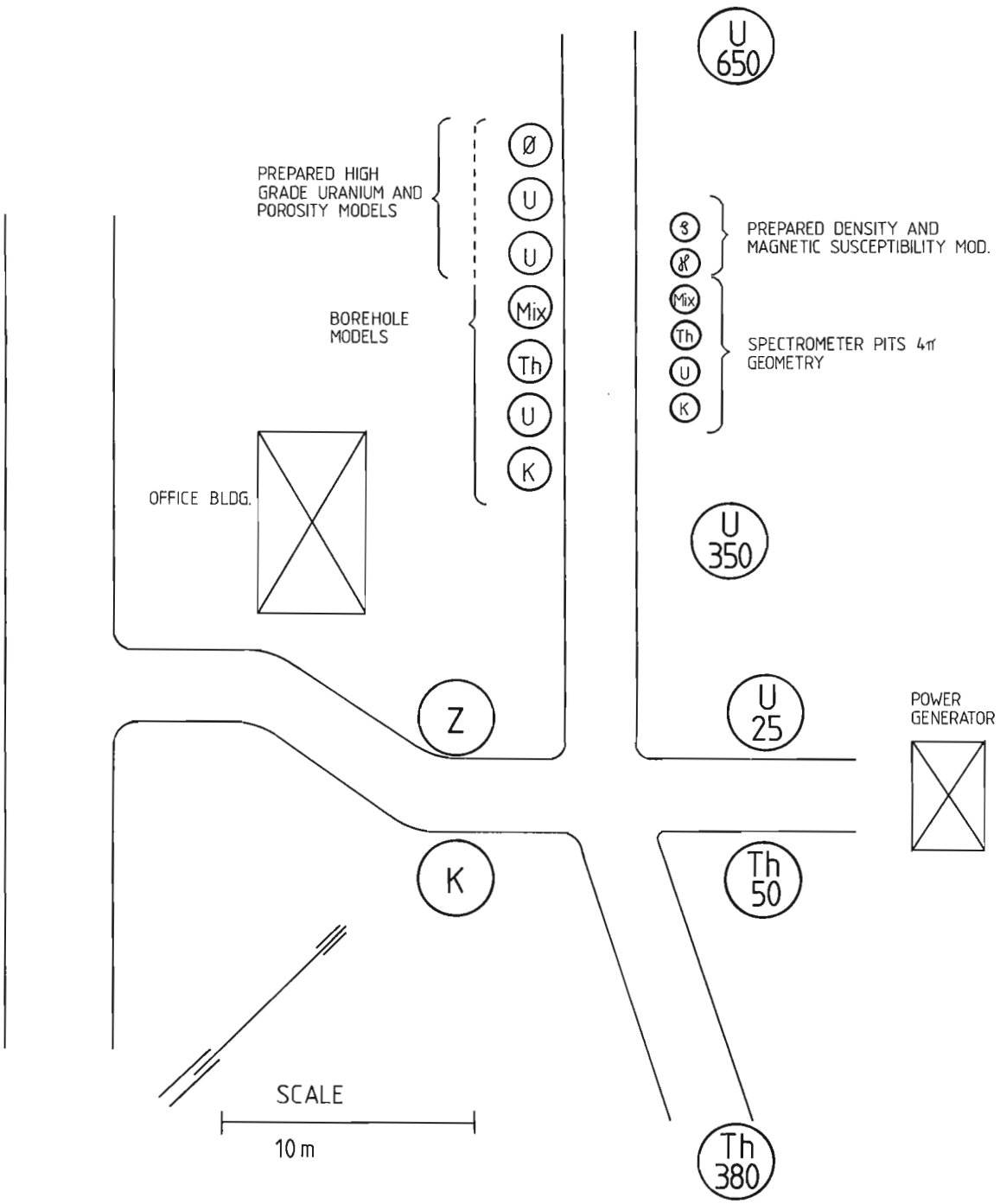

Figure 5.1. *Calibration facilities at Malå, Sweden.*

Introduction

Quantitative use of geophysical data has long been recognized as an important part of formation evaluation by the petroleum industry. Many of these methods, originally developed for large diameter holes in sedimentary rocks, have now become available for slim-hole applications in a hard rock environment. Hence, the traditional qualitative 'anomaly-searching' type of logging common in minerals exploration, has shifted towards more sophisticated use of the collected data. This calls for an accurate calibration of logs in absolute values. To meet these new requirements of the mining industry and of engineering geology it was decided to construct a calibration facility where logging-tools could be calibrated in an environment that as close as possible resembled the actual measuring situation in the field.

The site is located at Malå in northern Sweden, and was originally chosen for off-set adjustments of electromagnetic equipment since it provides a very low noise-level environment due to few man-made or natural disturbances in the surroundings. Also located there are seven calibration pads with known grades of the three radioelements,

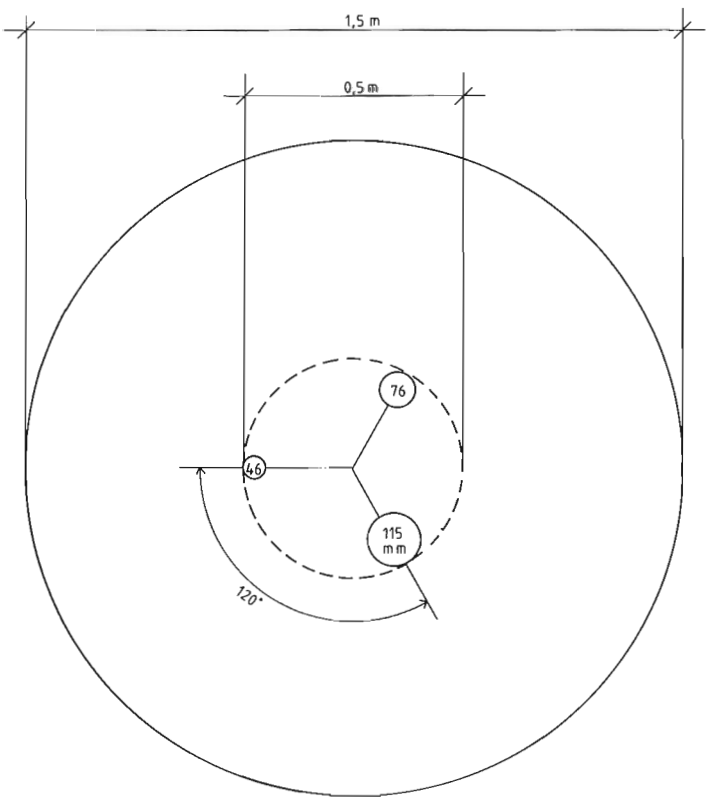

Figure 5.2. *Plan view of radiometric borehole model.*

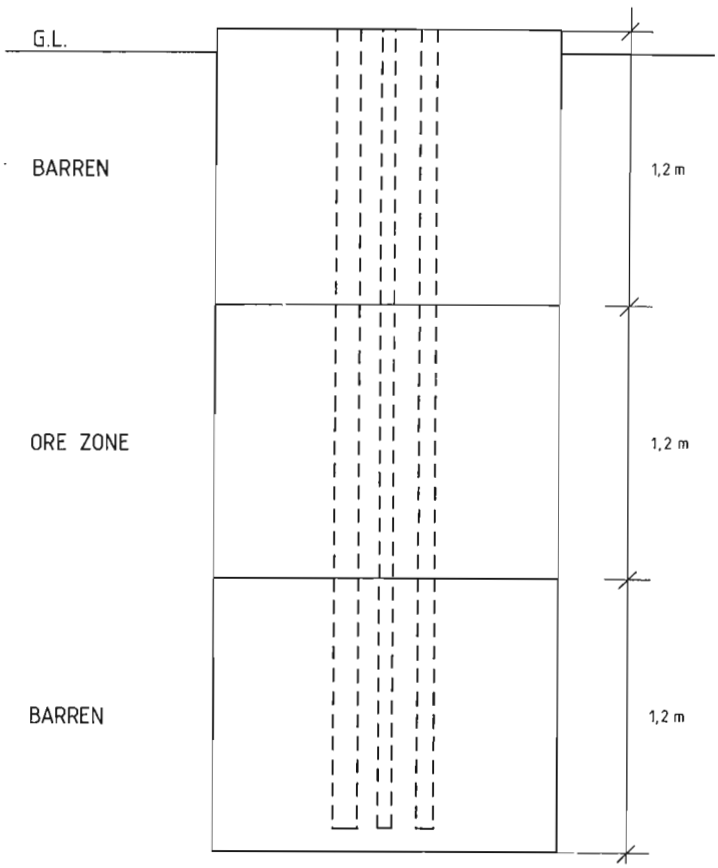

Figure 5.3. *Section through radiometric borehole model. G.L. indicates ground level.*

potassium, uranium and thorium. These are used for the calibration of scintillometers and spectrometers. The pads are 3 m in diameter and consist of concrete spiked with aggregate rich in potassium (K), uranium (U), thorium (Th) plus one blank pad (Z) (Fig. 5.1).

The borehole models consist of a KUT-suite for the calibration of both total count and spectrometer tools. The geometry of the models is shown in Figures 5.2 and 5.3. The models were poured as three separate layers of concrete with subsequent coring by diamond drilling. The nominal grades for the ore zones are 7.5% K, 650 ppm eU, and 380 ppm eTh respectively.

The Swedish Geological Company is also constructing borehole models for the determination of such parameters as porosity, density and magnetic susceptibility, using neutron, gamma-gamma and induction devices. Furthermore two high grade uranium models will be added to the test site.

6. DRILLHOLE EM MEASUREMENTS IN MINERAL EXPLORATION*

A.V. Dyck[1] and J.G. Hayles[1]

Dyck, A.V. and Hayles, J.G., Drillhole EM measurements in mineral exploration; in Borehole Geophysics for Mining and Geotechnical Applications, ed. P.G. Killeen, Geological Survey of Canada, Paper 85-27, p. 57-58, 1986.

Abstract

Different aspects of three drillhole EM techniques are discussed. The techniques are:

1) Time-domain EM

Time-domain EM using a large loop source is a proven technique for detection of offhole massive sulphide conductors. The complexity of the targets can, however, produce discrepancies between observed responses and simple models, as shown by examples from the Sudbury basin. An appreciation of the discrepancies could help to refine an interpretation as may be required, for example, as a guide to advanced exploration drilling.

2) VLF-EM

Delineation of structural features, such as poorly conducting fault zones, can be accomplished by measurements of the electric field which is subject to distortion by relatively small conductivity contrasts (current channelling). Simple current-channelling models provide a useful first attempt at understanding field surveys with the United States military transmitters as sources. It appears that trend and lateral extent of structural features can be estimated using orthogonal primary fields. Preliminary results show that local VLF loop sources could be used to supply the orthogonal fields when the military transmitters cannot.

3) Drillhole AFMAG (Audio Frequency Magnetic)

Using a method and hybrid computer developed by Marcel St. Amant of the Mineral Exploration Research Institute, Montreal, drillhole AFMAG is shown to give reproducible results in detecting a known massive sulphide deposit with naturally occurring primary fields. The coherence between downhole sensor and surface reference as a function of reference azimuth can be used to determine the geological strike of a conductor. As a relatively inexpensive and lightweight method, drillhole AFMAG could be useful in grassroots exploration, especially in low electrical noise environments.

These techniques could be considered individually for application to a mineral exploration problem or collectively as a multi-faceted approach to understanding the electrical structure of a large volume of rock. They can therefore supply both direct and indirect information to the explorationist.

Résumé

Divers aspects de trois techniques électromagnétiques appliquées aux trous de sondage sont exposés. Ces trois techniques sont les suivantes:

1) Le sondage électromagnétique à dimension temporelle

La technique électromagnétique à dimension temporelle et à large boucle de transmission a fait ses preuves dans la détection des gisements de soufre massif conducteur éloignés des trous. La complexité des gisements peut toutefois donner lieu à des écarts entre les observations et les modèles simples, comme l'indiquent des exemples tirés du bassin de Sudbury. L'examen de ces différences pourrait aider à perfectionner l'interprétation des données selon les besoins, par exemple, pour guider les forages d'exploration avancée.

2) Le sondage électromagnétique à très basse fréquence (VLF-EM)

La délimitation des composants de structure, tels que les zones de faille peu conductrices, peut se faire par la mesure du champ électrique, qui comporte des anomalies dues à de petites variations de conductivité (durant la transmission du courant). Des modèles simples de transmission de courant procurent une compréhension préliminaire utile des levés sur le terrain effectués à l'aide des émetteurs de l'Armée américaine. Il semble que les champs primaires orthogonaux puissent servir à

---

* Manuscript not submitted

[1] Geological Survey of Canada, 601 Booth St. Ottawa, Ontario

déterminer approximativement la direction et la dimension latérale des composants de la structure. Des résultats préliminaires indiquent que, faute de ne pouvoir utiliser les émetteurs militaires, on pourrait créer des champs électriques sur place au moyen d'une source de boucle à très basse fréquence.

3) Le sondage magnétique à audiofréquence (SMAF)

Effectué à l'aide d'une méthode et d'un calculateur hybride conçus par Marcel St. Amant, de l'Institut de recherche en exploration minérale de Montréal, le sondage magnétique à audiofréquence donne des résultats reproduisibles lors de la détection de gisements connus de soufre massif grâce à l'utilisation des champs magnétiques primaires naturels. Il est possible de déterminer la direction d'un corps conducteur en mettant en corrélation la lecture du détecteur, placé dans le trou, et la référence de surface, en fonction d'un azimuth de référene. Comme la méthode des sondages magnétiques à audiofréquence est peu coûteuse et utilise du matériel léger, elle peut faciliter l'exploration de base, en particulier en milieu où le bruit de fond électrique est peu élevé.

Ces techniques peuvent être prises en considération individuellement, en vue d'être appliquées à la résolution d'un problème d'exploration minérale, ou collectivement, comme un instrument polyvalent aidant à comprendre la composante électrique d'une formation rocheuse massive. Elles peuvent donc procurer des renseignements de façons directe et indirecte à l'explorateur.

7. FIELD EXAMPLES OF BOREHOLE PULSE EM SURVEYS USED TO DETECT AND OUTLINE CONDUCTIVE ORE DEPOSITS

J. Duncan Crone[1]

Crone, J.D., Field examples of borehole Pulse EM surveys used to detect and outline conductive ore deposits; in Borehole Geophysics for Mining and Geotechnical Applications, ed. P.G. Killeen, Geological Survey of Canada, Paper 85-27, p. 59-70, 1986.

Abstract

The first example is of a borehole Pulse EM survey in 1978 that led to the discovery of a small ore lens adjacent to a mine being prepared for production. This conductive sulphide body was located off to the side and below the bottom of the drillhole leading to the discovery. Depth to the body was 950 m.

The second illustrates how the use of multiple transmit loops on surface helps to determine the position of a conductive body relative to the drillhole and also to some extent its shape.

The third case history, from a recent quartz-vein copper discovery in Chibougamau, Quebec, is an excellent example of the unique type of anomalies obtained when a borehole cuts the edge of a body. Information derived from this type of survey response helps to define the continuity and extent of a deposit.

The final example consists of borehole survey results from the deep Ansil discovery of Corporation Falconbridge Copper in 1981, at a depth of 1266 m. The survey results are complex and illustrate the necessity for detailed correlation between geological and geophysical data to obtain a meaningful interpretation. One application of the survey was to determine how far the edge of the massive-sulphide deposit was from a borehole that missed the zone. This information was used to decide if the hole should be "wedged" in an attempt to obtain an intersection through the deposit. Since a wedged hole has a limited striking distance of approximately 50 m the borehole survey could evaluate the possibility of it intersecting or missing the massive sulphide zone.

Résumé

Dans le premier exemple, il s'agit d'un levé électromagnétique à impulsions entrepris en 1978 qui a mené à la découverte d'une petite lentille de minerai contiguë à une mine que l'on s'apprêtait à mettre en production. Cette masse conductrice de sulfure, située à une profondeur de 950 mètres, se trouve à quelque distance du sondage menant à la découverte et sous celui-ci.

Le deuxième exemple montre comment l'utilisation de boucles à transmission multiples installées en surface permet de déterminer la position et, dans une certaine mesure, la forme d'un corps conducteur par rapport à un sondage.

Le troisième exemple est tiré d'une découverte récente d'un filon de quartz cuprifère à Chibougamau, au Québec; c'est un excellent exemple de ce type unique d'anomalies obtenues lorsqu'un sondage traverse le bord d'une masse minéralisée. Les renseignements dérirés de ce genre d'étude permettent d'établir la continuité et l'étendue d'un gisement.

Le dernier exemple présente les résultats de l'étude d'un sondage foré à une profondeur de 1 266 m dans le gisement profond Ansil de la Corporaton Falconbridge Copper en 1981. Les résultats sont complexes et montrent qu'il est nécessaire d'effectuer une corrélation détaillée entre les données géologiques et les données géophysiques afin d'obtenir une interprétation utile. Le levé avait, entre autre, pour objet de déterminer la distance entre la marge du gisement de sulfure massif et un sondage qui n'avait pas atteint la zone. Cette information a servi à déterminer s'il fallait faire dévier le sondage de façon à ce qu'il arrive en contact avec le gisement. Puisqu'un sondage dévié ne peut se faire que sur une distance limitée d'environ 50 m, l'étude pourrait déterminer s'il est possible que le sondage puisse rejoindre la zone de sulfure massif.

[1] Crone Geophysics Limited, Mississauga, Ontario

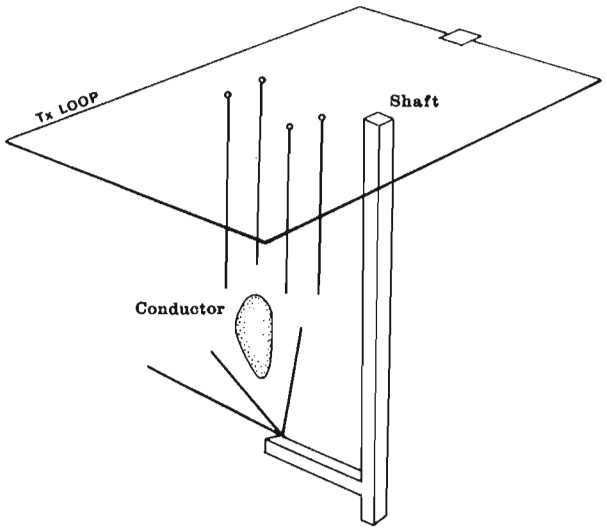

Figure 7.1. Large transmit loop borehole PEM system used for surveying a group of drillholes from surface or underground. The position of a conductor is determined from the response obtained from adjacent holes.

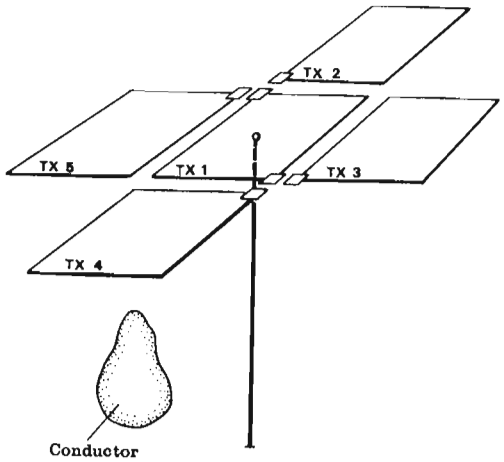

Figure 7.2. Multiple transmit loop borehole PEM system used for surveying isolated drillholes. Multiple small transmit loops must be used to determine the position of a conductive target.

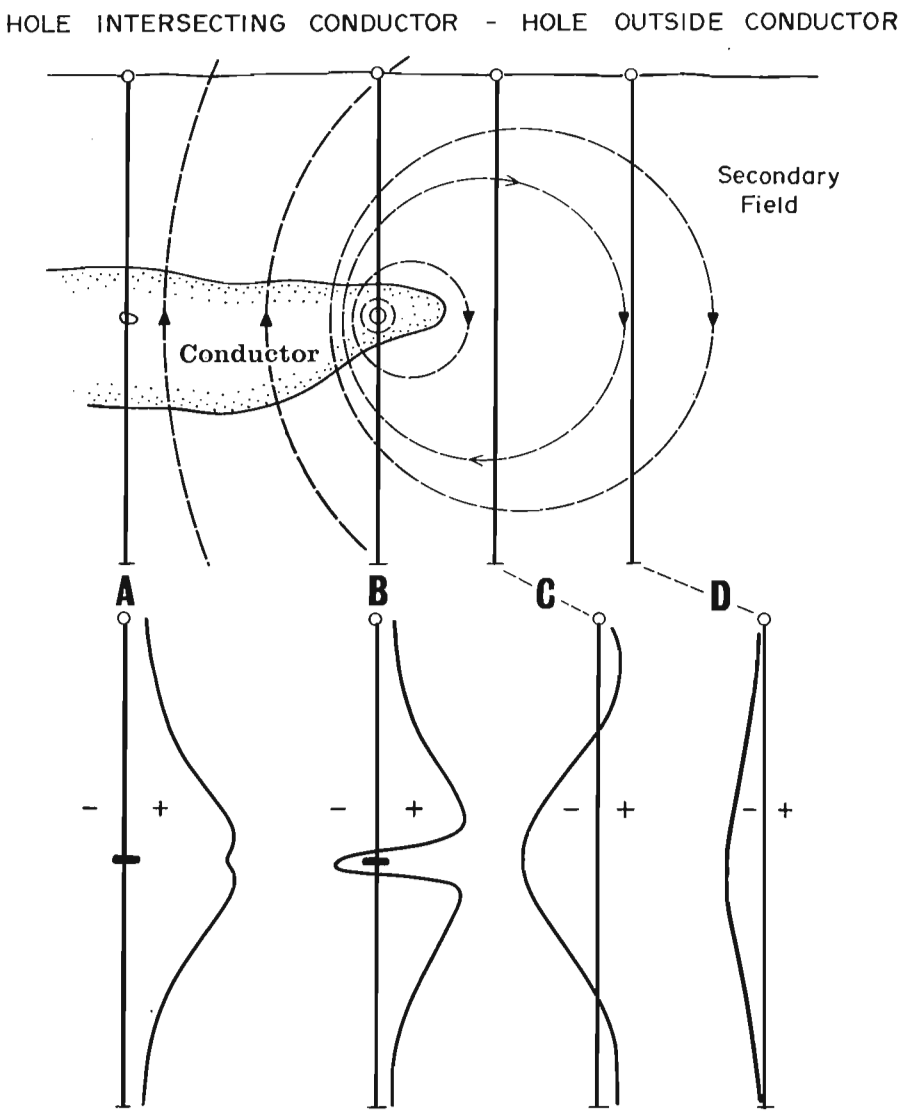

Figure 7.3. The four basic type response curves obtained when the transmit loop is located above the conductor.

Introduction

The role of a borehole Pulse EM (PEM) survey is usually thought of in terms of detecting a conductive ore deposit that exploration drilling has missed. The anomalous response measured by the system is however dependent on physical properties of the body other than its conductivity. These properties of size, shape, continuity and position provide valuable information in various stages of the exploration and mining process. As a result the industry is using the survey method not only in early exploration drilling but also as a guide in development drilling, tonnage estimation, shaft site location and searches at producing mines for satellite deposits. The following case histories illustrate some of these applications

Survey method

The PEM survey equipment consists of a single-turn transmit loop that is laid out on surface. Its size may vary from 100m x 100m to 1km x 1km. A pulsed current is placed through the loop with a peak current in the order of 10 to 20 amps. The receiver probe is lowered down the drillhole - the probe has a diameter of 3 cm. Eight measurements are taken during the time-off interval and one measurement during the current-ramp shut-off period. The eight sample measurements are proportional to the rate of change of the secondary field components along the axis of the probe.

Two basic survey methods are used. In areas where a group of holes are being surveyed (Fig 7.1) one large loop is laid out and all holes surveyed from the same loop. Information as to location of a conductive body is derived by the change in response from hole to hole. In the case of an isolated drillhole usually 5 transmit loops are laid out on surface (Fig 7.2) and the hole is surveyed from all 5 loops. Information as to shape and location is determined by the change in response from the 5 loops. In this type of survey the loop size is usually one third to one half the depth of the hole.

There are four basic type response curves (Fig 7.3) obtained when the transmit loop is located above the conductor. Model study curves have been produced by Woods (1975) and a computer model program by Dyck et al. (1980). An atlas of primary fields by Macnae (1980) for a fixed transmitter loop is also useful when planning surveys and interpreting results.

Case history of a small sulphide body at a depth of 950 m

This discovery was made as a result of a borehole survey for Corporation Falconbridge Copper in the Dufault area of Quebec. Included in the survey were a number of deep holes drilled from surface in the vicinity of a massive sulphide copper-zinc mine being prepared for production. A shaft had been sunk and underground levels established. As a mining plan was being formulated, it was important to locate any existing satellite ore lenses and fit them into this plan. A delay of two or three years in their discovery could result in their being uneconomic to mine.

One of the holes surveyed from surface (Fig 7.4) produced an anomaly at the bottom of the hole at 920 m indicating the presence of a conductive body off to the side and below the bottom of the hole. A nearby hole was then located and surveyed (Fig 7.5), obtaining a clear off-hole anomaly at a 950 m depth. The conductor was interpreted to be lying between the two vertical holes whose collars were only 70 m apart. This anomaly was tested by drilling from underground. Ore grade copper sulphides were intersected in the first hole. This ore lens has now been completely drilled off and incorporated into the mining plan. It was our first ore discovery with the Pulse EM borehole logging system.

Case history in the use of multiple transmit loops from surface to detect a massive lead-zinc deposit in Virginia

This was a test survey over a known massive-sulphide body. The results are typical of survey responses obtained when working in areas of extensive, scattered sulphide mineralization. The drillhole surveyed cut several sections of pyrite with low lead, zinc and minor copper values (Fig 7.6). The borehole surveys from 5 transmit loops are shown (Fig 7.7, 7.8). The first observation is that the early-time samples 1, 2 and 3 have completely different anomaly patterns than the late-time samples 6, 7 and 8. This means that the early time induced current paths are completely different from the late time paths - i.e., we have two separate conducting bodies. The upper conductor is detected as an in-hole, up-dip, edge (type B, Fig. 7.3) anomaly located at 155 m (510 feet) where bands of sulphides were cut by the hole. This zone of poor conductivity (thickness x conductivity = 10 mhos) would be expected to continue up-dip towards surface. It would also be expected to terminate just below the hole, in the down dip direction. The lower off-hole anomaly is located at 225 m (740 feet) in a section of the hole where no sulphides were intersected. The conductivity-thickness of this zone is 60 mhos which would imply massive sulphides in this area. The amplitude of the lower anomaly is strongest from the south and east transmit loops, indicating the zone occurs in this direction about 30 m from the hole. The reversed anomaly obtained from the west transmit loop can be explained by the reversed energization as shown in the primary field direction diagrams (Fig 7.9). Since the anomaly shapes are all similar (varying only in amplitude and sign) we conclude that the induced currents are restricted to flow along the same paths from all transmit loops. This means that the conductors are tabular in shape.

Case history of edge-type borehole anomalies obtained in two holes from a recent copper discovery in the Chibougamau area of Quebec

The Corner Bay deposit discovered by Riocanex consists of a steeply dipping quartz vein, mineralized primarily by chalcopyrite. It occurs in a host of intrusive rocks. The survey was run while the property was in the development drilling stage. Two of the surveyed holes were of particular interest since they both produced almost identical anomalies of the type where a borehole cuts the lower edge of a conductive body. In hole "A" (Fig 7.10) there is excellent geological control. The drillhole emerges from a gabbro dyke, then after a few metres, intersects 9 m of high grade copper mineralization. This is a classic example of an edge type anomaly, since we know the ore zone terminates abruptly against the dyke 5 to 8 m down dip from the core intersection of sulphides. In borehole "B" (Fig 7.11) a section 100 m away, a similar borehole PEM survey response is obtained at a depth of 390 m. The hole in this case cut 1 m of quartz vein at this depth; it contained only minor sulphides with no significant values. Farther down the hole at 450 m a small intersection of massive sulphides was cut that carried copper values. In this case our interpretation is quite clear - in hole "B" the massive mineralization must continue along the section to within a few metres of the quartz vein intersection at 390 m. The massive sulphide vein at 450 m is not related to the main mineralized vein and is of such a small size that it was not detected by the PEM survey.

* Text continues on page 69.

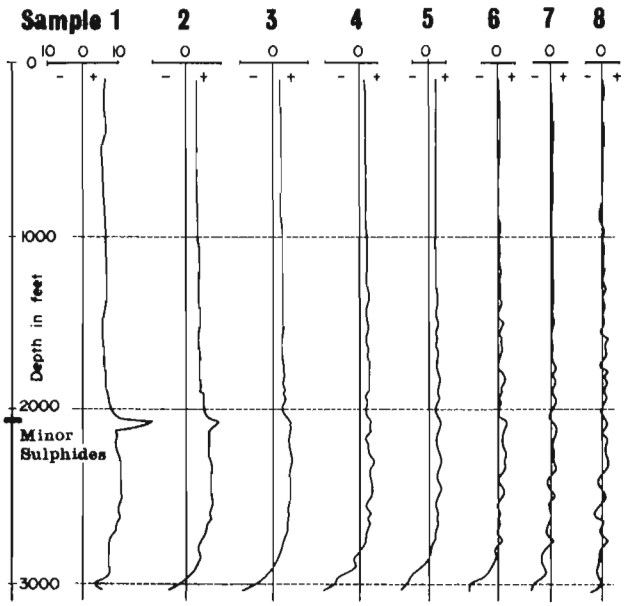

Figure 7.4. Results of a borehole Pulse EM survey for Corporation Falconbridge Copper in the Dufault area, Quebec. Conductive body detected, below and off to the side, from the bottom of the hole at 950 m (3100 feet).

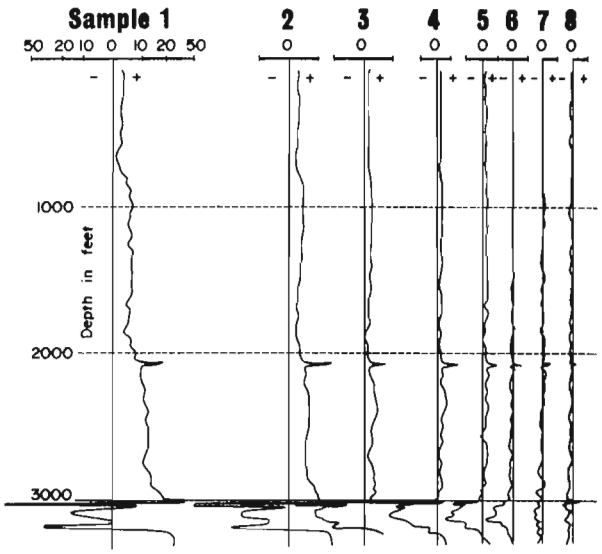

Figure 7.5. Results of a borehole Pulse EM survey for a hole collared only 70 m away from the borehole in Figure 7.4. Conductive body detected at 950 m (3100 feet) off to the side of the hole.

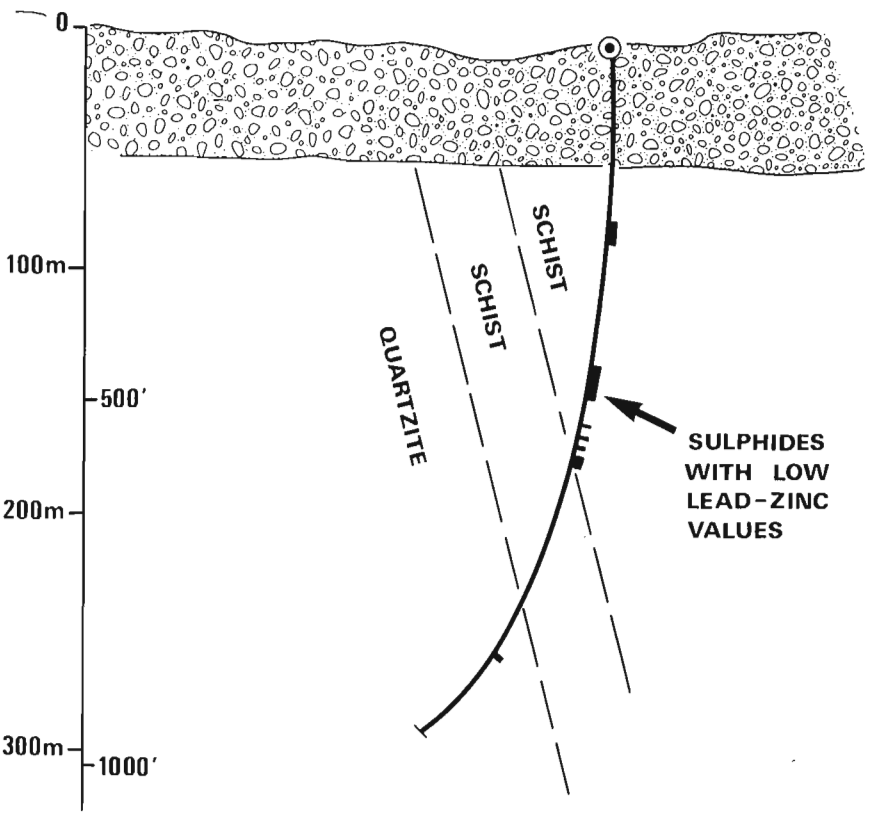

Figure 7.6. Geological section showing a borehole which intersects lead-zinc mineralization in Virginia, United States of America.

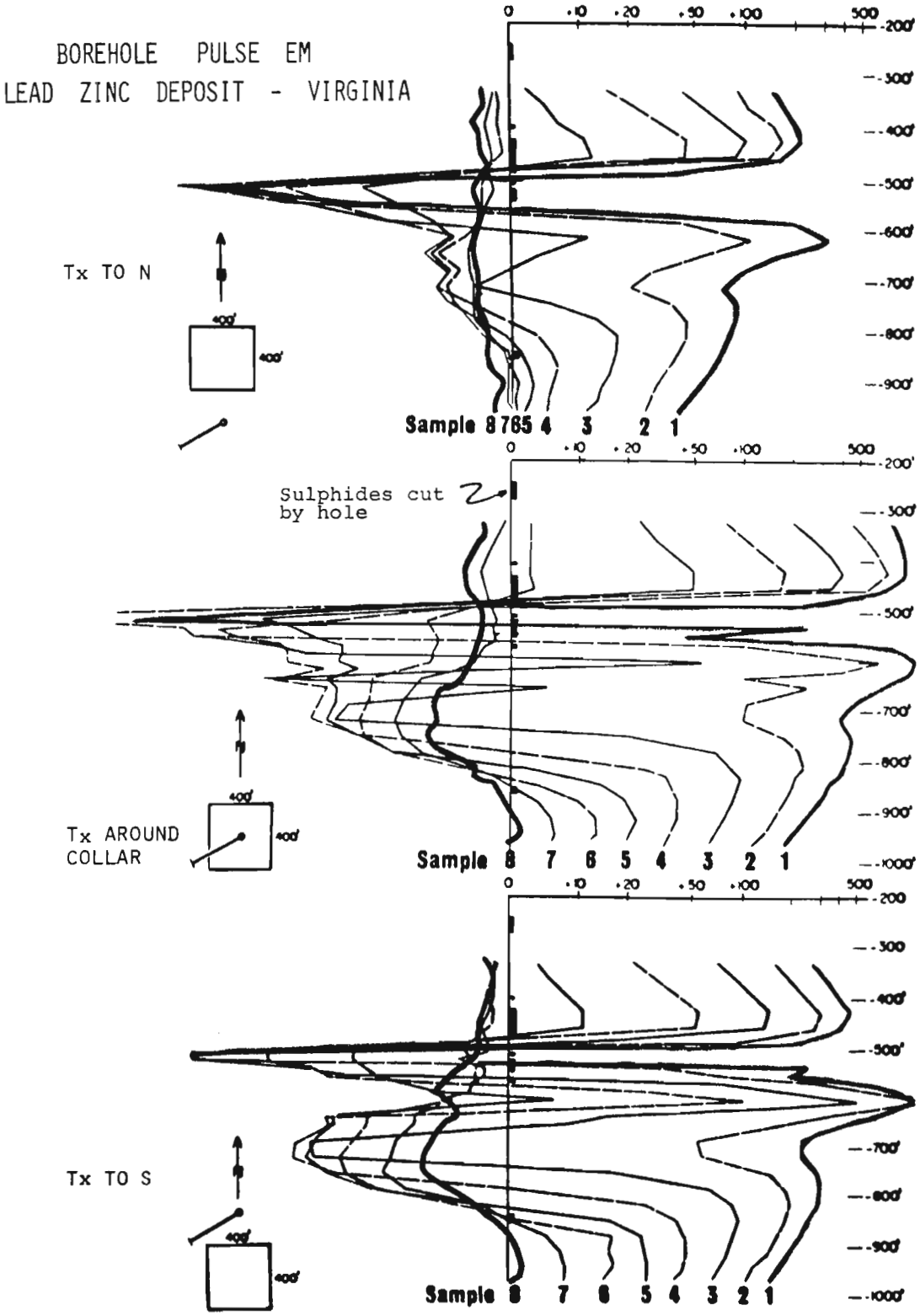

Figure 7.7. Results of Pulse EM logging of the borehole shown in Figure 7.6 with transmitter loop located to the north, south and around the borehole collar.

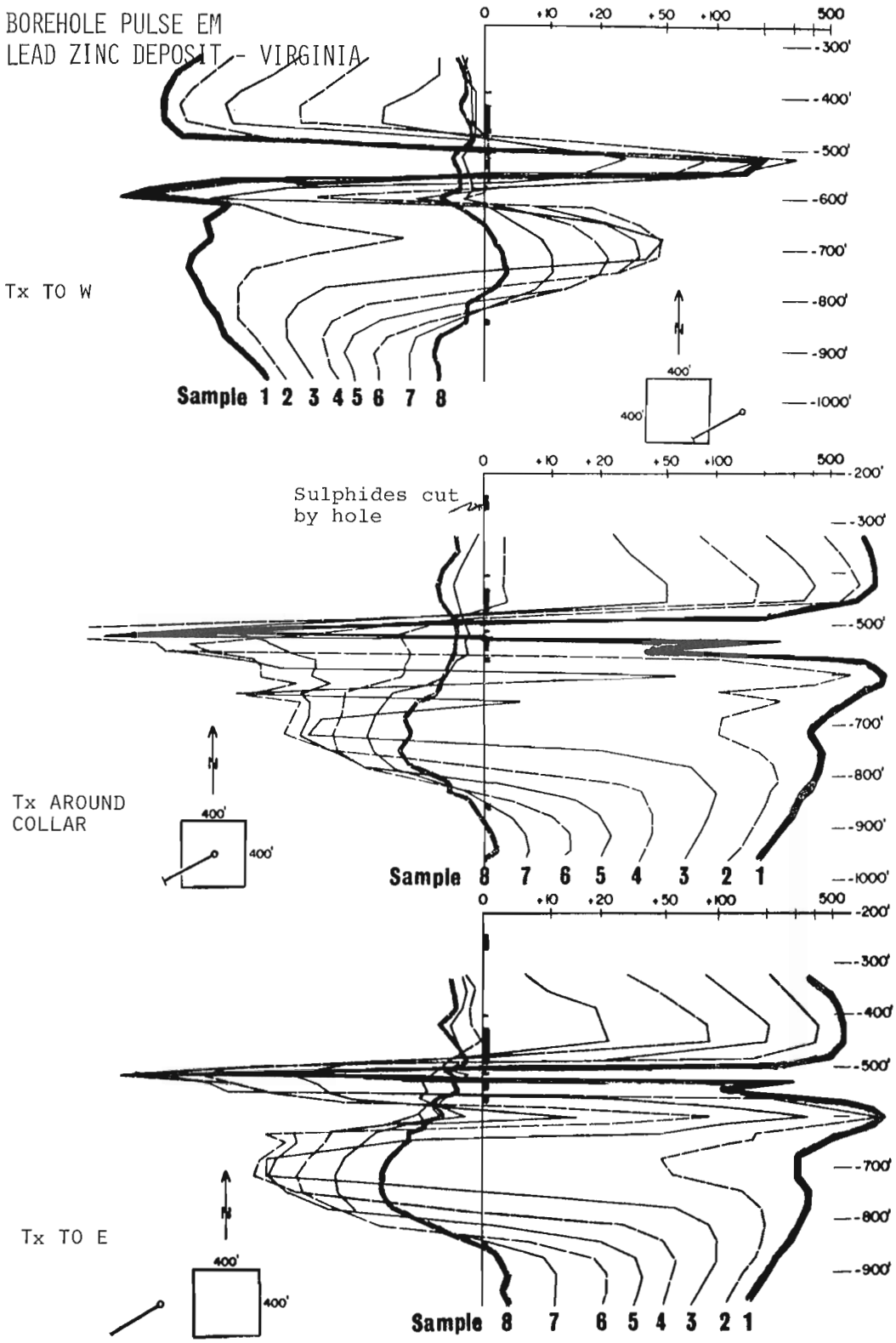

Figure 7.8. Results of Pulse EM logging as in Figure 7.7 for transmitter loops located to the west, east and around the borehole collar.

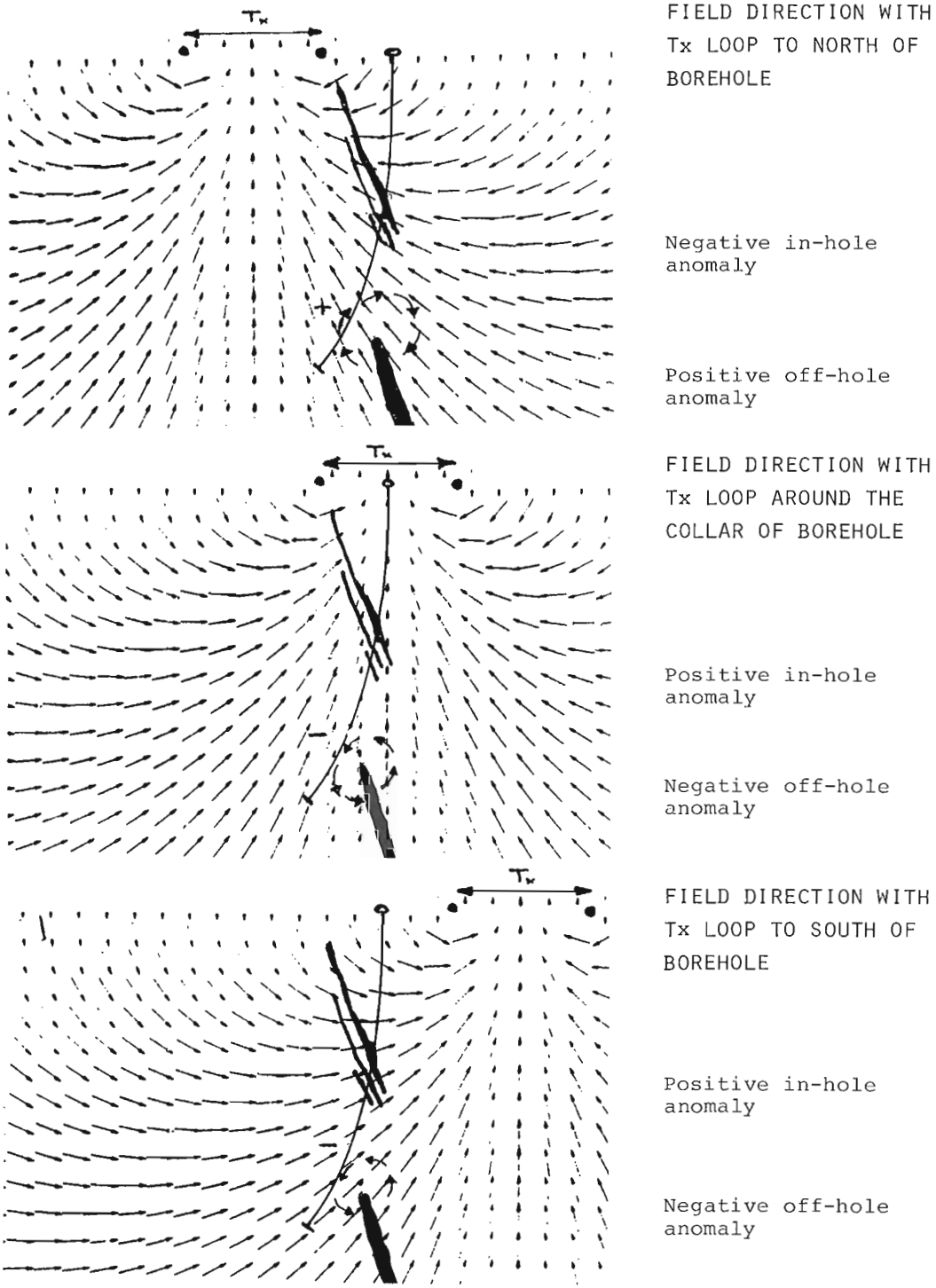

Figure 7.9. *Primary field direction diagrams for transmitter loops located to the north, south and around the collar of the Virginia lead-zinc borehole.*
top: Tx loop north of borehole; negative "in-hole" anomaly, positive "off-hole" anomaly.
middle: Tx loop around borehole collar; positive "in-hole" anomaly, negative "off-hole" anomaly.
bottom: Tx loop south of borehole; positive "in-hole" anomaly, negative "off-hole" anomaly.

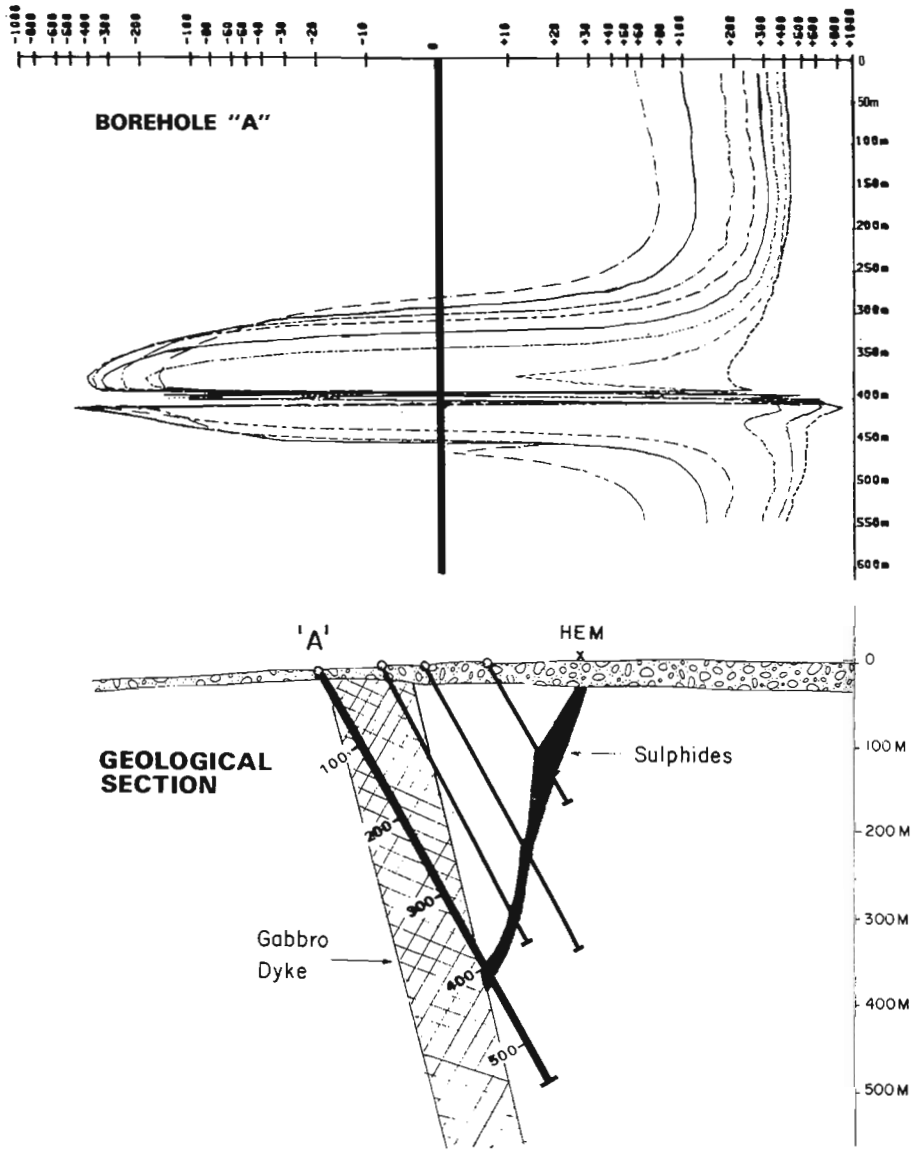

Figure 7.10. Pulse EM survey in borehole 'A', penetrating a massive sulphide deposit, Chibougamau area, Quebec. Geological section also shown.

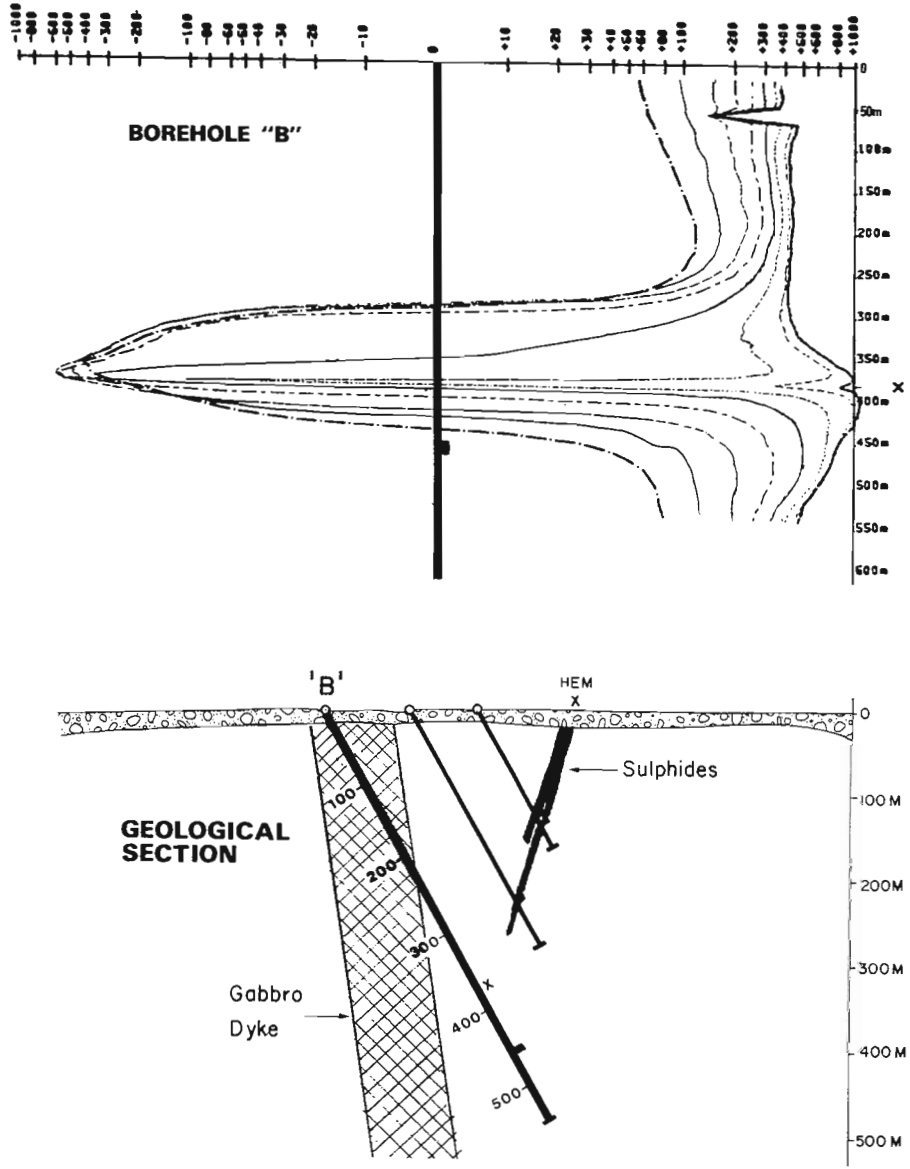

Figure 7.11. Pulse EM survey in borehole 'B', Chibougamau area, Quebec, with geological section 100 m away from the section in Figure 7.10.

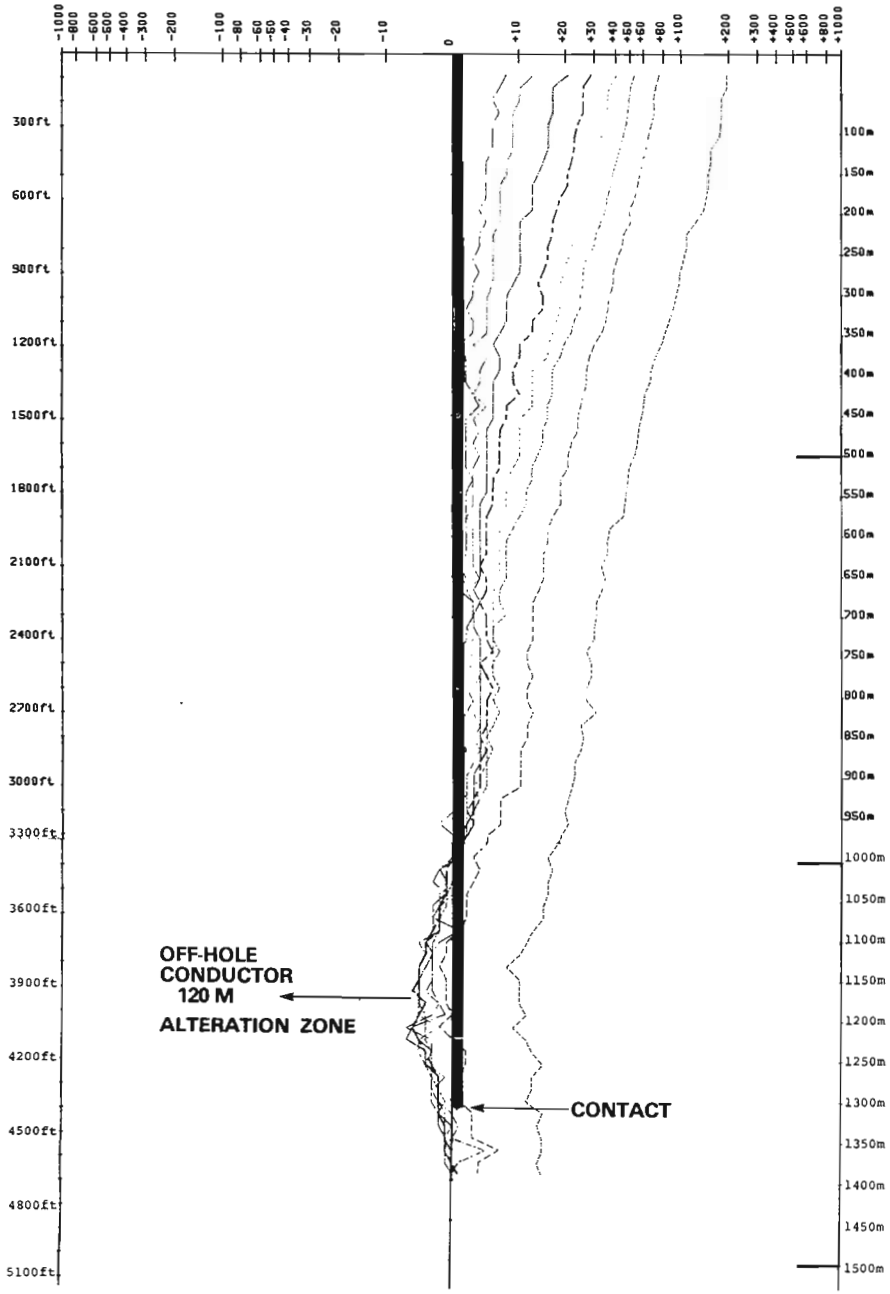

Figure 7.12. *Results of Pulse EM survey of borehole 'A', Ansil deposit, Noranda area, Quebec.*

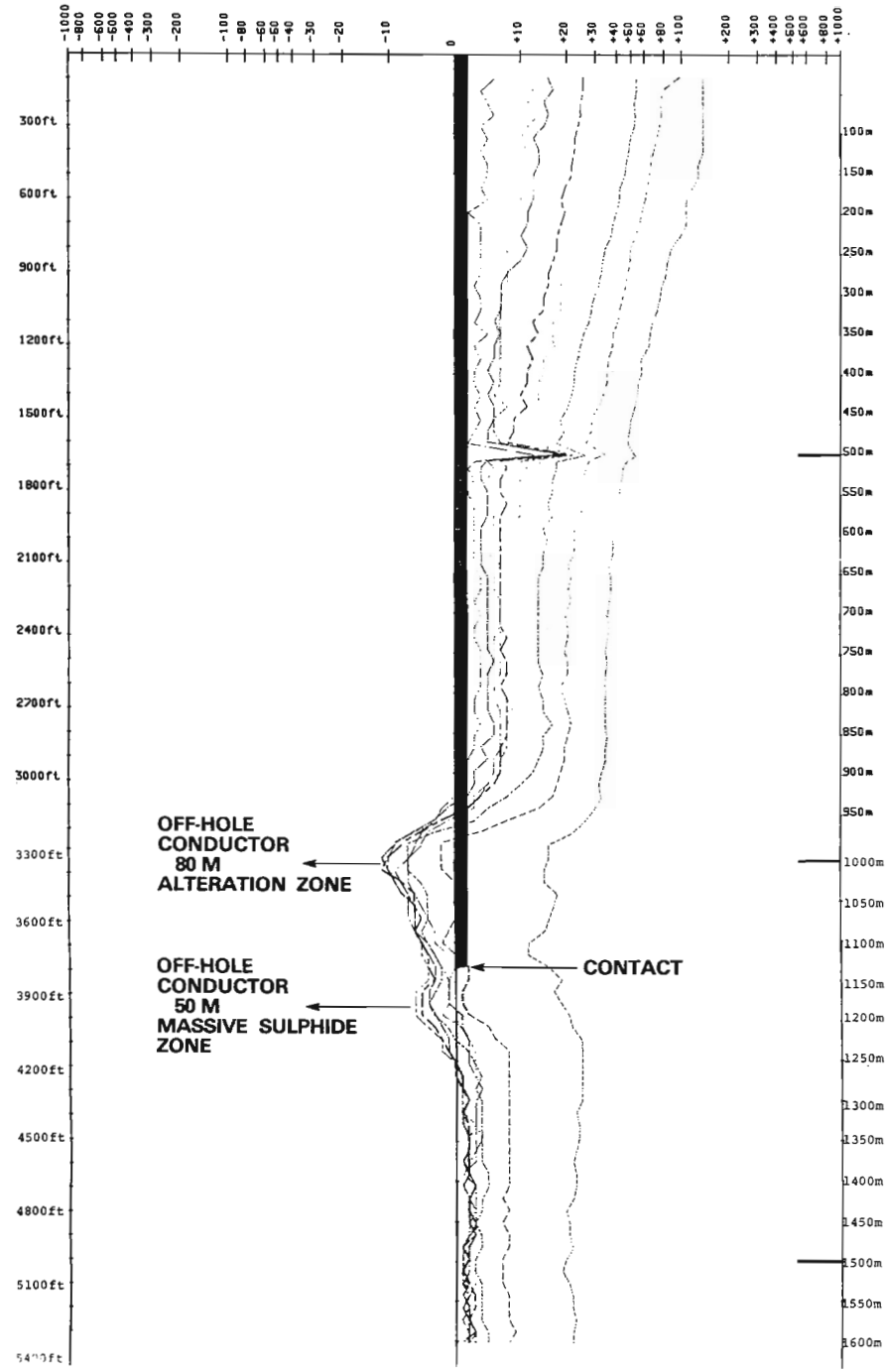

Figure 7.13. *Results of Pulse EM survey of borehole 'B', Ansil deposit, Noranda area, Quebec*

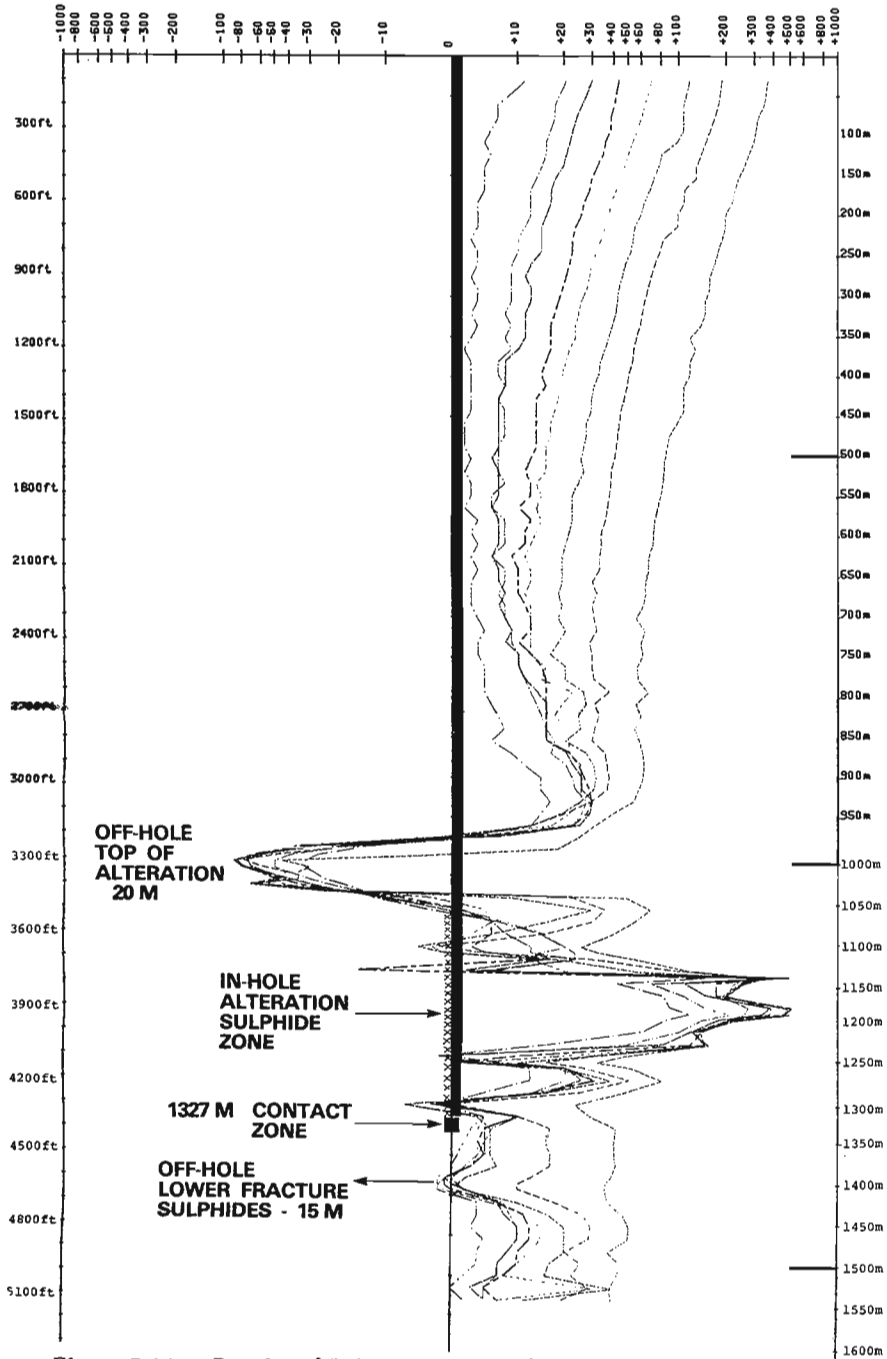

Figure 7.14. *Results of Pulse EM survey of borehole 'C', Ansil deposit, Noranda area, Quebec.*

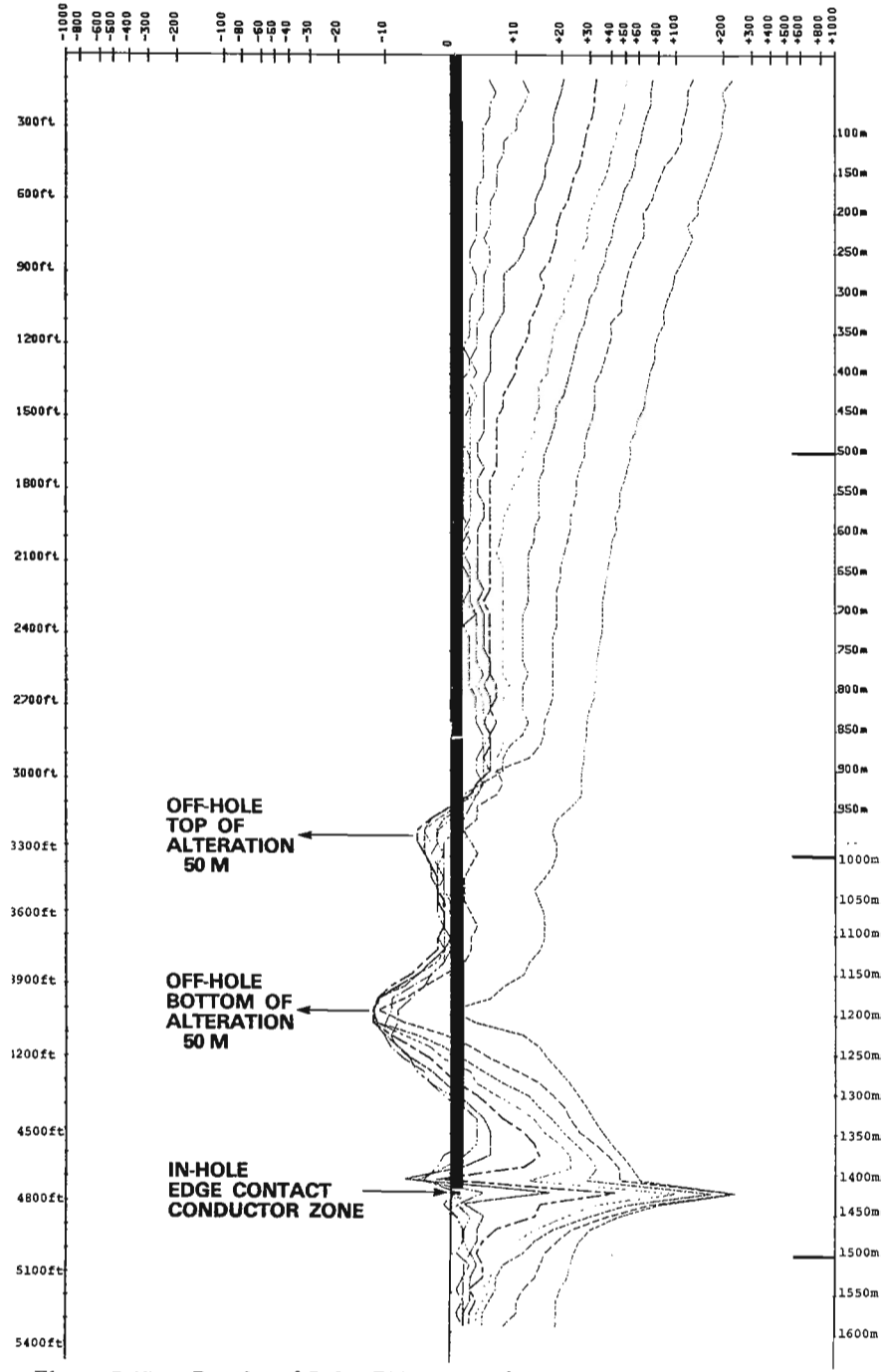

Figure 7.15. *Results of Pulse EM survey of borehole 'D', Ansil deposit, Noranda area, Quebec.*

Borehole Pulse EM at the Ansil discovery Noranda area, Quebec

In 1981, drilling from surface, Corporation Falconbridge Copper discovered a massive sulphide, copper, zinc deposit at a depth of 1266 m. This is probably a record for discovery of a massive sulphide body based on extrapolation of geological information. Corporation Falconbridge Copper were the early advocates of surveying deep exploration holes with Pulse EM. At the time of the Ansil discovery their equipment was limited by the cable length to 1000 m. After the Ansil ore grade intersection in borehole 63 their Pulse EM equipment capabilities were quickly increased to 2000 m and new records were also established for deep downhole EM logging.

The Ansil deposit was not a simple, textbook type geophysical target. Directly above the massive sulphides, occurring at the rhyolite-andesite contact, was an alteration pipe some 200 m high. This alteration zone carried fracture filling and pillow lining sulphides, predominantly pyrite and pyrrhotite. Although these sulphides were minor in content, they did interconnect to form a very large, complex zone of high conductivity. Also below the massive sulphides was a stringer copper zone of excellent conductivity. The early discovery boreholes, drilling down through the centre of this complex structure of alteration pipe, massive sulphides and footwall fracture zone produced strong erratic pulse EM anomalies extending over a distance of 500 m, from 1000 to 1500 m deep. The ore bearing massive sulphide zone

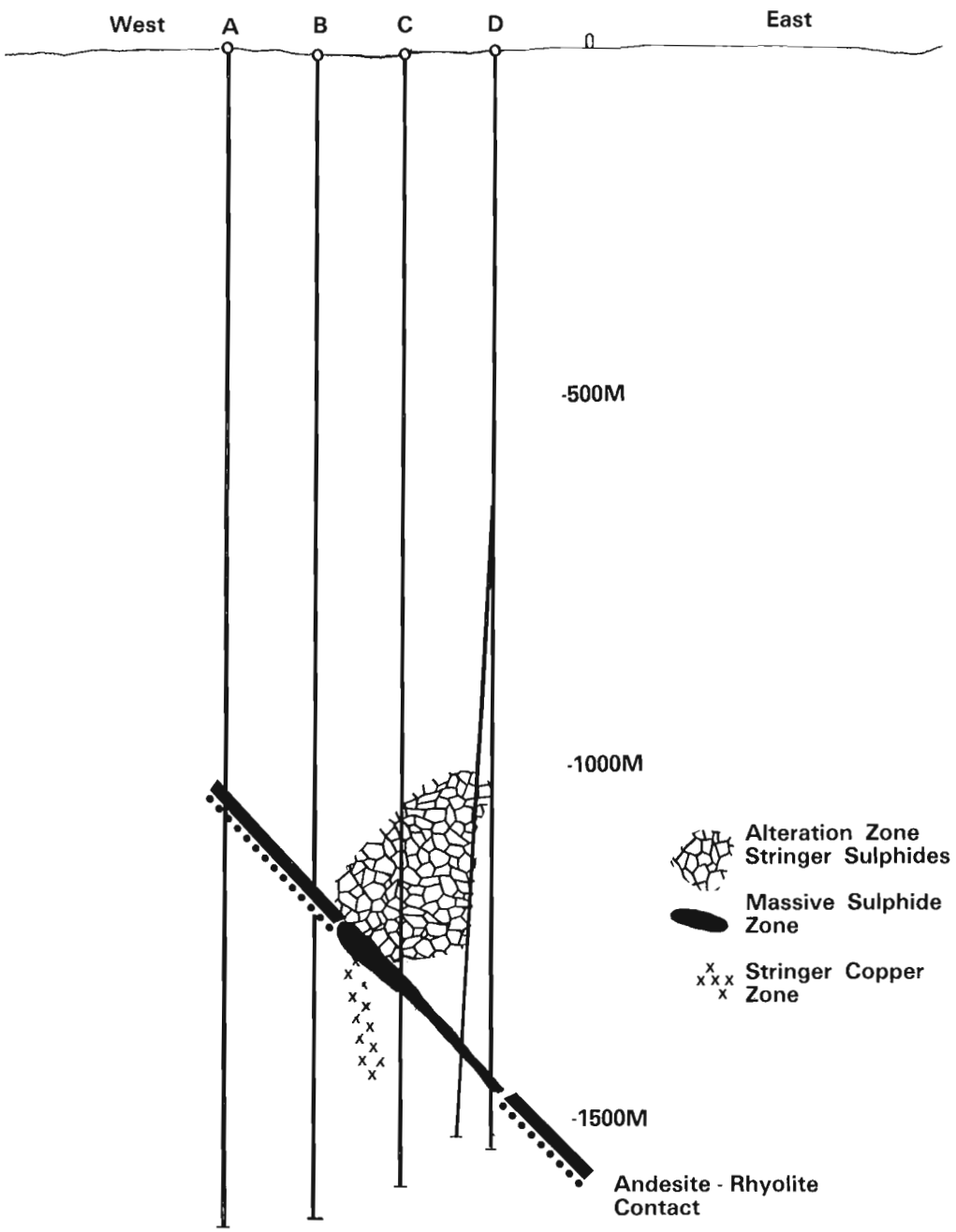

Figure 7.16. *Simplified geological section showing the Ansil deposit, a massive sulphide copper-zinc body, Noranda area, Quebec*

produced only a small "blip" in this complex zone of conductive anomalies. The pulse EM surveys from these early holes therefore did not contribute much information as to shape or size of the deposit. Fortunately where the geophysical information was minimal the geological information was very positive. With holes that missed mineralization the geophysical response patterns simplified and started to produce more positive information as to the boundaries of the various sulphide zones.

The borehole results from holes "A", "B", "C" and "D" are shown (Fig 7.12 - 7.15), along with a simplified geological section (Fig 7.16). The broad "off-hole" anomaly obtained in hole "A" is caused by the entire complex zone of conductivity not just the ore bearing massive sulphides. The distance to the nearest conductive edge would be in the order of 100 m. In hole "B" this broad anomaly separates into three zones, the lower of which, from geological correlation, is the massive-sulphide conductor at the contact. Distance to this edge is calculated at 50 m - the marginal reach of a wedged hole - the borehole PEM survey conclusion would be that wedging this hole could be risky in that the wedged hole may not intersect the massive sulphide zone. In borehole "C" the hole cut through and alongside the central alteration zone, then intersected the massive high grade sulphides and then went into the footwall stringer copper mineralization. As mentioned the anomaly from the massive sulphide zone is hidden within this complex pattern of EM responses. Wedging here is determined entirely on the basis of geological information. In borehole "D" the hole misses the alteration zone detected as "off-hole" conductors. At the contact a narrow intersection of sulphides carrying weak zinc values was intersected. The borehole PEM anomaly is however a typical "edge" type indicating the sulphides are part of the main massive-sulphide body. In this case wedging of the hole was definitely recommended. The wedged hole subsequently cut a wide intersection of good grade copper mineralization.

The Ansil borehole EM survey program is an excellent example of where accurate interpretation of the complex geophysical data is completely dependent on detailed correlation with the known geological information. The interpretation is carried out by comparison of the downhole PEM logs with geological sections - in most cases every "wiggle" of the geophysical log could be attributed to known or extrapolated sulphide zones. The important anomalies then by this process could be recognized and evaluated accordingly.

Acknowledgment

Thanks is directed to the following companies for giving permission to publish survey results: Corporation Falconbridge Copper, Callahan Mining Corporation, and Riocanex.

References

Dyck, A.V., Bloore, M., Vallee, M.A.
1980: User Manual for programs PLATE and SPHERE: Research in Applied Geophysics no. 14, Geophysics Laboratory, Department of Physics, University of Toronto.

Macnae, J.C.
1980: An atlas of primary fields due to fixed transmitter loop EM sources: Research in Applied Geophysics no. 13, Geophysics Laboratory, Department of Physics, University of Toronto.

Woods, D.V
1975: A model study of the Crone borehole pulse electromagnetic (PEM) system: M.Sc. Thesis, Queen's University.

8. TRANSIENT ELECTROMAGNETIC BOREHOLE LOGGING

G.M. Levy[1] and J.D. McNeill[1]

Levy, G.M. and McNeill, J.D., Transient electromagnetic borehole logging: in Borehole Geophysics for Mining and Geotechnical Applications, ed. P.G. Killeen, Geological Survey of Canada, Paper 85-27, p. 71-77, 1986.

Abstract

Exploration for electrically conductive sulphides can be carried out using a transient electromagnetic technique in which the transmitter consists of a large loop laid out on the surface, and the receiver coil is lowered into a borehole. With the Geonics EM37, the transmitter waveform is a bipolar current pulse exhibiting a rapid turn-off, and measurement is made of the time derivative of the axial magnetic field in the borehole at 20 time intervals during the period that the transmitter is off. Since measurement is made during the off-time the system response is essentially invariant to changes in transmitter/receiver coupling, making it ideally suited for borehole work.

Several advantages arise from commencing the measurement at a short time after transmitter turn-off. For example poorer or smaller conductors exhibit a response which has large initial amplitude but decays rapidly, so that signal is lost at late times. Measurements made at early times on better conductors are diagnostic of conductor geometry, since the currents are essentially on the conductor surface; however, at early time, there is also significant response associated with currents induced in the overburden and host rock, even when they are quite resistive. It is necessary to distinguish between these responses and that from conductive targets. This paper presents the results of calculations illustrating the response from overburden, host rock, and confined targets. Techniques for separating out the responses using both spatial and temporal variation are demonstrated.

Résumé

La prospection des sulfures conducteurs peut être effectuée à l'aide d'une technique électromagnétique transitoire qui utilise un émetteur constitué d'une grande boucle installée en surface et d'une bobine réceptrice déposée au fond du trou. Dans le cas de l'appareil Geonics EM37, la forme d'onde de l'émetteur est une impulsion bipolaire à blocage rapide; on mesure la dérivée temporelle du champ magnétique axial dans le sondage à 20 reprises pendant que l'émeteur est fermé. Puisque les mesures sont prises lorsque l'émetteur ne fonctionne pas, les résultats sont essentiellement insensibles aux changements dans le couplage émetteur-récepteur, ce qui rend cette méthode idéale pour les travaux dans les sondages.

Il y a plusieurs bonnes raisons de commencer à prendre les mesures peu après avoir fermé l'émetteur. Par exemple, les conducteurs de moindre qualité ou de plus petit calibre donnent une réponse à forte amplitude initiale qui s'amortie rapidement de sorte que plus tard, le signal se perd. Les mesures effectuées tôt sur de meilleurs conducteurs sont caractéristiques de la géométrie du conducteur puisque les courants se trouvent essentiellement à la surface de celui-ci; toutefois, au début il y a aussi production d'un écho associé aux courants induits dans la couverture et la roche encaissante même lorsque celles-ci sont très résistantes. Il est nécessaire de faire la distinction entre ces réponses et celles qui proviennent des cibles conductrices. Cette étude présente les résultats des calculs montrant la réponse provenant du terrain de couverture, de la roche encaissante et des cibles retreintes. Elle décrit des méthodes de séparation des réponses qui utilisent à la fois les variations spatiales et les variations temporelles.

[1] Geonics Limited, 1745 Meyerside Dr., Unit 8, Mississauga, Ontario L5T 1C5

Introduction

The technique of transient or time domain electromagnetic (TEM) surveying is finding ever wider application in the field of resource exploration and development. This paper describes the technique as embodied in the Geonics EM37/BH43 borehole system, outlining the basic physical principles which come into play. The nature of the instrument response to conductive overburden, host rock, and confined bodies are discussed. More detailed treatments can be found in the references listed at the end of the paper.

Measurement technique

The procedure used in borehole logging is to lay a large loop transmitter (Fig 8.1), typically hundreds of metres on a side, in the vicinity of the borehole. Several different loop positions commonly are used to aid in interpretation. The receiver is lowered into the borehole, and data are collected at each station chosen for measurement, using a magnetic tape data logger located at the surface. An HP85 computer is used for final data editing and reductions.

Transient EM is distinguished from the more familiar frequency domain EM by the transmitter waveform, and by the way in which the receiver signal is analyzed (Fig 8.2). In the case of the EM37, a steady current of up to 30 amperes is caused to flow in the transmitter loop, for a time sufficiently long to allow transients induced in the ground by the switched current essentially to dissipate. This current is then turned off sharply, which results in currents being set up in the surrounding medium so as to oppose any instantaneous change in the magnetic field. These currents then decay away according to the conductivity structure of the medium (as will be discussed in more detail below) and it is the field due to these currents - or more precisely the time derivative of this field, dB/dt, - which is measured at the output of the receiver coil.

The EM37 receiver divides the time period after turnoff into 20 segments or gates, covering a range of 2 decades in time from the earliest to the last, or 3 gates per "octave". The signal for each gate is added to the signal for the same gate for previous repetitions of this basic cycle (stacking), until adequate signal-to-noise is reached.

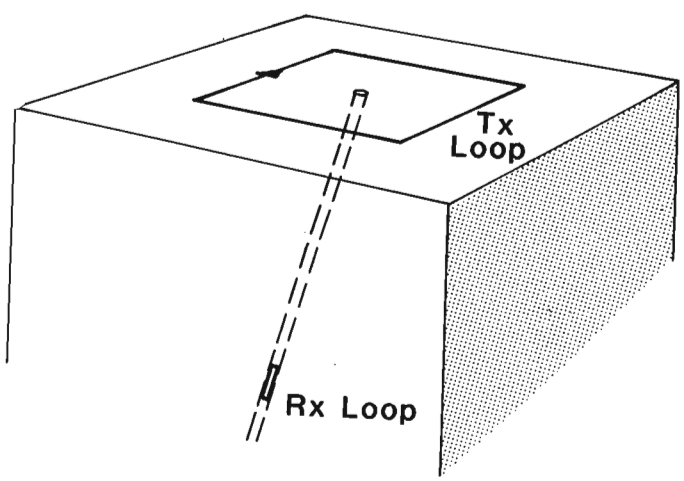

Figure 8.1. *Typical borehole Transient EM logging arrangement showing large transmitting loop on the surface near the hole and receiver lowered downhole to make measurements.*

One principle advantage of TEM over frequency domain EM is that, in the above manner, responses which are analogous to responses for 20 single frequencies ranging over 2 decades, are gathered at the same time, rather than having to be recorded separately. With the EM37 operating at a base frequency of 30Hz, the earliest gate is centred 89 μs after the end of turnoff, and the latest gate at 7.2 ms. If later times are important a lower base frequency may be used.

Another advantage is that, since measurements are made while the TX current is turned off, the measurements are insensitive to small variations in the RX orientation, which could other wise produce changes in coupling with the primary field.

One complication in analyzing the response arises due to the fact that the transmitter turnoff is not actually instantaneous, but rather takes place over a finite period of time. In fact, for the 30Hz base frequency, the turnoff ramp is typically 300 μs long, whereas the 1st gate starts less than 100 μs after the end of turnoff. This means that the response measured by the instrument is not quite the same as would be expected for an ideal impulse, but is rather the ideal impulse response convolved with a rectangular waveform of width equal to the duration of the turnoff. As the difference can be quite significant for the earlier gates, this must be taken into account, and a deconvolution operation may be carried out as part of the data reduction procedure.

Other TX waveforms are used in TEM work as well. One particular case of interest is the UTEM system, in which the waveform used is essentially triangular in shape. The effect is to provide a response which corresponds to the B field which would be obtained for the case of an EM37 type of waveform, as opposed to dB/dt. The cost is having to make measurements while the TX is on.

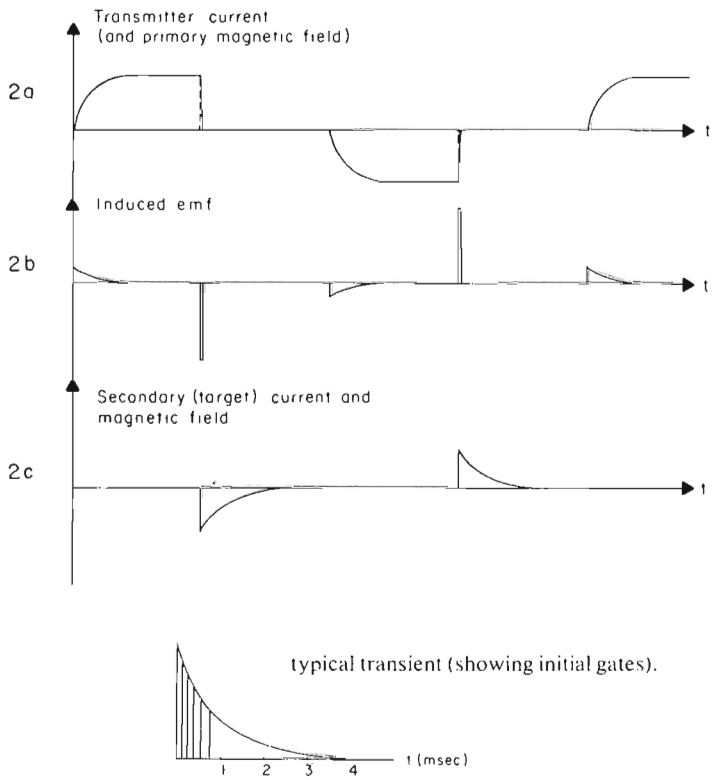

Figure 8.2. *Transient EM (TEM) wave form, showing induced emf, the secondary magnetic field, and initial sampling time gates for a typical transient.*

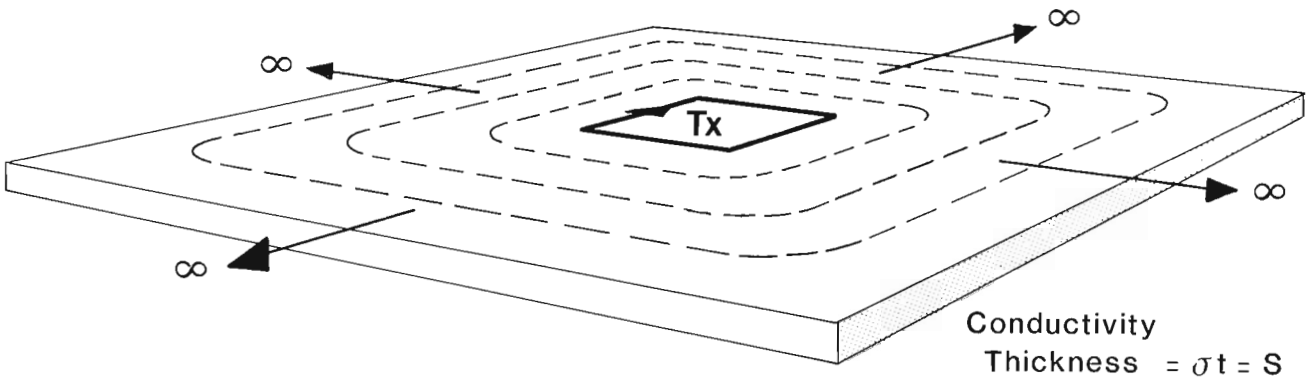

At late time (horizontal coil receiver)

$$\text{Signal voltage} \propto \frac{S^3}{t^4}$$

Figure 8.3. *Current flow for the unconfined situations of a thin conductive horizontal sheet overlying a highly resistive medium considered as free space.*

The EM37 reduction software routinely provides B, as it is automatically calculated in the process of deconvolving the waveform, and so may be used with interpretation techniques based on this quantity rather than dB/dt.

Secondary responses

Resistive environment

Returning to the secondary response due to currents set up in the surrounding medium, it is instructive to examine what we might expect in some idealized situations. The simplest case is, of course, free space. In practice this means an environment with resistivity so large that the currents have decayed to levels below the detection limit by the time the 1st gate begins; rather uninteresting except to note that this has happened.

Thin sheet

Not quite so trivial is the situation of a thin conductive overburden, overlying a highly resistive medium which may be considered again as essentially free space (Fig 8.3). In this case a current flow is set up in the sheet which at very early times is concentrated very closely in the vicinity of the TX loop. (This distribution mirrors the field which existed immediately prior to turnoff). However, the current rapidly diffuses across the sheet and the field eventually decays as t^{-3}. The field for the thin sheet may be easily calculated, as image theory tells us that the response is that which would be obtained for a current loop which is the size and shape of the TX loop, but which moves away from the measurement point, in a direction perpendicular to the sheet, with a velocity inversely proportional to the plate conductance.

Half-space

In the case of a conductive half-space, the current distribution is again initially confined to the vicinity of the TX loop; in this case, however, the diffusion of the current proceeds downards as well as outwards. Figure 8.4 shows current density contours calculated by Nabighian (1979). (Hoversten and Morrison, 1982, have published similar contours for up to 3 layers.) The peak current density is seen

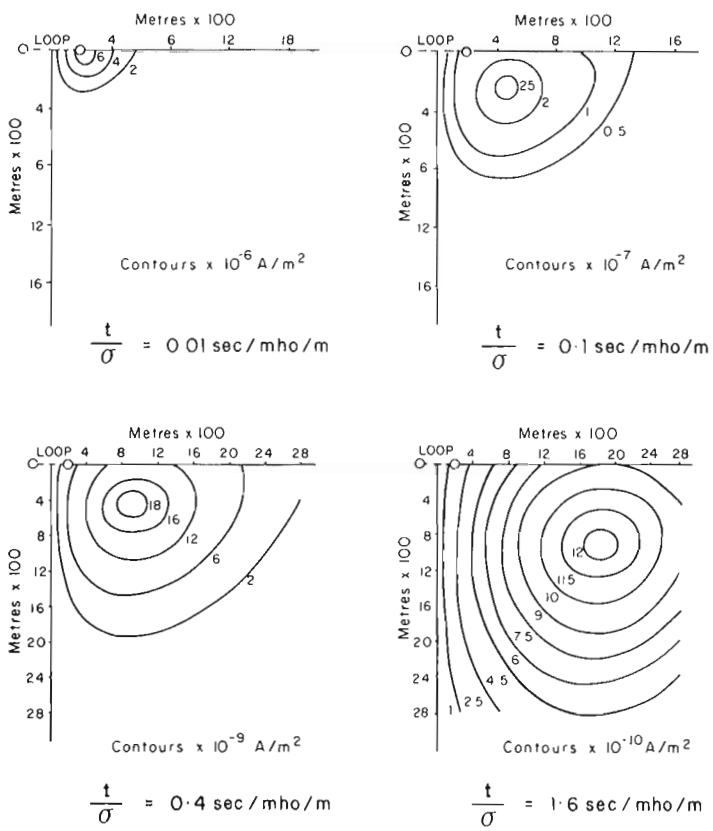

Figure 8.4. *Current density contours, computed by Nabighian (1979), passing through the loop centre for a loop of dimensions 400 x 800 m.*

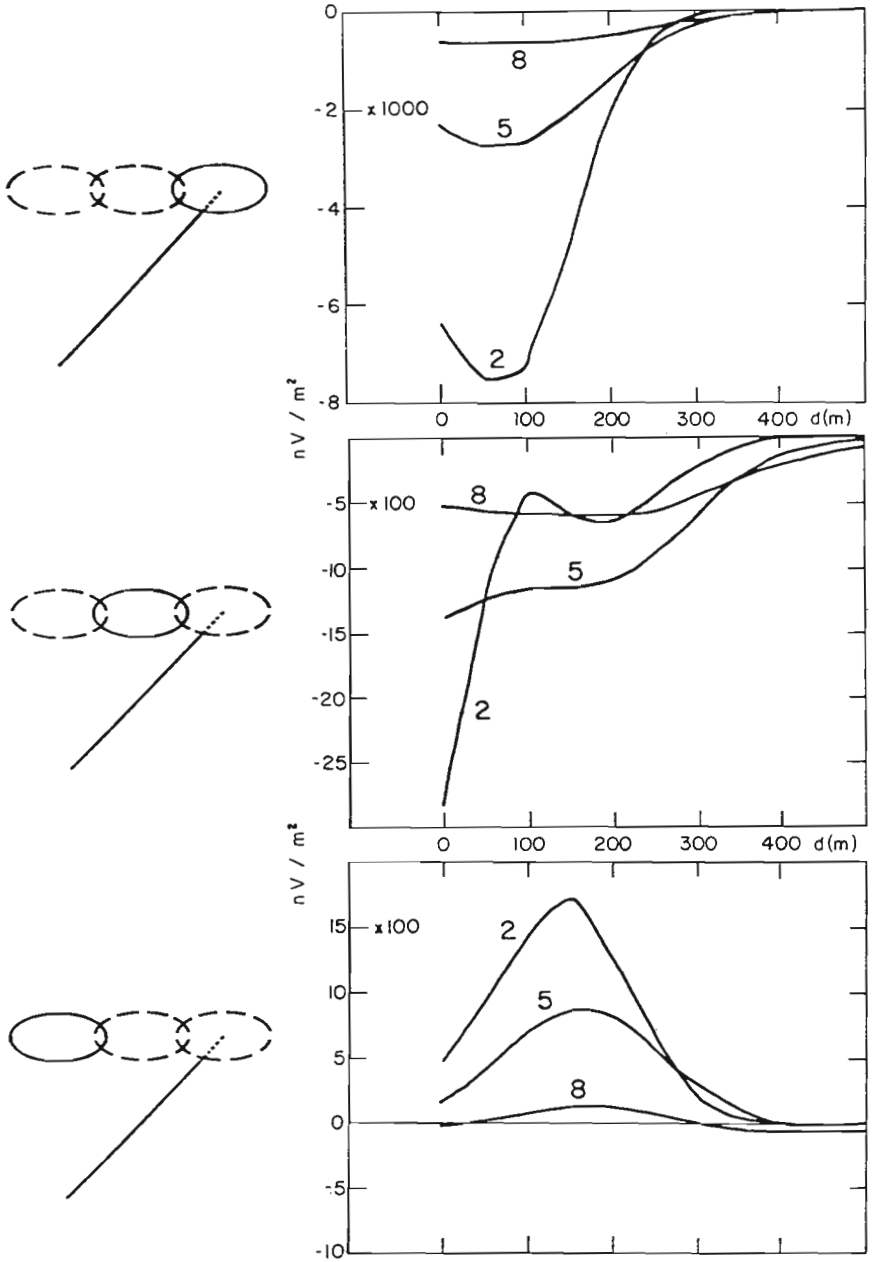

a. *Responses for earlier gates 2,5, and 8, corresponding to* ρt *values of approximately 0.005, 0.01 and 0.02 ohm-m-s.*

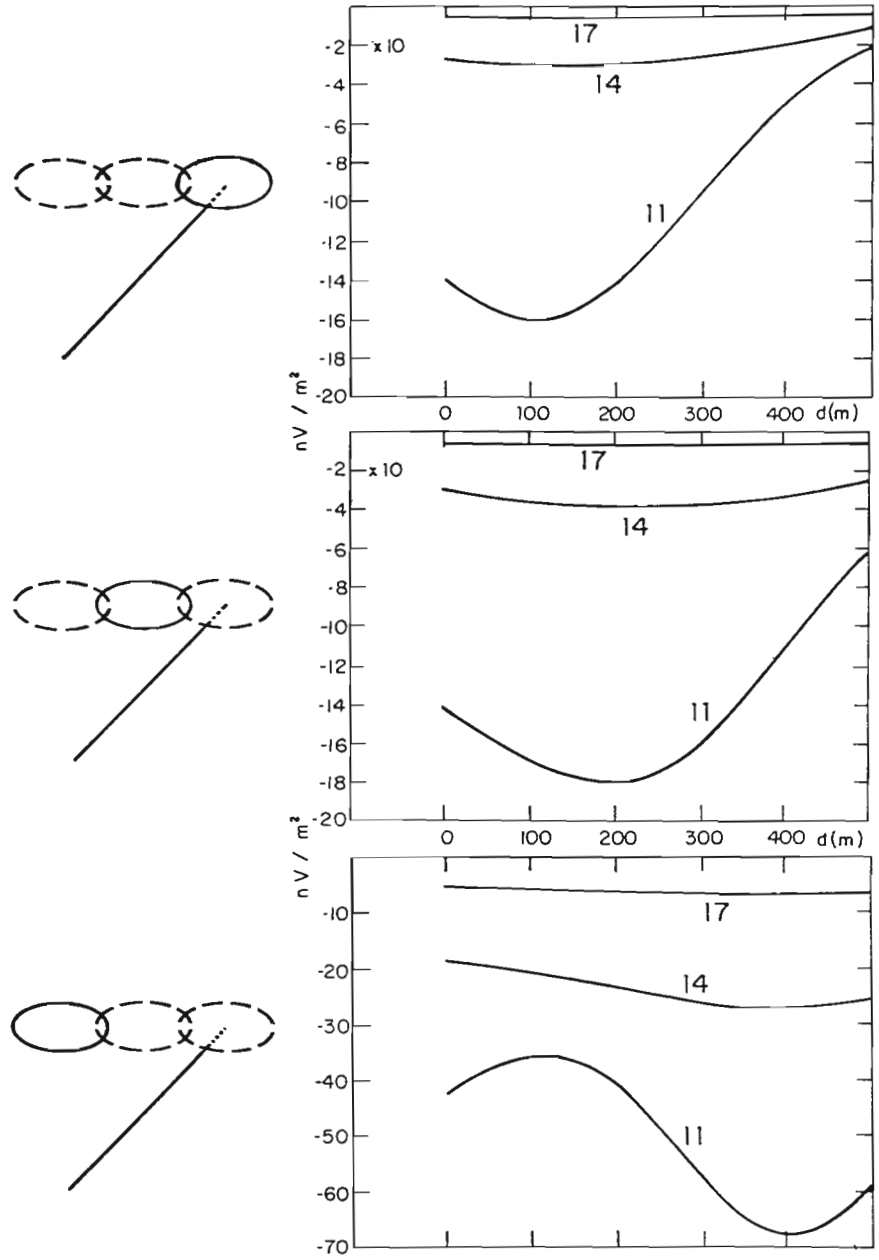

b. *Responses for later gates,* ρt *being 0.04, 0.08 and 0.16 for gates 11, 14 and 17.*

Figure 8.5. *Responses along a 45° borehole extending to a depth of 500 m in a 50 ohm-metre half-space, for 3 different positions of a 200 m radius circular TX loop; centred over the upper end, middle portion and deep end of the borehole respectively. The responses plotted are for the axial downhole component of the field in units of* nV/m^2 *for a 1 amp TX current.*

to move downwards and outwards at about 30° from horizontal. The shape of the current distribution in the ground is a function of ρt, the product of the resistivity and the measurement time: indeed the peak in current density occurs at a horizontal distance from the TX given by $1.6\,(\rho t)^{\frac{1}{2}}$ km. Nabighian also pointed out that the field as measured at the surface at late time, is in fact close to that due to a current loop decaying as 1/t and travelling downward and outward at 47°. This is a simplification which is useful in understanding the type of response we see in practical cases.

Figure 8.5 shows responses along a 45° borehole extending to a depth of 500 m in a 50 ohm-metre half-space, for 3 different positions of a 200 m radius circular TX loop: centred over the upper end, middle portion and deep end of the borehole respectively. The responses plotted are for the axial downhole component of the field in units of nV/m^2 for a 1 amp TX current. (EM37 noise levels are not discernable with this plotting scale, so these responses will occur at high signal-to-noise ratio). In Figure 8.5a we see results for earlier gates 2,5, and 8, corresponding to ρt values of approximately 0.005, 0.01 and 0.02 ohm-m-s. The response tends to peak in the upper portion of the drillhole, although there is some indication of the peak becoming deeper and broadening towards the later times. At points within the borehole, it can be seen that at earlier times the response may actually increase in amplitude with time. The detailed shape of the response, as might be expected, depends very much on Tx position. In fact, for these gates, the response with the TX loop centred over the deep end of the hole is opposite in sign to the responses for the other 2 TX positions: the upper portion of the borehole is outside the effective current loop in the ground for the one Tx, inside for the other 2.

Figure 8.5b shows the responses for later gates, ρt being 0.04, 0.08 and 0.16 for gates 11, 14 and 17. As the currents move farther from the original TX positions, the responses become smaller, deeper, and broader, and the differences in TX position become less and less important.

Confined conductors

The response of confined conductors is of considerable interest, as this is a model which can often be used to represent ore bodies. Figure 8.6 illustrates the physical effects which combine to set up current flow in confined conductors. The important factors to be considered are the electric field vector, $\bar{E}$, and the rate of change of the magnetic field vector, $d\bar{B}/dt$ or $\bar{B}$.

The effect of the $\bar{E}$ field is rather involved, and dependent on the conductivity and shape of the target body, and the conductivity of the host rock as well (Edwards, 1974; Kaufman, 1978); however the net result is current flow in the conductive body in the direction of and in proportion to the field itself – the so-called current gathering effect or Galvanic response – accompanied by a diffuse return current in the host medium. Note that if the host medium is highly resistive, the field dies away rapidly, as does this current, according to a $t^{-5/2}$ power law.

The secondary field produced by the Galvanic component of the current can be useful in determining the position of the body; much more information, however, can be obtained about the body if effects of vortex currents, produced by $d\bar{B}/dt$, can be observed. As in the case of the thin sheet or half-space, any change in the magnetic field sets up currents which initially are confined to the surface of the body and which oppose the change in the field. The currents at this time can be considered as loops at the surface of the body, circulating in planes perpendicular to the $\bar{B}$ vector excitation. Once the initial $\bar{B}$ disappears, these currents diffuse to the interior of the body in a manner which is determined by its shape and conductivity. Conceptually, the currents may be resolved into component currents, the paths of which are characteristic of the body's shape (eigencurrents). These eigencurrents each decay exponentially at rates which reflect the effective L/R time constants for the different current paths. At sufficiently late time (late stage), the current path with the largest decay time constant will dominate (Kaufman, 1978).

In the case of a thin, plate-like body, the currents will quickly be reduced to those in the plane of the plate, although the distribution within the plane will continue to change until the late stage for the largest loop is reached.

Examination of the secondary field due to vortex currents in a confined conductor can reveal several properties. The longest decay time constant is proportional to the conductivity times the smallest cross section of the body. The spatial variation of the field is indicative not only of the position of the body, but also of the orientation of the effective plane of the vortex current. For example, a thick

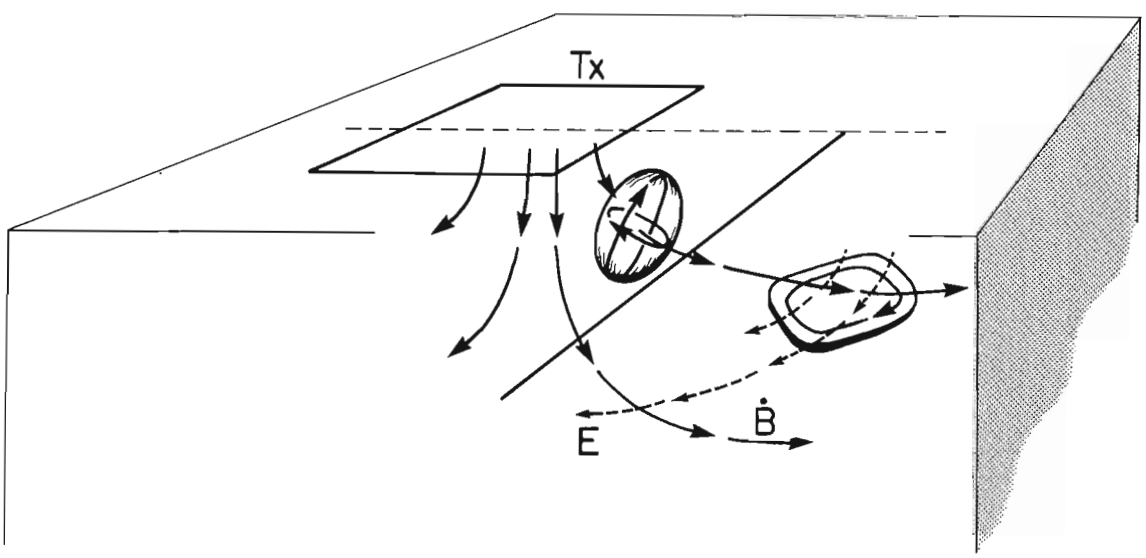

Figure 8.6. *Current flow for the situation of a confined conductor showing induced currents and secondary electric and magnetic fields at the receiver.*

body will produce a response which corresponds to currents in a plane determined initially by the direction of the primary field, but which eventually rotates to a direction characteristic of the body's own geometry. It may often be distinguished by this type of behaviour from a thin plate-like target in which the vortex currents always remain in the plane of the plate.

At sufficiently early and sufficiently late times, the Galvanic currents due to the $\bar{E}$ field will dominate the vortex currents set up in the confined conductor by $\bar{B}$. Under favourable conditions, however, the vortex response may be strong enough to be useful in interpretation. It can be shown that the ratio of the vortex current to the Galvanic current is at its maximum at a time after turnoff equal to a few vortex decay time constants.

Figure 8.7 shows the borehole response for the late stage vortex currents in a plate-like confined conductor. The shape is constant, but the amplitude decreases exponentially with time. The asymmetry of the shape is characteristic of a body which is dipping with respect to the borehole direction, while the width of the response reflects the distance from the borehole. The actual plate-borehole geometry is shown in Figure 8.8 – the curves of Figure 8.7 being generated by the plate with the solid boundary. An interpretational problem arises in borehole work when only the field component along the borehole axis in measured, as the response produced by currents in a body in one particular position does not change if the body is rotated arbitrarily about an axis along the borehole. Thus the flat-lying plate (dashed boundary in Figure 8.8), when suitably excited, can produce the same shape response as the vertical plate. The main difference will be the amplitude of the response. Indeed, by using several different positions of the TX loop it is possible to resolve such ambiguities, through consideration of the response amplitudes for different possible body positions and how these vary with the TX positions.

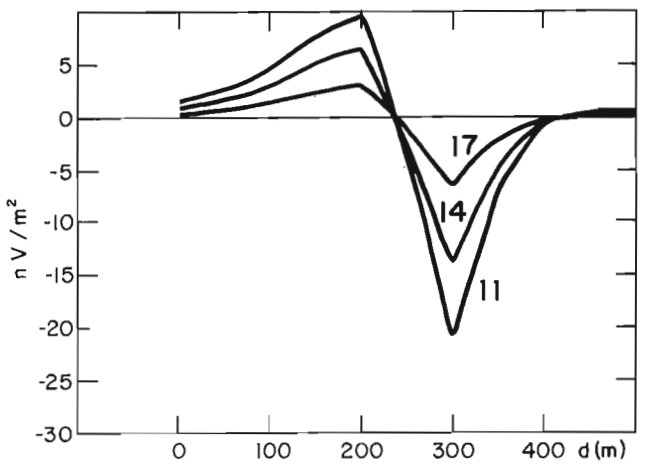

Figure 8.7. *Borehole TEM response for late stage vortex currents in a plate-like confined conductor.*

Figure 8.9 shows the vortex response of the vertical plate in Figure 8.8, combined by simple addition with the response for the 50 ohm-metre half-space, for the same 3 TX positions used earlier. (Simple adding of the responses is not strictly correct, but often close enough.) The late gates only are shown; at the earlier times the plate response is almost completely lost in the half-space response. As can be seen the plate response is strongest with the TX to the left. Note also the change in sign of the response between the left and the other two TX positions. The variation in behaviour would be very different were the plate lying in the horizontal position.

Another point illustrated by this set of responses is the importance of recognizing the influence of the half-space on the profile shapes. Any attempt to determine attitude parameters for the plate, for example from the shape of the curves with the left TX position, is likely to be considerably in error if the effect of the half-space response is not first removed with sufficient accuracy.

In conclusion, transient EM can be a powerful tool in borehole applications; however, attention must be given to the various interpretational complications if it is to be used most effectively.

Special acknowledgement is extended to Mark Goldman of the Institute for Petroleum Research and Geophysics, Holon, Israel, who provided the original computer programs for calculating the borehole half-space fields.

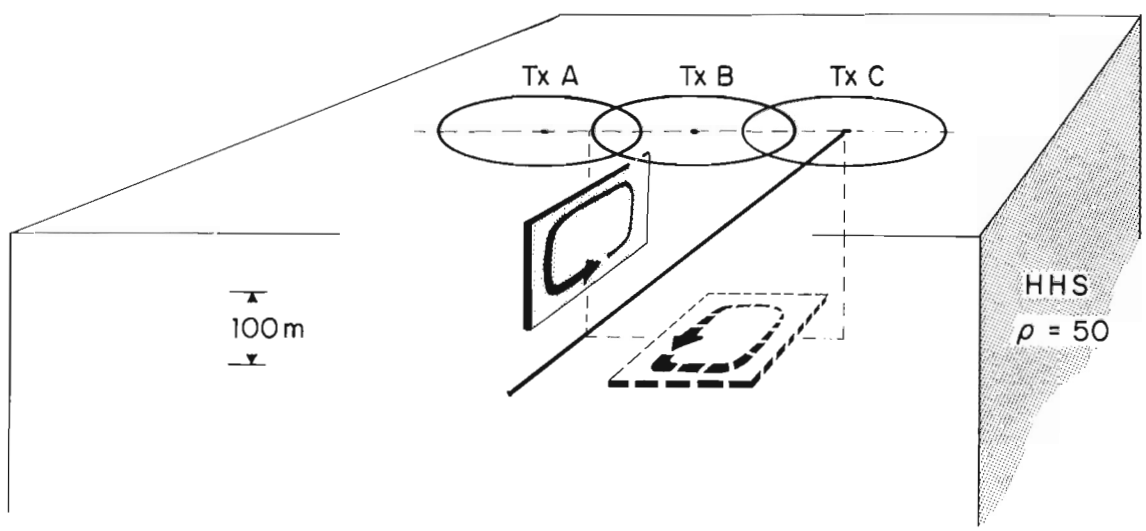

Figure 8.8. *Plate-borehole geometry. The curves in Figure 8.7 were generated by the plate with the solid boundary.*

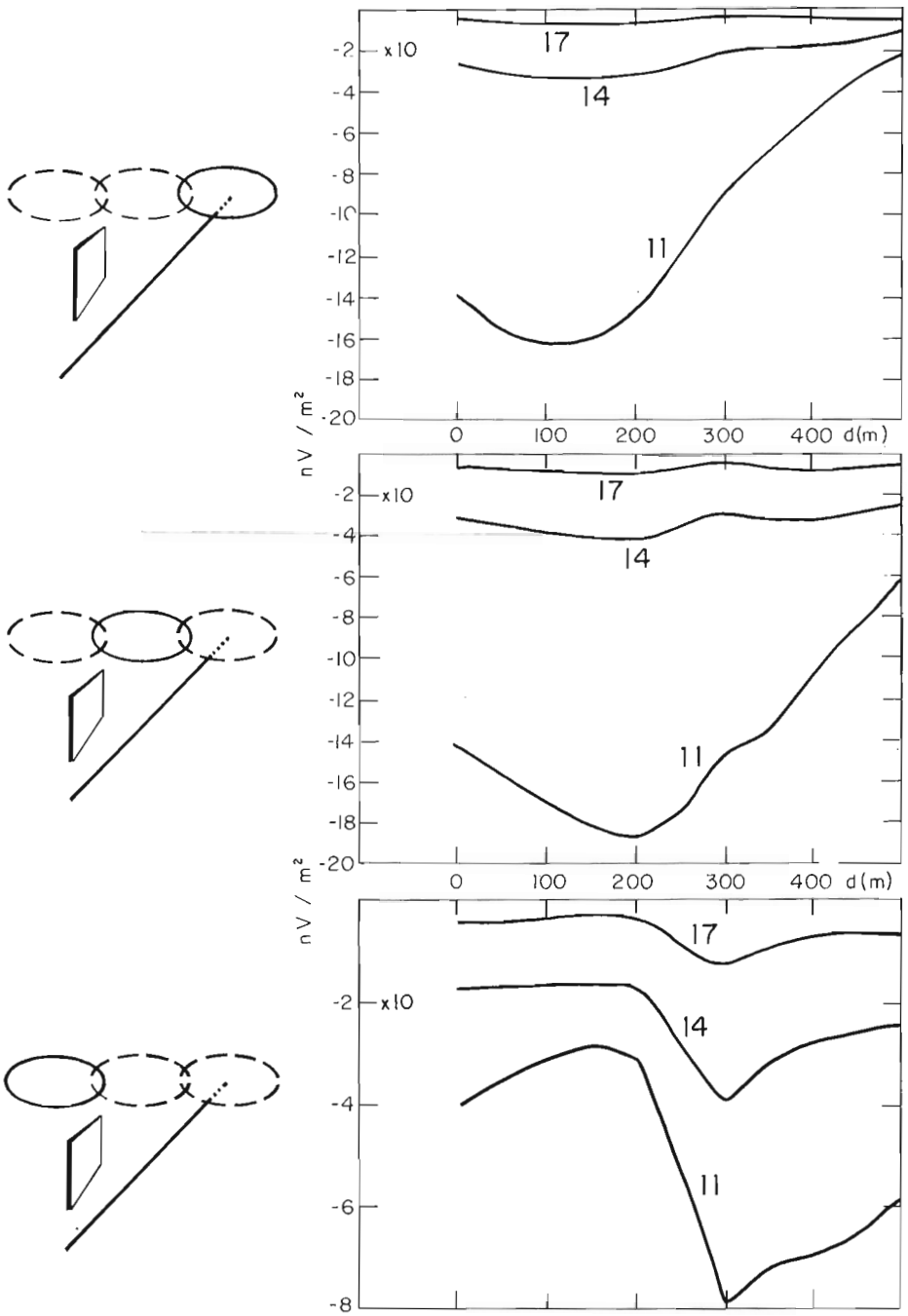

Figure 8.9

The vortex response of the vertical plate in Figure 8.8, for the same three transmitter positions as used for Figure 8.5. Late gates only are shown.

References

Edwards, R.N.
1974: The magnetometric resistivity method; Canadian Journal of Earth Sciences, v. 11, no. 8, p. 1136-1156.

Hoversten, G.M. and Morrison, H.F.
1982: Transient fields of a current loop source above a layered earth; Geophysics, v. 47, no. 7, p. 1068-1077.

Kaufman, A.A.
1978: Frequency and transient responses of electromagnetic fields created by currents in confined conductors; Geophysics, v. 43, no. 5, p. 1002-1010.

Kaufman, A.A. and Keller, G.V.
1981: The magnetotelluric sounding method, Chapter 9; Elsevier, Amsterdam.

McNeill, J.D.
1980: Applications of transient electromagnetic techniques; Geonics Ltd., Technical Note TN-7, Toronto, 17p.

Nabighian, M.N.
1979: Quasi-static transient response of a conducting half-space – an approximate representation; Geophysics, v. 44, no. 10, p. 1700-1705.

Wait, J.R.
1982: Geo-Electromagnetism (inductive transients) Chapter VII; Academic Press, New York.

Woods, D.V.
1975: A model study of the crone borehole Pulse Electromagnetic (PEM) system; M.Sc. Thesis, Queen's University, Kingston, Ontario.

9. DIRECTIONAL EM MEASUREMENTS IN BOREHOLES

Robert Pantze, Lennart Malmqvist[1], and Gerhard Kristensson[2]

Pantze, R., Malmqvist, L., and Kristensson G., Directional EM measurements in boreholes; in Borehole Geophysics for Mining and Geotechnical Applications, ed. P.G. Killeen, Geological Survey of Canada, Paper 85-27, p. 79-88, 1986.

Abstract

The objective of geophysical exploration from boreholes is to indicate direction and distance to promising targets. To improve the possibilities for 3-D interpretation of the surrounds, a system capable of measuring three magnetic field components in the hole has been developed.

The system generates a continuous wave electromagnetic field from a large ground transmitting loop, working at 2 frequencies, 200 and 2000 Hz. An efficient noise reduction is performed in the receiver. This makes measurements in mines possible even when mining operations take place.

The probe measures the EM-field parallel to the hole and the horizontal field perpendicular to the hole. The third component is perpendicular to the two other components. The three components create a right-hand system. The amplitude and phase are recorded for each component. Phase reference is transmitted to the receiver by a radio communication link. In underground work a separate small loop can be used to provide a local phase reference.

Measurements have been made down to a depth of about 1000 m. Continuous operations have been undertaken during the last 3 years. The potential range for the detection of a conductive target of economic size is at least 75 m.

The interpretation scheme has been developed according to two lines. In general everyday work a computerized interactive system based on graphics and simplified fast calculations is used. In addition, a more advanced interpretation system has been developed, describing all components and their phases in the presence of an infinite surface, a layered earth, and a buried bounded inhomogeneity.

Résumé

L'exploration géophysique des sondages a pour objet d'indiquer la direction et la distance des cibles prometteuses. Un système pouvant mesurer les trois composantes du champ magnétique dans un sondage a été mis au point en vue d'améliorer les possibilités en matère d'interprétation tridimensionnelle des environs.

Le système produit un champ électromagnétique à ondes continues au moyen d'une grande boucle au sol qui transmet 2 fréquences, soit 200 et 2000 Hz. Le bruit est atténué efficacement dans le récepteur, ce qui permmet de prendre les mesures dans les mines même pendant les travaux d'exploitation.

La sonde mesure le champ électromagnétique parallèle au trou et le champ horizontal perpendiculaire à celui-ci. La troisième composante est perpendiculaire aux deux autres. Ces trois composantes créent un système à droite. L'amplitude et la phase de chaque composante sont enregistrées. La référence de phase est transmise au récepteur par liaison radioélectrique. Pour les travaux souterrains, on peut utiliser une petite boucle distincte pour fournir une référence de phase locale.

Les mesures ont été effectuées à une profondeur maximale d'environ 1000 m. Les travaux se sont poursuivis sans interruption depuis trois ans. Le rayon de détection possible d'une cible conductrice de dimension rentable est d'au moins 75 m.

Le plan d'interprétation a été mis au point en utilisant deux méthodes. Pour les travaux courants, on utilise un système interactif informatisé fondé sur des graphiques et des calculs rapides et simplifiés. On a également mis au point un système d'interprétation plus détaillé qui décrit toutes les composantes et leurs phases en présence d'une surface infinie, d'un terrain stratifié et d'une hétérogénéité limitée enfouie.

[1] Boliden Mineral AB, S-936 00

[2] Institute of Theoretical Physics, S-412 96 Gothenburg, Sweden

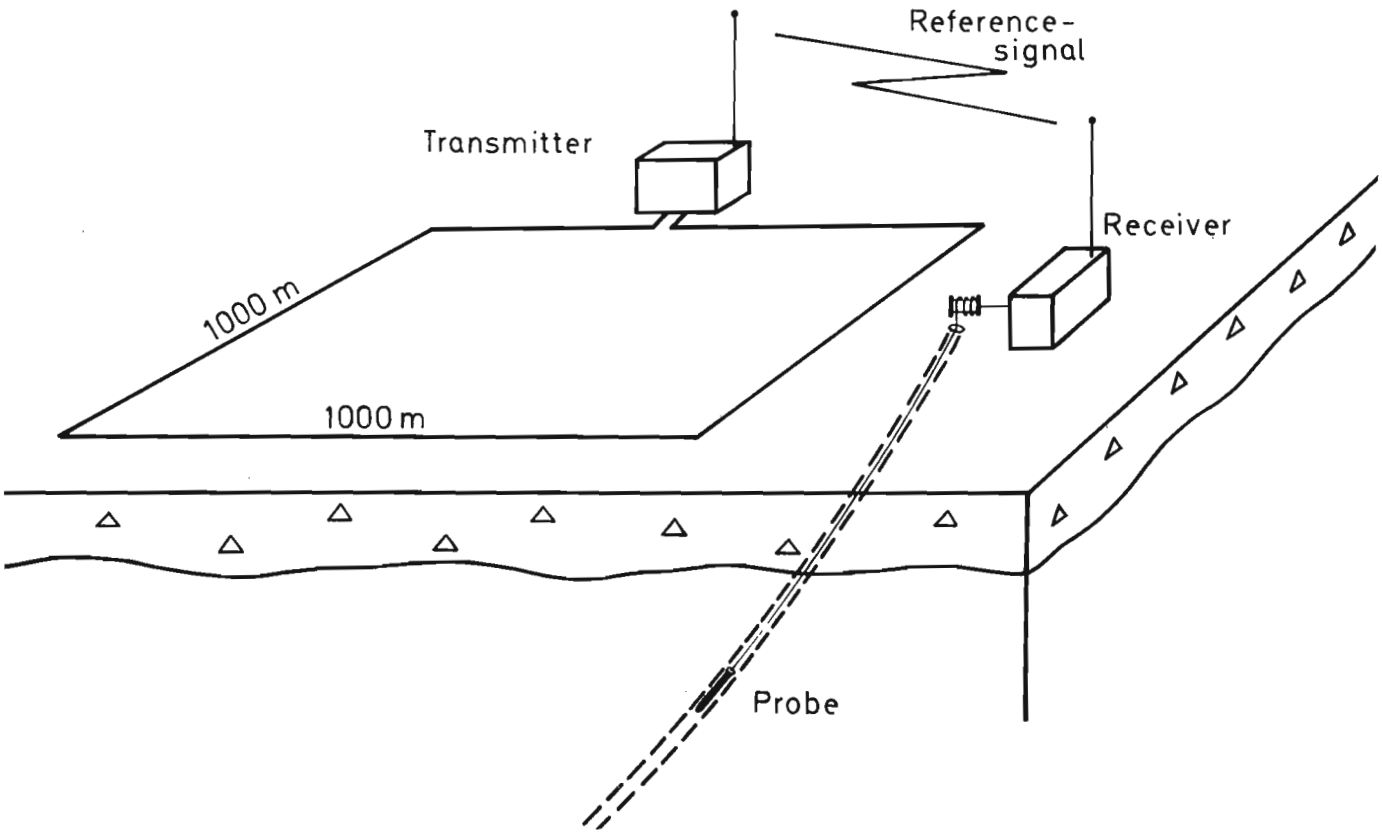

Figure 9.1. *A sketch of the system arrangement in a field application.*

Introduction

The exploitation of outcropping massive sulphide ore bodies is the basis for the 9 productive mines in the Skellefte field in northern Sweden. Exploration has been carried out during more than 60 years and probably the most important outcropping deposits have been found today. To maintain the ore reserves beyond the year 2000 we have to find some new deposits. Such deposits can probably be found at greater depth.

To access the deeper parts of an old mining district we have to improve the performance of the exploration technique and to a larger extent use expensive boreholes to gain new information. Geophysical borehole techniques therefore become of great importance (Malmqvist and Malmqvist, 1983).

The pyrite dominated massive sulphide ore bodies of the Skellefte field are generally steeply dipping and have a high conductivity (Rickard and Zweifel, 1975). Consequently, they are ideal targets for EM-techniques.

To gain new information from measurements in a borehole we specified, at the beginning of the work, the system to have an ability to locate a massive conductive sulphide deposit of economical size 50 to 100 m from

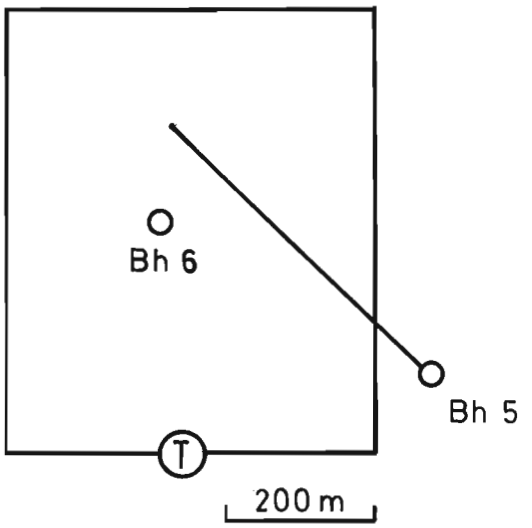

Figure 9.3. *Finnsjön area. The horizontal projection of the ground loop and the boreholes investigated.*

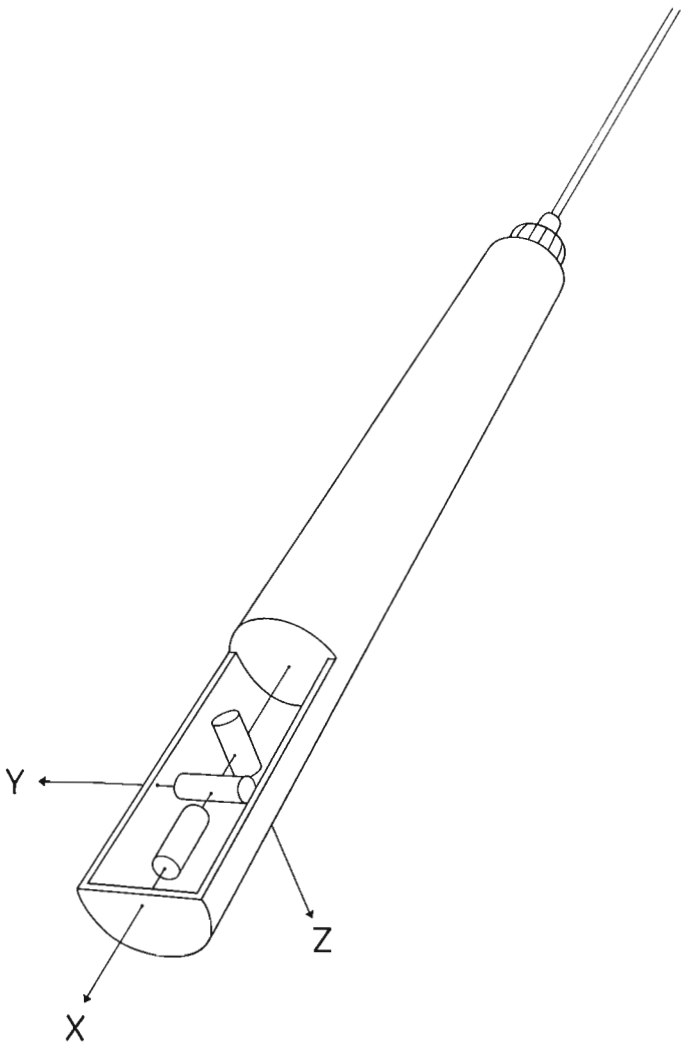

Figure 9.2. *The arrangement of the coils and the definition of the x-, y- and z-directions.*

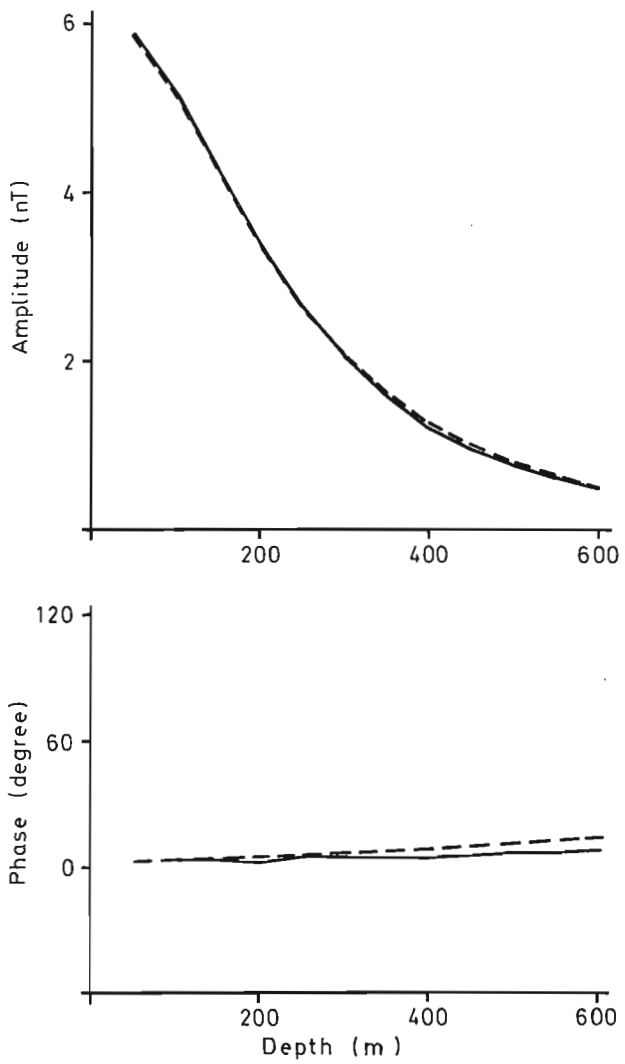

Figure 9.4. *Finnsjön Bh 6. A comparison between the theoretical model and the measured data for the x-component at 2000 Hz. The solid line represents the measured data and the broken line the theoretical model.*

the hole. We also wanted the system to have the ability to determine the attitude of the target, and the direction to the target from a single hole. We also required the system to be usable in an operating mine. By now, it has been operating for 3 years. In this paper we present a brief review of the system.

Equipment

The system basically consists of a large ground loop transmitter and a receiver registering the three perpendicular components of the magnetic field. A sketch of the system is given in Figure 9.1.

The transmitter can feed the loop with a 4 ampere alternating current. Its maximum power is 1000 W and it operates at two frequencies, 200 and 2000 Hz. A characteristic size of the transmitting ground loop is 1000 m X 1000 m.

The receiver measures the magnetic field in three perpendicular directions. The coils are placed within the 32 mm wide probe and form a righthanded co-ordinate system. One coil measuring the x-component is fixed with its axis parallel to the hole. The other two, y and z, are fixed on a gimbal mounted frame using gravity as a reference. In the system the y component is chosen to be horizontal (Fig. 9.2).

The coils are tuned to a bandwidth of 150 Hz. The signals from the three coils are preamplified and transmitted to the surface through a coaxial cable. A reference signal is transmitted to the receiver from the transmitter by a radio communication link. In the receiver, located on the ground, the signals are processed and the amplitude and phase for the three components are computed. To improve the signal to noise ratio the bandwidth of the detector is reduced to 1 Hz.

The accuracy of the instruments is of the order of ± 2% of the measured amplitude and ± 2 degrees in phase within the range 0.05-16 nT.

The data are recorded in the instrument. At the end of the day the data are transferred to floppy disk and sent to a central computer for processing. Together with information about the attitude of the borehole the measured components are transformed to a co-ordinate system suitable for presentation.

To be able to find low amplitude anomalies caused by distant targets, and to be able to interpret the information inherent in the phase measurements, a quite general theoretical model of the propagation of the electromagnetic field in the ground has been developed. Such calculations consume much computer time and are mainly used to guide the interpretation under specific circumstances. Therefore, a simplified model for the treatment of the borehole data is also applied. This procedure is much faster and allows interactive interpretation work. We have found it possible to use it in areas of well known bedrock properties. Examples will be given from both models.

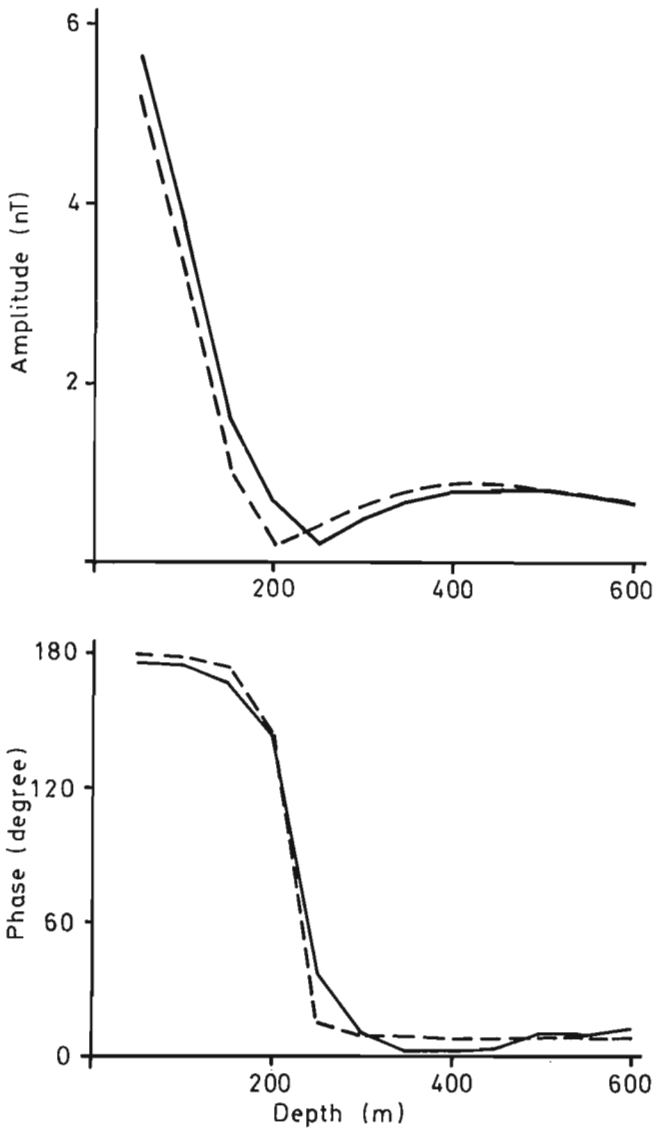

Figure 9.5. *Finnsjön Bh 5. A comparison between the theoretical model and the measured data for the x-component at 2000 Hz. The solid line represents the measured data and the broken line the theoretical model.*

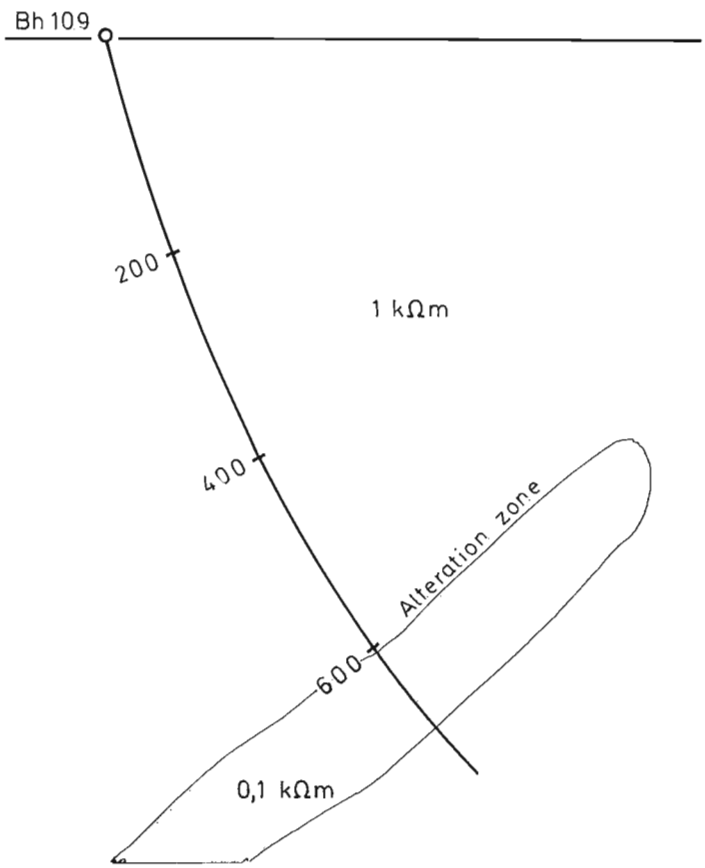

Figure 9.6. *Kankberg Bh 109. Vertical projection.*

Theoretical modelling

Consider a completely homogeneous space with dielectric constant ε, permeability μ and conductivity σ. A current density $\vec{j}(\vec{r})$ in a volume V will create a radiation field H. If we assume stationary time conditions with frequency f (a factor $e^{-i\omega t}$ is suppressed throughout the paper, $\omega = 2\pi f$) we have the following representation of the radiating magnetic field $\vec{H}(\vec{r})$ according to Kristensson, 1983:

$$\vec{H}(\vec{r}) = \iiint \vec{j}(\vec{r}') \times \nabla' \left[\frac{\exp(ik|\vec{r}-\vec{r}'|)}{4\pi|\vec{r}-\vec{r}'|} \right] dV' \qquad (1)$$

k is here the wave number defined by

$$k^2 = \varepsilon\mu\omega^2 + i\mu\sigma\omega \qquad (2)$$

The magnetic field $\vec{H}(\vec{r})$ in Equation (1) satisfies radiation conditions for large distances from the sources in V, i.e. the field $\vec{H}(\vec{r})$ is essentially an outgoing spherical wave e^{ikr}/r for large $r = (\vec{r})$. The boundary conditions are continuity of the horizontal or tangential electric and magnetic fields $\vec{E}$ and $\vec{H}$, respectively.

When introducing the ground as an interface the situation will become somewhat more complicated and by using Maxwell's equation (3) we obtain the following boundary condition (4)

$$\nabla \times \vec{H} = \vec{j} + \frac{\partial}{\partial t}(\varepsilon\vec{E}) = \frac{k^2}{i\mu\omega}\vec{E} \qquad (3)$$

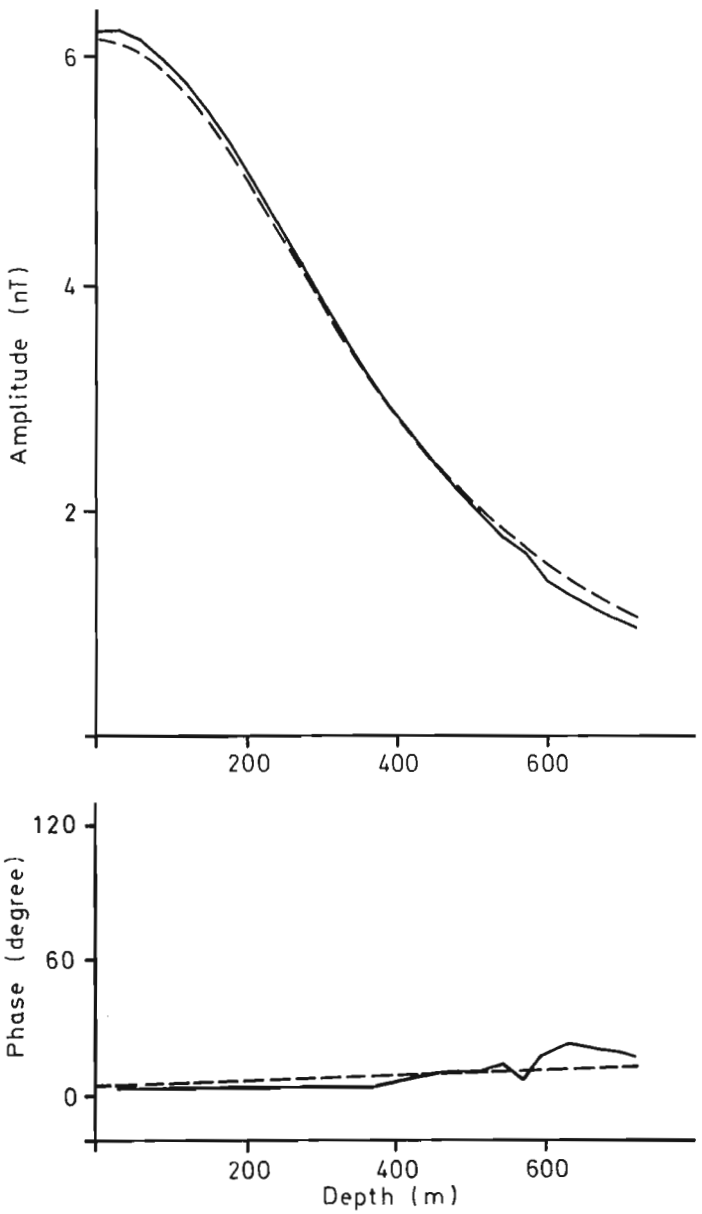

Figure 9.7. Kankberg Bh 109. A comparison between the theoretical model and the measured data for the x-component at 200 Hz. The solid line represents the measured data and the broken line the theoretical model.

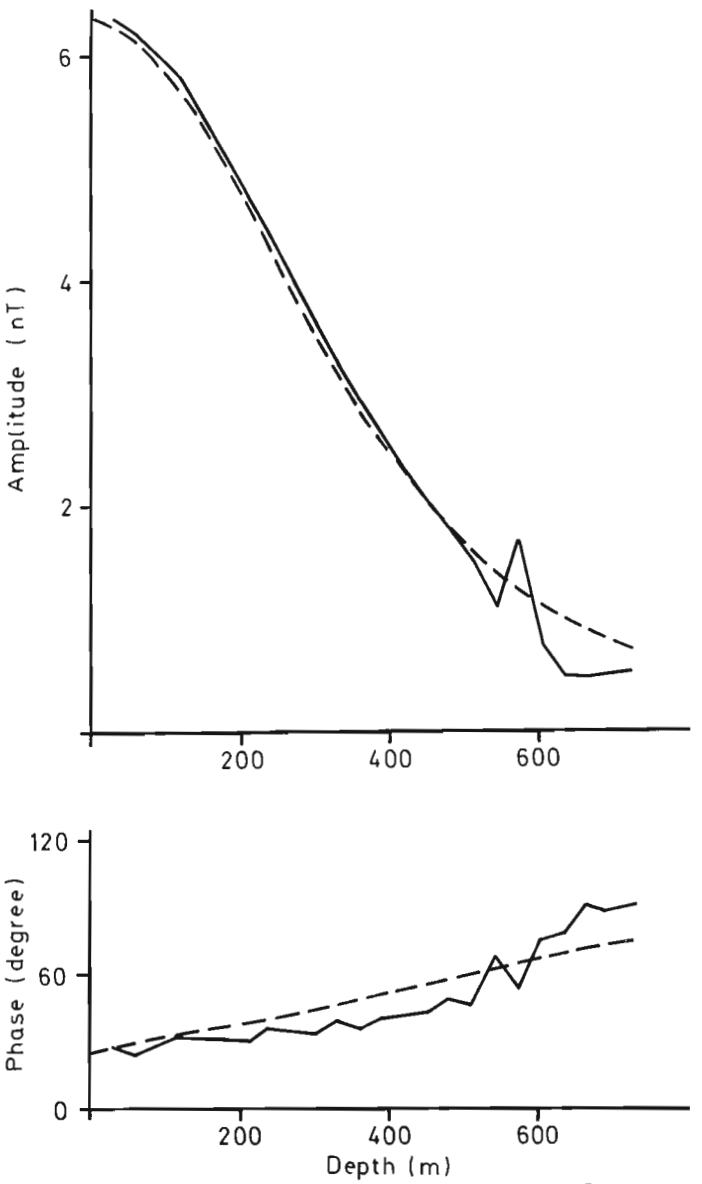

Figure 9.8. Kankberg Bh 109. A comparison between the theoretical model and the measured data for the x-component at 2000 Hz. The solid line represents the measured data and the broken line the theoretical model.

$$\left.\begin{array}{l}\hat{H}\times\hat{n}\\ \frac{\mu}{k^2}\,(\nabla\times\vec{H})\times\hat{n}\end{array}\right\}\ \text{continuous} \qquad (4)$$

n is here a normal vector to the interface.

On the other hand, if the source is a plane wave, generated outside V, the effect of the interface can be handled as a reflected and a transmitted part, such that the boundary conditions in Equation (4) are satisfied. The radiating magnetic field $\vec{H}$ in Equation (1) is decomposed in plane waves. The mathematical details are given by Kristensson (1983). In conclusion, we can write the field in Equation (1) as a superposition of plane waves, formally as

$$\vec{H}(\vec{r}) = \int h(\vec{k})\,\vec{\varphi}(\vec{k};\vec{r})\,d\vec{k} \qquad (5)$$

where $\vec{\phi}(k;r)$ are the plane vector waves and $h(\vec{k})$ is the amplitude for each plane vector wave.

The mathematical analysis soon becomes rather complicated and has to include such things as complex angles of propagation. The field represented in Equation (5) can now very easily be generalized to include the effect of an interface.

The effect of each plane wave i.e. $\vec{\phi}(\vec{k};\vec{r}$ upon reflection and transmission at the interface will simply be a multiplication by a reflection and a transmission coefficient, respectively. Thus, we get

$$\vec{H}(\vec{r}) = \int h(\vec{k})\left\{\begin{matrix}R(\vec{k})\\ T(\vec{k})\end{matrix}\right\}\vec{\varphi}(\vec{k};\vec{r})\,d\vec{k} \qquad (6)$$

for the reflected and the transmitted field, respectively.

The advantage of this formulation is that the amplitudes $h(\vec{k})$ in Equations (5) and (6) are the same functions. We have essentially

$$h(\vec{k}) = 2ik\iiint_V \vec{j}(\vec{r})\cdot\left(\nabla\times\vec{\varphi}(\vec{k};\vec{r})\right)dV \qquad (7)$$

This is a volume integral over the sources of the antenna. For a wire antenna this integral will reduce to a single integration. For some simple shapes of the wire loop e.g. magnetic dipole, horizontal circular and rectangular loops, the single integral can be evaluated exactly (Kristensson, 1983). The remaining step for the calculation of the total magnetic field, given by Equation (6), is the synthesis of the plane waves. For the wire antennas mentioned above (e.g. magnetic dipole, horizontal circular and rectangular loops) this synthesis eventually reduces to a single integration over an infinite interval.

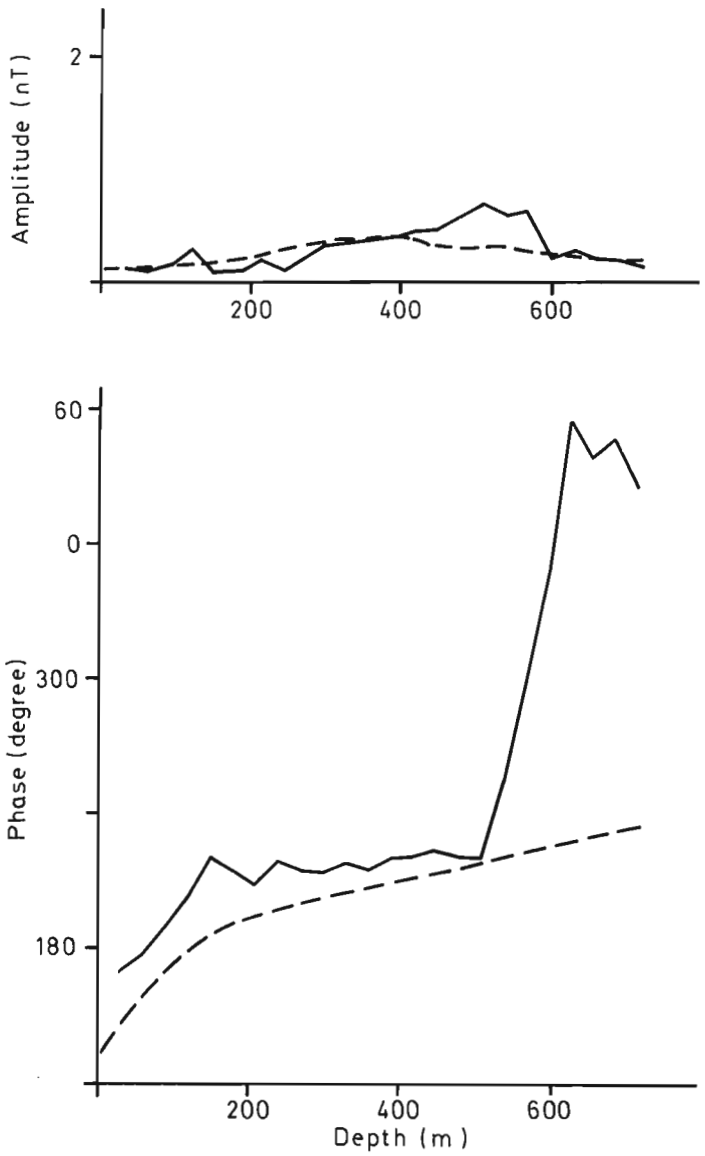

Figure 9.9. *Kankberg Bh 109. A comparison between the theoretical model and the measured data for the y-component at 2000 Hz. The solid line represents the measured data and the broken line the theoretical model.*

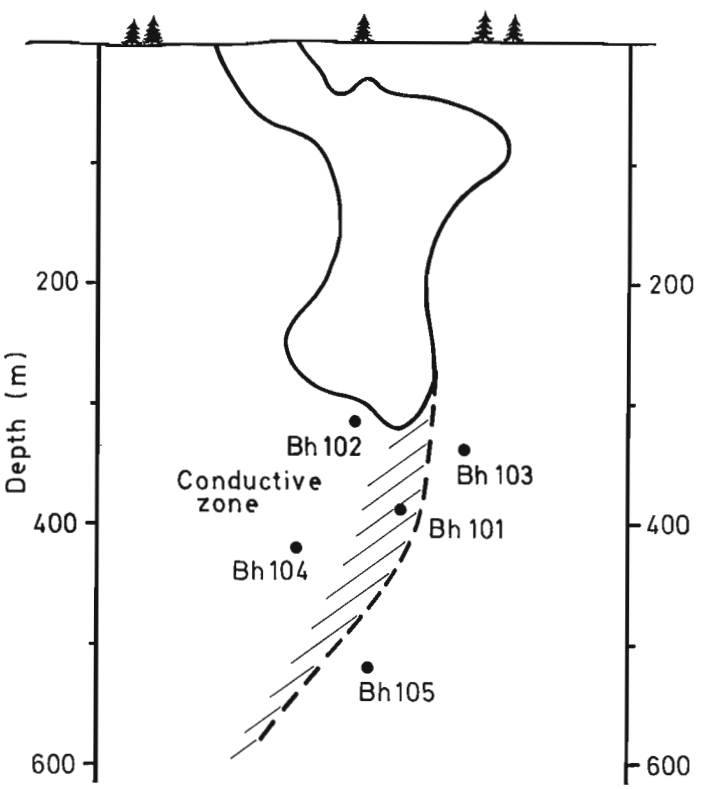

Figure 9.10. *Vertical projection of the Kankberg orebody and an interpretation of the conductive alteration zone. The points where the boreholes are intersecting or passing the mineralized zone are marked by dots.*

Calculation and tests of the model in a homogeneous half-space

The first step is to compare the measured fields and the theoretical model in a situation when the geology has a degree of homogeneity. We think these comparisons to be important to establish the modelling of the background as the basis for the shape and amplitude of any anomaly expressed as residuals. In the following we will give two examples.

In the Finnsjön area in central Sweden a number of holes, about 600 m deep, had been drilled in a large granitic body to investigate the rock properties as part of a program for nuclear waste disposal in geological formations (Fig. 9.3). The transmitting ground loop is placed almost symmetrically around the vertical borehole 6. In the figure a second hole, Bh 5, dipping about 50 degrees towards the edge of the loop, is also shown.

A comparison between the theoretical model of a homogeneous half-space and the measured data for the x-component from Bh 6 is shown in Fig. 9.4. The resistivity used in the model is 10 kΩ-m which corresponds to the mean value of the apparent resistivity recorded in a downhole Schlumberger survey (Öquist, 1981).

The agreement between the model and the measured data is almost perfect for both the amplitude and the phase. However, a small difference between the curves for the x-component in Bh 5 appears in Figure 9.5. It is probably caused by the small topographical irregularities. The irregularities in the area are of the order of 5-10 m. Nevertheless, the results show that the theoretical model can also handle the situation very close to the edge of the loop.

A second test in more conductive rocks was made in the Kankberg area where the acid volcanics have a typical apparent resistivity of 1 kΩ-m. Bh 109 is intersecting an alteration zone at a depth of 600 m with an apparent resistivity down to 0.1 kΩ-m (Fig. 9.6). In this case the transmitter is a square loop, 800 m x 800 m. At 200 Hz there is a good correspondence between the measured data and the theoretical calculation (Fig. 9.7). Using the higher frequency, 2000 Hz, the influence fromt the alteration zone, becomes, as expected, stronger (Fig. 9.8). The phase of the y-component fits reasonably well to the model in the first 500 m of the homogeneous bedrock, but it is shifted about 180° under the approach of the conductive zone (Fig. 9.9). This shift takes place along a 100 m section of the hole ahead of the conductive zone which probably reflects the increasing influence from the eddy currents in the conductor. Thus, measuring and modelling the phase give in this case additional information to the interpretation of the measured amplitudes.

Tests in areas with conductive targets

In another example from the Kankberg area, we have included a buried conductive target (Fig. 9.10). It is a massive sulphide body mainly composed of pyrite and pyrrhotite bearing traces of Cu, Zn and Pb. EM-measurements were carried out in exploratory holes no. 101-105 towards the deeper parts of the ore body.

Figure 9.10 shows a vertical projection of the ore and an interpretation of the conductive alteration zone based on geological and geophysical information. The points where the holes intersect or pass by the mineralized zone, are marked by dots in the figure.

In the following examples we have used a simplified model for the calculations, which allows us to work interactively with the computer.

A horizontal projection of the ore body and the boreholes intersecting the zone at the vertical depth of about 350 m is given in Figure 9.11. The vectors shown in the figure represent a horizontal projection of the residual field measured at 200 Hz.

In the vectorial representation the magnetic field induced by the eddy currents in the two conductive zones is clearly demonstrated in Bh 103 which misses the target by about 30 m. The superposition of the fields from the two current centres is also revealed.

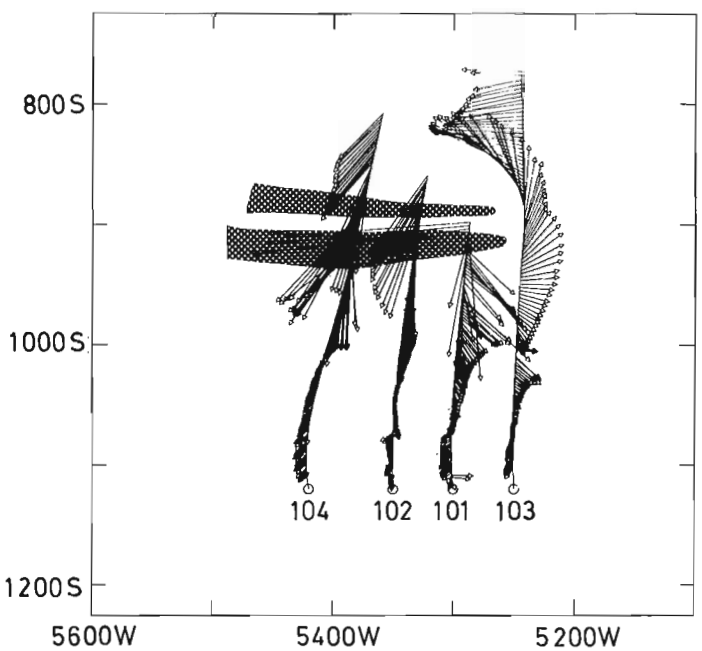

Figure 9.11. *Horizontal projection of the Kankberg orebody at about 350 level. The vectors are representing the in-phase residuals at 200 Hz.*

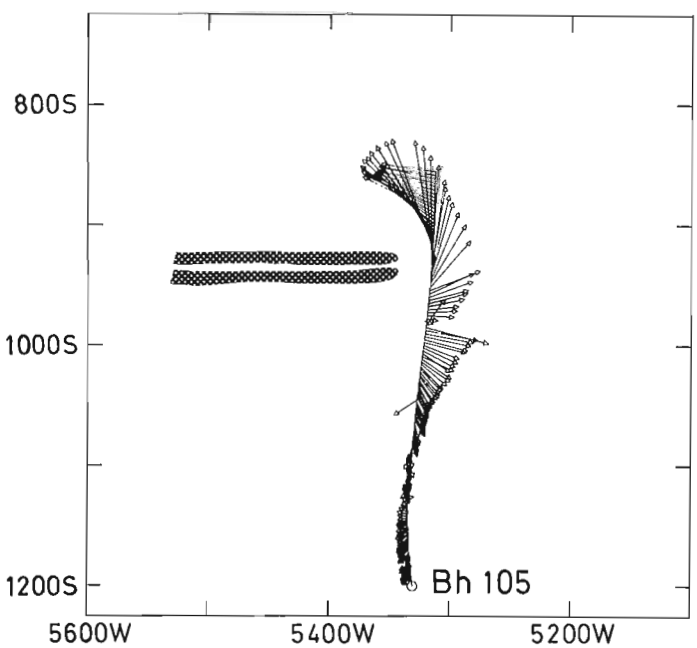

Figure 9.12. *Horizontal projection of the in-phase rediduals at 200 Hz in Kankberg Bh 105. The residuals are represented by vectors. The interpreted good conductors at about 500 m level are shaded.*

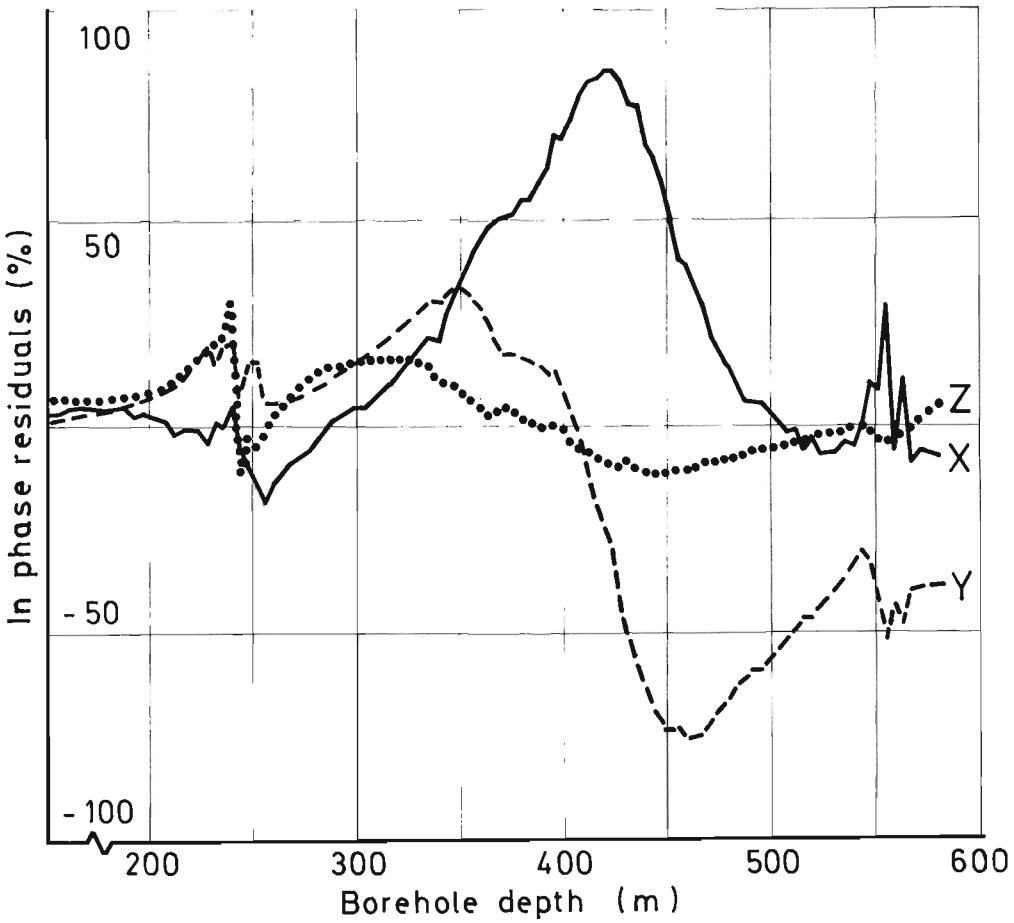

Figure 9.13

Kankberg Bh 103. In-phase residuals for the x-, y-, and z-component at 200 Hz.

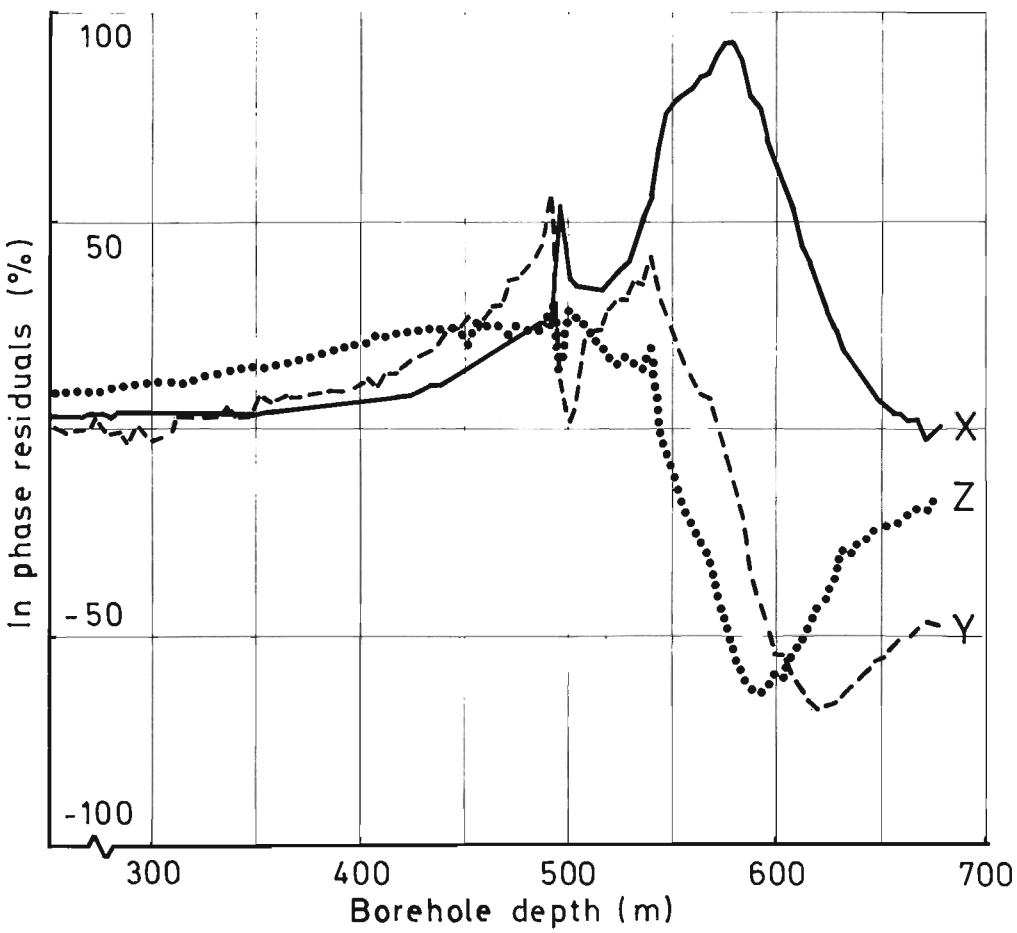

Figure 9.14

Kankberg Bh 105. In-phase residuals for the x-, y-, and z-component at 200 Hz.

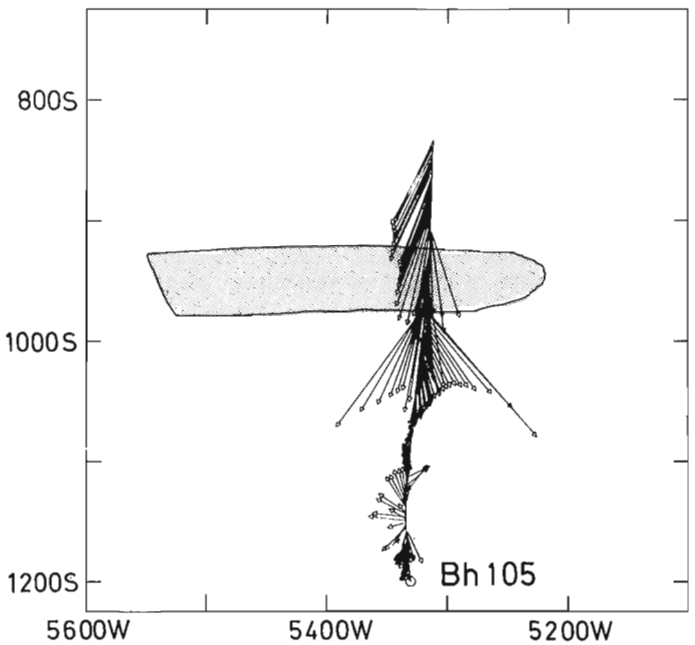

Figure 9.15. *Horizontal projection of the in-phase residuals at 2000 Hz in Kankberg Bh 105. The residuals are represented by vectors. The interpreted alteration zone is shaded.*

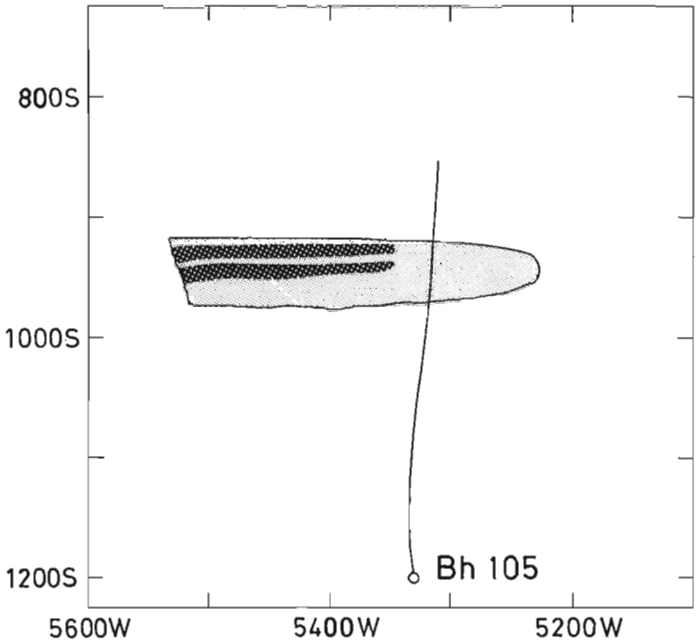

Figure 9.16. *Horizontal projection of the interpreted situation around Kankberg Bh 105. The alteration zone is shaded and the structures of high conductivity are black*

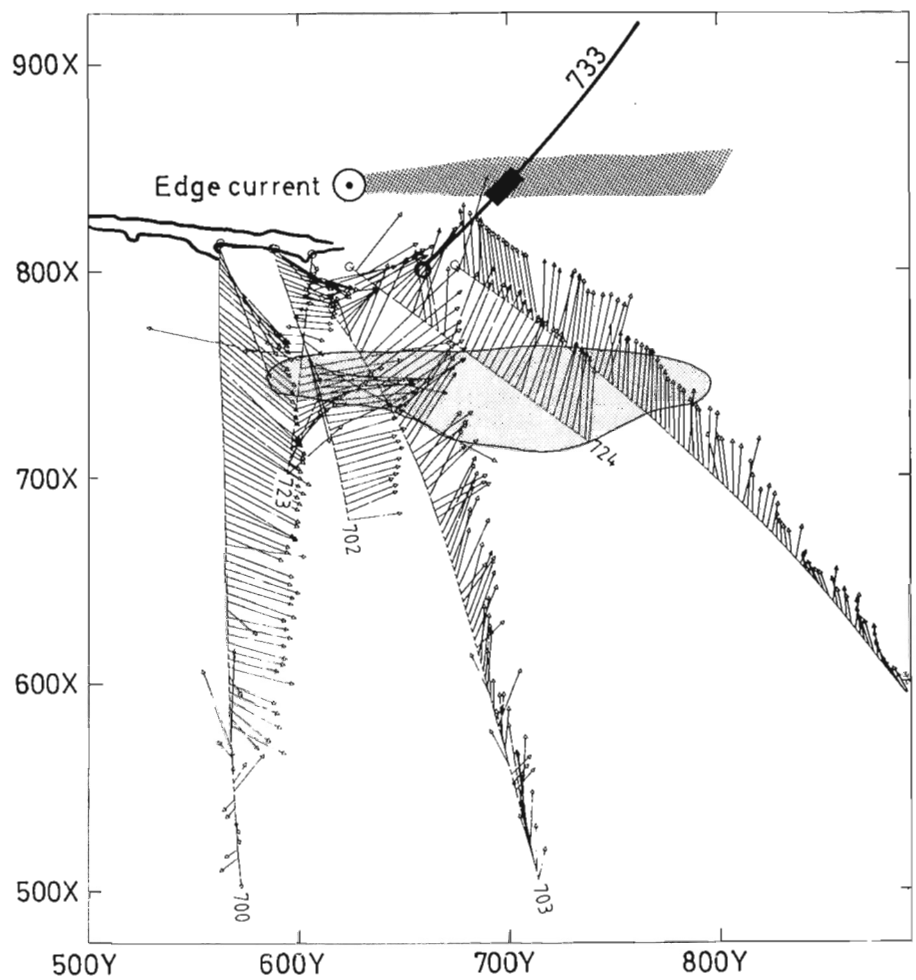

Figure 9.17. *Horizontal projection of the 610 m level in the Långsele mine. The vectors are representing in-phase EM-residuals at 2000 Hz. The lowest level of the orebody, coloured grey, is situated about 70 m above the measured boreholes. The interpreted conductive target is coloured black.*

The primary field imposed on the conductor is directed to the north. From the measurements in the holes intersecting the target the southerly directed secondary field is demonstrated. Superimposed on this is the influence from the eddy current in the eastern part of the target which reveals that Bh 104 still is situated in the eastern half of the target.

An even deeper intersection of the alteration zone at the vertical depth of 500 m is shown in Figure 9.12. The horizontal projections of the residual vectors show that Bh 105 passes east of the conductor. Here again the residual vector diagram indicates an unchanged situation with conductors.

These two situations are chosen also to demonstrate the information inherent in a simultaneous interpretion of the x, y and z-residuals. The residuals measured in Bh 103 are given in Figure 9.13. The y-residual is antisymmetric and it is zero at the point where the x-residuals have its maximum. The amplitude of the z-component is very small. This means that the direction of the eddy current is almost parallel to the z-direction in the borehole system giving the attitude of the edge of the conductor at the depth of 350 m.

By comparing the y- and z-residuals in Bh 105, at a depth of 500 m, it is seen that their peak-to-peak values are the same (Fig. 9.14). This means that the edge of the conductor is dipping about 45 degrees in the borehole system. The fact that both the y- and z-components have their positive peaks before the maximum of the x-component together with the relations in amplitude differences gives us an opportunity to locate the conductor. Thus, it is situated to the left of the hole and it is dipping about 45 degrees down to the left. The half peak width of the x-anomaly or the half distance between the positive and negative peak of the y-and z-components give us a rough estimation of the distance to the conductor from the hole to be approximately 30 m.

These results however were measured at a frequency of 200 Hz. Since the Kankberg ore body is surrounded by disseminated pyrite it is an interesting environment for showing the differences at the two frequencies of 200 and 2000 Hz and how these frequencies can give us information about the conductivity of the targets.

At the higher frequency the system will be more efficiently coupled to targets of lower conductivity than at a lower frequency. Figure 9.15 shows the corresponding residuals at 2000 Hz from Bh 105. At 2000 Hz the measurements show a southerly directed secondary field originating in the secondary currents in the target. This indicates that the borehole intersects the conductor, whereas the 200 Hz residuals indicate that the hole passes about 30 m to the right of the conductor (Fig. 9.12).

Considering the results from the two frequencies we may conclude that the borehole intersects the outer parts of a pyrite dissemination and that there is a much better conductor about 30 m to the west. Summarizing, we conclude that the most conductive part of the target is approximately perpendicular to the borehole and that it has a plunge of about 45° (Fig. 9.16).

As a final example we will show a situation which appeared when we measured a number of boreholes made under the known deposit of Långsele.

EM-measurements were carried out in five boreholes drilled from the 610 m level in the Långsele mine. The holes were drilled in order to investigate deeper parts of the ore body about 70 m below the deepest level of earlier investigations. None of the boreholes struck any ore. However, the results of the EM-measurements gave a very unexpected pattern of residual vectors shown in Figure 9.17. The source of this residual field was interpreted to lie behind the boreholes.

To check the anomaly Bh 733 was drilled. It showed that there were banks of massive pyrite altogether about 20 m thick.

Over the last 3 years of operation we have found the system to be useful in many situations. The possibility of determining the direction to and the attitude of conductive targets is of great importance for geological interpretation. In fact, it also reduces the number of expensive boreholes in our exploration work.

Acknowledgments

We are sincerely grateful to the Geophysical Laboratory and Dr. Bruno Nilsson for their skillful work with the equipment. We also thank the National Swedish Board for Technical Development for financial support.

References

Kristensson, G.
1983: The electromagnetic field in a layered earth induced by an arbitrary stationary current distribution; Radio Science, v. 18, p. 357-368.

Malmqvist, K. and Malmqvist, L.
1983: Simulation as a tool for planning of exploration for deep seated base metal deposits; European Journal of Operational Research, v. 14, p. 163-168.

Öquist, U.
1981: Electrical properties of a granitic pluton in the Finnsjön area – a comparison between borehole logging results and drillcore measurements. Part III in measurement of electrical properties of rocks and its application to geophysical investigations of ores and of waste disposals; Dissertation Royal Institute of Technology, Stockholm, Sweden 1981.

Rickard, D.T. and Zweifel, H.
1975: Genesis of Precambrian sulfide ores, Skellefte district, Sweden; Economic Geology, v. 70, p. 255-274.

10. INDUCTION LOGS APPLIED TO MINERAL EXPLORATION AND DEVELOPMENT

B. Frignet[1]

Frignet, B., Induction logs applied to mineral exploration and development; in Borehole Geophysics for Mining and Geotechnical Applications, ed. P.G. Killeen, Geological Survey of Canada, Paper 85-27, p. 89-100, 1986.

Abstract

Two induction probes ("ROMULUS" and "ERIC") have been developed for slimhole logging in mineral exploration. Both have fixed coaxial transmitter-receiver geometry and an external diameter of 40 mm. They may be operated in dry and plastic cased holes.

The ROMULUS probe operates at 4 kHz with a transmitter-receiver spacing of 0.85 m. The resulting low induction number permits "In phase" and "Quadrature" secondary fields to be related to magnetic susceptibility and electric conductivity, respectively. Penetration is about 1 m for conductivity, and several decimetres for susceptibility. Hole effect is negligible on both parameters. In sulphide exploration problems the method has proved effective in determining the conductivitv contrast between sulphides and surrounding rocks. Theoretical and experimental comparisons between induction and normal array resistivity logs have been made and indicate that induction is more reliable for determining conductances of intersected veins.

The ERIC probe has been designed for penetrating up to 10 m around the hole. It has three spacings (5, 10, 20 m), and an operating frequency of 1 kHz. The induction number is high enough that conductivity may affect both "Quadrature" and "In phase" secondary fields. Penetration is such that conductive bodies narrowly missed by the hole may be detected. As well the geometry of an intersected conductive target may be inferred.

Résumé

Deux sondes à induction "ROMULUS" et "ERIC" ont été développées pour la prospection dans les sondages miniers. Elles ont un diamètre de 40 mm, sont composées d'un émetteur et d'un récepteur co-axiaux et peuvent être utilisées en trou sec et tubé plastique.

La sonde "ROMULUS" opère à la fréquence de 4 kHz avec un espacement émetteur-récepteur de 0.85 m: le faible nombre d'induction qui en résulte permet de relier séparément la phase et la quadrature du champ magnétique secondaire à la susceptibilité magnétique et à la conductivité électrique des roches autour du forage. La pénétration est métrique en conductivité et pluri-décimétrique en susceptibilité; l'effet de trou est négligeable pour les diamètres courants. La technique s'est révélée efficace pour déterminer les conductances relatives des veines sulfurées et de leur encaissant. Des comparaisons théoriques et expérimentales entre les diagraphies de conductivité par induction et de résistivité avec le dispositif normal montrent que la sonde à induction est mieux adaptée à la détermination des conductances.

La sonde ERIC a été conçue pour l'investigation des dix premiers mètres autour du forage. Sa fréquence est de 1 kHz et des séparations émetteur-récepteur de 5, 10 et 20 m sont utilisées. Le nombre d'induction devient suffisamment élevé pour que la conductivité électrique affecte simultanément la phase et la quadrature du champ secondaire. La pénétration décamétrique apporte une information sur la géométrie de corps conducteurs recoupés par le forage et permet de détecter des cibles non intersectées.

Introduction

In principle, an induction probe is similar to loop-loop electromagnetic prospecting systems used in airborne or ground mineral surveys. Induction logging was introduced by Doll as an alternative to resistivity measurements (Doll, 1948). Induction tools are widely used in the oil industry, but their large diameter makes them impractical for mineral applications.

The ROMULUS and ERIC induction probes described in this paper have been developed for slimhole logging (40 mm in diameter). They are derived from a ground system used for electrical conductivity and magnetic susceptibility mapping in archeological investigations (Clerc and Frignet, 1982).

[1] Bureau de recherches géologiques et minières, Orléans, France

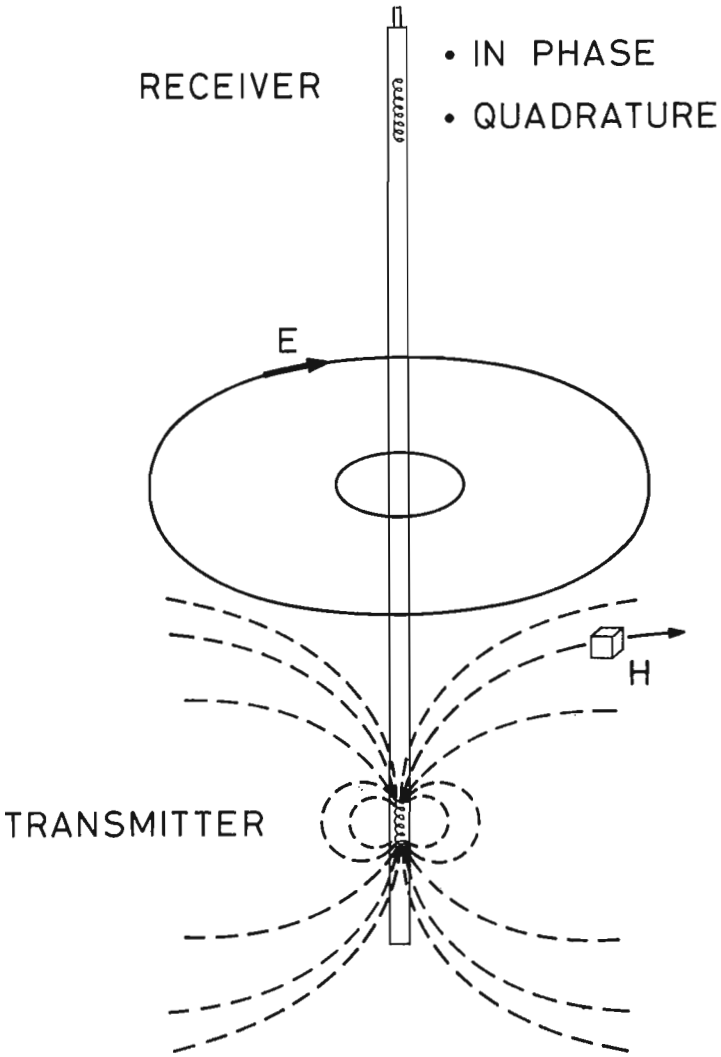

Figure 10.1. ROMULUS and ERIC induction probes are co-axial loop-loop EM systems. In-phase and Quadrature secondary field are detected at the receiver.

Table 10.1. Characteristics of ROMULUS and ERIC induction probes

Probe	ROMULUS	ERIC
Frequency	4 kHz	1 kHz
Spacing	0.85 m	5 m 10 m 20 m

Each probe is composed of a coaxial transmitter and receiver coils (Fig. 10.1). In the presence of magnetic or conductive rocks, the transmitter coil induces magnetic and electric fields in the rocks around the hole. These fields generate In-phase and Quadrature secondary magnetic fields at the receiver. ROMULUS has been designed for electrical conductivity and magnetic susceptibility logging within 1 m of the hole. ERIC has three different spacings to investigate conductive rocks up to 10 m from the hole. Their frequency and transmitter-receiver spacings are listed in Table 10.1.

Simplified theory of induction probes

Each probe may be approximated by a pair of coaxial dipoles, characterized by their half-spacing, L, and frequency, f or $\omega(\omega = 2\pi f)$.

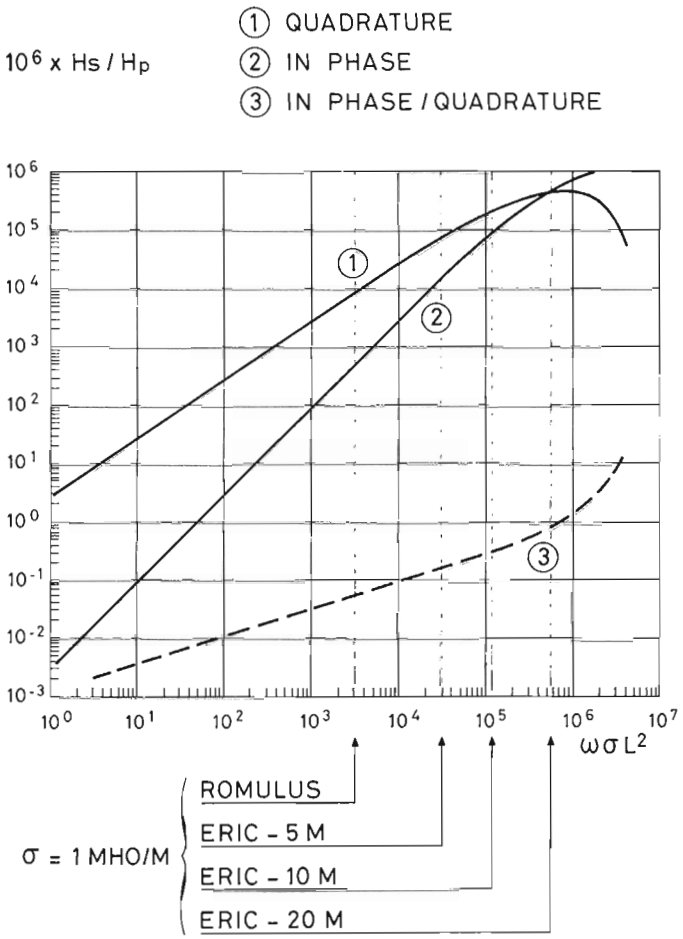

Figure 10.2. Response of conductive and nonmagnetic homogeneous earth to an induction probe (σ is conductivity of the earth, probe is characterized by its angular frequency, ω, and half-spacing, L. Hp and H_S are primary and secondary fields at the receiver).

In free space, the transmitter of magnetic moment, M, will generate a primary magnetic field Hp at the receiver:

$$Hp = \frac{M}{32L^3} \qquad (1)$$

In the presence of magnetic or conductive rocks, a secondary field H_S is produced. We shall describe its relationship to the magnetic susceptibility and electrical conductivity in simple cases.

Effect of conductive rocks

The theoretical response of an induction probe buried in a homogeneous, nonmagnetic conductive medium was first calculated by Duesterhoeft (1961) and is shown in Figure 10.2.

At low conductivities, the In-phase secondary field is negligible compared to the Quadrature field, which is proportional to conductivity. This is the "linear" or "small induction number" domain. Induced current flows along the electrical field lines, which are concentric circles perpendicular to the hole axis (Fig. 10.1); linearity of response expresses lack of mutual inductance between loops of induced current.

As conductivity increases, the In-phase secondary field reaches and ultimately dominates the Quadrature field, and linearity between conductivity and Quadrature field disappears. This is the "non-linear" or "large induction number" domain.

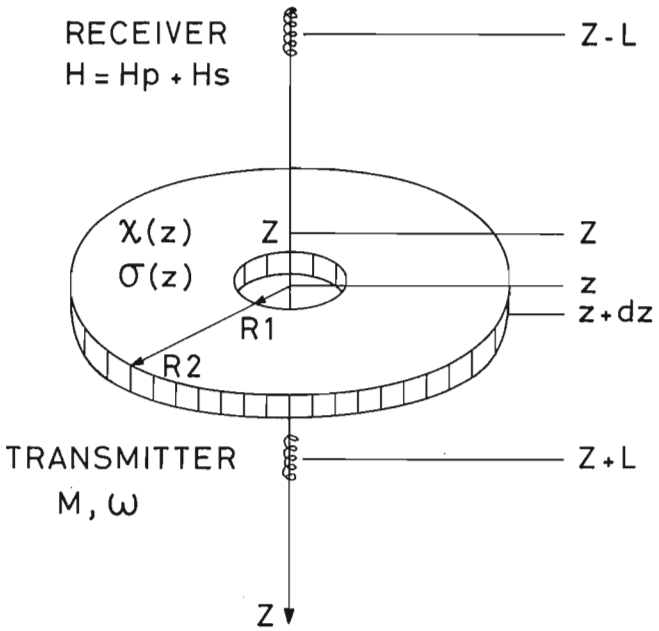

Figure 10.3. The earth is decomposed into a stack of thin discs at depth z characterized by electrical conductivity σ(z), magnetic susceptibility X(z), and internal and external radii R1 and R2. The probe centre, receiver and transmitter are at depth Z, Z-L, Z+L.

Responses for both probes are shown for a conductivity of one mho/m, which is representative of sulphide mineralization. ROMULUS clearly remains in the "linear domain" for conductivities up to 10 mho/m. In contrast, In-phase and Quadrature fields for ERIC differ by less than an order of magnitude at 1 mho/m, particularly for 10 m and 20 m spacings.

Effect of magnetic rocks

The Primary field, $\vec{H}$, generated around the probe by the transmitter within any elementary volume, dv, characterized by magnetic susceptibility, X, will induce an elementary magnetic moment, $d\vec{m} = X dv \vec{H}$, which itself generates secondary field, $d\vec{H}_s$, at the receiver. Provided that magnetic viscosity is very rarely encountered, X is real and the secondary field, H_s, at the receiver will be in phase with primary field Hp. When X is small enough ($<10^{-3}$ SI units, Parchas, personal communication, 1978), the mutual interaction between elementary induced magnetic moments is negligible, and $\vec{H}_s$ may be calculated by volume integration of $d\vec{H}_s$. The ROMULUS probe, which records the In-phase component, will measure the magnetic susceptibility of rocks around the probe, provided that there is no In-phase secondary field due to electrical conductivity.

Quantification

In order to calculate the response of an induction probe (specifically ROMULUS) to magnetic and conductive rocks, we shall make the following assumptions:

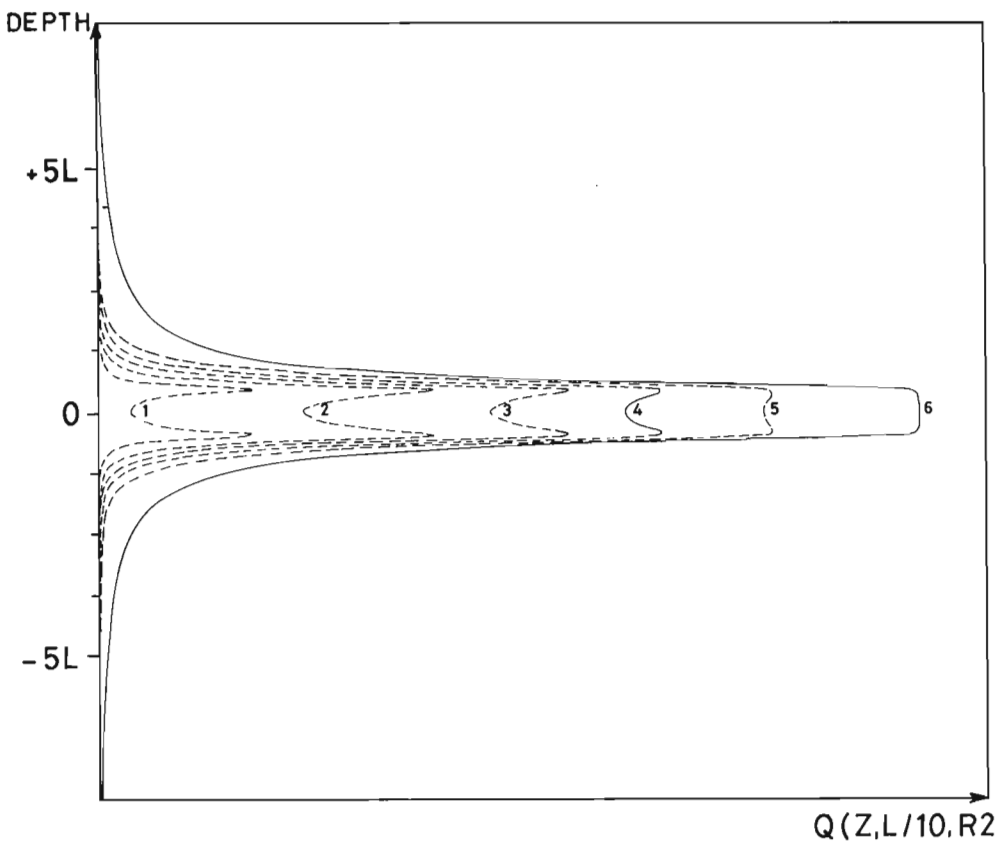

Figure 10.4. Quadrature response of a thin conductive disc of fixed internal radius (R1 = L/10) and variable external radius R2:

1: L/2
2: L
3: 1.5 L
4: 2 L
5: 2.5 L
6: 500 L

1) conductivity is low enough to be in the "low induction number" domain, and

2) susceptibility and conductivity are homogeneous along toroids perpendicular to the hole axis.

The space around the probe may be divided into a stack of elementary discs characterized by conductivity, $\sigma(z)$, susceptibility, $X(z)$, internal and external radii, R1 and R2 respectively (Fig. 10.3). With such a model, induced current lines will be coaxial with the electric field. The secondary field at the receiver has been expressed by Clerc and Frignet (1981) as a function of conductivity and susceptibility.

$$H_s(Z-L) = \int_{-\infty}^{+\infty} X(z)\,P(z-Z, R1, R2)\,dz + j\mu_0\omega \int_{-\infty}^{+\infty} \sigma(z)\,Q(z-Z, R1, R2)\,dz \quad (2)$$

(low induction number approximation)

with

$$P(Z, R1, R2) = \frac{M}{8\pi}\int_{R1}^{R2} \frac{\left[2(L+Z)^2 - R^2\right]\left[2(L-Z)^2 - R^2\right] - 9R^2(L^2 - Z^2)}{\left[R^2 + (Z+L)^2\right]^{5/2}\left[R^2 + (Z-L)^2\right]^{5/2}}\,dR \quad (3)$$

$$Q(Z, R1, R2) = \frac{M}{8\pi}\int_{R1}^{R2} \frac{R^3}{\left[R^2 + (Z+L)^2\right]^{3/2}\left[R^2 + (Z-L)^2\right]^{3/2}}\,dR \quad (4)$$

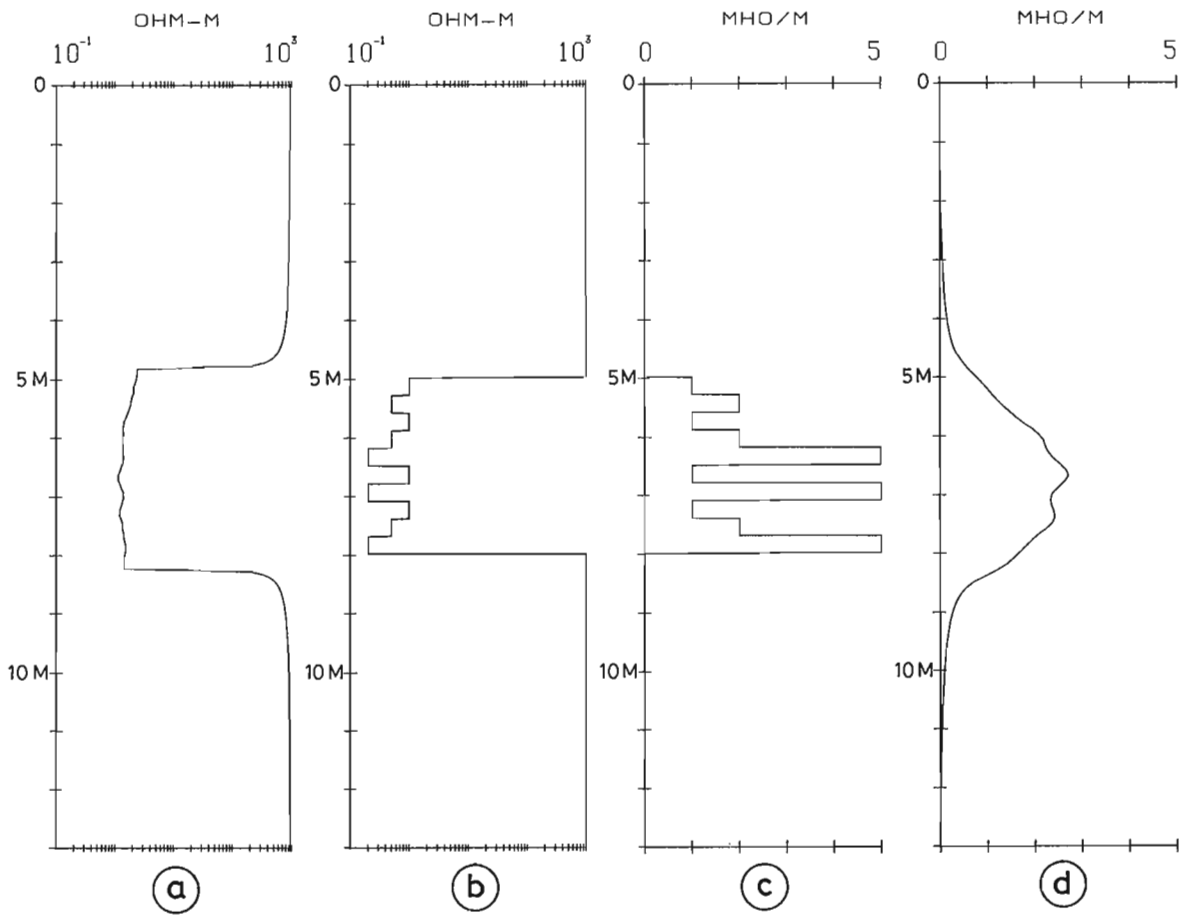

Figure 10.5. *Simulation of ROMULUS and normal array electrical probe responses to a complex, conductive stratified model:*

a - 16 inch synthetic normal resistivity log
b - stratified model (resistivity)
c - stratified model (conductivity)
d - ROMULUS quadrature synthetic log

P and Q functions are the In-phase and Quadrature responses of the probe to a thin magnetic and conductive disc, respectively. Both are analytic expressions and possess even symmetry in Z (Clerc and Frignet, 1981). Equation (2) expresses the secondary field at the receiver as a correlation (or convolution) product of the vertical susceptibility (or conductivity) distribution by the instrumental filter P (or Q).

Figure 10.4 shows the Quadrature response of an induction probe to a thin conductive disc of varying external radius R2 when R1 is equal to the hole radius.

Homogeneous conductive or magnetic earth

In the case of a homogeneous conductive earth, we have R1 = 0 and R2 = ∞. Equation (2) reduces to:

$$H_s = j\,\mu_0\omega\sigma\int_{-\infty}^{+\infty} Q\,(z, 0, \infty)\,dz \qquad (5)$$

which may be analytically integrated:

$$H_s = j\,\mu_0\omega\sigma\,\frac{M}{8\pi L} \qquad (6)$$

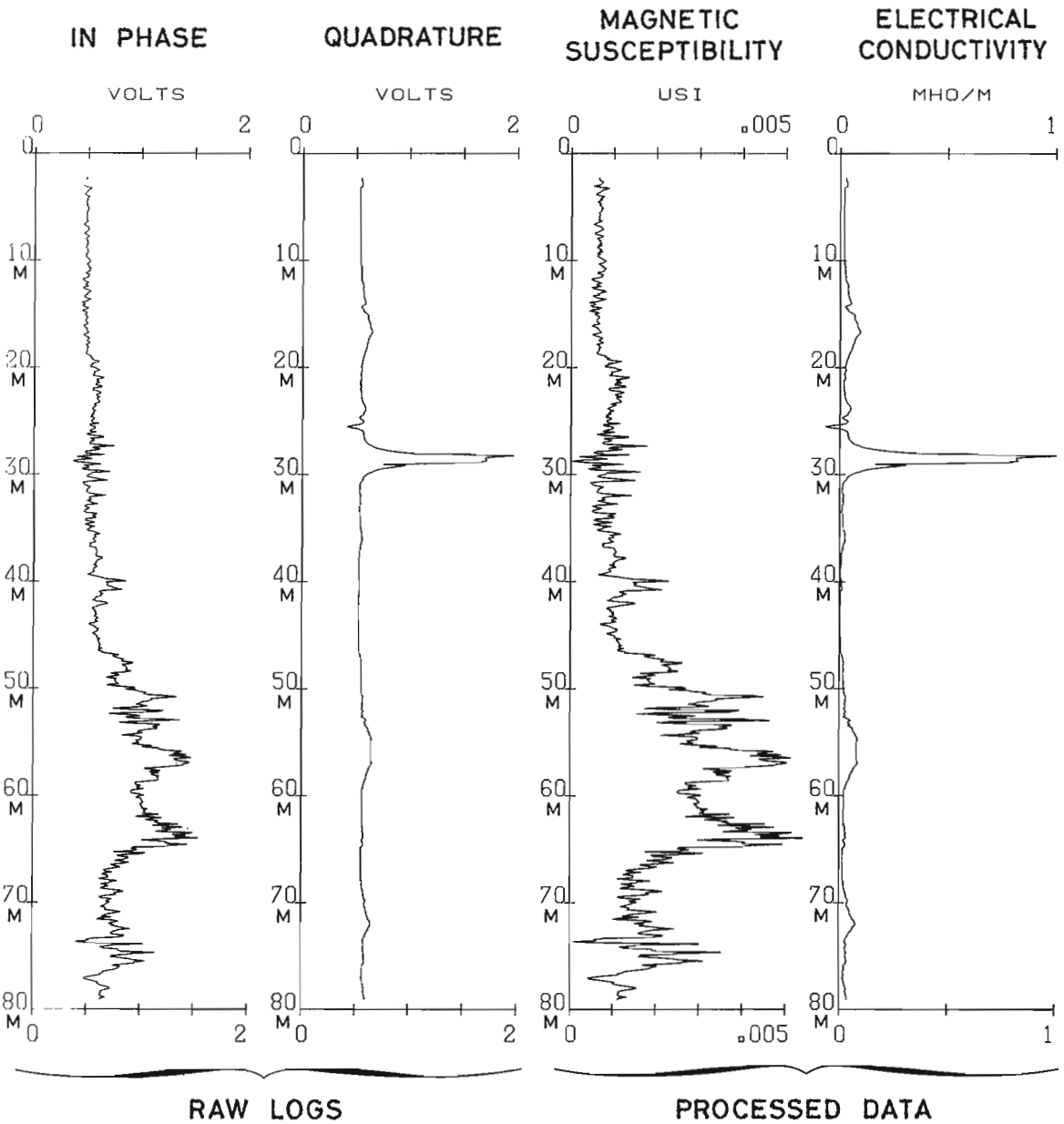

Figure 10.6. *Example of a ROMULUS data set: In-phase and Quadrature raw logs are corrected for offset and thermal drift, and converted to magnetic susceptibility and electrical conductivity.*

From equations (6) and (1), we deduce:

$$\sigma = \frac{1}{2\mu_0 \omega L^2} \frac{\text{Imag}(H_s)}{Hp} \qquad (7)$$

Equations (5), (6), (7) express the relationships previously observed in Figure 10.2 in the "linear domain".

In the case of a homogeneous magnetic earth, no analytic expression has been founded. It is not possible to take R1 = 0 because of a numerical singularity. We approximated the homogeneous earth intersected by a hole by a cylinder having a height of 10 L, an external diameter of 1000 L and a hole diameter of L/5. Numerical integration was performed with a vertical step of L/50 giving:

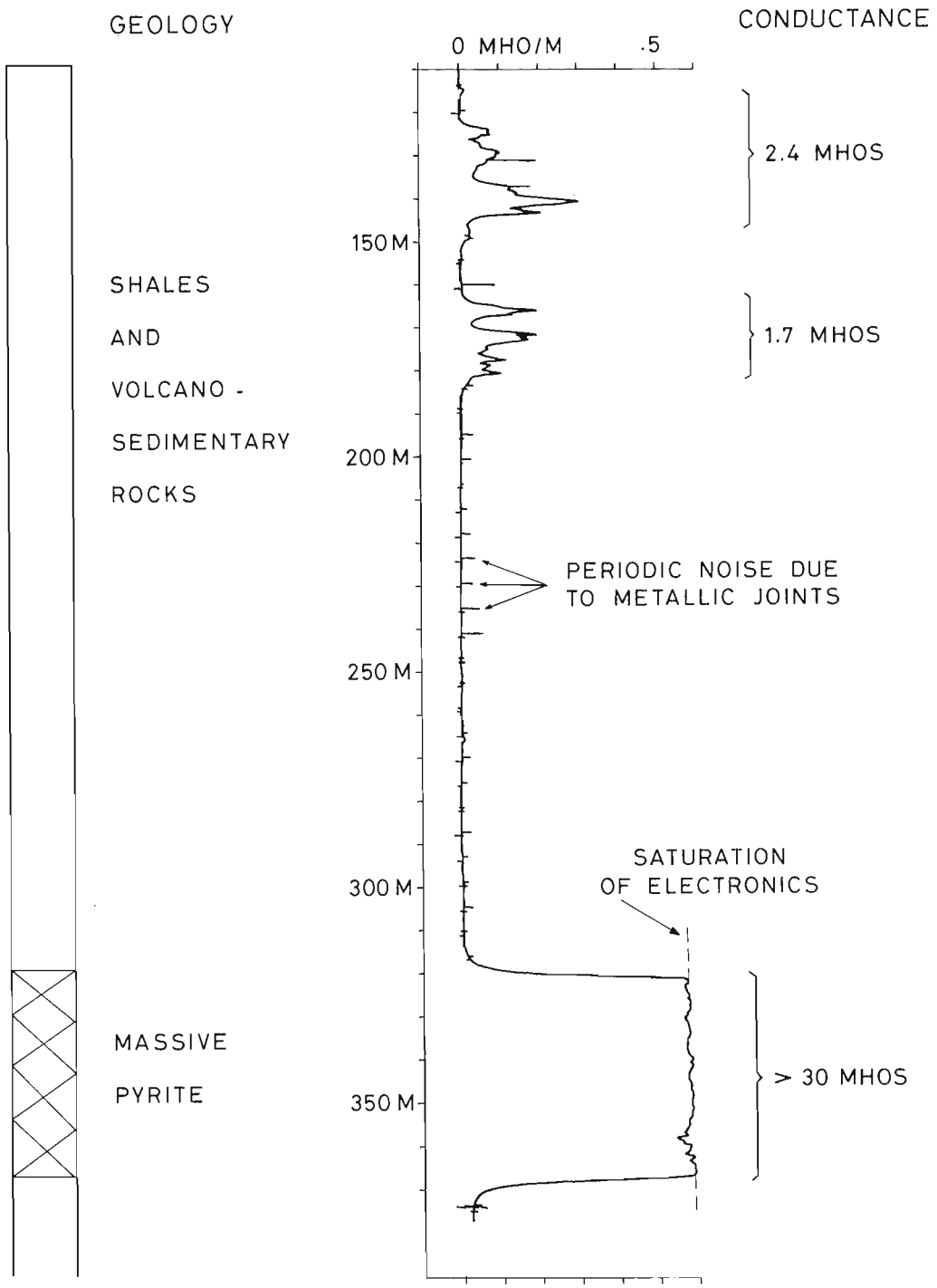

Figure 10.7. *Example of ROMULUS conductivity log in hole 1 intersecting a thick massive pyrite zone surrounded by volcano-sedimentary cover. Conductance contrast between mineralization (> 30 mhos) and graphitic shales (2.4 mhos, 1.7 mhos) suggests that remote detection of the ore body by EM or resistivity techniques is possible from the surface.*

$$H_s = X \int_{-5L}^{5L} P(z, L/10, 500\,L)\, dz \qquad (8)$$

from which we obtain:

$$X = 0.52 \frac{\text{Real}\,(H_s)}{Hp} \qquad (9)$$

Equations (7) and (9) are used to compute apparent magnetic susceptibility Xa and electrical conductivity σa from the secondary magnetic field.

Conductance evaluation of a stratified earth

Taking R1 = 0 and R2 = ∞ in equation (2), we get the probe response to stratified earth expressed in term of apparent conductivity:

$$\sigma a\,(Z) = \frac{8\pi\,L}{M} \int_{-\infty}^{+\infty} \sigma(z)\, Q\,(z - Z, 0, \infty)\, dz$$

If we integrate this apparent conductivity in Z, we see that apparent conductivity calculated from an induction probe is equal to true conductance of the stratification:

$$\int_{-\infty}^{+\infty} \sigma a(Z) dZ = \frac{8\pi L}{M} \int_{-\infty}^{+\infty} dZ \int_{-\infty}^{+\infty} \sigma(z)\, Q(z - Z, 0, \infty) dz$$

$$= \frac{8\pi L}{M} \int_{-\infty}^{+\infty} \sigma\,(z) dz \int_{-\infty}^{+\infty} Q(z - Z, 0, \infty) dz$$

$$= \int_{-\infty}^{+\infty} \sigma(z) dz$$

This property is particularly important in the presence of thin conductive layers. Their contribution to conductance will be fully taken into account, even though they are not individually resolvable by the probe.

The example in Figure 10.5 illustrates this. A layered model composed of an irregularly conductive zone bordered by resistive layers simulates heterogeneous mineralization of 7.5 mhos in conductance (integrated conductance). The simulated response of the ROMULUS probe is a smoothed anomaly with no resolution of individual layers. However, the exact conductance of the mineralization is easily determined by integration of the conductivity log. The same model, converted to resistivity, was used to simulate a 16-inch normal resistivity probe response (Straub, personal communication). The conductive zone appears without resolution of individual beds, because they are thinner than the probe spacing. The integrated conductance from the latter method is 2.4 mhos, which is only one third of the true value.

Lateral penetration

Integration of the P and Q functions allow us to calculate the contribution of rocks at different distances from the hole to the secondary field. For the In-phase component, 75% of the signal comes from the region R<L, and for the Quadrature component, 70% of the signal originates from R<3L. It shows that ROMULUS radius of investigation is no greater than 1 m, whereas ERIC penetrates to more than 10 m around the hole. Hole effect is negligible when hole diameter is less than 20% of probe spacing.

Operation of the probes

ROMULUS is a single sonde while ERIC is composed of two sondes (transmitter and receiver) linked by 5, 10 and 20 m jumpers. Both are 40 mm in diameter and used with standard armored four-conductor cable. Two conductors supply power from the surface, while the other two transmit DC signals proportional to In-phase and Quadrature secondary field. Primary field is compensated within the probe. A micro-computer monitors data acquisition, storage and plotting. One practical advantage of induction probes is that they can be used in water or air filled holes, either plastic cased or uncased. Operational logging speed is 6 m per minute.

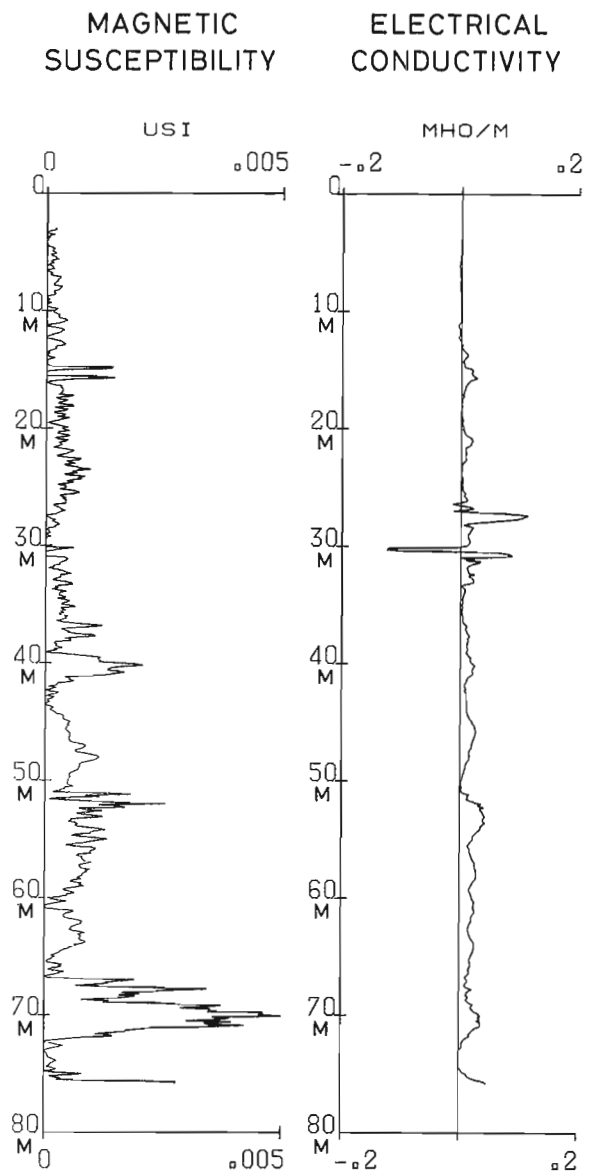

Figure 10.8. Example of ROMULUS logs in mineralized volcano-sedimentary rocks in hole 2. Sulphide zone at 30 m is moderately conductive but not magnetic. Surrounding rocks are locally magnetic (due to pyrrhotite), and do not correlate with the conductive mineralization.

Temperature variations have a slight effect on the probe electronics, generating zero offset and weak drift for both In-phase and Quadrature. Provided that the probe is at thermal equilibrium at the bottom of the hole, drift becomes linear with depth and may be removed. Processing of data includes offset and drift removal, and conversion of voltages to conductivity or susceptibility. An example of raw and converted ROMULUS logs is presented in Figure 10.6.

Field cases

Experimentation with ROMULUS

Hole 1 intersected thick mineralization (315-375 m) under volcano-sedimentary cover. It was logged with ROMULUS and the conductivity log is presented in Figure 10.7. Metallic joints between the plastic pipes created low amplitude periodic noise. Several conductive

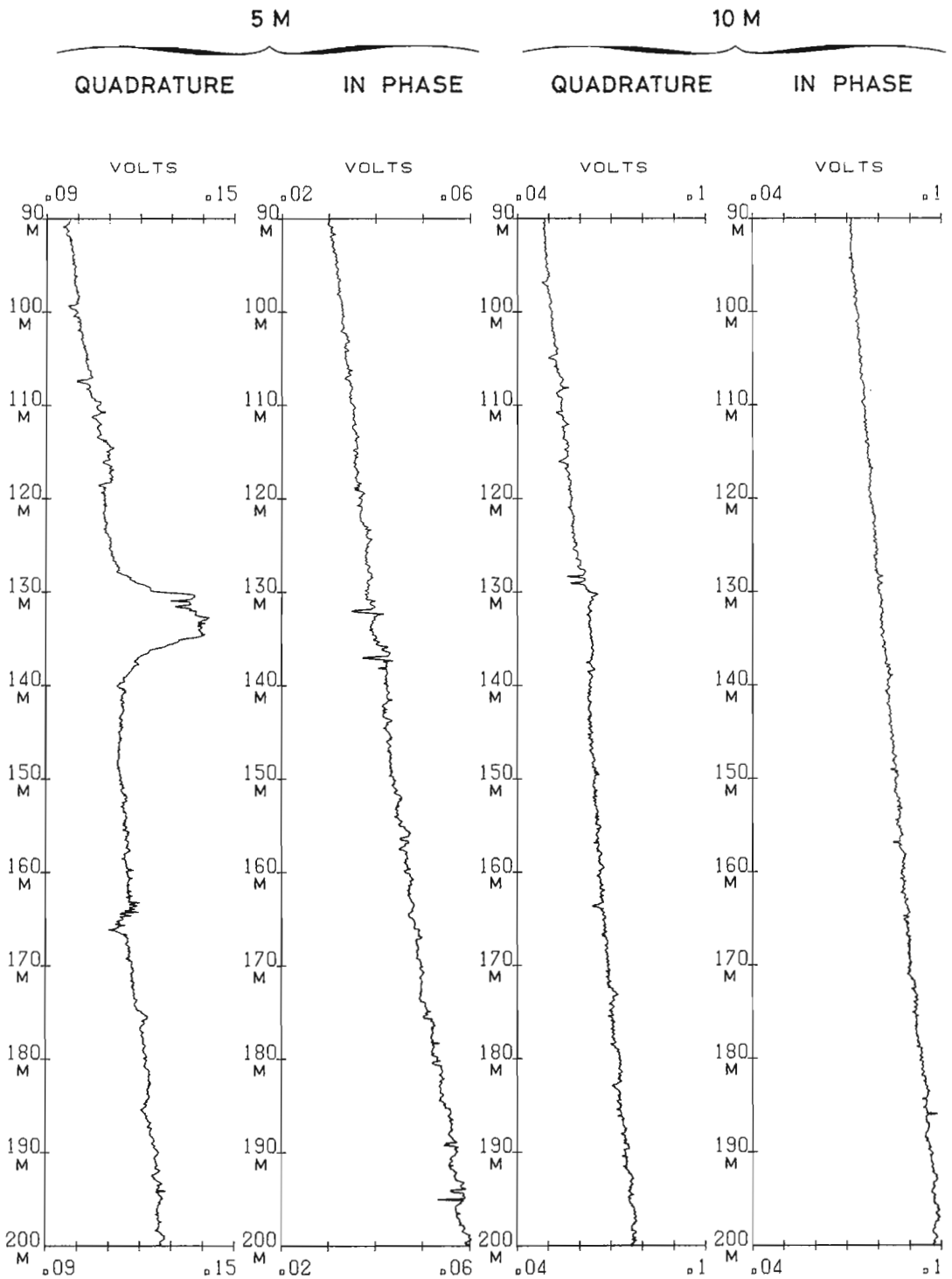

Figure 10.9. *Example of ERIC raw logs in hole 3 with 5 m and 10 m spacings. Linear offset with depth is due to temperature variations. The In-phase signal is below the noise level showing that the conductivity is low enough to stay within "low induction number" domain.*

zones appear in the surrounding rocks and correspond to graphitic shales. Their conductance (integrated conductance) is less than 5 mhos. Unfortunately, the probe saturated within the pyrite zone so that only minimum conductance (30 mhos) could be evaluated for the mineralization. These data were used to model an EM surface survey, which has shown that the encountered conductivity contrast is high enough to allow detection of the mineralization from the surface.

Hole 2 was drilled through volcano-sedimentary shales and sandstone. Interbedded massive sulphide layers contain economic mineralization. Pyrite and pyrrhotite are irregularly disseminated within the shales. ROMULUS logs in Figure 10.8 show the magnetic susceptibility and electrical conductivity distribution along hole. Both conductive zones at 28 and 30-31 m correspond to mineralized beds; their conductivity contrast with surrounding rocks is moderate, making their detection from the surface difficult. The negative conductivity at 30 m (associated with the positive at 31 m) is due to a geometrical artifact: the earth is not horizontally stratified and a negative anomaly indicates that the detected conductor has one boundary close to the hole and dips. (Due to transmitter-receiver symmetry, any conductor perpendicular to the hole would generate a symmetric anomaly). The magnetic susceptibility log shows that magnetic rocks are not correlated with economic mineralization. Surface magnetic and EM surveys over this area have provided a complex pattern of uncorrelated magnetic and conductive anomalies. Logging data confirm

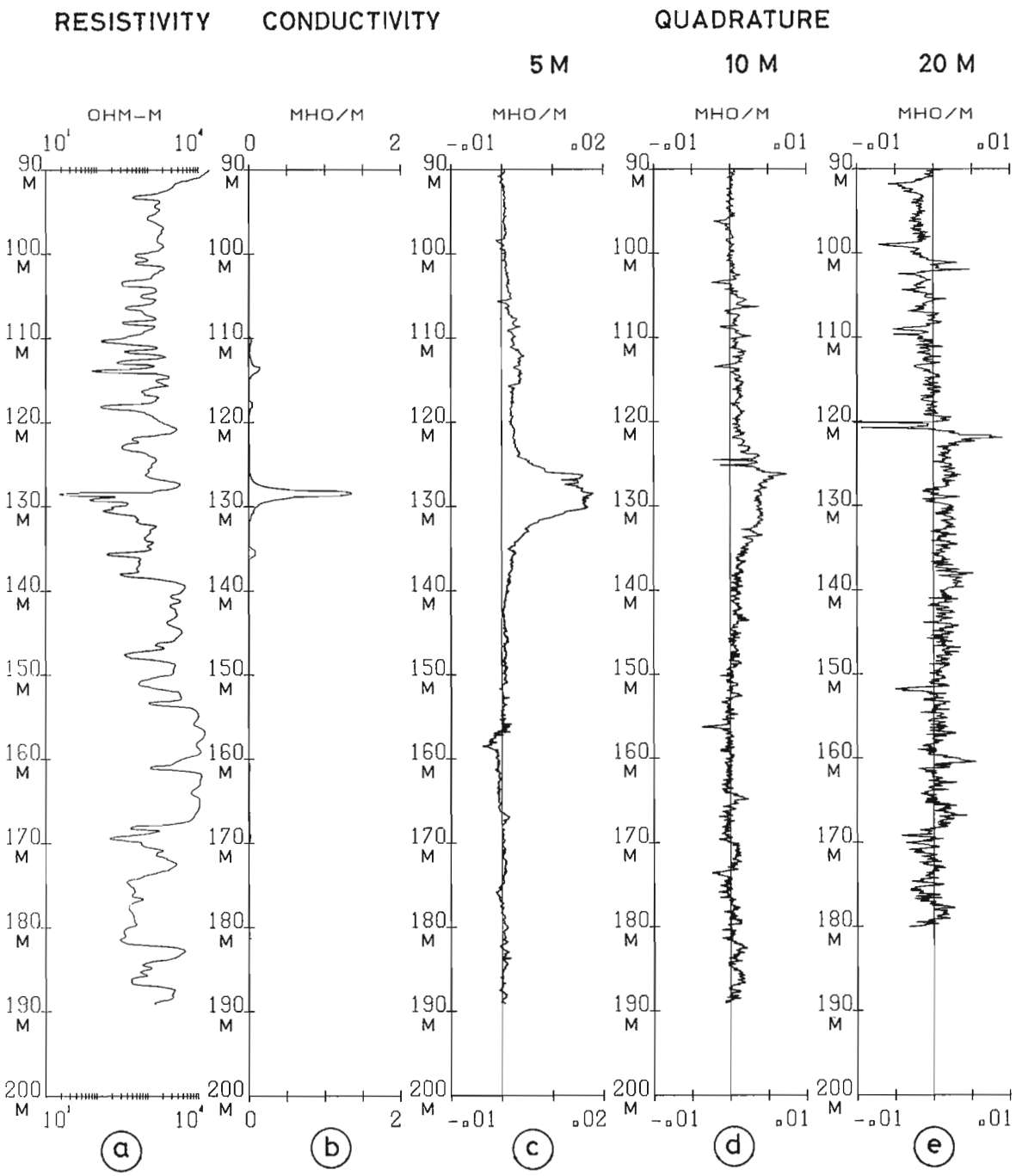

Figure 10.10. *16-inch normal resistivity (a), ROMULUS conductivity (b) and ERIC quadrature logs (c, d, e) in hole 3. Conductive anomaly at 130 m disappears with ERIC 10 m and 20 m spacings.*

this poor correlation; they further indicate that in the search for mineralized extensions, priority should be given to the drilling of EM targets.

Combined use of ROMULUS and ERIC

We have shown that the In-phase component of ERIC may be affected by both magnetic susceptibility and electrical conductivity. Here, we shall limit ourself to field cases where the In-phase to Quadrature ratio is small enough that the Quadrature is in the "linear domain". This situation has been encountered in many areas.

A raw set of ERIC Logs (5 and 10 m spacing) in hole 3 is presented in Figure 10.9. The Quadrature anomaly at 130 m has a negligible In-phase counterpart. The anomalies have very low amplitude and instrumental drift due to temperature variation is clearly visible. Processed ERIC Quadrature logs (converted to apparent conductivity) are presented in

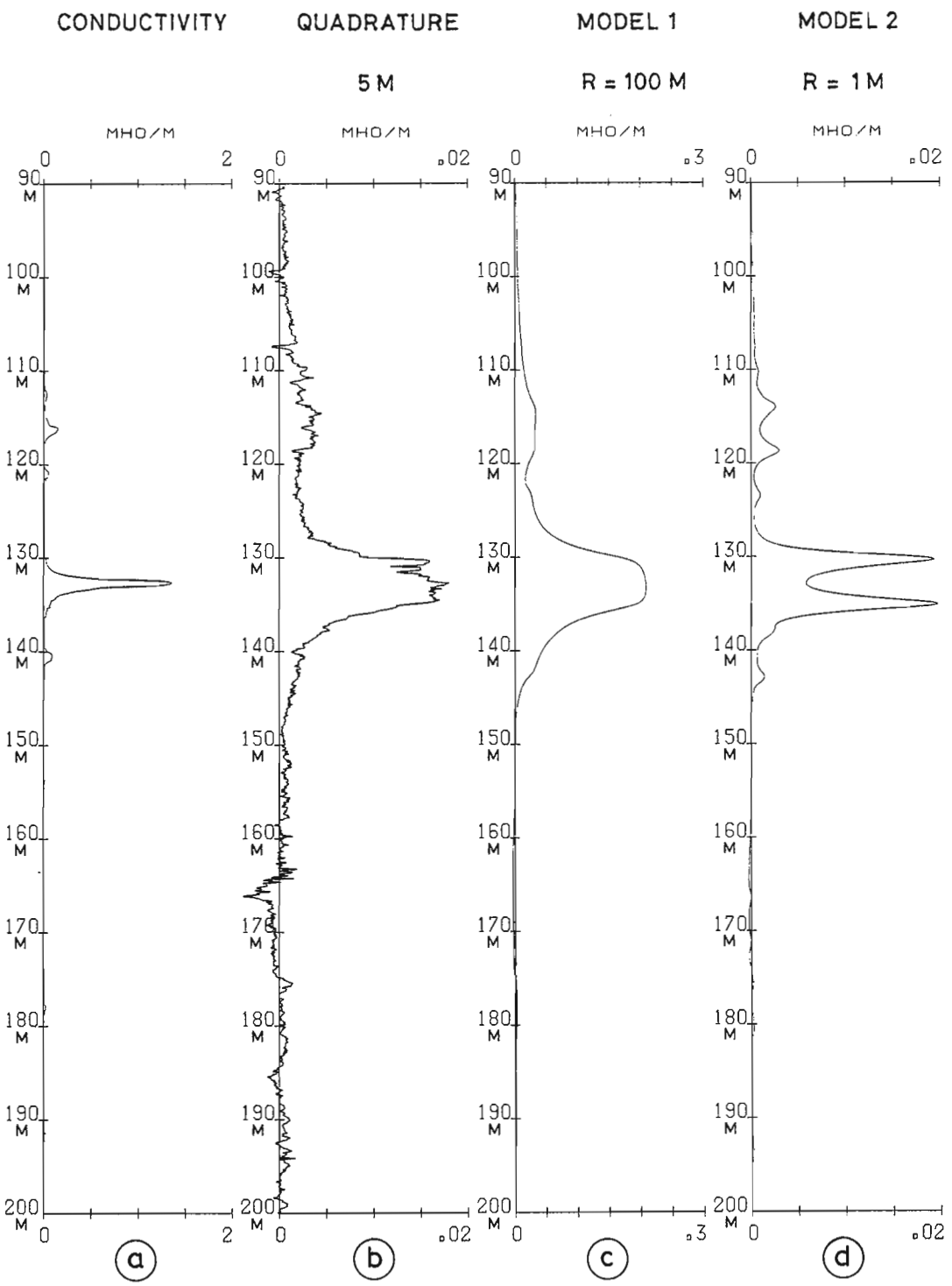

Figure 10.11. *Hole 3 - Starting from ROMULUS conductivity log (a), it is possible to simulate ERIC response (5 m spacing) in a stratified cylinder having ROMULUS conductivity vertical distribution and limited external radius (c: 100 m, d: 1 m). Simulated responses are compared to field log (b).*

Figure 10.10, together with 16-inch normal resistivity and ROMULUS conductivity logs. Hole 3 was drilled into a pipe of microgranite mineralized by a network of sulphide stringers. A major conductive zone detected by ERIC appears on both the normal resistivity and ROMULUS conductivity logs. Maximum conductivity is more than 1 mho/m with ROMULUS, while the normal resistivity minimum is 10-20 ohm-m. This confirms experimentally that the conductance of a heterogeneous conductive zone is underestimated by the normal resistivity log (see theoretical model in Figure 10.5). The ERIC conductivity anomaly is clearly visible with 5 m spacing, but it fades out with 10 m

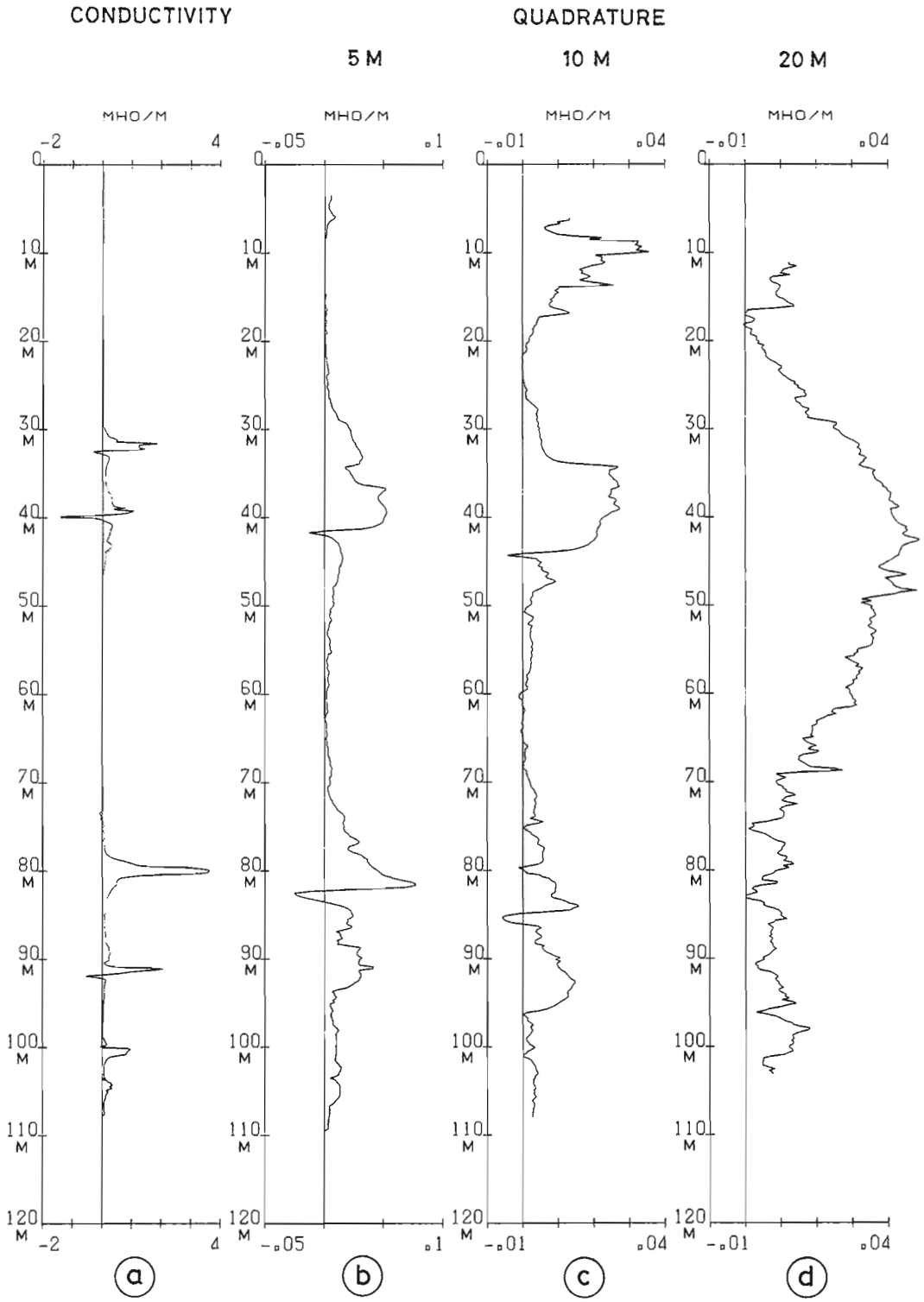

Figure 10.12. *ROMULUS conductivity (a) and ERIC quadrature (b, c, d) logs in hole 5 intersecting several conductive mineralized veins. At 40 m, the ERIC log with 20 m spacing reveals significant extension of the mineralization.*

and 20 m spacings. This indicates that the conductive zone crossed by the hole at 130 m has no significant lateral extension. To confirm this, we simulated the ERIC Quadrature log with 5 m spacing in the following models: vertically bounded cylinders having two different external radii (model 1: R = 100 m or infinite extension and, model 2: R = 1 m or no extension) and a vertical conductivity distribution taken from the ROMULUS log (Fig. 10.11). The model 1 simulation is very similar to the experimental data in shape, but the amplitude is overestimated by a factor of 10. With model 2, the simulated anomaly has the right amplitude, but the shape is very different from the field data. None of the models is satisfactory suggesting that the conductivity probably diminishes gradually away from the borehole. These models, however, indicate poor lateral extension of conductive rocks intersected by the hole.

Hole 4 is located 100 m from hole 2 and intersects several mineralized veins (Fig. 10.12). They are clearly indicated on ROMULUS conductivity log. The ERIC Quadrature logs give significant new information. Close to surface, one down-dipping conductor is particularly visible on the 10 m spacing log. Two veins intersected about 80 and 90 m generate low amplitude anomalies, lessening with larger spacings of ERIC. They have moderate lateral extension. Conversely, a high amplitude anomaly is revealed with 20 m spacing. It is caused by significant extension and probable lateral thickening of a mineralization crossed at 40 m. This suggests good mineral potential in the area, and invites further geophysical development work (mise-à-la-masse, hole to surface EM survey, etc.).

Conclusions

We have shown several examples of combined use of ROMULUS and ERIC logs in mineralized zones. ROMULUS is used to investigate physical properties (conductivity and susceptibility) which may be compared with core information. It allows the correlation of geophysical and geological logs, and the selection of geophysical targets of mineral interest. Use of the ERIC probe is restricted to the investigation of conductors lying within ten metres of the hole. Though qualitatively interesting, our interpretation of ERIC data remains poor. In the future, numerical modelling of complex geometries should enable us to extract more quantitative information from the logs.

References

Clerc, G. and Frignet, B.

1981: Diagraphies de conductivité électrique et susceptibilité magnétique avec la sonde à induction "ROMULUS". Applications en recherche minière; in seventh European logging symposium transactions, paper n° 19, S.A.I.D., Paris.

1982: Transmitter-receiver induction techniques and probes developed for surface and borehole measurements: application to archeology and mineral exploration; in sixth electromagnetic induction workshop transactions, I.A.G.A., Victoria, B.C. (in press in a special issue of Journal of Geomagnetism and Geoelectric).

Doll, N.G.

1949: Introduction to induction logging and application to logging of a well drilled with oil base mud; Petroleum transaction American Institute of Mining, Engineering.

Duesterhoeft, W.C.

1961: Propagation effects in induction logging; Geophysics, v. 26, n° 2, p. 192-204.

Parchas, C.

1971: Personnel Communication.

11. FIBRE OPTIC DATA LINKS FOR BOREHOLE EM APPLICATION

Y. Lamontagne and J.C. Macnae[1]

Lamontagne, Y. and Macnae, J.C., Fibre optic data links for borehole EM application; in Borehole Geophysics for Mining and Geotechnical Applications, ed. P.G. Killeen, Geological Survey of Canada, Paper 85-27, p. 101-106, 1986.

Abstract

A borehole EM system using a fibre optic cable has been designed, constructed and tested in field surveys. In this system, a large loop on the surface generates a magnetic field and the downhole sensor detects the field distorted by the ground. It was decided that a fibre optic link would best suit the system because of the problems associated with conventional electrical cables in a downhole application, particularly with respect to common mode signals, cable channelling and signal degradation. Although these problems can be overcome with difficulty with electrical cables, fibre optic cable does not have any potential for similar problems. As well, fibre optic cable has an additional advantage in that it is lighter in weight and lower in cost than conventional shielded electrical cable. These advantages must be balanced against the cost of additional downhole electronics and battery operation, however, leading to a more expensive probe than is usual for borehole systems. Our results show that a fibre optic cable of this design can be used in many borehole applications particularly where the data rate is high and where signal degradation can be a problem.

Résumé

Le système de carottage électromagnétique des sondages qui utilise un câble en fibre optique a été conçu, construit et essayé sur le terrain. Ce système comporte une grosse boucle en surface qui produit un champ magnétique; le capteur de fond décèle le champ déformé par le sol. On a décidé qu'il serait préférable d'utiliser des fibres optiques étant donné les problèmes associés à l'utilisation de câbles électriques classiques dans les sondages, notamment en ce qui a trait aux signaux. Bien que ces problèmes puissent être difficilement résolus dans le cas de câbles électriques, il en va autrement avec des câbles en fibre optique. En outre, ceux-ci sont plus légers et moins dispendieux que les câbles électriques blindés classiques. Il faut cependant comparer ces avantages au coût additionnel de l'alimentation par pile et de l'alimentation électronique qui augmente les dépenses engagées dans le sondage. Nos résultats montrent que ce genre de câble en fibre optique peut servir dans bien des cas, notamment lorsque les données relevées sont nombreuses et que l'amortissement du signal peut présenter un problème.

Introduction

With the success of the UTEM system in surface applications (West et al., 1984; Lamontagne, 1975), it became clear that there was a need for an EM sensor which could be lowered into boreholes. Some of the unique characteristics of the system made adaptation to a borehole system perhaps more difficult than for other systems. These difficulties arise from the unusually large bandwidth of the UTEM system and the unique fact that the transmitter is always on during measurements. An additional problem posed by a borehole system, is the spurious response likely to be caused by the long cable connecting the sensor to the surface equipment. The way in which this problem was solved by the use of a fibre optic cable and the advantages and drawbacks of this technology are discussed in this report.

Conventional electrical cable problems

Initial analysis of existing borehole systems indicated that the task of supressing stray coupling effects to the required accuracy over the desired bandwidth was almost impossible using conventional electrical cable. Some initial tests by Dyck (1981) using a conventional borehole probe confirmed this suspicion. Three main areas of difficulty detected in this analysis are summarized in Table 11.1.

Common mode interferences

With a transmitter loop excited by several hundred volts at the surface, it is difficult to achieve a sufficiently high common mode rejection ratio, and the complete system balance needed to avoid spurious responses where conductive zones provide an electrical link to parts of the loop by capacitive or resistive coupling. Some of the very sharp responses, commonly seen even on late channels when crossing minor conductive zones, are probably caused by these effects.

Cable related signal degradation

Over a long electrical cable, mechanical and/or environmental effects caused by motion of the cable, flowing water, mechanical stress, temperature differences etc. can

[1] Lamontagne Geophysics Ltd., 49 Spadina Ave., Toronto M5V 2J1

introduce noise signals or change the electrical characteristics of the line (e.g. resistance), thus affecting any critical adjustment of common mode rejection.

Current channelling in the cable

When the probe depth is very large, a long shielded cable acts as a long antenna which can channel appreciable currents which are capacitively coupled to it. This disturbance in the induced current flow is more acute for early sampling times, where, depending on the symmetry of the channelled current flow in the vicinity of the probe, a variety of artificial responses may result.

These effects can not only introduce stray responses, but can also affect the system gain and fidelity, which would be interpreted as long time constant responses in UTEM.

The need for an all-dielectric link

From the start, the possibility of using fibre optic transmission was considered as a way around all these problems. Since an optical link can be all dielectric, complete electrical isolation can be realized, thus avoiding common mode problems and cable channeling effects. Also, one way to avoid signal degradation is signal encoding which is not only necessary for an optical link, but also can be done without introducing much noise in driving the long transmission line, as would be the case for electrical transmission (Hewlett-Packard, 1978).

When the possibility was studied further, there appeared a number of additional advantages for the use of an optical link. A good number of disadvantages were also discovered, mostly having to do with the use of a new technology. Both are summarized in Table 11.2.

Design problems associated with the use of a fibre optic cable

Once the decision to use a fibre optic cable had been taken, it became necessary to find satisfactory solutions for various aspects of system design. These can be summarized as follows:

- incompatibility of presently available standard fibre optic with high hydrostatic pressure tolerance and tensile strength needed in logging operations
- method of digital data encoding to be used
- modifications required to a conventional winch to accommodate the special requirements of a fibre optic cable

Table 11.1. Problems with conventional electrical borehole cable

LONG CABLE EFFECTS ON BH MEASUREMENTS

PROBLEM	EFFECT	MEASUREMENTS AFFECTED	SOLUTIONS
1- COMMON MODE	- SYSTEMATIC ERROR - NOISE	- 'ON' TIME WORSE - WIDEBAND	- BALANCED DIFFERENTIAL TRANSMISSION - SHIELDING - ELECTRICAL ISOLATION
2- SIGNAL DEGRADATION	- DISTORTION - GAIN VARIATION	- HF WORSE - 'ON' TIME	- ENCODING - CONTROLLED IMPEDANCE LINE
3- CABLE CHANNELING	- ARTIFICIAL RESPONSE	- HF H FIELD - ALL E FIELD	- ELECTRICAL ISOLATION

UTEM CHARACTERISTICS

- 'ON' TIME MEASUREMENTS
- WIDEBAND
- GAIN CALIBRATED
- E FIELD MEASUREMENTS

- types of electro-optical transducers required to modulate and demodulate the optical carrier used to transmit the "H" field signal from the borehole sensor.

The first two of these are discussed below and the third is addressed in the subsequent section which describes the overall system.

Cable construction

It was found surprisingly, that fibre optic cables can be considerably cheaper than electrical cables for a comparable data handling capability. They are also much lighter since no metallic members are needed. The effective density of a fibre optic cable is near 1, giving it a near zero weight in a water-filled borehole. This means that the winch system must only support the weight of the probe. One of the main difficulties encountered at the beginning was that there existed no fibre optic cable capable of withstanding a sufficiently high pressure without damage. This was due to the fact that in normal construction, the cables are made to resist crushing rather than hydrostatic pressure. It was then necessary to specify a special cable that could withstand high pressures and also have a greater tensile strength to weight ratio than usual. After several attempts, we arrived at a construction which could be made by our supplier and had the required properties. The normal fibre optic cable construction is shown in Figure 11.1 and consists of: A. Tough outer jacket (high density polyethylene); B. Soft plastic inner jacket to help cushion crushing loads; C. Strength member (usually braided Kevlar); D. Rigid buffer tube (air filled); E. Fibre. The special fibre optic cable custom designed for borehole/high pressure work has a modified construction:

A. Tough outer jacket as above.
B. Heavier Kevlar strength member.
C. Semi-rigid buffer tube.
D. Freeze proof gel filling with density of 1.
E. Fibre spiraling in buffer tube.

The overall cable diameter and weight is reduced and the tensile strength/weight is greater than for a standard cable. The physical properties are summarized in Table 11.3.

Table 11.2. Advantages and disadvantages of using fibre optic cable

ADVANTAGES
– NO LONG CABLE EFFECTS
– NO MECHANICAL EFFECTS
– HIGH THROUGHPUT
– LOW WEIGHT
– LOW COST
– LIGHTER WINCH
DISADVANTAGES
– MORE DOWN-HOLE ELECTRONICS
– BENDING RADIUS LIMIT
– TERMINATION PROBLEMS
– NEW TECHNOLOGY

The overall system

The system consists of the following functional blocks: downhole probe, optical link, winch assembly, and winch controller.

Probe

The sensor is physically distinct from the other downhole electronics as shown in Figure 11.2. Only an axial magnetic sensor has been constructed so far, but an electric field sensor and transverse magnetic sensors will be implemented in the future.

Optical link

The analogue-digital-analogue data link (Fig. 11.3) contains a signal encoder, optical transmitter, fibre optic cable, optical receiver and decoder. Physically, the encoder is in the borehole, as is the optical transmitter. The optical receiver is in the hub of the removable winch spool and the decoder is in the controller box. The signal going through the slip-rings is thus a digital pulse coded electrical signal. The decoder reproduces the analogue signal for normal sampling by the receiver. The analogue signal at surface lags that downhole by 20 μs; this time delay is caused by encoding, decoding and transmission through the 2 km of fibre optic cable.

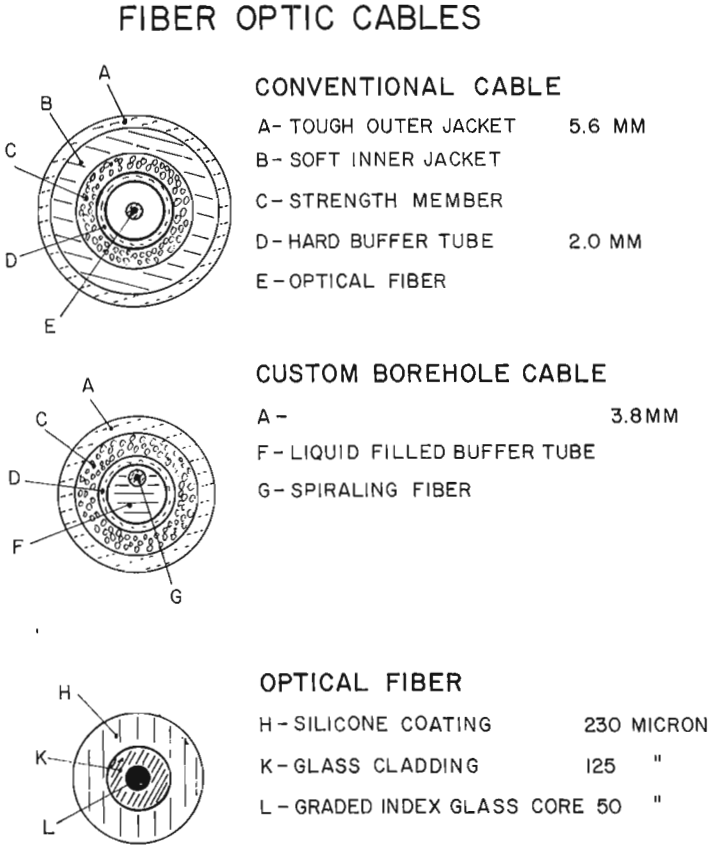

Figure 11.1. *Construction of conventional and custom designed fibre optic cable.*

Table 11.3. Specifications of custom designed borehole cable

– OD 3.8 MM		
– ATTENUATION 5 db/km		
– WEIGHT 14 KG/KM		
– STRUCTURAL STRENGTH	3390 N	(760 LBS)
– DAMAGE FREE LOADING	1160 N	(260 LBS)
– BENDING RADIUS	75 MM	
– DENSITY 1 G/CM^3		

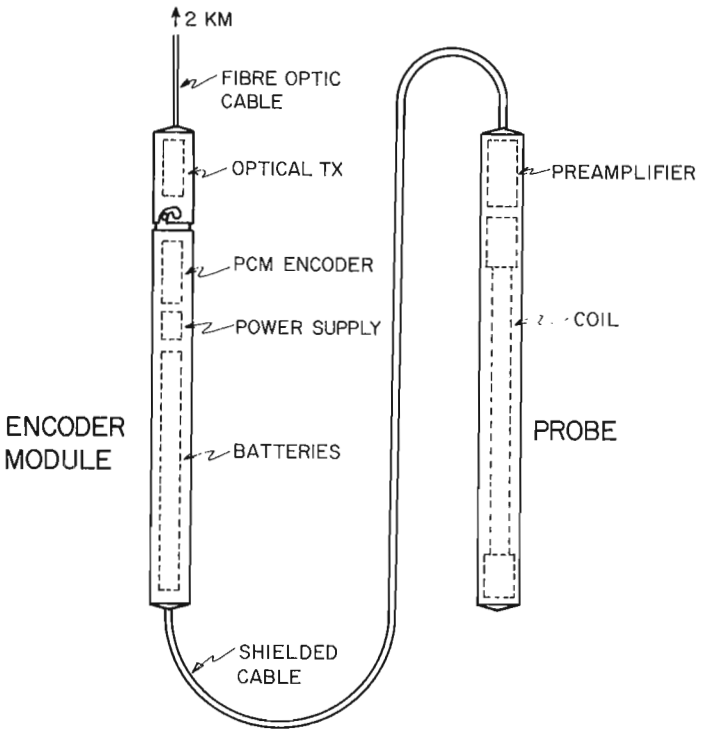

Figure 11.2. The downhole components of the UTEM borehole system.

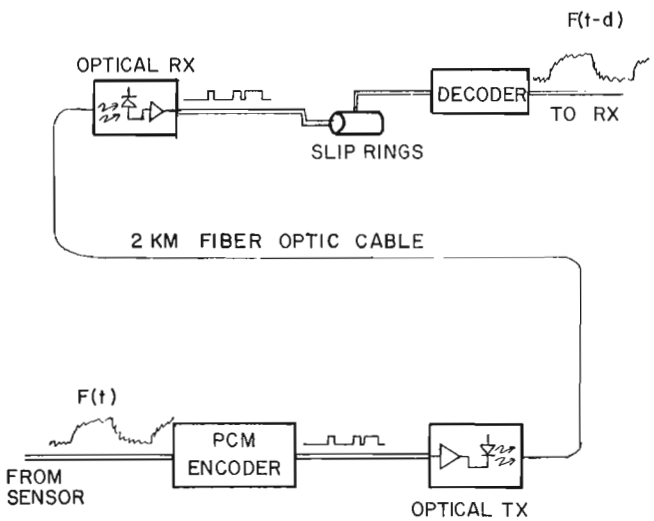

Figure 11.3. Block diagram of ANALOGUE-DIGITAL-ANALOGUE data link.

Winch assembly

The winch system was designed to include all components necessary for complete automation of the system (Fig. 11.4). The winch is driven by a servo motor and brake system. Optical shaft encoders are used to measure the probe position and the tension on the cable. The rack-and-pinion tensiometer also acts as a shock absorber. It comprises a pulley mounted on a spring-loaded arm. The spool and pulleys were made reasonably large in diameter to avoid undue bending of the fibre optic cable. The winch has a maximum torque limit set by the hardware, but this corresponds to actual cable tensions varying over a range of 2.7:1, depending on how full the spool is. For this reason, a tensiometer is nedded. The speed and braking of the winch is regulated by the winch controller unit. An upper tension limit is entered on the keyboard of the controller and determines the threshold at which the winch will slow down or stop to reduce the actual tension on the cable. This normally occurs when the probe is being pulled up. While the probe is being lowered, the tension is maintained by the controller above a fixed 5% minimum limit.

Winch controller

This unit provides intelligence for the whole system, although its main purpose is to control the winch. The controller can be operated manually from the keyboard or set automatically. The keyboard layout is shown schematically in Figure 11.5 and illustrates the controller operation functions. One set of entries is necessary to initialize the controller and a second set permits on-line intervention by the operator.

Entries initializing the controller are:

VMAX: sets the maximum velocity of the probe in centimetres/seconds (limit of 150)

TENSION: sets the maximum tension in per cent of probe weight in air

HOLE: sets the hole depth (controller will refuse to go to any greater depth)

SET: initializes the depth register from the keyboard

Entries permitting on-line intervention by operator are:

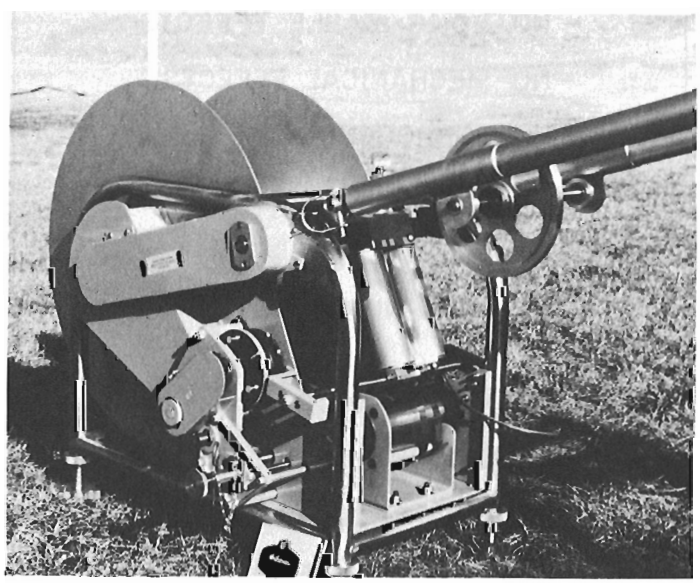

Figure 11.4. The winch. (GSC 203811)

DEPTH: enters probe target depth (initiates movement of probe upon entry)
STOP: controlled stop (gradually slows winch to complete stop)
MAN: emergency manual stop
START: re-initiates movement of the probe toward current target depth (used after STOP and MAN or automatic stoppage)

In addition to the essential functions outlined above, the following functions are provided for convenience in routine keyboard operation:

INCR: sets depth increment
UP: moves probe up by depth increment (INCR)
DOWN: moves probe down by depth increment (INCR)
THRESH: sets an anomaly threshold depth above which automatic detailing is performed

The probe speed is limited to the value specified by VMAX and by the tension monitoring system. During descent, the tension is maintained above 5% probe air weight whereas during ascent the tension limit is entered by the operator. When approaching these limits the winch is slowed by the controller, which regulates the rate of descent or ascent of the probe to keep the tension on the cable within the specified limits. Thus, the winch acts as a slip clutch during probe ascent and prevents cable spillage during probe descent. The controller digital loop characteristics are such that the speed is regulated steadily when the drag is viscous in nature.

A conservative hole depth limit is usually entered before logging a hole. Once the probe reaches that depth, the controller warns the operator. The hole depth is then increased and the maximum velocity reduced until the controller detects the bottom of the hole by means of the tensiometer and stops the winch. In a greasy hole, the same mechanism slows down the probe during probe descent in order to keep a slight tension on the cable. The whole cable retains some tension in such cases since the fibre optic cable itselt has a null buoyancy in water.

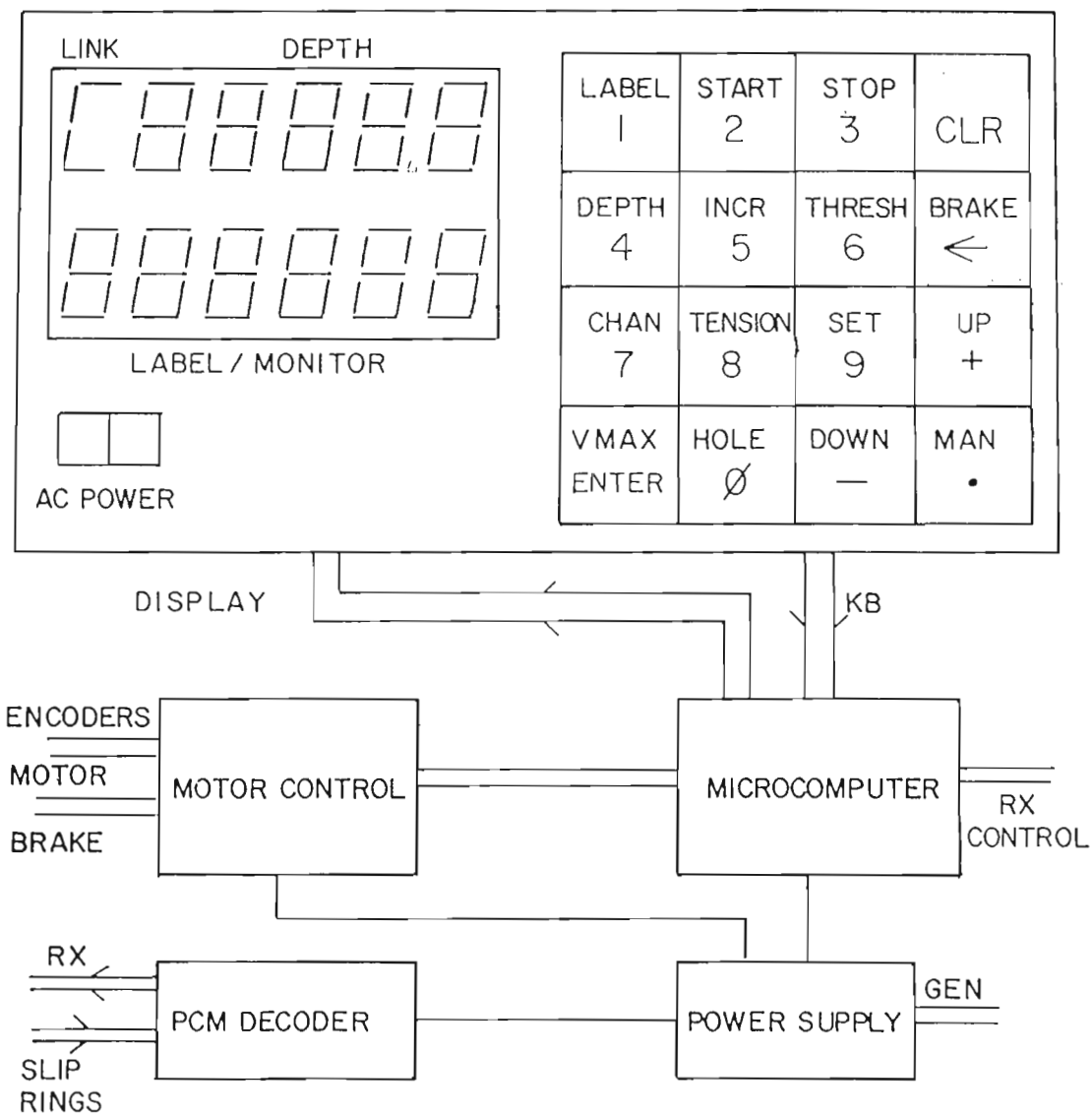

Figure 11.5. *Schematic diagram of the UTEM borehole system controller.*

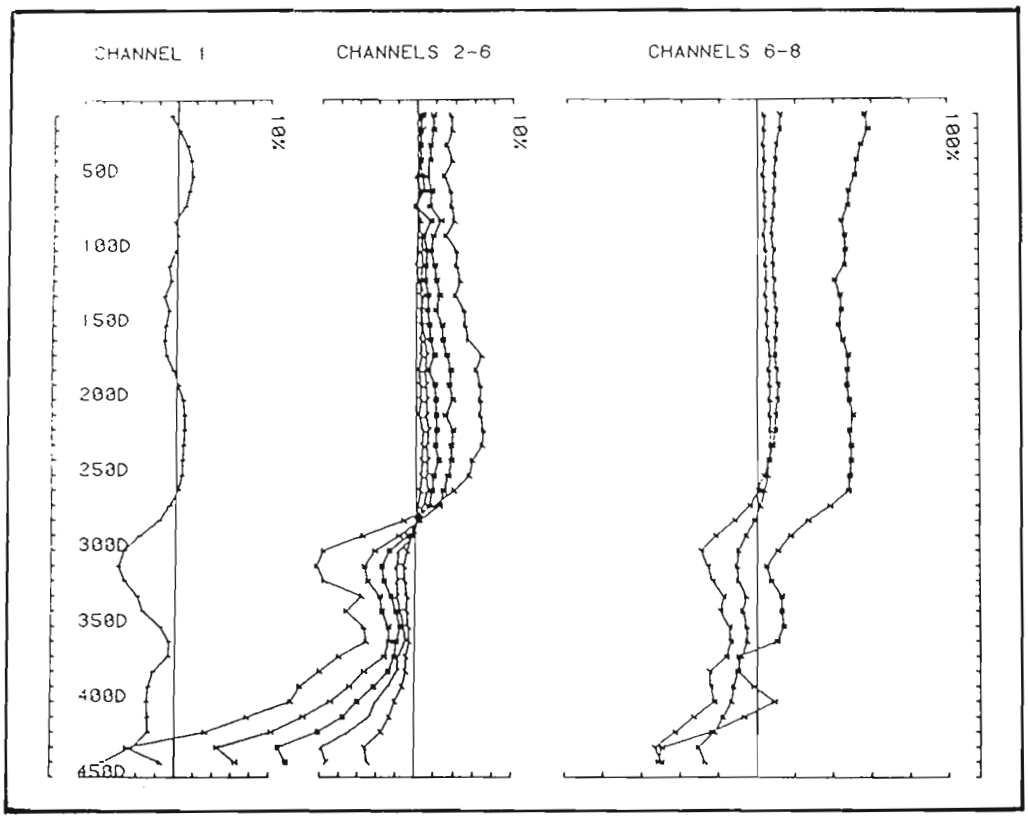

Figure 11.6. *Results from the first test logging using the UTEM system.*

The signal connection from the downhole coil to the UTEM 3 receiver is identical to that from the UTEM 3 surface coil. There is also an interface for automatic logging in which the winch controller unit can signal the UTEM 3 receiver to start reading and, upon completion of the reading, move the probe to a new depth. In both keyboard and automatic operation, the usual UTEM response and depth data (together with the standard header information) are stored on magnetic cassette in the receiver.

Field testing

Figure 11.6 shows the results from the first hole logged with the UTEM borehole system. The data collected in this hole did not include any compensation for the 20 μs delay of the analogue-digital-analogue link, which caused the large response on channel 8. A subsequent receiver program modification corrects for this time delay.

Conclusions

The development of a fibre optic data link proved to be more of a challenge than initially anticipated. However, the technological problems have now been solved, and the data link should prove to be a cheap, lightweight alternative to electrical wire data links with none of the usual problems of common mode rejection, capacitive pickup or grounding. Many other applications for the data link such as borehole IP measurements are likely developments in the near future.

Acknowledgments

Development of the borehole system at Lamontagne Geophysics was supported by Cominco Ltd., Texasgulf Inc., Kidd Creek Mines, St. Joe American, Sulpetro Minerals and the Ontario Geological Survey through an ETDF grant GR-010 to Lamontagne Geophysics. The careful work of two critical reviewers is also gratefully noted.

References

Dyck, A.V.
1981: A method for quantitative interpretation of wide-band, drill-hole EM surveys in mineral exploration; PhD thesis, University of Toronto (available as RAG 23, Geophysics Laboratory, University of Toronto).

Hewlett-Packard
1978: Digital transmission with the HP Fibre Optic System; Application note 1000, Hewlett-Packard, Palo Alto, California.

Lamontagne, Y.
1975: Applications of wideband, time-domain EM measurements in mineral exploration; PhD thesis, University of Toronto (available as RAG 7, Geophysics Laboratory, University of Toronto).

West, G.F., Macnae, J.C. and Lamontagne, Y.
1984: A time-domain electromagnetic system measuring the step/response of the ground; Geophysics, N. 79, no. 7, p. 1010-1026.

12. TIME DOMAIN IP BOREHOLE LOGGING

Blaine Webster[1]

Webster, B., Time domain IP borehole logging; in Borehole Geophysics for Mining and Geotechnical Applications, ed. P.G. Killeen, Geological Survey of Canada, Paper 85-27, p. 107-118, 1986.

Abstract

Borehole logging for mineral exploration has been gaining acceptance slowly over the past 30 years. The ready availability of off-the-shelf electromagnetic loggers for massive sulphides and IP loggers for disseminated sulphides (time domain and frequency domain) have made their use much more accessible to explorationists.

In IP logging, multi-dipole arrays are employed to obtain a representation of the variation of chargeability and conductivity with distance from the borehole, along its length. Remote detection of non-intersected bodies can be made, as well as the determination of the potential importance of sections of sulphides which are intersected by the hole. This type of survey constitutes the "detection log". A second type of survey, using only current electrodes on surface, provides a "directional log" for sources of potential interest in and around the hole.

The use of multi-input, microprocessor controlled IP receivers has speeded up IP borehole logging considerably.

Spectral IP parameters, obtained from computer analysis of the transient decay form, help to resolve and identify different sources of IP response in the borehole.

Examples are given of IP borehole logs from Greece and Canada.

Résumé

La diagraphie des sondages appliquées à l'exploration minérale est une méthode qui gagne progressivement en popularité depuis 30 ans. Les enregistreurs électromagnétiques utilisés pour l'exploration des sulfures massifs et les enregistreurs à polarisation induite (PI) utilisés pour la prospection des sulfures disséminés (domaine temporel et domaine harmonique) sont devenus beaucoup plus accessibles pour la prospection parce que ces appareils sont gardés en stock.

Dans les diagraphies à PI' des réseaux à multiples dipoles sont utilisés pour obtenir une représentation de la variation de la capacité d'accepter une charge électrique et de la conductibilité en fonction de la distance du sondage, parallèlement à la longueur de celui-ci. Il est possible de déceler à distance les corps non traversés et de déterminer l'importance éventuelle des masses de sulfures traversées par le sondage. Ce genre d'étude donne lieu à une "diagraphie de détection". Un deuxième genre d'étude utilise uniquement des électrodes de courant en surface et produit une "diagraphie de direction" qui indique les zones d'intérêt possibles dans le sondage et autour de celui-ci.

L'utilisation de récepteurs à PI et à donnés multiples, contrôlés par des microprocesseures, a accéléré de beaucoup la diagraphie par PI des sondages.

Les paramètres spectraux de PI, obtenus par une analyse informatisée de la forme de dégradation transitoire, aident à déceler et à identifier les diverses sources de PI dans les sondages.

Des exemples sont donnés de diagraphies de PI recueillies en Grèce et au Canada.

Introduction

Induced polarization/resistivity logging has been gaining acceptance over the past 30 years. Presently the method is used routinely in the Viburnum lead-zinc belt in Missouri, United States and in the Cu-Ni mining district in Sudbury, Ontario, Canada.

The multi-dipole arrays employed result in a large volume of data. Recent advances in microprocessor based receivers such as the Scintrex IPR-11 (Seigel et al., 1980) have simplified and accelerated the data gathering process. Efficient data editing and posting facilities are available with the Scintrex Soft II program written for the Apple IIe computer. In addition, the Soft II program calculates

[1] Scintrex Limited, Toronto, Ontario, Canada

spectral parameters which yield additional information on the detected anomaly's cause using measurements routinely obtained with the IPR-11 receiver.

Survey methodology

In IP logging, multi-separation electrode arrays are employed to determine the variation of chargeability and electrical conductivity with distance from the borehole. IP logging techniques commonly are of two types: detection and direction. The detection log explores about the hole for non-intersected bodies and determines the relative importance of intersected zones. The directional log gives an azimuth to non-intersected bodies.

Detection logging

Figure 12.1 illustrates the detection log electrode configuration. The inter-electrode "a" spacings are 2.5, 5, 10, 20 and 40 m. One current electrode is located at the bottom of the electrode array and the other is located remotely on surface.

The 2.5 and 5 m separations provide information on the lithologies in the vicinity of the drillhole. The near-hole log will usually reflect informatoin comparable with that obtained from the core. The 10, 20 and 40 m spacings provide information on the lithologies up to a radius of approximately 20 m about the drillhole.

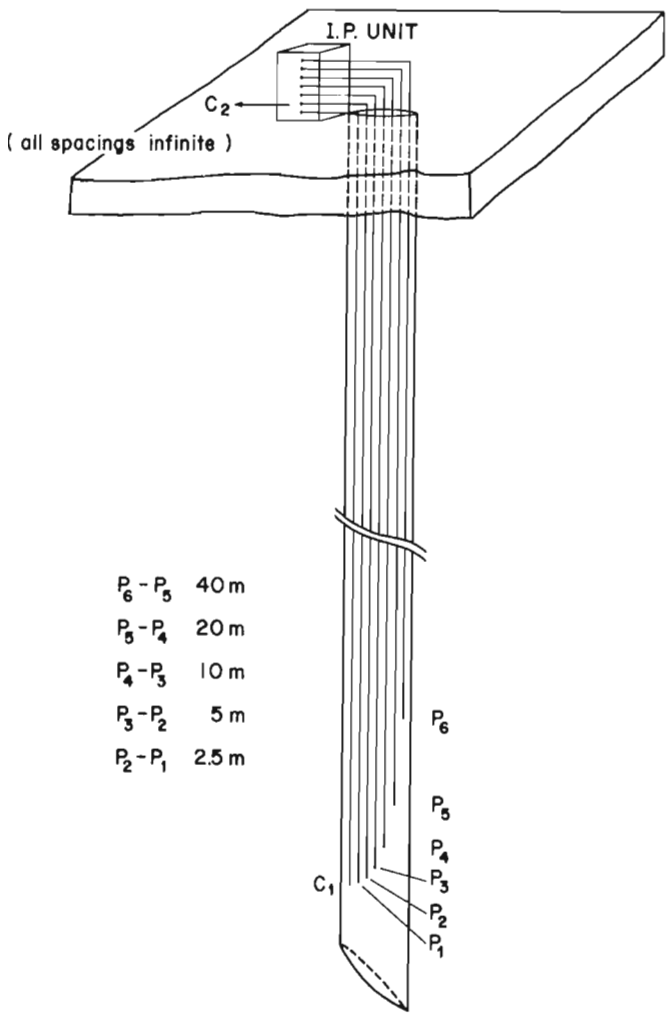

Figure 12.1. *The detection logging electrode array.*

Direction logging

Figure 12.2 illustrates the electrode configuration for the directional array. Current electrodes are placed away from the drillhole on surface at a distance some two-thirds of the hole depth. A reference potential electrode is fixed at the borehole collar and single search potential electrode is lowered down the drillhole. Current is passed through the current electrodes in east-west and north-south pairs.

The detection and directional logs are reviewed in a paper by Wagg and Siegel (1963).

Instrumentation

The following instrumentation is normally employed, either mounted in a truck or assembled on site (see Fig. 12.3a). All are of Scintrex manufacture.

1) Receiver

An IPR-11 Time Domain Receiver measures up to 10 slices of the chargeability decay on up to 6 potential dipoles simultaneously.

2) Transmitter

On detection surveys an IPC-8/250 Watt Crystal Controlled Battery Powered Time Domain Transmitter is employed. On the directional survey a TSQ-3 (3 kw) or TSQ-4 (10 kw) transmitter is employed depending on the power required.

3) Interface

A DHIP-2 interface unit is used to interface current from the transmitter to the current electrode and signal from the potential electrodes to the receiver.

4) Winch

A CLW-2 winch with 500 m of 8 conductor cable consisting of 6 potential wires, two shielded current wires and three kevlar strain members is used.

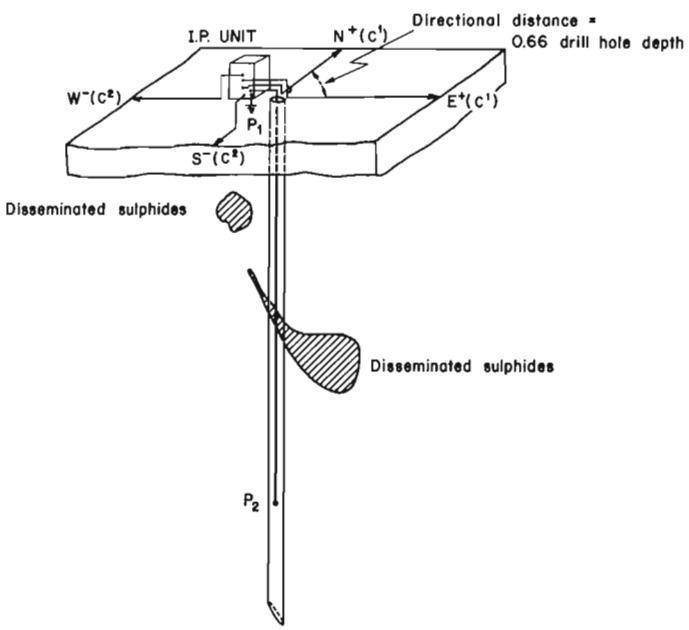

Figure 12.2. *Electrode configuration for a directional array.*

5) Electrode Array

An 80 m electrode string with a current electrode and six potential electrodes, separated by 2.5 m, 5 m, 10 m, 20 m and 40 m respectively is used.

Measured parameters

A direct current is applied across the current electrodes with a 2 second "on" 2 second "off" pulse duration with the polarity automatically changing every 4 seconds.

A primary voltage (Vp) is measured across the potential electrodes. Given the transmitted current and the array geometry, the apparent resistivity may be calculated.

After current shut off, the secondary voltage decay is measured. The secondary decay is subdivided into multiple slices for integration (see Figure 12.3a). The chargeability is given by:

$$Ma = \frac{V_s}{V_p} \cdot 1000 \quad Mv/v \qquad (1)$$

where

V_s = secondary voltage
V_p = primary voltage

The secondary voltage is defined as

$$V_s = \frac{1}{(t_2 - t_1)} \int_{t_1}^{t_2} V(t)\, dt$$

where t_2, t_1 are the time limits of the integration. By adjusting such times, the chargeability is sampled at different points of the decay. The times used for the IPR-11 are listed in Figure 12.3b.

Spectral IP parameters are determined by the shape of the measured decay (Johnson, 1983). The decay is compared against a suite of master curves which describe the IPR-11 decay for an idealized Cole-Cole model earth. The best fit of measured and master curves gives the Cole-Cole parameters of time constant, exponent and true chargeability.

Survey examples

Several examples of drillhole surveys illustrate how drillhole IP logging can be applied.

1) Carbonate hosted lead-zinc deposits

Historically, surface induced polarization surveys have been successfully used in exploring for these deposits. The targets are difficult ones because:

i) They are very irregular and are often associated with karst systems and slump breccias in reef complexes.
ii) Most of them contain significant amounts of sphalerite which is non-conducting and which lowers the overall chargeability response of the mineralization.

The first example (see Fig. 12.4, 12.5) shows the IP/resistivity logs of three holes drilled on a lead-zinc deposit located in northern Greece. These holes are from a fence of holes crossing the deposit and separated by 50 m. With respect to the mineralization. the holes are variously located as;

a) entirely within the main sulphide body,
b) in apparently significant volume percent of sulphides on or near the edge of the main sulphide body. Here the intersected mineralization may be much higher grade than that located about the hole (i.e. misleading high grade),
c) in an apparently insignificant volume percent of sulphides but where the hole may in fact pass near the main sulphide zone (i.e. near miss).

The IP/resistivity logs of hole D show strong responses between 185 and 205 m on both the near-hole (a = 2.5, 5 m) and on the far-hole logs (a = 10, 20 m). The chargeabilities decrease at the main intersection due to the low resistivity of the sulphide body which short circuits the potential electrodes.

The IP/resistivity log of hole C shows a strong IP response with a moderate resistivity low in the near-hole log and a moderate IP response on the far-hole log. These logs reflect a lower volume percent of chargeable/conductive mineralization located about the hole. Interpretation of thee logs would lead to a downgrading of economic mineralization intersected in hole C.

The IP/resistivity log of hole G gives a strong IP response and a moderate resistivity low on the near-hole logs. The response of the near-hole logs is similar to the near hole log of hole C even though the intersected mineralization is of a much lower grade. The far hole logs are much more significant as their IP and resistivity responses are almost as large as those obtained on the far-hole log of hole D which intersects the main sulphide body. Results show that the 10 and 20 metre separations are seeing a much higher volume percent of sulphides than is indicated in the drill core.

A second example of an IP/resistivity log in a carbonate hosted Pb-Zn deposit is taken from Nanasivik Mines located at 70°N latitude on the northern end of Baffin Island.

The Nanasivik ore body strikes east-west and is located south of the drillhole. The ore body is composed of two sulphide lenses. One is located at a depth of some 120 m and is called the upper zone; the other is located at a depth of 150 m and is called the lower zone. The drill log intersected 2% pyrite from 100 to 118 m (upper zone). From 145 to 160 m up to 3% sphalerite was intersected in a zone without pyrite (lower sulphide zone).

The project had two primary goals. They were, a) to determine if the upper and lower sulphide zones were detectable; b) to determine if the IP/resistivity log would be valid as the entire hole was drilled in permanently frozen rock and filled with salt brine.

A secondary, research oriented goal was the study of the correlation between surface IP spectral data over mixed sulphide and barren pyrite zones with chargeability anomalies located in mixed sulphide zones and barren pyrite zones in the drillhole.

Near-hole and far-hole logs for the Nanasivik drillhole are shown in Figures 12.6 and 12.7 Both the near-hole and far-hole IP/resistivity logs have moderate responses at 120 m and 150 m which correlate with the upper and lower ore lenses. The response at 150 m is likely caused by the lower ore lens which, from drill information, is from 0 to 40 m away from the hole. The response at 120 m is quite complex because there is significant pyrite mineralization in the hole. However, the 40 m spacing does give a large response at 135 m which could be a response caused by both sulphide lenses. The marked resistivity low between 80 to 110 m on the 40 m log could also be partially due to the conductive drilling fluid penetrating a fracture zone. The water return was lost from 0 to 100 m. The effect of the brine can also be

IPR-11Receiver

Apple II with Scintrex Soft II Software

IPC-8 - 250 Watt Transmitter

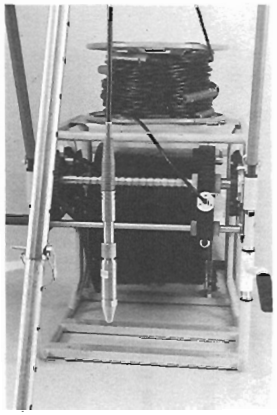

Detail of current electrode showing winch and electrode cable spool.

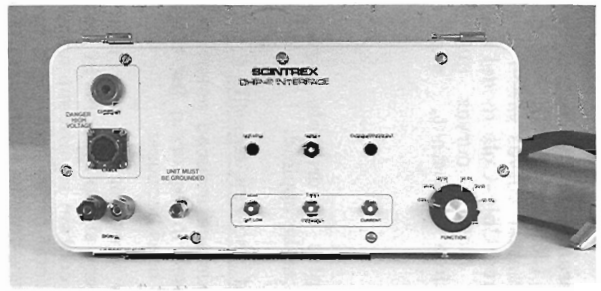

DHIP-2 Interface Unit

Figure 12.3a. *Instrumentation employed for downhole I.P. logging showing the receiver, transmitter, current electrode with winch, and the interface unit.*

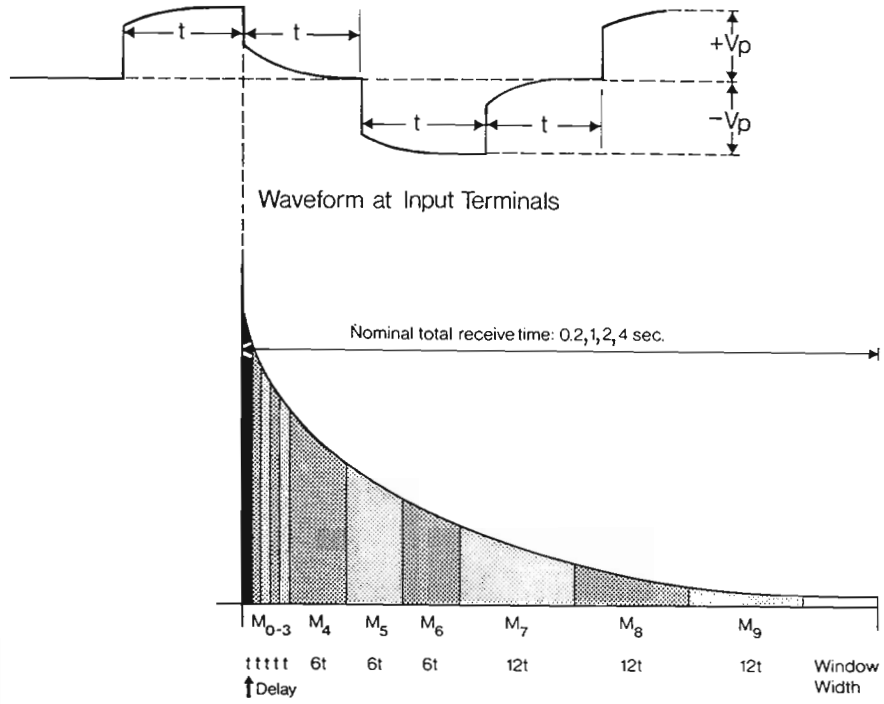

IPR-11 Timing for the Slices of an IP Decay Curve, where t represents t_{TX}.

IPR-11 Timing Data

MODE Sec.	SLICE	DURATION ms	FROM ms	TO ms	MID-POINT ms
t=2.0	0	30	30	60	45
	1	30	60	90	75
	2	30	90	120	105
	3	30	120	150	135
	4	180	150	330	240
	5	180	330	510	420
	6	180	510	690	600
	7	360	690	1050	870
	8	360	1050	1410	1230
	9	360	1410	1770	1590

Figure 12.3b. *The secondary decay voltage showing its subdivision into multiple time-slices.*

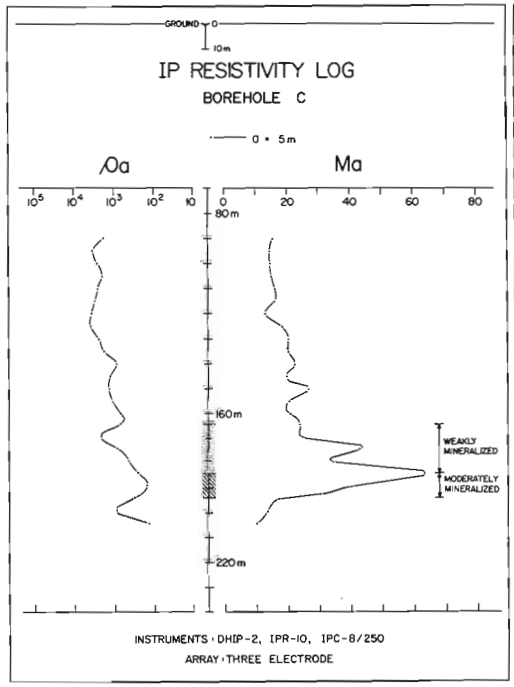

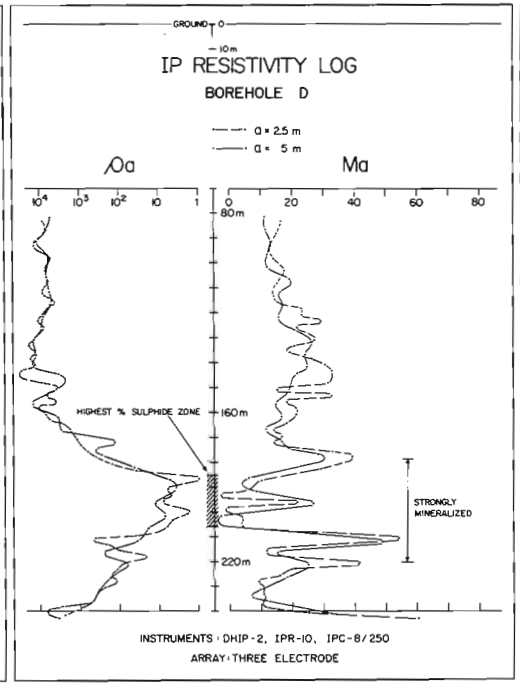

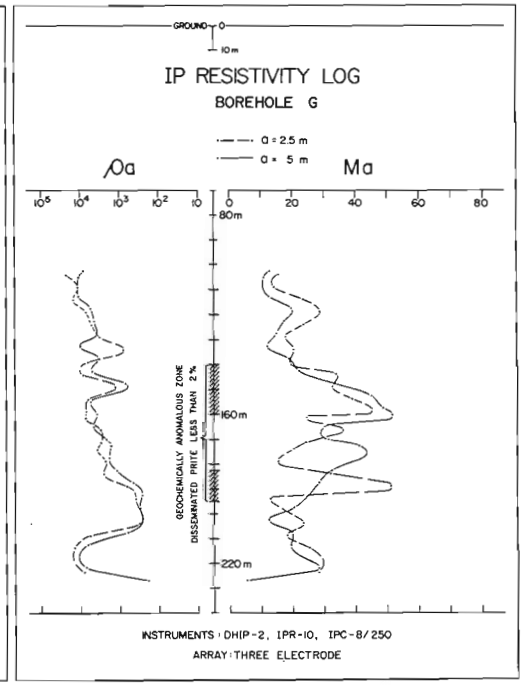

Figure 12.4

IP/resistivity logs of boreholes C, D, and G in a lead-zinc deposit in northern Greece. ('a' spacing of 2.5 m and 5.0 m)

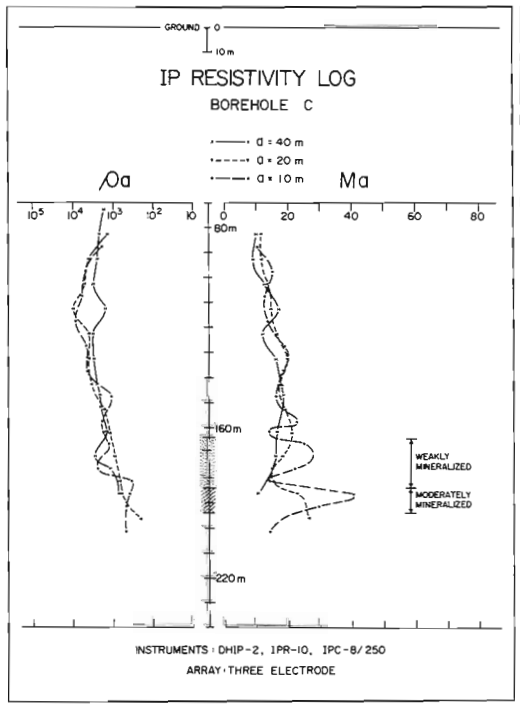

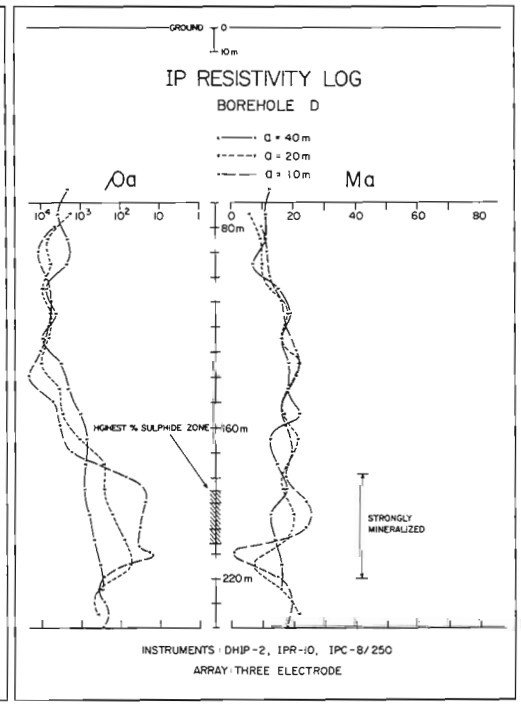

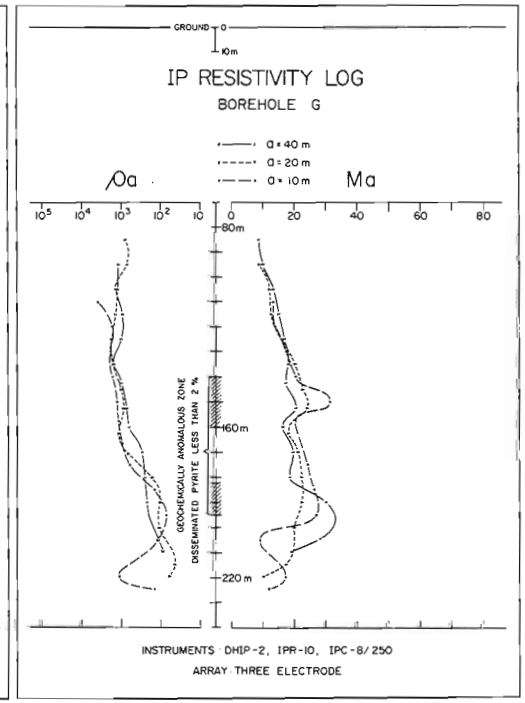

Figure 12.5

IP/resistivity logs of the same holes shown in Figure 12.4 with 'a' spacing 10 m, 20 m, and 40 m.

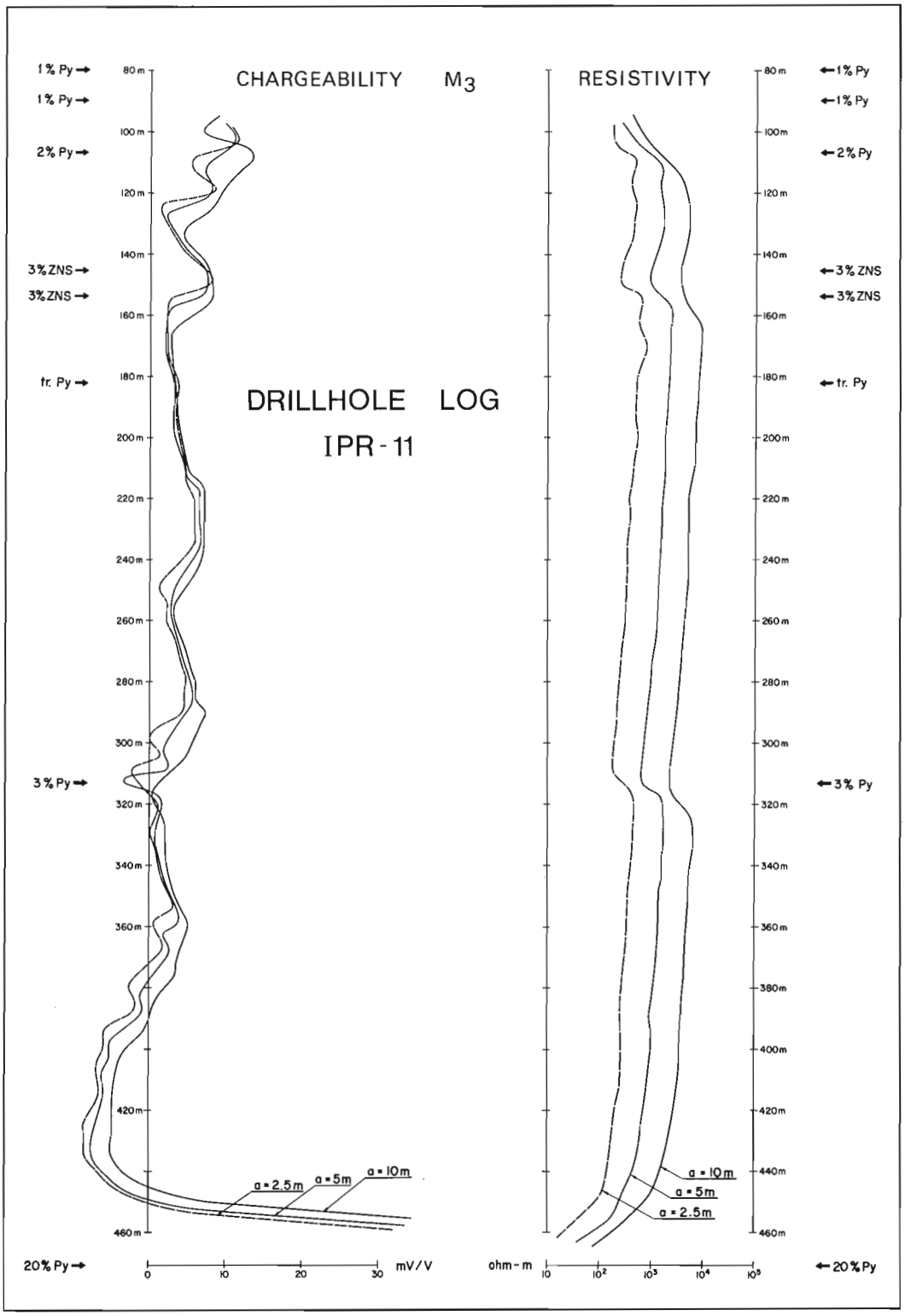

Figure 12.6. *Near-hole results ('a' spacing 2.5 m, 5 m, and 10 m) for drillhole IP logging of the Nanasivic carbonate hosted lead-zinc deposit.*

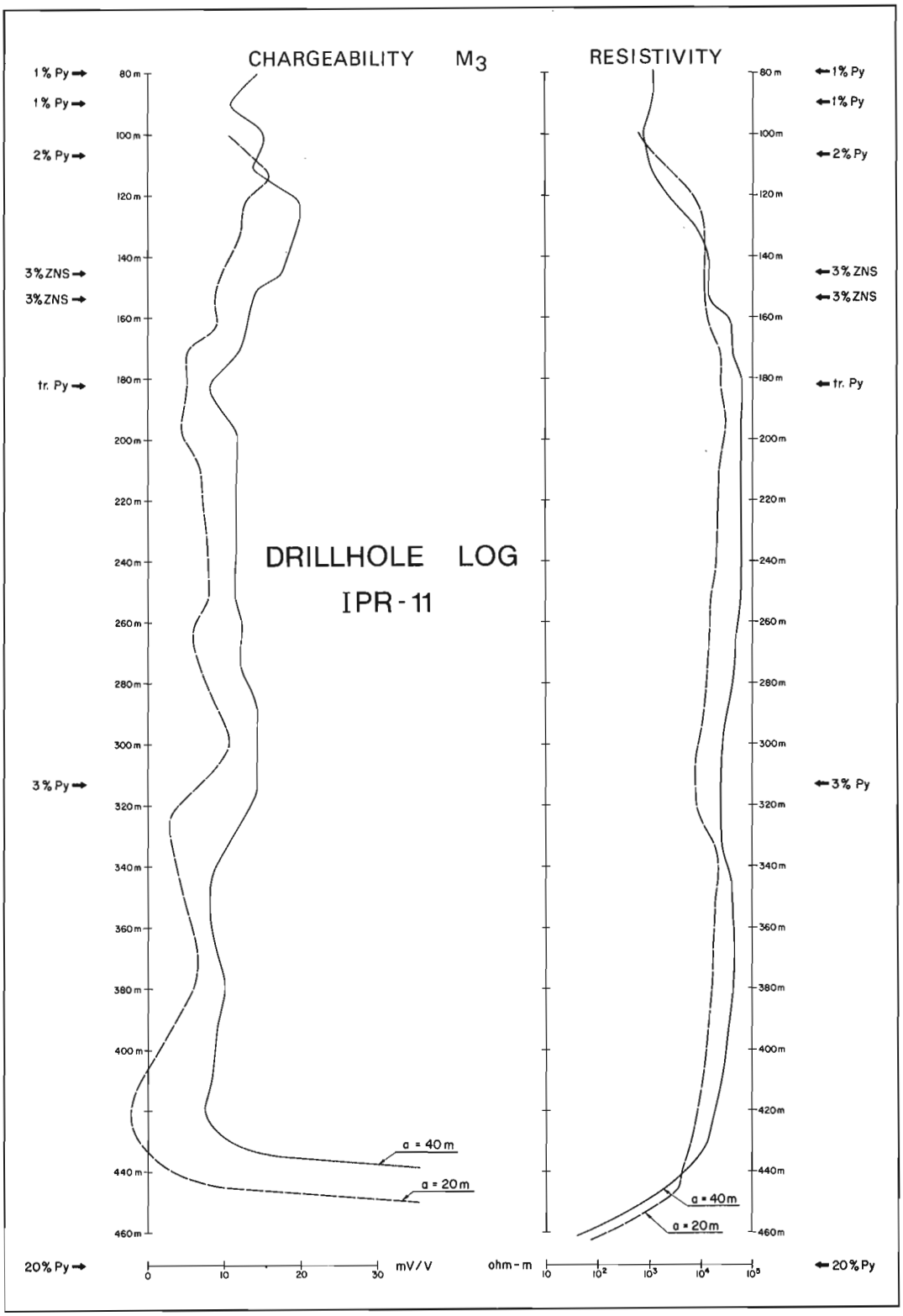

Figure 12.7. *Far-hole results ('a' spacing 20 m and 40 m) for the Nanasivic drillhole IP logs.*

observed on the resistivity profiles where the resistivity progressively increases with electrode separation. The increase in apparent resistivity is caused by a larger volume of highly resistive, permanently frozen rock being measured with increasing electrode separation.

At the bottom of the hole a large chargeability/resistivity anomaly is associated with a pyrite zone that occurs at the contact between the Society Cliff Dolomite – Arctic Bay Shale.

The directional array results are shown in Figure 12.8. The ore body strikes east-west and lies 0 to 40 m south of the drillhole. The east-west current line gives ambiguous results possibly due to the various pyrite zones in the hole which may not be associated with ore zones. Some anomalous values, however, occur between 120 and 160 m. The north-south directional log profiles are active between 120 and 160 m. The Vp/I (normalized potential) profile on the north-south log points to a body south of the drillhole at 150 m.

Spectral induced polarization information was also recorded on three surface test sites and these results were compared to spectral information data obtained from the IP responses recorded in the drillhole log.

The surface tests consisted of three test sites, for which the spectral data are summarized in Figure 12.9. The dipole-dipole array was employed with a 1 m electrode separation for n = 1 to 4.

The pyrite zone (1111) has a moderate time constant (tau = 1 sec.) and the mixed sulphide zone (3333) has a long time constant ranging between 30 and 100 seconds. These results suggest that the spectral data may allow a discrimination between the pyrite and the mixed sulphides. The Shale unit (2222) was not abnormally chargeable and its response is characterized by a short time constant (0.01 to 0.1 s).

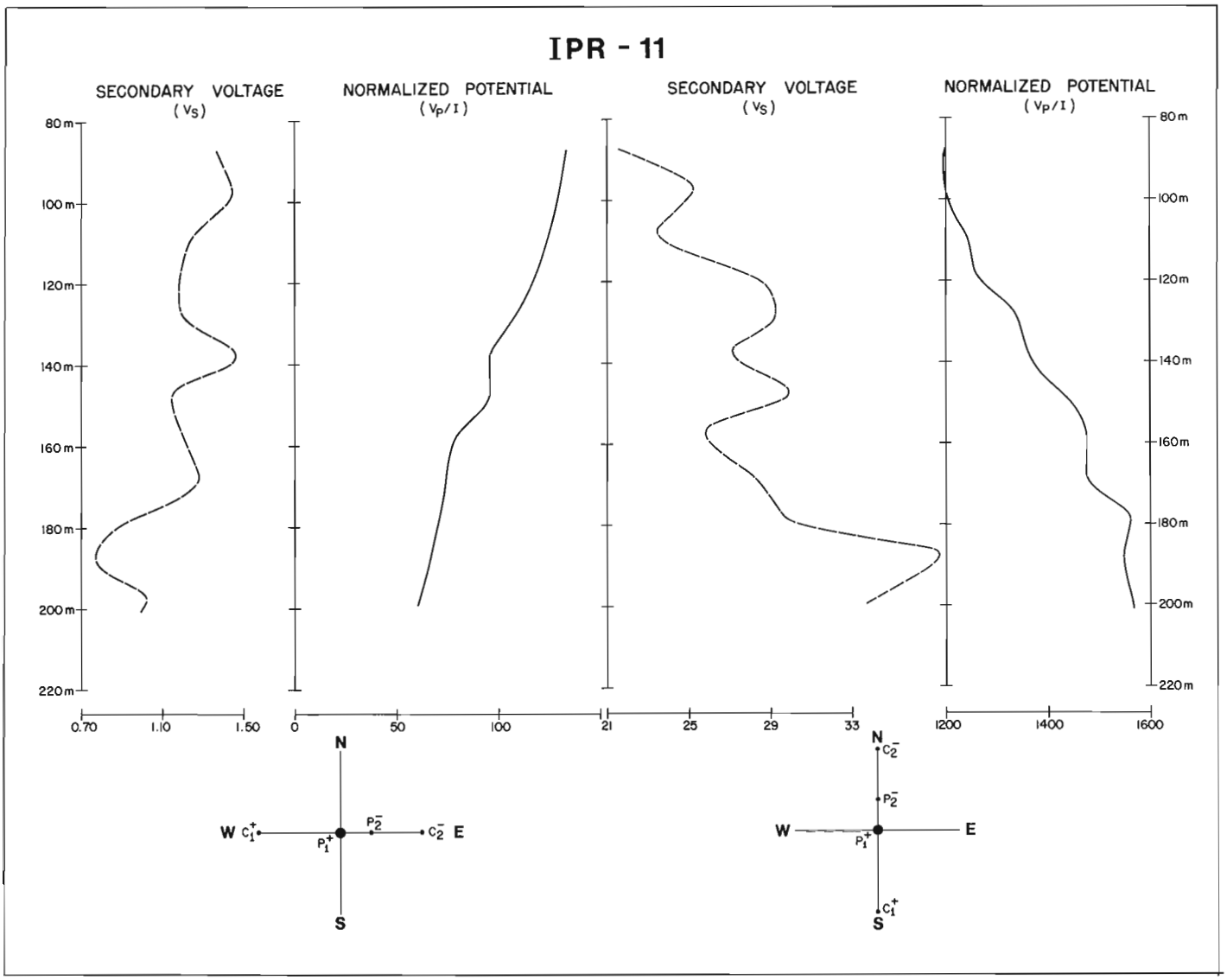

Figure 12.8. *Directional array results of drillhole IP logging of the Nanasivic deposit.*

Spectral parameters were also determined for several IP anomalies in the drillhole log. The time constants at 150 m, which are associated with Pb-Zn sulphide mineralization, are similar in the 2.5 m spacing to the response obtained on the surface Pb-Zn sulphide site (3333). The spectral data from an IP anomaly which was associated with pyrite mineralization at a hole depth of 460 m, give moderate time constants similar to those recorded on the surface pyrite test (1111).

2. Copper deposit - Quebec

The following example illustrates how a drillhole IP/resistivity survey can aid the interpretation of surface surveys.

The deposit was indicated to be a sheet dipping north at approximately 10°. Figure 12.10a shows the gradient array chargeability, resistivity and time constant profiles on two lines which cross the main mineralization (high grade sections are indicated by solid bars). The main chargeability and resistivity anomalies do not correlate to the highest concentrations of sulphides intersected by drilling. It is disconcerting that the high grade sulphide zone correlates only to a shoulder of the main anomaly at station 2S.

A drillhole was logged at station 1 + 75 north on line 00. The drillhole log (Fig. 12.10b) clearly shows that there are two significant chargeable sulphide zones with associated resistivity lows. The lower anomaly correlates with the main sulphide zone which was the exploration target. The upper anomaly correlates with a less concentrated sulphide zone which is chargeable and moderately resistive. The drillhole log proves that the upper sulphide zone responds geophysically and likely is the main source of the strong chargeability anomaly on station 00.

The time constants were also calculated from the drillhole data. The surface data indicate that the two zones have different time constants. It is important to note the time constant profiles are similar on both lines 00 and 2. This is contradictory to the drillhole data which indicates that both zones have long time constants. Additional drillhole spectral IP data from other holes may clarify this contradiction.

3. Uranium deposit - Saskatchewan (Fig. 12.11)

This example is taken from a fence of holes drilled on a uranium prospect. The resistivity and chargeability profiles show the associated geophysical response of the various lithologic units. These logs would be useful in quantifying the conductivity of various structural features (shear zones) so that the relative porosity of different horizons can be estimated. Similarily, the relative amount of chargeable material may be important in establishing the relative sulphide/graphite content of the various lithologic units. The sulphides may have formed a favourable reducing environment for uranium deposition.

IP/resistivity logging can provide accurate in situ physical properties of the various lithologies. Physical property determinations of resistivity and chargeability from core samples can be unreliable. This is particularly so in the case of rock types with variable or high porosity such as a sandstone.

MINERAL	ARRAY	SPACING (m)	n value	SPECTRAL PARAMETERS		
				C	M(mV/V)	(sec.) τ
1111 PYRITE SURFACE	DIPOLE - DIPOLE	1m	1	0.4	472.15	1.0
			2	0.4	408.00	1.0
			3	0.4	405.00	1.0
			4	0.2	650.83	30.0
2222 SHALE SURFACE	DIPOLE - DIPOLE	1m	1	0.3	122.20	0.03
			2	0.3	114.52	0.01
			3	0.3	98.12	0.03
			4	0.3	110.82	0.1
3333 ECONOMIC MINERAL PbS, ZnS, FeS_2 SURFACE	DIPOLE - DIPOLE	1m	1	0.2	606.59	30.0
			2	0.1	1027.73	30.0
			3	0.2	797.26	100.0
			4	0.2	820.24	100.0
20% PYRITE at 465m DRILL HOLE	POLE - DIPOLE	2.5m		0.3	373.88	3.0
		5.0m		0.3	377.52	3.0
		10.0m		0.3	380.69	3.0
3% SPHALERITE & 1% D_3 at 150m DRILL HOLE	POLE - DIPOLE	2.5m		0.1	128.90	100.0
		5.0m		0.1	114.64	0.3
		10.0m		0.4	30.14	0.3

Figure 12.9. *Summary of spectral IP data based on surface tests of three Nanasivic test sites.*

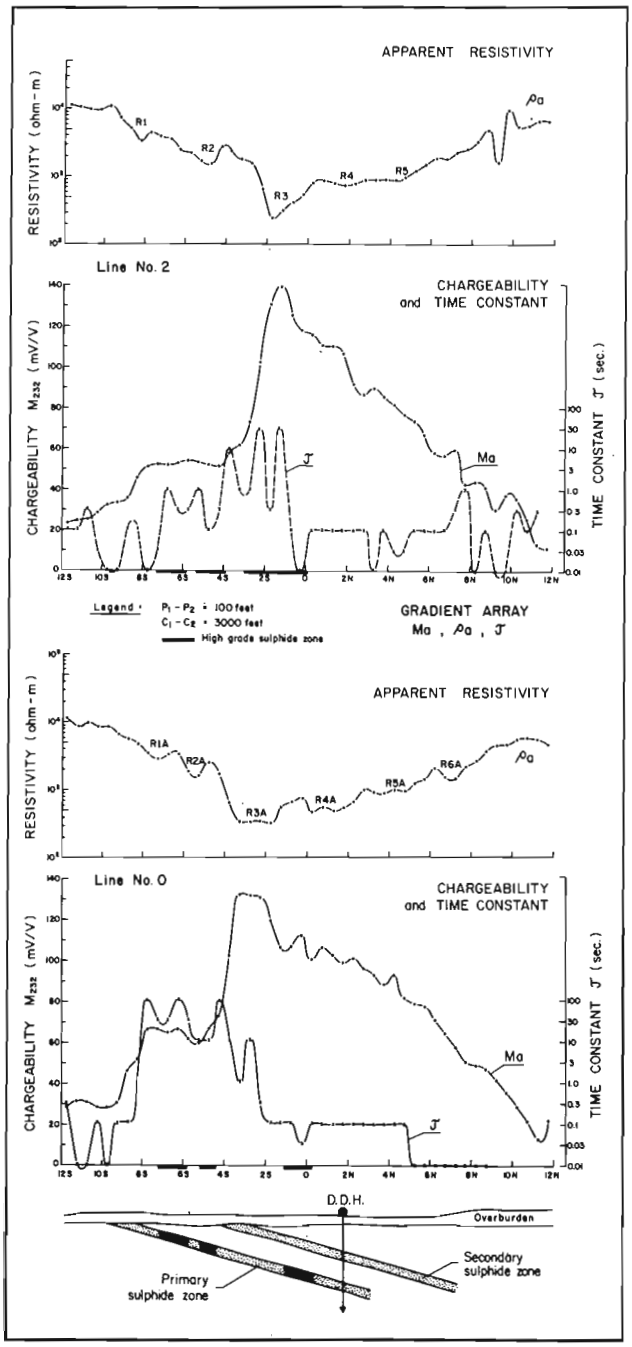

Figure 12.10a. *Surface IP results across the main mineralization of a copper deposit, Quebec.*

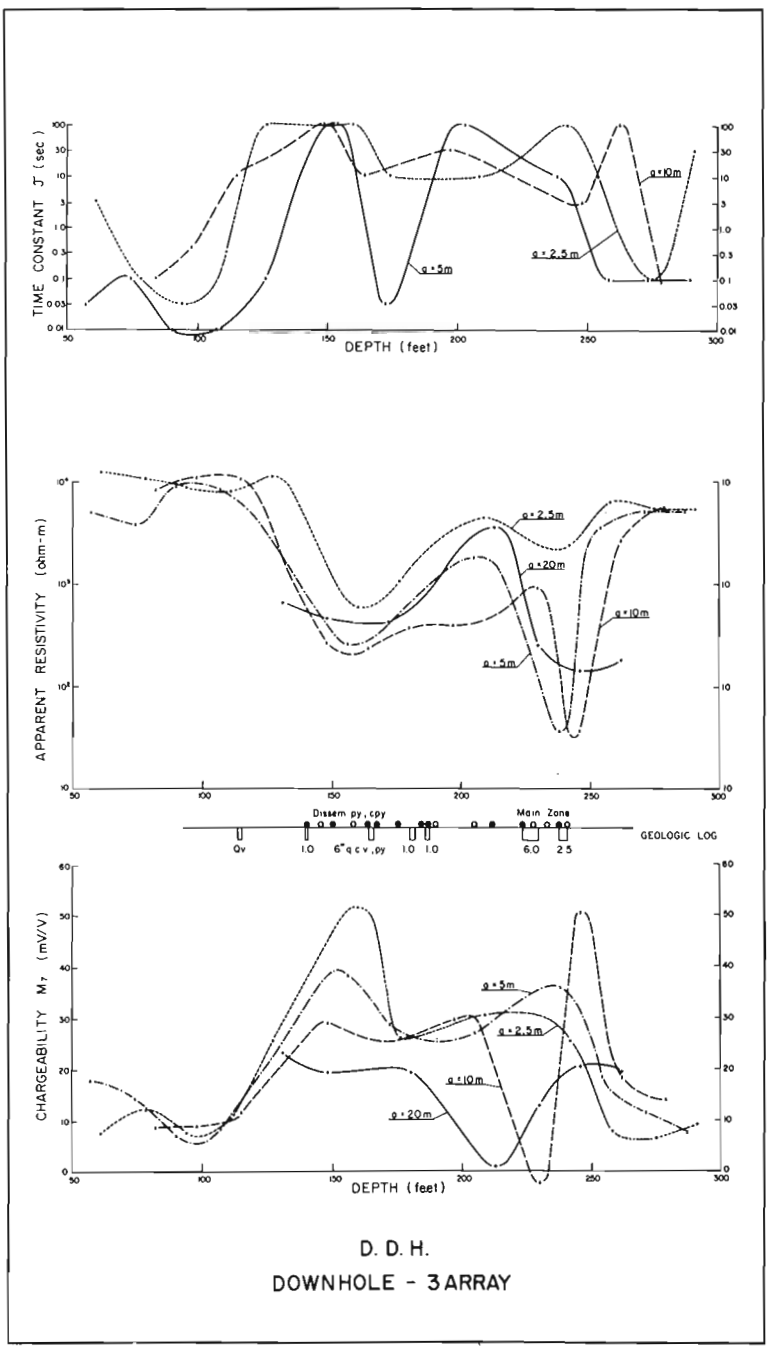

Figure 12.10b. *Drillhole IP results for the deposit shown in Figure 12.10a.*

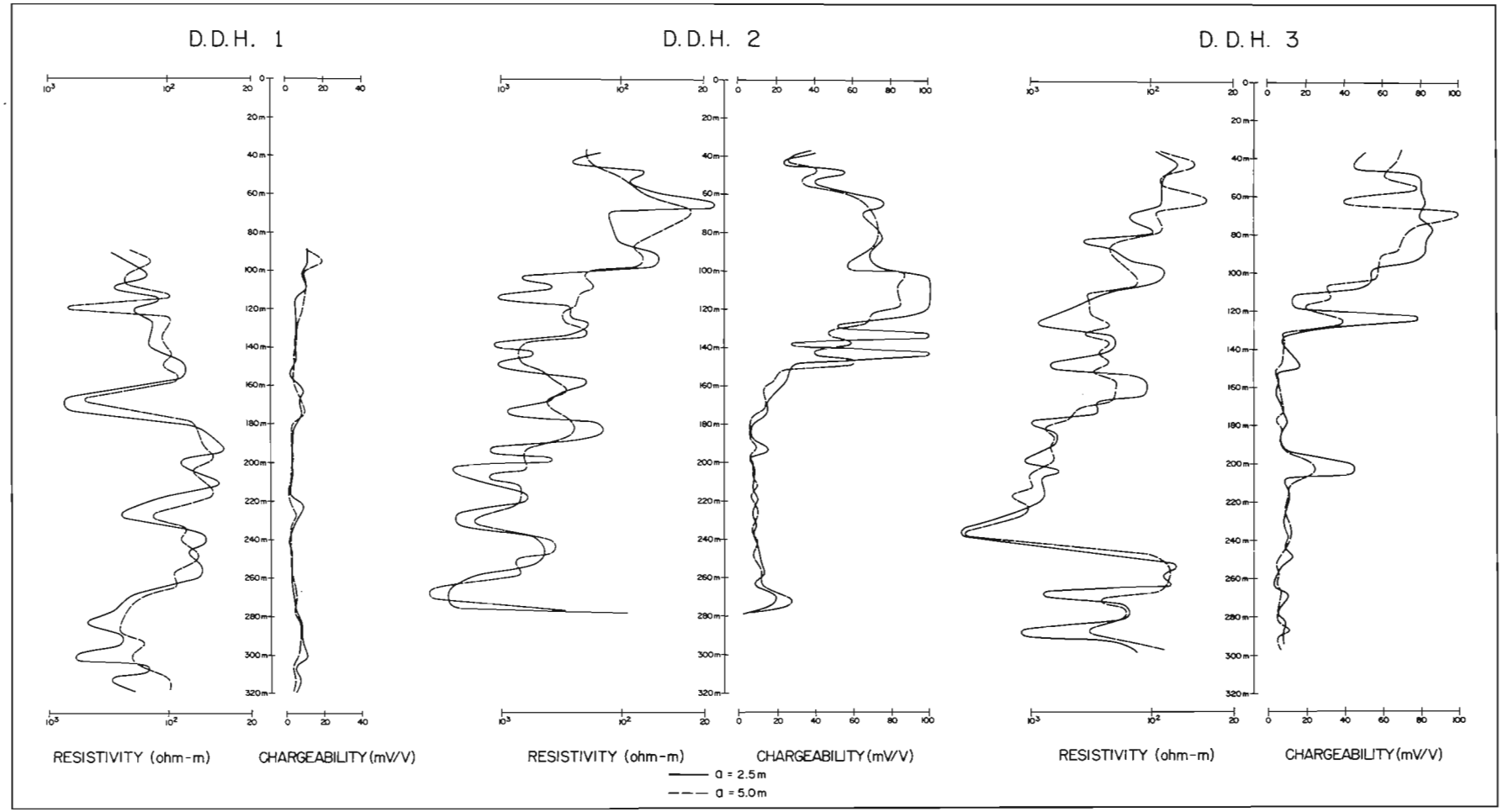

Figure 11

Figure 12.11. *Drillhole IP results for three holes in a uranium prospect in Saskatchewan.*

Economics of drillhole IP/resistivity logging

As with any drillhole logging method the economic benefits of drillhole logging can best be realized on multihole surveys. Today in a lead-zinc district in North America, holes may be drilled to 600 m at a cost of $40 000 to $60 000 each. A detection log and directional log will run approximately 5% of the drilling cost. The core radius is approximately 5 cm; the radius of exploration for the detection log is approximately 20 m. Drillhole IP/resistivity logging increases the effective exploration radius of the drillhole by 400 times at an increase in cost of only 5%.

This is, of course, oversimplified. Stratigraphic drilling is commonly, however, the main exploration methodology for carbonate hosted lead-zinc deposits. Induced polarization/resistivity logs decrease the probability of abandoning a barren hole which in fact is near mineralization.

Conclusions

Current developments in IP/resistivity instrumentation now allow multi parameter IP/resistivity drillhole surveys to be conducted economically. When modern receivers are coupled with microcomputers the data can be compiled and presented quickly.

Such surveys can be beneficial when applied in or near ore bodies to assist in the accurate definition of ore body boundaries and consequently the optimization of the mine plan and therefore the maximization of profits. In exploration projects drillhole IP/resistivity logs assist the geologist in evaluating zones of mineralization intersected by drilling.

Acknowledgments

The co-operation of the Institute of Geology and Mineral Exploration of Greece, Nanasivik Mines Limited and Campbell Resources Limited is gratefully acknowledged.

References

Johnson, I.M.
1983: Spectral IP parameters as determined through time domain measurements; Presented at the 53rd Annual Meeting of the Society of Exploration Geophysicists in Las Vegas.

Seigel, H.O., Ehrat, R., and Brcic, I.
1980: Microprocessor based advances in time domain IP data collection, in-field processing and source discrimination; Presented at the 50th Annual Meeting of the Society of Exploration Geophysicists in Houston.

Wagg, D.M. and Seigel, H.O.
1963: Induced polarization in drill holes; Canadian Mining Journal, V. 84, no. 4, p. 54-59.

13. TWO-AND-ONE-HALF DIMENSIONAL MODELS IN RESISTIVITY AND IP SIMULATION ON MICROCOMPUTERS

J. Wong[1]

Wong, J., Two-and-one-half dimensional models in resistivity and IP simulation on microcomputers; in Borehole Geophysics for Mining and Geotechnical Applications, ed. P.G. Killeen, Geological Survey of Canada, Paper 85-27, p. 119-125, 1986.

Abstract

The surface integral equation technique can be used to calculate the secondary electric potentials from bodies with polygonal cross-sections and finite strike lengths. With some approximations, the calculations can be done quickly (tens of minutes on 16-bit microcomputers with sufficient memory. Comparison with analog scale models and with results from more intricate numerical modelling schemes on mainframe computers indicate agreement (within 10 to 15%) with the present method when resistivity and induced polarization are simulated using the dipole-dipole array. Examples presented indicate how efficient and fast simulations of resistivity and induced polarization on microcomputers can assist survey planning, provide interpretational insight, and suggerst nonstandard procedures for special situations involving downhole electrodes.

Résumé

La méthode de l'équation de la surface intégrale permet de calculer les potentiels électriques secondaires des masses aux coupes polygonales et aux longueurs limitées. En utilisant certaines approximations, les calculs peuvent être effectués rapidement (dizaine de minutes) sur des micro-ordinateurs à 16 bits dont la capacité de mémoire est suffisante. Les résultats tirés de modèles réduits analogiques et de modèles numériques plus complexes produits sur de gros ordinateurs concordent (de 10 à 15% près) avec les résultats de cette méthode lorsque la résistivité et la polarisation induite sont simulées à l'aide d'un dispositif dipole-dipole. Les exemples présentés montrent comment la simulation efficace et rapide sur micro-ordinateur de la résistivité et de la polarisation induite peut aider à planifier les travaux, à fournir des indices à des fins d'interprétation et suggérer des méthodes inhabituelles dans le cas de situations spéciales demandant l'utilisation des électrodes de fond.

Introduction

Several schemes of modelling numerically the resistivity and induced polarization responses of two- and three-dimensional bodies have been formulated. They include finite element and finite difference techniques (Coggon, 1971; Dey and Morrison, 1979; Pridmore et al., 1981), volume integral techniques (Hohmann, 1975) and surface integral techniques (Barnett, 1972; Snyder, 1976; Gomez-Trevino and Edwards, 1979). All these methods involve approximations which limit the validity of the numerical results and their applicability to real geophysical exploration problems. Nevertheless, numerical modelling of resistivity and IP is both useful and important in that it provides a means of estimating the induced polarization and resistivity responses of hypothetical exploration targets. Thus, it can assist in choosing optimal electrode arrays during the survey planning stage as well as provide valuable background knowledge for the interpretation stage.

In order for numerical modelling of IP and resistivity responses to be generally useful to the resource exploration community, the methods must be readily accessible and easy to use by geophysicists who are not experts in modelling theory. In addition, the methods must be flexible enough to accommodate a wide range of geometries and conductivity contrasts but still be inexpensive in terms of computational time. Of the various formulations for IP-resistivity modelling, the surface integral method appears to be the best compromise when such factors as memory requirements, speed, flexibility, ease of implementation, and accuracy are considered. It is therefore the best algorithm to be implemented on relatively inexpensive desk-top computers.

Modelling by surface integral equation

Figure 13.1 is a schematic diagram of a two- and one-half dimensional model, i.e., a prismatic body with constant cross-section and finite strike length residing in a host rock with an overburden of uniform thickness. The modelling for a fully three-dimensional body has been discussed by Barnett (1972). Specification of the geometry of a fully three-dimensional body is a complicated task and would require cumbersome input routines in a computer program. For this reason, we will restrict our discussion to the two- and one-half dimensional target.

Referring to Figure 13.1, a galvanic current source (I) will generate a primary electric field given by

[1] Department of Physics (Geophysics), University of Toronto, Toronto, Ontario, Canada M5S 1A7

$$\vec{E}(\vec{r}) = \nabla\left\{\frac{I}{4\pi}\rho_1 G^P(\vec{r},\vec{r}_s)\right\}$$

where

$\vec{r}$ is the position vector of the observation point,

$\vec{r}_s$ is the position vector of the source I,

ρ_1 is the resistivity of the host rock, and

$G^P(\vec{r},\vec{r}_s)$ is the Green's function for the primary field.

The component of primary electric field, which is normal to the surface of the body with resistivity ρ_2, induces image charges on the surface of the body. These image charges interact with each other through secondary electric fields and modify the surface charge density distribution on the body. If we denote this surface charge density by $q(\vec{r}')$, then

$$q(\vec{r}') = 2\lambda\left\{\nabla'_n \frac{I\rho_1}{4\pi} G^P(\vec{r}',\vec{r}_s) + \int_{s''} q(\vec{r}'')\nabla'_n G^I(\vec{r}',\vec{r}'')ds''\right\} \quad (1)$$

where ∇'_n denotes the gradient normal to the surface of the body, and $\vec{r}''$ denotes position vectors on the surface. The integral is over the surface S'' of the body. $\lambda=(\rho_2-\rho_1)/(\rho_2+\rho_1)$ is the reflection coefficient of the body (Snyder, 1976), and G^I is the Green's function for charge-to-charge interaction.

If equation (1) is solved to find the surface image charges on the body, then the secondary electric potentials and fields can be calculated anywhere in space from

$$V^s(\vec{r}) = \frac{1}{4\pi}\int_{s''} q(\vec{r}'')G^s(\vec{r},\vec{r}'')ds'' \quad (2)$$

By using suitable arrays of current and potential electrodes and combining primary and secondary potentials with the appropriate geometrical factors, the apparent resistivity of the body can be found. The induced polarization effect can be considered to be the change in secondary potential (normalized by the primary potential) associated with a perturbation in the true resistivity of the target body. This change can be found directly by calculating the secondary potentials twice, i.e., once with the unperturbed body resistivity and once with the perturbed value and taking the difference. A faster but more approximate way of finding this difference is to differentiate equation (1) with respect to ρ_2 and then multiply by $\Delta\rho_2$ to find $\Delta q(\vec{r})$ and hence ΔV^s.

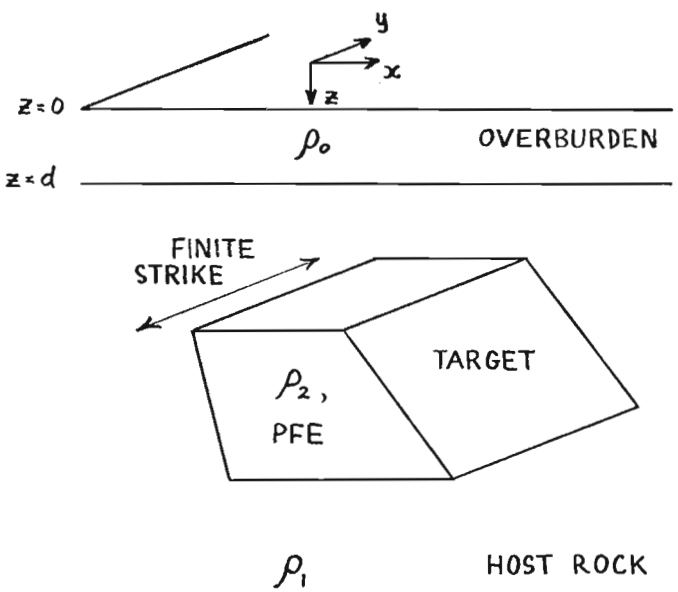

Figure 13.1: Schematic of a 2-1/2 dimensional model. The intrinsic induced polarization response of the body is characterized by a percent frequency effect (PFE).

Discretization of the surface integral equation

Equation (1) can be written in discrete form as described by both Barnett (1972) and Snyder (1976). The surface of the body is divided into small subsections with area dS_i and the charge density on each subsection is approximated by a constant or a bilinear function. With the constant approximation (which is adequate to yield good results for the dipole-dipole array), equation (1) has the discrete representation

$$q_i = 2\lambda\left\{\nabla_n \frac{I\rho_1}{4\pi} G^P(\vec{r},\vec{r}_i) + \sum_{j:\vec{r}_j \notin \vec{r}_i} q_j \nabla_n G^I(\vec{r}_j,\vec{r}_i)dS_j\right\} \quad (3)$$

where the subscripts refer to each surface subsection, and ∇_n is the normal gradient at surface element dS_i with charge q_i and position vector $\vec{r}_i$.

Equation (3) is a matrix equation which should be properly solved by matrix inversion. In order to represent the continuous surface charge density reasonably well by the

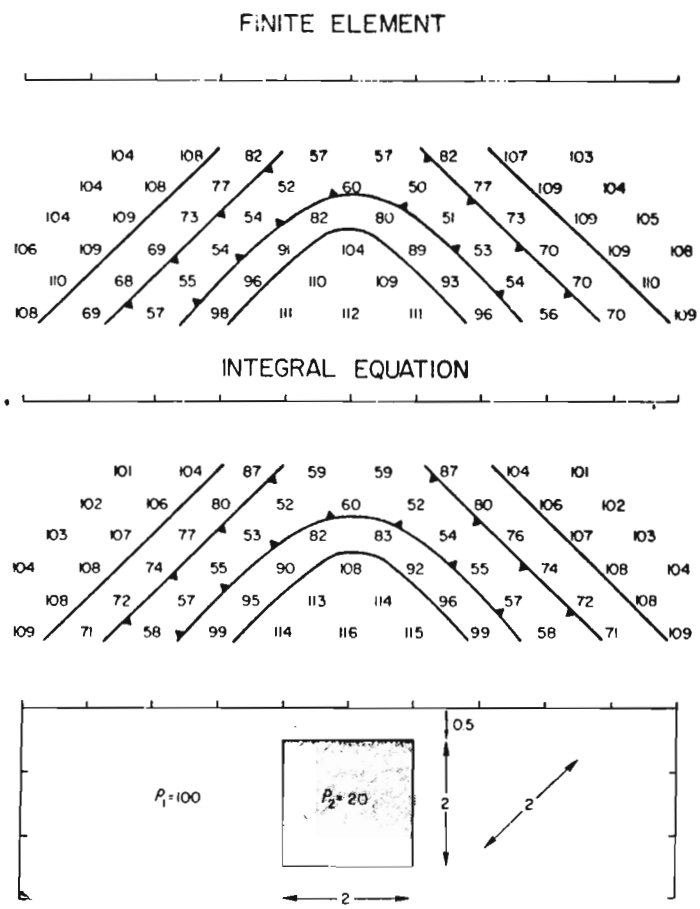

Figure 13.2: Comparison of numerical results for a standard model (after Pridmore et al., 1981).

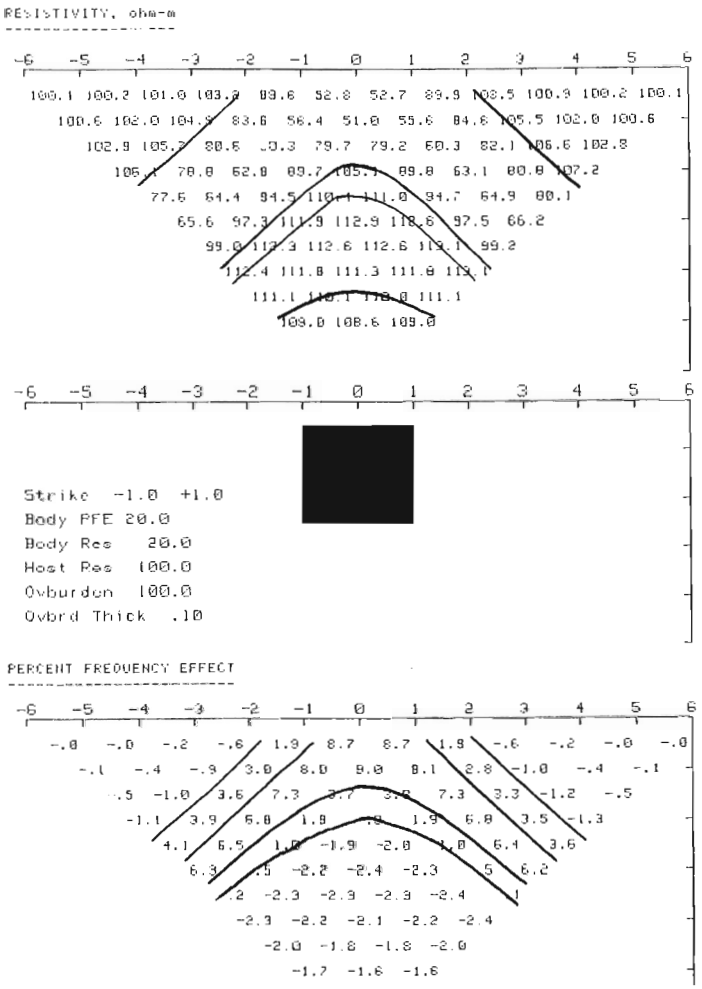

Figure 13.3: *Resistivity and IP response of the standard model modelled using the surface integral equation technique with the Born approximation.*

discrete quantities q_i, the number of surface elements must be fairly large, in the order of 200 or so. This means that the matrix to be inverted has dimensions 200 x 200, and direct inversion would be time-consuming even on a mainframe computer. We can, however, obtain approximate solutions for q_i by using Jacobi or Gauss-Seidel iterative methods. These are discrete equivalents of the Born approximation commonly used in mathematical physics to obtain approximate solutions to integral equations (Morse and Feshbach, 1953).

Iterative solutions to matrix equations work well when the matrices are diagonally dominant, a condition which is met by equation (3) when the reflection coefficient is less than about 0.8 (this is dependent somewhat on the subsectioning of the surface). Since the reflection coefficient approaches 1 when the target becomes much less resistive than the host, the iterative solution for the charge densities tends to become less accurate as the target becomes extremely conductive in comparison with the host rock. However, examples to be shown later show that, even in this case, the apparent resistivities resulting from the approximate solution to equation (3) compare favorably with those from more elaborate and expensive modelling schemes. When the approximate values q_i have been found, the secondary potential at an arbitrary observation point $\vec{r}'$ can be found via

$$V^S(\vec{r}') = \frac{1}{4\pi}\sum_i q_i dS_i G^S(\vec{r}_i,\vec{r}') \qquad (4)$$

Green's functions

For the case in which the host medium is a homogeneous half-space, the Green's functions for the primary potential, interaction potential, and secondary potential all have the same form

$$G^P(\vec{r},\vec{r}') = G^I(\vec{r},\vec{r}') = G^S(\vec{r},\vec{r}') = \left[(x-x')^2+(y-y')^2+(z-z')^2\right]^{-1/2}$$

$$+\left[(x-x')^2+(y-y')^2+(z+z')^2\right]^{-1/2}$$

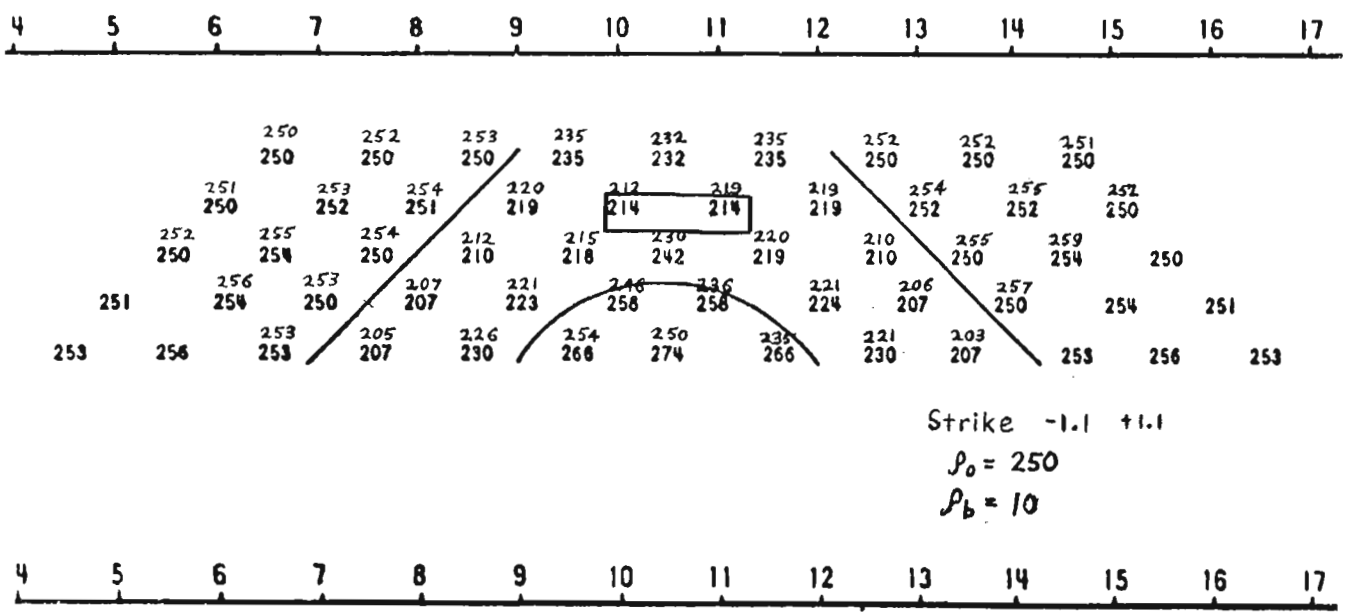

Figure 13.4: *Comparison of results from analog scale modelling with surface integral equation modelling.*

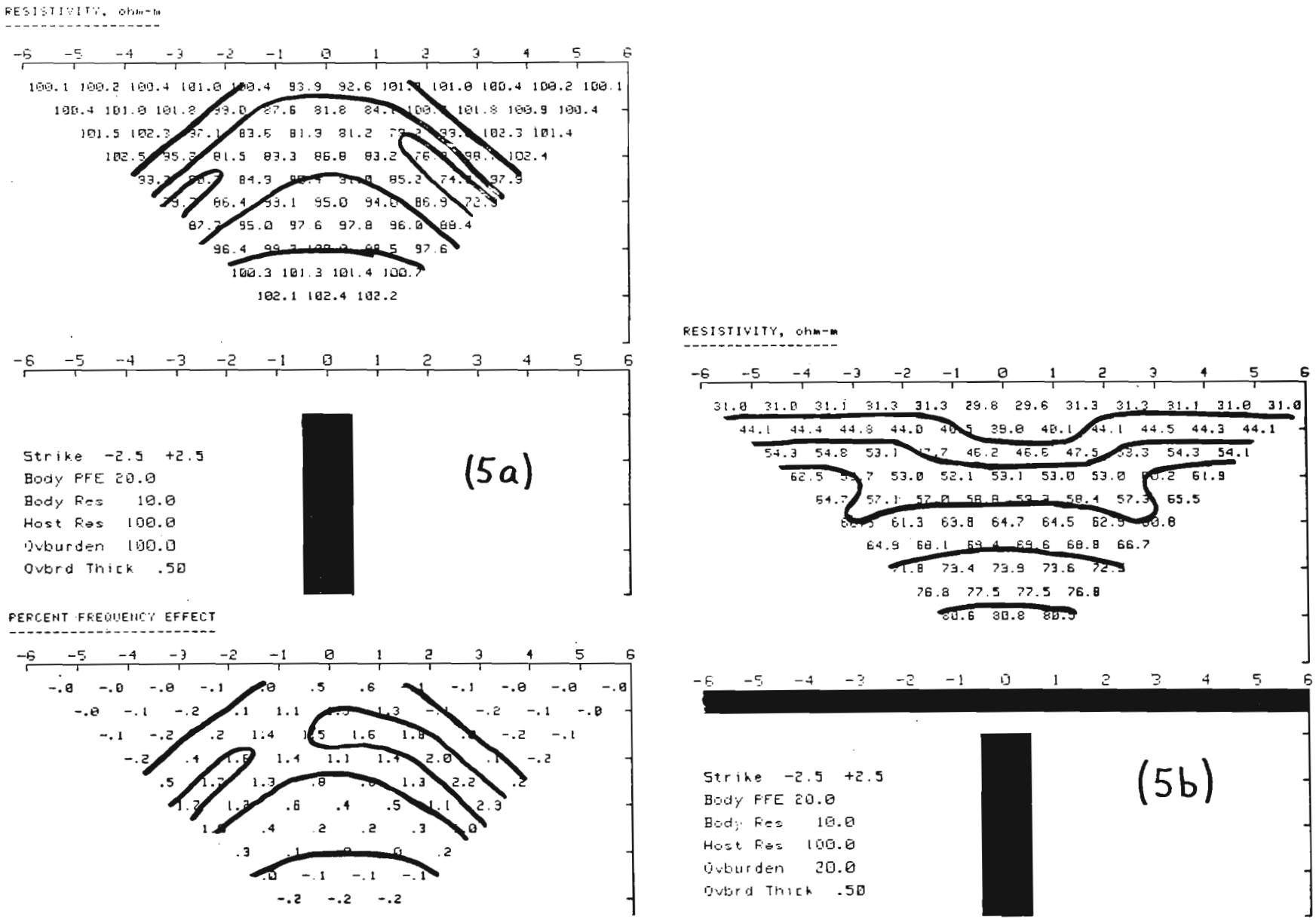

Figure 13.5a,b: *Modelling of overburden effects on the resistivity and IP response of a conductive target.*

The unprimed co-ordinates refer to the observation point, while the primed co-ordinates refer to the source point.

When the host medium includes a uniform overburden, the various Green's functions differ depending on where the source current or charge is situated and where the observation points are. These Green's functions are easily determined as convergent series by using the method of images with the appropriate boundary conditions (Van Nostrand and Cook, 1966). For example, when the source current is on the surface of the overburden (thickness d and resistivity ρ_0), the potential anywhere in the overburden is given by

$$V(r) = \frac{I}{4\pi}\rho_0 \sum_{n=0}^{\infty}\left\{\frac{k^n}{[(x-x)^2+(y-y)^2+(z-nd)^2]^{1/2}} + \frac{k^n}{[(x-x)^2+(y-y)^2+(z+nd)^2]^{1/2}},\right\}$$

$$k = \frac{\rho_1-\rho_0}{\rho_1+\rho_0}, \quad z \lesssim d.$$

while in the underlying host rock, the potential is

$$V(r) = \frac{I\rho_0}{2\pi}\sum_{n=0}^{\infty}\frac{2\rho_0}{\rho_1+\rho_0}\left\{\frac{k^n}{[(x-x)^2+(y-y)^2+(z+nd)^2]^{1/2}}\right\},$$

$$z > d.$$

Similar expressions can be written for a current source lying below the overburden. These potentials determine the Green's functions G^P, G^I, and G^S to be used in equations (3) and (4) when the host consists of an overburden over a half-space.

Results

Figure 13.2 shows the theoretical dipole-dipole resistivity pseudo-section calculated by the finite element and volume integral equation methods. The dimensions of the model are normalized by the dipole length. Figure 13.3 shows the pseudo-section resulting from the surface integral equation with the Born approximation as implemented on a Hewlett-Packard 9845 desk-top computer. The resistivities from the three different modelling techniques generally agree within 10%. The calculations on the desk-top computer took about 15 minutes; this is much more efficient and less expensive than the calculations involving the finite element and volume integral equation methods implemented on a mainframe computer (Pridmore et al., 1981).

Figure 13.4 shows a comparison between scale modelling and numerical modelling using the surface integral equation. The scale model is a salt-loaded gelatin body in a water solution. The pseudo-section is across the centre of the target. The experimental resistivities are the lower numbers on the pseudo-section, while the upper numbers are the corresponding numerically-determined resistivities. The agreement between the two sets of numbers is very good.

Numerical modelling via the surface integral equation method can be used to predict the effects of conductive overburden on the pseudo-section response of a target. Comparison of Figures 13.5a and 13.5b shows that, as expected, a conductive overburden dramatically decreases the detectability of a target and changes the pattern of the dipole-dipole pseudo-section contours.

Modelling of downhole IP and resistivity

As mentioned previously, the secondary potentials due to a target can be found anywhere in space once the surface charge densities on the target are known. Thus, although only central pseudo-sections were shown in the above examples, results along profiles with any orientation and at any location with respect to the target could be calculated as easily. This is an improvement on the finite element or finite difference techniques, where the numerical values generally are accurate only within the central portions of the mesh. In particular, the surface integral equation method could be used with current sources either on or beneath the surface of the host medium (or within the target body in the misé-a-la-masse configuration) to find potentials or potentials gradients along vertical and subvertical profiles in the host rock. In this way, it is possible to model downhole resistivity and IP responses (Daniels, 1977, 1978).

Figure 13.6a shows the cross-section of a conductive target (ρ_2 = 10 ohm-m) in a homogeneous host rock (ρ_1 = 100 ohm-m) and the position of a downhole

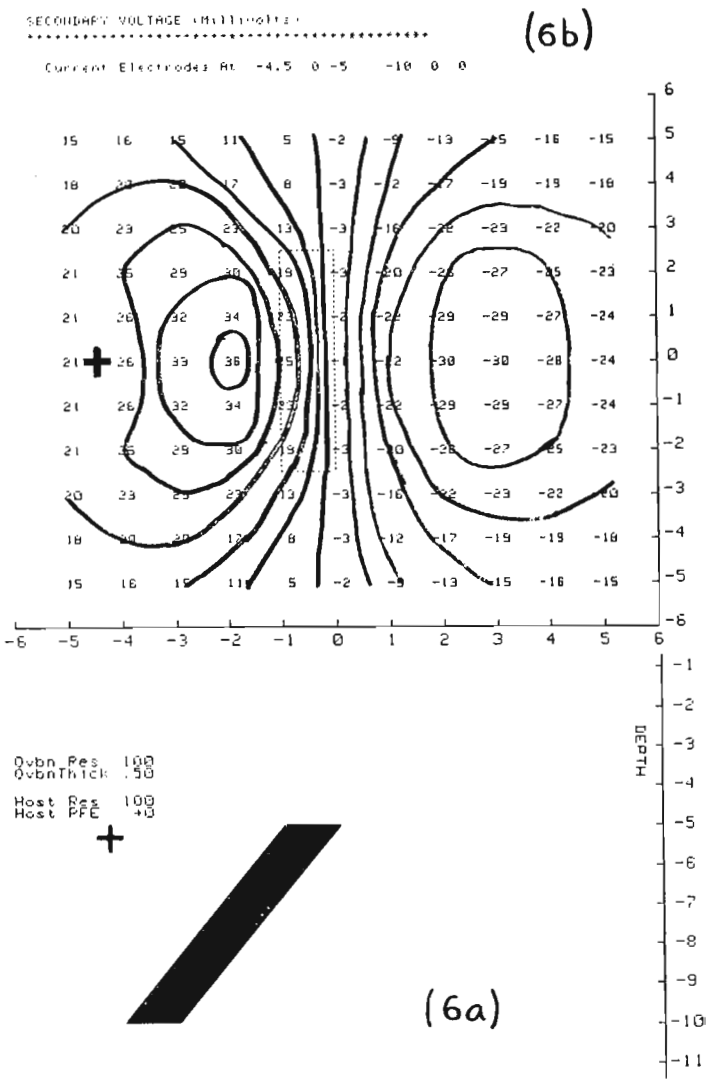

Figure 13.6a,b: Secondary potentials between two electrodes 1 unit apart due to a buried target influenced by a buried current source (location marked by +).

current source. Figure 13.6b shows the plan view of the top of the target and the location of the source. It also includes the secondary potentials as mapped out by two electrodes space one unit apart in the x-direction (the secondary potential differences are plotted at the midway point between electrodes). These numbers are related to the decay voltages due to a polarizable target. It can be seen that the location in plan view of the top of the target corresponds to a transition from positive induced polarization to negative induced polarization. This example suggests that drillhole-to-surface IP surveying could prove useful in trying to locate a suspected target near a number of barren drillholes.

Figure 13.7 shows a second example in which vertical gradient resistivities are calculated for a number of vertical profiles (i.e., along drillholes) near the target in Figure 13.6. The spacing between the downhole potential electrodes is one unit, and the source current is on the surface at -6. The resistivity profiles demonstrate the complex anomaly shapes that can be expected for drillhole electrical surveys. It must be emphasized that where the profiles penetrate the target, the modelled resistivity values are not likely to be very accurate because of the use of the discrete form of the surface integral equation and the solution of it by the Born approximation. However, the profiles are still useful and informative in a qualitative sense.

Conclusion

The surface integral equation method with the Born approximation is an efficient and useful technique for modelling the IP and resistivity responses of 2-1/2 dimensional targets in a host rock with or without a uniform overburden. The numerical results are probably accurate to about 10% as long as the current or potential electrodes are not too close to the target. For the dipole-dipole array, this means that the calculated resistivities are valid if the depth to the top of the target is not less than half a dipole unit. For shallower targets, finer subsectioning of the surface integral and matrix inversion of equation (3) is required for good results. However, as long as only semiquantitative modelling is required, the Born approximation approach will still be useful in the near-target zone. With some modifications and further approximations, it should be possible to generalize the method to include varying topography and overburden thcikness as well as multiple targets in the host rock.

Acknowledgments

The author wishes to express gratitude to the New South Wales Geological Survey and Utah Mines International Limited for their support of this research.

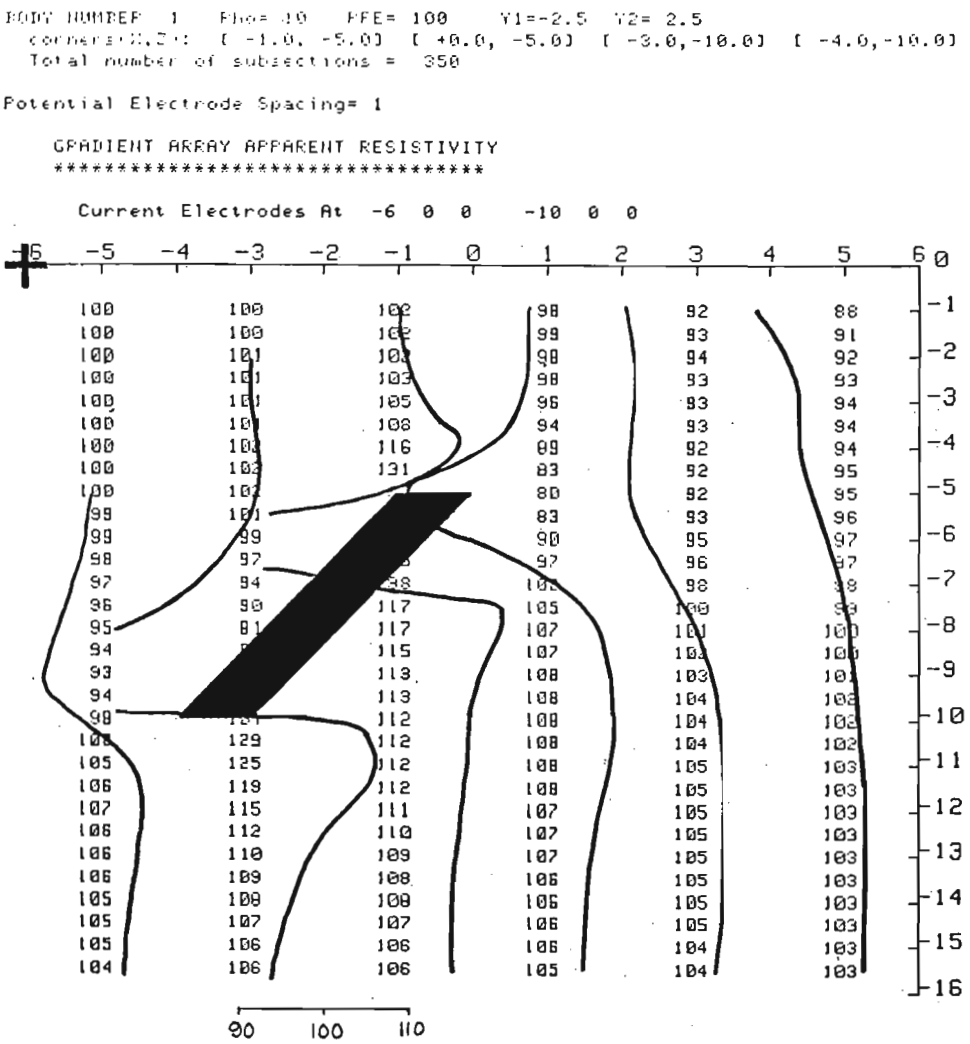

Figure 13.7: *Vertical gradient apparent resistivity profiles along drillholes near a conductive target influenced by a surface current source.*

References

Barnett, C.T.
1972: Theoretical modelling of induced polarization effects due to arbitrarily shaped bodies: D.Sc. thesis T-1453, Colorado School of Mines.

Coggon, J.H.
1971: Electromagnetic and electrical modelling by the finite element method; Geophysics, v. 36, p. 132-155.

Daniels, J.J.
1977: Three dimensional resistivity and induced polarization modelling using buried electrodes; Geophysics, v. 42, p. 1006-1019.

1978: Interpretation of buried electrode resistivity data using a layered earth model; Geophysics, v. 43, p. 988-1001.

Dey, A. and Morrison, H.F.
1979: Resistivity modelling for arbitrarily shaped three-dimensional structures; Geophysics, v. 44, p. 753-780.

Gomez-Trevino, E. and Edwards, R.N.
1979: Magnetometric resistivity (MMR) anomalies of two-dimensional structures; Geophysics, v. 44, p. 947-958.

Hohmann, G.W.
1975 Three-dimensional induced polarization and electromagnetic modelling; Geophysics, v. 40, p. 309-324.

Morse, P.M. and Feshbach, H.
1953: Methods of Theoretical Physics, McGraw-Hill Book Co., New York.

Pridmore, D.F., Hohmann, G.W., Ward, S.H., and Sill, W.R.
1981: An investigation of finite-element modelling for electrical and electromagnetic data in three dimensions; Geophysics, v. 46, p. 1009-1024.

Snyder. D.D.
1976: A method for modelling the resistivity and IP response of two-dimensional bodies; Geophysics, v. 41, p. 997-1015.

Van Nostrand, R.G. and Cook, K.L.
1966: Interpretation of resistivity data; United States Geological Survey, Professional Paper 499.

14. A SYSTEM FOR THE DIGITAL TRANSMISSION AND RECORDING OF INDUCED POLARIZATION MEASUREMENTS IN BOREHOLES

Q. Bristow[1]

Bristow, Q., A system for the digital transmission and recording of induced polarization measurements in boreholes; in Borehole Geophysics for Mining and Geotechnical Applications, ed. P.G. Killeen, Geological Survey of Canada, Paper 85-27, p. 127-143, 1986.

Abstract

A system has been developed at the Geological Survey of Canada for acquiring time domain induced polarization (IP) borehole logs which transmits data from the downhole probe in digital form. A surface transmitter generates conventional "positive-off-negative-off" current waveforms with amplitudes from 1 to 254 milliamps controlled by a computer according to received signal amplitude. The signal waveforms are recorded as 256 channel spectra with depth data on magnetic tape at minimum intervals of one second. A lightweight, shielded, twisted pair cable with a neoprene jacket is used. Field tests to verify the performance showed that it was also possible to record a useful "Single Point IP" signal, analogous to Single Point Resistance, with only a current electrode downhole. Test logs are presented which show excellent repeatability and illustrate the versatility of the system.

Résumé

La Commission géologique du Canada a conçu un système permettant de transmettre les données d'une sonde de fond sous forme numérique afin de réaliser des diagraphies de trou de sondage par l'enregistrement de la polarisation induite (PI) en fonction du domaine du temps. À la surface, un émetteur produit des formes d'onde classique de courant "positif-fermé-négatif-fermé" dont les amplitudes, qui vont de 1 à 254 mililampères, sont contrôlées par un ordinateur en fonction de l'amplitude du signal reçu. Les formes d'onde du signal sont enregistrées sous l'aspect de 256 spectres de bande, avec l'indication de la profondeur, sur une bande magnétique à des intervalles minimaux d'une seconde. On utilise pour ce faire un câble léger consistant en un câble à paires torsadé, blindé et gainé de néoprène. Les essais de rendement effectués sur le terrain ont révélé qu'il est également possible d'enregistrer un signal de polarisation induite en un point unique, comme pour la résistance en un point unique, à l'aide d'une seule électrode émettrice installée dans un trou de sondage. Les diagraphies d'essai qui sont présentées ont un excellent indice de répétition et témoignent de l'excellente polyvalence d'utilisation du système.

Background

The Resource Geophysics and Geochemistry Division of the Geological Survey of Canada has a continuing program of R&D aimed at improving and standardizing measurement and interpretation techniques in borehole logging. One of the borehole logging techniques is natural gamma ray spectrometry, for which instrumentation based on a Data General NOVA minicomputer has been used. This vehicle-mounted system has been described previously (Bristow and Killeen, 1978; Bristow, 1979a). The same system, and much of the same software, have been adapted to record induced polarization measurements in boreholes with accompanying resistivity and spontaneous potential (SP) data. The waveforms are recorded in digital format with the highest possible fidelity on a continuous basis. Off-line processing can then be carried out as often as required on the same data using digital techniques to optimize interpretation methods. This paper describes the equipment and the features which are considered to represent improvements over that which is presently available for borehole IP measurements.

Summary of the principles of induced polarization

When a current is passed through a metal-electrolyte interface an overvoltage is developed across the interface which increases nonlinearly with time to a limiting level dependent on the current. This is due in part to a continuing accumulation of ions of one polarity close to the metal interface. If the current source is removed and replaced by a short circuit, then a reverse current will flow until an electrically neutral equilibrium of positive and negative ion concentrations is restored. The interface thus behaves in some respects like a capacitor containing a polarizable dielectric which can be charged and discharged (see e.g. Telford et al., 1976).

The same phenomenon occurs at the myriad interfaces formed between metallic minerals and pore fluids in formations containing disseminated sulphides when a current is passed through them. The diagnostic property is the time dependent voltage increase observed after current turn-on and the corresponding decay after current turn-off,

[1] Geological Survey of Canada, 601 Booth Street, Ottawa, Ontario K1A 0E8

(see e.g. Sumner, 1976). The phenomenon was first investigated by Conrad Schlumberger in France who obtained a patent in 1912 for application of the technique for mineral exploration. The underlying principles were investigated extensively by a group at Newmont Exploration after World War II and publications which resulted from this work stimulated widespread use of the method as a base metal exploration tool (Wait, 1959; Seigel, 1959; Bleil, 1953; Madden and Marshall, 1959). The vast majority of IP surveys are carried out using electrode arrays on the surface, with relatively few workers using downhole electrodes.

In both modes of operation, current is injected into the ground from a suitable transmitter by means of one pair of electrodes, while the resulting potentials are sensed with a second pair. The time dependent parameters can be observed either by applying the current as a square wave function (with alternate polarity reversals to avoid the cumulative effects of polarization), or by applying it as a series of sinusoidal waveforms of different frequencies. In the first case (time-domain IP), the time dependent polarization parameters can be observed directly in the signal recorded by the potential electrodes as departures from the square waveform generated by the exciting current. In the second case (frequency domain IP), the time dependent polarization parameters are determined indirectly by measurements of shifts in amplitude and phase of the received signal with respect to the exciting current waveform as the frequency is changed.

A considerable body of published literature on the subject of induced polarization exists, however only a small part of it is concerned with techniques or equipment for borehole IP measurements (e.g. Dakhnov et al., 1952; Wagg and Seigel, 1963; Bacon, 1965; Brant et al., 1966; Snyder et al., 1977; Hallof, 1980; Ogilvy, 1984). Two interesting papers have recently appeared in print: Vinegar et al. (1985) described a system similar to the one which is the subject of this paper, and Ogilvy (1985) described anomalous negative IP effects recorded in boreholes. His explanation closely parallels one presented in this paper.

Some aspects of present borehole logging technology

Borehole logging equipment has been extensively developed for oil and gas exploration and is a universally accepted technique in that industry. An inevitable consequence has been the establishment of de facto standards in equipment design and manufacture appropriate for large diameter holes. This presents difficulties in adapting off-the-shelf systems to mineral exploration, where costly diamond drilling in relatively inaccessible terrain places severe constraints on the overall weight of equipment and the diameter of the tools which can be used.

One such standard component is the four conductor steel armoured cable designated as "4HO" (now 4H18RB), which weighs 91 kg/km and requires a substantial winch for raising and lowering the logging tool. Logging systems for gamma ray spectrometry and pulse EM developed to GSC specifications by McPhar Geophysics and Crone Geophysics respectively, incorporate neoprene-jacketed, shielded, twisted pair cables weighing only 35 kg/km. The lighter cable allows a corresponding reduction in the size and weight of the winch and power source required. Since in any logging system the cable, winch and power source account for the bulk of the weight, the reduction in size and weight of all three is a considerable dividend.

Oil and gas wells are usually a minimum of 100 mm in diameter and as a result the various logging tools designed for use in them are rarely less than 50 mm in diameter. Diamond-drill holes for mineral exploration by contrast are typically "BQ" size (60 mm diameter), which limits logging tool diameters to approximately 40 mm.

Conventional logging systems for time-domain IP and/or SP and resistivity measurements use tools with electrodes only (normally made from lead), and no active electronics. The signals are transmitted directly to the surface equipment as analogue voltages. The possibilities for noise pick up in a long cable with the low signal levels involved are considerable, and in the case where a current electrode is being fed via an adjacent conductor, some interference is almost inevitable.

The use of the "4HO" cable, with its conductive steel wrap, limits operational flexibility in the selection of electrode configurations for some electrical measurements. For example one useful configuration is to have both current electrodes remote from the downhole potential electrodes, either on the surface or in adjacent holes. The presence of an equipotential line (the cable) running from the surface down to the tool might then cause undesirable effects by distorting the potential field in the vicinity of the borehole.

Surface processing of signals received from the tool has of course been revolutionized by the availability of high quality and relatively inexpensive A/D converters and microcomputers. More and more data will undoubtedly be processed on-line as this revolution progresses. In the interim however field data must be stored for off-line processing and the most universal, compact and reliable of available mass storage devices for field use continues to be nine-track magnetic tape. The storage capacity and reliability far exceed that of flexible discs and almost all data processing centres support the nine track tape medium.

System design objectives

The equipment to be described was designed for use in a research program to increase the level of knowledge and understanding of IP phenomena observed in boreholes and their relation to the presence of mineralization. Sufficient flexibility was required to cover a wide variety of experimental modes of operation and configurations. It was also desirable to be able to examine raw data which had been recorded with the minimum of preprocessing and with the best possible signal-to-noise ratio. Since the system would be experimental, it was reasonable to consider incorporating any recent advances in technology or new approaches which appeared likely to improve the accuracy and reproducibility of the measurements, even if their reliability record was as yet unproven. This is an entirely different approach from that used in the design of commercial equipment, where the emphasis must be on proven technology and techniques, a minimum of costly options, streamlined packaging with operator convenience in mind, and presentation and recording of data in nearly final form as possible. With the above requirements in mind the design objectives were set as follows:

- Time-domain rather than frequency domain operation, with a constant current transmitter generating a conventional "positive-off-negative-off", waveform in order to minimize the time required for a single measurement and to permit continuous rather than stepwise logging.
- Recording of complete received signal waveforms digitized at a minimum of 256 samples per complete cycle; with a maximum rate of one complete cycle per second.
- Tool diameter to be less than 40 mm, with provision for easy connection of a variety of different electrode arrays.
- In-tool signal conditioning and A/D conversion in order to eliminate any noise injection or signal distortion occurring in the signal path from tool to surface.

- The use of chemically reversible (non-polarizing) electrodes in the tool as potential sensors rather than the traditional lead ones.
- Electrical isolation of the potential electrodes and associated analogue signal conditioning circuitry from the surface equipment. The rationale here was to avoid the necessity of impressing the large common-mode voltage signals generated between the tool and the surface, onto the low level signals which are being transmitted between them. By isolating the measurement circuitry, the possibility of referencing potential measurements to a point on the surface is precluded, so that only potential gradients can be transmitted.
- Transmitter/receiver (T/R) unit and logging tool to be developed as far as possible as an independent subsystem, with a view to making the technology available to Canadian industry, with standard interfacing to commonly used data acquisition systems or personal computers.
- Compatibility with the insulated shielded twisted pair logging cable already in use by the GSC research group for the measurement of other parameters. It is also an overall objective to make this lightweight cable standard for all tools which are used in the continuing borehole logging research program.
- Compatibility with an existing truck-mounted, research-oriented data acquisition system based on a Data General Corporation NOVA minicomputer.

Overview of experimental borehole IP system

The IP system, which was assembled and is now being used for preliminary studies, is shown in block diagram form in Figure 14.1. The top section of the logging tool consists of a stainless steel tube containing the signal conditioning and A/D conversion electronics plus a dry battery pack. Current and potential electrodes were constructed in several commonly used configurations using gold plated brass cylinders. The electrodes are separated by insulating sections machined from PVC material for closely spaced electrode pairs. Flexible rubber covered cable of appropriate length is used to make the connections between these assemblies for widely spaced electrodes.

The T/R unit contains a programmable constant current supply with provision for connecting the output terminals to two remote electrodes, or to one remote electrode and one in the downhole array. The potential signal is received from the tool as a modulated frequency and fed to circuitry in the T/R unit via an optical coupler, thereby electrically isolating the entire potential measurement circuitry in the tool from the surface equipment. The current waveform is fed to the tool current electrode via one conductor of the twisted pair when the array configuration requires a downhole current source. The shield and second conductor are used to transmit the frequency signal to the optical coupler.

The data acquisition system consists of the following components:

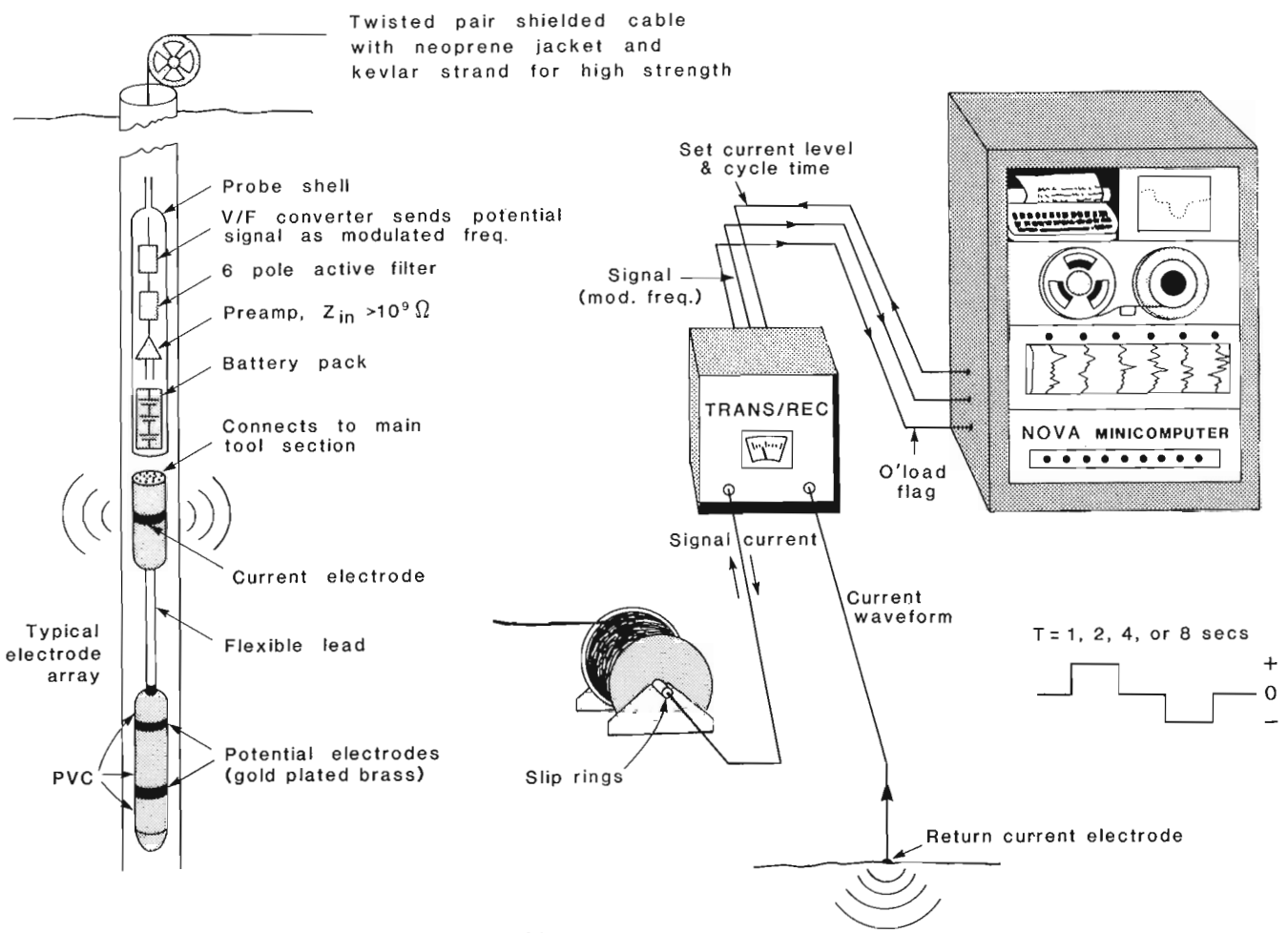

Figure 14.1. System block diagram.

- NOVA 1220 minicomputer (Data General Corp.).
- Nine track magnetic tape transport (DIGIDATA Inc. with NOVA interface board).
- CRT display consisting of a Tektronix model 604A X-Y monitor which provides a continually refreshed display of "pages" of alphanumeric or graphic data stored in various blocks of NOVA memory. The necessary character generation, raster scan and D/A conversion circuitry to implement text and/or graphic display modes is built onto an interface board contained in the NOVA chassis. Operation is by direct memory access with keyboard entries for selection of pages of data to be displayed.
- An RMS Instruments chart recorder with alphanumeric print capability. This microprocessor controlled instrument allows real time plotting of up to six parameters with depth printout at specified intervals and fiducial lines across the chart.
- Texas Instruments "Silent 700" Model KSR743 data terminal for operator communication with the system.

A software operating system, written in assembly language for maximum speed in on-line processing and easy adaptation to non-standard interfaces, allows complete control by the operator via keyboard entries of all system parameters while logging.

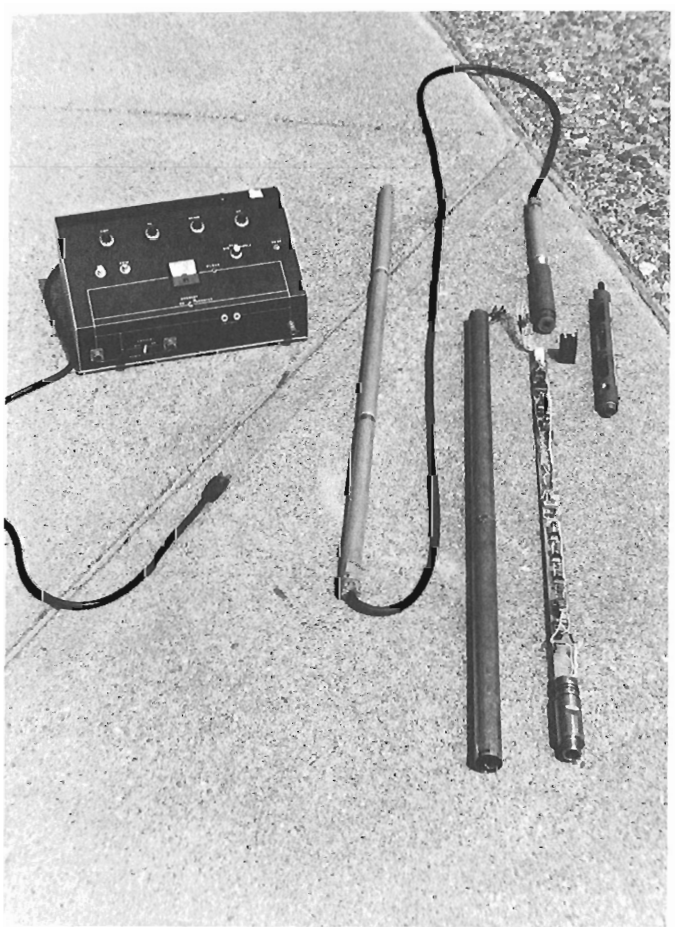

Figure 14.2. *The T/R unit, a pole-dipole electrode array, and the disassembled logging tool showing circuit board containing amplifier, filter and V/F converter. Battery pack is shown with one of the three 9V transistor batteries beside it.*

A key feature of the software is the automatic control of the transmitter current, which is done on the basis of received signal amplitude. If a transmitter overload occurs, the current is automatically reduced to 75% of the value which caused the overload. This value is then stored as the maximum allowed current unless or until this upper limit is revised by a keyboard entry. The option of a fixed current (specified from the keyboard) can be selected as an alternative to the auto-current mode.

Depth data are recorded from a shaft encoder driven by the well-head pulley as the logging cable moves over it. This data acquisition system has been used to record gamma ray spectral data, temperature data and electrochemical parameters with various logging tools since 1978.

Detailed system description

IP logging tool

A photograph of the logging tool and contents is shown in Figure 14.2. There are four functional blocks of electronics as follows:

- Regulated ± 10V power supply, operated by three standard 9 volt transistor radio alkaline cells. These provide at least 8 hours continuous operation of the tool at a temperature of 10°C. Transmission is switched off automatically when the battery voltage falls to a predetermined level to avoid recording unreliable data.
- High input impedance (10^{10} ohm) preamplifier for potential electrode signals with switch selectable gains of X2; X10; X100. The device used is a premium quality bipolar monolithic IC operational amplifier with low noise and drift characteristics (Monolithics Corp. OP-07).
- 6 pole Butterworth active low-pass filter with a 3db cutoff set at 30 Hz. This is incorporated to ensure rejection of 60 Hz ground current noise contributions to the signal. The filter is implemented with three low power IC operational amplifiers and associated RC networks and has zero insertion loss in the pass band.
- Analogue to digital conversion of the signal following the filter is accomplished by a monolithic IC voltage-to-frequency converter (Analog Devices Inc., Model AD537). The device is biased so that the zero signal level corresponds to a frequency of approximately 75 kHz. Full scale negative and positive inputs at the potential electrodes generate frequencies of 20 kHz and 130 kHz, respectively. The frequency signal is in the form of a 20 mA current square wave derived from the battery operated power supply, and is transmitted to the surface via the shield and one conductor of the twisted pair in the logging cable.

The stainless steel portion of the tool is in two sections separated by a bulkhead with "O" ring seals on each side. The upper section houses the circuit board with the electronics and is terminated with a standard Gearhart Owen cable connector having four connector pins. The lower section of tubing houses the battery pack (3 batteries slotted into a solid PVC rod as shown in Fig. 14.2) which is easily removed for battery replacement by means of a bayonet lock. This pack also contains the switch for changing the preamplifier gain. A connector at one end of the pack engages with a mating connector in the bulkhead and makes the necessary connections for the electrode leads, gain switch and batteries. The electrode leads are routed past the batteries and out at the lower end to the electrodes via pressure tight "O" ring seals. Chemically reversible electrodes have not yet been fitted to the tool and to date gold plated brass cylinders have been used instead in order to minimize unwanted contact potential variations. Gold is considerably less

chemically active than lead in this respect, although still not chemically reversible. Figure 14.3 shows details of the electrode assemblies.

Transmitter/Receiver (T/R) unit

A block diagram of this unit is shown in Figure 14.4; the functional blocks are as follows:

- Programmable constant current supply controlled by the NOVA minicomputer.
- Overload sense and flag circuitry.
- Optical coupler for electrical isolation of tool measurement electronics from current generating circuitry.
- Current switching circuitry controlled by the NOVA via optical couplers to allow electrical isolation of the T/R unit from the rest of the data acquisition system.
- Differential amplifier to allow recording of the voltage waveform between the supply terminals.
- IP signal waveform simulator.

The constant current supply is of conventional design except for the use of a power MOSFET rather than a bipolar transistor as the current generator. These devices are rugged, relatively inexpensive and by their nature draw no power from the control circuitry connected to the gate electrode. A further advantage in this application is the assurance that since there is no gate current, the drain and source currents are always equal, even at the 1 mA level. The voltage measured across the source resistor thus accurately reflects the current actually delivered to the current electrodes over the full design range, which in this case is 1-254 mA.

The current level is set by a 12 bit D/A converter of which only the most significant 8 bits are used. This generates a reference voltage which is used by an error amplifier to maintain the voltage across the MOSFET source resistor (marked "R" in Fig. 14.4), at the same level, thereby setting the current delivered to the formation. If the formation resistance encountered between the output terminals (i.e. between the current electrodes) requires a voltage greater than the supply can provide (approximately 150 VDC), then the reference voltage and that across "R" will no longer be matched and an overload sense circuit will be triggered, flagging the computer that the received signal waveform is invalid. A second D/A converter, identical with the current-setting unit and driven in parallel with it, is used to vary the sensitivity of the overload sense circuit with current level, so that it can be set to trigger for a deviation which is a fixed percentage of the level set at any time. The system presently operates with the overload trigger set for detection of a 2% difference between the current set and the current delivered.

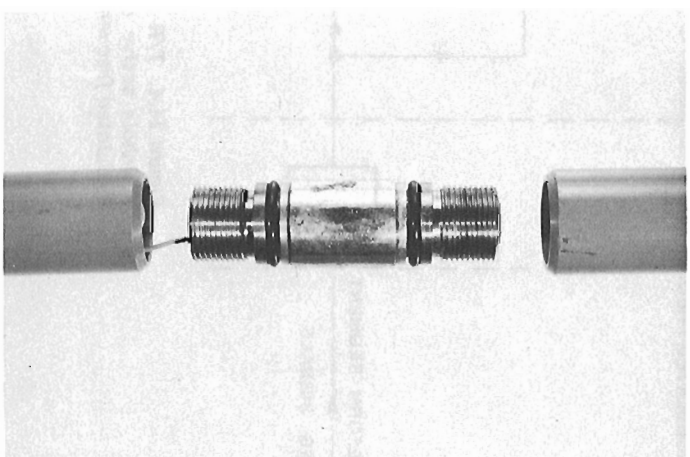

Figure 14.3. *The electrode arrays use gold-plated brass cylinders for the potential electrodes. They are screwed into sections of PVC rod with "O" ring seals.*

One terminal of the supply is normally connected to the tool current electrode, while the other one may be connected to a surface electrode some distance from the surface equipment, or to an electrode down an adjacent hole. In either case an unknown alternating potential difference can be expected between the ground on which the surface equipment is situated and the current supply circuitry, as the current is cycled through the positive-off-negative-off sequence. Optical isolators are therefore used to provide electrical isolation between the NOVA control signals and the supply itself. The overload signal to the NOVA is similarly isolated. This prevents an undesirable voltage difference between the chassis of the data acquisition system and the area of ground where it is located.

The frequency signal from the tool is isolated from all other circuitry by an optical coupler in the T/R unit, from which it is routed to the frequency measurement circuitry in the NOVA.

An IP signal waveform simulator is incorporated into the T/R unit which can be switched in to replace the waveform received from the tool at any time. Provision is included for varying the amplitude, rise and decay times, and the zero level of the signal. This simulates variations in resistivity, IP effect and SP respectively. The waveform is applied to a separate V/F converter in the T/R unit so that the NOVA receives a signal as if it had been generated in the logging tool.

A differential amplifier with a high input impedance (40 Megohms), is connected across the current supply terminals. The signal from it is connected to a second V/F converter in the T/R unit. A front panel switch allows selection of this waveform for recording as an alternative to the one generated by the downhole tool. The voltage between the current electrodes has traditionally been recorded as "single point resistance" in unsophisticated systems. It also provides "Single Point IP" information, which is discussed in a later section of this paper.

Current switching signals are generated in the NOVA interface, these actuate relays in the T/R unit which reverse the polarity of the electrode terminal connections during the OFF periods. A front panel meter displays current level and an LED indicator flashes when overloads occur. A safety switch is provided to short circuit the current supply while electrode connections are being made. The unit also has a main AC power switch. The current supply terminals are accessible as front panel banana jacks, in addition one of the terminals is routed to the logging cable connector. This provides adequate flexibility for any configuration of current electrodes that may be required.

Acquisition of received waveforms

Figure 14.5 shows a typical potential waveform that would be sensed by the potential electrodes in the tool as the current cycles through the "Positive-Off-Negative-Off" sequence. The horizontal line labelled "BASELINE LEVEL" represents the potential seen by the electrodes in the absence of any transmitter generated current. If no SP is present this will be zero, in which case the V/F converter will transmit a steady frequency of approximately 75 kHz. This frequency will shift to a full scale maximum of 130 kHz if the potential electrodes sense a full scale voltage difference when the

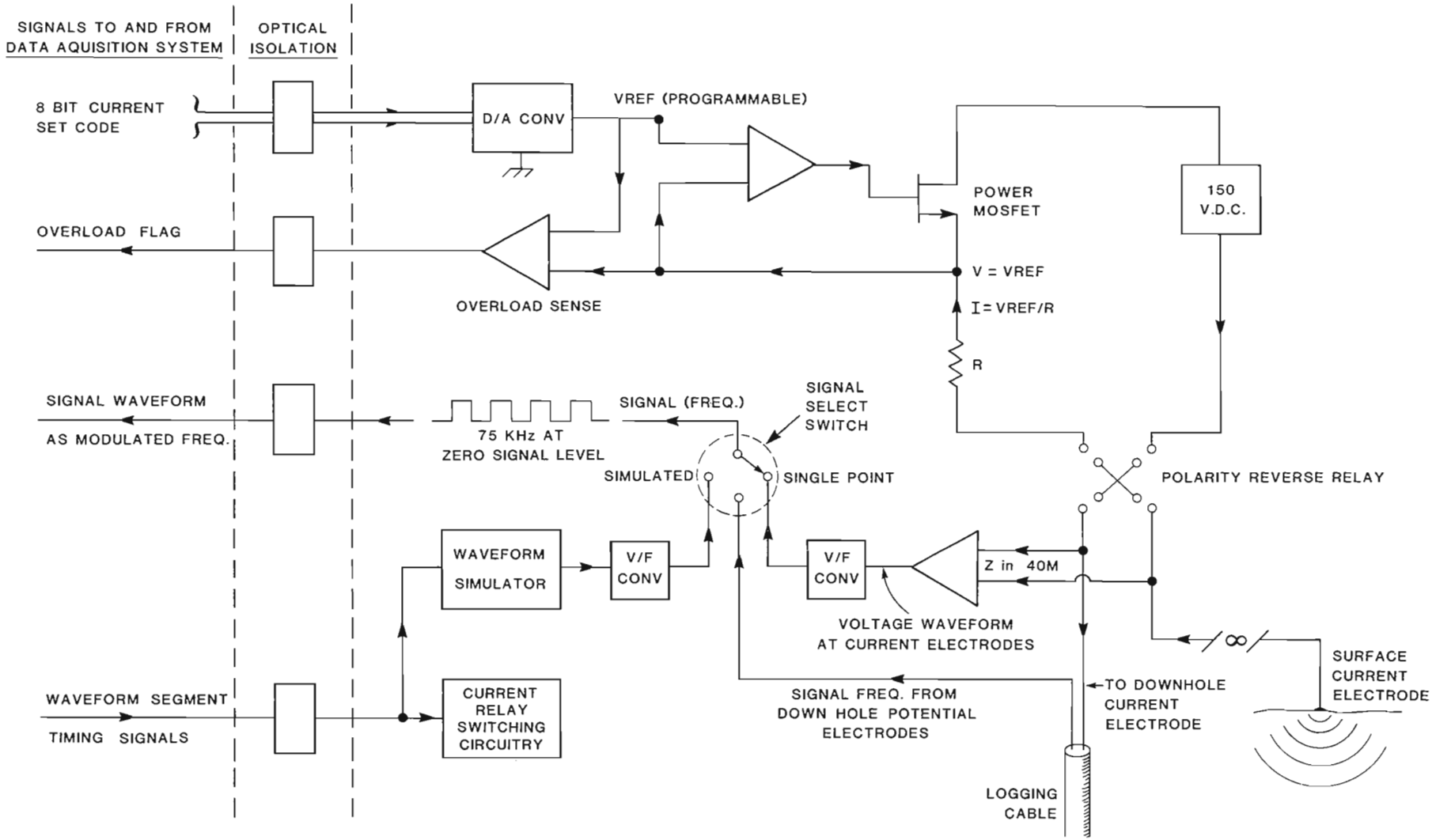

Figure 14.4. *T/R unit block diagram. Signal select switch (centre) can feed simulator signal, downhole active amplifier signal, or signal measured at transmitter terminals, to computer as a modulated frequency. Constant transmitter current level is set by computer.*

transmitter current is positive, similarly it will fall to a minimum of about 20 kHz for a full scale negative voltage when the transmitter current is negative.

If the continuously changing frequency from the tool is sampled for a series of short intervals, then the resulting counts for each successive interval will be proportional to the original analogue voltage averaged over each one, thereby forming a histogram or digitized version of the waveform. The waveform (Fig. 14.5) is digitized in this fashion into 256 data points per second. The available waveform duration times (periods), are 1, 2, 4 or 8 seconds and are set by keyboard entry. The number of data points per complete waveform are thus 256 for a one second time, up to 2048 for an eight second time. It should be noted that the measurement resolution of each data point is a function of the length of each counting interval and the number of pulses per second (i.e. frequency) being transmitted by the V/F converter. The longer the counting interval the larger the number of counts -but also the fewer the number of data points. There is thus a trade-off between signal amplitude resolution and number of points defining the original analogue waveform. The comparatively low frequency range of the V/F converter used in the tool of this system did not allow an acceptable compromise, so that another means of achieving adequate resolution had to be found. One solution would have been to use a V/F converter having a much higher frequency. An off-the-shelf device was not however available which would fit into a slim-hole tool.

The approach, adopted for this system, was to use a phase-locked-loop circuit at the surface to multiply the incoming frequency signal by an appropriate factor, so that the desired resolution in terms of signal amplitude could be achieved without sacrificing resolution of the waveform by having too few data points. Multiplying the V/F converter base frequency by a factor of 10 using the phase-locked-loop circuit, allows a full scale amplitude resolution of approximately one part in 2000. This corresponds to a sensitivity of about 0.5 mV/volt which is considered adequate.

Figure 14.6 illustrates the principle of transmitter control and waveform acquisition which in this system is implemented on a NOVA general purpose board contained in the NOVA chassis. At the top is shown the timing chain which begins with a crystal controlled clock. The frequency (163.84 kHz) is divided down initially to a frequency of 256 Hz. The resulting marker pulses, spaced 3.9 ms apart, define the successive counting intervals for counting the incoming signal frequency (bottom left of Fig. 14.6). Synchronizing logic ensures that coincidence occurs between a clock pulse and a signal frequency pulse before counting commences in each time interval. Counts are deposited in successive locations of NOVA memory via the direct memory access "Data channel", thereby building a digitized version of the waveform in memory. This can be seen on the display monitor as it progresses. Further division of the same timing chain (top of Fig. 14.6) is carried out to produce timing signals for switching the transmitter current through its sequence. Thus the digitizing of the received signal is synchronized with the transmitter waveform.

The use of voltage-to-frequency conversion as the digitizing technique offers some significant advanages over successive approximations converters for this application:

- V/F converters have better linearity and do not suffer from any discontinuities in the transfer function.
- They are relatively inexpensive and available as 14 or 8 pin monolithic ICs which are physically compatible with the restricted space available in a "slim hole" logging tool. A/D converters of comparable performance are generally larger, more expensive, and consume much more power.
- Data transmission as a continuously varying frequency is simple to implement and does not require parallel-to-serial conversion in the tool, or any two-way communication with the surface equipment.
- Measurement resolution can be as good as the sophistication of the surface equipment allows. This can be accomplished in short time intervals either by measuring period (rather than frequency) using a high speed clock, or by means of a phase-locked-loop circuit, as was done in this system.
- The analogue signal being sampled is automatically averaged over the counting interval chosen. The requirement for analogue integration with sample-and-hold circuitry in the tool is thus avoided.

On-line control of transmitter current

The measurement resolution of the received signal amplitude is approximately 0.05% of full scale when measured in either the positive or negative quarter cycle from the zero signal level. For a given current setting the signal amplitude is proportional to formation resistivity, within the volume of investigation for the chosen potential

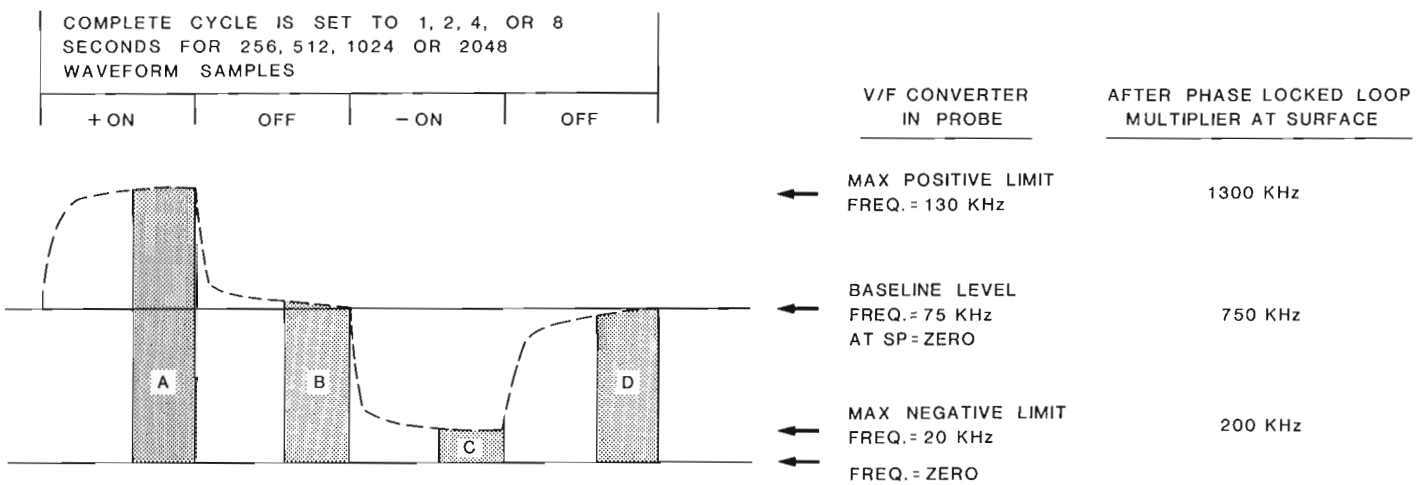

Figure 14.5. *Downhole A/D conversion. Wave form at left is converted to a proportional frequency with ranges indicated at right.*

electrode spacing. Experience indicates that in mineral exploration environments, where boreholes intersect sequences of sedimentary and igneous rocks, resistivity contrasts of the order of 10^4:1 can occur.

The transmitter current range (1 to 254 mA) in conjunction with the 0.05% measurement resolution of the received signal amplitude allows for an overall dynamic range of greater than 5 x 10^5:1 in resistivity. In order to realize these limits the current setting must be changed as necessary to track the rapid changes that occur as the tool moves across contacts between different rock types. An algorithm has been developed and used in the system software which accomplishes this function.

The signal waveform in Figure 14.5 is typical of that which might be obtained in a formation containing disseminated sulphides. If the SP gradient (the potential effectively measured by the relatively closely spaced potential electrodes) is zero, then the "BASELINE LEVEL" in Figure 14.5 will correspond to a V/F converter frequency of approximately 75 kHz, as explained previously. Any departure of the line from this predetermined level is therefore due to the presence of an SP gradient superimposed on the alternating signal caused by the transmitter current.

A reasonably accurate measure of the SP gradient signal can be made by computing the mean of the sum of the data points contained in the regions marked B and D in Figure 14.5 and subtracting the predetermined zero level, thus:

$$SP \propto (B + D)/N - K \qquad (1)$$

where "N" is the number of data points in B and D, and "K" is the zero signal level count.

The resistivity is proportional to the absolute full amplitudes of the positive and negative lobes of the waveform with respect to the "BASELINE LEVEL" in Figure 14.5, divided by the current level generated by the transmitter as set by the NOVA. A good measure of this quantity is given by:

$$RES \propto (|A - C| + |B - D|)/(NxI) \qquad (2)$$

where "RES" is a quantity proportional to resistivity; A and B are regions having N data points each; I is the transmitter current and the vertical bars denote absolute values. If there is no significant IP effect, then the term $|B - D|$ will be zero and the curve will be at full amplitude for the full widths of regions A and C.

The signal level recorded thus consists of a resistivity component and an SP component:

$$SIG \propto RESxI + SP \qquad (3)$$

The NOVA must be able to separate these two components in order to set current levels. The composite signal must not be allowed to exceed certain predetermined positive and negative levels (which can be set in the software), or non-linear operation will occur. If the actual amplitude excursion of the signal from the predetermined zero level is "SIG" as above, but the desired or optimum value is (say) "S_O", then the current "I" which produces a signal level of "SIG" should

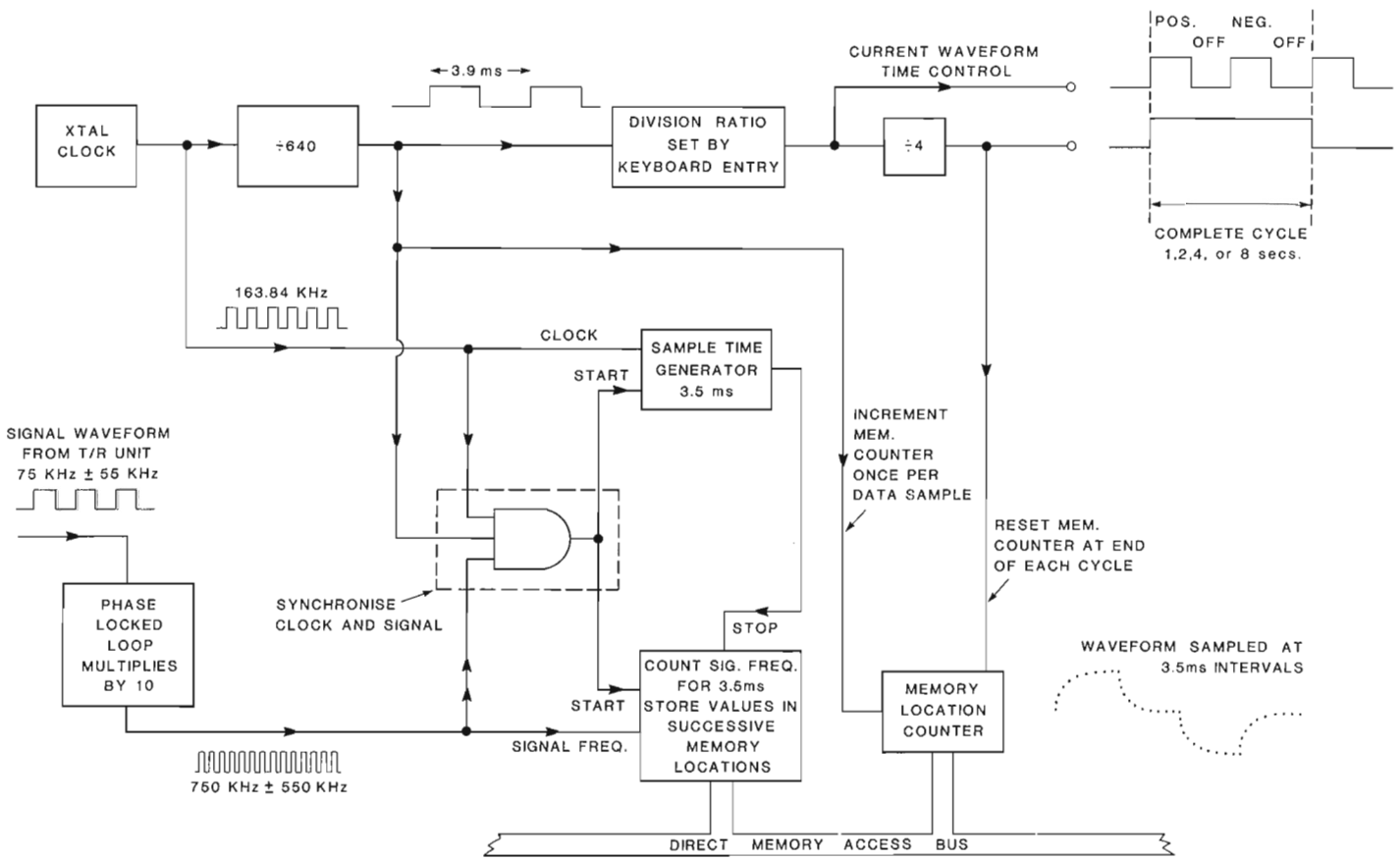

Figure 14.6. *Acquisition of IP wave forms as digital data. Incoming modulated frequency (left) is multiplied to enhance measurement resolution and counted over 4 ms. time slices to produce digitized wave form at right.*

be changed to bring it to the level "S_0". The factor "F" by which the current must be changed to accomplish this is given by:

$$S_0 \propto F(RES \times I) + SP \quad (4)$$

(Changing the current does not alter the SP component.)

from which the factor "F" is given by:

$$F \propto (S_0 - SP)/(RES \times I) \quad (5)$$

Continuous on-line corrections are made to the transmitter current on this basis to maintain the received signal in a predetermined working range for variations in either formation resistivity, or SP.

IP measurements are based on integration of the the current "OFF" segments from 0.285 T to 0.55 T, where T is the time for each OFF segment. This applies for the four complete waveform times which are available in this system.

Summary of software capability

As indicated earlier a software operating system for the NOVA based data acquisition equipment already existed, having been developed primarily for use in airborne gamma ray spectrometry measurements (Bristow, 1979b). The routines required to process 256 channel gamma ray spectra (integration of regions etc.) were directly applicable to the processing of the digitized IP waveforms. The computation required to determine resistivity, SP, and current adjustment factor is carried out on waveform number N (stored in memory), while waveform N + 1 is being acquired in another block of memory, and while waveform N-1 is being dumped to tape with other related data.

On line processing and monitoring facilities include the following:

- Integration and live display of the numerical values of ten regions of the waveform, six of which are operator defined by keyboard entries.
- Graphic display of individual waveforms as they are acquired, or of composite waveforms after stacking for a number of cycles set by keyboard entry. In the latter case any or all of the integration regions selected can be shown as intensified portions of the display.
- Live display of depth; cable velocity; resistivity; SP; transmitter current, and correction factor computed as described above. The present value of maximum allowed transmitter current as set by the system following an overload, or as revised by the operator is also displayed. All these parameters are updated on the screen as each new waveform is acquired.
- Warning to the operator from data terminal horn when a transmitter overload condition persists for more than a predetermined number of data points in a given waveform. The displayed waveform is also intensified for the portions where transmitter overloads occur. All overload data points in a waveform are flagged on the magnetic tape record.
- The operator can define simple algebraic functions of parameters to be plotted out on the six channel strip chart recorder. The parameters are: resistivity, SP, IP, current, and the numerical values of the integrations over the six selectable regions. Functions can include for example simple scaling of amplitudes, ratios, products, sums, or differences of any of the above parameters. Functions already defined on other channels can also be included as parameters.

In addition to on-line capabilities, the operating software allows recorded data to be read back, with digitized waveforms being dumped into the same areas of memory that are used in the acquisition mode. Essentially the same code

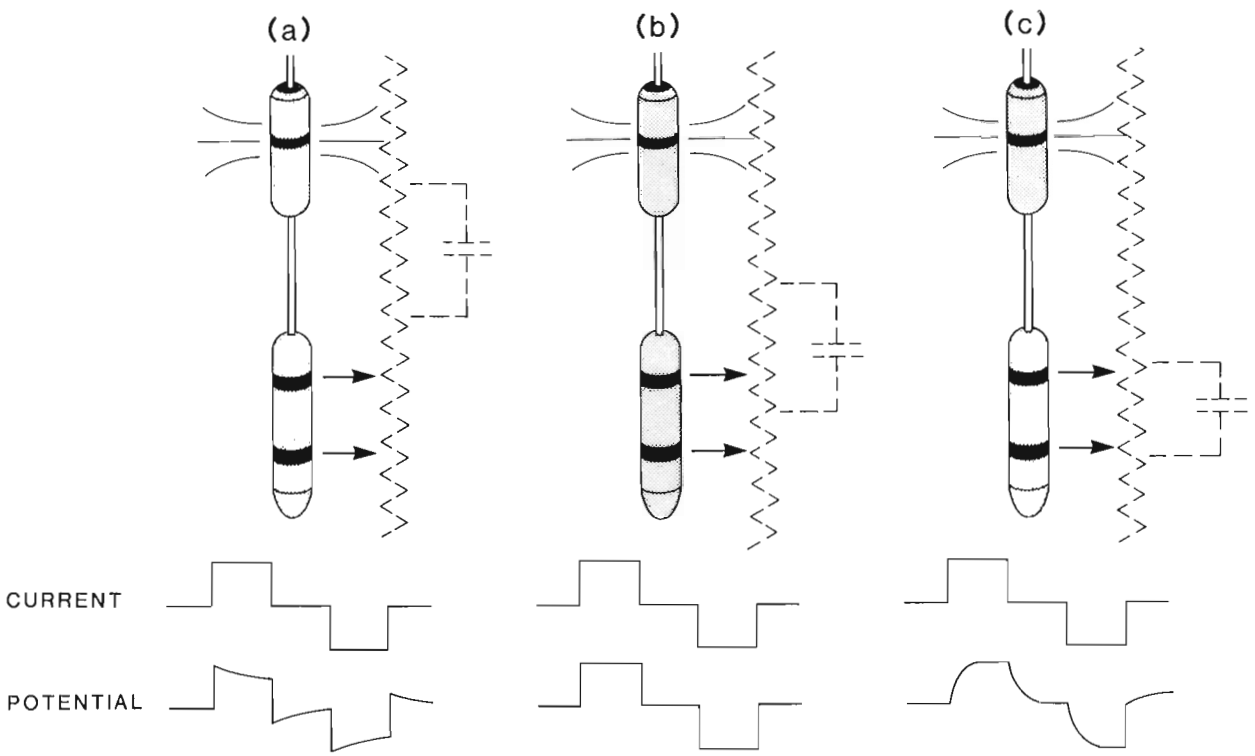

Figure 14.7. *(a) Negative IP effect. With polarizable body between current and potential electrodes. (b) Zero IP effect. When potential electrodes partially intersect the polarizable body. (c) Positive IP effect. When potential electrodes are within the polarizable body.*

then processes these raw waveforms; providing the same display and strip chart facilities as outlined above. One of the valuable features of this "instant replay" capability is the opportunity to view each complete waveform on the graphic display as it is read back (at a maximum rate of about five records per second) and to stop the action and plot a waveform on the recorder if any significant characteristics or peculiarities are observed. Another advantage is the option to refine strip chart functions and re-run the data as often as desired in order to maximize discrimination of desired parameters from background noise. More sophisticated processing of the raw recorded data is done in our case with the aid of a Data General Corp. Eclipse S-130 based system.

A simple predictive model for some borehole IP responses

Analytical modelling of surface and borehole IP responses has received extensive attention in the literature over many years (e.g. Seigel, 1959; Loeb, 1970; Snyder and Merkel, 1973; Hohmann, 1975; Nabighian and Elliot, 1976; Daniels, 1977; Lytle, 1982; Majumdar and Dutta, 1984), resulting in the publication of response patterns to be expected in the vicinity of polarizable bodies of various shapes under a variety of conditions. It is usually difficult to visualize from such analyses the equivalent electrical circuit behaviour which causes the various IP effects which are predicted and do indeed occur. In order to gain some physical insight into borehole responses and relate them to waveforms generated by familiar electrical networks, a simple resistance-capacitance model was adopted to explain the transition from a negative to a positive IP effect – a transition which can occur under certain conditions in borehole work.

Figure 14.7 shows a tool with a pole-dipole array in three positions with respect to a polarizable body (the capacitor) in an essentially resistive formation. If the current waveform is a square wave sequence as shown, then when the polarizable body lies between the current electrode and the nearest potential electrode (Fig. 14.7a), the uncharged capacitor acts as a temporary short-circuit between the two when the current is turned on. Consequently the initial potential seen between the potential electrodes is greater than it would otherwise be, eventually decaying back to the level it would normally be at as the capacitor charges up and no longer offers an additional path for current conduction. The resulting potential waveform in Figure 14.7a is a classic "negative IP" effect. Figure 14.7c shows the situation where the capacitor representing the polarizable body is between the potential electrodes. By the same reasoning it is apparent that initially the resistivity seen by the electrodes is lower than normal as the capacitor acts to short-circuit a portion of the resistive medium when the current is first turned on. Again as the capacitor charges, the alternate conductive path disappears and the waveform in Figure 14.7c results, which is the familiar "positive IP" effect.

Somewhat less obvious is the situation shown in Figure 14.7b, where the potential electrodes straddle portions of the resistive medium which are affected in opposite senses by the two capacitive effects shown in Figures 14.7a and c. A point will be found where the two effects almost cancel, giving essentially a square wave potential waveform (Fig. 14.7b), with no indication that a polarizable body is in the vicinity of the tool.

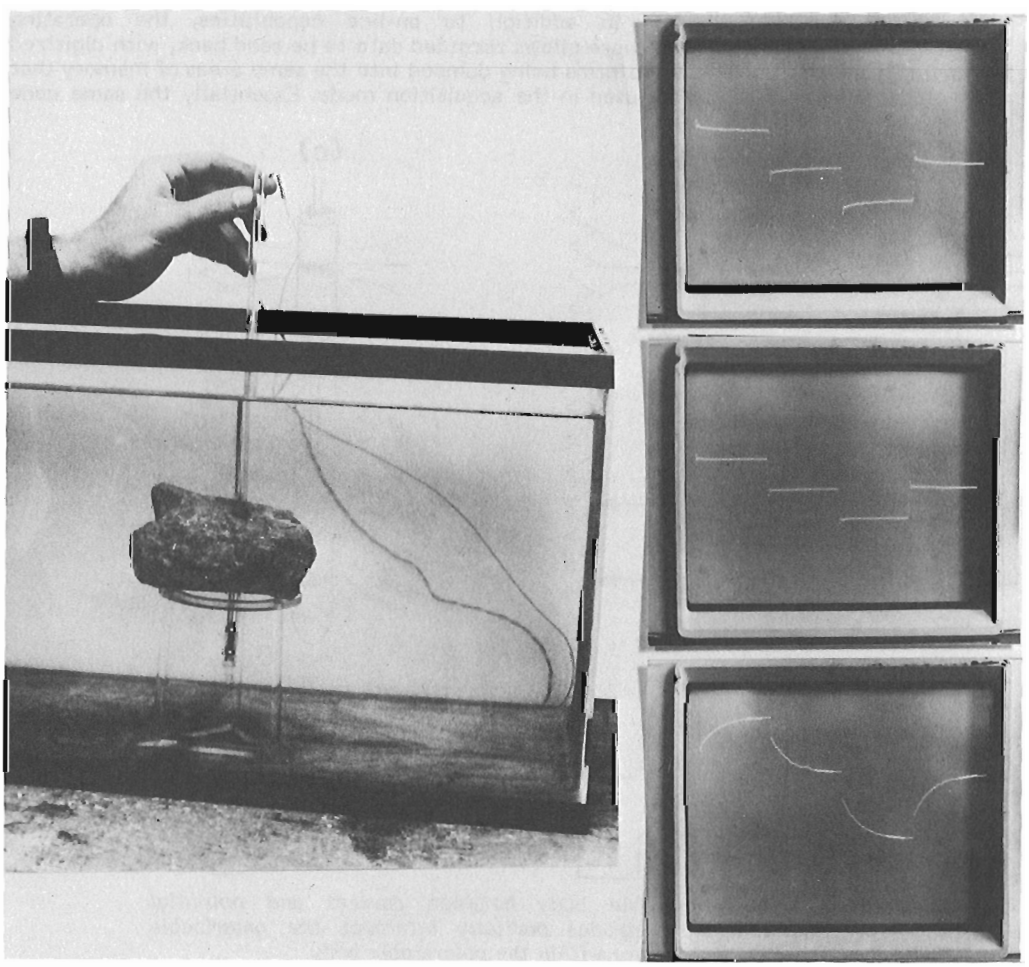

Figure 14.8

A miniature electrode array, connected to the data acquisition system, (not shown) convincingly demonstrates the negative-zero-positive IP effects predicted in Figure 14.7, as it is passed slowly through a pyritized rock sample in a water tank.

A simple experiment designed to show this as a demonstration piece has proven to be a useful aid. A mini-probe was constructed from 5 mm diameter plastic tubing with metal rings mounted on it to serve as electrodes with separations of a few centimetres only. A rock sample containing less than 10% sulphides was drilled through with a 10 mm diameter hole and mounted in a tank filled with tap water and lined with metal mesh to provide an "infinite" current sink. The apparatus is shown in Figure 14.8, along with waveforms actually recorded. As the mini-probe was moved through the rock sample the waveforms shown in Figure 14.7 were obtained in sequence as predicted.

Basic field tests

To date field tests have been conducted in the GSC test boreholes at Bells Corners near Ottawa, a facility which has been described by Bernius (1981). The Bells Corners holes intersect 65 m of sedimentary strata, underlain by Precambrian gneiss which contains disseminated sulphides with concentrations up to 2%. These sulphides do not provide any well defined anomalies, so that it was not possible to make a quantitative assessment of the detection capability of the equipment. Nevertheless a number of logs were run to test the repeatability of the measurements, the effect of different transmitter current levels on the IP signal, and the efficacy of the auto-current algorithm.

Figure 14.9a shows three stacked resistivity and IP logs over a 60 m segment in Precambrian strata, made with a "lateral" array. The logs are offset for clarity of presentation. This array has a current electrode uppermost, with two potential electrodes 40 cm apart, their centre line being 3.0 m from the current electrode. The first log was run with the current fixed at 1 mA; the second with the current fixed at 5 mA, and the third in "auto-current" mode with the current being set by the system using the algorithm described earlier. The actual current trace for the third log is shown alongside the IP and resistivity traces.

These show excellent repeatability for the resistivity logs, regardless of the current level. This indicates that the purely resistive component of the overall impedance is at least constant and not current dependent over the range from 1 mA to the maximum current set by the system, which was 35 mA in this case.

The IP logs show slight differences in the range of amplitudes which indicate that the IP effect is not strictly independent of current even at these low levels, but that the essential response profile is maintained over the current range from 1 to 35 mA. It is also worth noting that the IP log made with the current fixed at 1 mA involved the processing of a signal which was only 3% of the amplitude the system determined as optimum in some places. In these instances the current log shows that the system had called for 35 mA in order to produce a satisfactory signal amplitude. The high level of repeatability on both the resistivity and IP logs under these conditions is an indication of the overall precision of the system, both in current generation and signal processing.

In order to provide maximum flexibility, provision was made in the T/R unit for operation with the current electrodes either shorted during the current-off segments of the cycle, or open circuit during these periods. Sumner (1981) has speculated on the possible value of operation with the current electrodes shorted if one of them is immersed in a polarizable body. Although the opportunity to do that particular experiment has not yet arisen, a simple comparison was made by running logs in the two different modes. Two logs are shown superimposed (not offset) in Figure 14.9b. The log made with the current electrodes short-circuited during the current-off segments, is seen to have a significantly lower mean level than the one with the electrodes open circuit. Apart from this level difference the two are essentially identical. H.O. Seigel (personal communication, 1984) attributed this difference to depolarization of the current electrodes in the "short circuit" mode. Since this process would produce a signal of opposite polarity to that being measured in the formation, and one which is essentially constant from cycle to cycle, the result would be the subtraction of a constant level from the entire log, as is indeed evident in this case. This comparison was repeated in other holes with similar results.

SP measurements

In principle the potential electrodes record an SP gradient function as the tool progresses along a borehole. The data which were obtained in practice however were less than satisfactory unless the transmitter was turned off.

One of the advantages of a built-in simulator is the ability to generate SP, resistivity and IP signals individually, or in any desired combination in order to check the efficacy of processing software. The algorithm used to extract the SP signal performed satisfactorily using signals from the simulator, even when long time constant IP signals were added to distort the baseline. It seems, therefore, that the spontaneous potential gradient as seen by the potential electrodes may well be distorted by the transmitter current. The SP measurements recorded so far with no transmitter current have been entirely satisfactory.

Evaluation of "single point IP"

Reference was made earlier to some additional circuitry which was incorporated into the T/R unit to allow recording of the complete waveform appearing across the current electrodes during the current-on and current-off segments. The main purpose of this was to compare the quality of the IP signal obtained in this way with that measured by the tool using separate potential electrodes.

Dakhnov et al. (1952) indicated that the IP signal seen at the current electrodes during the current-off segments is susceptible to interference from variable electrode depolarization effects and from inductive effects, and is therefore not useful unless the target is highly polarizable.

Figure 14.10 shows three repeat logs of single point resistance and IP (offset for clarity). The repeatability is clearly excellent, although some low level noise is evident on the IP traces. Figure 14.11 shows two logs, made in a different hole from that in Figure 14.10. One log was made using the single point mode for resistance and IP, while the other was made using the active logging tool with a 3 electrode array. Both were made in the auto-current mode. The electrode array used was an inverted 40 cm normal configuration, with current electrode uppermost and a potential electrode spacing of 2.6 m, with the upper one being 40 cm from the current electrode. The second current electrode was at a point on the surface approximately 0.5 km from the borehole. For each log there are three parameters shown: current, resistance, and IP. The normal array resistivity versus the single point resistance is a familiar comparison for well log analysts, the exaggerated peaks in the resistivity log are almost certainly due to the complicated impluse response of the normal array (see Keller and Frischknecht, 1966).

The two IP logs show a good correlation over the entire record, despite the fact that the current variations in the two cases are mostly uncorrelated. The amplitude of the IP signal for the single point IP log is only about one half that from the normal array log. Such a reduction would occur if, for example, the IP effect were not linearly related to the exciting current at the very high current densities which

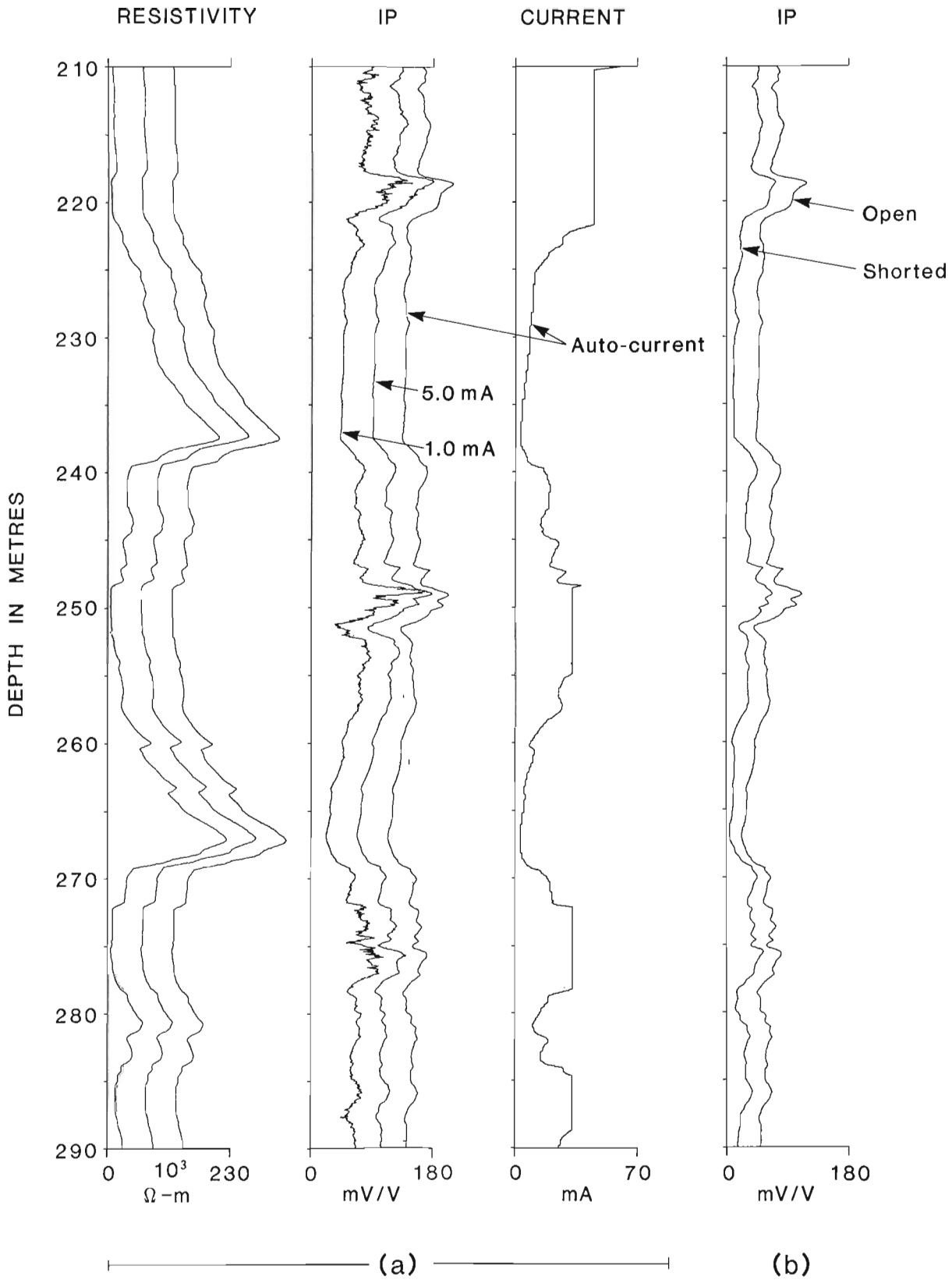

Figure 14.9. ***a)*** *IP and resistivity logs with different excitation current, logs are offset for clarity.* ***b)*** *IP logs, one with current electrodes shorted, and one with them open during current-off segments, (superimposed and not offset, level difference is real).*

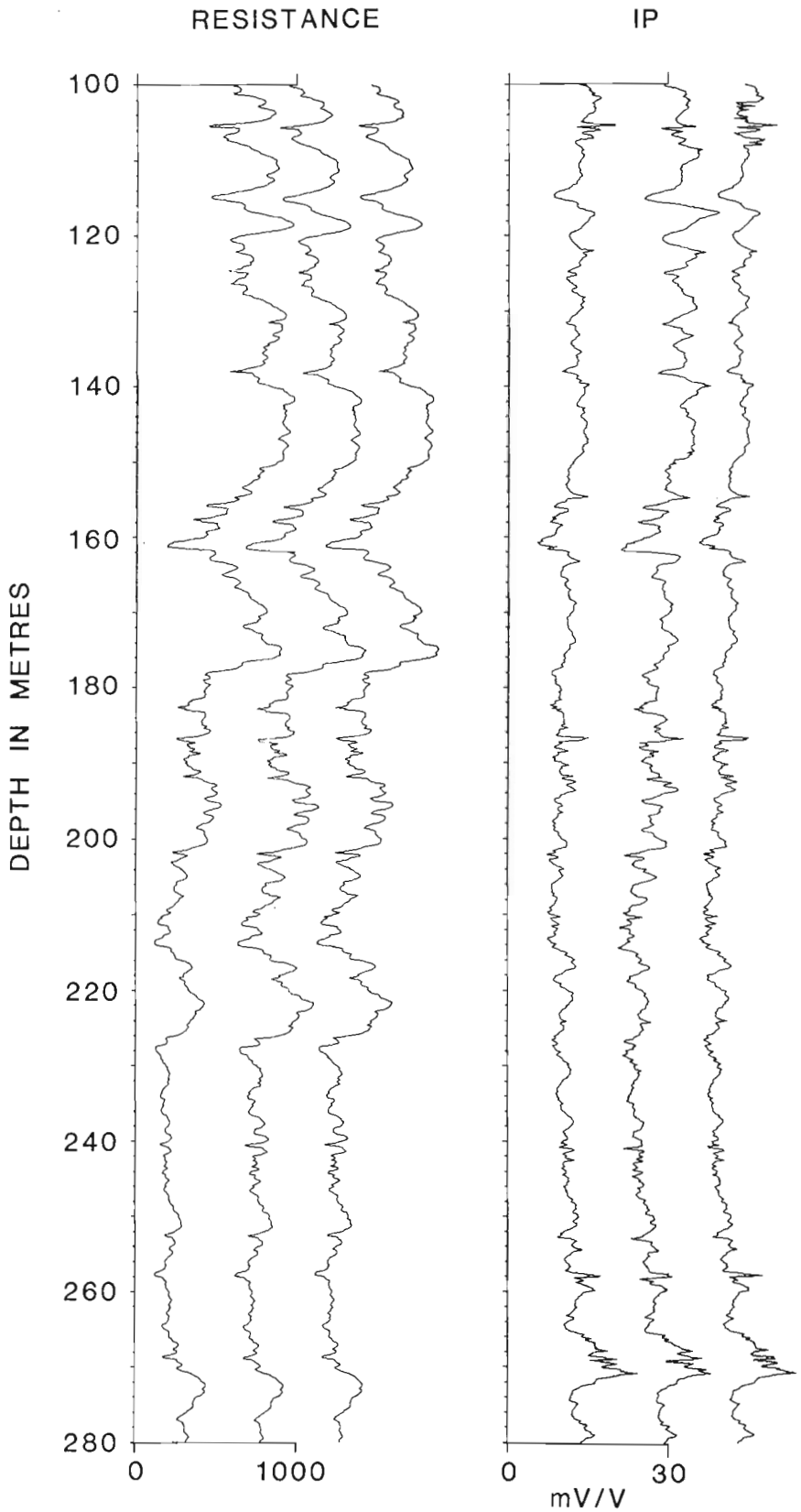

Figure 14.10. *Single point resistance and Single point IP logs. Repeat runs (offset; single point resistance scale is arbitray).*

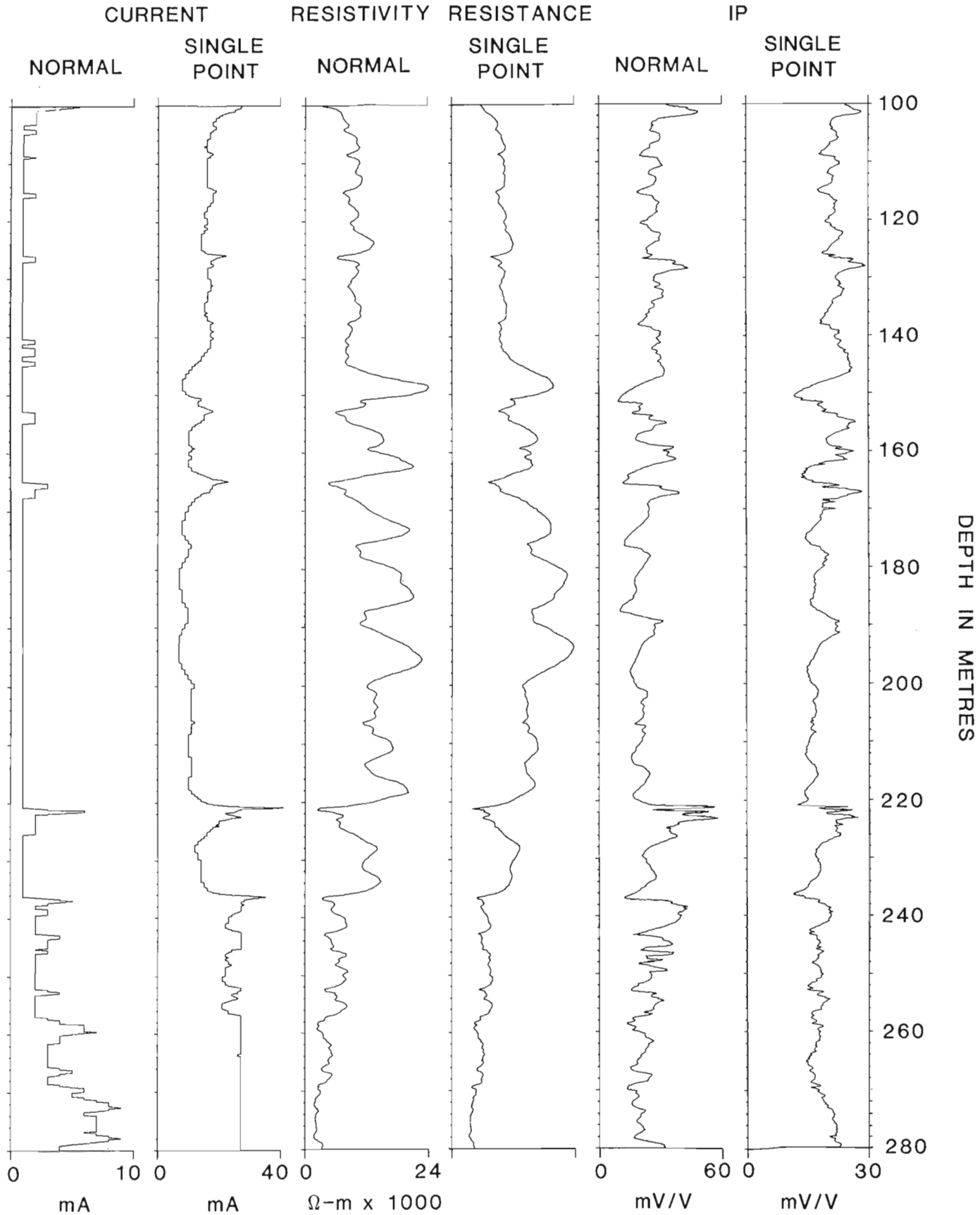

Figure 14.11. *Single point vs. normal array logs for resistivity and IP (Single point resistance scale is arbitrary).*

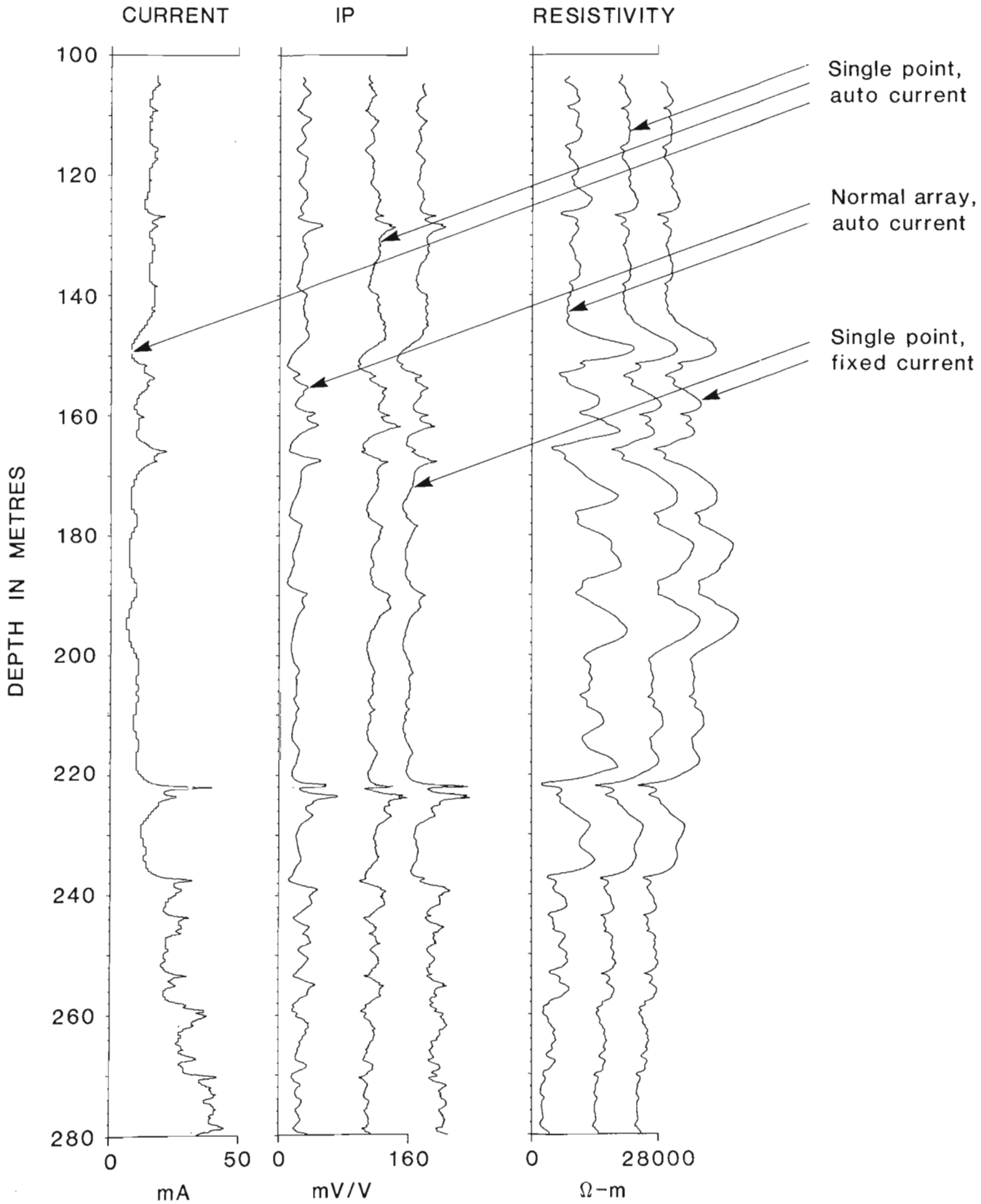

Figure 14.12. Normal array auto-current log vs. Single point auto-current and Single point fixed current logs. (Resistivity and IP scales apply to Normal array log only; logs offset for clarity).

occur in the region of the current electrode itself. Under these circumstances the IP signal, when expressed in terms of mV/volt according to the usual definition, would be relatively lower in the high current density region where the single point measurement is being made.

In order to investigate the effects of variable electrode depolarization in single-point IP measurements, three more logs were run in the same hole as those in Figure 14.11. The first two were single point logs, one with the current fixed at 15 mA, and the second with the system in auto-current mode. The third log was a repeat run of the normal array log shown in Figure 14.11. The resistive and IP components of the three logs are shown stacked and offset for clarity in Figure 14.12, with the current log for the single-point auto-current log only shown. From this it is clear that despite large current fluctuations over the course of the auto-current log, (which might be expected to cause variable inductive and electrode depolarization effects), the fixed and auto-current single point IP logs are essentially identical, and that both correspond very closely with the normal array, auto-current IP log.

The single point IP measurement involves the regions in the immediate vicinities of both the current electrodes. The one that is not moving will only contribute some overall level shift to the log which will be a function of the polarizability of the medium it is in. In general it would be unlikely that in a borehole IP survey, the remote current electrode would inadvertently be placed in an area having a significant concentration of sulphides.

The data presented in Figures 14.10, 14.11, and 14.12, although somewhat preliminary, suggest that single point IP measurements may well be a useful alternative to the more precise data acquired by the more elaborate logging tool, in circumstances where a large separation between the downhole current and potential electrodes is not required. The obvious advantage is that only a single conductor cable, terminated with a simple current electrode, is required downhole. This means lighter and less expensive equipment; easy access to small diameter holes, not possible with the larger tool and electrode array; and virtually no risk of anything becoming wedged in a borehole. These are all crucial considerations when undertaking mineral exploration in typical Precambrian terrane where diamond-drill holes are of small diameter and where sites are difficult to reach, even with a 4-wheel drive vehicle.

Conclusion

A system has been described for continuous or step-wise IP logging which offers considerable research-oriented flexibility. The ability to record data in different operating modes and with a fixed or automatically varying exciting current has already made possible an initial re-evaluation of the "single point IP" method, which it appears has not been tried since the early 50s. This preliminary work indicates that electrode depolarization effects may not be as serious as had previously been thought and that the technique may provide a viable and less expensive alternative for mineral exploration applications, in situations where small current-to-potential electrode separations are acceptable.

The logging tool and T/R unit have been designed in such a way that interfacing to any one of the popular personal computers would not be difficult.

Acknowledgments

The author is indebted to J. Parker and Y. Blanchard for assembly and testing of the system hardware; to W.G. Hyatt for acquisition of field test data; and to C.J. Mwenifumbo for much helpful discussion during the development phase and a valuable critical reading of the manuscript.

References

Bacon, L.O.
1965: Induced polarization logging in the search for native copper; Geophysics, v. 30, p. 246.

Bleil, D.F.
1953: Induced polarization: a method of geophysical prospecting; Geophysics, v. 18, p. 636-662.

Brant, A.A. and Newmont Exploration Staff
1966: Examples of induced polarization field results in the time domain; in Mining Geophysics, v. 1, Tulsa, Society of Exploration Geophysicists.

Bristow, Q.
1979a: NOVA-based airborne and vehicle mounted systems for real time acquisition, display and recording of geophysical data; in Proceedings of Data General Corp. Users Group Conference, New Orleans, Dec. 1979.

1979b: An airborne gamma ray spectrometry system for airnborne geological research; Geological Survey of Canada Paper 79-1C, p. 55-61.

Bristow, Q. and Killeen, P.G.
1978: A new computer-based gamma-ray spectral logging system; Society of Exploration Geophysicists, 48th Annual International Meeting, Abstracts, p. 117-118.

Dakhnov, V.N., Latishova, M.G., and Ryapolov, V.A.
1952: Well logging by means of induced polarization; The Log Analyst, v. 8, 1967, p. 3-18; Translated from Promishovaya Geofizika, p. 46-82, 1952 by G.V. Keller.

Daniels, J.J.
1977: Three dimensional resistivity and induced polarization modelling using buried electrodes; Geophysics, v. 42, p. 1006-1019.

Hallof, P.G.
1980: Use of the I.P. method for exploration in drill holes; practical geophysics for the exploration geologist, Ch. 2; Northwest Mining Association, Spokane, Washington, USA.

Hohmann, G.W.
1975: Three dimensional induced polarization and electromagnetic modelling; Geophysics, v. 40, p. 309-329.

Keller, G.V. and Frischknecht, F.C.
1966: Electrical methods in geophysical prospecting; Pergamon Press.

Loeb, J.
1970: Note on induced polarization models; Geoexploration, v. 8, p. 105-112.

Lytle, R.J.
1982: Resistivity and induced polarization probing in the vicinity of a spherical anomaly; IEEE Transactions on Geoscience and Remote Sensing, v. GE-20, no. 4, p. 493-499.

Madden, T.R. and Marshall, D.J.
1959: Induced polarization, a study of its causes; Geophysics, v. 24, p. 790-816.

Majumdar, R.K. and Dutta, S.
1984: Induced polarization time domain equipment and some model studies over thin dikes of finite strike extent; Geophysics, v. 49, p. 291-296.

Nabighian, M.N. and Elliot, C.L.
1976: Negative induced polarization effects from layered media; Geophysics, v. 41, p. 1236-1255.

Ogilvy, R.D.
1984: Down-hole I.P. surveys applied to off-hole mineral exploration - some design considerations; Geoexploration, v. 22, p. 59-73.

1985: Down hole IP/Resistivity prospecting in mineral drill-holes - some illustrative field examples; Geoexploration, v. 23, p. 257-273.

Seigel, H.O.
1959: Mathematical formulation and type curves for induced polarization; Geophysics v. 24, p. 547-565.

Snyder, D.D.
1976: A method of modelling the resistivity and I.P. responses of two dimensional bodies; Geophysics, v. 41, p. 997-1015.

Snyder, D.D. and Merkel, R.M.
1973: Analytic models for the interpretation of electrical surveys using buried current electrodes; Geophysics, v. 38, p. 513-529.

Snyder, D.D., Merkel, R.H., and Williams, J.T.
1977: Complex formation resistivity - the forgotten half of the resistivity log; Transactions of Society of Professional Well Log Analysts 18th Annual Logging Symposium, Paper

Sumner, J.S.
1976: Principles of induced polarization for geophysical exploration; Elsevier Scientific Publishing Co.

1981: The Mise-a-la-masse induced polarization method; Society of Exploration Geophysicists; 51st Annual International Meeting and Exposition; Extended Abstracts v. 2, Paper M3.2.

Telford, W.M., Geldart, L.P., Sherriff, R.E., and Keys, D.A.
1976: Applied Geophysics; Cambridge University Press.

Vinegar, N.J., Waxman, M.H., Best, M.H., and Reddy, I.K.
1985: Induced polarization logging - borehole modelling, tool design and field tests; Transactions of Society of Professional Well Log Analysts 26th Annual Logging Symposium.

Wagg, D.M. and Seigel, H.O.
1963: Induced polarization in drill holes; Canadian Mining Journal, April, p. 54-59.

Wait, J.R.
1959: Overvoltage research and geophysical application; J.R Wait, ed; Pergamon Press.

15. DRILLHOLE MISE-À-LA-MASSE INDUCED POLARIZATION AND POTENTIAL MEASUREMENTS IN A Zn-Pb-Cu SULPHIDE DEPOSIT

C.J. Mwenifumbo[1]

Mwenifumbo, C.J., Drillhole mise-à-la-masse induced polarization and potential measurements in a Zn-Pb-Cu sulphide deposit; in Borehole Geophysics for Mining and Geotechnical Applications, ed. P.G. Killeen, Geological Survey of Canada, Paper 85-27, p. 145-158, 1986.

Abstract

Drillhole mise-à-la-masse potential and induced polarization (IP) measurements were conducted underground in the MacLean Extension orebody at the Buchans mine in Newfoundland. The MacLean Extension orebody is a Zn-Pb-Cu sulphide deposit. Parts of this polymetallic sulphide deposit were found to be highly conductive and polarizable. Correlation of ore intersections between holes was easily accomplished with the mise-à-la-masse method. The ore lying between the three sections surveyed was shown to be electrically continuous and forms a single ore lens. The time domain mise-à-la-masse IP measurements showed an inverse relationship to the mise-à-la-masse potentials. Low, almost constant IP effects were observed across the sulphide mineral intersections. External to the energized sulphide mineralization, higher apparent chargeabilities were measured.

Résumé

Des mesures du potentiel et de la polarisation induite (PI) ont été effectuées au moyen de la méthode de sondage souterrain dite "mise à la masse" à l'emplacement du corps minéralisé MacLean Extension de la mine Buchans (Terre-Neuve). Ce corps minéralisé est un gisement de sulfure de Zn-Pb-Cu. On a constaté que certaines parties de ce gisement de sulfure polymétallique sont très bonnes conductrices et polarisables. La mise en corrélation des intersections transversales a été chose facile grâce à la méthode de la mise à la masse. L'étude a révélé que le minerai compris entre les trois sections examinées est un conducteur électrique homogène et forme une seule lentille de minerai. Les mesures de polarisation induite par mise à la masse dans le domaine du temps ont révélé une relation inversement proportionnelle aux potentiels de mise à la masse. Des effets de polarisation induite faible, presque constants, ont été observés entre les points de sondage du gisement de sulfure. Des capacités de charge apparente plus élevées, extérieures à la minéralisation de sulfure mise sous tension, ont été mesurées.

Introduction

The mise-à-la-masse (MALM) electrical method of prospecting is generally used after a conductive mineralized zone has been located. It involves placing a current electrode directly in contact with the mineralized zone, and then mapping the resulting electric potential field distribution either at the surface or in the subsurface via drillholes or underground openings. The potential field reflects the shape, size and orientation of the energized conductive zone. This technique is used mainly for mapping the size and orientation of a deposit and for determining the continuity of the mineralization from hole-to-hole. It is also possible to detect conductive orebodies in the vicinity of the energized body that are not directly connected. The MALM method has been extensively and successfully applied during detailed mapping of massive sulphide ore bodies with high electrical conductivity (McMurry and Hoagland, 1956; Parasnis, 1967; Ketola, 1972; Mansinha and Mwenifumbo, 1983). Although most of the present systems used for resistivity and MALM measurements are equipped for Induced Polarization (IP) measurements, there have been no reports of field examples of the MALM IP method. Recently, however, Sumner (1981) has presented a theoretical analysis of the MALM IP results to be expected from a simple geometric model, a polarizable sphere.

MALM IP and potential measurements were carried out underground in the MacLean Extension orebody, at the Buchans mine in Newfoundland. The MacLean Extension orebody is structurally and stratigraphically complicated. A number of ore intersections cannot be easily correlated from section-to-section or from hole-to-hole along a given section. There is also a high degree of variability in the proportions of lead, zinc and copper sulphides (galena, sphalerite and chalcopyrite). Some of the sulphide ores contain a high percentage of sphalerite, barite and rock fragments which are poor electrical conductors. The overall conductivity of the ore, however, is fairly high relative to that of the host rock. The MALM potential field measurements were conducted to investigate the possibility of using the technique to trace sulphides from hole-to-hole and to determine any possible extension of the orebody that may have been missed by drilling. The MALM IP measurements were carried out to evaluate the merits of the method and to verify some of the peculiar IP results (e.g. negative IP) expected from the theoretical analysis of Sumner (1981).

Geology

The geology and ore deposits of the Buchans area have been described in detail by Thurlow and Swanson (1981) and the geology of the MacLean Extension deposit has been

[1] Geological Survey of Canada, 601 Booth Street, Ottawa, Ontario K1A 0E8

described by Binney et al. (1983). The Buchans ores are barite-rich, polymetallic massive sulphide deposits associated with submarine felsic volcanic rocks. They are mainly zinc-lead-copper sulphides. Three major ore types occur at Buchans; 1) stockwork, 2) in situ ore, and 3) mechanically transported fragmental ore. The MacLean orebody is mechanically transported ore and consists of low to high grade accumulations of sulphide fragments derived from an unknown massive sulphide source. The ore has apparently been transported by debris flows for considerable distances from its source and deposited in paleotopographic depressions. In the MacLean Extension orebody, some sections consist of massive, high grade, copper-rich ores and others are mainly low to high grade lead-zinc ores. In general, the ore comprises varying proportions of sphalerite, galena and chalcopyrite in different ore lenses.

Figure 15.1 is a map of level 20 of the MacLean Extension orebody where the MALM experiments were carried out. Three sections where these measurements were taken (W2300, W2350 and W2400) are indicated on the map. Figure 15.2 shows the cross sectional geology of section W2300, where the ore consists of moderate to high grade ore breccia (mainly galena and sphalerite) within the dacitic tuff unit. The ore zone approximates a curved tabular body, dipping to the south at about 40 degrees. The geology of section W2350 is shown in Figure 15.3. The ore outline is approximately elliptical and the ore consists of moderate to high grade Cu-Pb-Zn sulphides. Figure 15.4 shows the geology of section W2400. The ore along this section is massive Cu-rich, high grade Cu-Pb-Zn ore. The ore outline is circular, only 100 feet away from the curved, tabular ore zone of section W2300. These three geological sections indicate the complex morphology of the MacLean Extension orebody. Only the geology below the drift level is displayed in these figures, although there are ore lenses above the drift level. There has been extensive drilling in all these sections and the holes used in the experiments are indicated on the sections.

Equipment and field procedure

The equipment used in the MALM measurements consisted of a battery operated Huntec M4 LOPO transmitter and a Huntec M4 receiver. Both the receiver and the transmitter can be used for time and frequency domain IP and complex resistivity measurements. However, the MALM IP and potential measurements conducted in the MacLean Extension orebody were carried out in the time domain only. Primary voltages, self potentials (SP) and chargeability information from ten windows of equal width (175 ms) were recorded on cassette tapes. The complete waveforms were also recorded on the tapes. The period of the transmitter current waveform was 8 s (two repeat cycles of 2 s current on and 2 s off, with polarity reversed after each cycle).

Figure 15.5a shows a typical complete IP waveform recorded on cassette tape with the M4 receiver. Note that the first channel does not coincide with the start of the current-on cycle. This means that the complete waveform data has to be rearranged before any subsequent processing of the decay waveform and Figure 15.5b shows the rearranged waveform of Figure 15.5a.

The electrode configuration used throughout the measurements was the pole-pole array consisting of an energizing current electrode implanted in the conductive sulphide in one hole and a moving potential electrode in a second hole. The current electrode used to energize the sulphide zone was a copper clad steel rod about 1 m in length. The electrodes used for potential measurements were made of platinum wire mesh about 5 cm in length and 1.25 cm in diameter. The remote potential electrode was a non-polarizable copper-copper sulphate electrode whereas the other distant current electrode was a copper clad steel electrode. Accurate depth measurements along the hole lengths were accomplished with a mechanical depth encoder having a resolution of 10 cm. MALM IP and potential measurements were made at 1 m intervals downhole using a two conductor shielded cable. All the holes logged were water-filled. Geological logs and contact resistance measurements were used to locate the current source in the ore intersections. The locations of the remote potential electrode (P ∞) and the distant current electrode (C ∞) are shown in Figure 15.1. All measurements were made with reference to these remote electrodes. Electrode layouts for measurements in underground workings were dictated by accessibility into various drifts. Metal objects such as steel pipes, railway tracks and operating machinery also constrained the electrode layouts and measurements underground.

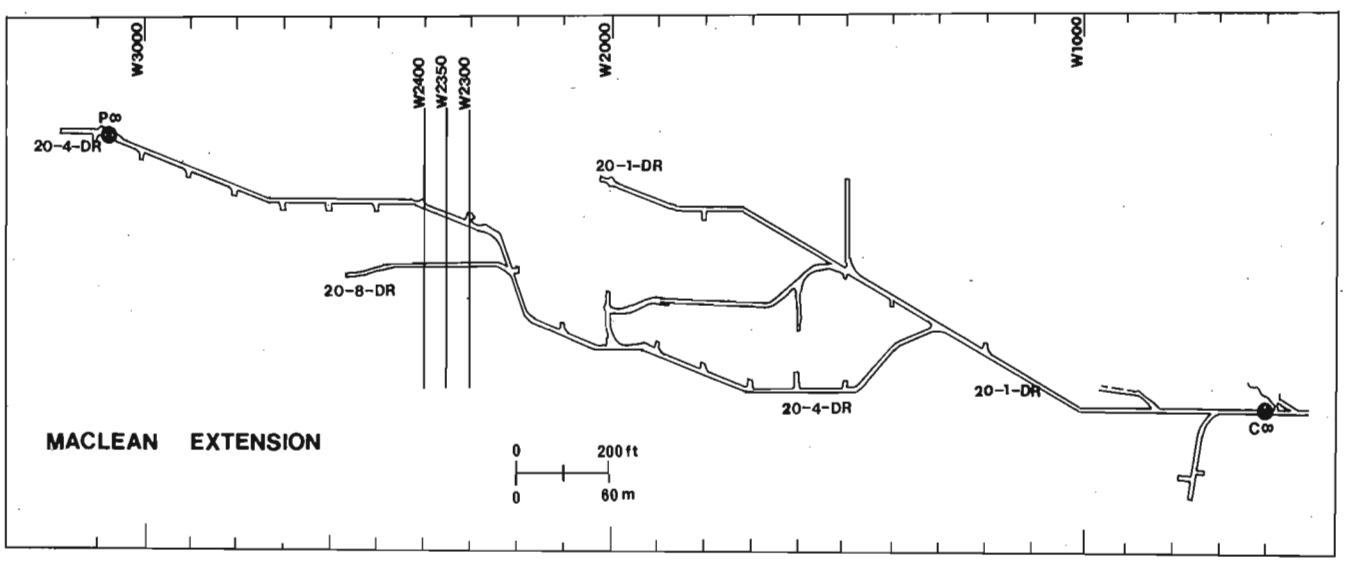

Figure 15.1. Plan map of level 20 of the MacLean Extension orebody showing the location of remote electrodes and the location of the geological sections shown in Figure 15.2-15.4 where mise-à-la-masse measurements were carried out.

Data presentation

For each energizing current source location, the following data are presented: MALM potential, MALM IP (Newmont chargeability parameter), self potential (SP) and chargeabilities for 10 other windows. The chargeabilities are the normalized time integral of the decay voltage and the standard IP chargeability is integrated from 0.45 to 1.1 s after current switch off. The other 10 windows are adjacent and of equal width (175 ms) with the first window integrated from 100 to 275 ms. In all the figures to follow, the IP window with the highest chargeability is the first window (W1) and with the lowest chargeability is the last window (W10). All chargeability values are expressed in milliseconds. The MALM potentials in each drillhole are measured at a constant current. However, in order to compare potentials measured in different holes within the orebody, the potentials are normalized to one current value and are expressed in volts/ampere.

Normally only the measured mise-à-la-masse potentials are presented. However, these are easily converted to apparent resistivities, ρ_a.

$$\rho_a = 4\pi RV/I$$

where V = measured potential,
I = applied current,
R = distance between the source and the measurement points.

The effect of the distant current source, C ∞ and that of the reference potential electrode, P ∞, are assumed to be negligible and hence not included in the computation. The apparent resistivity profiles are indicated by a dotted line superimposed on the MALM P profiles (see Figures 15.7, 15.12 and 15.15).

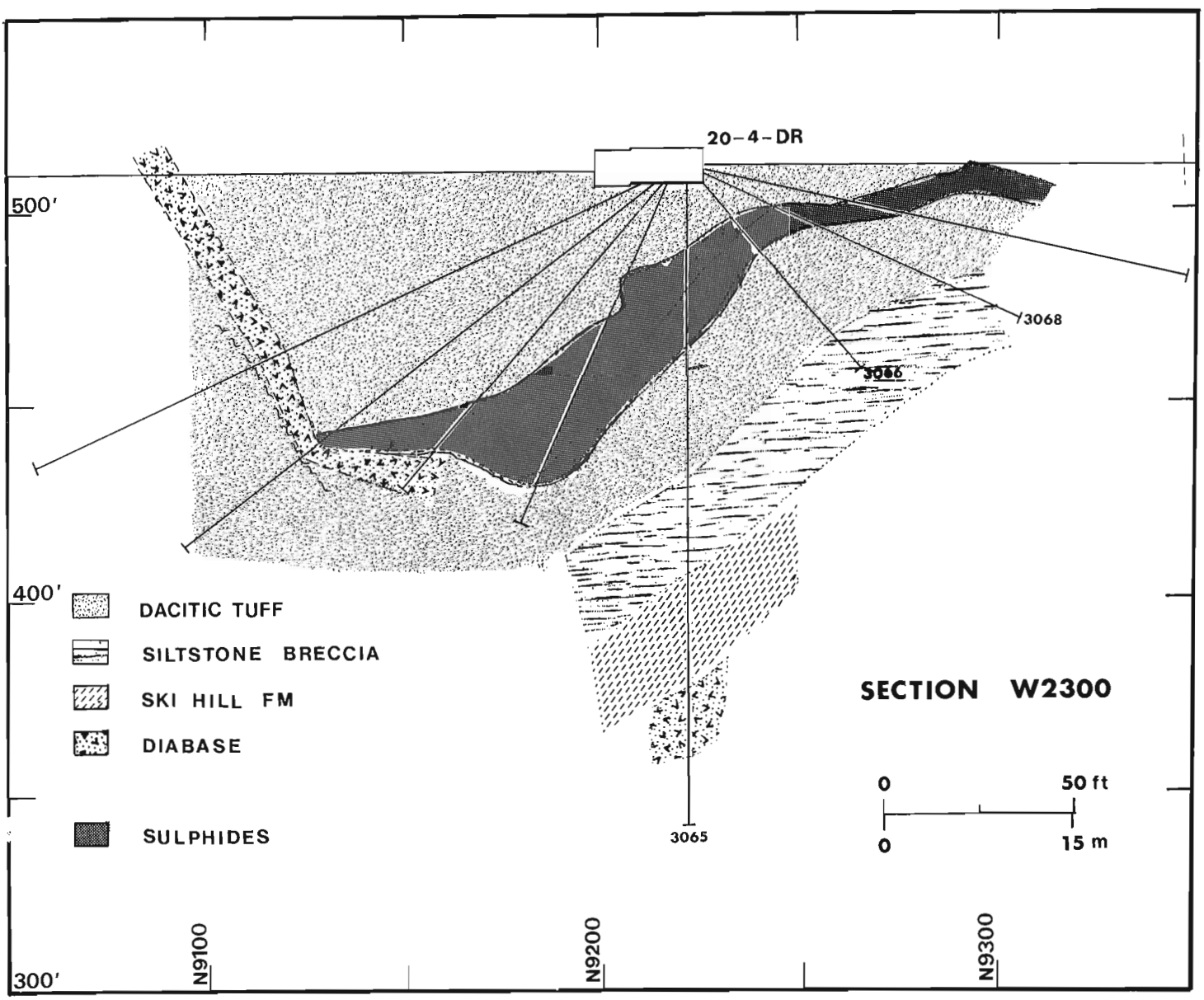

Figure 15.2. Geological section along W2300 on level 20, MacLean Extension orebody (geology from company sections). The holes used in the present study are numbered.

The distances along the depth axis do not represent the true vertical depths but lengths along the drillhole. The location of the sulphide mineral intersections (ore zones) are displayed as shaded areas along a column next to the depth axis.

Mise-à-la-masse potential and IP measurements - section W2300

Figure 15.6 shows the current source locations for MALM potential and IP measurements carried out along section W2300. Source C1 and C2 are located within the conductive sulphide and source C3 is located outside the sulphide mineralization.

Mise-à-la-masse potential

Figure 15.7 shows MALM potential and IP measurements along hole 3065 in section W2300 with the energizing current electrode in the ore zone in hole 3068, at a depth of 7.5 m (C2) along the hole. A constant input current of 500 mA was applied. The MALM potential results show a flat, potential high outlining the position of the ore intersection. This indicates that the ore intersections in holes 3068 and 3065 are in electrical continuity. An almost constant potential high across the intersection indicates that the ore is highly conductive. The sulphide-host rock interface is clearly defined by the marked change in potentials. It should be noted that the potentials decrease at a slower rate downhole as would occur for a dipping orebody which agrees with the geological section in Figure 15.2. Across the ore intersection, higher apparent resistivity values are observed near the bottom edge and lower values near the top edge. Because of the nearly constant potentials across the ore, the lower apparent resistivities near the top edge indicate that the current source is located closer to this edge of the conductor (see Fig. 15.6 and refer to the ρ_a equation). The ore limits are not as well defined in the apparent resistivity profile as in the MALM potential profile but its presentation in this case, provides an approximate resistivity value of the host rock. The SP results show a low potential zone in the centre of the ore but the edges of the ore intersection are not well defined from this data.

Mise-à-la-masse IP

The MALM IP profile shows an inverse relationship to the MALM potential profile. A decrease in apparent polarizability is observed within the energized sulphide conductor. Constant chargeabilities across the ore intersection indicate that the current densities and therefore the potentials are fairly uniform within the conductor as shown by the MALM potentials. This assumes homogeneous intrinsic polarizability of the sulphide mineralization. The IP

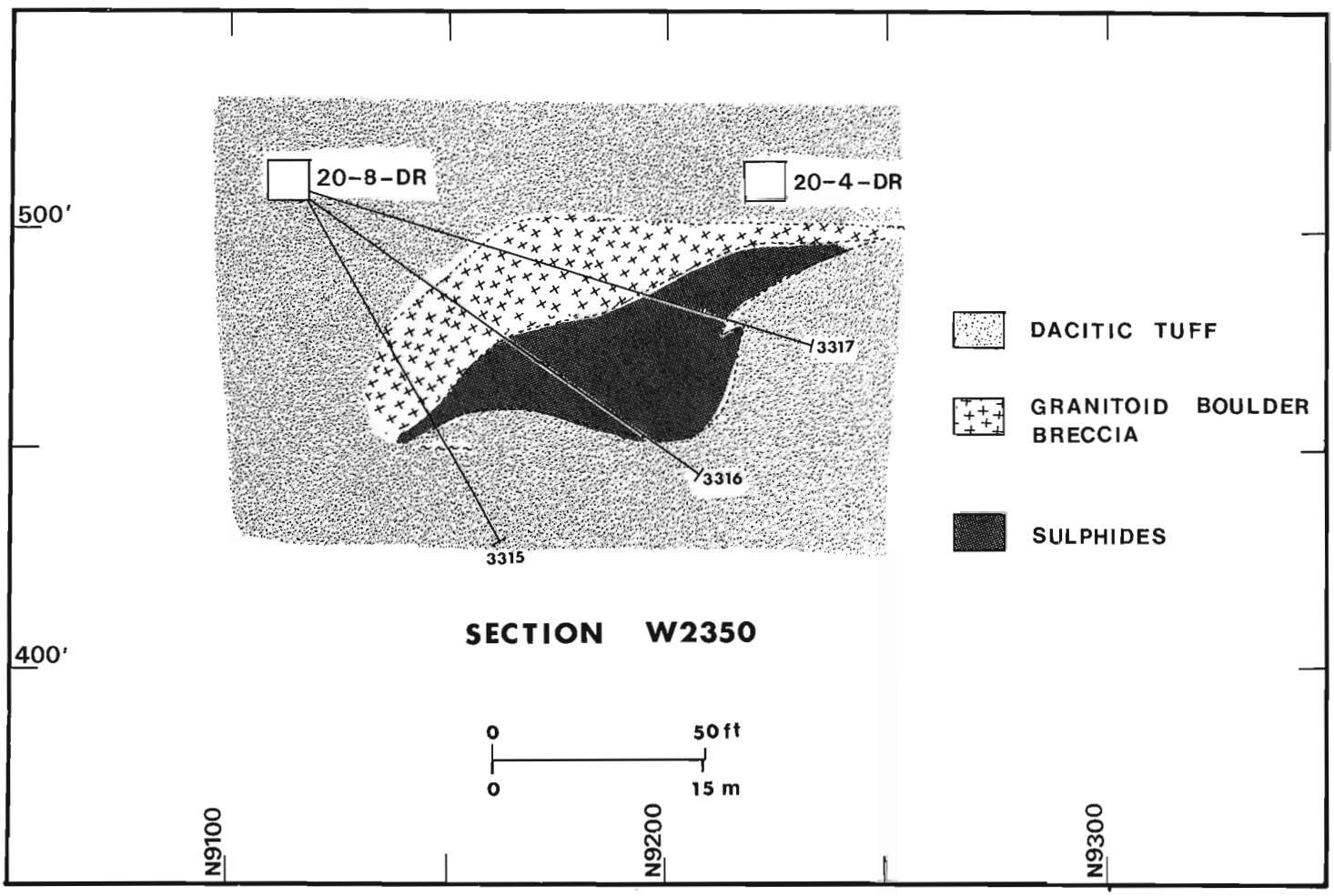

Figure 15.3. *Geological section along W2350 on level 20, MacLean Extension orebody (geology from company sections). The holes used in the present study are numbered.*

profile is asymmetric about the ore intersection. A steep rise in the apparent polarizability is observed on the upper boundary of the ore while the lower boundary shows a slow rise. This indicates that the conductor is not flat but extends towards the bottom of the hole. This observation is consistent with the conclusions drawn from the MALM potential data. In the absence of other drillholes, this information would prove valuable in directing subsequent drilling aimed at defining the extent of the sulphide intersection. Even though the ore intersection shows low apparent polarizability, the intrinsic polarizability of the sulphide mineralization is higher than that of the host rock. It is well known that for a given conductive and polarizable target (same shape, depth of burial, same intrinsic polarizability and resistivity contrast with the host rock) the shape of the IP anomalies depend on the array used. This has been called the electrode effect by Bertin and Loeb (1976). In the case of an array with a single current electrode (the second current electrode is assumed to be at "infinity") low apparent polarizabilities are measured above the polarizable body when the source is located close to the centre of the body (Komarov, 1970). For the MALM method, Sumner (1981) has presented a theoretical analysis of the IP response to be expected for a simple polarizable sphere. He stated that when a current source is located at the centre of a polarizable sphere, polarization can be detected external to the sphere during the current-on cycle. However, when the current is cycled off, the internal depolarization field collapses on itself so that no external polarization field is observed and that there is asymmetry or non linearity in the IP charge and decay curves.

In the present study, IP waveforms measured inside and outside the sulphide mineralization, with current source located within the conductor did not show this kind of polarization behaviour. Figures 15.8 and 15.9 show the complete voltage waveforms and transient voltage decay curves, respectively, observed within the energized conductor (waveform 1) and outside the conductor (waveform 2 and 3). Polarization is detected both within and external to the energized sulphide mineralization and there is symmetry in the IP charge and decay curves. It is interesting to note that although amplitudes of decay voltages observed inside the conductor are higher than those observed outside (Fig. 15.9), the corresponding primary potentials (Fig. 15.8) show even higher amplitudes inside, relative to those observed outside. Since the apparent polarizability depends on the primary potential (the area under the decay curves is normalized by the primary potentials) it is easy to see how low values are measured inside the conductor. Higher current densities and hence higher potentials are observed within the energized conductor resulting in lower computed apparent polarizabilities relative to the host rock.

The polarization levels observed during the positive current-off cycle were always higher than those observed during the negative current-off cycle for measurements

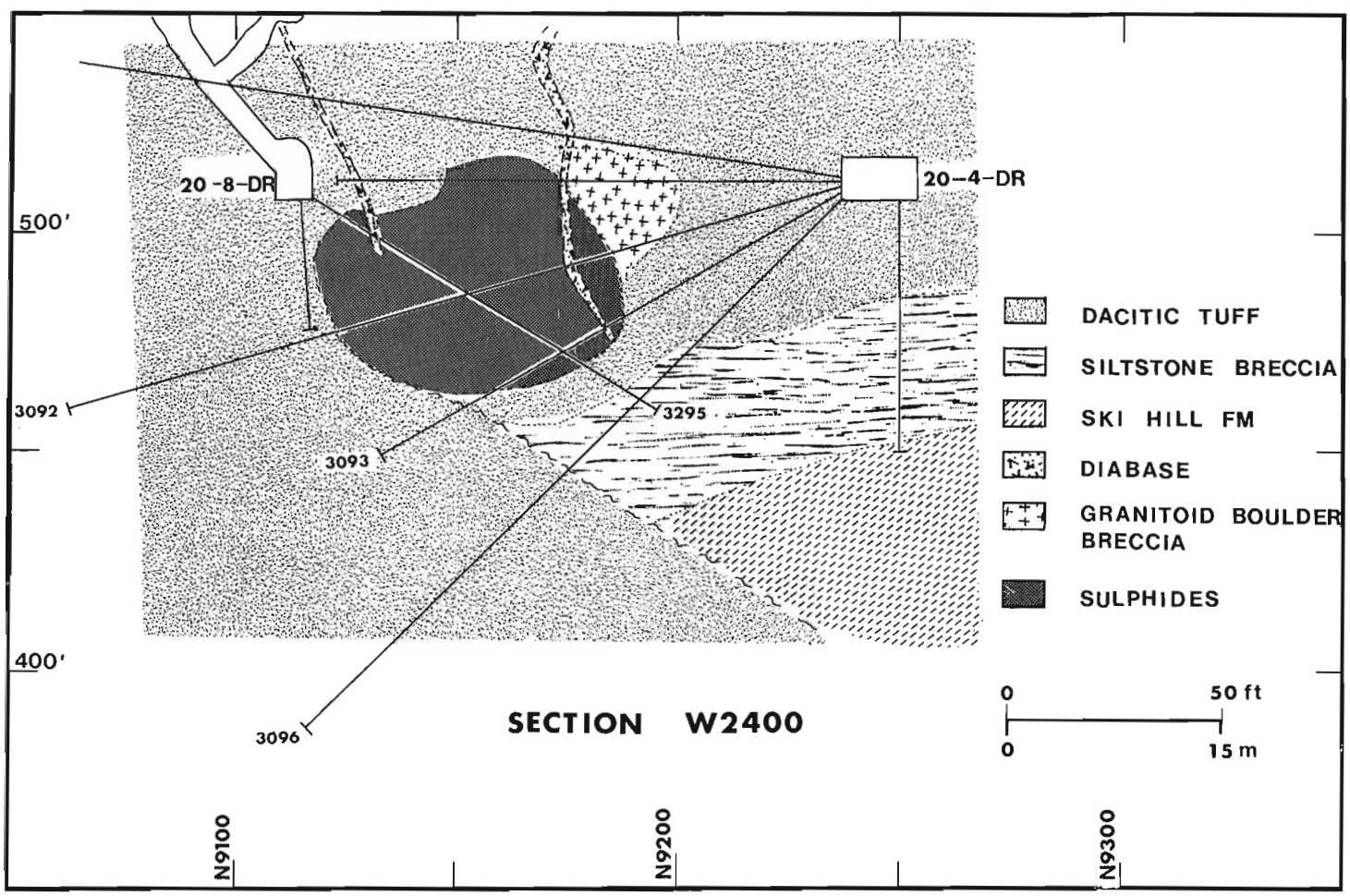

Figure 15.4. Geological section along W2400 on level 20, MacLean Extension orebody (geology from company sections). The holes used in the present study are numbered.

within or outside the conductor. This was also true for current sources either inside or outside the sulphide conductor (Fig. 15.10). The decay curves for the negative current-off cycle have been inverted to facilitate comparison. This asymmetry in the IP decay curves indicates the IP phenomenon is not totally reversible when the polarity of the current is changed. The non-reversibility suggests that the assumption that the sulphide minerals are true metallic conductors is not valid. Most ore minerals are semiconductors (Shuey, 1975). Bertin and Loeb (1976) and Dakhnov et al. (1967) have also noted that the induced polarization of a rock may not be the same when measured with negative current as when measured with positive current.

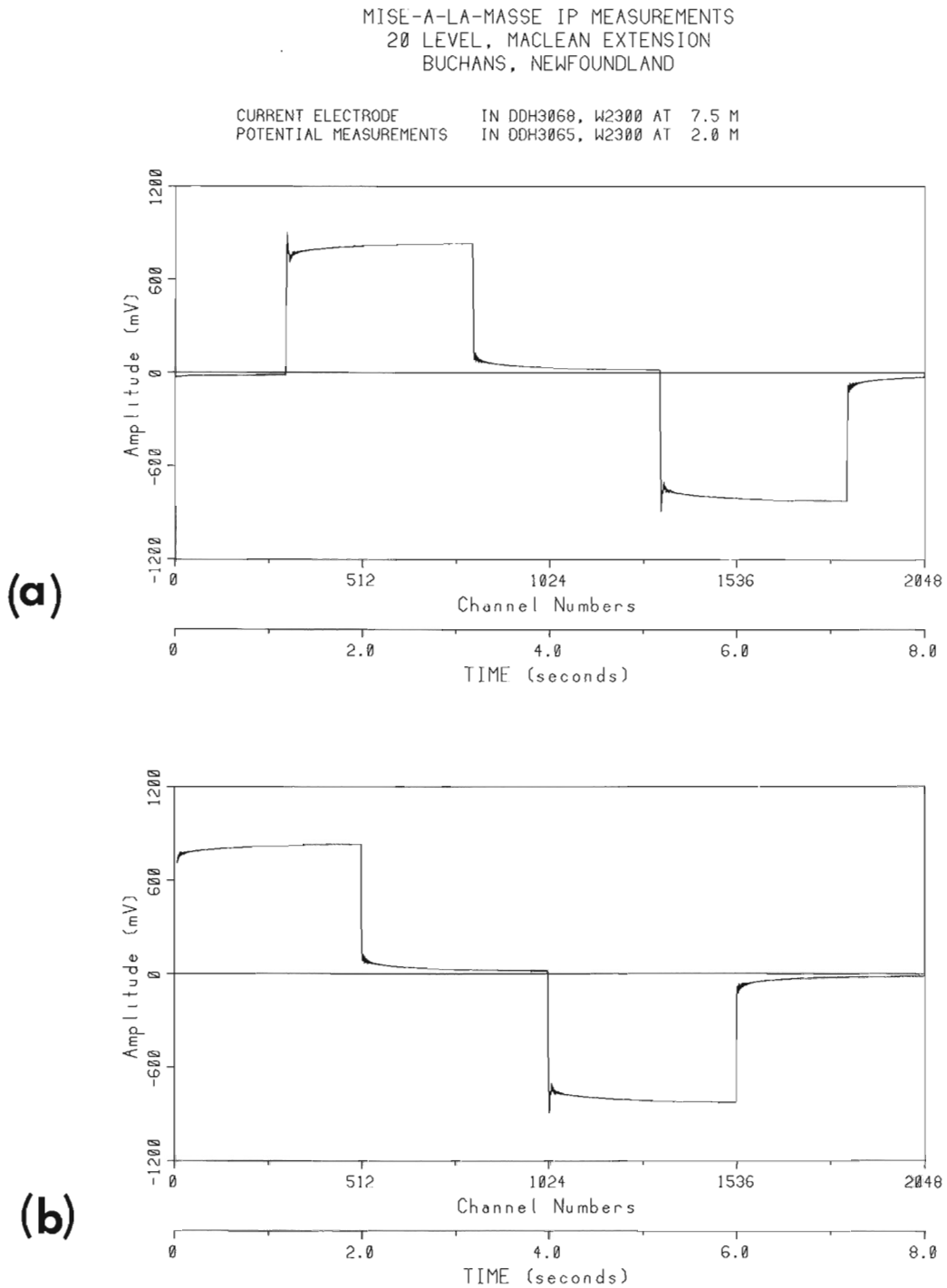

Figure 15.5. *Typical time domain complete IP waveform recording with the Huntec IP system. (a) voltage waveform as recorded on cassette tape of the Huntec M4 receiver. (b) rearranged waveform with the onset of the positive current-on time at the beginning of the cycle.*

Reciprocity in MALM potential measurements

With the MALM method, the continuity of the sulphide zone between current source and potential electrodes is established when the location of the potential maximum coincides with that of the indicated location of the ore. However, this does not always happen. In many cases the ore deposit consists of a number of ore lenses with differing resistivities and dimensions, and also within the limits of the ore deposit other conducting structures such as faults may be present. In such complex geological situations the potential field distribution is complicated, and in order to determine accurately the geoelectrical structure between drillholes, measurements of the potential field are carried out in a number of holes with the energizing current electrodes at different locations. In order to verify the continuity of the energized ore section from hole 3068 to hole 3065, a current electrode was placed in hole 3065 at 9 m (C1) and potential measurements were made in hole 3068. The results presented in Figure 15.11 show the location of the potential maximum coinciding with the ore intersection.

Potential and IP Results - Source Outside Conductor

The potential, apparent resistivity, and IP measurements made with the current source located outside the conductive and polarizable sulphides are shown in

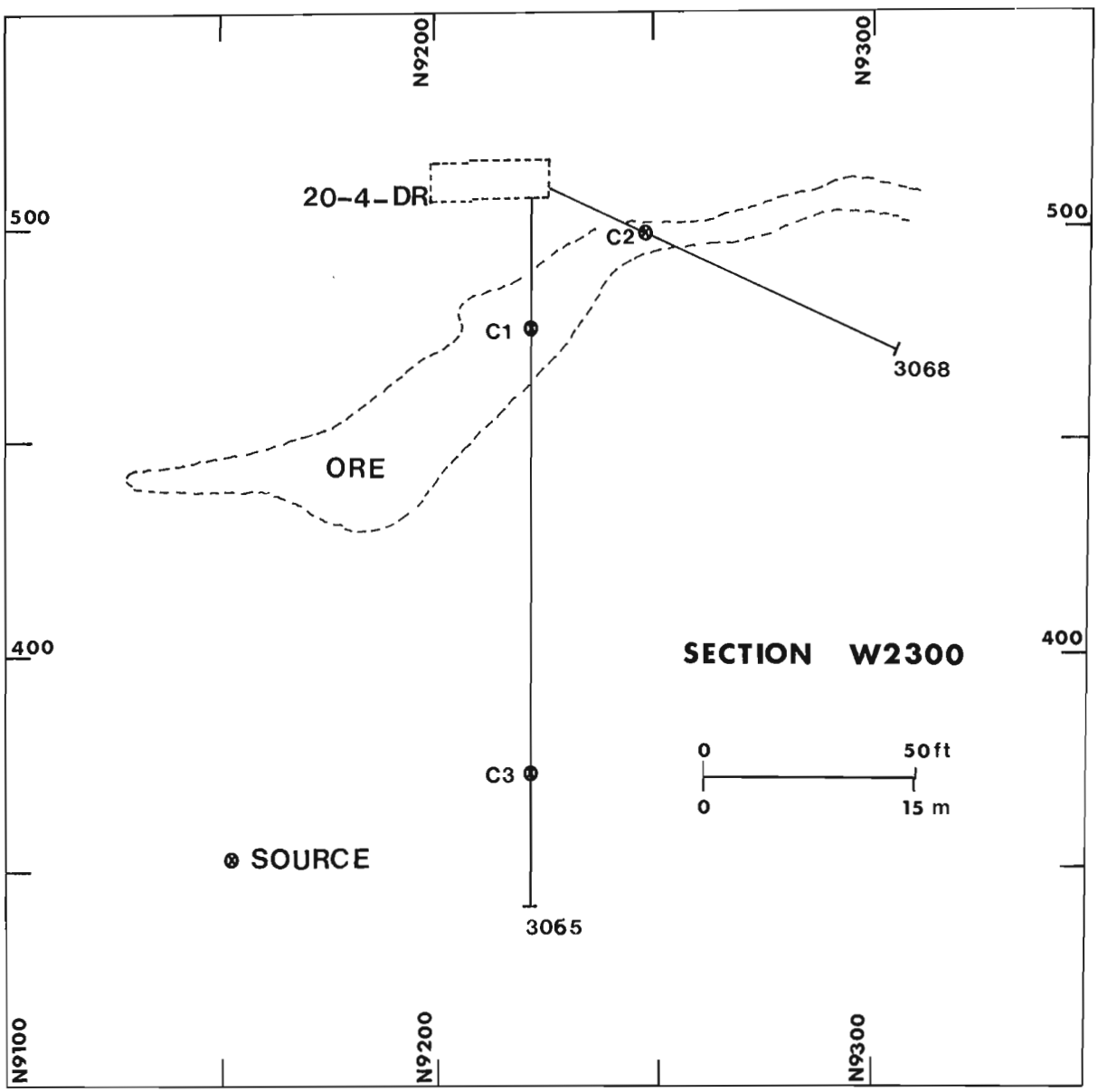

Figure 15.6. Section W2300 showing the drillholes and the location of current sources used in the potential and IP measurements carried out along this section. The ore outline is also indicated.

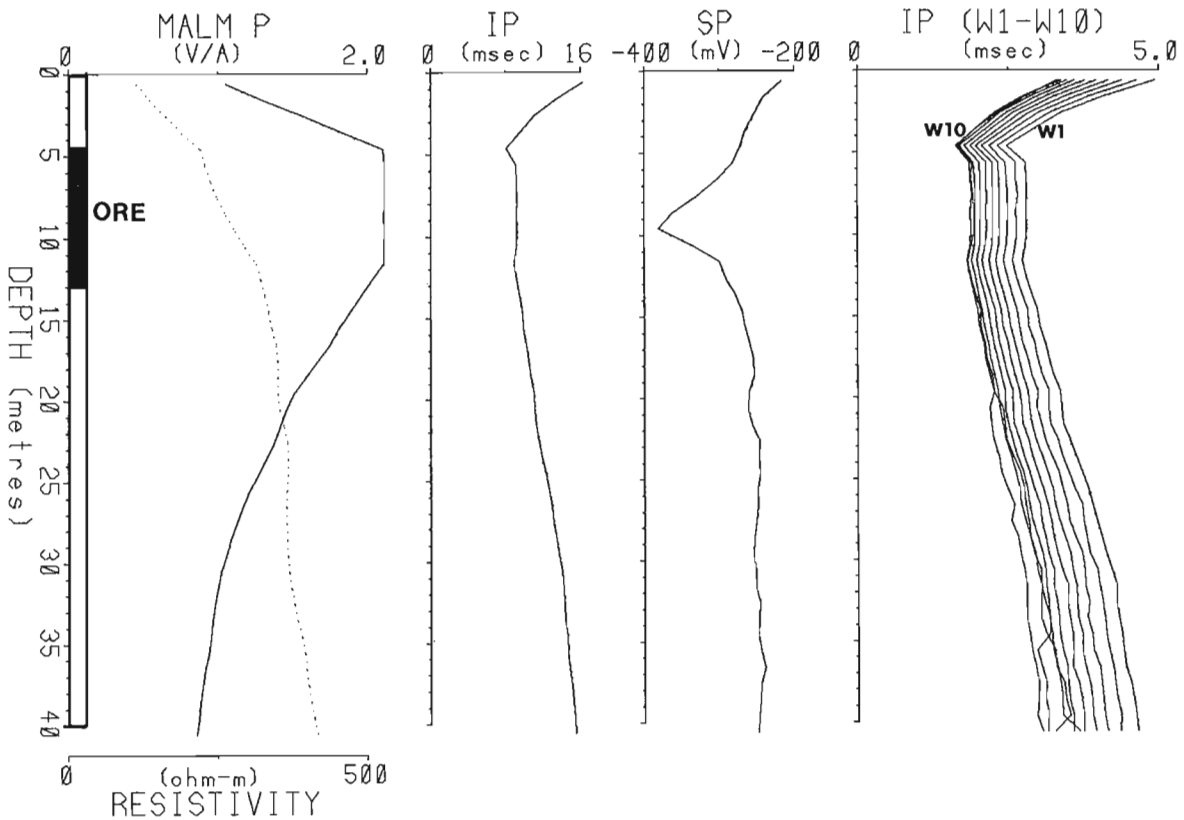

Figure 15.7. *Mise-à-la-masse potential and IP measurements along hole 3065-W2300 with the energizing current electrode (C2, Fig. 15.6) in ore at 7.5 m in hole 3068-W2300. The MALM potential values are normalized with respect to the applied current and expressed in volts/ ampere. IP values are in milliseconds.*

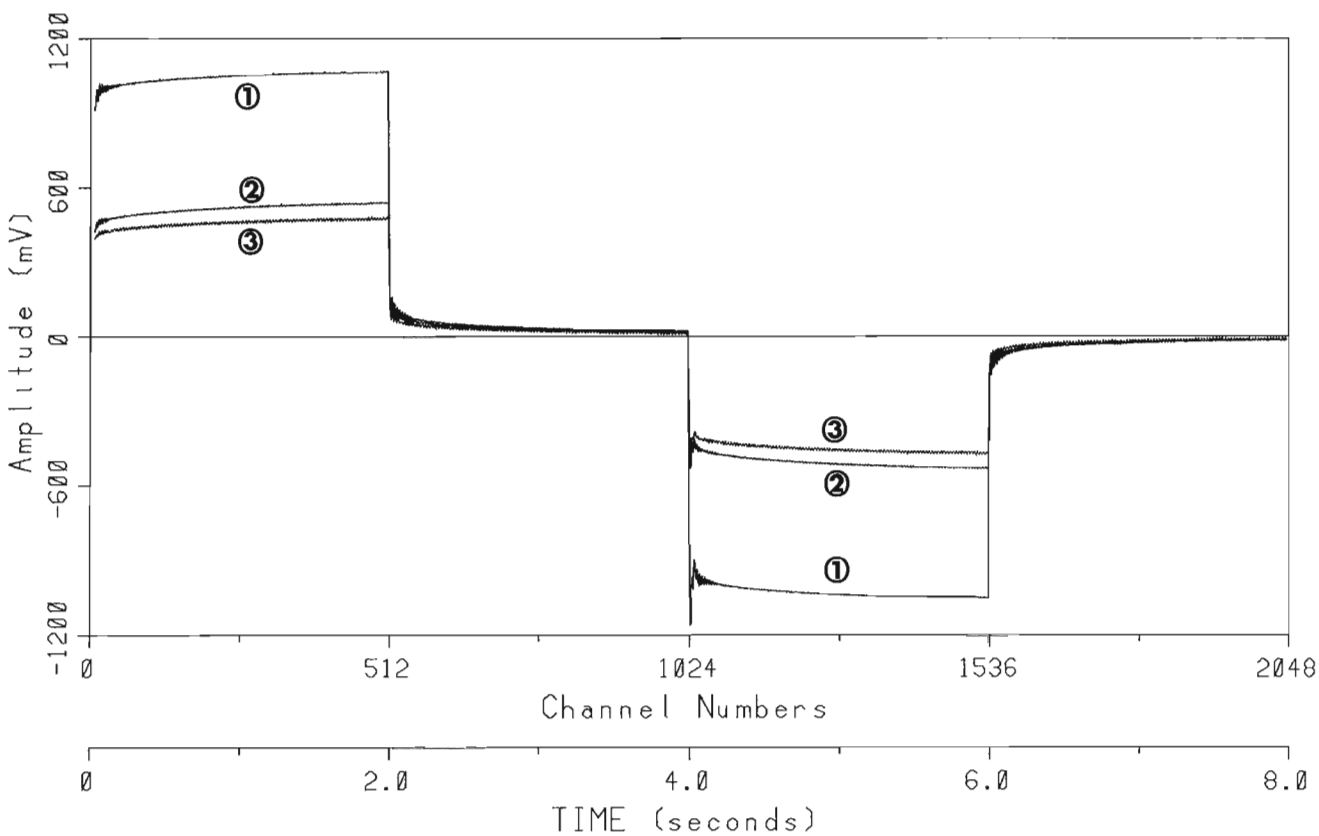

Figure 15.8. *Mise-à-la-masse IP waveforms observed in hole 3065-W2300 with the current source in ore at 7.5 m in hole 3068-W2300. (1) waveform observed inside ore at 7 m. Waveforms observed outside ore at 1 m (2) and at 35 m (3).*

Figure 15.12. The source is located at a depth of 41 m in hole 3065 (C3) and potential measurements were carried out in the same hole. The potential field attenuates with distance away from the source in the normal fashion (i.e. Vα1/R, where V is the potential and R is the distance away from the source) except across the ore intersection. Low, almost constant potentials, are observed across the intersection. This is a typical response for a highly conductive zone that is not in electrical continuity with the energized zone (Mwenifumbo, 1985). The apparent resistivity profile shows an anomalous resistivity low on the conductor boundary close to the source and an anomalous resistivity high on the boundary opposite the current source. The conductor boundaries are clearly defined by these low and high resistivity anomalies. In this case the apparent resistivities provide a better resolution of the conductor boundaries than the potentials.

The IP profile shows an inverse relationship to the potential profile. The apparent polarizability within the ore is higher than that observed within the host rock below the ore. Above the ore intersection, the apparent polarizability increases steeply in a similar manner to that observed in the mise-à-la-masse data in Figure 15.7. There is a marked change in the IP at the edges of the ore making it fairly easy to estimate the ore width. A comparison between the 10 window data in Figures 15.7 and 15.12 indicates that there is a difference in the decay rate for the two source positions. This observation has not been fully investigated in the present study. The differences in the apparent polarizability curves illustrates the strong dependence of the polarizability on the current source positions with respect to the centre of the polarizable body. Distortions of the primary field by the conductive polarizable body are dependent on the location of the current source relative to the body and consequently the depolarization field (IP effect).

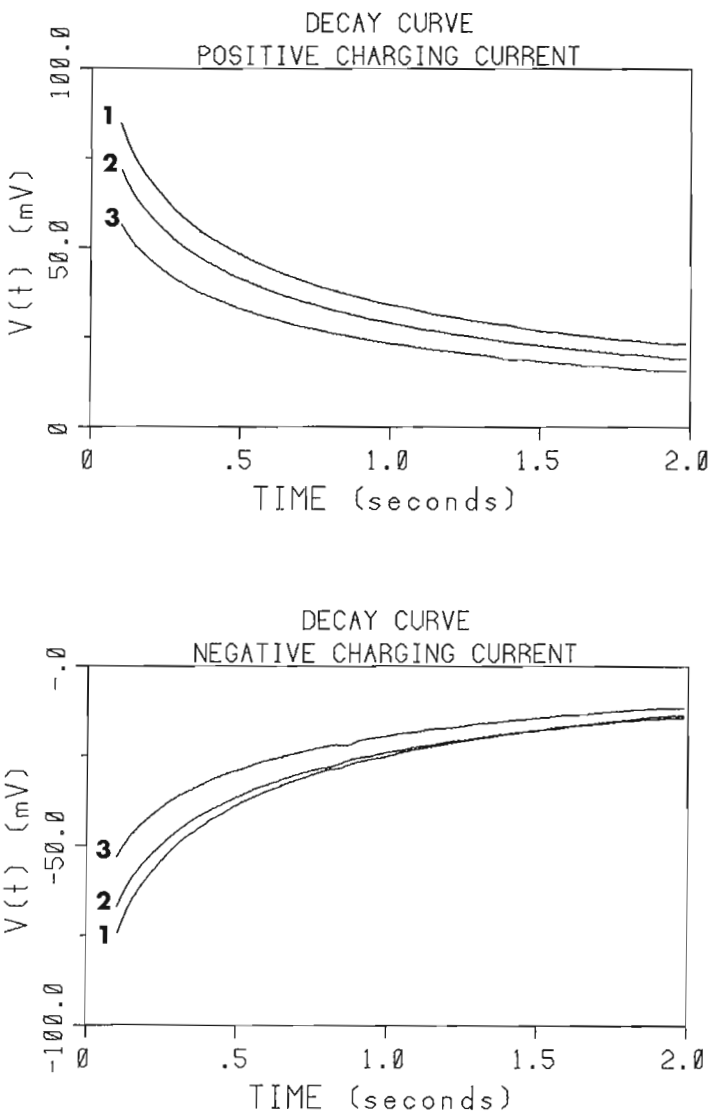

Figure 15.9. *IP decay curves for the positive and negative charging currents. The curves correspond to the off-cycle voltages of the waveforms presented in Figure 15.8.*

Mise-à-la-masse IP and potential measurements between sections W2300, W2350, W2400

To study the continuity of the ore intersections between the three sections, a number of measurements were made along holes in all the sections with the current

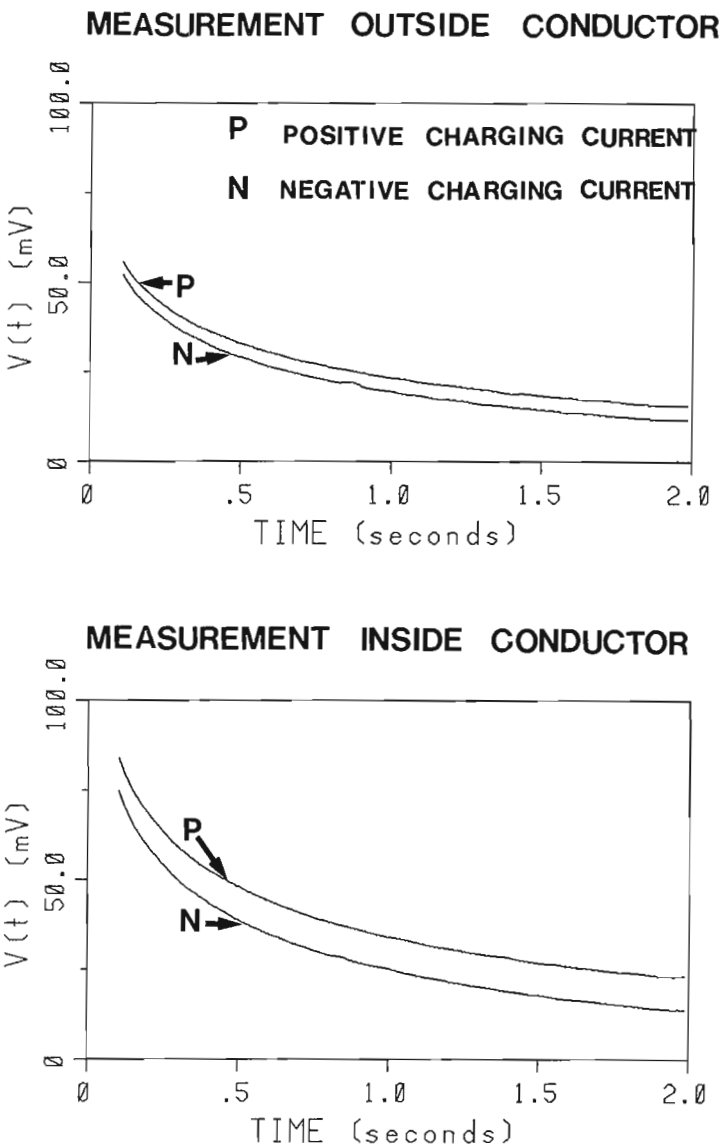

Figure 15.10. *IP decay curves observed outside and inside the energized sulphide conductor illustrating that the IP is not completely reversible with polarity reversal of the charging current. The decay curves for the negative charging current are inverted for ease of comparison.*

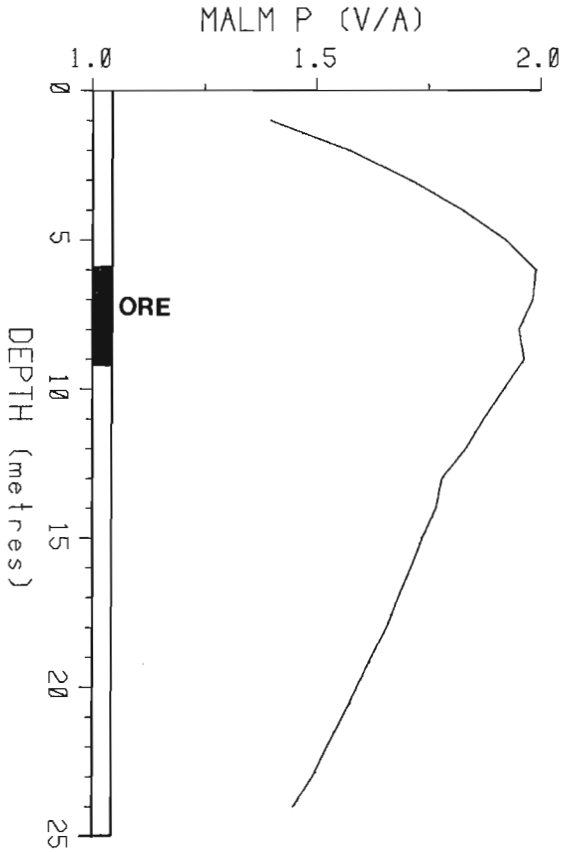

Figure 15.11. *Mise-à-la-masse potential measurements along hole 3068-W2300 with current electrode in the ore at 9 m in hole 3065-W2300 (C1, Fig. 15.6).*

electrodes placed in different mineral intersections. MALM IP and potential measurements were made in hole 3295, section W2400 with the current electrodes located in ore intersections in hole 3065, section W2300 at 9 m and in hole 3316, section W2350 at 24 m. The results are shown in Figure 15.13a and b, respectively. An almost constant potential maximum is observed across the ore intersection for both the current electrode positions indicating that the orebody is electrically continuous between these holes (sections W2300 and W2350 to section W2400). The potential curves for the two source locations are practically identical. The IP measurements similarly show an inverse relationship to the potential measurements. The form of the apparent polarizability profiles is identical for the two current source locations. The noticeable differences are in the amplitude and the rate of decay of the discharge curves (see IP W1-W10). The amplitude difference is a result of the differences in the current densities due to changes in distances of the source to the measurement hole. Lower apparent polarizability values are observed for the current source closer to the measurement hole. The constant apparent polarizability across the sulphide intersection indicate fairly uniform current densities within the sulphide mineralization.

MALM IP and potential measurements along hole 3093, section W2400 are presented in Figure 15.14 with the current source in the sulphide zone in hole 3316, section W2350 at 24 m (Fig. 15.14a) and with the current electrode in hole 3096, section W2400 at 23 m (Fig. 15.14b). There is a gradual increase in potential values with increasing depth. The potentials reach a maximum at about 14 m and then flatten out. This depth coincides with the upper boundary of the ore intersection. The potential field distribution could not be determined below the lower contact because the hole was plugged at about 23 m. The gradual increase in the potentials indicates that the conductive ore comes close to the hole

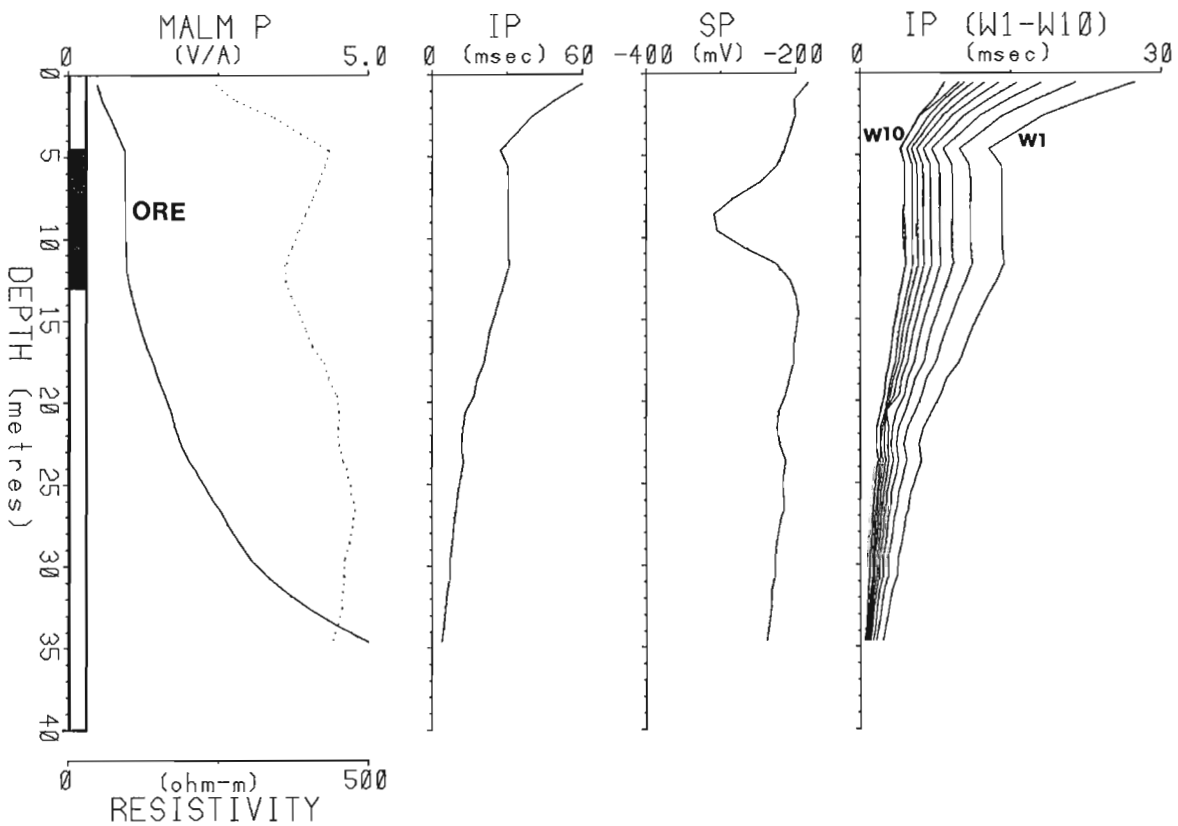

Figure 15.12. *Potentials, apparent resistivity, SP and IP measurements carried out in hole 3065-W2300 with the current source fixed outside the sulphide mineralization at 41 m in the same hole (C3, Fig. 15.6).*

above the upper contact, in contrast to an almost step-like change in the observed potentials along hole 3316 (see Fig. 15.13). The distinct potential maximum and constant potentials within the ore intersection indicate that the ore is highly conductive and forms a single continuous ore zone between the holes. The potential field distribution was also studied along hole 3065, section W2300 with current sources located in holes in sections W2350 and W2400. The potential maxima were observed to coincide with the ore intersections indicating, conclusively, the continuity of conductive sulphides between these sections.

Potential and IP measurements between barren holes

When drillholes do not intersect ore, it is often necessary to determine whether ore is located between the holes. With current electrodes grounded at various positions in one hole, and potential measurements recorded in another hole, comparison of the observed measurements with theoretical results from simple models can establish the presence of conductive bodies between the holes. Figure 15.15 shows IP and potential measurements along barren hole 3096 in section W2400 with the current source grounded in an unmineralized top part of hole 3295 at a depth of 1 m. The measurements were not carried out past the projection of the sulphide zone because the hole was plugged. A broad potential high is observed directly opposite the projection of the ore zone onto the drillhole. The apparent resistivity values are anomalously high across the broad potential high. This observation could be misinterpreted to indicate the presence of a resistive target between the source and the measurement hole. The apparent resistivity high, however, indicates that a conductor lies between the source and observation hole. Lytle (1982) and Yang and

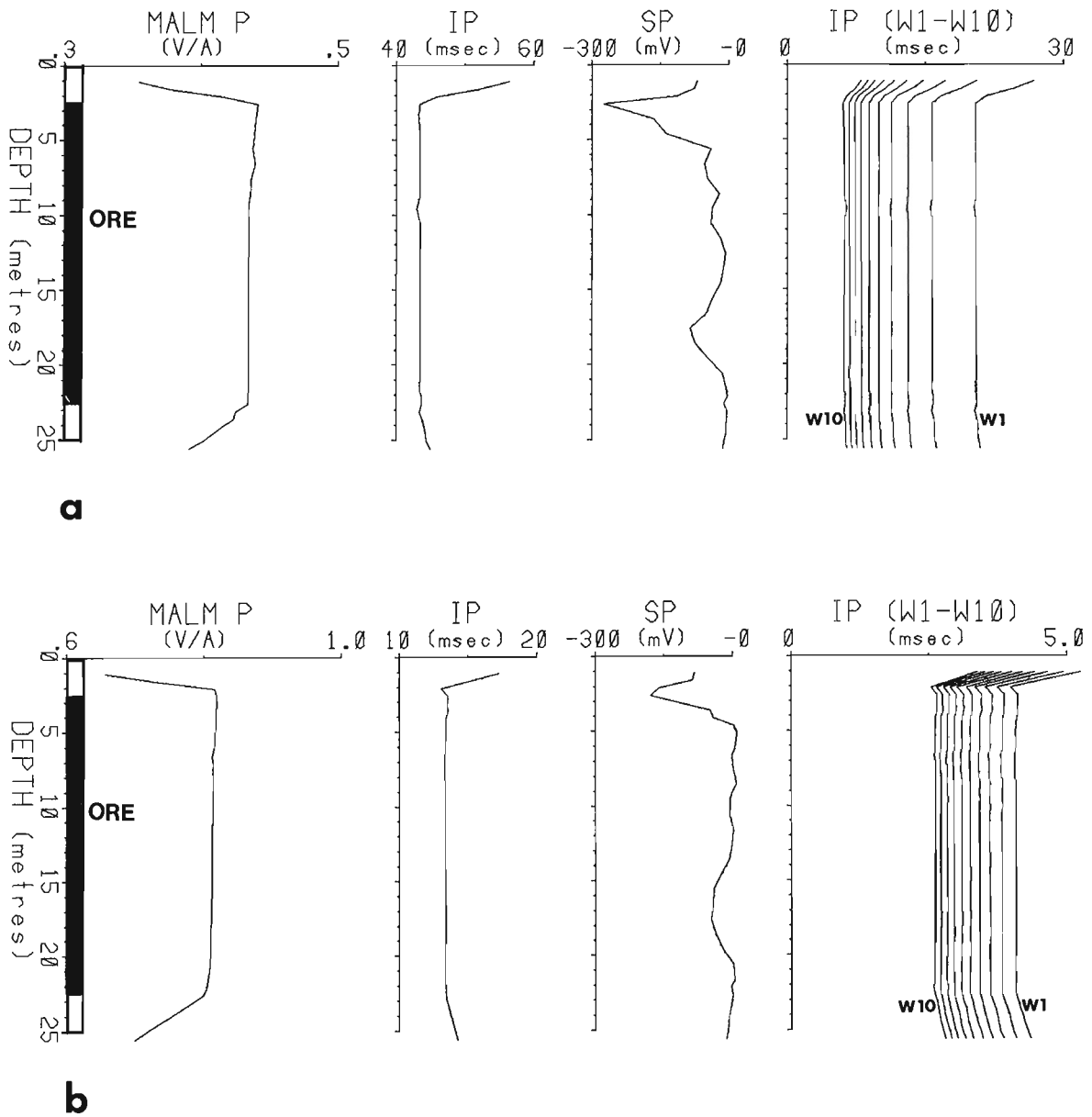

Figure 15.13. *Mise-à-la-masse potential and IP measurements made along hole 3295-W2400. (a) with the current electrode in ore at a depth of 9 m in hole 3065-W2300. (b) with the current electrode in hole 3316-W2350 at a depth of 24 m.*

Ward (1985) have presented hole-to-hole resistivity responses for a pole-pole array for a spherical body located between the source and the measurement hole. The apparent resistivities computed on the current source side of a conductive spheroid are low whereas, on the side of the spheroid opposite the current source, an apparent resistivity high is observed. In the case of a resistive spheroid, the converse is true. The geology of section W2400 shows a circular outline of the conductive sulphide mineralization between the source (hole 3295) and the measurement hole 3096. The projection of the sulphide onto hole 3096 is approximately defined by the apparent resistivity high. Interpreting where the target lies relative to the current source and receiver locations needs to be carried out with caution. The above observation alone does not conclusively indicate the presence of conductive mineralization between the holes. Other geophysical and/or geological data are needed to establish the possible occurrence of sulphides between the holes. The high negative SP values observed along hole 3096 are an indication of sulphides in the vicinity.

Conclusions

The MacLean Extension orebody is a complex assemblage of polymetallic sulphides. A number of faults within the ore area seem to offset some ore lenses. A number of holes drilled above and below the drift intersected base metal sulphides, while others were barren. The MacLean Extension appeared to present an ideal situation for the study of the MALM potential field distribution. Unfortunately all drill holes except those studied were plugged.

The MALM IP and potential measurements carried out in the MacLean Extension orebody, although limited to three sections and a few holes, indicate that the sulphide zones

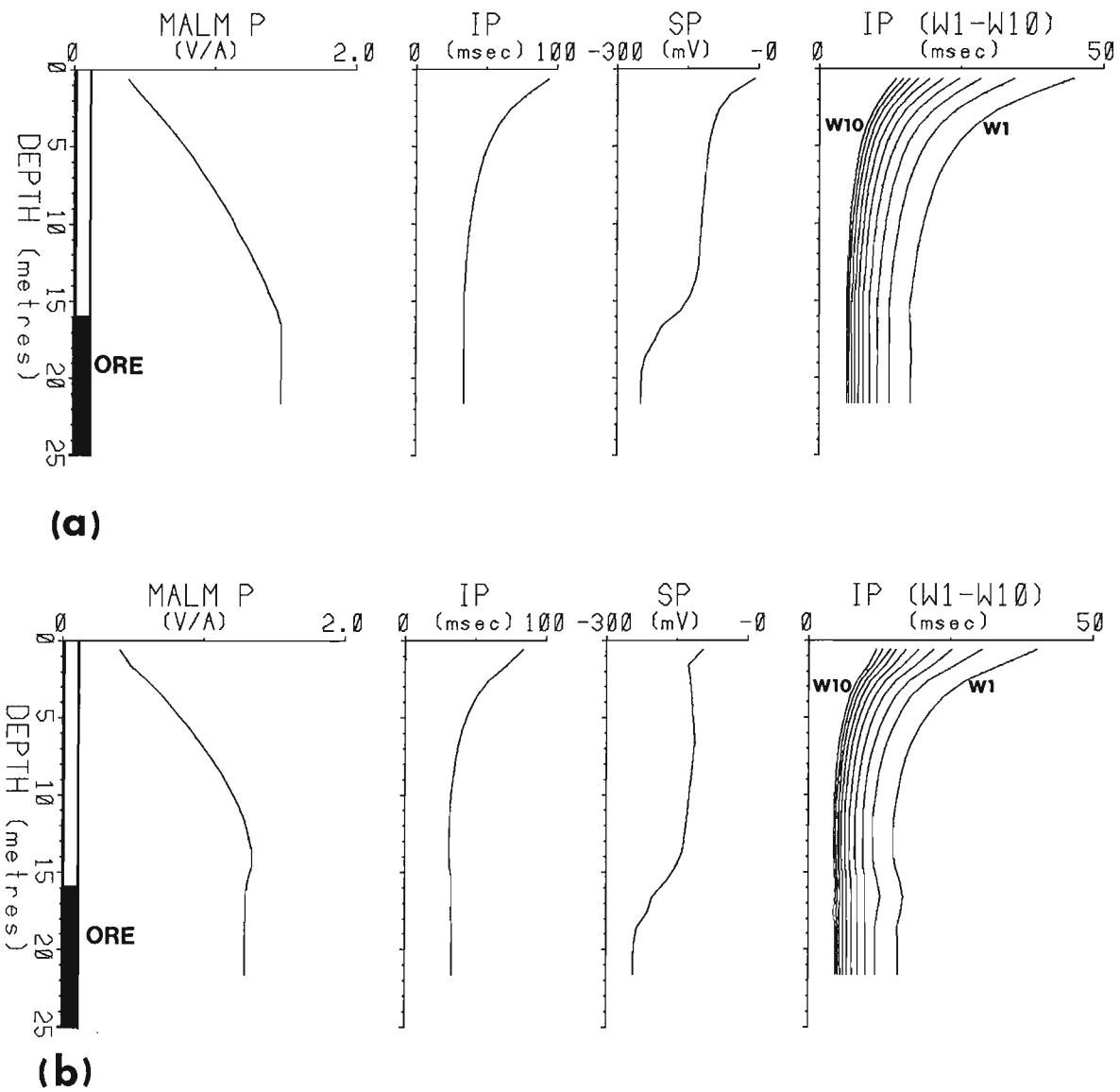

Figure 15.14. *Mise-à-la-masse potential and IP measurements along hole 3093-W2400. (a) with the current electrode in the ore section at a depth of 24 m in hole 3316-W2350. (b) with the current electrode at a depth of 23 m in hole 3096-W2400.*

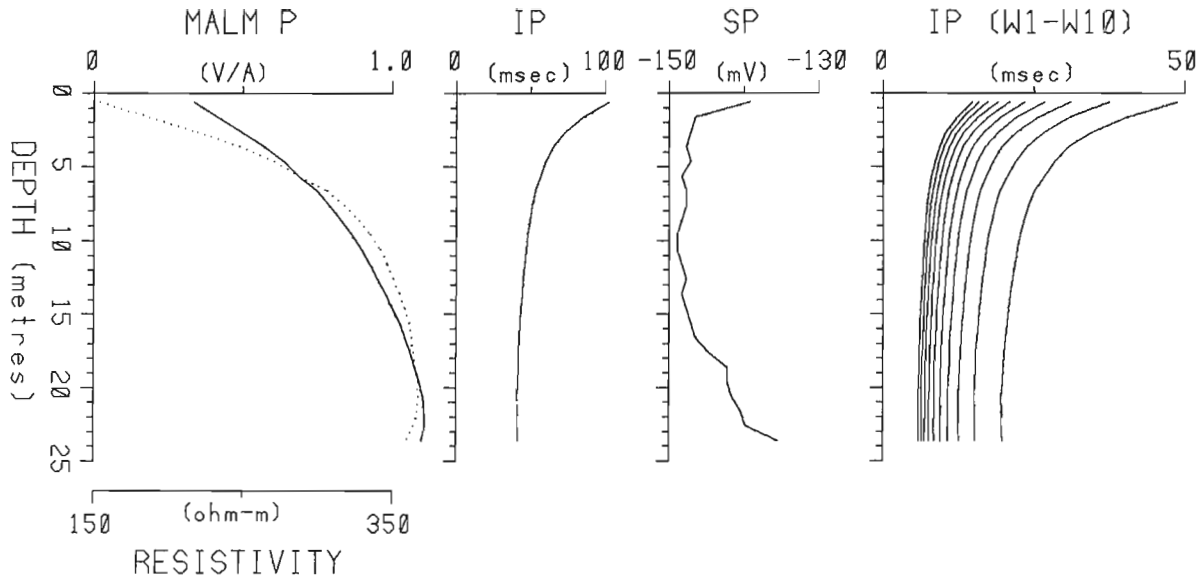

Figure 15.15. *Mise-à-la-masse potential and IP measurements along a barren hole 3096-W2400 with the energizing current electrode placed in an unmineralized section at 1 m depth in hole 3295-W2400.*

within this part of the orebody are highly conductive and the ore sections can be correlated easily between holes. The normalized MALM IP data show an inverse relationship to the potentials, low IP coinciding with high potentials across the mineral intersections. No additional information can be obtained on the geometry and nature of the ore zones from the IP data. A more comprehensive analysis of the decay waveforms (time constants) may reveal additional information on the polarizability of the sulphides. The unusual MALM IP effects (negative IP and non-linearity in charge and discharge curves) reported by Sumner (1981) were not observed in the present study. This could be due to the complex morphology of the sulphide mineralization.

The MALM measurements can answer a number of questions encountered in mineral exploration and development. In cases where an orebody consists of a number of ore lenses, the MALM measurements can be used to determine which of the lenses are connected between drill holes. This information is useful in planning mining operations. The MALM measurements can also be used to determine the direction of dip of a discovered conductor and to evaluate its extension within a given area. This information is again useful in siting subsequent drill holes aimed at intersecting the same sulphide lense. The MALM measurements can also be used to determine the structure between holes which may aid in the discovery of missed ore zones.

Acknowledgments

This work was carried out under the Canada-Newfoundland co-operative mineral program 1981-84. Thanks are due to the staff of ASARCO and ABITIBI-PRICE Mineral Resources for providing the geological information and logistical help required for carrying out this study.

References

Bertin, J. and Loeb, J.
1976: Experimental and theoretical aspects of induced polarization; Geoexploration Monograph, Ser. 1, no. 7, volume 1, Geopublication Associates, Berlin, 250 p.

Binney, W.P., Thurlow, J.G. and Swanson, E.A.
1983: The MacLean Extension orebody, Buchans, Newfoundland; in Current Research, Part A, Geological Survey of Canada, Paper 83-1A, p. 313-319.

Dakhnov, V.N., Latishova, M.G. and Ryapolou, V.A.
1967: Well logging by means of induced polarization (electrolytic logging); The Log Analyst, v. VIII, no. 3, p. 3-18.

Ketola, M.
1972: Some points of view concerning mise-à-la-masse measurements; Geoexploration, v. 10, p. 1-23.

Komarov, V.A.
1970: The importance of induced polarization method for the exploration of ore deposits; in Mining and Groundwater Geophysics 1967, Geological Survey of Canada, Economic Geology Report 26, p. 138-147.

Lytle, R.J.
1982: Resistivity and induced polarization probing in the vicinity of a spherical anomaly; IEEE Geoscience and Remote Sensing, Volume GE-20, p. 493-499.

Mansinha, L. and Mwenifumbo, C.J.
1983: A mise-à-la-masse survey at the Cavendish geophysical test site; Geophysics, v. 48, p. 1252-1257.

McMurry, H.V. and Hoagland, A.D.
1956: Three dimensional applied potential studies at Austinville, Virginia; Geological Society of America, Bulletin, v. 67, p. 683-696.

Mwenifumbo, C.J.
1985: Mise-à-la-masse mapping of gold-bearing alteration zones at the Hoyle Pond gold deposit, Timmins, Ontario; in Current Research, Part A, Geological Survey of Canada, Paper 85-1A, p. 669-679.

Parasnis, D.S.
1967: Three dimensional mise-à-la-masse surveys of an irregular lead-zinc-copper deposit in Central Sweden; Geophysical Prospecting, v. 15, no. 3, p. 407-437.

Shuey, R.T.
1975: Semiconducting ore minerals; Developments in Economic Geology, Volume 4, Amsterdam, Elsevier.

Sumner, J.S.
1981: The mise-à-la-masse induced polarization; Fifty-first Annual International Meeting and Exposition, Los Angeles, Society of Exploration Geophysicists, Technical Papers, Paper M3.2, p. 741-763.

Thurlow, J.G. and Swanson, E.A.
1981: Geology and ore deposits of the Buchans area, central Newfoundland; in The Buchans Orebodies: Fifty Years of Mining and Geology, E.A. Swanson et al., ed., Geological Association of Canada, Special Paper 22, p. 113-142.

Yang, F.W. and Ward, S.H.
1985: Single- and cross-borehole resistivity anomalies of thin ellipsoids and spheroids; Geophysics, v. 50, p. 637-655.

16. CROSSHOLE AUDIO-FREQUENCY SEISMOLOGY*

P. Hurley[1], J. Wong[1], and G.F. West[1]

Hurley, P., Wong, J., and West, G.F., Crosshole audio-frequency seismology; in Borehole Geophysics for Mining and Geotechnical Applications, ed. P.G. Killeen, Geological Survey of Canada, Paper 85-27, p. 159, 1986.

Abstract

A high resolution borehole to borehole seismic system has been developed at the University of Toronto for the detailed study of the mechanical properties of rock masses. In a method that is similar to the vibrator source techniques of surface reflection seismology, a low power continuous source is used, and the seismic impulse response estimated by cross-correlation of the received waveform with the transmitted one. Both the transmitting and receiving sondes utilize piezo-ceramic transducers, and were designed to operate in NQ size or larger holes, at depths of up to 1 km.

The system operates in the 1 to 6 kHz band, in part to achieve very high timing resolution. In the surveys that have been completed, compressional arrivals with a signal to noise ratio of better that 5:1 have been recorded along paths of 250 m through the intact granitic rock of the Lac Dubonnet batholith at Pinawa, Manitoba. Similar signals have also been detected on 100 m paths in Nepean sandstone at the Geological Survey of Canada calibration facility near Ottawa, Ontario. Shear waves are heavily attenuated in both of these rock masses, but have been detected on paths of up to 50 m in near surface granite, and are clear on short paths.

Information about both the velocity and the attenuation of the seismic waves in the rock mass can be extracted from the data. These parameters reflect the mechanical properties of the material penetrated, and can be strongly affected by lithology or by the presence of faults and fracture systems. By collecting these data from many different positions of the transmitter and receiver it is possible to construct a cross-sectional representation of the mechanical and geological information obtained in other ways in order to characterize the entire panel of rock between the holes.

Résumé

Un système de sondage sismique transversal à hautre résolution permettant d'étudier avec précision les propriétés mécaniques des masses rocheuses a été conçu à l'Université de Toronto. Comme dans le cas de l'étude de la sismique réflexion en surface qui utilise une source de vibration, une petite source d'énergie continue est utilisée et les impulsions sismiques provoquées sont estimées par la mise en corrélation de la forme d'onde reçue et de la forme d'onde émise. Les sondes émettrices et réceptrices comportent des transducteurs en piézo-céramique et ont été conçues de manière à être utilisées dans des trous de dimensions NQ ou supérieures, à des profondeurs allant jusqu'à 1 km.

Le système fonctionne dans la bande 1-6 kHz, notamment pour permettre d'obtenir une synchronisation très précise. Durant les levés qui ont été terminés, des ondes de compression dont le rapport signal-bruit était meilleur que 5/1 ont été enregistrées le long de parcours de 250 m dans la roche granitique non altérée, dans le batholithe du lac Dubonnet à Pinawa (Manitoba). Des signaux semblables ont également été captés le long de parcours de 100 m dans du grès de Nepea, à l'installation d'étalonnage que la Commission géologique du Canada a aménagée près d'Ottawa (Ontario). Les zones transversales sont très atténuées lorsqu'elles franchissent ces masses rocheuses, mais elles ont été captées le long de parcours allant jusqu'à 50 m dans du granite situé près de la surface et elles peuvent être détectées nettement dans de brefs parcours.

Les données prélevées renseignent sur la vitesse et l'atténuation des ondes sismiques qui se propagent dans la masse rocheuse. Ces paramètres traduisent les propriétés mécaniques de la matière sondée et ils peuvent varier considérablement selon la lithologie ou en raison de la présence de failles et de systèmes de fractures. La cueillette de ces données au fil des nombreux déplacements de l'émetteur et du récepteur permet de réaliser une vue en coupe des propriétés mécaniques de la roche entre les trous. Jointe aux renseignements géophysiques et géologiques obtenus d'autres façons, cette information permet de connaître les caractéristiques de tous les plans verticaux de la roche entre les trous.

* Manuscript not submitted

[1] University of Toronto, Toronto, Ontario

17. AN EXPERIMENT WITH THE SEISMIC CROSSHOLE METHOD IN AN IRON MINE

Matts Gustavsson, Hans Israelson, Sven Ivansson,
Per Morén and Jörgen Pihl[1]

Gustavsson, M., Israelson, H., Ivansson, S., Morén, P., and Pihl, J., An experiment with the seismic crosshole method in an iron mine; in Borehole Geophysics for Mining and Geotechnical Applications, ed. P.G. Killeen, Geological Survey of Canada, Paper 85-27, p. 161-166, 1986.

Abstract

Seismic techniques have so far been only sparsely employed by the mining industry for ore prospecting. There is, however, a growing interest in geophysical techniques for ore prospecting which allow depth penetration of 1 km or more. The known bodies usually dip very steeply and for direct mapping the standard seismic reflection method has probably to be modified substantially. This paper presents an experiment with the seismic crosshole method which can be used to map steeply dipping structures provided that suitable boreholes or galleries are available.

In this experiment an attempt was made to detect a steeply dipping magnetite orebody at the Research Mine in Kiruna, Sweden. Geophone recordings of some 50 microexplosions in slim boreholes were collected with recording distances up to about 175 m. A tomogram of the P-velocity across a vertical section of 50 x 165 m, intersecting the magnetite body, shows good agreement with geological and geophysical observations in the galleries of the mine as well as E-modulus determinations of drilled core samples.

Résumé

Jusqu'à présent, l'industrie minière s'est très peu servie des méthodes sismiques pour la prospection des minerais. Toutefois, on s'intéresse de plus en plus aux techniques géophysiques qui permettent de pénétrer un kilomètre ou plus dans le sol. En général, les masses minéralisées connues ont un pendage très raide et pour les cartographier, il faudrait probablement modifier considérablement la méthode classique de sismique-réflexion. La présente étude décrit une expérience qui utilise une méthode transversale, laquelle peut servir à cartographier des structures à pendage abrupt pourvu qu'il y ait des trous et des galeries appropriés.

Au cours de cette expérience, on a essayé de déceler la présence d'une masse de magnétite à pendage abrupt dans la Research Mine à Kiruna, en Suède. Quelque 50 micro-explosions ont été enregistrées dans des sondages étroits, les distances d'enregistrement atteignant près de 175 m. Un tomogramme de la vitesse de l'onde P en travers d'une section verticale de 50 m, par 165 m, qui coupe la masse de magnétite concorde bien avec les observations géologiques et géophysiques recueillies dans les galeries de la mine et avec les chiffres du module E déterminés pour les échantillons carottés.

Introduction

Seismic techniques have so far been only sparsely employed by the mining industry for ore prospecting. In the last few years, however, a growing attention has been drawn to the seismic reflection method which is the most powerful geophysical tool in terms of resolution and depth penetration for hydrocarbon exploration. At least in Sweden there is an increasing interest in geophysical techniques for ore prospecting which allow depth penetration of 1 km or more. Known bodies in Sweden, however, usually dip steeply and the standard seismic reflection method has probably to be modified substantially in order to perform well for such formations.

This paper describes an experiment with the seismic crosshole method which can be used for mapping steeply dipping structures provided that suitable boreholes or galleries are available. In short, the area between two boreholes are systematically scanned by seismic signals, which are generated by microexplosions in one hole and recorded by borehole geophones in the other hole. This method has previously been tried out in a crystalline rock body with two vertical holes separated by 625 m (Gustavsson et al., 1983). The application here describes an experiment to detect a slanting magnetite ore body in the Research Mine in Kiruna in Sweden.

[1] National Defence Research Institute, Box 27322, Stockholm, S-102 54 Sweden

Field experiment

The purpose of the experiment was to apply the crosshole method to a geological structure which is reasonably well known, and to test the principle of "reversed" crosshole measurements. In addition it provided an opportunity to gain experience at shorter distance ranges with a hole separation of about 165 m.

Figure 17.1 shows the setting in the Kiruna Research Mine for the experiment, which was performed between two vertical holes at a level of 320 m below the ground. The core-drilled holes are about 165 m apart and 50 m deep, and have a diameter of 56 mm. They are waterfilled and uncased. As can be seen in figure 17.1, they are on both sides of the magnetite ore body which takes the shape of a thin (20-25 m) sheet, dipping about 60 degrees towards the vertical line. There are also galleries almost along a line between the two holes and perpendicular to the magnetite sheet. These galleries run at the 320 and 370 m levels.

Microexplosions (10 g) were set off in the holes at various depths to generate seismic signals. The firing design allows very accurate timing of the instant of detonation. To minimize the effects on the borehole walls a centring device was utilized to keep the charge at the centre of the holes during detonation. Shooting was also avoided at places along the hole where the core logging indicated fractures.

The signals form microexplosions in hole R1 (Fig. 17.1) were recorded by a borehole geophone array with three elements separated by 10 m. This equipment has been described by Bergh et al. (1983). The elements of the array were locked at various depths in hole R2.

In addition recordings were obtained by 14 geophones along a line in the 320 m gallery between the two holes.

The spikes of the geophones in the gallery were wedged into handdrilled holes (diameter 8 mm and depth about 70 mm) on the walls of the gallery. Only one component, vertical or horizontal depending on the nature of the surface

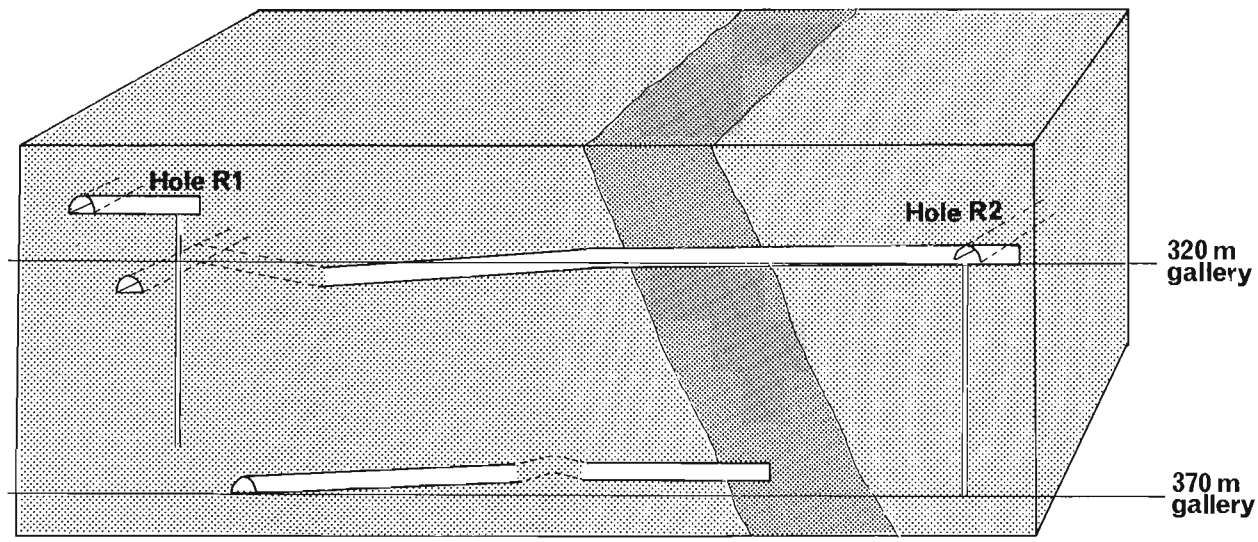

Figure 17.1. Schematic view of the area with seismic crosshole measurements at the Kiruna Research Mine. The two holes, R1 and R2, and the galleries at the 320 m and 370 m levels are marked and the steeply dipping magnetite body is indicated as a dark zone.

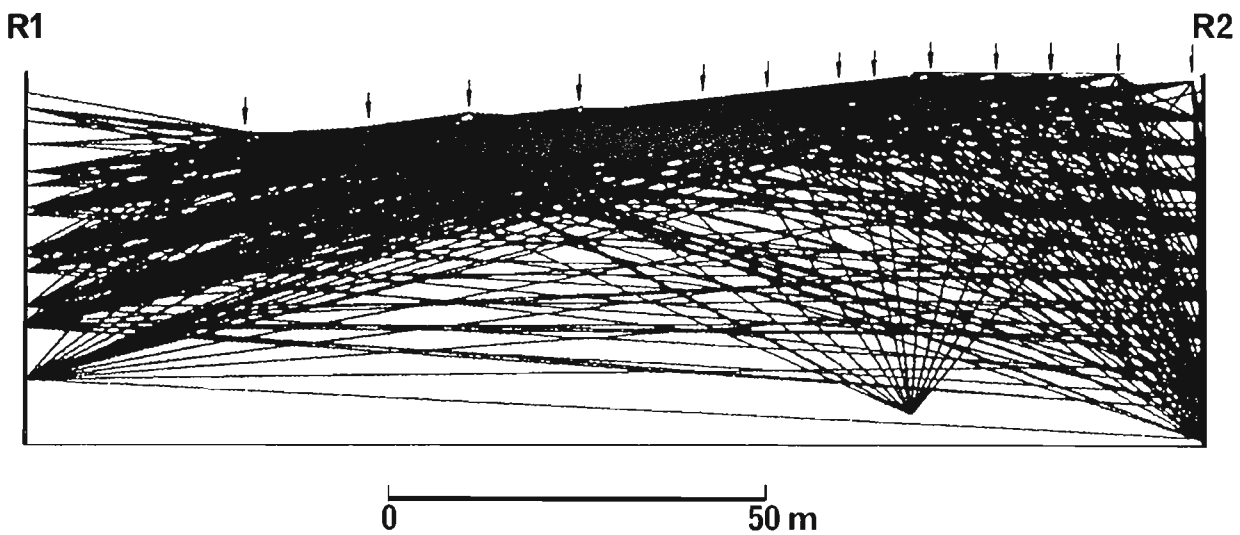

Figure 17.2. Raypath diagram linking positions of shot to geophones with straight lines. The arrows indicate the geophone positions in the 320 m gallery.

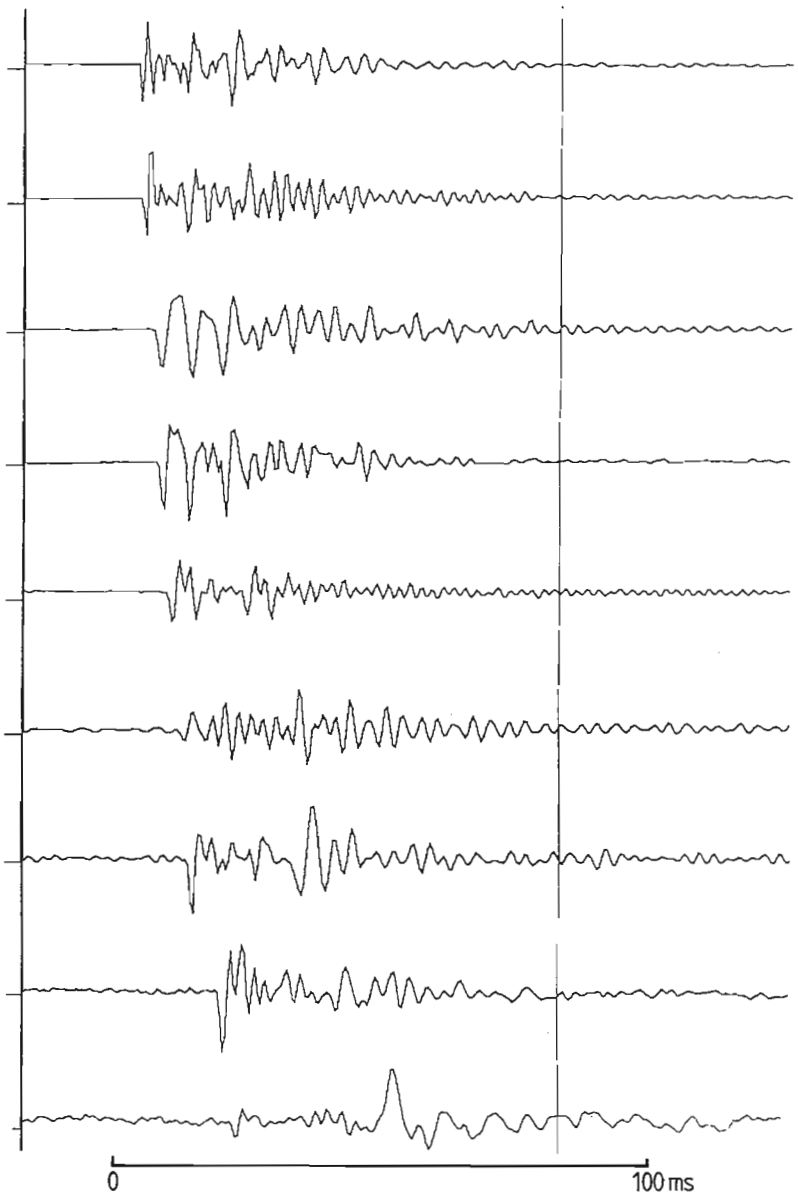

Figure 17.3a. Recordings at geophones in the gallery from an explosion in hole R1 and 14 m. The rock material for each geophone position is also indicated.

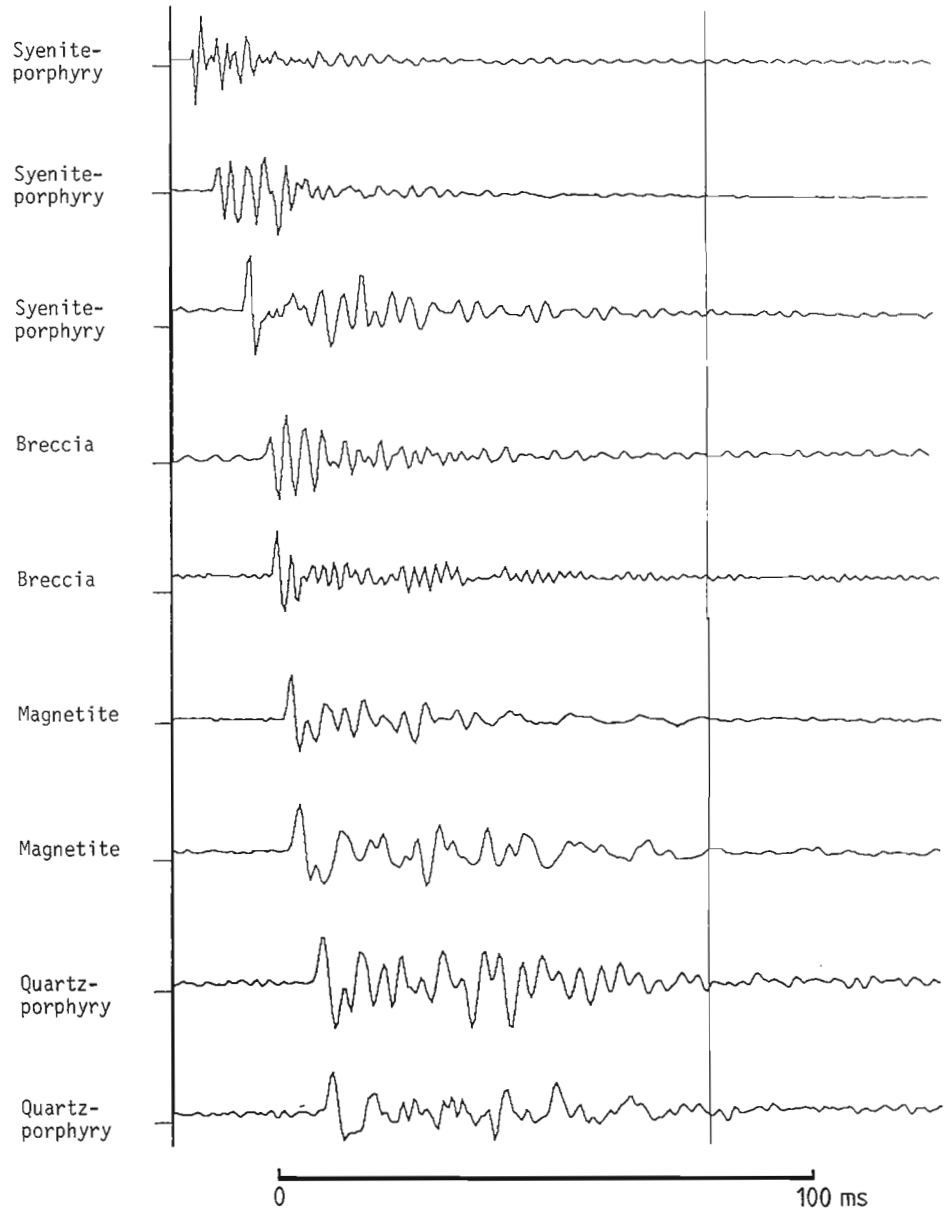

Figure 17.3b. Recordings at geophones in the gallery from an explosion in hole R2 at 44 m. The rock material for each geophone position is also indicated.

of the gallery wall, was used at each location. Figure 17.2 shows the raypath diagram linking positions of microexplosions and all gallery and borehole geophones by straight lines. The arrows indicate the geophone positions in the gallery.

Recordings were obtained from 50 explosions in all with 30 and 19 set off in holes R1 and R2 respectively. An additional explosion was set off in the gallery at the 370 m level (Fig. 17.1, 17.2). The array of borehole geophones was operated only for shots in hole R1. The shots in hole R2

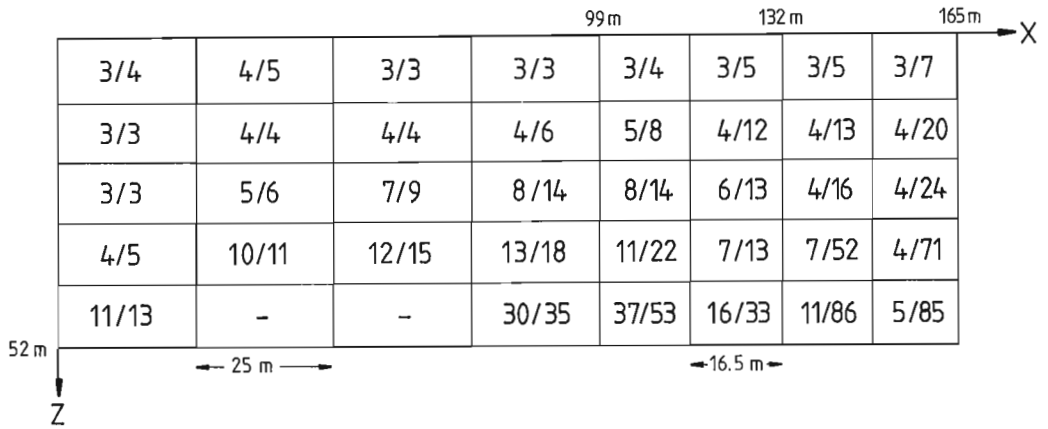

Figure 17.4. *Standard deviation of estimators in per cent of 0.2 s/km (equal to 5 km/s) for error standard deviation of 0.5 ms (assumed reading error of first arrivals). Numbers to the left of slash correspond to the case for all rays present, ie "reversed" shooting. Numbers to the right of slash correspond to the case with rays belonging to shots in hole R1 only. Note the large differences to the right in the cross section indicating the importance of "reversed" shooting.*

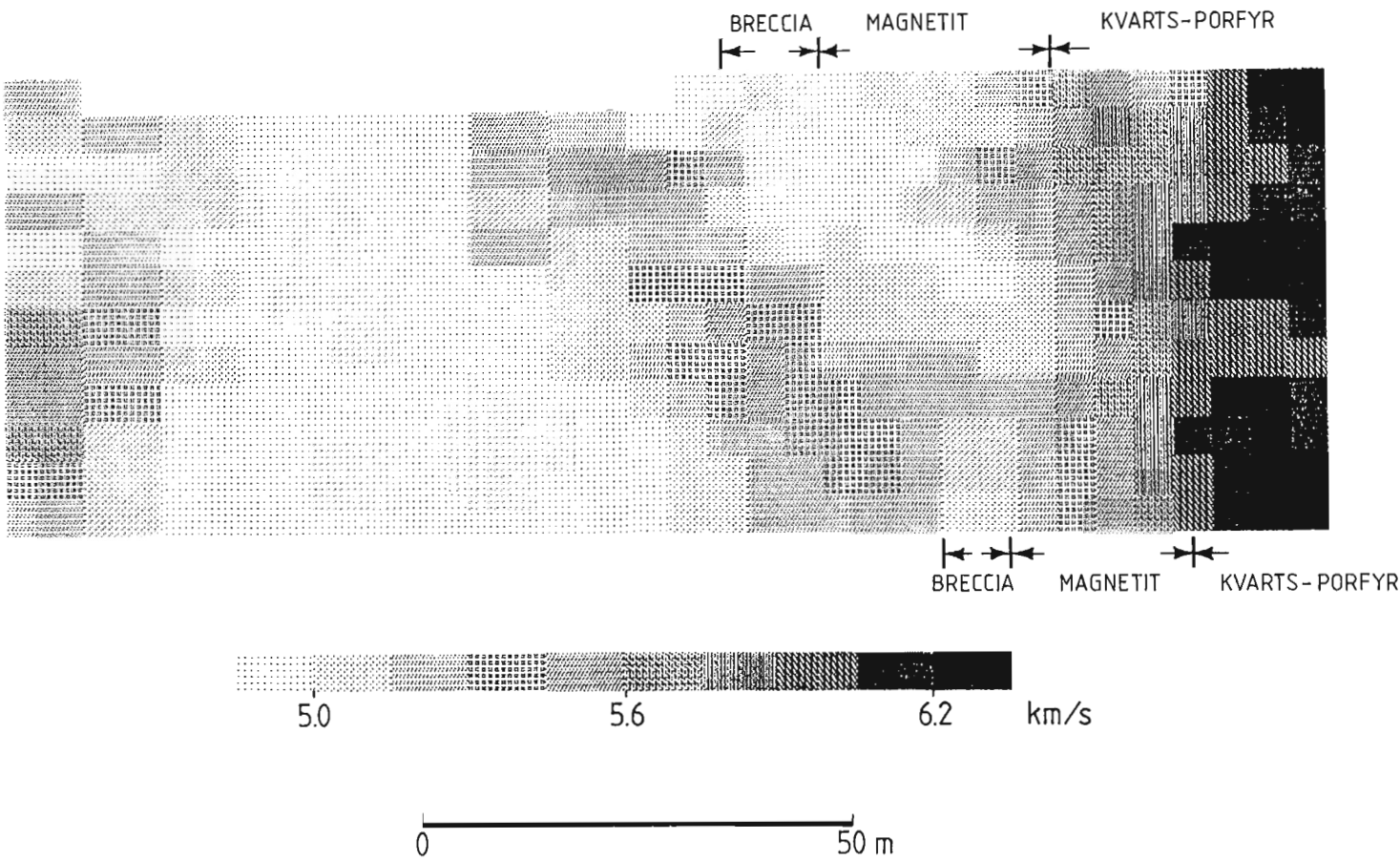

Figure 17.5. *Estimated velocity structure from travel times of first arrivals by a least squares procedure solution. The boundaries of the geological structures in the two galleries are also indicated.*

"reverses" the crosshole procedure with the additional ray paths to the geophones along the horizontal gallery and this improves the confidence of velocity estimates across the section.

The signals were recorded at a sampling rate of 2 kHz (25 channels) and with lowpass prefiltering at 0.5 kHz.

Figure 17.3 shows typical examples of recorded traces at some of the geophones in the gallery for explosions in holes R1 and R2. The initial onset of the P-wave is usually very clear and S waves can also be seen on some of the records primarily due to their dominantly low periods. Particularly interesting to note is the low frequency content of the P-waves recorded in the gallery where the magnetite body crosses. This can be seen in both examples in Figure 17.3.

Tomographic velocity mapping

Owing to the clear nature of the first arrivals of the recorded signals it was considered sufficient for a preliminary analysis to measure the arrival times from computer plottings with a high magnification. The reading error is estimated to be less than 0.5 ms. The arrival times (about 500) were used for a tomographic mapping according to procedures described by Ivansson (1983). Since all shots and geophones are not situated in the same plane the cross section is rather the projection of the positions of the shot points and geophones onto a plane. The cross section is divided into a number of cells and it is assumed that the veolcity is constant within each cell and that a ray propagates along a straight line between source and receiver.

The confidence of the estimated velocities in each cell can be specified and varies across the section due to the non uniform coverage of rays. The "reversed" shooting applied in this experiment significantly improves the results as is illustrated by Figure 17.4. If the division into cells of the cross section is carried too far stable unique velocity estimates will no longer be obtained unless additional assumptions are made. It is for example not unduly difficult to add to the equations based on the measured traveltimes the condition that nearby cells should have equal velocities. This will make it possible to obtain smoothed estimates with a fairly high resolution as shown in Figure 17.5. The cross section in Figure 17.5 is based on about 500 rays and the cells in the right and left half of the section are 5 x 5 m and 10 x 5 m respectively. The gross features are in full agreement with an unconstrained solution for a more coarse cell division, for which the changes from high to low velocities across the hanging wall are statistically significant. The boundaries of the magnetite and breccia as observed in the galleries at the 320 and 370 m levels are marked in the figure, and agree with the sharp velocity contrasts of the tomogram.

Table 17.1. P-velocities (km/s) computed from E-moduli and densities of core samples

	Magnetite	Quartz-porphyry	Breccia
Maximum	4.4	5.4	4.5
Minimum	3.9	4.5	3.6
Dynamic parameters	3.6	6.0	-

It is also interesting to note the increase in the velocity along a slanted structure as one proceeds towards the left in the section around the breccia zone.

In the picture there also occurs a large low velocity area within the syenite-porphyry boundary which is statistically significant. However, no other geological or geophysical investigations have been done in this part of the cross section that can confirm this variation.

The in situ P-velocities shown in Figure 17.5 can be compared with values computed from E-modules and densities obtained from measurements of core samples in the mine. These values (Table 17.1) show qualitative agreement with the data in Figure 17.5. In both cases the high and low velocities for quartz-porphyry and magnetite respectively are very pronounced. No values from the syenite-porphyry are available.

Concluding remarks

The results of the experiment with the seismic crosshole method in the Research Mine in Kiruna can be summarized as follows in relation to the objectives of the test:

- the tomographic mapping of P-velocities broadly agrees with other geological and geophysical observations of the structural properties in the mine
- the "reversed" crosshole principle improves significantly upon the confidence of estimated velocity structures
- the crosshole techniques with microexplosions and borehole geophones originally conceived for mapping crystalline rock volumes of a large dimension (0.5-1 km) could be applied with encouraging results at much shorter (100-200 m) distances.

Finally it can be noted that the inverted velocity structure is based only on first arrival time data. The recorded signals, however, indicate that their actual shapes indeed carry information about the geophysical properties of the structure as clearly illustrated by the change in dominant period of recordings across the gallery. This change in frequency content can be compared with the synthetic computational experiments by Bold and Smith (1976). Interpretation of such features may in the future improve the quality of the structural inversion procedure.

Better resolution of the magnetite target geometrically and also in terms of the true velocity would have been obtained if more shots could have been used in the 370 m gallery with recordings for each shot taken in both boreholes and on the 320 m gallery.

Acknowledgments

This experiment was sponsored by the Swedish Nuclear Fuel Supply Co (SKBF). Discussions during the planning and formulation of problems with the project manager Hans Carlsson at SKBF are much appreciated.

The microexplosions were carried out by Staffan Berglund and Rune Hank at the Division of Underwater Detonations of the Swedish National Defence Research Institute.

We would like to thank the staff at the Kiruna Research Mine for the preparation of the boreholes, and making available density and E-module determinations of drilled holes, and helping with practical matters during the experiments.

References

Bergh, S., Ekström, U., Gustavsson, M., Israelson, H., Morén, P. and Pihl, J.
1983: A vertical borehole geophone array; Geophysics, v. 48, no. 11, p. 1558-1559.

Bolt, B. and Smith, W.
1976: Short note on finite-element computation of seismic anomalies for bodies of arbitary shape; Geophysics, v. 41, no. 1, p. 145-151.

Gustavsson, M., Israelson, H., Ivansson, S., Morén, P. and Pihl, J.
1983: The seismic crosshole method in crystalline rock. Extended abstract in; Technical Program for 52nd meeting of Society of Exploration Geophysicsists, p. 471-472.

Ivansson, S.
1983: Tomographic velocity estimation for crosshole measurements; National Defence Research Institute, Stockholm, Report C20494-E1.

18. TOMOGRAPHIC MODELLING USED FOR CROSSHOLE DATA ANALYSIS

Sven Ivansson[1]

Ivansson, S., Tomographic modelling used for crosshole data analysis; in Borehole Geophysics for Mining and Geotechnical Applications, ed. P.G. Killeen, Geological Survey of Canada, Paper 85-27, p. 167-171, 1986.

Abstract

Seismic crosshole techniques for detection of fracture zones in crystalline rock bodies with a dimension of 0.5-1 km are being developed in Sweden. Seismic signals are thereby generated in one hole by microexplosions while recording is made in the other hole and on the surface.

As a first step in the analysis of the registrations from such a crosshole experiment, a tomographic approach for estimation of the seismic P-velocity distribution in the crosshole area has been used. Approximating the ray paths by straight lines one gets a linear equation system for the velocities. However, the solution obtained in this way cannot automatically be taken as a truthful picture of the crosshole area. This is due to the impact of certain sources of error: the uncertainty in traveltime measurements and the "straight ray path" approximation. These matters are discussed in connection with results from a field experiment.

Using a simple "trial and error" method of comparison with synthetics it is shown that a reasonable velocity map of the crosshole area can in fact be obtained, although the standard tomographic solution has several peculiarities.

Résumé

Des chercheurs suédois mettent au point présentement des méthodes sismiques transversales afin de pouvoir déceler les zones de fractures dans les masses cristallines dont la dimension varie de 0,5 à 1 km. Les signaux sismiques sont produits en déclenchant des micro-explosions dans un trou; l'enregistrement se fait dans un autre trou et à la surface.

La première étape de l'analyse des enregistrements provenant d'une telle expérience consiste à estimer, à l'aide d'un tomographe, la répartition de la vitesse des ondes P dans la zone étudiée. La représentation du parcours des ondes par des lignes droites donne un système d'équations linéaires pour les vitesses. Toutefois, la réponse obtenue ne donne pas automatiquement une image réelle de la zone examinée étant donné l'importance de certaines sources d'erreur, notamment l'incertitude des mesures du temps de parcours et l'approximation en ligne droite du trajet de l'onde. Ces questions sont examinées en tenant compte des résultats d'une expérience effectuée sur le terrain.

En procédant simplement par approximations successives avec des produits synthétiques, on a découvert qu'il est possible d'obtenir une carte plus ou moins raisonnable des vitesses dans la zone étudiée, bien que la solution tomographique ordinaire présente plusieurs particularités.

Introduction

Our aim is to discuss the problem of estimating the distribution of P-velocity for seismic waves in a crosshole section using measured first-arrival travel-times for explosion-generated waves. A tomographic approach has been used. The crosshole area is thereby divided into a number of rectangular cells, in each of which the P-velocity is assumed constant (Fig. 18.1). The ray paths, one for each shot/receiver-pair, are assumed to be straight (though this is only approximately true, see below). From the experimental registrations only the measured first-arrival travel-times are used.

Least-squares machinery

For simplicity we assume that the errors in the travel-time measurements are normally distributed with mean zero. In the tomographic approach described above one then directly arrives at a standard linear statistical model with the cell-velocities as unknown parameters (Aki and Richards, 1980). According to the Gauss-Markov theorem the least-squares method furnishes minimum-variance unbiased estimators for the cell-velocities. A computer program for convenient solution for the least-squares tomographic equations has been constructed and was used for the computation of forthcoming results.

[1] Division of Applied Seismology, National Defence Research Institute, Box 27322, S-102 54 Stockholm

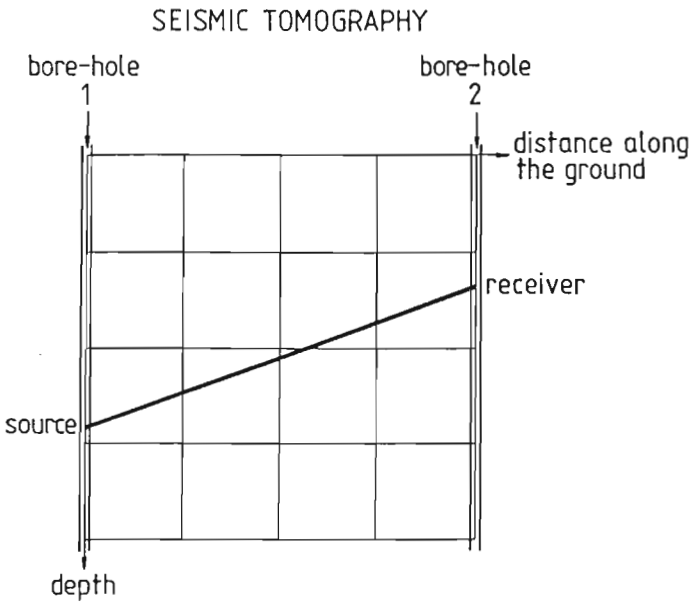

Figure 18.1. Seismic crosshole-section with cell-decomposition and an example of a ray path.

With a sparse coverage of ray paths within the crosshole area it is possible that unbiased estimators of certain cell-velocities simply do not exist. This is particularly true if no ground-geophones are present but only borehole geophones are used. (We assume here, of course, that the area is divided into at least two columns of cells.) In such a case no cell-velocity will have an unbiased estimator since it will be impossible to discover differences in velocity between different columns. The importance of having a dense coverage with geophones on the surface is thus apparent.

It is also important to note that the effect of the errors in the travel-time measurements will be more severe on certain cell-velocity estimators than on others. By the Gauss-Markov theorem one also gets standard deviations of the estimators. An example is shown in Figure 18.2 for a crosshole area of 625 x 625 m using 200 rays. (The corresponding ray-path diagram is easily visualized by connecting all the "S" to all the "R" in the figure.) Unbiased estimators do not exist for the velocities of the four shaded cells.

In advance of a planned field experiment it is therefore important to make an analysis in order to assess the statistical uncertainty of the obtainable estimators. This will help in determining the required number and location of shots and geophones for a reasonable cell-decomposition.

CONFIDENCE

	R	R	R	R	R	R	R	R	R	R	
S	1	1	3	5	6	6	6	6	6	4	R
S	1	2	4	6	7	7	8	8	8	6	R
S	1	2	5	7	8	9	10	11	10	8	R
S	1	2	6	10	10	11	14	14	13	10	R
S	1	3	8	13	12	13	18	17	15	12	R
S	1	4	11	18	16	17	22	20	17	14	R
S	1	5	15	24	21	22	28	23	18	15	R
S	1	7	19	31	27	28	34	28	20	17	R
S	2	11	25	38	33	36	42	34	23	20	R
S	3	19	39					40	35	26	R

62.5 m

S = source R = receiver

Figure 18.2. Standard deviation of estimators in per cent of 5000 m/s at a true velocity of 5000 m/s if the error standard deviation of the travel-time measurements is 0.5 ms.

Kråkemåla tomographic velocity map

A crosshole field experiment was performed at Kråkemåla in southern Sweden in late 1981. The two holes used were 450 m deep and 625 m apart. About 150 explosions were set off in one of the boreholes and registrations were collected at 24 geophones on the surface and 3 movable geophones in the opposite borehole (Fig. 18.3). In all P-wave travel-times were measured for 1583 rays. The errors in these measurements were not believed to exceed 0.5 ms by very much.

In Figure 18.4 the expected influence of statistical errors is shown. Due to the described shot/receiver-geometry the errors are small in the upper left corner whereas they are greater downwards in the middle and to the right. All velocities have unbiased estimators in this decomposition into 88 cells.

The obtained tomographic velocity-map (cells with anomalous velocity are shaded) is shown in Figure 18.5 and the following observations are made:

(1) The velocities in the leftmost column and in the upper left corner seem very reasonable. They increase with depth and are of expected magnitude. Note also that the influence of statistical errors is here very small.
(2) The sixth and seventh columns from the left are pronounced low-velocity columns. It is also to be noted that a marshy area is present at the surface of the seventh column. That this column is headed by a cell of low velocity (4.7 km/s) therefore seems quite reasonable.
(3) Some of the velocities in the cells to the right of the seventh column seem anomalously high. Such high velocities have never been observed so close to the surface and they cannot be explained by the statistical errors as is seen in Figure 18.4.
(4) At the bottom of the third and fourth columns the calculated velocity estimates indicate that cells of extremely high velocity occur just next to cells of quite low velocity. We note again (Fig. 18.4) that the statistical errors cannot be responsible.

It is apparent that Figure 18.5 cannot be believed to be a truthful velocity map of the crosshole area. The reason for the misbehaviour is the straight-path assumption used in the tomographic procedure and the discretization errors that ensue when the velocity is forced to be constant throughout each cell.

Paying attention to ray-bending

To be able to take ray-bending effects into consideration it is first necessary to know how to solve the direct problem, that is given a velocity-distribution for a crosshole area one must be able to calculate the "minimum" (ray paths and corresponding) travel-times. This can be done conveniently by using numerical solution of a boundary problem for the Euler equation of a "stationary ray" by e.g. the "shooting method", though required computer time will not be negligible. In doing this one usually uses a smoothed velocity-distribution with continuous velocity and first spatial velocity derivatives. We have used two-dimensional polynomials to interpolate between given values at the midpoints of the usual rectangular cells.

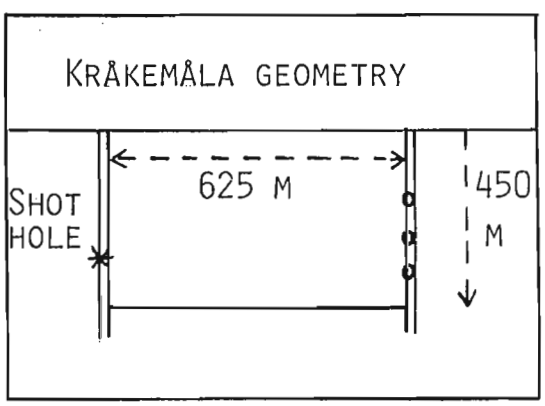

Figure 18.3. Sketch of crosshole experiment at Kråkemåla. Explosions were set off in left borehole.

horizontal distance

0.5	0.4	0.5	0.6	1.7	2.0	1.3	2.2	1.5	0.8	1.2
0.4	0.5	0.9	1.0	1.9	2.1	1.7	3.0	3.1	2.8	2.1
0.4	0.6	1.2	1.6	2.5	3.1	2.9	4.5	4.3	3.9	2.8
0.6	0.9	2.0	2.4	3.0	3.8	3.9	5.3	5.1	4.8	3.5
0.6	1.4	2.8	3.3	3.8	4.5	4.5	5.8	5.8	5.7	4.2
0.7	2.1	4.6	4.4	4.5	5.0	5.0	6.3	6.2	6.2	4.7
0.8	3.7	6.9	5.9	5.8	6.2	6.0	7.1	6.7	6.6	5.3
1.2	5.0	8.3	8.0	8.6	11.3	11.3	10.4	9.0	7.5	5.8

depth

Figure 18.4. Relative statistical errors, for Kråkemåla; the numbers are estimator-standard deviations, in per cent of the velocity 5000 m/s at a true velocity of 5000 m/s and an error in traveltime-measurements of 0.5 ms.

shot hole

horizontal distance

54	53	50	51	54	50	47	60	54	55	60
53	55	51	50	57	50	48	58	51	61	64
54	57	50	50	57	47	48	58	51	66	69
53	57	53	51	58	46	48	60	52	66	81
55	59	51	50	61	46	47	60	51	63	81
56	64	64	46	59	47	47	63	53	74	76
56	61	79	44	61	48	50	66	56	72	78
58	53	84	43	61	48	50	63	57	74	78

depth

Figure 18.5. Velocity solution, for Kråkemåla; cell-velocities in hectometre/second.

Iterative procedures for taking account of ray-bending have been proposed by Bois et al. (1971). The natural idea used by them is to solve a new tomographic equation-system in each iteration step. Essential features of each iteration are:

(1) Given the current velocity-distribution from the last iteration, the direct problem is solved. That is, the corresponding ray paths are calculated. These calculations are in principle performed as described above.
(2) Given the new ray paths it is then possible to write down a new "tomographic linear equation system" with the velocities at the centre of the cells as unknowns (the spatial velocity-distribution is still considered to be polynomial). The other side of the system is unchanged, it consists of the measured travel-times. Solution of the equation system now yields a new velocity distribution to be used in the next iteration.

This method has however not given any useful further information concerning the Kråkamåla case. In fact, synthetic calculations with the Kråkemåla geometry showed that the method only worked well when a reasonably accurate start-solution could be given. The solution obtained in Figure 18.5 is by no means very accurate.

Because of this a different but much simpler idea has been used to take ray-bending effects, and in fact discretization errors as well, into account.

The approach is as follows. We already have a kind of "filter" with which we can transform traveltime data into a "picture" in the velocity domain, viz. the tomographic least-squares procedure with no consideration of ray-bending. However, in the presence of velocity-heterogeneities the "picture" will become distorted. Now, instead of trying to design a "filter" giving the true velocity distribution, we try to learn how the distortions by our present filter behave. This will enable us to discover features of the real velocity-distribution by looking at the distorted picture.

Let us look at two examples. The Kråkemåla shot/receiver geometry is still used. To the left in Figures 18.6 and 18.7 is the synthetic velocity-distribution and to the right is the obtained velocity-map after calculating the corresponding synthetic travel-times and passing them through our filter. Cells with significant distortions are shaded, heavily and weakly for unrealistically high and low values respectively.

We note that in Figure 18.6 the distortions are quite small and the actual velocity-distribution is recovered rather accurately. The reason is of course that since almost all the ray paths are approximately horizontal, the rays which pass the low-velocity column must do so anyway, and cannot gain much time by choosing curved (or in this case rather: piecewise linear) paths.

In Figure 18.7, however, the distortions are quite severe.

Compare now with the tomographic map obtained from the experimental Kråkemåla data shown in Figure 18.5!

We must draw the conclusion that the "low-velocity columns" in the middle (slightly to the right) in Figure 18.5 are in fact not "real columns", rather the low-velocity zone is limited to the top of the region in question! (With the low-velocity zone reaching right to the bottom, the severe distortions in the right-hand side of the area would not have occurred).

By making more synthetic calculations of the same kind as in Figures 18.6 and 18.7 one arrives at the following interpretation of the experimental Kråkemåla data:

(1) The extreme velocities in Figure 18.5 are indeed not unusual. Instead they are quite normal expressions of the fact that ray-bending effects and discretization errors play a decisive role.
(2) The major part of the distortions are explained by introducing a low-velocity zone, size about 100 m (width) x 150 m (depth), at the top of the sixth and seventh columns with a velocity of about 4000 m/s.
(3) Apart from this there are also indications of two other low-velocity zones at the top, one to the left and one to the right. However, these are smaller and the interpretation is much more uncertain.

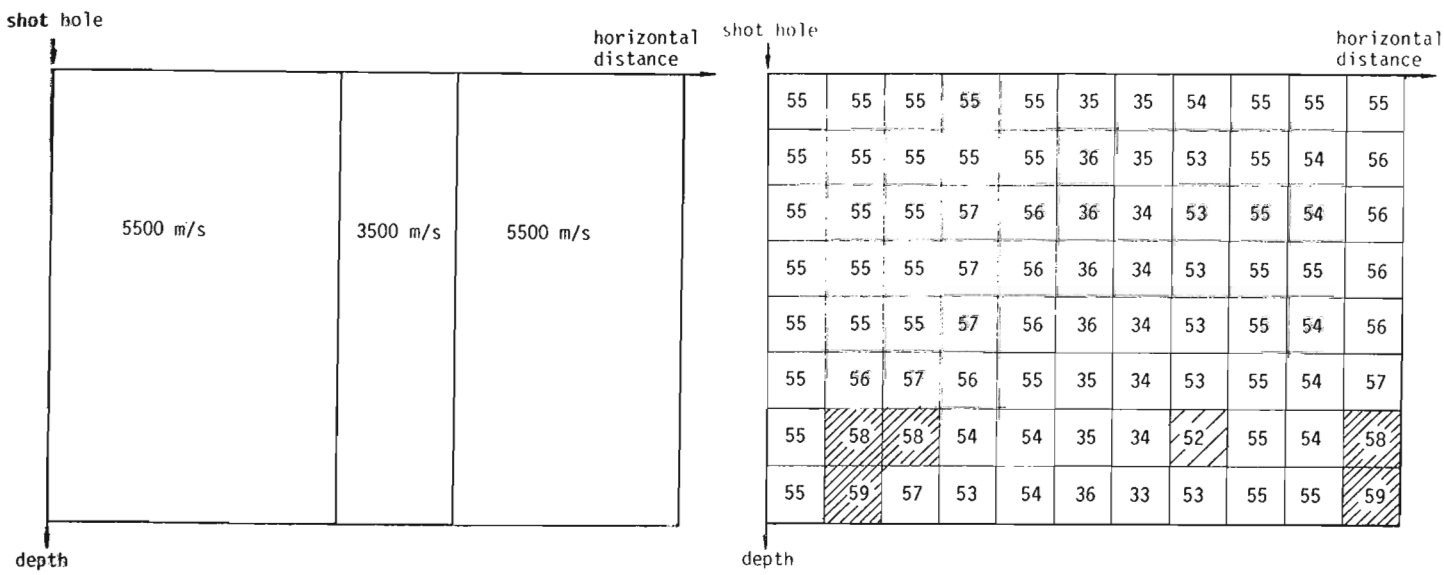

Figure 18.6. Synthetic velocity-model with a low-velocity column. Tomographic velocity-solution in hectometre/second with travel-times calculated for the model to the left. See text for detail.

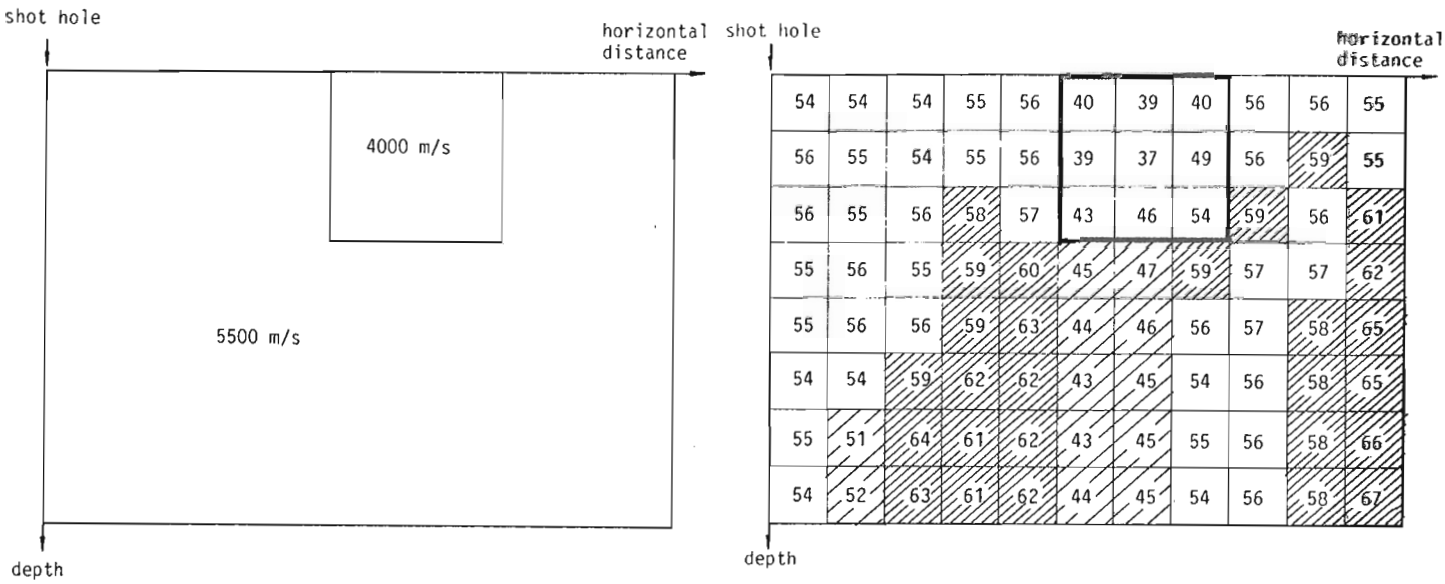

Figure 18.7. *Synthetic velocity-model with a low-velocity region. Tomographic velocity solution in hectometre/second with travel-time calculated for the model to the left. See text for detail.*

(4) An overall increase of velocity with depth is also manifested in the results. Due to the significant distortions it is however difficult to make precise statements.
(5) The velocities in an upper triangular region to the left, beginning at the shothole, are quite reliable and not seriously affected by either distortions or statistical errors.

Concluding remarks

Generally speaking the standard tomographic method is expected to be a good, reliable tool for detecting and studying crosshole structures where the velocity is only smoothly varying. It is also possible to allow sharp discontinuities if they cut through the whole area in a direction almost perpendicular to most of the ray paths.

When it comes to areas with pronounced but less favourable shaped inhomogeneities, the interpretation becomes less definitive. One, however, can detect that inhomogeneities are present and it is possible to give a rough determination of location, spatial size and velocity jump of at least the larger inhomogeneities.

Acknowledgments

The author is a member of the exploration group of the Division of Applied Seismology at the National Defence Research Institute of Sweden. This group is headed by Hans Israelson and other members are Matts Gustavsson, Per Morén and Jörgen Pihl.

Financial support was given by the Swedish Nuclear Fuel Supply Co.

References

Aki, K. and Richards
1980: Quantitative Seismology: Theory and Methods, Freeman, Chapter 12.3.

Bois, P., La Porte, M., Lavergne, M. and Thomas, G.
1971: Essai de détermination automatiques des vitesses sismiques par mesures entre puits; Geophysical Prospecting, v. 19, p. 42-83.

19. A SEISMIC TRANSMISSION TOMOGRAPHY TECHNIQUE FOR ROCK QUALITY EVALUATION

B.M. New[1]

New, B.M., A seismic transmission tomography technique for rock quality evaluation; in Borehole Geophysics for Mining and Geotechnical Applications, ed. P.G. Killeen, Geological Survey of Canada, Paper 85-27, p. 173-180, 1986.

Abstract

A simple technique for processing seismic data has been developed that provides a 'representative velocity' tomogram which may be interpreted in terms of the engineering properties of the subject rock mass. This transmission system is intended for use in cross-borehole surveys and has been successfully tested between subparallel mine roadways in a massive granite body.

The velocities of compressional waves between numerous source and transducer locations are analyzed and the interactive character of the observations is used to build a two-dimensional array of computed 'representative velocities' appropriate to specific areas within the intervening rock mass. Evaluation of the processed data is undertaken using site specific and more general rock mass classification systems.

The processing was carried out on a microcomputer and the program is readily adaptable to most field configurations. The program also allows various mapping and influence parameters to be varied and optimized to obtain the best resolution of rock mass inhomogeneities. The field data acquisition and processing techniques have been tested in a mine and the maps derived from the seismic data correlate well with the observable rock mass properties.

Résumé

Une méthode simple a été mise au point pour le traitement des données sismiques; cette technique fournit un tomogramme de la vitesse représentative qui peut être interprétée en termes des propriétés techniques de la masse rocheuse étudiée. Ce système de transmission, qui sera utilisé pour les levés transversaux, a été essayé avec succès dans les galeries subparallèles creusées dans un granite massif.

On a analysé les vitesses des ondes de compression se déplaçant entre de nombreuses sources et de nombreux transducteurs et, en tenant compte de la nature interactive des observations, on a établi un réseau à deux dimensions des vitesses représentatives calculées qui est propre à certaines parties de la masse rocheuse. Les données traitées sont évaluées en utillisant des systèmes de classification de la masse rocheuse particulières à l'emplacement et d'autres plus généraux.

Le traitement est effectué à l'aide d'un micro-ordinateur et le programme peut être facilement adapté à la plupart des configurations sur le terrain. Ce programme permet également de modifier et d'optimiser divers paramètres de cartographie et d'influence de façon à obtenir la meilleure résolution des hétérogénéités de la masse rocheuse. Les méthodes d'acquisition et de traitement des données recueillies sur le terrain ont été mises à l'essai dans une mine et une bonne corrélation a été établie entre les cartes produites à partir des données sismiques et les propriétés observées de la masse rocheuse.

Introduction

As part of the United Kingdom's radioactive waste management research programme the Ground Engineering Division of the Transport and Road Research Laboratory has carried out a short program of seismic velocity measurements at an experimental excavation in a massive crystalline rock mass at Carwynnan, Cornwall. This work was in collaboration with the Building Research Establishment who are using this site for testing a variety of techniques for subsurface site investigation. A pre-knowledge of rock conditions is vital to all aspects of underground construction and seismic methods provide a means of investigating large volumes of rock without the expense and undesirable penetration of the rock mass by frequent exploratory boreholes although some information obtained by direct access will still be required.

The objective of the seismic measurements was to map a specific section of the granite in terms of compressional wave velocity for comparison with other geotechnical properties determined using statistical techniques for rock structure assessment (Hudson and Priest, 1979; Lapointe and Hudson, 1985). The relationship between the seismic mapping and engineering rock mass classifications is also considered.

[1] Department of the Environment/Department of Transport, Old Wokingham Road, Crowthorne, Berkshire RG11 6AU

Resource considerations required that emphasis was placed on making straight-forward measurements and data processing was carried out using a simple tomographic algorithm. Although, in this case, access to the rock mass was provided by mine headings the technique used is equally applicable to interborehole measurements.

Field measurements

The experimental site is situated toward the northwestern margin of the Carmenellis Granite. This granite boss is one of several associated with the Cornubian batholith and is predominantly a coarse grained biotite-muscovite granite with potassium-feldspar phenocrysts. The rock is generally very strong and is faintly weathered. A predominant subvertical joint set, striking approximately 120° to grid north with a spacing usually greater than 1 m, is present throughout the area of the tests.

The procedure used was to locate a seismic source at a number of fixed 'reference positions' in turn and measure the time taken for the initial compressional pulse to reach each of the remaining reference positions. Thus 'forward' and 'reversed' calculations of compressional wave velocity were available between all reference points.

Twenty reference points were fixed along three sides of a rectangular section of rock some 900 m^2 in area. This horizontal section of rock is situated at a depth of about 30 m and the three headings may be considered as providing a geometrically similar configuration to two parallel boreholes with surface access to rock head between boreholes. A map of the test area is given in Figure 19.1 and the transmitting and receiving reference locations are indicated by the numbers 0 to 19. The reference points are spaced at approximately 5 m intervals around the section with two locations (5 and 6) in a short heading which penetrates the rectangular area. It was originally intended to use proprietary signal enhancement hammer seismographs to gain the data. However, laboratory trials revealed that both makes of equipment tested had inadequate frequency response to cope with the high frequency arrivals associated with hammer induced wave motions in the granite. It must be remembered that these instruments are designed mainly for seismic refraction work where the geophones are located on soils of low characteristic velocity and frequency (<200 Hz).

Although rock in general is not considered to exhibit compressional wave velocity variation with frequency changes, the waveform may change significantly in character with propogation due to frequency selective attenuation. Also the apparent dispersive effects of bounded and jointed media combined with wave packets comprising body waves of differing characteristic velocities causes material change in the duration of the wave packet and its component motions. It is therefore vital that the initial compressional wave motions are accurately identified through the adequate response characteristics of the instrumentation.

Further, it was not considered adequate to use the closure of inertial contacts on the hammer source to identify the initiation of the wave packet. The actual initiation moment was established by a geophone fixed about 1 m from the hammer impact point. This arrangement has the advantage that the time difference between observed arrivals at each geophone may be referenced to a similar point at the beginning of the wave packet at both near and remote geophones. Analysis of the data suggested that pathlength did not significantly influence the results at this site. The individual transit times between several adjacent locations were summed and found to be similar to the transit time

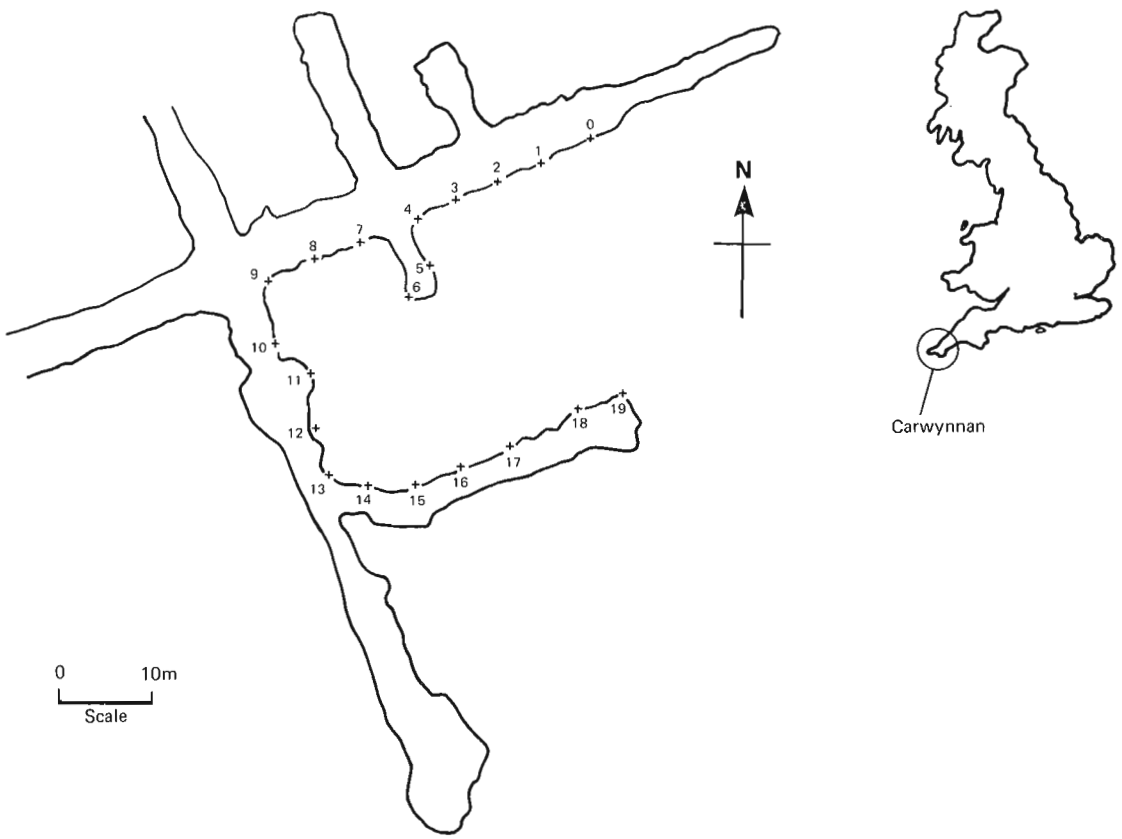

Figure 19.1. *Reference positions in test mine.*

between first and last locations of the linear sequence. The low pass filter characteristics of the rock mass had not materially influenced the observed rise time of the seismograms between 'near' and 'remote' positions.

The first arrivals from the geophones were captured and displayed on a dual beam digital storage oscilloscope and hard copy of the seismograms was taken for subsequent examination (Fig. 19.2). Inspection of the compressional waves from a preliminary hammer blow allowed the gain setting for each oscilloscope beam to be optimized and observation of two or three further blows provided a value for the difference in arrival times between the geophones. The variation in travel time between blows was generally less than 2% of the total travel time. Travel times between reference points varied between 0.8 ms and 7 ms and the standard deviation of the differences between forward and reversed paths was 60 μs.

The axes of sensitivity of the geophones were aligned toward the source to maximize sensitivity to compressional wave arrivals and where possible the direction of hammer impact was also arranged to stimulate compressional wavefronts in the direction of the remote geophone. The possibility of varying the direction and weight of the hammer blow was most useful when wave packets did not show the first arrivals clearly. The geophones were rigidly bolted to the rock and the reference positions surveyed to an accuracy of ± 0.5 cm.

The field data therefore comprised a series of grid references fixing each source/receiver position and a listing of point to point compressional wave timings.

A large intact fresh sample of the rock was taken for the laboratory determination of compressional wave velocity at ultrasonic frequency (54 kHz). This provided a basis for comparison with in situ wave velocity. The velocity was measured in seven directions through the sample and the mean velocity found to be 5540 m/s. The results did not indicate any significant velocity anisotropy. Ideally the testing of samples in this way should be carried out with the specimen confined at stresses similar to those imposed in the field. However, for strong rock samples free from discontinuities influencing stiffness these effects are small compared to those of the joints and other major mechanical discontinuities present in the rock mass as a whole (New and West, 1982).

Data processing

Initially it had been intended merely to measure the compressional wave velocity between adjacent reference points around the section of rock to be investigated. This would have provided a single velocity for comparison with observed conditions over a heading wall section about 5 m long. However it quickly became apparent that having mobilized a suitably equipped field team it was easy to provide considerably more information by measuring the velocity between each point and every other point. This provided velocities dependent on the interior of the rock mass and owing to the relatively large numbers of paths through the rock the considerable redundancy within the data could be utilized.

Techniques of tomographic reconstruction (literally, the drawing of a section) have been widely investigated particularly by the medical sciences. The processes often depend on the losses at sub-micron wavelengths of electromagnetic radiation during passage through a material of varying dielectric properties; they provide an image of electromagnetic opacity. The tomographic algorithms developed are potentially useful in processing both variations

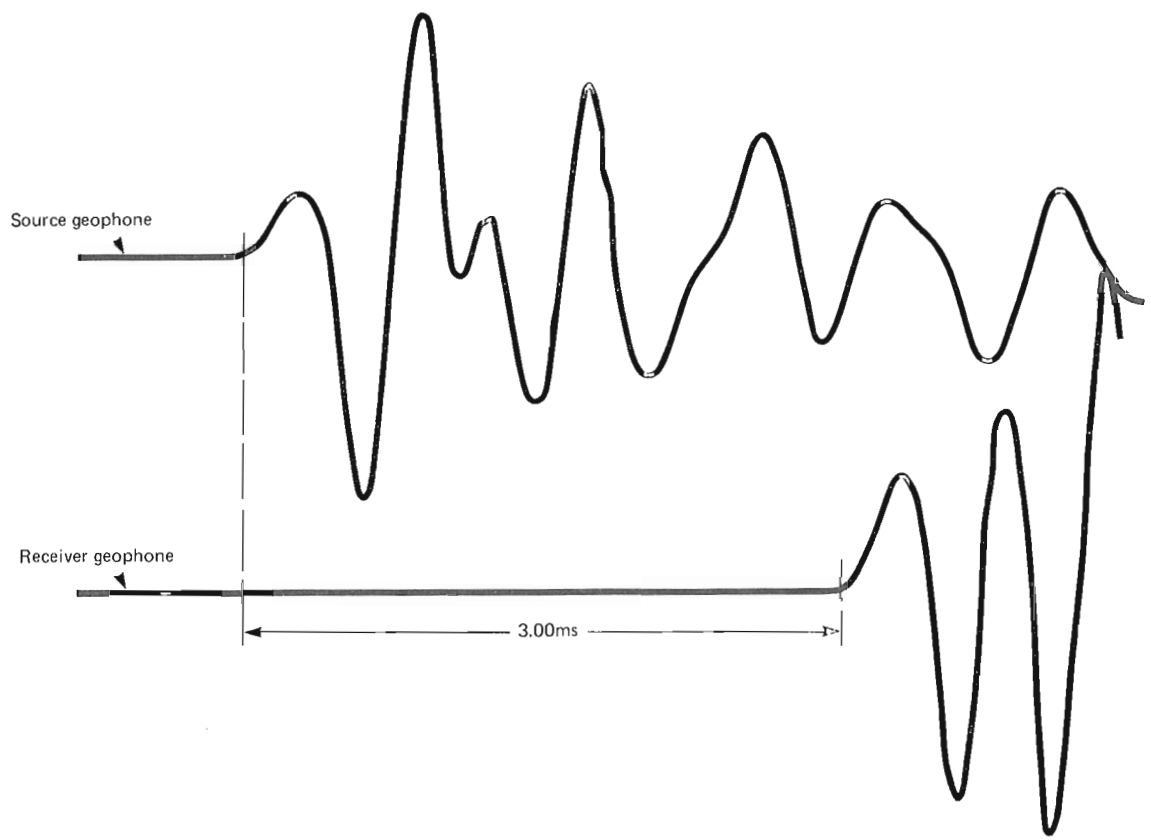

Figure 19.2. *Source/receiver seismograph for position 16 to 6.*

in attenuation and velocity at seismic wavelengths in rock masses. However there are a number of difficulties inherent both in these techniques and in their application to seismic data. Some of these problems are most usefully discussed by Wong et al. (1982). These difficulties are, in part, associated with the nature and size of the matrices involved. Further, the iterative or other methods of solution of tomographic problems are often extremely complex and require considerable computing resources.

Techniques used in medical science may not be directly applicable to seismic imaging for other reasons. For instance seismic wavelengths will commonly be similar in scale to the required resolution of the system whereas at X-ray wavelengths this will not be a problem. Also in geological strata path bending according to Snells law may need to be considered and the iterative application of ray tracing methods will inevitably increase the already high processing costs. Objections to the use of many algorithms can be based on the form or quality of the data available from the field. For instance, if ray paths through the host solid are not available in many varied directions then non-unique descriptions with the omission of major structural inhomogeneities may result.

It was decided to try a very simple algorithm that could be quickly programmed and run on a microcomputer. This method suffers from most of the problems discussed but has one notable advantage; it is easy to apply and is undemanding in terms of computer resources. The method calculations 'representative velocity' values for a grid of points at any specified spacing; for this work the grid spacing was 1 m. Iterative procedures would be required to yield actual velocities but where measured velocity variations are substantial and well above noise levels then little will be gained in the assessment of rock quality variation.

The representative velocity, V_R, for each grid point is calculated from the following equation

$$V_R = \Sigma V_i \frac{S-R_i}{S} \frac{1}{L_i} \Big/ \Sigma \frac{S-R_i}{S} \frac{1}{L_i} \quad \text{for } R_i < S$$

where V_i is the velocity between two reference points which are separated by distance L_i.

R_i is the distance of the closest point, on a direct path between reference points, to the particular grid point

S is a preselected parameter which determines the width of the influence corridor associated with each direct path.

Thus the representative velocity comprises a weighted mean of all measured velocities along direct paths which pass within a distance S of the particular grid point considered. The two weighting factors are:

(1) $\frac{S-R_i}{S}$ This factor attributes a significance to the velocity V_i which is linearly degraded (from unity to zero) with increase in distance of the grid point from the direct path.

(2) $1/L_i$. This factor attributes a significance to a velocity V_i which is inversely proportional to the length of the direct path.

It must be noted that, dependant on reference location layout, the number of velocity measurements and the relative significance attributed to them may vary considerably for each grid point, i.e. some points may have many direct paths passing close to them whereas others may have relatively few. The denominating factor $\Sigma \frac{S-R_i}{S} \frac{1}{L_i}$ merely normalizes all calculated values of V_R.

An ideal experimental configuration would provide closely equal numbers of measured point to point velocities passing each grid point in a wide variety of directions.

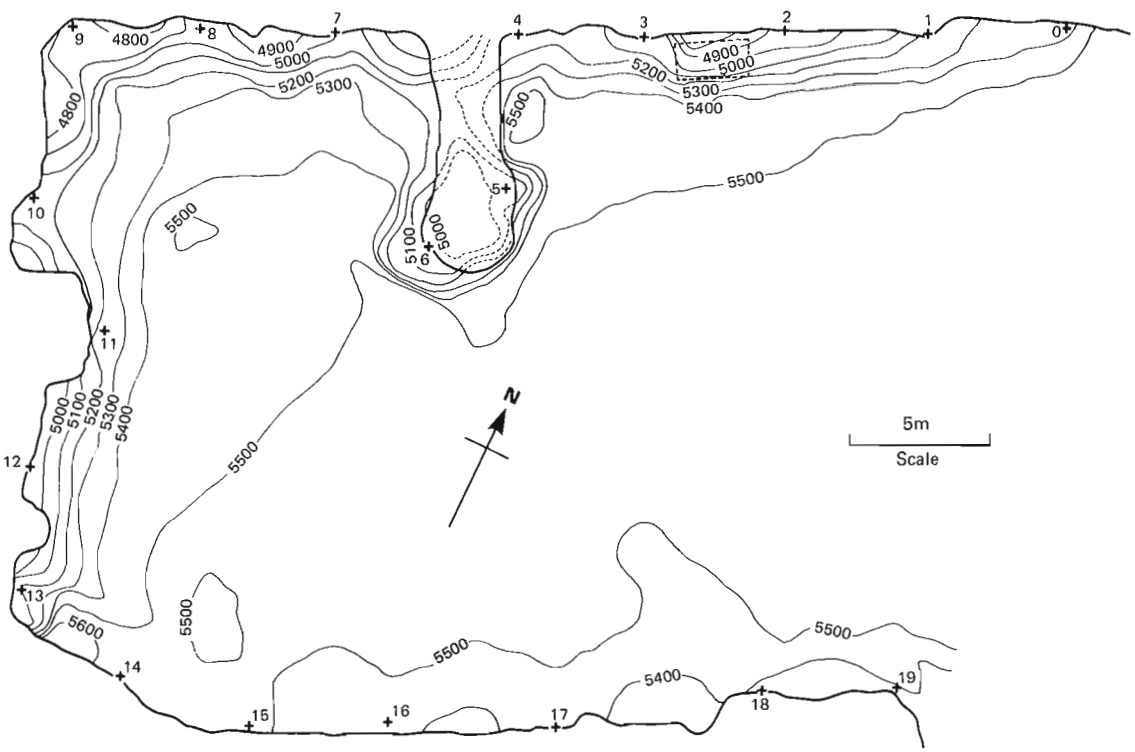

Figure 19.3. Representative velocity contour map (all data; S = 2).

The value of S determines the lateral extent of an influence corridor formed on either side of the direct path between two reference points. The choice of value for the factor S will be largely dependent on the wavelength of the seismic disturbances. The higher the frequency the lower the value of S may be made to improve the image resolution. However the smaller the value chosen for S the less advantage will be gained from the effects of large numbers of contributing measurements. The factor $1/L_i$ was chosen to favourably weight short pathlengths which necessarily sample smaller areas of rock than long paths. Clearly where a short path passes to close to a grid point the measured velocity must be more significant to that particular point than that indicated over a longer sampling path-length. Provision was made for various exponents to be applied to L_i in the representative velocity equation. The calculation of representative velocity for each grid point in the test area required a large number of simple calculations and was therefore ideally suited to solution by microcomputer. The computer program requires the following data input:

a) the north-south, east-west grid reference of each source/receiver location,
b) the time taken for compressional waves to travel between each location,
c) the specification of the representative velocity grid spacing and dimensions, and
d) the width of the influence corridor (defined by S).

The computer output yields:

a) individual source to receiver velocities,
b) representative velocities for each grid point,
c) a ranked scale mapping of representative velocity, and
d) a velocity rosette listing. (To show velocity variation with direction of wave propagation).

Results

Figure 19.3 gives a contoured map of representative velocity based on measurements between all 20 reference positions. This map was drawn from the listed (V_R) output from the computer. Figure 19.4 shows the same data presented as a ranked velocity mapping (the higher the ranking the higher the representative velocity) as computed and printed with the listing. These figures show clearly that velocity variation is primarily associated with the effect of the mine openings rather than the natural characteristics of the rock mass. This result was to be expected and is further discussed below.

The width of the influence corridor for this particular map was 4 m(S = 2), a value similar to that of the wavelength of the predominant compressional wave arrivals. Maps with wider influence corridors tended to smooth out the data losing resolution and narrower corridors did not noticeably improve resolution of observed rock variations. Indeed as corridor widths were reduced below 1 m many grid points were influenced by only one or two velocity measurements and the interactive character of many velocity determinations could not be used. Figure 19.3 shows several areas of significant representative velocity reduction:

a) a major anomaly associated with the short heading into the test area;
b) a significant local drop in velocity in the area between positions 2 and 3 where a small excavation (about 5 m^3) was present;
c) the lowest velocities occurred in the western corner of the test area;
d) low velocities were associated with the areas of rock adjacent to the wider headings ie, the northwest and southwest walls of the area; and
e) sliqht velocity reductions occurred along the southeast wall formed by the narrower heading.

Further, the representative velocity of rock away from the man-made openings was both high and uniform. Figure 19.5 presents a velocity contour map prepared without using data obtained at positions 5 or 6. These reference locations are within the test area and would not be available during interborehole investigations. This map shows all the features revealed by Figure 19.3 with the notable exception of (a). Instead of the major anomalies associated with the heading only a minor lower velocity intrusion is shown. It is most unlikely that this would have been interpreted as a large void. The rosette diagram in Figure 19.6 shows the variation of velocity with direction of propagation through the test area. Average velocities, over a span of ± 10° are plotted at 5° intervals and the diagram again shows how the influence of the large heading, running southwest to northeast, and to a lesser extent the heading, running southeast to northwest, dominate as causes of velocity reduction.

Rock quality classification

To assess the sensitivity of the seismic velocity measurements to variations in the engineering properties of the rock mass it was necessary to classify observed structural variations throughout the test area. Empirical techniques of classification (Bieniawski, 1979), which predict stand-up time and support requirements, are not sensitive enough in this case as they attempt to cover all rock types. For instance,

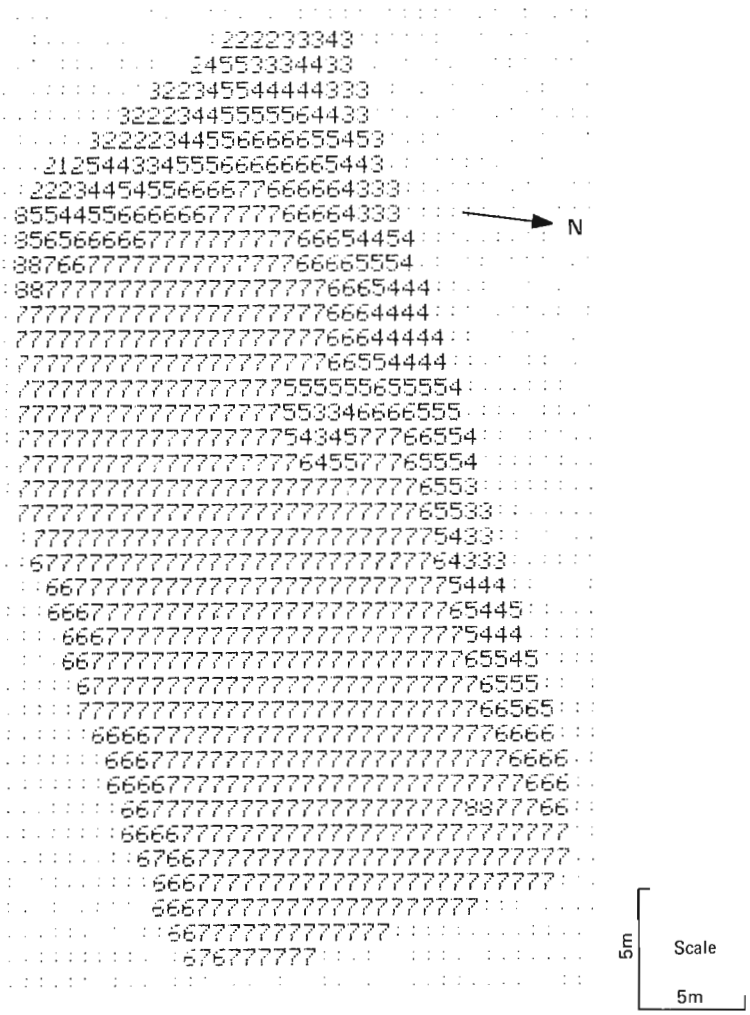

Figure 19.4. *Computer output of ranked scale representative velocity map.*

both Bieniawski's RMR and Bartons Q systems (see Bieniawski, 1979) of classification place the test area rock as being in the category 'very good' or better. Both systems indicate that the headings will require minimal support, applied as spot bolting; a prediction verified by post excavation observations.

A system specific to the field conditions appropriate to the test mine and the seismic observations was required. Site specific classifications of this type are becoming more widely used in the British tunnelling industry and provide a useful basis not only in the prediction of support requirements but as a measure against which payment may be made by the client to his contractor (Berry, 1980).

The velocity of propagation of compressional waves depends on the elastic modulus, Poisson's ratio and the density of the rock. For a massive granite formation the density may be regarded as a constant factor and any significant variation of velocity may be attributed to changes in the elastic properties of the rock mass. These changes of elastic properties will also be highly relevant to the engineering properties of the rock as they will be largely influenced by the effects of mechanical discontinuities.

Onodera (1963) proposed that the ratio of the dynamic elastic modulus of an in situ rock mass to that of an intact specimen could be used as an index of rock soundness; the dynamic moduli being derived from compressional wave (P-wave)velocities measured in the field and laboratory. Deere et al. (1966) correlated other experimental velocity ratios[1] with Rock Quality Designation (RQD)[2]. Subsequently Deere (1968a) suggested that the square of the velocity ratio may be used interchangeably with the RQD for engineering purposes. This seismic method has obvious potential for the site investigations carried out before tunnelling in rock and has also been proposed by Deere (1968b) as a method for determining the rock quality ahead of a tunnelling machine. The application and difficulties associated with seismic methods for determination of the engineering properties of rock in a tunnelling context, are discussed by New and West (1980).

A site specific system of rock classification was adopted which comprised observations of rock conditions though likely to materially affect the elastic properties of the rock mass in the test area. These factors were combined to give a numerical classification value, for each area of wall between reference points, dependent on the following characteristics:

a) the spacing of the joints,
b) the condition of the joints (aperture, filling, etc.),
c) the general intact rock condition,
d) the degree of excavation induced blast damage, and
e) the 'hole density' (the sidewalls in this mine have been extensively drilled to depths between 1 m and 3 m. The holes are, in places, drilled at such close spacing that they must materially affect the local elastic properties).

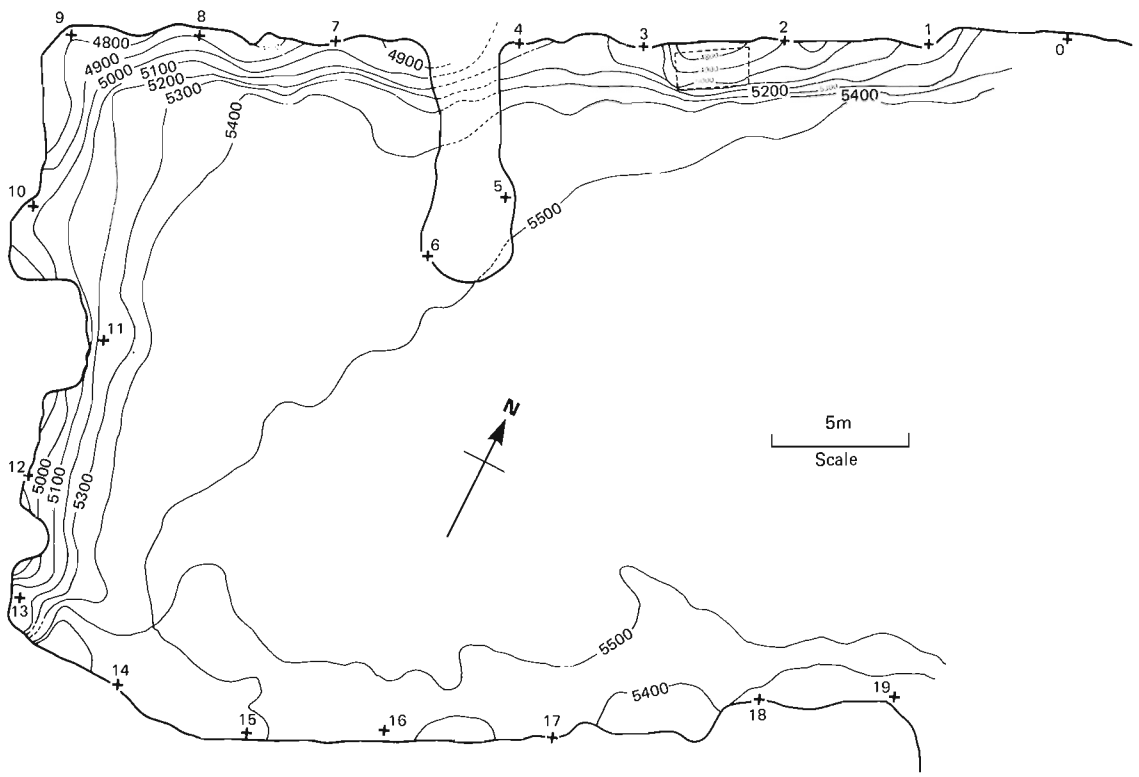

Figure 19.5. Representative velocity contour map (without data from positions 5 or 6; S = 2).

[1] The determination of the velocity ratio requires the measurement of the in situ P-wave velocity of the rock, using surface or borehole geophysical techniques, followed by measurement of the P-wave velocity of an intact core specimen taken from a borehole. The intact specimen should preferably be tested under an axial load equivalent to that estimated from its former depth in the field. The velocity ratio is the in situ velocity divided by the intact velocity; it is close to one for fresh rocks with few joints and less than one for sheared, altered or weathered rock or rock containing many joints.

[2] RQD = percentage of solid core recovered greater than 0.1 m in length.

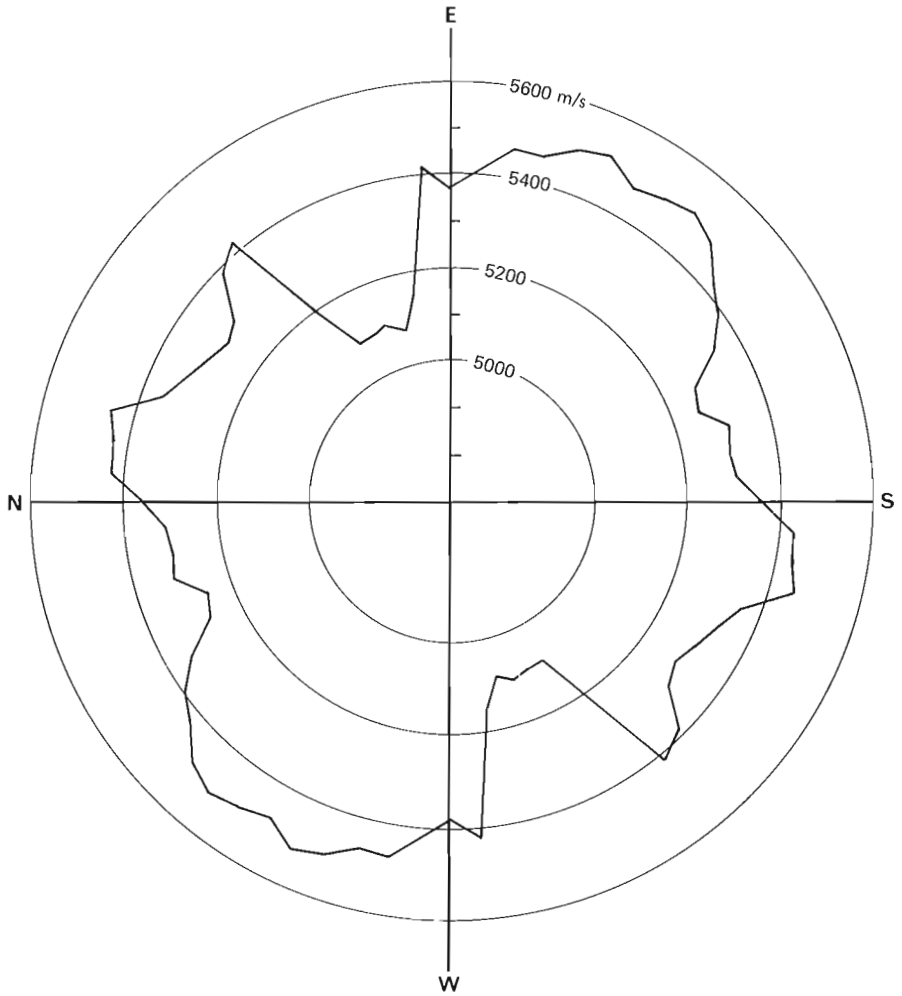

Figure 19.6

Rosette diagram of compressional wave velocity (5° increments, ± 10° span).

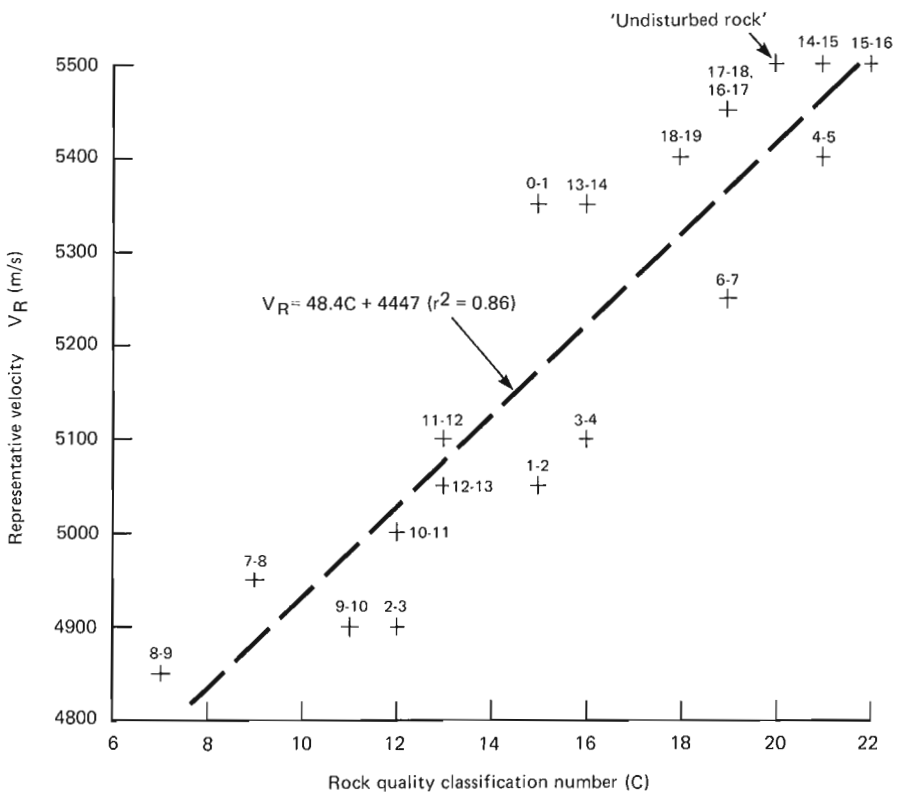

Figure 19.7. *Correlation of representative velocity with rock quality classification.*

Clearly the detailed effects of each of these factors will be very complex and in the absence of specific data each of the parameters were given equal weight in the calculation of a classification number. Each section of wall between reference points was given a score (1 to 5) reflecting the number of joints, joint condition, etc. and the total score (the classification number) calculated by the summation of the 5 factor scores. Upper and lower 'score' limits for each factor were set at maximum and minimum conditions observed in the test area. As with many methods of geotechnical classification this approach is necessarily rather subjective in application, however it does provide a numerical value associated with in situ modulus that may be compared with seismic velocity variation. It was felt that this approach was more useful than a purely qualitative correlation. Thus 19 wall areas were classified and a value for the undisturbed rock away from the heading walls also obtained. These values are plotted (Fig. 19.7) against the average compressional wave velocity in each area between reference point and are identified by their bounding reference locations.

Conclusions

Variations in velocity measured at this site were good indicators of areas of disturbed rock. However the influence of the excavations around the test area clearly dominated both the seismic velocity reduction and the classification attributed to each area. The results will be further analyzed with regard to rock mass structure and properties at depth as determined by statistical methods (Lapointe and Hudson, 1985). Care must be exercised when interpreting the velocity maps particularly with regard to the effective resolution of the system. For instance, although laterally extensive areas of highly discontinuous rock along the heading walls were identified, the small heading into the area (sectional dimensions of which were similar to the predominant compressional wavelengths) was not clearly resolved unless transducers were actually located within the cavity.

Figure 19.7 shows that the representative seismic velocity is well related to the rock classification at all the rock exposures examined. The northwest and southwest boundary walls of the test area are both heavily blast damaged and extensively drilled compared with the smaller heading along the southeast boundary. The very lowest velocities are associated with a heavily damaged and weathered area of rock with several major joints at the western extremity of the test area. These tests have confirmed that classification of rock by seismic methods can give a good indication of the engineering properties of a rock mass. In particular a low in situ velocity (compared to that of an intact sample) indicates disturbed rock in which excavation and support difficulties may be expected. Further trials will be carried out to determine if seismic wave attenuation would also provide a potentially useful measure of the engineering properties of a rock mass.

Acknowledgments

This work has been commissioned by the Department of the Environment and carried out in collaboration with J.A. Hudson and C.M. Cooling of the Building Research Establishment.

The author is grateful for the assistance provided by his colleague V.J. Ewan and by Mr. Lloyd Tunbridge of Golder Associates.

References

Berry, N. (as reported by R.W. Poole)
1980: Ground classifications: Continental and British Practice; Report of British Tunnelling Society meeting 21 Feb., Tunnels and Tunnelling, Vol. 12, no. 6, p. 59-62.

Bieniawski, Z.T.
1979: Tunnel design by rock mass classifications; Pennsylvania State University. US Army Engineer Waterways Experiment Station Geotechnical Laboratory, Box 631, Vicksburg, Mississippi, Technical Report GL-79-19.

Deere, D.U.
1968a: Report in Rock Mechanics in Engineering Practice, K.G. Stagg, and O.C. Zienkiewicz, Editors, Wiley, N.Y.

1968b: Indexing rock for machine tunnelling, Proceedings of Conference on Rapid Excavations: Problems Progress, p. 32-38.

Deere. D.U., Hendron, Jr., A.J., Patton, F.D., and Cording, E.J.
1966: Design of surface and near surface construction in rock; Proceedings Symposium on Rock Mechanics, 8th Minn.

Hudson, J.A. and Priest, S.D.
1979: Discontinuities and rock mass geometry; International Journal of Rock Mechanics and Mining Sciences, v. 16, p. 339-362.

Lapointe, P.R. and Hudson, J.A.
1985: Characterization and interpretation of rock mass joint patterns, Geological Society of America, Special Paper, v. 199, 37 p.

New, B.M. and West, G.
1980: The transmission of compressional waves in jointed rock; Engineering Geology, v. 15, p. 151-161.

Onodera, T.F.
1963: Dynamic investigation of foundation rocks in situ; Proceedings Symposium on Rock Mechanics, 5th Minn.

Wong, J., Hurley, P., and West, G.F.
1982: Crosshole audiofrequency seismology in granitic rocks using piezoelectric transducers as sources and detectors; Proceedings of Workshop. Geophysical investigations in connection with geological disposal of radioactive wate, Ottawa, September, Nuclear Energy Agency OECD.

20. BOREHOLE GRAVITY SURVEYING, CURRENT INSTRUMENTATION, CAPABILITIES AND APPLICATIONS

Andrew J. Black[1]

Black, A.J., Borehole gravity surveying, current instrumentation, capabilities and applications; in Borehole Geophysics for Mining and Geotechnical Applications, ed. P.G. Killeen, Geological Survey of Canada, Paper 85-27, p. 181-187, 1986.

Abstract

Present day borehole gravity instrumentation has been designed to operate in petroleum exploration and production wells. The majority of these surveys make use of the tool's ability to provide very high accuracy density measurements for large volumes of rock surrounding the borehole.

The current tools are miniature versions of the LaCoste and Romberg surface gravity meters. They are housed in 10.48 cm outside diameter pressure sondes and require at least a 4-conductor wireline. Operation is by remote control from a surface console.

Single reading accuracy for this system is about 7 microgals. Multiple reading sets often have standard deviations of less than 2.5 microgals. To obtain accurate densities over small intervals, the vertical depth interval must commonly be known to less than 2 cm.

The large outside diameter of the tool presently restricts the use of borehole gravity in many mining situations. If this difficulty were overcome, several applications such as locating faults within coal seams and providing density maps of sulphide ore bodies are attractive possibilities.

Résumé

Les appareils utilisés de nos jours pour les diagraphies gravimétriques des sondages ont été conçus pour les puits d'exploration et de production du pétrole. Dans la plupart des cas, on utilise des outils susceptibles de fournir des mesures très précises de la densité des énormes volumes de roche entourant le sondage.

Les outils utilisés aujourd'hui sont des versions miniatures des gravimètres LaCoste et Romberg employés en surface. Ils sont logés dans des sondes de pression dont le diamètre extérieur est de 10,48 cm et utilisent un câble à au moins 4 conducteurs. Ils sont actionnés à distance en surface à partir d'un tableau de commandes.

La précision des lectures simples est d'environ 7 microgals. Les lectures multiples ont souvent un écart-type inférieur à 2,5 microgals. Pour obtenir des chiffres précis de la densité sur de petits intervalles, l'intervalle vertical de la profondeur doit généralement être inférieur à 2 cm.

Le grand diamètre externe de l'outil limite présentement son utilisation dans bon nombre de cas. Si l'on parvenait à résoudre ce problème, il sera intéressant de pouvoir utiliser cette méthode de maintes façons notamment pour déceler les failles dans les filons houillers et fournir des cartes de la densité des masses sulfurées.

Introduction

Borehole gravity survey capability has been available since about 1964 when Shell Development and Esso Production Research Co. built operational meters utilizing the vibrating – string principle. These meters are no longer in use. The presently available meters were all manufactured by LaCoste and Romberg. There were twelve of these meters built of which eleven are currently operational. Four of these meters are available to prospective clients on a contract basis.

Two development efforts are now underway to manufacture borehole meters. Bodenseewerke of Germany is working on a meter similar to the Askania sea meter and Delta g Instruments, Inc. is pursuing a design related to the Worden land meter principle. These meters may be operating within the next two years.

The major users of borehole gravity surveys have been the major oil companies. These surveys have been used in a number of ways which could be broadly described as belonging to either a structural mapping type of survey or a formation evaluation survey type. Use of the tool for formation evaluation purposes is expected to be predominant in the future.

The tool has also been used for engineering surveys. In particular, several surveys have been performed at proposed nuclear waste disposal sites and also as a part of the

[1] EDCON Inc., 605 Parfet Street, Lakewood, Colorado 80215 USA

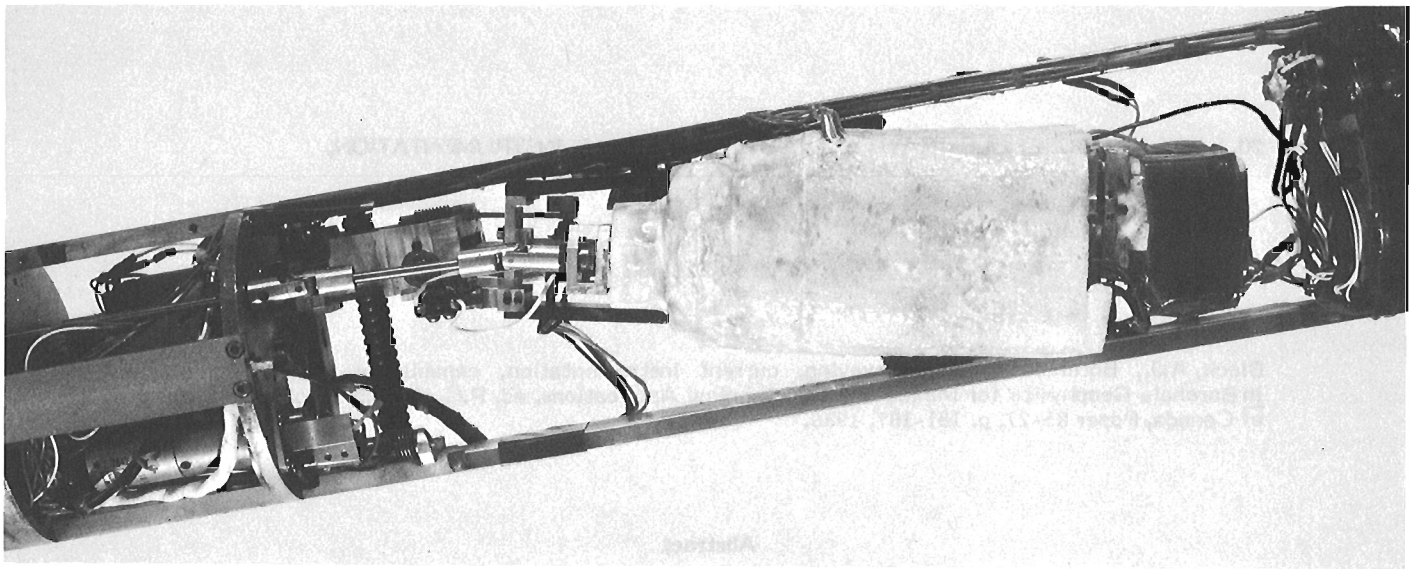

Figure 20.1. *Borehole gravity meter tilted for deviated holes.*

containment studies in conjunction with the testing of nuclear devices. The large external diameter of the tool and the high expense involved has up to now prevented its regular use within the mining industry.

Instrumentation

The present borehole gravity meters operate on exactly the same zero length spring and weighted beam principle as their well known land and sea counterparts. The first three of these meters used elements from LaCoste and Romberg geodetic meters. Subsequent meters have been miniaturized to enable them to operate within a 10.48 cm outside diameter sonde. All but the last produced meter (BHGM 12) have an operating range of about 2500 milligals corresponding to about 45 degrees of latitude range on the Earth's surface. BHGM 12 has a range adjustment facility to enable worldwide operation.

Figure 20.1 shows BHGM 8 outside its pressure sonde. The element is enclosed in polyurethene foam type insulating material. Suspended beneath the element are two capacitance/pendulum type levels used to ensure that the element is in a true vertical position when a reading is made. The element is placed in a vertical position by rotating and tilting it with respect to the pressure sonde. The rods feeding into the element from above move the meter screw to change the spring tension and clamp and unclamp the beam so the element can be moved without damage.

Immediately above the meter in the sonde lies the downhole electronics package. This contains a transformer which steps down the 440 v alternating current power supply sent down the line to several direct current levels which supply the positioning motors, the heater circuitry, the telemetry system and the receiving system for the telemetry from uphole.

The meter is operated by remote control from a surface console which sends tones of differing frequencies to a downhole filter bank to operate the desired motor. Information from the downhole system is relayed uphole as 10 kHz bursts riding on a voltage which is dependent on the position of the element beam. The length of the 10 kHz burst is related to the magnitude of the number being transmitted. This system requires 4 conductors in the supporting wireline to operate. The tool is normally supported beneath a natural

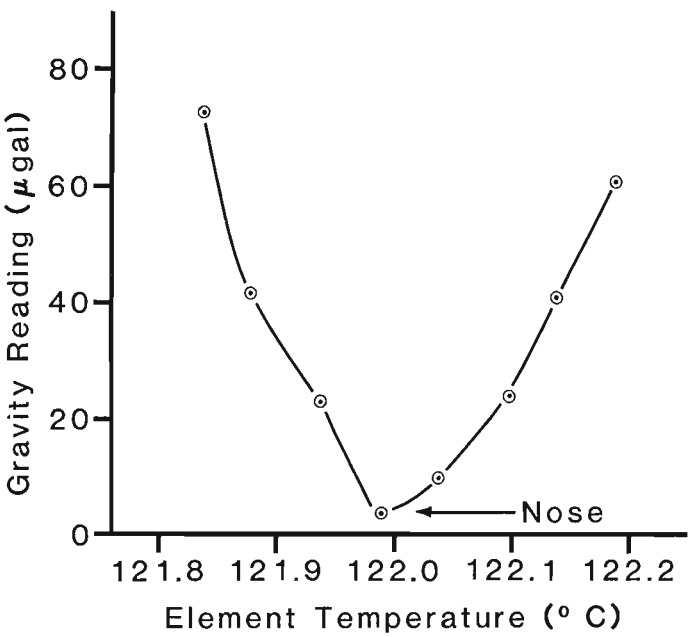

Figure 20.2. *Nose curve for LaCoste and Romberg borehole gravity meter no. 8.*

gamma tool and a casing collar locator (CCL) tool which require the remaining three of the normal oil industry wireline's seven conductors. The gamma and CCL tools are used for location of the gravity meter with respect to the other logs.

To take a reading the tool must be stationary in the hole. The element is leveled, the beam unclamped and the spring tension changed until the beam is balanced. The beam is then clamped and the tool is moved to the next station. This process normally takes from 4 to 10 minutes depending upon the distance moved from the previous station and the amount of noise due to fluid motion in the hole or seismic noise. If the distance from the previous station was large enough to produce a change in the well bore temperature near the sonde of 1° or more, the operator will often have to wait for a few extra minutes while the thermostatting system achieves equilibrium.

The accuracy obtained on a borehole gravity survey depends to a large extent on how well the element can be maintained at a constant temperature. Figure 20.2 is a diagram showing the variation in apparent gravity readings which will occur as a function of element temperature. This is the nose curve for BHGM 8. The temperature is kept at the point marked 'nose' by a bridge circuit which controls the current flow to the heater wiring beneath the element insulation. Thermistors within the insulation and a sensistor placed outside the insulation monitor the temperature difference across the insulation and are part of the bridge circuit. A reference thermistor placed under the insulation provides the operator with a continual monitor of the element temperature during the survey.

Further control of the temperature has been provided this year for the first time by the construction of a Dewar sonde to house the meter and the downhole electronics. This was designed with the primary aim of allowing the meter to be operated in oil and geothermal wells with hole temperatures in excess of the gravity meter nose temperature. It will also effectively isolate the meter from temperature variations between stations.

Figure 20.3 shows the Dewar flask and its contents. The small cylinders are fusible metal heat sinks which melt at about 97°C. Figure 20.4 shows how the temperature inside the Dewar flask increases due to the heat output of the gravity meter electronics and heater circuit. This smooth temperature increase allows the thermostatting temperature of the element to be well maintained until the nose temperature is approached. Then, electronic component failures are generally responsible for survey termination. The immersion time can be extended by cooling the electronics and the heat sinks to about 0°C before inserting them in the flask.

Borehole gravity data are normally presented not as a series of gravity values corresponding to station depths in the borehole, but as densities for the intervals between each of the gravity stations. The equation in Figure 20.5 shows how the gravity readings are converted to densities. The equation is derived by considering the difference in gravity, ΔG, in an infinite slab of uniform density, ρ, located a vertical distance, Δz, apart. By inserting the appropriate constant values (Robbins, 1980) we obtain an equation for this slab density in terms of ΔG and Δz. The value 3.6837 corrects for the free air gravity gradient. This varies with position on the Earth's surface and with depth.

In a complex geological environment, this computed borehole gravity density will be an apparent density as it is the density of a uniform slab of rock which produces the same ΔG to Δz ratio as measured in the actual complex situation. The accuracy of the density calculation depends on the accuracy of the ΔG and Δz measurements. This dependence is shown by the equation in Figure 20.6.

Operating experience has shown that relative depth measurements in a well can be obtained to an accuracy of less than 2 cm provided that the tool is able to move freely. Differences between repeat gravity measurements made at the same position are normally within the range from 1 to 7 microgals.

The density error equation has a Δz term in the denominator. Density measurement accuracy is therefore inversely proportional to the gravity station vertical separation.

To obtain highly accurate densities as required in, for example, residual oil saturation determinations, several repeat readings are taken alternately occupying stations at each depth. This produces two clusters of points on a plot of gravity against depth (Fig. 20.7). The slope of the line of best fit to these two clusters is proportional to the density and a confidence level may be assigned to each density value.

Two completely separate surveys were made over the same set of depths in a well to test the accuracies which could be obtained using this method (Fig. 20.8). Survey 1, shown by the dashed lines on this density log and survey 2, shown by the solid lines were performed with 10 repeated

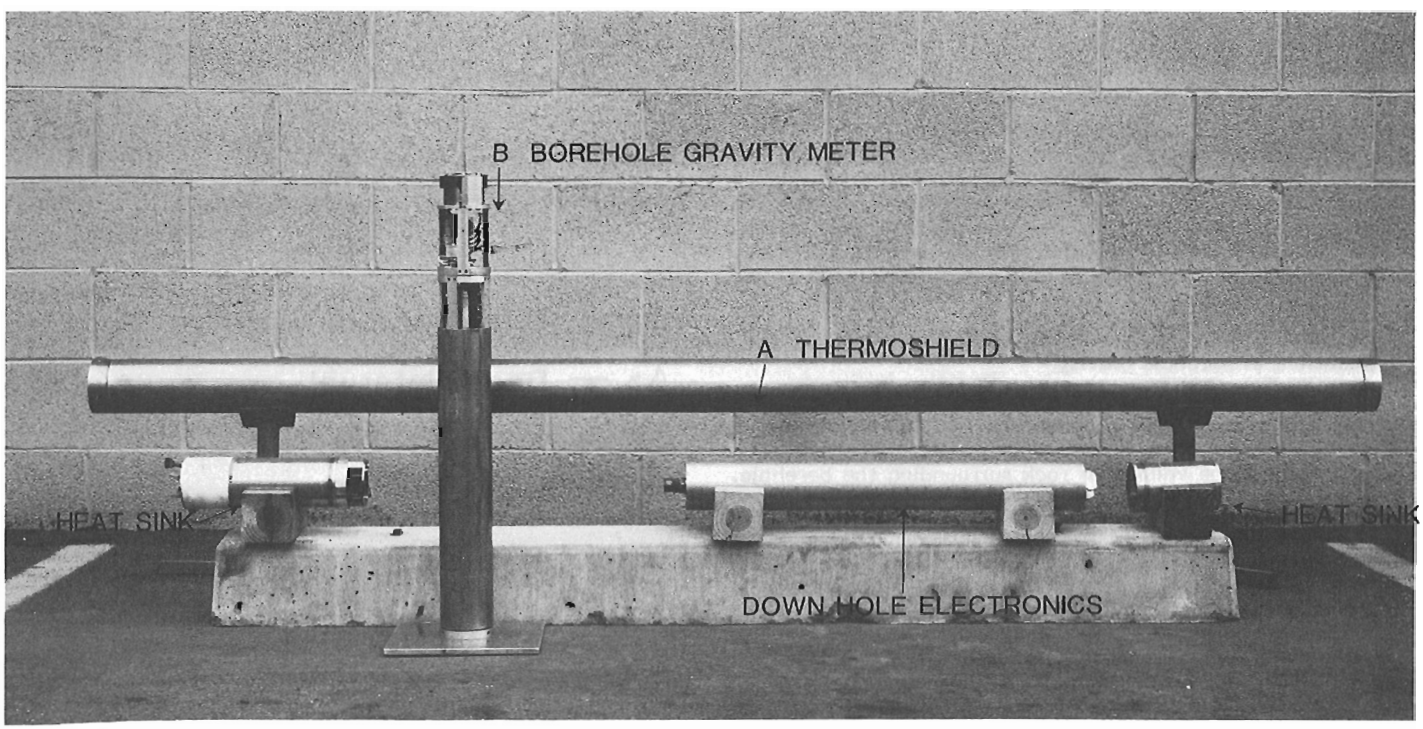

Figure 20.3. *Dewar flask (Thermoshield), borehole gravity meter, downhole electronics and fusible metal heat sinks.*

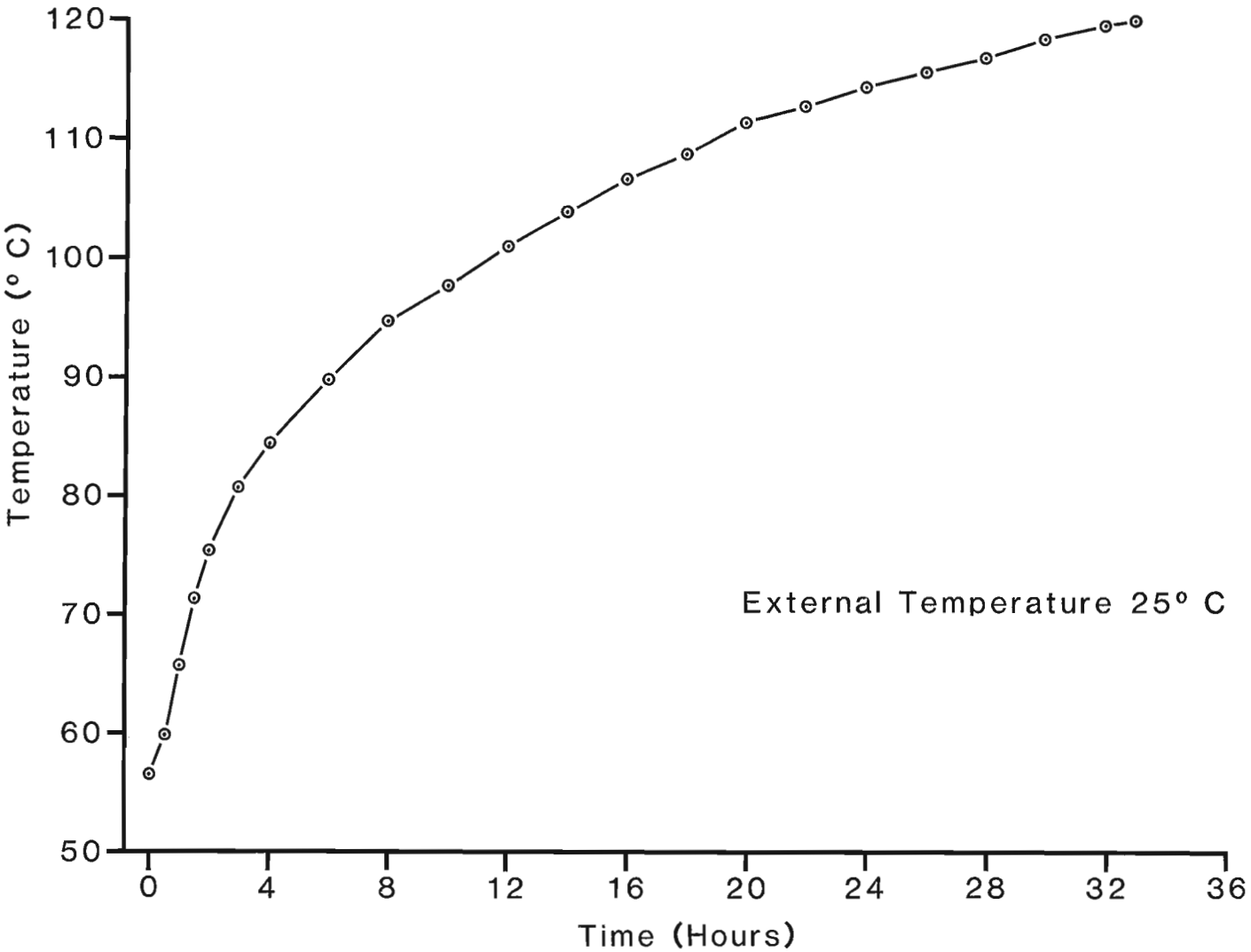

Figure 20.4. *Temperature increase due to heating of gravity meter electronics and heater circuit plotted against immersion time.*

gravity measurements at each depth. The 80% confidence limits for these densities are shown by the error bars. The density differences between the two surveys are written beside the appropriate intervals. The differences in density measurements for the two ten foot zones were 0.005 g/cm^3 and 0.004 g/cm^3.

Applications of borehole gravity

Borehole gravity surveys have been used to investigate remote discontinuities of rock density and to provide highly accurate measurements of rock densities or changes of rock density for a large volume of rock surrounding the borehole. Commonly, surveys have combined both these functions.

Surveys performed to investigate possible nuclear waste disposal sites in salt domes, for example, could use station spacings as close as 5 m to check for impurities in the salt which may provide access channels for ground water to mix with the waste material. Surveys with wider station spacings can provide a means of investigating the horizontal extent of the salt to ensure that sufficient room exists for a disposal chamber. This type of survey has been done in Denmark (LaFehr and Dean (1983); LaFehr et al. (1983)).

$$\rho = \frac{1}{4\pi K} \left\{ F - \frac{\Delta g}{\Delta z} \right\}$$

Δg — Difference in Gravity

Δz — Depth Interval

F — Free-Air Gradient

K — Universal Gravitational Constant

$$\rho_B = 3.6837 - 39.1308 \frac{\Delta g}{\Delta z}$$

Δg milligals, Δz feet

Figure 20.5. *Density calculation equations.*

$$\delta(\rho_B) = 39.1308 \left\{ \frac{\Delta g}{(\Delta z)^2} \delta(\Delta z) - \frac{1}{\Delta z} \delta(\Delta g) \right\}$$

If: $\delta(\Delta z) = .04$ feet

$\delta(\Delta g) = 2\ \mu$gal

$\Delta z = 10$ feet

$\rho = 2.3$ g/cc

Then: $\delta(\rho_B) = .014$ g/cc

Figure 20.6. *Error calculation equations.*

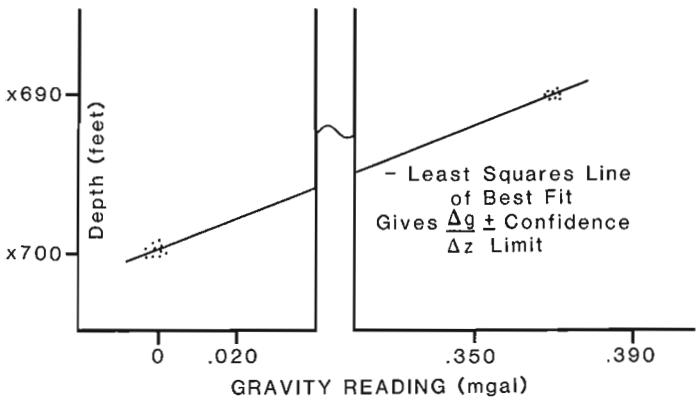

Figure 20.7. *Density calculation from multiple borehole gravity readings. Depth scatter is due to relocation errors.*

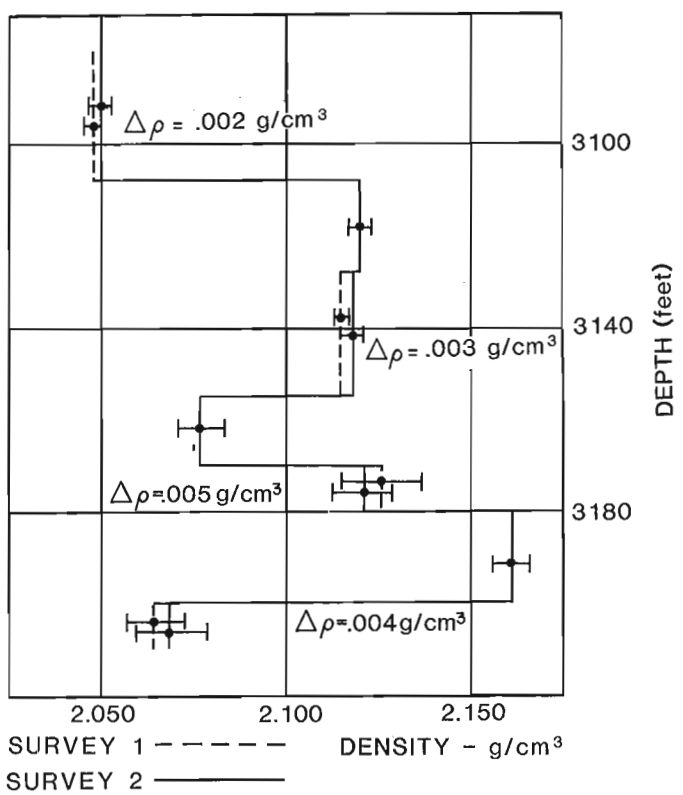

Figure 20.8. *Density logs from two independent borehole gravity surveys over the same section of a well.*

Hydrocarbons are often stored in salt domes in a similar fashion. Surveys with the borehole gravity meter have been performed during site selection processes for this type of storage. They have also been suggested as a means of monitoring leaching of the side walls of these storage caverns.

Borehole gravity surveys have been performed in investigations of hard rock storage sites for nuclear waste disposal. They are used here to detect fracture systems which will increase the bulk porosity of the rock and hence lower its density. Since fracture porosity is normally only about 2% to 8% of the rock volume, these surveys must be designed to achieve accuracies of about ± 0.01 g/cm^3. Multiple readings or wide station spacings are therefore necessary.

Situations where this type of survey could benefit the mining industry would most likely be in deep exploration areas where the region of investigation about each borehole should be as wide as possible. An example of this situation would be in a Mississippi Valley type lead zinc exploration program. Use of the gravity meter would help ensure that drillholes which narrowly missed a dense sulphide accumulation would not be written off as barren. In a situation where a mine is in the planning stage and several holes intersect the ore body, gravity surveys in those holes could provide an apparent density section of the body to indicate higher ore concentrations.

Figure 20.9 shows a hypothetical 'density-difference' section obtained by contouring the difference between the borehole gravity density and the nuclear density log in the vicinity of two bodies having densities of 2.0 g/cm^3 higher than the surrounding rocks. The densities were calculated using a two dimensional Talwani modelling algorithm.

The density pattern surrounding the two bodies is one which will be seen about any body of finite extent and positive density contrast. Above and below the body are apparent negative densities while to either side there are apparent positive densities. In a real world situation this would translate to lower than true densities being recorded above and below the body and higher than true densities recorded on each side. The ability to recognize this pattern is dependent upon how well the interpreter knows the rock densities immediately surrounding the drillhole. In this example, a positive density anomaly of 0.01 g/cm^3 exists about 50 m from the side of the body. A nuclear density log would probably be needed to provide accurate enough reference densities to enable this to be recognized.

Densities obtained with the gravity meter within an ore body will also be distorted by this low/high density pattern. Nearness to the edge of the body will also decrease the apparent densities recorded so it should be emphasized that this is an apparent density and not a true density measurement. True densities will only be approached in the case of very extensive flat lying bodies.

Borehole gravity could also be used to detect faulting in coal seams adjacent to a drillhole. This situation is illustrated in Figures 20.10A and B. Figure 20.10A shows a 6 m thick coal seam interrupted by a 4 m throw vertical fault. The density data are modelled for a drillhole 2 m from the fault on the up side. The presence of the fault causes a higher than true apparent density to be recorded within the coal seam and an asymmetric pattern of lower than true and higher than true apparent densities to be recorded above and below the seam respectively.

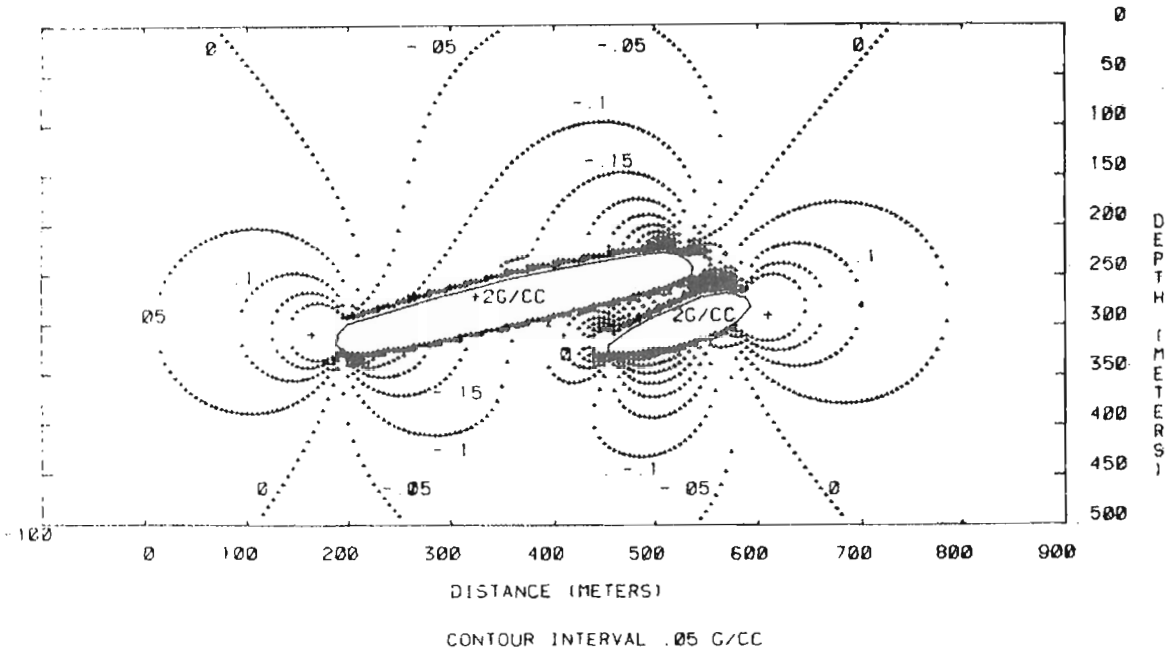

Figure 20.9. *Contoured density-difference data in the vicinity of two bodies of density 2.0 g/cm³ higher than surrounding rocks.*

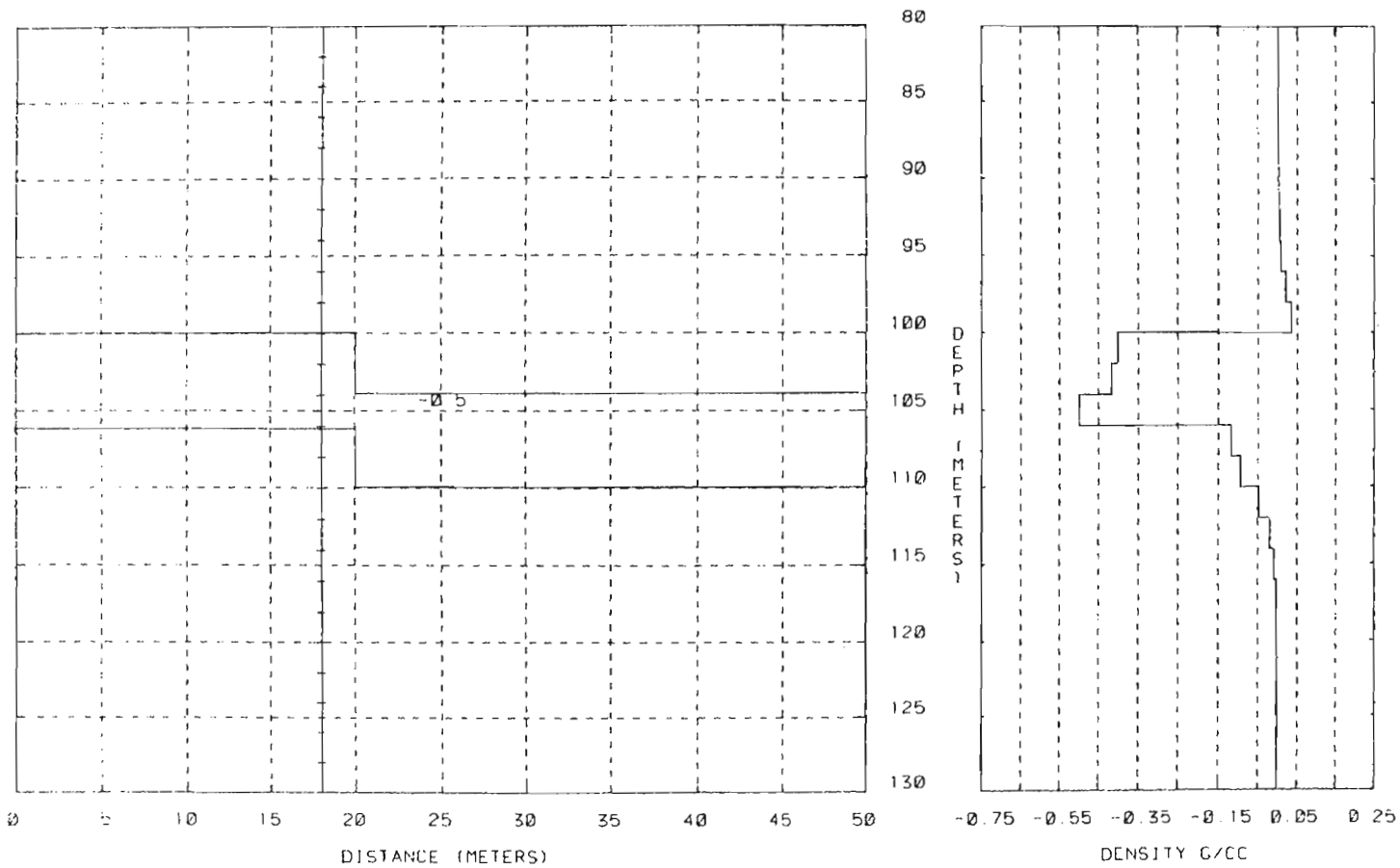

Figure 20.10a. *Hypothetical coal seam of thickness 6.0 m, interrupted by a 4 m throw vertical fault. The density data are modelled in Figure 20.10b for a borehole located 2 m from the fault on the up side.*

Figure 20.10b. *Density-difference data computed for the model of Figure 20.10a showing the apparent changes in density over the coal.*

Conclusions

Borehole gravity surveys are presently being performed for engineering studies and in particular those involved with selection of nuclear waste disposal sites. The data, in the form of high accuracy apparent densities, aid in the detection of rock fractures and salt impurities and help estimate the size of the storage volume.

Use of the tool in mining exploration and development is presently restricted by the large diameter of the sonde. Applications concerned with detection and mapping of sulphide bodies and detection of faulting in coal seams are possible but these await the introduction of smaller and less expensive tools.

References

LaFehr, T.R. and Dean, V.C.
1983: Borehole gravity case history of the Mors Salt Dome, Denmark; in Society of Exploration Geophysicists Expanded Abstracts with Biographies, 1983 Technical Program 53rd Annual International SEG Meeting, Las Vegas, Nevada, Paper BG7, p. 33.

LaFehr, T.R., Dean, V.C., and Davis, T.L.
1983: Seismic and gravity modeling of the Mors Salt Dome, Denmark; in Society of Exploration Geophysicists Expanded Abstracts with Biographies, 1983 Technical Program 53rd Annual International SEG Meeting, Las Vegas, Nevada, Paper S4.8, p. 301.

Robbins, S.L.
1980: Bibliography with abridged abstracts of subsurface gravimetry (especially borehole) and corresponding in-situ density determinations; United States Geological Survey, Open File Report 80-710, 47 p.

21. A NEW BOREHOLE RADAR SYSTEM

Bruno Nilsson[1]

Nilsson, B., A new borehole radar system; in Borehole Geophysics for Mining and Geotechnical Applications, ed. P.G. Killeen, Geological Survey of Canada, Paper 85-27, p. 189-195, 1986.

Abstract

A new pulse radar system permitting measurements in 46 mm boreholes has been developed by the Boliden Mineral Company. The system with its peak transmitted energy at 50 MHz has separate transmitter and receiver probes thus making both reflection and transmission measurements possible. The two probes communicate with the central unit situated on the ground surface via fibre optic links. This technique effectively eliminates the unwanted wave propagation along or reflections from a conventional conducting cable.

Presently the system operates with fibre optic links 300 m in length but is capable of using up to 1000 m. The central unit is equipped with a video memory feeding a CRT display with a resolution of 256 x 256 4-bit pixels, thus allowing a radar image presentation in 16 levels of gray-scale. Storage of data is accomplished by an integral digital cassette tape recorder. Playback of cassette data may be either on the CRT of the central unit or on an external image processing system. In the reflection mode, the radar system is able to detect discontinuities in the conductivity and/or permittivity parameters of the medium. In the transmission mode, on the other hand, the average absolute values of the two parameters along the propagation path are obtainable. Practical tests have proved the system to have a range of up to 100 m in the reflection mode in low conductivity rock such as granite.

Résumé

La Boliden Mineral Company a mis au point un nouveau système radar à impulsion qui permet d'effectuer des mesures dans les sondages de 46 mm. Le système, dont l'énergie maximale transmise est de 50 MHz, comprend un émetteur distinct et des sondes réceptrices lui permettant de mesurer les ondes réfléchies et les ondes émises. Les deux sondes sont reliées au moyen de fibres optiques à l'unité centrale qui est située à la surface du sol. Cette méthode élimine effectivement la propagation des ondes le long d'un câble conducteur normal ou la réflexion de ces ondes à partir de ce câble.

Le système utilise présentement des fibres optiques de 300 m de long mais peut utiliser des fibres de 1000 m. L'unité centrale est munie d'une mémoire à écran de visualisation qui alimente un écran cathodique ayant une résolution de 256 x 256 pixels à 4 bits, ce qui permet de présenter l'image radar en utilisant 16 niveaux de l'échelle de gris. Le stockage de l'information se fait au moyen d'un cassettophone numérique intégral. La reproduction des données peut se faire soit sur l'écran cathodique de l'unité centrale, soit sur un système externe de traitement de l'image. Dans le mode réflexion, le système radar peut déceler des discontinuités dans les paramètres de conductibilité, de permittivité ou des deux, du matériau. Par contre, dans le mode transmission, il est possible de calculer les valeurs absolues moyennes des deux paramètres le long du trajet de propagation. Des essais d'exécution ont montré que la portée du système atteint un maximum de 100 m dans le mode réflexion dans les roches à faible conductibilité telles que le granite.

Introduction

In recent years there has been a growing interest in geophysical methods utilizing electromagnetic fields of very high frequencies. In this case the wave aspect of the field is of prime importance. That is, the electromagnetic field may be described in terms such as propogation, attenuation, reflection, refraction and so on. In practice an electromagnetic field with a frequency, between 1 and 300 MHz may be regarded as a wave field, given proper geological conditions.

The earliest known proposal for the use of electrical shockwaves in subsurface investigations, seems to be that by Hulsenbeck et al. (1926) who were granted a German patent in 1926. Their idea was to use a spark-discharge device connected to a suitable antenna as the transmitter, and a high frequency oscilloscope connected to another antenna as the receiver. This principle was the basis of the pulse-radar technique used in World War II.

[1] Newmont Exploration Limited, 200 West Desert Sky Road, Tucson, Arizona 85704

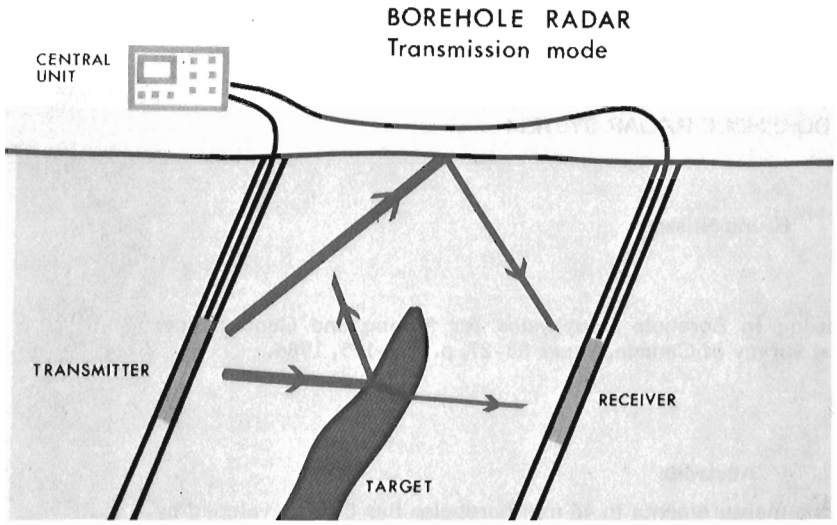

Figure 21.1
The borehole radar in transmission mode.

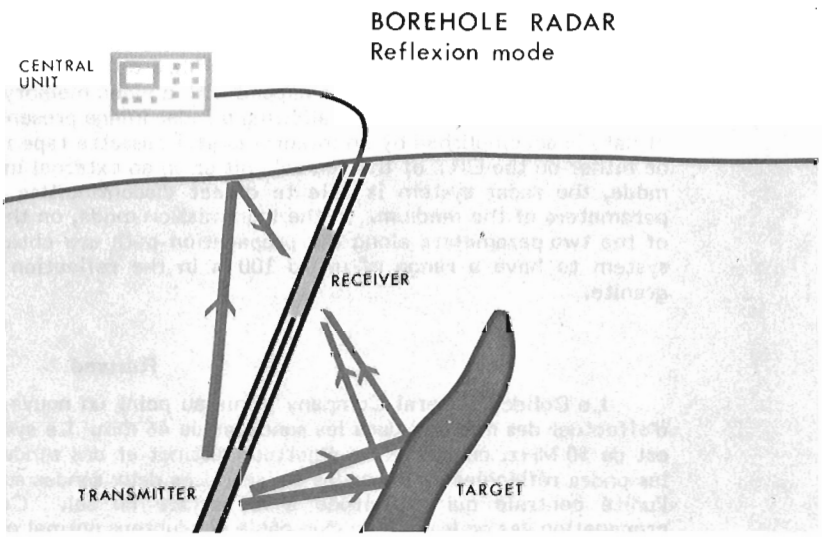

Figure 21.2
The borehole radar in reflection mode.

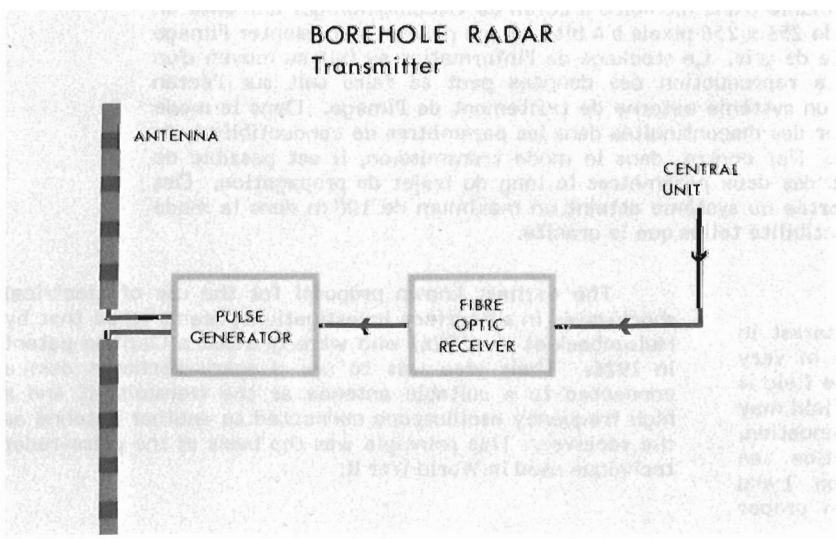

Figure 21.3
Schematic diagram of the transmitter.

The same basic principle is applied in most of the present systems for subsurface investigations. This includes the first widely available system, manufactured by Geophysical Survey System, Inc, which was introduced in the middle 1970s (Morey, 1974).

The Boliden Mining Co. in Sweden has been doing research in this area for the last 10 years (Nilsson, 1973, 1976, 1978) and in this paper our most recently developed borehole radar system is described.

Background

As with most geophysical methods, the borehole radar is a suitable tool only in proper geological environments. The most important requirement is the relatively high resistivity of the medium needed for wave propagation to occur.

The objective of our ongoing borehole radar project has been, on one hand, to develop the equipment itself and on the other to evaluate the possible use of such a system as a tool in mineral exploration. Figure 21.1 shows radar used in the transmission mode. The main items of interest in this situation are the amplitude and propagation delay of the direct pulse. In a homogeneous situation, the amplitude indicates the resistivity of the medium and the propagation delay indicates the permittivity.

A body with high conductivity located between the boreholes should manifest itself as a decrease in amplitude of the received pulse. This is due to both the reflection of the incident wave at the surface of the body and absorption within the body. Some of the energy may be reflected at the ground surface, as indicated, and reach the receiver behind the body. However, this component is easy to distinguish from the direct pulse due to its longer time delay.

In Figure 21.2 the radar is shown in the reflection mode. The target is detected by the reflected waves. The amplitude of these reflections is dependent upon the contrast of the target with the respect to its surroundings and the propagation delay gives the distance to the target.

In this case also we may have reflections from the ground surface as indicated.

Transmitter

The basic principle of the transmitter (Fig. 21.3) is very simple and is similar to that covered by the German patent from 1926 mentioned above.

To the right (Fig. 21.3) the fibre optic link from the central unit enters an optical receiver which converts the optical signal to a corresponding electrical signal.

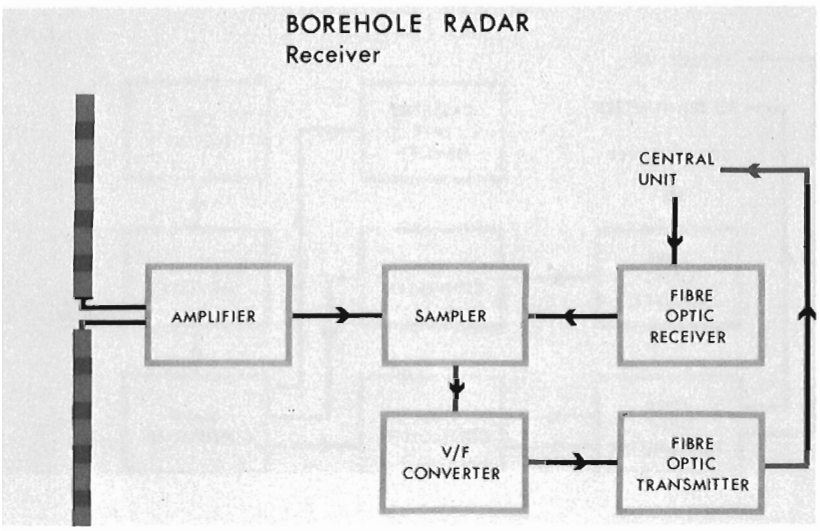

Figure 21.4

Schematic diagram of the receiver.

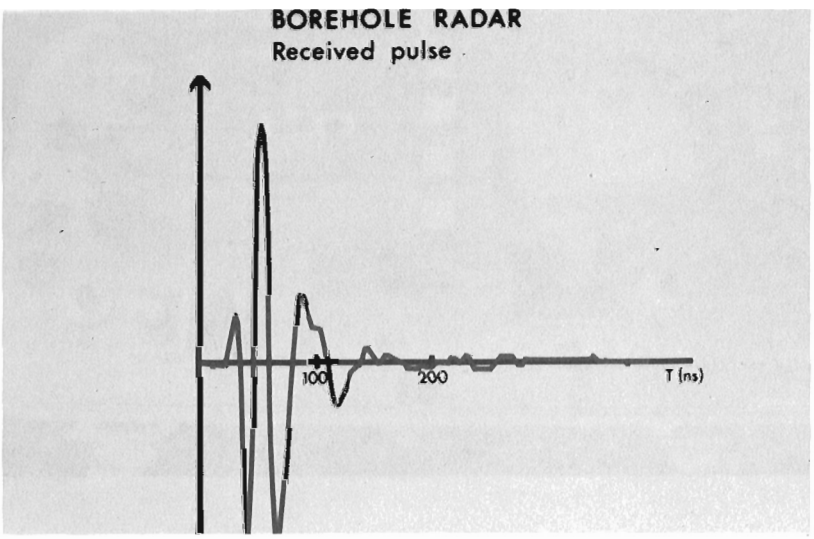

Figure 21.5

Receiver pulse.

Figure 21.6
Picture of the equipment.

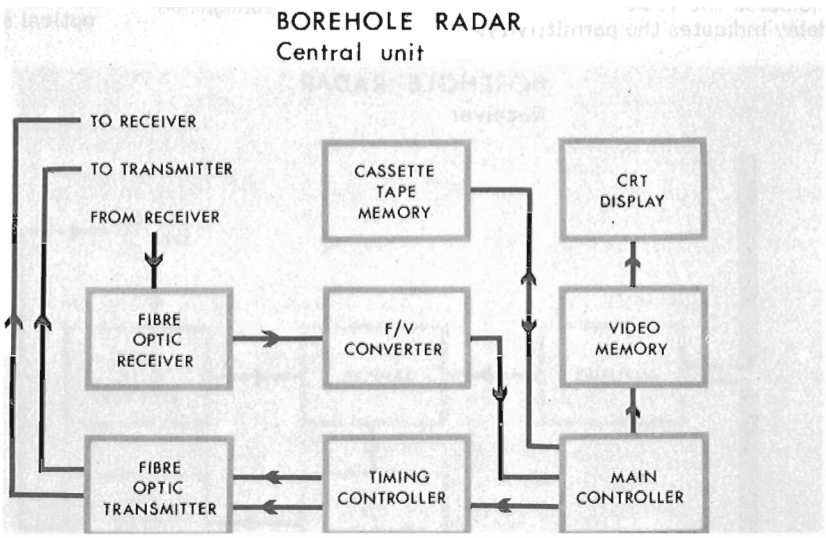

Figure 21.7
Schematic diagram of the central unit.

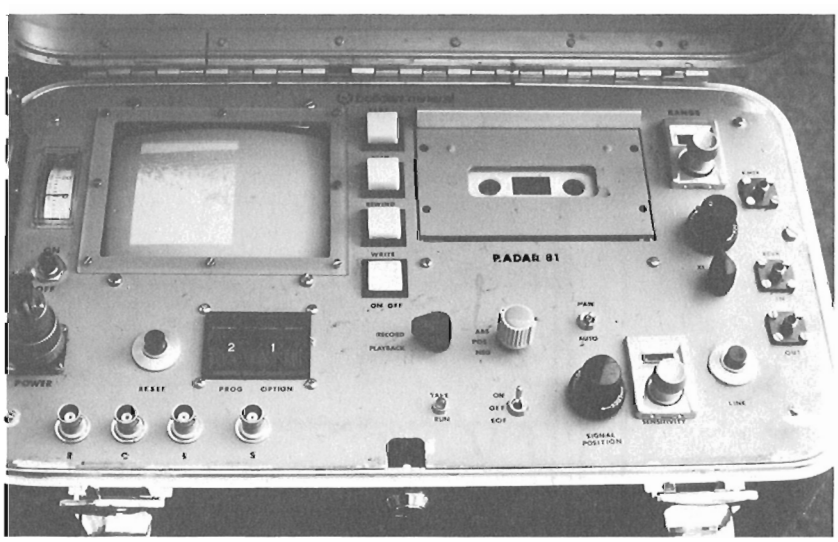

Figure 21.8
Picture of the central unit.

When the central unit commands the transmitter to send out a pulse, it sends an optical trigger pulse in the fibre. After propagation along the fibre and conversion in the optical receiver, the trigger pulse fires the pulse generator. This in turn feeds the antenna with a current pulse of 1 A having a rise time of a few nanoseconds thus causing an electromagnetic pulse to be radiated. The pulse repetition rate is 50 kHz.

The antenna is a periodically loaded travelling wave dipole structure that is capable of transmitting a pulse of short duration. The theory of this antenna, designed to achieve a purely outward travelling wave along the antenna elements, was studied by Wu and King (1965). The antenna structure is made of sections of copper pipe with resistive elements in between the pieces.

The probe has a diameter of 40 mm and a length of 4 m to accomodate the selected frequency range. In this system, the peak of the transmitted energy was selected to be 50 MHz in order to obtain a suitable trade off between wave attenuation and resolution.

Receiver

The receiver shown in Figure 21.4 is basically a sensitive high frequency oscilloscope of the sampling type connected to a suitable antenna. The antenna signal is amplified by a low noise preamplifier with a bandwidth of 60 MHz.

The central unit furnishes timing information to the sampler in the receiver on one of the two fibre optic links connected to the receiver. The sampler produces a low frequency replica of the amplified antenna signal. For the purpose of transmitting this signal on the fibre links to the central unit, the signal is converted to a pulse train by means of a voltage-to-frequency converter. The converter generates a pulse train with an instantaneous frequency proportional to the instantaneous signal output from the sampler. The electrical pulse train is converted to a corresponding optical and then, finally, fed on the fibre link to the central unit.

The antenna of the receiver is identical to that of the transmitter.

Figure 21.5 shows a receiver pulse after penetration of 40 m of quartzite. The degree of dispersion is found to be very low; that is, the pulse shape will normally remain very stable along the path of propagation.

Figure 21.6 shows the receiver going down into the borehole and the central unit standing to the right.

Central unit

The central unit is illustrated in Figures 21.7 and 21.8. The controller supervises the timing controller which, in turn, controls the timing of the two probes via the optic links.

After the central unit has commanded the transmitter to send out an electromagnetic pulse, it starts the receiver sampling process for reception of the pulse (and possible echoes of it) at the receiver. This is done by converting the optical pulse train on the fibre back to a corresponding electrical pulse train by the optical receiver. The low frequency replica of the receiver signal is sent to the central unit by using a frequency-to-voltage converter.

The replica signal is conveyed as an analog input to the main controller and is transferred to the video memory for presentation on a CRT screen. The video memory has a resolution of 256 x 256 4-bit pixels, thus allowing presentation in 16 levels of grayscale. The data may also be stored in the mass memory which is of the digital tape cassette type. One cassette may store four separate radar images.

Image processing system

In order to analyze the radar measurements in more detail, the radar data are transferred to a separate image processing system (Fig. 21.9), developed by Boliden Mineral Co. This system has 3 image planes, each 4-bits deep, connected to the RGB inputs of a regular colour video monitor. The resolution is 256 x 256 pixels.

A computer, based on the 8073 microprocessor manufactured by National Semiconductor, controls the image memories. For data storage both 8 inch and 5 1/2 inch diskettes are used.

The system is equipped with two graphics copiers. One is the Tektronix 4695 ink jet colour copier for high quality colour graphics. The other is the Honeywell VGR 4000 for fast black and white continuous-tone images.

The system software has a number of interactive tools available for the enhancement of the radar images. These include various routines for arithmetic and logical processing, correlation and filtering.

Field results

Figure 21.10 shows the results from a radar reflection survey in the Saxberg mine in central Sweden. This mine is a zinc-lead sulphide mine operated by Boliden Mineral Co.

The receiver was located in horizontal borehole 613 and the transmitter in borehole 608 parallel to it. The two probes were then moved in unison in the boreholes. The separation between the two boreholes was 15 m.

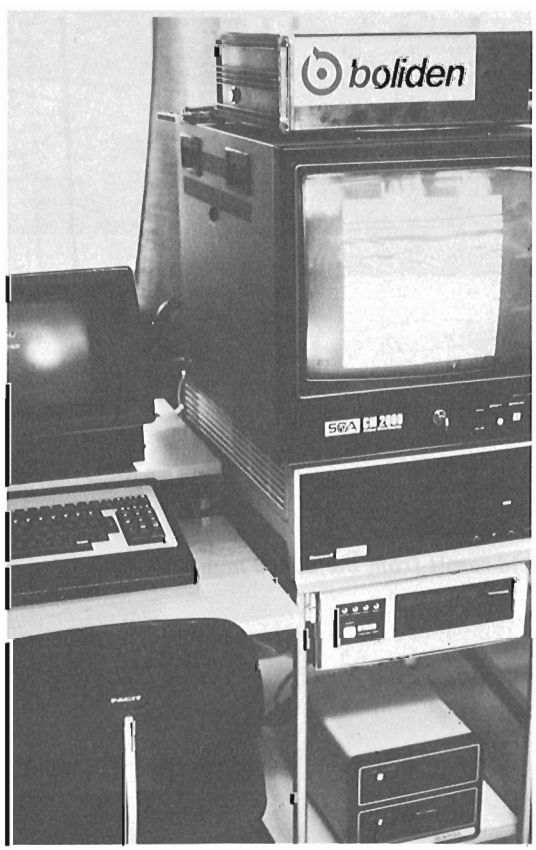

Figure 21.9. *Picture of the image processing system.*

The holes traverse a rock formation made up of parallel layers of quartzite, granite, pegmatite, and amphibolite. The layers dip at an angle of about 30 degrees to the boreholes with a strike perpendicular to the plane containing them.

One dominant feature is the reflection from the drift from which the two boreholes originate. The angle between the drift and the boreholes is 30 degrees. Since the geometry is known, this reflection allows the wave velocity to be measured, and thus also the permittivity. In this case the wave velocity was 10^8 m/s, giving a relative permitivity of 9.

The reflection from a sloping interface will show up as a hyperbola in this grayscale image. However, since the separation between the two probes is relatively small, the two branches of the hyperbola do not deviate much from straight lines.

The various interfaces show up in most cases relatively well. Certain rock interfaces not traversed by the borehole can also be distinguished.

The various rock types along the borehole have very low conductivity. The reflections are thus due to the different permittivites of the various rock types involved.

At a point between 50 and 60 m down the borehole, a strong echo was observed from a body between 25 and 30 m from the borehole. This is interpreted as a highly conductive sulphide lens, due to its high reflectivity.

Figure 21.11 illustrates a radar reflection survey from borehole F1 on the 360 level in the Stripa mine in central Sweden. Stripa is an old iron mine which is now used as a research site of the OECD/NEA International Stripa Project.

The bedrock consists of a medium grained monzogranite (Carlsson et al., 1982). The dominant reflection extending from the beginning of the borehole down to more than 150 m is caused by an aluminum tube inserted into borehole E1. Since the angle between E1 and F2 is 15 degrees, range calibration is possible.

The hyperbola shaped reflection at 175 m is caused by a drift at the 410 level, perpendicular to the borehole. The measured distance to the drift is 12 m.

A number of weaker, linear reflections are also observed. These correspond to known tectonized sections penetrated by the borehole (S. Carlsten and K-Å Magnusson, personal communication, 1983). At 117 m a 9 m wide

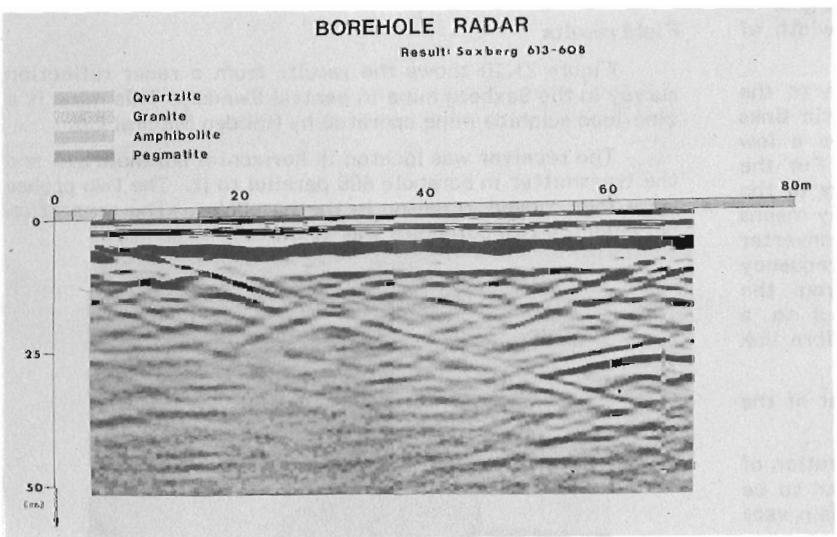

Figure 21.10
Field result from the Saxberg mine.

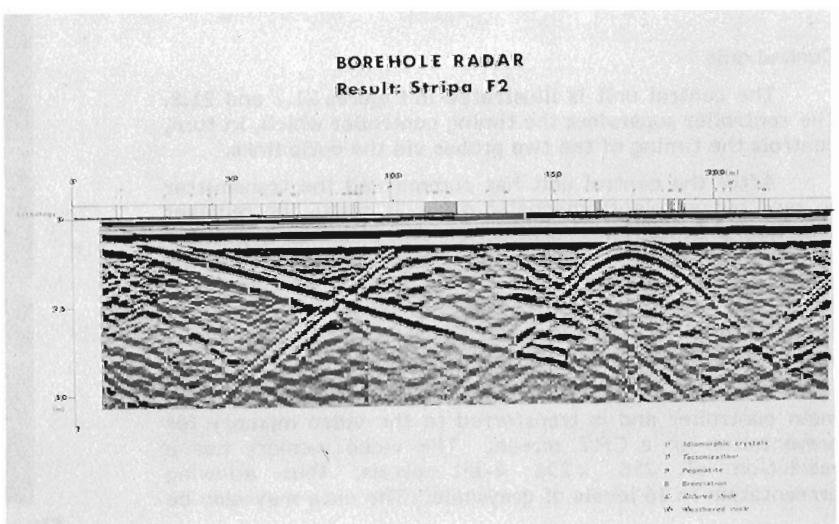

Figure 21.11
Field result from the Stripa mine.

tectonized zone of weathered rock gives rise to a relatively strong reflection. Another relatively strong reflection is found near the end of the borehole, however the hole was not deep enough to actually penetrate this reflector.

Conclusions

The work carried out to date on this borehole radar probe development project has proved that the VHF pulse-radar is capable of providing valuable information not easily obtainable with other geophysical methods.

One major advantage with the method is that it allows a simple and straight forward technique to be used for the interpretation of measured results.

Another advantage is the possibility of locating boundaries between different low conductivity rocks provided there is a contrast in permittivity. A drawback of the method is the necessity of restricting operation to media with relatively low conductivity in order to obtain useful propagation.

In low conductivity media, the system has a range of up to 100 m.

Acknowledgment

A considerable part of this work was financially supported by the Swedish Board of Technical Development, which is gratefully acknowledged.

References

Carlsson, L., Stejskal, V., and Olsson, T.
1982: Core-logs of the subhorizontal boreholes N1 and E1; Stripa project, Report 82-04.

Hulsenbeck et al.
1926: Verfahren zur elektrischen Bodenerforschung; Deutches Reichspatent Nr 489434.

Morey, R-M.
1974: Continuous subsurface profiling by impulse radar; Proceedings Engineer Foundation Conference on Subsurface Exploration for Underground Excavation and Heavy Contruction, American Society of Civil Engineers, p. 213-232.

Nilsson, B.
1973: Using pulse-radar for prospecting with a large penetration: a theoretical study; Boliden Mineral Co. Report (GP 73 0069).

1976: Geophysical prospecting by radar; Swedish Board of Technical Development, Report 74-3286.

1978: Two topics in electromagnetic radiation field prospecting; Doctoral Thesis, University of Luleå, Luleå, Sweden.

Wu, T.T. and King, R.W.P.
1965: The cylindrical antenna with nonreflecting resistive loading; Institute of Electric and Electronic Engineers, Transactions on Antenna and Propagation.

22. SOME EXAMPLES FROM BOREHOLE RADAR MEASUREMENTS

O. Olsson[1] and B. Nilsson[2]

Olsson, O. and Nilsson, B., Some examples from borehole radar measurements; in Borehole Geophysics for Mining and Geotechnical Applications, ed. P.G. Killeen, Geological Survey of Canada, Paper 85-27, p. 197-206, 1986.

Abstract

A new borehole radar system has been developed by Boliden Mineral AB in Sweden. The system consists of a control unit and separate units for transmitter and receiver antennas. Thus the system may be used both for single hole and crosshole measurements. The communication of data and control signals between the control unit and transmitter and receiver is made using optical fibres.

The measurements have mainly been performed in the form of single hole measurements with a transmitter-receiver spacing of 13 m. Attenuation and delay of the direct wave between transmitter and receiver have been observed in connection with fracture zones which penetrate the borehole. Fracture zones also cause reflections which have given information on the orientation of the fracture zones relative to the borehole. The maximum two way travel distance for which a reflection was observed was 88 m. Reflections have also been observed from an air filled drift 30 m from the borehole. In the present system, resolution is limited by ringing on the antenna, however, significant enhancement of the radar data has been obtained by deconvolution filtering.

Résumé

La société suédoise Boliden Mineral AB a mis au point un nouveau système de diagraphie radar des sondages. Ce système comprend une unité de contrôle et des unités distinctes pour les antennes d'émission et de réception. Il peut donc être utilisé dans un seul sondage et d'un sondage à un autre. La communication des données et des signaux de contrôle entre l'unité de contrôle et l'émetteur et le récepteur se fait au moyen de fibres optiques.

La plus grande partie des mesures ont été effectuées dans un seul sondage à la fois avec un espacement émetteur-récepteur de 13 m. L'onde directe transmise entre l'émetteur et le récepteur est atténuée et ralentie près des zones de fractures traversant le sondage. Ces zones de fractures produisent également des échos qui fournissent des données sur l'orientation des zones par rapport au sondage. La distance maximale du parcours allée-retour pour lequel on a observé un écho est de 88 m. On a également observé des échos provenant d'une galerie remplie d'air située à 30 m du sondage. Avec ce système, la résolution est limitée par des oscillations parasites sur l'antenne; toutefois la déconvolution a beaucoup amélioré les données radar.

Introduction

The new pulse radar system developed by Boliden Mineral AB was initially intended for use mainly in mineral prospecting. In this application reflections are expected from conductive mineralizations at a distance from the borehole. Detectable mineralization supposedly has a large conductivity contrast relative to the surrounding bedrock. The transmitted frequency has been kept low (less than 50 MHz) with the intent to reduce reflections from and attenuation due to supposedly low contrast anomalies such as fractures.

Borehole radar may also be used for engineering applications where the main interest is to detect fracture zones at a distance from the borehole. In this case, the resistivity contrasts are small compared to mineralizations but reflections will also be due to changes in the relative dielectric constant, e.g. caused by a higher water content in fracture zones. At least in low conductive rock such as granite the borehole radar system has a potential to detect fracture zones or single fractures. However the conductivity of water increases significantly at frequencies greater than 100 MHz (Nilsson, 1978), thus frequencies greater than 100 MHz should be preferred for the mapping of water-bearing fracture zones.

Experiments with borehole radar have recently been performed in granite by Wright and Watts (1982) and in salt domes by Nickel et al. (1983). In the salt dome experiments radar ranges of up to 600 m were reported. There are also possibilities for detection of fractures between boreholes by use of the tomographic technique (Okada et al., 1980).

To test the capabilities of the borehole radar system for engineering applications, measurements have been performed in some boreholes in crystalline rock. The objective of the tests was the mapping of fracture systems, which are of significance in the geological storage of spent nuclear fuel. Measurements were made at the Swedish test site at Finnsjon and at the Stripa mine.

[1] Swedish Geological Co., Box 1424, S-751 44 Uppsala, Sweden
[2] Boliden Mineral AB, S-936 00 Boliden, Sweden

The borehole radar system

The technical characteristics of the borehole radar system are only described briefly here as a detailed presentation was given by Nilsson (1986).

The pulse radar system employs separate transmitter and receiver borehole probes and may thus be used both for single hole reflection and crosshole transmission measurements. The borehole probes are 40 mm in diameter and contain transmitter and receiver electronics respectively and identical resistively loaded dipole antennas. Resistively loaded antennas are used to obtain a larger bandwidth compared to ordinary dipoles, thus well defined pulses should be obtained. The system is designed to transmit signals with a centre frequency of 50 MHz.

Transmission of pulses and recording of the received signal are controlled by a central unit located at the ground surface. The communication between the probes and the central unit is made on optical fibre links. The fibres effectively eliminate the unwanted wave propagation along or reflections from conventional conducting cables.

Theoretical responses from simple targets

When the radar system is used in the reflection mode, the transmitter and receiver are moved along the borehole with a fixed separation distance, 2c. The radiation pattern of the antennas is rotationally symmetrical around the borehole, thus the origin of a reflection may be any point on a rotational ellipsoid with the focuses at the transmitter and receiver antennas respectively. When the antenna array is moved along the borehole the distance to a reflector is varied and a characteristic reflection pattern will be generated.

In the case of pointlike reflector the two way travel distance, 2a (the measured travel-time has been converted to distance by multiplying with the velocity), will vary when the array is moved along the borehole according to the equation

$$2a = d^2 + (x+c)^2 + d^2+(x-c)^2 \qquad (1)$$

where: 2c is the distance between the antennas;
x is the distance along borehole; and
d is the closest distance from the borehole to the point reflector.

In the case of a planar reflector, such as a fracture crossing the hole, the two way travel distance, 2a, will vary according to

$$2a = 2\ x^2 \sin^2 \theta + c^2 \cos^2 \theta \qquad (2)$$

where θ is the angle between the borehole and the fracture plane.

Equation (2) is valid when both transmitter and receiver are on the same side of the fracture. Also note that the reflection from a fracture plane is symmetrical with respect to the intersection of the fracture plane and the borehole. Equation (2) is actually the equation of a hyperbola but when transmitter-receiver separation, 2c, is small or when the angle between the hole and the fracture plane is nearly perpendicular it degenerates into a line. With the use of the equations given above it is possible to calculate the distance between the borehole and a point reflector and the angle between a fracture plane and the borehole.

The characteristic signatures of the point and planar reflectors are shown in Figure 22.1.

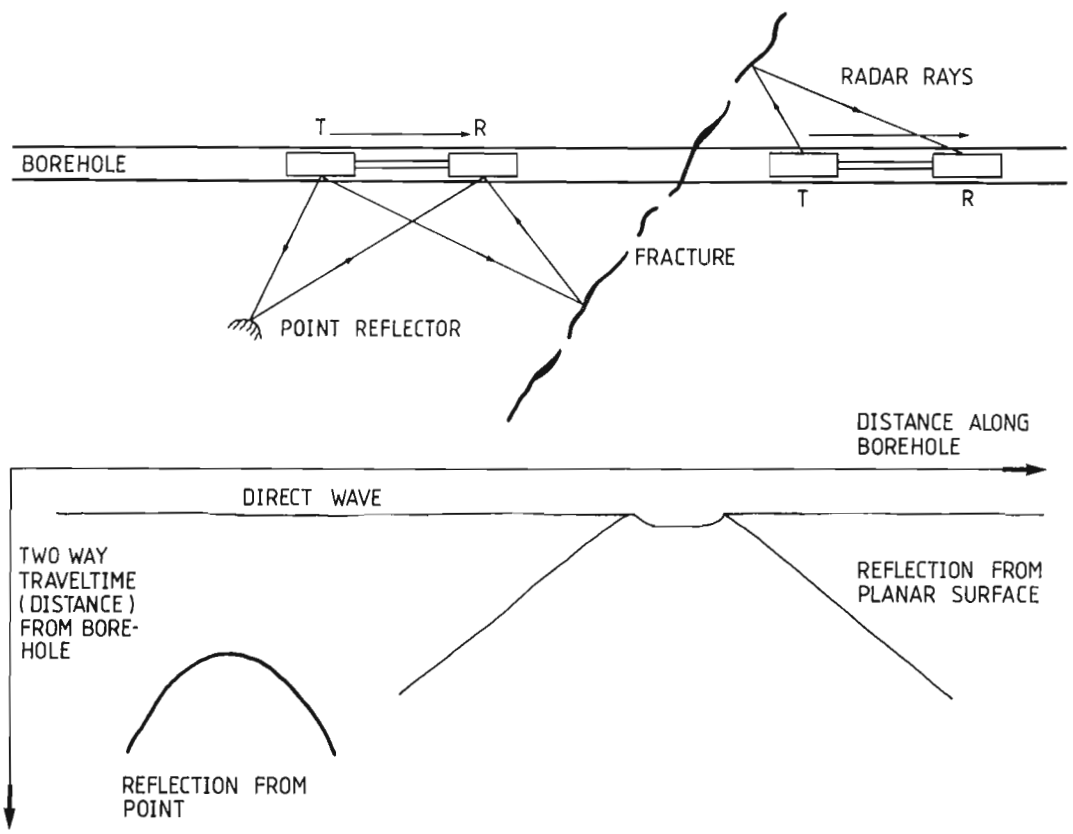

Figure 22.1. *Expected radar signatures from point and plane scatterers in reflection measurements along a borehole.*

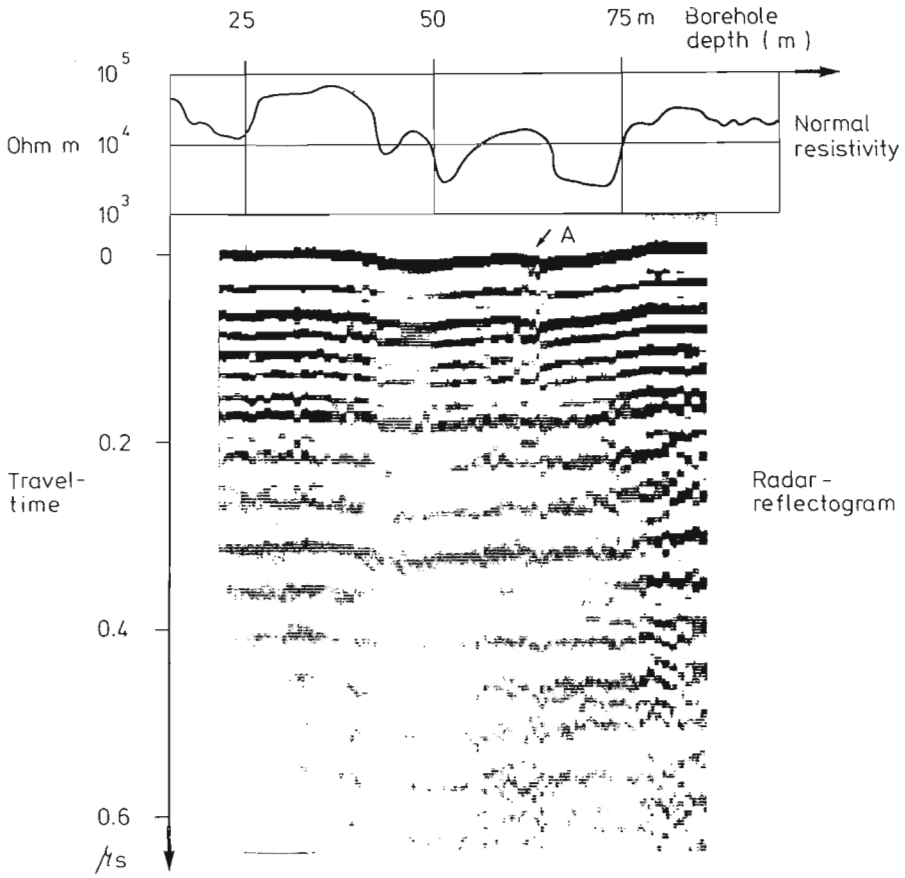

Figure 22.2

Radar plot and resistivity log for the borehole G4 in Finnsjon. Transmitter-receiver spacing 13 m.

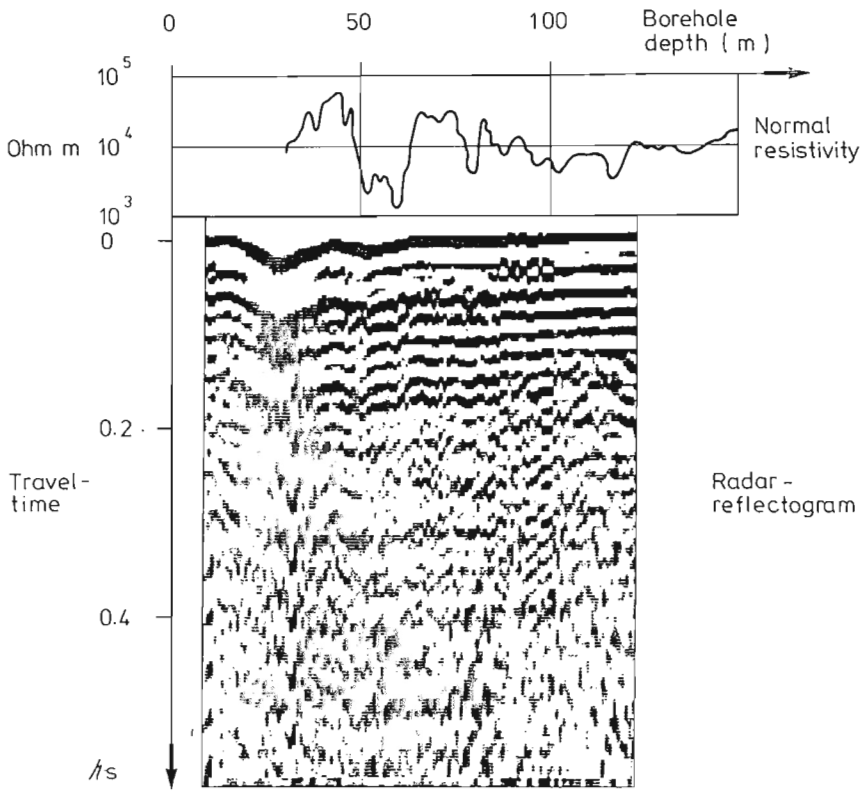

Figure 22.3

Radar plot and resistivity log for the borehole Fi8 in Finnsjon. Transmitter-receiver spacing 13 m.

Results from field tests at Finnsjon

The first tests for engineering purposes were made at the Swedish test site at Finnsjon, which is situated about 150 km north of Stockholm. The bedrock at Finnsjon consists of a grey medium grained granodiorite (Carlsson et al., 1983). The bedrock at the site is heavily tectonized with mylonites and breccias and has a high fracture frequency.

Borehole G4 is a percussion drilled vertical borehole with a diameter of 155 mm. The hole is drilled close to a major regional lineament passing through the site. The hole is generally fractured containing zones of more intense fracturing. These zones may be seen in the normal resistivity log (electrode spacing 1.6 m) shown in Figure 22.2.

The radar measurements were performed with transmitter and receiver in the same borehole. The transmitter-receiver spacing was fixed at 13 m and the array was moved along the hole.

The first horizontal band on the radar recording shown in Figure 22.2 is the arrival of the direct wave propagating along the borehole. The later horizontal bands are due to antenna resonance, ringing. The data are displayed with a time variable gain; i.e. gain increases with time. Thus the latter part of the pulse, i.e. the ringing, will appear stronger than it really is.

The travel time of the direct wave is seen to vary along the borehole where the increase in travel time is associated with increased attenuation of the wave. The time delay and attenuation has a clear correlation with low resistivity zones of the medium. This is in agreement with Maxwell's equations which predict increased attenuation for increased conductivity and decreased velocity for increased dielectric constant (due to higher water content also normally associated with increased conductivity).

There is only a faint reflection to be seen at A, which seems to be associated with the lower (deeper) of the two fracture zones intersecting the borehole.

Borehole Fi8 is a dipping core drilled hole 56 mm in diameter. The borehole is positioned close to the regional lineament penetrated by borehole G4. The hole is directed towards the lineament and penetrates it, but not in the part of the hole measured by radar. The radar plot shown in Figure 22.3 is similar to the one obtained in G4. A time delay and increased attenuation is observed at the two fracture zones penetrated by the borehole, indicated by the resistivity lows, close to the surface. A few faint reflections are seen (they are more easily seen if the radar plot is viewed at a glancing angle). It has not been possible to make a definite correlation between the observed reflections and any distinct geological feature.

The similarity between the results obtained in the boreholes Fi8 and G4 indicates that influence of the borehole fluid is comparatively small. The DC resistivity of the borehole fluid is approximately 100 ohm.m, still there seems to be only a small effect due to the different amounts of borehole fluid surrounding the antennas (borehole diameters are 56 and 115 mm respectively).

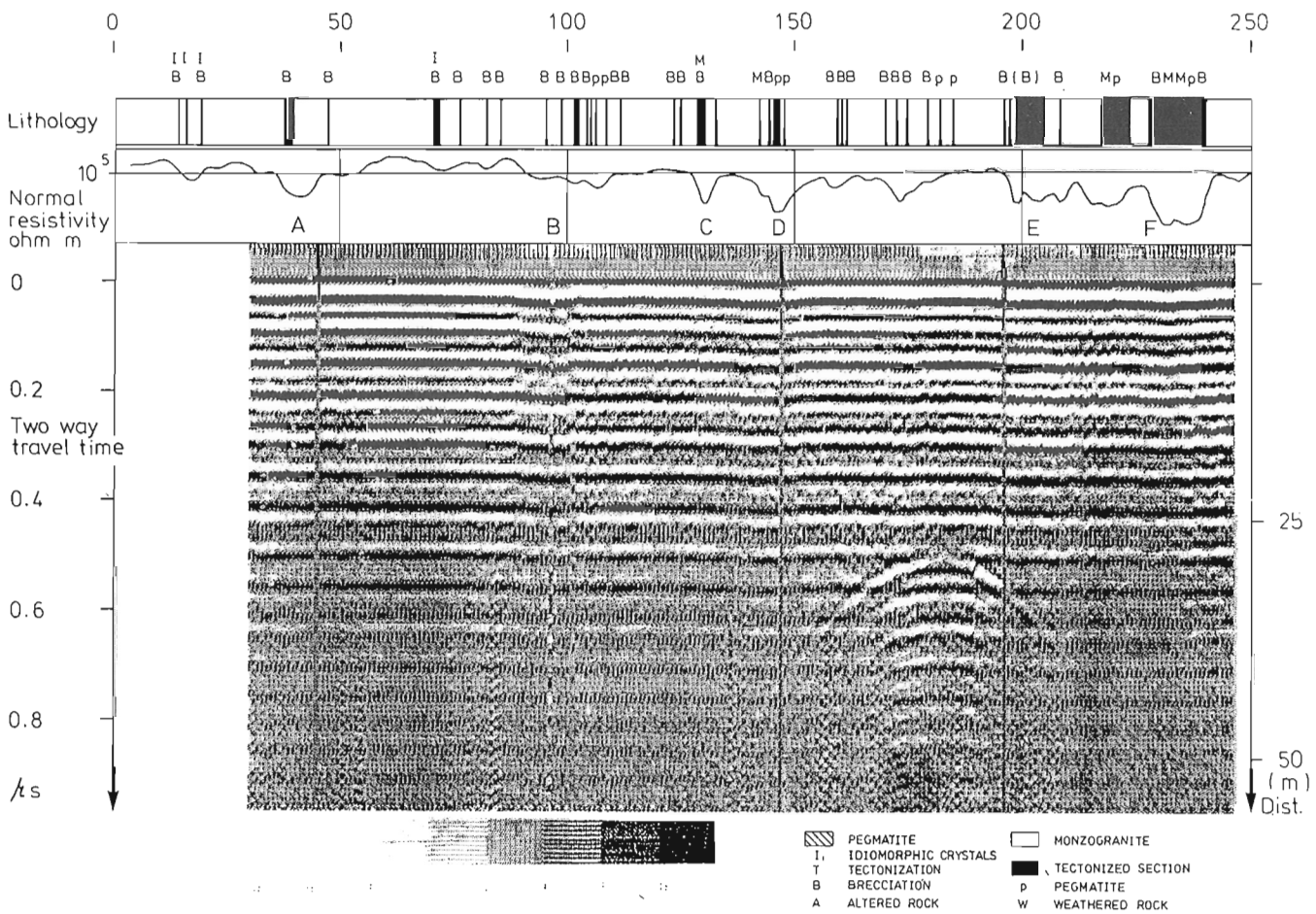

Figure 22.4. Radar plot, tectonic log and resistivity log for the borehole E1 in Stripa. Transmitter-receiver spacing 13 m.

A crosshole experiment was also conducted between two vertical percussion drilled holes separated by 40 m. However, it was not possible to detect any signals passing between the holes. This negative result is probably caused by high attenuation in the generally fractured rock at Finnsjon.

Results from field tests at Stripa

Stripa is an old iron mine which is now used as a research site of the OECD/NEA International Stripa Project. The Stripa mine is situated about 200 km west-northwest of Stockholm, Sweden. Measurements have been performed in boreholes E1 and N1, drilled as a part of a hydrogeological investigation program of the Stripa Project.

Boreholes E1 and N1 are semihorizontal and perpendicular with a diameter of 76 mm; N1 directed to the north and E1 to the east. The bedrock consists of a medium grained monzogranite (Carlsson et al., 1982). Borehole E1 penetrates several tectonized zones such as breccia, mylonite, and weathered and altered rocks. In borehole N1 there are only a few minor tectonized zones. The boreholes are also intersected by pegmatite dykes usually with a width of less than 1 m. The fracture frequency in borehole E1 is 4.3 fractures/m which is larger than in N1 where it is 1.6 fractures/m. The fracture orientations are concentrated in two main groups, one steeply dipping with a strike to the northeast and one semihorizontal.

Figure 22.4 shows the results from a radar reflection survey in E1 in which the distance between the antennas is 13 m. The dominating feature of the radar plot is antenna resonance, ringing, showing up as horizontal bands. The ringing naturally obscures some of the reflections obtained.

The first notable feature on the radar plot is a 12 m wide section, B, centred at 98 m in the borehole, characterized by increased attenuation and a time delay of the direct wave propagating along the borehole. There are no evident reflections from this feature, indicating its extension outside of the borehole. In the core, a highly fractured section of the borehole between 93 and 106 m is observed. Within the same section there is also a decrease in resistivity, the largest decrease being at 106 m. From the core and the resistivity log, it is difficult to relate the attenuation and time delay to any outstanding feature within the section, but there is a thin brecciated zone at 98 m.

The next significant feature on the radar plot is the reflection from a planar structure, C, at 129 m. The reflection from the plane is seen a considerable distance from the borehole. At 180 m borehole length the two way travel distance of the reflected wave is 88 m. Towards decreasing borehole lengths the reflection is seen for a somewhat smaller distance. The angle between the planar reflector and the borehole has been estimated at 45° by use

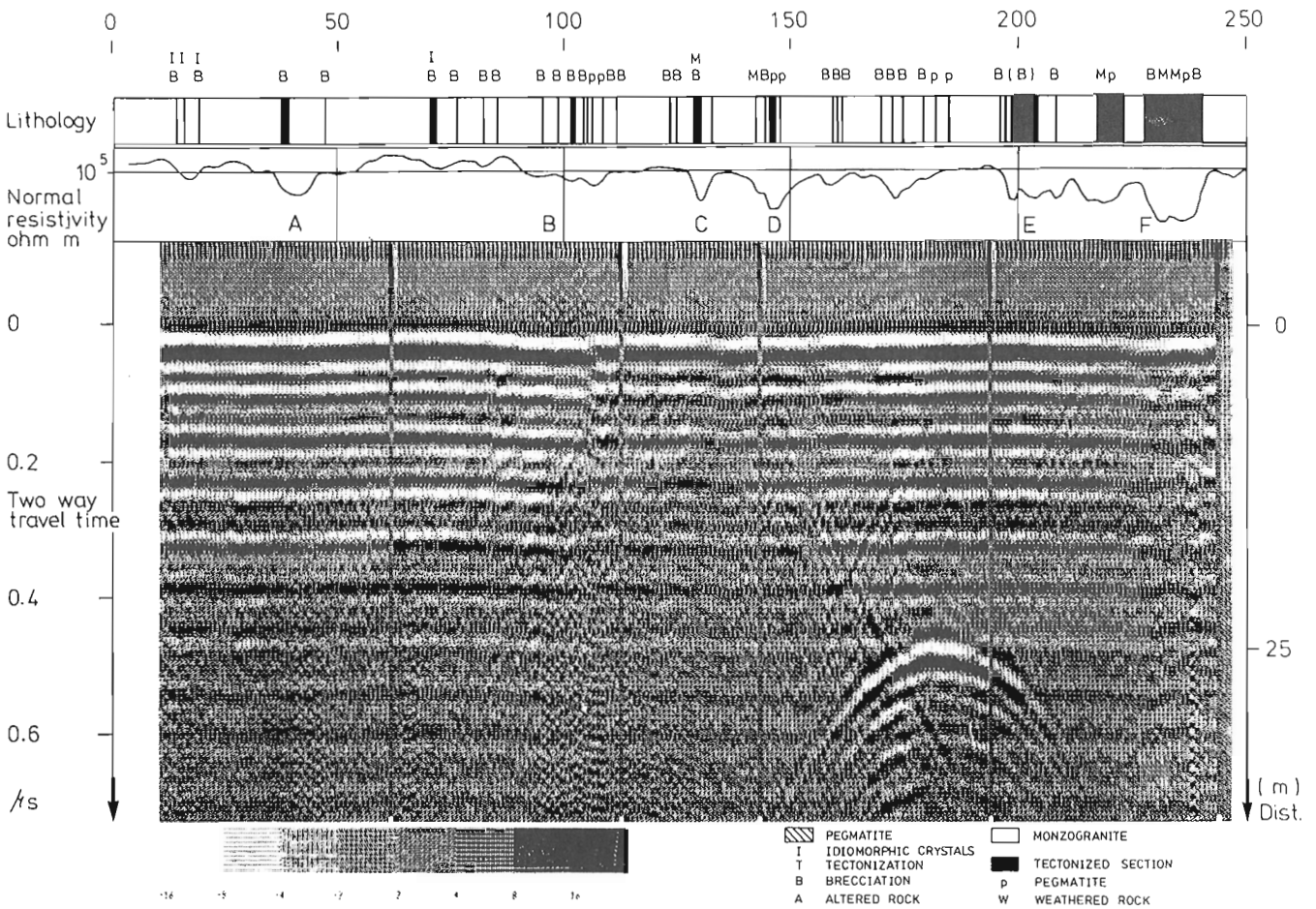

Figure 22.5. *Radar plot, tectonic log and resistivity log for the borehole E1 in Stripa. Transmitter-receiver spacing 23 m.*

of equation (2). The velocity of the radar waves used for this calculation were determined in a crosshole experiment described below.

The reflection is caused by a 1.2 m wide brecciated zone with sealed fractures. The zone is also associated with a marked decrease in resistivity.

The fracture planes observed in the core have an angle to the borehole axis in the range 40-60° which is in reasonable agreement with the orientation calculated from the radar measurements.

Centred at 145 m there is a reflection from a planar structure, D. This reflector is only seen on one side (smaller borehole lengths) of the reflector and at comparatively short distances from the borehole. The feature is also associated with a small time delay of the direct wave. The angle between the borehole and the plane is estimated at 37°. The reflection is caused by a 1 m wide brecciated zone with fractured pegmatite veins. About 0.5 m of the core consists of crushed rock. The zone is also associated with a decrease in resistivity. The fractures in this zone are hydraulically conductive, this zone constituting the most hydraulically conductive zone in the entire borehole (hydraulic conductivity 3×10^{-8} m/s). It is surprising to note that this zone, D, which is hydraulically conductive and is a crushed zone gives a much smaller reflection compared to zone C which is a brecciated zone with sealed fractures.

The most outstanding feature on the radar plot from borehole E1 is the hyperbola shaped reflection centred at 182 m. The reflection is evidently caused by a point or cylindrical shaped object with its axis perpendicular to the borehole. The distance from the object to the borehole has been calculated at 30 m. The origin of this reflection is an air filled drift at the 410 m level in the mine. The borehole is dipping slightly downwards so the closest distance between the borehole and the drift is 30 m, which is in agreement with the distance calculated from the radar measurements.

Centred at 201 m is a reflection, E, from a planar structure which is seen only to the side of shorter borehole lengths. The angle between the plane and the borehole is estimated at 51°. The reflection is caused by several thin zones of brecciation which are associated with intense fracturing.

The last reflection seen, F, is caused by a planar structure crossing the borehole at 229 m. This reflection is also associated with a time delay of the direct wave propagating along the borehole. The angle between the plane and the hole is estimated at 47°.

There is a tectonized section from 229 to 240 m containing fracture zones with marked slickensides and thin zones of mylonite. Associated with this section is also a marked decrease in resistivity along the total length. That the reflection is seen only on one side may be because the

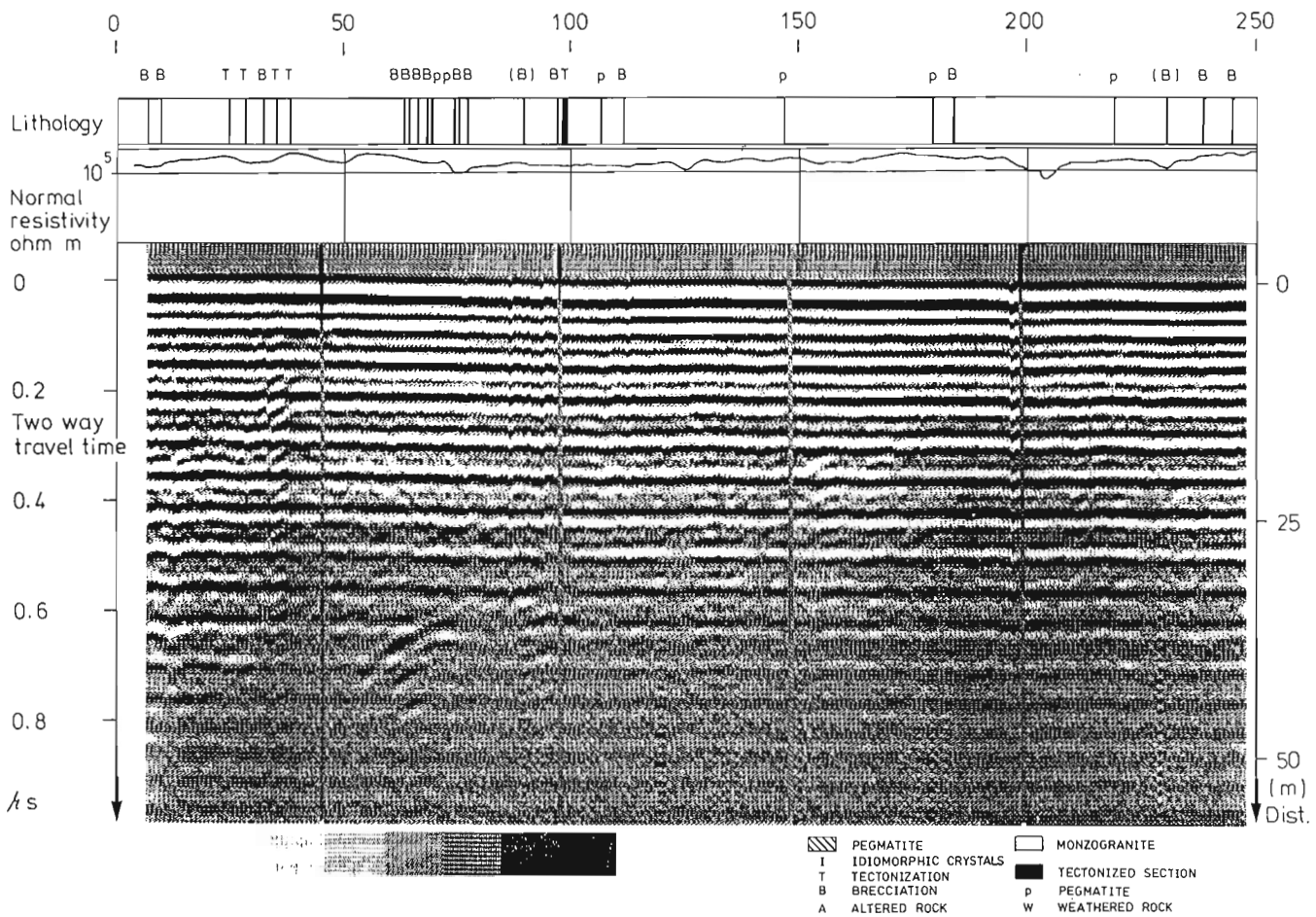

Figure 22.6. *Radar plot, tectonic log and resistivity log for the borehole N1 in Stripa. Transmitter-receiver spacing 13 m.*

reflection was obtained from only one side of this thick tectonized section. The eventual reflection from the other side is not seen because the measurement in the hole was stopped before the entire antenna array had gone far enough on the other side of the zone.

The planar reflectors found in E1 have been associated with tectonized sections of the borehole where brecciation or mylonitization and high fracturing is present. The reflectors are also associated with low resistivity conditions shown by the ordinary resistivity log. The fracture zones have also been observed in a recently drilled borehole adjacent to E1. Thus, the extension of the fracture zones outside of the borehole have been verified. The orientation of these fracture zones interpreted from the radar measurements, are in general agreement with observations in the new borehole. There are however also a few tectonized sections which cause no detectable radar anomalies, most notably the tectonized section at 38 m.

A measurement has also been made in E1 with a transmitter-receiver spacing of 23 m as shown in Figure 22.5. (Note that the time/distance scale is different from Fig. 22.4). Due to the increased transmitter-receiver separation the amplitude of the direct wave has decreased significantly and consequently the amplitude of the ringing is reduced proportionally. Thus the ringing becomes less dominant. In this diagram the same characteristic reflectors are more clearly evident than in Figure 22.4. The increased transmitter-receiver separation causes an increase in distance between the reflection limbs of reflector, C, and the small time delay caused by reflector D is widened. It is also interesting to note that the time delay associated with fracture zone B is now widened to 22 m which is approximately the transmitter-receiver separation. This indicates that the time lag is due to lower wave speed in the thin brecciated zone at 98 m rather than a change in antenna properties due to increased fracturing in the section 93-106 m. The magnitude of the time delay is approximately 6 ns, which should be compared to a total travel time of 122 ns for a transmitter receiver separation of 13 m and 219 ns for a separation of 23 m. As an example a time delay of 6 ns may be caused by a 1.4 m wide zone with a velocity two thirds of the average velocity of the granite.

Estimates have been made of the angle between the borehole axis and the fracture planes. The difference between these estimates and the estimates made for a transmitter-receiver separation of 13 m is less than 10°.

Measurements were also made as shown in Figure 22.6 in borehole N1 which is perpendicular to E1. Transmitter-receiver separation was 13 m. The rock penetrated by this borehole is also monzogranite, but the fracture frequency is much lower compared to E1. There are only a few minor zones of tectonization. On the resistivity log there are only a few small indications of low resistivity. Since there are no distinct zones of fracturing no radar reflections are seen. There are only a few weak reflectors at a distance of about 30 m from the borehole between borehole positions of 50 and 100 m. The origin of these reflections is not known.

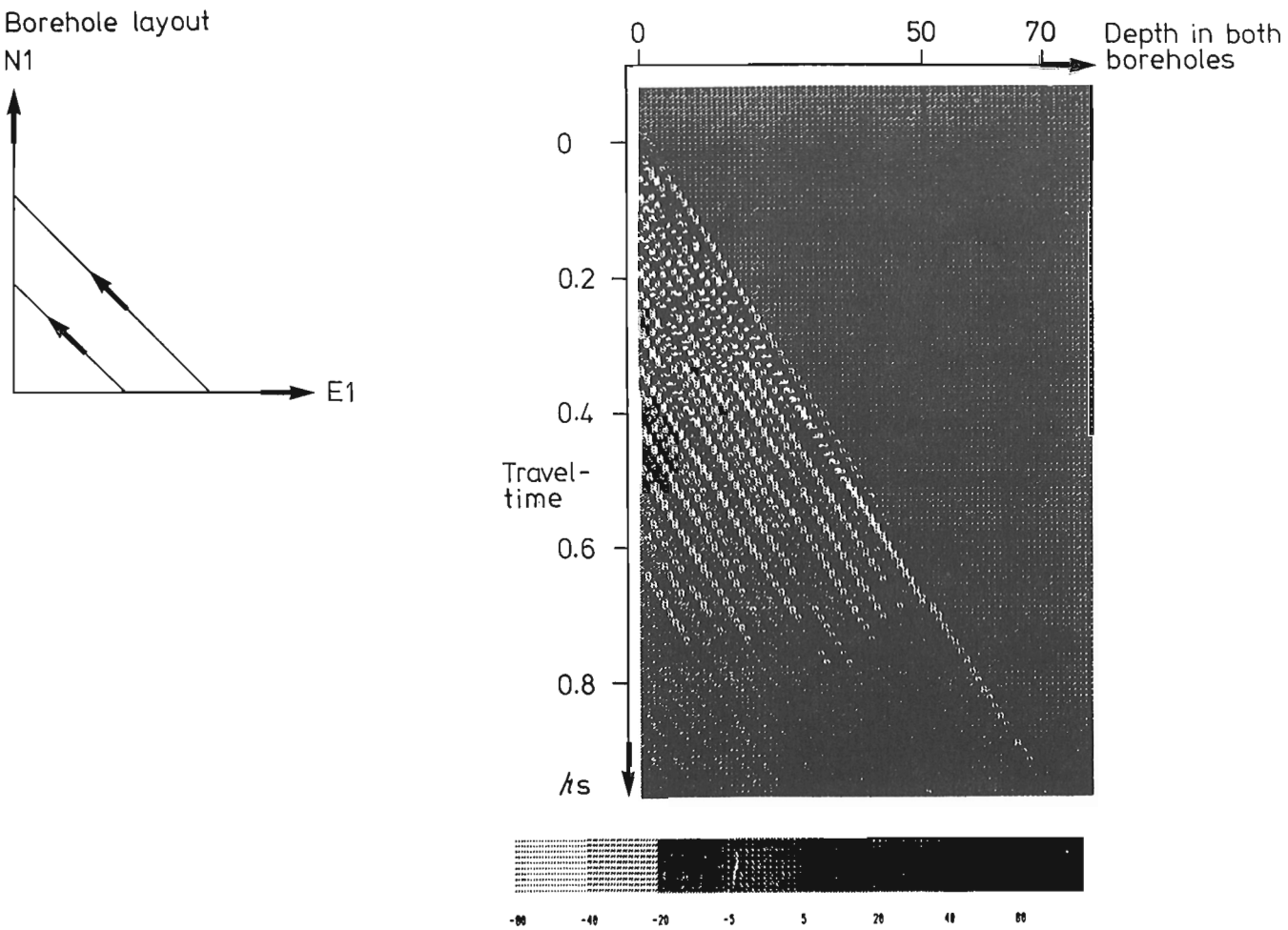

Figure 22.7. *Radar plot from the crosshole measurement between E1 and N1 in Stripa.*

A crosshole measurement was made between the perpendicular boreholes E1 and N1 as shown in Figure 22.7 The main purpose of this measurement was to obtain a time-distance calibration of the recorded data. The transmitter was put into E1 and the receiver into N1. Both transmitter and receiver were then moved in each hole simultaneously in 1 m increments. Since the holes are perpendicular, the distance between the probes is increased by 2 m between each measurement, while the relative orientation of the antennas is kept the same. This orientation gives a larger coupling between the antennas compared to when both antennas are in the same hole, consequently the amplitude of the received signal is considerably larger. Amplitude is also seen to decrease with distance. However there is a time variable gain which has not been calibrated, thus no definite conclusions can be drawn concerning the attenuation properties of the rock.

As noted from the radar plot, the time-distance curve is virtually a straight line. This indicates that there are no large low velocity zones between the boreholes to cause detectable changes in time delay. Thus the rock mass between the boreholes seem to be relatively homogeneous with respect to the propagation of radar waves.

From this crosshole experiment the velocity of the radar waves has been estimated to 106 000 km/s, which corresponds to a relative dielectric constant of 8.

Frequency analysis

To analyze the frequency content and to test some signal processing techniques, a Fourier transform has been made of the received signals. It is important to note that signals are recorded with a time variable gain where the gain is increasing with time. The Fourier transform has been made on the raw data and no correction has been made of the change of gain with time. The displayed spectrum is thus somewhat distorted.

The frequency spectrum from E1 with a transmitter-receiver separation of 23 m (Fig. 22.8) has the energy concentrated in the frequency band 10-40 MHz with peaks at approximately 19 and 35 MHz. There is also a third minor peak outside the main frequency band in about half of the recorded traces. The frequency of this peak is at 64 MHz. The observed antenna ringing evidently corresponds to the dominance of the two main frequency peaks.

It is interesting to note that the spectrum is relatively independent of the position in the borehole. Most reflections do not seem to be associated with any changes in the spectrum.

In an attempt to improve the radar images so that the reflections stand out more clearly, different signal processing techniques have been applied. Different passband, correlation, and deconvolution filters have been tested and resulted in some improvements of the radar image.

The best improvement so far is obtained by a deconvolution filter with prewhitening. The deconvolved radar plot is shown in Fig. 22.9. The improvement in the radar image is substantial, showing that the reflections previously seen with some difficulty now stand out more clearly (compare Fig. 22.5) and a few new reflections may be seen. The brecciated zone, B, only associated with a time delay in Figure 22.5 is now associated with a reflection indicating that it is a planar structure. In the deconvolved

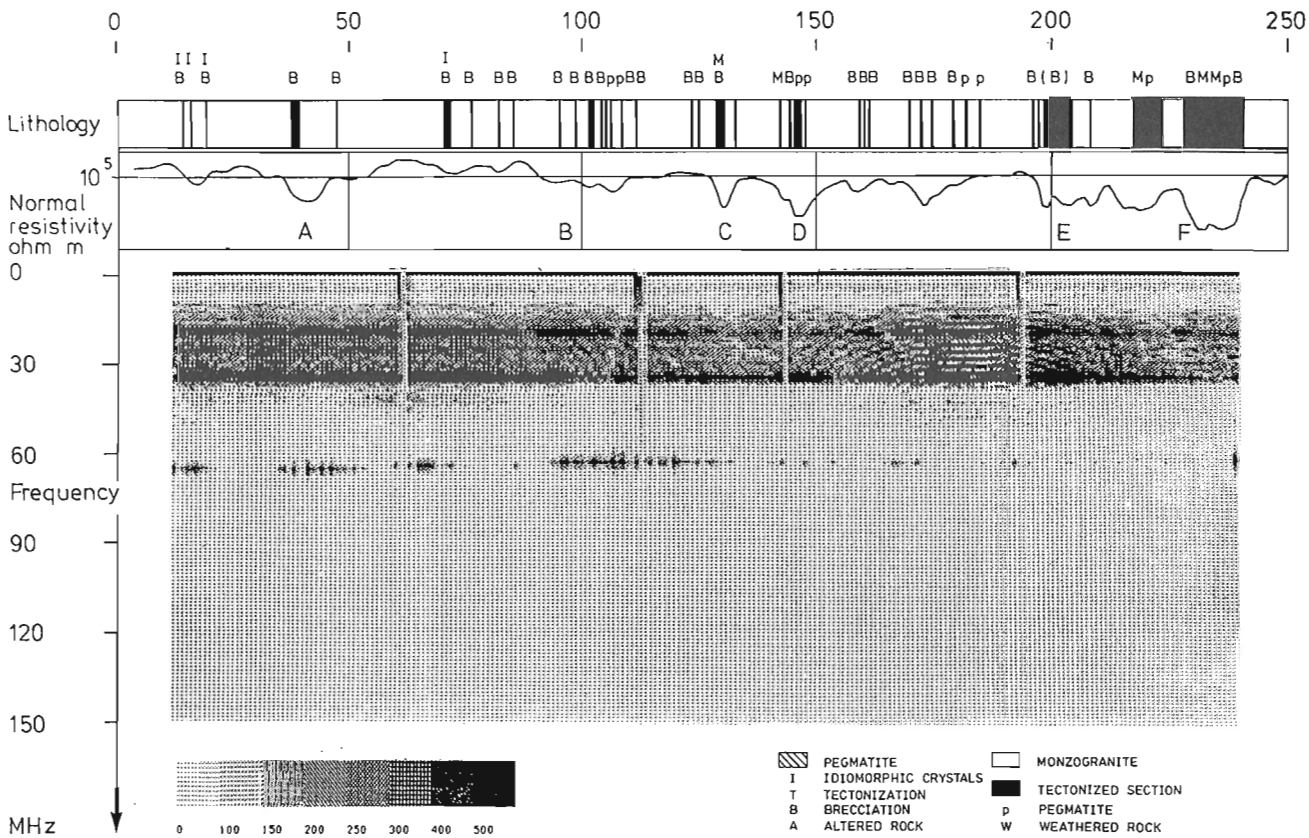

Figure 22.8. *Frequency spectrum from the radar measurement in E1 with a transmitter-receiver spacing of 23 m.*

plot, the resolution is greatly improved close to the borehole. Note that the reflections from the planar structures show a tendency to be slightly curved close to the borehole, which is to be expected from equation (2).

Concluding remarks

The experiments performed so far with the radar system have been a preliminary test of the capabilities of single-hole pulse radar for engineering purposes. Crosshole measurements have only been made for calibration purposes. Reflections from fracture zones crossing the borehole have been obtained in the granite at Stripa where there are a number of relatively well defined tectonized zones. It has also been possible to calculate the orientation of the fracture zones relative to the borehole. In the boreholes at Finnsjon, where the bedrock is generally more fractured, only a few indistinct reflections were observed.

A reflection was obtained at Stripa from an air filled drift at a distance of 30 m from the borehole and a reflection from a fracture zone was obtained after a two way travel distance of 88 m. Considering the obtained results it is estimated that the present radar system has a range of about 50 m in this type of rock.

These tests have shown that borehole radar may be a valuable tool in the mapping of fracture zones, especially in relatively high resistivity bedrock. However, studies will have to investigate what properties of the fracture zones actually cause the reflections. Possible causes of the reflections are the increased water content of fracture zones, conductive fracture minerals, or the tectonization associated with the fracture zones. Considering that the present system was designed for mining purposes rather than engineering applications the results obtained may be considered promising. With an increase in the centre frequency of the transmitted pulse it is likely that the resolution of fracture zones will be improved. A better defined pulse will also improve resolution especially close to the borehole. Increase in transmitted power and dynamic range will improve the range of investigation.

Further work with borehole radar will be performed within the framework of the OECD/NEA International Stripa Project where more emphasis will be put on the crosshole applications of pulse radar.

Acknowledgments

The main part of the project has been funded by the Swedish Nuclear Fuel Supply Co. (SKBF/KBS) while some of the final evaluations have been performed with the OECD/NEA International Stripa Project.

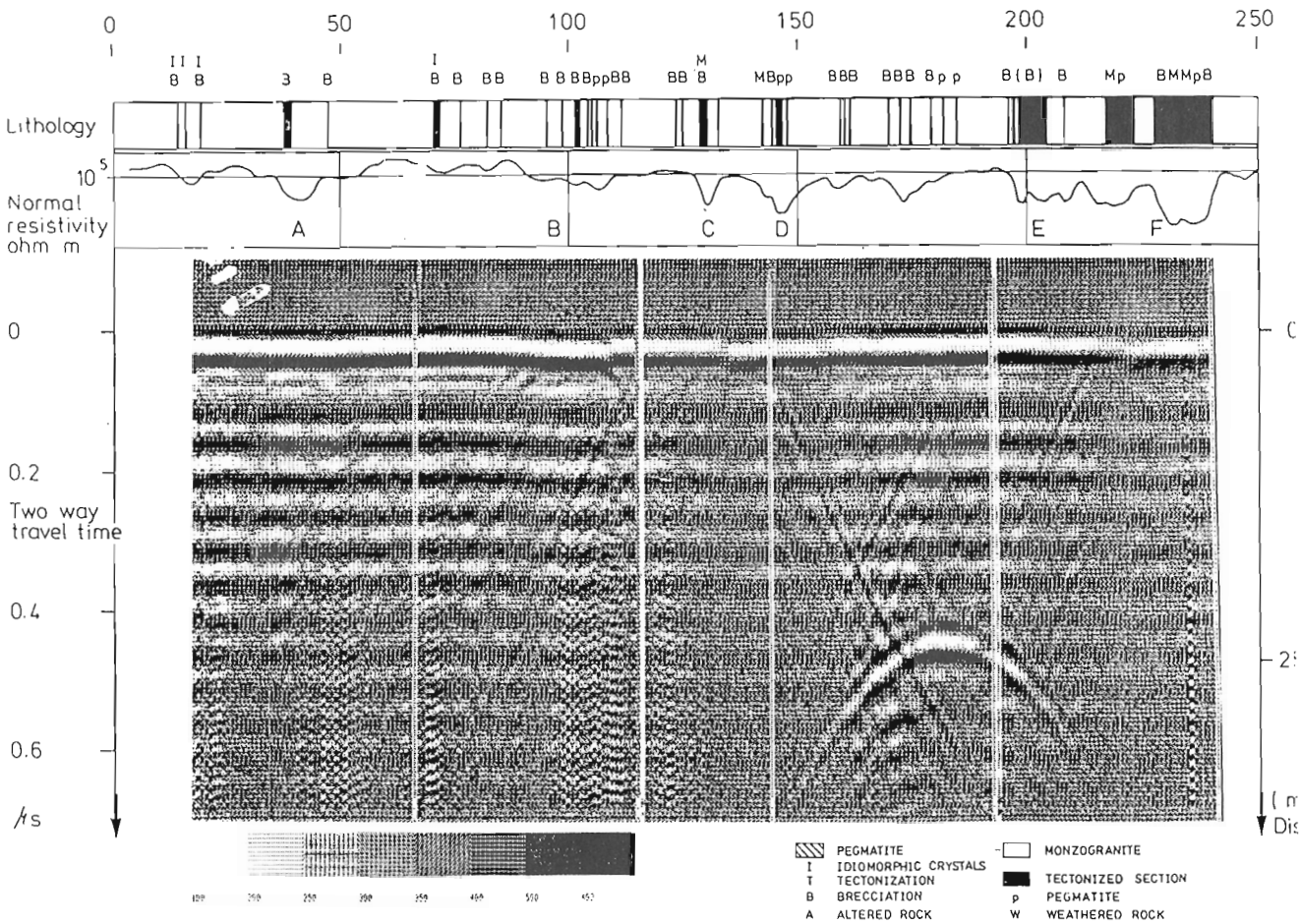

Figure 22.9. *Enhanced radar plot from E1 due to a combination of bandpass and deconvolution filtering.*

References

Carlsson, L., Gudlund, G., and Hesselstrom, B.
1983: Evaluation of the hydrogeological conditions at Finnsjon; Swedish Nuclear Fuel Co. (SKBF/KBS), Technical Report 83-56.

Carlsson, L., Stejskal, V., and Olsson, T.
1982: Core-logs of the subhorizontal boreholes N1 and E1; Stripa Project, Report 82-04.

Nickel, H., Sender, F., Thierbach, R., and Weichart, H.
1983: Exploring the interior of salt domes from boreholes; Geophysical Prospecting, v. 31, p. 131-148.

Nilsson, B.
1978: Two topics in electromagnetic radiation field prospecting; University of Lulea, Lulea, Sweden. PhD thesis 1978:03D

Nilsson, B. (cont.)
1986: A new borehole radar system; in Borehole Geophysics for Mining and Geotechnical Applications; Geological Survey of Canada, Paper 85-27, report 21.

Okada, J.T., Laine, E.F., Lytle, R.J., and Daily, W.D.
1980: Geotomography applied at the Stripa Mine in Sweden; Lawrence Livermore National Laboratory, Report UCRL-52961.

Wright, D.L. and Watts, R.D.
1982: A single-hole, short-pulse radar system; in "Geophysical investigations in connection with geological disposal of radioactive waste", OECD/NEA, Ottawa, Canada.

23. SINGLE-HOLE SHORT-PULSE BOREHOLE RADAR EXPERIMENTS AND A CROSSHOLE TRANSPONDER

D.L. Wright, R.D. Watts, and E. Bramsoe[1]

Wright, D.L., Watts, R.D., and Bramsoe, E., Single-hole short-pulse borehole radar experiments and a crosshole transponder; in Borehole Geophysics for Mining and Geotechnical Applications, ed. P.G. Killeen, Geological Survey of Canada, Paper 85-27, p. 207-216, 1986.

Abstract

We have developed a single-hole short-pulse radar system for use in deep fluid-filled or dry boreholes. Experiments using this system were conducted at the Underground Research Laboratory site of Atomic Energy of Canada Ltd. Two boreholes in granite were logged. Preliminary analysis of the data shows that the radar was sensitive to major fracture zones intersecting the boreholes, and to many lesser features as well. Besides detecting fracture zones intersecting the borehole, the system detected an anomalous zone which appears to extend from near the borehole to more than 20 m away.

To extend the capability of the radar to crosshole as well as single-hole operation, we have designed, built, and tested a borehole transponder (active reflector). The transponder triggers when a wave is incident from the radar, generating a pulse which propagates back to the radar. Unlike other time-domain crosshole radar systems, which use fibre-optic or metallic cables to establish a time reference between transmitter and receiver, the transponder requires no cables. The time reference is established automatically by the radar wave propagated through the medium. The transponder requires no modifications to the radar itself, and provides a means of simultaneously acquiring both reflection-mode and transmission-mode data if adjacent boreholes are available. The transponder is battery powered and is suspended on a dielectric rope, thus avoiding cable-guided waves which propagate on steel-armored logging cable. Field tests using the transponder yielded crosshole observations through almost 20 m of inhomogeneous and moderately lossy granite at a test site near Gold Hill, Colorado.

Résumé

Nous avons mis au point un système radar à courtes impulsions susceptible d'être utilisé dans des sondages simples, secs ou remplis de fluide. Ce système a été mis à l'essai au Laboratoire de recherches souterraines d'Énergie atomique du Canada Limitée. Deux sondages forés dans du granite ont été diagraphiés. L'analyse provisoire des données montre que le radar peut déceler les grandes zones de fractures qui intersectent les trous ainsi qu'un grand nombre d'éléments moins importants. En plus de déceler les zones de fractures, le système a décelé une zone anormale qui semble se prolonger à plus de 20 m du sondage.

Afin de pouvoir utiliser ce système dans les travaux effectuées dans un seul sondage et dans plus d'un sondage, nous avons conçu, construit et mis à l'essai un transpondeur (réflecteur actif), qui est déclenché lorsqu'il est touché par une onde provenant du radar, et produit une impulsion qui se propage jusqu'au radar. Le transpondeur n'utilise pas de câble, contrairement à d'autres systèmes radar à domaine temporel qui servent à étudier plus d'un sondage à la fois et qui emploient des câbles métalliques ou des câbles en fibres optiques pour établir un temps étalon entre l'émetteur et le récepteur. Ce temps étalon est établi automatiquement par l'onde radar qui traverse le matériau. L'utilisation du transpondeur n'exige aucune modification du radar et offre un moyen d'obtenir simultanément des données en mode réflexion et en mode transmission dans les sondages contigus. Le transpondeur est alimenté par piles et suspendu à un câble diélectrique, ce qui évite la création d'ondes qui se propagent le long des câbles de carottage à armature d'acier. Des essais pratiques effectués à l'aide du transpondeur dans plus d'un sondage ont donné des observations dans presque 20 m de granite hétérogène et plus ou moins dissipatif à un emplacement près de Gold Hill, au Colorado.

[1] United States Geological Survey MS 964, Box 25046, Federal Center, Denver, Colorado 80225, USA

Introduction

Borehole geophysics is widely used to study potential nuclear-waste disposal sites. However, many of the standard borehole logging techniques gather information from only a thin cylindrical region around the borehole. It is desirable to gather information from a larger volume around a borehole and to do it with high resolution. High frequency electromagnetic techniques, such as radar, offer good resolution and can have reasonable range in high resistivity, relatively homogeneous media. Attenuation of electromagnetic waves may arise from inhomogeneities in the dielectric permittivity, which scatter energy, and from ohmic losses due to electrical conductivity of the medium. Ohmic losses are generally controlled mainly by the amount of pore water in the material. A nuclear waste host rock material, however, should be relatively dry and homogeneous. Thus, high frequency electromagnetic methods may be expected to be useful in waste repository studies. Seismic waves at kHz or higher are also useful for such studies; they offer comparable resolution and range and are complementary to radar in that they respond to different physical properties.

Because the electrical properties of proposed host media for nuclear waste repositories are often favorable for use of high frequency electromagnetic waves, the United States Geological Survey designed and built a prototype borehole radar system for use in deep fluid-filled or dry boreholes. Although the system design assumed that the radar would be used in salt, to date only tests in granitic rocks have been conducted. Early tests were made at sites at

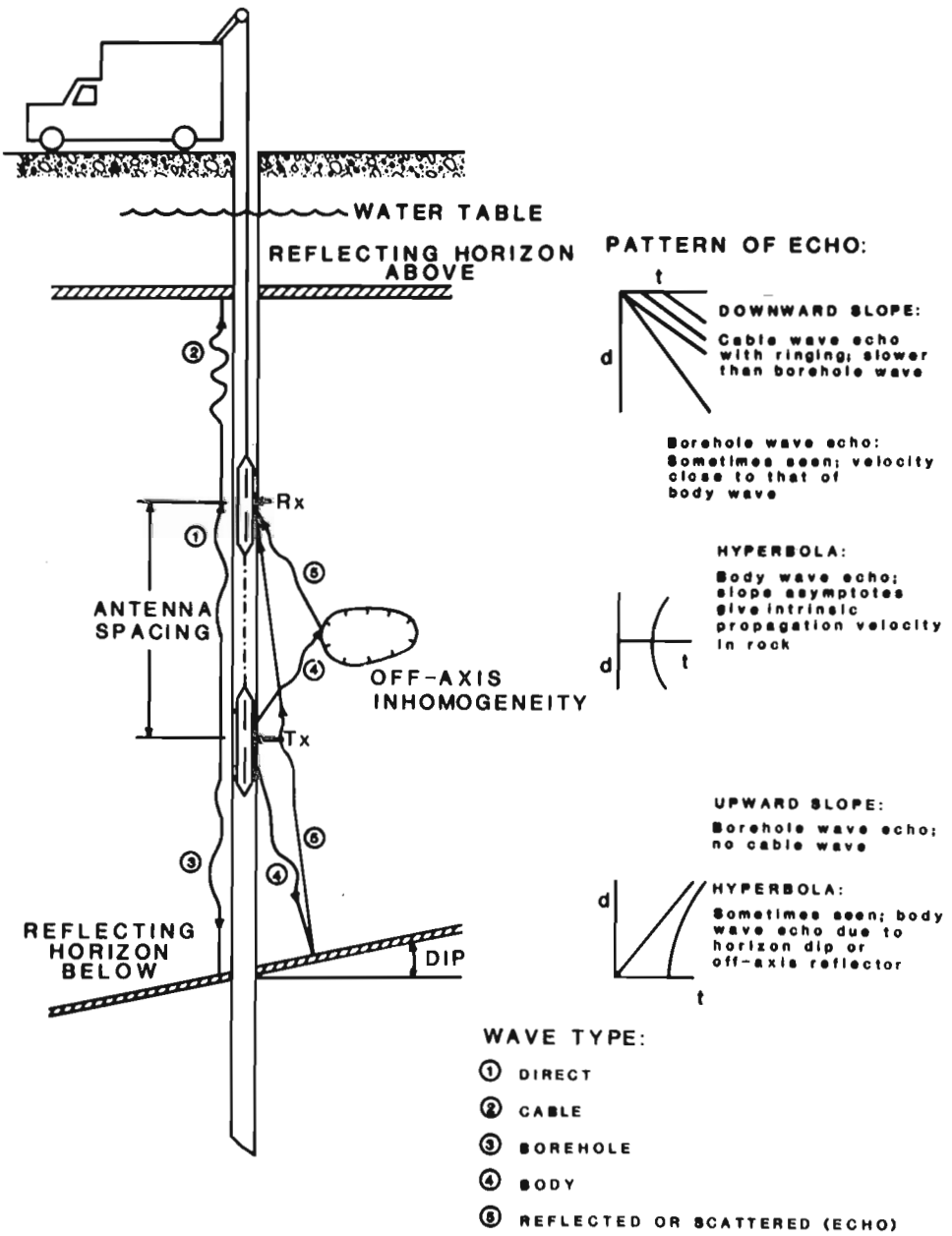

Figure. 23.1. *The borehole radar system transmits short pulses of electromagnetic energy. When an inhomogeneity is present, some of the incident energy is backscattered to the receiving antenna. Some of the transmitted energy will be guided along the cable and borehole. Possible echo patterns from various kinds of reflectors are shown in the right-hand part of the figure.*

Gold Hill and Idaho Springs, Colorado. These tests demonstrated that the radar was functioning, but were not suitable for performance evaluation because the rock is inhomogeneous and comparatively lossy at the radar operating frequencies and because geophysical logs for comparison purposes were not available from these sites. The Underground Research Laboratory (URL) site of Atomic Energy of Canada Ltd., near Pinawa, Manitoba, had suitable boreholes in which geophysical logs had been run. Radar tests were performed in two boreholes at the URL site in August 1983.

If more than one borehole is available, crosshole experiments are desirable. In short-pulse crosshole experiments a time reference is necessary between the transmitter and receiver. Usually this reference is provided through fibre-optic or metallic cables. The radar system which we developed is operated on a 2000 m long 7-wire steel-armored logging cable. The bandwidth characteristics of this cable are too poor to pass fast timing pulses up and down the cable. For this reason, it appeared that the existing system was not capable of crosshole work without a different cable. However, we conceived, built, and tested a borehole radar transponder which circumvents the need for a timing cable and permits simultaneous acquisition of single-hole reflection-mode and crosshole transmission-mode data. The borehole transponder senses the arrival of the wave transmitted by the radar pulser and sends a similar signal back to the radar receiver. Field tests using the transponder yielded crosshole observations through nearly 20 m of inhomogeneous lossy granite at Gold Hill, Colorado.

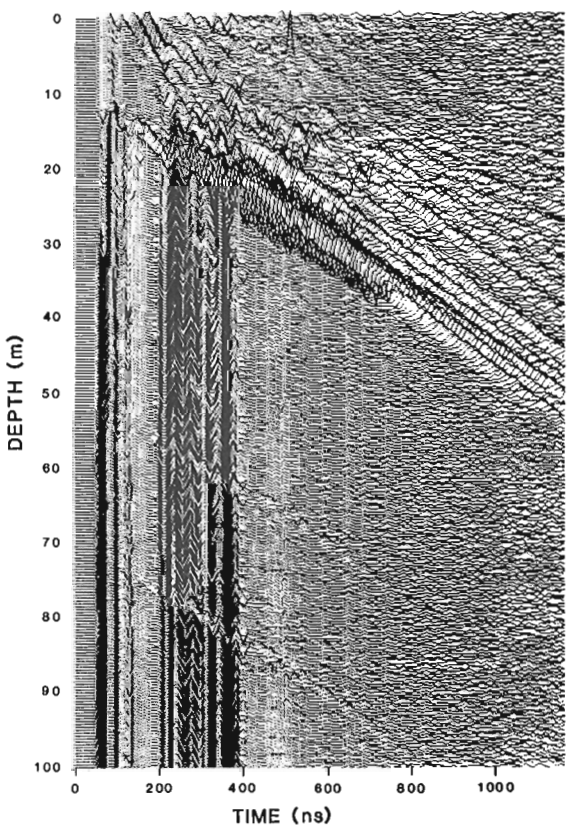

Figure 23.2. Data from URL borehole M8. Antenna spacing = 3 m. The depth is from the top of the borehole casing to the top of the radar. The vertical stripe which begins at approximately 49 ns represents the directly coupled wave from the transmitting antenna. The change noted at about 12 m depth is due to the entry of the radar probe into water in the borehole.

Borehole radar

The borehole radar system shown in Figure 23.1 uses identical, but separate, transmitting and receiving antennas. Each antenna is a 1.5 m long resistively loaded electric dipole. The transmitting antenna radiates a short electromagnetic pulse. Ideally, the pulse would be a single cycle of a sine wave, but ringing usually persists for some time due to imperfect antenna damping, coupling between antennas, and reflections from the ends of the probe body. The peak of the power spectrum is probably between 20 MHz and 30 MHz, but we have not yet transformed our data into the frequency domain. If the radiated pulse encounters a region whose permittivity or conductivity differs from that of the surrounding medium, some of the energy will be back-scattered to the receiving antenna. If the back-scattered energy is sufficient, the presence of the inhomogeneous region will be detected in the received waveform. The time between the transmitted pulse and the received return may be converted to range if the propagation velocity in the medium is known or measured.

Figure 23.1 shows wave types and propagation paths that may occur with borehole radar, and the character of the echos that are produced by various reflectors. Cable and borehole waves are guided waves which may be excited by the transmitter and propagate along the borehole. The differences between the two types of waves are in the axial propagation velocity, attenuation, and spatial distribution of the electromagnetic field in the surrounding rock. Since the borehole is small compared to a wavelength in the rock, the

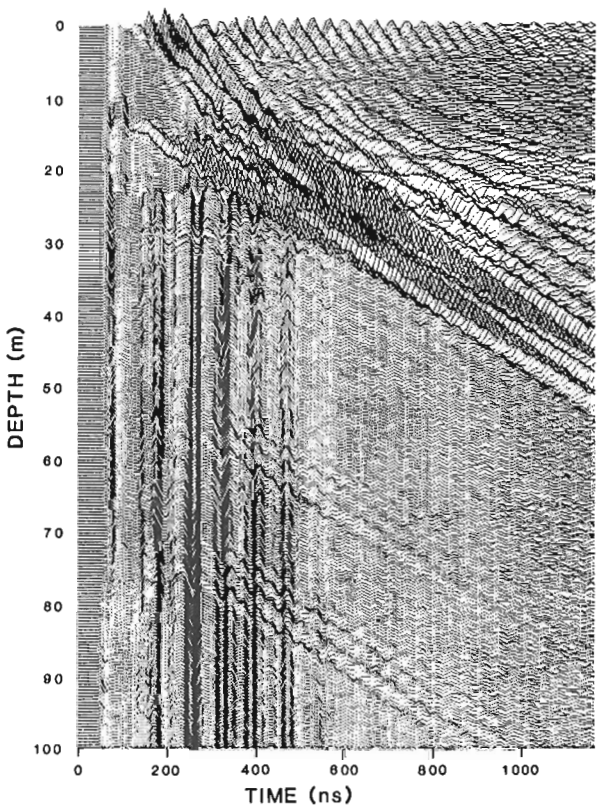

Figure 23.3. Data from URL borehole M8. Antenna spacing = 5.4 m. The increased spacing reduces direct antenna coupling and permits the operator to select a higher gain setting on the receiver. The results are increased sensitivity to reflections, but more pronounced oscillatory ringing.

propagation velocity of borehole waves is only slightly slower than the intrinsic propagation velocity in the rock. Cable waves, on the other hand, propagate considerably more slowly and do not occur without a centre conductor such as the steel-armored logging cable. The direct wave is a borehole guided wave from the transmitting antenna to the receiving antenna. Multiple reflections often occur between the ends of the probe body and perhaps between the antennas. The multiple reflections occur later in time than the direct wave arrival. Examples of multiple reflections are shown in Figures 23.2 and 23.4. The direct wave arrival and following reflections are referred to as "direct wave coupling." Body waves are waves which are not bound to the borehole guiding surface, but propogate in the body of the rock. If a wave of any type encounters a discontinuity in electrical properties, energy will be reflected or scattered from the discontinuity. Reflected or scattered energy detected by the receiver will produce characteristic patterns in a time-depth plot (which has an appearance much like that of a borehole seismogram) depending on the nature and location of the reflector or scatterer. The patterns in the time-depth plot are often loosely and interchangeably referred to as "reflections," "returns", or "echos". The right side of Figure 23.1 depicts patterns which will be produced by three types of reflectors or scatterers. A reflecting horizon above the radar will produce a downward-sloping echo. Reflecting horizons below the radar will produce upward-sloping echos. Dipping horizons and localized off-axis inhomogeneities will produce hyperbolas. The downward-sloping echos are generally cable waves which have a distinctly slower velocity than the upward-sloping borehole waves, but in echos from some horizons above the radar both cable and borehole waves may be seen.

The transmitting and receiving antennas are housed in tubular fiberglass-epoxy pressure vessels 114.3 mm in diameter. The antennas may be in one continuous tube 4.9 m, 6.1 m, or 7.3 m long, or placed in two separate tubes an arbitrary distance apart. The timing signals between the receiver and the transmitter are passed through a fibre-optic link. The transmitter is battery powered, so that no metallic cables run between the transmitter and the receiver. When the radar is configured in two parts, the transmitter is suspended from the receiver by a dielectric rope. Avoidance of a metallic cable between the antennas reduces, but does not eliminate, coupling between the antennas in the borehole. The direct wave between antennas should be minimized to avoid saturating the receiver preamplifier and masking desired reflection signals. However, the direct wave can provide useful information about the borehole wall material.

The radar system communicates to the surface through a standard 7-wire logging cable. The measured frequency response of the cable indicated that signals with frequency content to about 1 kHz could be passed through the cable with little distortion, but serious attenuation and cross-talk

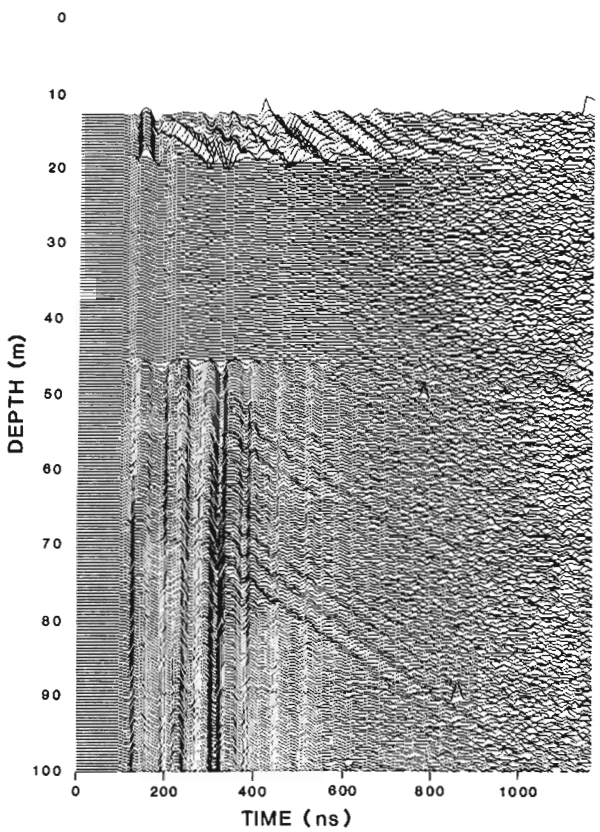

Figure 23.4. *Data from URL borehole M8. Antenna spacing = 7 m. On this log the radar antennas were packaged in physically separate tubes, as opposed to a single continuous tube. Timing pulses were passed between receiver and transmitter by means of a fibre-optic cable. Segments from 0 m to 11 m and 17 m to 44 m are missing or deviant due to an electronics malfunction. In other respects this log is similar to the log shown in Figure 23.3 with a minor improvement in the oscillatory ringing due to reduced antenna coupling.*

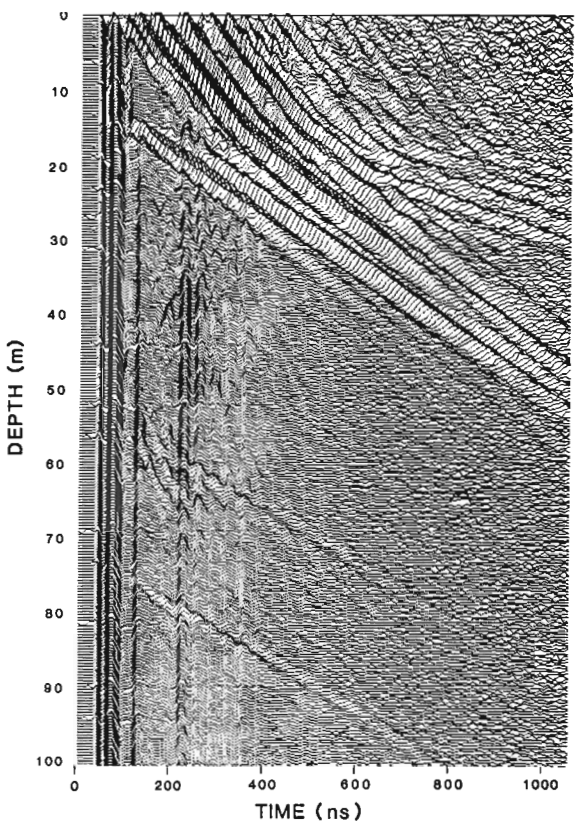

Figure 23.5. *Data from URL borehole M8. Antenna spacing = 20 m. These data were obtained with separate tubes as in Figure 23.4, but with increased separation. The directly coupled wave and following ringing is diminished relative to the desired reflections. Subtle features of reflections are visible in this log which can not be seen in the previous logs.*

between wires occurred at frequencies as low as 2 kHz. For this reason it was decided not to attempt to pass fast timing pulses or digitized data pulses through this cable. Rather, the radio frequency (RF) signal is sampled downhole as in a sampling oscilloscope and an audio frequency replica of the repetitive RF signal is transmitted through the cable to the logging truck for recording.

Recording is currently done on an analog FM instrumentation tape recorder. Digitization and processing is done as a separate step, but a real-time digital data acquisition system is being developed.

Further details and estimated theoretical limits for this radar system are given by Wright and Watts (1982). A similar system operated in dry salt has produced recognizable reflections at ranges of up to 600 m (Nickel et al., 1983).

Experiments at the underground research laboratory

Initial tests of the radar system were made in shallow (50 m) boreholes in inhomogeneous granite at sites near Denver, Colorado. These tests were useful, but not adequate to fully evaluate the performance of the radar in granites which might be acceptable for nuclear waste repositories.

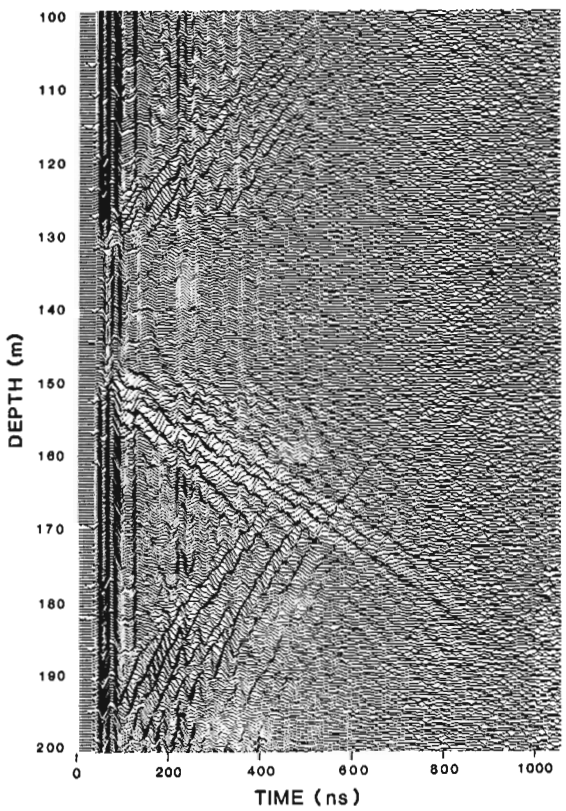

Figure 23.6. *Data from URL borehole M8. Antenna spacing = 20 m. In this part of the log the response from a known fracture zone may be seen. The transmitting and receiving antennas staddle the zone from 130 m to 150 m. The direct wave is diminished in amplitude in this zone. Reflections from the top side and bottom side of the fracture zone result in upward and downward-sloping signatures. Two distinct downward slopes may be seen indicating the presence of both a cable wave and a borehole or body wave. The fact that the positive and negative slopes generally differ in magnitude is attributed to the effect of the steel-armored cable on wave propagation along the borehole.*

A more suitable site was sought and, in August 1983, we were granted access to several 152.4 mm diameter boreholes in granite at the Underground Research Laboratory of Atomic Energy of Canada Ltd. near Pinawa, Manitoba. We logged boreholes M8 and M9 which are 400 m and 350 m deep, respectively.

The URL tests had three objectives. First, we wanted to try the radar in deeper fluid-filled boreholes to see what operational and mechanical difficulties might be encountered. Second, we wanted to study the effects of various antenna separations and packaging on radar performance. Third, we wanted to correlate our radar logs with other geophysical logs to see how well our radar system could detect known geological features and whether it might detect features missed by other techniques.

We found that the fiberglass-epoxy pressure vessels withstood the hydrostatic pressure (3900 kPa), and no "O" ring failures occurred. One electronics failure occurred that was repaired in the field. We experienced several fibre-optic cable failures. Modifications involving a different type of fibre-optic cable will be required before the system can be considered to be reliable.

Borehole M8 was logged with the radar in four different configurations. In the first configuration the antennas were housed in a single continuous pressure vessel 4.9 m long with 3 m between antenna centres. In the second configuration the antennas were in a continuous pressure vessel 7.3 m long with a 5.4 m antenna spacing. In the third configuration each antenna was housed in a separate pressure vessel 2.5 m long

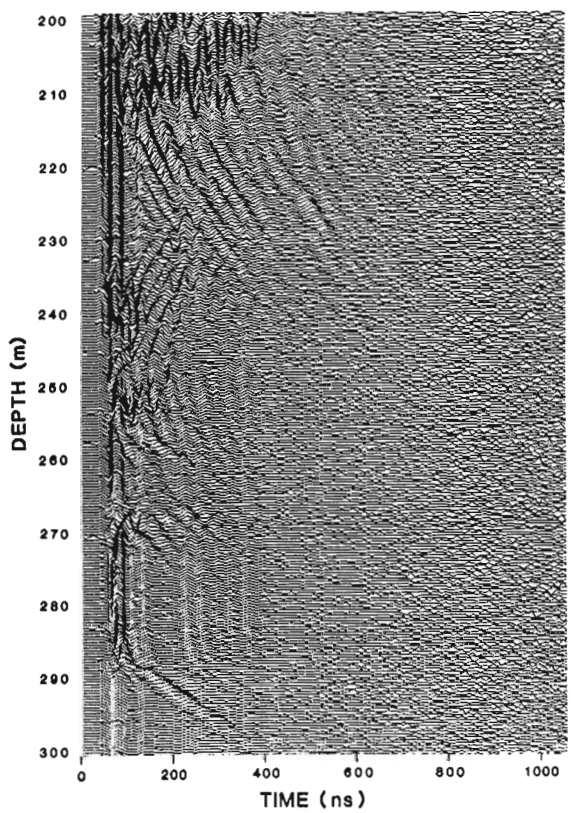

Figure 23.7. *Data from URL borehole M8. Antenna spacing = 20 m. In the 200 m to 300 m segment of the log a number of responses occur. A distinct change in the strength of the direct wave occurs at an indicated depth of 288 m. The rock below this depth attenuates waves more strongly than that above the boundary.*

with a 7 m antenna spacing. In the fourth configuration the antennas were in separate pressure vessels with a 20 m antenna spacing. Pressure vessel lengths are significant because both the pressure vessels and the antennas will influence borehole-guided waves and the transmitter-receiver coupling. Figure 23.2 shows data obtained with the antennas spaced 3 m apart. Figure 23.3 shows data obtained with a 5.4 m antenna spacing. In Figures 23.4 and 23.5 the data were obtained with the antennas housed in separate pressure vessels with antenna spacings of 7 m and 20 m, respectively. All data in Figures 23.2 through 23.5 were obtained in borehole M8. The numbers along the left margin indicate the depth in metres in the borehole measured from the top of the borehole casing to the top of the radar probe. These depths are only approximate and are based on an assumed constant logging speed. (The electronic depth encoder on the draw works failed intermittently and could not be relied on.) The horizontal axis represents time. In these figures, the vertical stripes near the left side represent the direct wave from the transmitting antenna and subsequent reflected waves between antennas and pressure vessels. Our objective was to maximize the sensitivity of the radar to returns from inhomogeneities that are off the borehole axis while minimizing the direct wave coupling between the antennas.

We concluded that the greatest antenna spacing that we tried was better than the smaller spacings. This is not unexpected, since antenna coupling decreases with increasing antenna separation. Antenna coupling in boreholes depends on frequency, borehole diameter, the electromagnetic properties of the surrounding rock and borehole fluid, the diameter, length, and electrical properties of the insulating tube, antenna characteristics and separation, and type of electromagnetic wave suppressors which may be used between the antennas. Although many of these factors can be addressed theoretically, the total problem depends on so many variables that precise analysis is difficult. In particular, the performance of a borehole radar system may depend as heavily on the environment as on the system.

Since the best results were obtained with the greatest antenna separation, we concentrate on that data set for further discussion. Figure 23.6 shows the 100 m to 200 m segment, Figure 23.7 shows the 200 m to 300 m segment, and Figure 23.8 shows the 300 m to 375 m segment. Besides the vertical stripe near the left margin representing the arrival of the direct wave, the prominent elements in the data are the approximately straight lines sloping downward and upward. The downward-sloping features are caused by reflections off the bottom side of fractures, and the upward-sloping features are caused by reflections from the top sides. The asymmetry in slopes is because the radar probe has the steel-armored logging cable above it, but no cable beneath it. A metallic cable supports a mode of propagation along the borehole that is not possible where there is no cable (i.e., below the radar probe). We have tested several devices to suppress these cable-guided waves, but none was used here.

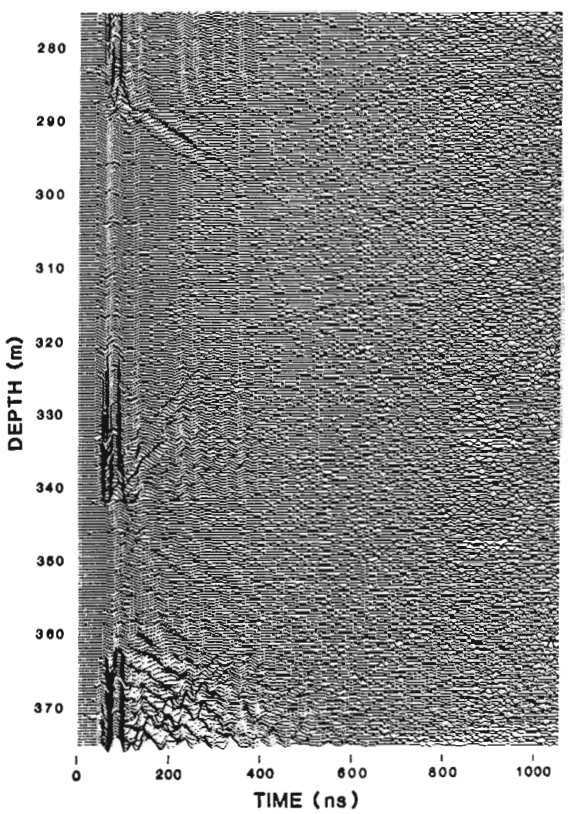

Figure 23.8. *Data from URL borehole M8. Antenna spacing = 20 m. In the 300 m to 342 m part of this segment the directly coupled wave gradually increases. A second known fracture zone causes the wave to abruptly drop in amplitude and be delayed in time in the 342 m to 362 m section.*

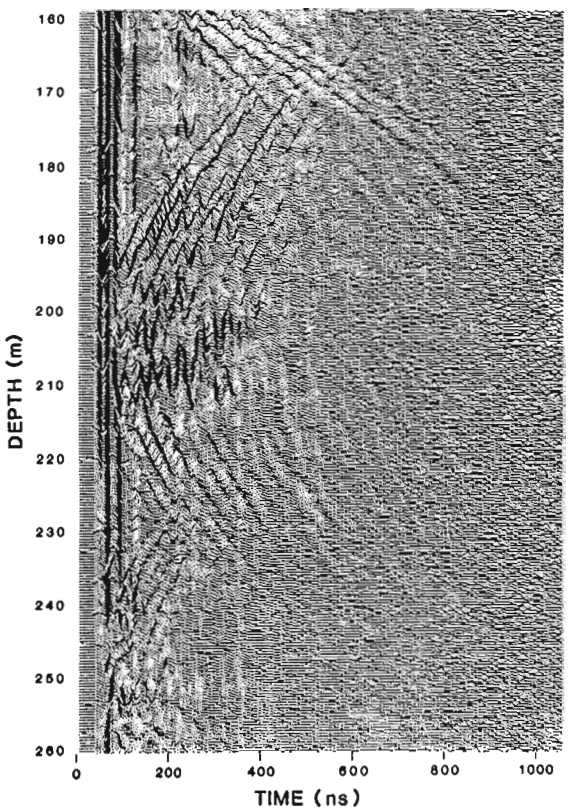

Figure 23.9. *Data from URL borehole M8. Antenna spacing = 20 m. This segment of data is dominated by the wide curving feature centered at an indicated depth of 205 m. It is not clear from the data whether the anomaly causing this feature intersects the borehole, or just comes close. The signature of the anomaly persists for more than 350 ns, indicating that the anomaly may extend to a distance of more than 20 m from the borehole. An acoustic televiewer log of this zone does not show fractures intersecting the borehole, and standard geophysical logs do not indicate a major anomaly.*

The cable wave turned out to be a fairly sensitive means of detecting fractures that intersected the borehole. The velocity calculated from the downward slope is neither the propagation velocity of the rock nor that of water, but depends on both as well as on the diameter of the cable and the borehole. The velocity calculated from the upward-sloping features is essentially the propagation velocity in the rock mass. Since the winch speed could not be held precisely constant, and because the electronic depth encoder was unreliable, velocities calculated from the slopes of echos in this data set are only approximate. Propagation velocities ranging between 139 m/μs and 123.5 m/μs were calculated from the data. These velocities correspond to relative permittivities ranging between 4.7 and 5.9. It is thought that the variations are mainly due to winch speed variations rather than actual changes in the rock permittivity. At a velocity of 123.5 m/μs, a return at 1000 ns would correspond to a reflector distance of 62 m.

The strong echos at depths of up to 50 m in Figures 23.2 through 23.5 are reflections from the top of the water column at about 12 m depth, and from the top of the borehole. Electrical, acoustic, nuclear, and caliper logs indicate two major fracture zones intersecting borehole M8. The radar responds strongly to these fracture zones at depths of 130 m to 150 m (Fig. 23.6) and 342 m to 362 m (Fig. 23.8). The 20 m apparent thickness of the zones is due to the separation between transmitting and receiving antennas, and does not represent the true thickness of the fracture zone. The thickness of the zones to which the radar is responding is difficult to determine from these logs since the thickness is probably much less than the antenna separation. The true depths (if our depth scale were accurate) would be about 151 m and 363 m. Whenever the transmitting and receiving antennas are on opposite sides of a fracture, the direct wave is usually diminished. In addition, the direct wave is often noticeably slowed, as may be seen in the 130 m to 150 m data. Both effects are probably caused by water in the fracture zone.

The radar also responds to gradual changes in electrical resistivity of the rock as indicated by the gradual increase in amplitude of the direct wave in the 310 m to 340 m section. This increase correlates with gradually increasing DC resistivity in the rock as measured by conventional electrical resistivity logs, and probably indicates a decrease in the amount of pore water in the rock.

The curving echos centred at about 205 m in Figure 23.9 appear to be caused by an inhomogeneity that does not intersect the borehole. The conventional logs show nothing unusual at this location, nor does an acoustic televiewer log show any fractures in this zone. The time duration of the return from this anomalous zone indicates that it extends to over 20 m from the borehole axis. We speculate that this zone may contain a vertical pegmatite, a xenolith with relatively vertical faces, or block fractures with some vertical facets. The major importance of this feature is that it demonstrates the capability of radar to detect off-axis anomalies tens of metres from the borehole that would not be observed by standard geophysical logs.

Crosshole transponder

In cases where two adjacent boreholes are available, it is desirable to do crosshole studies of the intervening material. Because of the design of our single-hole radar system it was thought that crosshole data could not be obtained with that system without extensive modifications and a new cable. However, we have developed a borehole transponder (Fig. 23.10) which, in many cases, will allow both single-hole and crosshole data to be simultaneously acquired

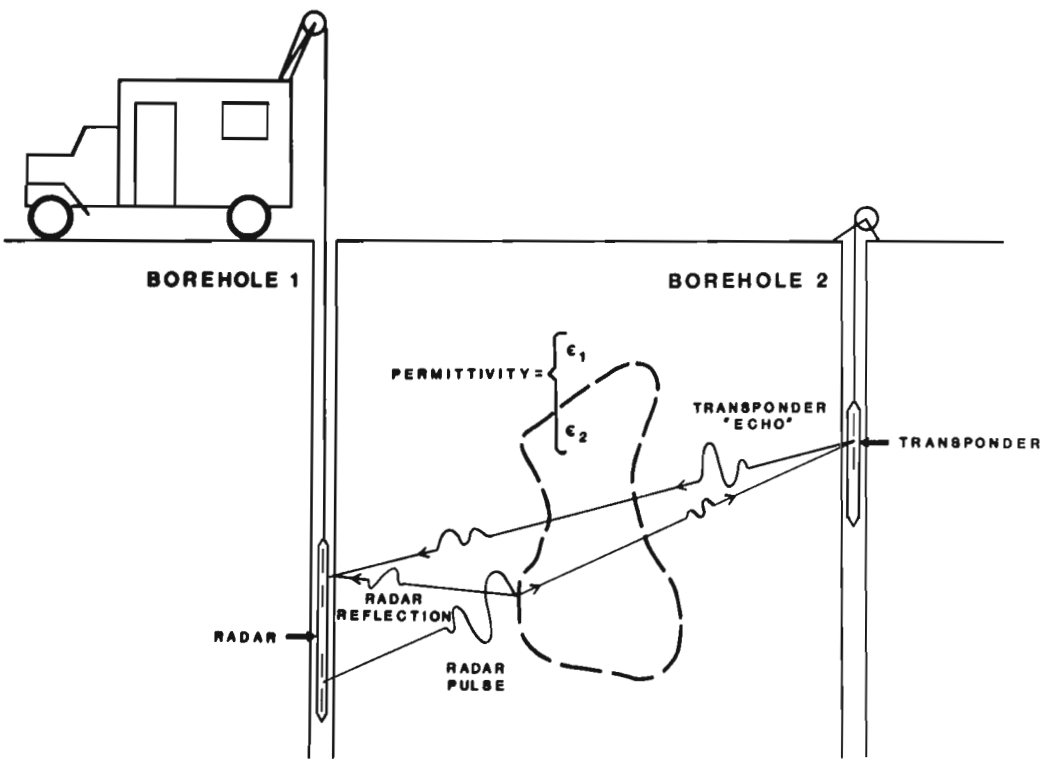

Figure 23.10. *A borehole transponder extends the capability of a short-pulse radar system so that both single-hole and crosshole data may be acquired simlultaneously. Since the transponder transmits when it senses a signal incident from the radar, the requirement for a timing cable in the transponder borehole is eliminated.*

with no modifications to the radar itself. The transponder may be thought of as an active reflector. When a wave is incident from the radar, the transponder is triggered and generates an "echo" which returns to the radar receiver and is recorded. The incident signal at the transponder input terminals may be millivolts in amplitude, whereas the pulse at the transponder output antenna terminals is about 1 kV. Thus, the ratio between the incident and returned signal can be as much as 120 dB. This amplification greatly enhances the ability of the radar to detect and characterize inhomogeneities between two boreholes.

The transponder shown schematically in Figure 23.11 requires no sampling or timing circuits. It consists simply of two antennas, an amplifier, a pulser, a battery pack, a multivibrator, and a diode-bridge clipper circuit. The monostable multivibrator serves two functions: first, it triggers the pulser; second, it blocks any further inputs which might trigger the pulser by remaining in its quasi-stable state for a pre-set period. This feature ensures that antenna transients from the transponder pulser have decayed to very low levels before another trigger pulse is accepted. Otherwise, the transponder will go into spontaneous and perhaps self-destructive firing. The diode-bridge clipper circuit protects the video amplifier from high-voltage transients when the pulser fires. Low amplitude signals are passed unhindered by the diode-bridge circuit. The transponder is housed in a dielectric tube, is battery powered, and is suspended on a dielectric rope. Because metal cables are not present, cable-guided waves in the transponder borehole are avoided.

Since the transponder operates by sensing an incident signal and returning a similar but larger signal, the electronic delay time between transponder excitation and response must be known if absolute propagation time is important. In many cases relative times are sufficient. The measured electronic delay time is 40 ns if the incident signal is large, but is amplitude dependent for small signals, and may increase to as much as 50 ns for signals at the limit of detection. For signals of a given amplitude the delay time is consistent, so jitter is not a problem. The maximum 10 ns difference would amount to a range error of 0.75 m in a medium having a relative permittivity of 4, less if the permittivity is higher. In one sense the change of delay time with amplitude is a source of error, but it might also be used to indicate cases where the propagation path attenuation changes spatially.

The sensitivity of the transponder video amplifier cannot be increased without limit, particularly since pulsed systems are wideband systems. The particular video amplifier we employ has external gain select pins, a maximum gain of 52 dB, and a bandwidth of 120 MHz. When tests in air were conducted near Denver, the presence of television and FM radio stations generally made it necessary to operate the transponder with reduced sensitivity. In boreholes, the maximum available sensitivity was sometimes used successfully. Care must be taken to avoid internally generated electronic noise. For example, switching dc-to-dc converters often radiate sufficiently, even when filters are added to their terminals, to preclude their use in this application. All voltages, including the high voltage for the pulser, are derived directly from batteries. The maximum range at which the transponder will be usable depends on the radiated power from the radar, the length and radiation pattern of the antennas including any cable and borehole fluid effects, the attenuation of the intervening material, and the maximum gain of the transponder amplifier which can be tolerated without spurious triggering. The incident signal from the radar must substantially exceed background levels for the transponder to trigger properly.

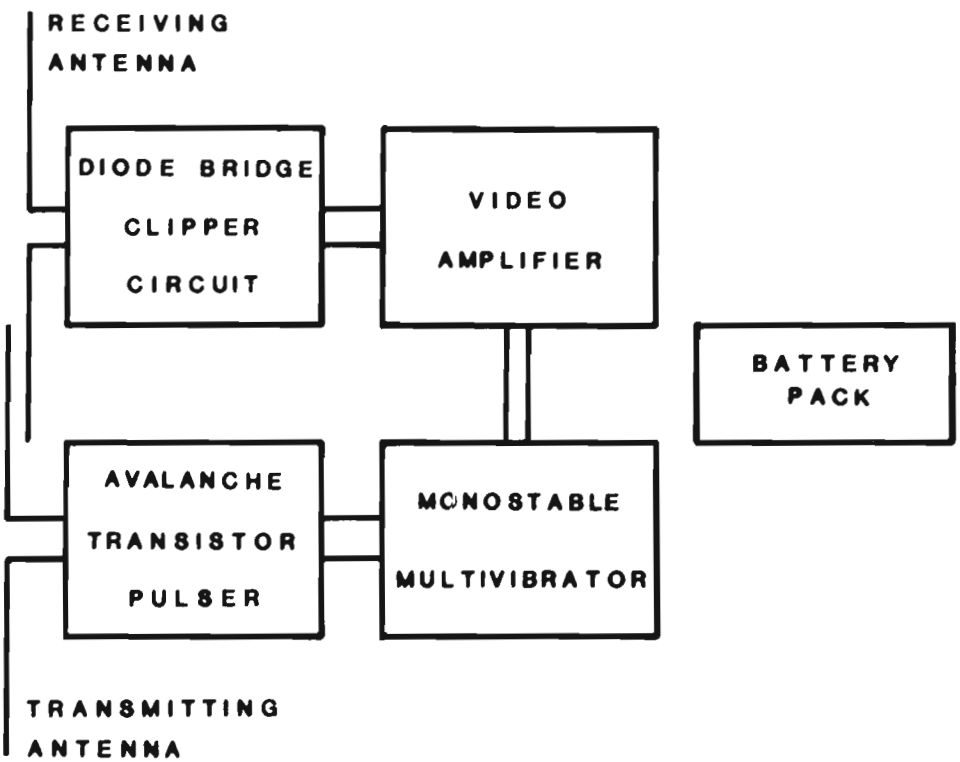

Figure 23.11. *The transponder consists of only four electronic functional blocks. All power is derived from batteries to minimize internally generated electronic noise.*

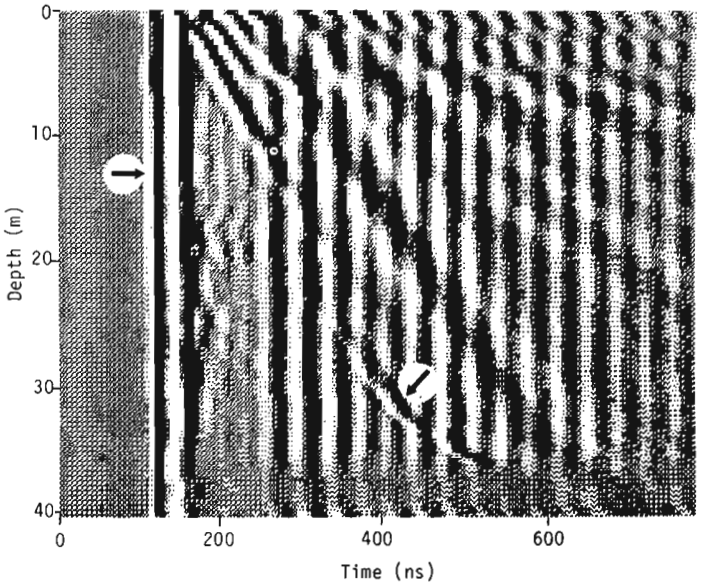

Figure 23.12. *Density plot of raw data when transponder is at fixed depth and radar is in motion. The indicated depth refers to the depth of the radar in the borehole. The time axis may be converted to distance if propagation velocity is known. The data sampling begins prior to the arrival of the direct wave from the radar transmitter to receiver, indicated by the horizontal arrow. Strong oscillations, resulting in the vertical stripes, largely obscure the transponder return indicated by the diagonal arrow.*

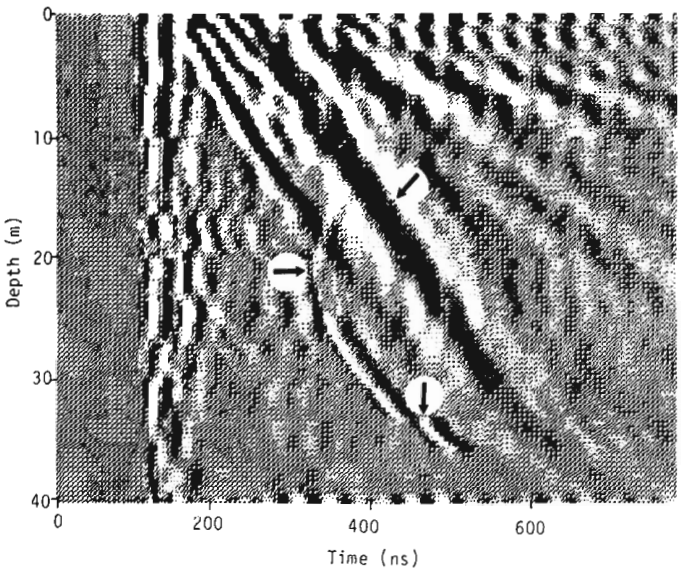

Figure 23.14. *Data derived from Figure 23.12 by subtraction of the average of all the waveforms. The vertical stripes are largely removed. The broad diagonal band, indicated by the diagonal arrow, is caused by the part of the radar signal that couples to the cable resulting in waveguide-mode propagation up to the borehole, reflecting at the surface, and propagating back down. The transponder signal, indicated by the horizontal arraw, is more evident. The vertical arrow points to a jump in time which may be caused by a zone with slower velocity.*

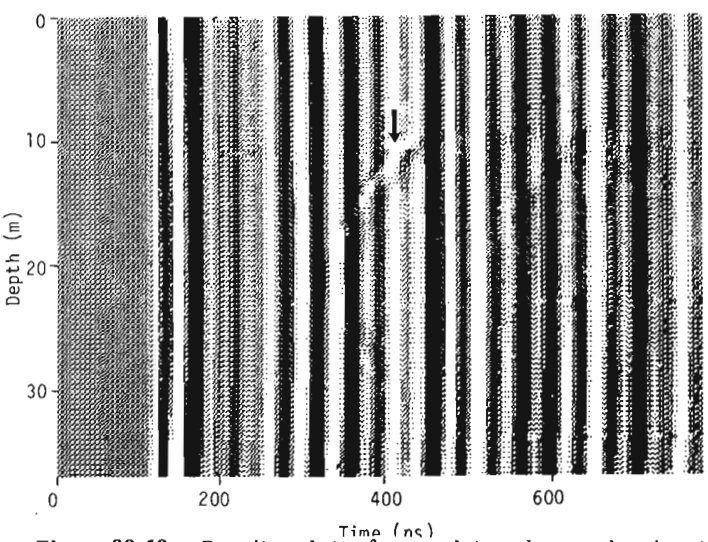

Figure 23.13. *Density plot of raw data when radar is at fixed depth and transponder is in motion. Depth refers to depth of the transponder and is approximate, since speed control on manually operated transponder winch was not precise. If the radar and data sampling are completely consistent the vertical stripes will be exactly uniform since the radar is not moving. The vertical arrow indicates the partially obscured transponder signature.*

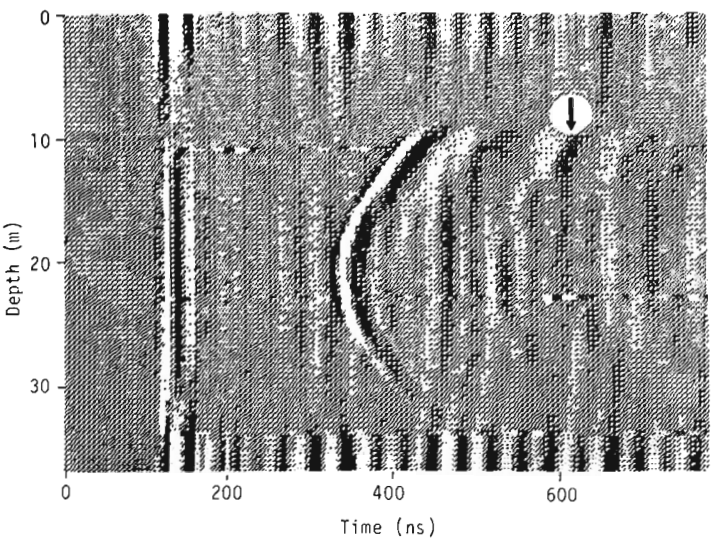

Figure 23.15. *Data derived from Figure 23.13 by subtraction of the computed average waveform. The fact that the vertical stripes are not entirely removed is an indication of some variation in the radar performance. The result does make the transponder signature quite clear, however. The faint replica of the transponder signal, indicated by the arrow, was not expected. The source of this replica is a cable-guided wave reflecting from the top of the borehole.*

Transponder field test results

The transponder was first tested at a site near Gold Hill, Colorado in dry boreholes in granite spaced 12.2 m apart. The bulk dc resistivity of the rock is reported to be in the order of 1000 ohm.m with VHF (30 MHz – 300 MHz) velocity of about 127 m/μs and attenuation of 1.2 dB/m (Myers and Leckenby, 1983). The granite is quite inhomogeneous, however, containing gold ore vein deposits, aplite and pegmatite dykes, and other inclusions (Goddard, 1940). Lerner et al. (1983) reported that the attenuation at higher frequencies is anomalously high and has an unexpected frequency dependence.

The transponder was tested using two methods: first the transponder was lowered to a fixed depth while the radar was continuously moved; second, the radar was lowered to a fixed depth while the transponder was moved. The raw data shown in Figures 23.12 and 23.13 for the two cases is dominated by ringing in the radar. The transponder signature is barely visible.

By digitally subtracting the average waveform from the data some improvement is evident both when the radar is in motion as shown in Figure 23.14 and when the transponder is in motion as shown in Figure 23.15. The broad diagonal stripe in Figure 23.14 is the result of the cable-guided wave previously discussed. Subtraction of the average waveform in the case where the radar is stationary ought to yield only the transponder signature. The fact that there is some residual waveform associated with the radar in Figure 23.15 indicates that the radar is not completely consistent in its behavior.

From the known spacing between boreholes a propagation velocity of 129 m/μs was calculated from the data after subtraction of the 40 ns electronic delay time. This compares well with the previously mentioned value of 127 m/μs.

In an attempt to remove the effects of the cable-guided wave in Figure 23.14, the radar logged the same hole a second time without using the transponder in the second hole, and the data from this run were subtracted from that with the transponder in place. If the radar could log the hole twice in exactly the same fashion, the result would be only the transponder signature. For a number of reasons, including an inability to precisely control the speed of the hydraulic winch on the truck, complete repeatability is not achieved. Nevertheless, the result presented in Figure 23.16 does show that the transponder was triggering over a greater portion of the borehole than was apparent in the raw data.

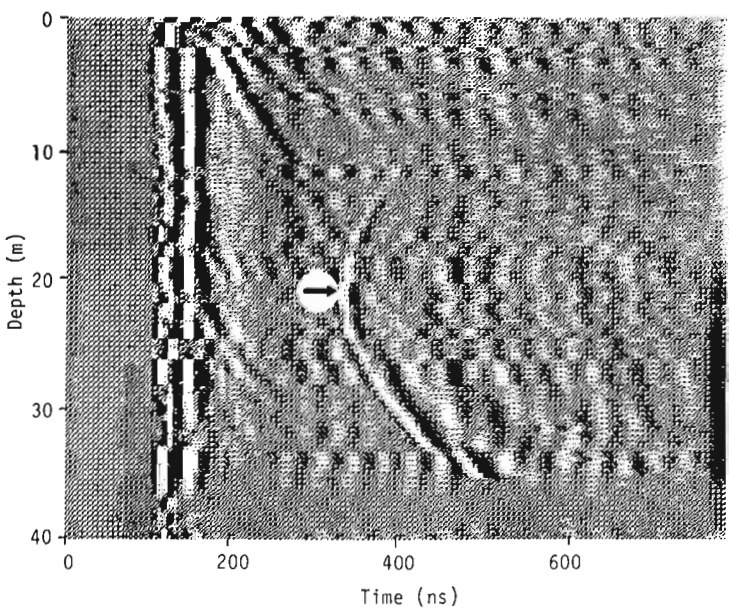

Figure 23.16. Data derived from Figure 23.12 by repeating the radar run with no transponder in the second borehole and subtracting the second data set from the first. As discussed in the text, the result is not perfect but does make the transponder signal indicated by the arrow much more visible.

Conclusions

The tests in granite of the borehole radar operating in a single-hole configuration at the Underground Research Laboratory were encouraging. Although considerable analysis remains to be done, it is clear that the radar was responsive to known major fracture zones intersecting the hole and to many lesser fractures as well. The cable-guided wave, which is an annoyance in many respects, seems to be sensitive to horizontal fractures which intersect the borehole. In addition, the radar detected what appears to be an anomalous zone extending from near the borehole to more than 20 m from the borehole axis. It is this capability of detecting, with good resolution, inhomogeneities some distance off the borehole axis which makes radar a useful supplement to other geophysical techniques.

The borehole transponder extends the ability of the radar so that it can be used to gather both single-hole and crosshole data. Field tests have shown that the device works and can help detect inhomogeneities in a rock mass. The signal-to-noise ratio at the transponder input terminals determines the maximum distance at which the transponder may be used. The signal-to-noise ratio, in turn, is governed by the radar radiated power in the direction of the transponder, attenuation in the rock between the boreholes, external RF cultural noise, and internal electronic noise. The simplicity of the transponder makes it an attractive alternative to timing cables which can be electromagnetically or operationally undesirable except in cases where large borehole separations and/or high attenuation is encountered. In such cases the use of timing cables is necessary.

Acknowledgments

We thank C.C. Davison and N.M. Soonawala of the Whiteshell Nuclear Research Establishment, Atomic Energy of Canada Ltd. for their generous assistance in arranging for our use of boreholes at the Underground Research Laboratory, for arranging access to geophysical logs, and for their interest and encouragement.

References

Goddard, E.N.
1940: Preliminary report on the Gold Hill mining district, Boulder County, Colorado; Colorado Scientific Society Proceedings, v. 14, no. 4, p. 103-139.

Lerner, R.M., Landers, T.E., Zettler, W.R., and Brown, J.R.
1983: Observations and measurements related to the use of airborne UHF CW radar for underground tunnel detection; Massachusetts Institute of Technology Lincoln Laboratory Report TRE-1, 111 p.

Myers, R.L., and Leckenby, R.J.
1983: Unpublished data; United States Bureau of Mines, Denver, Colorado.

Nickel, H., Sender, F., Thierback, R., and Weichart, H.
1983: Exploring the interior of salt domes from boreholes; Geophysical Prospecting, v. 31, no. 1, p. 131-148.

Wright, D.L. and Watts, R.D.
1982: A single-hole, short-pulse radar system; in Geophysical investigations in connection with nuclear waste; Nuclear Energy Agency Organization for Economic Co-operation and Development, Ottawa, p. 267-279.

24. THE INFLUENCE OF FISSURING ON SALINE INCURSION IN A LIMESTONE AQUIFER AS REVEALED BY FLUID LOGGING

K.W.F. Howard[1]

Howard, K.W.F., The influence of fissuring on saline incursion in a limestone aquifer as revealed by fluid logging; in Borehole Geophysics for Mining and Geotechnical Applications, ed. P.G. Killeen, Geological Survey of Canada, Paper 85-27, p. 217-225, 1986.

Abstract

The Cretaceous Chalk is a major source of potable water for rural and industrial communities in east central England. Concern arose for the future of these supplies when water quality began to deteriorate in high abstraction areas.

Instrumental well logging was carried out as part of a detailed hydro-geological study initiated to investigate temporal and spatial relationships between fresh groundwater and saline groundwaters of several possible origins. Logging was conducted in over 70 existing and purpose drilled wells. Logged parameters include S.P., multi- and single-point resistivity, gamma ray, temperature, differential temperature, fluid conductivity and impeller flow.

Temperature and differential temperature logs identify fissure flow as the dominant groundwater flow mechanism. Fissuring is mainly confined to two distinctive zones towards the top of the geological unit where its development appears unrelated to the chalk unit stratigraphy as defined by geophysical logs. Flow meter measurements suggest that the lower fissure zone contributes very little to the cumulative transmissivity of the aquifer. In rare instances the formation of deeper fissures can be related to the presence of occasional, thin but persistent, argillaceous bands.

Particularly important is the influence of fissuring on the behaviour of old saline water prevalent at depth in the east of the area. According to classical understanding the saline groundwater body should give rise to a single fresh/saline water interface, the elevation of which is controlled by density/head relationships. Fluid conductivity logs suggest the classical ideal is approached only in the southeast where pumping is minimal. In high abstraction areas fresh water inflows at fissures transform the borehole salinity profile into a series of steps unrepresentative of conditions in the formation. By contrast it is significant that the saline water of recent seawater origin tends to be confined to the upper, well-developed fissure zone where, due to preferential horizontal flow, it gives rise locally to a hydrostatically unstable salinity profile.

Résumé

La craie d'âge crétacé est une importante source d'eau potable pour les collectivités rurales et industrielles de la partie centrale de l'Angleterre. L'approvisionnement futur en eau suscite de l'inquiétude depuis que la qualité de l'eau a commencé à se dégrader dans les zones à perte élevée.

Les sondages ont été diagraphiés dans le cadre d'une étude hydrogéologique détaillée visant à examiner les liens temporels et spatiaux entre l'eau douce souterraine et l'eau saline souterraine pouvant provenir de diverses origines. Les diagraphies ont été effectuées dans plus de 70 sondages existants et forés. Les paramètres comprennent le potentiel spontané, la résistivité en un et en plusieurs points, le rayonnement gamma, la température, la température différentielle, la conductibilité des fluides et la circulation provoquée par une roue à aubes.

Les diagraphies de température et de température différentielle montrent que la circulation à travers les diaclases est le principal mécanisme d'écoulement des eaux souterraines. La fissuration se produit surtout dans deux zones caractéristiques situées vers le haut de l'unité géologique et ne semble pas être liée à la stratigraphie de l'unité de craie telle qu'elle est définie par les diagraphies géophysiques. Des mesures au fluxmètre laissent croire que la zone de fissuration inférieure contribue très peu à la transmissivité cumulative de l'aquifère. Dans des cas rares, la formation de fissures plus profondes peut être reliée à la présence de bandes argileuses intermittentes, minces mais persistantes.

L'influence de la fissuration sur le comportement d'anciennes eaux salines que l'on trouve souvent en profondeur dans la partie est de la région revêt une importance toute particulière. D'après la théorie classique, la masse d'eau salée souterraine devrait donner lieu à un seul interface eau fraîche-eau salée, dont l'élévation serait contrôlée par les liens entre la densité et la tête. Les diagraphies de conductibilité des fluides laissent croire que cet idéal classique est atteint uniquement dans le sud-est, où il y a très peu de pompage. Dans les zones à perte élevée, l'apport d'eau fraîche dans les fissures transforme le profil de salinité en une série d'étapes qui ne sont pas caractéristiques des conditions existant dans la formation. Par opposition, il est important de noter que l'eau salée d'origine marine récente tend à se trouver uniquement dans la zone supérieure de fissures bien développées où, en raison d'un écoulement horizontal préférentiel, elle donne lieu par endroits à un profil de salinité hydrostatiquement instable.

[1] Department of Geology, Scarborough College, University of Toronto Scarborough, Ontario, M1C 1A4, Canada

Introduction

The Cretaceous Chalk of east central England supplies some 170 ML/d of good quality potable water to local industrial and agricultural communities. Concern arose for the future of these supplies when water quality began to deteriorate during the 1950s and 1960s in high abstraction areas around Grimsby and Immingham (Gray, 1964; Lloyd et al., 1978). Although it was speculated that saline water was being drawn in from the adjacent Humber Estuary and North Sea, such a source could not be reconciled with slightly saline water later identified at depth in a production well over 6 km from the coast.

Instrumental well logging was carried out as part of a comprehensive hydrogeological investigation of the saline groundwater problem and its effects on resource management (University of Birmingham, 1978; Evans et al., 1979). Other fundamental elements of the investigation included hydrochemistry (Lloyd and Howard, 1978; Howard and Lloyd, 1983), surface geophysics (Barker, 1978; Barker and Griffiths, 1981) and numerical modelling. The overall objectives of the study were: i) to determine the origin of the saline waters; ii) to develop an understanding of the regional flow system; and iii) to represent aquifer behaviour using a finite difference model.

The well logging program was planned with more specific objectives in mind: i) to define the geological structure of the area; ii) to evaluate the importance of fissure flow on a regional and local scale; and iii) to determine spatial relationships between the fresh and saline groundwater bodies. In this paper emphasis is placed upon the use of temperature, differential temperature, fluid conductivity and flowmeter logs as means of satisfying the last two well logging objectives.

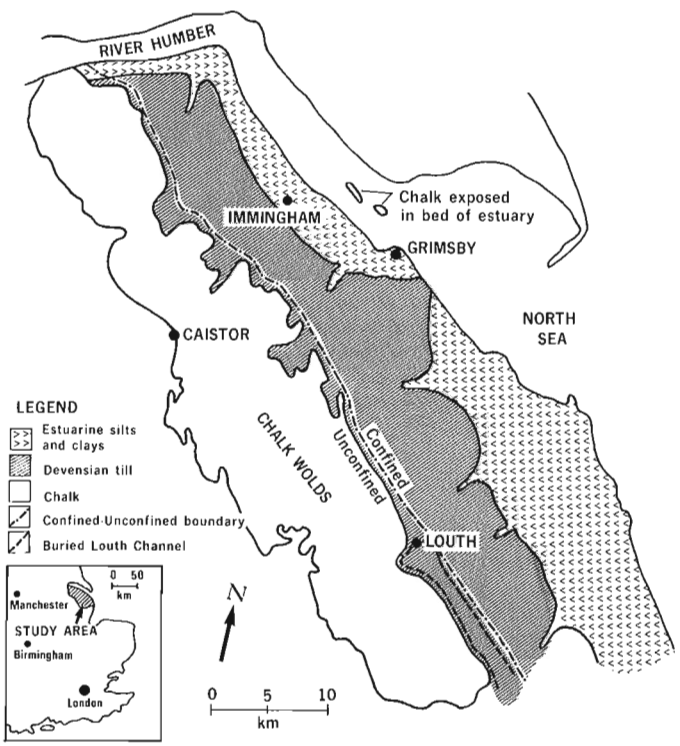

Figure 24.1. Location of study area and feature maps.

Geology and hydrogeology

The study area is shown in Figure 24.1 and a generalized east-west hydrogeological section across the area is given in Figure 24.2.

The Cretaceous Chalk is a massive white, finegrained Upper Cretaceous limestone containing an irregularly spaced sequence of thin, but persistent, argillaceous bands (Wood and Smith, 1978). These bands are very rarely observed in drilling returns but proved to be excellent geophysical marker horizons during logging operations, giving sharp responses on the resistivity logs (Fig. 24.3). As indicated further by Figure 24.3, the chalk unit varies little in character across the study area and single point resistivity logs allow stratigraphic correlation to be accomplished easily over distances of 25 km or more (University of Birmingham, 1978).

In the west (Fig. 24.2) the chalk unit is well exposed, has high relief and recharge of a predominantly direct nature occurs (Howard and Lloyd, 1979). Groundwater heads in this region locally exceed 100 m above sea level and flow occurs in a generally northeasterly direction towards the coast. As in most limestone aquifers flow is predominantly associated with fissures developed by chemical dissolution.

By contrast the eastern part of the area has been considerably affected by recent Quaternary events. A major transgression during the Ipswichian interglacial (120 000 BP) resulted in the formation of a cliff-line and extensive wave cut platform which are now buried beneath a mantle of Devensian tills up to 30 m thick. The tills date between 18 000 and 13 000 BP (Penny et al., 1969) and presently confine groundwaters throughout the eastern seaboard. With two small, but notable exceptions (McQuillin et al., 1969), the tills also extend as a virtually impermeable cover across the Humber Estuary and North Sea floor where they significantly reduce the potential for hydraulic interaction between aquifer and the sea.

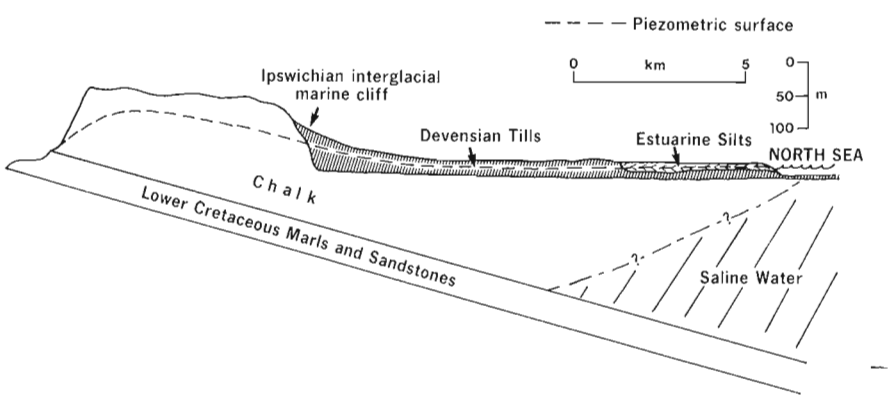

Figure 24.2

Generalized east-west hydrogeological section.

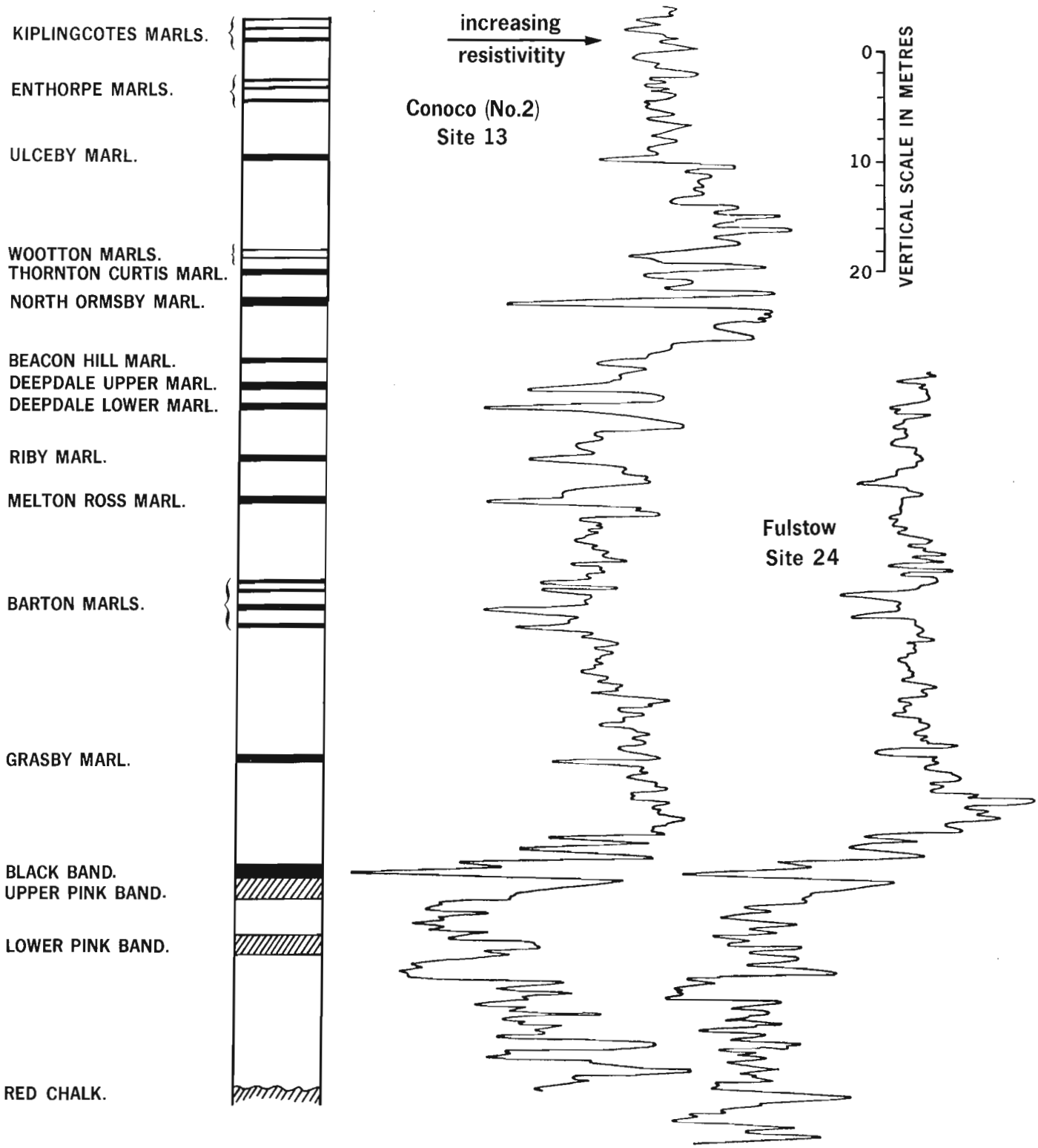

Figure 24.3. Correlation of single-point resistivity logs in wells 25 km apart with chalk lithology (after University of Birmingham, 1978).

Well logging operation

Well logging was conducted in over 70 existing and purpose drilled wells using an early series Wuidard Hydrologger. This equipment, as described by Robinson (1974), was designed specifically for narrow diameter water wells and is capable of logging S.P. (spontaneous potential), multi- and single-point resistivity, natural gamma, temperature, differential temperature, fluid conductivity and impeller flow. The sondes were lowered and raised on a six-conductor reinforced cable connected to a two-channel chart recorder via a manually operated winch. Electrical power was provided by a 12 volt heavy duty storage battery. Although the equipment lacked the reliability and electronic sophistication of its modern-day counterpart, it did prove to be extremely versatile and provided reasonably complete sets of logs for over 60 wells. The locations of the wells logged are shown in Figure 24.4. For clarity only those wells referred to in the text are numbered.

Fissure flow study

Carbonate aquifers such as the chalk unit rely on narrow openings, known as fissures, as the primary means of transmitting water. These fissures tend to develop preferentially close to the water table where the water is chemically most aggressive and flow rates are frequently high. Deeper fissures may form when groundwater levels are lowered for a considerable period of time as experienced during glacial episodes. A knowledge of fissure distribution is essential as it allows the vertical extent of the aquifer to be determined. In many carbonate systems the aquifer, as defined by the zone of fissuring, comprises only a small proportion of the total thickness of the formation.

Differential temperature logging is a valuable means of investigating fissure flow, particularly in the absence of a caliper tool. In a borehole devoid of fissure flow the vertical temperature profile shows a smooth variation corresponding to the local geothermal gradient. When fissures are present, very small differences in temperature between fissure water and water in the borehole column cause slight inflections in the temperature profile that can be greatly amplified when differentiated with respect to vertical distance. In modern instrumentation, differentiation of the signal from a single temperature sensor is achieved by computer processing. In the study described differential temperature was satisfactorily determined by measuring the small difference in temperature between two carefully matched thermistors lowered at a fixed 1 m separation.

Previous fluid logging investigations in Cretaceous Chalk of southern England have revealed a single zone of fissuring towards the top of the geological unit. Along the south coast of Sussex the fissure zone extends to a depth of 100 m below the water table (Monkhouse and Fleet, 1975). In Berkshire, west of London, exhaustive work by Robinson (1975) has shown that fissure development reaches a maximum between a depth of 20 and 35 m below ground level and reduces considerably below a depth of 45 m.

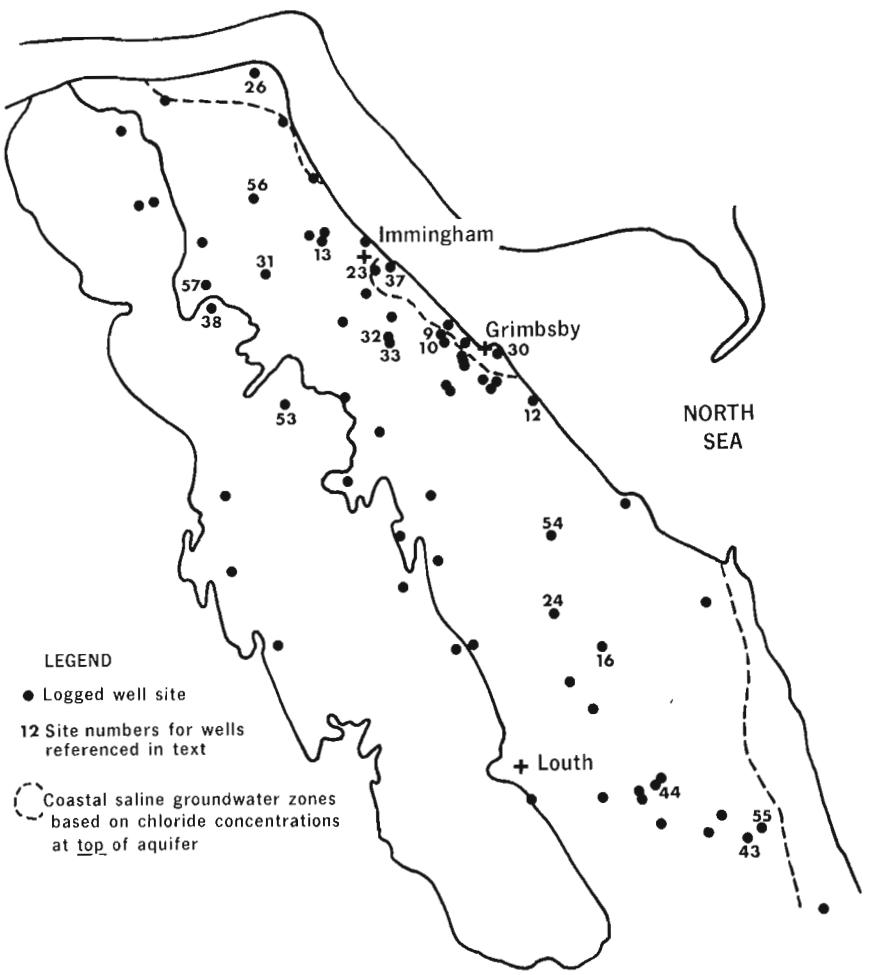

Figure 24.4. Location of logged well sites and coastal saline zones. Numbered wells are discussed in the text.

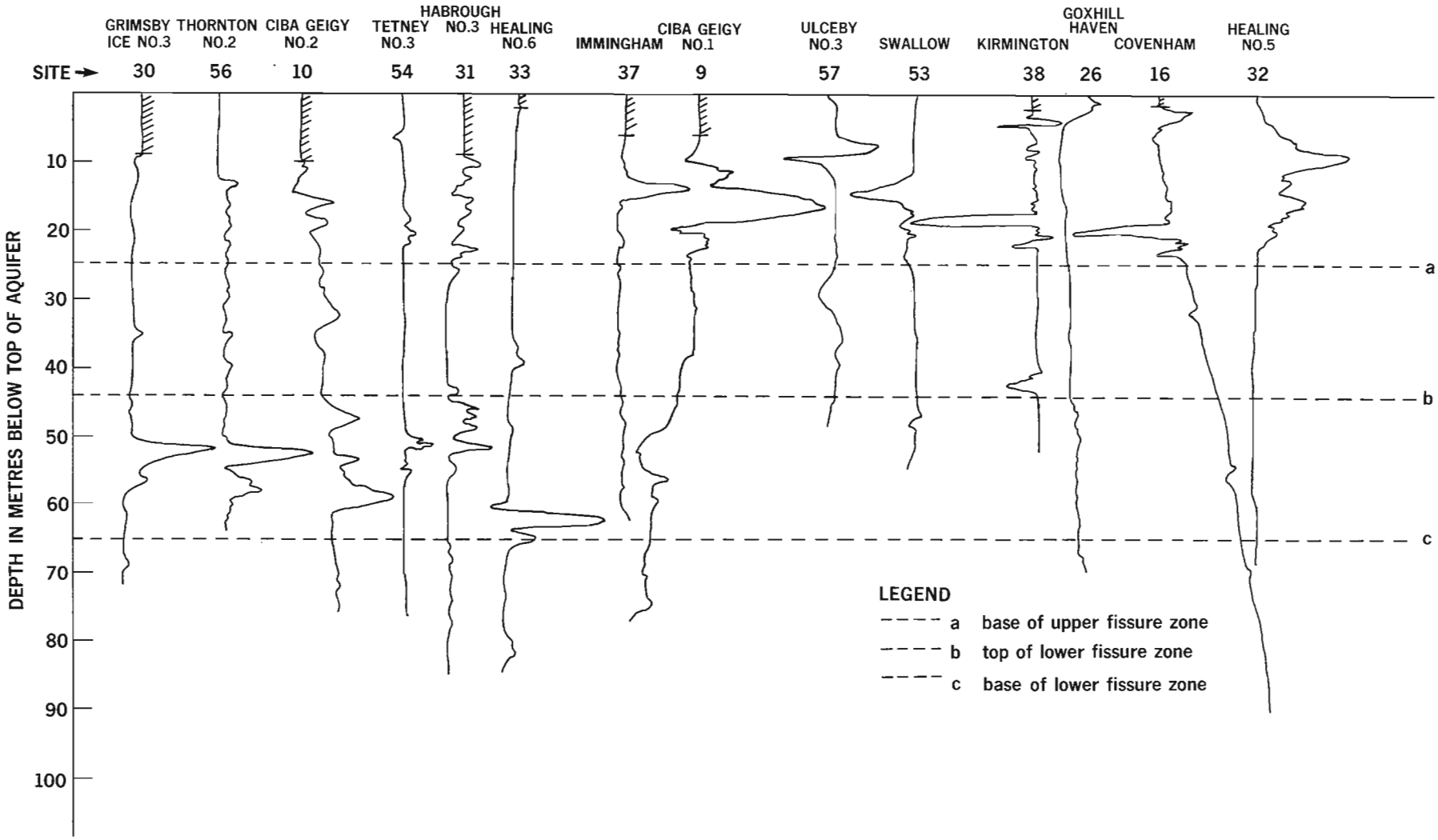

Figure 24.5. *Fissure zones as indicated by uncalibrated differential temperature logs.*

Uncalibrated differential temperature logs from the study area are displayed in Figure 24.5. To allow comparison and correlation between the logs the top of the aquifer as defined by either the water table or base of the till confining layer has been taken as a common datum.

The logs displayed clearly reveal the presence of two major zones of fissuring. The upper fissure zone occurs to a depth of about 25 m below the top of the aquifer and can be recognized throughout the study area. The zone shows no correlation with chalk unit stratigraphy and was presumably developed by circulating waters at a time when groundwater levels were close to their present elevation. More unusual is a deeper zone of fissuring occurring throughout the area at a depth of between 45 and 65 m below the top of the aquifer. There is some evidence to suggest that the development of certain individual fissures within this lower zone may be associated with specific argillaceous bands, in particular the North Ormsby Marl. In general, however, the lower fissure zone cannot be correlated with the chalk unit and must have formed regionally when sea and groundwater levels were about 50 m below their present elevations. Such a condition is known to have persisted in eastern England during the Early and Middle Devensian (115 000 – 26 000 BP) (Mitchell, 1977) when due to the onset of glaciation the coastline receded to leave much of the southern North Sea Basin dry. In neighbouring North Humberside, Foster et al. (1976) have postulated the existence of a similar lower zone of fissuring at a depth comparable to that revealed by the present study. The zone was identified on the basis of relatively limited information and was thought to occur only in the unconfined region to the west.

Despite the presence of the deeper zone of fissuring, impeller flow meter logs indicate that most of the groundwater flow occurs in the upper fissure zone towards the top of the aquifer. Figures 24.6 and 24.7 compare temperature logs with impeller flow meter measurements obtained in flowing artesian wells at Kirmington (site 38) and Tetney (site 54) respectively. At Kirmington most of the water enters the well at a major fissure 20 m below the top of the aquifer and at other shallower fissures. Although a deeper fissure occurs 45 m below the top of the aquifer, the inflow at this level was so small as to be below the threshold level of the flow meter. At Tetney (Fig. 24.7) the situation is more complicated in that there is evidence of minor flows between fissures at different levels. Again, however, virtually all the water discharging at the well-head originates at fissures just a few metres below the base of the well casing.

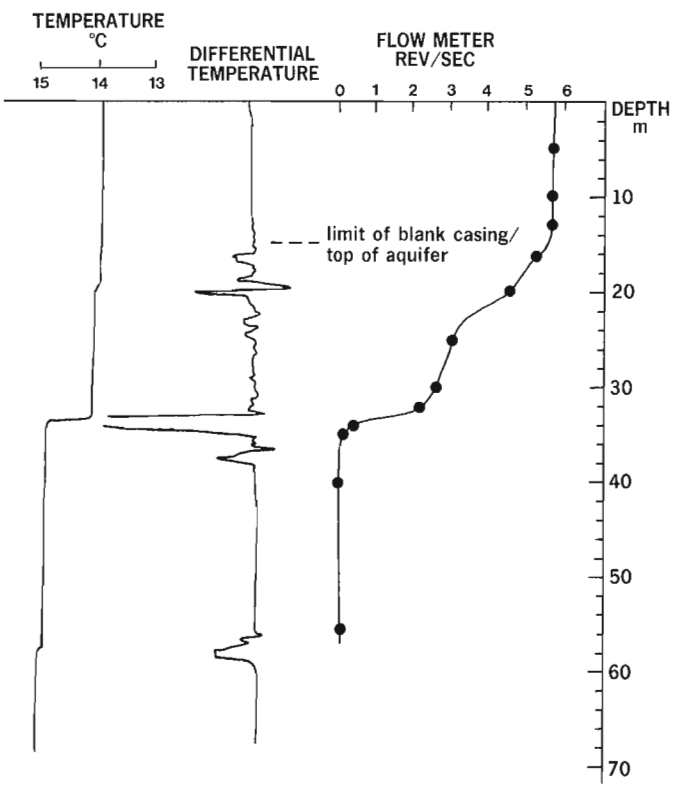

Figure 24.6. Temperature, differential temperature and flow meter logs at Kirmington (site 38).

Saline groundwater study

To investigate the spatial distribution of saline groundwater in the study area, fluid conductivity logging was carried out by means of a throughflow conductivity cell attached immediately beneath the thermistor on the temperature sonde. Particular attention was paid to the three coastal saline zones defined in Figure 24.4. General characteristics and origins of the saline waters in these zones are shown in Table 24.1. Conductivity logs from the two saline zones of greatest concern (Grimsby and East of Louth) are displayed in Figure 24.8.

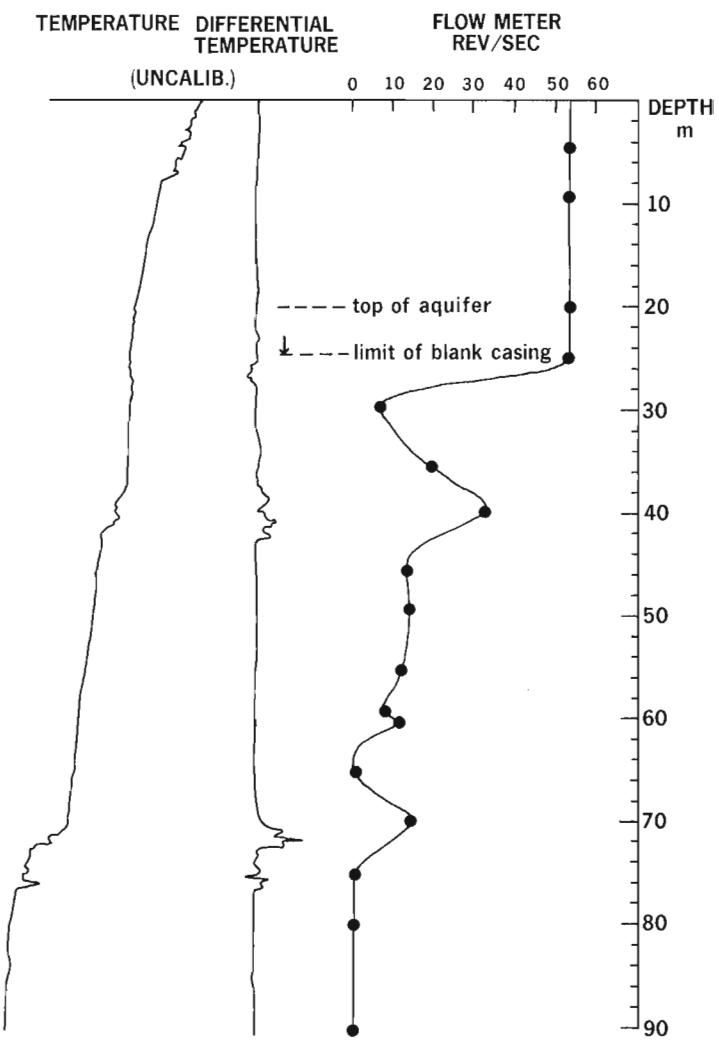

Figure 24.7. Temperature, differential temperature and flow meter logs at Tetney No. 3 (site 54).

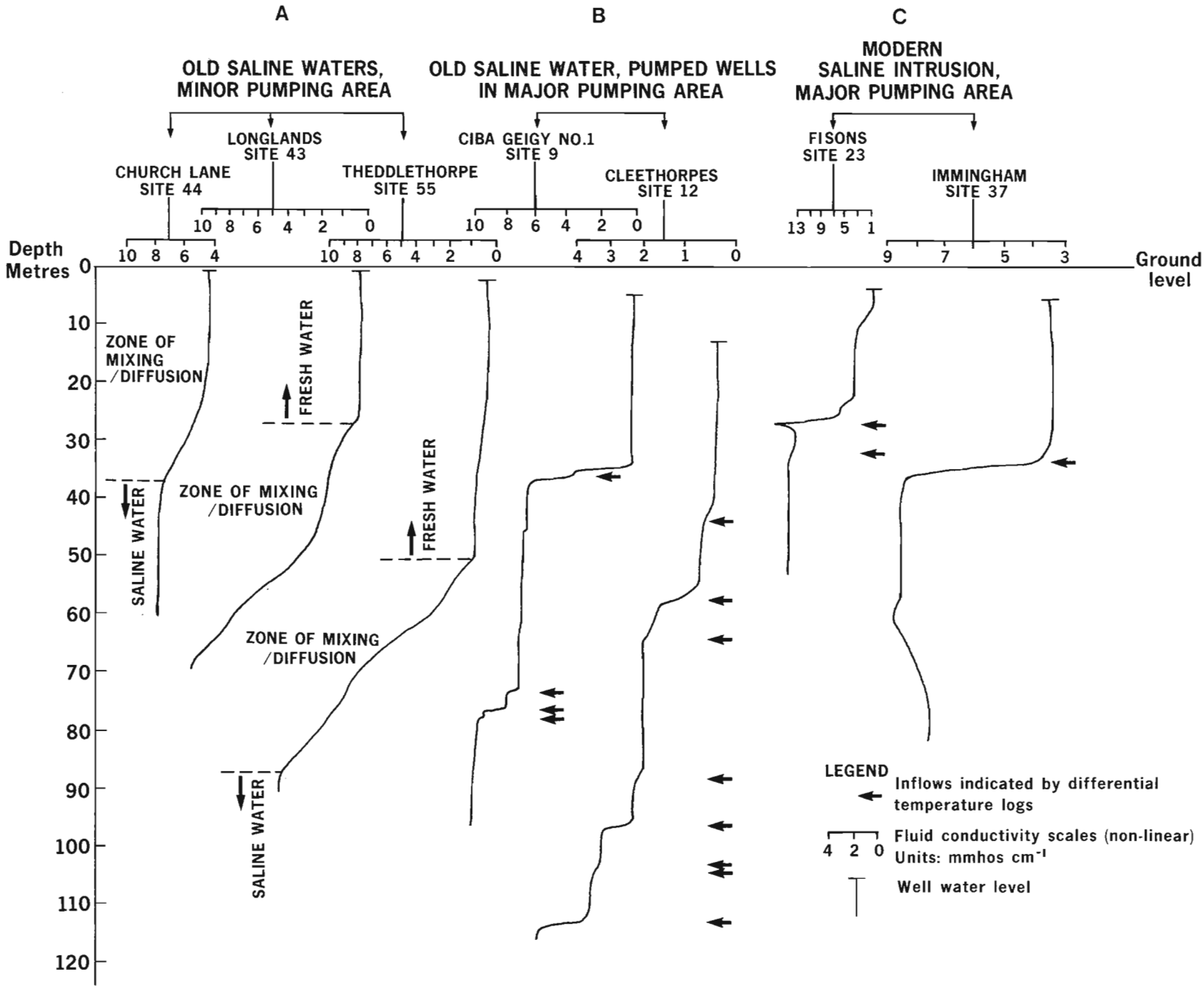

Figure 24.8. *Influence of fissure flow on saline groundwater incursion.*

Table 24.1. Characteristics and origins of the saline groundwaters

Saline zone	Maximum salinity at depth mg/L chloride	Origin (Howard and Lloyd 1983)	Abstraction in area	Degree of concern
Northern	800	Seepage from estuarine silts	Minor	Moderate
Grimsby	11 000	i) Old seawater intruded during Ipswichian interglacial	Minor	Major
		ii) Modern seawater intrusion		
East of Louth	8 000	Old seawater intruded during Ipswichian interglacial. Occurs up to 8 km inland	Major	Major

The study and prediction of saline groundwater behaviour is commonly, and sometimes routinely, approached by assuming a sharp fresh/saline water interface and adopting techniques based on the Ghyben-Herzberg hydrostatic equilibrium relationship (Hubbert, 1940). Modern developments of these techniques now permit representation of zones of diffusion, mixing and transient flow conditions (Cooper et al., 1964; Segol and Pinder, 1976). Rarely, however, do such analytical advances cope adequately with aquifers that are anisotropic and heterogeneous.

The problem, indeed the futility of adopting an analytical approach to the study of saline groundwater in fissured Cretaceous Chalk is well illustrated by the conductivity logs in Figure 24.8. As shown in Figure 24.8A only old saline groundwaters in a minor abstraction area east of Louth display in any way the classical ideal of a single (though diffuse) transition from fresh to saline water. In a major pumping area around Grimsby (Fig. 24.8B) minor inflows at fissures have transformed the salinity profile of similar deep, saline groundwaters into a series of steps that mask the true position of the saline groundwater body. Remarkably, regular logging at several wells has shown that the stepped salinity profiles are virtually unaffected by the pumping condition of the well. This is a further indication of preferential flow in the upper fissured zone with only minor flow activity at depth.

Although preferential flow in the upper zone of fissuring tends to reduce the incidence of upconing of old saline groundwater from depth, the zone can also provide an effective flow path for the lateral intrusion of modern seawater. Fortunately this condition has been observed only to the south and east of Immingham where the chalk unit is exposed in the bed of the Estuary (Fig. 24.1). Figure 24.8C shows salinity profiles in wells affected by modern seawater intrusion. Characteristically they show highest salinity at levels corresponding to the inflow of saline water through the upper fissure zone and a moderation of salinity with depth. Salinity profiles displaying similarly hydrostatically unstable conditions have been recorded in association with modern seawater intrusion along the south coast of England (Monkhouse and Fleet, 1975).

Conclusion

Fluid logs including temperature, differential temperature, fluid conductivity and impeller flow have proved an invaluable means of investigating the influence of fissuring on fresh and saline groundwater behaviour in the chalk unit of east central England.

Temperature and differential temperature logs reveal the importance of fissuring as the dominant groundwater flow mechanism. Two major fissure zones are identified but flow meter measurements indicate that the majority of flow is confined to the upper zone immediately below the top of the aquifer. Neither fissure zone can be correlated with Chalk stratigraphy, but there is some evidence to suggest that the development of certain individual fissures within the lower fissure zone may be associated with specific argillaceous bands.

Particularly important is the influence of fissuring on the behaviour of old saline water prevalent at depth in the east of the area. According to classical understanding the saline groundwater body should give rise to a single fresh/saline water interface, the elevation of which is controlled by density/head relationships. Fluid conductivity logs suggest the classical ideal is approached only in the southeast where pumping is minimal. In high abstraction areas fresh water inflows at fissures transform the borehole salinity profile into a series of steps that disguise the true location of the saline groundwater body. Below the upper zone of fissuring the inflows are minor and in most cases the old saline groundwater body is barely disturbed.

By contrast it is significant that the saline water of recent seawater origin tends to be confined to the upper fissure zone where, due to preferential horizontal flow, it gives rise locally to a hydrostatically unstable salinity profile.

Acknowledgments

The author gratefully acknowledges the support of University of Birmingham colleagues J.W. Lloyd, project supervisor, and R.D. Barker who undertook much of the logging work and was responsible for the geophysical interpretations. Thanks are also extended to the Anglian Water Authority for their permission to publish.

References

Barker, R.D.
1978: The reduction of lateral effects in resistivity sounding; Geophysical Journal, Royal Astronomical Society, v. 53, p. 143-144.

Barker, R.D. and Griffiths, D.H
1981: Surface geophysical methods in hydrogeology; in J.W. Lloyd, ed., Case studies in Groundwater Resources Evaluation, Oxford University Press. 206 p.

Cooper, H.H., Jr., Kohout, F.A., Henry, H.R., and Glover, R.E.
1964: Sea water in coastal aquifers; United States Geological Survey, Water-Supply Paper 1613-C, 84 p.

Evans, D., Lloyd, J.W., and Howard, K.W.F.
1979: A study of saline intrusion and its influence on groundwater management in the Lincolnshire Chalk, England; International Hydrological Programme, 6th Salt Water Intrusion Meeting (SWIM), Hannover, p. 87-103.

Foster, S.S.D., Parry, E.L., and Chilton, P.J.
1976: Groundwater resource development and saline water intrusion in the Chalk aquifer of North Humberside; Institute of Geological Sciences Inst. Geol. Sci. (U.K.), Report 76/4, 34 p.

Gray, D.A.
1964: Groundwater conditions of the Chalk of the Grimsby area, Lincolnshire; Water Supply Paper, Geological Survey of Great Britain, Resource Report No. 1,24 p.

Howard, K.W.F. and Lloyd, J.W.
1979: The sensitivity of parameters in the Penman evaporation equations and direct recharge-balance; Journal of Hydrology, v. 41, p. 329-344.

1983: Major ion characterization of coastal saline groundwaters; Ground Water, v. 21, no. 4, p. 429-437.

Hubbert, M.K.
1940: The theory of groundwater motion; Journal of Geology, v. 48, p. 785-944.

Lloyd, J.W. and Howard, K.W.F.
1978: Environmental isotope studies related to groundwater flow and saline encroachment in the Chalk aquifer of Lincolnshire, England; Isotope Hydrology 1978, v. 1 IAEA-SM-228/18, p. 311-325.

Lloyd, J.W., Rushton, K.R., Taylor, H.R., Barker, R.D., and Howard, K.W.F.
1978: Saline groundwater studies in the Chalk of northern Lincolnshire; International Hydrological Programme, 5th Salt Water Instrusion Meeting, Medmenham, U.K., p. 87-97.

McQuillin, R., Arnold, S.E., Tully, N.C., and Hull, J.H.
1969: Cruise Report of the Humber Investigation 1968; Institute of Geological Sciences (U.K.), Science Report 69/3, 22 p.

Mitchell, G.F.
1977: Raised beaches and seal levels; in F.W. Shotton, ed. British Quaternary Studies. Clarendon, Oxford.

Monkhouse, R.A. and Fleet, M.
1975: A geophysical investigation of saline water in the Chalk of the south coast of England; Quaternary Journal of Engineering Geology, v. 8, p. 291-302.

Penny, L.F., Coope, G.R., and Catt, J.A.
1969: Age and insect fauna of the Dimlington Silts, East Yorkshire; Nature, v. 224, p. 64-67.

Robinson, V.K.
1974: Low cost geophysical well logs for hydrogeological investigations; Quaternary Journal of Engineering Geology, v. 7, p. 207-215.

1975: Groundwater Development Scheme. Report on borehole geophysical logging carried out during Stage 1.; Thames Water Authority, Internal Report, 29 p.

Segol, G. and Pinder, G.F.
1976: Transient simulation of saltwater intrusion in southeastern Florida; Water Resources Research, v. 12, p. 65-70.

University of Birmingham
1978: South Humberbank Salinity Research Project; final report to the Anglian Water Authority, 99 p.

Wood, C.J. and Smith, E.G.
1978: Lithostratigraphic classification of the Chalk in North Yorkshire, Humberside and Lincolnshire; Proceedings, Yorks. Geological Society.

25.

APPLICATION OF MAGNETIC SUSCEPTIBILITY WITHIN CRYSTALLINE ROCKS

B.A. Chomyn[1], P. Lapointe[2], W.A. Morris[3], and R.L. Coles[2]

Chomyn, B.A., Lapointe, P., Morris, W.A., and Coles, R.L., Application of magnetic susceptibility within crystalline rocks; in Borehole Geophysics for Mining and Geotechnical Applications, ed. P.G. Killeen, Geological Survey of Canada, Paper 85-27, p. 227-236, 1986.

Abstract

This review highlights some of the important features of bulk magnetic susceptibility measured on drillcore from the Lac du Bonnet in Manitoba and Atikokan and Chalk River in Ontario. The variations in susceptibility reflect changes in lithology, in particular alteration associated with fractured rock. Similar levels in susceptibility are observed in the Lac du Bonnet rocks: susceptibility minima characterize fractured and altered core; 'background' uniform susceptibilities correspond to non-fractured, unaltered core; and anomalously high susceptibilities coincide with magnetite-rich xenoliths. The Atikokan rocks exhibit generally higher and less varied susceptibilities than Lac du Bonnet rocks. The metamorphosed and highly fractured Chalk River granite-granodiorites give values several orders of magnitude lower than the other research areas, with the exception of anomalously higher susceptibilities coinciding with metagabbro lenses and diabase dykes.

Résumé

Le présent rapport fait ressortir certaines des caractéristiques importantes des mesures de susceptibilité magnétique faites à partir de carottes provenant de la zone du lac Dubonnet, au Manitoba, et d'Atikokan et de Chalk RIver, en Ontario. Les variations de susceptibilité traduisent des changements lithologiques, en particulier l'altération associée à la présence de roche fracturée. Des niveaux semblables de susceptibilité magnétique peuvent être observés dans la roche du lac Dubonnet: un niveau minimal de susceptibilité caractérise la roche fracturée et altérée; les susceptibilités uniformes ayant l'aspect d'un bruit de fond correspondent à la roche non fracturée et non altérée; enfin, les susceptibilités anormalement élevées coincident avec la présence de xénolites riches en magnétite. En général, la roche d'Atikokan affiche des susceptibilités plus élevées et moins variées que celle de la roche du lac Dubonnet. Les granites-granodiorites métamorphosés et très fracturés de Chalk River affichent des valeurs de plusieurs ordres de grandeur inférieures à celles qui ont été observées à d'autres endroits sondés, à l'exception des susceptibilités anormalement élevées coïncidant avec la présence de lentilles de métagabbro et de filons intrusifs de diabase.

Introduction

The Canadian Nuclear Fuel Waste Management Program was formally initiated in June 1978 and its prime objective is the disposal of nuclear waste deep underground in stable, hardrock formations of the Canadian Shield (Boulton, 1978; Boulton and Gibson, 1979; Boulton, 1980; Dixon and Rosinger, 1981; Sheng and Shemilt, 1981). There are six research areas being studied, five in Ontario and one in Manitoba (Fig. 25.1). In the context of the program the measurement of magnetic properties is one aspect of a series of comprehensive geological and geophysical investigations undertaken within a given area.

This review highlights some of the important features and correlations of bulk magnetic susceptibility measured on drillcore from the Lac du Bonnet batholith in Manitoba and from granitic-granodiorite gneisses of Chalk River, and the Eye-Dashwa granitic pluton of Atikokan in Ontario. Much of the research is ongoing. Some of the investigations, such as research on the Lac du Bonnet batholith and the Eye-Dashwa Lake pluton, are more comprehensive than others. In view of this, the authors have used some examples (Table 25.1) taken from a large collection of data to illustrate some of the important features that have come to the fore.

Magnetic susceptibility

Magnetic susceptibility is the measure of the ability of a sample to become temporarily magnetized in a magnetic field. The observed variation in bulk susceptibility is controlled largely by the presence of iron and iron-titanium oxide minerals, their composition, grain size, and relative abundance. Magnetite is the most important of the iron oxides based on its abundance and high values of susceptibility. Variations in susceptibility may arise from changes in lithology, and in particular, from the alteration of primary iron oxide and possibly iron sulphide species, and from the introduction of secondary iron oxide and/or iron sulphide species via fluid migration along fracture planes. The recognition of particular susceptibility signatures associated with alteration about fractures may provide a direct qualitative estimate of the significance of individual fracture sets for fluid movement (Coles, 1981).

[1] Atomic Energy of Canada Ltd., Energy Mines and Resources
[2] Earth Physics Branch, Energy Mines and Resources
[3] Morris Magnetics, Lucan, Ontario

Methodology

The magnetic susceptibility of the cores was measured using a Bison Instrument Susceptibility Bridge model 3101A, with a 63.5 mm diameter accessory coil, model 3110-6 (Bison Instruments, 1970). The quantity determined is the volume susceptibility, i.e. the magnetic moment per unit volume (A/m) per unit magnetizing force (A/m). Thus, "true magnetic susceptibility" is a dimensionless quantity.

Every 2 m, a group of three measurements 0.1 m apart was made on core samples from the research areas. In cores URL 1, -2, and -5 (Underground Research Laboratory, Lac du Bonnet Batholith), measurements were taken every 0.1 m within fracture zones and within intervals of marked lithological change to record the near continuous change in susceptibility in these zones.

Lac du Bonnet batholith

The WN and URL cores are from drillholes at the Whiteshell Nuclear Research Establishment (WNRE) and Lac du Bonnet, Manitoba respectively. These boreholes intersect the Lac du Bonnet batholith, a high-level granitic intrusion within the Winnipeg River batholith belt of the English River subprovince in the Archean Superior Province (Beakhouse, 1977; Tammemagi et al., 1980). The batholith has been described by Tammemagi et al. (1980), as a pink, medium- to coarse-grained, slightly porphyritic, granite-granodiorite, which attains a maximum width of 25 km and an areal extent of over 1000 km^2.

Generally, susceptibility plots show that the cores can be divided into regions of differing magnetic character. Hence, susceptibility signatures in the first 140 m of core within WN-1, WN-2 (Fig. 25.2) and WN-4 (Fig.25.3), are similar: "background", uniform susceptibilities (7 to 10 x 10^{-3} SI) occurring within the interval 0 to 20 m correspond to non-fractured rock; susceptibility minima (0 to 2 x 10^{-3} SI) in the interval 40 to 90 m correspond to highly fractured rock (fracture frequency 5-35 fractures/metre) and a grey foliated tonalite zone (Coles and Morris, 1981). In WN-2 fractured rock prevails throughout the length of core from 35 m to approximately 150 m, coinciding with generally variable and low susceptibilities with the exception of a susceptibility increase at 100 m. The high (25 x 10^{-3} SI) corresponds to a magnetic anomaly which is notably present in all cores. Uniform background susceptibilities (7 to 10 x 10^{-3} SI) occur in the interval 140 m to 480 m in WN-1, with except for a low at 380 m to 440 m. This region of susceptibility minima coincides with a major fracture zone, also observed in WN-4, exhibiting fracture frequencies in the order of 4 to 48 fractures/metre. Many of the fractures are open. Core WN-4 exhibits more variable susceptibility. Intermittent lows occurring in the interval 100 m to 200 m correspond to fractured and altered rock. Somewhat higher values in the intervals 200 m to 380 m and 500 m to 740 m coincide with less altered, less fractured and comparatively homogeneous core. The amplitude and shape of the magnetic signatures corresponding to the major fracture zones, the tonalite layer, and the magnetic anomaly at 100 m, are similar in all the WN cores.

The relation between susceptibility, lithology and fracturing is evident in the URL cores. We see from a three-dimensional plot of the smoothed susceptibility of cores URL-1 to -7 (Fig. 25.4), that similar levels and types of susceptibility are observed in all cores except URL-4 (a short core). The levels of susceptibility are grouped into four types (Chomyn and Lapointe, in press): (i) susceptibility minima (0 to 5 x 10^{-3} SI); (ii) "background" susceptibilities (7 to 10 x 10^{-3} SI); (iii) intermediate susceptibilities (10 to 20 x 10^{-3} SI) and (iv) susceptibility maxima (20 to 100 x 10^{-3} SI). The minima are common to all cores generally within the first 150 m, corresponding in most instances to zones of intense fracturing with fracture frequencies in the order of 32 fractures/metre and greater.

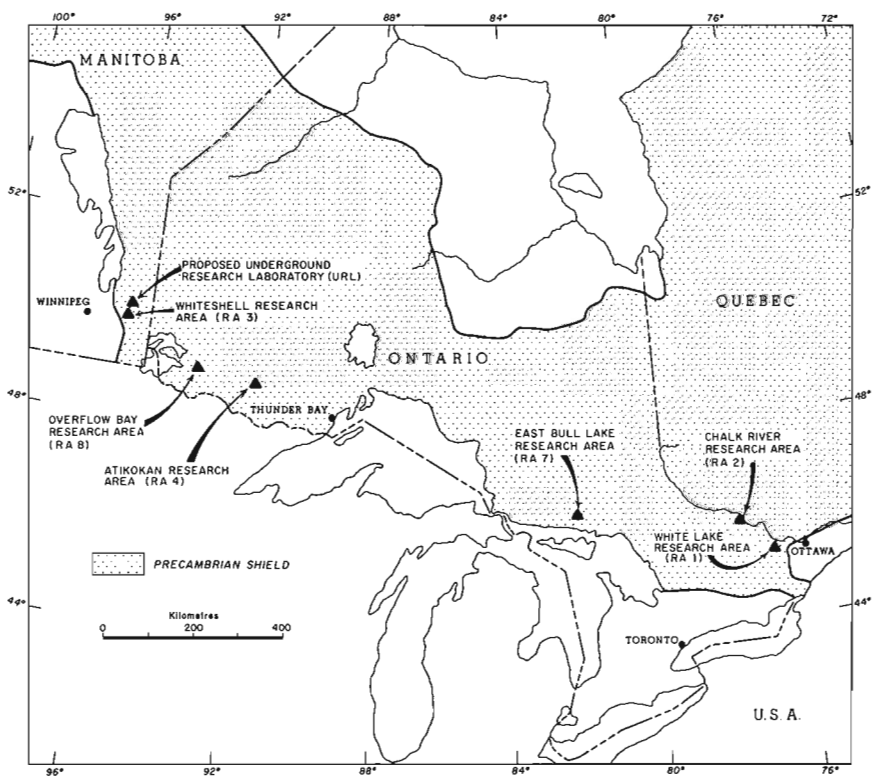

Figure 25.1

Locations of Atomic Energy of Canada Ltd., research areas in Manitoba and Ontario.

An example of a well-defined fracture zone in URL-1 between 80 m and 160 m and corresponding susceptibility minima is shown in Figure 25.5. The recorded bulk susceptibility values are low (0 to 4 x 10^{-3} SI) in comparison to the higher values measured in the enclosing less-altered, non-fractured rock. The relation between fracturing and susceptibility is well defined in Lac du Bonnet core because of the overall high magnetic content of the rock. Other occurrences of susceptibility lows that are not associated with major fracturing, coincide with hematite infilled hairline fractures (<3 cm), and intervals of core that are depleted in iron oxides. In contrast to the well defined susceptibility lows characterizing major fracture zones, these features produce poorly defined lows and are not common. Susceptibility maxima coincide with the presence of xenoliths and with intervals of core containing large and coarse-grained magnetic minerals. In URL-1 (Fig. 25.6) maxima predominate in the intervals 400 m to to 620 m. The uniform 'background' susceptibilities that characterize homogeneous, non-fractured unaltered rocks, for example in URL-1 at 60 m to 210 m and 630 m to 680 m, occur in varying amounts in all cores.

It is evident that comparable levels of magnetic susceptibility are found in the WN and URL cores. Susceptibility minima (0 to 5 x 10^{-3} SI) characterize fractured and altered rock; uniform susceptibilities ranging from 7 to 12 x 10^{-3} SI correspond to relatively homogeneous, unaltered core; and susceptibility maxima, that is anomalous values in susceptibility denote intervals of rock encompassing abundant magnetite. Susceptibility is more varied in the URL than in the WN, perhaps reflecting greater lithological heterogeniety within the batholith in the vicinity of the URL.

Table 25.1. Characteristic magnetic susceptibilities measured on drillcore from the respective research areas

Research Area	Borehole Depth (Metres)	Rock Type	Susceptibilities
Whiteshell Nuclear Research Establishment (Manitoba)		Lac du Bonnet Batholith	
WN-1	153	medium-to coarse-grained slightly porphyritic granite-granodiorite	minima: 0 to 4 x 10^{-3} SI
WN-2	474		maxima: 20 to 80 x 10^{-3} SI
WN-3	199		background: 7 to 12 x 10^{-3} SI
Underground Research Laboratory (Manitoba)		Lac du Bonnet Batholith	
URL-1	678.82	same as above	minima: 0 to 4 x 10^{-3} SI
URL-2	1099.80		maxima: 20 to 100 x 10^{-3} SI
URL-3	389.44		background: 7 to 12 x 10^{-3} SI
URL-4	157.60		
URL-5	500.47		
URL-6	400		
URL-7	200		
Chalk River, Ontario			
CR-1	269.2	garnetiferous quartz monzonite; amphibolite to granulite metamorphic grade	minima: 0 to 4 x 10^{-4} SI maxima: 20 to 100 x 10^{-4} S background: 5 to 7 x 10^{-4} SI
CR-2	213.5		
CR-3	159.8		
CR-4	113.0		
CR-5	230.1		
CR-6	304		
CR-7	152		
CR-8	304		
CR-9	704		
Atikokan, Ontario		Eye-Dashwa Lake Pluton	
ATK-1	1151	medium to coarse-grained porphyritic, hornblende-biotite granite	minima: 0 to 10 x 10^{-3} SI
ATK-2	199		maxima: 25 to 50 x 10^{-3} S
ATK-3	400		background: 17 to 22 x 10^{-3} SI
ATK-4	340		
ATK-5	1290		

Chalk River

The Chalk River research area lying within Atomic Energy of Canada Limited's (AECL) Chalk River Nuclear Research Establishment, is underlain by complex folded rocks of the Canadian Shield and overlain by Pleistocene deposits. The area is lithologically heterogeneous and structurally complex. The main rock unit, a folded sheet of garnetiferous quartz monzonite, comprises granitic monzonitic and syenitic phases, and is overlain and underlain by paragneisses and discontinuous pods of metagabbro (Dence and Scott, 1979). The rocks are of amphibolite to granulite regional metamorphic grade. The area is cut by numerous faults and fractures (Brown and Roy, in press). Susceptibility values of the CR cores are about 5×10^{-4} SI; an order of magnitude less than the average values of the Lac du Bonnet and Atikokan granites. However, caution is advised in the interpretation of the data, because the average magnetic susceptibility values are close to the resolution of the susceptibility instrument (Coles, in press).

In CR-1, minima predominate in regions of extensive fracturing and shear zones; in particular in the intervals 80 to 110 m, 160 m to 175 m, and 230 m to 240 m. Of the total length of core (270.6 m), the upper 160 m exhibits a higher level of susceptibility than the remaining 110 m. This feature reflects a higher mafic content in the former than in the latter.

CR-2 is more extensively fractured throughout its 213 m than CR-1, a characteristic reflected in its overall low susceptibility values ($0\text{-}2 \times 10^{-4}$ SI).

CR-3, like CR-2 is a short core (160.5 m). It exhibits somewhat higher values of susceptibility in the first 100 m of core than in either CR-1 or CR-2. The higher susceptibility reflects the predominance of mafic rich units: amphibolites and pyroxenites. A quartz monzonitic gneiss occurs in the

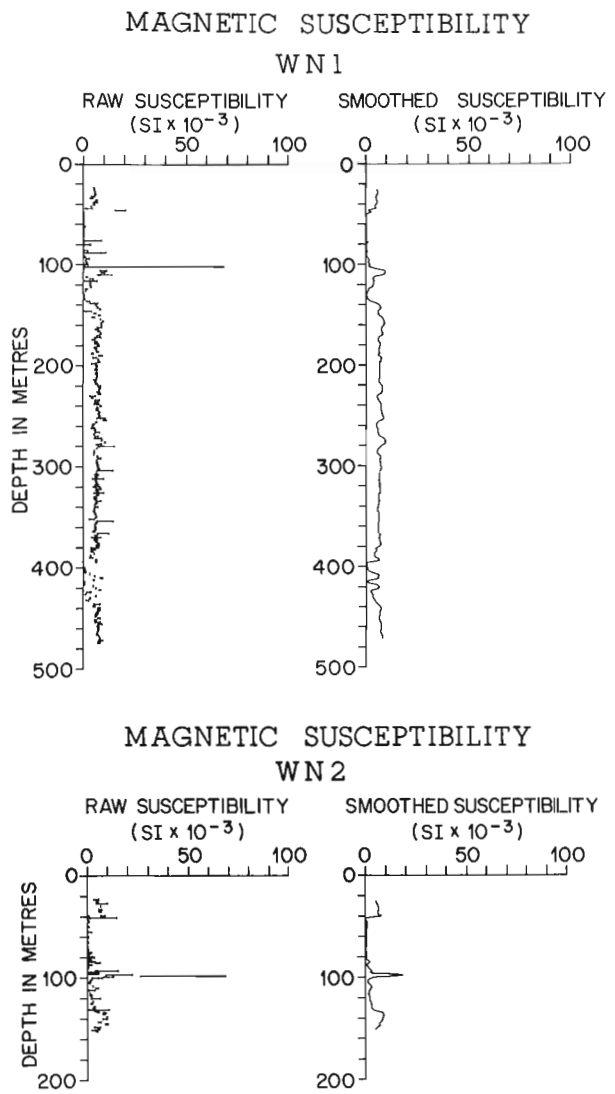

Figure 25.2. *Plots of raw and smoothed susceptibility of cores WN-1 and WN-2. The smoothed curve is obtained by averaging three measurements, 0.1 m apart, per susceptibility sampling interval. The horizontal lines in the raw data join maximum and minimum susceptibility measurements within the 2 m interval. This plotting technique applies to the smoothed susceptibility logs in subsequent figures.*

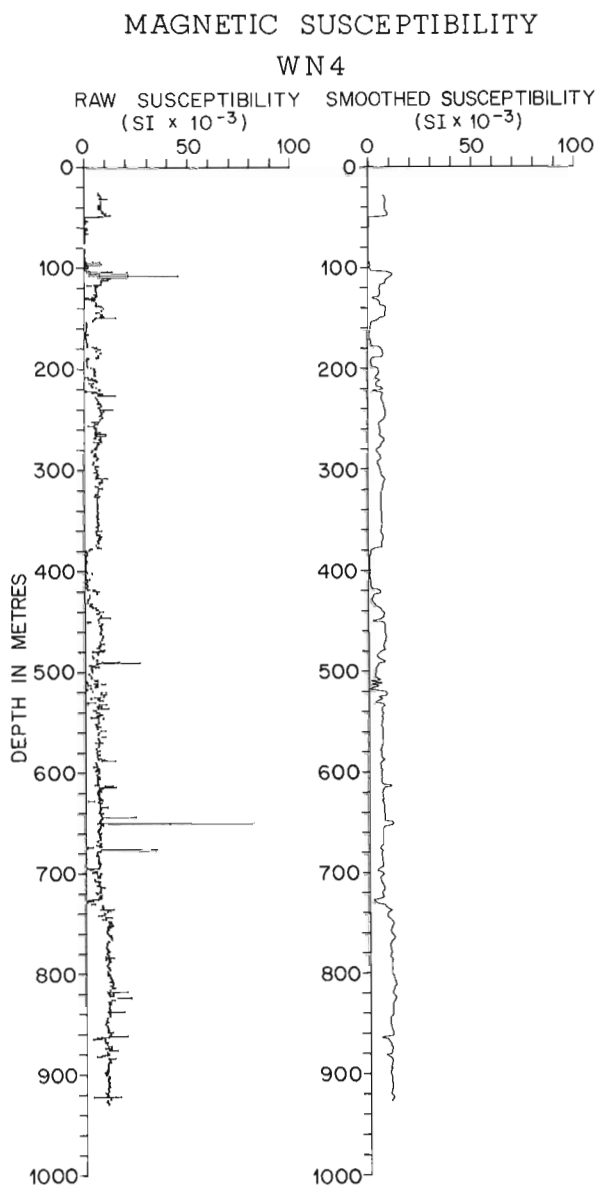

Figure 25.3. *Plots of raw and smoothed susceptibility for core WN-4.*

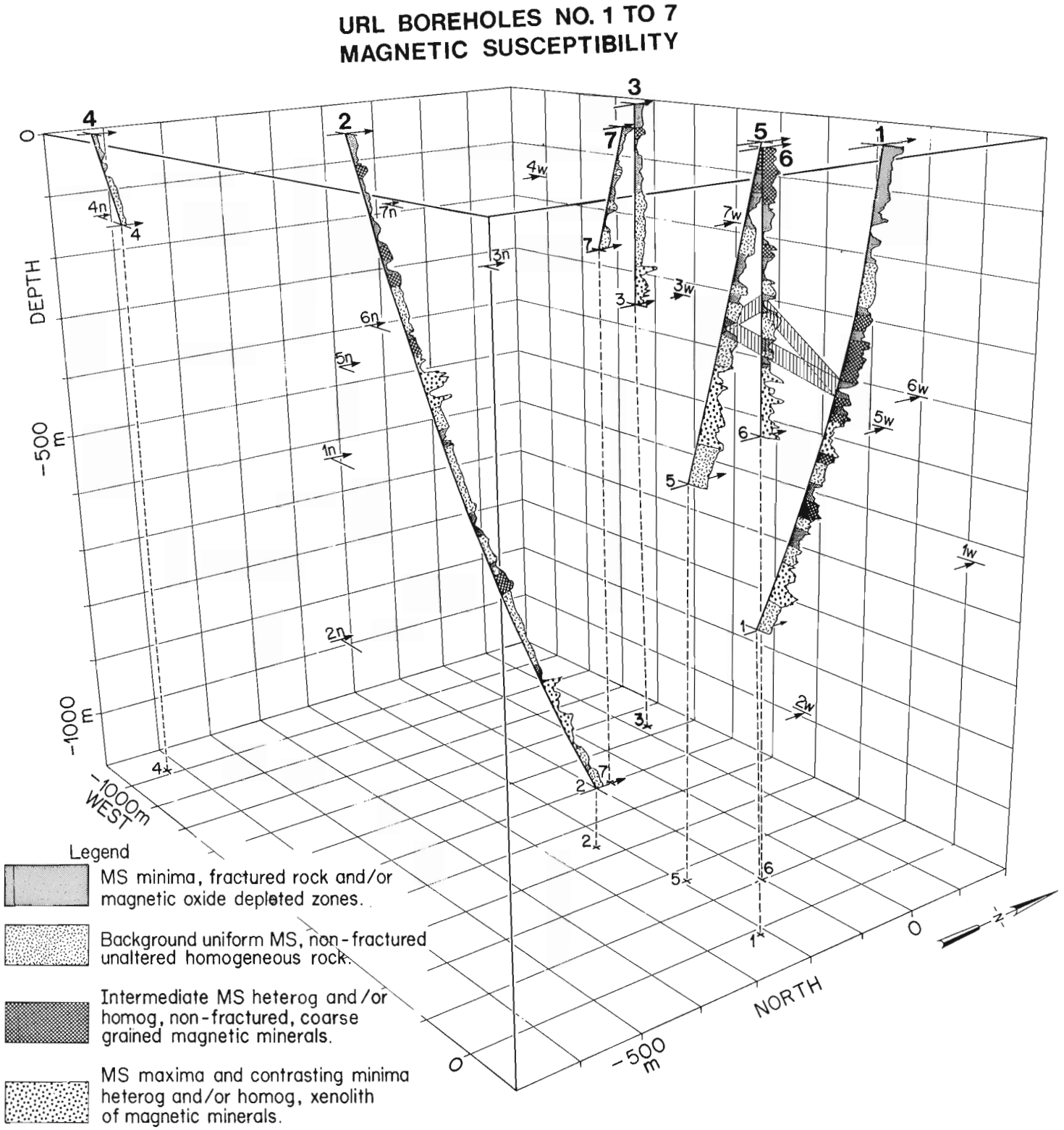

Figure 25.4. *Three dimensional plot of smoothed susceptibility of cores URL -1, -2, -3, -4, -5, -6 and -7, portraying characteristic susceptibility 'zones'.*

remaining 60 m of CR-3, and is also characterized by well developed fracturing and brecciation. This interval of fracturing is marked by decreased susceptibility in comparison with the less fractured core above 100 m.

CR-4 is similarly highly fractured. An extensive zone of fracturing and faulting occurs from 80 m to 100 m, containing several zones of open fractures that correspond to susceptibility near zero. A susceptibility maxima (greater than 100×10^{-4} SI) occurs at 100 m and denotes the intersection of the core by a diabase dyke. Pyroxenite and amphibolite units and less fractured rock occurring above this zone (shallower than 50 m) account for generally higher susceptibilities.

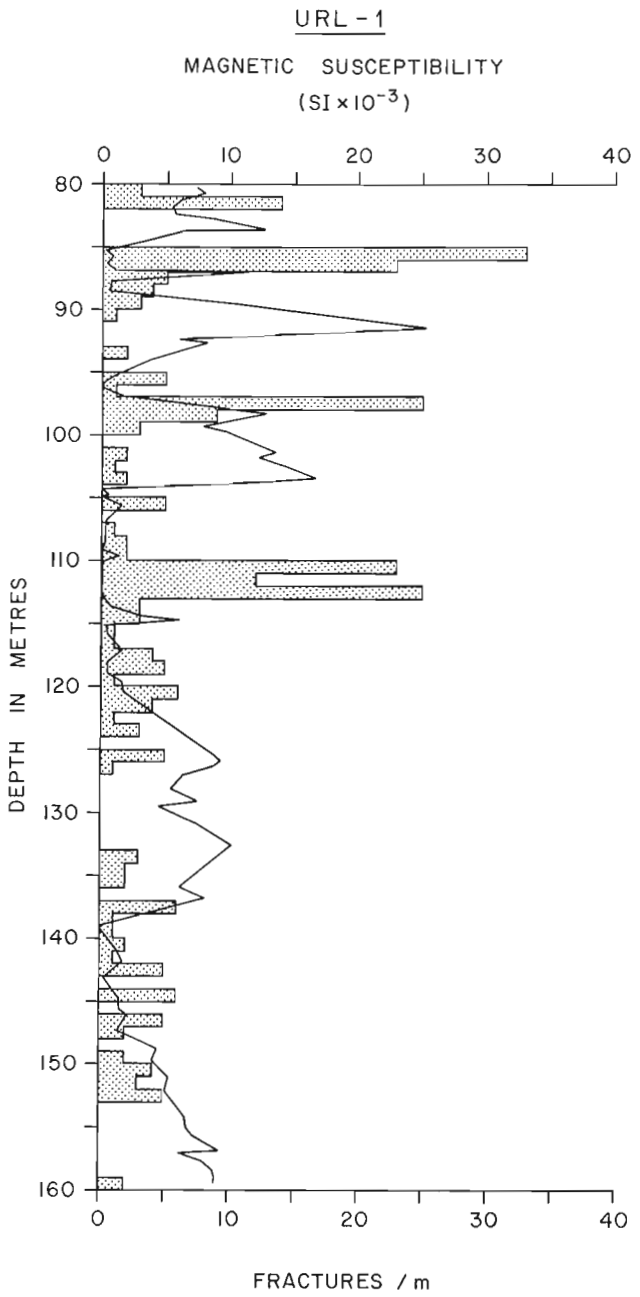

Figure 25.5. Plot of susceptibility measured at 10 cm intervals in URL-1 between 80 and 160 m. Note correlation between susceptibility minima (solid line) and fractured rock (stippled area).

Higher and somewhat more variable susceptibilities are observed in CR-5. Susceptibility maxima (20 to 80 x 10^{-4} SI) occurring in the intervals, 70 m to 105 m, 125 m to 140 m and 210 m to the end of the core (230.1 m), coincide with intervals of core that are less fractured (fracture frequencies 5 to 35 fractures/metre). By comparison the upper and middle portion of CR-5 is more fractured (25 to 100 fractures/metre) with corresponding susceptibility minima values of 0 to 2 x 10^{-3} SI.

In CR-6, a pronounced increase in susceptibility occurs from 200 m to 300 m which coincides with the presence of a diabase dyke (Fig. 25.7) (fracture and lithological logs of CR cores, Dugal and Kamineni, in press).

There are no diabase units or anomalous zones in CR-7. Low and relatively uniform susceptibilities characterize the 152 m of core.

In CR-8 several anomalous zones occur around 50 m and from 240 m to 270 m. The latter zone coincides with lenses of metagabbro; the former corresponds to an interval of less fractured rock (2 to 5 fractures/metre) as compared to the more extensively fractured rock (20 to 100 fractures/metre) and attendent susceptibility minima characteristic of the rest of the core.

Over its 704.3 m length, the susceptibility values of CR-9 are generally low except for a few zones. An unmetamorphosed diabase dyke coinciding with susceptibility maxima (40 to greater than 100 x 10^{-4} SI) occurs within the intervals 40 m to 60 m (Fig. 25.8) and a metagabbro with similar susceptibilities occurs from 480 m to 670 m (Chernis and Hamilton, in press). Two distinct magnetic zones which

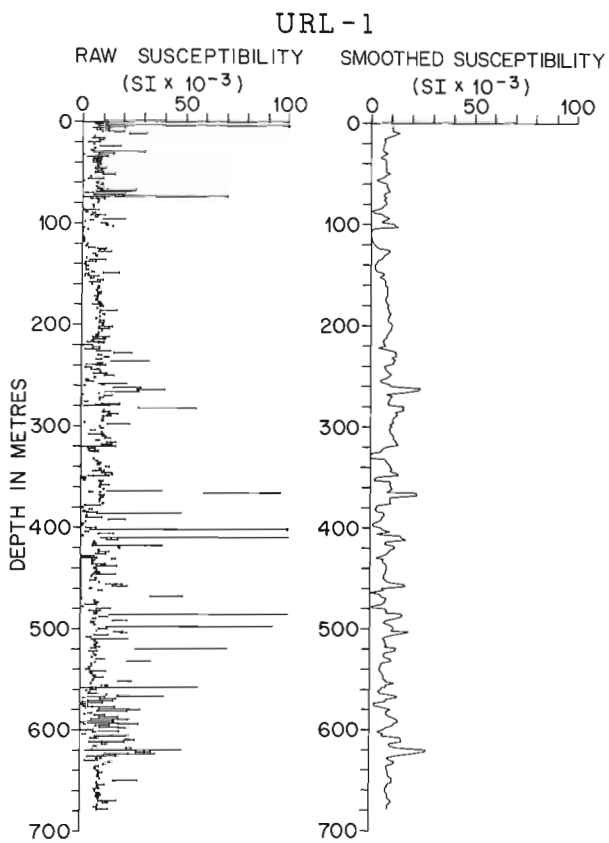

Figure 25.6. Plots of raw and smoothed susceptibility of URL-1. As in previous figures, the smoothed curve is obtained by averaging three measurements, 0.1 m apart per susceptibility sampling interval.

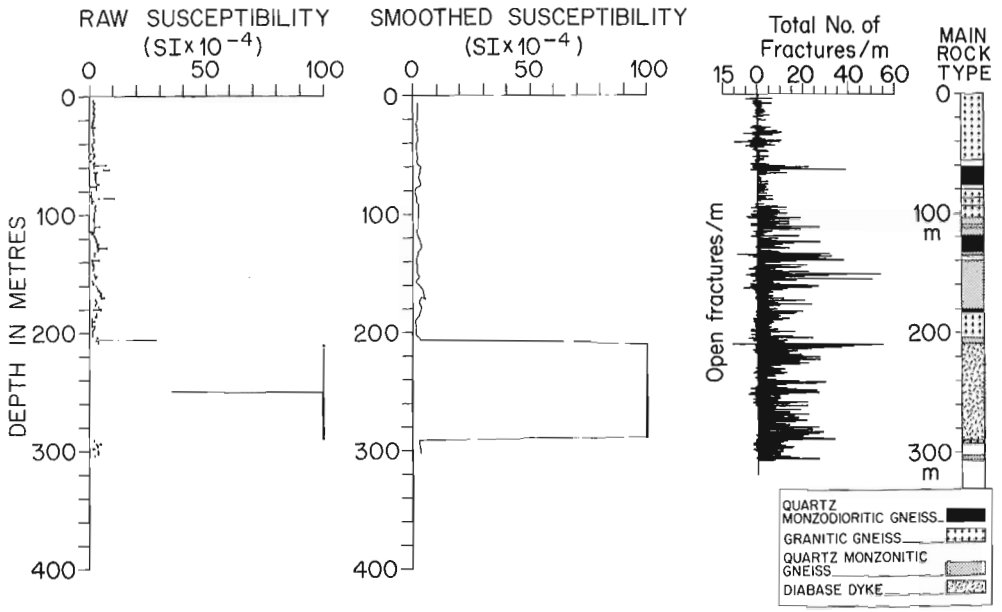

Figure 25.7

Raw and smoothed susceptibility plots, fracture and lithological logs of CR-6. Anomalous zone corresponds to diabase dyke. (Note, low levels of susceptibility are close to resolution of instrument).

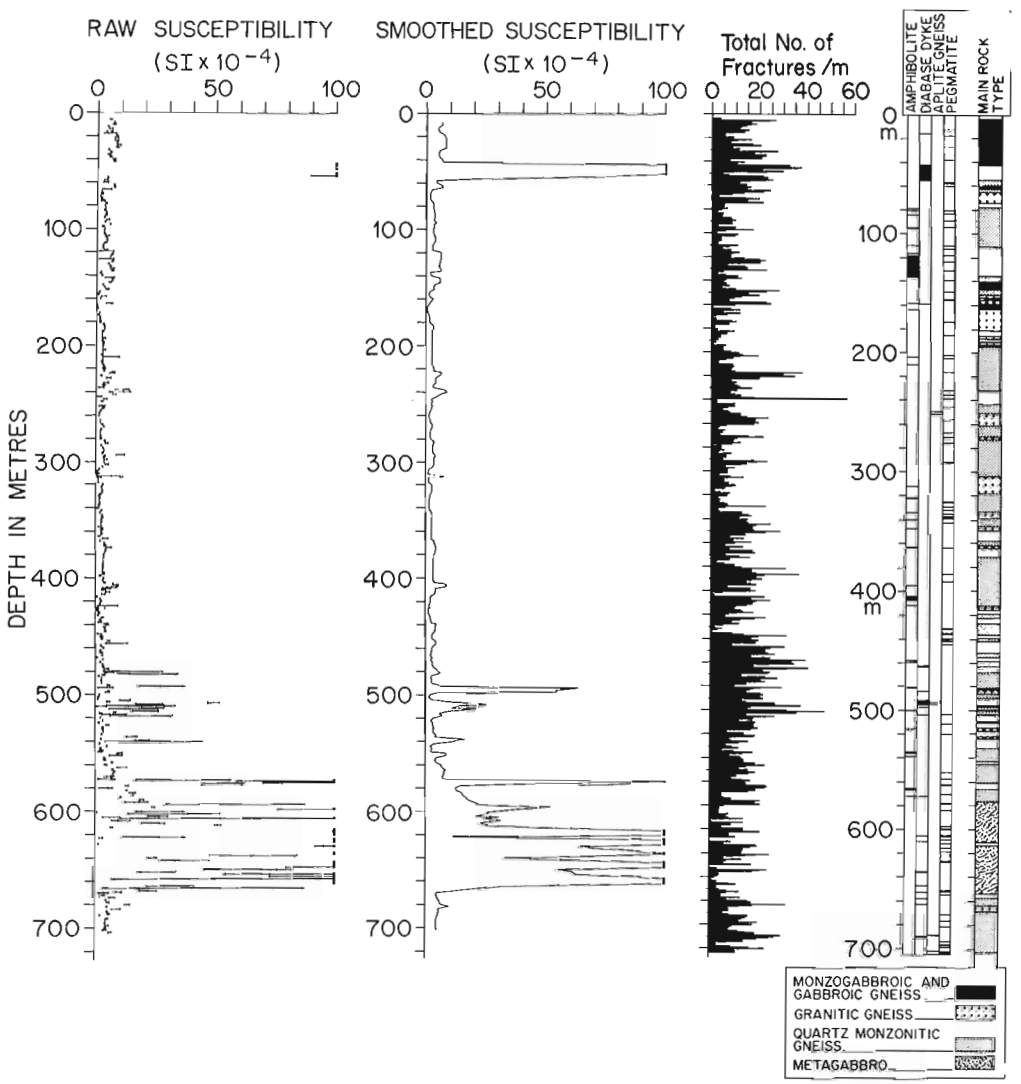

Figure 25.8. *Raw and smoothed susceptibility plots and fracture and lithological logs of CR-9. Anomalous zones correspond to an upper unmetamorphosed diabase dyke, and a lower metagabbro unit.*

are believed to be lithologically different are distinguished within the metagabbro unit (Coles et al., in press); one from 580 m to 615 m, and the second from 615 m to 670 m. The susceptibility signature of the remaining intervals of core is comparable to the signatures of the previous CR cores.

Eye-Dashwa pluton, Atikokan

Bulk magnetic susceptibility measurements were made on five cores drilled within the Eye-Dashwa granite pluton north of Atikokan. The pluton, averaging 14 km in length and 7 km in width, occurs within the Superior Province of the Canadian Shield. It is described as a massive medium- to coarse-grained porphyritic, hornblende-biotite granite

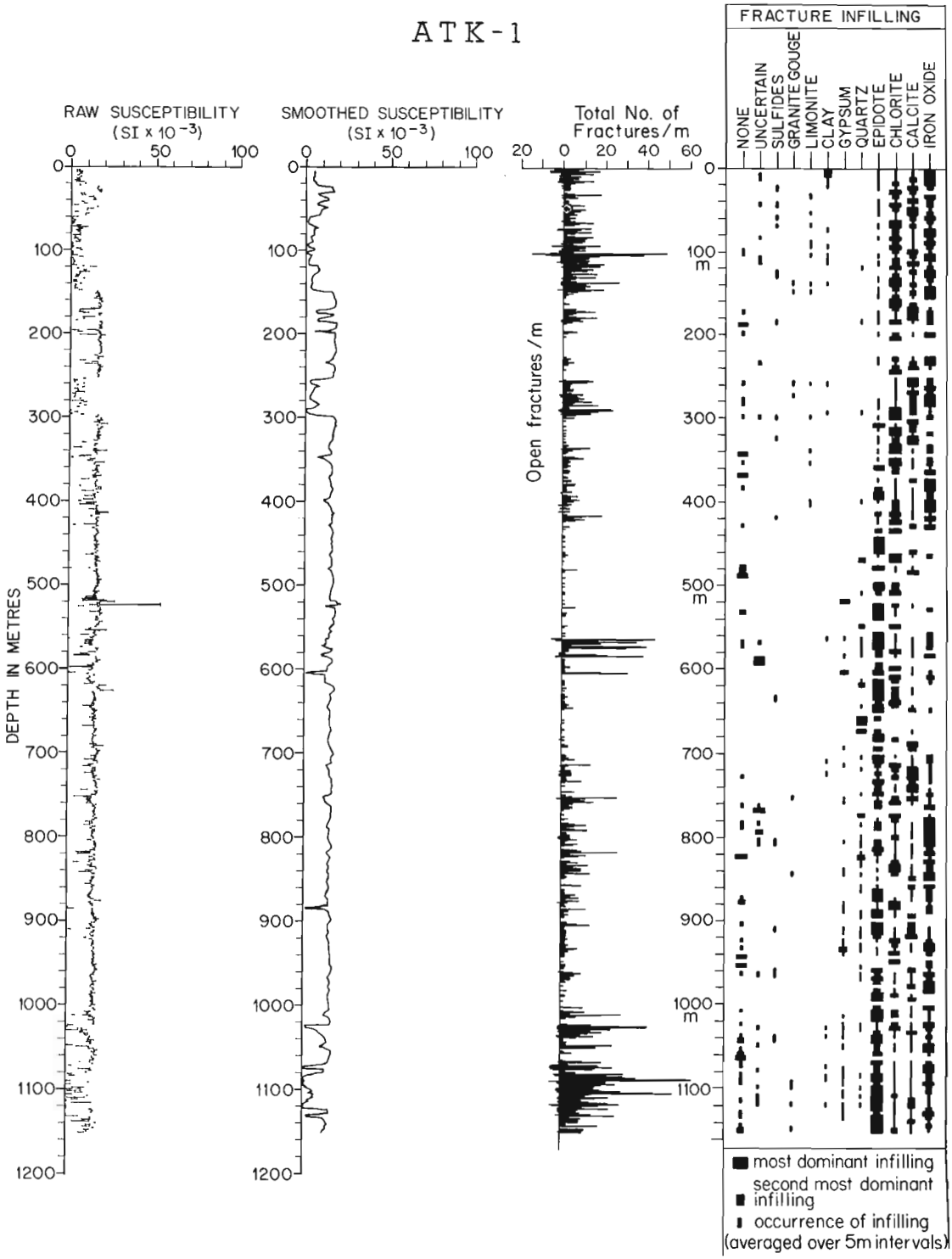

Figure 25.9. Raw and smoothed susceptibility for ATK-1 and fracture and lithological logs.

surrounded by tonalitic gneisses which are in turn enveloped by metavolcanics (Kamineni and Stone, 1983). The relatively homogeneous granite gives susceptibilities in the order of 17 to 18 x 10^{-3} SI, which are higher and generally more uniform in comparison with values from drillcore of the other research areas. Deviations from this value are indicative of lithologic change and/or alteration of the magnetic minerals by secondary geologic processes.

The magnetic susceptibility of core ATK-1 (Fig. 25.9) is variable throughout its 1160 m (fracture and lithological logs, Dugal et al., 1981). The first 0 to 150 m of core, as in ATK-2 and ATK-3, is marked by many minima (0 to 10 x 10^{-3} SI) that correspond to major fracture zones. Somewhat higher susceptibilities (20 x 10^{-3} SI) with several lows occur from 100 m to 1000 m reflecting the presence of less fractured rock. A major fracture zone at 1000 m to the end of the core (1150 m) is denoted by variable and low susceptibilities. Similarly, the occurrences of several fracture zones at 0 m to 180 m, and 185 m to 195 m in ATK-2, and 50 m to 140 m, 180 m to 260 m and 300 m to 380 m in ATK-3 coincide with susceptibility minima (0 to 4 x 10^{-3} SI). Fracture frequencies in these intervals range from 5 to 55 fractures/metre; the more extensive the fracturing and associated alteration, the lower the susceptibility value. Similar features are observed in ATK-4 and ATK-5; magnetic susceptibility lows at 20 m, from 80 m to 270 m in ATK-4, and 0 m to 530 m and 1230 m to 1270 min ATK-5, correspond to fractured rock exhibiting fracture frequencies ranging from 5 to 90 fractures/metre. The core immediately between this fracture interval in ATK-5 is less altered, and gives corresponding higher susceptibilities (18 to 22 x 10^{-3} SI), with relatively low fracture frequencies (0 to 10 fracture/metre). In the ATK cores, the fracture fillings are of several generations. The oldest being pegmatite, aplite and hornblende porphyry fillings. Those younger include epidote, chlorite, diabase, iron oxides, gypsum, carbonate and clay (Stone and Kamineni, 1981). The magnetic data show that ATK-5 is from an area that has a total field 100 gammas greater that the ATK-1 to 4 cores; a feature that could correspond to the higher levels of susceptibility measured in the ATK-5 core (J. Hayles, personal communication, 1984).

Summary

The magnetic susceptibility measurements on drillcore from the Lac du Bonnet batholith, the Eye-Dashwa Lake pluton and the Chalk River research area have been used to effectively characterize the differences in lithology of these various rock bodies. Although the levels of susceptibility vary from one research area to the next, the following significant similarities in the types of signatures are noted:

1. Fractured, brecciated and altered rock in most all cases correspond to susceptibility minima. This observation has been shown true with respect to the major fracture systems in ATK, WN, CR and, in particular, in the URL core.
2. Anomalous values of susceptibility reflect lithological changes, such as xenoliths comprising magnetite, dykes with high magnetite concentrations, etc.
3. Unaltered core gives corresponding uniform susceptibilities of about 7 to 12 x 10^{-3} SI for WN and URL, and 17 to 22 x 10^{-3} SI for ATK.
4. Variability in susceptibility arises as a result of lithological change. The more variable the susceptibility, the more heterogeneous the rock body. This feature is evidenced by the heterogeneity of URL core compared to homogeneity of ATK core.
5. Similarities in the types and levels of magnetic susceptibility are observed in the URL and WN cores. The ATK values are slightly higher, corresponding to a more magnetic rock type. The metamorphosed and highly fractured CR cores give the lowest values in susceptibility compared to the other research areas.

Acknowledgments

The authors thank J.K. Park and J.L. Roy from Earth Physics Branch (EPB), EMR, Ottawa for discussing and reviewing this paper. (EPB contribution 1128).

References

Beakhouse, G.P.
1977: A subdivision of the western English River Subprovince; Canadian Journal of Earth Sciences, v. 14, p. 1481.

Bison Instruments
1970: Instruction manual for magnetic susceptibility system Model 3101 and accessories; Bison Instruments, St. Louis Park, Minneapolis.

Boulton, J. (editor)
1978: Management of Radioactive Fuel Wastes; The Canadian Disposal Program; Atomic Energy of Canada Limited Report, AECL-6314.

1980: Second Annual Report of the Canadian Nuclear Fuel Waste Management Program; Atomic Energy of Canada Limited Report, AECL-6804.

Boulton, J. and Gibson, A.R.
1979: First Annual Report of the Canadian Nuclear Fuel Waste Management Program; Atomic Energy of Canada Limited Report, AECL-6443.

Brown, P.A. and Rey, N.A.C.
in press: Fractures and Faults at Chalk River, N.E. Ontario; in Proceedings of a Workshop on Geophysical and Related Geoscientific Research at Chalk River, Ontario, Atomic Energy of Canada Ltd., Technical Report.

Chernis, P.J. and Hamilton, K.T.
in press: Petrography and petrology of rocks in borehole CR-9, Chalk River, Ontario; Workshop on Geophysical and Related Geoscientific Studies at Chalk River, December 1983, Atomic Energy of Canada Limited, Technical Report.

Chomyn, B.A. and Lapointe, P.
1984: Magnetic susceptibility and lithological variations within the Lac du Bonnet Batholith, Manitoba, Canada; in Process Mineralogy III, W. Petruk, ed., Society of Mining Engineers, American Institute of Mining, Metallurgical and Petroleum Engineers, New York, p. 99-117.

Coles, R.
1981: Magnetic properties of rock: assessment of geoscience methods of rock mass evaluation; Earth Physics Branch, Energy Mines and Resources, internal report.

Coles, R.L., and Morris, W.A.
1981: Bulk and anisotropic magnetic susceptibilities applied to structural geological studies at WNRE; Atomic Energy of Canada Limited, Technical Report, TR-157.

Coles, R.L., Lapointe, P., Morris, W.A., and Chomyn, B.A.
– Magnetic susceptibility of rocks from boreholes CR-1 to CR-9 at Chalk River; in Proceedings of a Workshop on Geophysical and Related Geoscientific Studies at Chalk River, December 1983, Atomic Energy of Canada Limited, Technical Report. (in press)

Dence, M.R. and Scott, W.J.
1979: The use of geophysics in the Canadian Radioactive Waste Disposal Program, with examples from the Chalk River research area; Geoscience Canada, v. 6, no. 4.

Dixon, R.S. and Rosinger, E.L.J.
1981: Third Annual Report of the Canadian Nuclear Fuel Waste Management Program; Atomic Energy of Canada Limited, Report AECL-6821.

Dugal, J.J.B. and Kamineni, D.C.
– Lithology, fracture intensity and fracture filling of drillcores from the Chalk River research areas, Chalk River, Ontario; in Proceedings of a Workshop on Geophysical and Related Geoscientific Research at Chalk River, Ontario, Atomic Energy of Canada Ltd., Technical Report. (in press)

Dugal, J.J.B., Hillary, E.M., Kamineni, D.C., Simandl, G.J., and Sikorsky, R.I.
1981: Drilling and core logging programs at the Atikokan research area; Atomic Energy of Canada Limited, Technical Report, TR-174.

Kamineni, D.C. and Stone, D.
1983: The age of fractures in the Eye-Dashwa Pluton, Atikokan, Canada; Contribution to Mineralogy and Petrology, v. 83, p. 237-246.

Sheng, G. and Shemilt, L.W.
1981: Commentary on The Canadian Nuclear Fuel Waste Management Program; Geoscience Canada, v. 8, p. 16-20.

Stone, D. and Kamineni, D.C.
1981: Fractures and fracture infillings of the Eye-Dashwa Lakes Pluton Atikokan, Ontario. Canadian Journal of Earth Sciences, 19, p. 789-803.

Tammemagi, H.Y., Kerford, P.S., Requima, J.C., and Temple, C.A.
1980: A Geological Reconnaissance Study of the Lac du Bonnet Batholith; Atomic Energy of Canada Limited, Report AECL-6439.

26. MAGNETIC 3-COMPONENT BOREHOLE MEASUREMENTS IN FINLAND

A. Hattula[1]

Hattula, A; Magnetic 3-component borehole measurements in Finland; in Borehole Geophysics for Mining and Geotechnical Applications, ed. P.G. Killeen, Geological Survey of Canada, Paper 85-27, p. 237-250, 1986.

Abstract

Borehole magnetometry has been utilized at Rautaruukki Oy since the late 1950s using equipment developed by the company. Measurements of three orthogonal components of the magnetic field are used for ore prospectng and in the planning of mining operations. Interactive programs have been developed for data processing and for interpretation using the Hewlett-Packard 9845 desktop computer. The program uses 2-D models, but the effect of the third component of the magnetic field in a drilling profile that does not run perpendicular to the strike of the body can also be calculated. Results obtained from magnetite ores are described and the applicability of the method in the search for sulphide ores is discussed.

Résumé

La société Rautaruukki Oy poursuit la prospection magnétométrique des sondages depuis la fin des années 50 en utilisant des appareils qu'elle a elle-même mis au point. Les mesures obtenues des trois composantes orthogonales du champ magnétique sont utilisées pour la prospection des minerais et la planification des activités minières. Des programmes interactifs pour le traitement et l'interprétation des données ont été élaborés à l'aide d'un ordinateur de table Hewlett-Packard 9845. Le programme utilise des modèles en deux dimensions mais peut également calculer l'effet de la troisième composante du champ magnétique dans un profil de forage qui n'est pas perpendiculaire à la direction de la masse minéralisée. Le rapport décrit les résultats de l'étude des minerais de magnétite et la possibilité d'utiliser cette méthode pour la prospection des sulfures.

Introduction

Magnetic 3-component measurements in boreholes are not commonly used in mining and ore prospecting in the world, partly due to the fact that generally magnetite iron ore stoping blocks have increased to such a size that borehole measurements in them are no longer of any significance. On the other hand, interest has been aroused recently in the possibility of using the magnetic 3-component method in addition to electromagnetic borehole measurement methods to study polymetallic ores.

The stimulus for the development of the 3-component magnetometry technique at Rautaruukki Oy was the need to solve certain problems associated with the investigation and extraction of the complex ilmenite-magnetite ore at the Rautaruukki's Otanmaki mine in the mid-1950s (Paarma, 1954; Paarma and Levanto, 1958). This led to its establishment as a routine method at the company's mines and in its exploration work. The method is now used in all boreholes made for prospecting purposes, provided that the magnetic anomalies at the surface are sufficiently strong.

The simplest means of interpreting the results of magnetic 3-component measurements consists of examination of the measured magnetic field vector in two perpendicular planes. The location of the poles of the magnetized rocks can then be calculated from the convergence and divergence of the vectors by reference to the arcs of a circle (Levanto, 1963). A method based on the approximation of sheet models by means of line poles has also been proposed, in which the zero points for the horizontal and vertical components of the anomaly field are determined and the location of the pole or poles ascertained from these using a set of model curves (Lantto, 1973). However, such visual and graphical methods prove inadequate as soon as one is dealing with even slightly more complicated results, and thus computer technology has been introduced to develop better interpretation programs and calculation methods. It has been shown that the knowledge of two perpendicular components of the magnetic field yields new possibilities for using the inversion technique and an exact simplified formulation of the anomalous field (Kunaratnam, 1972; Hjelt, 1976a). An interactive program for processing and interpreting magnetic 3-component measurements on a Hewlett-Packard 9845 desktop computer have been developed (Hattula and Hjelt, 1981). The program uses the technique of the demagnetization factor for calculating magnetic anomalies of bodies with high susceptibility. A good basis to compare the rapid calculation methods used in interactive interpretations and to estimate accuracies is the technique where the surface integral equation is solved numerically by using the method of subsections. This enables precise solution of the inhomogeneous magnetization of complicated bodies (Eskola and Tervo, 1980).

[1] Rautaruukki Oy Exploration, P.O. Box 217, SF-90101 Oulu 10, Finland

Measurements and data processing

The borehole magnetometer 3DHM-4 comprises a borehole probe with inclinometer and an electronic unit. The 3 components of the magnetic flux density are measured in a co-ordinate system determined by the borehole itself: the first component in the direction of the borehole, the second in the vertical plane determined by the borehole and direction perpendicular to it, and the third at right-angles to the previous two, making up the horizontal component (Fig. 26.1). The diameter of the probe is 32 mm. The 3 fluxgate elements in the probe are fixed to the same frame, which is turned around an axis parallel to the first component by a servomotor controlled by a positioning element suspended from a torsion wire (a pendulum). The aim in the construction of the device was to achieve a mechanically durable structure which would enable measurements to be carried out in practically vertical boreholes (Hattula and Paarma, 1981). Measurements are performed stepwise along the borehole.

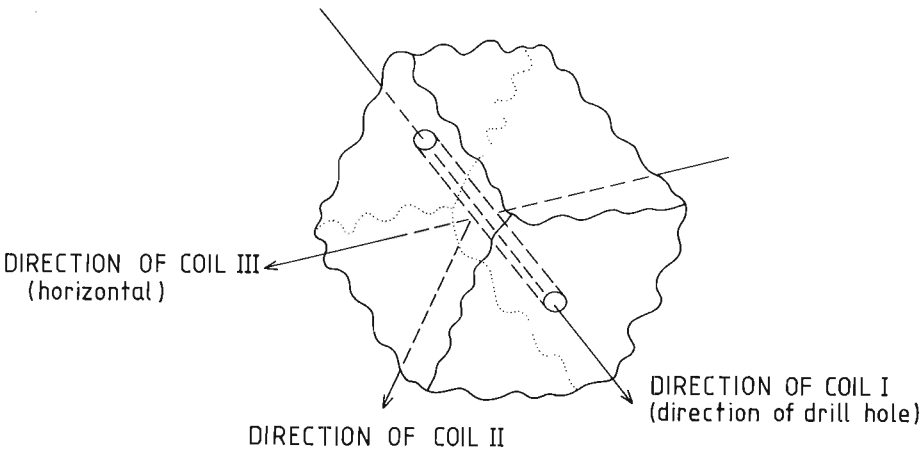

Figure 26.1. The components measured with the borehole magnetometer 3DHM-4.

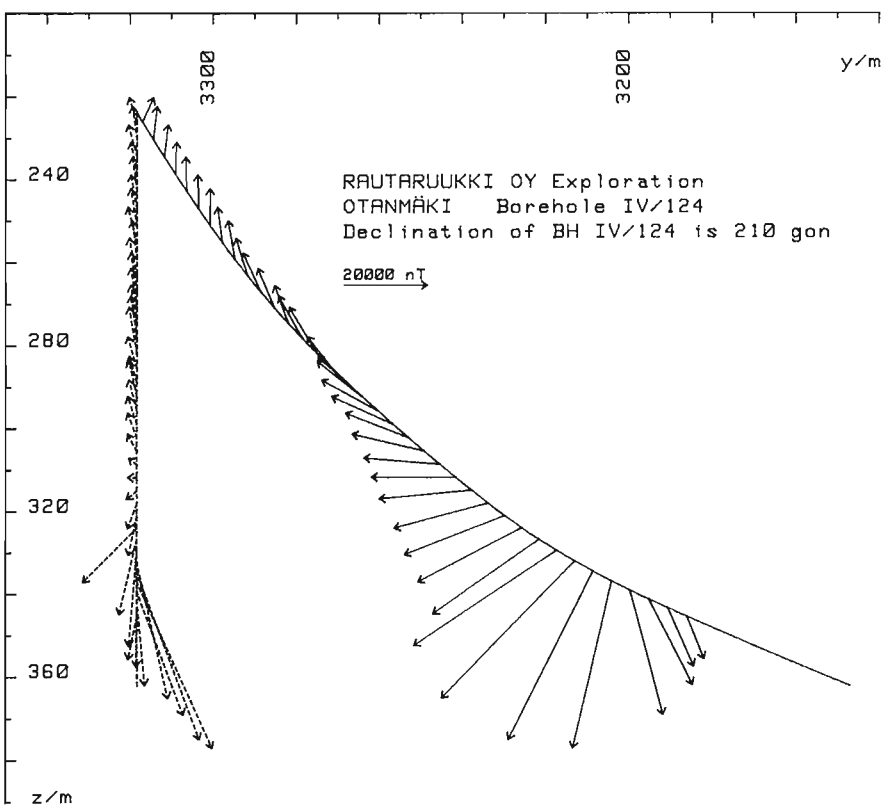

Figure 26.2. The form of presentation of measured anomaly field. Projections of the borehole from a side (solid vectors) and from back (dished vectors). y = distance to the east in metres, z = depth in metres, angle in gon (= grade). Note: 1 gon (grade) = 0.9°.

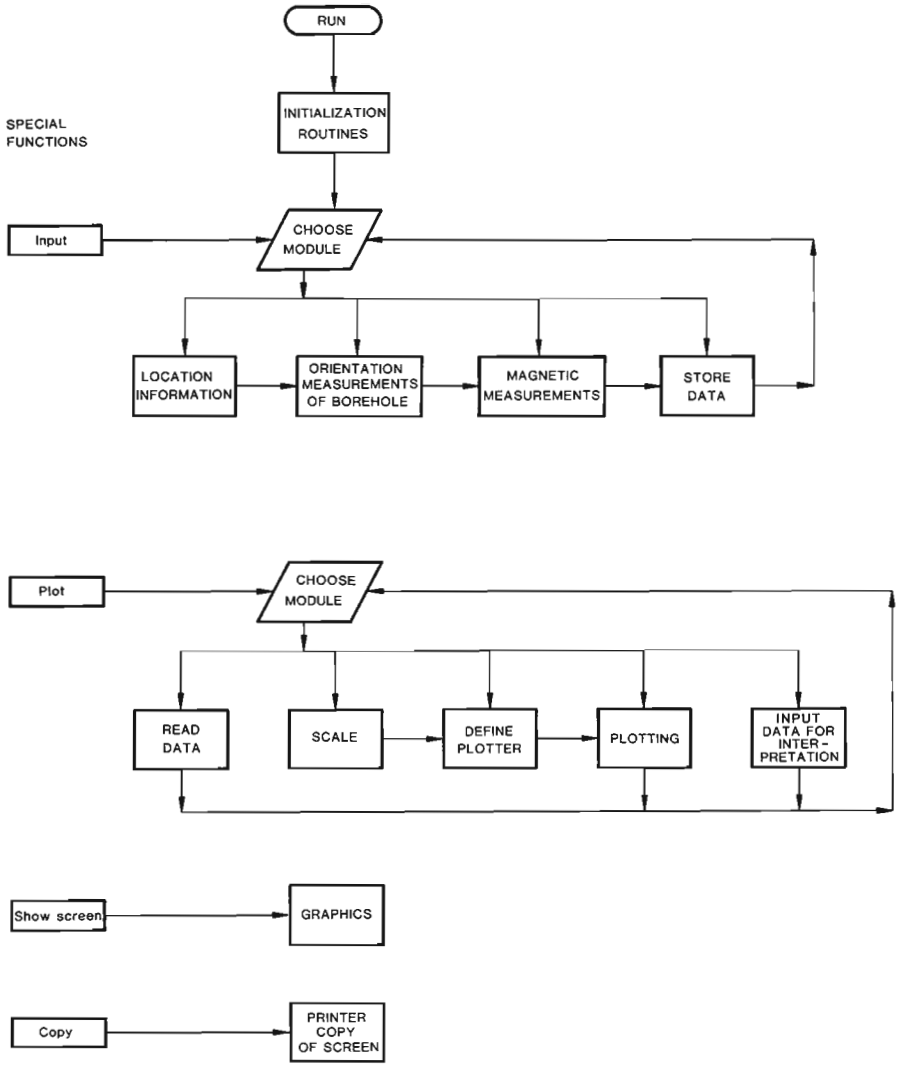

Figure 26.3. *The flow chart of the data processing.*

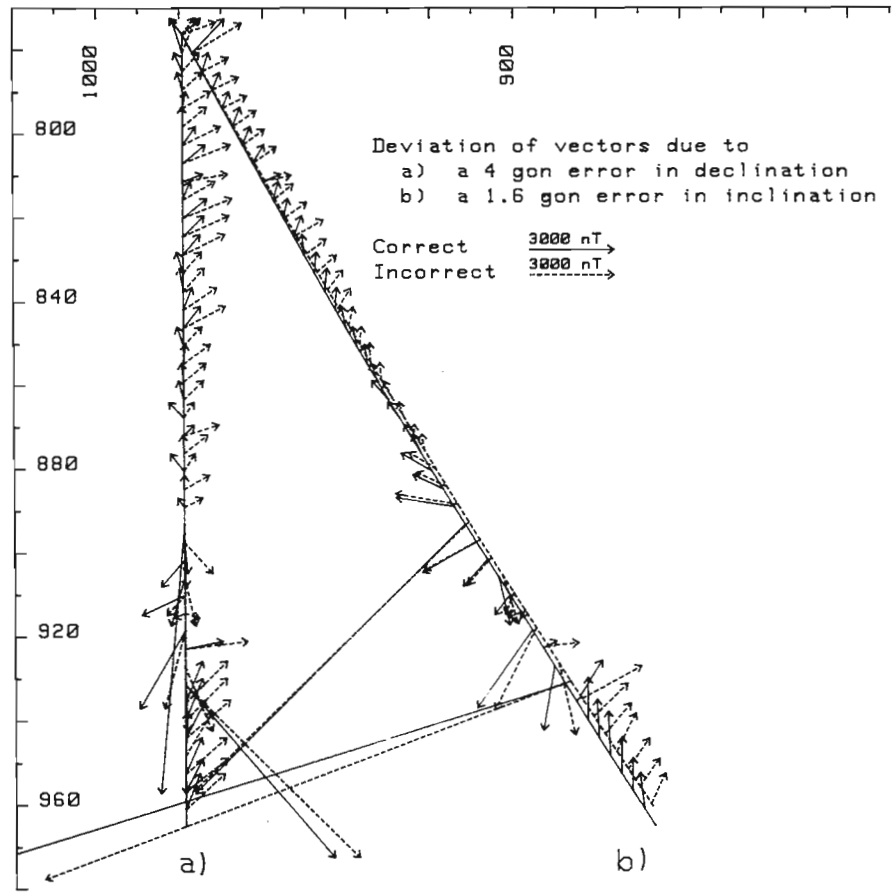

Figure 26.4. *Typical deviations of magnetic field caused by error in declination (a) or in inclination (b) of a borehole. The borehole runs to the south.* H_o *41.1 A/m and* I_o *= 82.4 gon (or grade). Note: 1 gon (grade) = 0.9°.*

The sensitivity of the magnetometer is approximately ± 100 nT for each component, and the measurement range ± 100 μT, although the actual limits of accuracy may run into hundreds of nanoteslas, due to various sources of error such as inaccuracies in the determination of the direction of the borehole, imprecisions in the positioning of the fluxgate coils, the difference in diameter between the borehole and the probe and temperature drift (Levanto, 1963).

The principal task in the processing of the results is the elimination of the regional geomagnetic field, which is best done for each measured component separately. Depending on the direction of the borehole in relation to the earth's field, any one component may emerge as critical for recognition of the true orientation of the probe at the moment of measurement. The decisive step is the determination of the correct orientation of the borehole, since the measurements take place on a system of co-ordinates related to this. Even quite small errors, the causes of which can be extremely hard to detect, can strongly affect the final results.

The results are presented in the form of anomaly vectors caused by bodies in the vertical cross-section and as projections onto the vertical plane running perpendicular to that determined by the borehole (Fig. 26.2). The aim of the latter is to illustrate the effect of the horizontal component. The results can conveniently be processed using the program devised for the HP 9845 desktop computer (Fig. 26.3).

The most typical errors are recognized as small constant vectors caused by horizontal component in the projection (Fig. 26.4a). This indicates that some mistake has probably been made in the determination of either the lateral direction of the borehole or in the horizontal components of the regional geomagnetic field. Even small inaccuracies in measuring the inclination of the borehole can seriously affect the results when dealing with weak magnetic anomalies (Fig. 26.4b). In the figure the borehole has been drilled towards the magnetic south, and it can be seen that even an error of just one degree in its angle of inclination can alter the results substantially, in this case causing an error in the computation of the depth of the lower pole. This serves to demonstrate that the question of the sensitivity of the instrumentation can easily take second place to the elimination of error factors when developing the 3-component technique for use with weakly magnetized ores.

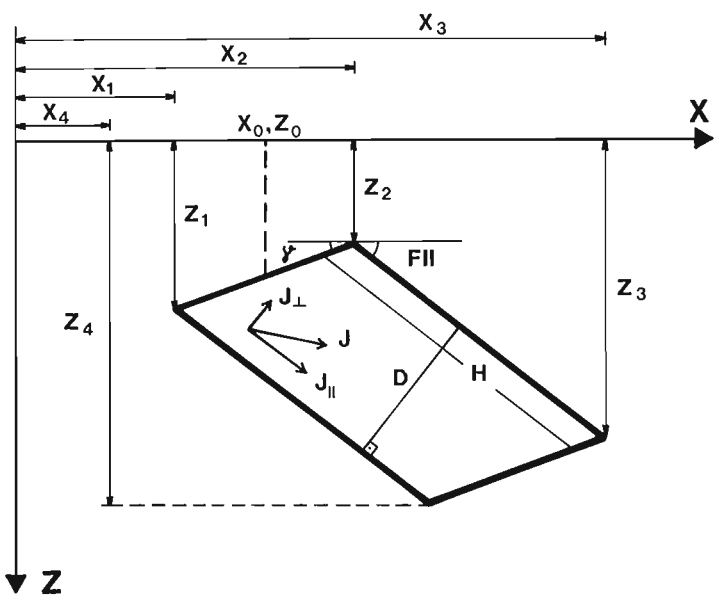

Figure 26.5. Basic coordinate and model parameters.

Interpretation

The main idea in constructing the interpretation program for magnetic borehole measurements was the achievement of speed, versatility, and the accuracy necessary in practical situations using an interactive system. The program is installed on a HP 9845 desktop computer and is intended to be a simple technical aid which will allow the geophysicist to concentrate his attentions on obtaining an overall solution to the geological/geophysical problem in hand. This is particularly important in the processing of borehole results, as one is already dealing with 3-dimensional structures in the source area itself.

The interpretation employs 2-dimensional plates with a parallelogram cross-section arranged in arbitrary attitudes (Fig. 26.5). Since the borehole will run at an angle to the geological strike, the model can be positioned in accordance with the actual geological structure and processed by means of the anomaly vectors in the section of the borehole. In reality the calculations are performed in sections perpendicular to the 2-dimensional model and the results are then transformed back into anomaly vectors corresponding to the section under examination. The algorithm employed in the calculations is a complex solution for a 2-dimensional thick plate (Hjelt, 1976b). The formulae are transposed into real and imaginary parts, since complex variables cannot be used in the BASIC language of the HP 9845 computer (Turunen, 1978). The demagnetization effect due to the shape of the body is taken into account on the basis of the dimension relations in the model (Joseph, 1967).

The interpretation program is made up of independent modules. After the input of the initial data (measurements, earth's field, etc.), the program execution resembles, with an interruption facility, that of a real-time system. The central blocks in the structure diagram (Fig. 26.6) indicate that the

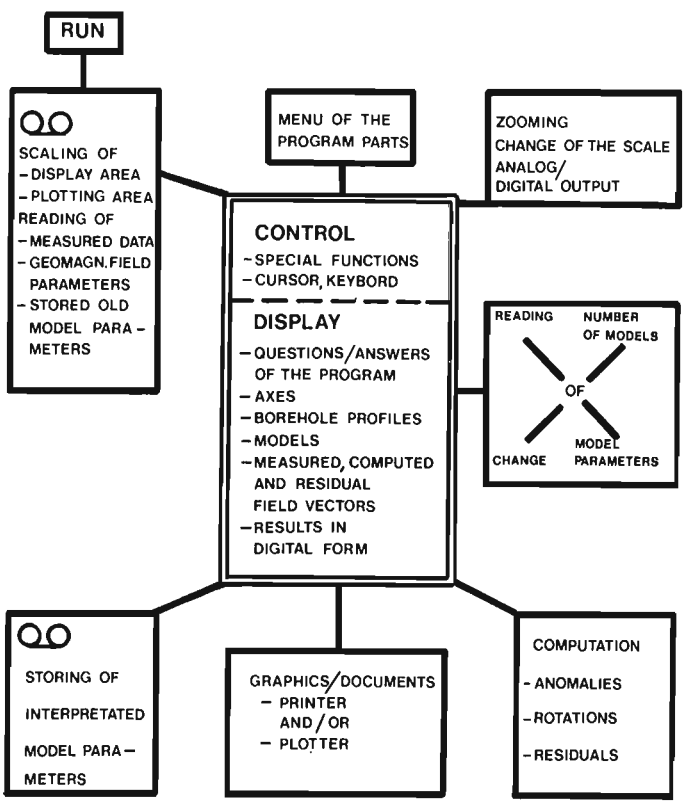

Figure 26.6. Block structure of the interactive magnetic interpretation system.

various functions are all equally accessible to the operator through the control and display facilities. The measured and calculated anomalies are compared on the CRT screen of the HP 9845 computer in the form of magnetic field vectors and recorded on a printer or plotter. In deciding upon the location of new models, assistance may be had from recordings of the differences between the measured and calculated vectors. The anomaly created by remanent magnetization can be accounted for together with the induced magnetism and its effect, which is also recorded separately.

The accuracy of the interpretation method can be illustrated best by reference to the anomaly field associated with certain theoretical models. The vector maps indicate the behaviour of the magnetic field at various distances from many causative bodies (Fig. 26.7, 26.8). The vectors inside the models denote magnetizations. The calculation method used in the interactive interpretation program is compared with the same results as obtained by the method of subsections. The effect of inhomogeneous magnetization upon the field is considerable near the corners of the magnetized units, but the errors diminish rapidly with

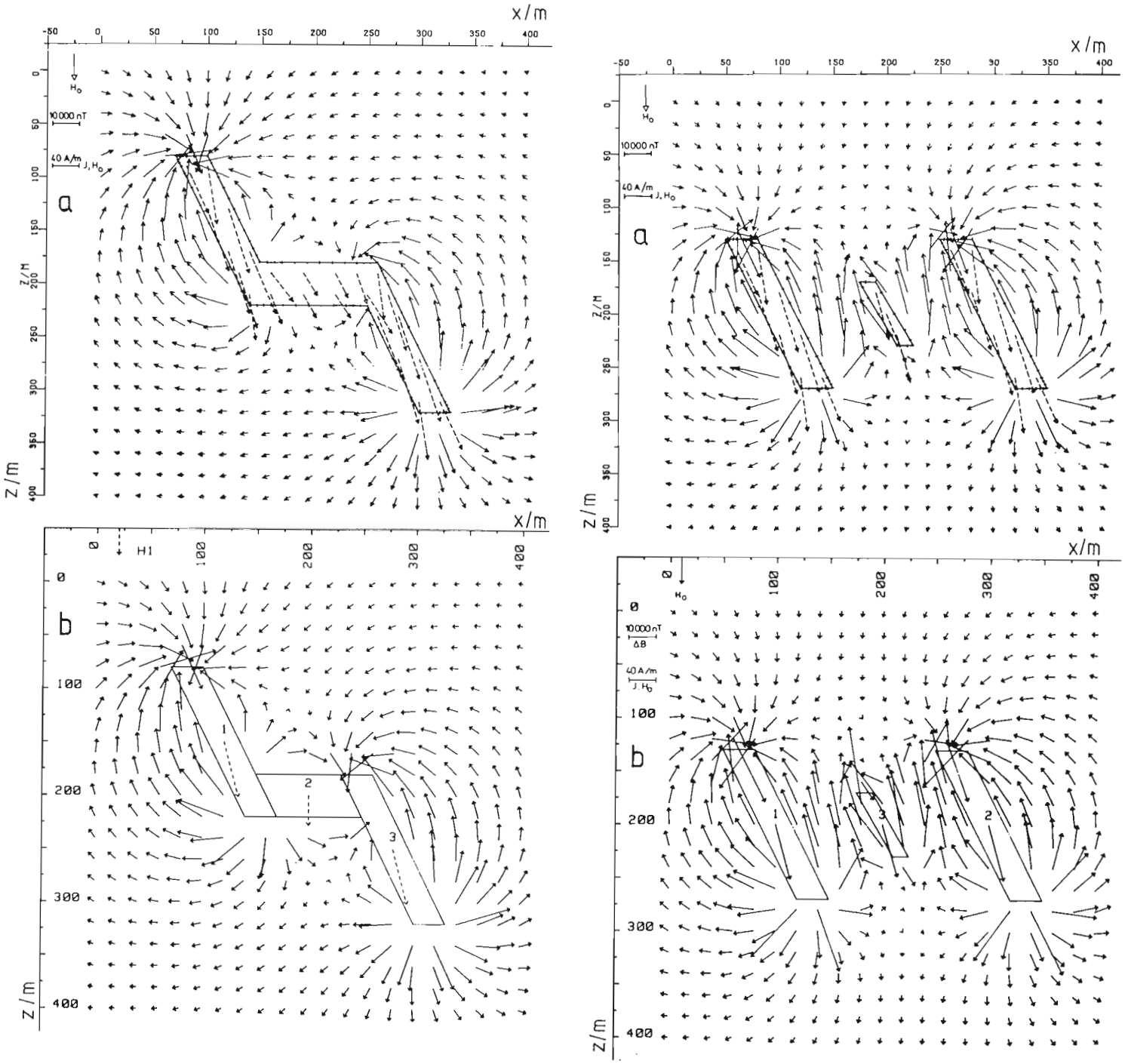

Figure 26.7 (left)-26.8 (right) *Magnetic anomaly field vectors maps of some models computed a) by the method of subsections and b) by the method based on homogeneous magnetization with demagnetization correction. The susceptibility of each model is 4 SI units. The point grid is 20 x 20 m. (Avdevich et al., 1981).*

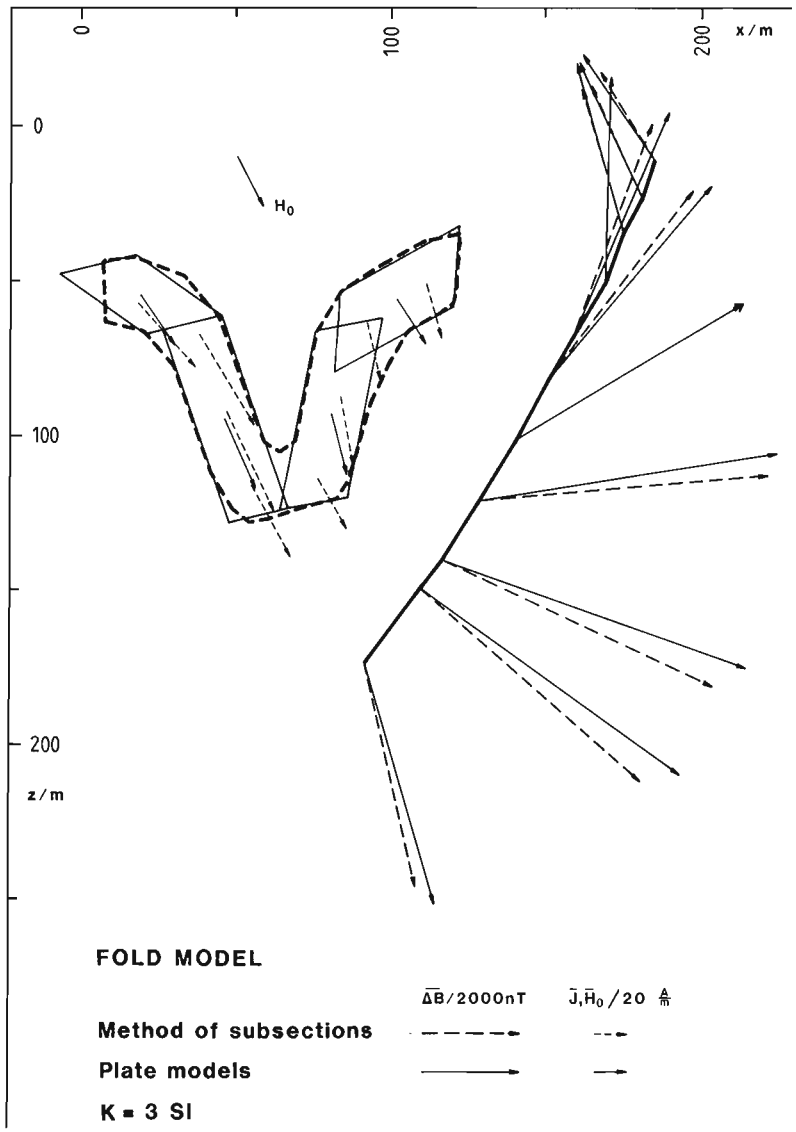

Figure 26.9. *Magnetization and anomaly fields in a borehole near a fold represented by polygons computed using the method of subsections and the method used in interactive interpretation system (Avdevich et al., 1981).*

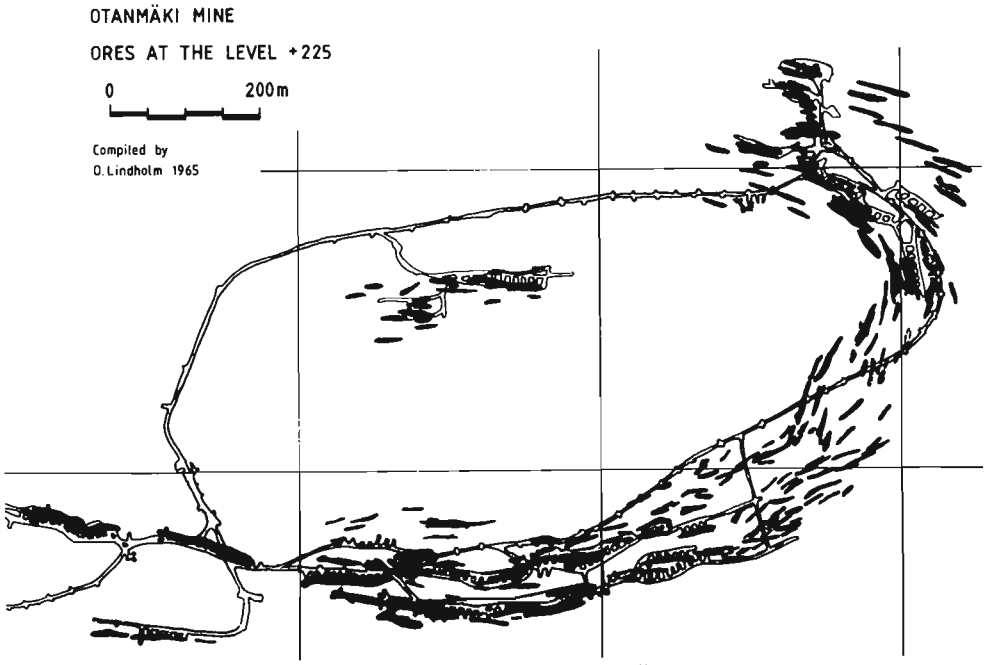

Figure 26.10. *Occurrences of ores at the Otanmäki mine, level +225 m.*

Table 26.1 Output parameters of the interpretation profile Y 5350 from the Välimalmi orebody at Otanmäki mine. Other parameters are described in Figure 26.5.

TØ = 51900 nT T1 = 51856 nT H1 = 41.3 A/m
IØ = 83.0 gon I1 = 83.2 gon
Declination of interpretation profile = 210 gon

N	XØ/m Q-ratio	D/m Ri/gon	ZØ/m Rd/gon	H/m KU/gon	FII/gon KK/gon	K/SI	J/(A/m)
1	3235.0	10.9	239.7	75.2	85.4	3.00	154.0
	1.2	64.0	344.0	300.0	70.0		
2	3215.1	11.1	228.7	104.5	92.6	3.00	172.4
	1.2	64.0	344.0	300.0	70.0		
3	3201.1	10.6	198.5	60.3	85.5	2.00	112.9
	1.2	64.0	344.0	300.0	70.0		
4	3249.3	5.1	231.2	27.4	88.0	3.00	148.4
	1.2	64.0	344.0	300.0	70.0		
5	3182.8	10.6	224.8	26.7	86.3	3.00	123.4
	1.2	64.0	344.0	300.0	70.0		
6	3171.7	4.6	194.0	51.1	92.3	3.00	176.9
	1.2	64.0	344.0	300.0	70.0		
7	3181.7	9.1	295.0	32.6	92.6	3.00	139.5
	1.2	64.0	344.0	300.0	70.0		

TØ = intensity of the main geomagnetic field
IØ = inclination of geomagnetic field
T1, H1 = magnetic field in interpretation cross-section
I1 = inclination of magnetic field in interpretation cross-section
N = number of model
K = susceptibility in SI units
J = magnetization
Q = ratio of remanent to induced magnetization
Ri = inclination of remanent magnetization
Rd = declination of remanent magnetization
KU = strike of body
KK = plunge of body

Table 26.2 Output parameters of the interpretation profile Y 1775 from the Huuhtijärvi orebody at the Kotalahti mine.

TØ = 51700 nT T1 = 51692 nT H1 = 41.1 A/m
IØ = 82.4 gon I1 = 82.4 gon
Declination of interpretation profile = 204 gon

N	XØ/m Q-ratio	D/m Ri/gon	ZØ/m Rd/gon	H/m KU/gon	FII/gon KK/gon	K/SI	J/(A/m)
1	907.0	8.8	852.3	49.5	105.9	.01	12.6
	30.0	82.4	0.0	320.0	0.0		
2	845.4	10.9	568.8	134.8	106.0	.01	12.7
	30.0	82.4	0.0	320.0	0.0		
3	869.5	15.9	734.5	56.1	119.4	.01	12.6
	30.0	82.4	0.0	320.0	0.0		
4	883.7	9.8	788.2	67.5	116.5	.01	12.7
	30.0	82.4	0.0	320.0	0.0		
5	856.0	6.7	703.0	32.7	117.3	.01	12.7
	30.0	82.4	0.0	320.0	0.0		
6	897.1	4.3	809.9	42.8	116.2	.01	12.7
	30.0	82.4	0.0	320.0	0.0		
7	888.1	12.6	888.6	166.4	104.8	.01	12.5
	30.0	82.4	0.0	320.0	0.0		
8	899.2	6.4	853.5	197.3	105.8	.01	12.7
	30.0	82.4	0.0	320.0	0.0		

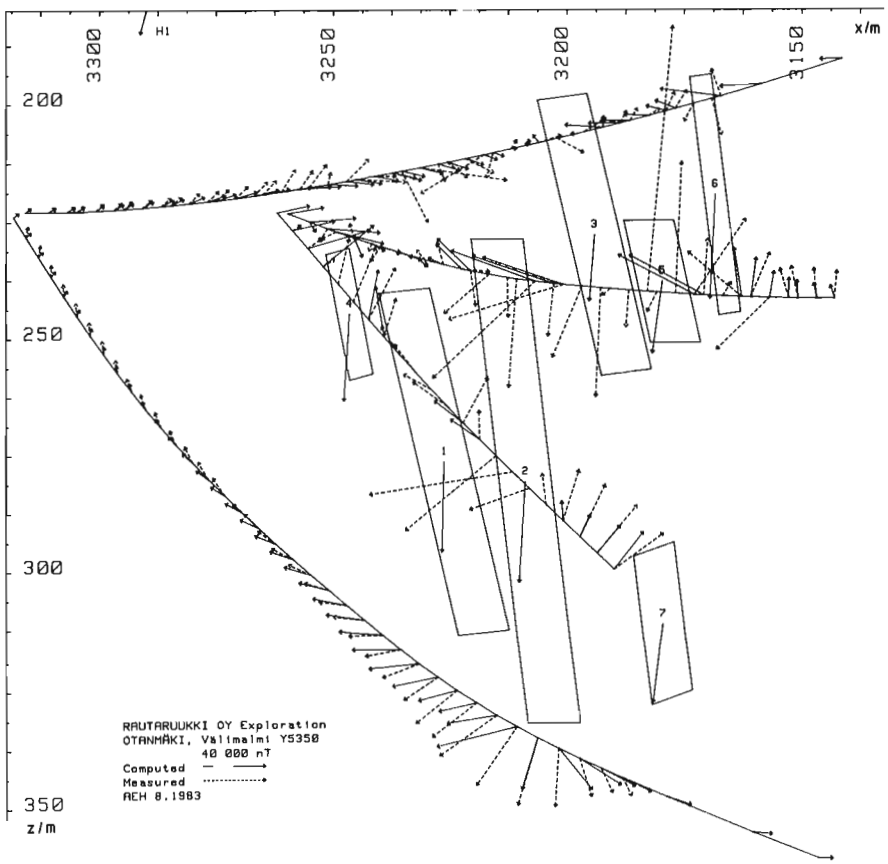

Figure 26.11. *Interpretation of borehole magnetic data in vector form from Otanmäki mine, section Y 5350 of Välimalmi orebody. Output parameters of interpretation are in numerical form in Table 26.1.*

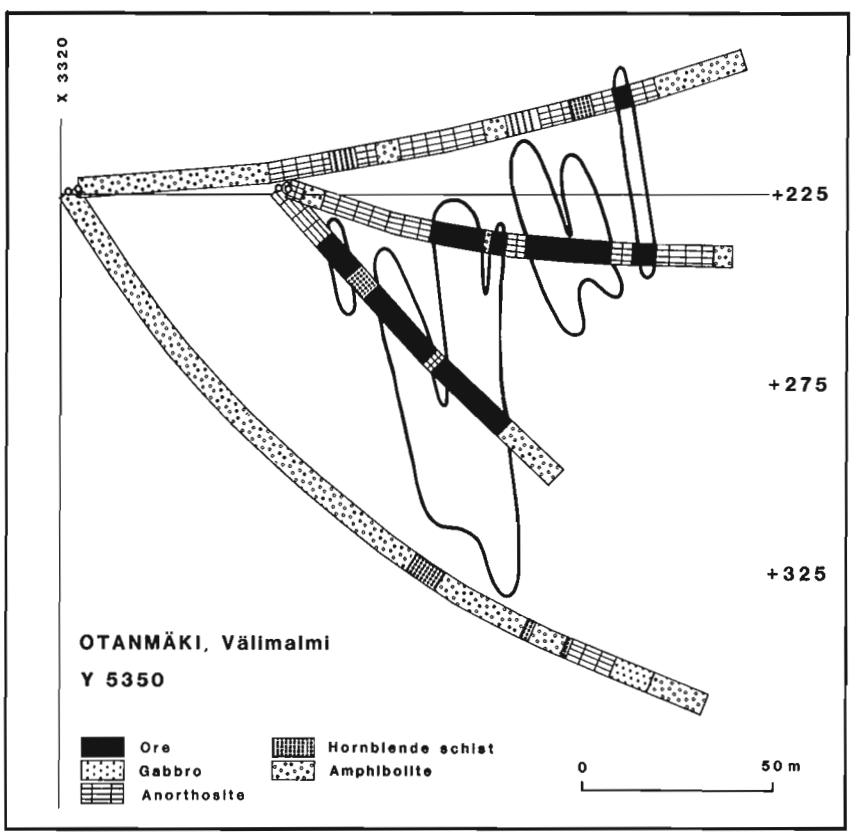

Figure 26.12. *Geological profile Y 5350 from Välimalmi, Otanmäki mine.*

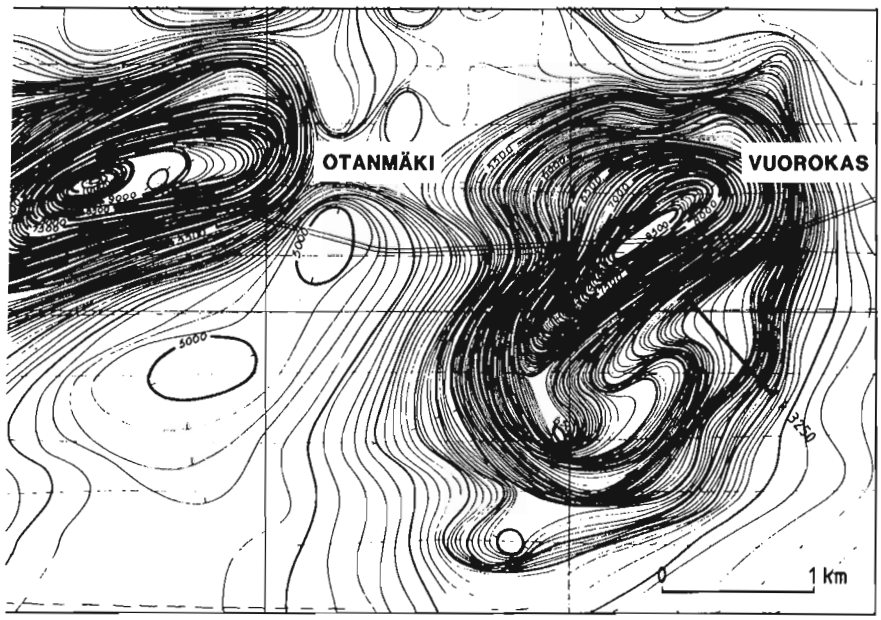

Figure 26.13. Aeromagnetic map of the Otanmäki Vuorokas area. Geological Survey of Finland, total intensity 150 m above the ground, basic contour-interval 20 nT.

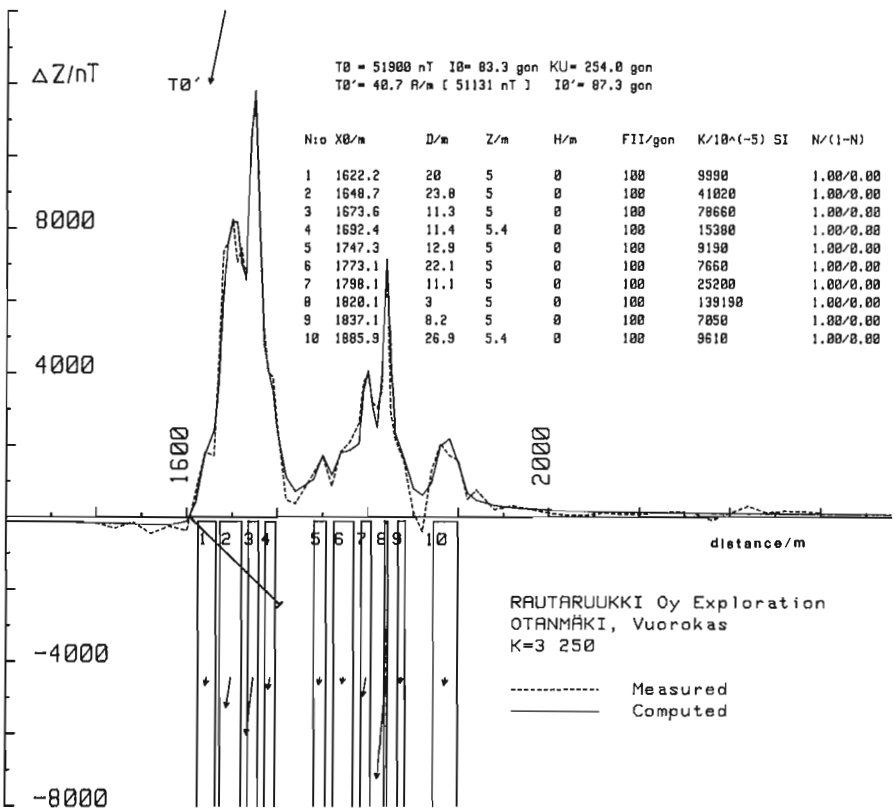

Figure 26.14. Ground magnetic interpretation profile K 3250 from the Vuorokas area and location of the drillhole BH-95. DZ = magnetic vertical intensity in nT, N = demagnetization factor (other symbols as in Fig. 26.5 and Table 26.1).

increasing distance. The vector anomaly maps also demonstrate that fields can vary a lot and may be weak even quite close to the magnetized body due to the masking effect of other bodies. Thus, by subtracting the theoretical fields of the known models from the total measured field, it is possible to reveal previously hidden bodies. The possibilities for interpreting more complex structures such as folds using plate models may be demonstrated in the form of a theoretical example of borehole results compared with the method of subsections (Fig. 26.9). The resulting magnetic field proved fairly consistent even without any attempt being made to reconstruct the fold from the parallelograms in any great detail, and the difference is reduced further at lower levels of susceptibility. The magnetic field, excluding the corners of the bodies, may be taken to be reproducible from other boreholes, since the magnetizations in the centres of the bodies are very close to being exact. Since actual geological structures are not regular in shape, this method of interactive interpretation based on homogeneous magnetization, with a constant demagnetization correction according to shape of the body, is sufficiently accurate for practical purposes. Where necessary, one can always resort to theoretical anomaly fields resolvable by the method of subsections.

Examples

Otanmäki

The Otanmäki mine exploits a vanadium-bearing ilmenite-magnetite deposit which is associated with gabbroic intrusions. It consists of hundreds of small, irregular ore lenses spread over a broad, heterogeneous zone (Fig. 26.10). The individual lenses, most of which are steeply dipping, vary in length from 20 to 200 m and in width from 3 to 30 m (Lindholm and Anttonen, 1980).

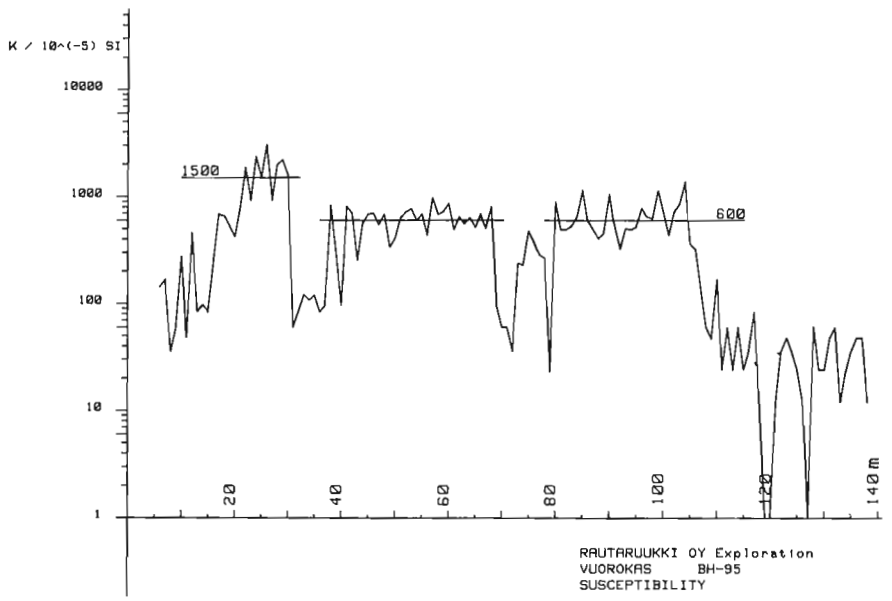

Figure 26.15. *Susceptibility at the Vuorokas BH-95 measured from core samples.*

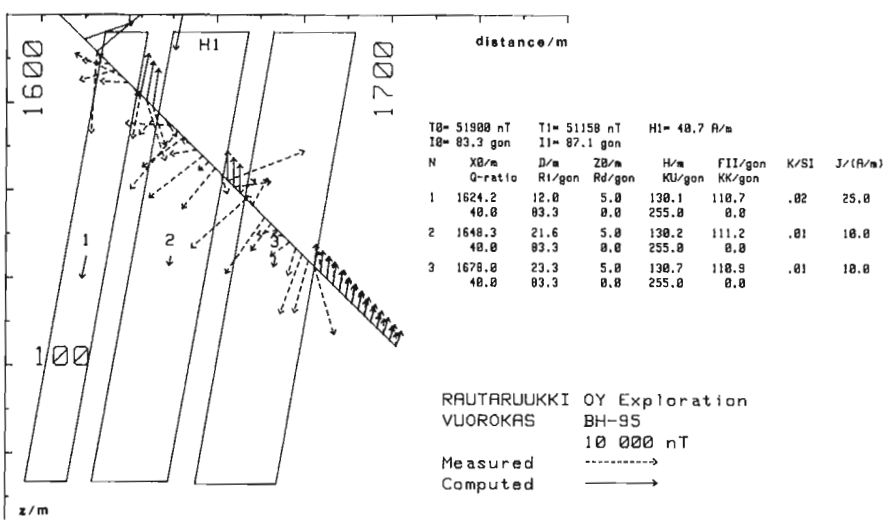

Figure 26.16. *Interpretation at magnetic 3-component data measured from the Vuorokas BH-95. Declination of the profile is 155 gon. (Symbols as in Fig. 26.5 and Table 26.1).*

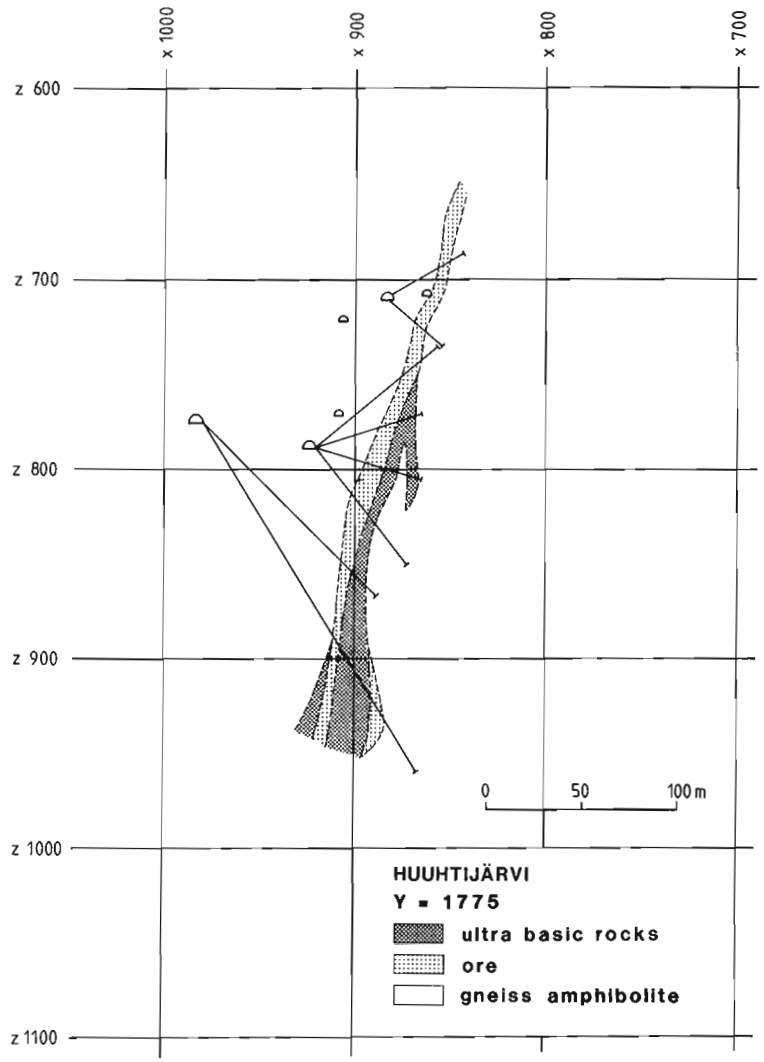

Figure 26.17. Geological cross-section Y 1775 at the Huuhtijärvi orebody of the Kotalahti mine.

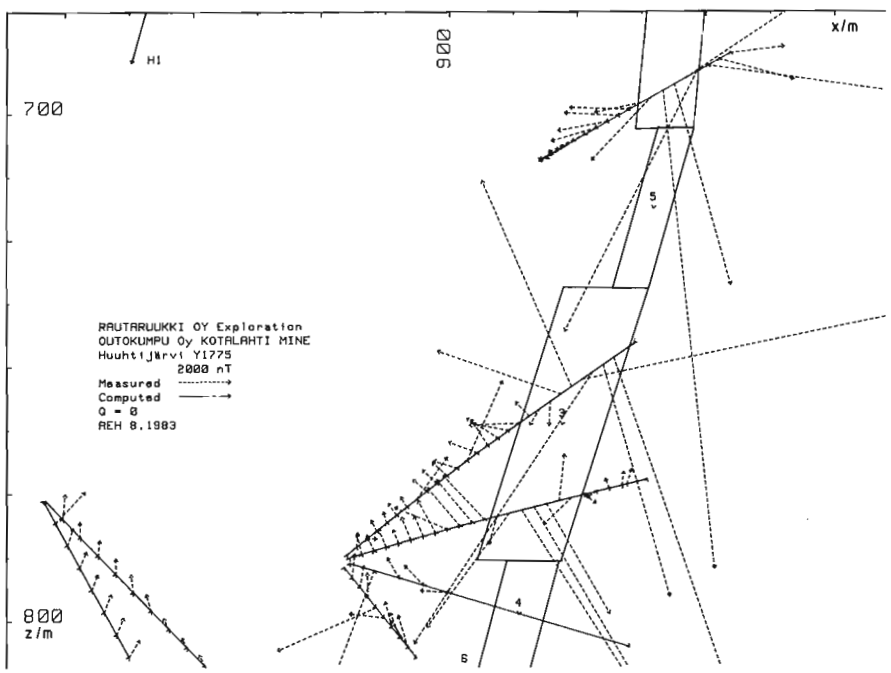

Figure 26.18. Magnetic 3-component data of the drilling profile Y 1775 from the Huuhtijärvi orebody and computer anomaly vectors, which are very small without remanent magnetism.

The susceptibility range corresponding to the magnetite content of the ore, 20 - 60% by weight, is 0.5 - 3 SI units, and the ratio of remanent to induced magnetization Q = 1.2. The rich ore in this deposit contains 35 - 40% magnetite and 28 - 30% ilmenite.

Percussion drilling is frequently employed to complement the diamond drilling used in geological investigations of the mine, being usable at only one fifth of the cost. Magnetic 3-component measurements and susceptibility measurements are performed in all diamond drillholes. The magnetite content of the ore is determined in the percussion drillholes by susceptibility logging. In view of the constant magnetite/ilmenite ratio, the ilmenite content can also be estimated from the same susceptibility/magnetite calibrations (Paarma and Lindholm, 1980).

Since the ore body is composed of lenses of different sizes and occurring at different distances apart, 3-component magnetometry constitutes an important method for connecting the ore penetrations and predicting new lenses. Thus a typical result would include evidence of a number of separate lenses (Fig. 26.11). Susceptibility measurements can be used to delimit the ore penetrations. The more small lenses make up the drilling sections, the more complex will be the magnetic anomaly field, as there will be a continual alteration of internal and external magnetic fields. The vectors measured inside ore bodies cannot be used quantitatively. When attempting to interpret the magnetic evidence it is thus important to bear in mind which results are the most essential in overall terms. The interactive mode of interpretation for 3-component readings offers an excellent aid in the construction of geological sections (Fig. 26.12).

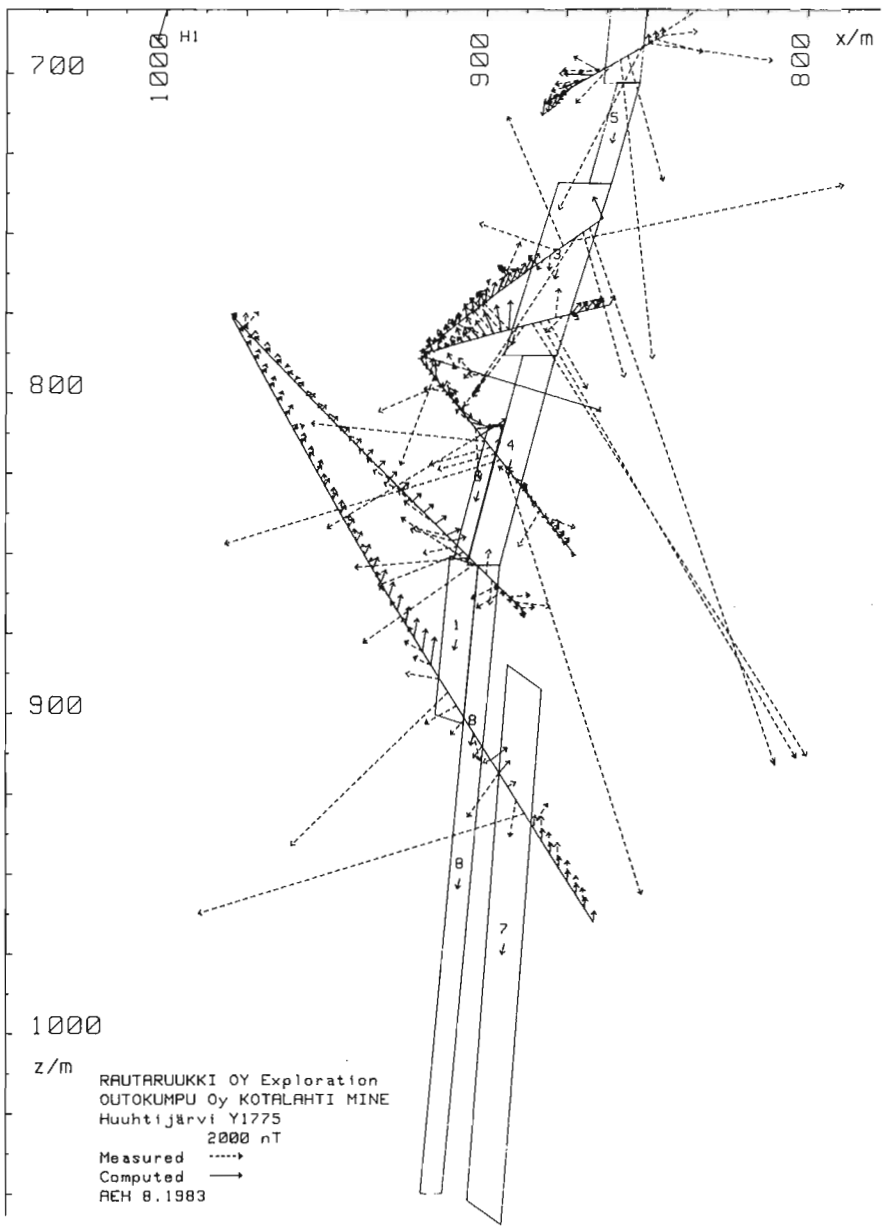

Figure 26.19. Interpretation of magnetic 3-component data measured from the profile Y 1775 of the Huuhtijärvi orebody at the Kotalahti mine. Output parameters of interpretation are in numerical form in Table 26.2.

Otanmäki, Vuorokas

The other magnetite-ilmenite ore body in the Otanmäki area being mined is located in the centre of the Vuorokas gabbro intrusion, and a few years ago exploration was carried out on the margins of this gabbro to ascertain the prospects for small-scale open-pit mining. One of the sites used, the profile K = 3250, is indicated on the airborne magnetic map in Figure 26.13. Ground magnetic measurements had suggested a possibility of finding thin magnetite-bearing layers here (Fig. 26.14), but the boreholes did not penetrate any magnetite ore but, only gabbro and anorthosite, with susceptibility readings of 600 - 1500 x 10^{-5} SI units (Fig. 26.15). This raised the question of how the boreholes could have missed the assumed magnetite target. Three component magnetometry, however, soon revealed what had happened. The magnetized zone had indeed been penetrated almost exactly at the point expected, but the magnetism had been largely remanent in kind. Thus, fitting of the intensities of the measured and calculated magnetic field vectors in the interpretation of the borehole results gave a Q (ratio of remanent and induced magnetizations) value of approximately 40 (Fig. 26.16), with parallel orientations for the remanent and the induced magnetizations.. Determinations of remanent magnetization from borehole core samples gave Q values in the range 30 - 100. The cause of this magnetization was found to be a very fine grained disseminated pyrrhotite.

Kotalahti

The Kotalahti ore deposit is a mafic complex showing differentiation from peridotite to diorite. The area forms part of a major tectonic belt characterized by subparallel swarms of shear fractures trending northwest. The Ni-Cu-bearing rocks are related to transcurrent faults, and the contact between the intrusion and the wall rocks, which consists of migmatitic gneisses and amphibolites, is generally sharp, but locally gradational. The mineralization varies from massive to disseminated with subgrade dissemination extending beyond the economic limits. The main ore minerals are pyrrhotite, pentlandite and chalcopyrite. The total sulphur content averages 10 - 15% (Koskinen,1980).

The magnetic 3-component technique was employed at the Kotalahti mine of Outokumpu Oy to determine the possibility of downward extensions of the Huuhtijärvi ore body. The mineralization zone had been penetrated by boreholes to an approximate level of +900 m (Fig. 26.17). Loggings done from the deepest two holes gave susceptibility readings for the ore body of about 1000 x 10^{-5} SI units, except for a few thin horizons in which the figure was higher. The magnetization of the country rocks was very weak.

A simple model was solved to describe the known ore zone for the levels between +700 and +850 (Fig. 26.18). The induced magnetization (K = 1000 x 10^{-5} SI) is too small to explain the measured magnetic field, but the extent of the remanence can be estimated by fitting the intensities of the measured anomaly vectors to those of the calculated vectors. This gives a Q value of 30. Comparison of the measured and computer anomalies suggests that the direction of the remanent magnetization coincides adequately with the earth's magnetic field. In an area where identification with the earth's field does not prove satisfactory, one could try the directions of geological lineation as the next alternative, but the testing of other directions on a trial-and-error basis is too unreliable a procedure for the present purpose. A better approach would be to take oriented samples from the ore, since pyrrhotite may carry remanence with a direction that differs strongly from that of the induced magnetization. The occurrence of a different direction of remanent magnetization can normally be deduced from the 3-component readings although it may still not be possible to determine unambiguously what this direction is.

The magnetic 3-component measurements indicate that the mineralization zone continued below the +900 level. According to the interpretation, the lower-surface lies at around +1050 m (Fig. 26.19). Since the magnetic field given by the models for the ore zone lying above the +900 level can be derived accurately in the lowermost borehole, the effect of the depth extention upon the results from this borehole can be examined relatively reliably. The main risk factors are minor fluctuations in the quality of the ore or its dimensions and the extension of the distances involved beyond the range of accurate measurement. As far as the magnetized zone is concerned, the depths obtained may be regarded largely as minimum depths.

The readings from within the ore body, show disproportionately strong fields, due to the occurrence of thin horizons whose susceptibility can be many times greater than the average although the Q ratio may remain constant.

Conclusions

Three-component magnetometry is applicable not only to magnetite-bearing deposits but also to sulphide ores containing pyrrhotites, in which a significant part is often played by the magnetic field caused by remanence. Such measurements can be of direct assistance in identifying remanent magnetization and determining its magnitude. In investigations of sulphide ores it is needed to develop more sensitive equipment. Improvement of the instrumentation is not the most difficult thing to achieve, however, as the question of increasing the accuracy of the orientation measurements regarding the borehole and the probe remains a problematical one, since the regional geomagnetic field has to be separated from the measured field in retrospect.

The best interpretation results can be obtained using an interactive interpretation system in which the measured and calculated anomalies are compared in vector form. It is characteristic of all borehole results, however, that the magnetic fields can vary rapidly in intensity and direction due to the distribution of sources around the borehole. Thus automatic inversion procedures are difficult to apply as anything more than an aid in the optimization of certain parameters in interactive interpretation. Perhaps the most important step for the future development of the method will be the inclusion of 3-dimensional models in the program and some new instrumentation.

Acknowledgments

The author would like to thank Rautaruukki Oy and Outokumpu Oy for permission to publish their data. Sincere thanks are due to Juhani Nuutilainen for the valuable work in encouragement and support which he has given to development work in the Exploration Department of Rautaruukki Oy.

The author also acknowledges the excellent computer programming of Veijo Snellman and wishes to thank Hannu Autio for critically reading the manuscript.

References

Avdevich, MM., Tervo, T., Hattula, A., and Turunen, P.
1981: Theoretical models and comparison of interpretation results obtained by different methods; in Interpretation of borehole magnetic data and some special problems of magnetometry, S.E. Hjelt, A.Ph. Phokin, ed., Department of Geophysics, University of Oulu, Report No. 1, p. 27-40.

Eskola, L. and Tervo, T.
1980: Solving the magnetostatic field problem (a case of high susceptibility) by means of the method of subsections; Geoexploration, v. 18, p. 79-95.

Hattula, A. and Hjelt, S.E.
1981: Main principles of interactive computer interpretation in mining geophysics; in Interpretation of borehole magnetic data and some special problems of magnetometry, S.E. Hjelt, A.Ph. Phokin, ed., Department of Geophysics, University of Oulu, Report No. 1, p. 70-83.

Hattula, A. and Paarma, H.
1981: Equipment used in borehole magnetometry at Rautaruukki Oy, in Interpretation of borehole magnetic data and some special problems of magnetometry, S.E. Hjelt, A.Ph. Phokin, ed., Department of Geophysics, University of Oulu, Report No. 1, p. 51-59.

Hjelt, S.E.
1976a: A new compact formulation of the two-dimensional magnetic interpretation problem; Geoexploration, v. 14, p. 1-20.

1976b: A new approach to magnetic profile interpretation; Geophysical Prospecting, v. 24, p. 1-18.

Joseph, R.I.
1967: Ballistic demagnetizing factor in uniformly magnetized rectangular prism; Journal of Applied Physics, v. 38, p. 2405-2406.

Koskinen, S.
1980: Geology of the Kotalahti Ni-Cu deposit; in Guide to excursions 078 A + C, Part 2 (Finland), 26th International Geological Congress Paris 1980, Geological Survey of Finland, p. 42-48.

Kunaratnam, K.
1972: An iterative method for the solution of a non-linear inverse problem in magnetic interpretation; Geophysical Prospecting, v. 20, p. 439-447.

Lantto, V.
1973: Characteristic curves for interpretation of highly magnetic anomalies in borehole measurements; Geoexploration, v. 11, p. 75-85.

Levanto, A.E.
1963: On magnetic measurements in drillholes; Geoexploration, v. 1, p. 8-20.

Lindholm, O. and Anttonen, R.
1980: Geology of the Otanmaki mine; in Guide to excursions 078 A + C. Part 2 (Finland), 26th International Geological Congress Paris 1980, Geological Survey of Finland, p. 25-33.

Paarma, H.E.
1954: The ilmenite-magnetite ore deposit of Otanmaki; in The Mines and Quarries of Finland, Geologinen tutkimuslaitos, Geoteknillisia julkaisuja No. 55, p. 36-42.

Paarma, H.E. and Levanto, A.E.
1958: Underground exploration at Otanmaki mine; Mine and Quarry Engineering, v. 24, p. 545-554.

Paarma, H.E. and Lindholm, O.
1980: The possibilities of geophysical measurements in drill holes to control the waste rock dilution; in Waste rock dilution and its economic significance in mining, The Mining and Metallurgical Society of Finland, No. 25 b 1980, p. 53-55.

Turunen, P.
1978: On the interpretation of many component measurements in boreholes (in Finnish). Thesis, University of Oulu, Department of Geophysics, 99 p.

27. DEVELOPMENT OF A 3-COMPONENT BOREHOLE MAGNETOMETER PROBE WITH GYROSCOPIC ORIENTATION

James H. Scott[1] and Gary G. Olson[2]

Scott, James H. and Olson, Gary G., Development of a 3-component borehole magnetometer probe with gyroscopic orientation; in Borehole Geophysics for Mining and Geotechnical Applications, ed. P.G. Killeen, Geological Survey of Canada, Paper 85-27, p. 251-259, 1986.

Abstract

A magnetometer probe was developed for measuring the direction and intensity of the Earth's magnetic field in boreholes drilled for mineral resource assessment studies and for geological research. The 5.1 cm diameter probe contains a 3-component fluxgate magnetometer with a sensitivity of approximately 50 nanoteslas (nT) and a range of ± 80 000 nT, and a gyroscopic and inclinometer orientation system for determining the angular position of the magnetometer to a readout resolution of 0.2°. The probe also contains signal conditioning, digitizing and multiplexing modules for transmitting digital data from the inclinometer, magnetometer, and temperature sensors to the surface. Azimuthal orientation of the probe is determined by a gyroscope whose digitized readout is transmitted to the surface along with other multiplexed data. The uphole power and signal conditioning circuitry collects and formats information from the downhole sensor modules and presents it to a digital computer in the logging truck for editing and storage on magnetic tape.

Two tests were made to determine the stability, repeatability, and overall sensitivity of the probe. The first test was made in a borehole drilled in nonmagnetic rock where the only expected anomaly was produced by steel surface casing. The other test was made with a small pod of magnetic ore fastened near the middle of an aluminum test stand on which the probe was raised and lowered so that it passed by the magnetic pod. The tests indicated that the probe can detect anomalies that are 1 μT or larger, and therefore should be useful for locating pods of magnetic ore associated with mineral deposits, and for determining the direction and intensity of magnetization of bedded volcanic rocks.

Résumé

Une sonde à magnétomètre a été mise au point en vue de mesurer la direction et l'intensité du champ magnétique de la Terre dans des sondages forés à des fins d'évaluation des ressources minérales et de recherche géologique. La sonde, dont le diamètre est de 5,1 cm, contient un magnétomètre électronique à sursaturation à trois composantes dont la sensibilité est d'environ 50 nanoteslas (nT) et la portée de ± 80 000 nT; elle comporte également un système d'orientation à gyroscope et à inclinomètre qui permet de déterminer la position angulaire du magnétomètre à une résolution de 0.2°. La sonde contient également des modules de conditionnement, de numérisation et de multiplexage du signal pour la transmission à la surface des données numériques recueillies par l'inclinomètre, le magnétomètre et les capteurs de température. L'orientation azimutale de la sonde est déterminée au moyen d'un gyroscope qui produit des données numérisées qui sont transmises en surface en même temps que les autres données multiplexées. Le circuit de puissance et de conditionnement du signal de tête de puits prélève et met en forme les données provenant des modules de capteur de fond et les transmet à un ordinateur numérique dans le camion-laboratoire à des fins d'édition et de stockage sur ruban magnétique.

Deux essais ont été effectués en vue de déterminer la stabilité, la répétabilité et la sensibilité globale de la sonde. Le premier essai a été effectué dans un trou foré dans une roche non magnétique où la seule anomalie prévue était produite par le tubage de surface en acier. L'autre essai a été effectué à l'aide d'une petite lentille de minerai magnétique fixée près du centre d'un support en aluminium sur lequel la sonde était soulevée et abaissée de façon à passer près de la lentille magnétique. Les essais ont révélé que la sonde peut déceler des anomalies d'au moins un μT et qu'elle devrait permettre de déceler les lentilles de minerai magnétique associées aux gisements minéraux et de déterminer la direction et l'intensité de l'aimantation des roches volcaniques stratifiées.

[1] U.S. Geological Survey, Denver, Colorado, 80225
[2] OWL Technical Associates, Inc., Longmont, Colorado, 80501

Background

The first borehole measurements of the Earth's magnetic field were reported by Broding et al. (1952), who described a total-field fluxgate magnetometer probe with a sensitivity of 1 nT developed for petroleum exploration in the United States. Later, Levanto (1959) described a 3-component fluxgate magnetometer probe with a sensitivity of 100 nT that was developed to map magnetic anomalies in boreholes drilled from within the Otanmaki underground iron mine in Finland. At about the same time a similar 3-component probe was developed by the Swedish Geological Survey and the Swedish Mining Association, also for use in iron mines (Bergdahl, 1963; Hood and Dyck, 1975). The design of these early systems has been refined, and a number of improved probes have been manufactured by Craelius in Sweden and Metex in Finland (Hood, 1970). The commercial units have fixed or selectable sensitivities of 50-150 nT and corresponding measurement ranges of ±100 000 nT and ±300 000 nT. Probe tilt is determined by a pendulum inclinometer installed in the magnetometer probes, or by separate borehole inclination surveys. The azimuth of the probe is estimated by sighting along the axis of the borehole at the hole collar and assuming that there is no azimuthal deviation with depth. Probes are constructed with one of the three perpendicular fluxgate magnetometer elements aligned with the axis of probe. When measurements are made, the other two coils, which can be rotated on the probe axis, are oriented so that one is horizontal and the other is in the vertical plane, either by a servo system or by a pendulum suspension system. Because of uncertainties in probe position and sensor orientation, the overall accuracy of surveys made with these probes is estimated to be 500-1000 nT (Levanto, 1963).

No significant improvements have been reported in 3-component magnetometer probe design since the early 1960s, although several papers have been published on interpretation of measurement data (Zuber, 1962; Ponomarev and Bakhvalov, 1964; Lantto, 1973; Parasnis, 1973; Silva and Hohmann, 1981). In a paper that describes procedures for locating a magnetized prism in the vicinity of a borehole, Silva and Hohmann (1981) recommended using a gyroscopic reference for determining the orientation of a 3-component magnetometer probe, although they did not do so in their study. To our knowledge, the probe described in this paper is the first 3-component magnetometer probe to use a gyroscope as an azimuthal reference.

The objectives of the USGS and OWL Technical Associates in developing the new, improved 3-component magnetometer probe were (1) to detect and locate weakly magnetized pods of sulphide minerals (with associated magnetic pyrrhotite and/or magnetite) occurring some distance from the borehole, and (2) to obtain magnetic signatures from volcanic rocks polarized in the direction of the Earth's present magnetic field (normal polarization) or opposite to it (reverse polarization). In order to accomplish this, it was decided to use a gyroscopic reference and sensitive inclinometers to determine the azimuth and tilt of the probe, and to use a 3-element fluxgate magnetometer to determine the direction and magnitude of the magnetic field. Probe temperature was to be monitored so that corrections could be applied to the magnetometer and inclinometer measurements. Probe measurement data were to be digitized and encoded downhole, then transmitted serially to the surface for decoding and interfacing to a computer in the logging truck. The computer would edit and store the data on magnetic tape, together with time and depth information obtained from the computer clock and the probe depth measurement system of the logging truck.

This report describes the results of preliminary tests of the 3-component borehole magnetometer measurement system, the methods developed for data acquisition and data reduction, some examples of experimental measurement data, and future plans for improving the system.

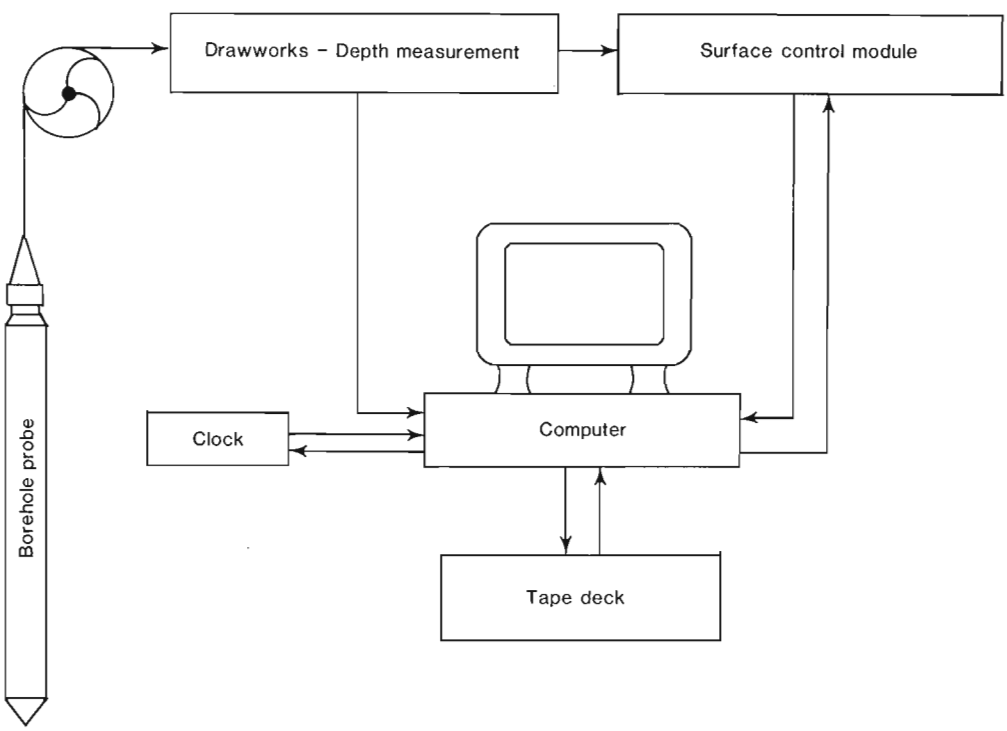

Figure 27.1. *Flow diagram of 3-component borehole magnetometer measurement system.*

Apparatus

The 3-component borehole magnetometer system consists of a borehole probe and surface control module designed and fabricated by OWL Technical Associates, a Hewlett-Packard 9845B desktop computer[1], and the USGS logging truck-winch system with digital depth readout. A block diagram of the system is shown in Figure 27.1.

The borehole probe is 5.1 cm in diameter and 2.3 m long. It contains gyroscopic, magnetic, inclination, and temperature sensors for making downhole measurements; also power conditioning, signal conditioning, and digitizing and multiplexing circuitry for transmitting data to the surface. Sensor output signals are digitized sequentially over a period of less than 1s. A layout diagram of the probe is given in Figure 27.2.

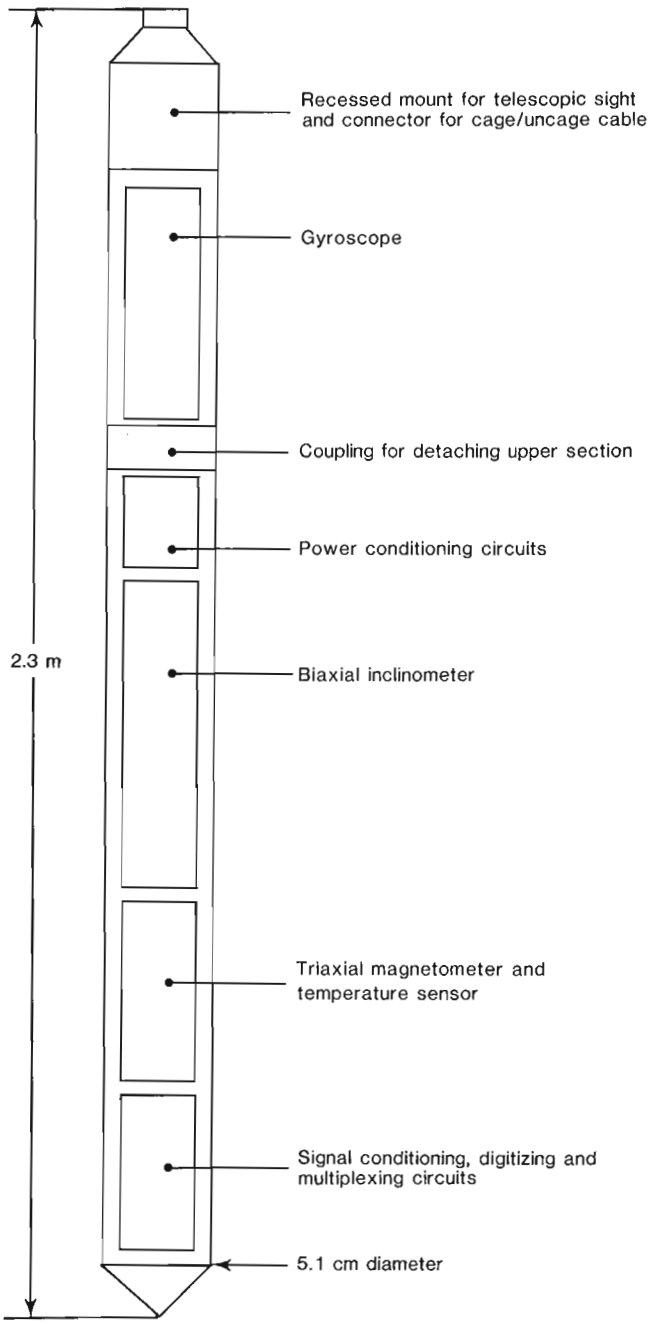

Figure 27.2. *Layout diagram of probe (not to scale).*

The gyroscope module, Humphrey model DG29-0701-2, is located in the top section of the probe which can be detached for transport in a cushioned case. Near the top of the probe is a recessed mounting bar for temporarily attaching a telescopic sight parallel with the spin axis of the gyroscope, and a recessed electrical connector for temporarily connecting a power source for caging and uncaging the gyroscope. The mounting bar and connector are covered by a water-tight metal sleeve during logging. The gyroscope is driven by an electric motor powered by a direct current (325 mA) sent downhole from a power supply in the logging truck. The outer gimbal of the gyroscope contains a circular potentiometer that is used to measure the angle of rotation of the probe from 0° to 358°. There is a 2° gap in the potentiometer from 358° to 360°. A voltage output representing the angle of probe rotation (positive from 0° to 358°, negative from 358° to 360°) is presented to the downhole digitizer-multiplexer for encoding and transmission up the logging cable to the surface control module.

The long axis of the probe is taken as the Z-axis. The other mutually perpendicular axes are the X- and Y-axes, respectively. The X-axis of the magnetometer, the X-axis of the inclinometer, the spin axis of the gyroscope and the mounting bar for the telescopic sight are all aligned within 0.5°.

The magnetometer is a three-component fluxgate magnetic field sensor developed by OWL Technical Associates, Inc. Three voltage outputs representing the three orthogonal magnetic-field components measured along the probe's X-, Y-, and Z-axes, are processed by the digitizer-multiplexer for encoding and transmission to the surface control module.

The two-axis inclinometer is a commercially available flexure-mounted force-motor accelerometer. Two voltage outputs representing the two orthogonal components of the Earth's gravitational field parallel with the probe's X- and Y-axes and perpendicular to the probe's Z-axis are sent to the digitizer-multiplexer for encoding and transmission to the surface.

Probe temperature is measured by a commercially available 2-terminal integrated-circuit temperature sensor. The voltage output of the sensor is processed by the digitizer-multiplexer and then transmitted to the surface.

The surface module is 9 cm high and mounts in a standard instrument rack 48.3 cm wide. It supplies power to the downhole magnetometer, inclinometer and temperature sensors, and to the downhole digitizer-multiplexer. Raw data transmitted up the cable by the probe are decoded and formatted in the surface module, and are then made available to the computer in the logging truck via an RS-232 link. At depth intervals designated by the operator, the computer requests the latest available set of probe measurements (updated every second or less) for recording on magnetic tape along with time and depth information.

Measurement accuracy

Small magnetic anomalies can be masked by measurement uncertainties which are considered system noise. The effects of uncertainties in probe orientation data from the gyroscope and the inclinometers are examined here. In Denver, Colorado, the magnitude of the Earth's magnetic field is approximately 56 000 nT (Fabiano and Peddie, 1981), the magnetic inclination is approximately 67° (Peddie et al., 1976), and the declination is approximately 12° E (Fabiano and Peddie, 1980). Simple calculations show that, for these values of magnitude and inclination, the vertical field strength is 51 548 nT and the horizontal field strength is 21 881 nT. If the probe is positioned vertically with the

[1] Use of trade names in this report is for descriptive purposes only and does not constitute endorsement by the U.S. Geological Survey.

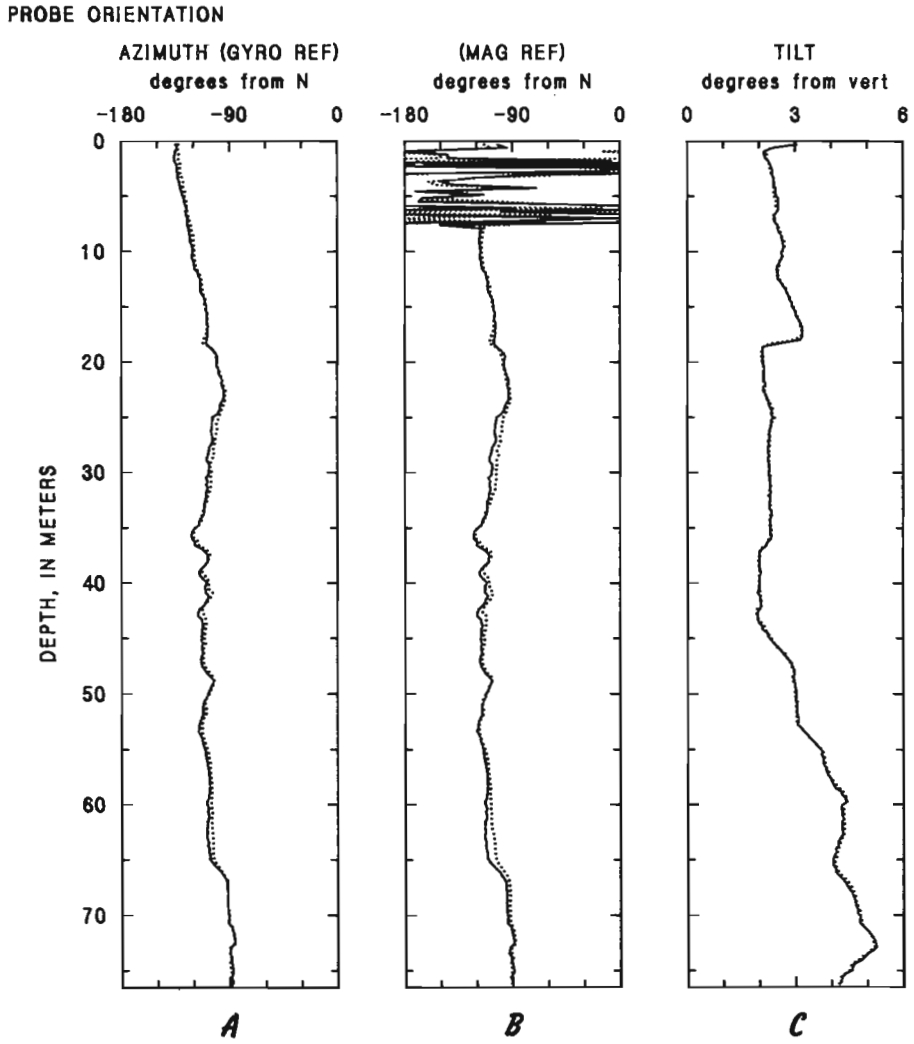

Figure 27.3. Logs showing the orientation of the Z-axis of the probe as it was lowered and raised in test hole drilled in nonmagnetic rock, Longmont, Colorado. Hole contains steel casing from surface to depth of 7.5 m. (A) Azimuth relative to gyroscopic reference to surface magnetic north. (B) Azimuth relative to downhole magnetic north determined from 3-component magnetometer readings. (C) Tilt from vertical. Solid line indicates logging down, dotted line logging up. Azimuths: -180° is south, -90° is west, 0° is north.

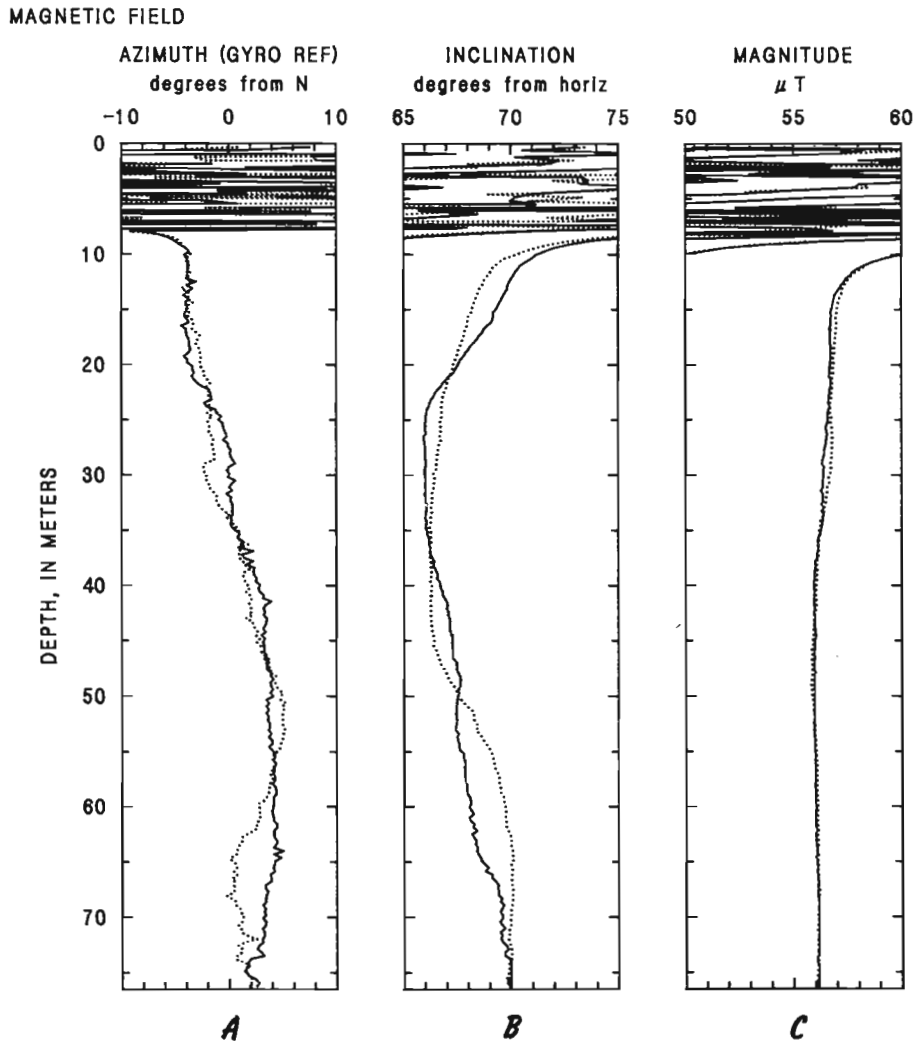

Figure 27.4. Logs showing direction and magnitude of magnetic field in test hole drilled in nonmagnetic rock, Longmont, Colorado. Hole contains steel casing from surface to depth of 7.5 m. (A) Azimuth referenced by gyroscope to surface magnetic north. (B) Inclination from horizontal. (C) Magnitude of total field. Solid line indicates logging down, dotted line logging up. Azimuths: -10° is N10°W, 0° is north, 10° is N10°E.

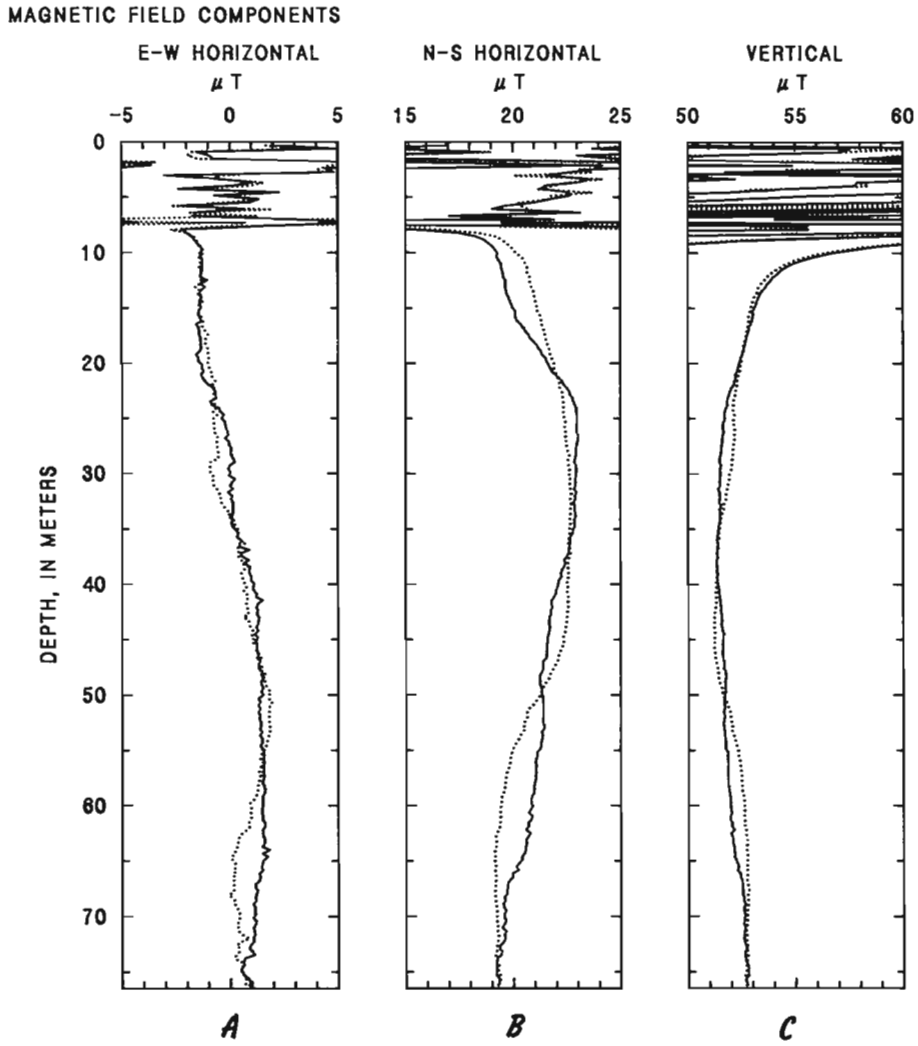

Figure 27.5. Logs showing magnetic field components in test hole drilled in nonmagnetic rock, Longmont, Colorado. Hole contains steel casing from surface to depth of 7.5 m. (A) East-west horizontal component. (B) North-south horizontal component. (C) Vertical component. Solid line indicates logging down, dotted line logging up.

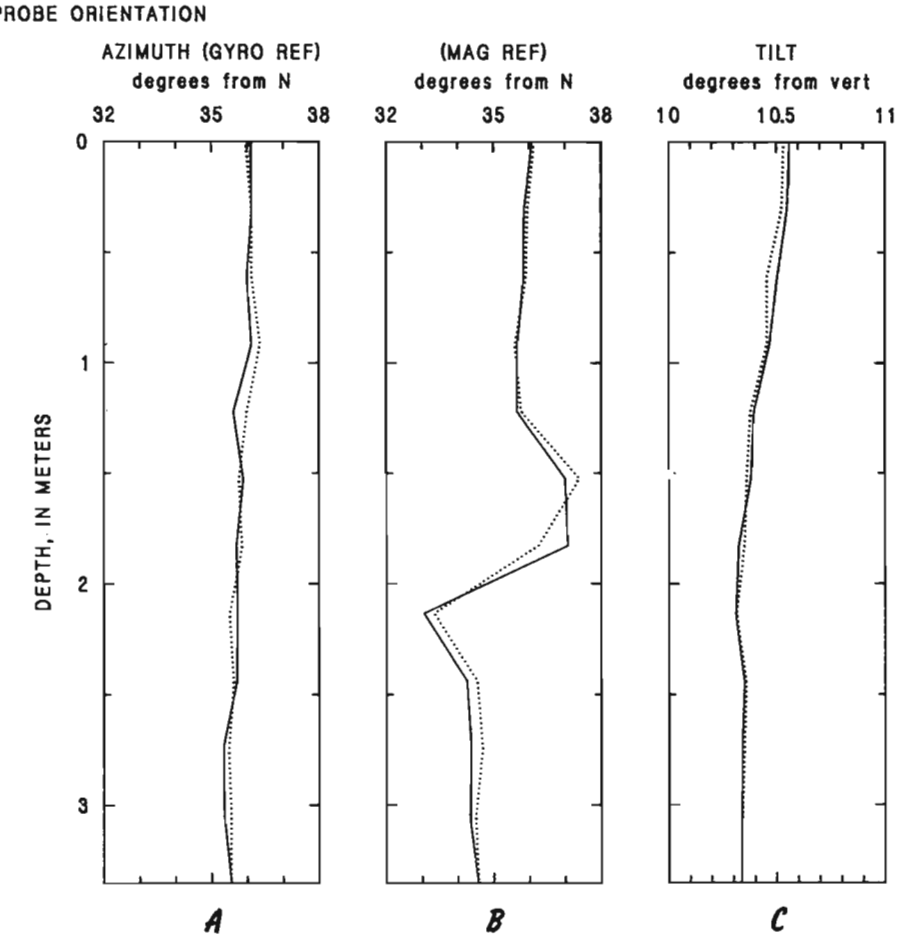

Figure 27.6. Logs showing the orientation of the Z-axis of the probe as it was lowered and raised. Magnetic dipole source is located 0.4 m S36°W of probe at depth of 2.0 m. (A) Azimuth relative to gyroscopic reference to surface magnetic north. (B) Azimuth relative to downhole magnetic north determined from 3-component magnetometer readings. (C) Tilt from vertical. Solid line indicates logging down, dotted line logging up. Azimuths are in degrees northeast.

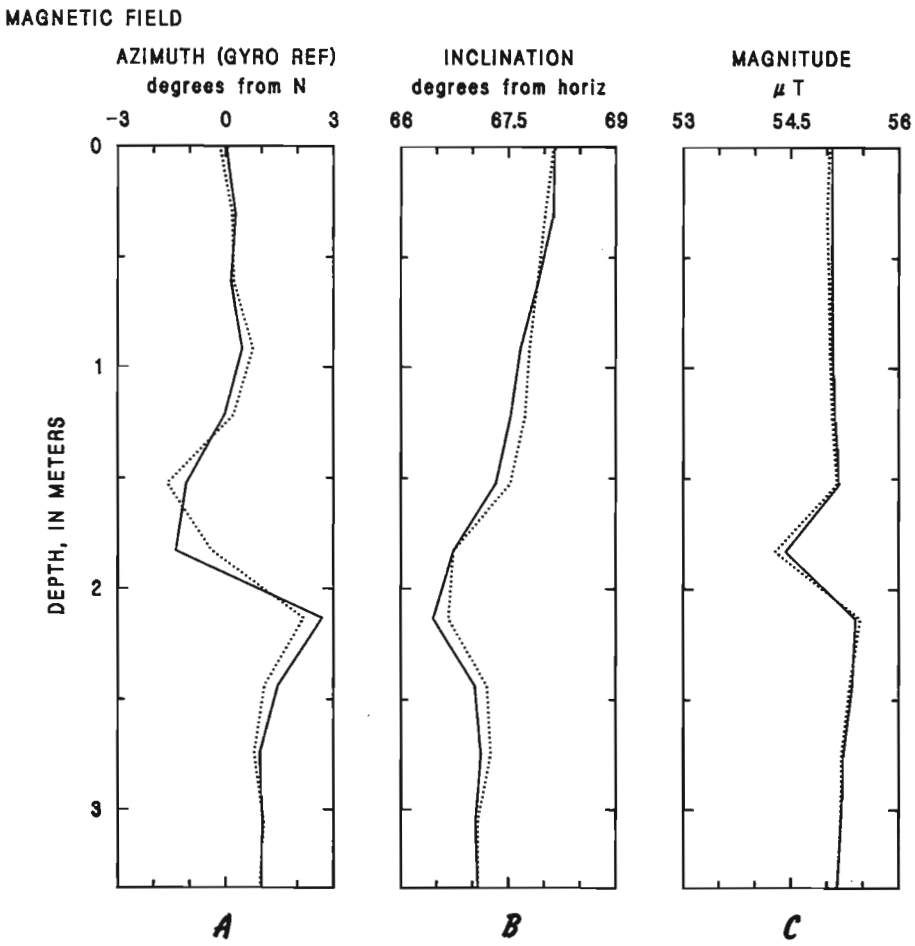

Figure 27.7. Test stand logs showing direction and magnitude of magnetic field. Magnetic dipole source is located 0.4 m S36°W of probe at depth of 2.0 m. (A) Azimuth referenced by gyroscope to surface magnetic north. (B) Inclination from horizontal. (C) Magnitude of total field. Solid line indicates logging down, dotted line logging up. Azimuths: -3 is N3°W, 0 is N, 3 is N3°E.

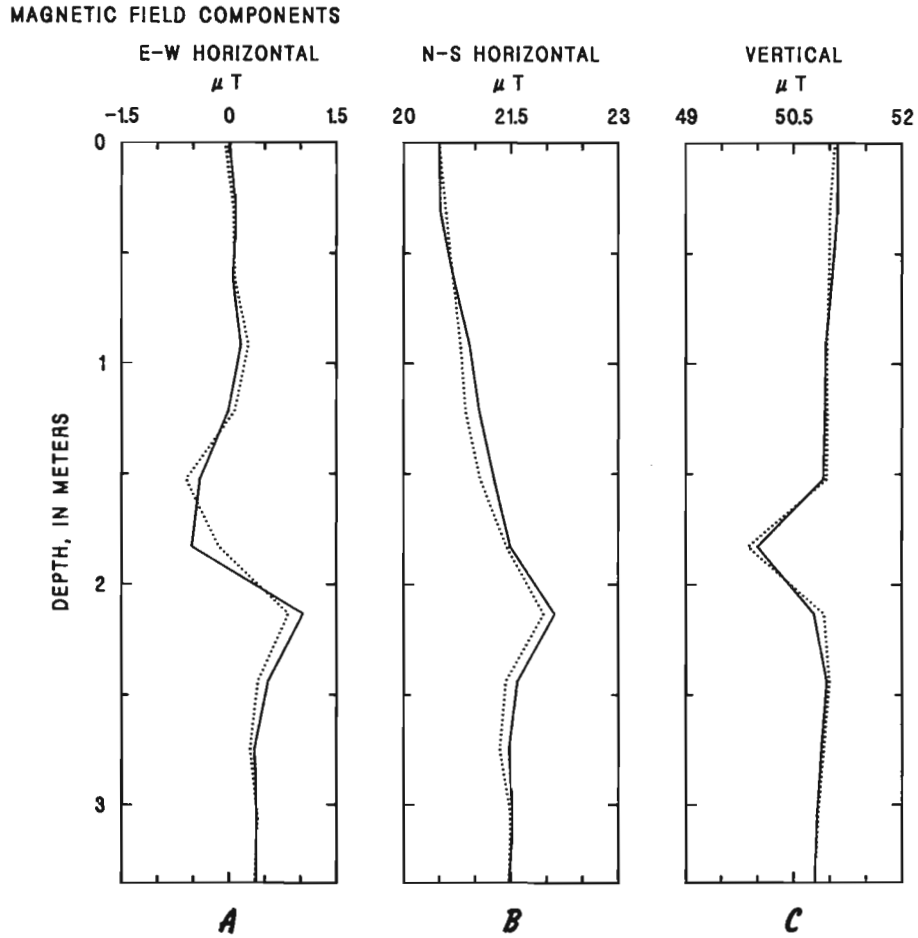

Figure 27.8. Test stand logs showing magnetic field components. Magnetic dipole source is located 0.4 m S36°W of probe at depth of 2.0 m. (A) East-west horizontal component. (B) North-south horizontal component. (C) Vertical component.

Y-axis pointing toward magnetic north, the Z-axis magnetometer will measure the vertical magnetic field and the Y-axis magnetometer will measure the horizontal magnetic field. If the uncertainty in the probe tilt is 0.1°, which is typical of the probe described in this report, the apparent magnetic dip could be 67.1°. In this case the vertical magnetic field perceived by the probe would be 51 586 nT and the horizontal field, 21 791 nT. Thus an uncertainty of 0.1° in probe tilt will cause an uncertainty of 38 nT in measurements of the vertical and 90 nT in the horizontal magnetic field components.

In the above example, the Y-axis was assumed to be aligned with the horizontal component of the magnetic field. Suppose, however, that the probe is vertical but rotated about the Z-axis so that the Y-axis is oriented 1° west of the direction of the horizontal field component. This is equivalent to a 1° uncertainty in the gyroscopic reading which is typical of the probe described in this report. Now the Y-axis magnetometer will report a field strength of 21 878 nT and the X-axis magnetometer will report 382 nT. Thus 1° rotational uncertainty will cause an uncertainty of only 3 nT in the north-south component, but an uncertainty as large as 382 nT in the east-west component.

Preliminary data indicate that the observed levels of measurement noise in the vertical, north-south and east-west magnetic vector components are in the approximate ratio of 1:2:10 (38:90:382). This ratio suggests that the vertical component can be estimated 2 times more precisely than the north-south component, and 10 times more precisely than the east-west component.

Data acquisition

The following procedure is used when a borehole is logged with the 3-component borehole magnetometer system:

1. After the probe has been attached to the logging cable, the logging truck boom and cable are positioned so that the probe is sidewalled in the hole at the zero-depth reference point (sighting position).
2. The gyroscope motor is turned on and allowed to stabilize at operating speed (30 min).
3. The telescopic sight and the caging-uncaging cable are attached to the probe. If the hole is not vertical the probe is rotated so that the telescopic line of sight (parallel to the X-axis) is horizontal, making the spin axis of the gyroscope horizontal. Then a sighting is taken on an azimuthal reference point some distance (at least 10 m) from the hole and the gyroscope is uncaged (1 s). After the gyroscope has stabilized (3 min), the probe is re-sighted, and an initial reading is taken and recorded. A compass reading is later taken on the reference point to determine its bearing from the hole collar with respect to magnetic north.
4. The telescopic sight and the caging-uncaging cable are then removed from the probe, and the probe is lowered into the hole, either continuously at a low speed (<6 m/min), or in a stop-to-read mode. Probe readings are taken and recorded at depth intervals of 0.3 to 10 m from the top to the bottom of the hole. Then the direction of probe travel is reversed, and readings are recorded at the same depth points while the probe is raised to the surface at the same speed and in the same mode. At a typical logging speed of 3 m/min the probe travels about 0.05 m during the time required to obtain one complete set of readings. This sometimes causes an error in the computed probe orientation, and a subsequent error in the magnitude of the resultant magnetic vectors in the Earth's coordinate system (vertical, N-S, and E-W). Therefore, more accurate results are obtained in the stop-to-read mode.
5. After the probe has been returned to the sighting position at zero depth, the telescopic sight and the caging-uncaging cable are re-attached and another sighting is taken on the azimuthal reference point. A final reading is recorded while the probe is held in the reference position. Then the gyroscope is caged (10 s) and its motor is turned off and allowed to slow down and stop (15 min) before the probe is moved or detached from the logging cable. This prevents excessive wear on the gyroscope bearings when it is caged and unable to move freely. The initial and final gyroscope readings are used later to correct for gyroscope drift which may be as great as 10°/h exclusive of the effect of the Earth's rotation.

At each depth measurement point, probe data readings consisting of three magnetometer values, two inclinometer values, the Gyroscope reference angle, probe internal temperature, and power supply voltage are automatically entered into the computer along with depth and time readings from the logging truck's winch system and the computer clock. Each data set is then recorded on digital magnetic tape by the computer. After the final reading has been made and recorded, a playback program is used for data reduction, either at the field site or later in the office.

Data reduction

The playback computer program accomplishes input, output and data reduction for all measurements of a logging run as follows:

1. Enter measurement data and apply basic corrections.
   a. Read the data acquisition magnetic tape.
   b. Check for invalid numbers beyond the range of permissible values, and discard readings containing invalid numbers.
2. Apply temperature corrections.
   a. Correct the 3-component magnetometer readings.
   b. Correct the 2-component inclinometer readings.
3. Convert the magnetometer and inclinometer readings to Système International units, and apply gyroscope drift corrections.
   a. Convert the magnetometer readings to microteslas (μT) and compute the magnitude of total magnetic field (1 μT=1000 nT).
   b. Convert the inclinometer readings to degrees of arc and compute the angle of tilt of probe axis from the vertical.
   c. Distribute the apparent gyroscope drift (difference between readings taken at the initial and final probe sightings), assuming linear drift with time during logging. Drift is reasonably linear for periods of 30-60 minutes. Corrections for nonlinear drift are required for logs requiring longer periods of time (described below).
4. At every point in the borehole where a reading was taken, compute the azimuth of the downward pointing Z-axis of the probe, the azimuth, inclination, and magnitude of the Earth's magnetic field, and the components of the magnetic field in the Earth's

co-ordinate system. These computations are made in the following sequence using standard techniques of rotation of co-ordinate axes (Korn and Korn, 1961).

a. Compute and store the azimuth of the downward pointing Z-axis of the probe, using (1) the gyroscope and (2) the 3-component magnetometer as two independent directional references. Call the azimuth referenced to the gyroscope Agyro, and the azimuth referenced to the magnetometer Amag.

b. Plot the difference Adif = Agyro - Amag as a function of time, and using the computer interactively, select three or more points along the time axis where Adif is smooth and has a constant slope, indicating that these points are in nonmagnetic sections of the hole.

c. Using these points as magnetic directional check points, correct the gyroscope readout for nonlinear drift during logging.

d. Using the corrected gyroscope readout as a directional reference, compute the magnetic components in the Earth's coordinate system (vertical, E-W, and N-S), and compute the magnitude and direction (azimuth and inclination) of the resultant magnetic vector representing the Earth's total magnetic field.

5. Plot, print, and/or record reduced data on magnetic tape.

Experimental measurements

Experimental logs have been made in two borehole environments: (1) nonmagnetic sedimentary rock penetrated by a nearly vertical hole, and (2) small magnetic dipole close to an inclined borehole.

The first experimental logs were made to examine system noise and repeatability in a 77 m test hole drilled through nonmagnetic sediments in Longmont, Colorado. The entire hole was lined with nonmagnetic plastic casing with an inside diameter of 10.2 cm and a wall thickness of 0.5 cm. The upper 7.5 m was also lined with steel casing with an inside diameter of 21 cm and a wall thickness of 0.5 cm. Measurements were made at 0.3 m depth intervals in the stop-to-read mode, first logging down and then up. The results of these experimental logs are shown in Figures 27.3-27.5. The data in Figure 27.3 indicate that the system noise and repeatability of the down and up logging runs are within 2°-3° for the azimuth of the probe axis and within about 0.1°-0.2° for probe tilt. System noise is estimated by observing the maximum range of non-repeatable measurement fluctuations (wiggles) occurring over short depth intervals (2-3 m). Repeatability is estimated by observing the maximum spread between measurements made during down and up logging runs. As expected, large and erratic magnetic anomalies occur in the steel-cased section of the hole as indicated by the extreme fluctuations of the probe azimuth referenced to downhole magnetic north (Fig. 27.3B). The data in Figure 27.4 indicate that below the steel casing the magnetic noise is about 2°-3° for the azimuth of the magnetic field and about 0.5° for the inclination of the magnetic field. Repeatability is within about 4° for the magnetic azimuth, 2° for the magnetic inclination and 0.4 μT for the magnitude fo the total field. The data in Figure 27.5 indicate that the noise level of the east-west component of the magnetic field is about 0.5 μT with repeatability within about 1.5 μT. The noise level of the north-south component is much lower, about 0.1 μT, but repeatability is about the same as that of the east-west component (1.5 μT). The noise level of the vertical component is even lower than that of the north-south component, (<0.1 μT), and the repeatability is better than 1 μT. Additional logs (not shown) were made with the probe moving continuously at 3-5 m/min. The noise levels and discrepancies in repeatability of these logs were several times larger than those of the stationary-reading logs shown in Figure 27.3.

The second set of experimental logs was made with the aid of a nonmagnetic test stand and a small, brick-shaped piece of magnetite-rich rock with a volume of about 1000 cm^3. The polarized rock was roughly equivalent to a magnetic dipole 20 cm long with a magnetic moment of 0.5 A m^2 (C.E. Jahren, personal communication). The strong polarization had a much greater effect on the measurements than the susceptibility of the rock sample. The magnetic rock was fastened to the test stand with its north pole pointing downward, and was positioned about 0.4 m directly behind and below the centreline of the path of the probe. The probe was lowered and raised along a track made of angle aluminum tilted about 10° from the vertical. The test logs were made with the probe first moving down, then up, at about 1 m/min, with readings taken at 0.3 m intervals. Results are shown in Figures 27.6-27.8. The distortion of the magnetic field in the vicinity of the magnetic rock produced a 4° S-shaped anomaly in the apparent azimuth of the probe referenced to magnetic north (Fig. 27.6B), and in the azimuth of the magnetic field (Fig. 27.7A). It also produced a 1° anomaly in magnetic inclination (Fig. 27.7B), and anomalies of 1 μT or more in magnitude of the magnetic field (Fig. 27.7C) and the east-west, north-south, and vertical components (Fig. 27.8). The direction and magnitude of these measured anomalies agree approximately with theoretical anomalies computed for the strength and geometry of the dipole source in relation to the logging probe.

The test stand logs demonstrated that the probe is capable of detecting small pods of magnetic ore that occur close to the borehole. They also indicated that the probe is capable of detecting polarized volcanic flows, because anomalies from thick tabular sources are commonly much larger than the test stand anomalies, typically ± 5 μT in the total field (Bath, 1976). The magnetic anomaly measured in a borehole within a polarized volcanic flow is opposite in sign to the anomaly measured by a surface or airborne magnetometer survey made over the same flow. The result of this paradox is that normally polarized flows produce negative anomalies that decrease the magnitude of the total field, and reversely polarized flows produce positive anomalies that increase it, making it easy to distinguish one from the other (Bath, 1976).

Conclusions and future plans

Results of recent measurements made to test the noise level, repeatability, and response characteristics of the 3-component borehole magnetometer probe indicate that the system is capable of detecting anomalies produced by strongly magnetized rock masses that are close to the borehole. In its present stage of development the probe's measurement noise level and drift are not low enough to assure the detection of weakly magnetized rock masses that occur more than a few metres from the borehole and produce anomalies less than 1 μT.

Future plans call for reducing the noise level and improving the overall accuracy of probe measurements by sampling all downhole sensors in a period of a few milliseconds rather than nearly a second, and by increasing the resolution of downhole digitizers. Tests will be made to identify the cause of drift that limits the repeatability of down and up logging runs, and attempts will be made to reduce the effects of drift by electronic circuitry or computer software compensation. Accurate calibration studies will be made to determine the sensitivity of the downhole measurement systems and to define possible nonlinearities so that appropriate corrections can be applied.

References

Bath, G.D.
1976: Interpretation of magnetic surveys in intermontane valleys of Nevada and southern New Mexico; United States Geological Survey, Open File Report 76-440, 37 p.

Bergdahl, S.G.
1963: The drill hole magnetometer and its use for magnetic prospecting; Colorado School of Mines, Quarterly, v. 58, no. 4, p. 253-258.

Broding, R.A., Zimmerman, C.W., Somers, E.V., Wilhelm, E.S., and Stripling, A.A.
1952: Magnetic well logging; Geophysics, v. 17, no. 1, p. 1-26.

Fabiano, E.B. and Peddie, N.W.
1980: Magnetic declination in the United States – epoch 1980; United States Geological Survey, Map I-1283.

Fabiano, E.B. and Peddie, N.W.
1981: Magnetic total intensity in the United States – epoch 1980; United States Geological Survey, Map I-1370.

Hood, P.J.
1970: Magnetic surveying instrumentation; a review of recent advances; Proceedings of the Canadian Centennial Conference on Mining and Groundwater Geophysics, Niagara Falls, October 22-27th, 1967; Mining and Groundwater Geophysics 1967, editor L.W. Morley, Geological Survey of Canada, Economic Geology Report 26, p. 3-31.

Hood, P.J. and Dyck, A.V.
1975: Magnetic drillhole measurements in mineral exploration; in Borehole Geophysics Applied to Metallic Mineral Prospecting: A Review, Geological Survey of Canada, Paper 75-31, p. 35-38.

Korn, G.A., and Korn, T.M.
1961: Mathematical Handbook for Scientists and Engineers; McGraw-Hill Book Co., p. 411-414.

Lantto, V.
1973: Characteristic curves for interpretation of highly magnetic anomalies in borehole measurements; Geoexploration, v. 11, no. 2, p. 75-85.

Levanto, A.E.
1959: A three-component magnetometer for small drillholes and its use in ore prospecting; Geophysical Prospecting, v. 7, no. 2, p. 183-195.

1963: On magnetic measurements in drill holes; Geoexploration, no. 2, p. 8-20.

Parasnis, D.S.
1973: Mining Geophysics; 2nd Edition, Elsevier Scientific Publishing Co.

Peddie, N.W., Jones, W.J., and Fabiano, E.B.
1976: Magnetic inclination in the United States – epoch 1975; United States Geological Survey, Map I-912.

Ponomarev, V.N. and Bakhvalov, A.N.
1964: Determination of the attitude of a thin bed from internal magnetic field measurements; Bulletin (Izvestiya), Academy of Sciences, USSR, Geophysics Series, no. 3, p. 214-219, p. 360-369 (Russian).

Silva, Joao B.C., and Hohmann, Gerald W.
1981: Interpretation of three-component borehole magnetometer data; Geophysics, v. 46, no. 12, p. 1721-1731.

Zuber, J.A.
1962: Magnetische Bohrlochmessungen als Hilfsmittel bei der Erzprospektierung. (Magnetic well logging as a tool in ore prospecting); Bergund Huttenm. Monatsh, v. 107, p. 299-306.

28. ASH DETERMINATION OF BLACK COAL IN EXPLORATION BOREHOLES BY THE NEUTRON-GAMMA METHOD

M. Borsaru, C. Ceravolo, J. Charbucinski, P. Eisler, and S. Youl[1]

Borsaru, M., Ceravolo, C., Charbucinski, J., Eisler, P., and Youl, S., Ash determination of black coal in exploration boreholes by the neutron-gamma method; in Borehole Geophysics for Mining and Geotechnical Applications, ed. P.G. Killeen, Geological Survey of Canada, Paper 85-27, p. 261-268, 1986.

Abstract

The theoretical bases are considered for measuring ash contents in strata of black coals by borehole logging methods. The theoretical bases considered were transport theory, the relative spectral sensitivities for the elemental constituents of coal-ash and a statistical analysis of a large sample of Australian black coals as regards the major elemental constituents determining coal-ash content.

An appropriate spectrometric neutron capture borehole logging method, based on the use of a ^{252}Cf source and a bismuth germanate detector, was tested at two coal deposits, about 250 km apart in eastern Australia. The results showed that the method was suitable for coal strata having a minimum width of 40 cm. The values of standard deviation and correlation coefficient obtained from regression analysis with 37 independent data were 2% ash and 0.97 respectively.

Résumé

On a examiné la possibilité de mesurer, par diagraphie des sondages, la teneur en cendre des couches de charbon en fonction des bases théoriques suivantes: la théorie du transport, les sensibilités spectrales relatives des constituants de la cendre de houille et l'analyse statistique d'un gros échantillon de charbon australien pour y déterminer le rôle des principaux constituants élémentaires dans le calcul de la teneur en cendre de houille.

La diagraphie des sondages par capture spectrométrique de neutrons, méthode fondée sur l'utilisation d'une source de ^{252}Cf et d'un détecteur au germanate de bismuth, a été mise à l'essai dans deux gisements de houille situés à environ 250 km l'un de l'autre dans l'est de l'Australie. Les résultats montrent que cette méthode peut servir pour les couches de houille dont la largeur minimale est de 40 cm. L'écart-type et le coefficient de corrélation, fondés sur une analyse de courbes de régression qui utilisait 37 données indépendantes, étaient de 2% de cendre et de 0,97 respectivement.

Introduction

The economic value of coal deposits, the mine planning and the production schedules are determined by a number of factors. Three important parameters in this respect are the thickness of the coal seams, their depth below the surface and the ash content in the coal.

In the past, these parameters were determined by geological inspection and chemical analysis of the material extracted from drill holes. However, this type of evaluation is costly, because in order to obtain representative samples for chemical analysis from the boreholes, core drilling, accurate sampling and careful sample preparation are necessary. As a consequence, the conventional chemical methods have been supplemented increasingly, in recent years, by in situ measurements based on borehole logging technology. Nuclear techniques are particularly effective in these applications because they are based on the interactions of deeply penetrating gamma rays or neutrons with the nuclei in the coal seam.

Currently, the gamma-gamma borehole logging techniques are those most commonly used in evaluating these parameters in coal deposits. In one configuration of the probe, it can be used to locate accurately the interface between coal layers and sedimentary strata. In a different configuration the probe gives accurate measurements of density. On the basis of the correlation generally observed between density and coal-ash content, this borehole logging measurement for density provides a measure of coal-ash content. Although the method is indirect, it has been used effectively in many coal exploration and mining applications. However, the method also has the following shortcomings:

(a) In rough, cavitatious boreholes, the measurement of density (and hence of ash content) has reduced accuracy. This effect applies to both sidewall and centralized probe-operation.

(b) The correlation between ash content and coal density is by no means universal (Agostini, 1977). It varies for different coal deposits and to a lesser extent for different seams within the same deposit.

[1] CSIRO Division of Mineral Physics, P.O. Box 124, Port Melbourne, Vic. 3207, Australia

Prompt neutron-gamma logging provides an alternative method that is less sensitive to either boreole rugosity or the difficulties of correlating probe response with ash content (Nargolwalla et al., 1977, Senftle et al., 1978). The basis of the ash-analyzing technique described in the present paper is neutron capture. By using ^{252}Cf as the source of primary neutrons, the prompt gamma rays generated in coal lithologies are dominated by photons excited in neutron capture reactions. The fission neutron spectrum of ^{252}Cf, which peaks at about 1 MeV and has a mean energy of about 2.2 MeV, is distributed over energies that are too low to excite sufficient 4.43 MeV gamma rays from inelastic scattering with carbon to compete with the 4.93 MeV gamma rays due to silicon capture. This choice of neutron source forms the basis of the technique presented in this paper (Senftle et al., 1979).

While both neutron activation and neutron inelastic scattering produce photons with an energy distribution mainly below 3 MeV, the neutron capture process produces photons with energies ranging up to 10 MeV. In fact, most of gamma rays that characterize the constituents of coal-ash have energies greater than 3 MeV. This contrasts with photons measured in gamma-gamma techniques where photon energies are largely below 500 keV. The greater penetration of the neutron capture photons enables this logging method to sample larger volumes in the coal strata than the other methods, particularly the gamma-gamma method. It also renders the neutron capture method the least sensitive to diameter variations in fluid-filled boreholes, especially where significantly large annuli of fluid surround the probe.

Preliminary considerations

Prompt neutron-gamma logging theory

The theoretical basis for neutron capture gamma logging is radiation transport theory applied to the logging situation. While the results of a theoretical analysis are too complex for direct application, a simplified analysis is useful in suggesting the variables for a regression model. The simplified theoretical analysis also suggests reasons why the method is relatively insensitive to borehole effects.

Consider an idealized borehole logging probe, consisting of a point spectrometric detector shielded from the direct radiation of a point source (^{252}Cf), located at a distance ℓ from the detector. If the borehole is water filled, as is likely in any coal deposit in eastern Australia, the probe is surrounded by borehole fluid (water) of annulus, R. Provided that R is appreciably smaller than the slowing down length in the coal, the borehole effect can be neglected, as a simplifying approximation. Thus, the probe is contained in an infinite homogeneous matrix of coal. The chemical concentration of any element j is given in this case by the simplified expression (J.A. Czubek, personal communication, 1976).

$$c_j \propto I_{kj} A_j \Sigma / (N_{kj} \rho \sigma_j F) \qquad (1)$$

for a source-detector separation, ℓ, where

- I_{kj} is the intensity of gamma rays detected at the characteristic energy, k, for this chemical element, j,
- A_j is the atomic weight of element j,
- N_{kj} is the number of photons emitted at energy k for each capture event in a nucleus of element j,
- ρ is the coal density,
- Σ is the macroscopic crosss-section of the coal (or rock), and
- σ_j is the microscopic cross-section of element j.

The function, F, has the form $\int_V \phi G_k dV$.

Both ϕ, the thermal neutron flux and G_k, the gamma ray transmission in the coal are exponential functions. In fact, the neutron capture logging method provides no direct measure of G_k. This, together with the mathematical complexity of equation (1), makes it impossible to determine c_j directly by substituting the measured parameters in the theoretical expression (In fact, the theoretical expression for c_j, which would satisfy the situation of an actual probe located in a real borehole, is even more complex than equation (1).

However, the above analysis is useful in suggesting the response variables of a linear regression model for c_j. I_{kj} is one of the selected variables because c_j is shown to be proportional to it. c_j is also inversely proportional to the average neutron flux and also to the average photon transmission in the zone of investigation. As previously stated, the photon transmission function, G_k, cannot be measured directly by the method. However, the neutron count rate, ϕ', can be monitored in the probe to give a measure of variations in the average neutron flux within the zone of investigation. Consequently, we selected I_{kj}/ϕ' and ϕ', in addition to I_{kj}, as the variables for regression analysis to calibrate for the probe coal-ash determinations. The variations in G_k can only be taken into account by correlation with the above response parameters.

Statistical investigation of ash composition

The second hypothesis underlying the present capture logging method is that the variation in coal ash content is predominantly determined by variations in the concentrations of the Si, Al and Fe coal constituents. We tested this hypothesis using the chemical and ash assays of 174 Australian black coals and fitting with a linear regression equation of the form

$$\% \text{ ash} = b_0 + b_1 X_1' + b_2 X_2' + b_3 X_3',$$

where b_0, b_1, b_2, b_3 are constant coefficients and X_1', X_2', X_3' are the weight fractions of SiO_2, Al_2O_3 and Fe_2O_3 in the coal ash (Joint Coal Board and Queensland Coal Board, Australian black coals, 1976). The analysis showed excellent correlation between ash content and these particular elemental constituents, which supported the hypothesis. The value of the correlation coefficient was 0.99, while that of the standard deviation was 0.7% ash. The correlation was significantly reduced, but still good, when only the concentrations of Si and Fe were considered. In that case, the value of the correlation coefficient was 0.97 while that of the standard deviation was 1.4% ash.

Effect of variation in spectral sensitivity for Si, Al and Fe

Two relevant points emerge in this context if the theoretical analysis is applied to the spectral data shown in Table 28.1. This table gives the gamma ray line energies E_k for the principal chemical elements in coal ash (j) and N_{kj}. In fact, quantitative interpretation for the neutron capture method presented was based on count rates in spectral windows preset to include selected line energies.

(a) The emission probabilities for the Fe and Al constituents in coal, determined by $N_{kj}\rho_j/A_j$, are in the ratio of about 14:1 (i.e. for Fe/Al), for equal weight fractions of the elements.

(b) The emission probabilities for the Fe and Si constituents of coal are in the ratio of about 2:1 (i.e. for Fe/Si), for equal weight fractions. However, because the peak efficiency of the detector is expected

Table 28.1 Neutron capture parameters for aluminum, silicon, iron and titanium.

Element (Atomic mass)	Cross section σ (barn)	Major gamma rays (MeV)	Intensity (I) (photons/100 neutrons)
Aluminum 26.98	0.23	7.72 7.69	20.10 4.17
Silicon 28.09	0.16	7.20 6.38 4.93 3.54	7.2 12.6 70.5 79.6
Iron 55.85	2.62	7.65 7.63	22.1 27.2
Titanium 47.90	6.1	1.38 4.88 6.42 6.56 6.76	65.5 5.7 36.5 6.5 54.0

Table 28.2. Variation of ash and major constituent elements in a large sample of Australian coals.

	% Al	% Si	% Fe	% Ash
Mean	1.83	3.38	0.45	12.53
Sigma	0.94	1.65	0.37	5.47
Max.	5.6	9.00	2.48	35.5
Min.	0.59	0.45	0.004	2.6

Note: Mineral concentrations are given as weight percent of coal.

Table 28.3. Variation of SiO_2, Al_2O_3 and Fe_2O_3 for almost constant ash in Australian coals.

	% Ash	% SiO_2	% Al_2O_3	% Fe_2O_3
σ'	1.64	2.2	1.32	0.93
$\bar{x}$	22.4	13.4	5.9	1.24
n = 11				
σ'	1.07	1.76	1.22	0.38
$\bar{x}$	16.2	10.4	4.05	0.62
n = 21				
σ'	0.7	1.0	0.64	0.32
$\bar{x}$	9.7	5.85	2.83	0.48
n = 47				

Note: (i) σ', $\bar{x}$ and n are the r.m.s. deviation, the arithmetic mean and the number of samples respectively.

(ii) Mineral concentrations given above are expressed as weight percent of coal.

to be substantially greater for the Si capture photons than for the Fe capture photons, the spectral sensitivity for Si would be roughly comparable with that of Fe.

From Table 28.2,the mean Al content in the Australian coals investigated is about 4 times that of Fe. On average, therefore, Fe makes a larger spectral contribution than Al. This is supported by the data, shown in Table 28.3, for coals of similar ash content. This table shows that the ratio of the variation (i.e. σ) of Al to Fe concentrations in these coals is significantly less than 4:1. Consequently, the variation in spectral response above 5 MeV, in coals of given ash content, is dominated by the variation of Fe content.

However, from the tables we expect that the spectral contribution from 4.93 and 3.54 MeV Si capture gamma rays will dominate all other spectral contributions, including that of Fe in the energy window from 2.6 to 5.2 MeV. As a consequence, the variation of count rates in the spectral windows present around the silicon capture peaks and above 5.2 MeV, are largely a measure of the variation in the Si and Fe contents of the coal respectively. The method is relatively insensitive to variations in the aluminium concentration. However, the work described below provides some test of the hypotheses discussed above.

Considerations governing the choice of detector

Current technology offers four types of spectrometric detectors for borehole logging. They are: high resolution Ge, NaI(T1), CsI(Na) and $Bi_4Ge_3O_{12}$ (BGO). While the Ge detector is purely a solid state device, the last three types are all scintillation detectors.

The borehole logging application described in the present paper required high detection efficiency and, particularly, high peak to compton ratios for photons with energies up to 8 MeV. Although good energy resolution is desired, it is relatively unimportant for routine determinations of ash content by continous logging.

While Ge detectors offer excellent energy resolution, both detection and peak efficiencies are slightly inferior to the conventional NaI(T1) detector on a volume basis. However, it is also significant that on a volume basis, the Ge detector is nearly two orders of magnitude more costly than the premium grade NaI(T1) detector.

Consequently, costs prohibit the use of Ge detectors having detection and peak efficiencies that are comparable with those of 51 x 51 mm NaI(T1) detectors. The cost factor is particularly significant with Ge detectors for logging techniques using neutron sources. In these applications, the useful life of the detector is limited by radiation damage. If the source-detector spacing is increased to limit the rate of degradation in detector performance, both the detection efficiency and the spatial resolution of the probe are degraded.

Apart from the difficulties due to high costs and radiation damage, Ge detectors must be operated at cryogenic temperatures. The logistical problem of organizing reliable liquid nitrogen supplies to mining leases is a further disincentive to using these detectors for routine borehole logging. However, Ge detectors would certainlly find valuable application for identifying impurities in coal lithologies.

The premium grade NaI(T1) detector, which has been used almost exclusively in spectrometric borehole logging for many years, achieves an energy resolution that is typically only 1/50 the resolution of the germanium detector. Nevertheless, it has advantages, common to all the scintillation detectors considered, of simple operation at normal ambient temperatures, good detection efficiency at low cost and performance characteristics that remain largely unaffected with accumulated radiation exposure. However, the probes used for logging narrow boreholes (of smaller diameter than NQ) place constraints on the dimensions of the NaI(T1) detectors used, which consequently limits both their detection and peak efficiencies, particularly for high energy photons (Stromswold, 1980, 1981; Killeen, 1982; Conaway et al., 1980).

CsI(Na) has appreciably greater detection and peak efficiency than NaI(T1) on a volume basis, largely because of its greater density and greater effective atomic number. It is also mechanically the more robust material and, unlike NaI(T1), it does not deliquesce on exposure to air.

However, CsI(Na) is only marginally the more attractive scintillator for borehole logging applications because it has significantly inferior energy resolution and only a slightly larger peak to compton continuum ratio than NaI(T1).

In spite of its particularly poor energy resolution, on balance, the BGO detector has the most suitable spectral response characteristics for the application described in this paper. On a volume basis, both the detection efficiency and the peak to compton ratio are much larger than for the other detectors considered, particularly for high energy photons. These characteristics of BGO are due to its high density (7.1. g/cm^3) and its high effective atomic number, (Z_{eq} = 70). By comparison, Ge, NaI and CsI have Z_{eq} values of about 32, 48 and 54 respectively, while their densities are 5.3, 3.7 and 4.5 g/cm^3.

In practice, small stripping ratios, relatively large peak efficiencies (Borsaru et al., 1983) obtained at high energies and relatively low sensitivity for neutron activation (Drake et al., 1981) support the choice of BGO as the most suitable scintillator for routine quantitative coal-ash measurements carried out in a continuous logging mode.

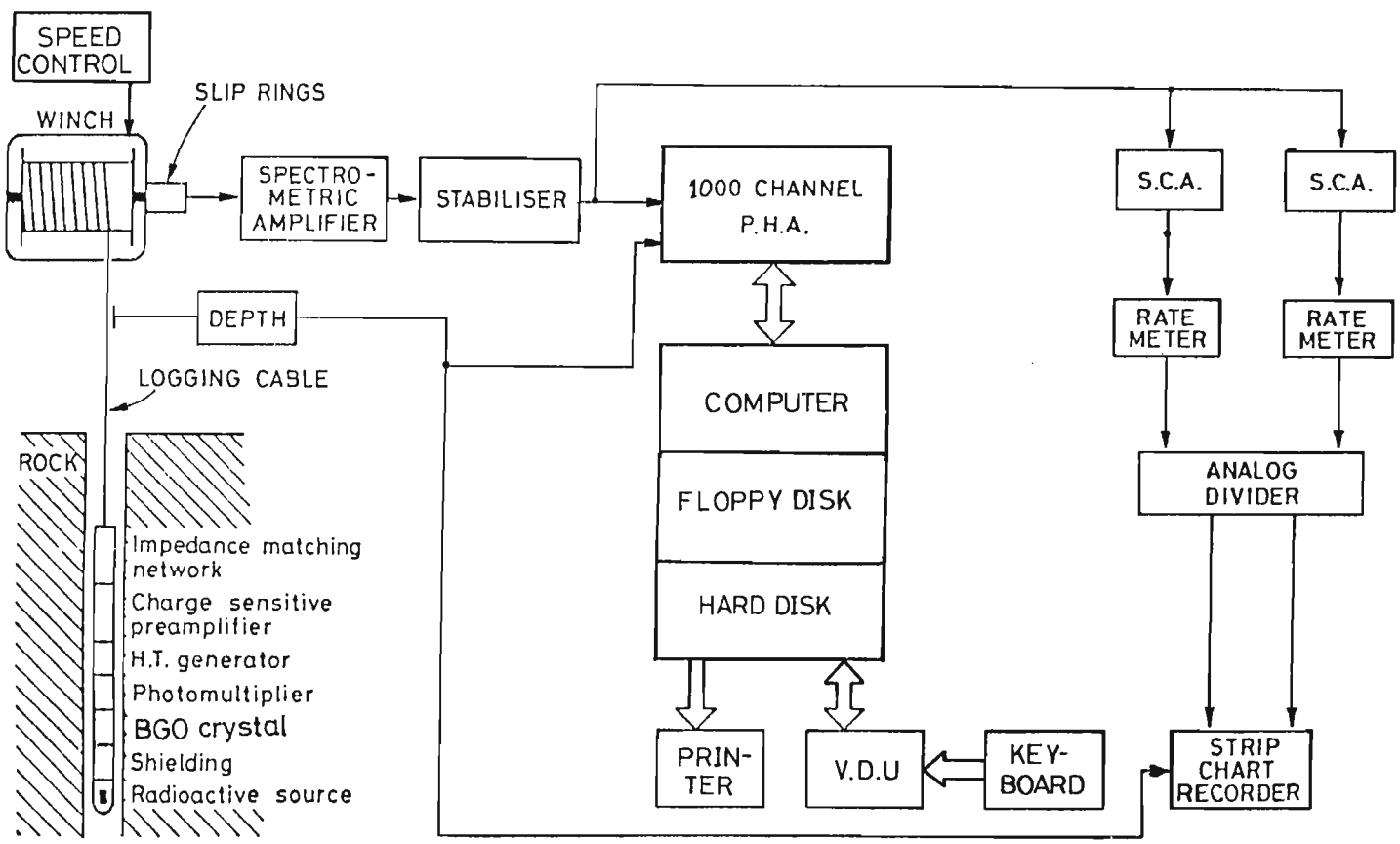

Figure 28.1. *Schematic of borehole logging system.*

Method

General

The neutron capture logging technique was field-tested at two coal deposits in southern Queensland, about 250 km apart. The test data were obtained from drill-cored boreholes that intersected 37 strata varying in width from 40 to 200 cm. These data consisted of both the chemical assays of core samples intersecting these strata and the corresponding digital records of the neutron-capture logging spectra. All spectral records used in the investigation were obtained in water-filled boreholes, although it was occasionally necessary to replenish the water in the boreholes to compensate for the daily variation in the level of the water table.

The ash content of the strata measured in the investigation varied from 7 to 31% ash, with a standard deviation, σ_t, of 8.3% ash. The diameter of the boreholes used in the tests varied from 12.5 to 17.5 cm.

Equipment

A schematic of the equipment used for prompt neutron-gamma logging is shown in Figure 28.1. It comprised the borehole logging probe connected via 300 m of standard 4-core cable with instrumentation for analogue signal processing, data storage and data interpretation. This instrumentation and the winch equipment were contained in an air-conditioned 4-wheel drive truck (Ford F100). Power was supplied by a 4.5 KV generator mounted on the bull bars at the front of the truck.

The logging probe, of external diameter 70 mm, was fabricated of aluminium alloy. It housed electronic instrumentation, and a 51 x 51 mm BGO detector shielded by a 150 mm length of bismuth against the primary gamma radiation of a ^{252}Cf source (2.5 µg). A coating of ^{10}B (16 mg/cm^2) for the scintillation detector provided it with both shielding against thermal neutrons and the means of obtaining a measure of the thermal neutron flux at the detector via the 478 keV capture peak of ^{10}B. The probe electronics included a preamplifier and high voltage supply. Gain stabilization was obtained by using the 2.2 MeV capture line of hydrogen for the reference peak because of its prominence in the spectra recorded.

Analog signal processing consisted of pulse shaping, amplification and multichannel pulse height analysis to measure and record the neutron capture gamma ray spectra. The "accumulate" and "output" functions of the analyzer were controlled by depth-marker pulses from the winch instrumentation. The control system was preset to transfer the digital spectral records, accumulated while logging contiguous 5 cm increments of borehole, to hard disk via the microcomputer (Cromemco Z-2D), at the end of each increment logged. At the beginning of logging each 5 cm increment, there was a 0.35 s period when spectral accumulation was halted for the destructive readout of the spectral record to the computer. For a typical logging speed of 1 cm/s, this represented only a 7 per cent loss of information in each increment.

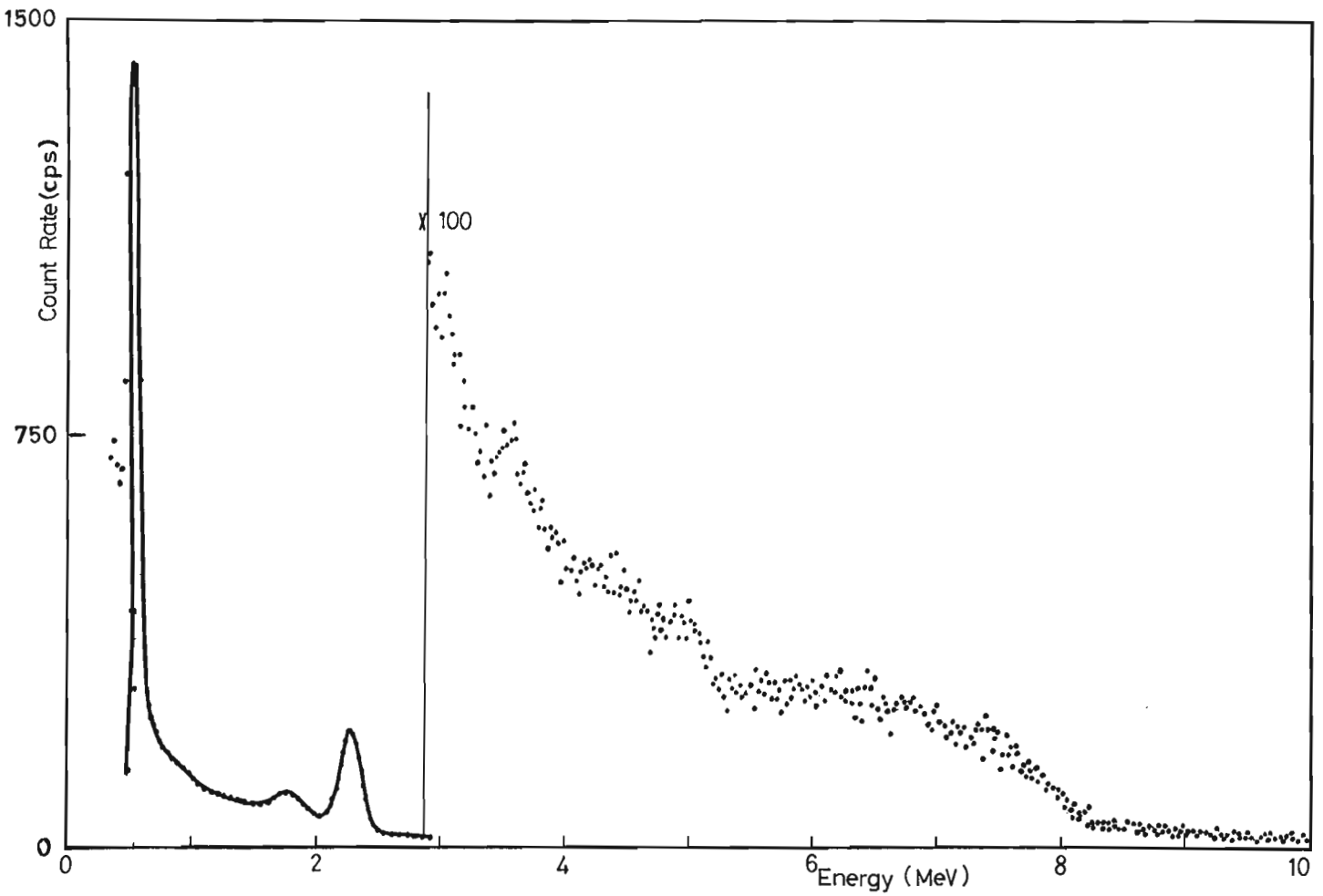

Figure 28.2. A neutron-capture spectrum for a typical layer collected for 3 minutes.

Results and discussion

Spectral response in coal

The neutron-capture spectrum recorded in a typical coal layer is shown in Figure 28.2. It features the prominent capture peaks of hydrogen and ^{10}B at 2.22 and 0.478 MeV respectively. Although less well defined than the above, the full absorption and first escape peaks due to 4.93 and 3.54 MeV capture gamma rays of silicon are also evident. Spectral peaks are also noticeable or discernable above the continuum at higher energies due to gamma rays at 7.72 and 7.64 MeV due to capture in Al and Fe, also at 6.76 and 6.42 MeV due to capture in Ti, but these require computer processing or enhancement to extract the spectral information.

The spectral sensitivity of the probe for the mineral matter in coal is sufficient for its application to the delineation of coal layers and seams, and also to the determination of coal-ash content.

Delineation of coal seams

The position and thickness of coal layer and seams can be determined by monitoring the spectral response of the probe to the Si, Al, Fe and Ti constituents in both the coal and the interlayer and interseam sediments. Because these constituents are more concentrated in the sediments than in the coal, the gamma ray count rate in the relevant spectral windows of the probe is expected to vary correspondingly.

The principal gamma ray energies and cross-sections for these constituent elements (Table 28.1) suggest that the energy window from 3 to 10 MeV is appropriate for monitoring stratigraphy. An example is shown in Figure 28.3 of the correspondence between the geophysical log, obtained with this spectral window setting, and the geological log obtained by inspection of core samples. From the figure, it appears that the geophysical log is accurate both in defining the position of coal-strata and their width.

The preliminary considerations of the paper indicated that the variation of ash content in eastern Australian bituminous coals is predominantly determined by the chemical concentrations of Si, Al and Fe. Consequently, we considered it unnecessary to use separate spectral windows corresponding to the energy peaks of Ti, Ca and other elements for defining the regression variables. The variables, $X_1, \ldots, X_n$, used in the regression model were the total count rates in spectral windows defined by software. The four windows used encompassed: (1) the 0.478 MeV peak of ^{10}B, (2) the full absorption peak of H at 2.22 MeV, (3) the full absorption and escape peaks of Si due to 3.54 and 4.93 MeV gamma rays, and (4) all gamma rays detected above 5.2 MeV.

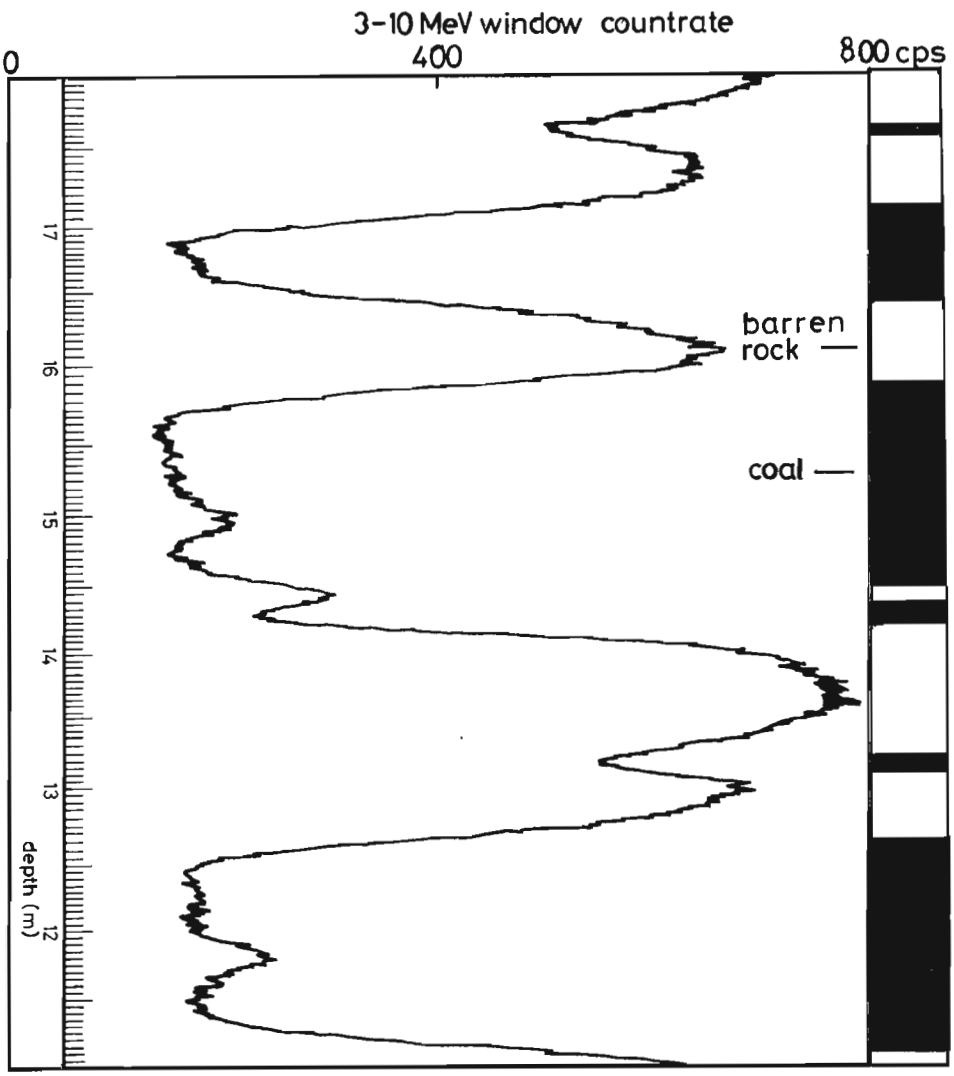

Figure 28.3.

Comparison of geophysical and geological logs.

It is worth stressing again that this last spectral variable is determined largely by the variation of Fe and Al concentrations. The other variables included in the model were the ratios of the count rates in the various windows with the count rate in the window for ^{10}B-capture, as indicated from previous theoretical considerations.

The linear regression model used was of the form

$$\pm \text{ ash} = a_o + a_1X_1 + \ldots + a_nX_n$$

The actual regression equation was determined by the stepwise regression technique.

Regression analysis indicated that the count rates in all the spectral windows, except that encompassing the 2.22 MeV hydrogen capture peak, were statistically significant regression variables, as were also the ratios of these count rates with that of the ^{10}B capture window. Thus, the best regression equation obtained consisted of 5 variables based on the count rates recorded in 3 spectral windows. The apparent insensitivity of the technique to hydrogen was probably due to the dominant spectral contribution of the hydrogen constituent in the borehole fluid, because the boreholes used were appreciably wider than the probe.

The accuracy of measurement (σ), represented by the r.m.s. deviation between the chemical and nuclear assays, was 2% ash, for data from the two coal deposits. The correlation coefficient (r) obtained from the same regression analysis, was 0.97. The cross plot of ash content values predicted by chemical and nuclear methods is shown in Figure 28.4. Where only one deposit was considered, with 23 coal strata varying form 7 to 25% ash, the values of σ and r obtained from regression analysis were 1.6% ash and 0.93 respectively.

The precision of the method(s), based on reproducibility testing of logging measurements, was determined from repeated logging runs at one of the two coal sites. This involved testing the reproducibility in 23 strata. The value of s obtained from this analysis was 0.6% ash. Consequently, the accuracy achieved was not limited by the procedures of measurement.

Summary and conclusion

Transport theory and considerations of the spectral sensitivities for the various elemental components in coal-ash suggest that the neutron capture borehole logging method is suitable for determining the ash content of Australian black coals. The reasons for this are that the variations in Si and Fe concentrations in coal generally predominate the coal-ash content variation. Also, Si and Fe are the chemical elements that cause the greatest variation in spectral shape of the capture spectra obtained in coal strata.

The BGO detector, which has a relatively large peak efficiency, particularly at high energies and also a large peak-to-compton ratio, was found to be particularly advantageous for the logging method. Further, the relatively low energy distribution of primary neutrons emitted by ^{252}Cf allowed the emission of Si capture photons to predominate that of photons due to inelastic scattering of neutrons with nuclei of C.

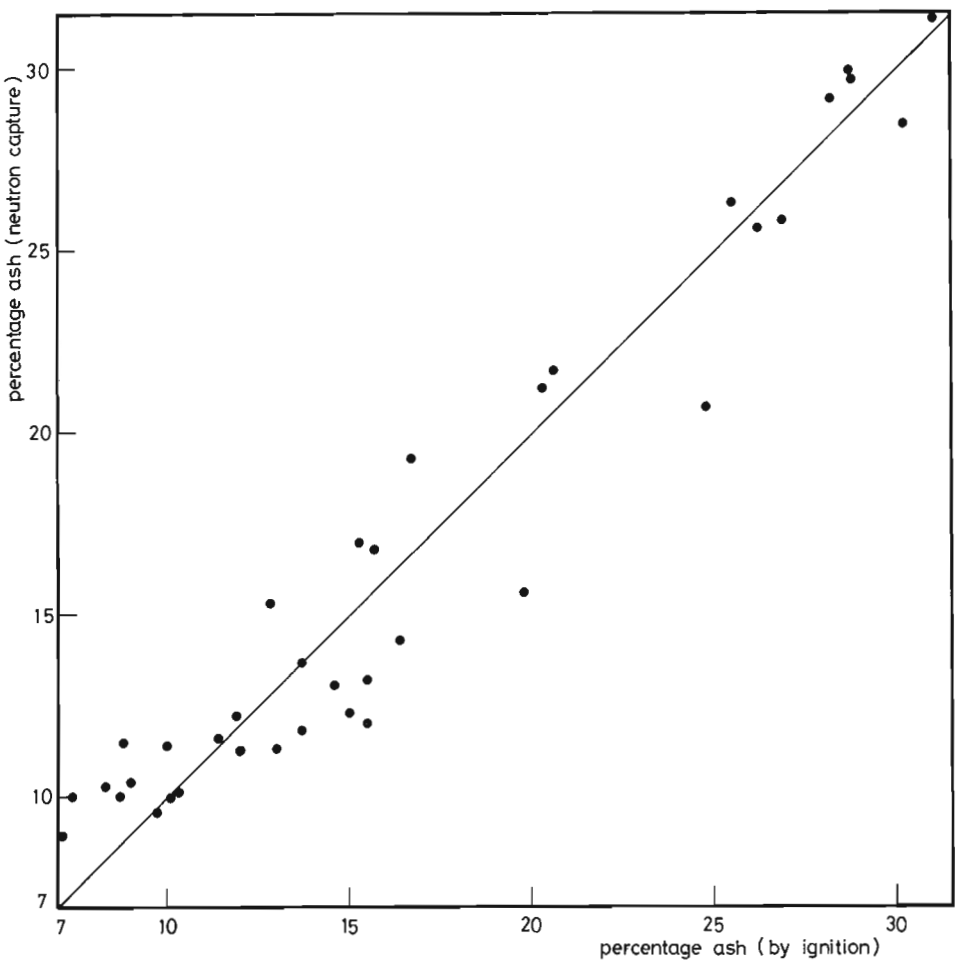

Figure 28.4.

Comparison of coal-ash assays obtained by neutron capture and chemical analysis method.

The method was tested at two coal deposits, 250 km apart in eastern Australia. The diameter of the boreholes used varied from 12.5 to 17.5 cm, while the ash content in the 37 strata tested varied from 7 to 31%, with a standard deviation of 8.3% ash. The result of a regression analysis using a linear model gave values for the standard deviation and the correlation coefficient of 2% ash and 0.97 respectively. A test for the reproducibility of the measurements showed that the precision of the technique was 0.6% ash, which could not have been a determining factor for the accuracy obtained. However, the value obtained for the accuracy could be explained by the nature of the correlation between ash content and the combined concentrations of Si and Fe. The logging method was also advantageous in another respect; it showed little sensitivity to the variations in diameter of the boreholes tested.

Acknowledgments

The authors wish to thank John Miles, the Divisional Engineer responsible for the mechanical design of the logging probe and ancillary equipment, the Workshop staff of the CSIRO Port Melbourne laboratory for fabrication, and The Shell Company of Australia Limited, Coal Division for providing collaborative assistance in the organization of the field trials. The work described was supported under the NERDDC program.

References

Agostini, A.
1977: Correlation of high resolution density log counts and ash content of coal in the Goulburn Valley, N.S.W.; Australian Society of Exploration Geophysicists, Bulletin, v. 8, p. 26.

Borsaru, M., Ceravolo, C., Charbucinski, J., Eisler, P., and Youl, S.
1983: Comparative performance of BGO and NaI(Tl) detectors for identifying coal sediments by gamma ray logs; Transactions Eighth European Formation Evaluation Symposium, London, Paper O.

Conaway, J.G., Killeen, P.G., and Hyatt, W.G.
1980: A comparison of bismuth germanate, cesium iodide, and sodium iodide scintillation detectors for gamma ray spectral logging in small diameter boreholes; in Current Research, Part B, Geological Survey of Canada, Paper 80-1B, p. 639-652.

Drake, D.M., Nilsson, L.R., and Faucett, J.
1981: Bismuth germanate scintillators as detectors for high-energy gamma radiation; Nuclear Instruments and Methods, v. 188, p. 313.

Killeen, P.G.
1982: New Scintillation detectors: a review of comparisons of bismuth germanate, cesium iodide and sodium iodide; Proceedings of the Symposium on Uranium Exploration Methods, Review of the NEA/IAEA R&D Programme, Paris, p. 639-652.

Nargolwalla, S.S., King, A., Legrady, O.J., Strever, J., Csillag, A. and Siegel, H.O.
1977: Nuclear Metalog grade logging in mineral deposits; Nuclear Techniques and Resources 1977, IAEA, Vienna, Austria, p. 229-264.

Senftle, F.E., Tanner, A.B., Philbin, P.W., Boynton, G.R. and Schram, C.W.
1978: In-situ analysis of coal using a Cf-252-Ge(Li) borehole sonde; Mining Engineering (AIME), v. 30, no. 6, p. 666.

Senftle, F.E., Macy, R.J., and Mikesell, J.L.
1979: Determination of the optimum size Cf-252 neutron source for borehole capture gamma ray analysis; Nuclear Instruments and Methods, v. 158, p. 293.

Stromswold, D.C.
1980: Comparison of scintillation detectors for borehole gamma ray logging; Proceedings 21st SPWLA Symp. (July 1980), Paper EE.

Stromswold, D.C.
1981: Comparison of sodium iodide, cesium iodide, and bismuth germanate scintillation detectors for borehole gamma ray logging; IEEE Transactions, Nuclear Science, NS-28, p. 290.

29.

A GAMMA-GAMMA METHOD FOR MEASURING THE DIAMETERS OF AIR-FILLED BOREHOLES

P.J. Mathew[1] and M.R. Anderson[1]

Mathew, P.J. and Anderson, M.R., A gamma-gamma method for measuring the diameters of air-filled boreholes; in Borehole Geophysics for Mining and Geotechnical Applications, ed. P.G. Killeen, Geological Survey of Canada, Paper 85-27, p. 269-275, 1986.

Abstract

Diameter is an important borehole parameter used not only for correcting other geophysical logs but also for providing information about the borehole and surrounding formations. A backscattered gamma ray technique has been developed for determining the diameters of air-filled boreholes. The method is based on the observation that the shape of the upper energy region of the backscattered gamma ray spectrum changes with borehole diameter. The shape of the spectrum can be measured by the ratio of the intensities of two spectral energy windows in this region. This ratio, called the S-factor, can be used to determine the diameter of model boreholes ranging from 11 cm to 22 cm with a standard deviation of 0.26 cm. The S-factor is virtually independent of the density and composition of the medium surrounding the borehole. An important advantage of this technique is that density, composition (P_Z), and the S-factor can be determined simultaneously from the same backscattered gamma ray spectrum. Extensive field trials have proved the veracity and usefulness of the technique, and it appears that the technique is also applicable to fluid-filled boreholes.

Résumé

Le diamètre d'un sondage est un important paramètre qui sert non seulement à la correction d'autres diagraphies géophysiques mais qui fournit également des renseignements sur le sondage et les formations qu'il traverse. Une technique aux rayons gamma rétrodiffusés a été mise au point pour déterminer le diamètre des sondages remplis d'air. Cette méthode est fondée sur l'observation suivante: la forme de la portée supérieure du spectre à rayons gamma rétrodiffusés varie en fonction du diamètre du sondage. La forme du spectre peut être mesurée en se servant du rapport qui existe entre les intensités des deux fenêtres spectrales de cette région. Cette proportion, appelée facteur-S, peut servir pour déterminer le diamètre des maquettes de sondage variant de 11 à 22 cm, l'écart-type étant de 0,26 cm. Le facteur-S est presque complètement indépendant de la densité et de la composition du matériau qui entoure le sondage. Cette méthode offre un avantage important: il est possible de mesurer en même temps la densité, la composition (Pz) et le facteur-S en utilisant le même spectre à rayons gamma rétrodiffusés. Des essais intensifs ont prouvé la véracité et l'utilité de cette technique qui s'appliquerait également aux sondages remplis de fluide.

Introduction

A variety of nuclear geophysical borehole logging techniques have been developed in the past for the evaluation of physical properties and chemical composition of formations to assist geological prospecting and mineral exploration (Berzin et al., 1966). The gamma-gamma method of density measurement has been widely used as a borehole logging technique for more than two decades. In recent years, the P_Z technique of composition measurement (Czubek, 1966; Blyumentsev and Migunov, 1967) has increased the scope and usefulness of the gamma-gamma method in mineral exploration. The diameter of a borehole varies due to drilling techniques and rock characteristics and, in common with so many other geophysical techniques, the gamma-gamma probe response is strongly influenced by variations in hole diameter. Consequently, an accurate knowledge of borehole diameter is needed to correct the probe response for quantitative evaluation of rock properties. Diameter or caliper logs also assist in the estimation of mud cake thickness, in the identification of caved-in regions, and in the calculation of the volume of cement needed to fill the annular behind casing (Hilchie, 1968). Electro mechanical calipers (Hilchie, 1968) have been the most widely used type in borehole logging, although techniques based on acoustic (Helander, 1966) and radiation calipers (Charbucinski et al., 1976) have been reported in the literature. Few eixsting borehole calipers, however, provide hole diameters with sufficient accuracy for the quantitative evaluation of rock properties.

In the work presented here a method called S-factor is described to measure air-filled borehole diameter from the shape of the upper energy region of the backscattered gamma ray spectrum of a gamma-gamma probe. The change in the spectral shape in this region is caused by the variations in borehole diameter. A significant advantage of this technique is that density, composition (P_Z), and hole diameter can be measured simultaneously from the same backscattered gamma ray spectrum of the gamma-gamma probe.

[1] CSIRO Division of Mineral Physics, P.O. Box 124, Port Melbourne, Vic. 3207, Australia.

The present technique was developed as part of this group's effort in developing techniques and instrumentation for borehole logging in iron ore mineralizations in the Pilbara region of Western Australia. A brief account of this technique has been reported earlier (Wylie and Mathew, 1976).

Principle of the technique

A typical backscattered gamma ray spectrum from a gamma-gamma probe, when placed in a borehole, is shown in Figure 29.1. The low energy region of the spectrum, i.e. <300keV, represents the P_z region (Charbucinski et al., 1977). The change in the shape of this region is a measure of the composition of the medium around the borehole. The region above 300 keV represents the well known density region (Aylmer et al., 1978). When corrected for changes in borehole diameter, the intensity of this region of the gamma ray spectrum is a measure of the density of the medium. The region of present interest is the higher energy region as indicated in Figure 29.1. The change in shape of this region as a result of variations in borehole diameter is explained below on the basis of the single scattering model (see for example, Homilius and Lorch, 1958; Taylor and Kansara, 1967).

Consider a borehole logging probe consisting of a monoenergetic gamma ray source S, separated a distance d from a gamma ray spectrometric detector D situated centrally in an air-filled borehole as shown in Figure 29.2.

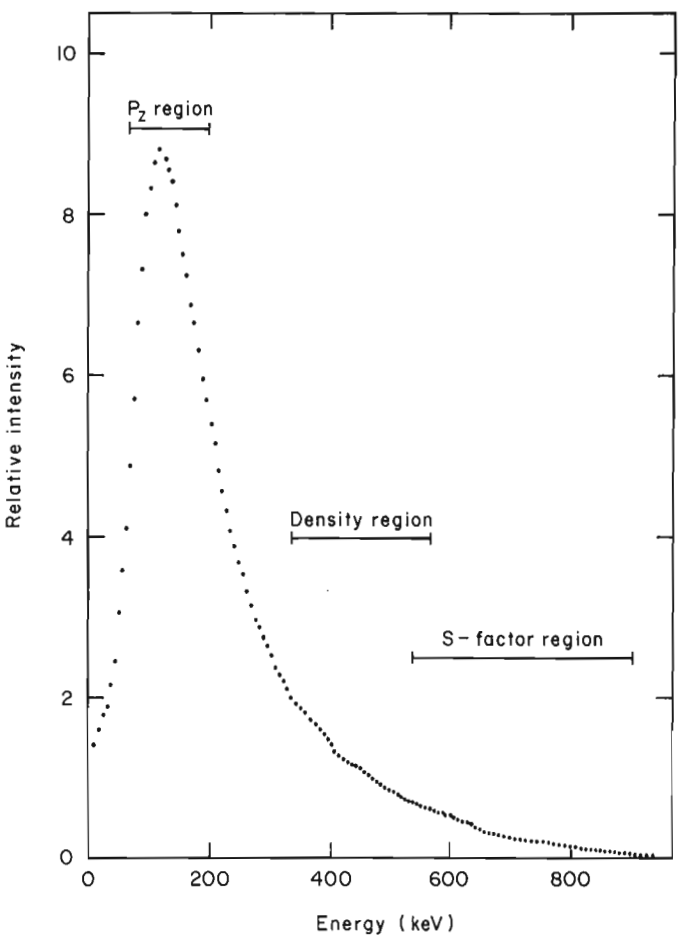

Figure 29.1. *Typical backscattered spectrum of ^{60}Co gamma rays obtained in a borehole of 13 cm diameter.*

W'W' represents the borehole wall. The energy of the gamma ray source should be between 400 keV and 1400 keV so that the only significant interaction is Compton scattering. A gamma ray photon of primary energy E enters the medium around the borehole and undergoes Compton scattering at an angle θ' at a point P'. The photon subsequently reaches the detector D with a degraded energy E' given by the well known Compton equation,

$$E' = \frac{E}{1 + \frac{E}{m_o c^2}(1-\cos\theta')} \qquad (1)$$

where $m_o c^2$ is the rest energy of the electron.

Equation (1) shows that the energy E' of the scattered gamma ray photon reaching the detector is solely determined by the scattering angle θ'. It is easy to see that all gamma

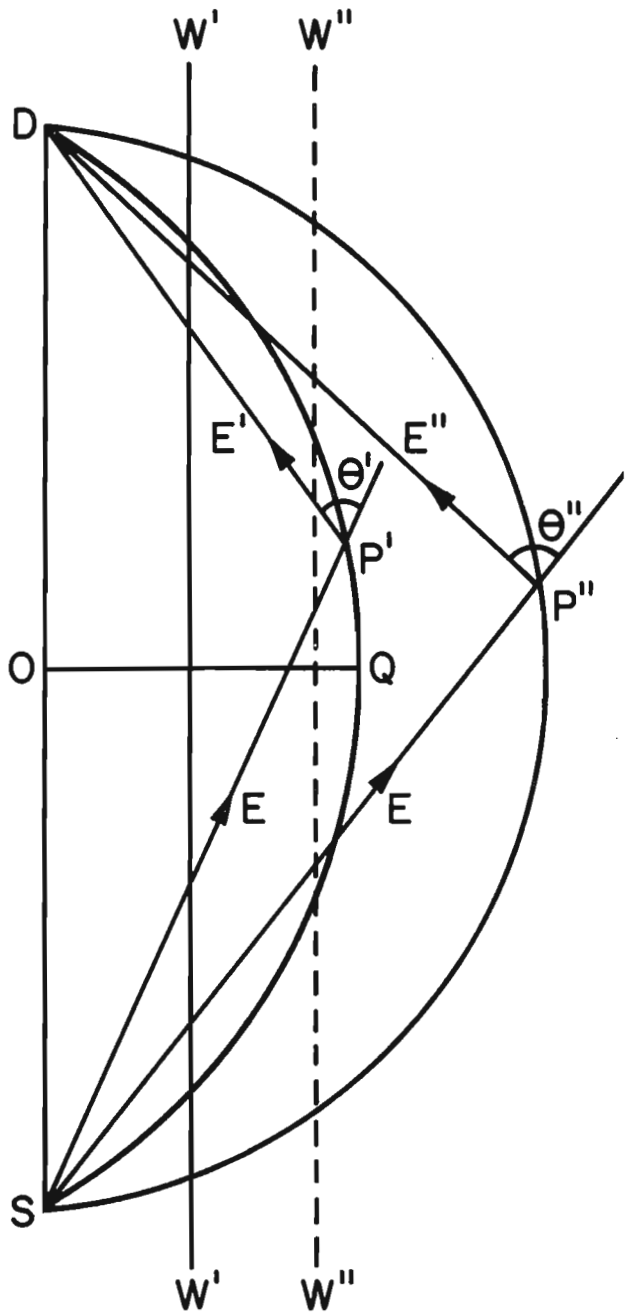

Figure 29.2. *Geometric relationship for the S-factor model.*

ray photons reaching the detector with energy E' after a single scattering event can originate only from the points P' along the arc of a circle SP'D of radius $R = d/2 \sin\theta'$. Also, the maximum height OQ of the arc SP'D from the probe SD is given by

$$OQ = \frac{d}{2} \tan\frac{\theta'}{2} \qquad .(2)$$

The intensity of the gamma rays reaching the detector D with energy E' can be computed using the single scattering model (Homilius and Lorch, 1958), allowing for the attenuation suffered by the photons in reaching the points P', further attenuation suffered by the scattered photons in reaching the detector D and for the probability of photons undergoing a scattering event through an angle θ' at points P' in the direction of D.

Figure 29.2 shows a second arc of a circle through SP"D for a second set of scattering points P". The primary gamma ray photons, after scattering through an angle θ" at points P", reach the detector with energy E". Obviously, θ" is larger than θ' and from equation (1) the energy of photons scattered from points P" will be lower than those scattered from points P'.

If the borehole wall moves from W'W' to W"W", corresponding to an increase in borehole diameter, both sets of photons scattering at points P' and P" suffer less attenuation in the medium due to decreased path lengths. This should enhance their intensity in the backscattered spectrum. The increase in the borehole diameter, however, decreases the arc length SP'D more rapidly than the arc length SP"D in the medium. This results in a greater reduction in the number of scattering points P' available to generate scattered photons of energy E' than the number of scattering points P" and the corresponding energy E". Thus, in the backscattered gamma ray spectrum recorded by the detector, an increase in the borehole diameter reduces the intensity of the photons with energy E' and increases the relative intensity of photons with the lower energy E" resulting in a change of the spectrum shape. It should be noted that when the borehole radius exceeds $d\tan(\theta'/2)/2$, the arc SP'D will be completely within the borehole, and in the absence of a scattering medium in an air-filled borehole the intensity of photons with energy E' becomes zero.

Figure 29.3 represents a computer simulation of backscattered gamma ray spectra, based on the single scattering model as exemplified by Homilius and Lorch (1958), but for the following conditions:

(a) a point source and a point detector separated by 38 cm situated centrally in a borehole within a medium of density 2 g/cm^3,

(b) a gamma ray source of energy 1250 keV to simulate a ^{60}Co source,

(c) a point detector with the response characteristics of a 50 mm x 50 mm NaI(Tl) detector (Marion and Young, 1968).

The spectra clearly illustrate the change in the shape in the upper energy region as the borehole diameter increases.

Experimental

An empirical approach was adopted to study the change in shape of the upper energy region of the backscattered gamma ray spectrum in relation to changes in borehole diameter. A major objective of this work has been to develop a gamma-gamma borehole logging probe for the simultaneous measurement of density, ore grade (P_z), and hole diameter of boreholes drilled in iron ore mineralization.

Borehole models

A large number of massive blocks (up to 6) with various diameter boreholes were available for laboratory investigation. Many of these were natural blocks collected from mines and quarries, while others were made from concrete containing various amounts of iron ore to produce blocks of different density and composition. Details of the borehole models, including borehole sizes, are given in Table 29.1. Two models had several boreholes of different diameters to study the variation of probe response with hole diameter. All models had more than 30 cm of material surrounding the hole to ensure that the sphere of influence of the probe remained within the material of the block.

The borehole logging probe

A schematic diagram of the apparatus used in this work is shown in Figure 29.4. It consists of a 51 mm x 51 mm NaI(Tl) gamma ray detector separated from a ^{60}Co gamma ray source by 38 cm with 20 cm of tungsten-lead shielding to prevent primary gamma rays from entering the detector. The strength of the ^{60}Co source was approximately 30 MBq. This particular geometry was chosen for the probe to facilitate the simultaneous measurement of density, ore grade (P_z) and borehole diameter in 13 cm nominal diameter boreholes drilled in iron ore mineralizations.

A weak ^{137}Cs gamma ray source was placed in a small well in the tungsten shielding near the detector to provide a gamma ray peak at 662 keV for stabilizing the gain using an electronic spectrum stabilizer. The signals from the probe were transmitted to the main amplifier-stabilizer-pulse height analyzer system by a multicore logging cable operated through a winch system. The analyzer was coupled to a minicomputer. This computer was programmed to read the backscattered gamma ray spectrum accumulated by the pulse height analyzer, subtract the background due to the ^{137}Cs source, divide the spectrum into windows of approximately 130 keV width and print out the results in counts per second in each of the spectral windows. It should be noted that a suite of other probe geometries was also examined in this

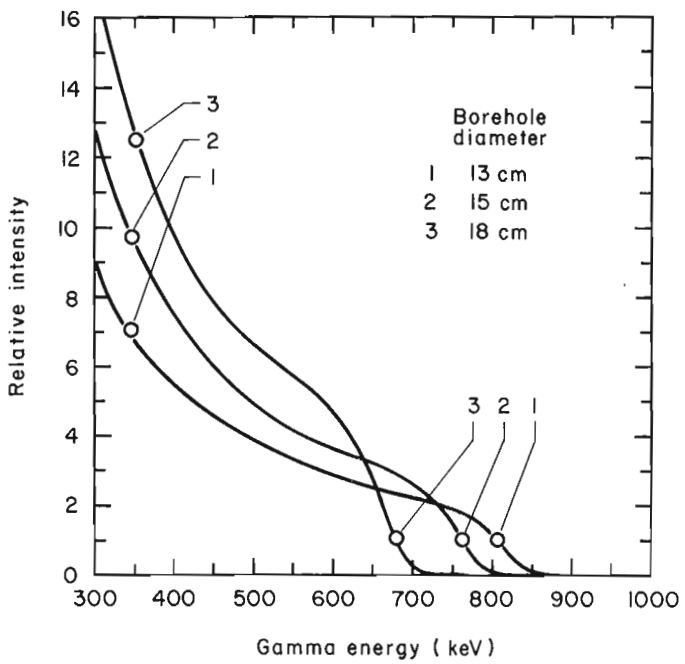

Figure 29.3. Upper energy region of the backscattered gamma ray spectra, obtained in different diameter holes, simulated by the computer.

Table 1. Details of borehole models and observed S-factors

Borehole model	Material	Density g cm^{-3}	%Fe	S-factors for various diameter holes					
				11.4 cm	12.7 cm	15.2 cm	17.8 cm	21.6 cm	31.7 cm
A	Natural basalt	2.62	8.6	4.86					
B	Natural granite	2.74	2.6	4.76					
C	Natural sandstone	2.42	1.9	5.11					
D	Natural shale	2.32	3.9	5.07					
E	Natural Hematite	4.39	68.7		6.46				
F	Natural Hematite	3.96	62.7		6.24				
G	Natural Hematite	3.52	53.0		6.10				
H	Natural Hematite	3.52	53.0		6.07				
	Hematite+concrete*	2.88	53.6		5.96	10.25	18.08	29.4	14.4
J	Hematite+concrete*	2.65	33.0		5.99				
K	Natural shale	2.45	4.6		6.89				
L	Concrete*	2.01			6.06	11.39	17.06		
			Mean	4.95 ±0.2	6.22 ±0.3	10.82	17.57	29.4	14.4

*Artificially prepared models.

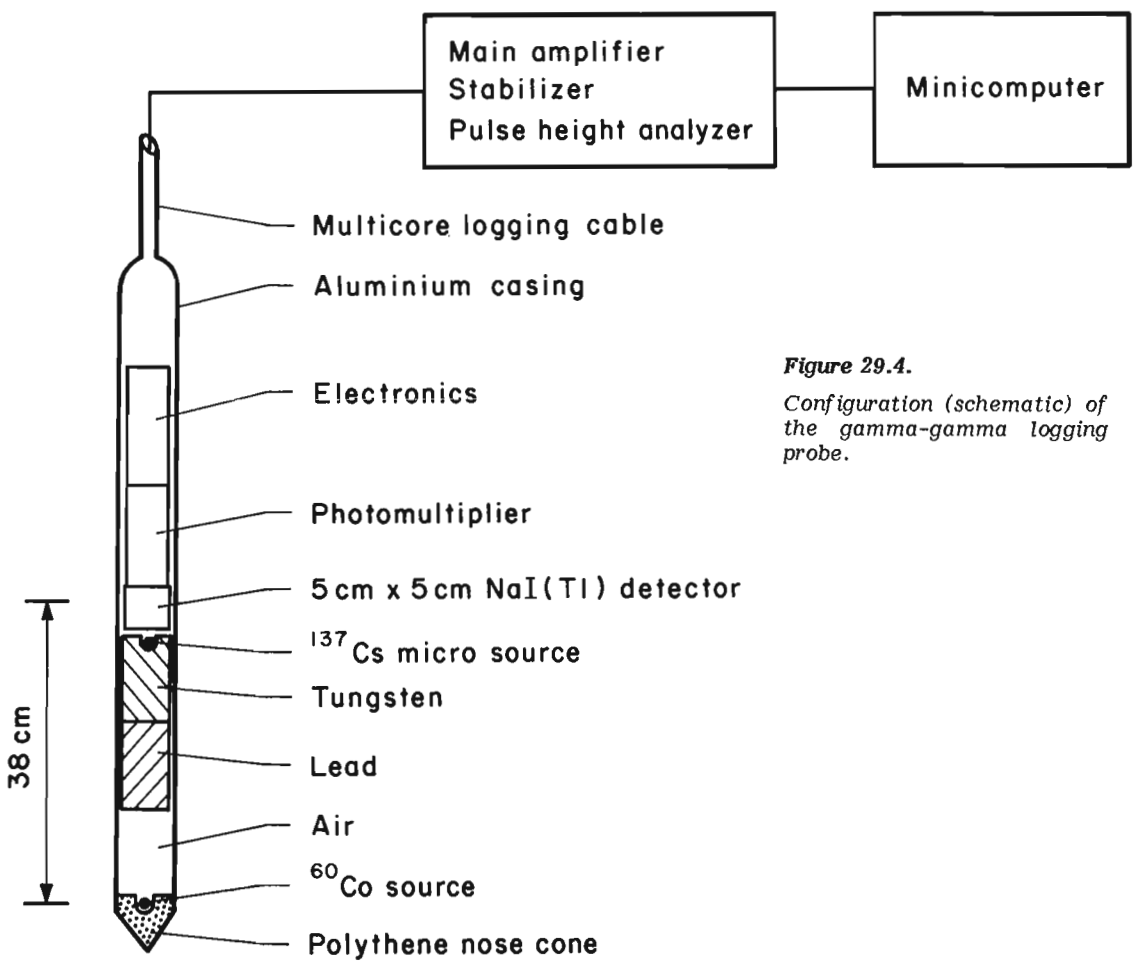

Figure 29.4.
Configuration (schematic) of the gamma-gamma logging probe.

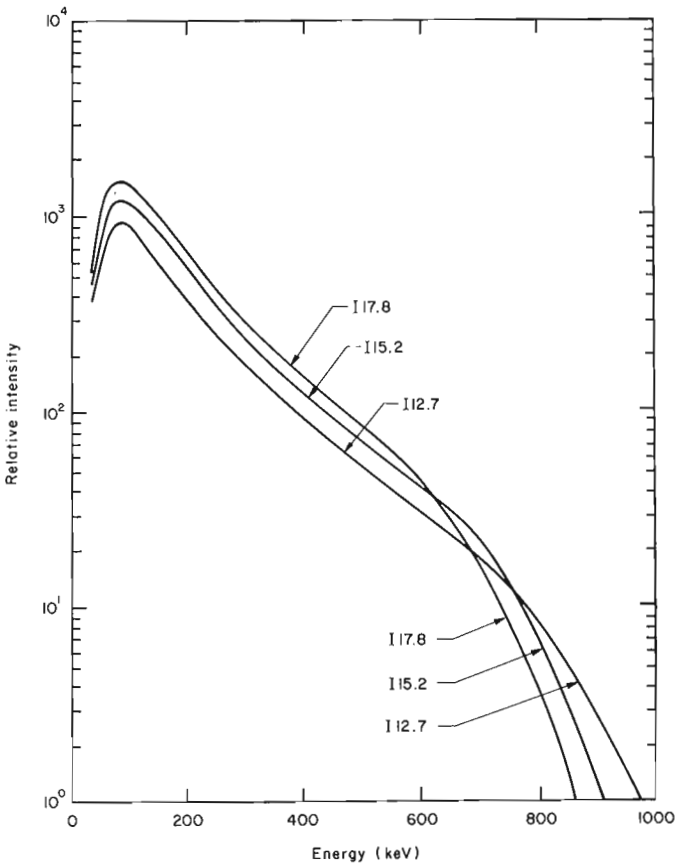

Figure 29.5. Backscattered spectra of ^{60}Co gamma rays obtained in borehole models I12.7, I15.2 and I17.8.

work, but was found to be inadequate because simultaneous measurement of density, P_z and hole diameter could not be effected. In some cases the S-factor was found to be dependent on density. In any measurement involving gamma techniques, it is impossible to completely eliminate the effect of density and elemental composition, but such effects can be minimized by suitable choice of source to detector distance, shielding geometry, the primary gamma ray energy and the energy regions selected for the spectral windows.

Experimental procedure

Experiments entailed placing the probe centrally within the holes of borehole models and collecting gamma ray spectra of 300 s duration. Some of the spectra illustrated in the next section were counted for longer periods of time. In the following section each model borehole is designated by a letter and the diameter of the hole. For example, the 15.2 cm diameter borehole in block I will be designated by I15.2

Results and discussions

Figure 29.5 represents backscattered gamma ray spectra taken from holes I12.7, I15.2 and I17.8. As shown in Table 29.1, these holes are in the same block of density 2.88 g/cm^3. In Figure 29.6, the spectra in Fgure 29.5 are normalized to the same intensity at 300 keV to illustrate the changes in the spectrum shape. As can be seen, the normalized spectra virtually overlap up to about 550 keV, beyond which the intensity of the spectra from the larger diameter holes fall more rapidly than for the small diameter holes. This change in shape qualitatively agrees with the results of the theoretical calculations.

Figure 29.7 shows backscattered gamma ray spectra taken from three borehole models of the same diameter but different density and composition viz., E12.7, I12.7 and J12.7.

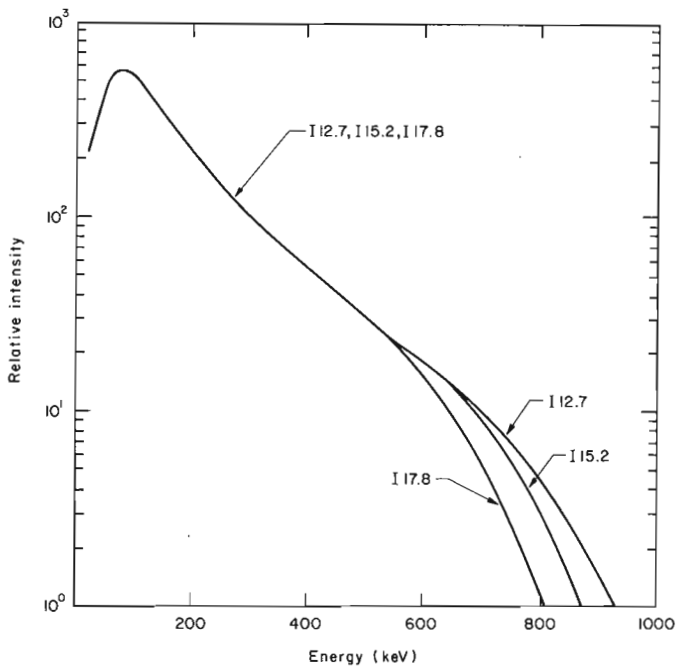

Figure 29.6. Spectra shown in Figure 29.5 normalized to the same intensity at 300 keV.

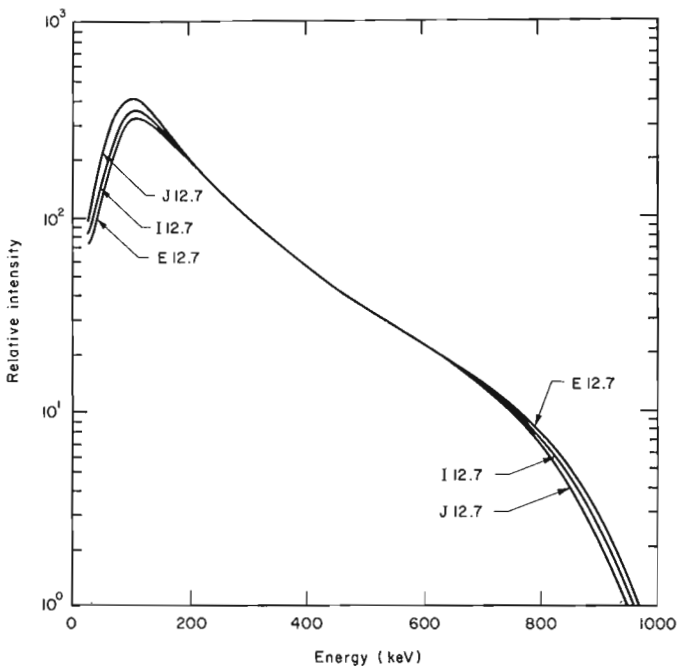

Figure 29.7. Backscattered spectra of ^{60}Co gamma rays in borehole models E12.7, I12.7 and J12.7 normalized to the same intensity at 300 keV.

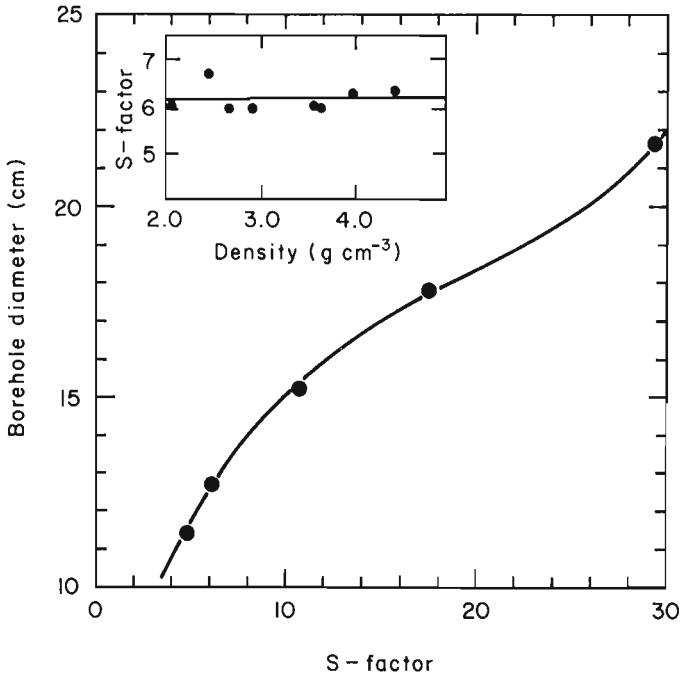

Figure 29.8. *Relationship between borehole diameter and S-factor. The solid line represents regression equation (3). Inset: S-factor vs. density for 12.7 cm diameter holes.*

These spectra are normalized to the same intensity at 300 keV illustrating very nearly the same shape to the upper energy region. It should be pointed out that the change in shape of the lower energy region of these spectra is caused by the composition or P_Z effect, due mainly to the variation in the iron content of the borehole models.

The shape of a backscattered gamma ray spectrum may be evaluated by curve fitting the entire spectrum, but this approach is not entirely satisfactory for a field technique as it would require utilization of large computers.

In the present work, a study of a large number of spectra showed that the ratio of the intensities of two windows in the upper energy region of the spectrum could serve as a measure of the spectral shape. This ratio, termed the shape factor or S-factor, was strongly correlated with the diameter of the borehole. For the present probe configuration, shown in Figure 29.4, the ratio of the intensity in the spectral regions 530 to 660 keV and 800 to 930 keV was found to be most strongly correlated with borehole diameter.

Measured S-factors for various borehole models are given in Table 29.1. S-factors for the 12.7 cm diameter holes may be used to evaluate the effect of changing density and elemental composition in the available models. The density of models range from 2 to 4.4 g/cm^3. In Figure 29.8, S-factors for the 12.7 cm boreholes are plotted against density. This plot shows virtually no significant correlation between S-factor and density. In addition, gamma rays of energy above 500 keV are used in the S-factor measurement and have negligible photo-electric cross-section.

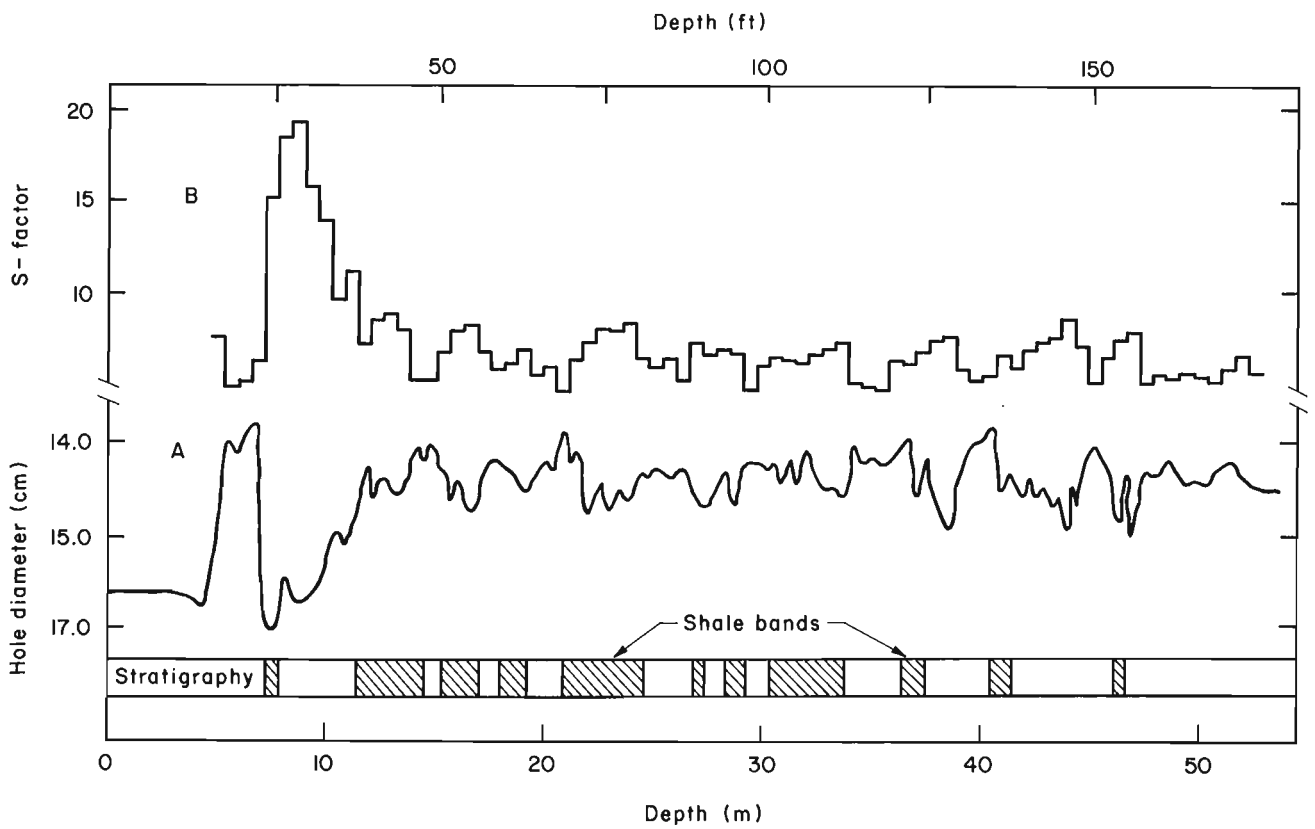

Figure 29.9. *A comparison of (A) S-factor probe response and (B) radiometric bowspring caliper response (Charbucinski et al., 1976) in a percussion drillhole in iron ore mineralizations. (Note reversal of diameter scale in lower trace).*

Consequently, the elemental composition of a medium constituted of the normal Earth's crust has no significant effect on the S-factor. An examination of Table 29.1 shows that the S-factor for the 12.7 cm model diameter holes has a standard deviation of 5%, resulting in an error of approximately ± 2% in the diameter measurement of 13 cm holes.

Figure 29.8 depicts the mean S-factors for various holes plotted against hole diameter. The data points from 11.4 cm to 21.6 cm diameter holes lie on a smooth curve. It can be proved using equation (2) that for a 32 cm diameter hole, the scattering points contributing to the spectral regions of present interest lie within the borehole. No gamma ray counts, therefore, should be expected in this spectral region due to the absence of a scattering medium. In practice, however, some gamma ray counts appear in this region from sources such as gamma rays leaking through the shielding entering the detector, natural gamma rays from the material around the borehole and from sum coincidence events taking place at the lower energy region of the spectrum. The S-factor for the 32 cm borehole is due to such background. In practice, sections of boreholes too large for the probe configuration can be easily identified from low count rate in the upper energy part of the backscattered gamma ray spectrum. It should be noted that a probe of given source to detector distance and shield configuration is suitable for diameter measurements only for a limited range of diameter variation. As pointed out in the section on field measurements, a source to detector distance of 58 cm is required for holes of nominal diameter 32 cm.

Regression analysis of the data set in Table 29.1 was carried out to establish the relationship between borehole diameter, D and S-factor, S of model boreholes. The data for the 31.7 cm diameter model were excluded. The results showed that borehole diameter can be represented by the regression equation

$$D = 6.16 + 1.36 \times S - 0.57 \times S^2 + 0.00097 \times S^3 \qquad .(3)$$

The standard deviation of D for a single diameter measurement using the S-factor technique was 0.26 cm. The density and iron concentration were found to be statistically insignificant in the regression equation. This shows that the borehole diameter can be determined from an easily measured parameter from the backscattered gamma ray spectrum of the present probe.

Field measurements

The gamma-gamma probe was subjected to extensive field trials in 13 cm nominal diameter development holes and 32 cm nominal diameter blast holes drilled in iron ore mineralizations in the Pilbara region of Western Australia. A source to detector distance of 58 cm was used for the gamma-gamma probe for the simultaneous measurement of S-factor, P_Z and density in the blast holes. Readers are referred to Aylmer et al. (1978) and Charbucinski et al. (1977) for full details of the field trials. A comparison of the S-factor log with a radiometric bowspring caliper log (Charbucinski et al., 1976) in a 55 m deep percussion hole, of nominal diameter 13 cm in iron ore, is shown in Figure 29.9. The field trials proved the veracity and usefulness of the S-factor method of borehole diameter measurement in the field environment. Recent field trials appear to show that the S-factor technique may be applicable also to fluid-filled boreholes (P.L. Eisler, personal communication, 1983).

Conclusions

Laboratory investigations based on a large number of borehole models and computer simulations of backscattered gamma ray spectra, based on a single scatter model, have shown that the shape of the upper energy region of the backscattered gamma ray spectrum of a gamma-gamma probe changes with borehole diameter. The ratio of the intensities in two spectral energy windows can be used as a measure of the shape of the spectrum in this region. This ratio is termed the S-factor. Using the present probe configuration, the diameter of the borehole in the range 11 cm to 22 cm can be determined with a standard deviation of 0.26 cm. Larger diameter holes would require a larger source to detector distance for S-factor measurements. The S-factor is virtually unaffected by the density or composition of the material used in the borehole models. Extensive field trials have proved the veracity and usefulness of the S-factor method of borehole diameter measurement.

References

Aylmer, J.A., Mathew, P.J., Wylie, A.W.
1978: Bulk density of stratified iron ores and its relationship to grade and porosity; Australasian Institute of Mining and Metallurgy, Proceedings, no. 265, p. 9-18.

Berzin, A.K., Bespalov, D.F., Zaporozhets, V.M., Kantor, S.A., Leipunskaya, D.I., Sulin, V.V., Feldmann, I.L., and Shimelevich, Yu. S.
1966: Present state and use of basic nuclear geophysical methods for investigating rocks and ores; Atomic Energy Review, v. 4, no. 2, p. 59-111.

Blyumentsev, A.M. and Migunov, B.B.
1967: Development of a method and apparatus for the quantitative determination of the iron content of rocks and ores using the data of borehole radiometry; Vsesoyuznyy Nauchin. Tekhn. Konf., 5th, Novosibirsk, 1963, p. 525-530, Nedra Publishing House, Moscow. (Trans. CSIRO).

Charbucinski, J., Jarrett, R.G. and Wylie, A.W.
1976: Radiometric calipers for borehole logging; Australasian Institute of Mining and Metallurgy, Proceedings, no. 258, p. 59-65.

Charbucinski, J., Eisler, P.L., Mathew, P.J. and Wylie, A.W.
1977: Use of backscattered radiation for determining grade of iron ores in blast holes and development drill holes; Australasian Institute of Mining and Metallurgy, Proceedings, no. 262, p. 29-38.

Czubek, J.A.
1966: Physical possibilities of gamma-gamma logging; in Radioisotope Instruments in Industry and Geophysics (proceedings of Warsaw Symposium, October 1965), v. 2, p. 249-275, IAEA, Vienna.

Helander, D.P.
1966: Caliper logging tools measure borehole size and shape; Oil Gas Equip., v. 6, no. 4, p. 11-12.

Hilchie, D.W.
1968: Caliper logging theory and practice; Log Analyst, v. 9, no. 3, p. 3-

Homilius, J. and Lorch, S.
1958: On the theory of gamma-ray scattering in boreholes; Geophysical Prospecting, v. 6, p. 342-364.

Marion, J.B. and Young, C.F.
1968: Nuclear Reaction Analysis, Graphs and Tables; North Holland Publishing Company, Amsterdam.

Taylor, D. and Kansara, M.
1967: A theory of the nuclear densimeter; Soil Science, v. 104, no. 1, p. 25-34.

Wylie, A.W. and Mathew, P.J.
1976: Borehole calipers; Australian patent 507495.

30. IN SITU MINERAL ANALYSIS IN BOREHOLES

C.A. Brott, W.A. Millard, J.M. Lively, and D.D. Goff[1]

Brott, C.A., Millard, W.A., Lively, J.M., and Goff, D.D., In situ mineral analysis in boreholes; in Borehole Geophysics for Mining and Geotechnical Applications, ed. P.G. Killeen, Geological Survey of Canada, Paper 85-27, p. 277-284, 1986.

Abstract

An X-ray fluorescence mineral logging system has been developed and field tested which detects and analyzes a broad range of in situ minerals on the borehole walls. The lower detection limit of the system varies with heavy, intermediate and light minerals. For heavy elements (e.g. lead, tungsten, etc.) the lower limit is less than 0.05 weight per cent (wt%), intermediate elements (e.g. molybdenum, bromine, etc.) less than 0.1 wt% and the limit for light elements (e.g. (cobalt, zinc, etc.) is uncertain but should be less than 0.5 wt%.

The logging sonde is 1.5 inches (38 mm) in diameter and about 5 feet (1.5 m) long; the weight of the sonde is less than 15 pounds (7 kg). The mineral logging system is installed in an Econoline 350 Ford van. The draw works contain about 3000 feet (1000 m) of cable and electrical power is supplied by a 5 kw gasoline generator.

The logging data consist of full X-ray spectra for each one foot (30 cm) depth increment which are displayed and recorded by a computer-controlled data acquisition system as the sonde is moving in the borehole. The maximum logging speed is about 360 feet per hour (110 m/h). Since a computer is part of the data acquisition system, qualitative and some quantitative analyses can be performed on the recorded data at the logging site.

The system was field tested by logging holes for which lithological and tungsten assay data were available from drill core. The system was evaluated by comparing the results of the logging data with the assays. For one hole which has almost continuous assays for 500 feet (150 m), there were 8 zones with tungsten assay values of 0.1 wt% or greater and 7 of these zones were detected. In addition 5 other zones with assays between 0.05 and 0.1 wt% were also detected.

Résumé

Un système de diagraphie minérale de fluorescence aux rayons X, qui permet de détecter et d'analyser un grand éventail de minéraux in situ sur les parois du trou de sonde, a été réalisé et soumis à des essais sur le terrain. La limite inférieure de détection du système varie selon que les minéraux sont lourds, intermédiaires ou légers. Dans le cas des éléments lourds (comme le plomb, le tungstène, etc.), la limite inférieure est de moins de 0,05% en poids; dans le cas des éléments intermédiaires (comme le molybdène, le brome, etc.), de moins de 0,1% en poids, et dans le cas des éléments légers (comme le cobalt, le zinc, etc.), non encore déterminée avec certitude, mais fort probablement de moins de 0,5% en poids.

La sonde de diagraphie a un diamètre de 1,5 po (38 mm) et une longueur d'environ 5 pi (1,5 m) et pèse moins de 15 lb (7 kg). Le système de diagraphie minérale est installé dans une fourgonnette Econoline 350, de Ford. Le treuil de sondage a un enroulement de câble d'environ 3000 pieds (1000 m) et son alimentation électrique est assuré par un groupe électrogène de 5 kW fonctionnant à l'essence.

Les données de diagraphie, qui sont affichées et enregistrées au moyen d'un système d'acquisition des données commandé par ordinateur à mesure que la sonde se déplace dans le trou de sonde, consistent en des spectres intégraux de rayon X correspondant à chaque pied (30 cm) de sondage parcouru dans le sens de la profondeur. Le rythme maximal de la diagraphie est d'environ 360 pi à l'heure. L'ordinateur dont est pourvu le système d'acquisition des données permet d'effectuer sur place des analyses qualitatives et certaines analyses quantitatives sur les données enregistrées.

Le système a fait l'objet d'essais sur le terrain à l'emplacement de trous de sondage à partir desquels des données d'analyse relatives à la lithologie et au tungstène avaient déjà été obtenues à l'aide de carottes. Pour évaluer le système, on a comparé les données de diagraphie et les données d'analyse. L'un de ces trous, qui a fait l'objet d'une suite presque continue d'analyses échelonnées sur 500 pieds (150 m), comportait huit zones où le tungstène affichait des valeurs d'analyse de 0,1% en poids ou plus et sept de ces zones ont été détectées. En outre, cinq autres zones affichant des valeurs d'analyse variant de 0,5 à 0,1% en poids ont été détectées.

[1] Phillips Petroleum Company, Bartlesville, Oklahoma 74004

Introduction

A prototype X-ray fluorescence mineral logging system was designed and developed in the early 1970s by Phillips Petroleum Company R&D personnel in order to detect and analyze in situ minerals intersected by boreholes (Barton and Gray, 1974). The system located mineral zones while the sonde was moving in the borehole. After the depth intervals of the mineral zones noted, qualitative and semi-quantitative analyses were done by obtaining full X-ray spectra in each of these zones. These spectra were obtained while the sonde was held stationary. The preliminary development was completed in 1974 and shelved for economic reasons until 1980 when the project was reactivated. At that time work was begun to improve the sensitivity (the ability of detecting lower mineral concentrations) and the resolution (the ability to better identify characteristic X-rays which are used for mineral identification).

One of the major improvements which has been made to the original mineral logging system is the development of a computer-controlled data acquisition system which continuously records full X-ray spectra over one foot (30 cm) increments on 9-track magnetic tape while the sonde is moving in the hole (Fig. 30.1). The maximum speed at which the system can record data is about 360 feet per hour (110 m/h). The X-ray spectra are displayed while logging the hole but more detailed analyses of the recorded data are done later by using a mini-computer which is part of the acquisition system. A second improvement to the logging system was the design and development of a detector housing on the sonde which causes less attenuation of the lower energies of the x-ray spectrum than the previous one, and which can withstand pressures equivalent to about 2400 feet (800 m) of standing water. Other modifications included the design of new electronic circuits and the use of different excitation sources to generate the X-rays.

The modified system was field tested by logging boreholes for which core assays were available for tungsten. Before presenting the results of these tests, the principles of operation and the methods used to analyze the data are presented.

Physical principles

The physical principles of the X-ray fluorescence (XRF) mineral logging sonde are the same as those for conventional XRF laboratory instruments where the sample being analyzed is irradiated by an external excitation source and the characteristic X-radiation of the desired elements is measured by a detector. In the case of the logging sonde, a radioactive isotope is used to generate the incident radiation and a scintillation detector consisting of a NaI crystal and photomultiplier tube (PMT) is used to detect the X-ray fluorescence (Fig. 30.1). Since the optimum excitation energy for different elements increases as a function of the atomic number seven (7) different sources are used for the detection of different minerals. The selection of suitable radioactive isotopes for different ranges of atomic numbers has been discussed by Rhodes (1971), Leman and Bolotova (1969), Bowie (1968), and many other authors.

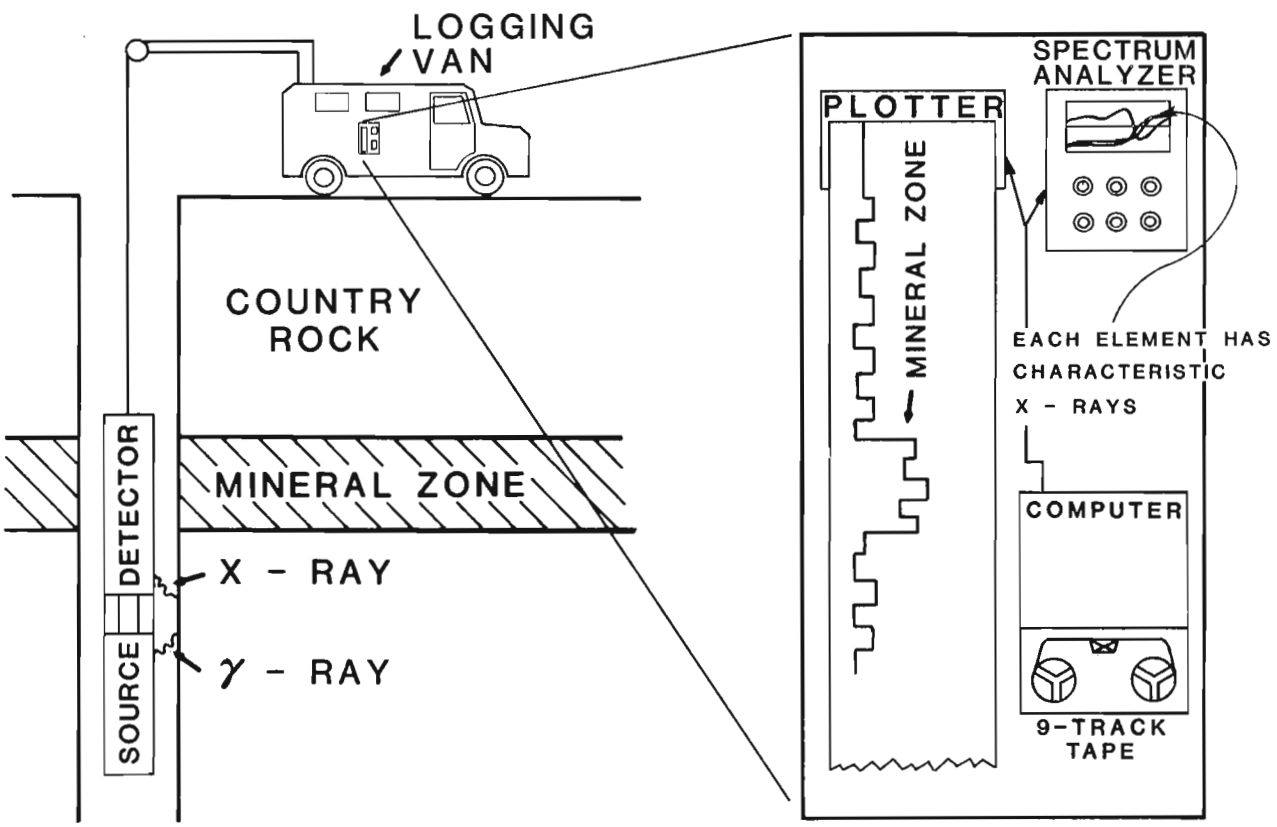

Figure 30.1. A diagrammatical drawing of the mineral logging system. The logging sonde contains a small radioisotope excitation source (10 mCi or less). Radiation from this source generates X-rays from minerals on the borehole walls. Some of these X-rays are detected and the sonde transmits the spectral signals uphole. The X-ray spectra are displayed and recorded for one foot (30 cm) increments while the sonde is moving in the borehole.

Each element of the periodic table has a characteristic X-ray spectrum and the wavelengths of these X-rays are proportional to the square of the atomic number (Mosely's Law). Thus if the fluorescent X-radiation of a particular mineral can be isolated and its intensity measured, the element can be identified and its concentration determined. In the case of mineral logging, the K X-rays are analyzed since they normally are the most intense in an X-ray spectrum. A quantitative analysis of element concentrations from the X-ray spectrum is not straightforward because the incident photons (radiation from the radioactive isotope source) are Compton scattered. The energies of these scattered photons span the energies of the desired X-rays. The methods used in isolating the X-ray spectrum are presented in the next section.

Another problem that arises in measuring the energies of the detected X-rays is the lack of resolution of the NaI detector (the sharp X-ray energy peaks are spread out over several keV, Fig. 30.2). However, since the energy differences between K X-rays of adjacent elements in the periodic table is approximately 0.5 keV, the atomic number of a detected element can usually be determined with an error of less than ±4. Precise mineral identification can be obtained from drill cuttings or from rock samples from the area. Future modifications to the logging system could include the use of a solid-state detector (either silicon or hyper pure germanium), which would have the resolution needed to identify the different X-ray spectra. A disadvantage of the solid-state detectors is that they must operate near liquid nitrogen temperature (77°K). Methods for using solid-state detectors in well logging sondes have been developed (Tanner et al., 1971; Lubecki et al., 1982). The isolation of a single element can also be done by using a pair of balance filters (Broquet et al., 1967, discuss the techniques for the fabrication of balance filters for most minerals). The disadvantage of using balance filters is that additional filters and detectors or additional loggings of a borehole for each element of interest are required.

Analysis of spectra

The detection of minerals in a borehole is achieved by comparing spectra in mineralized zones with those acquired in non-mineralized or background zones. Before the spectra are compared, each spectrum is normalized to the total number of detected photons (Compton scattering and x-radiation). After normalization, a difference spectrum is computed by subtracting the background spectrum to remove the effect of Compton scattering (Fig. 30.2).

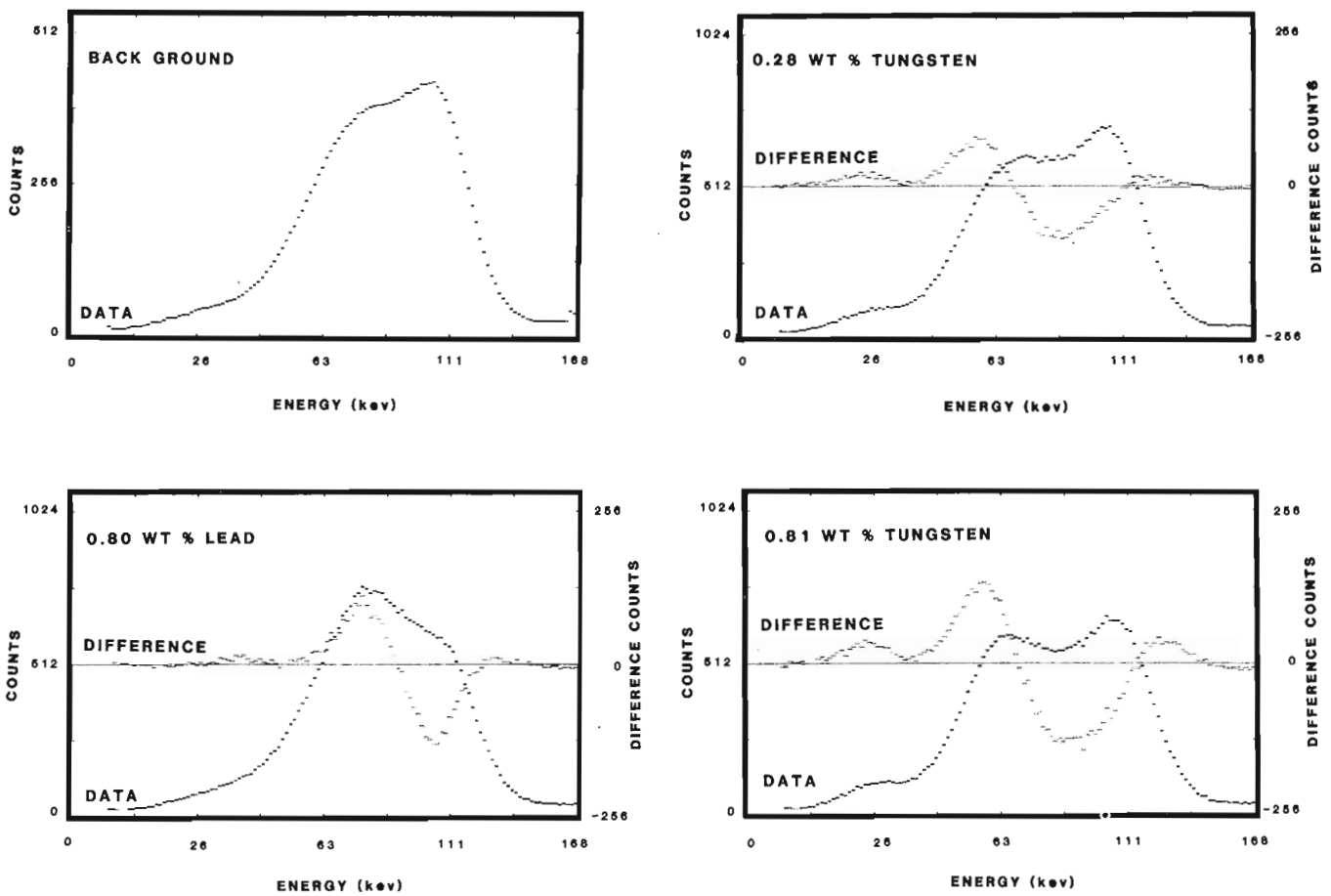

Figure 30.2. Spectra from calibration samples. The background spectrum is from a blank sample which was constructed from a concrete and sand mix. The three other data spectra are from samples to which lead or tungsten was added. The difference spectrum for each of the samples is the difference between the data and background spectra. Note that the energy of the peaks of the difference spectra can be used to identify the mineral and the intensities (the heights of the peaks) correspond to the concentration.

Complications in selecting a background spectrum arise because of the changes in lithology. Different mineralogy and other physical properties (porosity, grain size, crystal distribution, etc.) of the rocks cause the Compton scattering and the absorption of the energies in the X-ray spectrum to vary. In order to compensate for changes in the lithology without prior knowledge, the background spectrum is produced by averaging all the spectra in the depth intervals which are above and below a depth interval which appears to be mineralized. The selection of a background spectrum by this method assumes that the effects of the lithology on the X-ray spectrum are nearly the same over the selected depth intervals. Other methods used in X-ray spectroscopy for determination of the background spectrum include arbitrary polynomial function fits, applying low pass filters and by using Fourier transform techniques to construct a Wiener filter which can then be used to calculate a background function from the raw data (Semmler, 1977). Future work will include further investigating the application of some of these techniques.[1]

Another complication is that the rock matrix may contain other elements which absorb the X-rays of the desired element. Since the mineralogy varies, the absorption varies from location to location in a borehole. An indirect method for determining the absorption coefficients in rocks is by measuring the intensity of the Compton scattering (see Sumartojo and Paris, 1980; Lantor and Litchinsky, 1980; Reynolds, 1963, 1967). From empirical measurements, these authors showed a linear relationship between the X-ray absorption coefficients and Compton scattering intensity. Thus the ratio of the X-ray peaks to Compton scattering intensity can be used to correct for the absorption by the rock matrix.

In order to locate mineral zones in a borehole efficiently, semi-quantitative mineralization concentration traces for selected minerals are plotted in real time as logging proceeds. The values used in these plots are functions of the counts in selected energy ranges or windows in the X-ray spectrum. These energy windows are chosen in order to maximize the sensitivity for a desired element (i.e. one energy window spans the energy range under the major peak of the X-ray spectrum and two other windows span energy ranges on each side of the peak, Fig. 30.2). The sum of the number of counts in the energy windows on both sides of the peak is subtracted from the number of counts in the energy window under the peak. This difference is divided by the number of counts in the energy window on the high energy side of the peak. The ratio in the calculation tends to correct for the rock matrix effect. Since the full spectra are recorded on 9-track magnetic tape, mineralization plots for different minerals can be made after the borehole is logged.

Calibration for specific minerals can be accomplished with artificial samples. Figure 30.3 shows calibration curves and Figure 30.4 shows mineralization plots for molybdenum and tungsten calibrations. The samples were constructed from a concrete and sand mixture and different amounts of molybdenum or tungsten were added. A second order polynomial was fitted to the calculated mineralization values and the coefficients of this fit were used to estimate the weight percentages (wt%). The assayed weight percentages of the samples are listed on the left and the estimated percentages using the polynomial coefficients are listed on the right of Figure 30.4.

After the mineral zones in a borehole are located, the spectra from these zones are used for mineral identification and quantitative estimates. All the analyses of the spectral data are done using the mini-computer which is part of the mineral logging system.

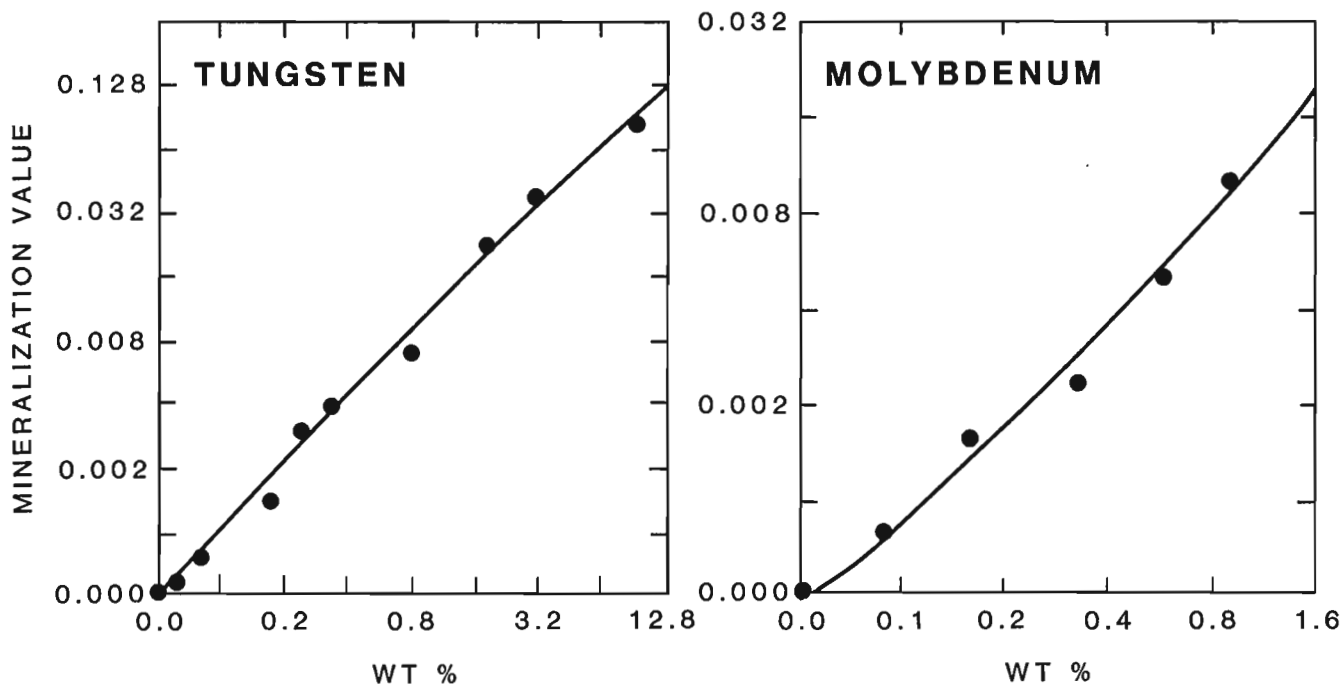

Figure 30.3. *Calibration curves for tungsten and molybdenum. The curves are from a second order polynomial fit of the mineralization values of artificial samples. The large dots on the plots show the location of the data points. The corresponding mineralization plots for the calibration curves are shown in Figure 30.4.*

[1] In 1985, due to changing economics, the further planned development of the XRF logging system described here has been suspended.

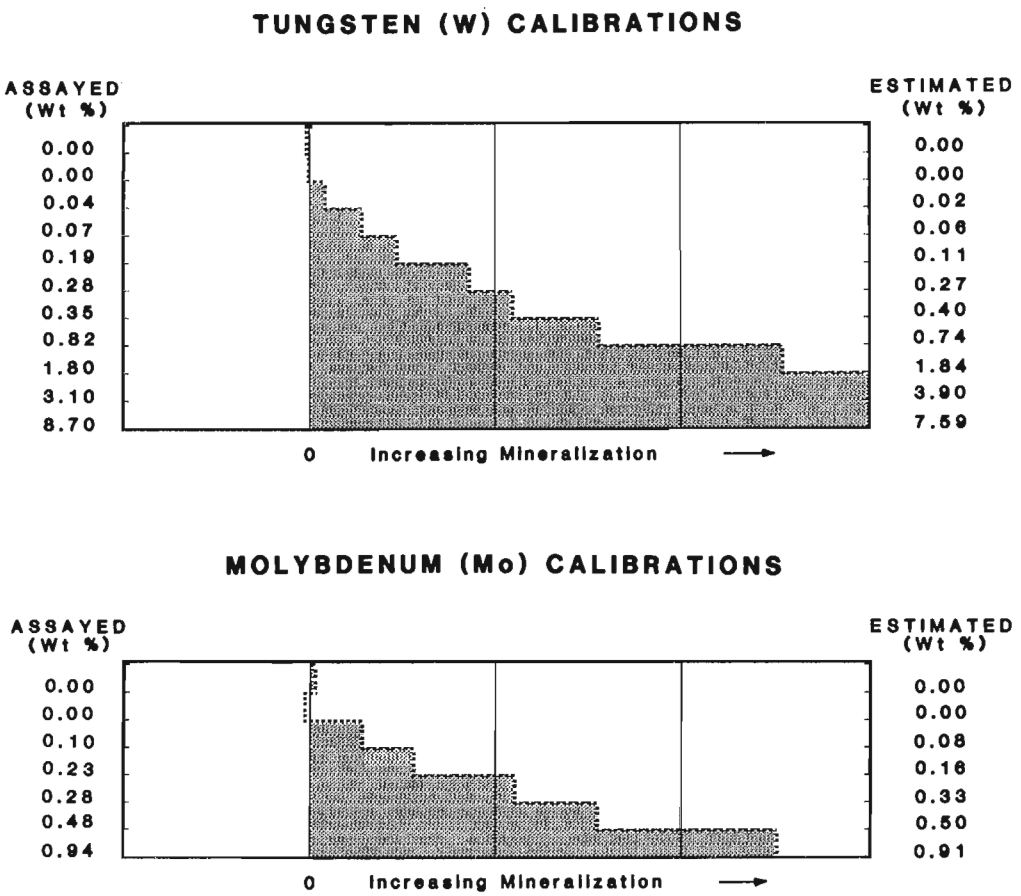

Figure 30.4. *Tungsten and molybdenum mineralization plots calculated from spectra of calibration samples. The tick marks on the vertical axes of the plots show the ranges for each of the calibration samples. The assayed weight percentages (wt%) are listed on the left and the estimated weight percentages from the calibration curves (Fig. 30.3) are listed on the right. The mineralization trace is shown as a dashed line and the positive areas under the trace are shaded. The amplitudes of the horizontal deflections are proportional to the relative mineral concentrations.*

Field tests

The X-ray mineral logging system was field tested by logging boreholes for which lithological and tungsten core assay data were available (Fig. 30.5). These holes were drilled in a skarn near Ely, Nevada. The evaluation was done by comparing the logging results to the assayed values. A problem was encountered in that the gain of the sonde varied while logging the boreholes. Thus the quantitative results are limited, but over short depth increments, the relative amount of mineralization can be estimated by comparing the deflections of the mineralization traces. These gain variations are most likely due to temperature and voltage changes and future modifications to the logging sonde will incorporate some form of spectrum stabilization.

Figure 30.6 shows a mineralization plot for hole PH-19 from 1050 to 1085 feet (320 to 330 m). The energy windows used to calculate the mineralization traces were chosen to maximize the sensitivity for the detection of tungsten. The tungsten trioxide (WO_3) assayed values for weight percentages over 0.05 weight per cent (wt%) are listed to the right of the plot. No assay values were available for the depth intervals from 1080 to 1085 feet (328 to 330 m) and from 1050 to 1065 feet (320 to 325 m). The large deflections of the mineralization traces from 1065 to 1072 feet (325 to 326.7 m) correspond to WO_3 assay values from 9.64 to 26.25 wt%.

Figure 30.5. *Logging a mineral hole near Ely, Nevada. The computer controlled data acquisition system is in the van. The draw work contains 3000 feet (about 1000 m) of cable. Electric power is supplied by a 5 kw gasoline power generator which is installed in the van.*

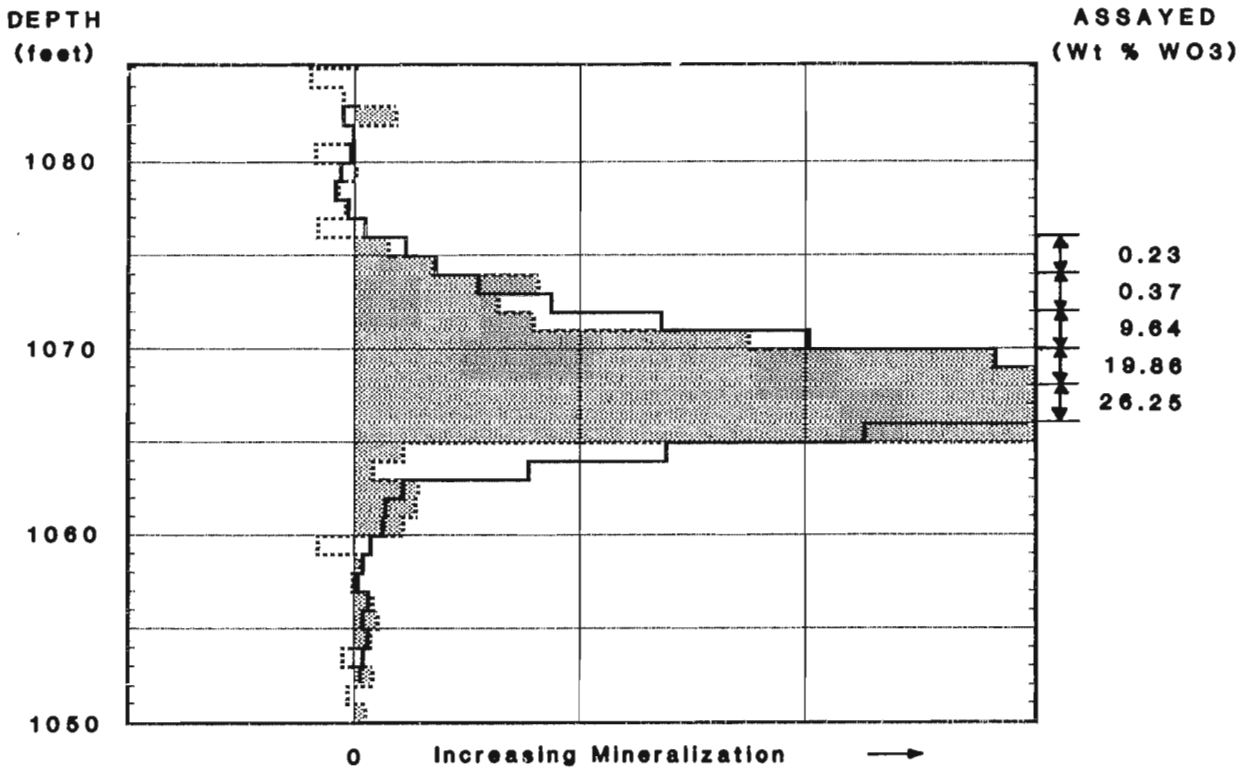

Figure 30.6. Mineralization plot of hole PH-19. Since the hole was logged from the bottom to the surface, the depths decrease from the top of the plot. The tungsten trioxide (WO_3) assays which are greater than 0.05 wt% are listed to the right of the plot. The solid trace on the plot shows the running average of the mineralization values over 5 foot (1.5 m) increments. The dashed line, whose positive areas are shaded, shows the mineralization values for each one foot (30 cm) increment. The deflections of the traces have good correlation to the assay values.

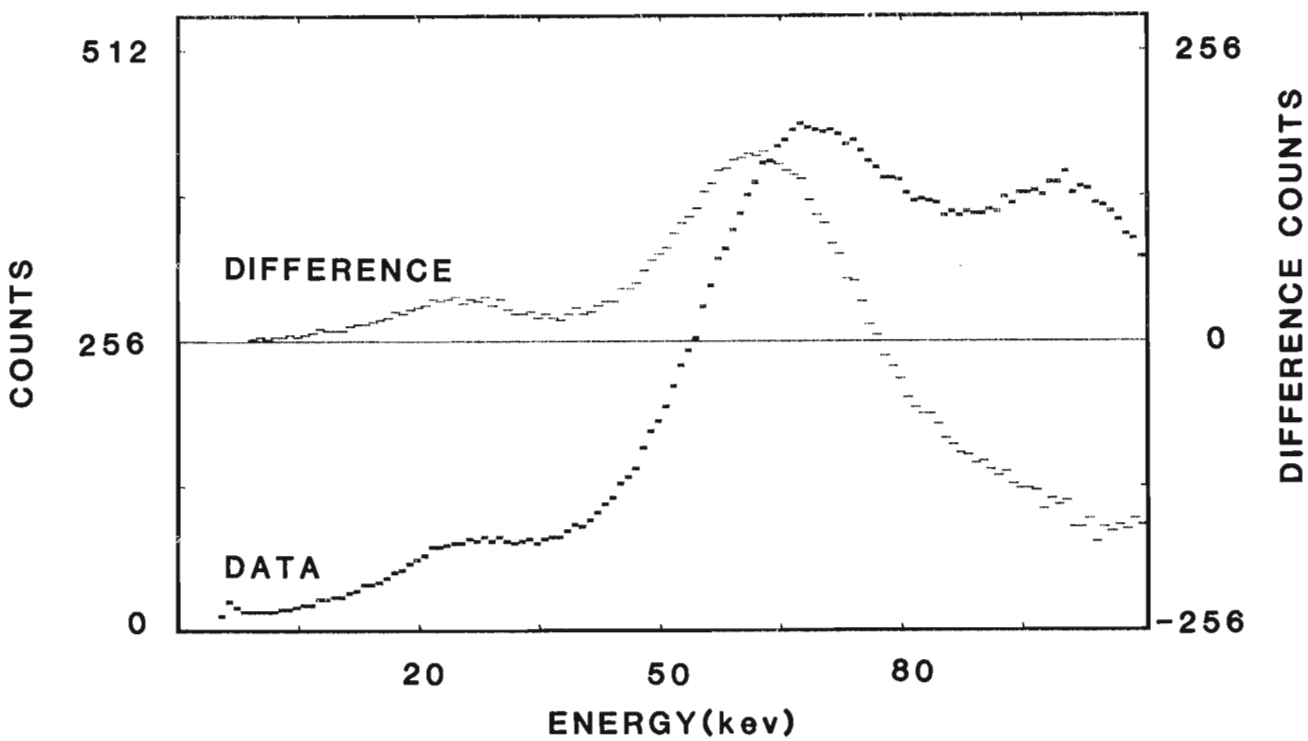

Figure 30.7. Data and difference spectra for hole PH-19. The data spectrum is the average of the spectra from 1065 to 1070 feet (325 to 326.1 m) which were recorded while logging. The background spectrum (not shown) used to obtain the difference spectrum, is the average of spectra taken from 1050 to 1060 feet (320 to 323 m) and from 1076 to 1085 feet (328 to 330 m).

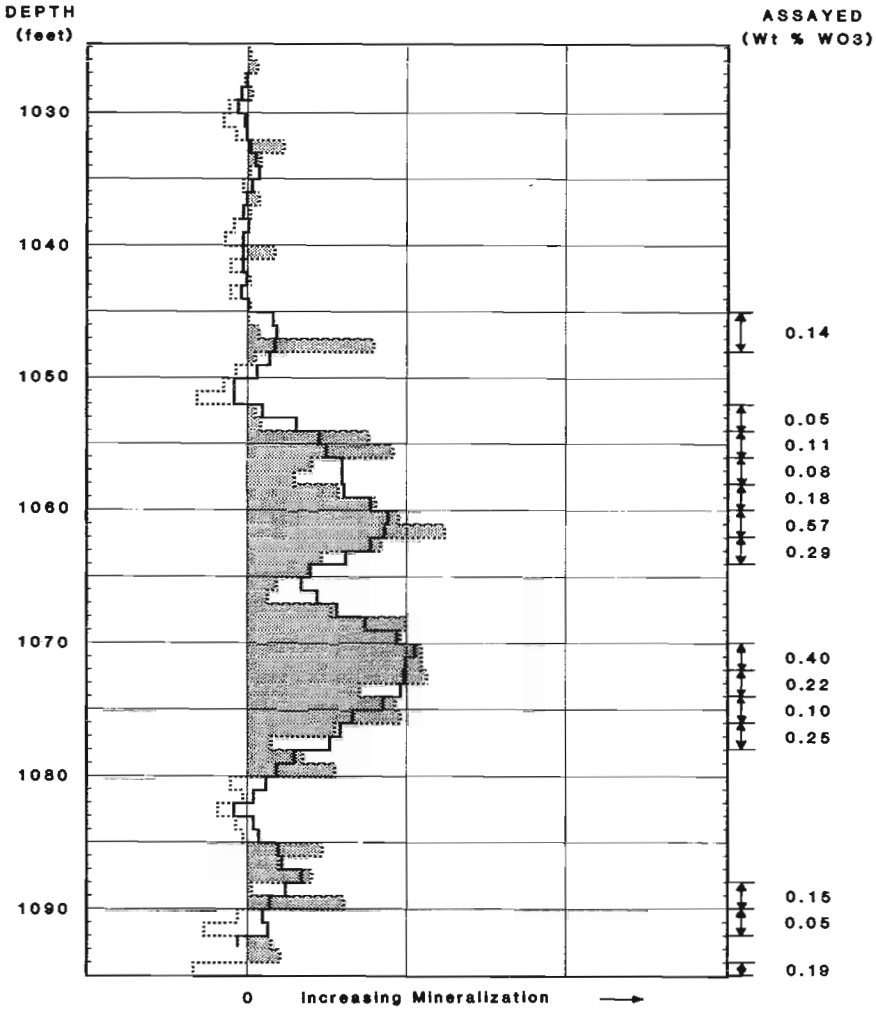

Figure 30.8. Mineralization plot for hole PH-57. The plot is for the depth interval from 1030 to 1095 feet (314 to 333.8 m). The solid trace is a running average of the mineralization values over 5 foot (1.5 m) increments and the dashed line whose positive areas are shaded is the trace of the mineralization values for one foot (30 cm) increments. The depths (listed to the left of the plot) increase going down and the tungsten trioxide (WO_3) assays which are greater than 0.05 wt% are listed on the right. The deflections of the traces correlate with the assay data.

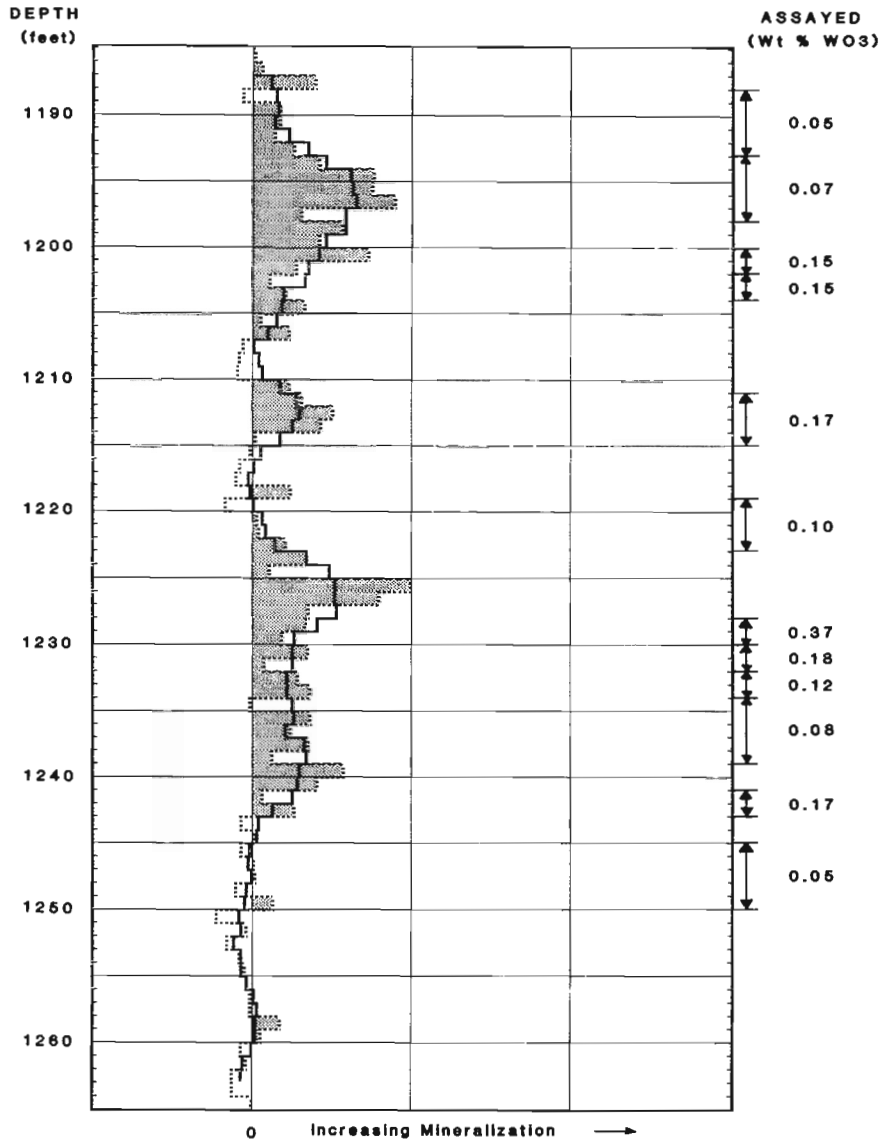

Figure 30.9. Mineralization plot for hole PH-57. The plot is for the depth interval from 1185 to 1265 feet (361.2 to 385.6 m) (depths are listed to the left of the plot). The tungsten trioxide (WO_3) assays greater than 0.05 wt%, are listed on the right. The solid trace is a running average of the mineralization values over 5 foot (1.5 m) increments. The dashed line whose positive areas are shaded is the trace of the mineralization values for one foot (30 cm) increments.

The spectra from 1065 to 1070 feet (325 to 326.1 m) were averaged and the result is shown in Figure 30.7 along with the difference spectrum. The background spectrum used to obtain the difference spectrum was obtained by averaging the spectra from 1050 to 1060 feet (320 to 323 m) and from 1076 to 1085 feet (328 to 330 m). The large energy peak at about 60 keV on the difference spectrum is due to the tungsten K X-rays.

Hole 57 was logged over a 500 foot (150 m) interval where available WO_3 assay data were almost continuous (Fig. 30.8, 30.9). In this interval there were 8 zones with assay greater than 0.1 wt% and mineralization traces have corresponding deflections for 7 of the 8 zones. In addition, there are 5 other large deflections which correspond to assays between 0.05 and 0.1 wt% and 3 anomalous deflections which appear to be due to lithological changes. These anomalous deflections appear to correspond to breccia in a fault zone, a thin igneous intrusion and thin hornfels bedding in the skarn. Figures 30.8 and 30.9 show the mineralization plots for the depth intervals from 1030 to 1095 feet (313.9 to 333.8 m) and from 1185 to 1265 feet (361.2 to 385.6 m). The deflections of the mineralization functions of both plots show good correlation with the assay values listed to the right. None of the assays for the logged interval of hole PH-57 exceeded 1 wt%.

The background of the mineralization traces will have dc offsets which correspond to lithological changes. These dc offsets are distinguishable from the more irregular deflections due to the mineralized zones. In addition the full spectra data of the dc offset will not display any sharp energy peaks.

Potential of the logging system

The X-ray fluorescence mineral logging system can be a useful tool in obtaining data for mine expansion and control as well as for mineral exploration. A commercial logging system could be used to log rotary drillholes which can be drilled faster and less expensively than core drilled holes. Since the logging system has the ability to analyze the data at the drill site, results necessary to make decisions regarding future drill sites can be readily obtained. Even with a commercial logging tool, some core holes would be recommended for data correlation.

The main limitation of the X-ray fluorescence technique is that X-rays are easily absorbed. Any mud or moisture on the borehole walls can absorb the X-rays before they are detected by the sonde. When logging in water, the detection of light minerals (elements with small atomic number, i.e., zinc, copper, etc.) is not possible and the sensitivity of the sonde for the heavy minerals (large atomic number, i.e., tungsten, lead, etc.) is reduced.

In order to provide a commercial system, the design and development of a new modular logging sonde is planned. The modular sonde would digitize the spectral data before transmitting the data to the surface. Since the detection of different minerals requires different radioactive sources, multiple detector and source modules are proposed. Each of these modules would be optimized for a given range of minerals. Since the gain of each module would be preset, major calibrations of the system could be routinely done in a laboratory and only minor functional tests of the system would need to be performed at the logging site. The logging sonde would contain a microprocessor which would control the flow of data. Additional modules which measure caliper, temperature, natural gamma and other parameters which affect the operation would be installed.

Acknowledgments

The authors of this paper are indebted to P.R. Gray, H.R. Barton, Jr., and V.L. Moore who performed the earlier work with the X-ray mineral logging system. The personnel in Analysis Branch were helpful in analyzing the calibration samples and for giving helpful advice in performing the analysis of the data. The Mineral Personnel and the Geology Branch involved in the mineral prospect near Ely, Nevada were helpful in locating the holes and supplying the lithological and assay data.

References

Barton, Jr., H.R. and Gray P.R.
1974: Detection of elements by irradiating material and measuring scattered radiation at two energy levels; U.S. Patent No. 3843881.

Bowie, S.H.U.
1968: Portable X-ray fluorescence analysers in the mining industry; Mining Magazine, v. 18, p. 1-6.

Broquet, C., Robin, G. and Vachen, M.
1967: Realization and use of X-ray filters, in OR NL-II C-10; R.S. Barker and M. Gerrard, ed., Oak Ridge National Laboratory, Oak Ridge, Tenn., p. 393-423.

Lantor, J. and Litchinsky, D.
1980: In situ rock analysis; Advances in X-ray Analysis, v. 23, p. 37-43.

Leman, E.P. and Bolotova, N.G.
1969: Radioactive isotopes and gamma-ray sources for X-ray sampling of ores (in Russian); Voprosy Razvedochnoy Geofiziki, v. 11, p. 3-11.

Lubecki, A., Doebele, R., and Herrmann, W.
1982: Direct uranium logging using X-ray fluorescence technique; in Proceedings of the Symposium on Uranium Exploration Methods, Review of the NEA/IAEA R&D Programme, Paris, 1-4 June 1982, p. 821-835.

Reynolds, R.C.
1963: Matrix corrections in trace element analysis by X-ray fluorescence: estimation of the mass absorption coefficient by Compton scattering; American Mineralogist, v. 48, p. 1133-1143.

1967: Estimate of mass absorption coefficients by Compton scattering: improvements and extensions of the method, American Mineralogist, v. 52, p. 1143-1502.

Rhodes, J.R.
1971: Design and application of x-ray emission analyzers using radioisotope x-ray or gamma ray sources; Energy Dispersion X-ray Analysis: X-ray and Electron Probe Analysis, ASTM STP 485, American Society for Testing and Materials, p. 243-285.

Semmler, R.A.
1977: Determination of the background in proton-excited X-ray spectra in the absence of blanks; in X-ray Fluorescence Analysis of Environmental Samples, T.G. Ozubay, ed., Ann Arbor Science Publications Inc., Ann Arbor, Michigan, p. 269-281.

Sumartojo, J. and Paris, M.W.
1980: A method for measuring X-ray mass-absorption coefficients of geological materials; Chemical Geology, v. 28, p. 341-347.

Tanner, A.B., Moxham, R.M., Senftle, F.E. and Baicker, J.A.
1971: A borehole sonde using a 252 Cf source and a Ge(Li) detector cooled by a melting cryogen, Proceedings of the American Nuclear Society, Topical Meeting, Neutron Sources and Applications, CONF-710402, Augusta, Ga., v. III, p. 1-6.

31. THERMAL ABSORPTION CROSS-SECTION MEASUREMENTS ON BOREHOLE SAMPLES[1]

J.M. Harris[2], P.J. McDaniel, R.W. Barnard, and D.H. Jensen

Harris, J.M., McDaniel, P.J., Barnard, R.W., and Jensen, D.H., Thermal absorption cross-section measurements on borehole samples; in Borehole Geophysics for Mining and Geotechnical Applications, ed. P.G. Killeen, Geological Survey of Canada, Paper 85-27, p. 285-287, 1986.

Abstract

Exploration for mineral and hydrocarbon-bearing formations often requires the use of logging tools which rely on neutron irradiation. Interpretation of the data from these tools is aided by knowledge of the thermal neutron absorption cross-section of the formation. Therefore, exploration and service companies have developed a variety of methods to determine the absorption cross-section in the formation from measurements taken in the borehole. One such method is the pulsed neutron dieaway technique, as is used in a commercial neutron capture logging tool.

Thermal absorption cross-sections from neutron dieaway measurements made with the NLL probe (trademark of the Dresser-Atlas Company) at a site near Pana Maria, TX, have been compared with measurements made of core samples. The cross-sections of the core samples were derived from reactivity measurements made at the Advanced Reactivity Measurement Facility located at the Idaho National Engineering Laboratory. A model based on an analytic infinite-medium solution to the time-dependent Boltzman equation was used to relate a dieaway measurement to the absorption cross-section.

Résumé

L'exploration des minéraux et des formations contenant des hydrocarbures requière souvent l'utilisation des appareils de sondage à activation neutronique. L'interprétation des données provenant de ces appareils est facilitée par la connaissance de l'absorption thermoneutronique de la coupe de la formation. De ce fait, les entreprises d'exploration et de services ont mis au point des méthodes afin de déterminer l'absorption de la coupe d'une formation à partir de mesures prises dan les trous de sondage. Une de ces méthodes est celle de la technique des neutrons pulsés dite «dieaway», c'est cette méthode qui est utilisée par les outils commercialisés de sondage à capture neutronique.

Les mesures d'absorption thermique des coupes par la méthode neutronique pré-citée ont été effectuées par la sonde NLL (marque déposée par la Dresser-Atlas) sur un site près de Pana Maria, TX; celles-ci ont été comparées aux mesures faites à partir de carottes. Les mesures effectuées sur les profils des carottes provenaient de mesures de réactivité de l'«Advanced Reactivity Measurement Facility» du laboratoire de l'Idaho National Engineering. On a utilisé un modèle de solution analytique à milieu indéfini en accord à l'équation à fonction temporelle de Boltzman pour mettre en relation les mesures neutroniques «dieaway» et l'absorption dans les coupes.

Introduction

Neutron capture logs have been commercially available since 1963 (Youmans et al., 1964). They are commonly used to locate the oil-water interface in a cased well hole, and when combined with the neutron absorption cross-section for the formation fluids, the residual oil saturation can be determined. Both applications are based upon measurement of the absorption cross-section. Since the thermal absorption cross-section of chlorine is much larger than that of carbon, hydrogen, or oxygen, the formation water, which normally contains NaCl, can be distinguished from hydrocarbon.

The neutron-capture logging tool incorporates a pulsed neutron source and a gamma ray detector. Neutrons with energies of about 14 MeV are injected into the formation and lose energy by scattering until their energy is comparable to the thermal energy of the nuclei. These thermal neutrons migrate through the formation until captured by one of the nuclei in the formation. Most capture events result in emission of a gamma ray which can be observed by the detector. The capture rate of the neutrons is a function of the thermal absorption cross-section in the formation; therefore, it is possible to determine the thermal absorption cross-section of a formation by measuring the time-dependent signal from the gamma ray detector.

Although the concepts on which the neutron capture log is based are easily understood, the actual relationship between the thermal absorption cross-section and the signal in the gamma detector can be quite complex. Variations in the borehole size, the thickness and type of the well casing, and the mud cake all affect measurements. Experiments were performed to determine the accuracy of the thermal absorption cross-section from borehole measurements. A commercial Neutron Lifetime Log (NLL) was run in a

[1] This work was supported by the U.S. Department of Energy under Contract No. DE-AC04-76DP00789.

[2] Sandia National Laboratories, Albuquerque, NM 87185

shallow borehole. The experiment was run in association with Chevron Oil Field Research Company during 1978. Chevron provided the data from the commercial NLL to Sandia Laboratories for analysis. The absorption cross-sections of samples taken from the formation fluids and rock matrix at various depths were measured and compared with the values from the NLL.

Experimental technique

The borehole was located in Karnes County, near Pana Maria, Texas. It was drilled with a 6.25 inch (15.9 cm) bit to a depth of about 275 feet (83.9 m) and was not cased. Fluids extracted from the borehole had a density of about 1g/cm^3. The measured salt content was less than 500 ppm, so the formation was treated as fresh water with no hydrocarbon content. The zone of interest was at a depth of 135-165 feet (41.2-50.3 m), and had a relatively constant borehole diameter. The porosity log of this zone showed an excursion of ±6 percentage points about the median value of 30%.

Several samples weighing about 120 g were taken from borehole cores. These samples were dried and pulverized to about 120 mesh. An aliquot of about 2 g from each sample underwent an elemental analysis using Prompt Gamma Activation Analysis (PGAA) (Harris et al., 1983). The remainder of each sample was sent to the Idaho National Engineering Laboratory for determination of the absorption cross-section using the Small Sample Reactivity Measurement (SSRM) technique (Farley et al., 1981).

Table 31.1 Analysis of typical core sample

Core 151.5 - 152.0 feet ϕ = 30%			
Element	Microscopic Cross Section (cm^2/g)	Concentration (μg/g)	Macroscopic Cross-Section (c.u.)
B	4.27×10^{1}	4.18×10^{1}	3.09
Si	3.68×10^{-3}	3.62×10^{5}	2.31
H	2.00×10^{-1}	5.00×10^{3}	1.74
K	3.24×10^{-2}	2.46×10^{4}	1.38
Gd	1.88×10^{2}	3.73	1.21
Al	5.15×10^{-3}	6.90×10^{4}	6.16×10^{-1}
Na	1.39×10^{-2}	2.10×10^{4}	5.07×10^{-1}
Fe	2.76×10^{-2}	5.00×10^{3}	2.40×10^{-1}
Sm	2.33×10^{1}	5.30	2.13×10^{-1}
Cl	5.70×10^{-1}	2.07×10^{2}	2.05×10^{-1}
Ti	7.65×10^{-2}	9.00×10^{2}	1.20
Ca	6.47×10^{-3}	6.00×10^{1}	6.73×10^{-2}
Cd	1.35×10^{1}	1.40	3.28×10^{-2}
O	7.16×10^{-6}	5.06×10^{5}	6.28×10^{-3}
		Total	12.6 c.u.
		Formation Fluid	22.0 c.u.
		Formation Absorption Cross Section	19.2 c.u.

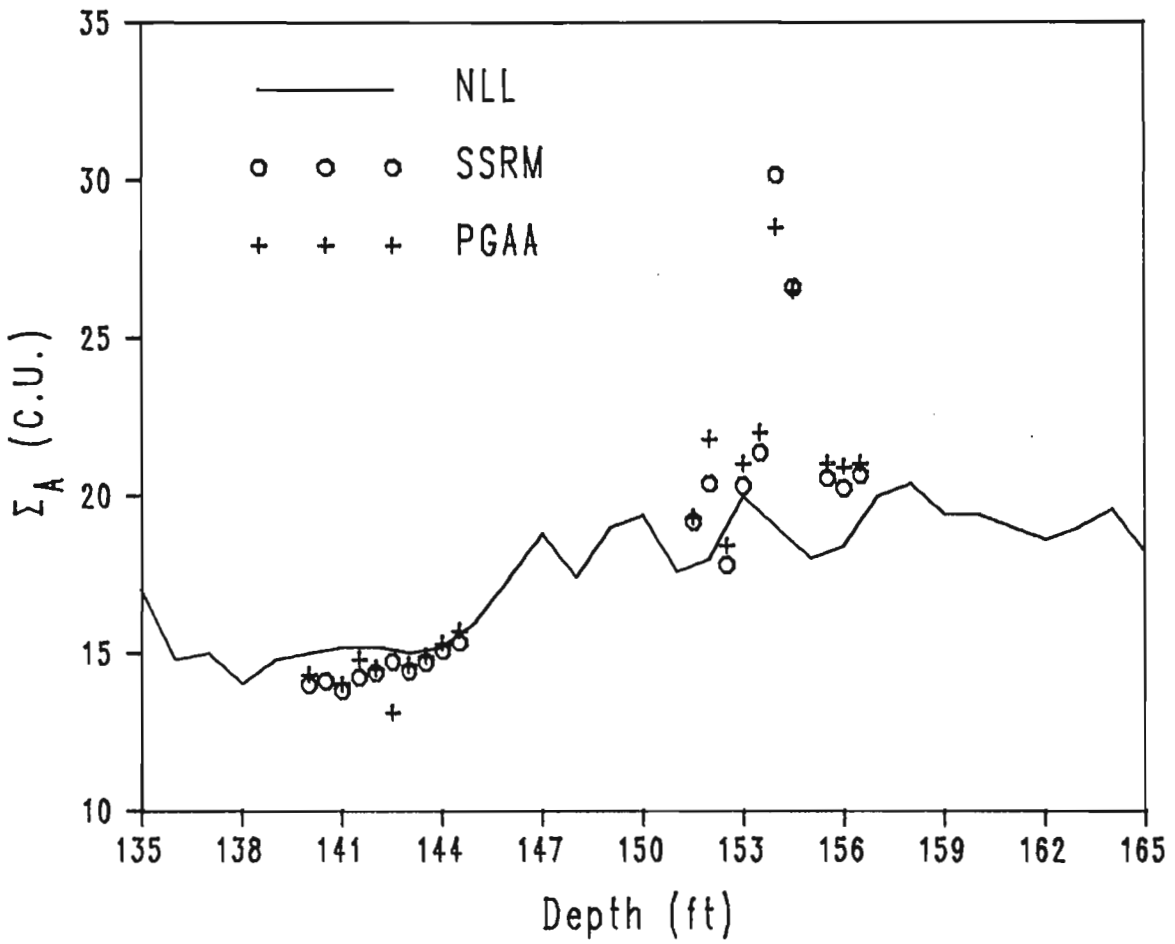

Figure 31.1. Formation cross-sections as a function of depth based on PGAA data and SSRM data, as well as the NLL.

The density of the rock matrix and the density of the formation fluid were calculated using the following:

$$\rho_m = (1 - \emptyset)\rho_g \quad (1)$$

$$\rho_w = \emptyset S_w \rho_f, \quad (2)$$

where

ρ_m = density of matrix in formation,
$\emptyset$ = porosity of formation,
ρ_g = measured grain density of matrix,
ρ_w = density of fluid in formation,
S_w = water saturation in formation, and
ρ_f = density of borehole fluids.

Since the zone of interest is below the water table, S_w was assumed to be 1.0. The thermal absorption cross-section for fresh water is $\Sigma_w = 22.2 \times 10^{-3}$ cm^2/g.

The absorption cross-section of the formation, Σ_A, is the sum of the matrix and the fluid absorption cross-section and is given by

$$\Sigma_A = \rho_m \Sigma_m + \rho_w \Sigma_w \quad (3)$$

and

$$\Sigma_m = \sum_{j=1}^{N} C_j \Sigma_j, \quad (4)$$

where

Σ_j = microscopic thermal absorption cross-section for the j^{th} element (cm^2/g),

C_j = concentration of element j (g/g),

N = number of nuclides in sample, and

Σ_m = microscopic thermal absorption cross section for matrix (cm^2/g).

The NLL data are digitized records of the count rates in five gates of 100 μs duration. These gates begin at 200, 300, 400, 600, and 800 μs after the neutron pulse. The macroscopic absorption crosss-section has been calculated from these data, based on the theory developed by Youmans et al. (1981). This theory is an infinite-medium approximation to the Boltzman transport equation, which predicts the neutron population in the formation will decay exponentially. An exponential dieaway has been fitted to the NLL data, and the absorption cross-section has been extracted from the exponent.

Results

At each depth in the borehole from which a core sample was taken, the absorption in the matrix was calculated from PGAA and also measured by SSRM technique. These results were combined with data from the porosity log to obtain the macroscopic thermal cross-section for the formation. The results of a typical core analysis from the PGAA are shown in Table 31.1. The microscopic cross-sections used for the individual elements were taken from the ENDF V compilation (Mughabghab et al., 1981). Contributions to the macroscopic cross-section for the rock matrix were calculated from equation (1) using a value of 1.74 g/cm^3 for ρ_m. Figure 31.1 shows the formation cross-sections as a function of depth based on PGAA data and SSRM data, as well as the NLL.

In the zone between 139 and 145 feet (42.4-44.2 m) the differences between the three techniques are less than 18%. In the region between 151 and 158 feet (46.1-48.2 m), the techniques agree within about 12%, except at one point. At 155 foot depth (47.3 m), the NLL measurement is only 60% of the other two values. No systematic differences are observed between the measurements made on core and the results obtained from the NLL. The differences obtained from the two techniques used on the core samples are less than 11% at any point.

Discussion and conclusion

The dominant contribution to neutron absorption in the formation is from capture in boron and silicon. Two core samples, taken at depths between 154 and 155 feet (47 and 47.3 m), contained almost twice as much boron as the sample shown in Table 31.1; consequently, their macroscopic absorption cross-sections are much larger than those obtained near 151 feet (46.1 m) (Fig. 31.1). The NLL did not accurately record this high-absorption zone. Two explanations for this discrepancy are possible; first, the core may not be representative of the formation volume which the NLL tool interrogates, or second, the high-absorption zone may be localized to a bed so thin that the NLL tool cannot accurately resolve it.

Comparison studies using core samples and log data would not be expected to yield pointwise agreement, but may be quite useful in detecting calibration or systematic errors. Using two independent techniques to obtain the absorption cross-section increases the confidence in the core analysis. The fact that cross-sections obtained from PGAA measurements and the SSRM data differ by up to 11% is expected since the latter are only accurate to about 10%.

In general, the NLL probe provides an accurate measurement of the absorption cross-section in this formation. Either of the methods used for analyzing the core can provide absorption cross-sections with an accuracy of about 10%. Additional work is necessary to completely understand the reason for the remaining discrepancies between the core measurements and the NLL measurements.

Acknowledgments

The authors acknowledge the assistance of Chevron Oil Field Research Company, La Habra, California, which provided the core samples and the NLL data obtained by Dresser-Atlas Company.

References

Failey, M.P., Anderson, D.L., Zoller, W.H., Gordon, G.E., and Lindstrom, R.M.
1979: Neutron-capture prompt γ-ray activation analysis for multielement determination in complex samples; Analytical Chemistry, v. 51, p. 2209.

Harris, J.M., McDaniel, P.J., and Widman, D.H.
1983: Thermal neutron absorption from reactivity measurements of selected geological materials; Society of Professional Well Log Analysts, 24th Annual Logging Symposium, Volume 2, Paper VV.

Mughabghab, S.F., Divadeenam, M., and Holden, N.E.
1981: Neutron Cross Sections, Volume 1, Academic Press, New York.

Youmans, A.H., Hopkinson, E.C., Bergan, R.A., and Oshry, H.L.
1964: Neutron Lifetime, a New Nuclear Log; Journal of Petroleum Technology, March.

32.

DESIGN AND FIELD TEST OF A SENSOR FOR THE CROSSHOLE MAGNETOMETRIC RESISTIVITY TECHNIQUE

B.B.H. Lo and R.N. Edwards[1]

Lo, B.B.H. and Edwards, R.N., Design and field test of a sensor for the crosshole magnetometric resistivity technique; in Borehole Geophysics for Mining and Geotechnical Applications, ed. P.G. Killeen, Geological Survey of Canada, Paper 85-27, p. 289-296, 1986.

Abstract

The Magnetometric Resistivity (MMR) method is an electrical method of exploration for conductive, mineralized bodies. In an MMR survey, low level magnetic fields caused by currents injected into the ground are measured. The crosshole variant, introduced in 1980 by Newmont Exploration Ltd. in conjunction with the University of Toronto, requires at least two boreholes in the vicinity of a target. In the first, two fixed current electrodes are located, one above the other. They are effectively joined by a single cable carrying the low frequency transmitter current. In another borehole, a sensitive coil measures, as a function of depth, the component parallel to the hole of the magnetic field of the transmitted current.

The design of a simple downhole probe is described. The radius of the finished probe is 1.6 cm and can fit into EX (1.8 cm radius) sized holes. The sensor consists of a 101 cm long ferrite core of relative permittivity of about 200. Twenty-four thousand turns of magnet wire are wrapped in ten equal sections about the core. Five tuned, active filter stages connected in cascade, amplify the received signal before transmission uphole in a Kevlar reinforced, shielded cable. The circuit diagrams of the probe assembly, as well as their Bode diagrams, are given.

Data collected on the first field test of the downhole probe are presented. They are corrected for primary current distortion caused by an overburden layer, and for the several effects of non-vertical boreholes. Anomalies, caused by current channelling, are evident in the reduced data. Targets identified occur at similar depths as those previously located with the downhole Crone PEM system.

Résumé

La méthode de la résistivité magnétométrique est une méthode électrique servant à la recherche des corps minéralisés conducteurs. Elle consiste à mesurer les champs magnétiques de faible intensité créés par l'envoi de courant dans les formations. La méthode transversale, que Newmont Exploration Ltd. et l'Université de Toronto ont présentées en 1980, nécessite l'utilisation d'au moins deux trous de sonde au voisinage de la cible. Dans le premier trou, des électrodes de courant fixes sont placées l'une au-dessus de l'autre. Elles sont reliées par un câble unique transportant le courant à basse fréquence émis par l'émetteur. Ce courant crée un champ magnétique et, dans un autre trou, une bobine sensible en mesure la composante parallèle au trou en fonction de la profondeur.

La mise au point d'une sonde de fond simple est décrite dans le présent rapport. Une fois assemblée, la sonde a un rayon de 1,6 cm et elle peut être insérée dans des trous de dimensions EX (rayon de 1,8 cm). Le détecteur consiste en un noyau en ferrite d'une longueur de 1,01 cm et d'une permittivité relative d'environ 200. Vingt-quatre milles tours de fil de bobinage sont enroulés de manière à former dix sections égales autour du noyau. Cinq filtres actifs et synchronisés, montés en étage et reliés en cascade, amplifient le signal reçu avant de le transmettre à la surface à l'aide d'un câble renforcé de Kevlar et blindé. Les diagrammes de circuit et les diagrammes Bode de la sonde sont fournis.

Les données recueillies au cours du premier essai de la sonde de fond sur le terrain sont exposées. Elles ont été corrigées de manière à tenir compte de la distorsion du courant primaire due à une couche de mort-terrain et à tenir compte de plusieurs effets propres aux trous de sonde non verticaux. Les données résumées font ressortir, de façon évidente, les anomalies causées par la transmission du courant. Les profondeurs indiquées pour les cibles sont les mêmes que celles que le système de fond Crone PEM avait indiquées auparavant.

[1] Geophysics Laboratory, Department of Physics, University of Toronto, Toronto, Ontario, M5S 1A7

Background

In an Magnetometric Resistivity (MMR) survey, the magnetic field caused by currents injected into the ground is measured. The current flowing out of a point source at the surface of a uniform earth produces a magnetic field on the earth's surface which is the same as that of a half infinite wire extending vertically downwards from the injection point. Further, the magnetic field when measured on the earth's surface is not perturbed by horizontal layering within the earth. However, the presence of lateral conductors does channel currents and produce an 'MMR anomaly'.

An advantage of the MMR technique occurs because a measurement of the magnetic field at a given location is due to all the current flow in space. Therefore, the technique is not as sensitive to the local conductivity structure at the measurement point as surveys which measure the electric field, which is strongly influenced by local charges. Consequently, an MMR survey can be more effective in areas of highly variable and conductive overburden than, for example, a resistivity survey.

Historically, the MMR method stems from a patent of Jakosky (1933). A viable system could not be built at that time because of a lack of magnetic field sensors of sufficient sensitivity. Extensive development of the method has taken place at the University of Toronto since the early 1970s when milligamma magnetometers became commercially available (Edwards, 1974; Edwards and Howell, 1976; Gomez-Trevino and Edwards, 1979; Edwards and Gomez-Trevino, 1980). The MMR technique of finding lateral conductivity changes in the earth has subsequently been applied successfully for mineral exploration.

With the commercial availability of low noise precision operational amplifiers, a sensitive coil may be used instead of a magnetometer. The design and construction of such an inexpensive sensor and electronics is presented. Our paper will concentrate on the crosshole variant of MMR and demonstrate the simplicity of the probe design.

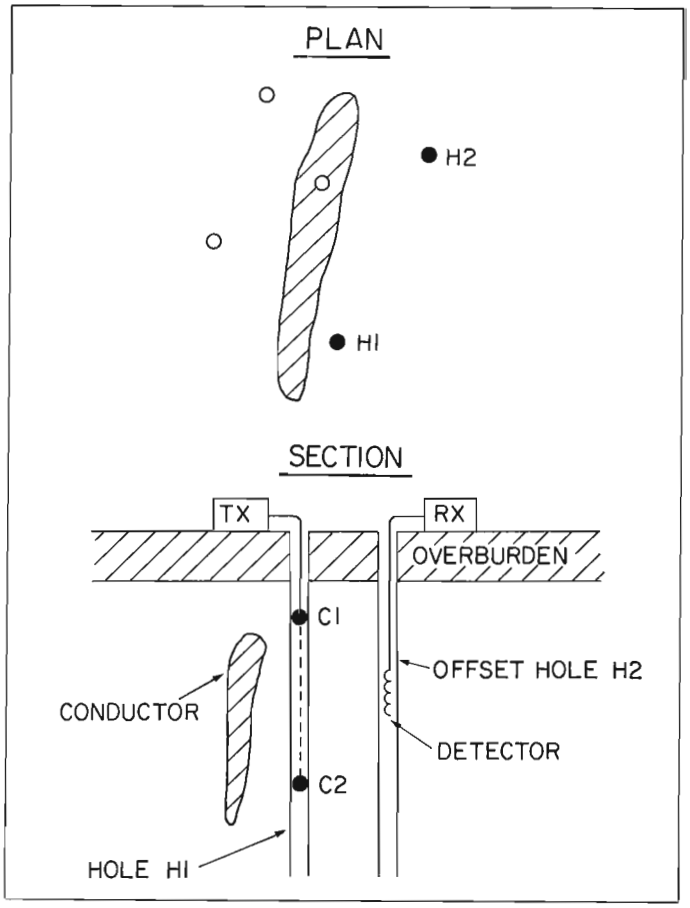

Figure 32.1. *The geometry of the crosshole MMR method.*

Introduction to crosshole MMR

The crosshole variant of MMR was developed initially to solve a particular geophysical problem encountered by Newmont Exploration Ltd., Tucson. Several holes were drilled in the vicinity of a certain prospect, but only one intersected the deep, mineralized target. Various geophysical techniques were used to obtain information about the conductor, including regular MMR surveys, in which magnetic fields at the surface of the earth were measured. Simple numerical modelling showed that improved resolution of the target might occur if both the current sources and, particularly, the sensor were located closer to the target in boreholes: the crosshole MMR method. The role envisaged for crosshole MMR was to add to the information already obtained by drilling.

In the idealized crosshole MMR survey (Fig. 32.1), a current source and sink are located in a vertical borehole. In

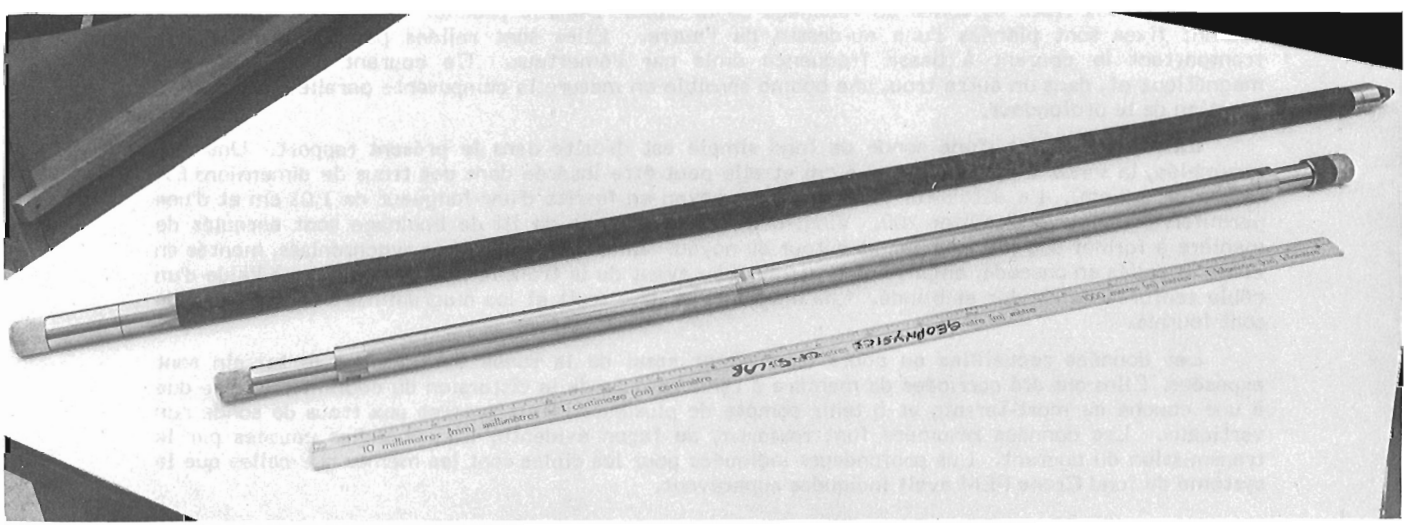

Figure 32.2. *The downhole probe.*

a second vertical borehole, a sensor measures the vertical component of the magnetic field as a function of depth. Inside a layered earth, using symmetry arguments, the currents generated in the earth by the current source and sink are independently axi-symmetric. Consequently, the associated magnetic field has only horizontal component. The magnetic field of the straight vertical current wire connecting the source and the sink is also horizontal in the ideal case for the same reason. Any vertical magnetic field measured must therefore be entirely due to current channelling caused by anomalous lateral conductivities.

In practice, boreholes are seldom vertical and primary fields generated by the current carrying wire are seen by the probe. Also, a non-vertical sensor measures a component of the horizontal magnetic fields produced by the current source and sink. These two geometric effects may be computed and removed in the first stages of data reduction.

Two useful numerical routines have been developed for making such a geometrical correction. They enable the magnetic field, due to injected currents of either a half-space or a layer over a half-space earth model, to be computed. The formulae derived by Edwards et al. (1978) for the vertical MMR response of a thick outcropping dyke of infinite vertical extent can be reinterpreted to give directly the magnetic fields of current sources and sinks in a layer over a half space earth. The magnetic field of the inclined current wire is evaluated from the fundamental Biot-Savart law. From dip, tropari and distance measurements along the borehole, the relative location and orientation of the sensor with respect to the current wire can be found. The coupling of the magnetic fields to the probe is then obtained through suitable co-ordinate transformations.

In practice, the distance scale of a typical crosshole MMR survey is the order of 1 km. Local effects of the drillhole, such as the effects of drilling muds, do not affect the downhole MMR measurements unless the muds are highly susceptible. Further, the receiver probe can be operated in plastic-cased boreholes.

Instrumentation

The equipment used in a crosshole MMR survey is easily adapted from instruments used in surface MMR (Lo, 1985). Our system includes:

1. A crystal controlled transmitter which injects an alternating square wave of the proper frequency into the ground. The transmitter operates from a 3 kW, 60 Hz Kohler motor generator.

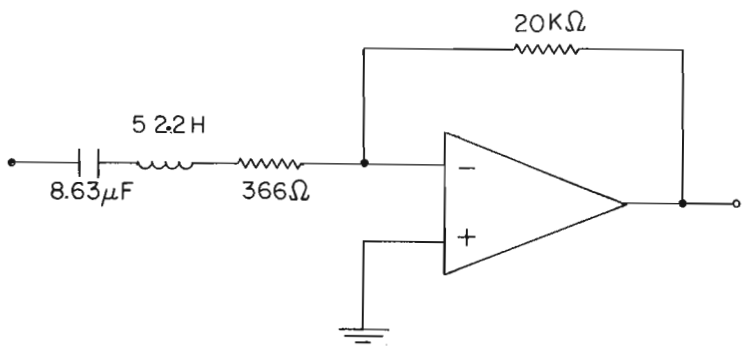

Figure 32.3a. *Circuit diagram of the first stage with the inductor and the resistor representing the coil.*

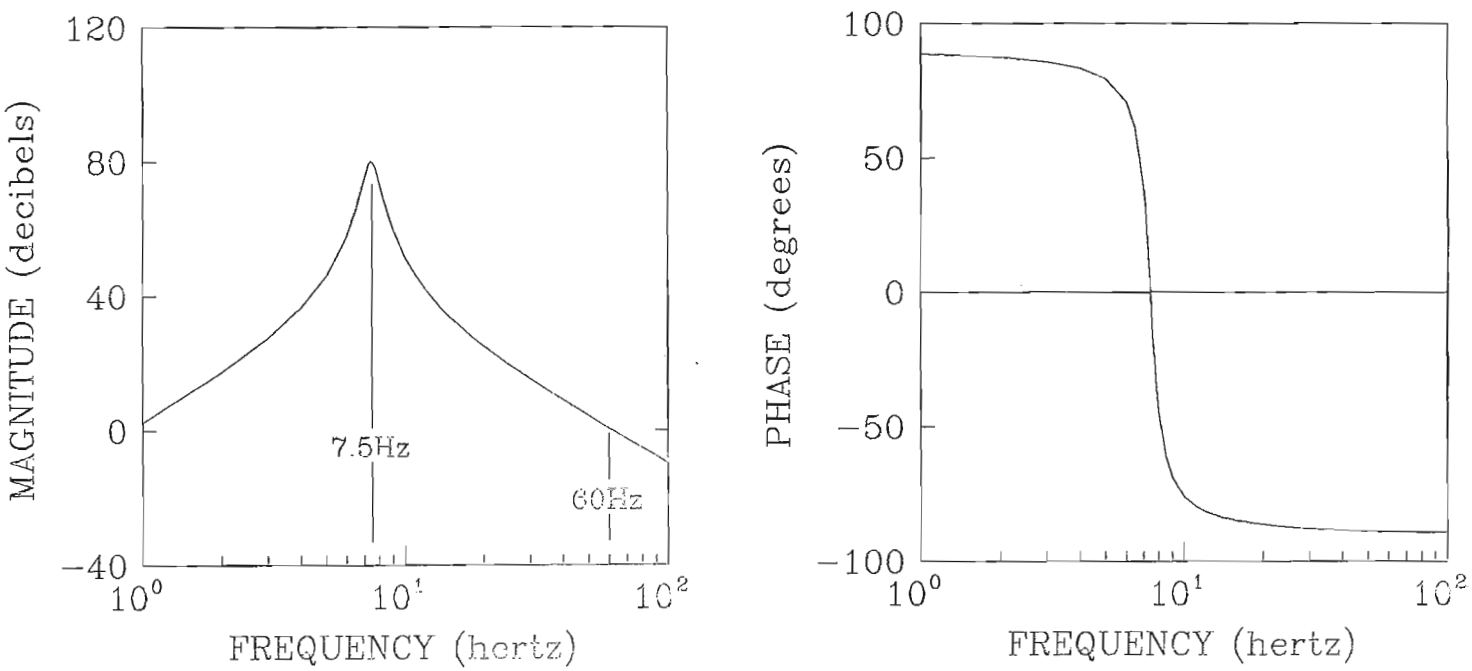

Figure 32.3b. *Bode plot of the first stage.*

2. A portable digital receiver which is phase-locked to the transmitter. The phase reference is carried and maintained by a local crystal oscillator synchronized with a similar oscillator at the transmitter.

A downhole probe and manual winch system are added to the above instrumentation for a borehole survey. One kilometre of Kevlar reinforced, two conductor, shielded cable is mounted on the winch. The probe's distance down the borehole is given by an attached counter calibrated in decimetres. The current-carrying wires, which form the transmitter bipole, are insulated, single conductor, steel-reinforced copper wire. Copper coated steel welding rods about 3 m in length are used for the current electrodes.

The complete downhole probe (Fig. 32.2), is 3 m long and 3.2 cm in diameter and as such, may be lowered in EX (a common drill size 3.6 cm diameter) size drill holes. The probe consists of a tuned ferrite coil sensor, pre-amplifiers and batteries. Operating life-time is 10 hours for a set of batteries. The coil is potted with fibreglass and the rest of the assembly is enclosed in a stainless steel casing. Operational depths of up to 1 km in water-filled holes have been achieved.

The sensor consists of a 101 cm length ferrite core which has a relative permeability of about 200. About this core is wound 24 000 turns of No. 28 magnet wire. The wire has an interwinding capacitance which forms a resonant circuit with the inductance of the coil. For operational stability reasons, the coil works in the linear region below the self-resonant frequency. Interwinding capacitance of the coil is minimized by pile winding in ten sections. This produced a coil with characteristics of 52.2 H (henries), 0.125 μF (microfarads) and a resistance of 377 ohms.

Before the emf induced in the coil by a changing magnetic field signal is transmitted uphole, the signal is amplified in stages. The coil is connected in series with capacitors of total capacitance of 8.63 μF (Fig. 32.3a) to resonate at the operating frequency of 7.5 Hz. The first stage has a three decibel passband width of 1.13 Hz centred about 7.5 Hz.

Up to four further stages each with a three decibel passband of 3.75 Hz may be connected in cascade with the first stage. Figures 32.3 and 33.4 show the circuit diagrams of the first coil stage, one subsequent tuned amplifier stage and their respective Bode diagrams.

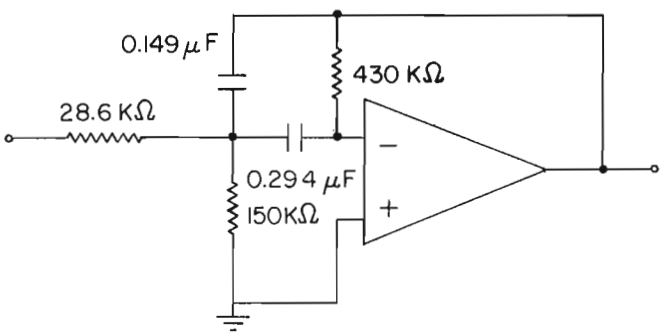

Figure 32.4a. *Circuit diagram of one of the following stages*

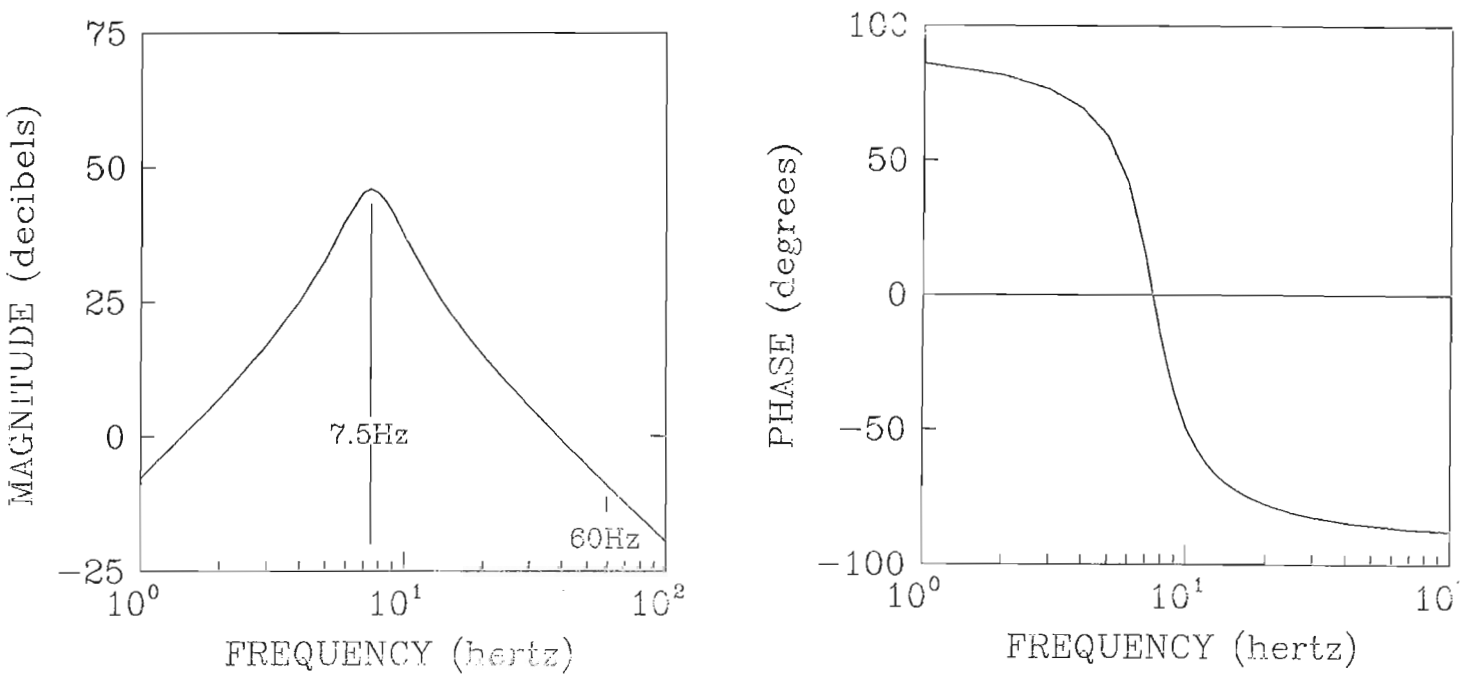

Figure 32.4b. *Bode plot of one of the following stages*

The smallest dynamic range of the probe (magnetic response), 300 pT (picotesla) peak to peak, corresponds to the greatest sensitivity, 31.3 V/nT, when all amplifier stages are cascaded. Each stage not used results in a ten-fold increase in the dynamic range, and a corresponding decrease in sensitivity.

Internal noise of the system determines the smallest signal which may be resolved. It originates from amplifier noise and from the thermal noise of the coil windings. Thermal noise could be reduced by using fewer windings but only at the expense of a decrease in the sensitivity of the coil. A high quality, low noise, precision operational amplifier (model OPA 27GT) manufactured by Burr-Brown Research Corporation is used in the first stage to reduce the amplifer noise to about the same level as the thermal noise of the coil. Noise from the system is 6 millivolts rms/root hertz. Consequently, for a 0.1 nT typical signal at 7.5 Hz, and a bandwidth of one hertz, the signal to noise ratio is 580 at the output of any of the four optional amplifier stages.

Electric field pick-up may mask the magnetic response or cause the amplifiers to saturate. It is avoided by grounding the electronics only at the input and running separate signal and ground wires to the surface.

Field test

Geology

A crosshole survey was conducted during July 1983, in conjunction with Noranda Exploration Co. The site is located near Sturgeon Lake, north of Ignace, in northwestern Ontario.

Here, about 5 m of overburden overlie the crystalline basement rock. Two work types, andesite and rhyolite form the major rock units in the region. Major sulphide minerals in rhyolite units are pyrite, pyrrhotite, chalcopyrite, and sphalerite. Some andesite units contain up to 5% euhedral magnetite. The topographic relief is small and the area is swampy. Access to the drill sites is provided by winter roads which, in the summer, are drivable to within 1 km of the drill sites.

Method

At the start of a survey, after the placement of the current electrodes, the crystal clocks in the transmitter and the receiver are synchronized. The sensor output is then calibrated against the field of a very long wire, carrying a known current, of which the magnetic field is known.

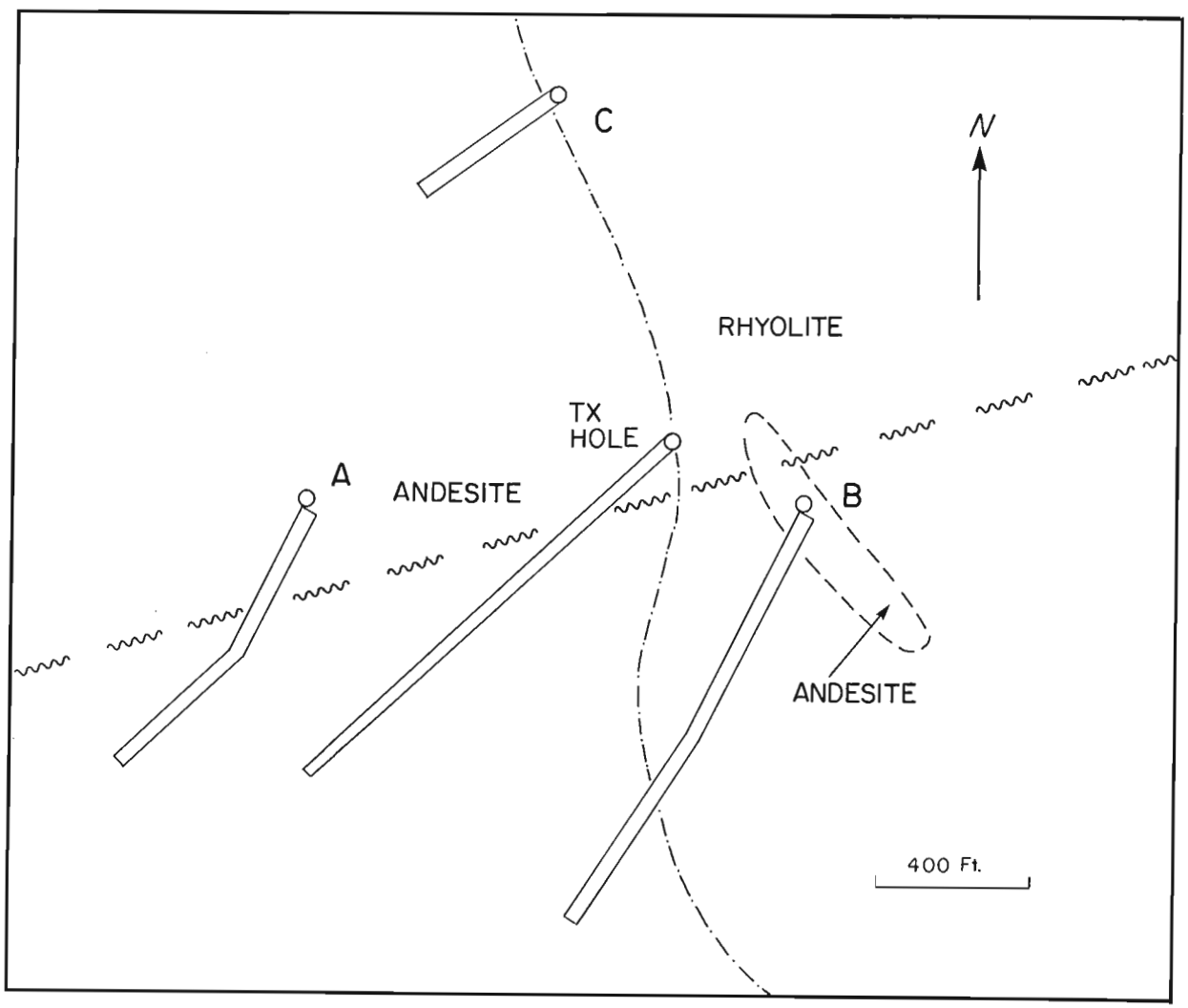

Figure 32.5. *Plan view of the boreholes logged in the first crosshole MMR test (400 feet = 122 m).*

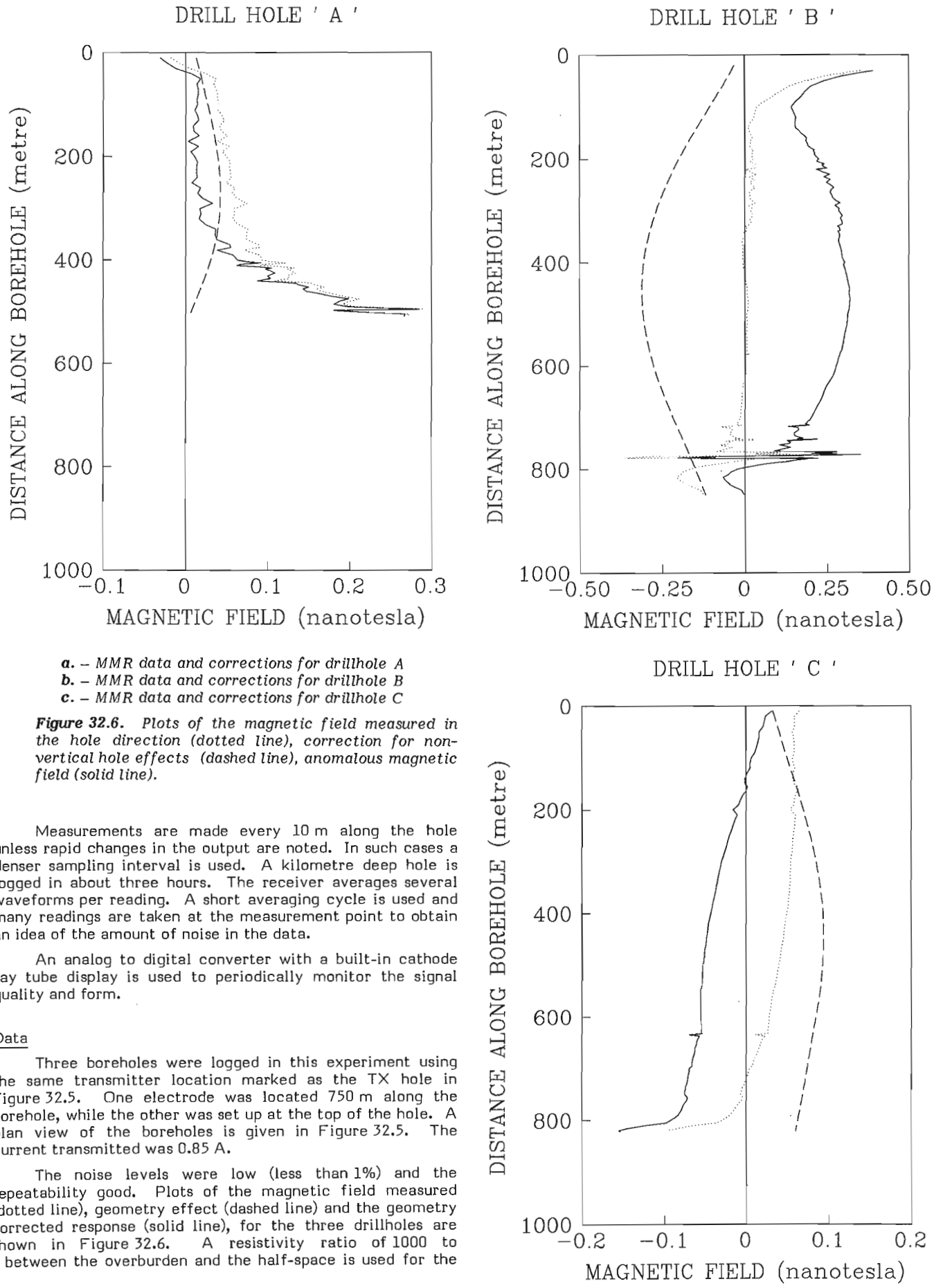

a. *– MMR data and corrections for drillhole A*
b. *– MMR data and corrections for drillhole B*
c. *– MMR data and corrections for drillhole C*

Figure 32.6. *Plots of the magnetic field measured in the hole direction (dotted line), correction for non-vertical hole effects (dashed line), anomalous magnetic field (solid line).*

Measurements are made every 10 m along the hole unless rapid changes in the output are noted. In such cases a denser sampling interval is used. A kilometre deep hole is logged in about three hours. The receiver averages several waveforms per reading. A short averaging cycle is used and many readings are taken at the measurement point to obtain an idea of the amount of noise in the data.

An analog to digital converter with a built-in cathode ray tube display is used to periodically monitor the signal quality and form.

Data

Three boreholes were logged in this experiment using the same transmitter location marked as the TX hole in Figure 32.5. One electrode was located 750 m along the borehole, while the other was set up at the top of the hole. A plan view of the boreholes is given in Figure 32.5. The current transmitted was 0.85 A.

The noise levels were low (less than 1%) and the repeatability good. Plots of the magnetic field measured (dotted line), geometry effect (dashed line) and the geometry corrected response (solid line), for the three drillholes are shown in Figure 32.6. A resistivity ratio of 1000 to 1 between the overburden and the half-space is used for the

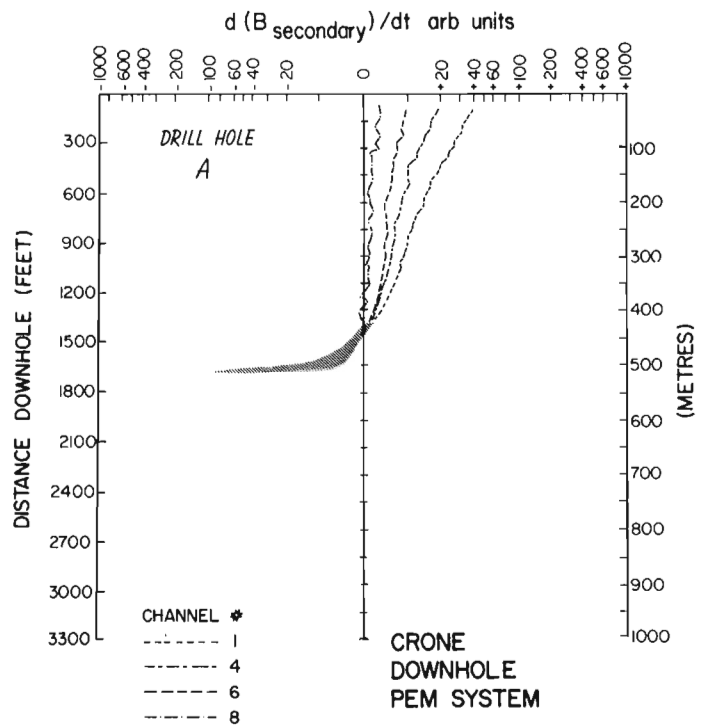

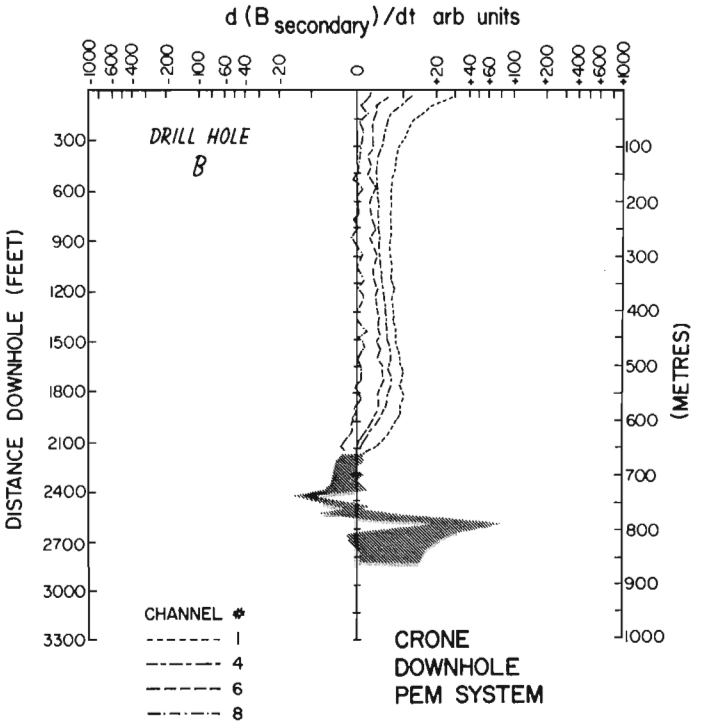

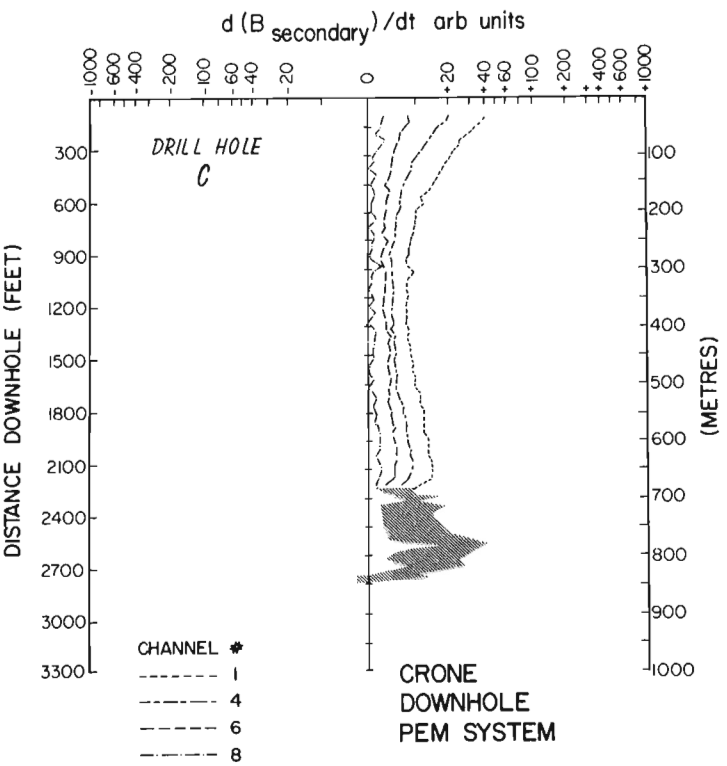

a. – *PEM data for drillhole A*
b. – *PEM data for drillhole B*
c. - *PEM data for drillhole C*

Figure 32.7. *Plots of Crone Pulse EM data collected previously for the same drillholes.*

earth model. Corrections for geometry are of the same magnitude as the data collected. Consequently, this correction may change the regional nature of the data curves.

Figure 32.7, shows Crone Pulse EM data collected by Noranda Exploration Co. for the same holes. For ease of presentation, only select channels of Crone PEM data are presented. The shaded areas in the plots are areas where the various channel responses are not easily distinguishable from each other.

Interpretation of the Crone PEM data for drillhole A shows a partially developed off-hole response at the end of the hole. Drillhole B has inhole responses at 731 and 769 m which correspond with known mineralization. A weak inhole response is detected near the bottom of drillhole C.

Interpretation

Both two and three dimensional numerical modelling routines are available for data interpretation. A very general two dimensional finite difference routine which has applications in regular resistivity methods is available (Pai and Edwards, 1983). Three dimensional modelling is at hand for either a discretized bendable plate or a conductive disc. Both of the three dimensional routines use integral equation techniques.

Due to a lack of a complete anomaly curve for the drillholes, many models may be used to fit the data. Lo (1985), in his M.Sc. thesis, provided a more detailed discussion of the interpretation.

Comparison of the crosshole MMR data with the Crone PEM data shows that both systems sense anomalies at the same place. High spatial frequency signals, located near 750 m along the borehole, caused by local current channelling beside the hole are seen in the MMR data for drillhole B. Also seen are high spatial frequency data in the section from 175 m to 350 m in the same drillhole. This zone consists of andesitic rocks which have significant amounts of magnetic materials. A magnetic or MMR anomaly is caused by magnetic flux gathering by the magnetite in this region. Also observed to a lesser degree in the PEM data is the same effect. Magnetic flux gathering is inseparable from the magnetic field produced by current gathering.

Conclusions

An inexpensive, simple downhole MMR sensor has been described. It can be simply built and operated. A successful field test of the crosshole system has been performed. Data show that crosshole MMR can detect current channelling which may be caused by mineralized bodies. Comparison with Crone Pulse E.M. data show that both systems detect anomalies in the same positions. Extensions and further testing of the equipment have to be done in order to fully develop this system.

Acknowledgments

This project is supported by the Government of Ontario through the Ontario Geoscience Research Funds, Grant no. 145. The authors thank the staff of Noranda Exploration Co. for their support and help with the survey.

References

Cheesman, S.J.
1983: The crosshole MMR Response of a bent lamella; Bachelor of Applied Science Thesis, University of Toronto.

Edwards, R.N.
1974: The magnetometric Resistivity (MMR) method and application to the mapping of a fault; Canadian Journal of Earth Sciences, v. 11, p. 1136-1156.

1983: An approximate model of the Magnetometric Resistivity (MMR) and Magnetic Induced Polarization (MIP) responses of dipping dikes beneath a conductive overburden; Bulletin of the Australian Society of Exploration Geophysicists, v. 14, p. 30-35.

Edwards, R.N. and Gomez-Trevino, E.
1980: MMR2D-A programme for the computation of Magnetometric Resistivity (MMR) anomalies of two-dimensional structures; Macquarie University, School of Earth Sciences, North Ryde, Australia.

Edwards, R.N. and Howell, E.C.
1976: A field test of the Magnetometric Resistivity (MMR) Method; Geophysics, v. 41, p. 1170-1183.

Edwards, R.N. and Nabighian, M.N.
1981: Extensions of the Magnetometric Resistivity (MMR) method; Geophysics, v. 46, p. 459.

Edwards, R.N., Lee, H. and Nabighian, M.N.
1978: On the theory of Magnetometric Resistivity (MMR) methods; Geophysics, v. 43, p. 1176-1203.

Edwards, R.N., Lo, B., Cheesman, S., Nabighian, M. and Opplinger, G.
1983: Crosshole Magnetometric Resistivity (MMR); in Ontario Geoscience Research Grant Program's Summary of Research 1981-1983.

Gomez-Trevino, E. and Edwards, R.N.
1979: Magnetometric Resistivity (MMR) anomalies of two-dimensional structures; Geophysics, v. 44, p. 1170-1183.

Jakosky, J.J.
1933: Method and apparatus for determining underground structure; U.S. Patent No. 1906271.

Lo, B.B.H.
1985: On the development of Downhole Magnetometric Resistivity; unpublished M.Sc. Thesis, University of Toronto, Toronto.

Nabighian, M.N., Opplinger, G., Edwards, R.N., Lo, B., Cheesman, S.
1984: Crosshole Magnetometric Resistivity (MMR); Geophysics, v. 49, p. 1313-1326.

Pai, D. and Edwards, R.N.
1983: Programme MMR2DFD: Finite difference modelling of MMR anomalies, Reports in Applied Geophysics No. 25, University of Toronto, Department of Geophysics.

33. DOWNHOLE PULSE EM-TWO RECENT FIELD EXPERIENCES

J.B. Boniwell[1]

Boniwell, J.B., Downhole pulse EM-two recent field experiences; in Borehole Geophysics for Mining and Geotechnical Applications, ed. P.G. Killeen, Geological Survey of Canada, Paper 85-27, p. 297-306, 1986.

Abstract

The challenge of geophysical measurement is always to recognize that which is unique to every exploration situation and to adapt the measuring procedures and subsequent interpretation accordingly. Two field cases are presented wherein the application of downhole pulse EM logging directly benefited each investigation but in different ways.

In the first example, a developing discovery of gold-bearing sulphides in Archean mafic volcanics on the Eastmain River in northern Quebec provided an ideal problem for downhole EM. After 27 holes, it became evident that there was more than a crude relationship between sulphides and gold occurrences, and that there existed a system of relatively narrow zones of ore-grade metallics extending over 300 m in depth. Downhole pulse EM logging was carried out to map the deep zones with very satisfactory results.

The second example is a base metal prospect with a history of sporadic exploration attempts. The area lies in the Shebandowan volcanic mineralization that was first discovered under 60 m of gravel overburden. Each unsuccessful borehole led to deeper exploration drilling. A unique arrangement of drillholes on one section has made it possible to predict, on the basis of downhole EM logging, that a large body of sulphides exists some 250 m from surface and lying outside all drilling to date. As a consequence, extensive further testng is in the offing.

Résumé

Les mesures géophysiques posent constamment un défi qui consiste à savoir déceler les caractéristiques uniques de chaque situation au cours de l'exploration et à savoir adapter en conséquence les procédés de mesure et l'interprétation subséquente de ces mesures. Dans les deux cas exposés dans le présent rapport, la diagraphie électromagnétique (EM) à impulsions de fond a profité directement à chaque recherche, mais de façons différentes.

Dans le premier cas, un gisement de sulfure aurifère en cours d'exploitation dans une zone de roche volcanique ferromagnésienne de l'Archéen, près de la rivière Eastmain, dans le nord du Québec, procurait un problème idéal à résoudre au moyen de la méthode des sondages électromagnétiques de fond. L'examen de 27 trous de sondage a indiqué qu'il y avait, de toute évidence, un lien plus que lointain entre la présence de sulfure et la présence d'or au même endroit et permis d'observer un système de zones étroites et métalliques à plus de 300 m de profondeur. Les zones profondes ont été cartographiées de façon très satisfaisante au moyen de la diagraphie électromagnétique (EM) à impulsions de fond.

Le second cas est celui d'un gisement prometteur de métal commun ayant fait l'objet de travaux d'exploration sporadiques. La zone étudiée s'étend dans la minéralisation volcanique de Shebandowan, qui a été découverte sous 60 m de mort-terrain constitué de graviers. Chaque trou de forage infructueux était suivi d'un forage plus profond. Un réseau unique de trous de sondage forés dans une partie de la zone a permis de prédire, selon les résultats de la diagraphie électromagnétique (EM) de fond, qu'un important gisement de sulfures se trouve à quelque 250 m de la surface à un endroit où aucun forage n'a été effectué jusqu'à maintenant. D'autres essais poussés sont donc en vue.

Introduction

Exploration provides numerous opportunities to enlarge geological knowledge by geophysical measurements. It is also true that no two exploration situations are exactly the same, especially in terms of geophysical response. In consequence, the exploration geophysicist has to recognize what is unique in every situation, and be prepared to adapt. This calls for an innate flexibility of approach, beginning with the field measuring systems and their application through to subsequent data handling and interpretation. Two recent field experiences with downhole pulse EM Eastmain River area, Quebec and Burchell Lake area, Ontario illustrate this point.

[1] Excalibur International Consultants Ltd., Mississauga, Ontario

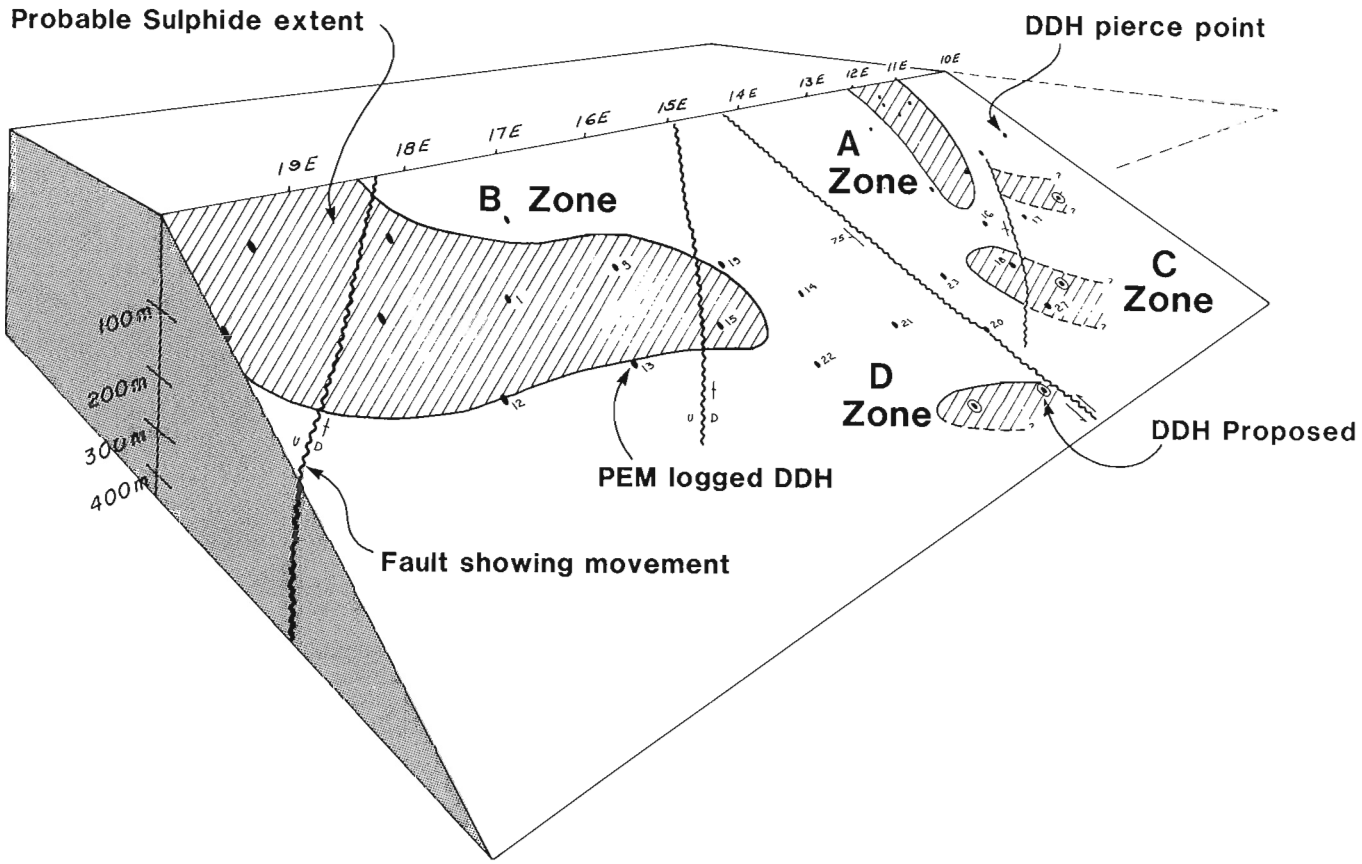

Figure 33.1. *Outline of sulphide zones in plane of ore horizon based on 1982 data Eastmain River area, Quebec.*

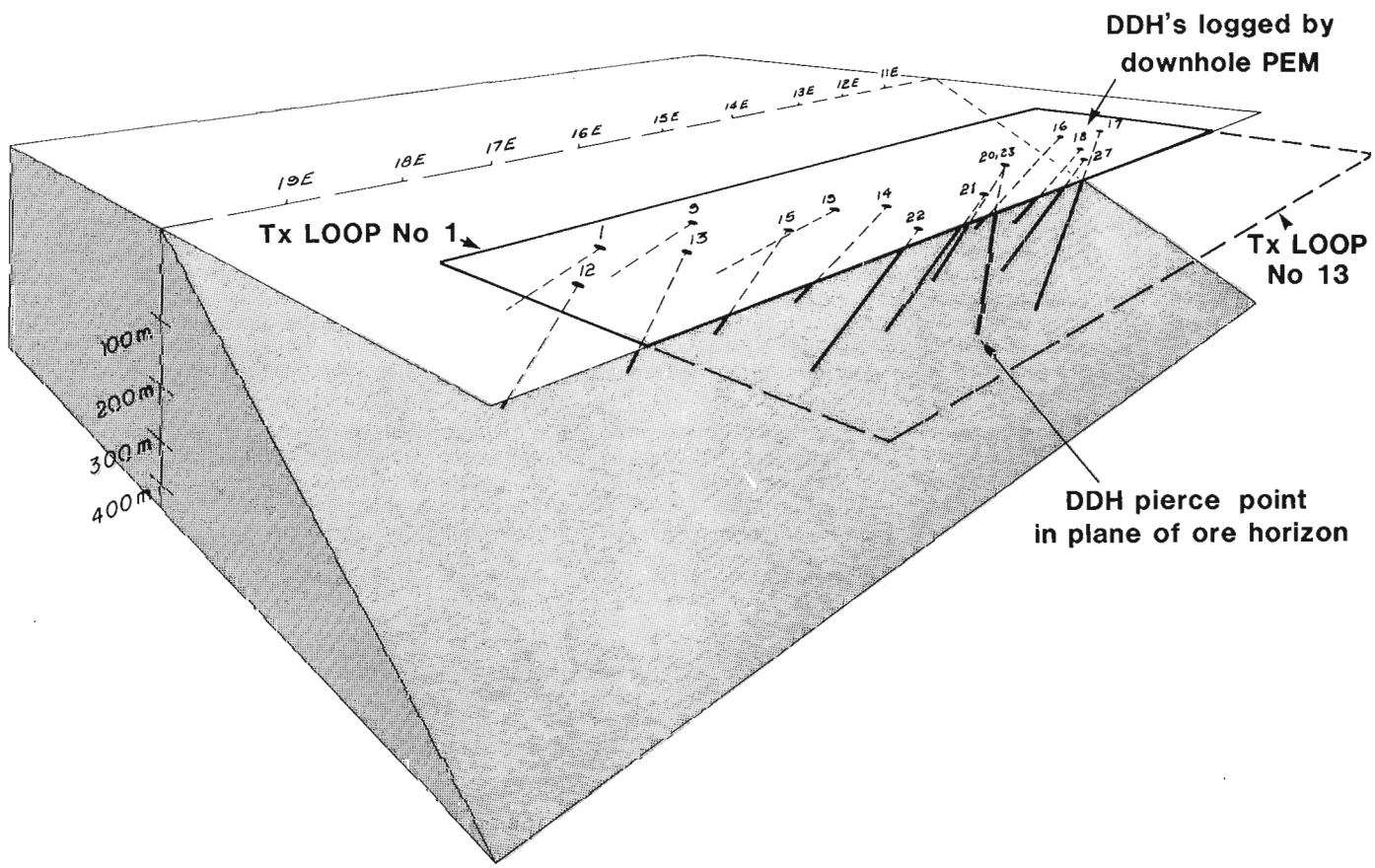

Figure 33.2. *Schematic showing transmitter loop locations relative to the diamond drill holes (DDH) for the Eastmain Project.*

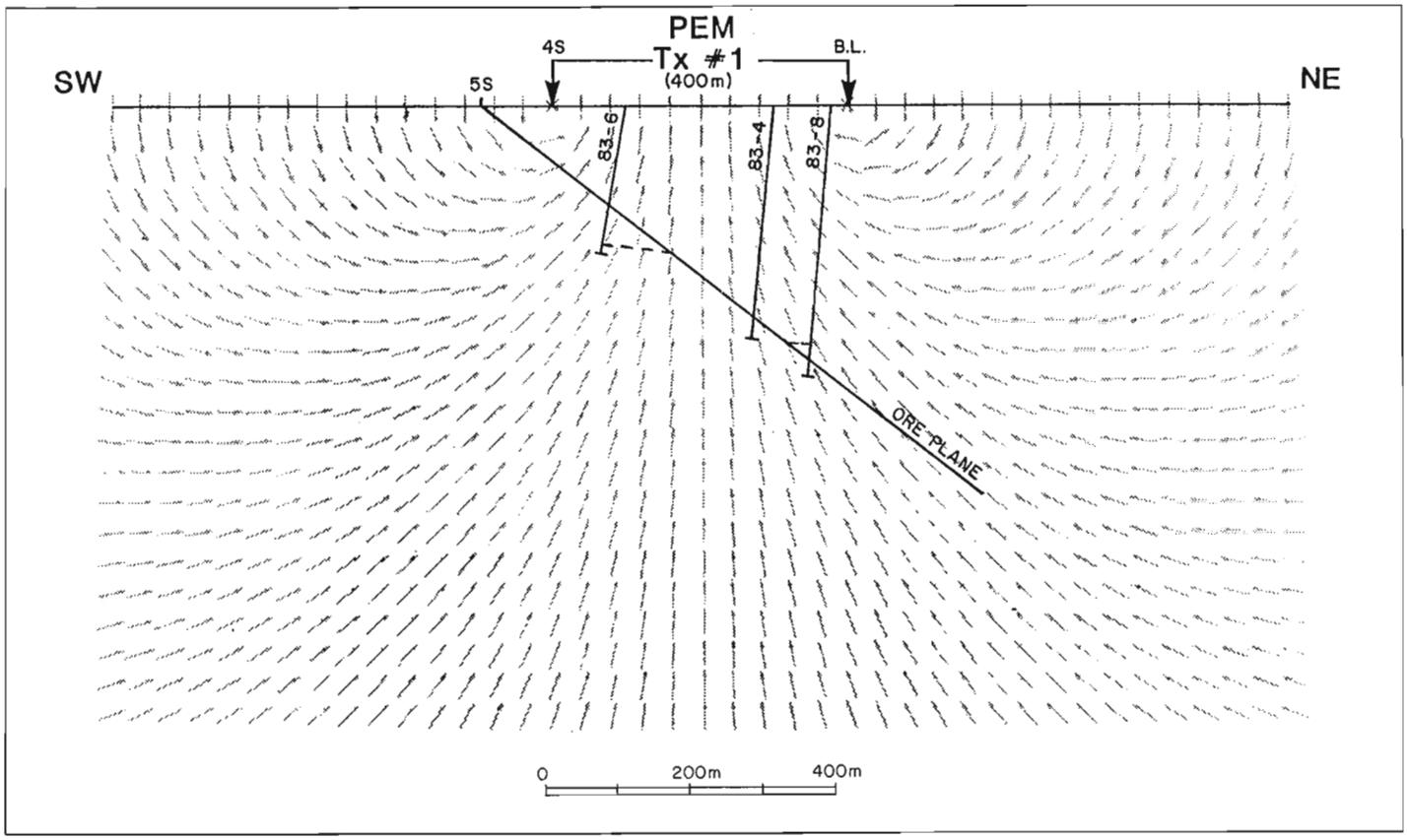

Figure 33.3. Typical pulse EM section showing transmitter no. 1 (Tx no. 1) and coupling of the field lines with the ore plane.

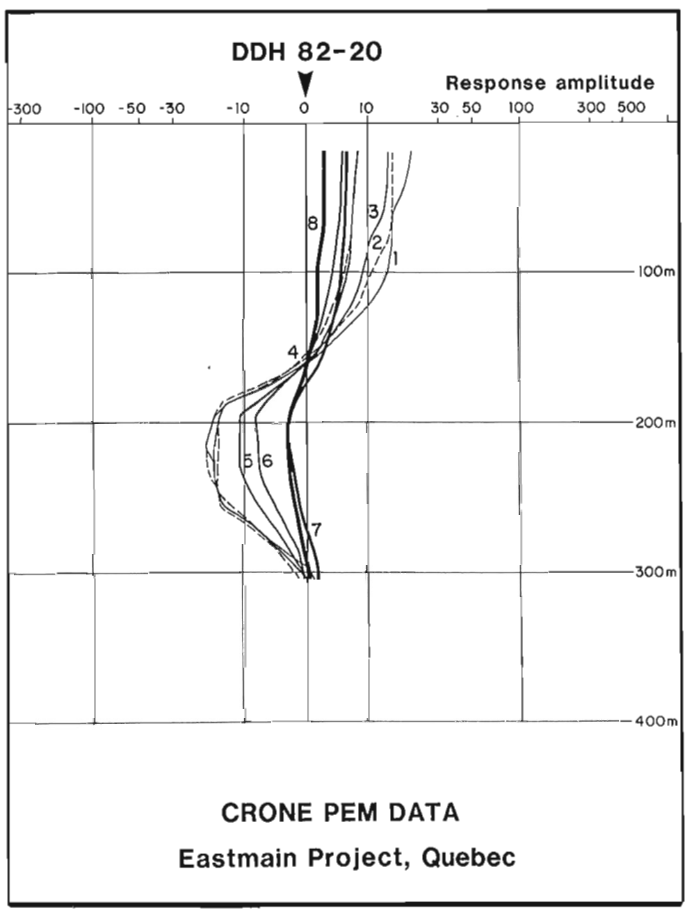

Figure 33.4. Downhole Crone pulse EM data for hole 82-20 using Tx no. 1 and a gain of 100.

Eastmain River, Quebec

On the Eastmain River in northern Quebec, the first small intersection of pyrrhotitic sulphides made relatively near-surface, based on conventional ground EM follow-up of an airborne survey, has led to further exploration because it was determined that these sulphides persistently carry grade-gold wherever they occur. The problem was that, although there exists a consistency to their geological setting, the sulphides form pods of irregular outline and apparently erratic distribution, and the drilling of them increasingly became a matter of guessing their shape and extent. At shallow depths pattern drilling could be justified as essential to defining the limits of the occurrences, but with increasing depth escalating costs demanded a greater degree of predictability.

After the completion of 27 holes in 1982, 21 of them aimed at defining the main zone (Fig. 33.1), it was clear that there exists a fairly direct relationship between sulphides and gold: the heavier the sulphides and larger their width, the greater the probability of an ore grade intersection. In order to map sulphides at depth downhole pulse EM logging of the accessible holes was undertaken.

Most of the surveying was carried out using a 400 x 800 m transmitter loop (Tx no. 1) laid out to encompass all the target holes (Fig. 33.2). A second loop (Tx no. 13), of similar size but placed adjacent to the downdip side, was used to reduce ambiguities in interpretation of Tx no. 1 responses. The primary loop Tx no. 1 was particularly cost effective, having a high transmitter power, a high vertical penetration, and for the middle range of depths at least, a reasonably uniform coupling (Fig. 33.3).

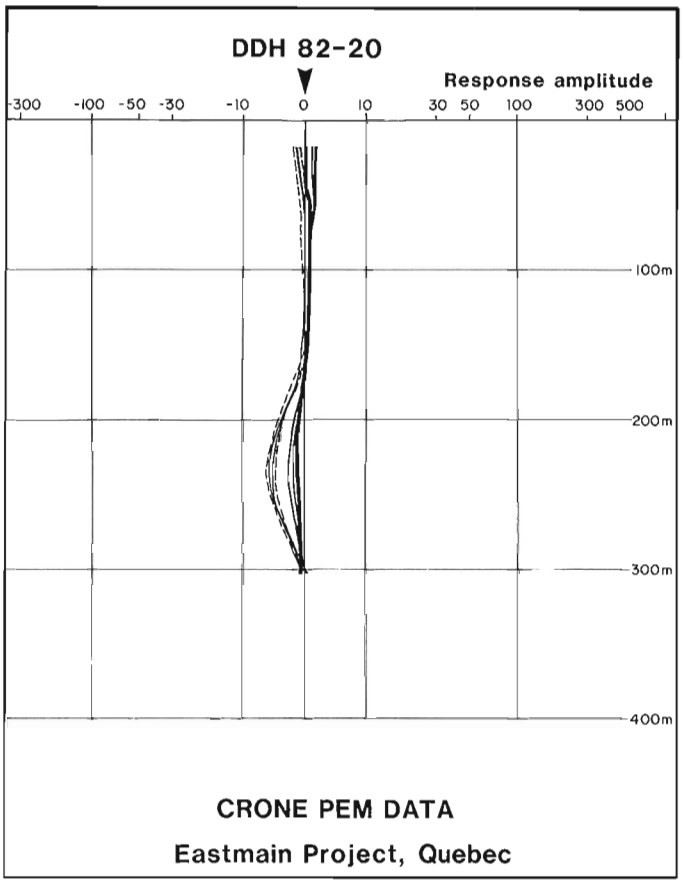

Figure 33.5. PEM results in hole 82-20 using Tx no. 13. (Same gain as in Figure 33.4)

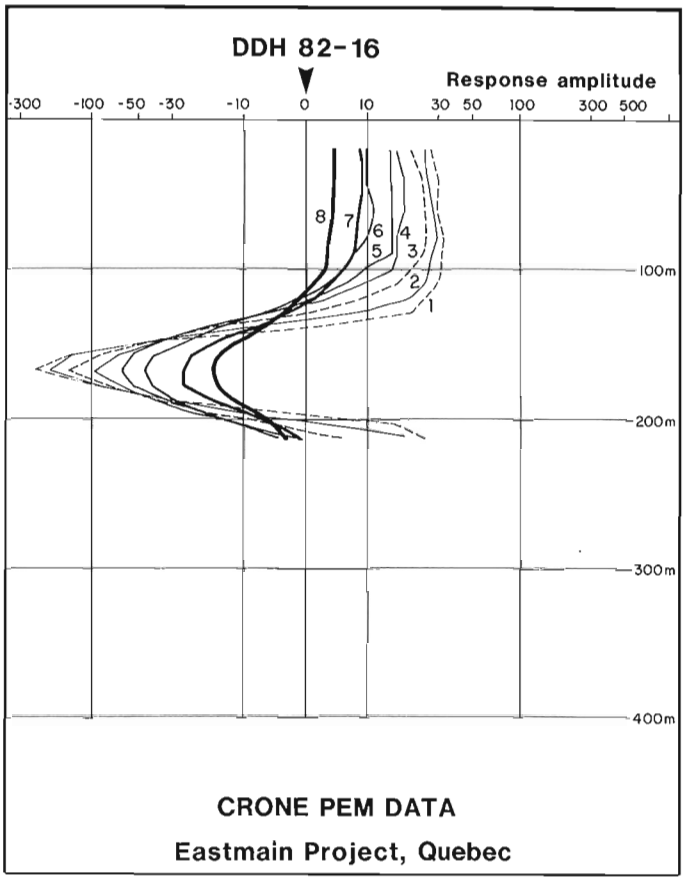

Figure 33.7. Downhole PEM data for hole 82-16, Tx no. 1, and gain of 100.

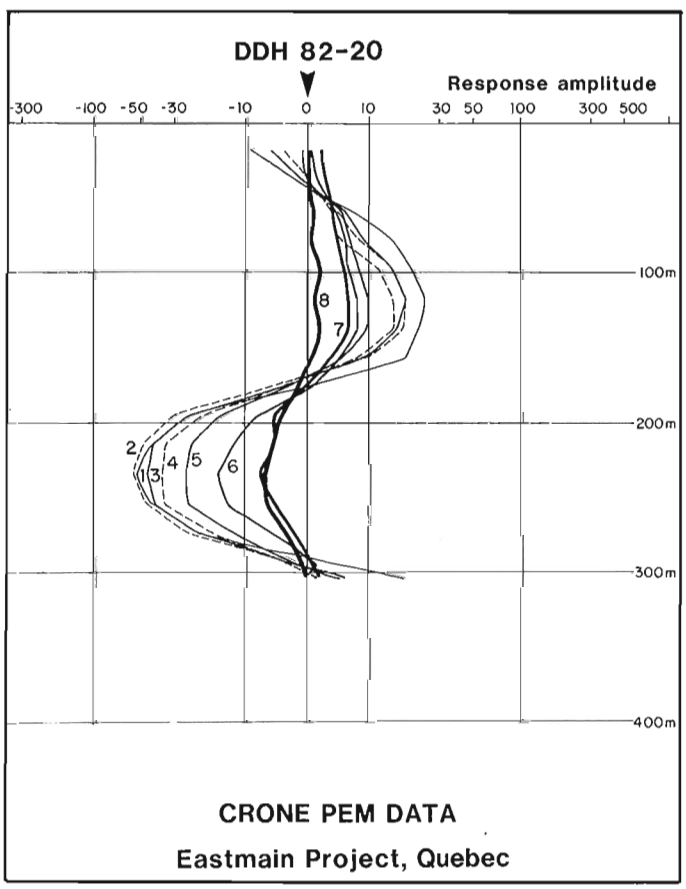

Figure 33.6. PEM results as in Figure 33.5 but with gain of 1000.

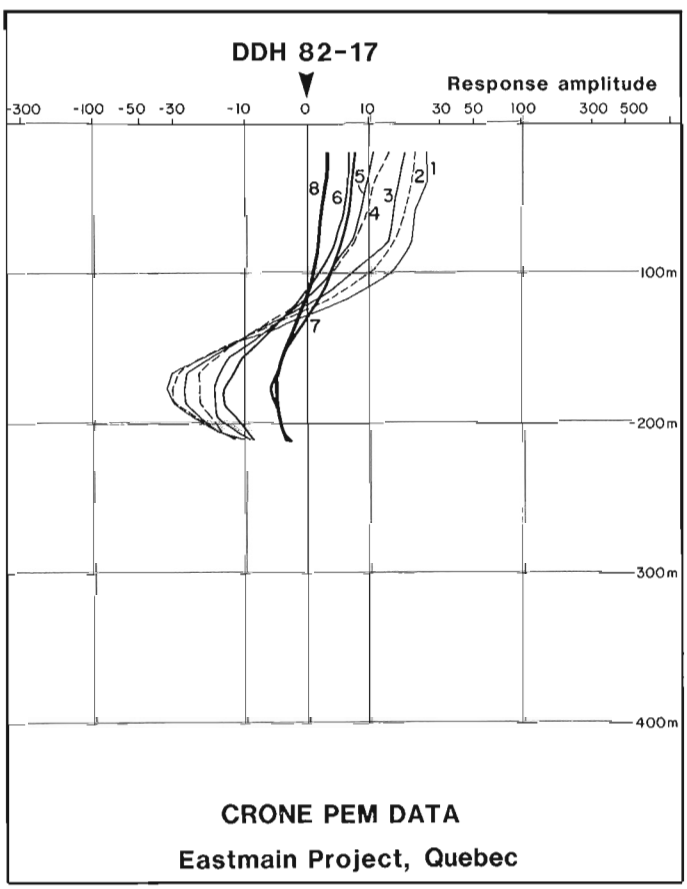

Figure 33.8. Downhole PEM data for hole 82-17, Tx no. 1, and gain of 100.

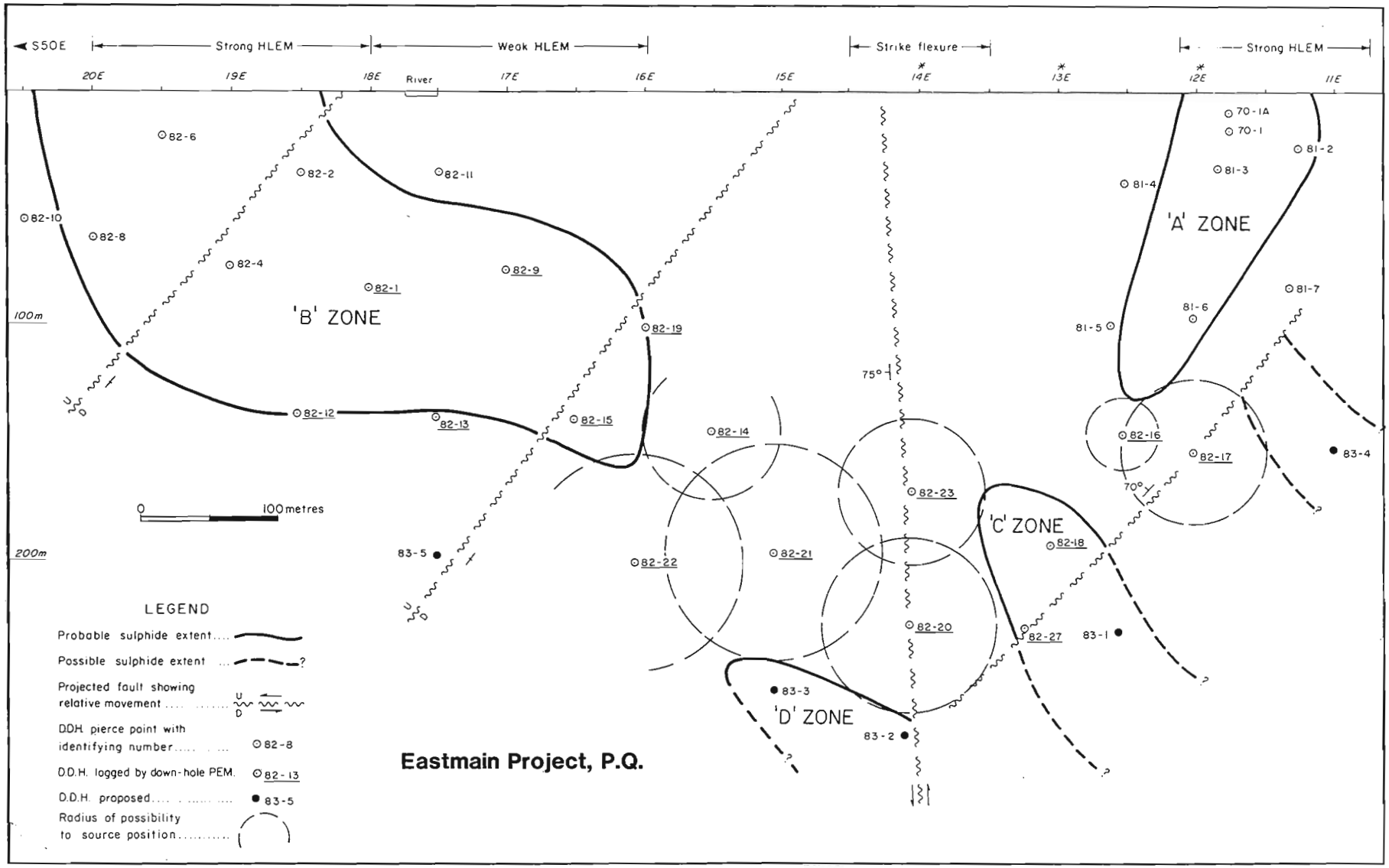

Figure 33.9. *Interpreted position of a sulphide occurrence called Zone "D", relative to the boreholes in the Eastmain Project.*

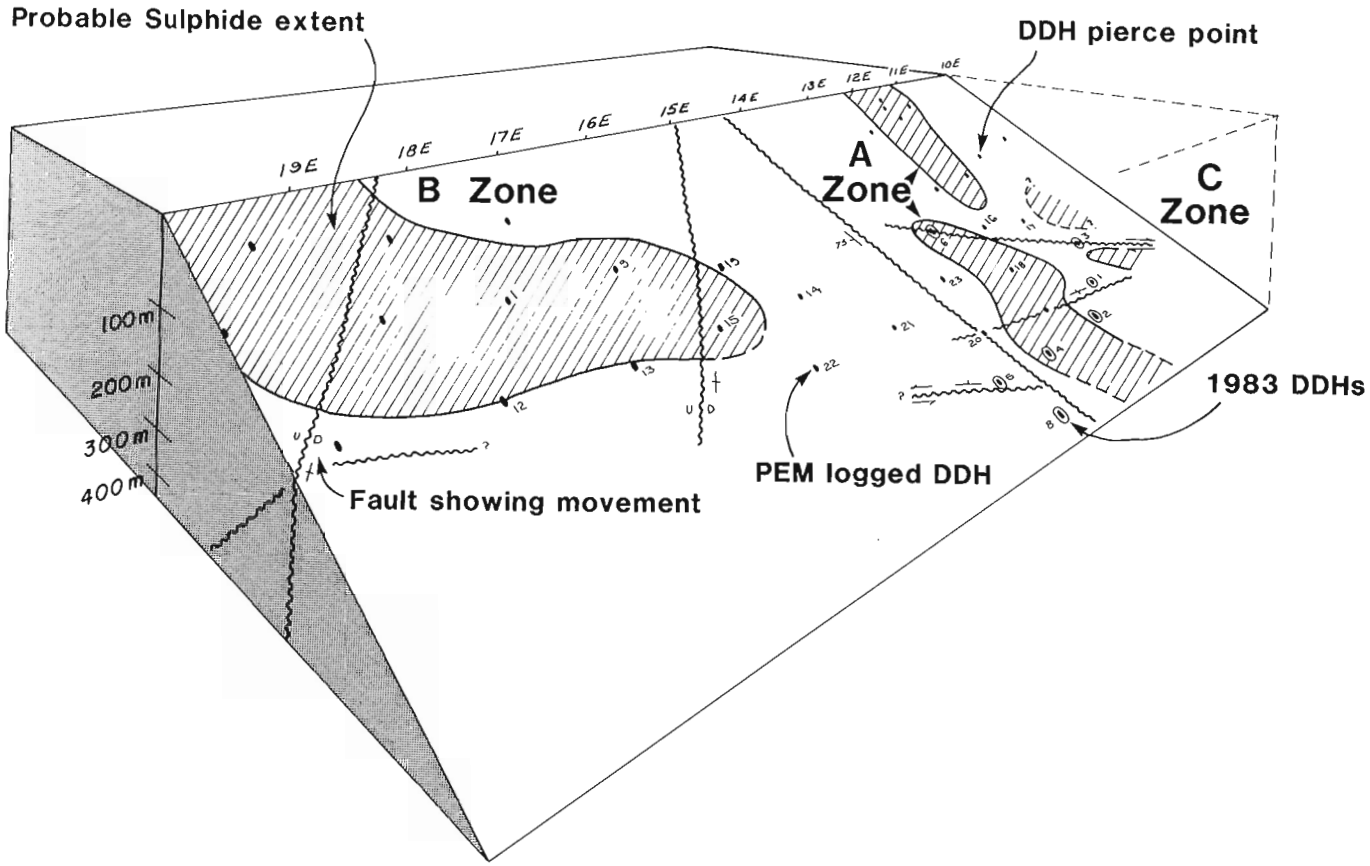

Figure 33.10. Outline of sulphide zones in plane of ore horizon amended to include 1983 data, Eastmain River area.

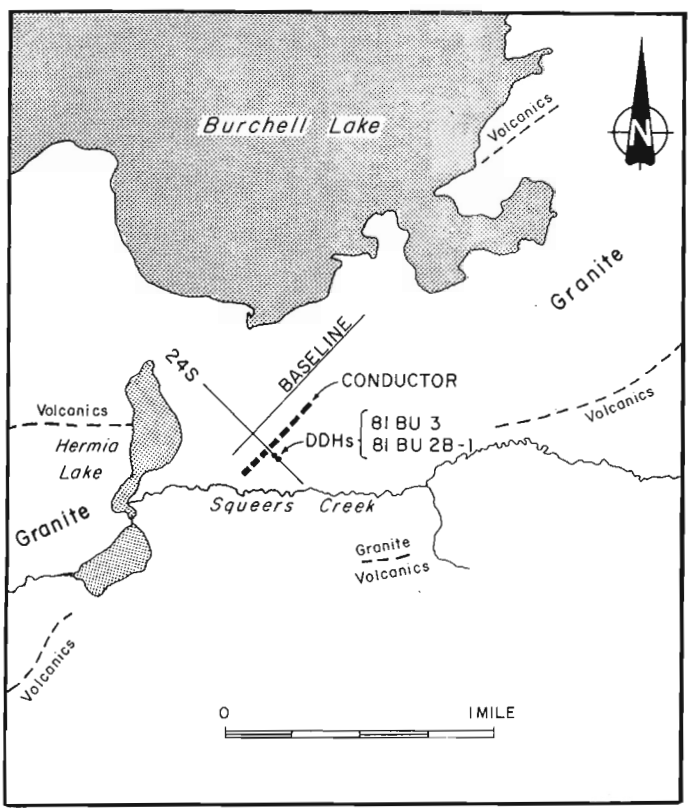

Figure 33.11

Burchell Lake area, Ontario showing locations of downhole pulse EM study.

What is significant about this mineral environment from the geophysical point of view is that the sulphides are restricted to a single, recognizable stratigraphic level and also there is no other conductive material in the host succession. By the end of the 1982 drilling, the plane of the sulphides was found to dip from 35° to 45° to the northeast, and the pods themselves had a thickness of 1 to 5 m. For the EM probe, they represented thin conductive sheets laterally separated by substantial sections of highly resistive material. Based on this information it was possible to interpret the recorded downhole EM responses. It is, of course, a paradox of borehole surveying that the most barren exploration holes are often the best for EM logging purposes. In this case, hole 82-20, which failed to intersect the target mineralization between the 'A' and 'B' zones, yielded the most information for predicting new extensions. The downhole EM log (Fig. 33.4) is dominated by an offhole anomaly that peaks 25 m lower than the geologically projected ore-plane pierce-point. It is nevertheless an unusually flat-topped anomaly, atypical for the environment and not at all like what might be expected from a sheet source. It in fact reflects faulting which, while recognized, was not at the time fully understood. Thus, a second log from Tx no. 13 with its improved coupling at this depth was needed to establish the peak position with more certainty (Fig 33.5, 33.6). Figure 33.5 is included to provide a comparison with Figure 33.4 at the same gain setting.

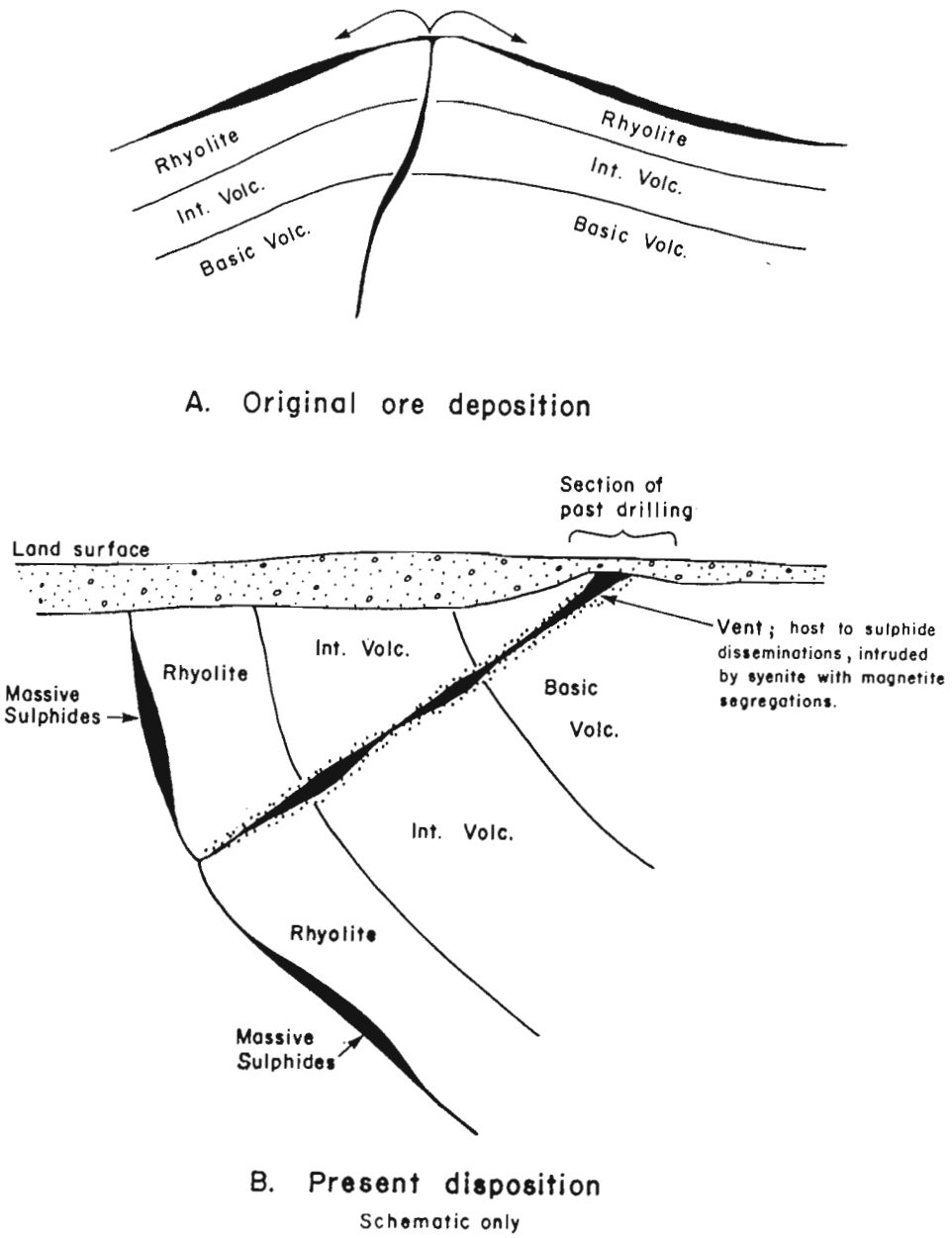

Figure 33.12. *Hypothetical ore occurrence for the Burchell Lake area, as depicted in relation to an overturned volcanic dome.*

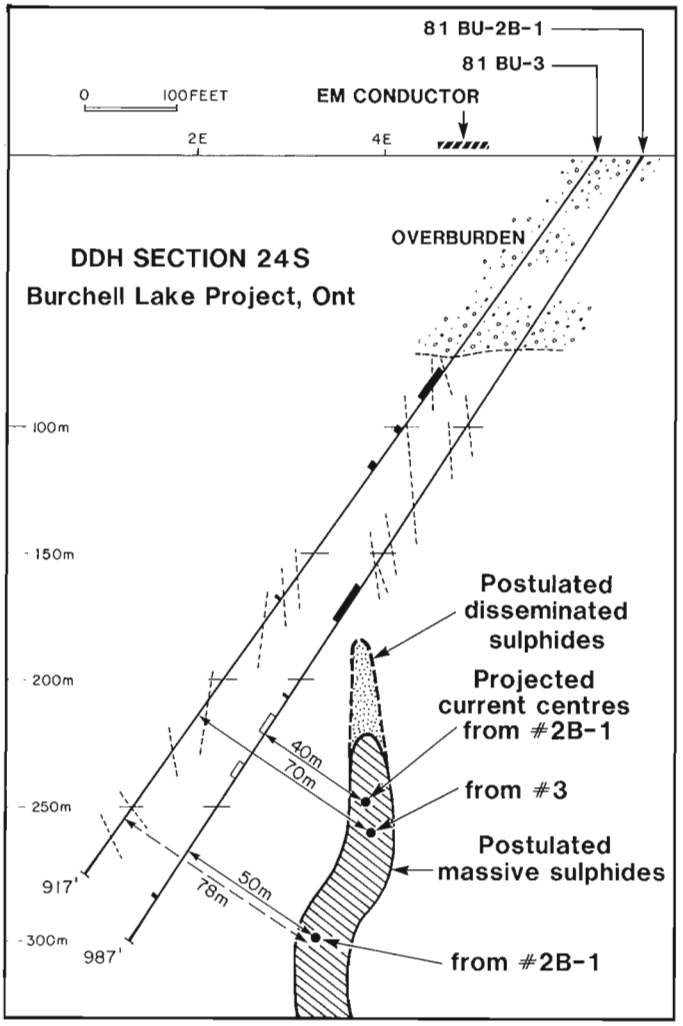

Figure 33.13. Section 2400S, Burchell Lake project, showing the two closely spaced, subparallel boreholes investigated with downhole PEM.

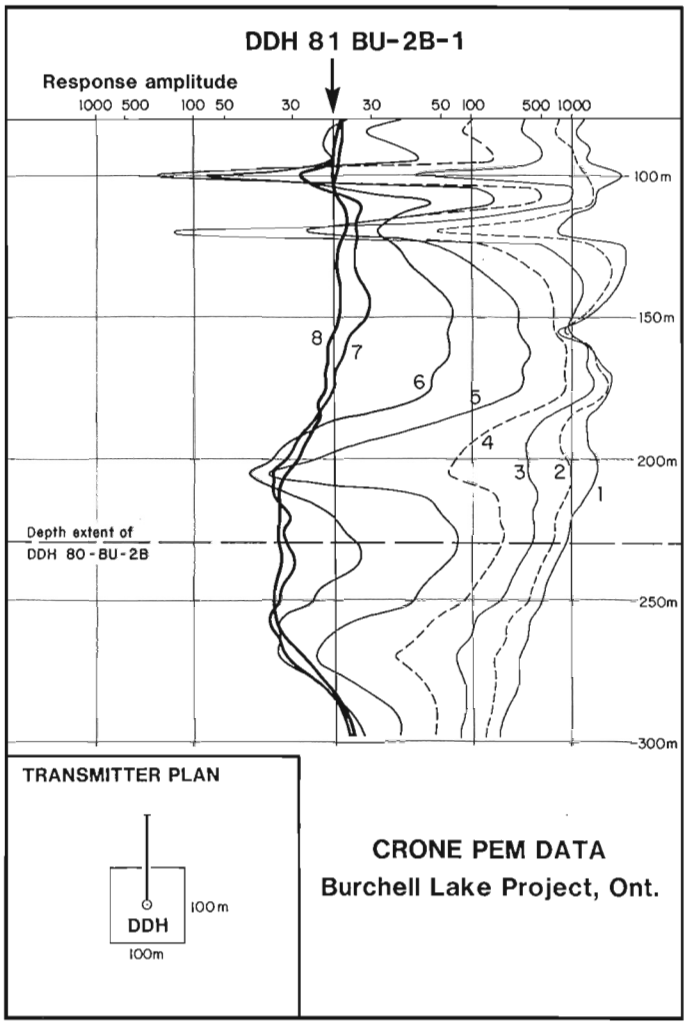

Figure 33.14. Results of Crone PEM logging of hole 81BU-2B-1. Note transmitter loop location centred around the drill collar for comparison with Figure 33.15.

By this stage in the investigations, it had become possible to estimate what fall-off rates might apply for a response from an offhole source in this setting. For instance, logs from holes 82-16 and 82-17 (Fig. 33.7, 33.8) show clean, single-peaked offhole anomalies at approximately the level where the holes pierce the ore-plane. These anomalies can be reasonably interpreted as due to the same source, viz. the bottom extremities of the upper 'A' zone sulphides as defined by drilling. If distances of 28 m and 55 m respectively to the common current centre are assumed, then it is observed that the channel 1 anomaly response falls off with distance according to an inverse cube law. This is reasonable in view of the limited size of the 'A' zone. As a consequence, more confident estimates could be made of the location of any new source recorded in the logs. Thus, in DDH 82-20, the displaced peak and the amplitude of the offhole anomaly allowed the prediction of a further significant sulphide occurrence at least 50 m below previous drilling in the ore-plane. This was the principal conclusion to emerge from the first-stage logging at Eastmain. This new source was labelled the 'D' zone. On the basis of hole 82-20 and nearby holes 82-21 and 82-22 (both barren holes) zone 'D' was conjectured to be positioned as shown in Figure 33.9.

Subsequently, two holes (83-4 and 83-5) were drilled to test the validity of this interpretation. The first hole successfully intersected a zone of semi-massive sulphides, containing a 5 m section of high grade ore, at a depth of approximately 340 m. As a result of this hole in particular, as well as companion drilling in early 1983, the at-depth sulphide distribution was amended to show extensions to the 'A' zone; however, the downdip limits are still open (Fig. 33.10).

Burchell Lake, Ontario

A problem of a different kind arose at Burchell Lake in the Shebandowan volcanic belt which runs west from Thunder Bay, Ontario (Fig. 33.10). There, a sequence of intrusive volcanic rocks and sediments disappears under a cover of gravels 65 m thick. Near the edge of the cover a dyke-like porphyry intrusion intrigued early explorationists because it carries a rather consistent 0.3% Cu over widths of 40-50 m. It has been drilled repeatedly but no higher grade sections have been found. It is the present thesis that this intrusion occupies an old vent in an overturned volcanic dome and, consequently, that its mineral grade is consistently low.

What is seen to be far more important is the possibility that stratiform volcanogenic sulphides were deposited on the flanks of the dome (Fig. 33.12).

A weak airborne (INPUT) EM anomaly had been detected on the posssible flank of the dome but either the anomaly was too weak and mediocre (1-7 mhos) to attract much attention, or the geology was not considered attractive. Early work by Noranda in 1965, and by Freeport Sulphur in 1971 had failed to locate economic mineralization. The third company to become interested was Gulf Minerals in 1979. However, they too were disappointed with their results and eventually (in 1982) relinquished their holdings. However, as part of their geophysical program, Gulf did carry out downhole EM logging of virtually all their drillholes. It is these logs which form the data base for the present discussion.

In section 2400S (Fig. 33.13), the first hole drilled by Gulf was targeted at the source of the horizontal loop EM anomaly which corresponded to the INPUT anomaly. It failed to encounter the expected near-surface, heavy sulphide mineralization. Instead, only weak stringers were intersected but the hole was continued to a coring depth of 229 m in the search for more information. Further scattered stringers of sulphides were intercepted but with decreasing frequency. Consequently, geological interest was directed to other, on-strike targets in the region.

Eventually this hole (no. 80-BU-2B) was logged by pulse EM, using five transmitter loops, 100 m square, grouped around the hole. Numerous anomalous responses, both offhole and inhole, from local sources were detected in the top half of all logs. There was nothing very significant about any of this since it indicated that within the detection range of the system nothing much better could be expected in the way of mineralization than had already been revealed by drilling. However,in the bottom half of the log, an intriguing offhole anomaly was detected. Gulf, in fact, hypothesized that a sulphide body of some size lay vertically below the bottom of the hole. They also postulated that the source of the surface horizontal loop EM anomaly lay updip above the hole, squeezed in a 30 m space between the hole and the updip distance to bedrock surface. A long second hole was drilled to test this second possibility. Also, the first hole (now designated no. 81-BU-2B-1) was extended in depth. Thus, at the end of the second summer of drilling on section 2400S, there were two subparallel holes, no more than 20 m apart, drilled to a depth of approximately 290 m (Fig. 33.13). To a downhole EM investigation, this represented a unique and golden opportunity: the chance of measuring in-depth the response from an offhole source (or sources) from two traverses marginally apart. Gulf extended their downhole pulse EM surveying to both the second hole and the extension of the first.

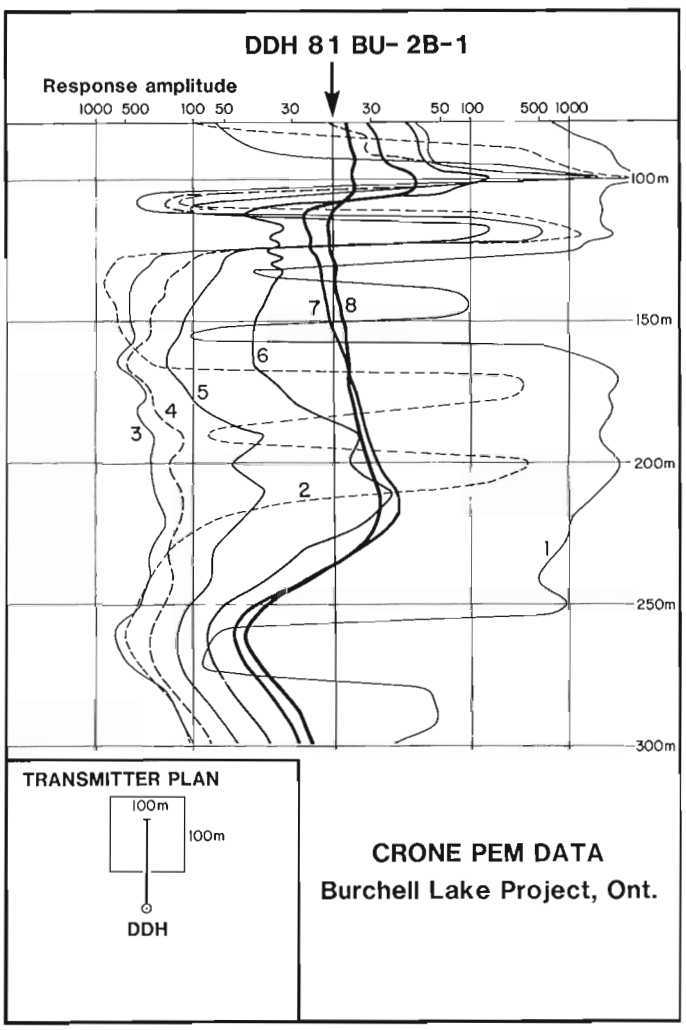

Figure 33.15. *Downhole Crone PEM data as in Figure 33.14 but with transmitter loop moved updip of hole 81BU-2B-1.*

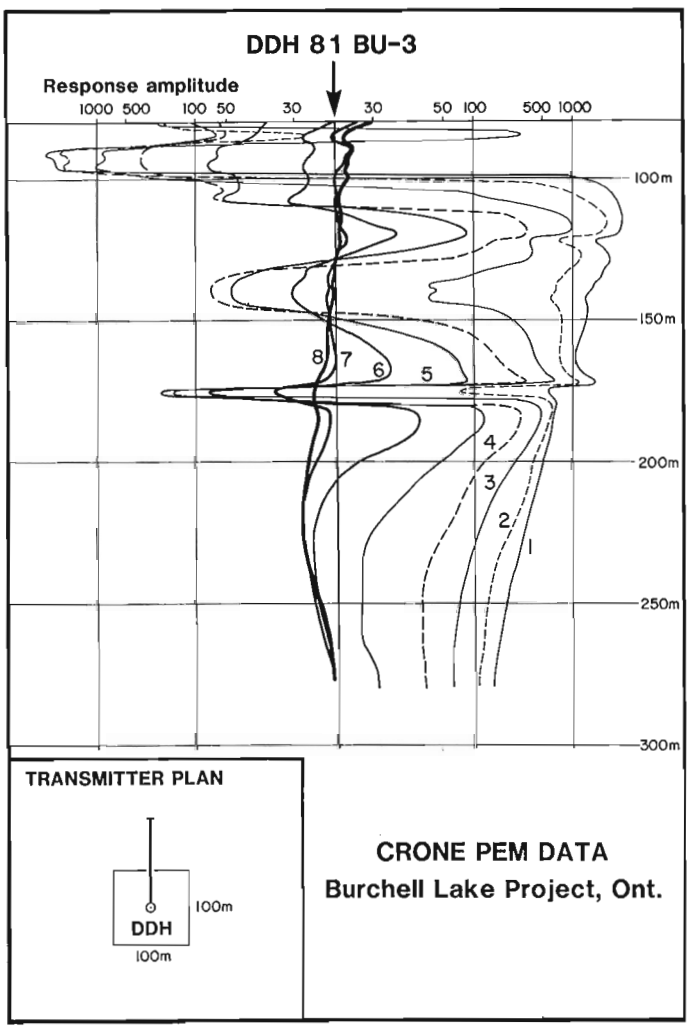

Figure 33.16. *Downhole Crone PEM data for hole 81BU-3, transmitter loop centred on the borehole collar.*

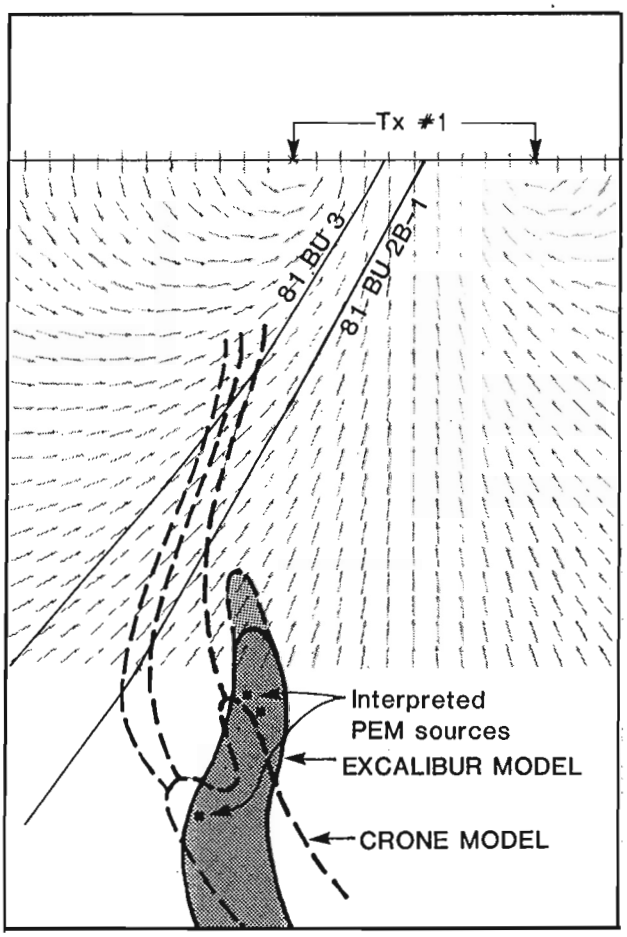

Figure 33.17. Two independent interpretations of the downhole PEM data showing their basic similarity.

The results obtained in this second stage logging of hole 81-BU-2B-1 are shown in Figure 33.14. First, it ought to be noted that for the same transmitter loops, the profiles in the upper portion of the hole closely duplicate the results of the previous survey. Secondly, the broad anomaly at depth on the later channels now has a lower edge, thus making its definition complete. This anomaly can be interpreted as being due to a single body 65 m wide and flat-topped, or to two separate sources 65 m apart and roughly parallel with each other. The first interpretation is preferred because the large, cohesive late time responses (channels 7 and 8) imply a source that is large, extensive and well removed from the hole. However, for the source body to be a uniform distance from the hole, even a relatively short section (viz. 35 m), requires that the body be folded. Fortunately, the core angles measured in the two holes allow for the possibility of such folding (Fig. 33.13).

When the transmitters were located in the other four quadrants, the most interesting results came from the transmitter loop updip of the hole (Fig. 33.15). Here, with the primary excitation directly over the sulphides and supplying maximum field strength, all the small stringers and the disseminated zone(s) above the main zone show strong responses. It was this result in the first logging of this hole that led Gulf to conclude that above the hole there exist more sulphides than had been seen in the core.

The second hole (no. 81-BU-3) was logged from the same transmitter locations as for the first. It is immediately evident from the collar central case (Fig. 33.16) that the amplitude of the anomaly from the deep source is about half what it was in hole 81-BU-2B-1. Thus, the source must be to the east of the holes. Moreover, the fall-off in response from the first to the second hole allows a determination of distances to current centres because, as the same transmitter loop was used, the current centres must be identical. Finally, it is noticeable that there is only one anomaly peak. The second one, 40 m deeper, is not detected in this more removed and slightly flatter hole. On the assumption that a rough inverse cube law is again operative (determined for channel 8 amplitudes in this case), it is projected that the deeper current centre lies in excess of 78 m from this second hole. Combining this with indications from the lateral transmitter locations that the source feature plunges to the northeast it is postulated that the source is a body of massive sulphides, up to 15 m wide, open at depth, conformable with the host volcanic succession and located at vertical depth of more than 226 m.

This situation is extraordinarily interesting for a venture group prepared to drill deep on the basis of geophysics. Two exploration companies have seriously considered the possibilities and both, quite properly, wanted to check out the Gulf data before proceeding. In the first case, Duncan Crone of Crone Geophysics Ltd., the manufacturer of the equipment employed, and a well-known practicing geophysicist, was called in to undertake an independent interpretation. As can be seen in Figure 33.17, although his interpretation differs in detail from the preceding Excalibur model the main features of the two models are encouragingly similar. Still, in the end, it was the second exploration group who consummated a deal. They did so after undertaking their own downhole EM logging to verify the Gulf data. Their results were so close a fit, and so indicative of massive sulphides according to their experience, that they acquired an option on the property.

This is where things stand now. Unlike many histories of exploration, this is not an account of how wise one can be after the event. It is instead a progress report; indeed, the eventual outcome of this geophysically defined bet at depth, yet belongs very much to the future.

Acknowledgments

The support and permission of Placer Development Ltd., and of Julian Boldy in particular, to pursue and present the Eastmain data are gratefully acknowledged, as also are the help and co-operation received from Corporation Falconbridge Copper, Mike Knuckey and Barry Simmons specifically, and from the late Harold Hauf of Belore Mines to present the Burchell Lake material.

34.

A BOREHOLE ELECTROMAGNETIC SURVEY OF THE SOUTH BAY MINE, ONTARIO

Laurie E. Reed[1]

Reed, L.E., A Borehole Electromagnetic Survey of the South Bay mine, Ontario; in Borehole Geophysics for Mining and Geotechnical Applications, ed. P.G. Killeen, Geological Survey of Canada, Paper 85-27, p. 307-322, 1986.

Abstract

In 1979, Selco Mining Corporation's South Bay mine in Ontario was nearing the end of its mineral reserve. The orebody, which had been discovered by airborne and ground electromagnetic methods, consisted of lenses of massive sulphides (chalcopyrite, pyrite and sphalerite) which were for the most part electromagnetically conductive. In an effort to find new ore lenses, electromagnetic surveys were conducted in drillholes collared underground in the mine. A Crone Pulse EM instrument was used for these surveys.

The main part of the survey was undertaken using a 400 foot by 800 foot (122 x 244 m) transmitter loop which was laid out on the surface over the hanging wall of the orebody. A few deep holes were later surveyed with a higher power transmitter using a 1600 foot (488 m) square transmitter loop.

Eighty-five holes, all those accessible in the mine, were surveyed. Many of these holes were horizontal in attitude, so a procedure was devised to manually push the borehole probe into the holes. The length of survey in these holes was limited by the mechanics of the system and the strength of the operators. It was found that holes could be effectively surveyed to depths of greater than 2000 feet (610 m) from surface using the small transmitter. The larger transmitter was used to survey the deeper holes; one to a depth of 3550 feet (1083 m).

A number of offhole anomalies were seen in the initial survey. These were subsequently drilled using the EM response as a guide. While no new mineable ore was found, the surveys did find new sub-ore sulphides missed by previous drilling. As well, the surveys provided some confidence that no orebodies lay undetected near the developed parts of the mine.

The mine was closed in 1981 after a production life of 10 years.

Résumé

En 1979, la mine South Bay, que la Selco Mining Corporation exploite en Ontario, était en voie d'épuiser sa réserve de minerai. Le corps minéralisé, découvert au moyen de levés électromagnétiques aériens et de surface, consistait en des lentilles de sulfures massifs (chalcopyrite, pyrite et sphalérite) dont la plupart étaient bonnes conductrices électromagnétiques. Afin de trouver de nouvelles lentilles de minerai, on a effectué des sondages électromagnétiques à partir de trous de sondage souterrain commencés à la mine. Une sonde électromagnétique Crone Pulse a été utilisée à cette fin.

L'étude a été effectuée, en majeure partie, à l'aide d'une boucle de transmission de 400 pi sur 800 pi (122 m x 244 m) disposée à la surface, sur le toît du corps minéralisé. Ensuite, quelques trous profonds ont été sondés à l'aide d'un émetteur plus puissant utilisant une boucle de 1 600 pi carrés (488 m carrés).

Tous les trous accessibles de la mine, soit 85, ont été sondés. Vu qu'un grand nombre de ces trous avaient une orientation horizontale, les exécutants ont conçu une façon de pousser manuellement la sonde de fond dans les trous. Les sondages effectués dans ces trous ont été aussi étendus que le permettaient les possibilités mécaniques du système et la force des exécutants. Les résultats ont indiqué que l'on peut effectuer des sondages efficaces à des profoneurs supérieures à 2 000 pi (610 m), à partir de la surface, au moyen d'un petit émetteur. L'émetteur plus puissant a servi au sondage des trous plus profonds, dont l'un avait une profondeur de 3 550 pi (1 083 m).

Un certain nombre d'anomalies ont été repérées aux environs des trous au cours des premiers travaux de sondage. Les zones en question ont été forées selon les résultats des sondages électromagnétiques. Bien qu'aucune autre quantité de minerai exploitable n'ait été découverte, les sondages ont permis de découvrir de nouveaux dépôts de sulfures non exploitables de façon rentable qui avaient échappé aux sondages précédents. L'étude a également confirmé qu'aucun corps minéralisé ne se trouve à proximité des parties exploitées de la mine.

La mine a été fermée en 1981; elle avait produit du minerai pendant dix ans.

[1] Selco Division, BP Resources Canada Limited

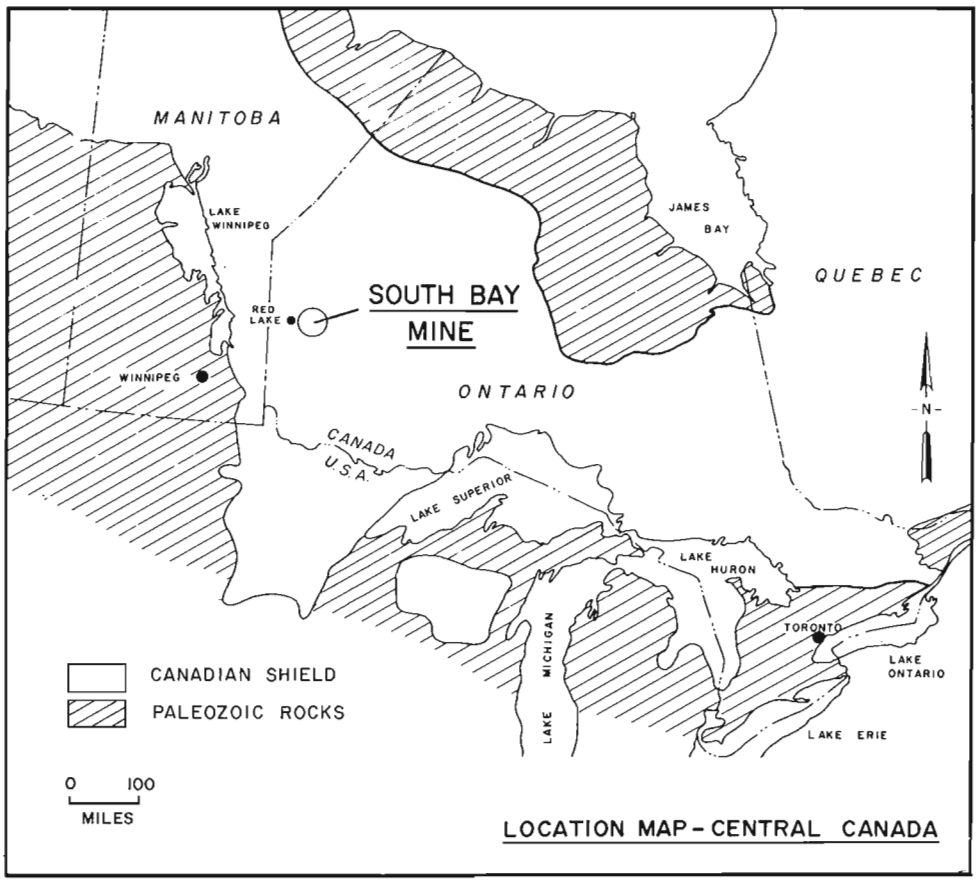

Figure 34.1. *Location of South Bay mine, east of Red Lake.*

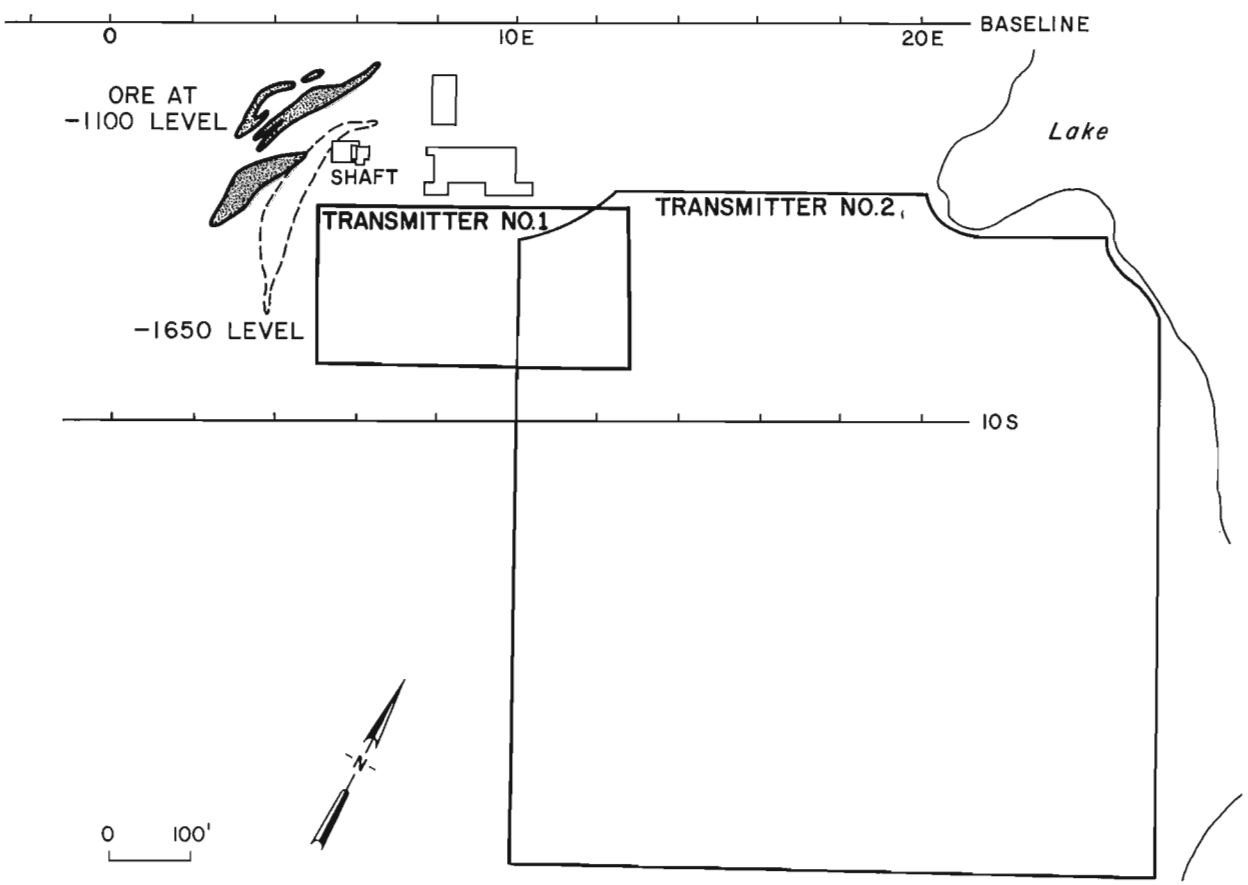

Figure 34.2. *Location of the Pulse Electromagnetic (PEM) transmitters on the South Bay mine grid.*

Introduction

The South Bay Mine is located in volcanic rocks of the Canadian Shield in Northern Ontario (Fig. 34.1). Its discovery by geophysics and its geology have been described by various authors (Auston, 1969; Pollock et al., 1972; Reed and Auston, 1973; Thurston et al., 1978; Wan and Warburton, 1979). Briefly, the deposit consisted of a series of massive sulphide lenses, lying in hydrothermally altered quartz-feldspar porphyry and dacite, along the contact between unaltered quartz-feldspar porphyry and overlying rhyolite. Lenses of massive fine pyrite with interstitial chalcopyrite and finely banded to coarse massive sphalerite occurred with a vertically elongate attitude. The ore lenses were up to 200 feet (61 m) in length horizontally, 10 to 70 feet (3.21 m) wide and up to several hundred feet vertically. The rocks are overturned with the lenses dipping steeply to the east. With the exception of the massive sphalerite, the orebodies were highly electrically conductive, while the enclosing rocks were highly electrically resistive.

The orebody was discovered in 1968 using the airborne Mark V Input Electromagnetic System. The South Bay mine was brought to production in 1971 and ceased production in 1981 with 1.6 million tons of ore having a grade of 2.3% copper, 14.5% zinc and 3.5% oz. per ton of silver produced.

During the later years of production, exploration in the immediate mine environment was intensified with the purpose of finding additional ore to extend its life. Over the life of the mine many exploration holes had been drilled. These fanned out from the working area, testing the favourable geological contact laterally and vertically. It was recognized, however, that ore lenses of sufficient size to be mined could lie undiscovered away from, or between the exploration holes and that it would be useful to conduct an electromagnetic survey in the holes to test this possibility. A search out to 300 feet (92 m) from the drillholes using the electromagnetic system was thought to be adequate for this investigation.

All accessible holes in the mine were surveyed during 1979, using the Crone Pulse electromagnetic system (Crone, 1979b, 1980). The primary survey employed a low power system (480 W). Eighty-two holes, totalling 45 000 feet (13 725 m) in length, were surveyed in two months. A second survey, employing a prototype high power transmitter (2.2 kW), investigated 3 deep holes totalling 5170 feet (1577 m). Useful data were acquired 3550 feet (1083 m) from surface in the deepest of these holes.

Instrumentation and method

The Crone Pulse downhole electromagnetic system has been described elsewhere (Crone, 1979b). The system transmits a pulsed electromagnetic field from a loop laid out on surface. In this investigation the loop was 400 feet by 800 feet (122 x 244 m) for the low powered survey, and 1600 feet (488 m) square for the high powered survey (Fig. 34.2). The transmitted pulse for both systems has a peak current amplitude of 20 A, with voltages of 24 V for the low power system, and 110 V for the high powered system. The current waveform is rectangular, with a cycle of 10.8 ms on and 10.8 ms off. Voltages at the receiver were sampled in eight channels with mid points at 0.15, 0.30, 0.55, 0.90, 1.45, 2.40, 4.00 and 6.40 ms after the current shut off.

Both transmitter loops were laid out on the surface over the hanging wall of the orebody in the best possible location, taking into account the positions of surface installations. It was felt that good coupling of the transmitted field to the ore lenses was achieved. Although low incidence angles between the field and the target bodies must occur at the greatest depths surveyed, there did not appear to be any problems in recording secondary field responses in the cases where coupling was poorest. Good data were recorded from depths of 2000 feet (610 m) from surface, and adequate data were recorded from 3000 feet (915 m) using the low power system. The large loop provides better coupling to the deeper targets. This, and the higher power, assured good quality secondary field data to be read to 3550 feet (1083 m).

A timing wire carrying a signal to synchronize the receiver with the transmitter was run from the transmitter on the surface down the shaft (in the manway and an unused compartment) to the receiver, which was located at the collar of each hole being surveyed. Figure 34.3 shows a partial view of the three dimensional projection of the mine, with some of the working areas employed in this survey. Holes surveyed were located throughout the mine.

All holes surveyed were AX size. The hole diameter was 1.89 inches (4.8 cm), and as the probe diameter was 1.14 inches (2.9 cm) adequate space was available inside the holes for the probe to move. As most of the holes to be surveyed had a horizontal attitude, a mechanism had to be devised to push the receiver probe into the holes. Push rods were devised using ten foot lengths of rigid PVC one inch diameter water pipe, slotted along their length and moulded at their ends into male and female snap fit locking couplings. The slot was made to allow the entry of the probe-to-receiver cable. The receiver probe was manually pushed into

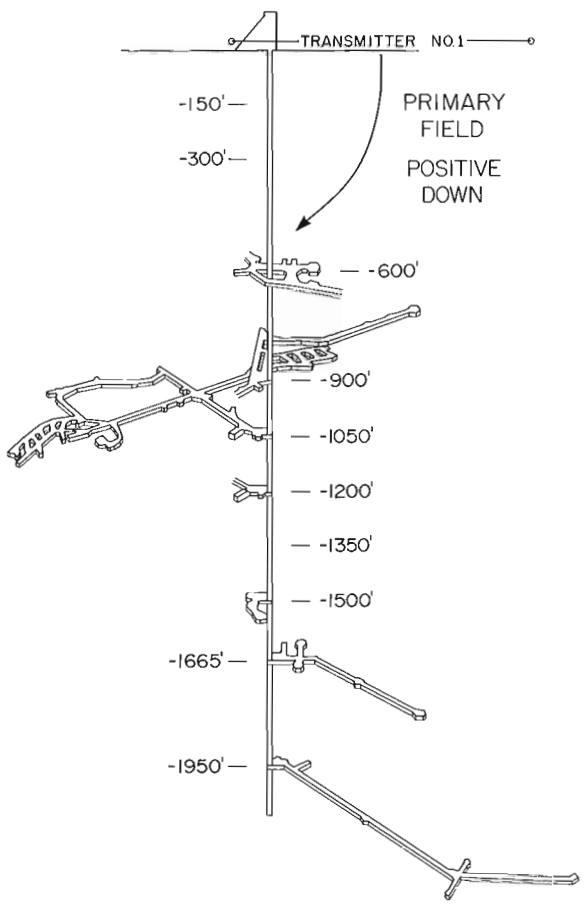

Figure 34.3. Pictorial three dimensional view of the area of interest at South Bay mine. The convention for the direction of the PEM field is shown.

the hole at the end of an assembly of these rods. Readings were taken at 30 foot (9.2 m) intervals, or less, in holes where the probe had to be pushed. In holes with inclinations greater than -30 degrees, the probe would slide under its own weight. In these holes the reading interval was usually 10 m (dictated by a metric cable length counter).

A variety of problems arose with the pushed probe operation, which limited the length of the survey in some holes. The friction between the push rods and the hole walls, especially later in the survey as the rods began to bow and weaken, was a major limiting factor. Dry holes were especially susceptible to high drag. Holes containing standing water were easier to survey. Holes with running water were difficult to work in, not only because the operator pushing the rods would often be under a steady stream of water, but also a head of water would build up against the probe and the push rods, which would prevent the probe from moving farther after a certain distance. High friction holes could be surveyed to a distance of from 400 to 700 feet (122-214 m), while low friction holes could be surveyed to 1000 feet (305 m). The major length limitation was the strength of the operator pushing and retrieving the rods; in addition, the plastic push rod assembly broke down under the pressure of pushing in the longer holes.

A dummy probe (steel bar) was lowered or pushed into all holes to be surveyed, to insure a clear hole for the more expensive receiver probe. The receiver probe was badly stuck on one occasion; sticking was probably due to small rock fragments falling off the hole wall. The probe was retrieved without damage with the assistance of a probe retrieving tool. One dummy probe was stuck and lost.

Data presentation

The results of the survey are presented in two ways. One way is shown in Figure 34.4, where a plot of the holes surveyed on the -900 level is shown with a profile of some of the data from these holes. In this case, hole SB662 shows responses for channels 1 and 8 while channel 1 responses are plotted for holes SB541 and SB677. Parts of some holes lying off the level are projected to the plane of the level in dashed form. On these plans will be seen the location of ore lenses (fine stippled), and interpreted sources (coarse stippled), as well as other geology of interest. Parts of the underground workings are seen in the plans. These can be referred back to the mine projection of Figure 34.3.

The other way data are presented is shown in Figure 34.5, where the eight channels of readings from the drillhole are plotted with separate zero levels in stacked profile form. A log-linear scale for the amplitude of the readings is shown in the figure. Profiles of the data are plotted horizontally across the page with negative down, positive up. Inhole electromagnetic data are more conventionally plotted in a vertical direction with negative to

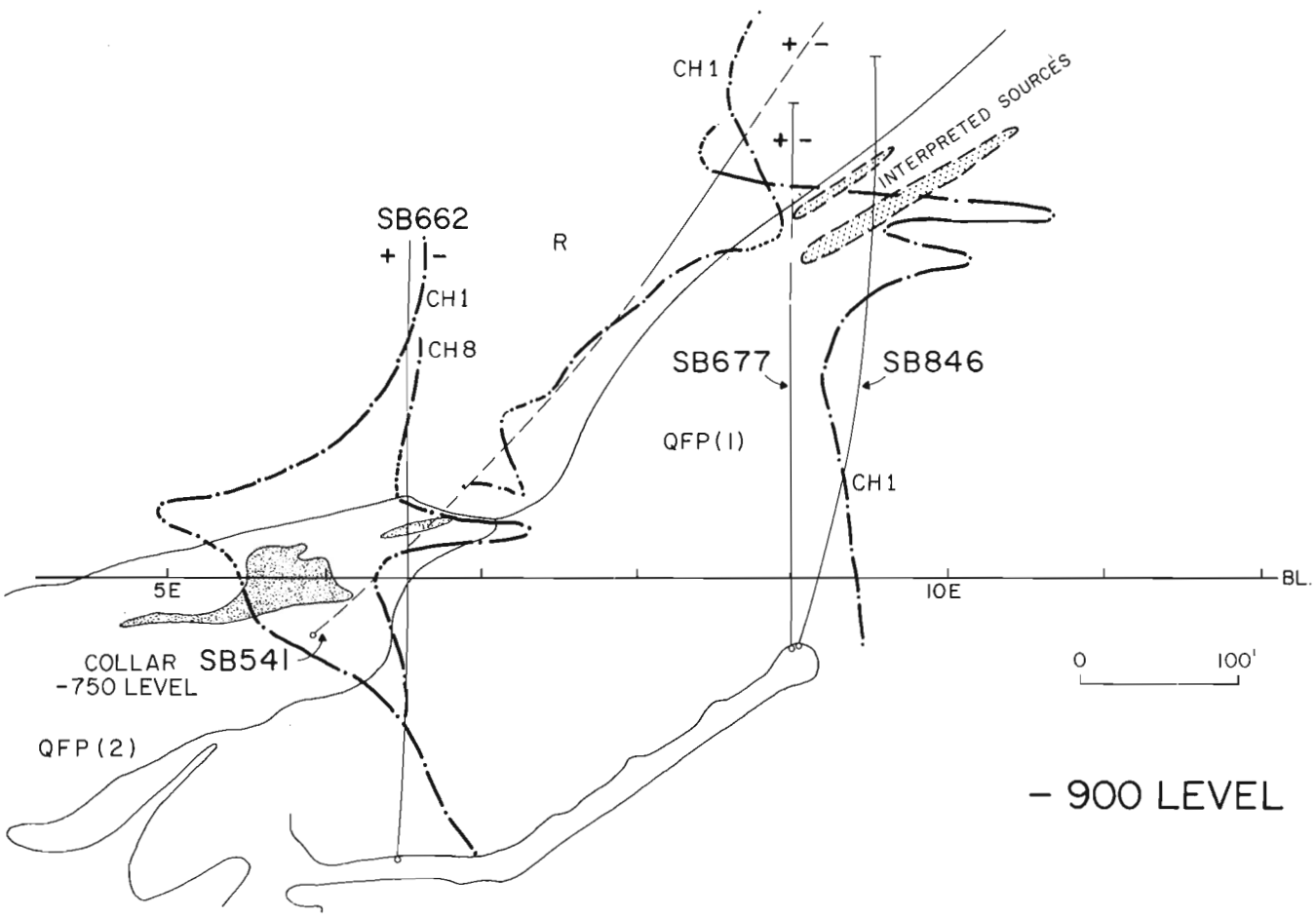

Figure 34.4. *-900 level. The line of the drillholes, along with their electromagnetic data profiles are projected to the plane of the level. Profile scale is in Figure 34.5. CH1 and CH8 are channels 1 and 8, R - rhyolite, QFP(1) - quartz-feldspar porphyry, QFP(2) - altered quartz-feldspar porphyry. Fine stippled units are massive sulphides. Coarse stippled units are bodies interpreted from the PEM data.*

the left. It is felt that the mode used here is more suitable for these data. The collar of the hole may be to the right or left in the figure depending on the orientation of the hole in the plan or section drawings.

Interpretation

The convention for the polarity of the field is defined as positive downward from the centre of the transmitter loop for the primary field, as drawn in Figure 34.3. The receiver probe was set upright inside the transmitter loop at the start of surveying to establish this calibration on the receiver. (Note this direction is the opposite of Macnae, 1980, which presents primary field directions for a variety of transmitter loops). As the transmitter was set to couple to ore lenses from the hanging wall side, then the secondary fields would be read as positive for a hole collared on the hanging wall side and passing through the conductor and away from the transmitter.

The polarity and strength of the secondary fields have been used to indicate the direction of those fields. The directions are identified by arrows on a number of the mine drawings including Figure 34.13. These field directions are qualitative, as only the component of the field strength axial to the hole is being measured. These field directions assist in locating the position and attitude of offhole bodies.

Readings were recorded at constant gain without normalizing to the primary field at the receiver. A log-linear channel amplitude scale is seen on each of the profile drawings. While these amplitudes are consistent within themselves in each hole and can reasonably be compared with nearby holes, amplitude comparisons of responses from sources widely separated in depth cannot be made as the primary inducing field will be different. This was not seen to be a difficulty as the most important consideration was to define the geometries of the source bodies derived from the shapes and dimensions of the secondary field profiles. The interpretation of the survey data from the South Bay mine was based mainly on matching these data with curves appearing in the thesis by Woods (1975). Interpretation nomograms from the thesis which indicate the size and distance of a body were also used. Three examples from the thesis are shown in this paper although many more comparisons were made in the overall interpretation of the survey. Subsequent to this study, several other papers on interpreting downhole electromagnetic data have been published (Woods and Crone, 1980; Woods et al., 1980; Dyck, 1981).

Only a few cases can be presented out of this very large survey. Few of the responses were simple, although in many approximate analogues of the Woods curves could be found. Some responses were made complex by multiple sources, while others appear complex from time-varying

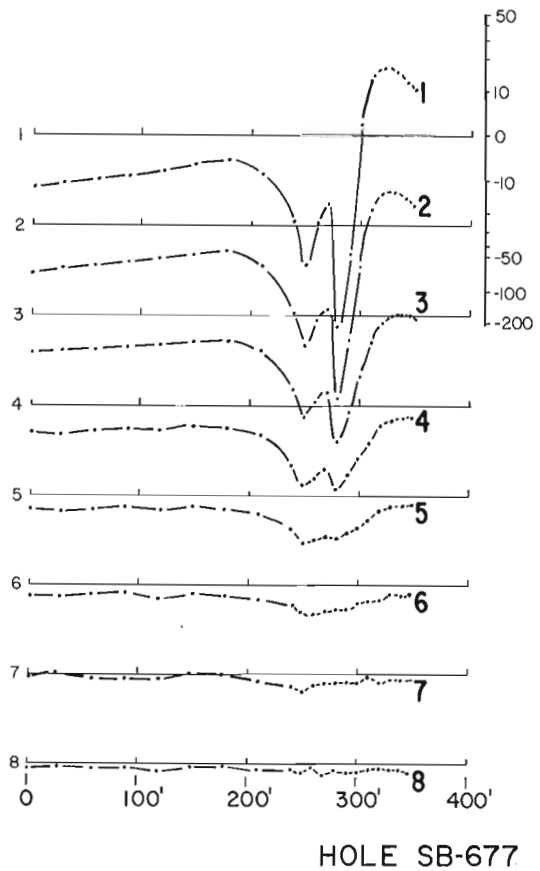

Figure 34.5. Hole SB677, PEM response profiles. Numbers 1 to 8 beside the profiles identify responses in each channel. The smaller numbers 1 to 8 identify the zero base level for each channel. For field data, the amplitude scale in the upper right hand corner is in arbitrary numbers derived from the induced voltage at the receiver. The distance along the hole is expressed in feet with the collar at zero.

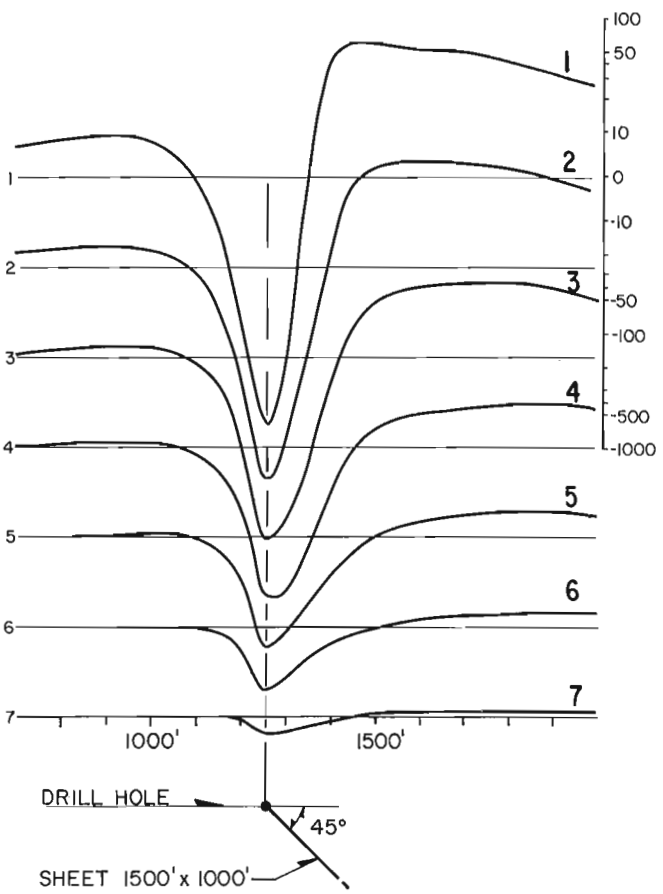

Figure 34.6. PEM model response profiles (after Woods, 1975, p. 205), in a hole passing a body at its top edge. For model data, the amplitude scale in the upper right hand corner gives the induced voltage in microvolts at the receiver.

characteristics of the conductors involved. A great advantage was the availability of many holes, so that quite a few of the offhole sources were seen from two or more locations. Some offhole sources were known in detail, as with the mapped orebodies. Other responses identified new extensions to known bodies, while still other responses identified completely new sulphide bodies, which were later confirmed by drilling.

The following examples illustrate some of the more important types of response as well as contributions made by the survey in finding new sulphide lenses.

Detail interpretation

-900 Level - Relatively uncomplicated cases

Figure 34.4 shows the responses along three holes in or passing through the -900 foot (275 m) level. The horizontal hole SB677 was drilled north at the end of the drift in order to investigate the rhyolite-quartz porphyry contact northeast of the orebodies. The channel one and later channel responses (Fig. 34.5) show a double-peaked negative response between 200 and 300 feet (61-92 m) along the hole. A distinctive asymmetry is evident, as a positive shoulder appears further along in the hole past 300 feet (92 m). Two offhole sources are indicated. Comparison of the profile to a profile from Woods (1975) indicates that the bodies have their top edge nearest the hole as shown in Figure 34.6. The general shape of the field curve compares favourably to the model curve for a 45° incidence angle. This compares well to the known angle between the hole and the geological contact at this location.

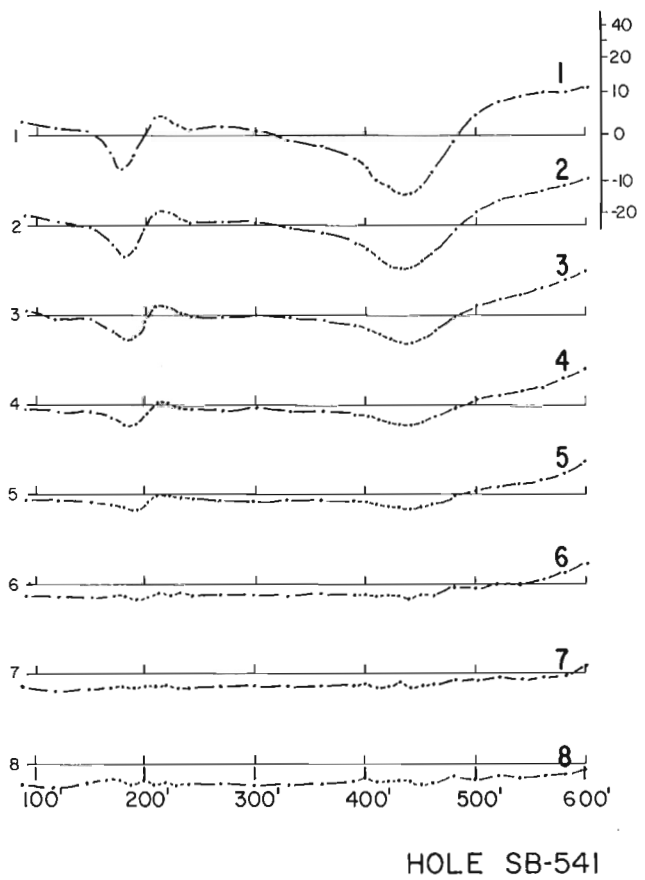

Figure 34.7. *Hole SB541, PEM response profiles.*

The sharp definition of the profile at 280 feet (85 m) in the SB677 hole is suggestive of a nearby or edge response. This is confirmed by the presence of one foot (0.3 m) of massive sulphides (pyrite with minor sphalerite) and a few feet of stringer sulphides in the hole at this point. The broader response at 250 feet (76 m) is indicative of a source slightly further away from the hole. The body at 280 feet (85 m) seems smaller than that at 250 feet (76 m) as the decay in the response is more rapid.

The location of the interpreted source bodies in Figure 34.4 is determined by the top edge aspect from the curves and by the necessity that any real bodies conform to the geology. In an arbitrary case where the geology is not known, the source bodies could lie anywhere in a 360° circle around the hole. Further, the bodies cannot lie along the contact to the left of the hole as such sources would generate bottom edge responses in which the asymmetry would be reversed to the observed profile.

Additional assistance in locating these bodies is provided by the response in hole SB541 between 400 and 500 feet (122-153 m)) (Fig. 34.7) which passes down through the level some 70 feet (21 m) west of the interpreted bodies. This response which merges the responses from the two sources, is not as sharply defined as in SB677, indicating that the source is farther away. Again, the asymmetry points to a top edge source. The decay of the responses in SB677 and SB541 is simple and uniform, as would be expected from offhole sources of regular geometry and uniform conductivity.

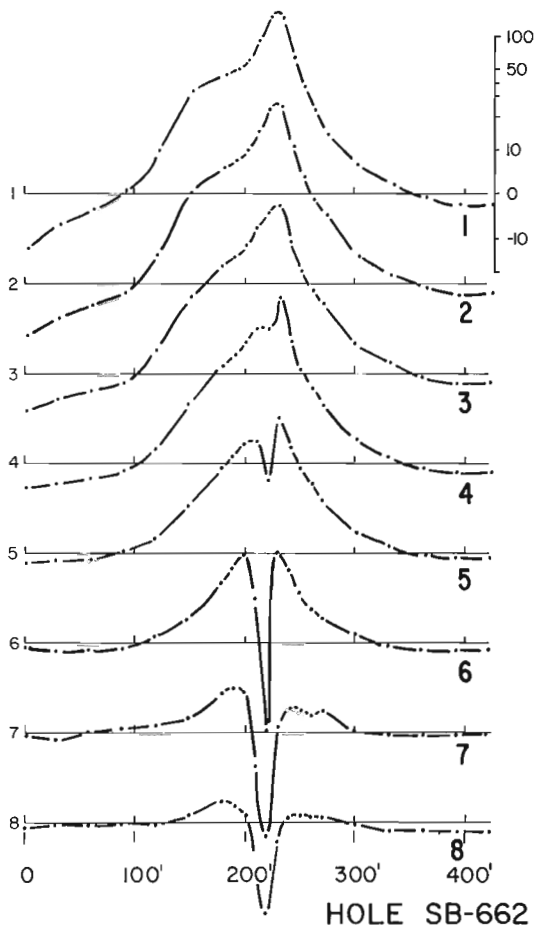

Figure 34.8. *Hole SB662, PEM response profiles.*

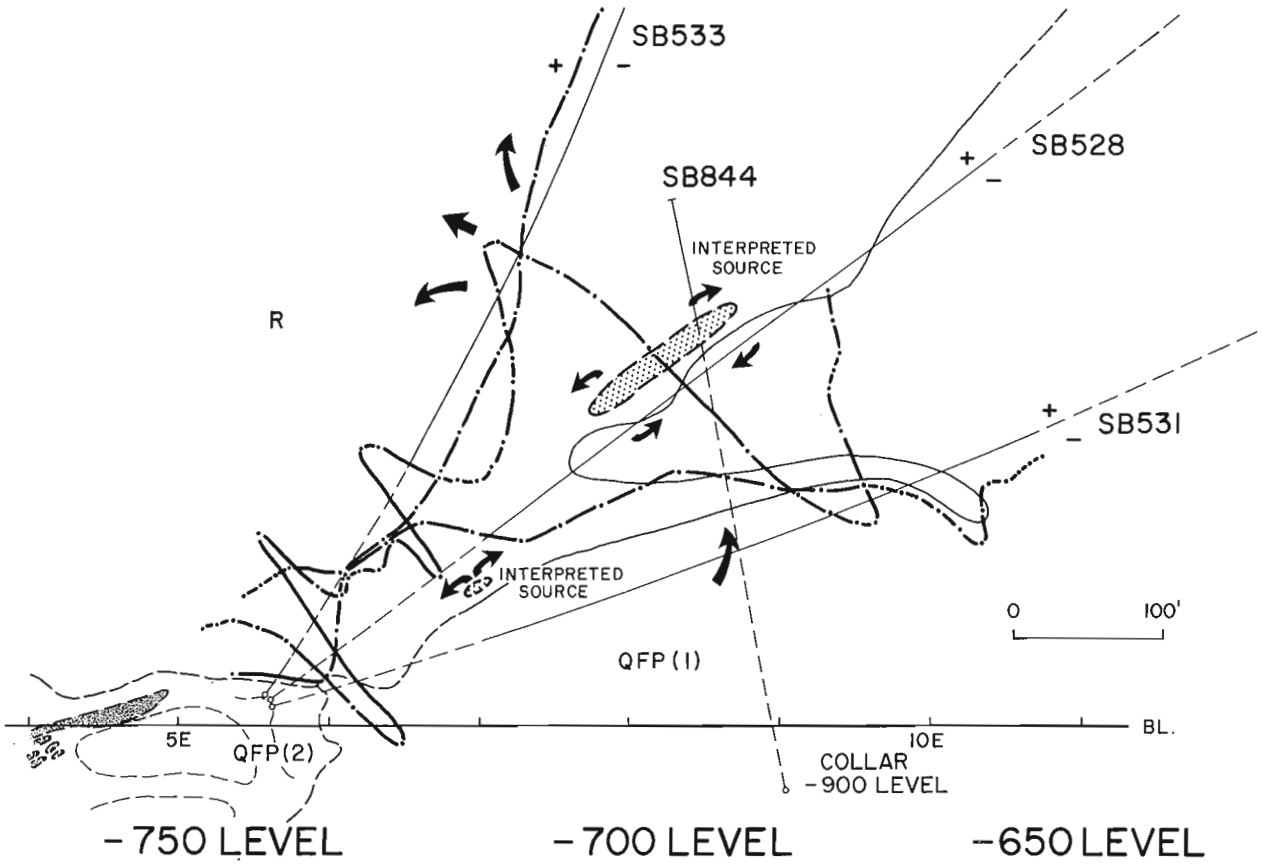

Figure 34.9. *-700 level with parts of the -650 and -750 levels (dashed lines) projected to the -700 level. The arrows represent the inferred directions of the secondary fields around conductive bodies.*

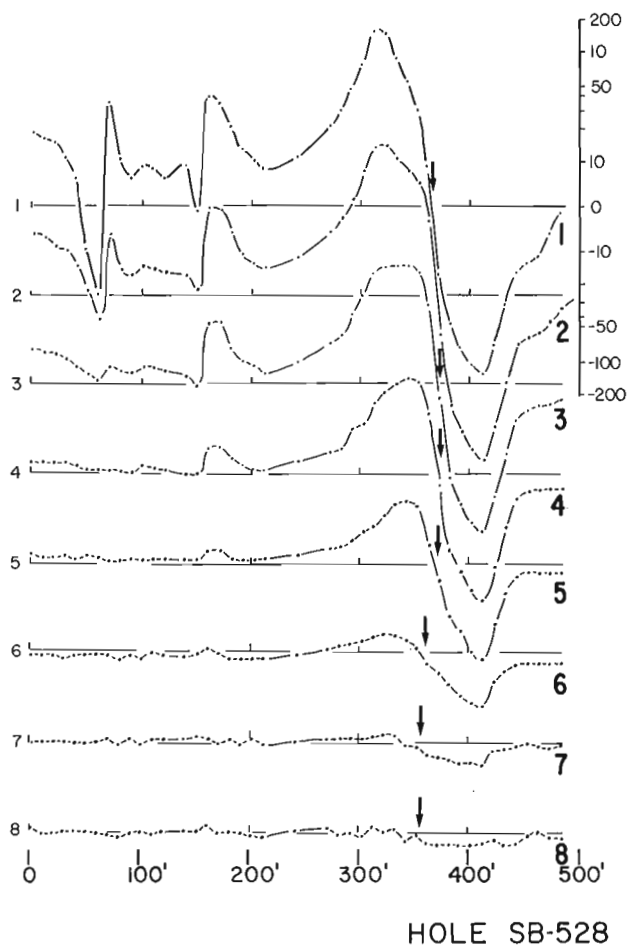

Figure 34.10

Hole SB528, PEM response profiles. Arrows identify response crossovers.

Hole SB846 (Fig. 34.4), drilled to test the interpreted sources near SB677, confirmed the presence of the conductors. Two intersections of massive pyrite with sphalerite (1.5 feet (0.5 m) and 1.2 feet (0.4 m), 20 feet (6 m) apart in the hole) were located at the larger interpreted source. Five feet (1.5 m) of massive pyrite with sphalerite were intersected at the location of the smaller interpreted source. More extensive stringer mineralization was identified in association with the masssive units. Further drilling would have been necessary to fully support the interpretation. This could not be justified, however, as the economic grade of the sulphides was low, and the potential for a much larger body was not indicated by the EM response. Hole SB846 was not surveyed with the EM system.

In Figures 34.4 and 34.7, an offhole response near 200 feet (61 m) in SB541 is interpreted to be from a small body lying near the hole but well above the -900 foot (275 m) level.

The response in hole SB662 (Fig. 34.4 and 34.8) is reasonably typical of a response which occurs when the hole has penetrated a conductor but has passed near its edge. The positive response in the early channels indicates that the body has been intersected while later channel negative responses show that much of the body lies off the hole. These negatives arise as the later time secondary current loops lie outside the hole. A profile from Woods (1975) used in a later comparison (see Fig. 34.24), illustrates this. Figure 34.4 shows that the hole intersected sulphides, which form part of the main ore lens seen just to the west on the drawing.

-700 Level - Source body parallel to hole

Figure 34.9 shows the results from three holes which are collared on the -750 foot (229 m) level. These were drilled up through the -700 foot (214 m) level and into the -650 foot (198 m) level.

Hole SB528 (Fig. 34.10) is very interesting. Between 250 feet (76 m) and 500 feet (153 m), there is a striking response from an offhole source lying very near the hole. The response profile is symmetrical on either side of the crossover which is indicated by the arrows at 370 feet. Note that the response is positive toward the collar and negative away from it. In Figure 34.9, the direction of the secondary field has been indicated by the arrows along hole SB528. The source body must lie to the north of the hole as the primary field direction is from south to north and the induced secondary field would lie in the same direction through the source body. The nearly symmetrical response and the indicated shape of the secondary field suggest that the hole passes parallel to the plane of the source body, and the ends of the body are identified by the peaks of the negative and positive responses. The position of the crossover which locates the point where the secondary field is normal to the hole (zero coupling to the receiver coil) represents the electrical centre of this body. It is very unusual to find a case where a conductive body happens to lie parallel to the drillhole as most holes are designed to cross the geological strike.

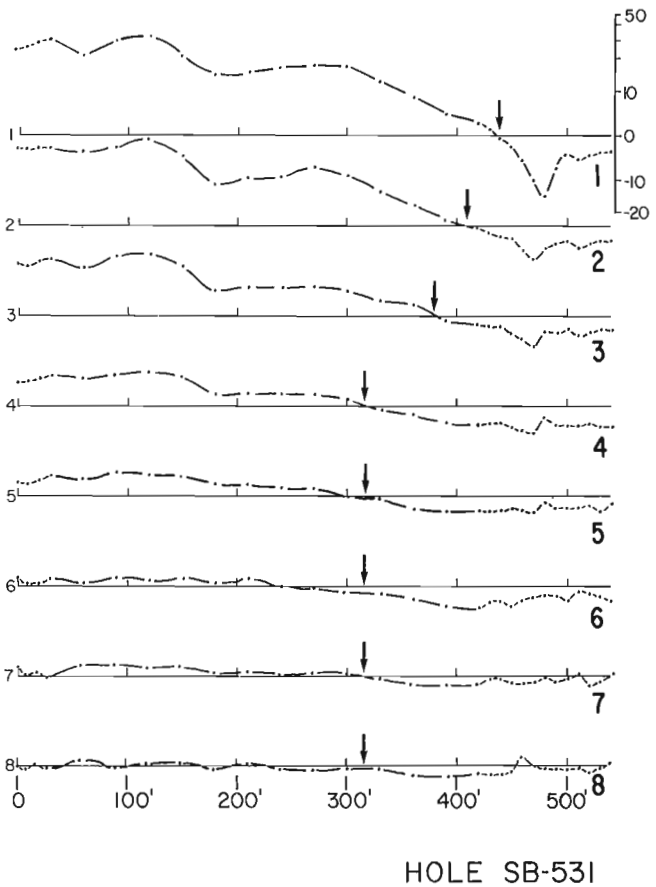

Figure 34.11. Hole SB531, PEM response profiles.

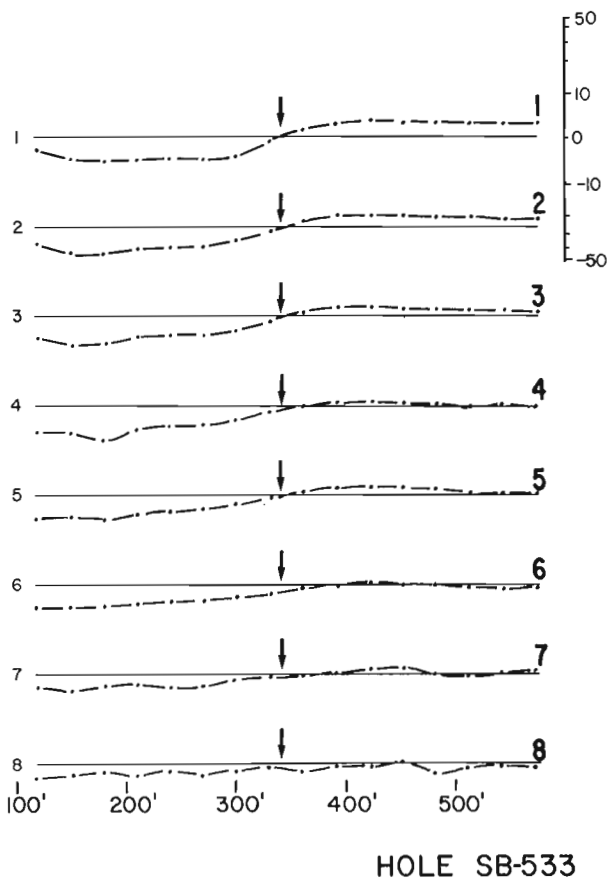

Figure 34.12. Hole SB533, PEM response profiles.

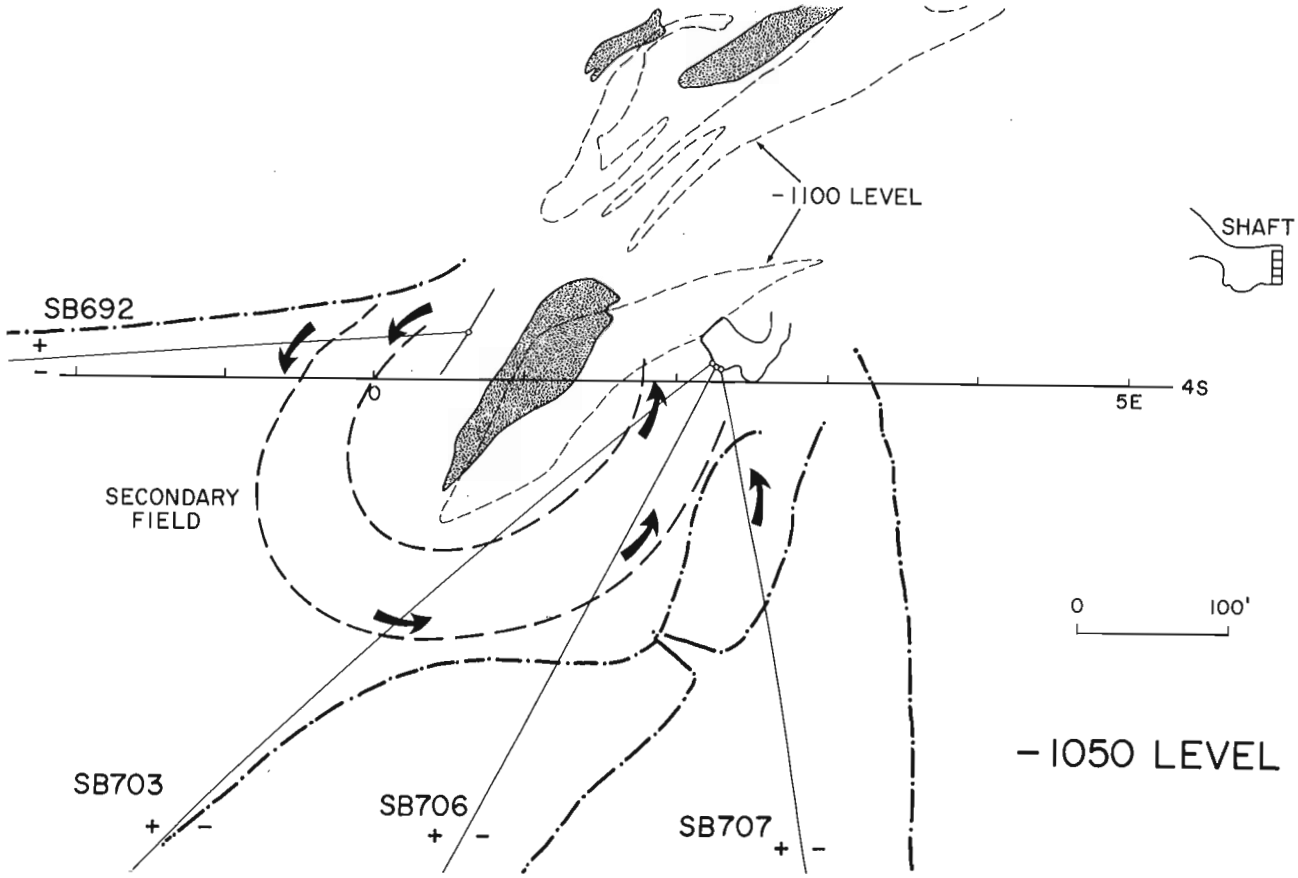

Figure 34.13. *-1050 level, ore on the -1100 level (dashed lines) is projected to the -1050 level. The inferred direction and location of the secondary field is indicated by arrows and dashed lines.*

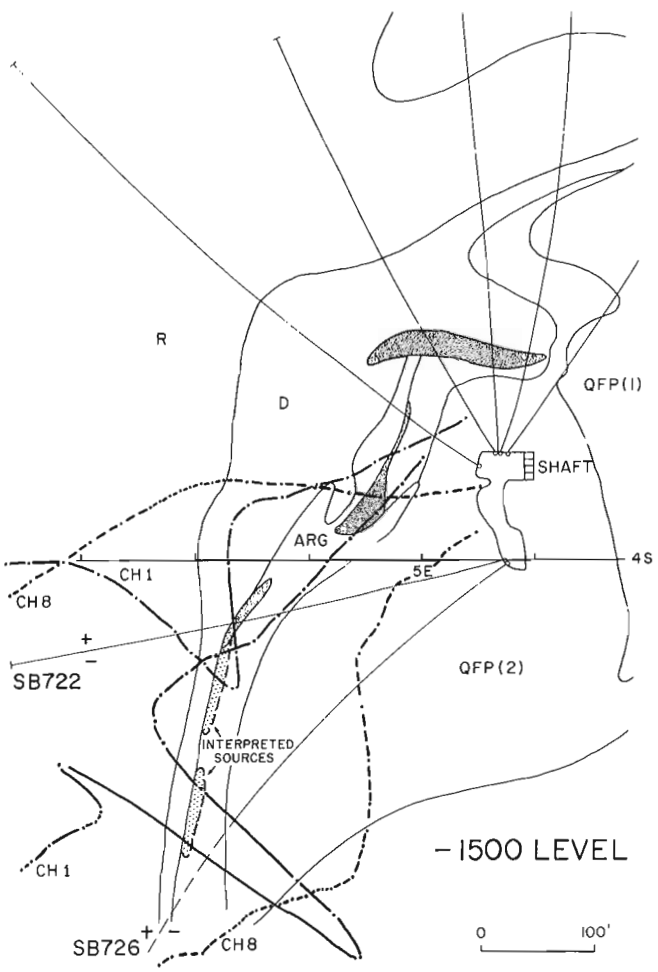

Figure 34.14

-1500 level, D - dacite, ARG - argillite.

The response in hole SB531 (Fig. 34.11) is somewhat complex, but a weak crossover at about 315 feet having the same polarity change as the strong response of SB528, indicates that the offhole source has been detected by both holes, and that both holes lie south of the source. In hole SB533 (Fig. 34.12), there is a broad crossover at about 340 feet. The polarity of the response is reversed to that in SB531 and SB528, which implies that this hole (SB533) lies on the opposite side of the source body from SB531 and SB528. The arrows in Figure 34.9 show the secondary field directions which these readings suggest. The reduced amplitude in SB533 indicates that the source body is some distance away.

The interpreted body lies along the rhyolite-quartz porphyry contact, and may be an upward extension of the body observed in SB677 on the -900 level. Hole SB844 (Fig. 34.9) was subsequently drilled up from the -900 level to test the -700 level response. Stringers and narrow massive veins of sulphides (mainly pyrite with minor sphalerite) were intersected as the hole crossed the contact and passed through the location of the interpreted source.

Responses from other offhole small bodies may be seen in these profiles. One (Fig. 34.9 at about 160 feet (49 m) shows opposing polarities in holes SB528 (Fig. 34.10) and SB531 (Fig. 34.11). This places the body between these holes. This interpretation is supported by the weak negative response in hole SB533 at this location.

-1050 Level - Direction of secondary fields

Figure 34.13 shows results from four holes which fan out around an ore lens on the -1050 foot (320 m) level. At the time of this survey the ore had been mined down to the -1050 level but massive ore was in place from this level down to -1120 feet (342 m). The outline of the ore on the -1100 foot (336 m) level (Fig. 34.13) shows that the lens becomes larger with depth. The response in these holes comes from this ore lens. The shape of the secondary field around the lens, indicated by the arrows and dashed line, is implied by the responses, which are positive in SB692 to the north, and negative in the holes to the south and east.

The responses shown in Figure 34.13, as well a others presented here, show that although the receiver measures a single axial component, a qualitative three dimensional view of the shape and direction of the secondary fields can be assembled by comparing diagrams on adjacent levels. This way of looking at the data can be of considerable value when unravelling sets of complex responses.

-1500 Level - Complex responses

At the -1500 foot (458 m) level (Fig. 34.14) the ore lenses are pinching out. The rocks of the ore horizon grade into argillite containing sulphide stringers (mostly pyrite with some pyrrhotite). This argillite plus sulphide unit generates complex responses. Two of these responses are seen in

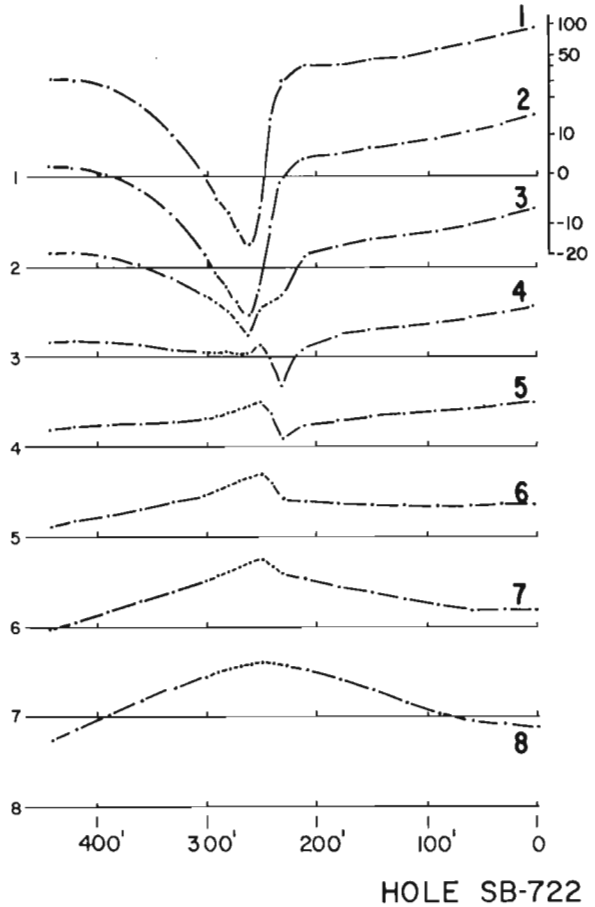

Figure 34.15. Hole SB722, PEM response profiles.

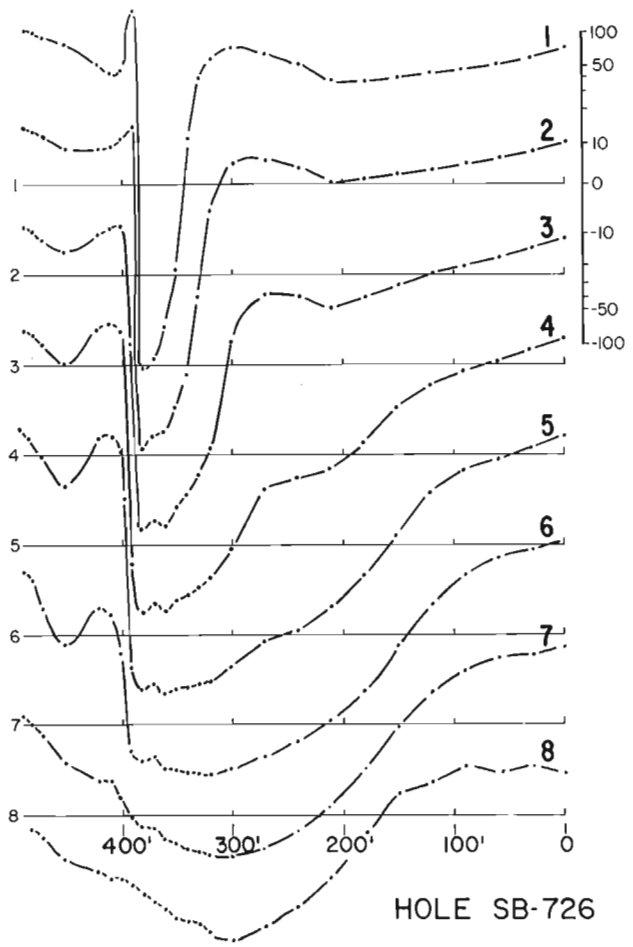

Figure 34.16. Hole SB726, PEM response profiles.

holes SB722 (Fig. 34.15) and SB726 (Fig. 34.16). SB 722 passes through the argillite and a sulphide body at the westerly contact between the argillite and dacite. The early channel responses in SB722 show a moderate negative anomaly near 250 feet (76 m) within a broad, nearly flat, positive background response. In later channels, the negative is replaced by a broad positive peak. This positive response, showing a inhole source, identifies the argillite with its concentration of sulphides at the west contact as a large conductor. An offhole source is indicated by the negative early channel responses. It appears to be caused by a smaller body, possibly more massive sulphides, near the hole. The shape of the negative suggests a top edge intersection, which is interpreted in Figure 34.14 as an extension of the sulphides south along the contact.

The responses in hole SB726 (Fig. 34.16) are of a somewhat different character, but derive from similar sources. The early channel, narrow negative is suggested in Figure 34.14 to arise from a nearby offhole body, likely sulphides, along the argillite-dacite contact. A broad negative with a crossover to a positive shoulder toward the collar develops in later channels. This is interpreted to originate from a large sheet conductor where the hole passes with a low incidence angle near the bottom edge. The argillite unit as the source, satisfies this interpretation quite well.

Figure 34.14 shows some of the other holes on the level not reported here. The fan distribution of the holes is typical of the access throughout the mine. Holes, such as those shown extending into the rhyolite, identified few offhole sources once these passed the dacite or quartz porphyry contact.

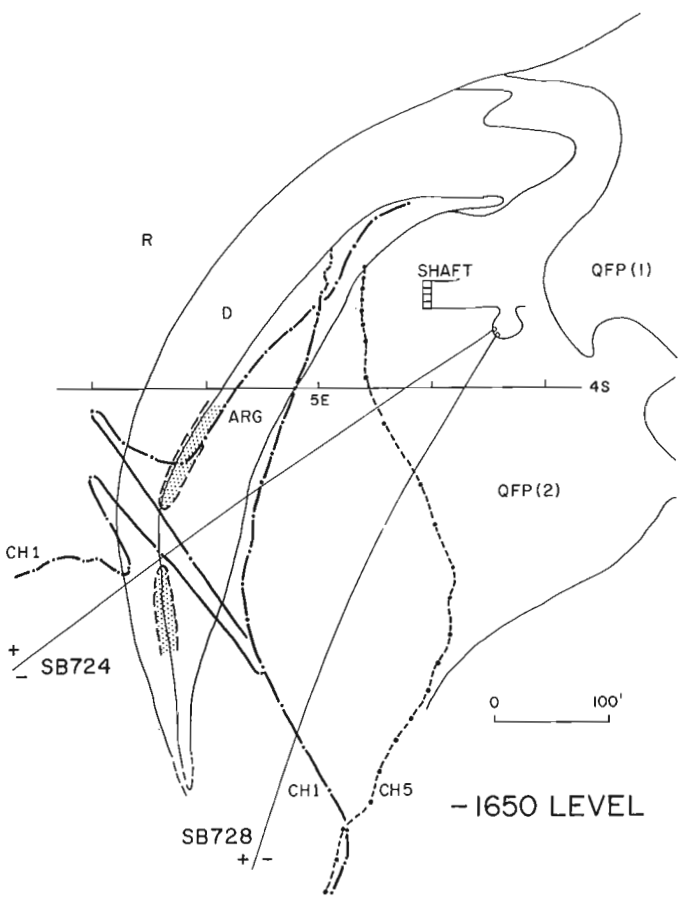

Figure 34.17. -1650 level.

-1650 Level - Response Migrating in Time

The responses in holes SB724 and SB728 on the -1650 foot (503 m) level (Fig. 34.17) are direct analogues of the responses seen above in holes SB722 and SB726 on the -1500 level (Fig. 34.14). The argillite with sulphides is the main source of electromagnetic response. Hole SB724 behaves much like the two holes reported on the -1500 level, with an early channel offhole type response from a small source, at the argillite-dacite contact.

The response in hole SB728 (Fig. 34.17, 34.18) provides a new kind of complexity. This hole lies essentially parallel to the large argillite body. The response is bipolar with the position of the positive and negative responses indicating a major secondary field around a source lying northwesterly from the hole. A somewhat similar pattern was developed in hole SB726 above, but a closer analogue was the parallel to the body response in hole SB528 on the -700 level (Fig. 34.10).

In SB728, however, the position of the crossover migrates in time from the first channel at about 400 feet (122 m) to channel 6 where it stabilizes at about 110 feet (34 m). Apparently, there is a migration in time of the centre of the secondary induced currents in the argillite, which are reflected in the migration of the position of the secondary fields. This is not seen to be a "smoke ring" effect (Nabighian, 1979), in part because the apparent movement of the secondary currents is not downward and outward, away from the transmitter. Instead, the centre of the secondary

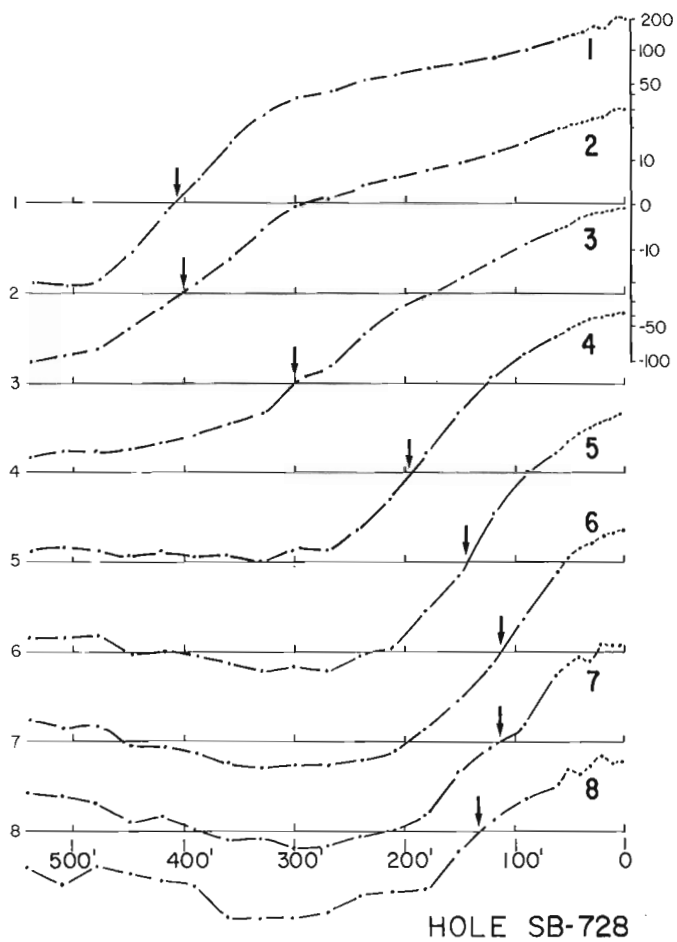

Figure 34.18. Hole SB728, PEM response profiles. Arrows identify response crossovers.

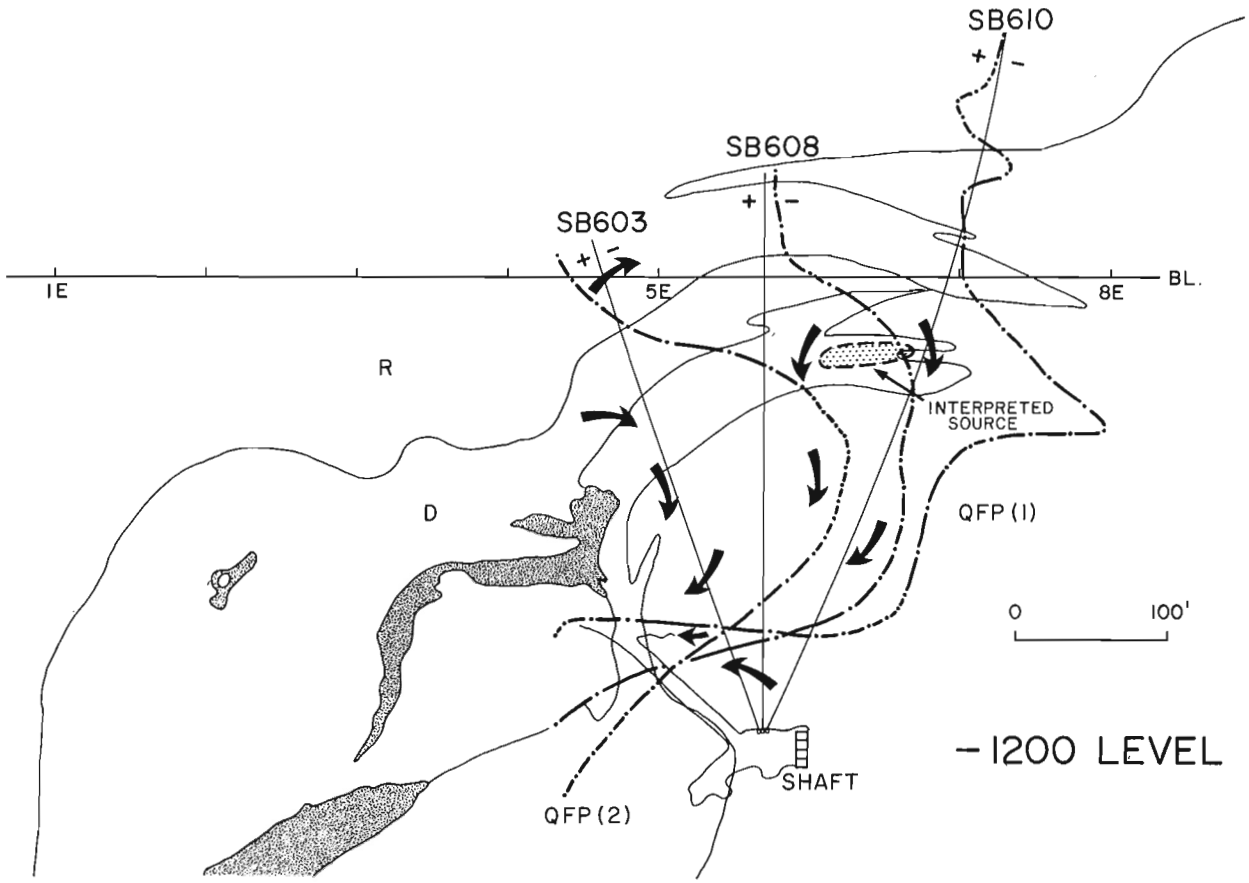

Figure 34.19. *-1200 level. Arrows indicate the inferred directions of the secondary fields. Profiles are for channel 1.*

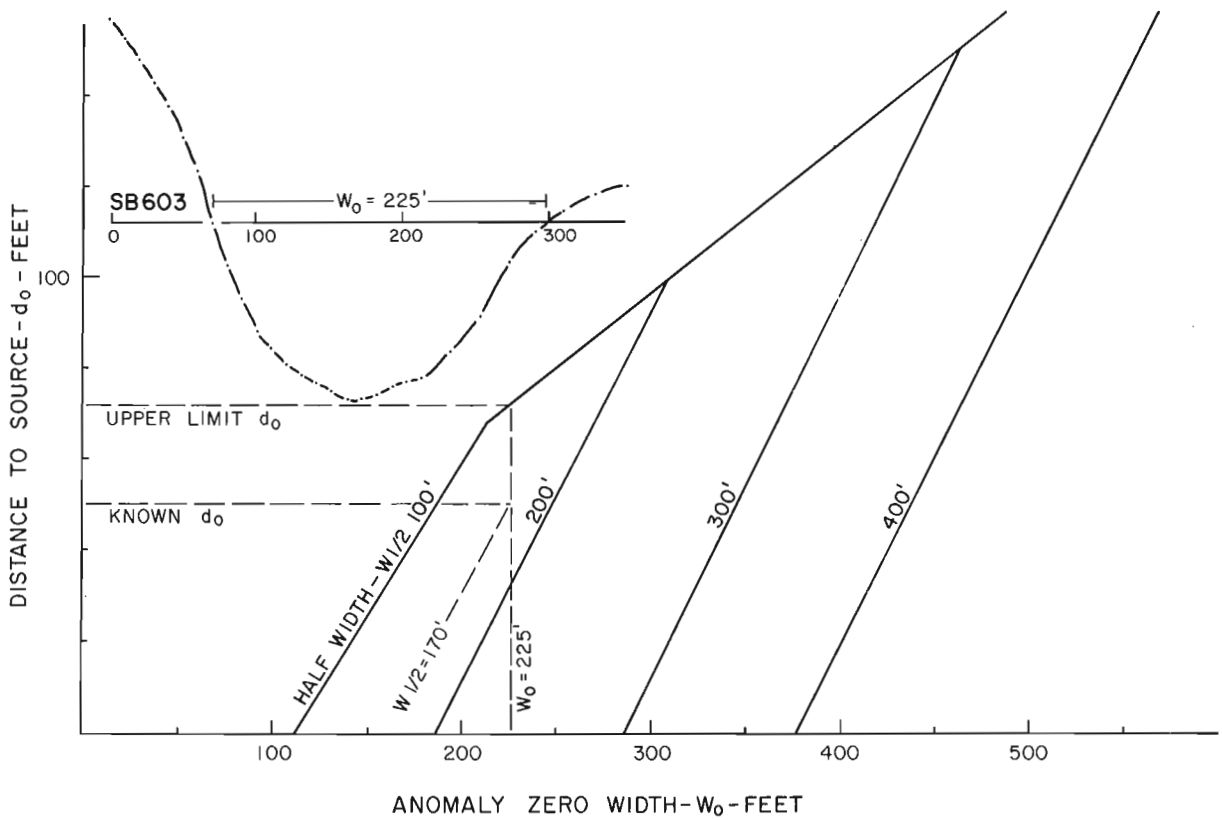

Figure 34.20. *Distance to the near edge of a conductor, versus zero width for conductors of various sizes, intersection angle 90° (after Woods, 1975, p. 67).*

currents moves in plan, maintaining an approximately constant distance from the transmitter. This behaviour would appear to be caused by non-uniform conductivity in the argillite. The collapse in time of the secondary field asymmetrically toward the north suggests that the argillite is more conductive in that direction. Crone (1979a), using a different detection procedure, has reported a similar migration of current centres in a body of varying conductivity.

-1200 Level - Estimation of size and distance to source

On the -1200 foot (366 m) level (Fig. 34.19), readings of channel 1 in a fan of three holes show responses from a main ore lens and from a small offhole source.

The somewhat irregular ore lens near hole SB603 had ore in place from -1075 to -1115 feet (328-340 m), from -1200 to -1300 feet (366-399 m) and from -1350 to -1500 feet (412-458 m) at the time of the survey. The exact electrical size of the orebody was uncertain as there may have been connections between the lenses in place through sulphides in stringers in the walls of the mined out areas. It is thought, however, that the main contribution to the responses on this level was from the 100 feet (30 m) of ore lying below this level.

The profile along SB603 provides a reasonable example to illustrate some parameters developed by Woods (1975) and used extensively in the interpretation and the development of drill targets in this survey. Usually, later channels are used in this interpretation. Channel 1 was used here, however, as there is little change in the shape of the anomaly from early to late channels. Figure 34.20 introduces three parameters. Zero width (W_0) is the anomaly width from crossover to crossover. This figure can be corrected for incidence angle; however, the example here assumes the body lies normal to the hole. The distance to source (d_0) is the shortest distance between the hole and the near edge of the body. The half width ($W_{1/2}$) is half the smallest dimension of a rectangular body.

As seen on the diagram in Figure 34.20 the zero width of the SB603 anomaly is 225 feet (69 m). This number provides a limit for the half width and the distance to source. The upper limit, which the diagram provides (about 70 feet (21 m)), is possible, but not real, as the approximate d_0 from Figure 34.19 is about 50 feet (15 m). The intersection of W_0 and d_0 gives an estimate of $W_{1/2}$ at about 170 feet (52 m). This would indicate a source body of rectangular aspect of about 340 feet (104 m) across. This is somewhat large as the strike of the orebody was about 240 feet (73 m). The possible larger dimension through the walls of the mined out areas may contribute to this overestimate. Also W_0 may be too large, as contribution from another offhole source is apparent. As well, the ore lens is not a simple thin sheet. However, a useful approximation to the size of the body has been achieved.

A limitation in the use of the diagram is the fairly large half width of 100 feet (30 m) as the smallest size available. Many significant responses in this survey were from bodies which were smaller than this. The diagram was extrapolated for the smaller events (not shown), but the results remain questionable. A modified version of the diagram in Figure 34.20 was presented by Woods et al. (1980). It was not available for this study.

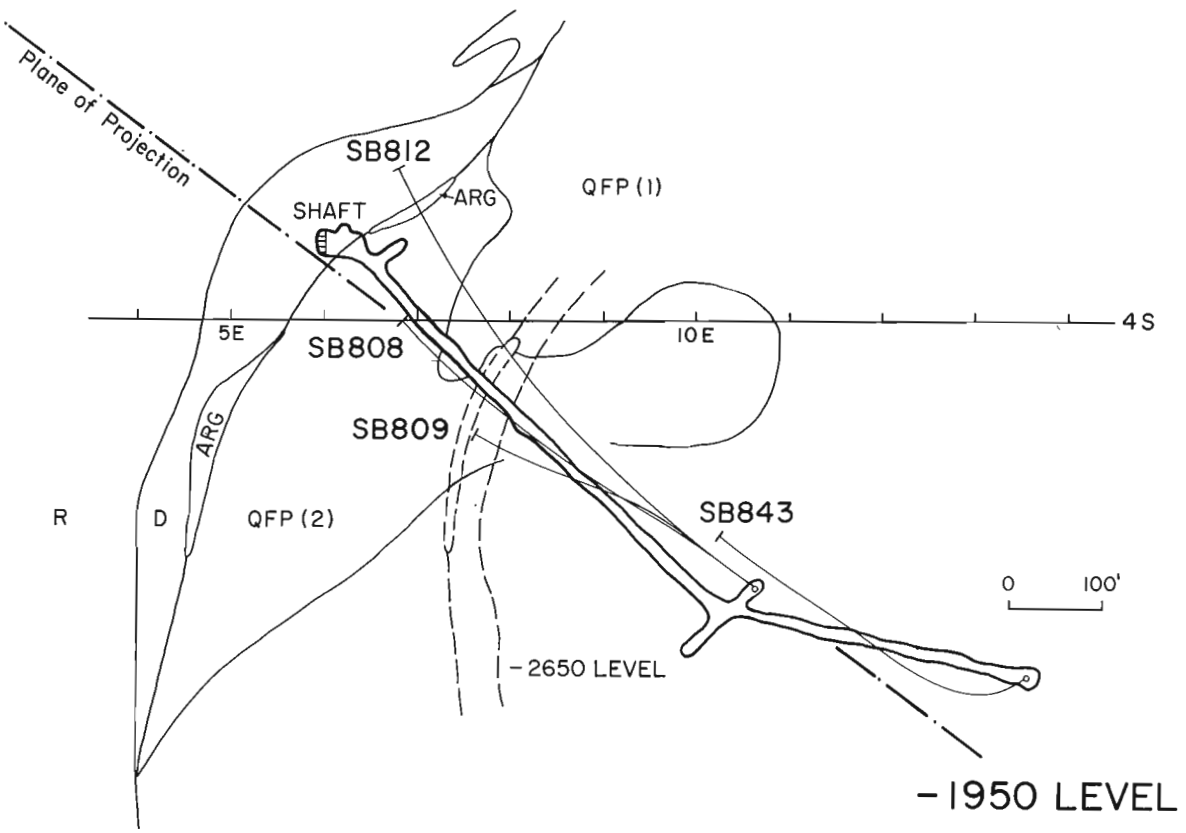

Figure 34.21. -1950 level.

-1200 Level - Three views of two bodies

The profiles on holes SB608 and SB610 on the -1200 foot (366 m) level (Fig. 34.19) show the response from the main ore lens to change character and diminish in amplitude as the geometry changes. An interesting event is an offhole source barely suggested in SB603 but appearing with increased amplitude in the other two holes. A source body has been interpreted in Figure 34.19, to lie between holes SB608 and SB610, approximately at right angles to the drillholes. The larger amplitude, and sharper definition of the response at about 270 feet (82 m) in SB 610, indicates that the body is closer to that hole. The arrows, indicating secondary field directions around the ends of the interpreted body, identify the source of the negative responses in the adjacent holes. The fied arrows also describe the field around the easterly end of the ore lens.

-1950 Level and below - Downholes from the deepest level

The deepest level in the mine was the -1950 foot (595 m) level. Holes drilled down from an exploration drift on this level provided access to levels as deep as -3350 feet (1022 m). Transmitter number 1 was almost directly over top of the -1950 drift (Fig. 34.2, 34.21), and over the target area being investigated (Fig. 34.22), but the easterly dip of the mineralized contact allowed some coupling of the primary field to bodies in this area, and valid data were obtained. Holes SB808, SB809 and SB812 were read with transmitter 1, and hole SB843 was read with the larger transmitter number 2 (Fig. 34.2, 34.21, 34.22). Transmitter 2 provided better coupling to the mineralized contact.

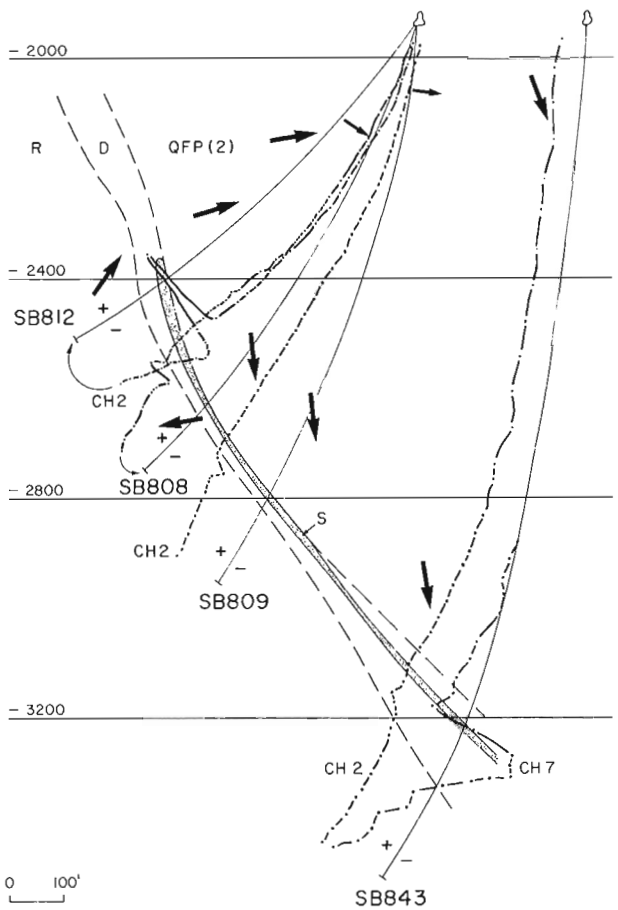

Figure 34.22. Projection to a vertical plane identified in Figure 34.21. Arrows indicate the inferred directions of the secondary fields, S - sulphides.

Holes projected to the -1950 level plan (Fig. 34.21) are projected to a vertical plane in Figure 34.22. Channel 2 profiles of SB808, SB809 and SB843, indicate by their broad positive response that the holes have passed through a large conductive sheet. Sulphides, in the form of 10% to 20% pyrite-pyrrhotite, were identified within dacite tuffs in these holes. The sulphides in each hole occur at the point where there is a notch or ripple in the early channel responses. Hole SB812 also passes through the sulphides indicated by the sharp bipolar response. The broad negative response, however, indicates that the hole passes through or just off the edge of the main electrical body. The direction of the secondary field is described by the arrows as it moves around the apparently large conductive sheet.

The later channel response in SB843 (Fig. 34.23) is interesting in that a negative, or offhole source appears. Comparison with the profiles in Woods (1975), as shown in Figure 34.24, suggests that the hole has passed a few tens of feet inside the bottom edge of the sheet. The broad negative developing in later channels, however, suggests an added complexity of a small conductive body lying somewhere offhole at about 1330 feet (406 m). This was considered to be too small to be of economic interest at that depth.

A more important response is that which develops toward the bottom of hole SB843 in the later channels, where responses rise instead of fall as would be expected from the simple sheet model of a body at 1280 feet (390 m) in the hole. A second conductor was projected to lie off the end of SB843. This interpretation, plus the known existence of a deeper quartz porphyry unit detected from other drillholes off the section in Figure 34.22, led to further drilling from the

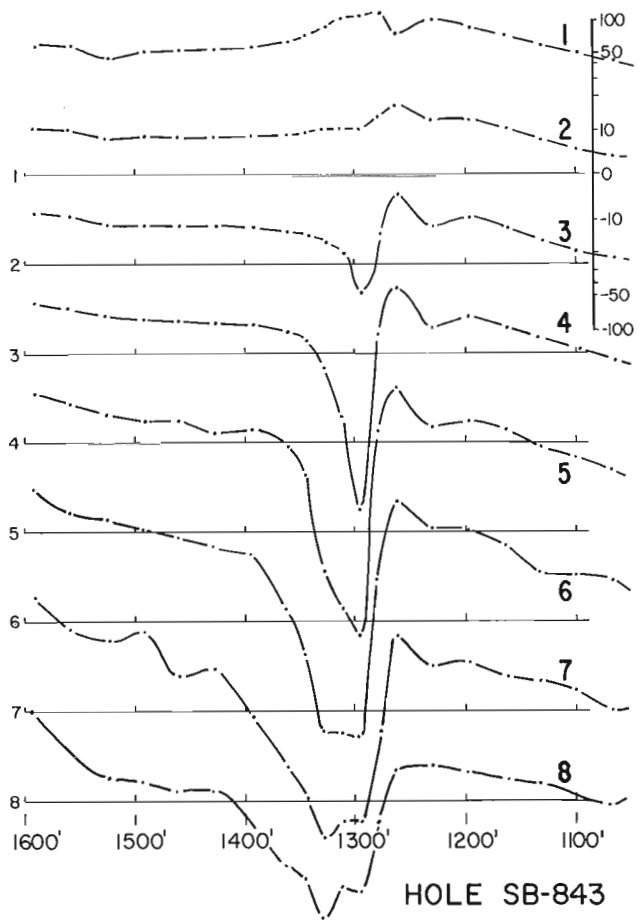

Figure 34.23. Hole SB843, PEM response profiles.

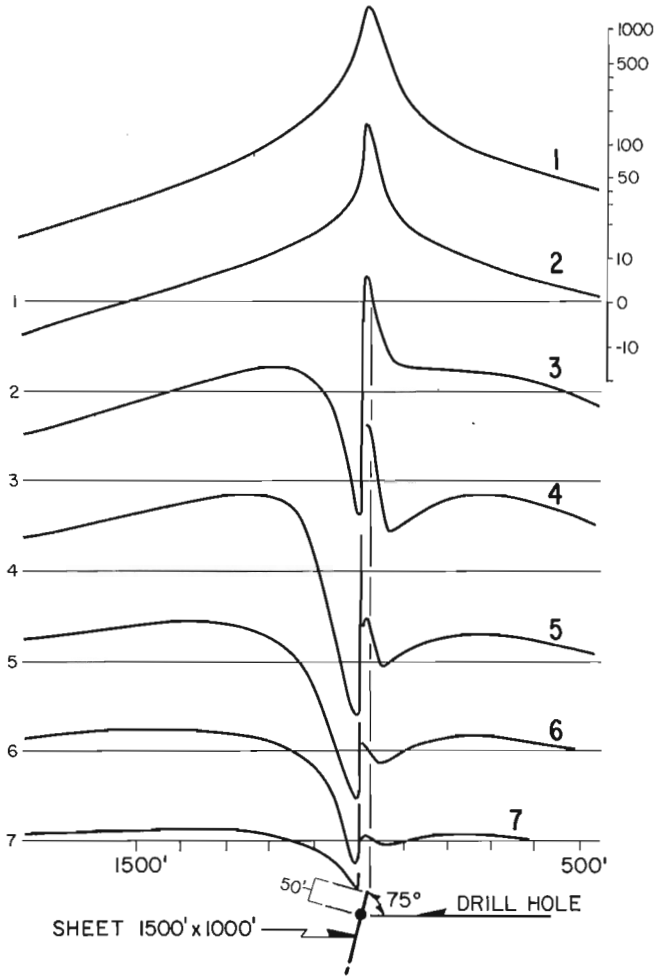

Figure 34.24. PEM model response profiles in a hole entering a body at its top edge, 50 feet (15 m) inside the body (after Woods, 1975, p. 258).

-1950 level. Hole SB843 was extended and a hole was drilled below and along strike from SB843. This drilling confirmed the existence of another sulphide sheet off the end of SB843. Unfortunately, the discovered sulphides were similar to the low grade pyrite-pyrrhotite seen higher up in these holes.

Conclusions

The life of a mine is determined by the ore it has in reserve. As with all mines, when the ore reserve at the South Bay mine dropped to zero, the mine was closed. The borehole electromagnetic survey carried out at South Bay near the end of it's life detected a number of previously unknown sulphide lenses. It did not, however, find any new ore. The survey did contribute to the last phases of exploration in the mine by giving confidence that no undiscovered orebodies lay nearby or just beyond some earlier exploration drillhole.

Acknowledgments

The author wishes to thank Selco Division and British Petroleum Minerals International Ltd. for permission to publish this paper.

Thanks are extended to Frank Hiebert, geophysical consultant, then of Crone Geophysics, for his direct participation with the author in this survey. Discussions with Duncan Crone of Crone Geophysics were of considerable assistance in planning and interpreting this survey. Thanks to Jim Wan of Selco, then South Bay mine geologist, for discussions about the geology, and to M. Safranek and S. Jakubowski for drafting, and R. Thalassinos for typing. Thanks are extended also to D.J. Reed for critically reading the manuscript.

References

Auston, J.S.
1969: Uchi Lake - A geophysical case history; paper presented at Society of Exploration Geophysicists, 39th Annual Meeting, Calgary, Alberta.

Crone, J.D.
1979a: Exploration for massive sulphides in desert areas using the ground Pulse EM method; in Geophysics and Geochemistry in the Search for Metallic Ores; Peter J. Hood, ed. Geological Survey of Canada, Economic Geology Report 31, p. 745-755.

1979b: Pulse EM - PEM and Borehole Pulse EM, information sheets; Crone Geophysics Ltd., Mississauga, Ontario.

1980: Field results using borehole Pulse EM method; Crone Geophysics Ltd., Mississauga, Ontario.

Dyck, A.V.
1981: A method for quantitative interpretation of wideband, drill-hole EM surveys in mineral exploration; Geophysics Laboratory, Department of Physics, University of Toronto, Research Applied Geophysics No. 23.

Macnae, J.C.
1980: An atlas of primary fields due to fixed transmitter loop EM sources; Geophysics Laboratory, Department of Physics, University of Toronto, Research in Applied Geophysics No. 13.

Nabighian, M.N.
1979: Quasi-Static Transient response of a conducting half-space - an approximate representation; Geophysics, v. 44, no. 10, p. 1700-1705.

Pollock, G.D., Sinclair, I.G.L., Warburton, A.F. and Wierzbicki, V.
1972: The Uchi Orebody - a massive sulphide deposit in an Archean siliceous volcanic environment; 24th International Geological Congress, Montreal, Section 4, p. 299-308.

Reed, L.E. and Auston, J.S.
1973: The Uchi orebody - a discovery using airborne and ground geophysical methods; paper presented at 75th Canadian Institute of Mining Metallurgy, Annual Meeting, Vancouver.

Thurston, P.C., Wan, J., Squair, H.S., Warburton, A.F. and Wierzbicki, V.
1978: Volcanology and mineral deposits of the Uchi - Confederation Lakes area, Northwestern Ontario; Field trip handbook, 1978 Joint Annual Meeting, Geological Association of Canada.

Wan, J. and Warburton, A.F.
1979: South Bay mine - a geological update; paper presented at Canadian Institute of Mining and Metallurgy Division IV, September 1979, Winnipeg, Manitoba.

Woods, D.V.
1975: A model study of the Crone borehole Pulse EM system; unpubl. M.Sc. thesis, Queen's University, Kingston, Ontario.

Woods, D.V. and Crone, J.D.
1980: Scale model study of a borehole Pulse EM system; Canadian Institute of Mining and Metallurgy Bulletin,, v. 73, no. 817, p. 96-104.

Woods, D.V., Rainsford, D.R.B. and Fitzpatrick, M.M.
1980: Analogue modelling and quantitative interpretation of borehole PEM measurements (abstract only); EOS, Transaction American Geophysical Union, v. 61, no. 17, p. 414-415.

35. INTERPRETATION OF CONDUCTOR COMPLEXITY WITH BOREHOLE APPLICATIONS

J.C. Macnae and Y. Lamontagne[1]

Macnae, J.C. and Lamontagne, Y., Interpretation of conductor complexity with borehole applications; in Borehole Geophysics for Mining and Geotechnical Applications, ed. P.G. Killeen, Geological Survey of Canada, Paper 85-27, p. 323-336, 1986.

Abstract

Surface surveys have the advantage over borehole EM surveys in that access to a grid is feasible, and any component of the EM field can be measured. However, borehole surveys generally approach closer to (or intersect) conductors of interest than do the surface surveys, which leads to the possibility of detailed local interpretation of the response measured in a borehole.

By careful estimation of the migration of characteristic points, it is often possible to identify regions of increased conductivity within a larger conductor. The observed data are first used to estimate the pattern of secondary current migration with delay time. If either the local thickening or increased conductivity is present, then the secondary current tends to migrate faster towards this location than if the conductor was uniform, and subsequently concentrates within the region for an extended range of time. If the borehole intersects the conductor, then the interpretation of tangential sheet current discontinuities may also be used as an indicator of local geometry.

Résumé

Les sondages de surface sont préférés aux sondages électromagnétiques de fond, en ce sens que les premiers permettent d'utiliser un quadrillage et de mesurer tout composant du champ électromagnétique. Par contre, les sondages de fond permettent, en général, d'examiner de plus près (ou de traverser) les conducteurs qui présentent de l'intérêt, ce qui permet une interprétation locale précise des mesures obtenues à partir d'un trou de sonde.

Une estimation soignée de la migration des points caractéristiques permet souvent de repérer, dans un plus grand corps conducteur, les zones de conductivité plus élevées. On utilise d'abord les données observées pour estimer la configuration de la migration du courant secondaire en fonction du temps de retard. Lorsqu'une zone plus dense ou meilleure conductrice est présente, le courant secondaire a tendance à se déplacer plus rapidement vers cet endroit que lorsque le conducteur est uniforme; une concentration de courant se produit ensuite dans cette zone durant une période prolongée. Lorsque le sondage traverse un milieu conducteur, l'interprétation des discontinuités de courant selon un plan tangent à la forme tabulaire de la masse peut également aider à en connaître la configuration locale.

Introduction

Electromagnetic (EM) exploration for massive sulphides in a borehole environment is a fairly recent development that has proven to be extremely successful. Reasons for conducting a borehole survey might include: 1) confirmation that any mineralization intersected in a borehole is the source of the surface anomaly, or detection and location of a main conductor if the drillhole has missed the target; 2) direct detection of conductors at depths too great to produce significant responses at the surface; and 3) interpretation of detailed conductivity structure as local thickening within a mineralized zone.

The most comprehensive interpretation studies to date have been the MSc. thesis of Woods (1975) and the PhD. thesis of Dyck (1980). This paper will concentrate on extending the developed interpretation methods to the third application above.

Comparison of ground and borehole EM interpretation

Figure 35.1 shows a schematic diagram of a conductor within the earth. EM measurements in boreholes are usually confined to the axial component along the hole. The process of interpretation for surface or borehole EM measurements should be identical since physical principals in operation are identical (with the added complication that boreholes may intersect the conductive source of an anomaly). In practice, a significant theoretical advantage of surface measurements is easy access to an adjustable grid of measurement points where a fixed, usually vertical, component may be measured. As with other potential field data, interpretation may be simply restricted to principal profiles crossing the anomalous zone. The advantage of a borehole survey lies simply in that it may afford a closer approach to an anomalous zone of conductivity than is possible from a surface survey.

[1] Lamontagne Geophysics Ltd., 49 Spadina Ave., Toronto M5V 2J1

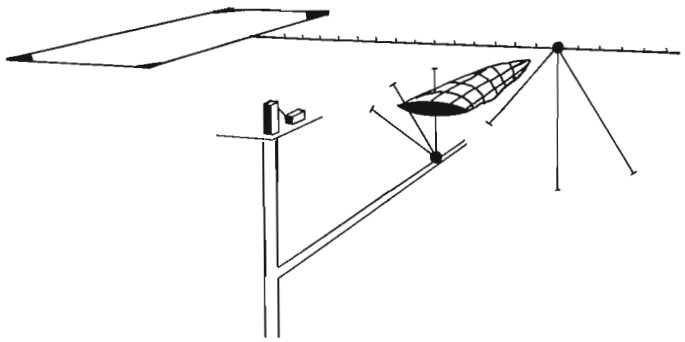

Figure 35.1. *Current practice for time domain EM logging is to lay out one or more surface transmitter loops and log the axial component of the resulting magnetic field in boreholes which may or may not intersect conductors of interest.*

Interpretation tools developed for surface measurement may in many cases be used in the borehole environment as shown in Figure 35.2. For example, the secondary EM response of the horizontal surface component in profile A due to conductor A alone is virtually identical to the secondary axial component response in borehole B from body B alone. Both conductors are of equal strike length, at identical relative dip and distance from the profile, and are maximum coupled to an approximately equal amplitude of primary field. Of course the primary fields measured in the drillhole and the surface will be quite different.

Interpretation of borehole data has been well discussed by Dyck (1980), and is based on the same features as surface EM interpretation namely 1) shape, 2) amplitude, and 3) migration. If a borehole intersects a conductor, then tangential discontinuities (Fig. 35.3) may be a fourth diagnostic parameter. Some of these features are indicated in Fig. 35.4 using the sign conventions of the UTEM system (West et al., in press).

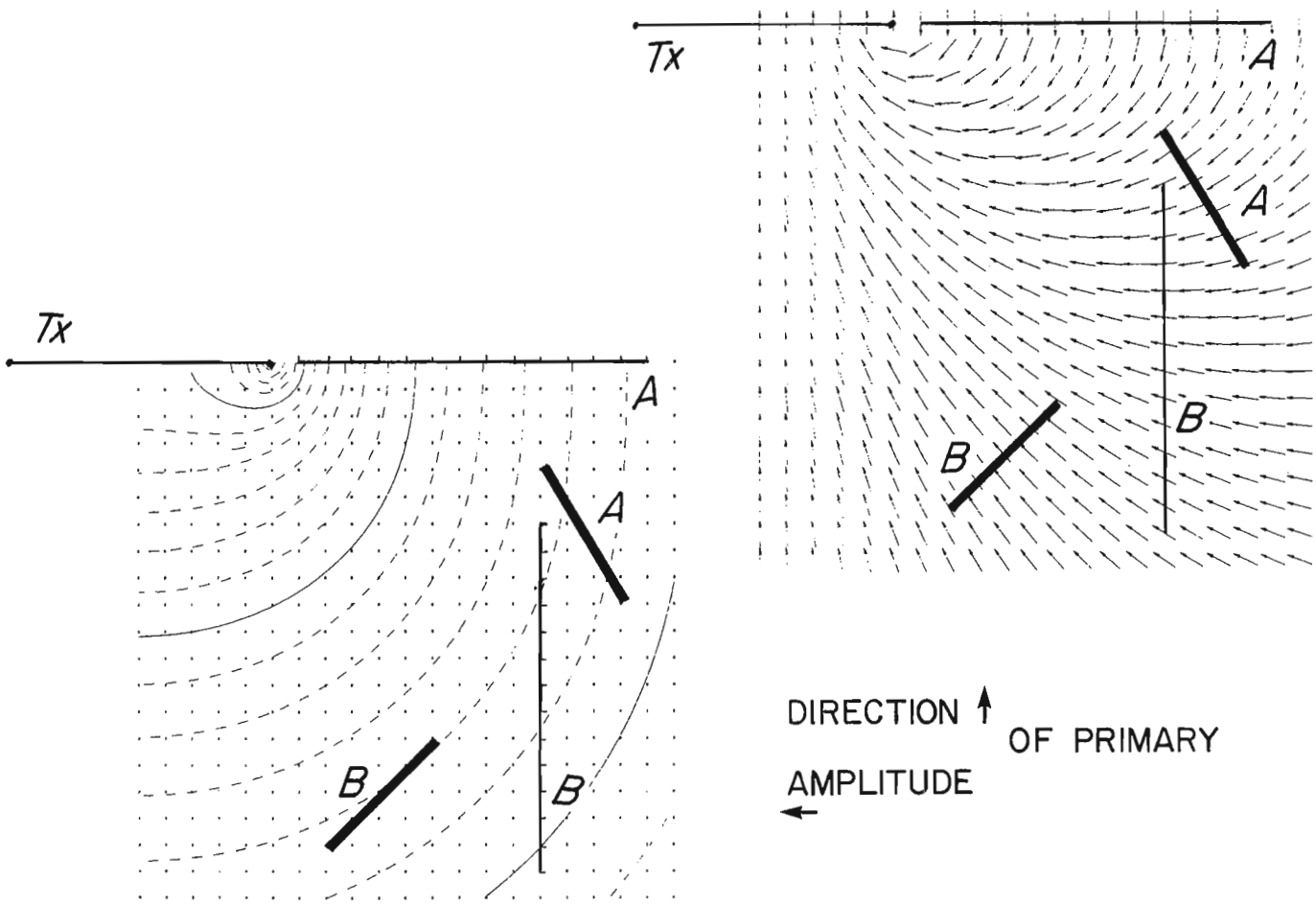

Figure 35.2. *Plot of direction (arrows) and amplitude (contoured) of the primary magnetic field from a square Tx loop on a vertical central profile (from Macnae, 1980). Conductors A and B are both very well coupled to an approximately equal average amplitude of primary field. Shown also are a surface profile A and a vertical borehole profile B.*

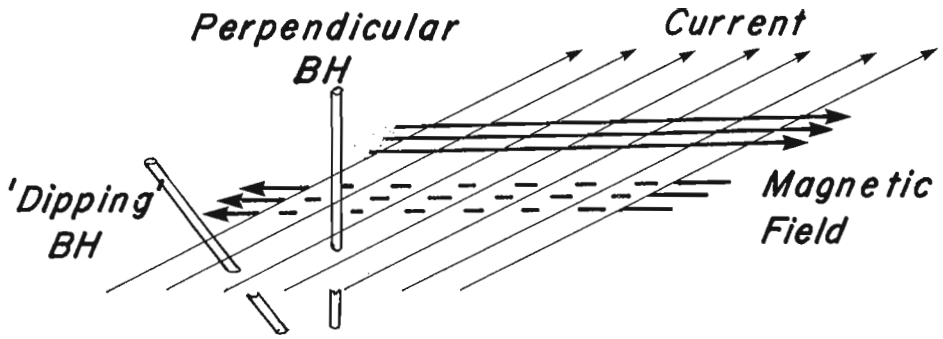

Figure 35.3

Above and below a sheet of current there is a discontinuous magnetic field perpendicular to it as shown. The axial component of the magnetic field in a borehole normal to the sheet of current will exhibit a continuous response, whereas the axial component in any dipping borehole will show a discontinuity across the sheet whose amplitude is controlled by a simple sine rule.

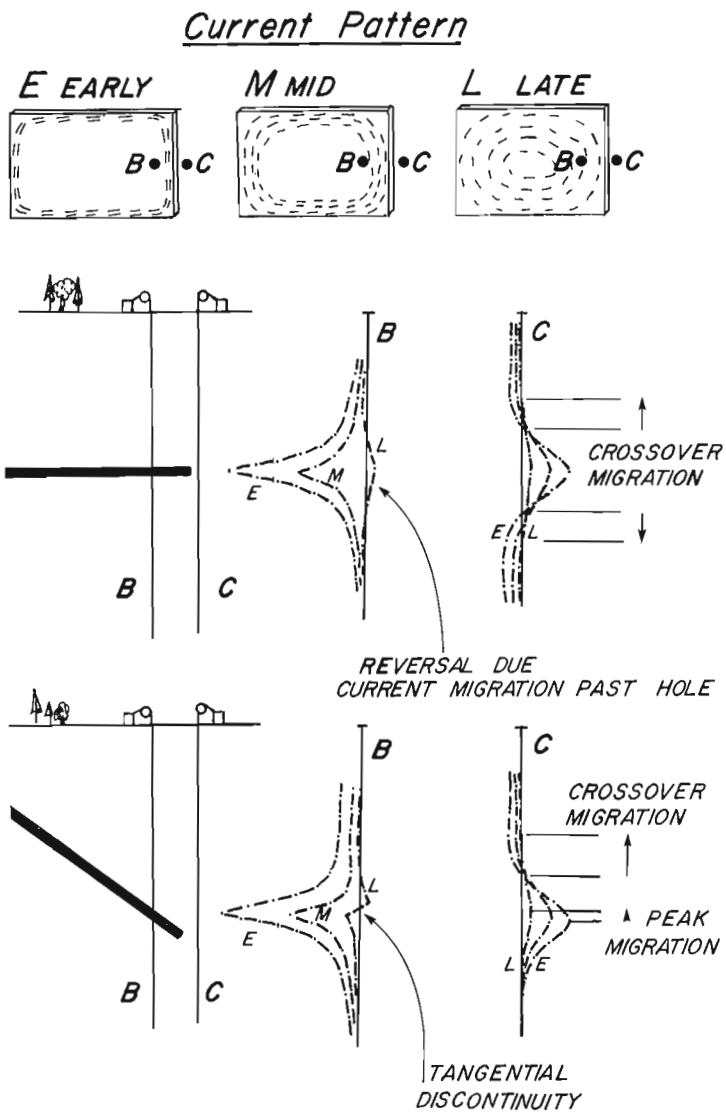

Figure 35.4. *In time domain EM systems with step or pulse excitation the induced currents at early delay times are concentrated at the edges of a conductor, and spread inwards with time at the same time as their amplitude decreases. The effects of this current migration on measured axial component borehole data are schematically shown here.*

Shape may be used as an indicator of dip, size and location of the eddy current system within a conductor. For example, a thin conductor perpendicular to the drillhole will give rise to a symmetrical anomaly. Shape information is often extracted at characteristic points in a manner similar to potential field data (gravity, magnetics) and interpretation is based on features such as half-widths, peak-to-trough ratios, or maximum-slope to peak-amplitude ratios.

Amplitude information is easily interpreted with UTEM or frequency domain data on the basis of a single profile (Macnae, 1983). In conjunction with shape information it can help define geometrical size parameters much better than shape alone. For all systems, the response amplitude as a function of transmitter location is very useful in estimating the relative coupling of body to transmitter and hence conductor location.

Migration keeps track of the movement of characteristic points such as peak location, location of slope maxima or half-widths as a function of delay time or frequency. This can be translated into keeping track of the migration of the induced eddy current system with time or frequency. With usual time-domain waveforms this is basically the collapse of the induced currents. The pattern of migration may be a clear indicator of dip and, as will be seen later, can be used as an indicator of inhomogeneity.

Figure 35.5 shows schematically how current migration in a conductor C may be related to a characteristic point migration in a drillhole. If the current in C moves inwards by an amount shown by the arrows, the amount of migration of a characteristic point in the drillhole will depend on the orientation of the drillhole, but is commonly closely comparable to the distance of current migration in the conductor. The radiating lines shown are the loci of the points where the component of the secondary magnetic field vanishes in the plane of the induced currents.

Tangential discontinuities can occur across a thin conductor only in the components of the magnetic field parallel to the interface as shown in Figure 35.3. Their amplitude depends on the relative dip of the conductor to the drillhole, and also on the amplitude of local current flow. Based on the sign of the response it is possible to say in many cases whether most of the induced current flow lies inside or outside the drillhole at any delay time, and if tangential discontinuities are present whether current flow is local or distant.

Geological complexity

Figure 35.6 shows four different simple geological targets whose outline is fairly similar, each of which may give similar thickness of intersection in a borehole. UN represents a fairly uniform plate-like body, CO is a geologically common case of a thick conductive core within a broader halo conductor. ET is a zone with edge thickening; geologically this could be a case of a larger conductor such as CO which has been cut by a fault. LT represents the case of a local "pod" or "lens" thickening within a wider zone. Since cases ET and LT were considered to be the most difficult to interpret from borehole data where the hole does not pass through the thickened part of the zone, it was decided to perform a scale model study to see what characteristics their response would have.

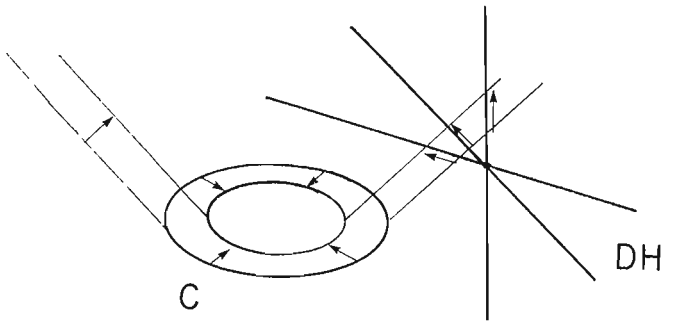

Figure 35.5. *Schematically, if a current system C migrates inwards, the characteristic points in its resulting magnetic field will also migrate by about the same amount. The lines moving away from the current system C are the loci of zeros in the magnetic field in the plane of C.*

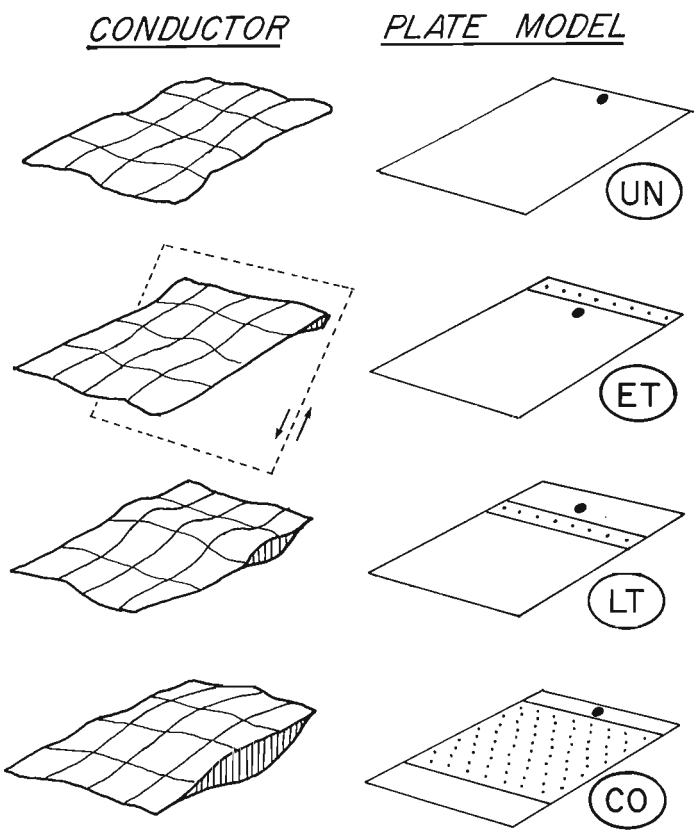

Figure 35.6. *Four geological models and corresponding thin plate conductors, from top to bottom Uniform, Edge Thickened, Locally Thickened and Conductive Core.*

A plate model was set up with geometry as shown in Figure 35.7, with the plate dipping at 45°. The local, or edge thickening was modelled by folding the metal model to form a triple width of the geometry as shown in Figure 35.6. This corresponds to a 3:1 zone thickening or, using the principal of equivalence, to a 3:1 conductivity increase with no thickening.

Scale model data

Rather than collect data along a number of different borehole profiles, it was decided to measure the response of all three components in a plane parallel to the plate, at the distance of closest possible approach. Using the standard upward continuation (Grant and West, 1965) it is possible then to predict the secondary magnetic field at any location in space above the plane of the plate. The standard boundary conditions imply that the field in the plane below the plate has even symmetry in its normal component, and odd

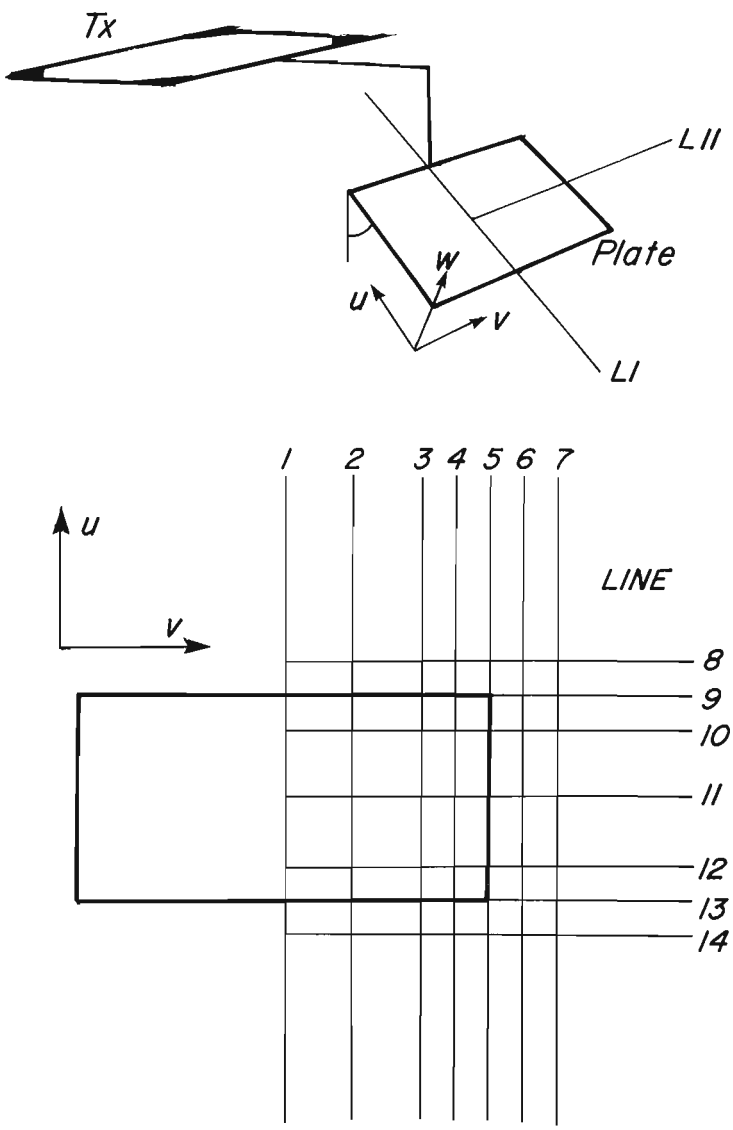

Figure 35.7. *Scale model geometry. Profiles were measured over half the u-v plane on 14 survey lines.*

symmetry in the components parallel to the plane of the plate. Thus, from a complete set of measurements in one plane we can predict the fields at any point in space, and hence if any particular borehole location is specified, we can generate the axial components that would be measured from the scale model. This procedure is in principal equivalent to the way program PLATE (Dyck et al., 1981) calculates the secondary fields at any point from the known eigencurrents.

Figures 35.8 to 35.13 contain the scale model results in the (u, v, w) components on 14 profiles whose locations are shown in Figure 35.7. The data were collected as close to the plate as physically possible: a perpendicular distance of w=0.005L where L is the strike length of the conductive sheet.

Clear in the data is that the expected response of the parallel (u, v) components is confined to the area directly above the plate as these components are basically null coupled at the ends of the profiles away from the plate. All data were collected using the UTEM waveform (West et al., 1984) and show the response from early (largest amplitude) to late (smallest amplitude) delay times. The response in the u, v components corresponds closely to the amplitude of the tangential magnetic field at each location, and will be half the total discontinuity from one side of the conductor to the other. The normal (w) component is continuous across the conductor; at zero delay time the induced current is such as to reduce the total normal component of the magnetic field at the conductor to zero. The w-component anomaly (in the plane of the conductor) persists to distances away from the conductor in contrast to the parallel components. Of course, the u, v components do have more extensive anomalies on any parallel plane not passing through the plane of the plate.

Careful examination of the profiles shows that the measured responses over the three types of conductor (UN, ET, LT) are different in detail. We will use the data to compute the current pattern in the plates as a function of time before describing the profile differences.

Migration of eddy currents

The parallel components (u, v) of the scale model data represented in Figures 35.8 to 35.13 were downward continued to the plane of the plate. In the plane of the plate, the only contribution to the parallel magnetic components comes from the local currents perpendicular to each magnetic component, i.e. the H_u anomaly is due to the planar current density I_v at the measurement point. From the surface magnetic field data, vectors in the plane of the plate were plotted that show point evaluations of the amplitude and direction of the local "sheet" current (Fig. 35.14) at early and late times. The late time currents are much smaller than the early time currents, but have been scaled up to show the current distribution pattern clearly.

For all three models, the current is concentrated at the conductor edge at early times, and little difference is evident between the models. At late delay times, the current in the non-uniform models is concentrated in the conductive strips relative to the currents in the uniform model. It is this characteristic which gives us the basis to differentiate between these models using field data. We note, of course, that migration of currents does occur even in the case of a uniform conductor, so it will be the difference in migration patterns with time that will be characteristic.

Figure 35.15 shows the location of the zero crossing in the w component (presented in Fig. 35.8 to 35.13) at three different delay times; early, mid, and late. The uniform case shows migration of characteristic zero crossing point of about 13% of the long side of the conductor in that direction (v). The edge thickening case shows distance migration of only 3% in the v direction. The conductor with local thickening (LT) shows distance migration of over 25% in the v direction. In the u direction, all three models show migration of about 20% of the width of the plate. Note that in all three cases there is little difference between early and middle times, but significant difference at late times.

Thus in the field, the method for interpreting local inhomogeneity will have to rely on the differences from early to late time. Interpretation of borehole data then for the presence and location of conductor improvement (thickening) would involve:

1) Estimation of location/size of target by conventional interpretation.
2) Measurement of the amount of migration of characteristic points on the profile as a function of time.
3) Estimation of the amount of migration of the induced currents as a function of delay time using simple geometry.
4) Comparison of this migration distance to the size of the conductor and looking for unusually fast or slow migration to locate local thickening.

As an example we can use the schematic data in Figure 35.4. From hole C for the horizontal conductor the outward crossover migration by a distance d would correspond to an inward migration of current of about the same distance d (to reduce the influence of background effects we should use maximum slopes rather than crossovers on real data). The data from borehole B indicate current migration from the edge past the drillhole. A suitable characteristic might be the half-width of the anomaly as a measure of the migration.

For the 45° dipping conductor, we note that the positive peak in borehole B data is located almost in the plane of the conductor and thus shows little migration. However, in the case of borehole C both the negative peak and crossover locations show clear migration effects. In detail, the migration may be seen to be relatively uniform from early to late times, as expected for the uniform conductor used to generate the data for Figure 35.4.

Field example

Figure 35.16 shows an example from an actual geological problem. The sulphide horizon was known to have significant thickening in a fold from shallow drilling and geological mapping. The bulk of the zone was however downfaulted and thus interpreted to lie at depth. Based on geological reasoning holes DH-A and DH-B were drilled, hole DH-A cutting the sulphides as expected and DH-B subsequently not intersecting any mineralization. The fold thickening was thus inferred geologically to lie between the two holes. A potential problem here, however, is the presence of a fault detected in the drillholes as marked, which, if it were shallowly dipping, would displace the inferred mineralization in the nose of the fold.

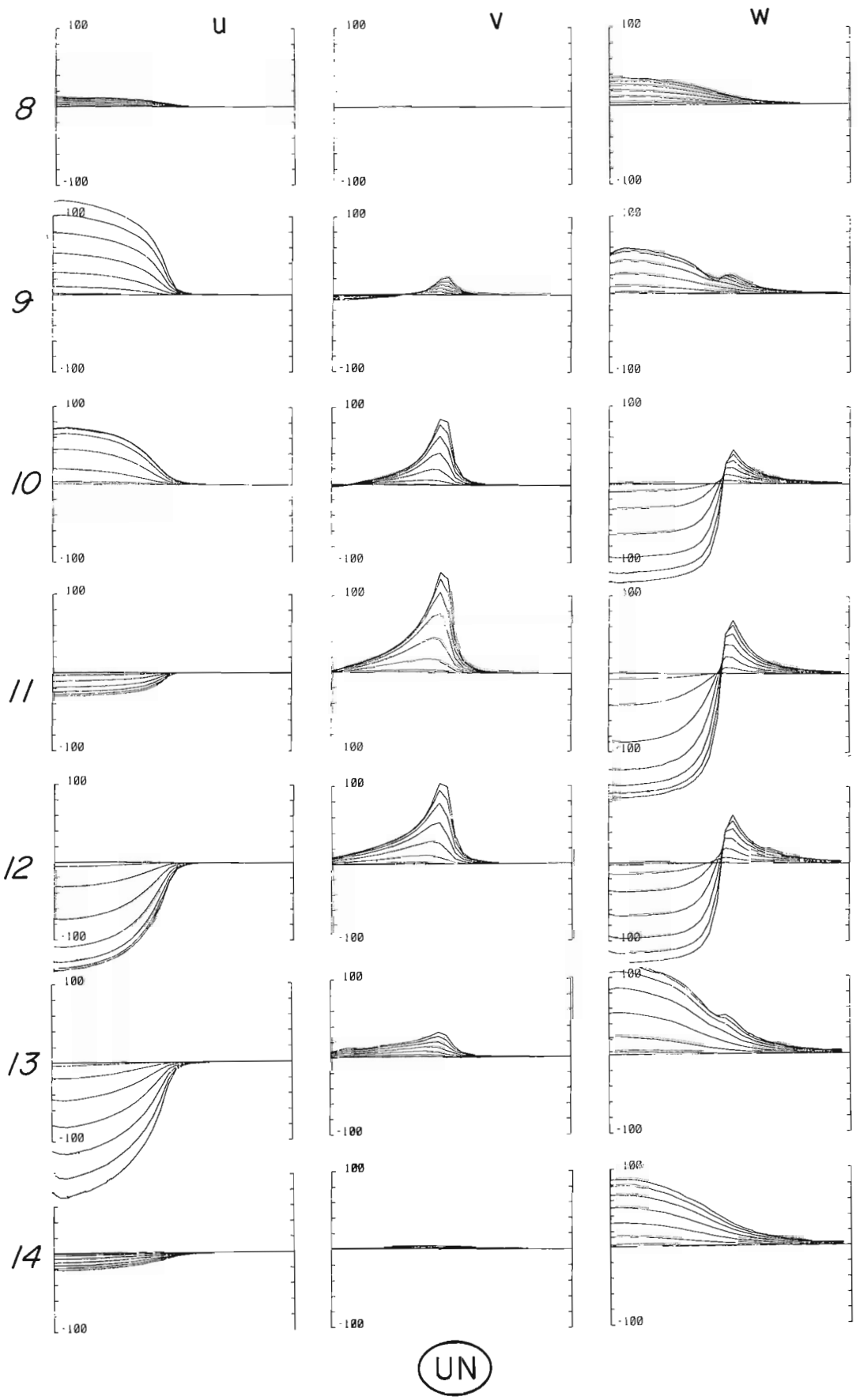

Figure 35.8. *UTEM scale model response over lines 8 to 14 with a uniform plate conductor.*

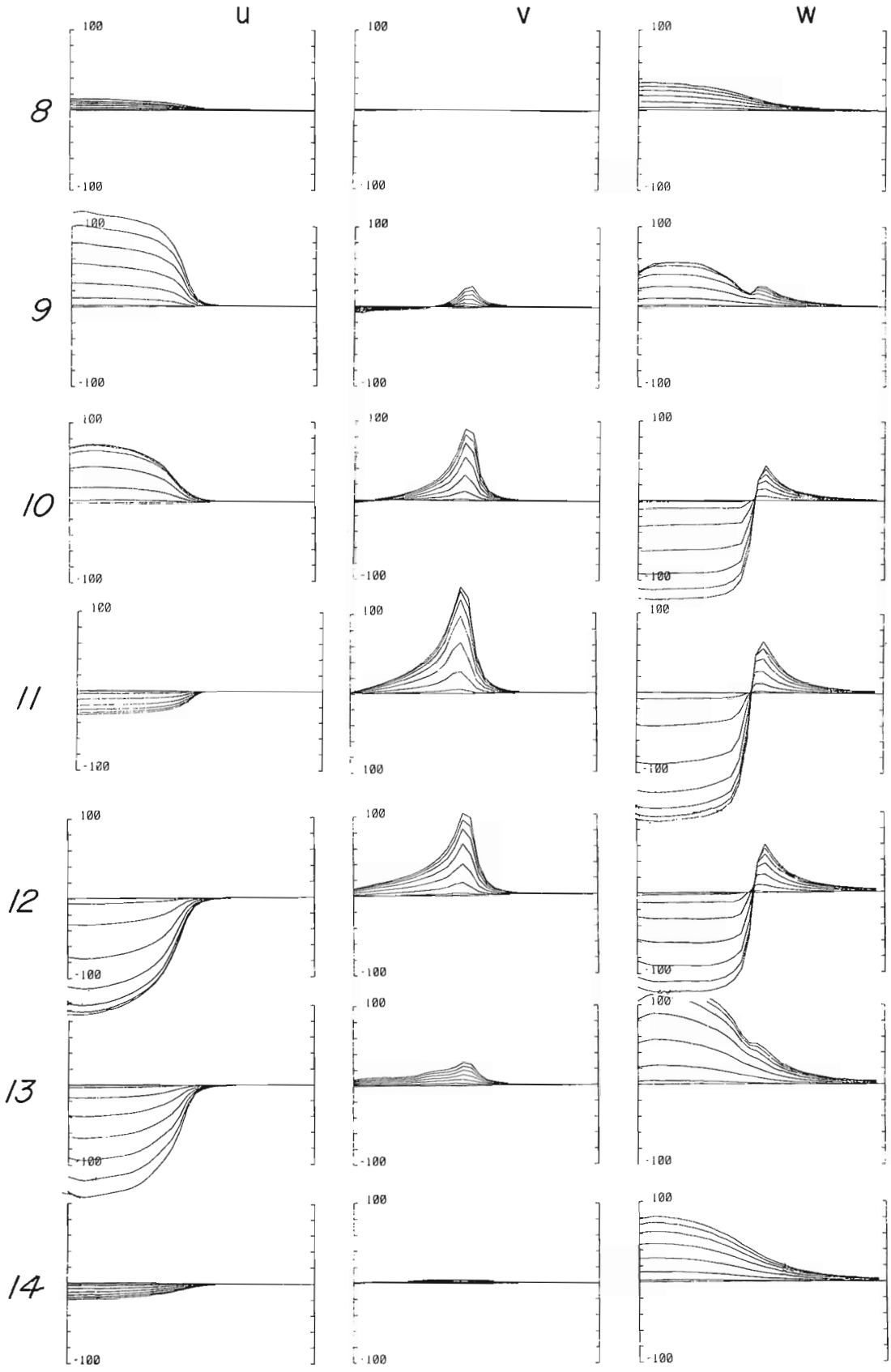

Figure 35.9. *UTEM response over an edge thickened conductor. Compared to the uniform conductor note the sharper crossovers in the w component, and extra late time amplitude in the v component over the thickened part of the zone.*

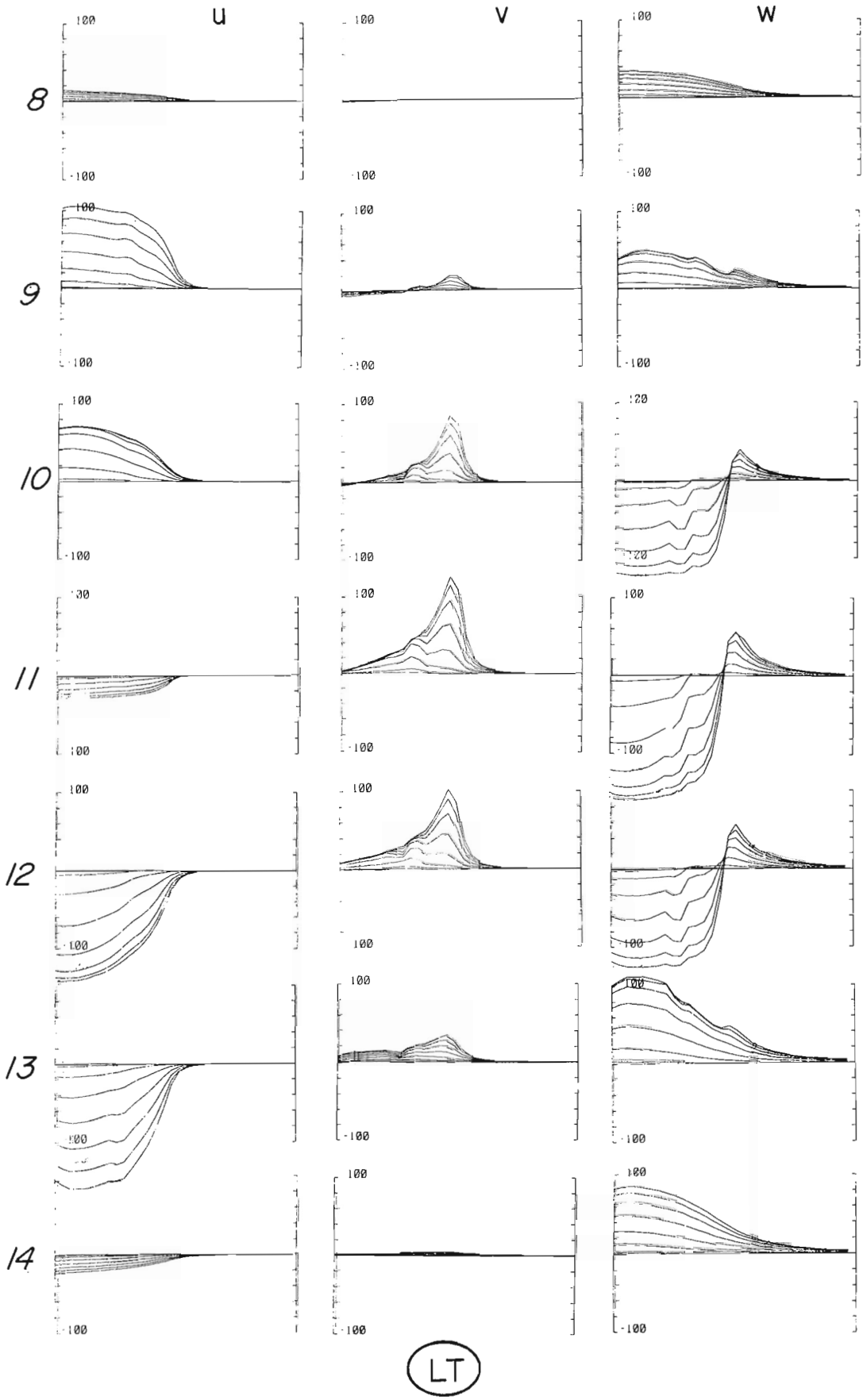

Figure 35.10. *UTEM response over the locally thickened conductor. Clear anomalies are present in the v and w components.*

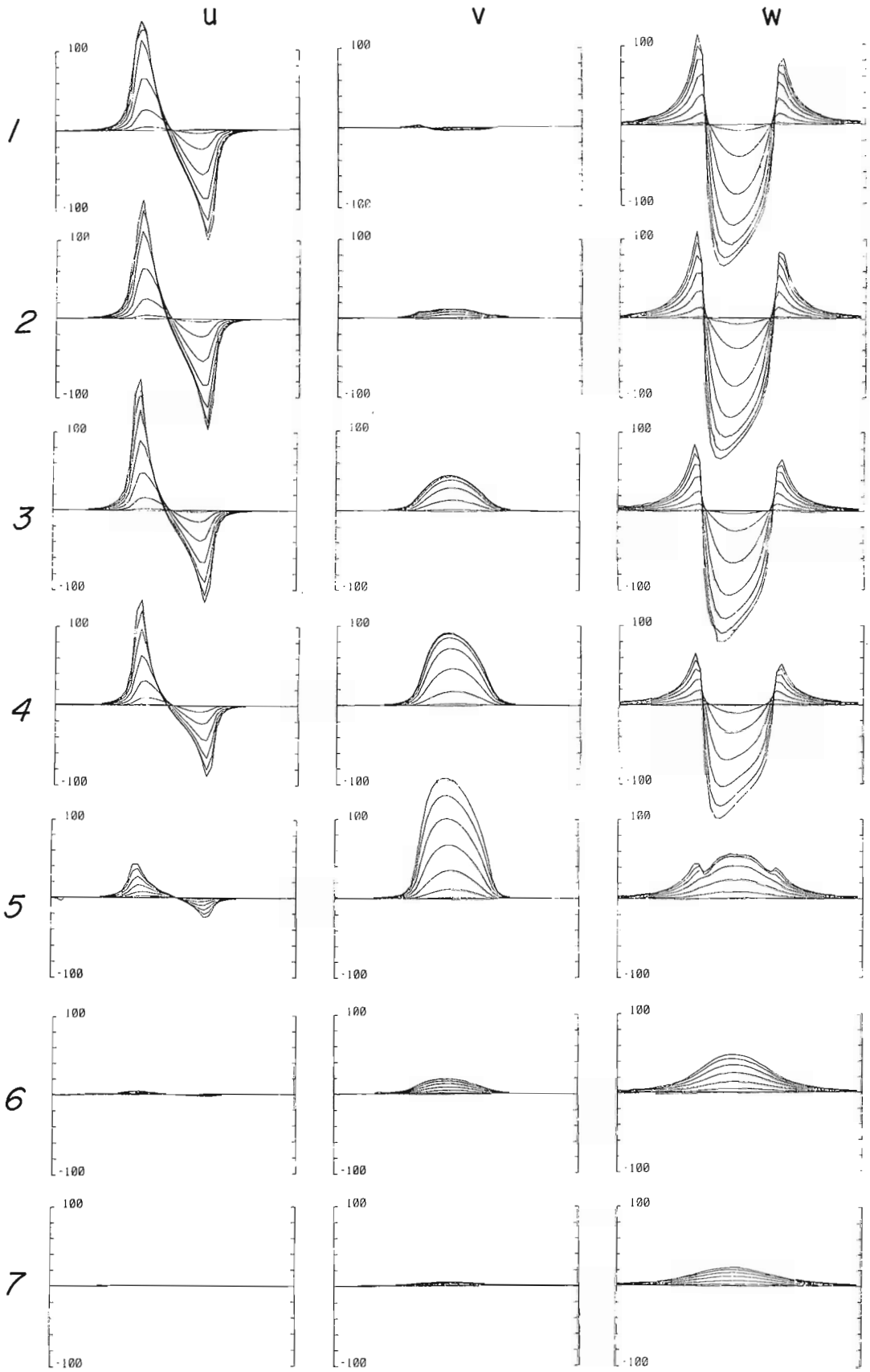

Figure 35.11. *UTEM response over the uniform conductor across the narrow dimension.*

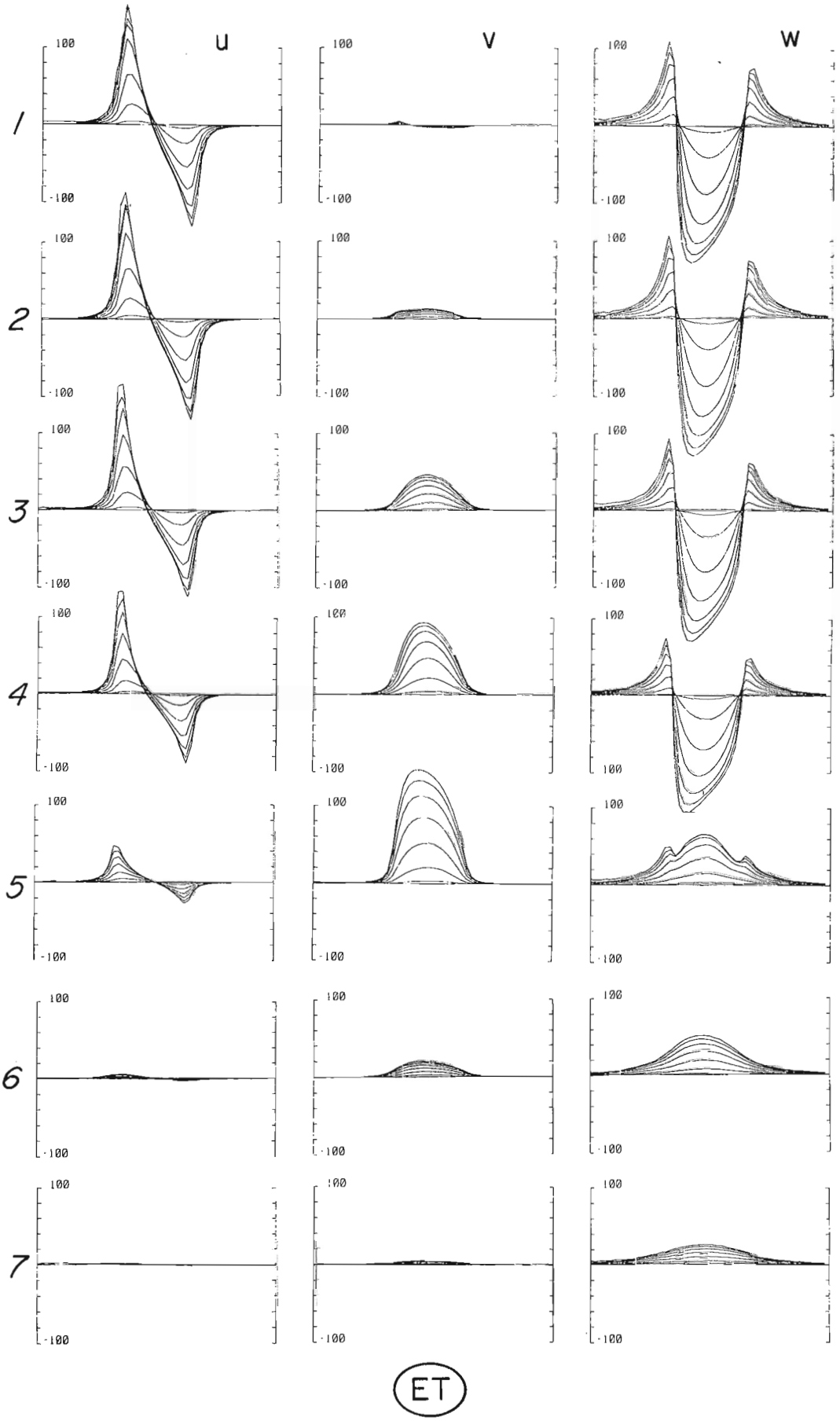

Figure 35.12. *UTEM response across the edge thickened conductor.*

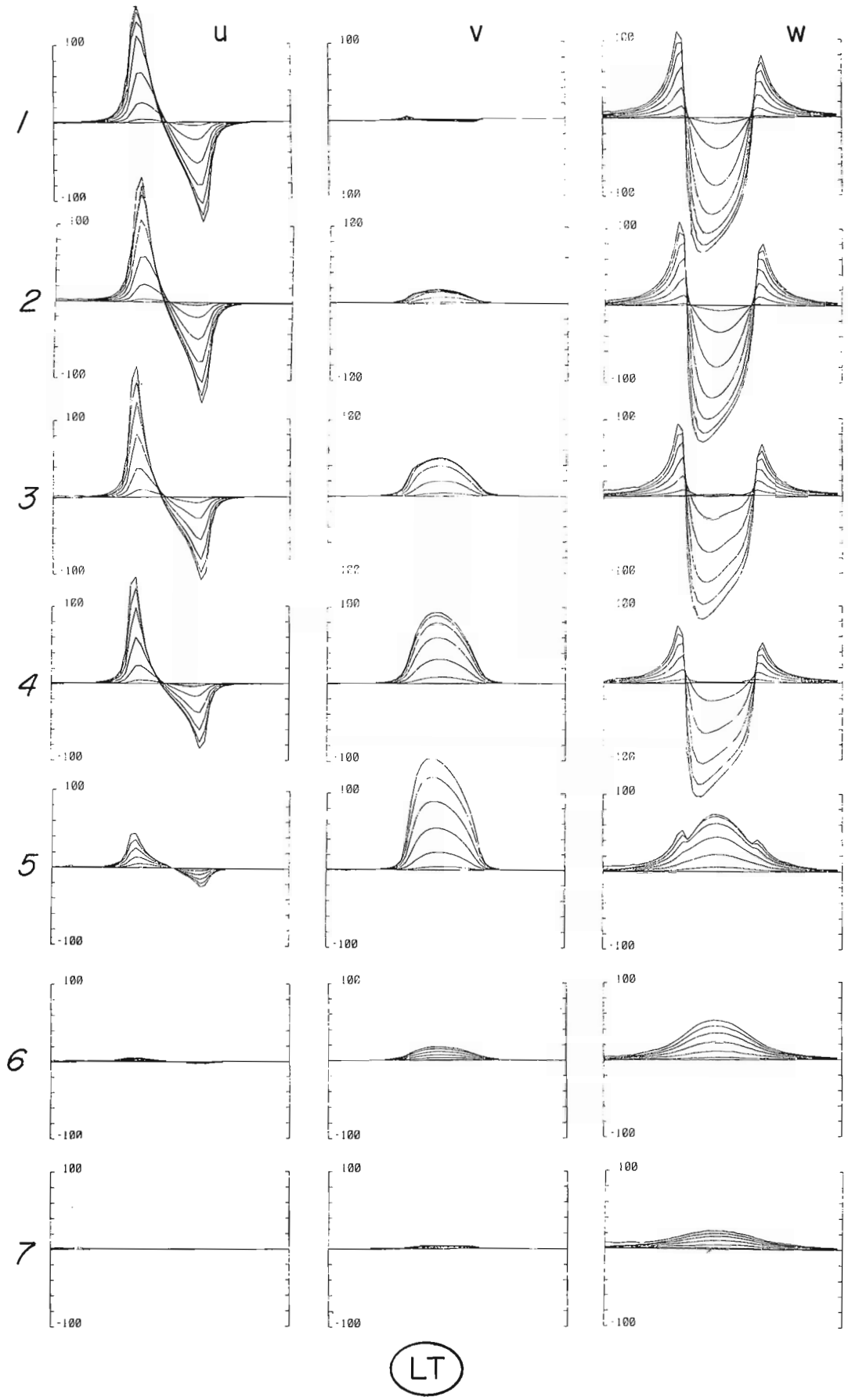

Figure 35.13. *UTEM response across the locally thickened conductor. Since the profiles are all parallel to the thickening, the anomaly is less obvious on these profiles than those in Figure 35.10.*

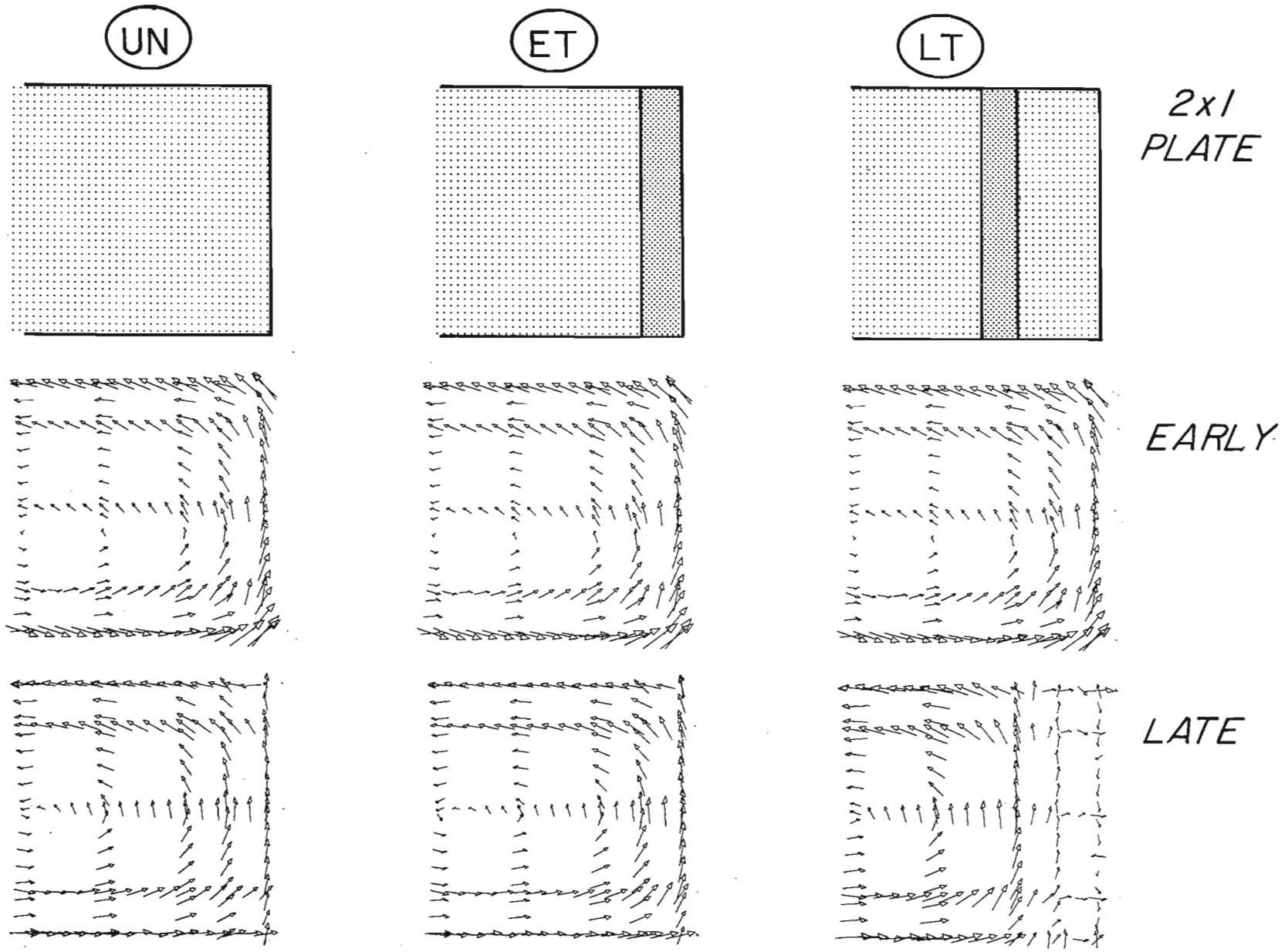

Figure 35.14. *Surface current vectors over half of a thin plate conductor. Amplitudes of the late time data are scaled up compared to the ear.y time data. Note the similarity in responses at early times and the increased concentration of current in the conductive strips at later times.*

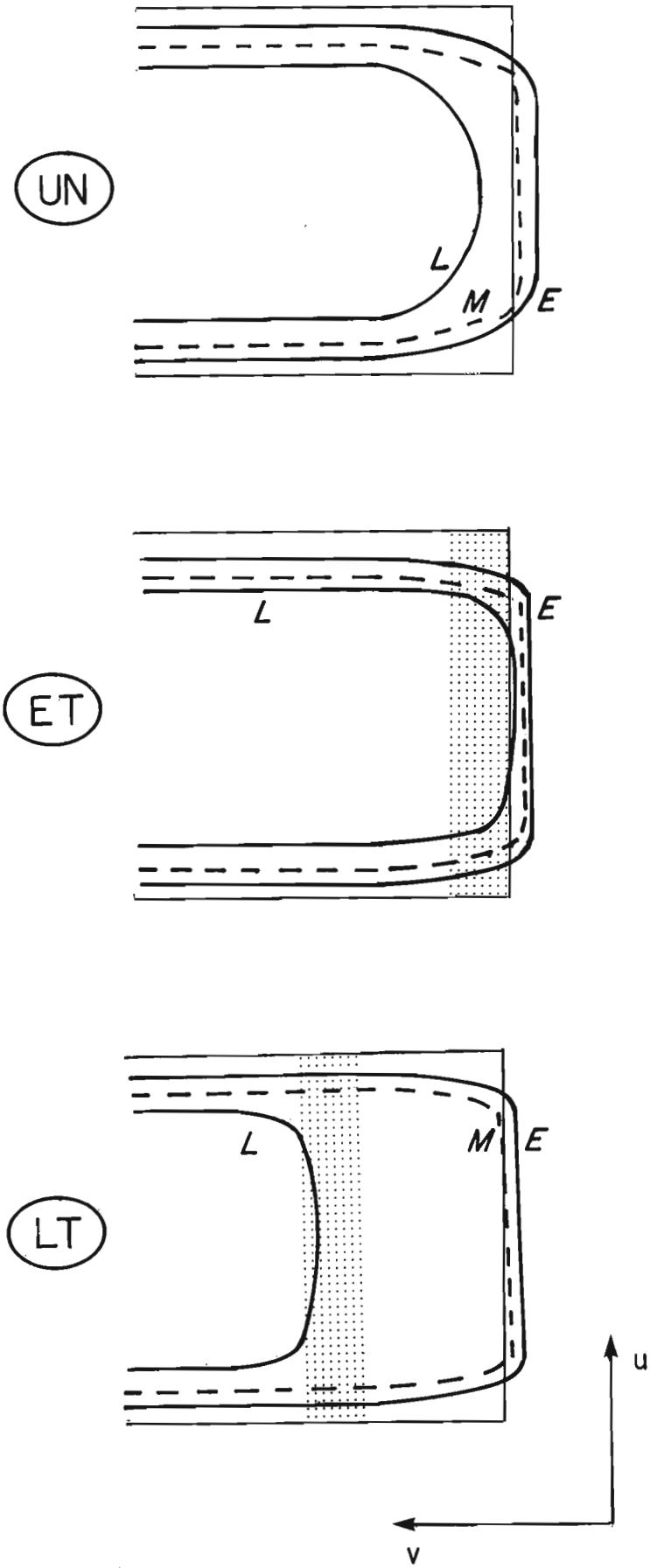

Figure 35.15. Migration of zero crossings with time over the three plate models. The plane of measurement is raised 0.1W above the plate where W is the width of the plate.

Borehole EM logging with the Crone PEM system using five different transmitter loop setups was done for both holes. The survey was conducted to determine whether the thickened zone of mineralization is present. To aid in the interpretation of the field data, a scale model study was run. The study would also determine if deepening the drillholes and then re-logging them with EM would detect any conductive mineralization in the inferred fold if the existing data were insufficient.

All available data were interpreted in order to constrain the conductor geometry and a scale model was constructed at the University of Toronto scale modelling facility. Figure 35.17 shows the selected profiles from the modelling using one transmitter loop with and without a projection on the plate model (Fig. 35.16).

Hole B was able to define the closest approach of the plate by both amplitude and shape data. It is clear from model data of DH-B that the width of the negative peak is increased by the presence of the vertical projection. However, field data show that the hole is obviously not deep enough to define the anomaly fully, thus deepening and re-logging the hole would aid in detecting any mineralization in the inferred fold.

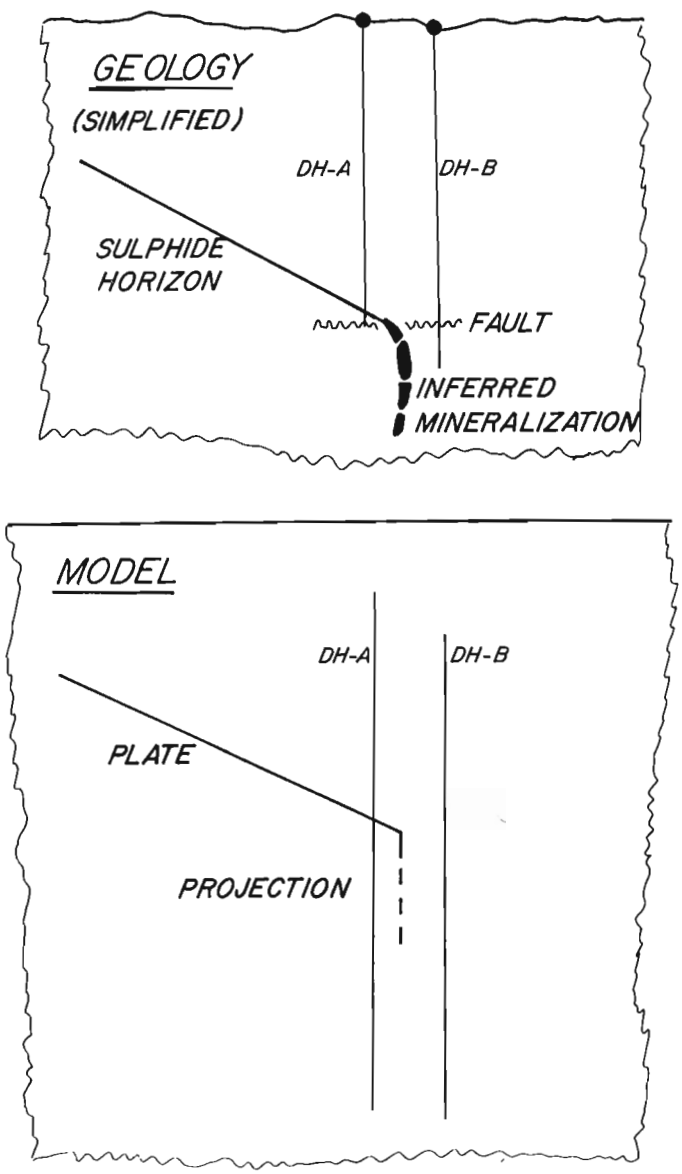

Figure 35.16. Simplified geology and corresponding thin plate model for drillhole data.

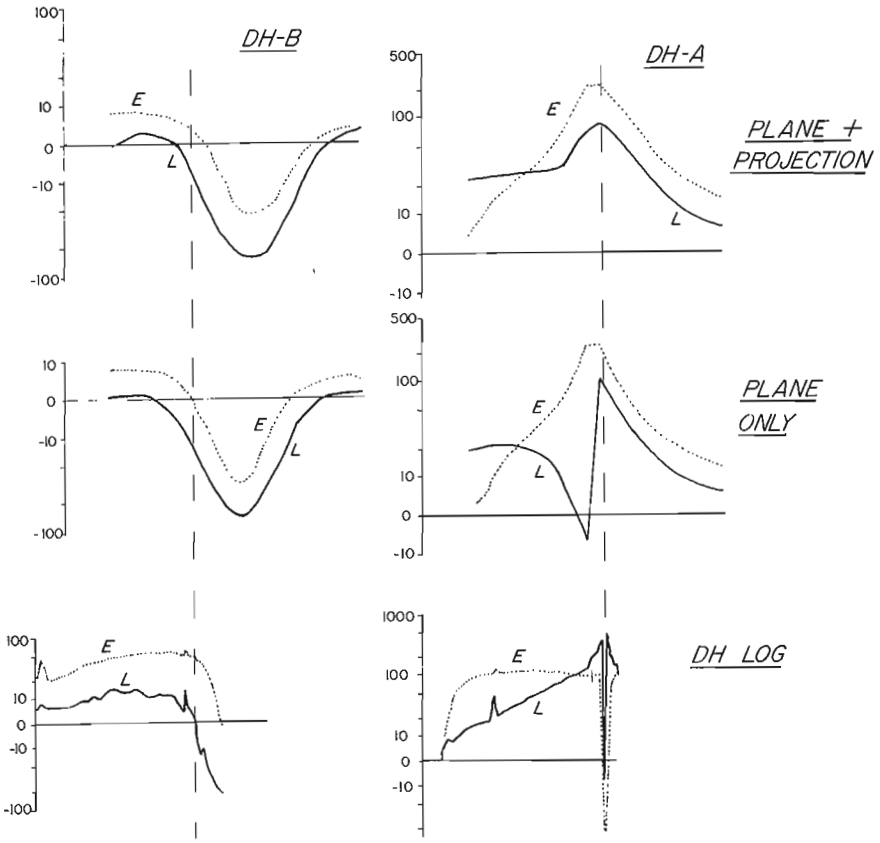

Figure 35.17

Field and model data using the Crone PEM system at early (E) and late (L) delay times. The absence of any late time tangential discontinuity in the DH data indicates that the plane only cannot fit the field data, and that either edge thickening or the modelled projection is present.

On the other hand, field data from DH-A show characteristic differences between the two models at the depths actually logged. Using the edge location fixed by DH-B, and matching the conductivity-thickness of the plate at 110S, if a uniform plate only were present, the current would have migrated inwards to the region of DH-A and produce a large tangential discontinuity as shown. The discontinuity cannot be observed in the field data. Thus, it is likely that either the edge of the zone is thickened and more conductive (case ET from earlier modelling) or the vertical projection is present which allows for current migration away from DH-A without too close an approach to DH-B. The interpreted results of the modelling study await testing by the drill.

Conclusions

By interpreting migration of characteristic points and amplitude of tangential discontinuities in drillhole EM data, it is possible to track the migration of induced eddy currents in a conductor. If local thickening or conductivity increase is present,the induced currents tend to migrate more quickly towards areas of increased conductance than if the body were uniform, and continue to concentrate within these regions.

Application of these principals to field data is not easy, as other geometrical complications may arise. Nonetheless, if we are able to take full advantage of the multichannel EM data available from current instrumentation, interpretation techniques for the complexities of the response are required.

Acknowledgments

The borehole interpretation research project at Lamontagne Geophysics is supported by the Ontario Geological Survey through the Exploration Technology Development Fund Grant GR-010. J.M. acknowledges support through an N.S.E.R.C. Industrial Research Fellowship.

The authors also wish to thank the two critical reviewers for their thoughtful comments and suggestions.

References

Dyck, A.V.
1980: A method for quantitative interpretation of wideband, drill-hole EM surveys in mineral exploration; Geophysics Laboratory, University of Toronto, Research in Applied Geophysics No. 23.

Dyck, A.V., Bloor, M., and Vallee, M.A.
1981: User manual for programs PLATE and SPHERE; Geophysics Laboratory, University of Toronto, Research in Applied Geophysics No. 14.

Grant, F.S. and West, G.F.
1965: Interpretation Theory in Applied Geophysics; New York, McGraw Hill.

Macnae, J.C.
1980: An atlas of primary fields due to fixed transmitter loop EM sources; Geophysics Laboratory, University of Toronto, Research in Applied Geophysics No. 13.

1983: EM interpretation manual for fixed transmitter systems; Lamontagne Geophysics, Toronto.

West, G.F., Macnae, J.C., and Lamontagne, Y.,
1984: A time-domain EM system measuring the step response of the ground; Geophysics, vol. 49, No. 7, p. 1010-1026.

Woods, D.V.
1975: A model study of the Crone borehole pulse electromagnetic (PEM) system; MSc. Thesis, Queens University, Kingston, Canada.

36.

EXAMINATION OF THE ELECTRICAL CONDUCTIVITY STRUCTURE IN THE REGION SURROUNDING A BOREHOLE BY A NATURAL SOURCE TECHNIQUE

Alan G. Jones[1]

Jones, A.G., Examination of the electrical conductivity structure in the region surrounding a borehole by a natural source technique; in Borehole Geophysics for Mining and Geotechnical Applications, ed. P.G. Killeen, Geological Survey of Canada, Paper 85-27, p. 337-341, 1986.

Abstract

Two major factors hinder mineral exploration at present: (1) a conventional resistivity borehole log is often more indicative of the resistivity of the pore-filled fractured rock in the close locale (<1 m) of the borehole than the actual resistivity of the layer in which the probe is located; and (2) ground-based EM techniques, both natural and controlled source, are often unable to locate a mineralized zone beneath another mineralized zone.

In this paper, the theory is presented for the basis of a conceptually new type of borehole technique based on the ratio of the measurement of the natural horizontal magnetic field variation to its gradient with depth, down the hole, viz. $V_{x,d}(\omega) = H_{x,d}(\omega)/(\partial H_{x,d}(\omega)/\partial z)$. Defining the "downhole apparent resistivity", $\rho_a(\omega,d)$ by

$$\rho_a(\omega,d) = \omega\mu_0 \left| V_{x,d}(\omega) \right|^2$$

it is shown that, for a 1D earth structure, as ω tends to infinity, then $\rho_a(\omega,d)$ tends to the actual resistivity of the layer in which the probe is located. Also, $\rho_a(\omega,d)$ is independent, in the 1D case, of any structure above it, and weakly dependent in the 2D case. The technique has the benefit of most borehole methods of being far superior at resolving structure at depth below it, e.g., a second good-conducting zone, than equivalent conventional ground-based methods (e.g., MT and/or GDS).

Application of the technique to some theoretical 1D and 2D structures is presented, as well as a discussion of the feasibility of constructing the necessary sensor for the proposed technique.

Résumé

Deux grands facteurs gênent l'exploration minérale actuellement: 1) il arrive souvent que la diagraphie de résistivité ordinaire décrive la résistivité de la roche fracturée poreuse au voisinage immédiat (<1 m) du trou de sonde, plutôt que la résistivité réelle de la couche où se trouve la sonde; et 2) il arrive souvent que les techniques de sondage électromagnétique au sol, qui utilisent des courants électriques d'origine naturelle et artificielle, ne permettent pas de repérer une zone minéralisée située sous une autre.

Dans le présent rapport sont exposées les bases théoriques d'un nouveau type de technique de sondage dont le principe met en rapport la mesure de la variation du champ magnétique horizontal naturel et son gradient en fonction de la profondeur, c'est-à-dire:

$$V_{x,d}(\omega) = H_{x,d}(\omega)/(\partial H_{x,d}(\omega)/\partial z)$$

La "résistivité apparente de fond", c'est-à-dire: $\rho_a(\omega,d)$ est déterminée de la façon suivante:

$$\rho_a(\omega,d) = \omega\,\mu_0 \left| V_{x,d}(\omega) \right|^2$$

Ainsi, dans le cas d'une structure 1D, la valeur $\rho_a(\omega,d)$ tend vers la résistivité réelle de la couche où se trouve la sonde à mesure que ω tend vers l'infini. On constate également que, dans le cas de 1D, la valeur $\rho_a(\omega,d)$ est indépendante de toute structure située au-dessus, et que, dans le cas de 2D, cette valeur est légèrement influencée par une structure située au-dessus. Dans le cas de la plupart des méthodes de sondage par trou de sonde, cette technique permet de déterminer beaucoup mieux les structures rocheuses situées sous la sonde, par exemple une deuxième zone possédant une bonne conductivité, que ne le peuvent les méthodes classiques de surface (par exemple la méthode MT ou la méthode GDS, ou les deux).

Le présent rapport décrit l'application de cette techique à des structures théoriques 1D et 2D et l'on y examine la faisabilité de construire le détecteur voulu.

[1] Geophysics Division, Geological Survey of Canada, 1 Observatory Crescent, Ottawa, Ontario, Canada, K1A 0Y3

Introduction

An examination of the electrical conductivity structure in the region surrounding a borehole can lead to delineation of zones of economic interest within the host rock. These zones either may have been interpreted from surface data and missed by the subsequent drilling operation, or their existence may not have been previously suspected due to the electromagnetic (EM) shielding effect of other conductivity anomalies. Also, the logging of a borehole to determine the in situ rock matrix resistivity is often hampered, and indeed is often erroneous, because of the infill, by the highly conducting drilling mud, of the near borehole fractured zone caused by the drilling itself. Furthermore, all active borehole procedures that rely on the generation and/or measurement of electrical fields cannot be utilized in plastic cased boreholes.

Active source induction logging techniques can be employed to circumvent the last two problems detailed above. The two probes developed by the BRGM of France (Frignet, 1986) - Romulus and Eric - are prime examples of such devices. However, the investigation within the vicinity of the hole by Eric is limited to some 10 m, and accordingly techniques in which the source is placed on the surface must be used (for example Worthington et al., 1981). Such surface active source methods suffer from the principal disadvantage of necessitating large loop or electrode configurations.

In order to evade problems associated with a controlled source, a conceptually new type of natural source borehole technique is herein described. The method, called Vertical Gradient Magnetometry (VGM), monitors the attenuation of the natural time-varying horizontal magnetic field components of the electromagnetic field as it diffuses

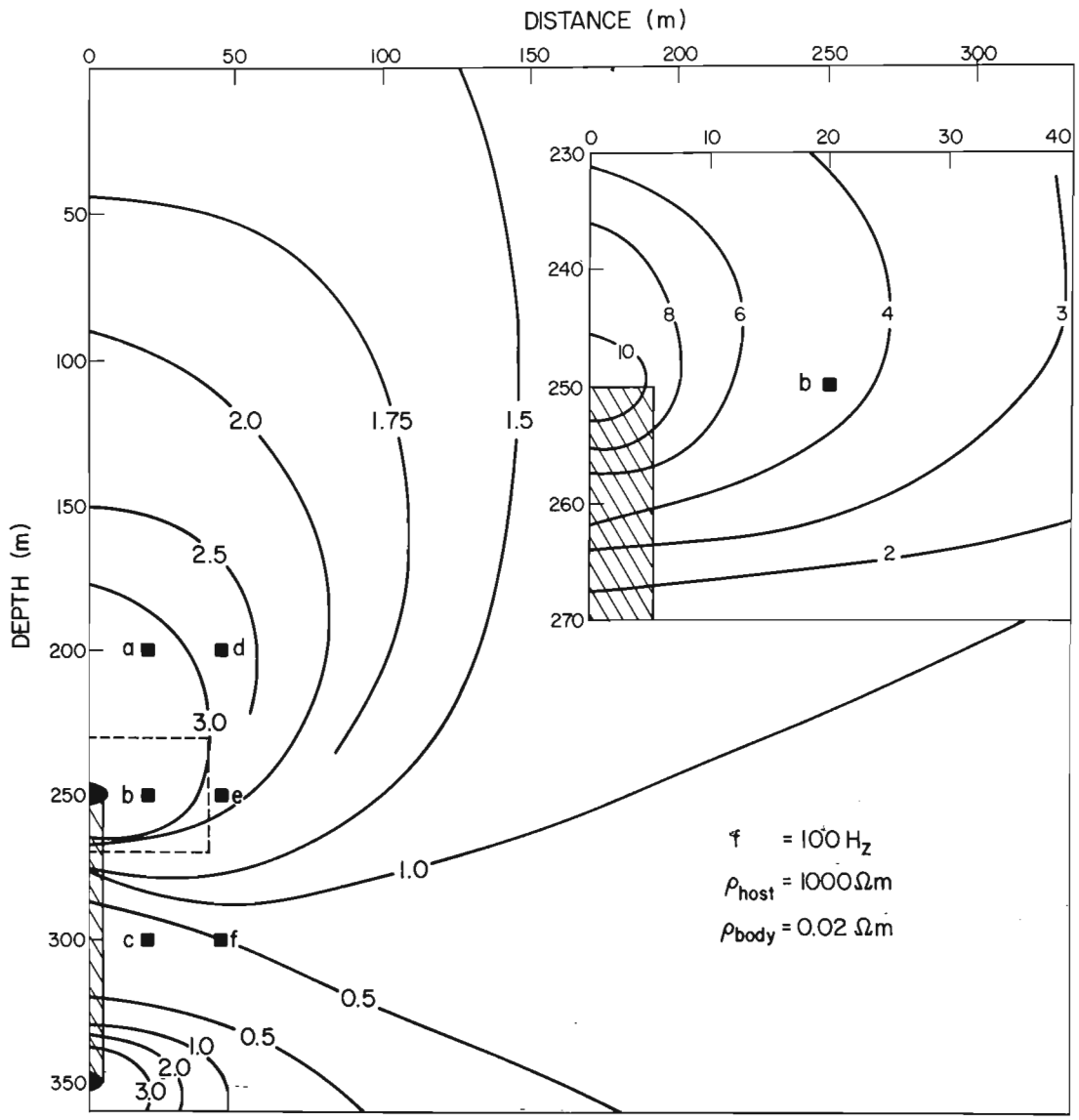

Figure 36.1. *Isolines of the horizontal magnetic field amplitude, at 100 Hz, in the y-z plane, due to E-polarization mode induction in a highly conducting anomaly (shaded) buried in a more resistive half space. The amplitudes are normalized to a value of unity on the surface at a distance of one skin depth away from the anomaly, i.e., at y,z co-ordinates (1500,0). The anomaly has a conductivity of 50 Sm^{-1} in a host country rock of 10^{-3} Sm^{-1}. Illustrated in the inset is a close-up view of the isolines around the top edge of the anomaly. Also shown are the six receiver positions (a,b,c,d,e,f) referred to in the text.*

downward through the earth. The VGM response function in a given direction, $V_y(\omega,d)$, is dependent on both the frequency of observation, ω, and the depth at which the observation is being made, d. This response function is given by the ratio of the horizontal magnetic field at that depth, $H_y(\omega,d)$, to its vertical gradient, $\partial H_y(\omega,d)/\partial z$, viz.,

$$V_y(\omega,d) = \frac{H_y(\omega,d)}{\partial H_y(\omega,d)/\partial z} \qquad (1)$$

(similarly for $V_x(\omega,d)$). From the response function can be defined, analogously to the magnetotelluric (MT) method, depth and frequency dependent VGM apparent resistivity and phase functions by

$$\rho_a(\omega,d) = \omega \mu_0 |V_{y,d}(\omega)|^2 \quad , \qquad (2)$$

$$\phi(\omega,d) = \tan^{-1}\left(\frac{\mathrm{Im}(V_{y,d}(\omega))}{\mathrm{Re}(V_{y,d}(\omega))}\right). \qquad (3)$$

As was shown in Jones (1983b), if the earth is truly one-dimensional (1D), then there exists an analytical recursion relationship for deriving $V_y(\omega,d)$ at any depth and frequency for a given layered earth. Two properties of the VGM response make it particularly attractive for a 1D earth. The response function is only dependent on the properties of the layer in which the observations are being made and on those below it – it is not dependent on the properties of any of the layers above it. Secondly, the high frequency asymptote of $\rho_a(\omega,d)$ is the actual layer resistivity in which the probe is located. At the surface of a 1D earth, the analogy between MT and VGM is complete as the Ampère-Maxwell law

$$\mathrm{curl}\ \underline{B} = \mu_0 \underline{J} + \frac{\partial \underline{D}}{\partial t} \qquad (4)$$

reduces to

$$\frac{-\partial H_y}{\partial z} = \sigma E_x \qquad (5)$$

on neglecting displacement currents and assuming that $H_z = 0$ – which is true for a 1D earth with a uniform source field. Accordingly, the MT impedance tensor element, $Z_{xy}(\omega) = E_x(\omega)/H_y(\omega)$, is related to the VGM response function at the surface of a 1D earth by

$$V_y(\omega,0) = \frac{1}{\sigma_1 Z_{xy}(\omega)} \qquad (6)$$

where σ_1 is the conductivity of the top layer. Thus, VGM may be thought of as an MT substitute. However, such a rôle for VGM is not the intended thrust of this present work, but rather its applications to borehole geophysics.

In a 2D earth, the term $\partial H_z/\partial y$ generally cannot be neglected from equation (4), and accordingly there is no simple relationship between VGM and MT. However, if $\partial H_z/\partial y << \partial H_y/\partial z$, which will be true at distances greater than the inductive scale length of the perturbations in the EM fields caused by the presence of the anomaly, then the remarks concerning the interpretation of the VGM response for a 1D earth are true. This means that whatever the conductivity distribution, given a sufficiently high frequency, the 2D/3D conductivity discontinuities are outside of the lateral inductive scale length, and accordingly the VGM apparent resistivity will be equal to the true resistivity of the zone in which the probe is placed. This comment is not true, however, if the rock matrix itself exhibits fabric anisotropy. In such a case, even at the highest frequencies possible, a 1D response will never be approached.

In a previous work, Jones (1983b) considered a 2D structure which represented a vertical sequence of two anticlinal traps, and he illustrated that the surface MT response was virtually unaffected by the parameters of the lower conducting body. Hence, although the upper body would be located and drilled, the lower body would be missed entirely. However, by placing a VGM probe below the upper body, the lower body would be successfully delineated. In this work, the author has chosen to investigate the VGM response of a 2D body representing a highly conducting vertical ore body in a resistive host medium. The body has dimensions and conductivity comparable to the Gertrude nickel-copper sulphide deposit in the Sudbury district of Ontario. The detection and delineation of the Gertrude deposit by surface controlled source and borehole logging techniques have been considered by Dyck (1981) and Worthington et al. (1981).

The validity of a 2D numerical modelling study of a 3D body has been considered in detail by Jones (1983a). In that work, Jones suggested that the important ratio to consider is the length of the 3D body to the electromagnetic skin depth in the host rock, where the latter is given by

$$\delta = \sqrt{\frac{2}{\omega \mu \sigma}} \ .$$

Provided that this ratio is greater than one, a 2D model appears to be satisfactory. For the 2D model used in the Gertrude deposit, the skin depths in the host medium at the

Table 36.1. Attenuation of the horizontal magnetic field at 100 Hz as observed at points a,b,c,d,e and f illustrated in Figure 36.1.

location	co-ordinates (y,z)	uniform half space	E-polarization mode	B-polarization mode
a	(20,200)	0.875	3.357	0.879
b	(20,250)	0.844	4.303	0.852
c	(20,300)	0.814	0.280	0.823
d	(45,200)	0.875	2.738	0.878
e	(45,250)	0.844	2.497	0.851
f	(45,300)	0.814	0.530	0.823

highest (10^4 Hz) and lowest (10^2 Hz) frequencies of interest in this work are 150 m and 1500 m respectively (assuming that the magnetic permeability of the host rock is that of free space). The known length of the Gertrude deposit is some 700 m, and it could be longer. Hence, a 2D study of this 3D geological body is valid in the frequency range used herein.

In this paper, the magnetic permeability of both the body and the host rock is assumed to be that of free space. The electromagnetic response of a magnetized 1D layer with parameters (μ, ρ, h) is exactly the same as that of an unmagnetized layer with parameters (μ_0, $\mu_r\rho$, μ_rh) (Kao and Orr, 1982). Accordingly, any magnetized zone would require an independent estimate of μ_r in order to derive correctly the resistivity of that zone. This is true of all EM techniques.

Numerical modelling study

For the 2D numerical modelling study, the structure chosen was one having characteristics comparable to the Gertrude deposit. The only significant difference between the actual and numerical structures is that herein the ore body is assumed to be vertical, whereas the deposit is known to dip at approximately 45 degrees. The numerical body is of 10 m width and 100 m depth extent, with its top surface at a depth of 250 m. The body was assigned a conductivity of 50 Sm^{-1} in a host country rock of 10^{-3} Sm^{-1}. Accordingly, the areal conductivity of the body, i.e., its conductivity X depth extent X width product, is 50 000 Sm. For a frequency of 100 Hz, then the inductive skin depth in the host rock is approximately 1500 m, and thus the appropriate areal conductivity of the host rock is 2250 Sm (given by $\delta^2\sigma$). Hence, the areal conductivity of the body dominates the observed response. Figure 36.1 shows the right half of the body in the host rock - the structure has a vertical plane of symmetry about y = 0.

Computations were made of the effect the body had on the natural EM fields. Two possible situations exist: one in which the incident magnetic field is parallel to the strike of the body (i.e., along the x-axis), called the B-polarization or TM mode; and the other in which the magnetic field is perpendicular to the strike of the body (i.e., along the y-axis), called the E-polarization or TE mode.

In the B-polarization mode, the presence of the body causes little variation in the horizontal magnetic field amplitude compared to what would be observed for a uniform half space (see Table 36.1). This is because there is little current induced in the body itself, and the EM effect of the alternating surface charge, which is being continually placed on the conductivity boundaries by the impinging current flow, is negligibly small.

In the E-polarization mode, however, there is substantial induction within the body which causes an extensive distortion of the lines of constant H_y within the half space. Figure 36.1 illustrates, in the y-z plane, the effect of the body on H_y at a frequency of 100 Hz, and Table 36.1 lists values for certain locations. The fields are normalized to unit horizontal magnetic field for an observer on the surface (z = 0) at a distance of one skin depth away from the body, i.e., for a frequency of 100 Hz, this

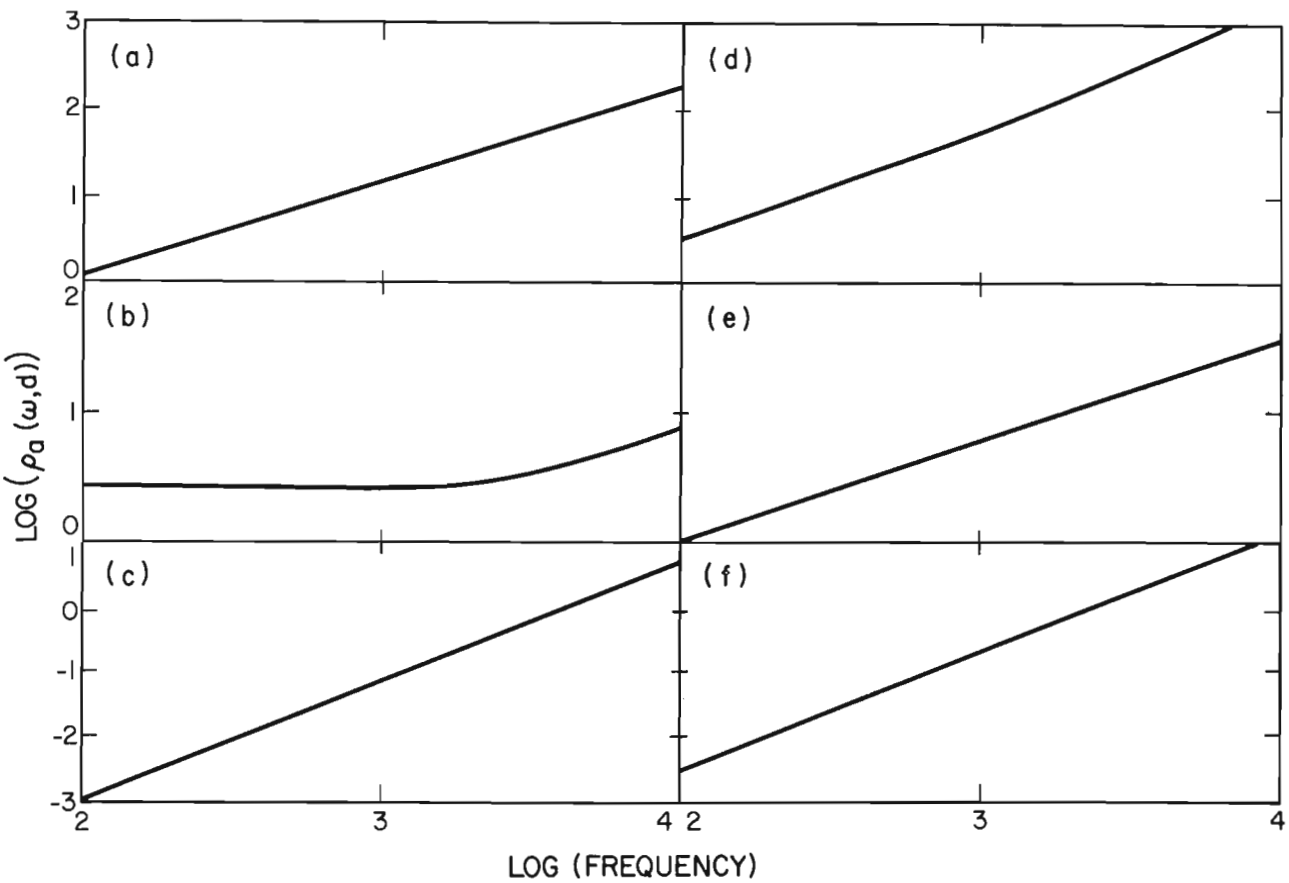

Figure 36.2. The VGM apparent resistivity curves that would be observed at the six receiver positions a-f, illustrated in Figure 36.1, in the frequency range 10-10^3 Hz for E-polarization mode induction. Note the differing ordinate scales.

corresponds to y = 1500 m. As can be seen in the illustration, the body creates a horizontal magnetic field amplitude pattern that resembles the total field that would be observed from two line currents at depths of 250 m and 350 m in the same vertical plane, i.e., y = 0. Numerical calculations were made of the VGM response function at six receiver positions. The first group of three (a,b,c in Fig. 36.1) represents observations of $V_y(\omega,d)$ made at depths of 200 m, 250 m, and 300 m, in a borehole which is 20 m from the plane of symmetry, i.e., 15 m from the body The second group (d,e,f) represents observations at the same depths in a borehole at y = 45 m, i.e., 40 m from the body. For those six receiver positions, the VGM apparent resistivities that would be observed in the frequency range 10 - 10^3 Hz are illustrated in Figure 36.2 (note the vastly differing ordinate scales). For a uniform half space, the VGM apparent resistivity would be constant over the whole frequency range, and for all receiver locations, at a value of 10^3 ohm-m. Figure 36.2 shows the extreme sensitivity of the VGM technique to the presence of the body.

The orientation of the body with respect to the borehole is also an extremely sensitive parameter that is well defined by the VGM method. At receiver position b, i.e., y,z co-ordinates (20,250), the E-polarization mode VGM apparent resistivity at 100 Hz is 2.2 ohm-m, whereas the B-polarization mode apparent resistivity, at the same position and frequency, is 1750 ohm-m. Hence, the orientation ellipse, given by rotating the VGM response function through 360°, is represented by an extremely linear ellipse in which the ratio of the major to minor axes is approximately 1000:1.

Hence, given two boreholes positioned approximately as shown in Figure 36.1, the presence, position, and pertinent characteristics of the body could be determined very accurately from VGM observations made at varying depths and frequencies. For the model studied here, there is a symmetry plane at y = 0. Therefore, should only one borehole exist, then all the characteristics of the body, e.g., distance from borehole, strike, areal conductivity, could be derived with the important exception of not knowing on which side of the borehole the body is. This is not considered to be a serious problem for the VGM technique however, as, for a more geologically realistic model the body will not have a vertical plane of symmetry. Also, surface measurements could be employed to resolve this ambiguity

Conclusions

In this paper it has been shown that a method relying solely on the natural source field is capable of delineating the pertinent characteristics of a buried ore body. The body considered bears a physical resemblance to the well-known Gertrude deposit in Sudbury, Ontario, with the major difference being that the numerical body was inclined vertically, whilst the true deposit is known to dip at 45°. The proposed new technique, named Vertical Gradient Magnetometry or VGM, relies on the ratio of the horizontal magnetic field at a given depth to the gradient with depth of the same magnetic field component, i.e., $V_y(\omega,d) = H_y(\omega,d)/(\partial H_y(\omega,d)/\partial z)$, and similarly for $V_x(\omega,d)$.

For the structure studied in this work, if the earth were a half space of constant conductivity of 10^{-3} Sm^{-1}, then the gradient at a depth of 250 m is approximately 0.06% of the surface field value per metre. The presence of the highly conducting ore body causes a departure from this value however, as illustrated in Figure 36.1. At depths of 200 m, 250 m, and 300 m, the gradients are 0.3%, 0.8%, and 3.0% of the surface field values per metre respectively, for both boreholes. At 100 Hz, the typical horizontal magnetic surface field amplitude is of the order of 100 mγ, and accordingly a sensor that can resolve 0.1 mγ is required for this particular study. In Jones (1983b) a fuller discussion is given of the feasibility of building the required sensors for deriving such small gradients, together with various solutions to practical deployment problems that may arise.

Acknowledgments

The author has received financial support from grants awarded to Professor G.D. Garland (NSERCC A2115) and to Professors R.N. Edwards and G.F. West (NSERCC G0501), for which he wishes to acknowledge his gratitude. This study was undertaken in the Geophysics Laboratory of the Physics Department, University of Toronto, Toronto, Ontario.

References

Dyck, A.V.
1981: A method of quantitative interpretation of wideband, drillhole EM surveys in mineral exploration; Geophysics Laboratory, Department of Physics, University of Toronto, Research in Applied Geophysics, vol. 23.

Frignet, B.
1986: Induction logs applied to mineral exploration and development; in Borehole Geophysics for Mining and Geotechnical Applications, P.G. Killeen, ed., Geological Survey of Canada, Paper 85-27, report 10.

Jones, A.G.
1983a: The problem of current channelling: a critical review; Geophysical Surveys, v. 6, p. 79-122.

1983b: A passive natural-source twin-purpose borehole technique: Vertical Gradient Magnetometry; Journal of Geomagnetism and Geoelectricity, v. 35, p. 473-490.

Kao, D. and Orr, D.
1982: Magnetotelluric response of a uniformly stratified earth containing a magnetized layer; Geophysical Journal of The Royal Astronomical Society, v. 70, p. 339-347.

Worthington, M.H., Kuckes, A., and Oristaglio, M.
1981: A borehole induction procedure for investigating electrical conductivity structure within the broad vicinity of a hole; Geophysics, v. 46, p. 65-67.

INSTRUMENTATION WORKSHOP

Q. Bristow

Bristow, Q., Instrumentation workshop; in Borehole Geophysics for Mining and Geotechnical Applications, ed. P.G. Killeen, Geological Survey of Canada, Paper 85-27, p. 343-348, 1986.

Chairman: Quentin Bristow, GSC

Panel Members: Bob Pavlik. Urtec Ltd.
R.D. Leask, INCO Ltd.
Yves Lamontagne, Lamontagne Geophysics
D.L. Wright, U.S.G.S., Denver

Introduction

The instrumentation workshop was organized with the idea of generating a dialogue between those who design and build geophysical instrumentation and those who use it. In the event the session which was very well attended, ran four an hour and a half and would have continued for much longer had time permitted. It will be apparent from the summary which follows that much ground was covered during the discussion with contributions from many knowledgeable people.

Unfortunately not all of the speakers were identified, and comments from those in this category are denoted simply "Floor". The chairman prepared this summary from a transcript of the tape recording. He has reproduced the discussion verbatim wherever that seemed appropriate, but for the most part comments have been edited to distil the essential points with economy of page space in mind.

The chairman opened the session by introducing the panel members and suggested that digital data storage be the first topic of discussion. He pointed out that five magnetic storage media are currently in use; audio-cassette tape, digital cartridge tape, ninetrack 1/2" tape, floppy and hard discs, and magnetic bubble memory. Comments were then contributed from the panel members and from the floor.

Bob Pavlik (Panel): Storage that involves mechanical parts is generally not very reliable and I think we all agree with that. To date there have been no technological advances which make it economic to store large volumes of data in any other way so we have to still live, probably for some time, with some storage media like magnetic tapes, cassettes, cartridges and so on. There were some advances made recently in some half inch tapes so it's possible probably within a year we will see some small units that will be using half inch tape recording on many more tracks than the standard 9-track tapes and so on with very high capacity but again these machines will have the same limitations as the other ones in terms of environmental specifications and so on, because all the machines that are commercially available are basically designed to operate down to a minimum of zero degrees centigrade and in a non-condensing environment. That's the major problem I think with all of the tapes that we are presently using. so we would like to hear some comments from you on your usage of tapes, and on your usage of some other storage media and what you consider to be the best.

Chairman: Any comment perhaps from other members of the panel?

R.D. Leask (Panel): My feelings coincide entirely with Bob's, we can't find any cheap method of storing other than magnetic tape.

Chairman: It does seem that 9-track mag tape is still the universal thing, it's awkward and clumsy and it's an old standard, but it's one that everybody has. Digital cassette is okay but the storage is limited, and they're not, I think, quite as reliable as 9-track.

J. Hallenburg (Consultant): I have a couple of comments on that. I don't have any argument about the quality of the 9-track tape. The trend I keep seeing though is that people, in our offices particularly but even in the field, are going to micros and I see in place after place I visit, that instead of people having terminals for the main frame in the company, they have an IBM-PC or something like that on their desk. When you start talking about 9-track tapes though, you're talking about cost for the tape transport being considerably higher than the cost of the computer together with the other peripherals very often. There are a number of disks for instance which are capable of storing very nearly enough material. I'm not sure about the Winchester disk. I would suspect that it could store enough for at least one borehole. Of course that is a fairly expensive storage medium compared to the floppy. The high density floppy disks will come fairly close to storing enough data for the borehole. I would like to see an effort in this direction toward less expensive storage media so that we can put all of the information on disks and use it easily without having to put a large investment into it.

Chairman: As a matter of interest can we see by a show of hands, how many people here do get involved with storage of digital data in the field at one point or another? That looks like about 80 per cent to me so we all face this problem to one degree or another.

Y. Lamontagne (Panel): We've had a fair bit of experience with storing data for field measurements and now we're starting to do the same sort of thing for borehole measurements for EM. In this we find that a Phillips type of cassette with incremental recording is quite adequate provided you protect it from the weather. We build it inside the receiver and it's environmentally protected, never to be opened in the field. Given the volume of data we have at present, we don't foresee that we could fill a cassette in a day, so the tape capacity is not a limitation at present.

D.L. Wright (Panel): I was just going to mention that one of the problems with radar is that you can generate an awful lot of data in a very big hurry and currently we're still using analog tapes and then digitizing later. We're developing a digital data acquisition system that will help somewhat by stacking on the fly in real time so that you have stacked data before you even put it on your storage medium.

Y. Lamontagne (Panel): Well that's really being done all the time for EM measurements basically. You wouldn't dream of getting the raw data on EM and then stacking it later on.

Chairman: That's an interesting comment that Dave made because there is still, amazingly, a place for analog recording. It's incredibly concise. If you take an ordinary gramophone disk and digitize that and put it into memory you've got a roomful of memory just to play half an hour's worth of music; so there's still a place as in Dave's application for recording analog data on tape and then digitizing after the fact.

At this point the chairman introduced the topic of borehole logging cables for discussion. He pointed out that the traditional standard has been the steel armoured 4 or 7 conductor cable designated "4HO" or "7HO", and that this has limited frequency response and is too heavy for use in any sort of portable logging equipment. Comments were then invited from the floor.

D.L. Wright (Panel): Well I've only worked on high frequency electromagnetic methods so my background is rather narrow but as I mentioned in the paper ("Transponder enhancement of short pulse borehole radar", ibid) the steel armoured cable is far less than ideal for what I want to do. Fibre optic cable would be superior. The reason we haven't gone to it is that we're not in a position to procure a system like that and also we're still somewhat concerned about its field worthiness in a rugged borehole environment, although it's clear, that great strides are being made in that area. We may look into procuring a fibre optic system but we're not there yet.

Chairman: If you had your choice of some more conventional cable, and there were no other limitations, which would you choose for your particular application? Or would you want to go to a fibre optic cable no matter what?

D.L. Wright (Panel): If I were looking to isolate things electromagnetically, I would really have no option other than a fibre optic cable. If that is not a consideration, then I would consider coaxial cables, although with the cable runs we've got, the attenuation would probably be unacceptable.

Floor: I think you might bring out the problem that a fibre optic cable raises with the design of the probe. If you look at conventional logging systems the cable is used to supply power down to your probe for whatever function you're running. With a fibre optic cable you have to have the power supply that drives the probe electronics contained within the probe itself so the choice may depend on the design of your probes.

Chairman: That's a very good point. It would indeed. Jim do you have a comment on that?

J. Hallenburg (Consultant): I would agree with that point and I'd like to remind you that probably about 80 per cent of the cable troubles would disappear if we went to downhole digitizing. These are pretty good techniques and allow you to use the cable (with the exception of the radar applications) almost entirely for getting power down to the tool depth.

R.D. Leask (Panel): A poor man's cable is a CTV cable. These low loss coaxial cables with foam dielectric are very cheap. I think we pay about 15 cents a metre for our cables, and you can get them in lengths of 6000 feet. They are not too bad to splice, the centre member is the strain member. The centre conductor presents a bit of a problem in some of the couplings and so on but you can select the cable to be almost neutrally buoyant in the borehole fluid, so that you don't have to worry about it supporting itself. The major problem with it is that the foam polyethelene, (in the one that we are using at least), compresses as you get down to 3000 metres. I don't really know how much the transmission characteristics change when you get down that deep, but losses do go up noticeably after about 2000 metres but it's quite usuable to that depth. It's a little more bulky than the fibre optic but it's also an awful lot cheaper. I think ultimately that the fibre optic cable and downhole digitizing is the way to go, but there are similarities with the coaxial cable approach. We use coax with VCO's (voltage controlled oscillators) passing up frequencies of 2, 4 and 6 megahertz. We probably should be using some sort of equalizer amplifier but we aren't at present. We use phase-lock loops to separate the VCO signals, coming from the different sensors in the probe and this seems a fairly good answer to cable problems.

Chairman: He has a point. I too have wondered about coaxial cable. After all they string it around the town by the mile and it's not that expensive. The frequencies involved are of the order of 100-200 megahertz so there can be no band-width problem with it, not as far as we're concerned at least, unless you get into something really exotic like radar, so that is a point to remember.

Floor: I think quite literally you are caught between a rock and hard spot on your coaxial cable and the fibre optic cable. When you get into the hole in a practical situation, and you have to put a couple of hundred pounds of tension on that cable to pull your probe out you may end up leaving your probe behind and regretting it. I think as I say you're caught between a rock and a hard spot in wanting to have the tensile strength in a cable which you can get, let's say with a Kevlar strength member and not sacrificing that probe.

P.G. Killeen (GSC): I'd like to ask Gus what was the breaking strength of that coaxial cable. I guess it's not too critical if you've only got a hundred dollar probe down the hole and your cable is only 15 cents a metre but if you've got maybe a $10,000 probe it might be a different consideration.

R.D. Leask (Panel): Our test showed a breaking strength of just under 300 pounds but I don't think that is the guaranteed value. I think the guaranteed breaking strength depends on that copper wire member that's in the centre. A point concerning the other bad feature of this thing: I tried at one time to find somebody that would make me a dielectric out

of glass beads and polyethelene so that the dielectric would not collapse under pressure. I don't know whether anybody in the audience has had any experience with glass beads and polyethelene. I wasn't able to find a manufacturer that would consider extruding a dielectric with these glass beads in it and I don't think anybody has tried it, but I don't see why it shouldn't work.

Y. Lamontagne (Panel): I have a point to add on the fibre optic cable. I'd say the fibre optic cable is probably a solution which is becoming even more viable now, but I would say the break even point is when you need a fairly long cable. Your major investment is in the cable termination. The middle - the two kilometre piece in the centre - is relatively cheap once you have the terminations at each end. It would be foolish to go to fibre optic if you're doing it only for a very short length, unless you really have a band-width infidelity problem, or ground isolation problem, but if it's just a matter of getting some signal from A to B cheaply or easily, then maybe it's better to do without it. However once it gets to a long length, then the weight of the cable and the price starts to tip the scales in favour of a fibre optic cable. There are three limitations really on the fibre optic cable: number one is attenuation, and that involves bending and stretching. Once you start stretching it past a given limit the attenuation increases drastically. However if you have a significant margin in signal power, then that will not affect you. On the other hand loss of signal is a warning that the cable is being stretched beyond a safe limit, so unless you have a transmitter that's too powerful, your signal will usually disappear before you damage the fibre, then you know to stop pulling so hard on it. The limitation is when you actually damage the fibre, and for our cable that would be around 250 pounds or so. The final limitation is the breaking strength of the Kevlar stress member which is about 750 pounds. Now that's adjustable. You can ask the manufacturer to incorporate a 1400 pound Kevlar stress member, which will be a bigger diameter, so the stress member is a matter of judgement and is no big technical problem. In my estimation fibre optic technology is probably the way to go for a long cable, but even though I have a fair bit of experience with it, I don't think I would consider it for a cable just a few hundred metres in length because of the investment required in the electro-optic terminations at each end. The big advantage is that it's light. Your winch is light; it's portable and less likely to break because you don't have to use brute force and ignorance to carry it around. After all you can afford to be more careful with something that weighs only 50 or 60 pounds or so.

D.L. Wright (Panel): Can I ask one question of the chairman with regard to cables. This had to do with insulation and with what you were doing. Did I understand that you were putting current down the shield?

Chairman: Yes that's right. In our particular case for that IP system I described, we did put a current down the shield of the table. It's apropos that you should ask that because just the other day we discovered that there was indeed a leakage problem at the bottom of the cable, probably via the termination where the cable entered the cable head (Gearhart Owen type). It appeared that the seal wasn't as good as it should have been, so we were getting some leakage and probably electrolysis between the shield inside, and the water outside. So unless the cable outer jacket is quaranteed to be waterproof all the way down, then passing currents down the shield is a thing to with caution. There doesn't seem to be any particular reason the cable jacket should not be waterproof, and if we get an appropriate connector with an "O" ring seal at the end, hopefully we'll solve that problem. I'd be interested in any other comment from the audience on that.

O. Olsson (Swedish Geological): I have a comment concerning the breaking strenght of the cable. I feel you overemphasize the importance of the breaking strength. As far as our experience goes if you get stuck in a borehole (especially if you are logging in hard rock environment), then you're usually stuck indeed, and even if you can pull with a hundred kilos or one ton it won't help you because the rock won't yield and I guess you'd need tens of tons to be able to pull the thing out otherwise.

Chairman: That's a very good point actually; if it's really stuck, then it doesn't really matter what the breaking strength is. Any comment on that from people in the field? Is it really that important; the breaking strength of the cable? - beyond a certain limit obviously.

B. Krause (INCO): We've had considerable experience in a lot of very deep work down 6000 feet and more in Sudbury and I agree totally. You're either stuck or you're free and if you're stuck all the horses in China couldn't pull you out. If you're going to do deep borehole work you have to face up to the fact you're going to lose a probe now and then and equate the value of your probe against the value of the information you're trying to get. If you're going to save a $20,000 borehole you can afford to lose a $10,000 probe now and then.

Chairman: Would you care to put a figure on the sort of breaking strength that you think is adequate. At what point do you stop pulling?

B. Krause (INCO): I don't know. I think certainly the 200 pound figure which people seem to talk about seems to me quite adequate. Basically you may have a chance to sort of jiggle it a bit, thereby working it loose but if you've pulled it up and snagged it on something, you're finished. We've had several cases where the main concern has been that if it's going to break, you want it to break at the probe. Particularly if you're going to be in these very deep holes and they are considering wedging; you don't want to leave any cable in the hole. The probe after all can be drilled out. We had one experience where we did leave cable in and it was about a $15,000-$16,000 error. The drilling company wasn't too impressed with it. I would emphasize therefore that you don't want to leave cable in a hole. So if you're going to have that kind of breaking strength, make sure you've got a weak point near your probe so if it breaks, it breaks at the probe.

B. Frignet (BRGM): We had several experiences when we had the probe stuck and we definitely needed more than 200 pounds to get the probe out. Several times we called a tractor and we got the probe out of the hole. So I think it's desirable to have a cable with at least 500 kilos breaking strength to be sure of getting the probe out.

Chairman: Judging from the comments so far, anywhere between 200 and 1000 pounds seems to be a reasonable figure for cable breaking strength and somebody made the point that you should have at least one weak spot near the probe.

A. Cicoria (Century Geophysics): We have quite a few logging tools that are pretty heavy, in the order of 60-70 pounds, some are even 90 pounds, so we have to stay away from a cable that's going to break at 200 pounds. We use a standard 4-conductor armoured cable and I think that's about a 2000 pound breaking strength and it has worked out well for us. I agree with Barry. We find our cable head tends to be the weak point and what happens is that a lot of our draw-ups can't break the cable. So we pull as hard as we want and if we do free it, fine, and if not then we can get the drill rig or whatever to pull on the cable. Sometimes we've had cases where they have freed the probe and brought it out and that's nice, because our probes are fairly expensive.

In the cases where the probe has been stuck the cable has always broken at the cable head, which tends to be the weak point and that's just as well, because you don't want that cable in the hole. It will ruin the hole and maybe get your drill pipe stuck if you're going to go back down, so we find we need a pretty strong cable.

Chairman: Thanks very much, that's worth knowing. So the other point is don't leave the cable in the drillhole whatever else you do.

J. Hallenburg (Consultant): I'm sorry to come up and make so many comments but this is something that I've had quite a bit of experience with. We used to deliberately set our weak point on the 4HO cable between 1000 and 1500 pounds and the loggers had orders never to pull more than 1000 pounds. If you're key seated in sediments, it's about like a hard rock situation. You're not going to pull free. You want to put enough pull on the cable to allow the driller to go down with an open ended drill pipe and wash over it. There is a whole family of excellent fishing tools and one of those which is very seldom used in the mineral business is a wireline overshot. I think a 250 pound breaking strength is probably a little too weak, but even with a 250 pound cable you can run a wireline overshot down the cable and come over the top of the tool. In order to do that you have to slack off before the overshot gets down to the tool. Of course an overshot on a drill pipe is much better but you don't always have the drill rig there. These fishing tools are something that are very sadly neglected and we should be using them more often. Even with the 4HO cable if you pull 1000 pounds you are going to have breaks in the conductors and you're certainly going to have to rebuild the cable head if nothing else.

Chairman: Fishing tools is on my little list here. Maybe now is as good a time as any to think about that. Does anybody have any comments on fishing tools?

Floor: Actually I want to make one point prior to discussing fishing tools, and it concerns the probes we use. I think one of the problems we have is maybe not so much the cable, but that we're limited in many respects by the comparatively large diameters of the probes. I think that's the greatest challenge to the technology - to reduce the size of the probes, especially when we're limited let's say to hard rock, where a lot of your holes are BQ. One of the areas which some people may have ideas on is whether or not it's a good idea to taper the end of the probe. In many cases when you get stuck, it's not because of partial collapse of the hole, but because at some point on the way down, rock chips have fallen down on top of the probe. Then as you bring it up, tapered end first, the rock chips get deflected to the side and jam the probe. There have been discussions on whether or not you should have a square end that would simply lift up any rock chips. Obviously if the chips are so large that they will not pass the side of the probe it doesn't make much difference whether it's tapered or square ended. However if there are small chips that might end up like gravel jamming on the sides, it would be better to lift them than to deflect them to the side of the probe.

M. Hammalainen (Geo Instruments): My experience is only from the hardrock environment but we never used tapered tools. We have a large chip collector. It's only a plastic tube screwed on top of the probe and if you get chips falling on the tool they usually land in the collector. We have had quite a few sticking problems because of the collector. However if the tools sticks then we use a quite simple fishing tool. It's an iron rod which is attached to a separate cable and it can be used as a hammer to drive the tool down. If you can get the tool go down a bit, then it usually comes free and then you can pull it up. If this won't succeed then it's better to pull the cable so that it breaks at the cable head, and then you can use a fishing tool attached to the drilling rig, but that usually means that you have to have the drilling rig on the site. The top of the plastic chip collector is cut at an angle to avoid catching the borehole casing. Usually the casing is short enough that even if it does catch, it can be freed by rotating the cable from the surface by hand.

A.V. Dyck (GSC): I can offer a slight variation on that last idea which was essentially a hammer. I was thinking more in terms of a cylindrical chisel of a diameter slightly larger than the probe. You lower that on another cable and use it to chip away at the rock or pieces that are around the probe. I actually got that to work once.

Chairman: Does anybody have any comment on any other reasons why they think probes might stick?

Floor: There are two other experiences to go along with this. We used to use heat-shrink tubing on the Crone Geophysics probe, and at one point one of the probes got stuck and I suspect it was clay or something. It was just left overnight and the water worked its way in so that just by pulling on it we were able to free it. So that was one probe which was rescued by just being left alone. And the second experience was using a retrieval tool that had a cutting edge on it. It was wedge-shaped all the way round, and circular with a slot in it, so you could put it over the cable. It also had three jaws inside it which would latch onto the probe as the device went down over it. Once these jaws had locked, then it was a matter of pulling everything back out with the steel cable. It's a functional system that's available from Crone Geophysics.

P.G. Killeen (GSC): Just talking about three jaws that grab the probe; we had a probe stuck at about 30 metres which wasn't very far down. We constructed a solid link betwen the surface and the probe out of threaded pipes with a three-arm jaw that grabbed the probe and a hydraulic affair on the surface with legs on it. I think we first of all broke the welds on the legs off, and then after we got that fixed we ripped the jaws off the solid connection that was to pull it up. I don't know how much foce we had but I think it was a house lifting jack we were using.

Chairman: And the jack got nearer and nearer to the probe.

Floor: We have used the Crone retrieval tool and it has worked out quite well. The only difficulty occurs when you get beyond I think about 350-400 metres, because then you have really got to be able to feel that Crone retriever catching onto the probe. I think it's the same with all these other ones. If you can actually feel it catching on to your probe you have a lot more chance of getting it up, but once you get down a very deep hole you can't tell that anymore cause there's too much slack in the line then.

Chairman: Jim Hallenburg, have you got any comment on that. You must have used a lot of fishing tools in your time.

J. Hallenburg (Consultant): Yes, my experience has been that if the hole is in reasonable condition you can pretty well tell what you're doing either with a drill pipe or with a wire line. You can feel the tool hit the top of the logging tool. It's when you have poor mud that you begin to get into trouble and incidentally along that line the comment was made about the reasons for sticking. When I was with Schlumberger we did a study of that and came to the conclusion that in sediments that most of the cases of getting stuck were because the cable key seats in a curve in the hole, and then because the tool is so much larger than the cable, it tries to cut through this narrow slot in the formation and it can't

make it. Now we also found, interestingly enough, that if the tool drags against the wall of the hole it can scrape the mud cake off opposite a permeable formation, or permeable zone, and when you start calculating the force plastering the tool up against the wall of the hole, it's tremendous. If you figure that you have a tool 120 inches long (a 10 ft long tool) and it's an inch in diameter, then if you have one psi differential pressure you're going to have 120 pounds plastering that tool up against the wall of the hole. Well you can figure that at 1000 feet you've got nearly 500 psi, so you have a tremendous force holding that tool down there. Now this is the kind of force that you're going to be working against and even with a steel armoured cable you usually do not have enough strength to pull it loose. Now if you can wash the formation away or get something between the tool and the formation then you stand a good chance of getting it out. However I think by far the most important thing in a fishing job is to have an experienced driller. He's really valuable. I've had drillers sit out there in the field and make fishing tools, things like a piece of 4-inch casing that has a little arm on it so that it could go down and rotate it and dig into the wall of the hole and scoop the tool into a slot on the piece of casing, things like that. It doesn't take much experience. After you've done it once or twice you can begin to feel what is happening down there. We had one location in the Powder River Basin where the loggers got stuck on an average of two or three times every hole. Now they were just terrible holes: poor mud. We found that by far the best way to get tools loose was to go down with an open ended drill pipe and just jet the tool away. Then pull 300-400 pounds on the cable and the tool will come free.

A. Cicoria (Century Geophysics): Again we're a logging company so we get tools stuck quite often and lose tools here and there. There are companies dedicated just to fishing tools, mostly geared for large holes, but a lot of times they will give you advice or they can even come up with something made especially for smaller holes. I've managed to save a few tools that way and it has helped me quite a bit and helped my clients quite a bit.

P.G. Killeen (GSC): A lot of people may not know that is there is a company that actually specializes in manufacturing those tools and they have a huge catalogue. It's called BOWENS. Their catalogue shows all kinds of methods of snagging probes with magnets, hooks, clamps, spirals and all kinds of overshots and other devices.

Chairman: Everything short of the indian rope trick, eh?

Floor: In a lot of areas I've been they've been using plastic pipe in the holes and that cuts down on the number of stuck probes. It also brings in a new problem of the pipe down the hole getting kinks in it and causing probes to get stuck. I'd also be interested if anybody has any ideas on how to keep the permafrost out of that type of hole.

C. Madsen (Spectronics): Well that's usually done with some salt water isn't it ? - for a few hours anyway. My comment was on small portable systems that seem to sustain more damage to the cable above the hole, than in the hole, because of a very poor design. Some of them have a very shallow groove in the well-head pulley, so when it starts moving, the cable can jump off to one side and get caught between the guard and the moving pulley itself. If there is a heavy load on the cable, then it can be severely damaged, probably somewhere in the middle. I have sold quite a few cables because of that.

Chairman: Another topic which we might discuss now is portability. The discussion on cables has led into this, and I'd be interested to know how many people here (again by a show of hands) regard portability of logging equipment as of some considerable importance. I'll put that down as about 65-70 per cent.

P.G. Killeen (GSC): Can you define what you mean by portability?

Chairman: I define portability as being light enough to be carried by no more than two strong students. Are there any other comments from the floor about the desirability of portability and how much that looms in one's mind when buying equipment?

Floor: I would have thought that if they got in to drill the hole, there should be some vehicle or means of transport to bring heavier logging equipment in.

Y. Lamontagne (Panel): Well my comment is that when you design equipment, you may want to ensure that it's transportable in a helicopter where weight and storage capacity is restricted. That's one thing that we kept in mind in our equipment design and I think others would do well to think along the same lines if they ever contemplate the kind of work that we have been doing.

Floor: It becomes rather important to me especially in the mountains. If you have to carry equipment through the mud from one site to the next, or if there are only two of you there and it's 300 ft. straight down, then it's rather important that it be easy to handle.

P.G. Killeen (GSC): I'd like to comment on the point that Rolf mentioned a minute ago. I think that just because a vehicle got in to drill the hole doesn't necessarily mean it is easy to get another vehicle there with logging equipment. It depends on the environment. For example in the Southwestern United States, they can drive to the hole with a 10-wheel truck, drill the hole and then move off. The logging vehicle then moves in right away. In Canada, and probably in a lot of other countries where drilling is done in the Precambrian, they drag the drill rig in on skids with a Caterpillar tractor of some sort and they stay there maybe months, depending on the depth of the holes to be drilled. By the time they are ready to have the holes logged, the vehicles that dragged the drill rig in have gone and no 4-wheel drive vehicle of any sort could get back in there. It would have to be a helicopter or some sort of all-terrain vehicle, or, extremely portable equipment that's man-portable. The two students that Quentin Bristow mentioned, for example, are necessary in many environments.

Chairman: I'll move on now to another topic, one that's of some interest to me, and that is the type of electrodes that one uses in resistivity and/or IP logging. Traditionally they are lead rings. It seems to me that it is highly desirable that they should be chemically reversible. That's why I gold-plated mine. Has anybody got any comments on a) the desirability, b) availability of chemically reversible non-polarizable electrodes for this kind of work?

A.V. Dyck (GSC): My understanding about lead is that it is desirable as an electrode because it oxidizes and once it is oxidized it is very stable.

Floor: I built an IP probe and what I'm using on that are stainless steel electrodes, but they spring outward to centre the probe in the hole. They do however get chewed up and I just replace them after a set period of time. It's quite easy to do it.

J. Hallenburg (Consultant): I've had some rather unfortunate experiences with stainless steel electrodes. It seems that stainless steel is stainless because it forms an oxide coating on the outside which has a fairly high dielectric constant, so you have an excellent capacitor between the electrode and the fluid in the hole.

Chairman: That's interesting. I believe the oxide is in fact chromium dioxide.

Floor: For several years we've been using naval brass, high quality naval brass, very successfully in place of lead electrodes and we've never been able to see any disadvantage in the use of naval brass.

Floor: Can I just ask if there is anybody who knows any theoretical reason why electrodes should be made from any particular material, because for something like IP logging or electrical logging you are looking at a symmetrical wave form, so any polarization effects should cancel out. Even for SP work you are looking at a constant error that isn't necessarily going to affect the log.

Chairman: My only comment to that would be that the potential which exists between a metal and a solution is dependent on the solution concentration and the type of metal, and if that is different or varies for whatever reason between the two electrodes, then you have a potential difference.

O. Olssen (Swedish Geological): The metal that you use for SP logging is important. We developed a geochemical probe which we have been using where we have a silver/silver chloride electrode as a reference. We have measured the potential relative to gold and platinum and graphite electrodes which are all supposed to be inert. But we have always observed a difference in the absolute voltages between these electrodes and the difference varies along the hole depending on the chemical properties of the water.

B. Frignet (BRGM): I think that the mechanical design of your probe is more important than the metal you use for the electrode, because when you encounter sulphide mineralization you will have a contact potential of up to 400 millivolts between a non-polarizable electrode and any other metallic electrodes that are in contact with the wall of the hole. This means that in order to make good IP measurements your potential electrode should not be in contact with the wall of the hole. This is more important than the nature of the metal of your electrode. This electrode dependent SP variation is a very important parameter in making IP measurements.

C.J. Mwenifumbo (GSC): Concerning SP measurements, there has been some work done by Collowin in the States. He tested the performance of a number of electrodes using different metals and came up with a design using silver/silver chloride electrodes. However the major problem that he had for SP measurements was that there was quite a bit of drift as he went downhole, due to changes in temperature and also to changes in the ionic content of the borehole fluid.

Chairman: The other topic, while the time lasts, is reliability, or lack of it. How serious a problem is this and what sort of steps could be taken by manufacturers or users to combat it, and are there any sort of standardized tests that one could do to ensure that equipment is working properly before attempting to acquire data.

C. Madsen (Spectronics): I would say train the people a bit better before you send them out in the bush. I have saved a lot of companies money by going out with them for a few days and actually getting the operators to know what they are doing.

Floor: A lot of intruments are done in by vibration in transporting them from site A to site B. Just transporting them around in their proper cases, (if they are properly packed with foam) or putting foam underneath them if you are travelling around in a truck, helps a great deal.

Chairman: Shock-mounted transport cases should be standard perhaps.

P.G. Killeen (GSC): I think in fact that the last two people who commented on it have hit the nail right on the head. It's partly transporting the equipment and making sure that you protect it carefully, and secondly making sure that the people who are using it are trained and taught that in fact it is important to follow a set of rules. Most of the time when we've broken any of our own equipment it was because we thought it would be alright on the floor of the logging truck just to travel from one hole to the next, but it only takes one bump to shake some components apart, and that's invariably what happens.

A.V. Dyck (GSC): The transportation problem notwithstanding, I'm usually (or quite often) sorry that I haven't taken the time to take the equipment, whatever it is, to a place where I know how it responds, (that's a real environment not a lab environment), before going to the survey area, and making sure that I'm still getting the same thing as I did the last time. Now obviously it could still, through vibration or whatever, suffer damage by the time you get to the real site, but at least then you could say in all truth: "it was working yesterday".

Chairman: This leads us to the question of simulators. I usually put a button in anything I design, which simulates the parameter that you're trying to measure and makes it appear to come from the probe or whatever. I wonder how many users would like the idea of test signal generators in button form, or whatever is appropriate, to make sure that at least the uphole stuff is working - a show of hands if people think that this is a good idea. Again that indicates about 70-80 per cent of people here think that this would be a good idea. Any comments on this perhaps from the panel members?

R.D. Leask (Panel): I think that all systems, especially drillhole systems and so on should have calibration signals, including communications with the downhole probes to check the calibration over the full range of the instrument. I also think that instrument designers nowadays could do an awful lot more with self-diagnostic programs like for example the EDA magnetometer, that is an excellent example. It has a few little LCD bars that tell you whether your gradient has gone to pot, or if your signal amplitude is down, and this indirectly tells you whether you've got the think misoriented, or whether you are in too high a gradient. This type of thing I think would be very beneficial for the users of a lot of the geophysical instruments.

Bob Pavlik (Panel): I would think that all of us actually share this opinion and that we will probably see more and more of these methods implemented. Until two or three years ago most people were using analog techniques of one sort or another. Now they are changing slowly to digital techniques which are much more amenable to the incorporation of hardware or software diagnostic features.

Y. Lamontagne (Panel): I would have to agree with this. There should be monitors for the most obvious faults like the battery getting low, and in our case the optical signal not getting through. Any system that has a carrier like that is very good because you know whether or not it is getting through. It is not always easy to build a calibration signal right in the probe of course because it is often hard to simulate a signal at such a low level, but you should definitely have one built in the receiver.

Chairman: Do we have any comment on that?

D.L. Wright (Panel): I guess my only comment is that I'm both a builder and a user and I've been my own worst enemy.

Chairman: Okay. Well on that note, I think if there are no more comments we will call it a day and I thank you for coming and it has been a most interesting session. It has lasted a lot longer than I had reason to expect that it would. Thanks very much indeed.

At this point the chairman had to bring the discussion to an end in order to allow the next event in the conference time table to proceed. It was apparent however that all concerned would have liked the session to continue had time permitted.

INTERPRETATION WORKSHOP

A.V. Dyck

Dyck, A.V., Interpretation workshop; in Borehole Geophysics for Mining and Geotechnical Applications, ed. P.G. Killeen, Geological Survey of Canada, Paper 85-27, p. 349-354, 1986.

Chairman: A.V. Dyck, GSC

Panel Members: Barry Krause, INCO
Jerry Roth, CANAMAX
Bernard Frignet, BRGM
James Macnae, Lamontagne Geophysics
Frank Hiebert, Quinte Geophysics
Joe Wong, University of Toronto

Introduction

This workshop was organized to promote interchange of ideas about interpretation of large-scale drillhole geophysical surveys, about interpretation of geophysical logs (small-scale surveys), and about how the two different sets of information might be integrated. The wide-ranging discussion clearly showed two different schools of thought and many interesting and knowledgeable comments were made.

This summary was prepared by the chairman from a transcript of the tape recording. The discussion has been reproduced in a somewhat distilled form with clarity and economy of page space in mind.

Chairman: Well, how about a nice general question to start with. Should the geophysicist talk to the geologist before or after the interpretation? Any geologists here?

J. Roth: The geophysicist should talk to the geologist as early and often as possible. The fact that he may be biasing his interpretation in favour of whatever the geologist's prejudices are or might be, I don't think should stand in the way of the potential benefits from communicating.

Chairman: There is perhaps a complication to that. Many times when we're trying to prove techniques, as we are all desperately trying to do in this field at this stage, the question arises at just what point do you get the information the geologist knows about.

L. Reed: I would like to know if anybody would really dispute Jerry (J. Roth) on that one. As exploration geohysicists we are from time to time placed in a position where exploration managers, geologists, will not tell us what's going on. They say you tell me and then we'll compare it later. I'd like to know if there are any geophysicists here who would take that kind of approach and think it's a correct one?

B. Krause: I couldn't believe Alf was serious because I think it's obvious that the geologists have to talk to the geophysicists. A very practical reason is that it's virtually impossible to design the survey properly if you don't have as much of that higher knowledge as you can.

J. Macnae: Actually you can never get away from geology. Every model that has been well studied, and that is useful, is normally based on some sound geological reasoning. Even if one does not communicate directly with geologists before trying to do an interpretation, the models you are fitting are in fact geologically biased.

Chairman: I fully agree. It's just that, again getting back to this idea of proving techniques, my feeling is that we're always trying to prove ourselves. If you actually do come up with an interpretation, which let's say is a sulphide body, and the intersection happens at the right place when they drill the next hole the geologist says, "well I told you it was there".

J. Roth: My response is that people who suffer from insecurity generally don't persist in exploration geophysics.

F. Hiebert: It's fair enough to make an evaluation of a new technique or a new system by withholding information to see what people can come up with. But it is important to emphasize that there is more than one way to interpret the data and had you been supplied with the information, you probably could have cut the number of alternatives down.

Y. Lamontagne: My opinion is that at times it's quite useful to look at the data without any preconceived idea of geology. It's a much better education for the geophysicist to have a few working hypotheses of the whole problem without knowing too much about what is there, and then see it.

Floor: I think you may be confusing apples and oranges here. I think that if we are trying to prove techniques they should not be confused with established techniques, let's say commercial or routine work. I think that if we are trying to convince someone that we have a workable technique and we are convinced that it does work, then we are obligated to start out with as much information as we can get. We should establish the idea of taking all of this input and then forming our own opinions on the basis of all of the information. Proving techniques is an entirely different thing.

B.M. New: I would like to second that idea. I said yesterday in my presentation that we kept rigorously apart the engineering geologist, who actually logged the piece of rock that we were looking at with regard to its structural properties, and the geophysical investigation of that, and it was in bringing them together, having kept them apart, that we were pretty confident that our predictions were correct. However, when you are presenting the results of some sort of site investigation, then they have to work together. I agree with what was said just now and for research purposes, I believe we've got to keep them apart; for overall site investigation, when you are bringing together groups of different disciplines to present an overall picture, then maybe they've got to get together.

Chairman: Written question from Rod Woolham: In comparing borehole data with geological logs how much importance does the geophysicist attach to (1) the accuracy of geological observations; (2) the detail of the geological observations; (3) the possibility that variations indicated by geophysical measurements are caused by mineral assembly changes that only can be identified by petrographic studies; and (4) assumption that core represents exactly the surrounding rock? In many cases I feel that the geologist and geophysicist ignore these factors.

B. Frignet: I think that very often mining geology is quite basic and the cores are not studied extensively and when we log the holes with a full suite – gamma-ray, neutron and sonic and all that, we find a lot of signatures of rocks that are related to geology, but for which the geologist has no time. An added complication is the changing way the geologic structure is understood over the life of an exploration project.

J. Wong: What kind of validity do the geologists put on their logs, how do they understand the information that the log gives them? If they take the same attitude that most of us do, that basically the core is just a sample of one point in the ground or one line in the ground and that you know there are possible variations in both lithology and structure away from the hole, then there is room for geophysical logs as extra input.

J. Roth: I'm reminded of a short, but fascinating paper that Ed Gaucher gave at the CIM about six or seven years ago where he took seven or eight boxes of different rocks and submitted them to ten or twelve different geologists and of course got the usual bell-curve distribution as to what the lithologies were in each box. So we should recognize that we all have a range of uncertainties in terms of the confidence we place in our observations and the interpretations derived. The types of questions we have been discussing are what I would call questions of meta-interpretation. in other words how do we as people who have some confidence that we are doing something useful in the way of indirect observation on rocks interface with our companions in the geological trades? Maybe we could move to more direct questions like. How do we better make use of the data that we are collecting and attempting to interpret?

R. Caven: As a geophysicist I would like to comment that a geologist logging a core, particularly in the exploration stage, does not consider all aspects of what is important for the location of a target and consequently misses details which are picked up in a geophysical survey whether it be ground survey or borehole survey. For instance if an exploration program is directed towards massive sulphides, the geologist who logs the core may only look at what is in fact, massive sulphides and miss any disseminated halos, changes in rock type and so on in the core. These things are often picked up by geophysical methods and if the drillhole misses the massive sulphide often the anomaly is not explained, when in fact if you go back and look at the core very carefully you can see that there are indications that there is an anomaly if not right in the core at least nearby, which has been overlooked.

Floor: Isn't it also a fact thought that if you get two or three geophysicists to interpret a particular set of curves, you'll also get two or three answers? I'm a geologist by the way.

J. Roth: I would disagree you will get at least three!

F. Hiebert: I think that was an important question because as we get more experienced in borehole work, particularly in the massive sulphide area, we are constantly being confronted with the question, is the mineralization that has been intersected in this hole enough to explain the anomaly? I think it's an important question. Sometimes in comparing sulphide intersections that carry equal volumes of sulphides, one will kick like a mule and the other one will be absolutely dead. I think that there are other factors to look into.

K. Morgan: We are beginning to see a proliferation of downhole tools, even in EM, and I'm wondering how badly, we as a group, need comprehensive interpretation schemes and diagrams, – I'd like to hear the panel's comments on that general problem.

J. Macnae: That happens to be one of my personal concerns and I think the only way we are ever going to be able to get things into reasonable form is to go right back to the underlying physics of everything, to really understand the type of behavior in conductors (I'm restricting this to EM for now). Once one has that physical basis one should learn what characteristics to look for. Now one can certainly go ahead and prepare volumes of type curves which just apply for one system but with not that much extra thought one can go on and work out things that are tied into more fundamental aspects of what's actually going on in the conductor and how that relates to things such as migration points. One should look carefully at what are fairly stable estimators. For example things like zero crossovers are fairly bad estimators because they are strongly affected by any background response. You are much better off looking at things like slope inflection points, and locations of peaks, which are much less affected. One has to use as much of the information as possible (for example, full shape of curves and full frequency or time dependence) rather than just one or two points on the curve. I think it's important that profile data be reduced to a smaller and simpler set of parameters based on things like shape alone or inductive limit amplitude. I think that is the type of interpretation knowledge that will start to be developed and to come out in the near future, but the only way I think one can do it is by going back to the physical aspects.

F. Hiebert: The basic questions we have to answer for the geologist are (1) is there something there and, (2) if so where do I drill the next hole? So we have to be quantitative enough so we can give that type of answer. Also it must be decided if it is worthwhile putting down another hole or has this hole cut a representative portion of the structure.

Chairman: I am not sure if that means that we need more refinement of interpretation or does it mean that a good solid seat-of-the-pants type interpretation, of which I think we've seen very good examples in the last few days, is very useful.

F. Hiebert: I think it's something that you can't generalize about. When you look at the Birk's Lake data that John Boniwell showed us it would be very difficult to accurately model that situation. You have so many responses that what you have to do is so-called seat-of-the-pants type interpretation. I discovered that it may be a mistake to try to interpret every little bump and squiggle in a profile. You may have to take a more distant perspective. There may be other features involved than what we are used to, so I really think it is important to judge on a case-by-case basis whether or not a more quantitative approach is required.

J. Roth: That seat-of-the-pants style interpretation ultimately rests on a base of modelling that has provided quantitative insight. I happen to be wrestling with a particularly obnoxious batch of drillhole EM date that has more than it's share of complications, and it seems to me (and this is restricting the discourse to drillhole EM), that responses in a conductive medium as well as multiple-conductor responses are two cases where we lack the kind of quantitative insight that will allow us to do seat-of-the-pants interpretation.

F. Hiebert: That's right. I think that there has been a lot of emphasis on numerical modelling, for instance, and a lot of those techniques don't allow for multiple conductor or the 3-dimensional type of conductor and certainly there is a greater need for those. You can certainly use intuition to a degree provided you are familiar enough with the system and extend what is already known.

J. Macnae: Once you understand the physics you can work anything out. Certainly it's geological targets we are dealing with which can be quite complex. But if you can understand particular physical phenomenon such as how coupling between multiple conductors is going to show up, or how does current gathering show up for a body in a conductive medium, you can get a reasonable idea of what's going on.

Floor: I've been on several surveys with a drill at my back and model studies in hand. Without a good understanding of what I'm working with, there were several targets that I would have missed completely, so the thing I see is that you have to understand what you're doing to start with and not be totally dependent upon model studies as the answer, but rather have a free-thinking mind.

Floor: I think I would agree with those remarks. We have to understand the basic process. I would like to suggest though, we need to carry that a step further. If we model on the basis of one system or one technique and then take a second one and make a similar analysis with that and these two models agree, we have increased the probability that our modelling is correct. If we add a third one then we have increased the probability to a very high degree. With some of the techniques that we use this is a fairly complex thing to do; I'm not familiar enough with your EM processes to know, but it appears to me that they might lend themselves to this type of technique. Some of the techniques that are already in use apply this very idea and I'm not suggesting that these particular techniques should be used but there are a number of techniques which can be considered. One of them for instance is a cross-plotting technique where you take the response from two entirely different curves which are looking at the same set of parameters and you don't add any information to what you have, you merely increase the readability of this information. In the cross-plotting technique for instance, the grouping of the points begins to give you an identification on, lithology, porosity, or whatever it is you want. This doesn't need to be restricted to two curves; there are techniques which use three or four curves in the same way and these do not have to be graphic solutions. I'm in the process of putting these on computer with alphanumeric readouts. There is a whole set of possibilities in combining these various systems which will increase the readability and the accuracy. We use the deviations of one system to apply a correction to another system or the deviations of the two combined. It's generally analogous to the use of two detectors on a density tool, or on a neutron tool, for compensation.

J. Roth: The general point is well taken, that if we can bring a multiplicity of observation to the problem we're likely to emerge with a strengthened and more confident interpretation. You phrased it, at least in terms of the discussion that was going on in respect to drillhole EM in a fashion that's perhaps a little difficult to translate, but I might for instance observe that, in general, there is a lack, in massive sulphide exploraton, of a slimhole device and induction log that one could measure the in-situ conductivity without the distraction of a large loop source. That might be a small niche in terms of instrumentation that someone might be moved to fill and by combining those two types of EM observations, one essentially an inhole measurement and the other with a large remote source, one might be able to improve on one's overall interpretation.

J. Wong: If we concentrate on EM, most interpretation knowledge is based on a number of very simple models. I sympathize with Jerry (J. Roth) with regard to that messy set of drillhole data which just does not in any way resemble the simple responses due to blocks or plates, in freespace. Maybe we should try to either scale model or numerical model more complicated situations such as bent plates; maybe there should be a whole program of modelling in conductive solutions. I know there has been a lot of talk about that but the projects never just seem to get off the ground in a serious way. It will require a big effort but if this is the kind of fundamental knowledge that the geophysicist needs in order to interpret his field data then maybe somebody should be doing something to provide that basis of information.

Q. Bristow: The more complicated the results or profiles, the more likely it is that there will not be a unique solution which will explain that data. In other words there may be any number of shapes and sizes of bodies all of which give the same thing and the more complicated the data profiles you get the more likely this is to be true. Is that a fair comment?

J. Roth: Yes and for that we should be thankful. If there were an immediately obvious solution to every case we would probably not have persistent employment.

Floor: There does seem to be a bit of a trend towards using multiple responses in a sort of automated interpretational system. I was thinking for example of ash content from a suite of logs and the coal industry as one example. The suite of logs is run and a specific quantity related to what the geologist wants comes out the other end. In miniaturized well logging for things like soil profiling, you buy little neutron probes that lower themselves down a hole from a small container, a microcomputer gives you water content as you go, there is no input by anybody-just an output from an automatic routine. Going a little further it seems to me that you could perhaps design a tool for the well driller, an SP log and a gamma log on one tool that went down the hole and could give back, in alphanumeric form, whatever it was you wanted to know, lithology or water content, for example. The microprocessor can work the algorithms. It can be done but it's dangerous and I guess I'd like some opinions as to whether or not automated interpretation is a desirable way to go. It's a trend we'll see more of because we see it in other areas of geophysics.

Y. Lamontagne: I think there are two different schools and two different types of problems that have not been stated. One is conventional logging wherein physical property measurements are made in-situ with the interference of having a hole there and the geometry of the hole and so on. The other one includes EM and other potential field methods wherein the whole problem is basically the same as measuring on the surface. You're not measuring a property by itself, you're measuring fields that are indirectly related to the property. That's completely different, so you have to worry about the complex geometry and you don't know the geometry but you're tryin to determine it. The differential equations are horrendous, as far as the geometrical aspects are concerned. They are well known on a physical basis, but complex geometry is the whole problem. On the other hand, in measurements of physical property, the actual underlying physical principles are known, sometimes only approximately depending on whether you are measuring a second order effect. So these are two different problems, two different approaches and I think we shouldn't mix the two. That's why you have apparently diverging opinions but people would agree if they were solving the same problem, I imagine.

Chairman: The interesting question is: what can be done about integrating those two schools.

Y. Lamontagne: If you take the example of EM, there is no doubt as to what is in the hole – there's a core there and it is the greatest piece of information you have in the hole. So you do the survey to determine what's happening off the hole and what's happening even further away from the hole, maybe hundreds of metres. So it's purely a question of how geometry interacts with the time varying process of EM induction. If you're talking of logging, which I know very little about, I imagine you're trying to make a property measurement in-situ. So it's different, you normally don't have a core. You have cuttings instead which makes it a little bit more difficult to understand what the structure is.

F. Hiebert: Getting back to the question that was originally asked, just how suitable would automatic processing or interpretation be, I think it probably could be useful but only in the simplest of cases and would require pre-screening to see what should be done automatically and what should not. You could run into trouble, at least in EM, by simply automatically submitting everything to an automatic interpretation. Whereas looking at the properties of the wall rock you may be confronted with a more regular situation than is otherwise encountered in EM prospecting.

Floor: One thing that hasn't been stated is that the two different cases are based on what we're trying to achieve. In the automated interpretation case we're looking for the norm of geology, for example, when you log a petroleum hole you're looking at sedimentary layers and the normal geologic sequence. When we're exploring for massive sulphides we're looking for the anomalies of nature and anomalies are in no way normal, they are usually very complicated and that sort of lends itself to more seat-of-the-pants interpretation.

Floor: The algorithms that would be used for automated interpretation would probably be designed by those three geophysicists with the three different opinions so you could still end up with several different possible interpretations of the same data.

J. Macnae: A useful distinction can be made between something like a straight automatic interpretation and a data transformation to a form in which the data are more easily interpreted. There are a number of data transformations that might exist. For example, resistivity and IP data presented as a pseudo-section make it a lot easier to visualize what's going on than a set of stacked profiles. I think there is great scope for procedures such as these to be automated and to be usefully implemented but only in as far as they do not destroy various parts of the data.

B. Frignet: There is no real danger with automatization because what is hard to do is to normalize your logs. You have to take your hole effects away and for that you have to calibrate your logs and transform your logs to correct for hole effect and casing effect, etc., and it is impossible to really automate it. Interactive programs are a better approach. The main problem is to calibrate the data. In mineral exploration I'm not aware of neutron or gamma tools that are really well calibrated, unlike in the coal exploration business, so that it is impossible to combine the logs and push the interpretation very far.

Chairman: Perhaps we could talk a bit about resistivity and induced polarization in drillholes. My impression, which is perhaps a bit naive I'll admit, is that one can do certain things with surface resistivity/IP surveys. I'm talking about large scale surveys from the point of view of detecting things at some distance away from the array. One can do certain things that we've seen, there are all kinds of interpretation schemes available using computer models and so on and that works a lot of the time because one has some sort of a buffer zone between the survey and the responding medium, for instance an overburden layer which is non-polarizable. But in the drillhole we get very close, we can come into intimate contact with that polarizable medium and the target halos and so on. Would somebody who has been working in IP either from the practitioners point of view, or the contractor or interpreter care to comment on just how far they think we're going to be able to take IP interpretation. Or will this be strictly what very often becomes, at best, "bump" identification?

B. Krause: I sense that's being directed at me. Inco has certainly done an awful lot of borehole IP through the years. I do think we sometimes get past the "bump" identification stage as well. In a barren hole modelling studies which are just done on surface tend to apply downhole and they are very useful. One of the biggest problems we do have, though, is the non-barren hole (mineralization in the hole) where you get very large effects, obviously right from the intersected mineralization, either in resistivity or charageability. There is a no modelling information or very little about that kind of a feature and to get an understanding of whether the response is due to a source which is very limited or has extent away from the hole, is something which the geologist is very interested in. In our experience we've tried to look at the effects as we build up towards that mineralization and essentially we're using the shoulders of the anomlies quite often to interpret what's happening away from the hole rather than the actual peaks of the anomalies.

F. Hiebert: I'm wondering what the limits of detectability (away from the hole) would be a polarizable body, be it resistive or not. There are numerous papers on detecting effects going right through the body and in some respects that makes the whole thing a little bit redundant.

J. Wong: It seems to me that detectability is ultimately related to the signal/noise of the instrumentation unit. I don't know exactly what the limits are on present electrical galvanic and IP equipment, but certainnly in EM, you're measuring in parts per million and airborne EM techniques are sensing things hundreds of metres away. If you could improve IP instrumentation to get your noise levels down you should be able to detect targets far from the drillhole. Also the effect of the intervening rock might attenuate some of the telluric noise or something and give you a bit more of a

margin than you would have when applying the same method on surface. On the other hand you have other effects like SP. But I would think that downhole IP should detect at the same kind of distances as surface work. I guess people are confident of IP down to a couple of hundred metres anyway from the surface.

Y. Lamontagne: I would think it depends a bit on how fortunate you are with the method you're using. If you take EM, suppose the hole caught some minor zones of sulphides that are conductive. One lucky thing about EM, and maybe that's why a lot of the borehole work is in EM for mining exploration, is that a minor conductor because of its small size has a fairly poor response parameter. That leads to small fundamental amplitude at a given distance relative to its size. What I'm trying to say is that in a borehole you are not really at much of a disadvantage in EM. In IP, I'm not sure about that, I think you would be limited by what's in the hole. That's just repeating a bit what we've heard before but I would say EM, and any potential field method – borehole gravity for sure, would probably detect things quite far away from the hole if there was such a thing to see. I'd like to hear more comments on that.

B. Frignet: I strongly agree that the conductive body has always sharp boundaries and it's very easy to check it when you do induction logs but when you do IP logs with a very small spacing, i.e. very little penetration, you will never see a very sharp boundary and IP is very irregular even within centimetres. I think that's why inhole IP is very difficult to interpret. Besides that we had very good experiences putting the electrode at the bottom of the hole and measuring potential gradient at the surface. But when you see IP logs it seems very difficult to say this body is polarizable and this body is not, whereas it's very clear for electromagnetism and conductivity.

J. Mwenifumbo: On the question of detectability in any geophysical technique that's mainly dependent on the contrast in the physical parameters that you're trying to measure. One must consider the target that you're looking for and the distance of the target from the measuring tool as well as the interaction of different bodies.

B. Krause: I agree with Jonathan. This is always a question that geologists ask "how far can you see"? It relates to the size of the target. But going back to the comment about IP I think the implication was perhaps small spacing and short holes – we don't really do much IP in holes less than a thousand feet, certainly less than a few hundred feet, because we feel we can actually see that from the surface. Our holes go anywhere from 4000 to 8000 feet deep so we're using separations which are quite comparable to what you use on surface and the interpretation, and hence the distance you can see from the hole, is quite comparable to what you can see from the surface – perhaps even better because you don't have variations due to overburden thickness. The only real problelm is the near-hole sulphides.

Floor: I'm not an expert on drillhole IP but I have a friend, Carl Bishop of Noranda, who worked on longtime charging. In other words he charged sometimes, in drillhole IP, for as long as 20 minutes and when massive sulphides were nearby the decay time might have been in terms of many hours. Perhaps one of our problems with drillhole IP is that we are not putting in enough charge to test the total capacity for chargeability of the area and therefore emphasizing the effects occuring very near the hole rather than looking at the long decay from the large things farther away.

J. Roth: It's too bad Gary Olhoeft wasn't here to enlighten us on what he's been doing in the realm of non-linear IP logging, but in addition to the usual linear aspects of IP behaviour, there is also the non-linear part that might be exploitable in a drillhole in some restricted settings.

Floor: We're taking what we know is a technique for operating on the surface – I'm talking about 2-dimensional way of doing things – and then trying to apply the same technique, down the borehole. Now can't we consider some other way of doing things. What springs to mind in electrical methods is the possibility of using some of the ideas presented here in the past few days for tomographic techniques. The ideas that Joe Wong presented in his paper, in moving one electrode around and, in this way, developing a different approach, may be possible. I'm wondering what the panel's idea may be on that.

Chairman: A lot of these things have been done but they may or may not have worked in isolated cases. One thing you have to do is design the experiment or the survey very carefully for what you think you might have but these techniques are not ones that have achieved any kind of routine application; tomography is in a different ball park. With respect to the business of putting electrodes in various places, there are examples in the literature.

J. Wong: I guess the problem with non-standard techniques is that people think that if you are taking a risk in terms of investing time then, at least in operations anyway, they would rather stick with the tried and true. The other aspect is that if you go to a standard technique you can get information out, but with non-standard techniques what do you do with the information? Probably people, like Inco, who have done a lot of borehole IP with large scale arrays know what's going on. I'm sure that there's a fair amount of cost in setting up some of these non-standard surveys.

Chairman: Is there anything that geophysicists supplying borehole techniques could do to influence the placing of holes. I don't mean just where the holes are collared, and then leaving it to the explorationist to decide how he's going to get that intersection that he's after. First of all, let me say, for steeply dipping or close to vertical features holes are drilled from the hanging wall to the footwall because that presents the largest area for probable intersection and secondly they're drilled to intersect the target. Is it worth trying to influence the drilling of the holes some other way. For example if one could drill a hole parallel to a plate-like conductor one can in fact stand back from it somewhat and get some kind of bulk estimate of its characteristics, perhaps with an improved geological signal/noise. From the point of view of large-loop EM with an axial-component receiver that is the optimum condition for determining where the target is. A plate which is perpendicular to the drillhole presents the most difficult situation.

F. Hiebert: What we have to do first is try to convince them to continue drililng past where the anomaly is. Usually they drill into the area of interest and no further and then you end up with a lot of profiles such as we've seen in this symposium where you're trying to interpret a fraction of the response. However, I think that trying to convince them of drilling a hole for its geophysical merits is the real question and the real problem.

B. Krause: This is one area where we have had some success. It seems that when you,re doing surface geophysics you're always finding surprises as far as the geologist goes. When you're doing borehole geophysics, in most cases they know the answers but if you can get a success somewhere along the way they start believing. It helps, because now in our deep

drilling they are quite happy to drill 500-600 feet past any geological area of interest so that we have room to survey the favourable contacts. Also we participate in their pattern drilling so that a drill pattern can serve not only a geological purpose but also a geophysical purpose.

J. Roth: We have cycled back here to what I would call a sort of metaphysics in terms of now do we deal with the other compatriots in this great game that we play. I was just going to raise, for a few seconds the other area that I think our geological compatriots find rather fascinating even if we don't regard it as technically challenging an adventure as drillhole EM, namely the potential for in-situ analysis. I think the work that Phillips Petroleum has done with XRF was to me the kind of fascinating direction that I hope someone builds upon. I'd like to say I have a sense that we have achieved, those of us interested in the non-petroleum, non-coal applications of mineral logging, a critical mass in terms of sustained activity and sustained interest and I'm pleased to see that occur. The last time Pat Killeen convened people of similar persuasion we only filled a small round table and clearly the group has grown in terms of number and contributions so I hope, if Pat is persuaded to repeat this exercise in a few years, we'll count on an even larger and more boisterous throng.

Chairman: I would like to thank the panel and everybody else for participating in the discussion.

MINERAL LOGGING WORKSHOP PAPERS

The following five papers have been selected from reports originally presented at an informal workshop on Mineral Logging held at the Geological Survey in 1981. The material, which has not been published elsewhere, is presented here so that a wider audience may benefit from some of the valuable experience in mineral logging discussed at that workshop.

SPATIAL DECONVOLUTION APPLIED TO GAMMA RAY LOGGING: A REVIEW

John G. Conaway[1]

Conaway, J.G., Spatial deconvolution applied to gamma ray logging: a review; in Borehole Geophysics for Mining and Geotechnical Applications ed. P.G. Killeen, Geological Survey of Canada, Paper 85-27. p. 357-360, 1986.

Abstract

The theoretical and practical development of the application of gamma ray logs for quantitative radioelement determinations is described and several spatial deconvolution techniques are outlined.

Résumé

On trouvera ci-après la description de l'évolution théorique et practique de l'utilisation des diagraphies de carottage radioactif pour la détermination quantitative des radio-éléments, ainsi qu'un exposé sommaire sur plusieurs techniques de déconvolution spatiale.

Introduction and background

Ideally, we would like gamma ray logs to give exact information regarding the quantity and distribution of radioactive material (say, uranium ore) with depth along a borehole. In this ideal gamma ray log, radiation intensity 'I' would be exactly proportional to the radioelement concentration or grade 'G' at any given depth, or $G = KI$ where K is the system calibration constant or K-factor. In practice, many factors interfere with this ideal, and distort the shape of the log. Several types of data processing techniques can be used to reduce this distortion, thereby causing the processed gamma ray log to approach the desired ideal. These techniques can be termed spatial deconvolution techniques.

Among the factors which limit spatial resolution in gamma ray logs are the effect of the analog ratemeter time constant (for analog systems), the effect of detector length, and the effect of borehole parameters including diameter, casing, and fluid. In general, the most significant distortion results from the fact that the gamma rays from a radioactive zone obviously are not constrained to travel in that zone, but, in fact, propagate in all directions; solid rock is translucent to gamma rays. Thus, a thin radioactive zone perpendicular to the borehole (Fig. 1a) does not cause a sharp anomaly as shown in Figure 1b, but rather a smeared anomaly spread over perhaps 1-2 m perpendicular to the thin zone (Fig. 1c). This smeared anomaly may be called the geologic impulse response, a term meant to indicate that the smearing is unavoidably inherent in the physical situation, and is not a result of instrument deficiencies or other external effects. The geologic impulse response is a function of gamma ray energy, and formation parameters such as density, fluid content, and equivalent atomic number.

The relationship between radioelement distribution and gamma ray log response has been considered theoretically and experimentally by a number of authors. Suppe (1957) summarized the Russian effort to that date. Further work by Suppe and Khaykovich (1960) and Davydov (1970) laid the foundation for the concept of the geologic impulse response, which was introduced by Conaway and Killeen (1978a). In addition, Davydov proposed an inversion (spatial deconvolution) scheme which, with some modification, has proven quite useful in dealing with the geologic impulse response. Roesler (1965) applied gamma ray logging for making quantitative determinations of K_2O in East German potash deposits. His work is notable especially for his consideration of the relationship between detector length and spatial resolution; Roesler did not suggest a solution for this problem. J.A. Czubek has expended considerable effort over the course of his career on describing theoretically the shape of gamma ray anomalies (Czubek, 1961; 1962, 1969) and on the spatial deconvolution problem (Czubek, 1971, 1972). Jonas (1975) attempted to apply some of Czubek's numerical deconvolution techniques: however, Czubek and Zorski (1976) reported that Jonas applied the techniques incorrectly. Jonas has certainly not been alone in his problems in applying Czubek's interpretation techniques. The level of knowledge in nuclear theory and mathematics required to follow much of Czubek's important work in nuclear logging is unfortunately beyond the experience of the majority of applied geophysicists.

In North America, parallel effort has led to other numerical interpretation techniques for gamma ray logs. In particular, Scott et al. (1961) demonstrated that, although the expression $G = KI$ is not valid for unprocessed gamma ray logs, under ideal conditions the average grade $\bar{G}$ over a complete gamma log anomaly having area A (from background to background) can be computed from $\bar{G} = KA/T$ where T is the total thickness of the radioactive zone, and K is the same calibration factor described earlier. Scott (1962) and Scott (1963) presented a computer program which was designed to improve the accuracy of gamma ray logs for determining the distribution of radioactive material. This was the well-known GAMLOG program, which represented the earliest application of spatial deconvolution to gamma logs.

[1] Los Alamos Scientific Laboratory, P.O. Box 1663, Los Alamos, NM 87545

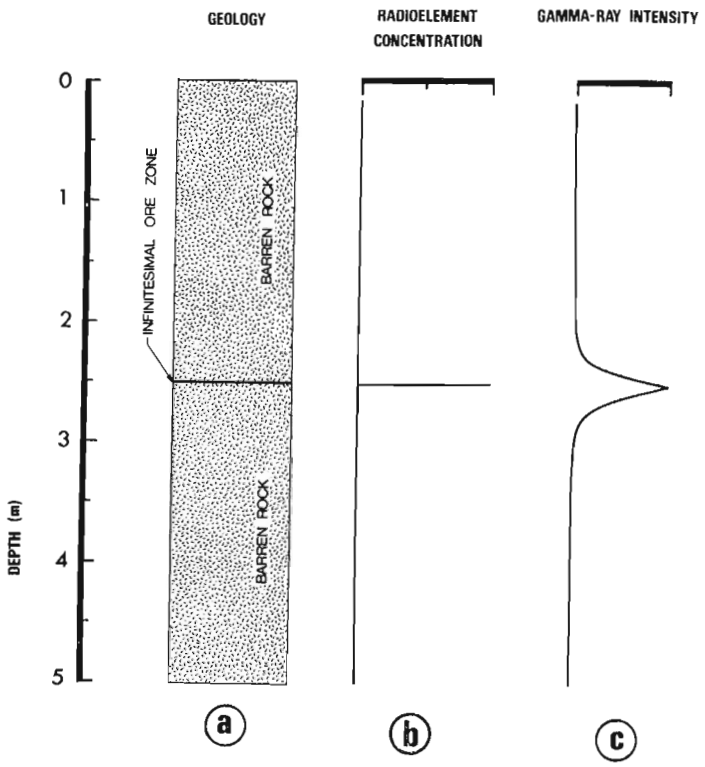

Figure 1.

(a) Geologic column showing an infinitesimally thin radioactive ore zone sandwiched between two thick barren zones, a 'geologic impulse' of radioactive ore.

(b) Plot of radioelement concentration with depth corresponding to Figure 1.

(c) Noise-free response of a point-detector to the thin ore zone, the 'geologic impulse response'.

GAMLOG, which is still in widespread use today, uses an iterative approach to the problem of improving the accuracy and resolution of gamma ray logs. The response of the logging system to a thin zone of radioactive material is first determined using data from model boreholes. Given that the equation $\bar{G} = KA/T$ is valid then the anomaly resulting from any complex sequence of radioactive zones is simply the sum of the anomalies resulting from the individual zones. The experimentally determined thin zone response function is applied to the raw field log and the result fed back in the form of an error signal. This process continues iteratively until the desired degree of improvement occurs, or until the practical limit imposed by noise is reached.

Through the efforts of the MIT Geophysical Analysis Group and others in the 1950s and 1960s, digital time series analysis was established as a powerful group of related techinques for the analysis of data gathered sequentially in time or space. In geophysics these techniques are associated largely with seismology, although they are equally applicable in other areas, including borehole logging. Drawing upon these techniques, and the work by Czubek (1971), Davydov (1970), and Suppe and Khaykovich (1960) mentioned earlier, Conaway and Killeen (1978a) considered separately the effects of the geologic impulse response, detector length, ratemeter time constant (analog systems) and sampling interval (digital systems). That paper also contained a number of computer-simulated gamma ray logs illustrating these effects both in the ideal case and in the presence of statistical noise (unavoidable in nuclear logging), using a combined inverse filter (spatial deconvolution) and smoothing technique.

Conaway and Killeen (1978b) compared the inverse filter technique (Conaway and Killeen, 1978a) with Scott's iterative technique (Scott, 1963). Theoretically the two techniques give identical results in the ideal case. In practice, slight differences between the processed logs result from unavoidable approximations made in applying both techniques. Inverse filtering has the advantage that it requires only about 3 per cent as much computer time as iteration. In addition, whereas iterative processing requires that an entire log (or at least a complete anomaly) be available to the computer before processing can begin, inverse filtering is a one-pass sequential operation and thus can be applied in real time during the logging operation, given suitable equipment.

The system response function

The log which is produced by a given logging system in the vicinity of a thin zone ("spatial impulse") of radioactive material perpendicular to the borehole is called the system impulse response, or the system response function. In an infinitesimally thin borehole using a point detector the system response function $\phi(z)$ would generally resemble Figure 1c, and could be approximated by the equation

$$\phi(z) = \frac{\alpha}{2} e^{-\alpha |z|} \qquad (1)$$

as given by Davydov (1970) based on Suppe and Khaykovich (1960). Here z is depth along the borehole and α is a parameter referred to as the shape constant.

Equation (1) describes a double-sided exponential, which has a corresponding simple exact digital inverse filter (Conaway, 1980a). The beauty of this equation for this application is its simplicity. By determining the behavior of α under various conditions, the exact inverse filter is adapted easily to changing conditions. Moreover, under favorable conditions α may be determined directly from field logs (Conaway, 1980b), thus providing a check on values arrived at by other means (model boreholes and theoretical studies).

Under the conditions considered by Scott et al. (1961) in their derivation of the relationship $\bar{G} = KA/T$, gamma ray logs obey the principle of superposition. This means that various distorting effects may be removed from the data separately, and in any order (at least to the limit that they may be removed at all). Thus, it is not necessary that the system response function correspond precisely with equation (1). In general, the radiation intensity outside of the radioactive zone will die away essentially exponentially with distance. This is a sufficient condition to use the inverse filter based on equation (1). After application of this filter, some residual distortion will exist in the log near the radioactive zone, the extent depending on borehole diameter, detector size ratemeter time constant, etc. These may also be considered individually.

Variations in the shape constant

The shape constant α in equation (1) provides a simplified means of studying the effects of borehole, formation, and instrumental parameters on the shape of the system response function. Such effects have been considered by many authors including Czubek (1961; 1966, 1969; 1971, 1972), Rhodes and Mott (1966), McDonald and Palmatier (1969), Davydov (1970), Conaway and Killeen (1978a), Conaway (1979, 1980a, 1980b, 1981), Conaway et al. (1979, 1980).

An increase in the value of α indicates a more rapid decrease in radiation intensity with distance from the radioactive zone. This condition may, in general, be brought about by:

(a) An increase in formation density.

(b) An increase in pore fluid density (e.g. from air to water).

(c) A decrease in dip angle between the radioactive zone and the normal to the borehole (until perpendicularity or 0° dip).

(d) An increase in borehole fluid density (e.g. from air to water to heavy mud).

(e) A decrease in borehole diameter (allowing proportionately less radiation to travel in the borehole).

(f) An increase in the equivalent atomic number Zeq of the formation.

(g) Restriction of the detected gamma rays to unscattered photons (e.g. the 1.76 MeV ^{214}Bi window of uranium).

(h) For unscattered gamma rays, a decrease in the energy of the spectral discrimination window.

The reader is referred to the abovementioned works for further information on these factors.

Conclusions

Improving the accuracy of gamma ray logs for quantitative radioelement determinations may be achieved by several spatial deconvolution techniques. These techniques have resulted from research in a number of countries over a period of more than 20 years. Appropriate choice of equipment, logging technique, and data processing can produce a log with markedly better accuracy and spatial resolution than normally obtained.

References

Conaway, J.G.
1979: Problems in gamma ray logging: The effect of dipping zones on the accuracy of ore grade determinations; in Current Research, Part A, Geological Survey of Canada, Paper 79-1A, p. 41-44.

1980a: Exact inverse filters for the deconvolution of gamma ray logs; Geoexploration, v. 18, p. 1-14.

1980b: Direct determination of the gamma ray logging system response function in field boreholes; Geoexploration, v. 18, p. 187-199.

1981: Deconvolution of gamma ray logs in the case of dipping radioactive zones; Geophysics, v. 45.

Conaway, J.G., Allen, K.V., Blanchard, Y.B., Bristow, Q., Hyatt, W.G., and Killeen, P.G.
1979: The effects of borehole diameter, borehole fluid, and casing thickness on gamma ray logs in large diameter boreholes: in Current Research, Part C, Geological Survey of Canada, Paper 79-1C, p. 37-40.

Conaway, J.G., Bristow, Q., and Killeen, P.G.
1980: Optimization of gamma ray logging techniques for uranium; Geophysics, v. 45, p. 292-311.

Conaway, J.G. and Killeen, P.G.
1978a: Quantitative uranium determinations from gamma ray logs by application of digital time series analysis; Geophysics, v. 43, p. 1204-1221.

Conaway, J.G. and Killeen, P.G. (cont.)
1978b: Computer processing of gamma ray logs: iteration and inverse filtering: in Current Research, Part B, Geological Survey of Canada, Paper 78-1B, p. 83-88.

Czubek, J.A.
1961: Some problems of the theory and quantitative interpretation of the gamma ray logs; Acta Geophysica Polonica, v. 9, p. 121-137.

1962: The influence of the drilling fluid on the gamma ray intensity in the borehole; Acta Geophysica Polonica, v. 10, p. 25-30.

1966: Physical possibilities of gamma-gamma logging; in Radioisotope Instruments in Industry and Geophysics, volume 2; International Atomic Energy Agency Proceedings Series, IAEA, Vienna.

1969: Influence of borehole construction on the results of spectral gamma logging: in Nuclear Techniques and Mineral Resources, International Atomic Energy Agency Proceedings Series, IAEA, Vienna.

1971: Differential interpretation of gamma ray logs: I: Case of the static gamma ray curve; Report No. 760/1, Nuclear Energy Information Center, Polish Government Commission for Use of Nuclear Energy, Warsaw, Poland.

1972: Differential interpretation of gamma ray logs: II: Case of the dynamic gamma ray curve: Nuclear Energy Information Center, Polish Government Commission for Use of Nuclear Energy, Warsaw, rep. no. 793/1.

Czubek, J.A. and Zorski, T.
1976: Recent advances in gamma ray log interpretation; International Atomic Energy Agency Advisory Group Meeting on Evaluation of Uranium Resources, Rome, Italy.

Davydov, Y.B.
1970: Odnomernaya obratnaya zadacha gamma-karotazha skvazhin (One dimensional inversion problem of borehole gamma logging); Izvestiya Vysshoya Uchebnoye Zavedeniya Geologiya i Razvedka, No. 2, p. 105-109 (in Russian).

Jonas, J.T.
1975: Digital data processing techniques applied to the natural gamma ray log; M.S. thesis T-1778, Colorado School of Mines.

McDonald, W.J. and Palmatier, E.D.
1968: Predicting nuclear log response; Journal of Petroleum Technology, v. 21, p. 1421-1426.

Rhodes, D.F. and Mott, W.E.
1966: Quantitative interpretation of gamma-ray spectral logs; Geophysics, v. 28, p. 410-418.

Roesler, R.
1965: Ein neues Auswerteverfahren fur radiometrische Bohrlochmessungen uter besonderer Berucksichtigung der K_2O-Bestimmung aus Messungen der naturlichen Gammastrahlung in Bohrlochern; Freiberger Forschungshefte, C180, Geophysik, VEB Duetsch; Verlag Fur Grundstoffindustrie, Leipzig.

Scott, J.H.
1962: The GAMLOG computer program: U.S. Atomic Energy Commission rep. RME-143, September, Grand Junction, CO.

1963: Computer analysis of gamma ray logs; Geophysics, v. 28, p. 457-465.

Scott, J.H., Dodd, P.H., Droullard, R.F., and Mudra, P.J.
1961: Quantitative interpretation of gamma ray logs; Geophysics, v. 26, p. 182-191.

Stromswold, D.C.
1979: Measurement of the deconvolution parameter "α" for uranium; Spectral Gamma Ray Borehole Logging Technical Note, Bendix Field Engineering Corporation, Grand Junction, Col.

Suppe, S.A.
1957: Gamma ray borehole logging: in Radiometric Methods in the Prospecting of Uranium Ores, V.V. Alekseev, A.G. Grammakov, A.I. Nikonov, and G.P. Tafeev, ed., Translation available as AEC-tr-3738 (Book 2), U.S. Atomic Energy Agency.

Suppe, S.A. and Khaykovich, I.M.
1960: Resheniye pryamoi zadachi gamma-karotazha v sluchaya slozhnogo raspredeleniya radioaktivnogo elementa v aktivykh plastakh (Solution of the linear problem of gamma logging in the case of a complex distribution of the radioactive element in the active strata); Voprosy Rudnoi Geofiziki, Issue I (in Russian).

Wilson, R.D.
1979: Log deconvolution with the inverse digital filter; Spectral Gamma Ray Logging Technical Note 9, Bendix Field Engineering Corporation, Grand Junction, Colorado.

APPLICATION OF APPLIED POTENTIAL AND DOWNHOLE PULSE EM TECHNIQUES TO EXPLORATION FOR MASSIVE SULPHIDE DEPOSITS IN EASTERN CANADA

K.E. Witherly[1]

Witherly, K.E., Application of applied potential and downhole pulse EM techniques to exploration for massive sulphide deposits in Eastern Canada; in Borehole Geophysics for Mining and Geotechnical Applications, ed. P.G. Killeen, Geological Survey of Canada, Paper 85-27, p. 361-374, 1986.

Abstract

During the last several years, Utah Mines Ltd. has been utilizing the Applied Potential (mise-à-la-masse) and the Downhole Pulse EM (DHPEM) techniques on a systematic basis to assist in its exploration efforts for massive sulphide deposits in Eastern Canada. To facilitate access to diamond drillholes for logging purposes, Utah Mines Ltd. had instigated a procedure whereby every hole drilled is left cased through the overburden either with the original steel casing used in drilling, or with a comparatively cheap plastic casing easily inserted in the hole immediately upon its completion.

The Applied Potential method involves the direct galvanic energization of a conductive body and the subsequent mapping of the resultant potential disturbance, either on the surface or in drillholes. The results are fairly simple to interpret and can provide information on the strike extent, depth and dip of a conductor.

The DHPEM technique, a Time Domain EM system, involves the logging of drillholes with transmitter loops laid out on the surface around the holes being logged. The results provide information on the dimensions and position of a conductor intersected by the drillhole and the conductor's attitude with respect to the hole. The survey data can also provide information about the location of conductors in the vicinity of the hole that have not been intersected.

The results presented are from a number of geological situations where Applied Potential and DHPEM have been used to elaborate on exploration of the results from corelogs. The results can verify the interpretation of surface geophysical data or extend information derived from exploration at depth with a resolution, not possible with surface geophysical techniques.

Résumé

La société UTAH MINES LTD. utilise depuis plusieurs années la technique de la mise à la masse et la technique du sondage électromagnétique à impulsions, d'une façon systématique, afin d'accélérer l'exploration de gisements de sulfure massif découverts dans l'Est du Canada. Afin de faciliter l'utilisation des trous de sondage au diamant servant à l'exécution des diagraphies, la Utah Mines Ltd. a mis au point une méthode selon laquelle chaque trou foré demeure chemisé en permanence dans la couche de mort-terrain, soit avec le revêtement d'acier original qui a été utilisé au cours du forage ou avec un revêtement fait de matériaux plastiques économiques que l'on peut insérer aisément dans le trou dès la fin du forage.

Les méthodes de la mise à la masse consistent en la mise sous tension directe d'un corps conducteur et à faire l'enregistrement graphique de la différence de potentiel observée à la surface ou dans les trous de sondage. Les résultats, dont l'interprétation se fait très simplement, peuvent renseigner sur l'ordre de grandeur et la profondeur du gisement ainsi que sur l'inclinaison du conducteur.

La technique du sondage électromagnétique à impulsions, qui s'applique au moyen d'un système électromagnétique du domaine du temps, comprend l'exécution d'une diagraphie de trous de sondage à l'aide de boucles de transmission déployées à la surface autour des trous étudiés. Les résultats renseignent sur les dimensions et la position du corps conducteur traversé par le trou de sondage ainsi que sur la position de ce conducteur par rapport au trou. Les données recueillies peuvent également renseigner sur l'emplacement des corps conducteurs non traversés situés aux environs d'un trou de sondage.

Les résultats présentés portent sur un certain nombre de cas géologiques où l'on a utilisé les techniques de la mise à la masse et du sondage électromagnétique à impulsions en vue de pousser l'étude des résultats d'exploration obtenus au moyen de carottages. Les résultats peuvent confirmer l'interprétation des données géophysiques de surface ou enrichir les renseignements issus de l'exploration en profondeur et, cela, à un degré de précision qu'il est impossible d'obtenir avec des données géophysiques de surface.

[1] Utah Mines Ltd. Toronto, Ontario

Introduction

Although Applied Potential has been used by geophysicists for decades, DHPEM equipment has only come into general availability in the last few years, largely as a result of a joint development program between Crone Geophysics Ltd. of Mississauga, Ontario and the Geological Survey of Canada.

In the course of exploration for massive sulphide deposits in Eastern Canada, Utah Mines Ltd. has for the past several years been performing applied potential (AP) or mise-à-la-masse and downhole pulse EM (DHPEM) surveys on a routine basis. It has been our experience that the two techniques used together as follow-up to drilling can be very helpful in resolving ambiguous surface geophysical responses, as well as extending exploration data away from the drillhole, with a resolution not possible with surface source-receiver techniques. The results presented illustrate a variety of situations where AP and DHPEM were used in a complementary fashion to assist in making exploration decisions. The author acknowledges with thanks the permission granted by Utah International Inc. to present this paper.

Logging philosophy

The decision to do AP or DHPEM in a given situation depends on what is intersected or sometimes not intersected in an exploration hole. A hole that encounters economic sulphides usually warrants rapid follow-up, but a barren hole can also warrant investigation. Generally, we cannot justify having a logging crew stand-by for routine drilling jobs, since most holes do intersect expected, albeit mundane, sources for the indicated surface response. However, we have often found that marginally interesting intersections can increase in exploration importance with subsequent drilling, delayed assay results or second looks at the geology and geophysics of an area. Thus to ensure later access to all holes drilled, we have instigated a policy whereby each hole is left either cased with the original steel casing in-place or the steel casing is replaced with a relatively inexpensive section of plastic pipe. This procedure ensures reasonable chance of getting back into most of our exploration holes. If rock conditions warrant, plastic pipe can be inserted through the entire length of a hole, but as yet this has not been much of a problem in the Precambrian Shield of Eastern Canada.

Equipment and techniques

Applied Potential (AP)

The equipment used for AP surveys by Utah Mines is one of the standard IP systems and consists of a transmitter, powered by either a battery or small motor generator and a receiver, commonly a Scintrex IPR-7. Use of AP has been primarily the variation which involves the energization of sulphide intersections in drillholes and the subsequent mapping out on the surface of the resulting potential pattern. Our survey technique has generally been to locate one current electrode in each of the sulphide intersections of interest, and place remote current and potential electrodes far away from the hole, at least 10 times the vertical depth of the deepest intersection being energized. Infinite electrodes are placed as orthogonal to local geology as possible. Both current and potential sites are generally within several hundred metres of each other. Potential readings are routinely taken at 30 m intervals along lines 60 m apart.

Downhole Pulse EM (DHPEM)

The system used for Utah Mines DHPEM work is manufactured by Crone Geophysics and consists of a Time Domain EM Receiver, a 2KW Time Domain Transmitter, a Downhole Probe and ancillary equipment. The downhole probe measures the axial component of the secondary magnetic field. The DHPEM is capable of logging holes to a depth of 1500 m. The survey procedure is to log the target hole with a number of loops laid out on the surface. Loop size varies but a square of 120 m on the side is convenient in most cases. A logging depth increment of 5 or 10 m is routinely used and occasionally 2.5 m for better resolution.

We have found a crew of three can log a 200 m hole with 5 transmit loops in one day. About 65 per cent of this time is spent in moving loops around the hole and moving equipment to and from the drill site. Only 35 percent is spent in actually logging the hole.

For most of our logging we have used the convention of constant gain for the receiver amplifier, set initially at the bottom of the hole for each loop. As well, we have set our primary pulse polarity positive at the bottom of each hole and recorded the polarity and amplitude of the primary field at every station logged in that hole for each loop. All the data shown were recorded in this fashion and were plotted exactly as observed. To sort out questions of true polarity in the primary and secondary fields, recourse to magnetic flux diagrams such as those drawn up by Woods (1975) or Macnae (1980), are very helpful. The type responses for DHPEM are fairly straightforward and have been studied by both scale modeling (Woods, 1975) and computer modeling (Dyck, 1981). The major challenge in interpreting DHPEM results is the 3-dimensional nature of the data. This aspect of the technique requires a considerable effort on the part of the interpreter to keep track of all the pertinent geophysical information and at the same time constrain solutions to those that are geologically plausible.

Figures 1 to 4 show some of the equipment used in AP and DHPEM surveying. Figure 1 shows the patch-panel for the 9-electrode survey in Property 1. The transmitter used was an Elliot 15A. Figure 2 shows the DHPEM cable winch assembly. Figure 3 shows the Crone 450W PEM XMTR., powered by a 3 HP Briggs & Stratton. Figure 4 shows the DHPEM downhole tool. A preamp is located in the upper part of the probe to improve signal quality.

Field Results

Property I

The first case history deals with a massive sulphide deposit that was extremely difficult to locate geophysically and to interpret structurally from drilling. Geophysical difficulties arose primarily due to the proximity of the economic sulphides to a much more responsive iron formation. Unfortunately, AP and DHPEM were not carried out on the prospect until the deposit had already been essentially outlined by considerable, somewhat redundant, drilling.

The AP survey conducted on this property involved eight different current electrodes in the deposit. The large number of electrodes were used primarily to investigate the overall electrical and structural continuity through the orebody. Figure 5 shows the AP results from the electrodes in holes R-21, R-46, and R-34, all within economic sulphides. Also shown for comparison, are the AP results for an

electrode placed in the adjacent iron formation, intersected in R-32. Several observations were immediately apparent from the data; firstly, electrical and presumably structural continuity through the deposit was apparent from a variety of current electrode locations; secondly, the strike extent, dip and plunge of the deposit was faithfully indicated by the AP data; thirdly, the adjacent iron formation was clearly distinguishable from the deposit, based on their respective responses.

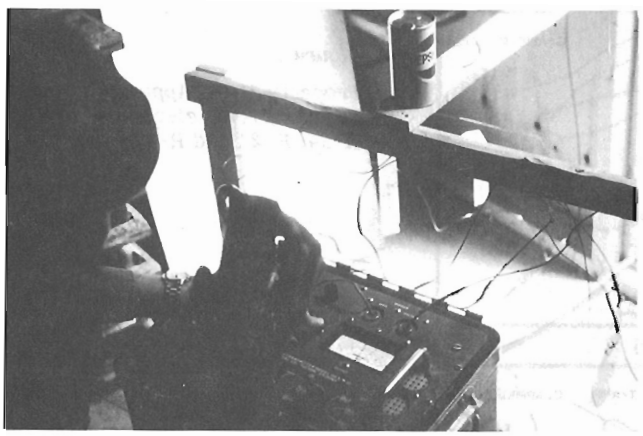

Figure 1. *Elliot 15 AIP transmitter and 9-electrode patch panel.*

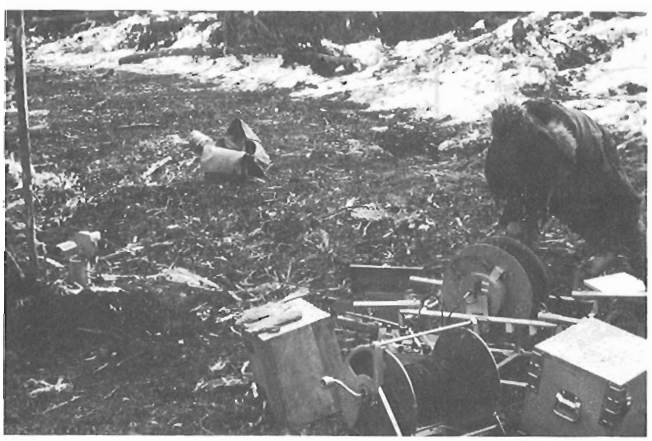

Figure 2. *Crone DHPEM draw works (winch assembly).*

Figure 3. *Crone 450W PEM transmitter and 3hp Briggs and Stratton gas powered engine.*

At the time DHPEM was first conducted on the prospect it was assumed that the western edge of the deposit ran diagonally between the two holes R-32 and R-34, shown in Figure 6. R-34 intersected economic sulphides at 145 m and R-32 passed by the target horizon at 104 m without encountering any economic mineralization. The two holes were logged with loops 1, 2, 8, and 9, also shown in Figure 6. The logs for R-34 are shown in Figure 7. It is apparent that all the loops excite a strong response from the banded iron formation, while the ore zone shows a strong response from loop 1, but much weaker and almost equal responses from loops 8 and 9. These responses appeared reasonable since it was known that loop 1 was much closer to the orebody than either of the other two loops. However, the comparable responses from loops 8 and 9 suggested that there may be a portion of the orebody southwest of R-34. The logs for R-32, shown in Figure 8, are quite similar to those of R-34; a predominant response through the iron formation on all three logs followed by varying degrees of responsiveness adjacent to the target horizon farther down the hole. Loop 2 showed the strongest response at the target horizon; the response of loop 9 was modest and that of loop 8 at this point was marginal. These observations lead to the interpretation that the edge of the orebody passed, not diagonally to the southeast between R-32 and R-34, but more steeply to the south and quite close to R-32. Based on this interpretation, R-49 was spotted (Fig. 6). This hole intersected the ore zone approximately 65 m below and 40 m west of the ore intersection in R-34.

Figure 4. *Crone DHPEM Probe.*

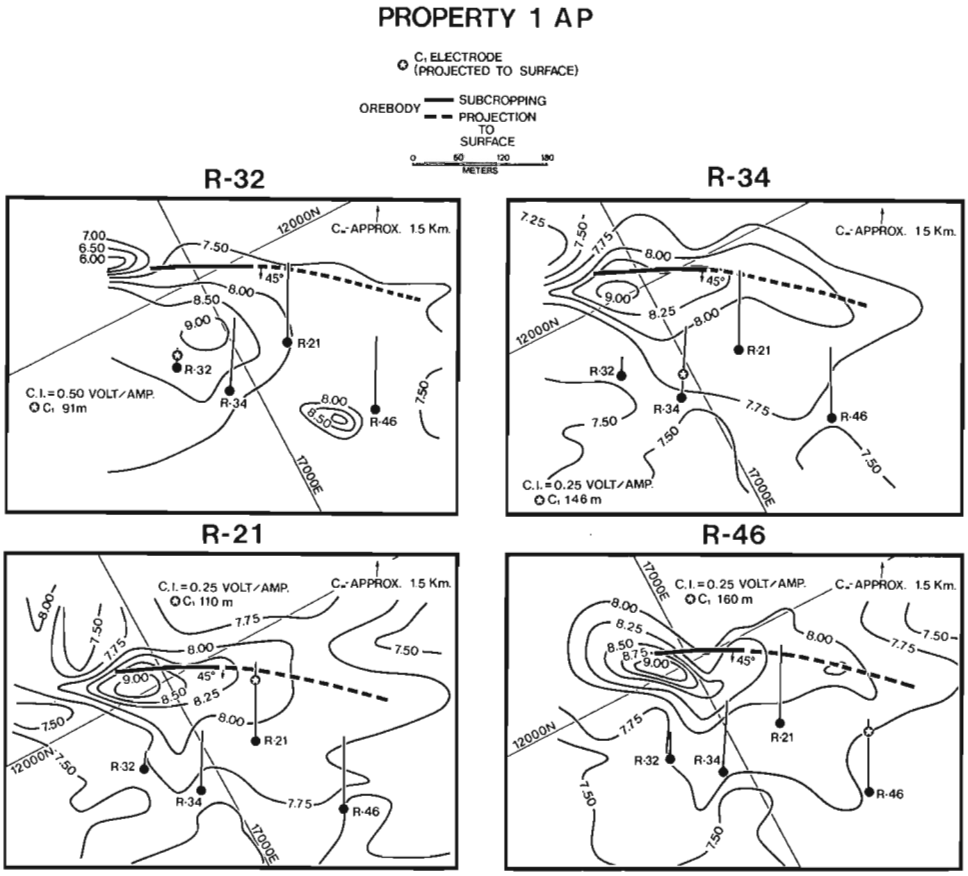

Figure 5

Property 1: Applied Potential data; current electrode in R-32, R-34, R-21 and R-46.

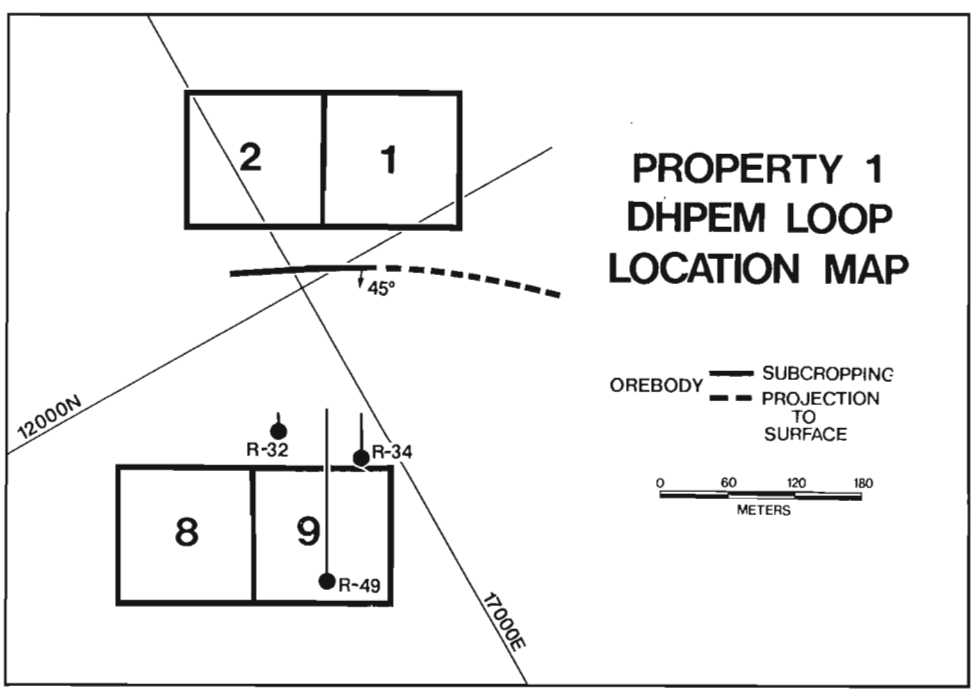

Figure 6

Property 1: DHPEM loop location map.

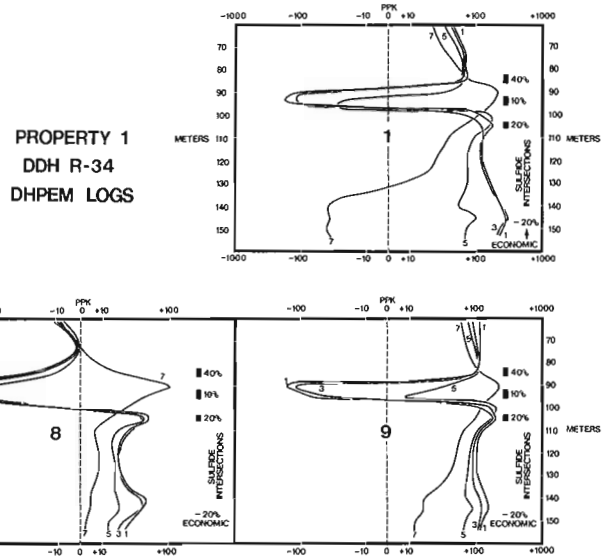

Figure 7

Property 1: DHPEM Logs in R-34.

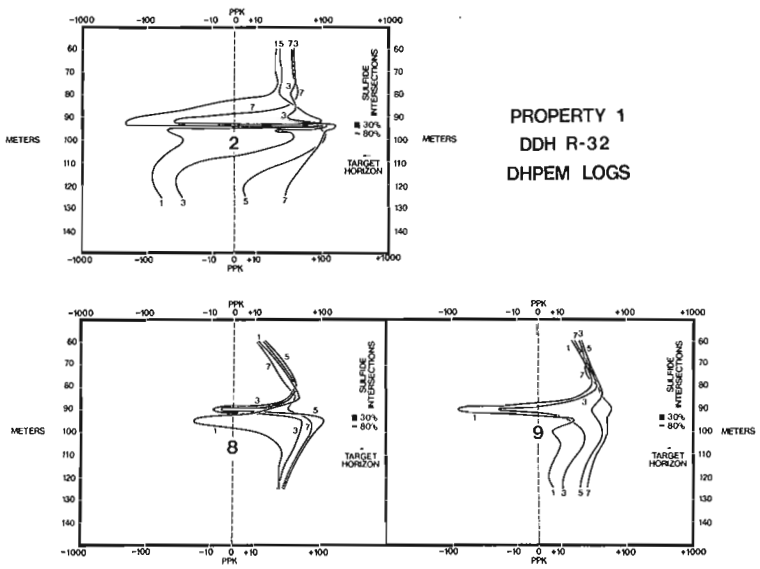

Figure 8

Property 1: DHPEM Logs in R-32.

Property II

The second property was initially drilled to test horizontal loop EM (HLEM) and magnetic anomalies with some consideration to an IP response associated with the conductors. The geological-geophysical section shown in Figure 9, illustrates the two holes drilled to test the indicated geophysical anomalies. The first hole, GU-3, was drilled some distance from the indicated conductor in order to concurrently test the observed IP anomaly. Although sufficient disseminated sulphides were encountered in the upper part of GU-3 to explain the IP anomaly, only one significant conductor was intersected, a zone of about 25 per cent total sulphides over 1 m, at a depth of 191 m. This conductor was, however, interpreted to be of a favourable geological nature, with some minor economic mineralization present. A directional survey done upon completion of GU-3 indicated that there had been a considerable azmithal drift from the original bearing and hence there was some question as to whether the surface geophysical response was arising from the intersected conductor. To confirm that the HLEM anomaly had been tested, and to further investigate the favourable intersection at a slightly higher elevation, GU-4 was spotted on line about 75 m from GU-3. GU-4 intersected a series of pyrrhotite-pyrite bands between 12 m to 52 m, followed by two minor sulphide intersections at approximately 88 m. Although the lower zone in GU-4 and the intersection in GU-3 appeared to line-up fairly well (Fig. 9), their different geological natures were felt sufficient to rule out their being the same horizon. Unfortunately, during the AP survey, the zone in GU-4 was not energized nor was GU-4 logged while the intersection in GU-3 was energized. However, other geological information and the subsequent DHPEM logging of both holes appear to support the original geological interpretation.

In an initial effort to sort out the various conductors with AP, the intersection in GU-3 along with the three upper intersections in GU-4 were energized. The results from GU-3 and a representative response from GU-4 are shown

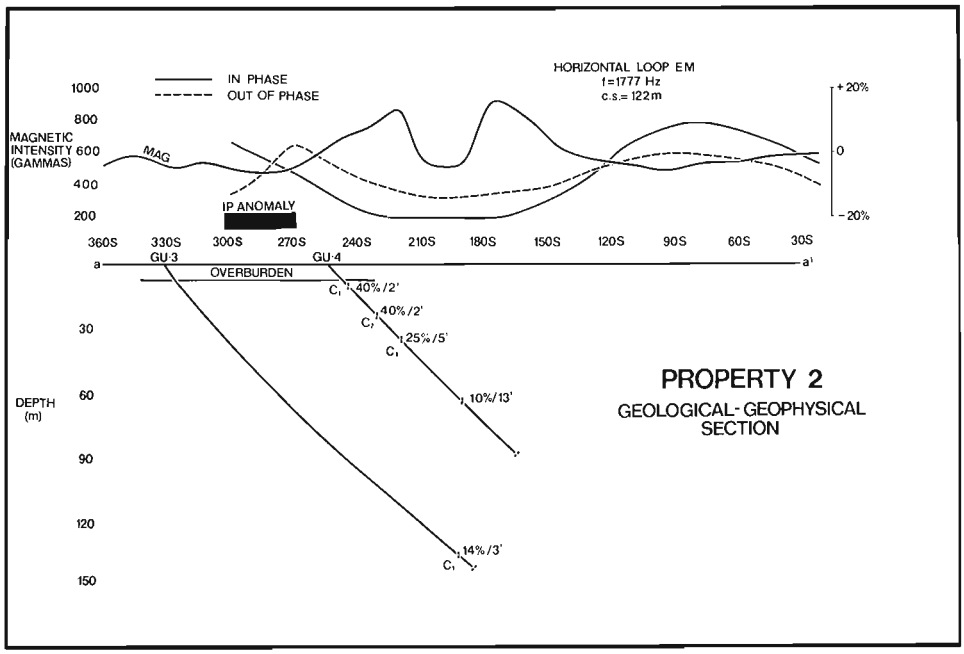

Figure 9

Property 2: Geological-Geophysical section.

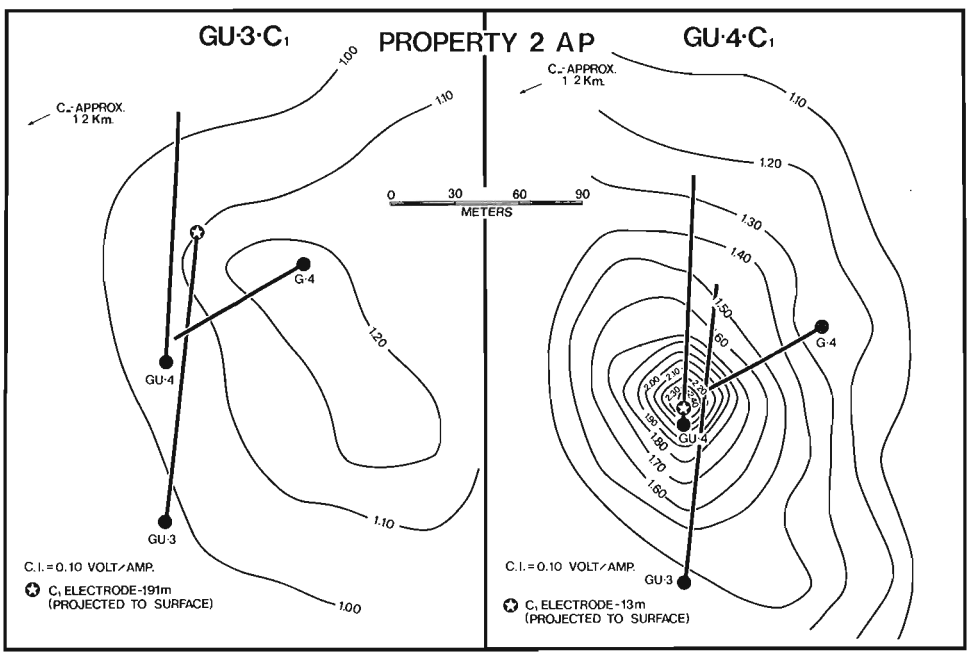

Figure 10

Property 2: Applied Potential data; current electrodes in GU-3 and GU-4.

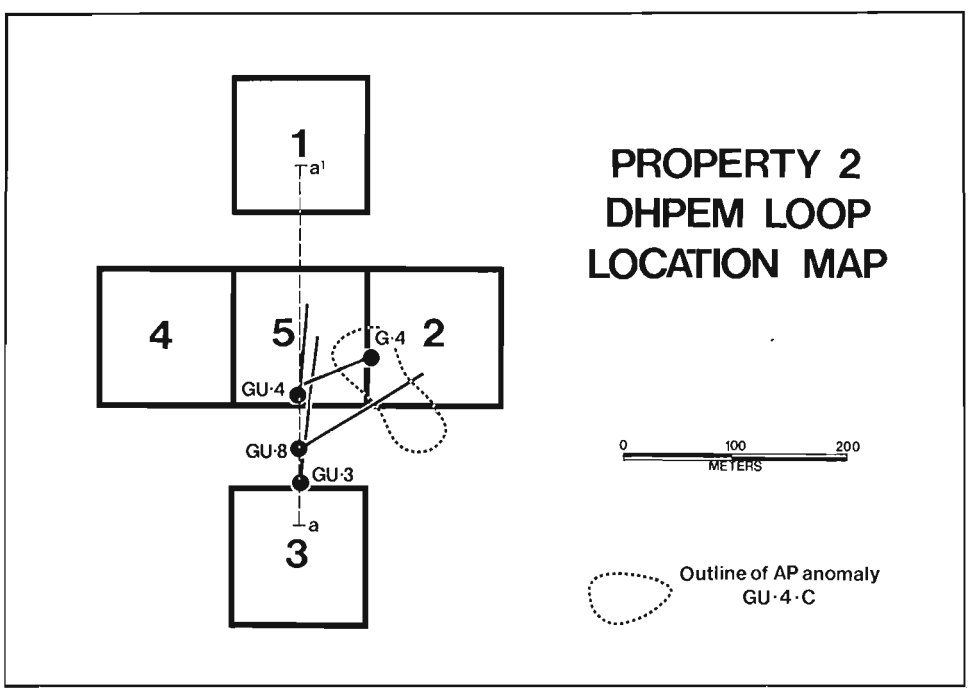

Figure 11

Property 2: DHPEM Loop Location Map.

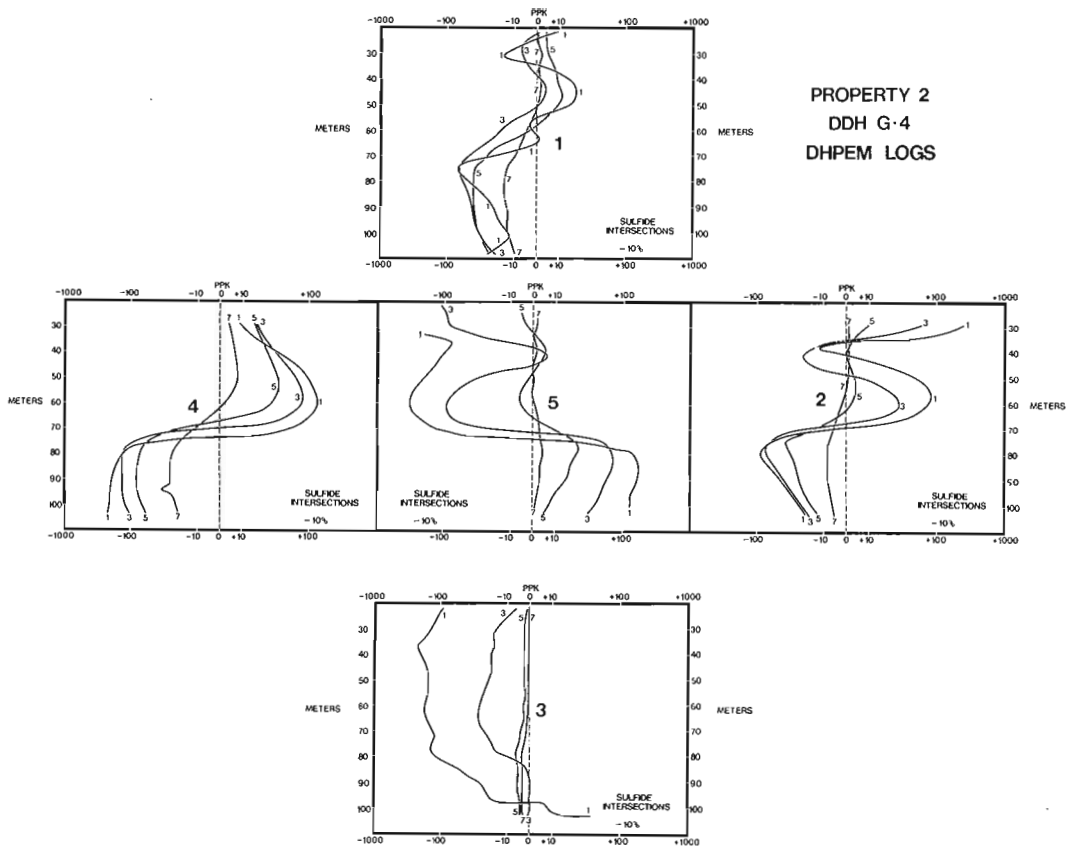

Figure 12. *Property 2: DHPEM Logs in G-4.*

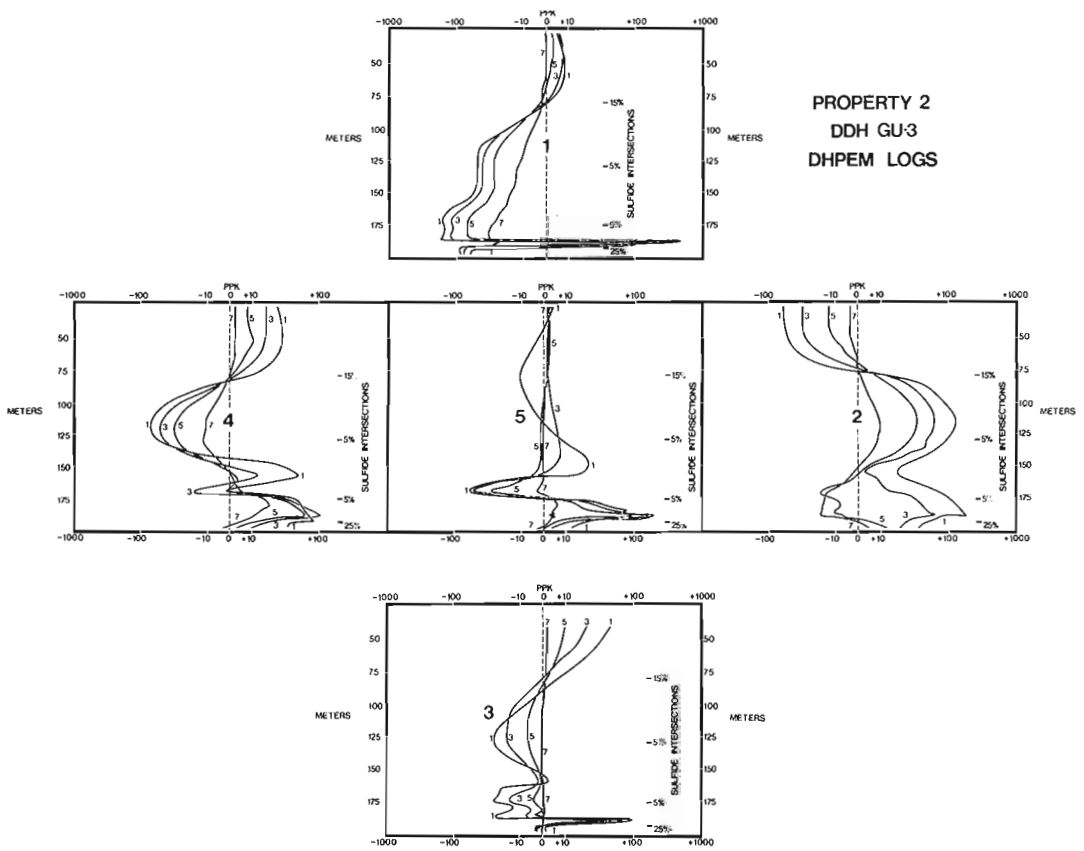

Figure 13. *Property 2: DHPEM Logs in GU-3.*

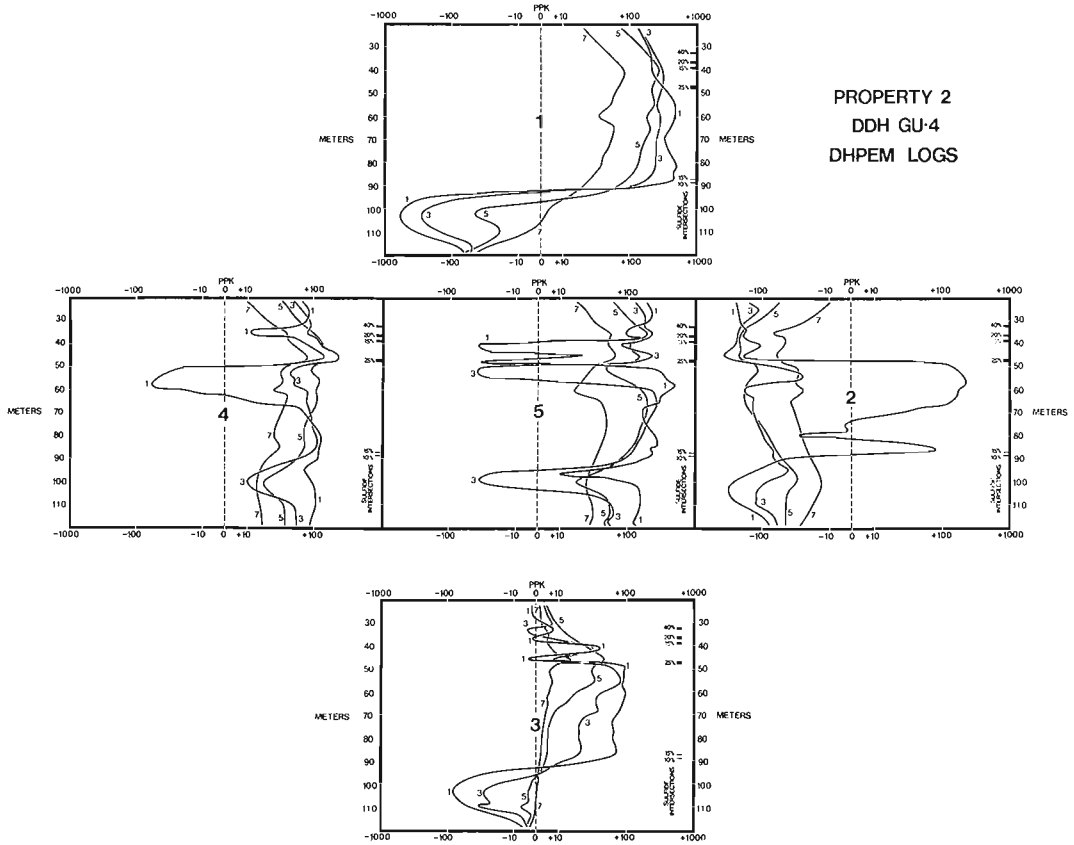

Figure 14. *Property 2: DHPEM Logs in GU-4.*

in Figure 10. The pattern produced from the electrode in GU-3 showed an elongate high, striking southeast at a distance of several hundred metres, from the surface projection of the electrode. The response from GU-4 however, showed a much more localized response, fairly symmetrical around the surface projection on the electrode. Downhole AP logging in GU-3, and G-4, (Fig. 11), was inconclusive. The interpretation was that the intersections in GU-4 were localized, although they could well have produced the observed HLEM response. The conductor in GU-3, however, showed a significant untested dimension. The fact that G-4 had not intersected this conductor and the lack of an HLEM response over the anomaly, indicated the zone probably did not subcrop.

To further investigate the intersection in GU-3, DHPEM was performed in G-4, GU-3 and GU-4, using the loops shown in Figure 11. The results for G-4 are shown in Figure 12; a strong off-hole conductive response was apparent, but varied considerably with loop position. The logs for GU-3, shown in Figure 13, revealed a complicated series of responses that were felt to be due to both off-hole and intersected massive sulphide zones. Loops 1 and 3, which had the most oblique coupling angle to the target zone (Fig. 11), both showed essentially narrow spikes adjacent to the zone of interest. These responses imparted little information with respect to the size or geometry of the zone. Loops 4, 5, and 2, however, showed considerably more character. The response from loop 4 suggested that the intersection was well inside the sulphide zone, since all channels are positive. The apparent up-hole migration of the channel maxima was considered to be due to the extension of the conductor above GU-3. The inferred dip of the zone was

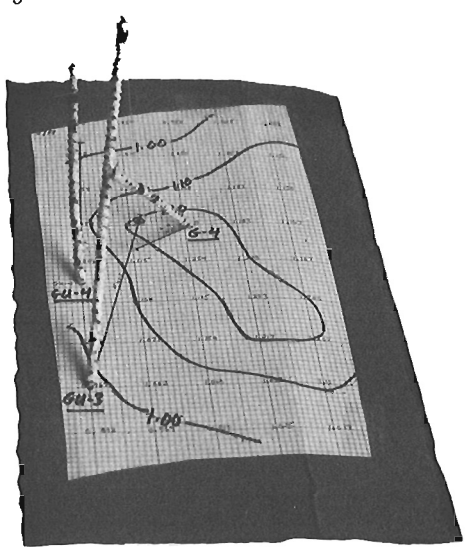

Figure 15. *Property 2: Three dimensional model showing sulphide intersections in Property 2: and surface applied potential contour map.*

steep and away from the collar. The alternative interpretation which implies an almost flat conductor lying below the hole, is geologically improbable. Loop 5 response was similar to loop 4 although at later channels, a polarity reversal occured. This suggested that an edge was nearby. Loop 2 in turn showed a pronounced reversal with channels 1 through 4 positive, while channels 5 through 8 were negative indicating an edge was even closer than the loop 5 response implied.

The logs for GU-4 are shown in Figure 14. These responses are considerably more complex than those for either G-4 or GU-3. In the upper part of the log the dramatic changes observed are attributed to strong gradients set-up by moving the loops around the rather pod-like (dimensions between 15 m to 125 m) conductors.

In the lower section of GU-4 however, two important observations were made. First, the sulphide intersections around 88 m showed very limited responses from all loops. This observation was felt to rule out the possibility that these intersections were directly connected to the intersecton in GU-3. Second, it was observed that a good off-hole response was obtained at about 102 m from all five loops. These responses were felt to be due to the upward extension of the sulphide horizon intersected in GU-3. Based on the descending channel maxima associated with this anomlay, the implied dip to the off-hole conductor was near vertical.

To try to tie together all of the downhole geophysical data, it was found helpful to construct the simple three-dimensional model shown in Figure 15. Based on the AP and DHPEM results, GU-8 was spotted to intersect the target horizon at approximately 90 m below the surface. Due to flattening of the hole in the course of drilling, the zone was intersected at 75 m below the surface but was still within 10 m of where the model predicted the zone would be penetrated by the drillhole. Intersected was 1.5 m of approximately 20 per cent total sulphides; although favourable alteration was still present, no significant base metal grades were encountered.

Property III

The third property involves a hole drilled on strike with a small massive sulphide deposit. The geological-geophysical section for this hole, NI-1, is shown in Figure 16. It is apparent that no significant surface conductor nor magnetic responses were present to guide the drilling. The lower half of the hole, however, encountered a series of minor pyrite-pyrrhotite intersections, all within strongly altered intermediate to felsic volcanics. Chalcopyrite was found in one of these zones at 185 m along with 10 per cent non economic sulphides. To investigate the possibility of a nearby massive sulphide deposit below the detection limits of surface geophysical techniques, downhole surveying was deemed worthwhile.

The AP results for NI-1 are shown in Figure 17. The pattern outlined indicates a potential high centred approximately 60 m to the right of the energizing electrode.

The DHPEM loops used to log NI-1 are shown in Figure 18, and the accompanying logs in Figure 19. In this survey, central loop over the hole was not used. Collectively, the logs mostly showed early channel responses. This was felt to be reasonable based on the amount of sulphides observed in the hole, although a stronger off-hole indication had been expected. Loop 1 response was interpreted to be due to the top edge of a conductor with a significant depth extent to explain the response lower in the hole. However, loop 3, which should have coupled well with the interpreted down-dip extension, showed only a marginal response. Responses from loops 2 and 4 were about the same; both seemed to be near an upper edge with loop 2 showing marginally better coupling.

Based on the AP and DHPEM results, NI-2 was spotted 60 m to the right of NI-1. In NI-2, two conductive zones were encountered, one a 3 m wide graphitic zone at about 135 m and a lower 2 m wide sulphide zone at 181 m. The sulphide zone contained about 10 per cent total sulphides and assayed significant base metal values.

AP was run using both intersections in NI-2 and the results are shown in Figures 20 and 21. In both cases, the responses obtained indicated anomalous centres located to the right of the intersections in NI-2. Also, the response from the graphitic zone appeared to have a significant down-dip extension. At this point, it seemed as if we were chasing the proverbial wild goose and this (see Fig. 21) was two of its eggs. DHPEM results in NI-2 were negative.

Of the work done in NI-2, only the AP left any hope for a possible extension to the mineralization of interest. However, the lack of reciprocity between the AP results in NI-1 and NI-2 strongly suggested that the two sulphide zones were not the same. This conclusion implied that the spotting of NI-2 based on the AP data from NI-1 and the resulting intersection was probably fortuitous, but then the geology looked good in NI-1, and follow-up drilling would have been done in any case.

Based largely on geological incentive, a third hole, NI-3, was spotted about 60 m to the right of NI-2 (Fig. 20). No significant sulphide intersections were encountered in NI-3, and the geologically favourable horizon which hosted the mineralization in the other two holes had essentially pinched out. DHPEM logging of NI-3 was negative.

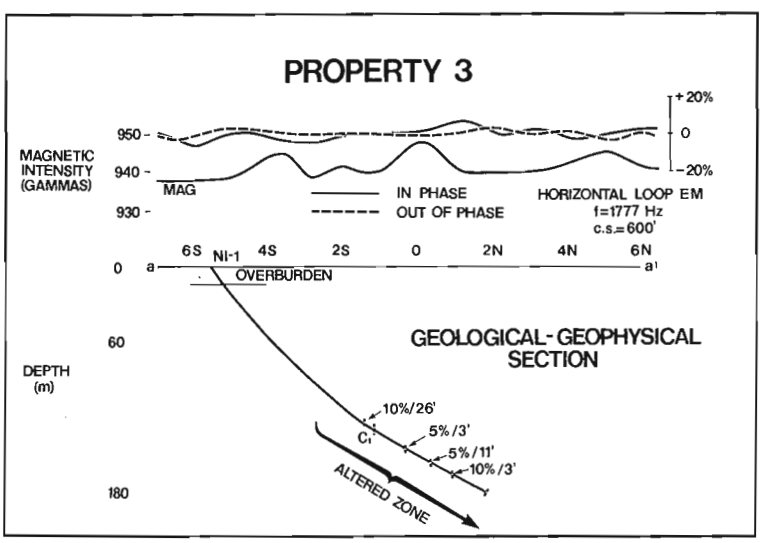

Figure 16

Property 3: Geological-geophysical section.

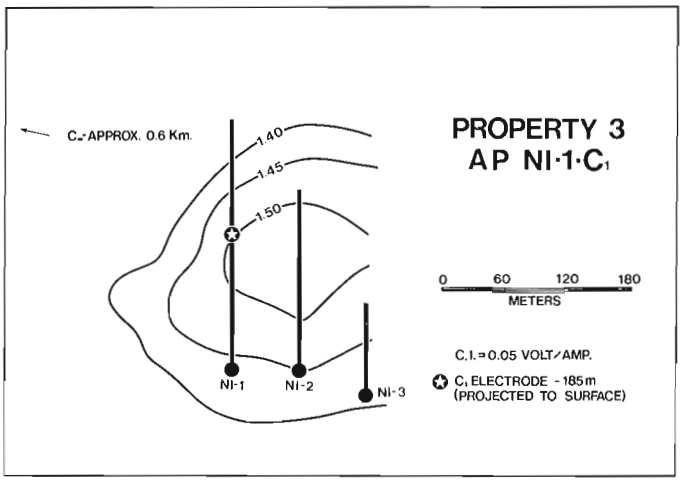

Figure 17. Property 3: Applied Potential data; current electrodes in NI-1.

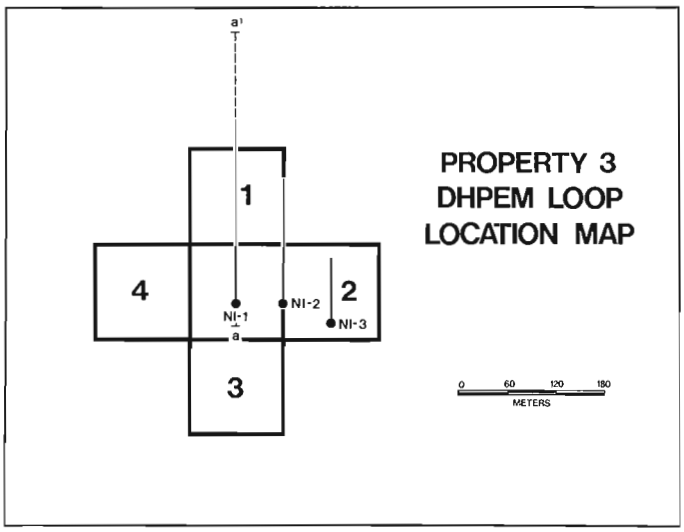

Figure 18. Property 3: DHPEM Loop Location Map.

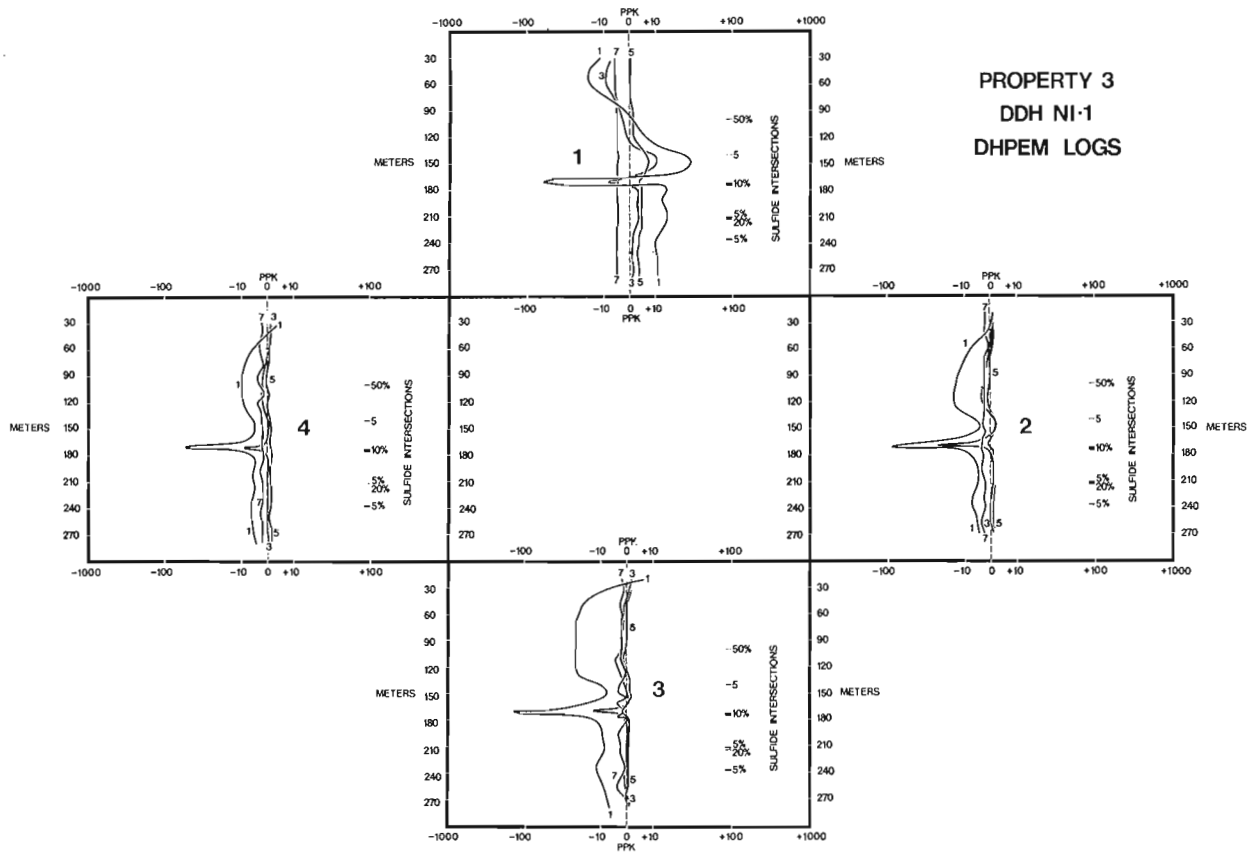

Figure 19. Property 3: DHPEM Logs in NI-1.

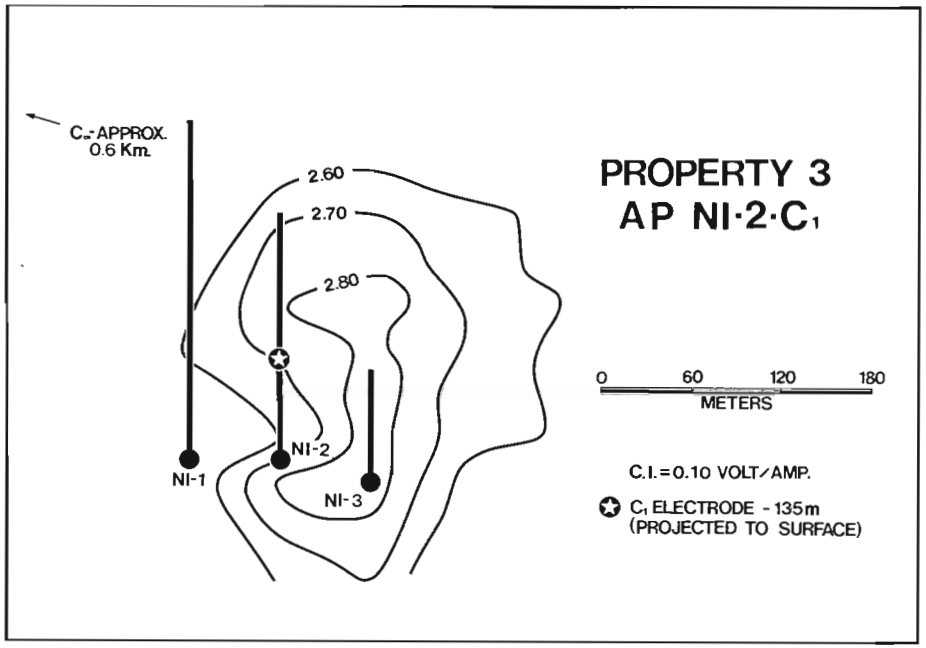

Figure 20. Property 3: Applied Potential data; current electrode at 135 m in NI-2.

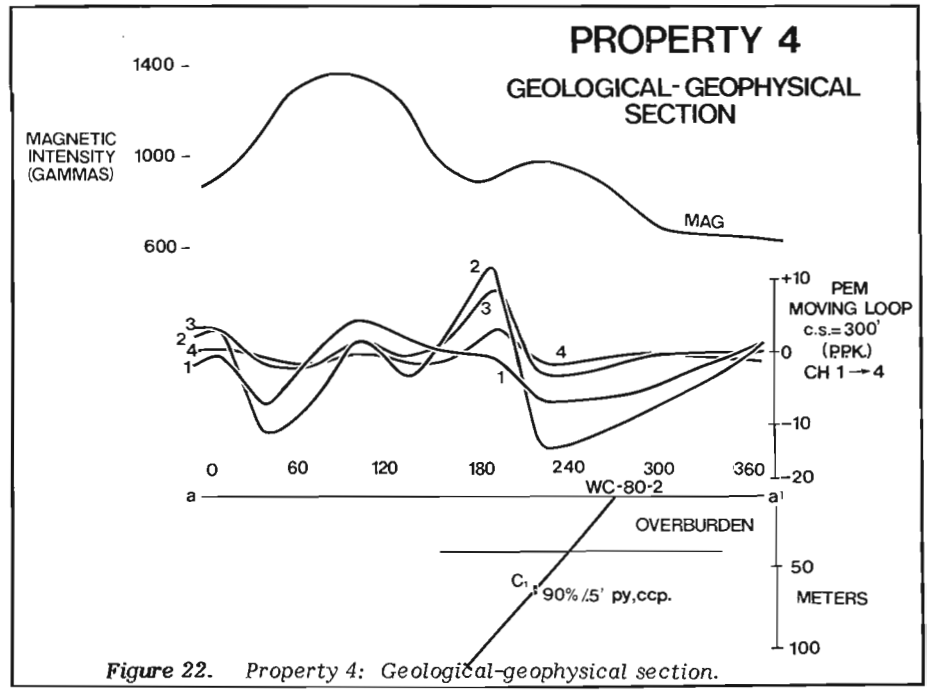

Figure 22. Property 4: Geological-geophysical section.

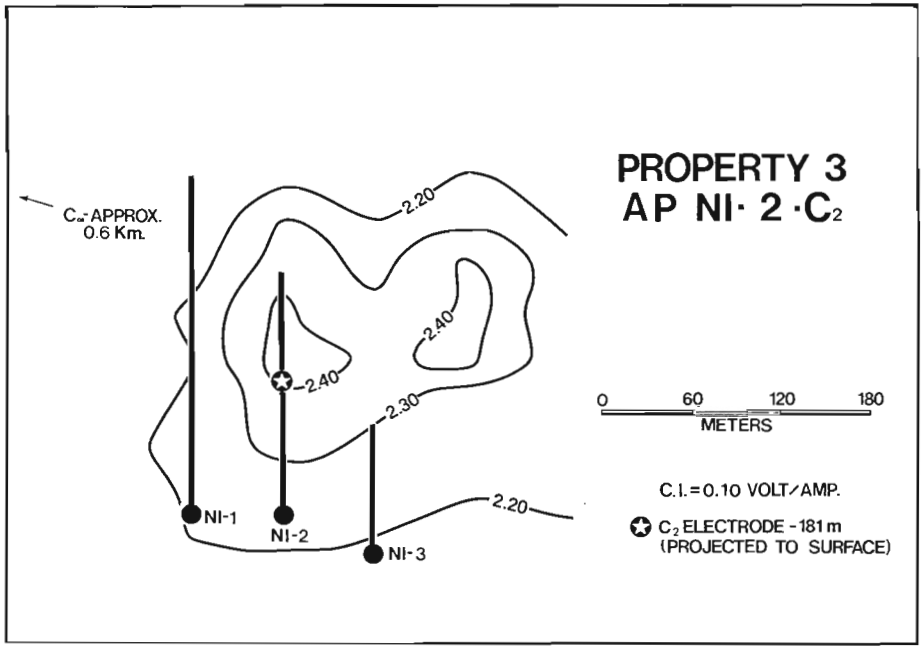

Figure 21. Property 3: Applied Potential data; current electrode at 181 m in NI-2.

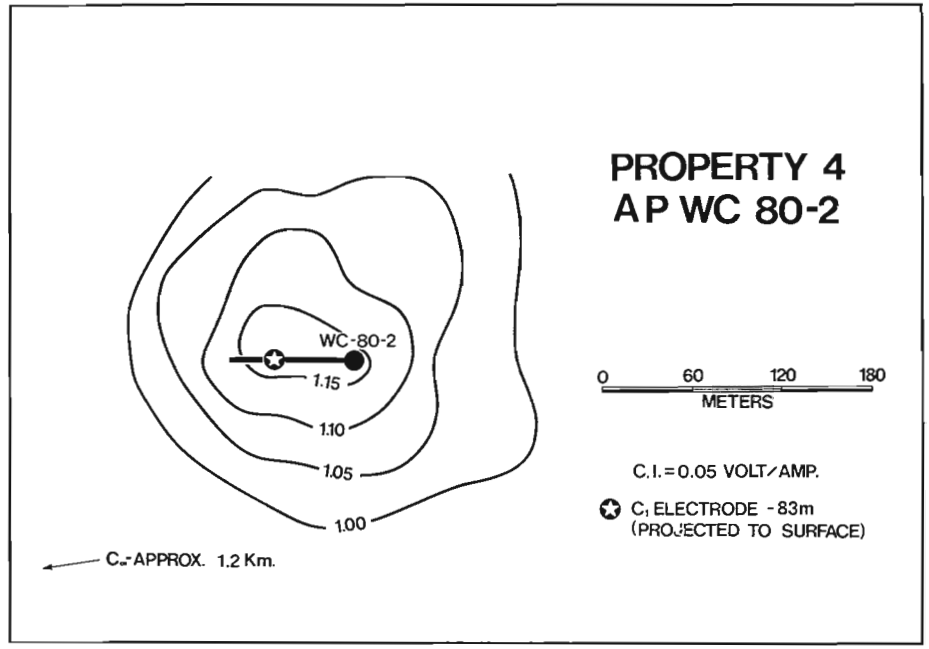

Figure 23. Property 4: Applied Potential data; current electrode in WC-80-2.

Property IV

The fourth situation deals with a hole that was spotted to test adjacent magnetic and PEM anomalies, shown in Figure 22. Intersected in this hole at 83 m was a 10 cm band of massive sulphides containing significant base and precious metal values. AP and DHPEM were run in this hole to investigate a possible extension to this zone, hopefully, a blowout of some greater thickness at depth.

The AP results are shown in Figure 23. A very localized, slightly elliptical anomaly was outlined, with its centre almost over the surface projection of the energizing electrode.

The DHPEM loops used to log the hole are shown in Figure 24 and the logs obtained are shown in Figure 25. No significant response was noted either adjacent to the intersection or throughout the remainder of the hole. The only feature of interest was the apparent overburden response visible on all of the logs and most prominent on loop 5 results. The overburden in this area is about 40 m thick and has a true resistivity of approximately 30 ohm-metres, as measured by small spacing resistivity soundings. Also noted on several of the logs was a weak response at the very bottom of the hole which was attributed to a lost steel dummy probe.

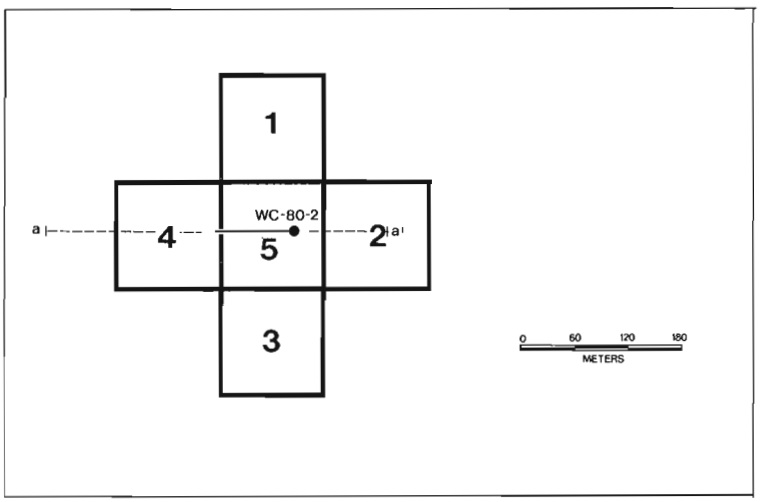

Figure 24. *Property 4: DHPEM loop location map.*

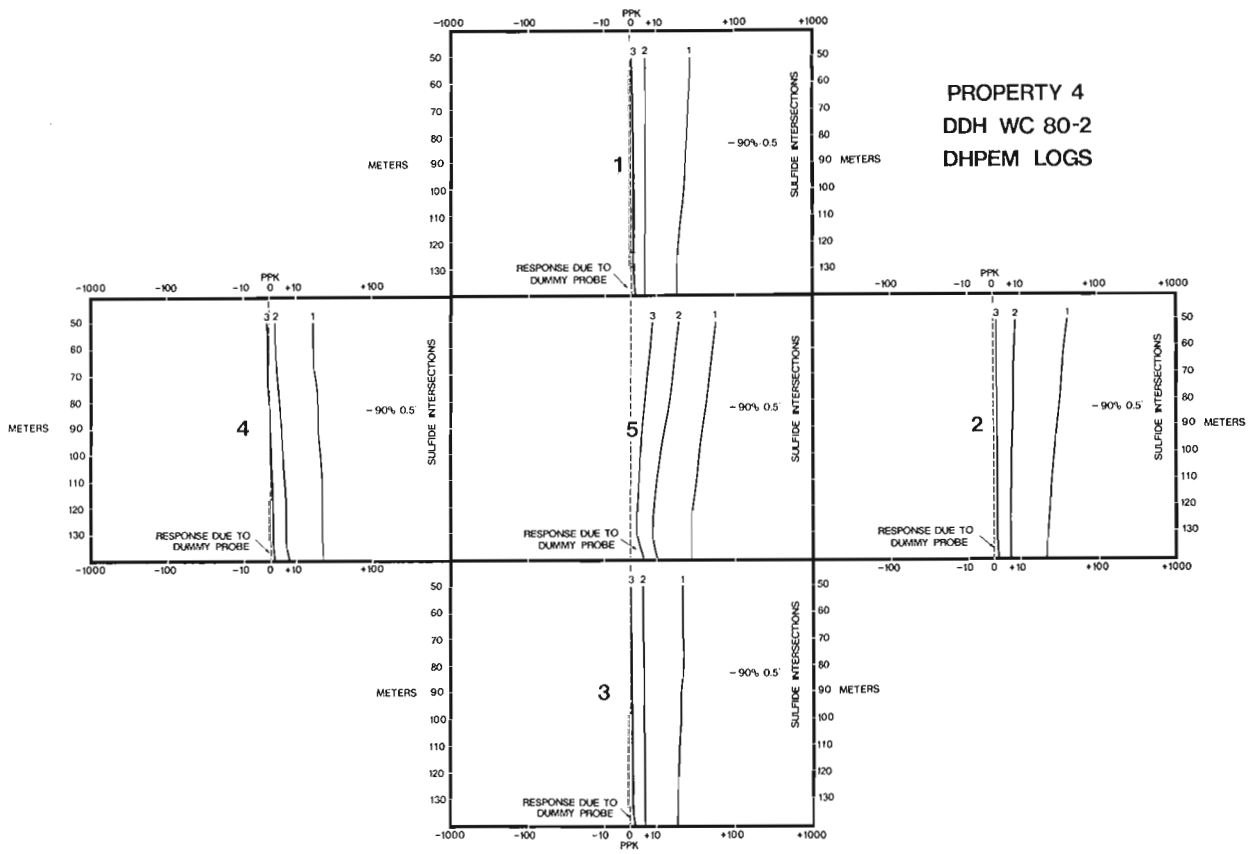

Figure 25. *Property 4: DHPEM logs in WC-80-2.*

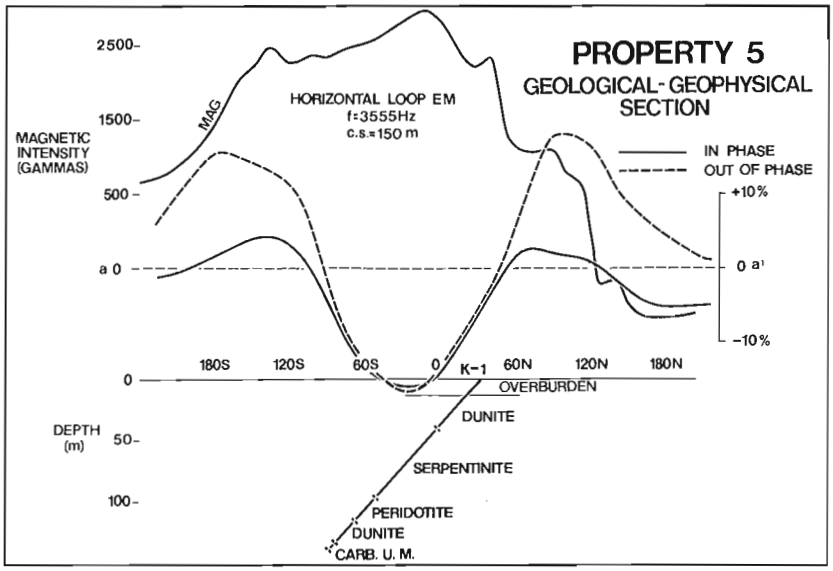

Figure 26. *Property 5: Geological-Geophysical Section.*

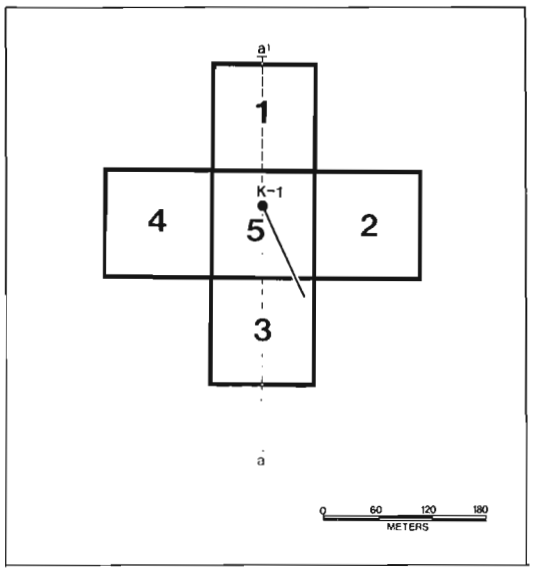

Figure 27. *Property 5: DHPEM Loop Location*

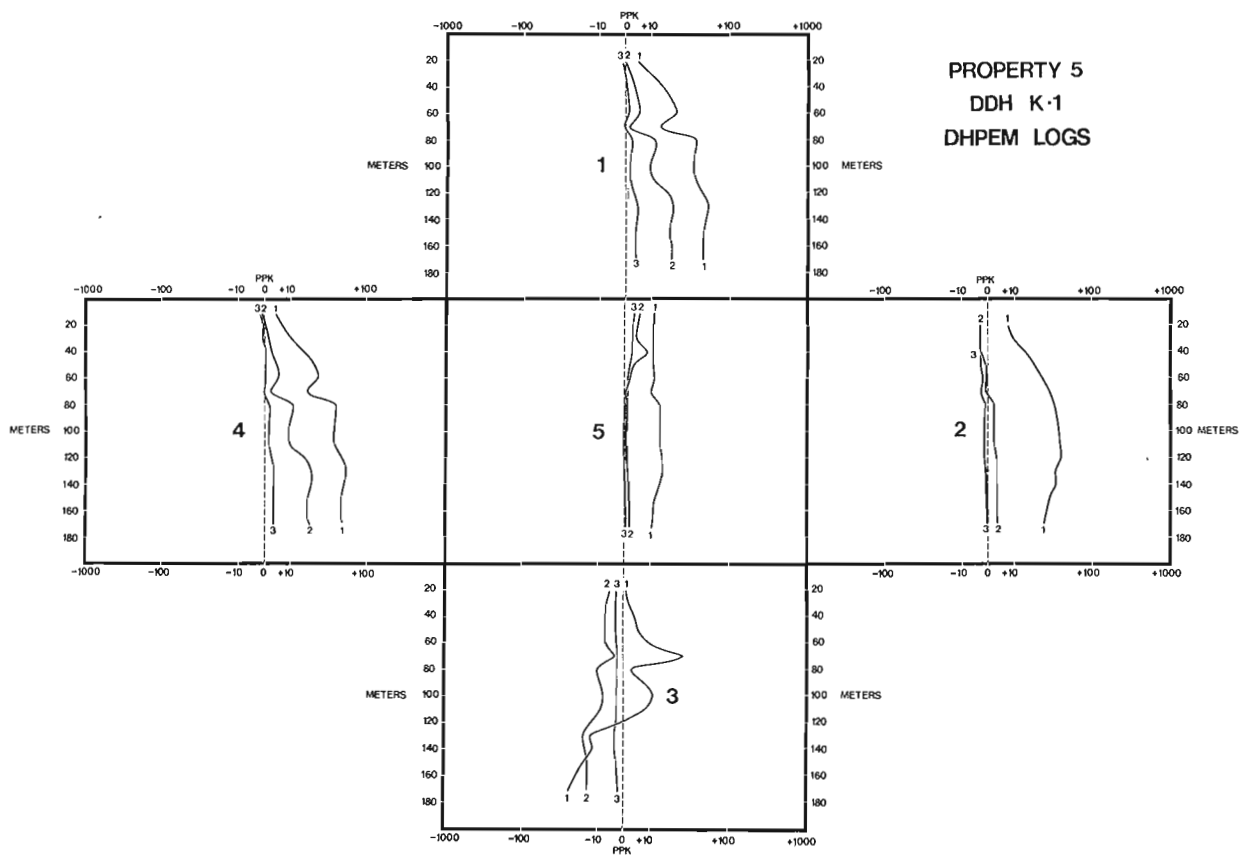

Figure 28. *Property 5: DHPEM Logs in K-1.*

Combining the geological opinion that the mineralization had only limited dimensional potential and the lack of any positive geophysical response either from the logging or from adjacent surface geophysical data, no further drilling was done.

Property V

The last example deals with a coincident HLEM-magnetic anomaly that was drilled, but where no initially obvious conductor was intersected in the hole. The geological-geophysical section for this hole is shown in Figure 26. Based on the drill log and the ground magnetic coverage, the tested anomaly was interpreted to be an ultramafic plug. As no identifiable sulphide conductor was located in the drill core, AP was not run.

The DHPEM loops used to log this hole are shown in Figure 27 and the accompanying logs in Figure 28. The logs showed a considerable early channel character throughout the entire length of the hole. The high frequency anomaly at about 70 m which shows up to some degree on all of the logs, seemed to be related to a change in the degree of serpentinization in the core. The conductivity-thickness product calculated from several of the logs gave a comparable value to the conductivity-thickness derived from the HLEM results (about 3 mohs-PEM versus 2 mohs-HLEM).

The conclusion from the logging was that no significant bedrock conductor had been missed by the drillhole. The observed conductive response was attributed to the abundant magnetite present with possible enhancement arising from the somewhat conductive serpentinized ultramafic host rock.

Conclusions

1. AP and DHPEM are a powerful set of tools to aid in the search for massive sulphides in the variety of environments found in Eastern Canada.
2. AP and DHPEM results can often be used for initial exploration purposes with minimum recourse to sophisticated interpretive models.
3. Significant quantitative information is contained in DHPEM results and to a lesser extent AP data, which does require recourse to sophisticated interpretive modelling techniques – some of which are generally not available; specifically a forward and inverse AP computer modelling program, a multibody DHPEM forward solution and a DHPEM single-body inverse solution.

Before any logging can be done, a drillhole must be left open. For downhole techniques such as I have discussed to be used effectively by the minerals industry, more effort must be made to make managers aware of the advantages of logging and hence be willing to spend the money to leave holes open.

References

Dyck, A.V.
1981: A method for quantitative interpretation of wide-band, drillhole EM surveys in mineral exploration; Ph.D. thesis, University of Toronto; available as Research in Applied Geophysics 23, Geophysics Laboratory, Department of Physics.

Macnae, J.C.
1980: An Atlas of Primary Fields Due to Fixed Transmitter Loop EM Sources; Research in Applied Geophysics Reports No. 13; University of Toronto.

Woods, D.V.
1975: A Model Study of the Crone Borehole Pulse Electromagnetic (PEM) System; Unpublished M.Sc. Thesis, Queen's University, Kingston, Ontario.

BOREHOLE INDUCED POLARIZATION AND RESISTIVITY

B.R. Krause[1]

Krause, B.R., Borehole induced polarization and resistivity; in Borehole Geophysics for Mining and Geotechnical Applications, ed. P.G. Killeen, Geological Survey of Canada, Paper 85-27, p. 375-378, 1986.

Abstract

The positive experience of INCO Limited with borehole Induced Polarization and Resistivity measurements is briefly reviewed. Three different electrode configurations with separations varying from 15 to 90 m have been used successfully in holes to depths of up to 1800 m.

Two examples are presented; one using a three-array in a single hole, and the other using a modified Schlumberger array in a hole-to-hole survey.

Résumé

Le présent rapport expose sommairement les résultats positifs que la société INCO Limitée a obtenus en effectuant des mesures de polarisation induite et de résistivité dans des trous de sondage. Des électrodes disposées selon trois configurations différentes et à des espacements allant de 15 à 90 m ont été utilisées avec succès dans les trous, dont les plus profonds étaient de 1800 m.

Deux exemples sont exposés: le premier décrit l'utilisation de trois appareils dans un seul trou, et la seconde, l'utilisation d'une configuration Schlumberger modifiée au cours d'un sondage transversal.

Introduction

Time Domain, borehole Induced Polarization and Resistivity surveys have been carried out annually in Sudbury by Inco Limited since 1974. Typical programs involve groups of 10 to 20 holes ranging in depth from 300 m to over 2500 m (1000 to over 8000 feet). Several electrode arrays may be required to fully investigate the environment around or between the holes. The co-ordinates and the dips and strikes of the collars, the surface or initial co-ordinates of all electrodes and the survey measurements are entered into a computer which calculates the co-ordinates for moving electrodes, geometric factors and apparent resistivities. A hard copy of all data and computer plots of profiles of the chargeabilities and resistivities aid interpretation which, on occasion, may be urgently required to minimize standby costs of a drill. Whether the geologist's interpretation is confirmed, blind targets detected or new ideas provided about the likely extent of intersected mineralization, the geophysical information is a valuable addition to that provided by the core.

The impetus to commence a program of borehole geophysical exploration in the Sudbury area was provided by several factors. Shallow exploration by geology, geophysics, target and grid drilling was almost exhausted. A long history of exploration had resulted in a large number of holes which, importantly, were all cased to bedrock and capped. New drill programs to greater depths were expected in ensuing years. As depth, and therefore cost per hole increased, so did the incentive to get the maximum amount of information from each hole. The exploration group already had a reasonable familiarity with a variety of borehole geophysical instrumentation, ancillary equipment and the rather hostile environment of high water pressure, caved holes, etc. Because the company was experienced in surface geophysical exploration, the advantages of increasing the depth (or radius) of exploration were readily explained and accepted.

Borehole IP surveying

There were several reasons for the choice of IP as an initial technique. The borehole programs were to start as soon as possible and start-up and operating costs were to be minimized. All target areas were at depths in excess of 600 m and often beyond 1500 m. The typical ore target was a massive, conductive, magnetic sulphide zone with, usually, a halo of similar but disseminated sulphides. In 1974, there were no known electromagnetic systems with any significant range of investigation that were reliable at the depths of interest and new developments or modifications would be time consuming and expensive. The massive sulphides are well suited to resistivity surveying and the disseminated halo offers a larger and equally suitable target for IP. The company already owned suitable IP instruments and the down-hole components were inexpensive, easily obtained and relatively insensitive to water pressure problems. All components could be kept light enough to allow a reasonable degree of mobility. Data interpretation, although obviously different in 'full space', was not expected to present radically new problems.

After seven years of operation involving hundreds of miles of survey, only a few really significant problems have been encountered and most were solved. Three electrode configurations, one of them of our own devising, have become

[1] Inco Ltd., Copper Cliff, Ontario

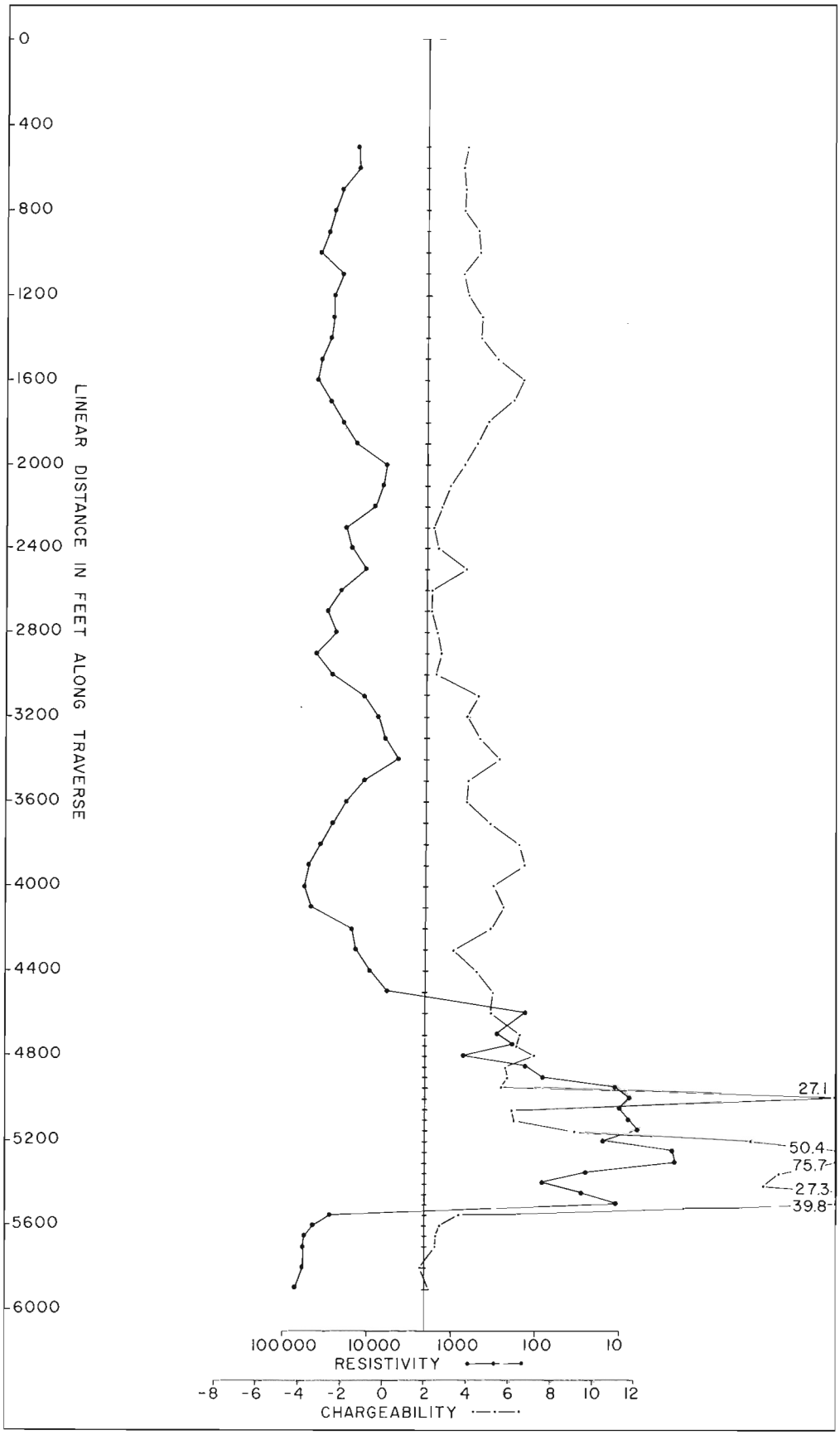

Figure 1. *Three Array survey in B.H.'C' with 'A' = 200 ft.*

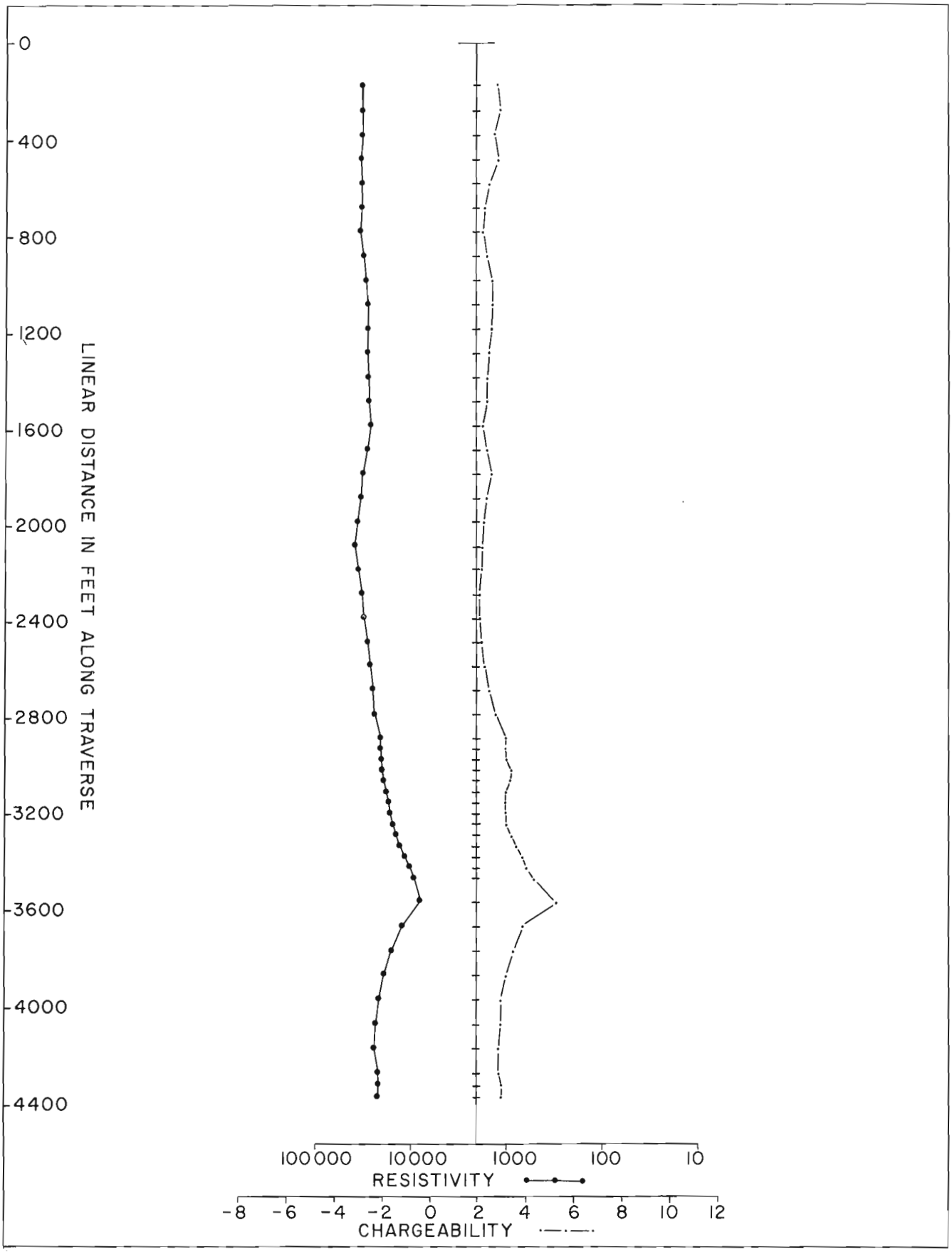

Figure 2. *Modified Schlumberger array with one pole starting in B.H.'A' at 100 feet and a second pole starting in B.H.'B'. at 250 feet using north-south current line.*

standard, and field procedures have become semi-routine. Costs vary with the number of holes and the complexity of a program but are generally in the range of 10 to 20 cents (1981 $Canadian) per foot. Short, stainless steel rods are used for down-hole electrodes and they are connected to standard, seven strand, field IP wire via a machined swivel to reduce wire twist. Short, stiff rubber bars are usually inserted in holes drilled through the rods perpendicular to the axis of the rods to minimize roll and friction. It has become standard procedure for all holes to be washed out with about 10 L of fuel oil before removing the drill rig since accumulated rod grease has, on occasion, gripped the wire and prevented the electrode from moving in the hole. The alternative of using a heavier electrode would require stronger, thicker cable and an unwieldy winch. Excessive washing should be avoided so that grease packed into fractures will continue to prevent any loose material from falling out and blocking the hole. A blocked hole, whether through accident or compliments of a 'tourist', is a major problem which can usually only be solved by re-drilling. Therefore, all recent holes are capped with special covers that require two 36-inch pipe wrenches to remove.

Electrode arrays

The three configurations of electrodes which have been found most useful are the Pole-Dipole or Three Array, the Single Pole and the Modified Schlumberger. The latter is a variation developed by Inco for exploration of pairs of holes.

The familiar Three Array, with separations varying from 50 to 300 feet, (about 15 to 90 m) is preferred for single, isolated holes. It is also used to determine the probable extent of intersected mineralization or the distance to a non-intersected source. With suitably chosen electrode spacings, it will provide true chargeability and resistivity values for the intersected units and aid lithological identification and correlation from hole to hole. Interpretation is similar to surface surveys with the exception that, at the depths involved, no directional information is provided. Chargeability noise within sulphides is an occasional minor problem and cable handling, using three wires as we do, must be dealt with carefully to avoid a tangled disaster. Figure 1, a drafted version of the computer plot, shows results from a 200 foot (60 m) Three Array in a 6000-foot (1830 m) hole. Background variations from geological changes are evident, although not sharply defined, due to the wide separation. There is excellent correlation between the intersected sulphides and the wide zone of strongly anomalous resistivities and chargeabilities.

The Modified Schlumberger Array was developed to take advantage of anomaly enhancement when a target lies between two holes. Surface current electrodes on opposite sides of a pair of holes and separated by at least twice their depth provide a uniform field. The potential electrodes, one in each hole, are aligned with the geology and then moved together at increments designed to maintain the alignment and thus explore the ground between and outside the pair. When the program involves a group of holes, numerous potential pair combinations can be read using one or both of two orthogonal current directions. Anomaly detection is very good and the determination of source location is fair and improves with the number of pairs which are surveyed. Distance of the target from a hole is poorly determined. Poor signal to noise ratios can result if the surface conductivity is too high or if holes are too close together. The primary potential gradient and hence signal can be increased if one of the current electrodes can be placed in an adjacent drillhole. In that event, it must be moved in the hole occasionally to maintain approximate alignment with the potential electrodes. Current location in a sulphide zone should, of course, be avoided to use this technique.

Figure 2, a Modified Schlumberger survey between two holes 1000 feet (305 m) apart, shows a typically quiet background and weak chargeability and resistivity anomalies near 3600 feet (1100 m) which coincide with a narrow intersection of disseminated sulphides. The broad nature of this anomaly combined with other surveys involving the same holes resulted in the conclusion that the intersected zone must increase in thickness and grade away from the hole. The recommended drilling proved that this was correct.

When anomalous results arise from Modified Schlumberger surveys, the Single Pole Array provides more specific and detailed information about the anomaly location, shape and strength. It can be considered as a variation of the Modified Schlumberger where one potential electrode is kept at a fixed location. When the fixed electrode is placed in a barren position while each of an anomalous pair of holes is read with a moving electrode, their relative contributions to a Schlumberger anomaly is readily determined. Then, if warranted, the hole nearer the source can be read with the Three Array to provide an estimate of distance. Alternately, the stationary potential probe may be located at resistivity lows or sulphide intersections and other holes surveyed to determine paths of low resistance. This information can be very useful for structural interpretation. Apparent resistivites of one ohm-metre or less are, for example, considered to be good evidence of continuity of sulphides from one intersection to another.

Conclusions

In conclusion, after seven years of exploration in holes as deep as 8600 feet (2600 m), we are convinced that IP and Resistivity surveys provide useful, interpretable data at a very modest cost. While most surveys merely confirm the geologist's expectations, there have been a rewarding number of occasions where distinctly new information has been provided. Ore grade mineralization has been discovered on the basis of geophysically recommended holes, and correct predictions of barren locations have provided the confidence required to increase the spacing in grid drilling or to lower the priority of, or even abandon, some holes. Another example of the degree of interest and confidence is a recent case where a drill rig was set up on an old hole for the sole purpose of clearing a blockage at a depth of 3800 feet (1160 m) so that a key survey could proceed.

GEOPHYSICAL WELL LOG CALIBRATION AND QUALITY CONTROL

D.G. Hill[1]

Hill, D.G., Geophysical well log calibration and quality control; in Borehole Geophysics for Mining and Geotechnical Applications, ed. P.G. Killeen, Geological Survey of Canada, Paper 85-27, p. 379-392, 1986.

Abstract

Quantitative use of wireline geophysical measurements requires assurance that the original data are of high integrity. Active on-site participation by the client representative can provide this assurance. Several examples of log quality problems and their resolution are discussed.

Résumé

L'utilisation, à des fins quantitatives, des mesures géophysiques résultant de carottages par câble exige que les données d'origine soient rigoureusement exactes. La participation active, sur les lieux, d'un représentant du client peut garantir cette exactitude. Plusieurs exemples de problèmes qualitatifs de diagraphie ainsi que leurs solutions sont exposés dans le présent rapport.

Introduction

Quantitative use of geophysical wireline log measurements has extended their utility far beyond simple hole-to-hole correlation. Geophysical wireline measurements are routinely used to provide quantitative estimates of commodity assays, porosity, water salinity, hydrocarbon saturation, and rock physical properties.

Quantitative use of geophysical wireline measurements requires original field data of high integrity. The drill site is the front line of geophysical log quality assurance. Drillholes are often cased or abandoned, after logging. Thus, there is usually only one chance to log an open borehole. No amount of clever data processing can restore data that were bad from the start.

Log Calibration

Improperly calibrated logs are good for little more than correlation. The logging contractor should demonstrate that the delivered products are logs which have been properly calibrated and run. The client should insist that the contractor provide signed and dated equipment calibration records for all delivered products.

Table 1 shows the basic steps to wireline log calibration. All systems, large or small, digital or analog, follow the same three basic steps. Geophysical logging tools are calibrated by creating an environment in which the correct tool response is known. The observed tool response is then adjusted to agree with the known response. The only time a logging tool is known to be working properly is during calibration. For this reason, calibration should be repeated often.

Figure 1 shows a temperature log calibration jig for temperature logging tools. In this sytem, the logging tool is sealed in a pressure vessel filled with water. The water is heated and continuously circulated during tool calibration.

Table 1. Wire line geophysical logging tool calibration sequence

1. Calibrate the hard copy recorder (zero and full scale).
2. Calibrate the system.
3. Calibrate the tool.

The logging tool temperature transducer is positioned adjacent to a National Bureau of Standards (NBS) rated Resistance Temperature Device (RTD). The logging tool response is then compared to the calibration jig RTD at several temperatures, as shown in Figure 2. In this case, the actual tool calibration is nonlinear. However, use of a current calibration chart, such as Figure 2, or a computerized "look-up table" can result in temperature measurements accurate to ±0.05 to 0.1°F. Figure 3 shows a "Rib-Spine" chart for a compensated density log calibration. This chart was created, using a variety of different density "formation" materials and mud cake situations, to record the individual detector responses to these situations (Wahl, et al., 1964). "Rib-Spine" charts, similar to Figure 3, can be used to calibrate field logs. Cross-plotting the near and far detector count rates yields a point on a "rib", which is followed down to the "spine" to yield the compensated density value.

Figures 2 and 3 show "true" calibration situations. While these cross-plots could be used to calibrate field measurements, in fact they are usually not. The "Rib-Spine" chart of Figure 3 is often approximated by a "Linearized Rib-Spine" model (see Fig. 4) which is programmed for either an analog or digital computer in the logging truck. In this case, the errors introduced for small departures from the spine, are minimal. Similarly, the temperature log calibration data of Figure 2 can be fitted with a series (two-three) linear segments. This allows use of a programmable calculator in the field to rapidly convert pulse rates to temperatures.

[1] Chevron Overseas Petro. Inc., Box 5046, San Ramon, CA 94583-0946

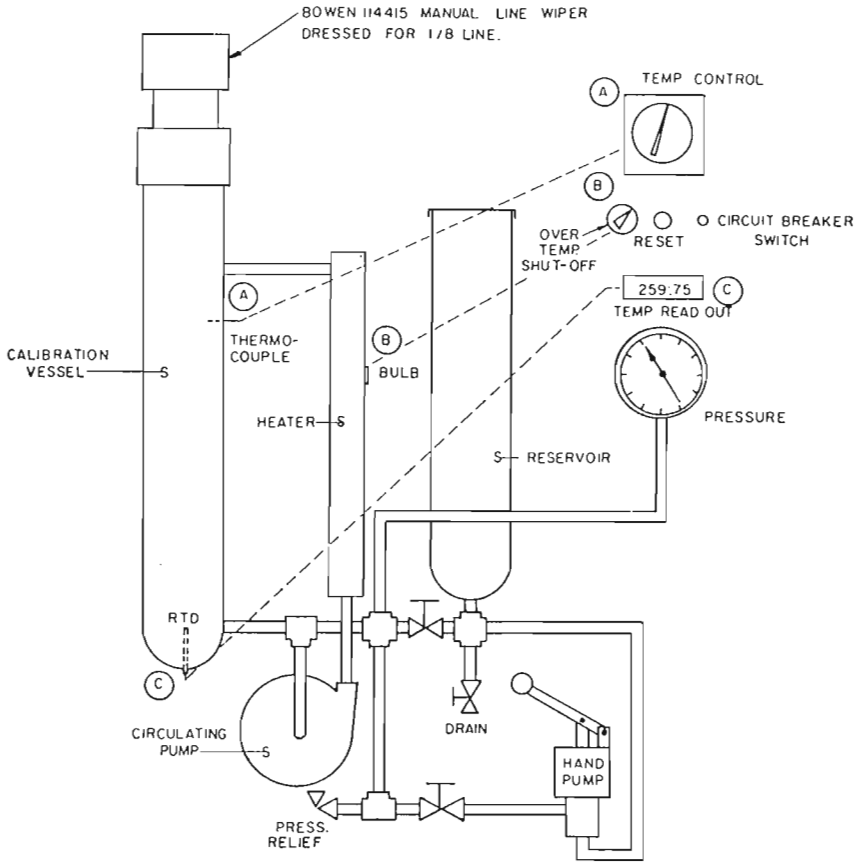

Figure 1. *Temperature log shop calibrator.*

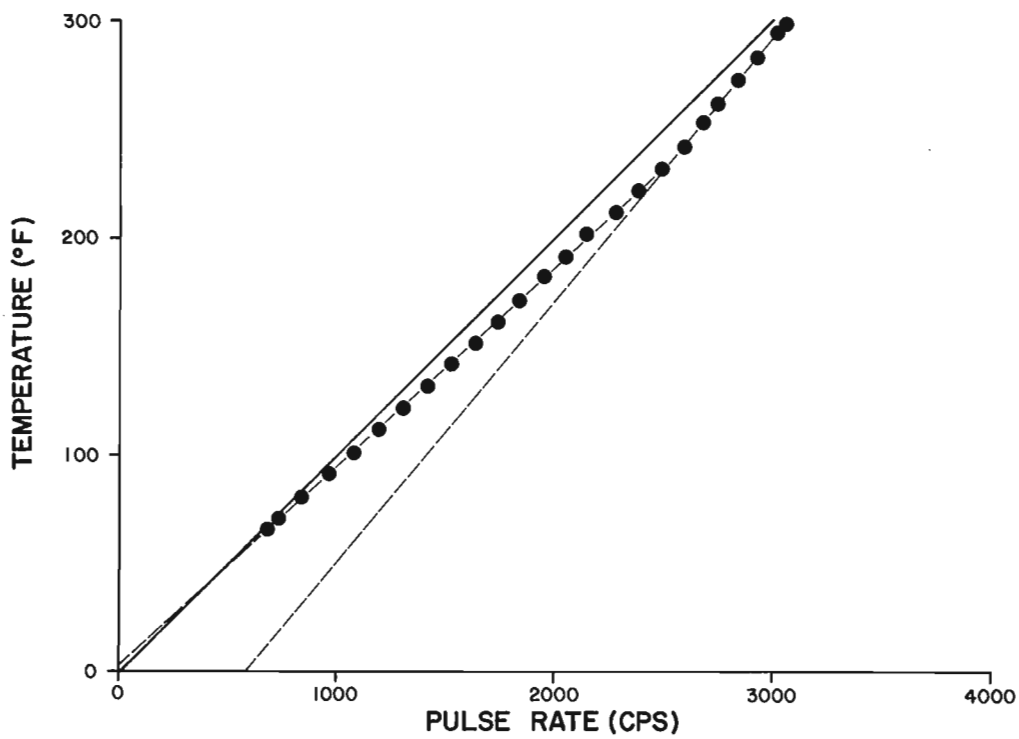

Figure 2. *Linearized temperature tool shop calibration.*

Sometimes logging tools are specifically designed to have a linear response. The additional expense involved in this added design must be justified by the need for increased accuracy in the results. Use of linearized calibration models also allows for rapid field calibration checks. Usually only one or two calibration points are required for this check (see Fig. 5.).

Both analog and digital logging systems are now in use. A digital logging system utilizes a microprocessor or minicomputer to calibrate tools and run the logging operations. Communication with the computer is via keyboard and all communications are usually stored on tape. An analog system utilizes a variety of analog computers to calibrate tools and run the logging operations. The operator communicates with this sytem by setting selector switches on the analog computers. These switch settings are then hand recorded in the operator's notes.

Digital logging systems are usually more stable, faster, and easier to calibrate, than analog systems. They are also less susceptible to operator error and only slightly more expensive than analog systems. Analog systems are slower, more error prone, less stable, and not that much cheaper than digital systems. Obviously, digital logging systems are preferable if the contractor can satisfy all other logging needs.

Table 2 summarizes the three basic types of logging tool calibration standards. The principal differences between these standards are in portability. Primary logging tool standards are environmental. They often consist of large blocks of known lithology and are usually not movable. The American Petroleum Institute (API) has established limestone, sandstone, dolomite and gamma ray "test pits" at the University of Houston campus, Houston, Texas. These test pits are the standards on which all major petroleum logging contractors' tools are calibrated. The U.S. Department of Energy (DOE) has established uranium, thorium and potassium calibration test pits at Grand Junction, Colorado, and George West, Texas. The Geological Survey of Canada (GSC) has established uranium, thorium and potassium calibration test pits at Ottawa, Ontario; Saskatoon, Saskatchewan, and Fredericton, New Brunswick. They are currently establishing granite, basalt, and sand-pack "test pits" at Ottawa. The South Australian Department of Mines and Energy (SADME) has established uranium, thorium and potassium calibration test pits in Adelaide, S.A. These three radionuclide calibration standards (DOE, GSC, and SADME) are used for radioactive assay logs. The Los Alamos Scientific Laboratory (LASL) and the U.S. Geological Survey (USGS) established granite and basalt calibration test pits at the Denver Federal Center, Denver, Colorado, in 1981. The new USGS and the GSC test pits will be extremely valuable for calibrating logs run in igneous and metamorphic rock environments.

Secondary calibration standards are usually also environmental in nature. In contrast to test pits, secondary standards are movable. All logging tool manufacturers and most larger logging contractor field shops have secondary calibration standards. For this reason they are often called

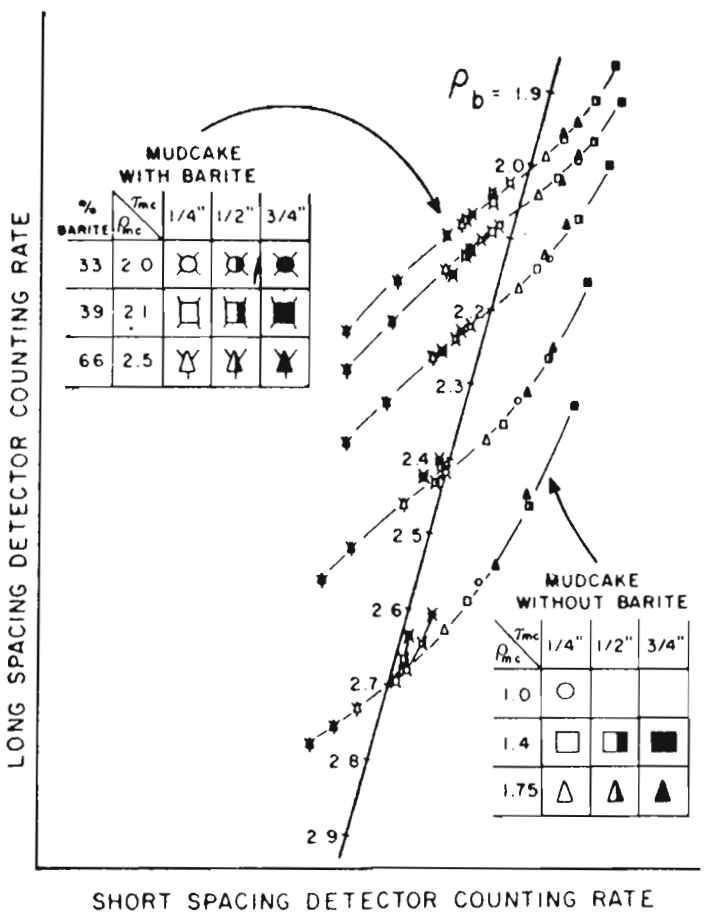

Figure 3. *Compensated density "Rib-Spine" chart (from: Wahl, et al., 1964).*

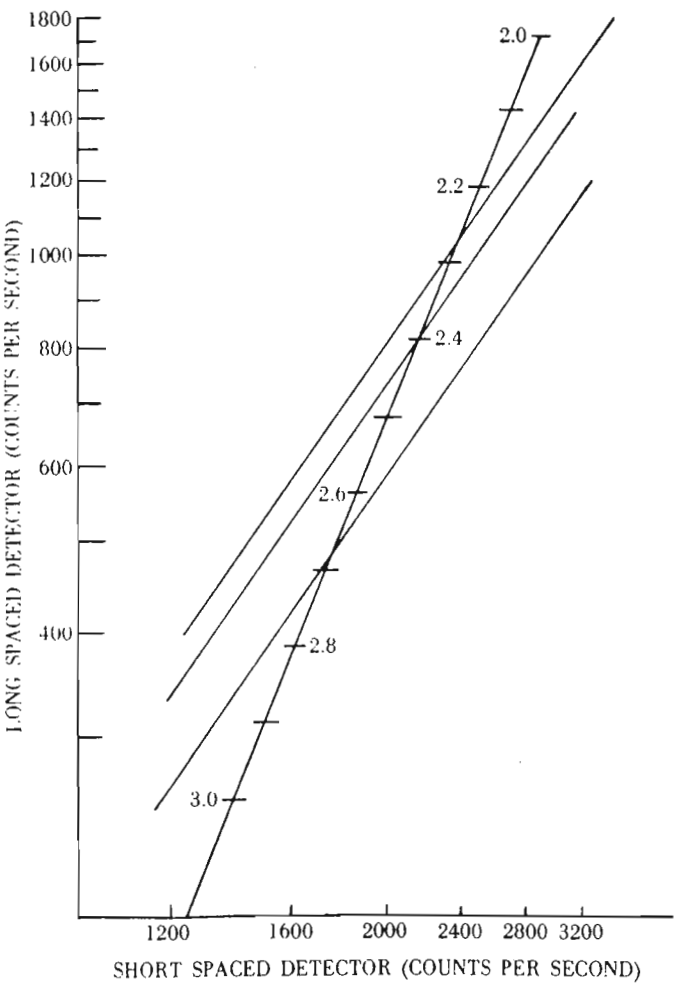

Figure 4. *Linearized compensated density log "Rib-Spine" model (from: Annon, 1979).*

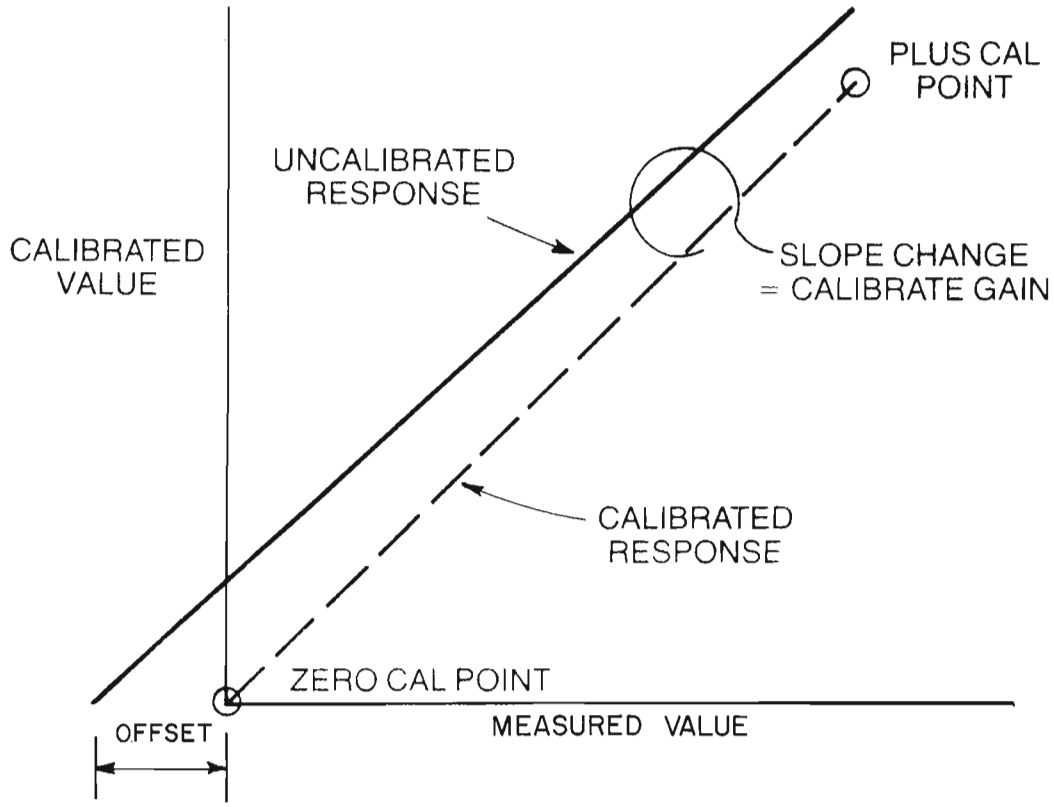

Figure 5. *Calibration of a linear response logging tool (from: Annon, 1978).*

Table 2. Wire line geophysical logging tool calibration standards

Primary:	Environmental. Usually not movable. Usually limited in number. Usually only used for prototype tools. Usually accepted industry-wide.
Secondary:	Referenced to primary standards. Usually environmental. Usually movable, but not portable. May vary from contractor to contractor. Located at all tool fabrication and most large field shops. Usually used to maintain tool calibration on a regular (e.g., monthly) basis. Secondary (shop) calibration records should travel with each tool and appear on all log products.
Tertiray:	Referenced to secondary standards. May or may not be environmental. Portable enough to be used at drill site. May vary from contractor to contractor. Usually (at least) one with every logging unit for each different type of tool. Used to field calibrate (or check calibration) before logging and check calibration after logging. Tertiary (field) calibration results should appear on all log products.

"shop standards". Secondary calibration standards are referenced to the primary standards. Usually, only prototype logging tools are calibrated in the primary calibration standards, with the exception of uranium assay logging tools. All logging tools, however, are calibrated with secondary standards on a regular basis. A good "Rule of Thumb" is to expect "shop calibrations" on a monthly basis. Log products should not be accepted if the "shop calibrations" are out of date, unless the contractor will recalibrate immediately after the logging job. Most logging contractors will "shop calibrate" before a logging job, if requested in advance.

Tertiary calibration standards are portable and brought to the drillsite. Because of this, they are often called "field standards". Tertiary calibration standards are used immediately before and after each logging operation. They are always referenced back to the last shop calibration. Some tertiary calibration standards are really calibration checks. The tool response is recorded, but it is not adjusted to any pre-set value. This course of action is followed to avoid contamination from the drill-site environment. Induction and neutron log calibrations are often field checked in this way.

Log products should have pre-log calibration, post-log calibration check, and the most recent shop calibration summaries attached. This is the only way a contractor can demonstrate that the delivered product was obtained with properly calibrated tools.

Logging operations – trying conditions

No logging contractor will knowingly deliver bad products. My own experience has been that most logging engineers are well trained and take great pride in their work. The log header, shown in Figure 6, serves to illustrate this point. Geologic conditions affected the drilling operations such that the acoustic log appeared to fail over large intervals of the hole. The logging engineer was so ashamed of the resulting acoustic log that he first declined to deliver it. The client representative had to convince the logging engineer that the product was good. Even then the engineer was so reluctant to claim it, that he cut the company logo off the film (see Fig. 6). This is not an isolated example. Most reputable logging contractors encourage their field borehole geophysicist and the drilling supervisor to design a drilling and logging program which will achieve the desired geologial and geophysical objectives. The logging contractor should be notified of the logging job at "spud-in" and periodically updated on expected "call-out". Written logging procedures help insure that calibrations, measurements, displays, and logging operations are performed to the client's specifications. These written procedures should be tailored to the specific needs of each drilling program and transmitted to the contractor well in advance of "call-out". Table 3 summarizes useful information to include in these requests.

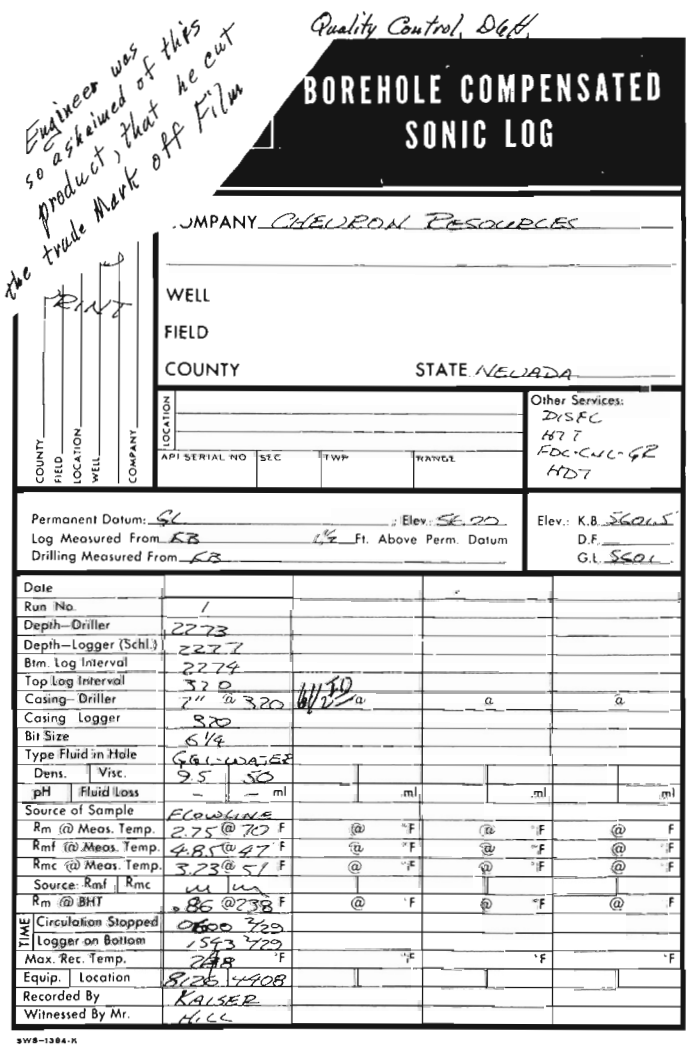

Figure 6. *Log header of a product reluctantly delivered because of field engineer's doubts about product quality.*

Logging job activities

Drilling and logging operations are among the more expensive exploration and evaluation activities. Because of this, drilling is usually one of the final activities involved in proving up a prospect. A well planned and executed drilling/coring and logging operation can maximize the information obtained. Crucial to its success, however, is drill-site log product quality control. Otherwise, the drilling operation may yield only expensive holes in the ground. The client representative should be prepared to remain on-site throughout the logging operations. Extended logging operations can benefit from multiple client representatives. By taking turns, the client representative will be alert, regardless of the condition of the logging contractor's crew.

The client representative should monitor all field calibrations, calibration checks, and the logging operations. They should be prepared to accept or decline the contractor products on-site. They should also be prepared to request reruns of unsatisfactory contractor products at no charge and select repeat intervals. Finally, they should be prepared to perform preliminary interpretations at the drill-site.

The client representative's notes on logging operations, product quality, and preliminary interpretations should be condensed into a brief report and filed with the logs. These client representative reports can prove to be invaluable, should questions arise during later log interpretation. Finally, the client representative should provide feedback to the logging contractor. This is an investment in the future. A small amount of time spent at the end of a logging job, reinforcing positive aspects of the operation, and pointing out shortcomings, will yield dividends on the next logging job.

Examples: problems and solutions

This section includes several examples of log quality problems and how they were resolved. Both calibration problems and tool failures are covered. Several field check

Table 3. Written Logging Procedures

1. Services requested.
2. Who will "call-out" the contractor.
3. Logging order.
4. Calibration expected:
   a. Contractor's normal calibrations.
   b. Client requested calibration checks.
5. Logging operations:
   a. Logging in or out of hole.
   b. Logging speeds.
   c. Repeat section selection.
   d. Copy requests.
6. Displays.
   a. Depth scales.
   b. Log format.
   c. Log scales.
   d. Copy requests.
7. Back-up and special equipment needs.
8. Specialist Engineer needs.
9. Contractor tape delivery.
10. Contractor processing requests.
11. Special conditions.

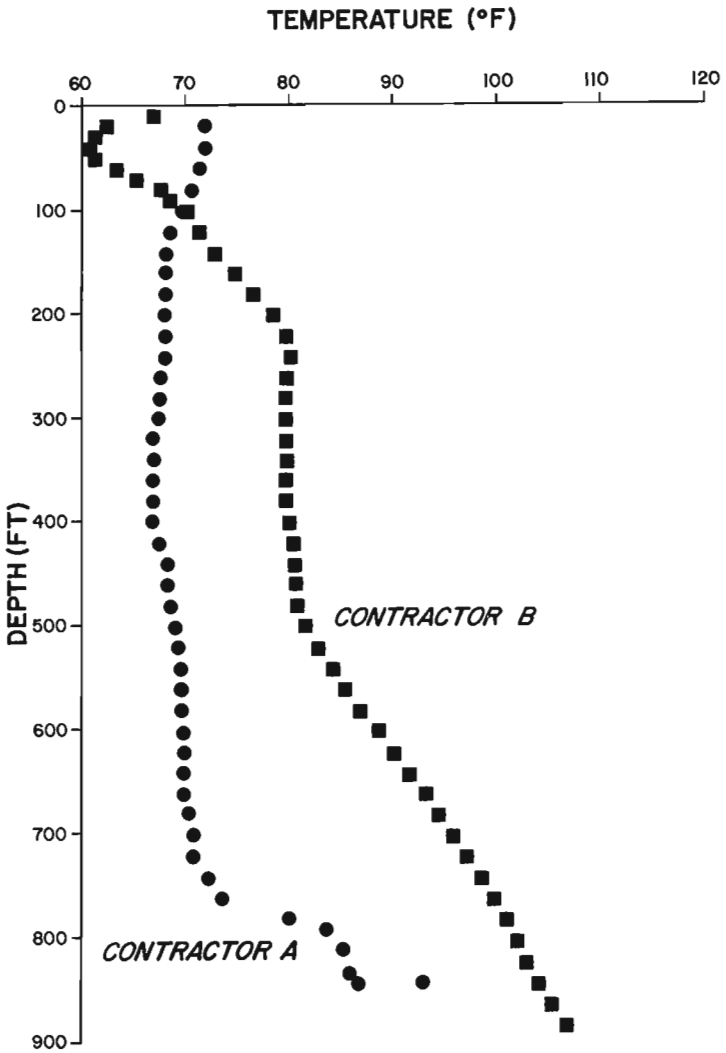

Figure 7. Repeat "Stabilized" temperature profiles in a single temperature gradient hole.

examples are also included. These examples are not intended to be exhaustive. Hopefully, they will serve as inspiration to others as they encounter their own specific log quality problems.

Temperature logs

The commodity sought in geothermal exploration is heat. A prime exploration tool is temperature gradient holes. Deeper and deeper temperature gradient holes are drilled as the prospect matures. The life and death of a geothermal prospect rides on temperatures and gradients measured from these temperature gradient holes. Figure 7 shows two supposedly "stabilized" temperature profiles by two different contractors in the same temperature gradient hole. The approximately 25°F temperature disagreement at about 750 feet could make or break this prospect. In this case, Contractor A had a tool failure which was not discovered until after Contractor B had also logged the hole. To overcome these types of problems, some operators purchase and operate their own temperature logging equipment. The calibration jig shown in Figure 1 was designed to calibrate one set of in-house equipment. Maintaining and running your own equipment is an extreme solution to the problem of log product quality. In some cases, however, the situation is serious enough to justify this type of solution.

Figures 8 and 9 show examples of a client-requested temperature tool calibration check which resolved a calibration problem. Many contractors calibrate their temperature logging tools at 32°F and 212°F assuming linearity between them (see Fig. 5). Commercial geothermal reservoir temperatures, however, are much higher (>340°F) than the boiling point of water. Temperature tool response could be nonlinear above the high calibration point (212°F). To test this concern, surface air-temprature and down-hole maximum recorded temperature (MRT) field calibration checks were requested (see Fig. 8, 9). Two documented calibration problems, similar to Figure 8, stimulated at least one contractor to invest in an oil bath calibration jig to raise the high temperature calibration point. Figure 9 is a field calibration check on this contractor's temperature tool, after this new calibration equipment was put into service. The problem shown in Figure 8 has now been resolved.

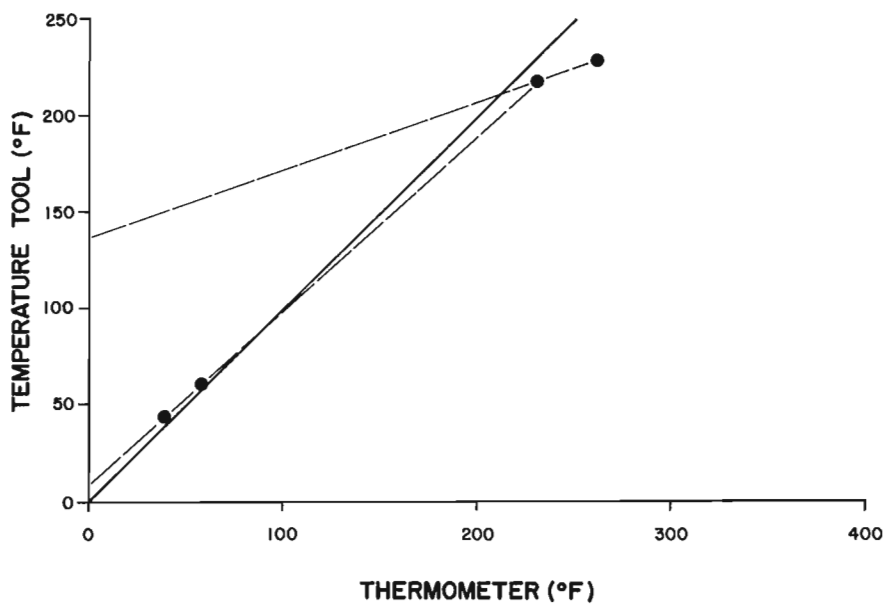

Figure 8

Temperature tool field calibration: non linear response case.

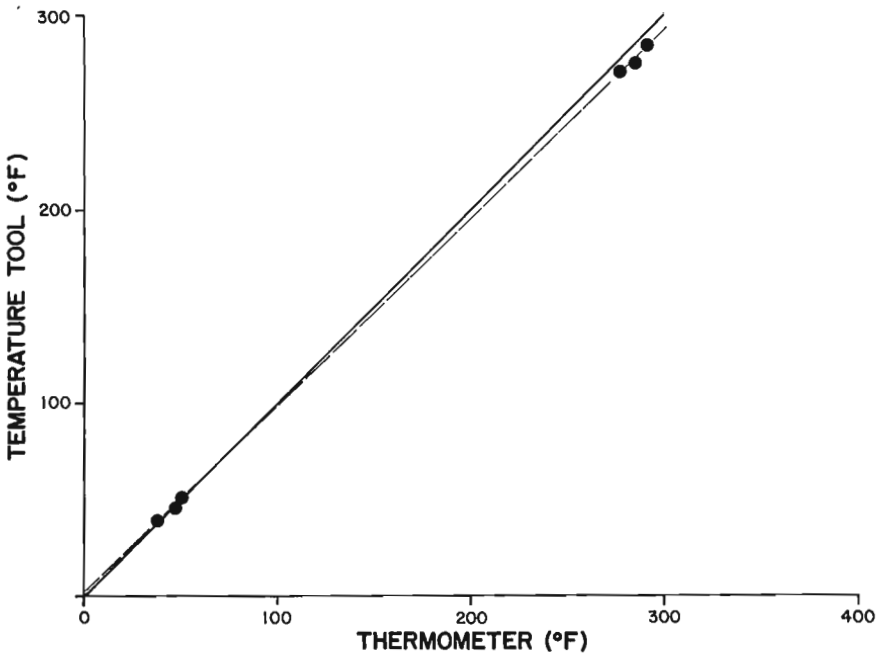

Figure 9

Temperature tool field calibration: linear response case.

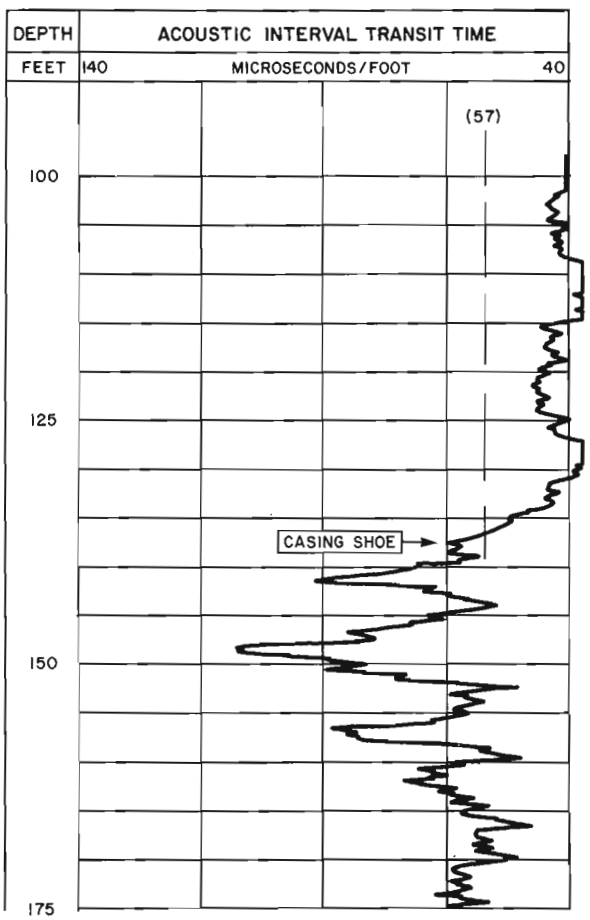

Figure 10. *Acoustic tool casing signal: improper calibration.*

Acoustic logs

Acoustic logs do not have secondary and tertiary calibration standards. These tools are essentially timing devices. The transmit time for acoustic energy, to travel from a transmitter to receivers at different distances, is recorded and converted into inverse velocity (μsec/ft). The principle involved is seismic refraction at the borehole wall. The only calibration involved is in the timing circuitry which is very stable. The operator, however, has several signal enhancement options at his disposal which can affect data quality. Because of this, acoustic logs are among the more difficult geophysical logs to run properly. It is well worth the time invested to allow the engineer to experiment with enhancement selection before running this log. The client representative can verify acoustic log quality in situations of known velocity. Table 4 lists representative transit times for several common acoustic log calibrators. A good operating practice is to require the contractor to record a casing signal both before and after logging. It is not worth running the log if a proper pre-log casing signal cannot be obtained.

Figure 10 shows the casing signal from an improperly run slim-hole acoustic log. The casing signal of less than 40 μsec/ft is much too low to be realistic. This is definitely an unacceptable product. The product should be declined and the contractor encouraged to repeat the measurement, preferably with another tool. Figure 11 shows a casing signal from a properly run acoustic log obtained by the same slim-hole contractor as Figure 10. This casing signal of approximately 187 μsec/m is acceptable. Figure 12 shows a casing signal from a major logging contractor. Tool design differences between Figures 11 and 12 account for the improved casing signal stability in Figure 12. Figure 13 shows the same log as Figure 11 in a massive anhydrite interval. The approximately 164 μsec/m signal indicates the log is operating properly.

Density logs

Density logs have both secondary and tertiary calibration standards. Drill-site calibration procedures vary from contractor to contractor. Some contractors use

Table 4. Acoustic Log Calibration Transit Times

Calibrator	Transit Time μ sec/ft	μ sec/m
Casing (iron)	57	187
Dolomite (massive, microcrystalline)	44	143
Anhydrite (massive, microcrystalline)	50	164
Halite (massive, microcrystalline)	67	219

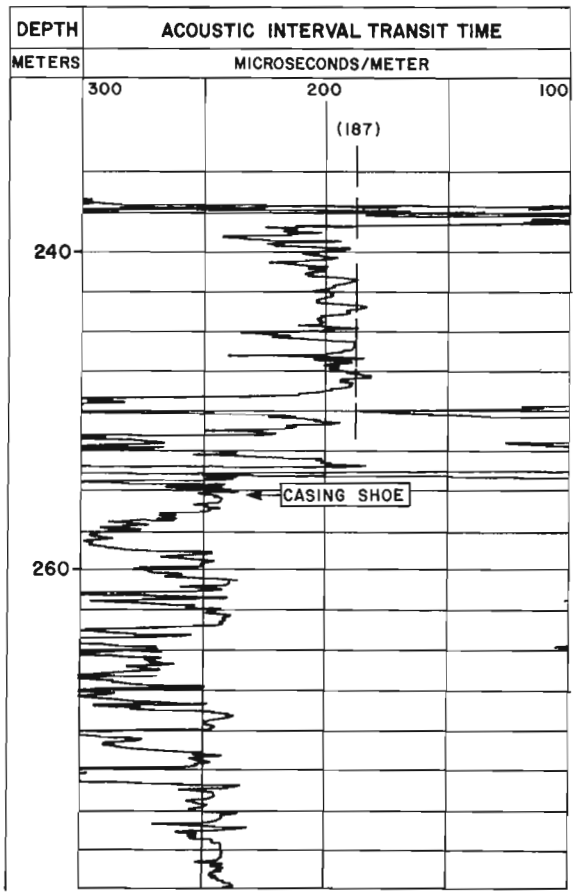

Figure 11. Acoustic tool casing signal: proper calibration but noisy tool response.

environmental calibrators at the drill-site. Others use two point drill-site calibrations. Still others use a single point drill-site calibration with the zero count rate as the second point. In all cases, these tertiary calibrations are referenced to the last shop calibration. The client representative should verify that:

1. There is no significant drift between the pre-log calibration and post-log calibration check.
2. The drill-site calibrations agree with the shop calibration.
3. The shop calibration is for the same equipment used for the logging job.
4. The shop calibration is current.

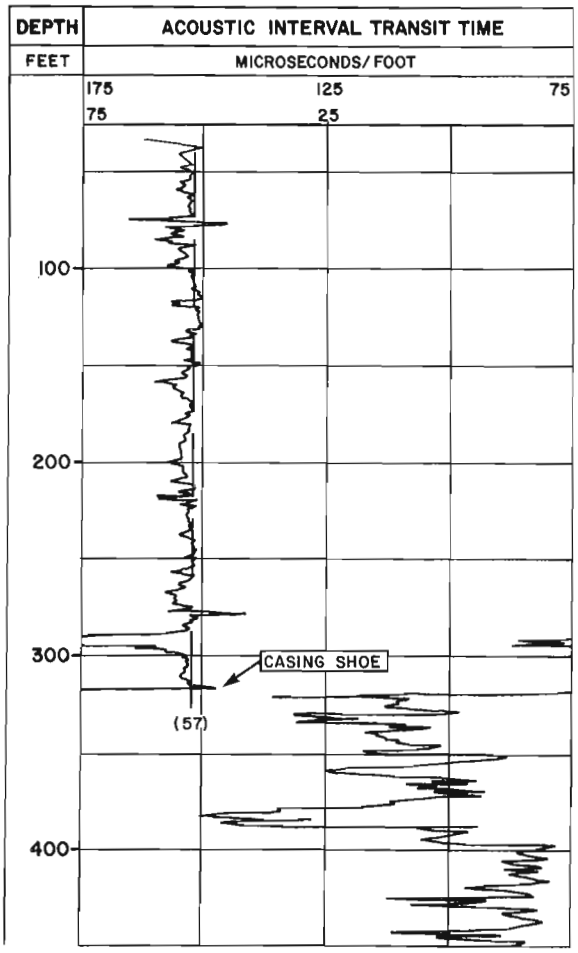

Figure 12. Acoustic tool casing signal: high integrity data.

Additional density log calibration checks can be made in massive lithologic intervals. Table 5 shows representative density log calibration lithologies. Evaporites tend to be the most reliable lithologies for these checks. Carbonates, quartzites, sandstones, and some fine grained igneous rocks may also work under certain optimum conditions. Figure 14 shows an example of a miscalibrated density log. Apparent bulk densities of over 2.7 gm/cm^3 for an unconsolidated sandstone aquifer are obviously in error. Figure 15 shows a density log anhydrite signal. Experience with specific formations and a specific contractor's tools is recommended before using lithology calibration checks. Figure 16 shows a problem which may occur in some high grade uranium ore zones. Enough gamma-radiation from the ^{238}U series decay is contaminating the Compton scattering energy window that the tool is reading erroneously low, apparent bulk densities.

Neutron logs

Neutron log calibration shares much of the variety of density logs. Both environmental and detector-only drill-site calibrations are used by various contractors. Some contractors use drill-site environmental calibrations only as calibration checks. Again, the drill-site calibrations are referenced to the last shop calibration. The client representative should verify the same things for neutron logs

Table 5. Density Log Calibration Checks

Calibrator	$\rho\beta$ (gm/cm^3)*
Fresh Water	1.000
Calcite	2.710
Dolomite	2.876
Anhydrite	2.977
Halite	2.032
Quartz	2.648
Gypsum	2.351

* (Multiply by 1000 to get kg/m^3. Tool design differences, between contractors, may change the values slightly.)

as for density logs. Neutron logs, in use by various contractors, exhibit considerable variety in design and in measurement principle. This variety makes use of lithology calibration checks somewhat more complicated. Massive rocks with extremely low porosity, no bound water, clay minerals, or hydroxol ions should show close to $\phi_N = 0\%$. Departures from $\phi_N = 0\%$, in these cases, are often taken to be bias shifts. Figure 17 shows a neutron log in a massive halite. In this case, the halite response ($\phi_N = -1.5\%$) was used as the $\phi_N = 0\%$ base line. Figure 18 shows an example of a hardware design failure in an uranium logging situation. The hardware configuration used by this contractor transmitted both gamma ray (bias) and far neutron detector count rate (ripple) on the same cable channel. The surface hardware did not anticipate the high count rates encountered in the uranium ore zone. Thus, the gamma ray signal (bias) raised the far neutron detector count rate (ripple) out of the expected signal window, resulting in an apparent "zero" count rate. This was interpreted as $\phi_N = 100\%$ by the surface electronics.

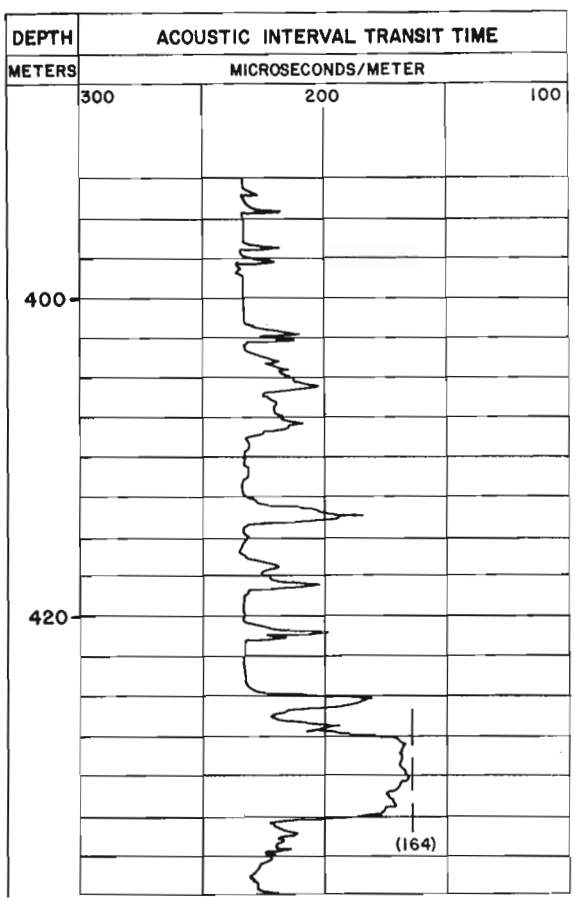

Figure 13. Acoustic tool anhydrite signal.

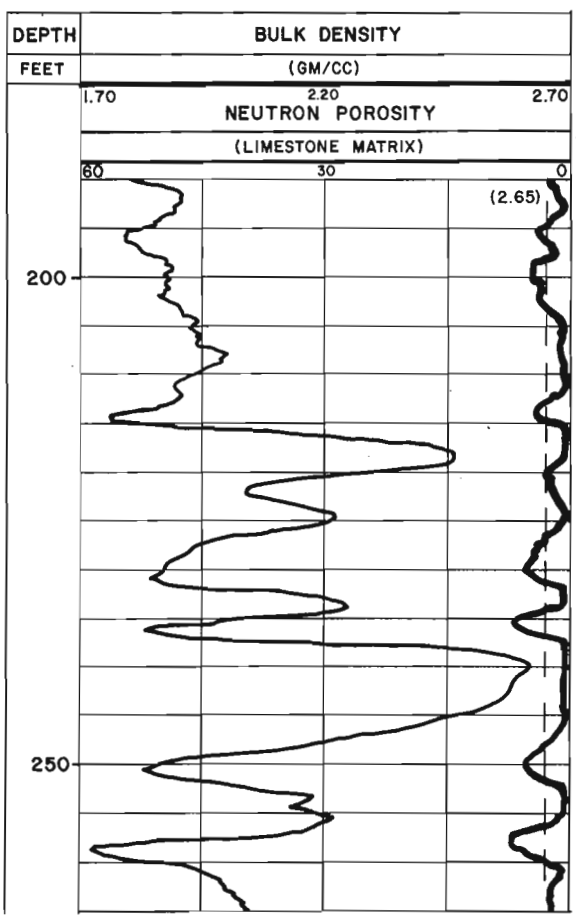

Figure 14. Miscalibrated density log in unconsolidated Gulf Coast clastics.

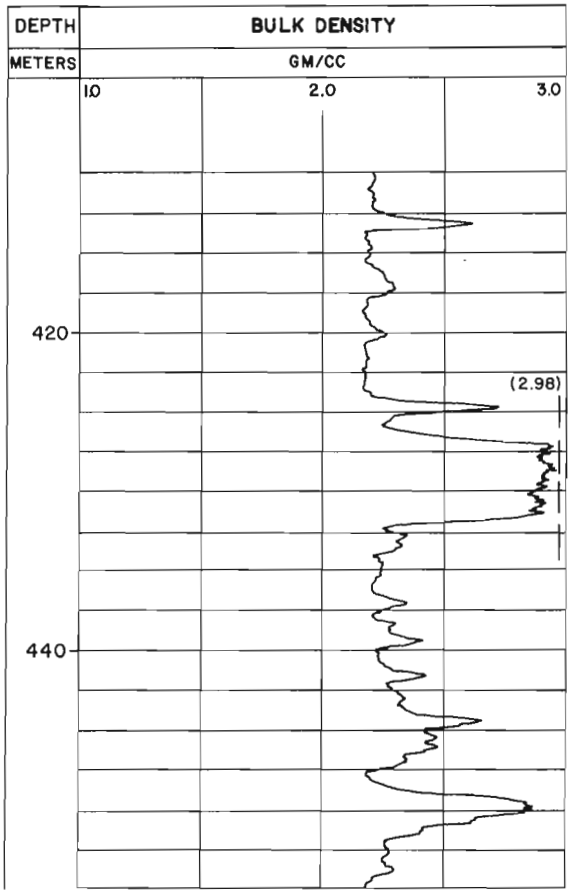

Figure 15

Density log: anhydrite signal.

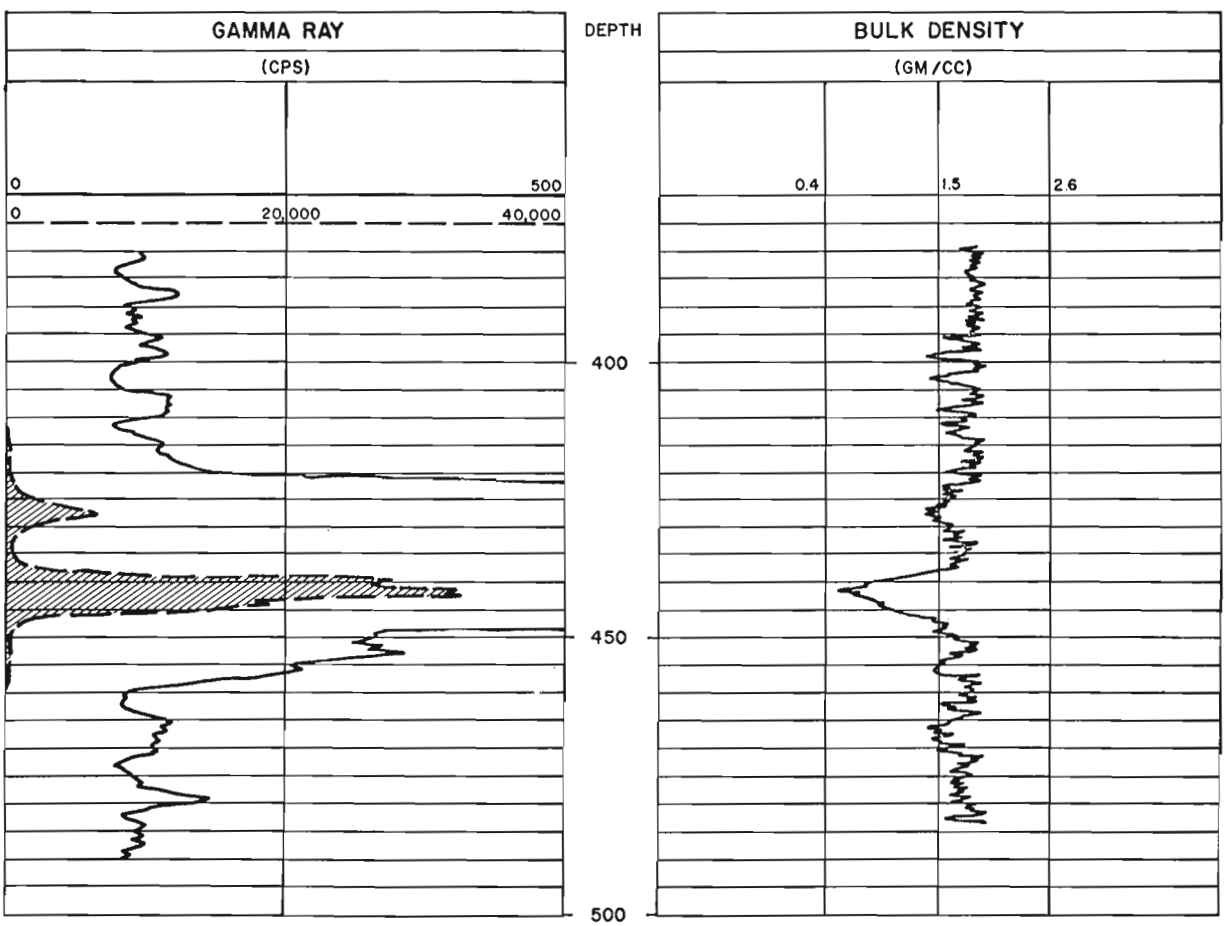

Figure 16. *^{238}U series gamma ray contamination of the density log.*

Gamma ray logs

Gamma ray logs are susceptible to logging speed and detector drift. Figure 19 shows an example of an unacceptable gamma ray detector drift. Figure 20 shows an example of a gamma ray log run with an inappropriate rate meter time constant (too long) for the logging speed used. The log at 3600 ft/hr is completely lacking in character.

Caliper logs

Caliper log primary standards are portable enough to be carried to the drill site. They are used to calibrate the tool prior to logging and check the tool calibration after logging. There should be minimal drift during the logging operation. The client should always specify that the contractor use calibration rings that span the bit and expected hole sizes. An independent check on the caliper calibration and linearity is to run the tool up into casing and compare the tool response to the casing I.D. Figure 21 shows an example where the caliper read larger than the casing I.D.

Fluid resistivity bridges

Formation fluid total dissolved solids (TDS) can be estimated from the SP log, or from resistivity and porosity logs. In either case, essential inputs are the resistivities of the mud (R_m) and mud filtrate (R_{mf}). These are obtained through use of a fluid resistivity bridge. Calibration of these bridges can be checked, using "standard" NaCl solutions. Figure 22 shows an example of such a calibration check where the bridge was not properly calibrated. The solid line in Figure 22 is the 1:1 line, indicating proper calibration. The actual measure points define a calibration line much different from 1:1. The true calibration line of Figure 22 was used to calibrate the R_{mf} and R_m values, and the contractor was notified about the bridge calibration problem. Figure 23 shows a similar calibration check conducted one month later with the same contractor. The calibration problem has now been rectified.

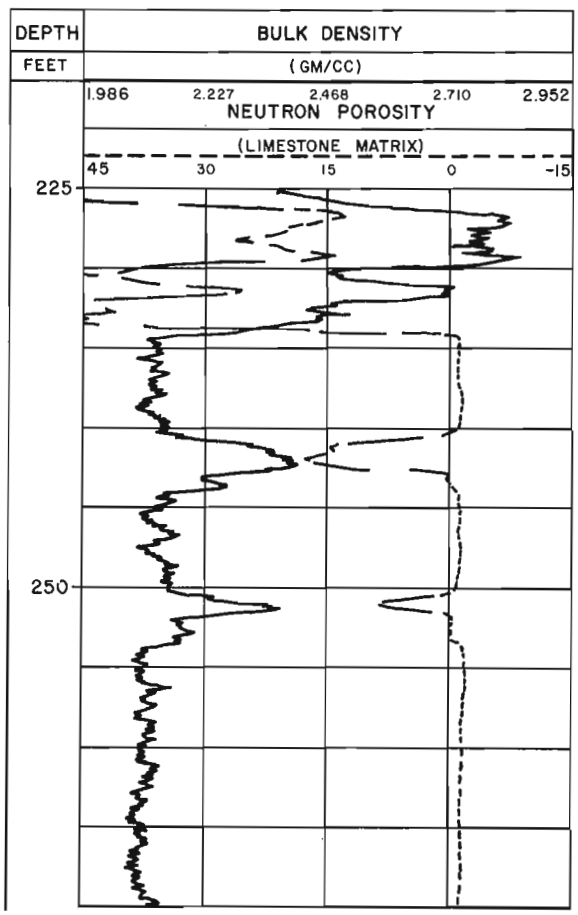

Figure 17. Neutron log halite signal.

Repeat logging intervals

Most geophysical wireline logs should yield the same values if logged through the same interval more than once. If the contractor cannot produce repeat intervals which agree, there is no sense in proceeding further. Figure 24 shows an example where the contractor could not produce a satisfactory repeat interval. Repeat intervals are selected by the client representative. Generally, these intervals should be of some geologic or economic significance. Successful repeat logs over these intervals builds confidence that quantitative interpretations made from these measurements will be valid.

Summary

The object of drill-site log quality control is improved product reliability. There is sometimes a fine line between a knowledgeable client representative helping to assure product quality and open harassment of the contractor. The key to obtaining this goal is open communication between client and contractor. Many of the calibration checks described in

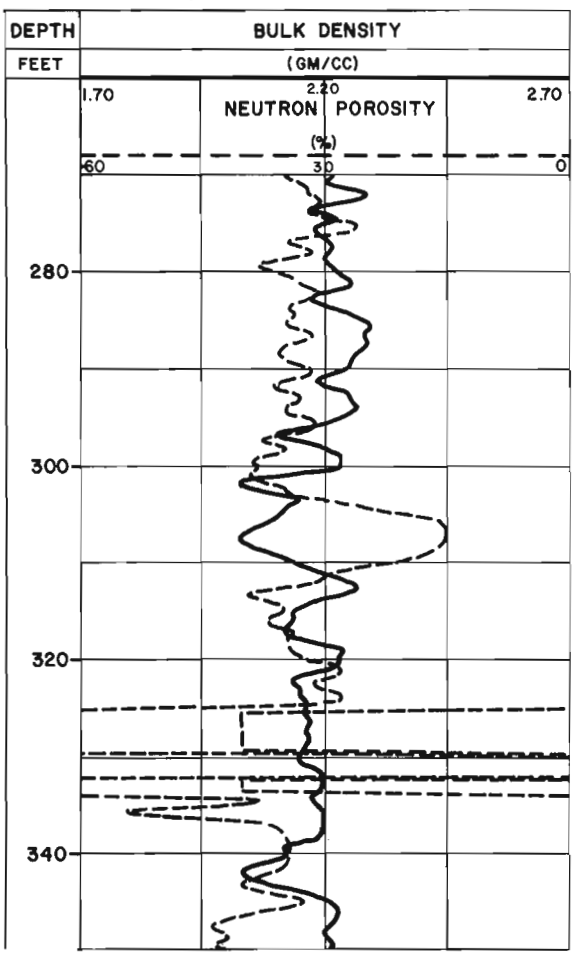

Figure 18. Neutron log hardware design failures due to gamma ray count rate saturation of far neutron detector cable channel.

	Tool Check			
	Before	After	Difference	Units
Gamma Ray	165	226	+61	GAPI
Caliper Small	6.0	6.2	+0.2	Inches
Caliper Large	12.0	12.2	+0.2	Inches

Figure 19

Gamma ray detector drift.

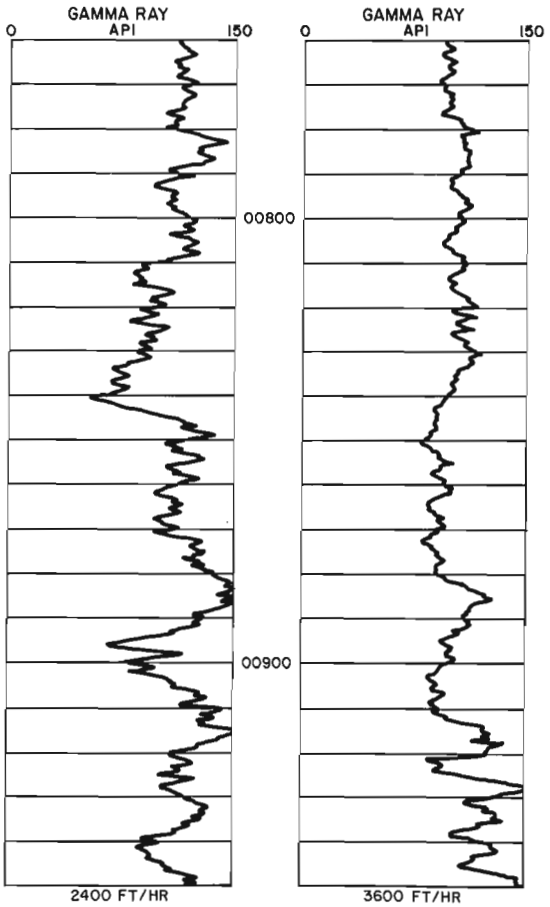

Figure 20. *Effects of logging speed on gamma ray response.*

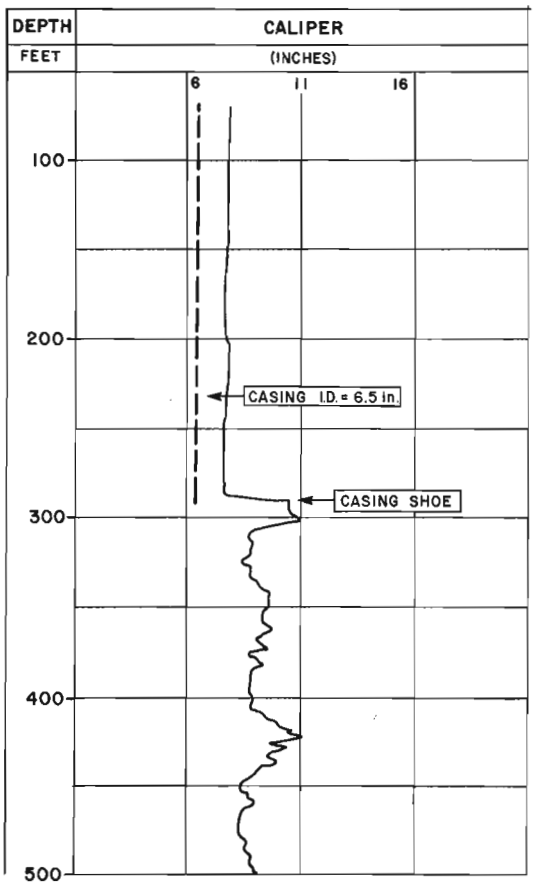

Figure 21. *Caliper log casing signal indicating improper calibration.*

this paper, go beyond those routinely employed by most contractors. The contractor should be informed of any special client-requested calibration checks, prior to "call-out". The goal of both client and contractor should be improved product quality. A partnership between contractor and client is an excellent way of insuring this goal. Many existing contractor calibration procedures originated from client requests for product quality assurance.

Active involvement by the client representative can greatly improve geophysical well-log product quality. High integrity log data will permit improved quantitative log interpretations.

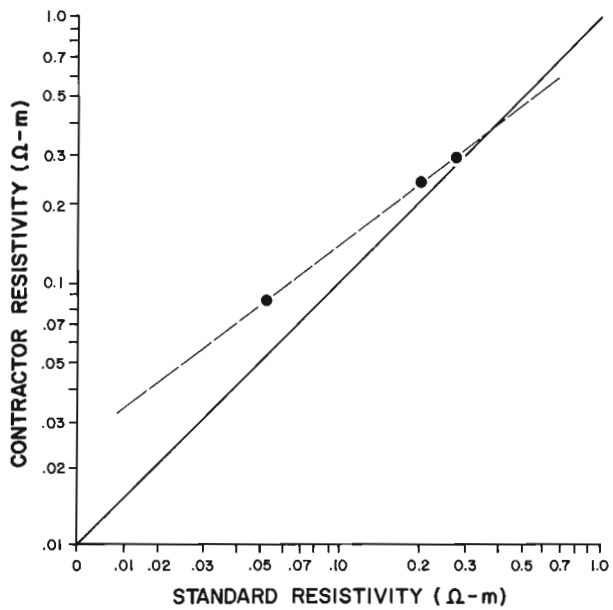

Figure 22. Fluid resistivity bridge field calibration check, indicating improper calibration.

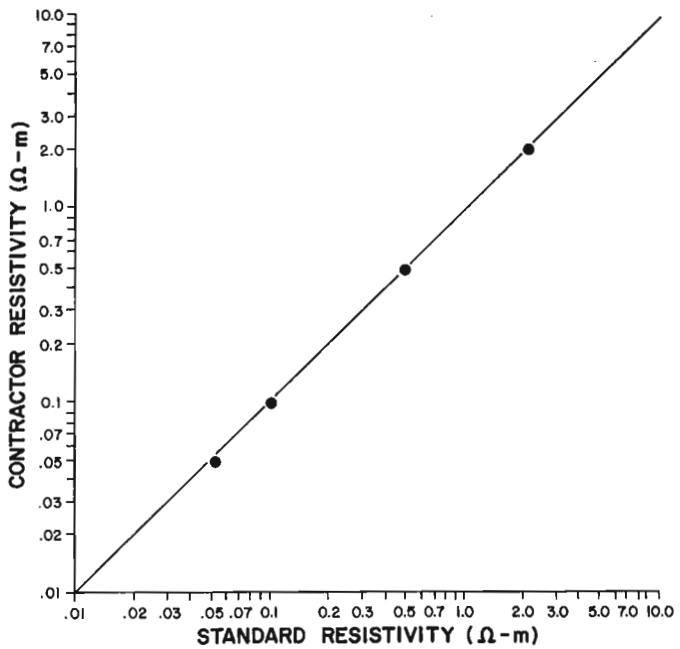

Figure 23. Fluid resistivity bridge field calibration check, indicating good calibration.

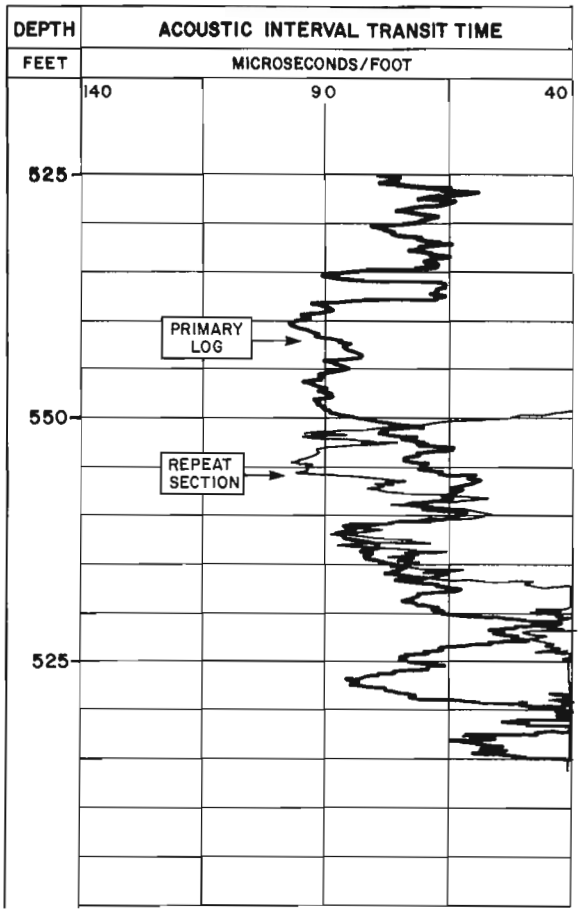

Figure 24. Example of inability to repeat logging measurements.

References

Allen, L.S., Caldwell, R.L., and Mills, W.R.
1965: Borehole models for logging; Society of Petroleum Engineers Journal, p. 109-112.

Annon.
1973: CSU Calibrations Guide, Schlumberger Well Services, Houston.

1974: Recommended practice for standard calibration and format for nuclear logs, API Recommended Practice 3.3.

Annon. (cont.)
1979: Calibration principles and field calibration procedures for Welex logs, Bulletin A-134, Welex, Houston.

1979: Calibrations Guide, Schlumberger Well Services, Houston.

Belknap, W.B., Dewan, J.T., Kirkpatrick, C.V., Mott, W.E., Pearson, A.J., and Rabson, W.R.
1959: API Calibration Facility for nuclear logs: Drilling and Production Practice, API, p. 289-316.

Bosworth
1972: Log calibrations surface and downhole, Canadian Well Logging Society Journal, v5, No. 1 (December), p. 39-68.

Cochrane, J.E.
1966: Principles of log calibration and their application to log accuracy: Journal of Petroleum Technology, p. 817-826.

Connolly, E.T.
1968: Standardization of large volumes of log data, Canadian Well Logging Society, Second Formation Evaluation Symposium.

1970: Interpretation and recognition of calibration and recording abnormalities on production logs, Canadian Well Logging Society Journal, v. 3, No. 1 (December), p. 89-122.

Czubek, J.A.
1976: Comparison of nuclear well logging data with the results of core analysis; Nuclear Techniques in Geochemistry and Geophysics, International Atomic Energy Agency, Vienna, p. 93-106.

Holt, O.R.
1975: Log quality control: Transactions, SPWLA, Sixteenth Annual Logging Symposium, June 4-7, New Orleans, LA, Paper BB.

Killeen, P.G. and Conaway, J.G.
1978: New facilities for calibrating gamma ray spectrometric logging and surface equipment, Canadian Mining and Metallurgical Bulletin (May), Vol. 71, No. 793, p. 84-87.

Maciula, E.A. and Cochrane, J.E.
1968: Quantitative use of calibration data to correct miscalibrated well logs: Journal of Petroleum Technology, p. 663-670.

Mathews, M.
1979: Log responses from the Geothermal Calibration/Test Well C/T-2: Transactions, SPWLA, Twentieth Annual Logging Symposium, June 3-6, Tulsa, OK, Paper SS.

Mathews, M.A., Koizumi, C.J., and Evans, H.B.
1978: DOE-Grand Junction Logging Model Data Synopsis: Bendix Field Engineering Report No. GJBX-76(78).

Mills, W.R., Hoyer, W.A., Tittman, J., and Wilson, B.F.
1977: A proposed calibration facility for pulsed neutron logging tools: The Log Analyst, V. 18, No. 1, p. 3-5.

Snodgrass, J.J.
1976: Calibration models for geophysical borehole logging: Bureau of Mines Report of Investigation, RI 8148.

Wahl, J.S., Tittman, J., and Johnstone, C.W.
1964: The Dual Spacing Formation Density Log, Journal of Petroleum Technology, December.

Waller, W.C., Cram, M.E., and Hall,J.E.
1975: Mechanics of log calibration: Transactions, SPWLA, Sixteenth Annual Logging Symposium, June 4-7, Paper GG, New Orleans, LA.

INTER-BOREHOLE SEISMOLOGY FOR GEOLOGICAL PROBING

J. Wong, P. Hurley, and G.F. West[1]

Wong, J., Hurley, P., and West, G.F., Inter-borehole seismology for geological probing; in Borehole Geophysics for Mining and Geotechnical Applications, ed. P.G. Killeen, Geological Survey of Canada, Paper 85-27, p. 393-399, 1986.

Abstract

A crosshole audiofrequency seismic system has been developed at the University of Toronto Geophysics Laboratory to be used for rock mass characterization. High-quality seismograms have been recorded with the system for distances up to 230 m in unaltered granites. It has been ascertained that travel times and signal amplitudes provide useful information about rock quality. It is anticipated that under favourable conditions systematic scanning of the rock between two boreholes can reveal or confirm structural and lithological details.

Résumé

Le Laboratoire de géophysique de l'Université de Toronto a réalisé un système de sondage sismique transversal à audiofréquences qui permet de déterminer les caractéristiques de la masse rocheuse. Des sismogrammes de haute qualité ont été enregistrés à l'aide de ce système pour des parcours allant jusqu'à 230 m dans des granites non altérés. On a confirmé que la connaissance des temps de parcours et des amplitudes de signal est très utile à la détermination des caractéristiques de la roche. Le sondage systématique de la roche entre deux trous de sondage devrait révéler ou confirmer des détails structuraux et lithographiques, pourvu que les conditions le permettent.

Introduction

Cracks, fractures, and joints have been shown both theoretically and experimentally to determine the mechanical and seismic properties of rocks (Hudson, 1981; Crampin et al., 1981; Stierman and Kovach, 1979; Walsh, 1965). For this reason, seismic methods are well suited for remote and non-destructive testing of rock quality in situ. Crosshole seismic techniques have been used in engineering and structural geological studies in a wide range of circumstances (Aki et al., 1982; Paulsson and King, 1980; Thill, 1978; McCann et al., 1975; Bois et al., 1972).

At the University of Toronto, a crosshole seismic system has recently been developed and implemented, incorporating a number of features which optimize resolution, data quality, and ease of field operation. Both the transmitter and receiver are based on piezoelectric transducers and are housed in sondes for use in 76 mm (NQ Size) or larger diameter boreholes. Once in a borehole, the transmitter can be activated continuously from the surface for the entire survey. The peak power is deliberately kept low so that the borehole is not damaged.

In order to be capable of resolving geological detail on the scale of 1 to 5 m in rocks with velocities ranging from 3 to 6 km/s, the operating frequencies of the system are in the mid-audio range, i.e., 1 to 6 kHz. Despite the low peak power and relatively high frequencies (which undergo stronger attenuation), crosshole distances of several hundred metres are feasible in unaltered and unfractured crystalline rocks. This is possible because signal-to-noise ratios can be increased dramatically through stacking and cross-correlation. The field data are stored digitally to facilitate on-site and post-survey processing.

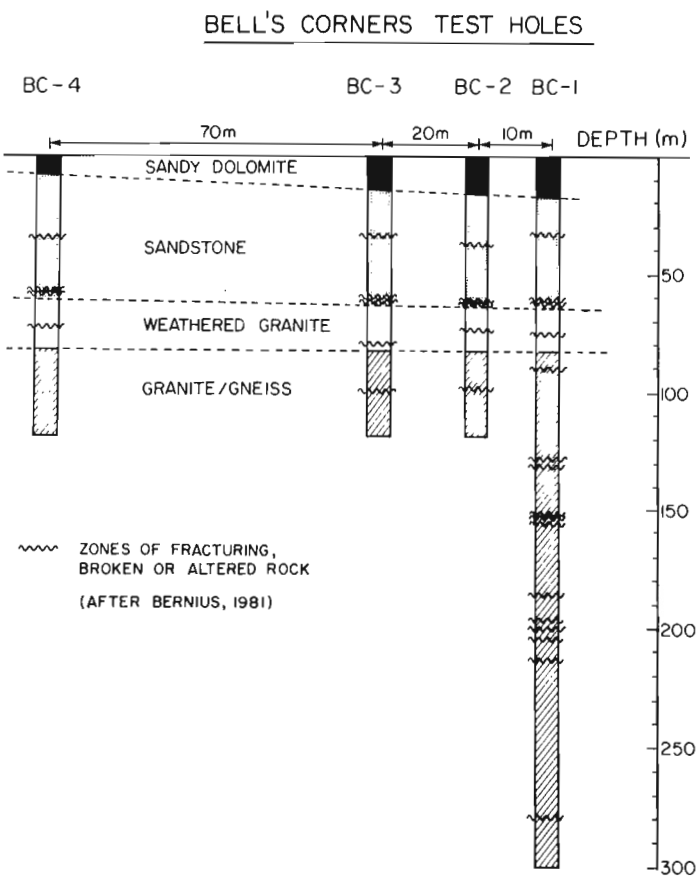

Figure 1. *Generalized geology in the boreholes at the GSC Borehole Geophysics Test Area in Bell's Corners, near Ottawa Ontario (after Bernius, 1981).*

[1] University of Toronto, Toronto, Ontario M5S 1A7

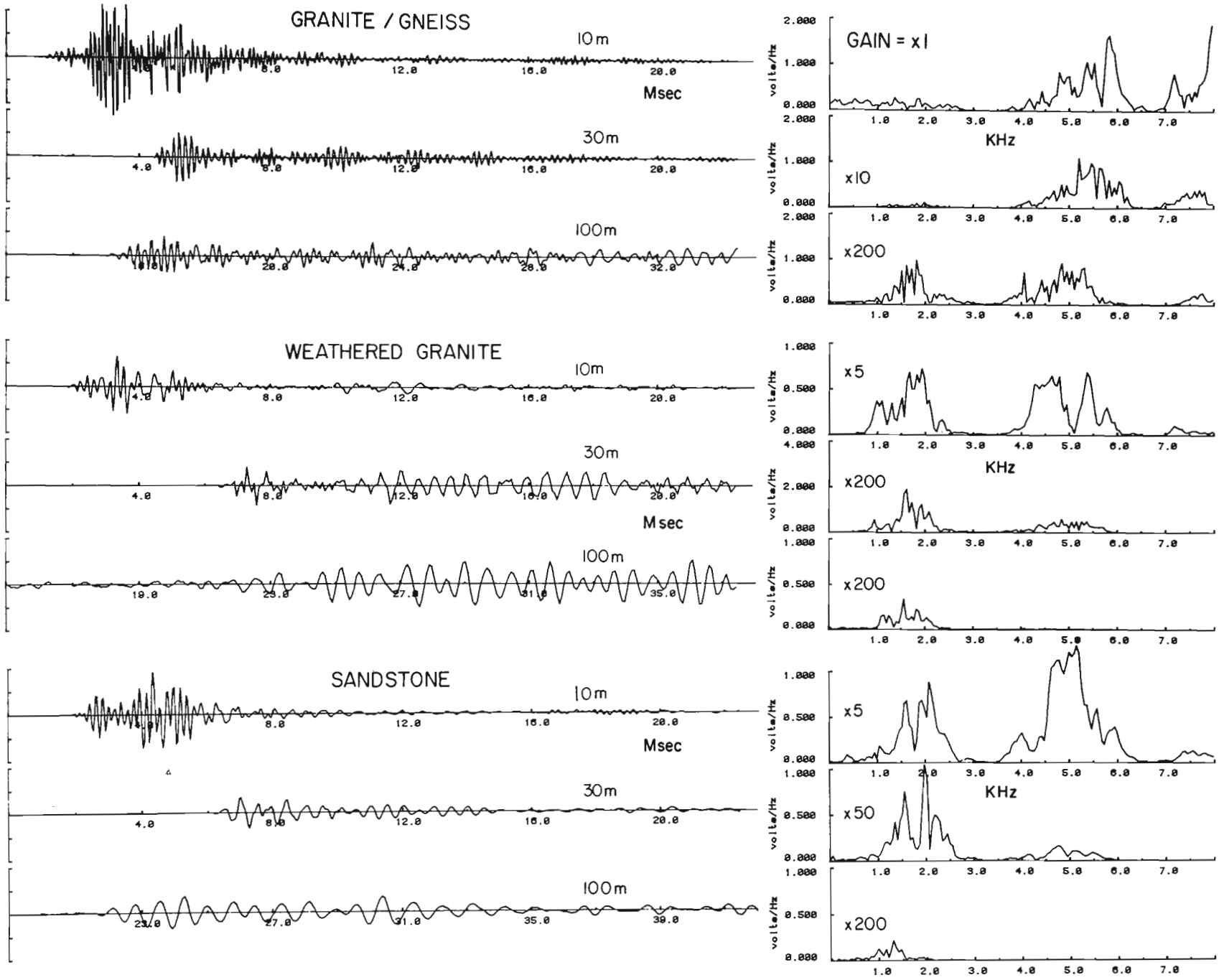

Figure 2. *Seismograms and their amplitude spectra for different rock types and at different ranges for the test boreholes.*

Field results

Figure 1 shows the geological logs (Bernius, 1981) of four near-vertical boreholes at the Geological Survey of Canada Borehole Geophysics Test Area at Bell's Corners, near Ottawa, Ontario. The top 65 m of rock is mostly sandy dolomite and sandstone. This is underlain by 17 m of severely weathered and altered Precambrian granite with abundant occurrences of chlorite, clay minerals, and altered feldspar. The alteration grades into unweathered granite and gneiss at about 80 m depth. Numerous small fractures and faults were observed in the core of all four boreholes.

Observations were made on how seismograms change as the path length between the receiver and transmitter increases for the different rock types: the sandstone at a depth of 50 m, the weathered granite at 70 m, and the granite-gneiss at 113 m. The transmitter and receiver sondes were placed in different borehole combinations (labelled as BC-1, BC-2, BC-3, BC-4) to obtain horizontal distances of 10, 30, and 100 m. Figure 2 shows the seismograms and their amplitude spectra estimated by the fast Fourier transform. The nulls in energy at 3.3 and 6.6 kHz occur because a driving waveform was chosen for the piezoelectric transmitting transducers with these nulls. It is clear that the high-frequency energy (>3.3 kHz) is rapidly attenuated in sandstone and altered granite, but it persists with relatively strong amplitude out to distances of about 100 m in unweathered granite-gneiss.

In Figure 3, first arrival times and logarithms of amplitudes (corrected for geometrical spreading and averaged over two frequency bands 1 to 3.3 kHz and 3.3 to 6.6 kHz) are plotted against range. The slopes of these plots give the apparent P velocities V_p and attenuation coefficients α_p. Both V_p and α_p strongly reflect the different mechanical properties of sandstone, weathered granite, and unweathered granite-gneiss.

Using the attenuation coefficients, velocities, and frequencies from Figure 3, we can estimate the rock quality factor $Q_p = \pi f/V_p/\alpha_p$. In the frequency band 1 to 6.6 kHz, Q_p is estimated to be between 85 to 95 for the unweathered granite, and between 30 and 45 for both the altered granite and sandstone. These Q_p estimates are noteworthy because they are derived from in situ measurements over distances of 10 to 100 m. They appear to be in general agreement with Q values determined in laboratory experiments using decimeter-sized rock specimens and ultrasonic frequencies (Johnston et al., 1979; Winkler and Nur, 1982). However, caution must be exercised in interpreting the significance of the apparent Q_p values since the loss of wave coherence and amplitude in the field experiment likely is caused by several physical processes, including, for example, anelastic absorption and scattering and diffraction by cracks and fractures of various sizes.

In Figure 4, we have shown constant-gain seismic fans of the two horizontal components (channels 2 and 3) of motion with the receiver sonde fixed at a depth of 113 m in BC-4 and the transmitter moved in one metre intervals from a depth of 113 to 213 m in BC-1. Direct arrivals on the upper parts of the fans and tube waves are obvious. There is a sharp decrease in direct arrival amplitude beneath the transmitter depth of 183 m where a major fracture intersection occurs. Random scattering by numerous small cracks and joints in the rock make these seismograms with longer travel paths extremely complicated and cluttered so that secondary arrivals such as S events or reflections are difficult to identify.

When the rock is relatively uncracked and unfractured, shear waves are identifiable as is shown in Figure 5. These seismograms were taken between two near-vertical 165 mm-diameter boreholes drilled 13 m apart in biotite granite at another test site. For these two seismic fans, the transmitter was fixed at 100 and 148 m in one borehole while the receiver was moved through 2.26 m intervals in the other. Both S and P arrivals can be seen clearly but the S is relatively much stronger for the upper transmitter position (fan on left side). This is because the lower transmitter position is located in a zone of fractured rock. For both seismic fans, the average S and P velocities were calculated to be about 3.1 and 5.5 km/s. Independent estimates for the density of the granite from gamma-gamma logs of 2.7 gm/cm^3 allow us to infer that the dynamic Young's

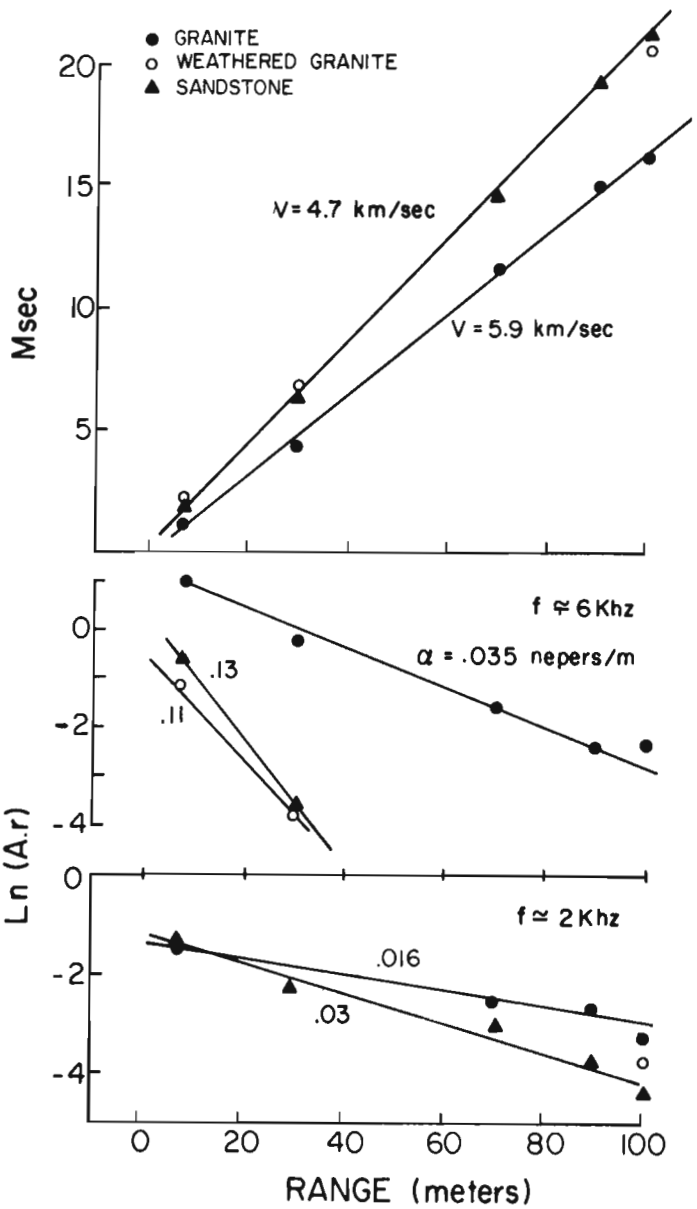

Figure 3. *Velocity and attenuation estimates for different rock types.*

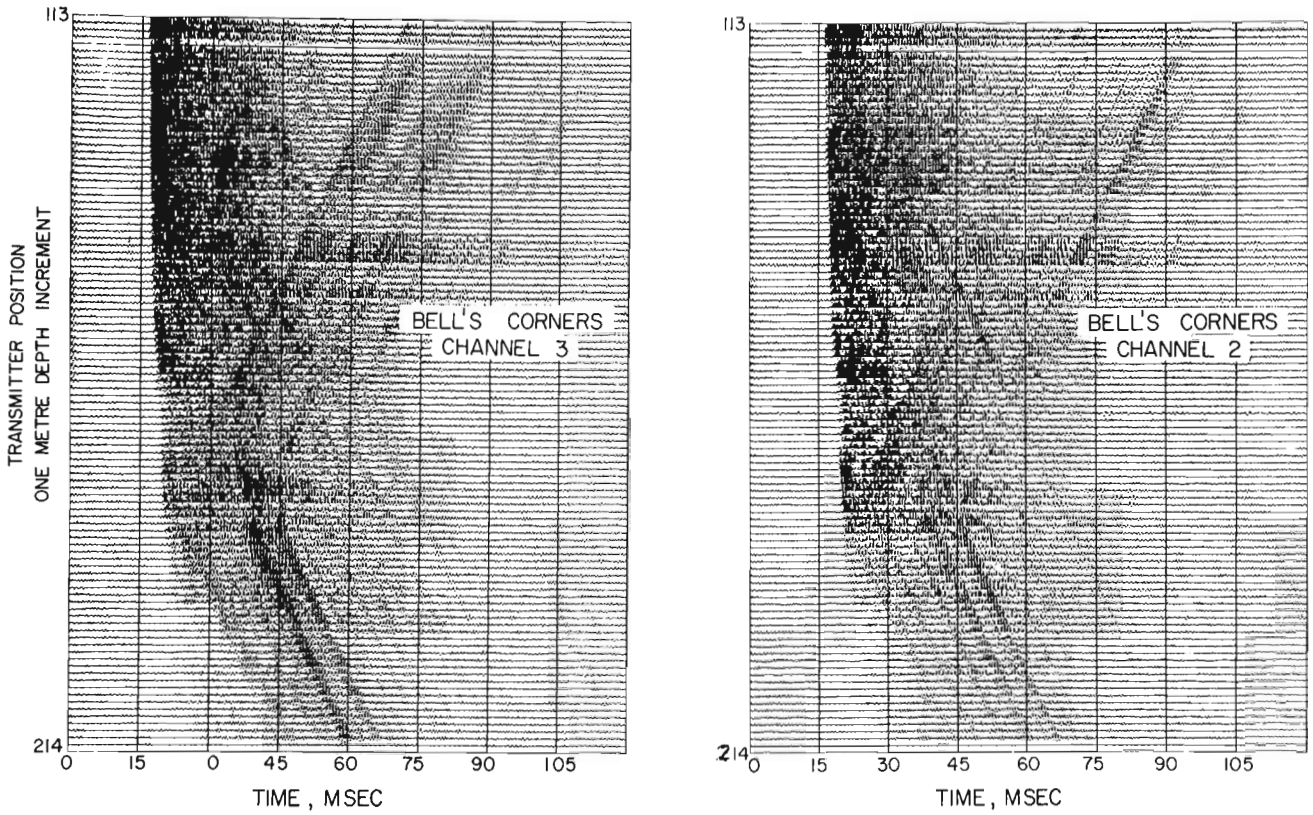

Figure 4. *Constant-gain seismic fan in granite/gneiss. The receiver is fixed at a depth of 113 m in borehole BC-4, while the transmitter is moved in one metre intervals in BC-1 from a depth of 113 m to 213 m.*

modulus and Poisson's ratio are 65 Gpa and 0.245 respectively. Such estimates of mechanical constants of rock may have important implications for mining and geological engineering.

Figure 6 shows a seismic fan observed between two boreholes 175 m apart. The transmitter is fixed in one borehole at a depth of 250 m while the receiver is moved from a depth of 100 m to 350 m in 5 m intervals in the other borehole. The maximum separation between the transmitter and receiver in these seismograms is about 230 m. The direct P arrivals can be seen clearly, and the average velocities of these granites is determined to range from 5.5 to 6.6 km/s. A sharp decrease in signal amplitudes for the lower receiver positions is also observed (approximately 305 m). For these seismograms, the receiver has moved below a fracture zone while the transmitter remains above it. The presence of broken and fractured rock in the seismic path between the sondes has severely attenuated the transmitted acoustic energy, creating a seismic shadow. The prominent low-velocity events in the fan originating at receiver depths of 245 and 300 m are tube waves due to the conversion of P energy by fracture intersections at these depths. There is no clear evidence of shear energy in this fan. It appears that small cracks and fractures along these longer travel paths have completely dissipated coherent S arrivals.

Conclusion

Field results using the crosshole system indicate the potential usefulness of the technique in rock mass characterization and determination of geological structure. They indicate that systematic scanning between two boreholes with many seismic fans would be capable of revealing geological details for distances away from the boreholes as great as 230 m in unaltered granites. This is significantly larger than the radii of investigation of standard geophysical logging tools.

Acknowledgments

This research was supported by Energy, Mines, and Resources Canada and Atomic Energy of Canada Limited.

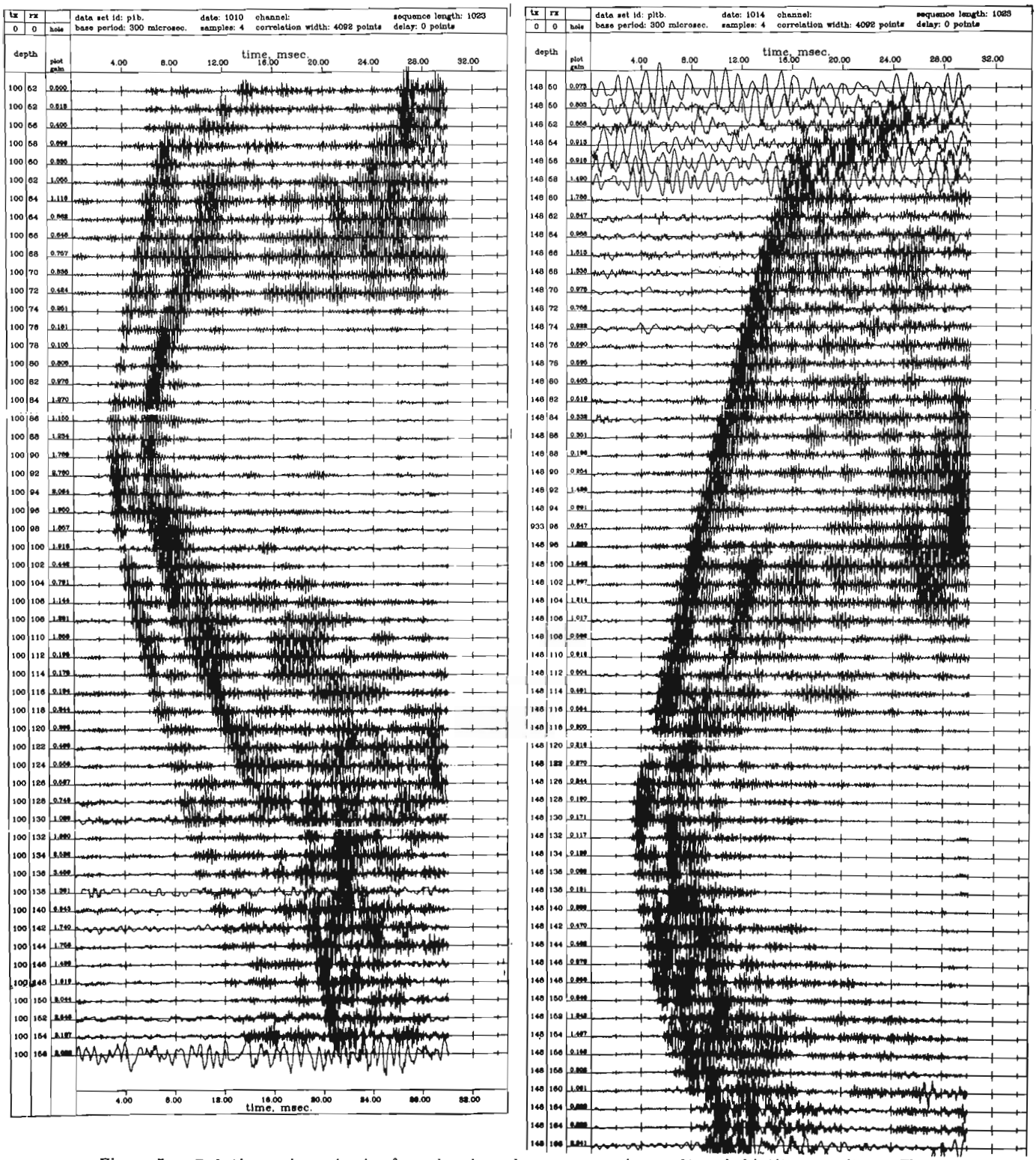

Figure 5. *Relative-gain seismic fan showing shear waves in unaltered biotite granite. The transmitter was fixed at 100 m and 148 m in one borehole while the receiver was moved in 2.26 m steps down to 214 m.*

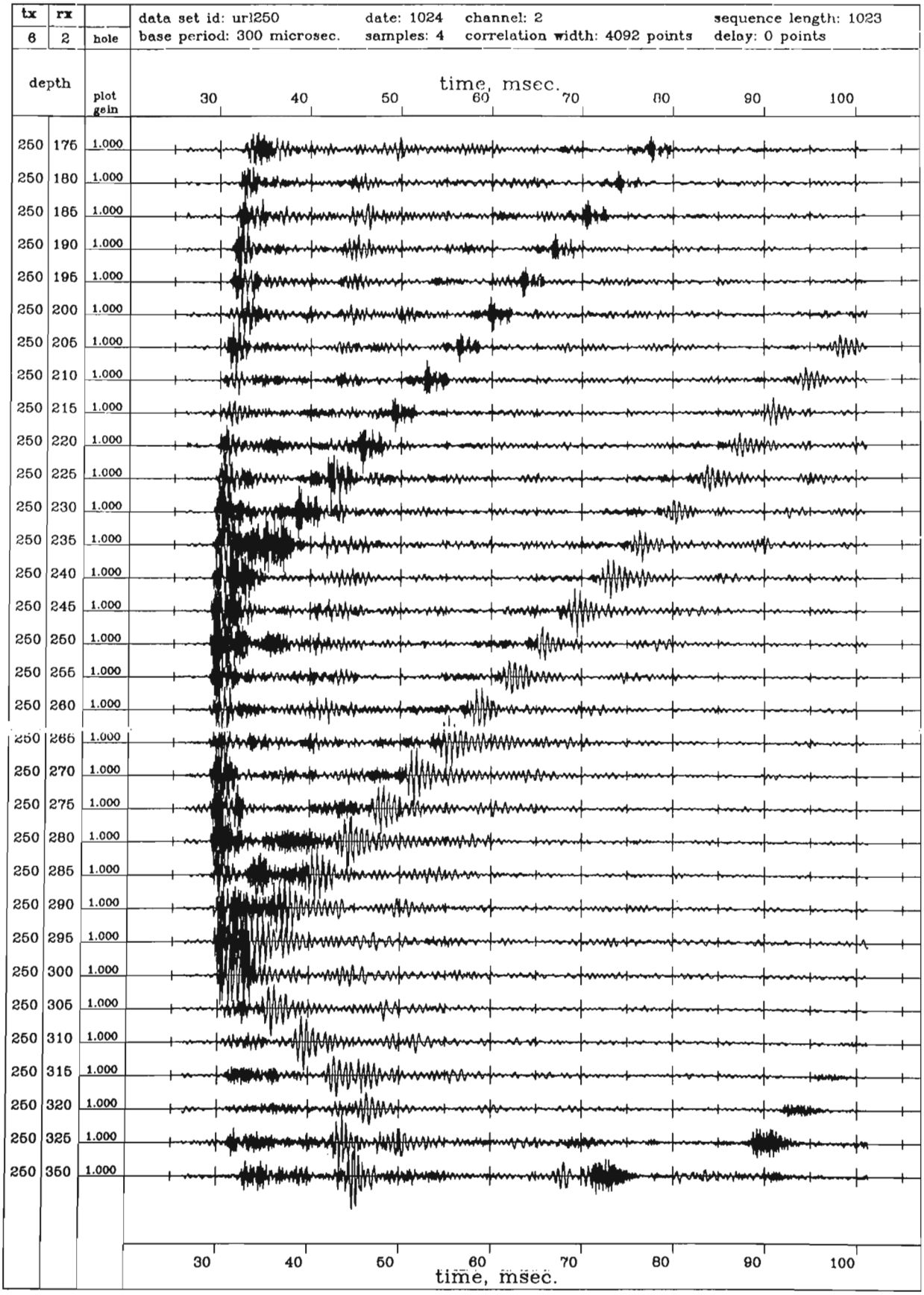

Figure 6. *Constant-gain seismic fan between two holes 175 m apart in biotite granite. The transmitter was fixed at 250 m while the receiver was moved in 5 m steps from 100 m to 350 m in the other borehole.*

References

Aki K., Fehler, M., Aamodt, R.L., Albright, R.N., Potter, R.M., Pearson, C.M., and Tester, J.W.
1982: Interpretation of seismic data from hydraulic fracturing experiments at the Fenton Hill, N.M., Hot Dry Rock Geothermal Site, Journal of Geophysical Researh, v. 87, p. 936.

Bernius- G.R.
1981: Boreholes near Ottawa for the development and testing of borehole logging equipment - a preliminary report; in Current Research, Part C; Geological Survey of Canada, Paper 81-1C, p. 51.

Bois, P., LaPorte, M., Lavergne, M., and Thomas, G.
1972: Well-to-well seismic measurements; Geophysics, v. 37, p. 471.

Crampin, S., McGonigle, R.M., and Bamford, D.
1980: Estimating crack parameters from observations of P-wave velocity anistropy; Geophysics, v. 45, p. 345.

Hudson, J.A.
1981: Wave speed and attenuation of elastic waves in material containing cracks; Geophysical Journal of the Royal Astronomical Society, v. 64, p. 133.

Johnston, D.H., Toksoz, M.N., and Timur, A.
1979: Attenuation of seismic waves in dry and saturated rocks; Geophysics, v. 44,p. 631.

McCann, D.M., Grainger, P., and McCann, C.
1975: Inter-borehole acoustic measurements and their use in engineering geology, Geophysical Prospecting, v. 23, p. 50.

Paulsson, B.N.P. and King, M.S.
1980: Between-hole acoustic surveying and monitoring of a granitic rock mass, International Journal of Rock Mechanics, Mining, Sciences and Geomechanics; Abstract, v. 17, p. 371.

Stierman, D.J. and Kovach, R.L.
1979: An in situ velocity study: the Stone Canyon well; Journal of Geophysical Research, v. 84, p. 672.

Thill, R.E.
1978: Acoustic cross-borehole apparatus for determining in situ elastic properties and structural integrity of rock masses, Proc.19th U.S. Rock Mechanics Symposium; University of Nevada-Reno Press, p. 121.

Walsh, J.B.
1965: The effect of cracks on the compressibility of rock, Journal of Geophysical Research, v. 70, p. 381.

Winkler, K.W. and Nur, A.
1982: Seismic attenuation: effects of fluids and frictional sliding, Geophysics, v. 47, p. 1.

Energy, Mines and Resources Canada
Énergie, Mines et Ressources Canada